Matthias Schädel
Dawn Shaughnessy
Editors

The Chemistry of Superheavy Elements

Second Edition

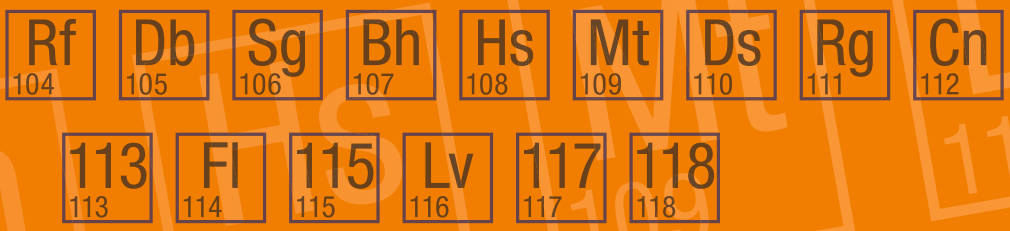

Springer

The Chemistry of Superheavy Elements

Matthias Schädel · Dawn Shaughnessy
Editors

The Chemistry of Superheavy Elements

Second Edition

Springer

Editors
Matthias Schädel
GSI Helmholtzzentrum für
Schwerionenforschung GmbH
Darmstadt
Germany

and

Advanced Science Research Center
Japan Atomic Energy Agency
Tokai-mura, Ibaraki
Japan

Dawn Shaughnessy
Physical and Life Sciences Directorate
Lawrence Livermore National Laboratory
Livermore, CA
USA

ISBN 978-3-642-37465-4 ISBN 978-3-642-37466-1 (eBook)
DOI 10.1007/978-3-642-37466-1
Springer Heidelberg New York Dordrecht London

Library of Congress Control Number: 2013950357

Printed on acid-free paper

Springer is part of Springer Science+Business Media (www.springer.com)

Preface to the Second Edition

Over the last decade, since the first edition of *The Chemistry of Superheavy Elements* appeared in 2003, the field of superheavy elements—chemistry and physics, experiment and theory—has made an enormously big leap forward. The discovery of elements 114 and 116, located in the center region of the long sought and highly desired "traditional" Island of Stability, was officially accepted and they were named flerovium (Fl) and livermorium (Lv). Further experiments provide strong evidence for the synthesis of all elements up to atomic number 118; a homolog of radon. With the complete filling of the seventh row of the Periodic Table of the Elements, experimenters set out to search for elements 119 and 120. They will be the first two elements of the eighth period followed by element 121, which would mark the beginning of the super-actinides. Technical advancements enable the beginning of a detailed nuclear spectroscopy of the first transactinides shedding more light on the nuclear structure and stability, including the shell effects, of these elusive elements. This helps to determine the position and strength of those nuclear shells which enable the existence of superheavy elements.

Chemistry has finally reached and is presently focusing on element 114. In addition, a new field of superheavy element chemistry has opened up entirely new perspectives—chemical studies after preseparation with gas-filled recoil separators. This includes metal-organic chemistry of superheavy elements and, potentially, aqueous phase chemistry beyond seaborgium. While advancements in fully-relativistic theoretical chemistry facilitate a much deeper understanding of experimental results, at the same time, experiments also challenge theory.

These are good reasons for an up-to-date second edition of this book. The first chapter of the previous edition was replaced by two completely new and much more extended ones highlighting the nuclear aspects much more than in the first edition.

Chapter 1 deals with nuclear synthesis of superheavy elements, including many production, separation, and identification aspects, and with the nuclear decay properties of the heaviest nuclides. Now, this chapter is focused much more on those nuclear reactions, which recently facilitated the production of the heaviest

elements and the more neutron-rich, longer-lived isotopes that are essential for chemical studies.

Chapter 2 outlines the present status of nuclear spectroscopy and nuclear structure studies in the transition region from heavy actinides into transactinides. It includes a detailed discussion of state-of-the-art techniques, provides basic nuclear structure and nuclear model information, as well as recent experimental results.

Chapter 3, which provides a summary of chemical properties of transactinides from a theoretical point of view, is significantly extended over the first edition. This reflects spectacular developments in relativistic quantum theory and computational algorithms, which provide improved information on atomic, ionic, and molecular properties of superheavy elements. It clearly demonstrates the importance of relativistic effects in the chemistry of superheavy elements and enables deeper insights into the architecture of the Periodic Table at its far end.

Chapter 4 discusses fundamental questions of the validity of chemical information obtained one atom-at-a-time. While still presenting concepts of statistical thermodynamics and fluctuation theory, and discussing limitations of atom-at-a-time chemistry, the revised version of this chapter includes a discussion of atom-at-a-time chemistry in more general terms.

Chapter 5 shows the progress made in experimental techniques including automated devices for chemical separations performed in the aqueous phase and the gas-phase as well as coupling of such devices to recoil separators.

Chapter 6 presents the wealth of information obtained about properties of transactinides up to element 106, seaborgium, in the aqueous phase. This includes new and detailed information on the chemistry of elements 104, rutherfordium, and element 105, dubnium.

As in the first edition, the revised version of Chap. 7 discusses thermodynamic data derived from gas-phase adsorption experiments and extrapolations into unknown regions including predictions of thermochemical properties.

Chapter 8 summarizes the results of chemical studies of superheavy elements in the gas-phase and their wall-adsorption properties. In addition to new results on lighter transactinides, first results on gas-phase and wall-adsorption properties of elements 112 and 114 are part of the focus of this chapter. It also provides new information on element 108, hassium, including interesting new nuclear data obtained with chemical methods.

The historical reminiscences of Chap. 9 are completed by one section bridging the gap between early attempts to synthesize superheavy elements and the success of recent experiments.

It is a great pleasure for me to thank my Coeditor Dawn Shaughnessy, who triggered this second edition and worked on many chapters and aspects, and Elizabeth Hawkins from Springer, who not only convinced me to again embark on this enterprise but helped me with her competence and friendliness most patiently through the process of making this edition possible. Many thanks go to the Authors of the individual chapters—the ones who already contributed to the first edition and again worked hard on the second one and the new Authors who helped to widen and deepen many perspectives in this book and bring it up-to-date. Last but

not least it is a great pleasure to again thank Brigitta Schausten for helping technically to get the project started and for her work on some graphics, especially the Periodic Table as a ball.

Wiesbaden, March 2013 Matthias Schädel

Preface to the First Edition

This book is the first to treat the chemistry of superheavy elements, including important related nuclear aspects, as a self contained topic. It is written for those—students and novices—who begin to work and those who are working in this fascinating and challenging field of the heaviest and superheavy elements, for their lecturers, their advisers and for the practicing scientists in the field—chemists and physicists—as the most complete source of reference about our today's knowledge of the chemistry of transactinides and superheavy elements. However, besides a number of very detailed discussions for the experts this book shall also provide interesting and easy to read material for teachers who are interested in this subject, for those chemists and physicists who are not experts in the field and for our interested fellow scientists in adjacent fields. Special emphasis is laid on an extensive coverage of the original literature in the reference part of each of the eight chapters to facilitate further and deeper studies of specific aspects. The index for each chapter should provide help to easily find a desired topic and to use this book as a convenient source to get fast access to a desired topic.

Superheavy elements—chemical elements which are much heavier than those which we know of from our daily life—are a persistent dream in human minds and the kernel of science fiction literature for about a century. This book describes in Chap. 1 how today this dream becomes true at a few accelerator laboratories, what the tools are to synthesize these elusive, man-made elements in heavy-ion nuclear reactions and how to detect the specific nuclear decays which terminate their existence shortly after they are created. The current status of experimental and theoretical insights into this very unique region of nuclear stability is briefly reviewed. The last chapter outlines historical developments, from first scientifically sound ideas about the existence of superheavy elements, which surfaced during the mid-50s, all the way to the beginning of the current research programs described in Chap. 1. It also discusses experimental attempts and prospects of the search for superheavy elements in Nature.

Today, one century after Ernest Rutherford and Frederick Soddy postulated that in the radioactive decay one chemical element transmutes into a new one, we know of 112 chemical elements. The discoveries of elements 114 and 116 are currently waiting to be confirmed and experimentalists are embarking to discover new and heavier elements. Now where are superheavy elements located on a physicist's

chart of nuclides and on the Periodic Table of the Elements—the most basic chart in chemistry?

The term "superheavy elements" was first coined for elements on a remote "island of stability" around atomic number 114 (Chap. 8). At that time this island of stability was believed to be surrounded by a "sea of instability". By now, as shown in Chap. 1, this sea has drained off and sandbanks and rocky footpaths, paved with cobblestones of shell-stabilized *deformed* nuclei, are connecting the region of shell-stabilized *spherical* nuclei around element 114 to our known world.

Perfectly acceptable, some authors are still using the term "superheavy element" in its traditional form; others have widened this region and have included lighter elements. It is generally agreed that the term "superheavy element" is a synonym for elements which exist solely due to their nuclear shell effects. From this point of view there are good arguments to begin the series of superheavy elements with element 104, rutherfordium. Because of the extra stability from nuclear shell-effects the known isotopes of rutherfordium exhibit half-lives of up to one minute. This is 16 orders of magnitude longer than the expected nuclear lifetime of 10^{-14} s these isotopes would survive without any extra shell stabilization. Taking 10^{-14} s as a realistic limit for a minimum lifetime of a system which can be called a chemical element, and assuming the absence of any shell effects, the world of chemical elements would be terminated at the end of the actinides. The appealing aspect of having the superheavy elements begin at element 104 is that this is identical with the beginning of the series of transactinide elements. The terms "superheavy elements" and "transactinide elements", in short "transactinides", are used with an equal meaning in this book.

One of the most important and most fascinating questions for a chemist is the one about the position of the superheavy elements in the Periodic Table of the Elements; how well accommodates the Periodic Table these elements as transition metals in the seventh period. Do the rules of the Periodic Table still hold for the heaviest elements? What is a valid architecture of the Periodic Table at its upper end? The main body of information to answer this question from our today's knowledge of the chemistry of superheavy or transactinide elements is embraced between the two mainly "nuclear" oriented chapters at the beginning and at the end.

One century after the beginning of most dramatic changes in physics and chemistry, after the advent of quantum theory and in the year of the 100th anniversary of Paul A.M. Dirac, modern relativistic atomic and molecular calculations clearly show the very strong influence of direct and indirect relativistic effects not only on electronic configurations but also on chemical properties of the heaviest elements. The actual state of the theoretical chemistry of the heaviest elements is comprehensively covered in Chap. 2. It does not only discuss most recent theoretical developments and results, where especially up to date molecular calculations dramatically increased our insights over the last decade, but it also relates these results to experimental observations.

The chemistry of superheavy elements always faces a one-atom-at-a-time situation—performing separations and characterizations of an element with single,

short-lived atoms establishes one of the most extreme limits in chemistry. While large numbers of atoms and molecules are deeply inherent in the statistical approach to understanding chemical reactions as dynamic, reversible processes Chap. 3 discusses specific aspects how the behavior of single atoms mirrors properties of macro amounts.

A large variety of tools, from manual separation procedures to very sophisticated, automated computer-controlled apparatuses have been developed and are now at hand to study the chemical properties of these short-lived elements one-atom-at-a-time in the liquid phase and in the gas phase. It is demonstrated in Chap. 4 how this can be achieved, what kinds of set-ups are presently available and what the prospects are for future developments to further expand our knowledge.

The known chemical properties of superheavy elements are presented and discussed in Chaps. 5 and 7 based upon experimental results obtained from the liquid phase and from the gas phase, respectively. It is quite natural that there is a large body of information on group-4 element 104, rutherfordium, and group-5 element 105, dubnium, which are now under investigation for three decades. However, recent detailed studies demonstrate that these elements still hold many surprises. They sometimes exhibit rather unexpected properties. The chemistry of element 106, seaborgium, was first tackled in 1995 followed by a series of experiments in the aqueous and the gas phase. While most of them revealed a "surprisingly normal" behavior, at least one experiment indicated a deviation from an extrapolation in group 6. Even more challenging, because of the only very few numbers of atoms produced per day, were recent investigations on elements 107, bohrium, and 108, hassium, performed in one gas phase experiment each. This is presented in Chap. 7 together with an attempt to get a first glimpse of the chemical property of element 112. Will it chemically react like mercury or will it be much more inert; presumably due to strong influence of relativistic effects?

Empirical models are frequently applied in chemistry to relate experimental observations to physicochemical or thermodynamical quantities. This has extensively been used over several decades for the interpretation of experimental results obtained from gas phase adsorption processes and is still used to interpret the gas chromatographic results discussed in Chap. 7. These empirical procedures and correlations are outlined in Chap. 6 for a deeper understanding of one of the possible ways to interpret experimental findings from gas phase chemistry.

All the authors of the individual chapters are describing the up-to-date ongoing research in their field where they are leading experts and give a thorough and comprehensive review of our today's knowledge. The individual chapters were finished between mid of the year and November of the year 2002. Pictures of the people involved in many of the described experiments, photos of the instruments and more details on experiments and results can be found on the web-page http://www.gsi.de/kernchemie.

I wish to acknowledge the contributions of Jan Willem Wijnen and Emma Roberts from the Kluwer Academic Publishers who started (JWW) and finalized (ER) this project with me. Many thanks go to the authors of the individual chapters

who enthusiastically agreed to contribute to this book and who spent so much time and effort to collect, judge and write up extensive amounts of material. Only thanks to them was it possible to provide such a far-reaching coverage of the chemistry of superheavy elements. Last, but definitely not least, its a great pleasure to thank Brigitta Schausten very much for helping me and the authors with hundreds of smaller or larger details which came up during the preparation of this book, and especially for her work on some of the graphics and for preparing the final format.

Darmstadt, December 2002 Matthias Schädel

Contents

Synthesis of Superheavy Elements

Kenton J. Moody

Abstract The Island of Stability of spherical superheavy nuclides exists at the extreme limit of the Chart of the Nuclides, beyond regions of nuclear stability associated with deformed nuclear shapes. In this chapter, the reactions that are used to synthesize these transactinide nuclides are discussed. Particular emphasis is placed on the production of nuclides with decay properties that are conducive to a radiochemical measurement. The cold- and hot-fusion reactions that lead to the formation of evaporation residues are discussed, as are the physical techniques that have been used in production experiments. Recent results from ^{48}Ca-induced fusion reactions are included. Speculative methods of producing the more neutron-rich nuclides that populate the approaches to the center of the Island of Stability are also presented.

1 Introduction

The known elements were organized into the Periodic Table in the nineteenth century, first by atomic weight and then by atomic number. In both versions, uranium was the most extreme element. Since that time, the possibility of extension of the Periodic Table to unknown atomic numbers has captured the imaginations of many people, among them scientists and students of chemistry and physics. Can they be produced? If so, what are their chemical and physical properties? Does the Periodic Table have an extreme limit? These questions are some of the most fundamental in the chemical sciences.

The discovery of the neutron and the development of the particle accelerator provided the means for exploration of the Periodic Table beyond uranium. In 1934,

K. J. Moody (✉)
Lawrence Livermore National Laboratory, Livermore, CA, USA
e-mail: moody3@llnl.gov

M. Schädel and D. Shaughnessy (eds.), *The Chemistry of Superheavy Elements*,
DOI: 10.1007/978-3-642-37466-1_1,

Fermi irradiated uranium with slow neutrons, and observed a variety of radioactivities that he tentatively identified as being transuranium elements [1]. We now know that these radioactive species were the products of the fission of the ^{235}U in the sample. Study of the chemical properties of these new nuclides led to the subsequent discovery of fission in 1939 [2, 3]. Explanation of the fission process was closely connected to the creation of the liquid-drop model [4–6], in which the nucleus is treated like an incompressible charged fluid with surface tension. See "Nuclear Structure of Superheavy Elements" for more information on nuclear structure and the stability of the heaviest nuclides.

The liquid-drop model was very successful in reproducing the beta-stable nuclei at a given atomic mass (A) as a function of atomic number (Z) and neutron number (N), and the global behavior of nuclear masses and binding energies. Early versions of the liquid-drop model predicted that the nucleus would lose its stability to even small changes in nuclear shape when $Z^2/A \geq 39$, around element 100 for beta-stable nuclei [6, 7]. At this point, the electrostatic repulsion between the protons in the nucleus overcomes the nuclear cohesive forces, the barrier to fission vanishes, and the lifetime for decay by spontaneous fission drops below 10^{-14} s [8]. Later versions of the model revised the liquid-drop limit of the Periodic Table to $Z = 104$ or 105 [9].

While the macroscopic liquid-drop model was successful in reproducing the gross features of nuclear stability across the known nuclides, there were local deviations between liquid-drop masses and those determined by experiment [10, 11]. The largest deviations were associated with nuclei containing certain defined numbers of protons and neutrons; these became known as the magic numbers. In the elements below uranium, the magic numbers for protons and neutrons are 2, 8, 20, 28, 50, and 82. There is an additional magic number for neutrons at 126. The deviation from the liquid-drop masses is especially pronounced for ^{208}Pb, which has 82 protons and 126 neutrons and is, therefore, "doubly magic". The attempt to explain the magic numbers led to the spherical shell model, in which the specific structure of the nucleus imparts an extra binding energy term (positive or negative) that is unique for each nuclide, and adds onto the mass prediction from the liquid-drop model [12, 13]. Though the forces involved are different in detail, nucleons in the nucleus behave like the electrons in atoms, with certain configurations that are extra stable. Complete filling of major proton or neutron shells in the magic nuclei is analogous to the stabilization of the electrons in the noble gases and their corresponding resistance to chemical processes [14, 15]. For more nuclear structure details, see "Nuclear Structure of Superheavy Elements".

After the magic numbers were reproduced by theory [14, 16], the obvious question to ask was: Where are the next ones? The initial prediction of the next magic proton number after $Z = 82$ (lead) was $Z = 126$, which matched the last magic neutron number [9, 10, 17, 18]. The next magic neutron number after 126 was predicted to be $N = 184$ [19–21]. In the mid-1960s, an improved theoretical treatment moved the magic proton number to $Z = 114$ [9, 10, 19, 20, 22, 23], resulting in the next doubly magic nucleus lying near the line of beta stability predicted by the macroscopic models; see, e.g., [24].

The microscopic stabilization of a $Z = 114$ nucleus results in a spherical nucleus that is more strongly bound than predicted by the macroscopic model. This effect produces a barrier to deformations leading to fission where there would otherwise be none [10, 12, 13, 23, 25–27]. At the time of these model calculations, the Periodic Table ended at the extreme limit of the actinides ($Z = 103$), with some experimental evidence for observation of the first transactinide elements. The overall trend with increasing atomic number was shorter half-lives and decreasing resistance to decay by spontaneous fission. The shell-model calculations indicated that well beyond the limits of the known elements the trends might reverse, allowing an extension of the Periodic Table [9]. This led to the concept of an "Island of Stability". The term "superheavy elements" was coined to describe the nuclides occupying the Island.

The prediction of the location of the Island of Stability was less problematic than the calculation of the magnitude of the effect, or the range in Z and N over which nuclides might derive some stability benefit from it [9, 22]. Under the guidance of theory, large extrapolations of nuclear properties to the region of the Island resulted in predicted half-lives that varied over tens of orders of magnitude and encompassed the age of the earth [10, 11, 13, 20, 21, 25, 26, 28, 29]. The conditions that lead to the production of heavy elements in the *r*-process involve a prolonged exposure to a high density of free neutrons and high temperatures such that beta decay can compete with neutron capture (and fission) [30, 31]. The *r*-process follows a path through the Chart of the Nuclides that is significantly removed from beta stability; these conditions can also result in the production of elements heavier than uranium, as shown in Fig. 1 [32]. Combined with the possibility of long half-lives, this led to searches for superheavy elements in Nature [9, 33–43] (see "Historical Reminiscences: The Pioneering Years of Superheavy Element Research"). The only transuranium element that has been convincingly demonstrated to exist in Nature is plutonium, both primordial and from radiogenic nuclear reactions [37, 44–46].

Attempts to synthesize superheavy elements began immediately after the development of the concept of the Island of Stability [22, 47]. Initially it was postulated that attaining the Island would involve a leap across an intervening channel of nuclei with little or no resistance to prompt decay by spontaneous fission. The discovery/prediction of neutron and proton subshells associated with non-spherical nuclear shapes provided the opportunity of approaching the region of the superheavy elements in a more stepwise fashion. The extra stability associated with a prolate-deformed subshell affecting the ground-state binding energy at $N = 152$ [12, 48–50] and deformed subshells at $Z = 108$, $N = 162$ associated with more complicated nuclear shapes [12, 19–21, 51–53] convert the Island of Stability to a peninsula, with the isthmus formed by nuclei that are resistant to decay by spontaneous fission. This resistance arises not only from the stabilization of the ground states, but also in transient structure imparted to the fission barrier as the nucleus deforms toward scission [52, 54, 55].

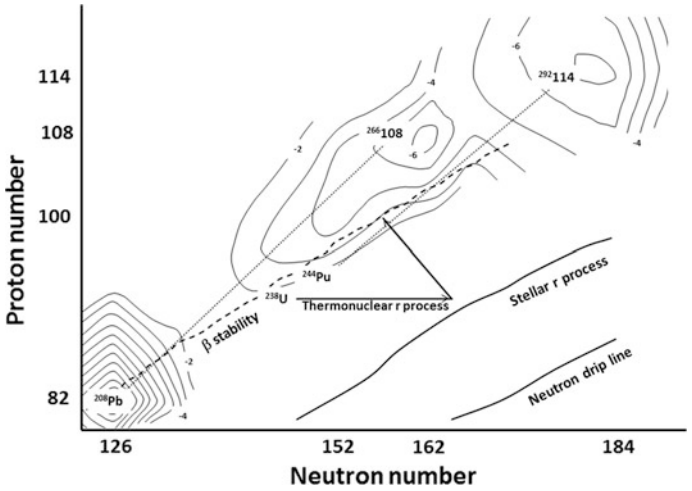

Fig. 1 The calculated microscopic corrections to liquid-drop masses [24, 56–59] for the heavy elements, showing a prediction of the location of the Island of Stability, centered at ^{298}114. Contours are labeled in MeV. The neutron-drip line is indicated, as are the pathways to the heavy elements followed by the stellar and thermonuclear *r*-processes. The compound nuclei produced in representative heavy-ion reactions are also shown, connected to the target nuclide by a *dotted line*

A calculation of the microscopic corrections to the liquid-drop masses for a limited section of the Chart of the Nuclides is shown in Fig. 1 [24, 56–59]. The predicted location and extent of the Island of Stability is evident.

The nuclear models that resulted in the prediction of an island of superheavy nuclei have evolved in response to experimental measurements of the decay properties of the heaviest elements. While the prediction of a spherical magic $N = 184$ is robust and persists across the models [8], the shell closure associated with $Z = 114$ is weaker, and different models place it at higher atomic numbers, from $Z = 120$ to 126 [60–69] or even higher [70] (see "Nuclear Structure of Superheavy Elements"). Interpretation of the decay properties of the heaviest elements may support this [71, 72], but the most part decay and reaction data do not conclusively establish the location of the closed proton shell. Because of this, the domain of the superheavy elements can be considered to start at approximately $Z = 106$ (seaborgium), the point at which the liquid-drop fission barrier has vanished [9]. For our purposes, the transactinide elements ($Z > 103$) will be considered to be superheavy (see "Nuclear Structure of Superheavy Elements").

The following sections will provide a discussion of nuclear reactions by which superheavy elements have been synthesized and the methods used in their isolation and detection. Since this chapter is part of a monograph on the chemistry of the superheavy elements, species with half-lives of more than one second will be emphasized; shorter-lived species are unlikely to survive the time required for chemical processes. Detailed information on nuclear properties, structure, and

radioactive decay will be found in "Nuclear Structure of Superheavy Elements". This chapter will conclude with a more speculative discussion of the possibilities for producing longer lived nuclides.

2 The Path to the Superheavy Elements

2.1 *Production of the Actinide Elements: Neutrons and Light Ions*

There are a number of excellent reviews of the history of the production of the actinide elements beyond uranium; e.g., [73–75]. The focus of this section will be on those aspects relevant to the production of superheavy elements.

The early history of the discovery of the transuranium elements involved a synergy between first-observation experiments involving irradiation of heavy-element targets with charged particles (mainly deuterons and alpha particles), followed by prolonged neutron irradiations in reactors to produce the element in bulk, suitable for use as a target in further charged-particle irradiations. Repeated neutron capture in reactors eventually results in neutron-excess isotopes that undergo β^- decay to the next higher element. By this method, isotopes of the elements through californium ($Z = 98$) can be produced in significant quantities, from tons of plutonium to kilograms of curium to grams of californium [37, 76]. The exotic preparations of single isotopes of these elements that are used as targets in superheavy element synthesis are available in much more limited amounts. Einsteinium ($Z = 99$) and fermium ($Z = 100$) are also produced in this fashion, but in much smaller quantities, on the order of hundreds of micrograms of 20.5-day ^{253}Es, micrograms of 276-day ^{254}Es, and sub-micrograms of 100-day ^{257}Fm. The capture-and-decay chain is terminated at element 100, either because of the α decay of lighter fermium isotopes or at ^{258}Fm, which decays by spontaneous fission with a very short half-life (380 μs) [77–79].

The last element discovered in a light charged particle irradiation was mendelevium ($Z = 101$) in 1955 [80]. A target containing 10^9 atoms of mixed Es isotopes was irradiated with α particles, and 1.3-h ^{256}Md was chemically isolated from the products that recoiled from the target and accumulated on a downstream foil. Determination of atomic number was through the elution position of the new activity in the eluant from an ion-exchange column (see "Fundamental and Experimental Aspects of Single Atom-at-a-Time Chemistry").

Though now produced in prolonged reactor irradiations, einsteinium and fermium were first detected in the debris of the 1952 above-ground thermonuclear explosion of the MIKE device [81]. In MIKE, uranium was subjected to an enormous flux of neutrons, and the *r*-process resulted in the production of heavy elements. One of the distinctions between the stellar *r*-process and the "thermonuclear *r*-process" is the time over which the neutron exposure is delivered. While

the stellar process is prolonged so that β^- decay can compete with other processes, the thermonuclear process is very short compared to the time required for β decay [82, 83]. As a result, the uranium target in MIKE captured as many as 17 neutrons in the early phases of the explosion, after which the uranium isotope inventory underwent a series of β decays to the nuclides that were ultimately observed in the debris, including 40-day ^{255}Es and its 20-h β-decay daughter ^{255}Fm (see Fig. 1).

Project Plowshare was a series of U.S. nuclear tests fired in the 1960s for the purpose of exploring the peaceful uses of nuclear explosives [84]. While the most attention was paid to their use as large-scale excavation devices, more than a dozen underground experiments were performed aimed at heavy-element synthesis, using a variety of actinide targets. Recovery of samples from the underground debris field and the time required for chemical processing set a lower limit of approximately 1 day on the half-lives of species that could be observed. There was no evidence for nuclides heavier than 100-day ^{257}Fm in any of the debris samples [37, 85–87].

The failure to produce superheavy elements in these experiments is not surprising. We now know that there are obstacles in some of the β-decay paths toward longer lived nuclei; e.g., the fermium isotopes with $A = 258$, 259, and 260, which decay by spontaneous fission. With increasing neutron number, the fission barrier of uranium isotopes is calculated to drop below 2 MeV at about mass 261 [24]. Though the method of the experiments avoided the high excitation energies that tend to wash out the shell effects that enhance the fission barrier [88, 89], it seems unlikely that many of the excited primary nuclei would survive deexcitation by fission [90]. The Q values (energy differences) for the β decays of these extreme uranium isotopes and their daughters are large compared to the fission barriers, leading to further depletion by β-delayed fission [30, 91, 92]. Finally, the neutron-separation energy decreases with increasing neutron number. The position of the drip line is uncertain, but probably occurs at a substantially lower neutron number than $N = 206$ [24, 30], the neutron number of the uranium isotope whose β decay would ultimately lead to ^{298}114 and the hypothetical center of the Island of Stability. The timed detonation of multiple nuclear explosives has been proposed as a method to tailor the neutron flux to more closely mimic the stellar r-process path, closer to the β-stable nuclei [93], although this seems improbable.

As researchers performed experiments that advanced them along the row of actinide elements on the Periodic Table, the general trends with increasing atomic number were smaller production probabilities expressed as cross sections (a consequence of the diminishing fission barrier and higher fission probabilities), an increased probability of decay by α-particle emission (a consequence of increasing α-decay Q values) and shorter half-lives. For the elements below fermium, spontaneous fission is not an important decay mode. Experimental work was dominated by radiochemical techniques in which atomic number was determined by chemical properties and atomic mass was determined by mass spectrometry and the connections of nuclei to one another by the processes of radioactive decay. The physical separation and detection methods that were used in later work were developed in the 1960s.

2.2 Transfermium Elements and the Complete Fusion of Heavy Ions: "Hot Fusion"

As discussed above, actinide target materials available in quantities sufficient for use as targets in charged-particle irradiations are limited to nuclides with $Z \leq 99$. Consequently, production of the elements beyond mendelevium requires projectiles with more protons than the α particle. Production of the heaviest elements was one of the early driving forces for the development of heavy-ion accelerators [37]. The first generation of these accelerators was limited to delivering beams of ions up to Ne with sufficient energy and intensity for heavy-element production experiments. This meant that it was still necessary to irradiate actinide targets, which where difficult to handle in the laboratory. The energy loss of heavy ions passing through matter is considerably greater than that of light charged particles, which limits the thickness of target deposits from the standpoints of both reaction kinematics and deposited heat (see Sect. 3.1 and "Experimental Techniques").

There are several important factors that must be considered in the production of heavy nuclei via heavy-ion irradiations. First and foremost is the reaction barrier. The projectiles must be accelerated to sufficient energies to overcome the Coulomb repulsion between the two positively charged nuclei. In a simple one-dimensional model [94, 95] adequate to describe reactions with heavy ions containing as many as 18 protons (argon) [96, 97], the Coulomb barrier (B_C) is roughly proportional to the product of the charges of the colliding nuclei, $Z_{\text{ion}} \times Z_{\text{target}}$. For a fixed compound nucleus (CN) proton number where $Z_{\text{CN}} = Z_{\text{ion}} + Z_{\text{target}}$, the highest asymmetry in the atomic numbers of the reactants in the entrance channel leads to the lowest interaction barrier.

The fusion of energetic heavy ions results in a CN in which excess collisional energy in the reactants has been converted into excitation energy in the product. The reaction Q value is calculated from the masses of the nuclei involved, and is defined as $Q = M_{\text{CN}} - M_{\text{ion}} - M_{\text{target}}$. The minimum excitation energy of the compound nucleus arising in a "light" heavy-ion reaction is $E_{\text{min}} = B_C - Q$. A simple argument based on the liquid-drop model shows that the Q value for complete-fusion reactions to produce the heaviest elements also decreases with asymmetry, resulting in a value of E_{min} that is between 35 and 45 MeV over a wide range of reactions involving light heavy-ion projectiles. Since E_{min} is much larger than the fission barrier in the product nucleus (typically 5–7 MeV), these reactions are referred to as "hot fusion". Unlike fusion reactions involving neutrons or light charged particles, the cross sections for production of the heaviest elements in heavy-ion irradiations are small, much less than the geometric sizes of the nuclei. This is a consequence of the relative magnitudes of the excitation energy and the fission barrier.

In light heavy-ion reactions, the cross section for the production of heavy-element reaction products depends on the probability of formation of the highly excited compound nucleus and on the probability for this nucleus to avoid the fission process as it sheds energy by predominantly emitting nucleons and photons

to become an "evaporation residue". The probability of forming the compound nucleus is often described by the classical description of the interaction of two charged spheres, $\sigma = \pi R^2 (1 - B_C/E)$, where σ is the reaction cross section, E is the center-of-mass energy of the reaction, and R is the internuclear distance defined by the Coulomb barrier. The classical description is justified because the reaction wavelength is small compared to the dimensions of the participants [98, 99]. The possibility of equating the complete-fusion cross section to the reaction cross section is a consequence of the potential energy of the reacting nuclei in contact being higher than the potential energy of the compound nucleus. At energies above the Coulomb barrier, peripheral reactions involving the exchange of nucleons between the reactants without formation of an equilibrated compound system comprise only a few percent of the geometrical cross section and occur at large impact parameters (high angular momenta) [100, 101]. Another way to say this is that collisions with angular momentum less than a critical value defined by E and R in the geometrical cross-section relationship lead to complete fusion.

Getting rid of 35–45 MeV of excitation energy requires the evaporation of several particles (mainly neutrons) and the emission of photons, which compete with the more probable fission process. The relative probabilities of neutron emission and fission are often expressed by their widths, Γ_n and Γ_f. Since Γ_f is significantly larger than Γ_n in the transactinides, Γ_n/Γ_f is approximately equal to the fraction of a collection of nuclei that undergo neutron emission in preference to fission [102, 103]. The relative widths of the competing processes in a hot nucleus can be approximated by $\Gamma_n/\Gamma_f = \exp[(B_f - B_n)/T]$, where B_f is the fission barrier, B_n is the binding energy of the neutron, and T is the temperature of the nucleus associated with its excitation energy. In addition to aspects like the neutron binding energy and the damping of shell effects with excitation energy, the uncertainty in the calculation of Γ_n/Γ_f is most strongly influenced by the choice of B_f, which is very model dependent [52, 60, 61, 104–106]. In extracting the height of the fission barrier from an experimental measurement of cross sections, it is often assumed that fission competes with each neutron emission equally so that the measured cross section of an evaporation residue is related to the geometrical reaction cross section by $(\Gamma_n/\Gamma_f)^x$, where x is the number of emitted neutrons. This is true when the relative decay widths do not change as the nucleus cools. Other than odd–even effects, B_n is slowly changing with neutron evaporation, but B_f can increase substantially as the nucleus cools if the ground state is shell stabilized [105, 107, 108] or if there are significant shell effects influencing the structure of the fission barrier [109]. The survival probability of the compound nucleus is significantly affected by the fission barrier, which is built solely from shell effects in the superheavy nuclei. The shell effects responsible for the stability of superheavy nuclei in their ground states are compromised at high excitation energies [110–114]. This will be important in the discussion of ^{48}Ca-induced reactions in Sect. 2.4. See "Nuclear Structure of Superheavy Elements" for a further discussion of fission barriers.

In the absence of shell structure in a highly excited nucleus, the height of the fission barrier as a function of intrinsic angular momentum is expected to trend with that of the rotating liquid drop [115, 116] and vanish at high angular momenta

[117]. Although, at energies well above the Coulomb barrier, the complete-fusion nuclei are produced in reactions out to large impact parameters [117–120], central collisions (low orbital angular momentum) most strongly contribute to the compound nuclei that survive the fission process to form evaporation residues [9, 121, 122]. Though the geometrical cross section for complete fusion increases with reaction energy, most of the added cross section results in compound nuclei with higher intrinsic angular momentum and does not contribute to the production of evaporation residues. This is substantial even at energies near and below the classical Coulomb barrier [123]. Combined with the overall depletion caused by increased nuclear temperature, there is no advantage in increasing the kinetic energy of the reaction much beyond the Coulomb barrier. Most hot-fusion studies of transactinide isotope production to date have been performed within 20 MeV of the 1-dimensional barrier calculated by the Bass model [95], favoring the evaporation of 3–5 neutrons.

The preferential depletion of high-angular momentum states in the highly excited nucleus has implications for the evaporation of particles other than neutrons contributing to the production of a superheavy evaporation residue. The intrinsic Coulomb barrier of the excited nucleus is high enough that neutron emission is expected to dominate over proton emission [124], and this is observed in the heavy actinides and light transactinides. Though α emission is even more hindered by Coulomb effects, there are advantages in energetics that might enhance the survival probability of the residual nucleus. However, α emission most successfully competes with neutron emission from states of high angular momentum [125], which are more susceptible to depletion by the fission process. The discovery of 58-min ^{259}No in the ^{248}Cm(^{18}O,α3n) reaction [126] is sometimes cited as a contradiction to this argument. The cross section for the reaction is much higher (20 nb) than that for the ^{248}Cm(^{18}O,xn) reaction products. However, it is not clear that the reaction proceeds through the formation of a complete-fusion nucleus, but might in fact arise directly in an extreme transfer reaction [122, 127–130] or involve precompound emission of an α particle [131] driven by the nuclear structure of the projectile. The limit on the cross section for the ^{248}Cm(^{18}O,α5n)^{257}No reaction is considerably lower [126], supporting this contention.

Hot-fusion reactions were employed in the discoveries of the elements beyond mendelevium as far as element 106, producing the first three members of the domain of superheavy elements. Higher transactinides have also been synthesized in these reactions. As before, the general trends with increasing atomic number were shorter half-lives and smaller production cross sections, a consequence of decreased survival probability in the evaporation process [132, 133]. The probability of decay from the nuclear ground state by spontaneous fission became significant in these elements. The techniques used in the experiments still included radiochemistry and off-line radiation counting [134]. As half-lives dropped below minutes into seconds it became more common to use direct techniques like transportation in gas jets to mechanisms like wheels and tapes (see Sect. 3.3 and "Experimental Techniques"). Detection of new nuclides resulted from the detailed

analysis of nuclear spectroscopy data, taking advantage of physical processes like the collection of decay-daughter recoils for background reduction [121, 135]. Determination of atomic number and mass was largely through the genetic connection of new species to the known nuclei by the radioactive decay processes. This technique could not be applied to spontaneous fission activities, whose identity was inferred (with varying degrees of success) through excitation functions (typically characterized by energy widths of less than 10 MeV) and reaction systematics.

The early history of experiments on the synthesis of the light transactinides is complicated by the report of results that could not be reproduced in subsequent experiments. The international union of pure and applied chemistry (IUPAC) and the international union of pure and applied physics (IUPAP) established a working group to answer questions of priority in the discoveries of the transfermium elements; the report generated by the group [136] provides a reasonable analysis (though not without flaws) of the pertinent literature and underlies the following discussion.

Rutherfordium, element 104, was first synthesized in hot-fusion reactions by research groups in Dubna (Russia) and Berkeley (USA). Early work in Dubna in which a spontaneous fission activity was assigned to ^{260}Rf [137–140] could not be reproduced by others. Later chemical experiments involving the formation of Rf in the ^{242}Pu(^{22}Ne,*x*n) reaction and the detection of a non-isotope-specific spontaneous fission activity in the chemical form of a volatile chloride demonstrated the fundamental change in chemical properties occurring beyond the end of the actinide series [141, 142]. The decay of ^{260}Rf was eventually determined to be spontaneous fission with a half-life of 21 ms, produced in the reactions ^{242}Pu(^{22}Ne,4n) [139, 143], ^{248}Cm(^{16}O,4n) [144, 145], and ^{249}Bk(^{15}N,4n) [145–148]. The α-emitting isotopes ^{257}Rf ($T_{1/2}$ = 4.7 s) and ^{259}Rf ($T_{1/2}$ = 2.8 s) were produced in Berkeley in 1969 in irradiations of ^{249}Cf targets with ^{12}C and ^{13}C ions, employing the technique of gas-jet transport to the periphery of a stepped wheel [144, 149] (see Sect. 3.3 and "Experimental Techniques" for more technical details). Though disputed at the time [150, 151], the results have stood up [152, 153]. The 9% SF branch in the decay of ^{259}Rf is the likely source of the detected fission events in the earlier Russian chemistry experiments. The SF activities ^{258}Rf ($T_{1/2}$ = 13 ms) [144] and ^{256}Rf ($T_{1/2}$ = 8 ms) [145] were observed in these same reactions, using the spinning-drum or tape-transport methods (see Sect. 3.3). A mainstay of subsequent chemical studies (see "Liquid-Phase Chemistry of Superheavy Elements" and "Gas-Phase Chemistry of Superheavy Elements"), 68-s α-emitting ^{261a}Rf is produced in the ^{248}Cm(^{18}O,5n) reaction with a cross section of 10 nb and in the ^{244}Pu(^{22}Ne,5n) reaction with a cross section of 4 nb [154–159]. A second long-lived state, ^{261b}Rf ($T_{1/2}$ = 2.6 s), has been reported in the ^{248}Cm(^{18}O,5n) reaction with a cross section of 11 nb [158]. Early experiments that reported the observation of ^{262}Rf as a 47-ms SF activity in the ^{248}Cm(^{18}O,4n) and ^{244}Pu(^{22}Ne,4n) reactions [145], were most likely detecting a *K* isomer and the ground state was subsequently reported to be a SF isotope with a half-life of 2.1 s, produced in the ^{244}Pu(^{22}Ne,4n) reaction with a cross section of 0.7 nb [160].

Ongoing work suggests that the 2.1-s activity may be an observation of ^{261b}Rf and that the ground state may be significantly shorter lived. The isotope ^{263}Rf ($T_{1/2} = 8$ s) can only be produced indirectly. At first it was reported as a 15-min SF activity in the ^{249}Bk(^{18}O,4n) reaction, as the decay daughter of a small EC branch in 27-sec ^{263}Db. However, 3% of the 6 nb evaporation-residue cross section results in an effective cross section of 180 pb for the production of the 15-min activity [161]. A single event consistent with an 8-s half-life was observed in an α decay chain of ^{271}Hs (see below), which is considered to be the more reliable observation of ^{263}Rf. Work is needed to sort out the decay properties of this isotope. Several of the Rf isotopes are also produced indirectly in hot-fusion reactions as daughters of the α decays of Sg isotopes (see below).

Dubnium, element 105, was first synthesized in hot-fusion reactions by the groups in Dubna and Berkeley. The first experiments were performed in Dubna in 1968 and involved the irradiation of ^{243}Am with ^{22}Ne ions producing a mixture of ^{261}Db and ^{260}Db in the 4n- and 5n-channels, respectively [162–164]. More-or-less contemporaneously, the Berkeley group reported the production of ^{260}Db ($T_{1/2} = 1.5$ s) in the ^{249}Cf(^{15}N,4n) reaction with a cross section of 3 nb, and observed its radiogenic connection to its decay daughter ^{256}Lr [165]. The Z of ^{260}Db was eventually confirmed through the detection of Lr X-rays coincident with the α decay [166]. The isotopes ^{259}Db ($T_{1/2} = 0.5$ s) and ^{258}Db ($T_{1/2} = 4.4$ s) have been produced in the ^{241}Am(^{22}Ne,xn) reaction with $x = 4$ (cross section of 16 nb) and $x = 5$ (cross section of 3.6 nb), respectively [167]. The isotopes ^{261}Db ($T_{1/2} = 1.8$ s) and ^{262}Db ($T_{1/2} = 34$ s) were produced in the ^{249}Bk(^{16}O,4n) and ^{249}Bk(^{18}O,5n) reactions, respectively, with corresponding cross sections of 5 nb and 6 nb [168–171]. The ^{248}Cm(^{19}F,5n) reaction has also been used to produce ^{262}Db [170] and the ^{250}Cf(^{15}N,4n) reaction has been used to produce ^{261}Db [168]. The SF decay branch of the isotope ^{263}Db ($T_{1/2} = 27$ s) was first observed in the products of the ^{249}Bk(^{18}O,4n) reaction with a cross section of 6 nb [168], and was positively identified in subsequent radiochemical experiments [161]. Until recently, chemistry experiments were usually performed with ^{262}Db (see "Liquid-Phase Chemistry of Superheavy Elements" and "Gas-Phase Chemistry of Superheavy Elements").

Seaborgium, element 106, was first synthesized in 1974 in Berkeley in the hot-fusion reaction ^{249}Cf(^{18}O,4n)^{263}Sg using the gas-jet technique [172]. Alpha decay produced recoiling daughter ^{259}Rf atoms that were collected and counted, providing a genetic link between the two nuclides. The half-life of the isotope is 0.9 s, and it was produced with a peak cross section of 300 pb [172] or higher [169]. The results were reproduced in 1994 [173]. The isotopes ^{263}Sg and ^{264}Sg ($T_{1/2} = 40$ ms) have been produced in the ^{238}U(^{30}Si,xn) reaction with cross sections of 70 pb and 10 pb for the $x = 5$ and $x = 4$ exit channels, respectively [174, 175]. The long-lived isotopes ^{265}Sg ($T_{1/2} = 8$ s) and ^{266}Sg ($T_{1/2} = 0.4$ s) have been produced in the ^{248}Cm(^{22}Ne,xn) reaction [159, 176–178] with peak cross sections of 240 pb for $x = 5$ and 25 pb for $x = 4$. The same isotopes are also produced in the ^{248}Cm(^{26}Mg,xn) reaction as the α-decay daughters of Hs isotopes [179, 180], as is ^{267}Sg ($T_{1/2} = 80$ s) produced in the 3n-reaction channel [181]. A

second long-lived state ($T_{1/2} = 14$ s) in ^{265}Sg has also been identified in the ^{248}Cm(^{22}Ne,5n) reaction [159], which was mischaracterized as ^{266}Sg in previous work [176, 177]. Recently, in the ^{248}Cm(^{22}Ne,5n) reaction, a total cross section of 380 pb was measured [159] for $^{265a+b}$Sg, the crucial isotopes for Sg chemistry experiments discussed in "Liquid-Phase Chemistry of Superheavy Elements" and "Gas-Phase Chemistry of Superheavy Elements".

Bohrium, element 107, has been produced in hot-fusion reactions. The isotopes ^{266}Bh ($T_{1/2} = 1.1$ s) and ^{267}Bh ($T_{1/2} = 17$ s) were observed in the ^{249}Bk(^{22}Ne,xn) reaction with peak cross sections of 25-250 pb for $x = 5$ and 100 pb for $x = 4$ [182–184]. The isotope ^{265}Bh ($T_{1/2} = 0.9$ s) was observed in the ^{243}Am(^{26}Mg,4n) reaction with an unreported cross section [185].

Hassium, element 108, has been produced in hot-fusion reactions. The isotopes ^{269}Hs ($T_{1/2} = 10$ s), ^{270}Hs ($T_{1/2} = 20$ s), and ^{271}Hs ($T_{1/2} = 4$ s) were observed in the ^{248}Cm(^{26}Mg,xn) reaction with peak cross sections of 7 pb for $x = 5$, 3 pb for $x = 4$ [179, 180, 186], and 2 pb for $x = 3$ [181]. See "Gas-Phase Chemistry of Superheavy Elements" for more details on the observed decay properties of these Hs isotopes and for the chemistry performed in these experiments. The ^{238}U(^{34}S,xn) reaction was used to produce ^{268}Hs ($T_{1/2} = 0.4$ s) and ^{267}Hs ($T_{1/2} = 50$ ms) with $x = 4$ and $x = 5$ and cross sections of 2 pb and 2.5 pb, respectively [187, 188].

Production of a single atom of darmstadtium, element 110, was reported following an extended irradiation of ^{244}Pu with ^{34}S ions [189]. The nuclide ^{273}Ds, produced with a cross section of $\sim$0.4 pb in the reaction ^{244}Pu(^{34}S,5n), constituted the first observation of a nuclide beyond the $N = 162$ deformed subshell closure. While the reported decay chain was not inconsistent with subsequent observations of ^{273}Ds as the second member of the ^{277}Cn decay chain [190] (see below), it was not considered sufficiently conclusive to stand by itself.

2.3 Beyond Element 106: The "Cold Fusion" Reactions of Heavy Ions

A drawback to heavy-ion fusion reactions derives from the bend of the line of β-stability toward neutron excess with increasing atomic number. Fusion of two β-stable species will by necessity form a compound nucleus that is neutron deficient, and the evaporation of neutrons in the deexcitation process only exacerbates the problem. This is particularly important when attempting to attain the Island of Stability, where the magic neutron number is at least as important to enhancing the stability of the nucleus as is the magic proton number. This "drift to the north" on the Chart of the Nuclides becomes more pronounced as the atomic number of the projectile increases and the neutron and proton numbers of the compound nucleus are controlled less by those of the target nuclide.

Even so, in the production of transactinide nuclei there is an advantage to using more symmetric reactions in which one or more of the reacting particles is stabilized by a shell closure; the microscopic correction to the liquid-drop mass acts as a heat sink, stealing excitation energy from the compound nucleus [191]. If one of the reactants is more tightly bound, the reaction Q value increases, resulting in a decreased $E_{\min}$ for the reaction. Although the Coulomb barrier is higher for more symmetric reactions, lower values of $E_{\min}$ can be attained. In reactions at the barrier with ^{208}Pb as a target, the values of $E_{\min}$ in the production of transactinide nuclides are on the order of only 10–15 MeV, leading to an evaporation residue after the emission of a minimal number of neutrons [192–196]. The mechanism of transactinide production from irradiation of targets near ^{208}Pb with very heavy ions is referred to as "cold fusion". The loss of shell stabilization in collisions leading to a loss of excitation energy in the compound nucleus was first observed in the production of Fm isotopes in the ^{208}Pb(^{40}Ar,xn) reaction [197]. Cold fusion was first proposed as a means of producing new transactinide isotopes as early as 1975 [122, 192, 197–200], shortly after accelerators that were capable of generating intense beams of the necessary heavy ions became available. Some of the early experimental work was radiochemical in nature, in which the concentrations of long-lived decay daughters were interpreted as an evaporation-residue cross section [201].

For example, the reaction of ^{13}C with ^{248}Cm produces the ^{261}No compound nucleus with $E_{min} \simeq 40$ MeV, leading to the evaporation of 3–5 neutrons [202]. In contrast, the reaction of ^{48}Ca with ^{208}Pb produces the ^{256}No compound nucleus with $E_{\min} \simeq 20$ MeV, leading to the evaporation of 2 neutrons [134, 203, 204]. As discussed above, the competition between neutron emission and fission goes as $(\Gamma_n/\Gamma_f)^x$, where x is the number of evaporated neutrons. Therefore, one might expect the cross section for production of nobelium from ^{48}Ca + ^{208}Pb to be substantially larger than that from ^{13}C + ^{248}Cm. In fact, the peak cross section for ^{208}Pb(^{48}Ca,2n)^{254}No is 3 μb, while the peak cross section for ^{248}Cm(^{13}C,4n)^{257}No is 1.1 μb, which is not substantially different.

While the lower excitation energies produced in cold-fusion reactions lead to an increased probability of avoiding fission during the deexcitation process, there is an extra potential barrier in the more symmetric reacting systems that diverts a significant fraction of the geometrical cross section to processes other than complete fusion [98, 99, 205–208]. This is sometimes referred to as an "extra push" [209–214] necessary to advance the reaction from the touching-sphere configuration at the Coulomb barrier to the compact, near-spherical compound nucleus. This is a consequence of the viscosity of hot nuclear material [215, 216] and the area of the shared nuclear matter at contact in the dinuclear system, which is much smaller than the surface area of the projectile in the more symmetrical reactions. This extends the period of time during which the dinuclear system is distinct and preserves some history of the entrance channel [217, 218]. It increases the probability of reseparation, a disruptive collective motion driven by the Coulomb potential. Reseparation paths include both the more peripheral nucleon-transfer-type reactions and the more central non-compound capture, or "quasifission".

In the latter process, substantial mass flow leads to near-symmetrical fragmentation that resembles the fission process, but does not necessarily involve an equilibrated compound nucleus.

In hot-fusion reactions, the cross section for producing heavy-element nuclides is determined by the probability that the highly excited compound nucleus will avoid fission in the deexcitation process. Cold fusion near the reaction barrier is qualitatively different; the formation of the compound nucleus comes about in two separate steps [105, 107]. The reacting nuclei come into contact, captured into a dinuclear configuration, which is separated from an equilibrated compound nucleus by a potential-energy barrier which is not reproduced by the one-dimensional Coulomb-barrier model [94, 95, 210, 219, 220]. This extra barrier diverts the trajectory of the reaction through multidimensional deformation space toward quasifission, making reseparation much more likely than complete fusion.

In lighter reacting systems, it is well known that there is a substantial fusion cross section at and below the Bass barrier [221–224], a consequence of nuclear deformation and nuclei not having a sharply defined radius [225]. In heavier systems, the extra push necessary to get from touching spheroids to a compound nucleus effectively adds to the Coulomb barrier, as does the spherical shape of the ^{208}Pb target nucleus, but there is still a substantial fusion cross section at subbarrier energies [226]. The maximum cross sections for heavy ion (HI) reactions of the (HI,*x*n) type to produce transactinide nuclides occur at or below the Bass barrier [227]. Tunneling through the barrier is facilitated by nucleon transfer and collective vibration between the reactants at contact [220, 228–233]. The angular momentum distribution introduced into the compound nucleus by the reaction impact parameter is narrow [234] and the reaction is very strongly constrained to a trajectory through deformation space that follows the path of minimum potential energy.

In the example above in which isotopes of nobelium are produced by hot and cold fusion, the difference between the observed cross sections and the geometrical cross sections derive from two different effects. In the hot-fusion reaction, the compound nucleus is unlikely to survive the competition between fission and each of the four neutron-evaporation steps, leading to a small cross section. In the cold-fusion reaction, the probability that the compound nucleus avoids the fission process is orders of magnitude higher than in the hot-fusion reaction, but the dynamical hindrance to complete fusion results in a lower probability for formation of that compound nucleus [227, 235–237]. It is a matter of some serendipity that the nobelium evaporation-residue cross sections for the two reaction types are approximately the same.

In the superheavy elements, the cold-fusion evaporation residues with the highest cross sections are the result of (HI,n) and (HI,2n) reactions. Evaporation of particles other than neutrons in a cold-fusion reaction is unlikely [192, 198, 201, 238, 239]. The same arguments that were made above for suppression of proton and α-particle emission from hot-fusion compound nuclei apply even more strongly to cold-fusion products. The height of the Coulomb barrier to charged-

particle emission is more comparable to the excitation energy and there are fewer chances for evaporation of charged particles to compete with neutron emission.

In spite of the lower excitation energies obtained in cold-fusion reactions, hot-fusion reactions produce evaporation residues that are more neutron rich, a consequence of the bend of the line of β stability toward neutron excess. For the purposes of studying nuclei whose stability is more strongly influenced by the spherical 184-neutron shell closure, hot fusion is the more viable path. If nuclei were constrained to be spherical, or deformed into simple quadrupole shapes like those that influence the properties of the actinide isotopes with $N = 152$, one would expect cold-fusion reactions to quickly veer into *Z*,*N* space where nuclides would be characterized by very short partial half-lives for decay by spontaneous fission. In fact, there is a region of nuclear stability centered at $Z = 108$ and $N = 162$ [12, 19–21], removed from the line of β stability toward proton excess, where the nuclei derive a resistance to spontaneous fission from a minor shell closure associated with complicated nuclear shapes, making α emission their most probable decay mode [133, 240].

The extension of the Periodic Table beyond seaborgium ($Z = 106$) to copernicium ($Z = 112$) was accomplished by means of cold-fusion reactions. Probing new-element space by hot fusion was characterized by producing nuclei that were becoming less stable to decay by spontaneous fission as they receded from $N = 152$. The switch to cold fusion took advantage of the approach to $Z = 108$ and $N = 162$, producing nuclei more resistant to spontaneous fission because of the shell stabilization of their ground states [227]. Although the cold-fusion superheavy nuclides are resistant to spontaneous fission decay, the increasing Q value for α emission has resulted in a trend of decreasing half-life with increasing atomic number, from hundreds of milliseconds near $Z = 106$ to hundreds of microseconds near $Z = 112$. Cross sections for the production of evaporation residues also tend to decrease with increasing atomic number of the product, attributed mostly to a hindrance to fusion in the entrance channel increasing with projectile mass, resulting in an increased probability of reseparation [235, 236]. However, the competition between neutron emission and fission in the exit channel exerts some effect on the cross sections as well, and may help to explain increased cross sections for production of darmstadtium ($Z = 110$) evaporation residues lying closer to $N = 162$ [195].

Decay by emission of α particles (with $\Delta N/\Delta Z = 1$) is a proton-rich process, and in the known transactinides results in daughter nuclei that lie closer to the line of β stability than do their parents. The decays of the superheavy cold-fusion nuclei lead to long chains of sequential α emissions and a progressive increase in neutron richness in the lower members of the chain. In this way, cold fusion can be used to produce isotopes that rival the neutron richness of those produced in hot-fusion reactions. This has been referred to as "overshooting" [22, 47]. For example, 10-s ^{269}Hs can be produced directly in the ^{248}Cm(^{26}Mg,5n) reaction with a cross section of 7 pb [179, 180]. The most neutron-rich isotope of hassium that can be produced directly by cold fusion is ^{265}Hs, in the ^{208}Pb(^{58}Fe,n) reaction [241–243]. However, ^{269}Hs is also the third member of the ^{277}Cn decay chain.

^{277}Cn is produced in the ^{208}Pb(^{70}Zn,n) cold-fusion reaction with a cross section of 0.5 pb. While the indirect production of ^{269}Hs proceeds with a cross section that is an order of magnitude lower than that for the direct process, in specific cases there may be disadvantages to the direct method involving, for example, reaction kinematics and radioactive target handling that might make the indirect overshooting reaction attractive in some applications.

Given the half-lives of the evaporation residues, physical detection methods that involved stopping the nuclides prior to transporting them (gas jets, wheels, and tapes) became less attractive. The development of recoil separation techniques (transporting then stopping) allowed experimenters to take advantage of the kinematics of the more symmetric reaction, which provided a means of isolating and detecting the evaporation residues. The differences in ionic charge and momentum among the reaction products are used to steer the evaporation residues in flight to position-sensitive detectors that allow for the reconstruction of the α-decay chains and the connection of the new product to the known members of the Chart of the Nuclides, providing a positive identification of Z and N [227, 243, 244]. This will be discussed further in Sect. 3.4. The momentum-acceptance criteria of the separators limit target thickness to $\leq$1 mg/cm^2. This is one fundamental limitation on production rate that prevents the application of the method to reactions with cross sections $\leq$0.01 pb [245], approximately 10^{-13} of the total inelastic-reaction cross section.

Rutherfordium ($Z = 104$), first synthesized by hot fusion (see Sect. 2.2), has also been produced in cold-fusion reactions. Early cold-fusion work was focused on demonstrating the disappearance of the effect of the $N = 152$ shell closure on the spontaneous fission half-life systematics of the heavy elements [198]. Rutherfordium isotopes are produced in reactions between Pb targets and Ti projectiles. The most neutron-rich cold-fusion Rf isotope is ^{257}Rf ($T_{1/2} = 4.7$ s), produced in the ^{208}Pb(^{50}Ti,n) reaction with a cross section of 5 nb [210, 246, 247]. This activity was first reported in the reaction of ^{12}C ions with ^{249}Cf [144]. An isomeric state, ^{257m}Rf ($T_{1/2} = 8$ s), was first observed in the cold-fusion reaction with a cross section of approximately 3 nb [246]. The SF isotope ^{256}Rf ($T_{1/2} = 8$ ms) has been produced in the ^{208}Pb(^{50}Ti,2n) reaction with a cross section of 10 nb [198, 201, 246] and in the ^{208}Pb(^{49}Ti,n) reaction [201]. The isotope ^{255}Rf ($T_{1/2} = 1.6$ s) has been produced in the ^{208}Pb(^{50}Ti,3n) reaction with a cross section of 0.5 nb [198, 201, 246, 248], in the ^{207}Pb(^{50}Ti,2n) reaction with a cross section of 5 nb [246, 249], in the ^{208}Pb(^{49}Ti,2n) reaction [201], and in the ^{208}Pb(^{48}Ti,n) reaction [201]. The SF nuclides ^{254}Rf ($T_{1/2} = 23$ μs) and ^{253}Rf ($T_{1/2} = 11$ ms) have been produced in the ^{206}Pb(^{50}Ti,2n) and ^{204}Pb(^{50}Ti,n) reactions, respectively, with corresponding cross sections of 2 nb and 0.1 nb [246, 250]. Rutherfordium isotopes also result from the α decays of seaborgium isotopes (see below), but with smaller cross sections than from their direct production. While the cold-fusion isotopes ^{257}Rf, ^{257m}Rf and ^{255}Rf all have half-lives in excess of one second, the production of longer lived ^{261a}Rf in hot-fusion reactions (Sect. 2.2) is of more interest to the radiochemist. However, one recent chemistry experiment used

physically preseparated ^{257}Rf (see "Experimental Techniques" and "Liquid-Phase Chemistry of Superheavy Elements").

Dubnium ($Z = 105$), first synthesized by hot fusion (see Sect. 2.2), has also been produced in cold-fusion reactions. Dubnium isotopes are usually produced in reactions between ^{209}Bi targets and Ti projectiles, but reactions between Pb targets and V projectiles and between Tl targets and Cr projectiles have been used as well [239]. The heaviest cold-fusion dubnium isotope is ^{258}Db ($T_{1/2} = 4.4$ s), produced in the ^{209}Bi(^{50}Ti,n) reaction with a cross section of 3 nb [239, 251] or in the ^{208}Pb(^{51}V,n) reaction [239]. The isotope ^{257}Db ($T_{1/2} = 2.5$ s) is produced in the ^{209}Bi(^{50}Ti,2n) reaction with a cross section of 2 nb [251] and in the ^{207}Pb(^{51}V,n) reaction [239]. An isomeric state, ^{257m}Db ($T_{1/2} = 0.9$ s), has also been observed in the ^{209}Bi(^{50}Ti,2n) reaction [248, 252]. The isotope ^{256}Db ($T_{1/2} = 1.6$ s) is produced in the ^{209}Bi(^{50}Ti,3n) reaction with a cross section of 0.2 nb [248] and in the ^{209}Bi(^{49}Ti,2n) reaction [239]. Dubnium isotopes also result from the α decays of bohrium isotopes (see below), but with smaller cross sections than for their direct production. While some of the cold-fusion isotopes have half-lives in excess of one second, the production of longer lived nuclides in other reactions is of more interest to the radiochemist.

Seaborgium ($Z = 106$), first synthesized by hot fusion (see Sect. 2.2), has also been produced in cold-fusion reactions. Early work involving the detection of short-lived spontaneous fission activities was not conclusive [200, 253]. The isotopes ^{259}Sg ($T_{1/2} = 0.3$ s), ^{260}Sg ($T_{1/2} = 4$ ms), and ^{261}Sg ($T_{1/2} = 0.2$ s) are all produced in cold-fusion reactions of lead isotopes with ^{54}Cr [247, 252, 254–256]. Cross sections of 320 pb for ^{207}Pb(^{54}Cr,2n)^{259}Sg, 400 pb for ^{208}Pb(^{54}Cr,2n)^{260}Sg, and 2000 pb for ^{208}Pb(^{54}Cr,n)^{261}Sg have been reported [121, 241, 247, 254]. The next lighter isotope, ^{258}Sg ($T_{1/2} = 3$ ms), was produced via the cold-fusion reaction ^{209}Bi(^{51}V,2n) with a cross section of 40 pb [246]. Seaborgium isotopes also result from the α decays of hassium isotopes, including ^{262}Sg ($T_{1/2} = 15$ ms). The directly produced cold-fusion isotopes of Sg all have half-lives of less than one second and are of limited interest to the radiochemist. The longer lived overshoot isotopes 0.9-s ^{263}Sg and (8-s + 14-s) $^{265a+b}$Sg occur in the decay chains of ^{271}Ds and ^{277}Cn (including ^{269}Hs), respectively (see below).

Bohrium ($Z = 107$) was first synthesized in 1981 at the GSI laboratory; earlier work involving the detection of a spontaneous fission daughter activity was not considered conclusive [199, 239]. The kinematic separator SHIP was used to isolate ^{262}Bh ($T_{1/2} = 20$ ms), produced in the ^{209}Bi(^{54}Cr,n) reaction [252, 257], and ^{261}Bh ($T_{1/2} = 12$ ms), produced in the ^{209}Bi(^{54}Cr,2n) reaction [258, 259], with cross sections of 400 pb and 60 pb, respectively. The decay properties of both isotopes have been confirmed [260, 261]. The lighter isotope ^{260}Bh ($T_{1/2} = 30$ ms) has been produced in the ^{209}Bi(^{52}Cr,n) reaction with a cross section of 60 pb [262]. Bohrium isotopes also result from the α decays of meitnerium isotopes [263–266]. The directly produced cold-fusion isotopes of bohrium all have half-lives of less than one second and are of limited interest to the radiochemist. Longer lived isotopes 1.0-s ^{264}Bh and 1.1-s ^{266}Bh occur in the decay chains of ^{272}Rg and ^{278}113, respectively (see below).

Hassium ($Z = 108$) was first synthesized in 1984 at the GSI laboratory with the SHIP apparatus, used to isolate ^{264}Hs ($T_{1/2} = 600$ μs) produced in the ^{208}Pb(^{58}Fe,2n) reaction with a cross section of 20 pb [195, 241, 242, 267]. Earlier work involving the detection of daughter activities was not considered conclusive [255]. Later, ^{265}Hs ($T_{1/2} = 0.8$ ms) was produced in the ^{208}Pb(^{58}Fe,n) reaction with a cross section of 60 pb [252, 268], as part of the effort that went into the search for element 110 (see below) [267]. The lighter isotope ^{263}Hs ($T_{1/2} = 0.7$ ms) was produced in the ^{208}Pb(^{56}Fe,n) reaction with a cross section of 20 pb [269]. Heavier isotopes ^{266}Hs ($T_{1/2} = 2$ ms) and ^{267}Hs ($T_{1/2} = 50$ ms) result from the α decays of cold-fusion darmstadtium isotopes ^{270}Ds and ^{271}Ds, respectively. The nuclide ^{267m}Hs ($T_{1/2} = \sim 1$ s) is populated in the α decay of ^{271m}Ds, but it is a rare process [270]. The directly produced cold-fusion isotopes of hassium all have half-lives of much less than one second. The longer lived isotope 10-s ^{269}Hs was first observed in the α decay sequence of ^{277}Cn decay (see below) [263, 271] and was confirmed in radiochemical experiments using hot fusion [179, 180].

Meitnerium ($Z = 109$) was first synthesized in 1982 at GSI with the SHIP apparatus, used to isolate ^{266}Mt ($T_{1/2} = 2$ ms), produced in the ^{209}Bi(^{58}Fe,n) reaction with a cross section of 8 pb [264, 272–274]. The same nuclide has also been produced in the ^{208}Pb(^{59}Co,n) reaction with a similar cross section (8 pb) [275]. More neutron-rich isotopes are produced in the α decay of roentgenium isotopes; ^{268}Mt ($T_{1/2} = 40$ ms) was first observed in the decay sequence of ^{272}Rg (see below) [263, 265, 266]. The isotope ^{270}Mt ($T_{1/2} = 0.5$ s) occurs in the decay sequence of the cold-fusion element 113 isotope (see below) [276–278]. All cold-fusion meitnerium isotopes have half-lives of less than one second.

Darmstadtium ($Z = 110$) was first synthesized in 1994 at GSI with the SHIP apparatus, used to isolate ^{269}Ds ($T_{1/2} = 180$ μs), produced in the ^{208}Pb(^{62}Ni,n) reaction with a cross section of 2.6 pb [267]. Later, the heavier $N = 161$ isotope ^{271}Ds ($T_{1/2} = 1.1$ ms) was produced using the ^{208}Pb(^{64}Ni,n) reaction [195]. Here, an increase in the neutron number of the projectile enhanced the production cross section by a factor of 5 to 15 pb. This work has been confirmed [270, 279, 280] as has the existence of a second α-decaying state with $T_{1/2} = 70$ ms, which is probably an isomer [67, 270]. The intermediate even–even isotope ^{270}Ds ($T_{1/2} = 100$ μs) was produced in the reaction ^{207}Pb(^{64}Ni,n) reaction with a cross section of 13 pb [281]. This nuclide may have a high-spin two-quasiparticle K isomer with $T_{1/2} = \sim 6$ ms [281, 282], which has interesting implications for structure effects on nuclear stability [98, 283]. Production of a single atom of ^{267}Ds ($T_{1/2} = \sim 3$ μs) via the ^{209}Bi(^{59}Co,n) reaction was reported tentatively in 1995 [284]; the unusual decay sequence proposed for the isotope needs further experimental elucidation. The α decay of ^{277}Cn results in ^{273}Ds ($T_{1/2} = 170$ μs) [190, 263, 271]. All cold-fusion darmstadtium isotopes have very short half-lives, though the isomeric state in ^{271}Ds has a half-life approaching 0.1 s [270].

Roentgenium ($Z = 111$) was first synthesized in 1994 at GSI with the SHIP apparatus, which was used to isolate ^{272}Rg ($T_{1/2} = 2$ ms) that had been produced in the ^{209}Bi(^{64}Ni,n) reaction [263, 265] with a peak cross section of 3 pb. The work was repeated at RIKEN with higher statistics [266]. The same nuclide was

produced at Berkeley in the ^{208}Pb(^{65}Cu,n) reaction with a cross section of 2 pb [280]. Three atoms of ^{274}Rg ($T_{1/2}$ = 13 ms) were reported in the decay sequence of ^{282}113 [276–278]. Both cold-fusion roentgenium isotopes have half-lives of much less than one second.

Copernicium (Z = 112) was first synthesized in 1996 at GSI with the SHIP apparatus, which was used to isolate ^{277}Cn ($T_{1/2}$ = 600 μs) previously produced in the ^{208}Pb(^{70}Zn,n) reaction [263, 271] with a cross section of 0.5 pb. The results were confirmed in an experiment performed at RIKEN [190]. An attempt to produce ^{275}Cn via the ^{208}Pb(^{68}Zn,n) reaction was unsuccessful [195].

Evidence for the cold-fusion production of element 113 was obtained at RIKEN in the ^{209}Bi(^{70}Zn,n) reaction [276–278]. An earlier effort at GSI was not sufficiently sensitive [227]. At RIKEN, three atoms of ^{278}113 ($T_{1/2}$ = 1.4 ms) were produced with a cross section of 0.02 pb, a phenomenal achievement. The element was also observed in the hot-fusion reaction ^{243}Am(^{48}Ca,xn) as the daughter of the decays of element 115 isotopes (see below) [285, 286].

The observation of element 118 was reported in 1999 at Berkeley with the BGS apparatus, which was used to isolate ^{293}118 produced via the ^{208}Pb(^{86}Kr,n) reaction [287]. The reported cross section was 2 pb, which was higher than expected from simple extrapolations of similar reaction systems, but consistent with certain theoretical calculations [288–291]. Subsequent attempts to reproduce the experiment were unsuccessful [227, 292–294] and the results were retracted in 2001 [295].

As mentioned above, there is an exponential downward trend in cold-fusion evaporation-residue cross sections with increasing atomic number of the product, attributed more to an increase in dynamical hindrance to fusion than to a decrease in $< \Gamma_n/\Gamma_f >$ [105, 108, 227, 232, 235, 236, 296]. For the transactinides, representative cross sections for 1n-channel cold-fusion reactions [198, 201, 246] are plotted in Fig. 2. In going from Z = 105 to Z = 113, the cross section decreases

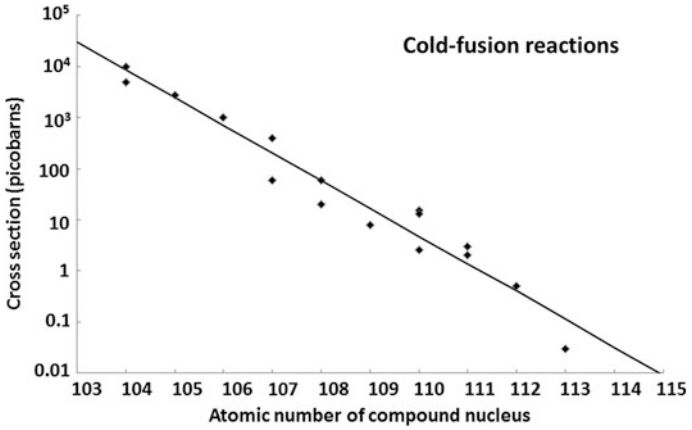

Fig. 2 Cold fusion cross sections for the 1n-evaporation reaction channel to produce transactinide nuclides from targets of ^{208}Pb or ^{209}Bi. An exponential fit to the data is included. Simple extrapolation would indicate that cross sections for synthesis of superheavy isotopes with $Z > 113$ are prohibitively low

from nanobarns to tens of femtobarns, a factor of $\sim 10^5$ [8, 195, 230, 276]. There is no significant deviation upward relative to the trendline for nuclei near $N = 162$ and $Z = 108$, supporting the idea that fission in the exit channel is less important than dynamical hindrance in the formation of superheavy evaporation residues in cold-fusion reactions. Extrapolation of Fig. 2 beyond $Z = 113$ leads to cross sections that are prohibitively low [245], ≤ 0.05 pb for nuclides with $Z \geq 114$. It has been speculated [282] that the increase in neutron number in going from ^{70}Zn to ^{76}Ge projectiles could result in a higher cross section than expected because of the evolution of ground-state nuclear shapes with changing neutron number. A fundamental change in method will be required to explore further using cold-fusion reactions.

2.4 Toward the Island of Stability—^{48}Ca-Induced Reactions

As described in the previous two sections, the mechanisms of cold and hot fusion of heavy ions are fundamentally different. Of course, there must be some smooth transition in reaction character as the projectile/target asymmetry evolves unit by unit from the irradiation of ^{208}Pb to the irradiation of actinides to make the same heavy-element product. In practice, the reaction mechanisms are distinct because of a lack of suitable target nuclides between ^{209}Bi ($Z = 83$) and ^{226}Ra ($Z = 88$). However, reactions involving the fusion of ^{48}Ca ions with actinide target nuclei probe an intermediate reaction mechanism.

The idea of irradiations with ^{48}Ca ions to produce superheavy elements is not new. In an examination of the lower end of the Chart of the Nuclides, ^{48}Ca stands out because of its unusual neutron richness, $N/Z = 1.40$, which is not found again among the naturally occurring nuclides at Z values below that of the far heavier element Se ($Z = 34$). The nuclide owes its existence as a 0.2% component of natural calcium to the spherical shell closures at $Z = 20$ and $N = 28$. Although ^{48}Ca is doubly magic, it is not actually a stable isotope; it is unstable to highly hindered β decays to states in ^{48}Sc, proceeding with a half-life that is too long to measure [297]. Its doubly magic character provides some of the same advantages in fusion reactions that are provided by ^{208}Pb, releasing the shell stabilization in the entrance channel, decreasing the excitation energy of the compound nucleus [8, 298, 299]. Nevertheless, in ^{48}Ca irradiations to produce transactinide isotopes, $E_{min} = 30$–35 MeV, requiring the evaporation of 3–4 neutrons in deexcitation, so these reactions are still classified as hot fusion.

Simple addition of protons and neutrons in the reactants indicates that the transactinide products of ^{48}Ca-induced fusion reactions derive the same advantage in neutron number over cold-fusion products that was observed in more asymmetrical hot-fusion reactions (see Sect. 2.2). In reactions that produce copernicium ($Z = 112$), the switch from the cold-fusion ^{208}Pb(^{70}Zn,n)^{277}Cn reaction to the hot-fusion ^{238}U(^{48}Ca,3n)^{283}Cn reaction effectively adds 6 neutrons to the evaporation residues. In terms of exploring Z,N space toward the center of the Island of

Stability at $N = 184$, ^{48}Ca-induced reactions provide, at present, the best experimental avenue.

Besides the effect of shell stabilization in the entrance channel on the $E_{\min}$ of the compound nucleus, the mechanism of ^{48}Ca-induced hot-fusion reactions shares another aspect of the character of cold-fusion reactions. While deexcitation of the hot compound nuclei is dominated by the competition between fission and neutron emission, attempts to reproduce the evaporation-residue cross sections by a simple Γ_n/Γ_f treatment results in values that are much higher than those that are observed experimentally [300–302]. It is necessary to invoke a significant dynamical hindrance to fusion and a two-step mechanism [303, 304] to reproduce the cross sections for ^{48}Ca-induced reactions that result in transactinide nuclides [305, 306], which increases as the atomic number of the target nuclide increases. Like the cold-fusion reaction intermediate, the reaction trajectory from nuclei in contact to a compound nucleus can be diverted into a more probable path leading to quasifission, even though the potential energy of the compound nucleus is lower than or approximately equal to that of the reacting nuclei in contact [8, 105, 123, 174, 220, 301, 307–312]. Only a small number of dinuclear intermediates reach the compact shape associated with the compound nucleus.

The concept of an "effective" potential barrier on top of the simple Coulomb barrier can be thought of as a requirement that the reacting nuclei have to achieve a closer center-to-center distance than touching hard spheres to achieve complete fusion. This has led to geometrical models based on the relative nuclear orientations of the near-spherical ^{48}Ca projectile and the prolate-deformed actinide target nucleus [305, 313–319]. The barrier for reactions involving an end-on collision is lower than that for reactions involving a collision at the waist of the target nucleus [319]. However, the end-on collisions lead preferentially to fast fission, while the more compact waist collision is more likely to result in complete fusion in spite of the larger Coulomb barrier. Quasifission dominates at lower reaction energies [320, 321]. Compared with cold-fusion reactions, the peaks of the excitation functions for producing superheavy evaporation residues in ^{48}Ca-induced reactions are shifted to energies several MeV above the spherical Bass barrier [8, 316]. At these higher energies there is a relaxation of the cold-fusion requirement that the colliding system evolves along the reaction coordinate of minimum potential energy; fluctuations in the reaction trajectory can also be related to nuclear orientation during the collision [119, 317, 318, 322].

It is expected that cross sections will *decrease* with increasing atomic numbers of the evaporation residues due to the increase in the probability of reseparation in the reaction entrance channel. Contrarily, it could be argued that cross sections will *increase* with increasing neutron number of the evaporation residues due to the increased height of the fission barrier in the reaction exit channel [8] and a corresponding increase in Γ_n/Γ_f for the nuclei as they approach $N = 184$. The increase in the fission barrier height with increasing neutron number is also expected to shift the maximum evaporation residue cross sections from (^{48}Ca,3n) to (^{48}Ca,4n) reactions, with an increase in the importance of the contribution of the (^{48}Ca,5n) reaction channel [8]. The interplay between dynamics and deexcitation

makes it impossible to predict the evaporation residue cross sections by simple extrapolation. The mechanism of the ^{48}Ca-induced reaction is being explored in theory [107, 230, 288, 296, 305, 323–327], with some success in reproducing excitation functions [105, 328].

Probing superheavy element space by ^{48}Ca-induced hot-fusion reactions is characterized by advancing beyond the $N = 162$ deformed subshell closure toward nuclei that are spherical and tightly bound. The macroscopic-microscopic model characterizes the ground-states of nuclei with $N > 175$ as having a prolate deformation parameter $\beta_2 \leq 0.1$, making them nearly spherical [8, 58, 60]. At neutron numbers below $N = 175$, any cross section benefit of the ^{48}Ca-induced hot-fusion approach to the Island of Stability is expected to decrease, as the shell stabilization of the ground state of the compound nucleus decreases. If a cold-fusion path to a particular superheavy nuclide is available, it is expected to be the better one; however, very little experimental evidence of this is available. As an example, the attempt to produce ^{277}Cn ($Z = 112$) in the ^{233}U(^{48}Ca,4n) reaction was unsuccessful (cross section limit $\leq$0.6 pb) [8, 316], in contrast to its production in the ^{208}Pb(^{70}Zn,n) reaction (cross section 0.5 pb) [263, 271].

Though the ^{48}Ca-produced transactinide elements can be relatively resistant to spontaneous fission decay, the local increase in α-decay Q value with an increase in atomic number results in an overall decrease in half-life [329]. The decays of the ^{48}Ca-produced superheavy nuclei lead to chains of sequential α decays to longer lived daughter nuclei lying closer to the line of β stability, some of which have surprisingly long half-lives. As an example, the decay of ^{288}115, produced in the ^{243}Am(^{48}Ca,3n) reaction, results in a chain of α-emitting superheavy nuclei that culminates in ^{268}Db ($Z = 105$), a nuclide with a half-life of one day [285, 286, 330]. This nuclide contains 7 neutrons more than the heaviest dubnium isotope that can be produced by either cold fusion or more asymmetric hot-fusion reactions.

The decay chains of the ^{48}Ca-produced superheavy nuclides span an interesting region of nuclear structure in which near-spherical nuclei gradually become more deformed as the neutron number decreases [58, 60]. Unlike the cold-fusion superheavy nuclides, the decays of these nuclei probe the $N = 162$ subshell closure and the transition region between $N = 184$ and $N = 162$ from the neutron-rich side. This results in a complicated structure in the α spectra of the lower-Z members of the decay chains arising from superheavy nuclides with unpaired nucleons [8]. There is a significant possibility of nuclear isomerism in these interesting nuclei, as has been reported for cold-fusion Ds isotopes (see Sect. 2.3). For a more comprehensive discussion of isomers and superheavy elements, see "Nuclear Structure of Superheavy Elements".

The expected half-lives of the evaporation residues with $Z > 112$ were sufficiently short that recoil-separation techniques and position-sensitive detectors similar to those applied in cold-fusion reactions were used in the discovery experiments. A fundamental drawback to the method is that the α-decay chains reconstructed from the detector data do not provide a connection to the known nuclei. The decay chains are terminated by spontaneous fission as they leave the

Z,*N* region of shell-stabilized nuclei. By themselves they provide no conclusive identification of the *Z* and *N* of the evaporation residues.

Collateral information is needed to make a definitive nuclide assignment. Excitation functions provide a means of determining the relative neutron richness of two nuclides produced in the same reaction. This is particularly important because the calculation of the reaction *Q* value depends on a compound nucleus mass excess that is the result of a theoretical model rather than a measurement. In comparing neighboring isotopes of the same superheavy element, the one with more odd nucleons will tend to produce the longer decay chain. This is a consequence of the relative magnitudes of the hindrance factors for alpha decay (1–10) and spontaneous fission (10^3–10^5) [133, 162] caused by single-particle effects and J^π conservation on the path through the barrier to spontaneous fission (see "Nuclear Structure of Superheavy Elements"). Cross bombardments, in which a given nuclide is produced by more than one reaction path, also provide information for nuclide identification. As an example, the superheavy isotope ^{287}Fl (flerovium, element 114) was produced by three paths: ^{244}Pu(^{48}Ca,5n), ^{242}Pu(^{48}Ca,3n), and ^{245}Cm(^{48}Ca,2n) followed by the α decay of the ^{291}Lv (livermorium, element 116) product [316, 331]. The resulting assignment of *Z* and *N* is therefore reasonably conclusive.

The decay properties of the superheavy nuclides themselves can also support an assignment of atomic number. The Geiger-Nuttall relationship between half-life and α-decay energy can be used for this. For the even-even nuclides, half-life and decay energy define a functional relationship that is unique for each atomic number [332–334], modified by the hindrance factors for α decay by nuclei with unpaired nucleons. The total kinetic energy released by spontaneous fission trends with fissility ($Z^2/A^{1/3}$) for asymmetric fission [335] (symmetric fission in a limited *Z*,*N* region in the heavy actinides follows different rules [77, 79, 148, 336]). The terminal spontaneous fission activities in decay chains arising from the decay of the superheavy nuclides are characterized by an unusually high energy release. If the number of members in a superheavy nuclide α-decay chain is well characterized in a physics experiment, a radiochemical determination of the atomic number of a chain member identifies the atomic numbers of its shorter lived parent nuclides (see for example [330, 337]).

Early efforts to produce superheavy nuclides in ^{48}Ca-induced reactions suffered from a lack of sensitivity [338–344]. Expectations for the production cross sections for evaporation residues in this work were optimistic, and experiments at that time had no chance of observing nuclides produced at the level of single-digit picobarns. Expectations for nuclide half-lives were similarly optimistic, and some of the work relied on radiochemical separations following irradiations of extended length. See "Historical Reminiscences: The Pioneering Years of Superheavy Element Research" for more details about these "historical" experiments.

The first credible hints of success in producing superheavy elements in ^{48}Ca-induced reactions were reported in 1999, when ^{238}U and ^{242}Pu targets were irradiated to attempt to produce the genetically linked isotopes ^{283}Cn and ^{287}Fl [345, 346]. The properties reported for the observed activities are not consistent with

those reported in later work [8, 316]. At approximately the same time, ^{244}Pu targets were irradiated in an attempt to produce ^{289}Fl via the (^{48}Ca,3n) reaction at 236 MeV. A single 4-member decay chain was reported [347] with a cross section of approximately 1 pb. The elapsed time between implantation of the potential flerovium isotope and its decay was 30 s. The long lifetimes of members of the decay chain resulted in a significant probability (about 1%) that the signature was due to an accidental correlated sequence of random events [347]. Nevertheless, the observed time intervals and α decay energies were consistent with expectations for flerovium and daughters by the Geiger-Nuttall relationship [8, 348]. In subsequent work in which excitation functions were measured, it was found that the optimum condition for production of flerovium isotopes was at higher reaction energies (a consequence of an underestimation of the dynamical hindrance of the reaction), peaking at around 243 MeV [316, 331, 349]. Furthermore, as the result of cross bombardments, it was determined that the shorter lived isotope produced at these higher reaction energies was ^{289}Fl rather than the $A = 288$ isotope as originally reported [349, 350]. There have been no attempts to reproduce the 30-s activity initially reported. The observed decay sequence is a candidate event for the decay of ^{290}Fl produced in the ^{244}Pu(^{48}Ca,2n) reaction, which should have a small but non-zero cross section under the experimental conditions [66, 351, 352]. The tentative assignment of the observed decay chain to an isotope of flerovium will not be included in the following discussion.

Rutherfordium ($Z = 104$) cannot be produced directly in ^{48}Ca-induced reactions, as it would require a polonium target. The isotopes ^{265}Rf ($T_{1/2} = \sim 160$ s) and ^{267}Rf ($T_{1/2} = 1.3$ h) are the terminating SF activities of the decay chains derived from ^{285}Fl and ^{287}Fl, produced in ^{242}Pu(^{48}Ca,xn) reactions with $x = 5$ and $x = 3$, respectively [8, 316, 353]. Rf activities produced in hot-fusion reactions with lighter heavy ions with much higher cross sections are generally more appropriate for radiochemical experiments (see "Liquid-Phase Chemistry of Superheavy Elements" and "Gas-Phase Chemistry of Superheavy Elements"). However, the long half-life of ^{267}Rf may provide the means for previously unexplored radiochemical investigations.

Dubnium ($Z = 105$) cannot be produced directly in ^{48}Ca-induced reactions, but long-lived isotopes occur in the decay chains of some of the heavier reaction products. The isotopes ^{268}Db ($T_{1/2} = 29$ h) and ^{267}Db ($T_{1/2} = 1.2$ h) are the terminating SF activities of the decay chains derived from ^{288}115 and ^{287}115, respectively. These nuclides are produced in ^{243}Am(^{48}Ca,xn) reactions with $x = 3$ and $x = 4$, respectively, with corresponding effective production cross sections of 8 pb and 2 pb, [8, 285, 286, 354]. Presently, it cannot be excluded that the SF activity assigned to ^{268}Db originates from a short-lived EC daughter nucleus ^{268}Rf. The isotope ^{266}Db ($T_{1/2} = 22$ min) is the terminal activity in the ^{282}113 decay chain, arising in the ^{237}Np(^{48}Ca,3n) reaction with an effective cross section of 1 pb [8, 355]. The isotope ^{270}Db ($T_{1/2} = \sim 23$ h) is the terminal SF activity in the ^{294}117 decay chain, arising in the ^{249}Bk(^{48}Ca,3n) reaction with an effective cross section of 0.5 pb [356, 357]. The 34-s isotope ^{262}Db, usually used for chemical studies (see "Liquid-Phase Chemistry of Superheavy Elements" and "Gas-Phase

Chemistry of Superheavy Elements"), is produced in hot-fusion reactions with lighter heavy ions with a much larger cross section (a factor of 10^3). However, the ^{48}Ca-produced overshoot Db isotopes offer distinct advantages in radiochemistry experiments, particularly in chemical systems in which reaction kinetics play a decisive role.

Seaborgium ($Z = 106$) cannot be produced directly in ^{48}Ca-induced reactions, as it would require a radon target. The 1.9-min isotope ^{271}Sg occurs in the decay chains arising from ^{283}Cn and ^{287}Fl, best produced in the reaction ^{242}Pu(^{48}Ca,3n) [316]. The α-decay branch of the intermediate nuclide ^{279}Ds is only 10%, so the effective production cross section is reduced from 4 pb to 0.4 pb. The 0.4-s isotope ^{266}Sg is the decay daughter of ^{270}Hs produced in the ^{226}Ra(^{48}Ca,4n) reaction [133]. A single atom of ^{269}Sg has been reported in the ^{285}Fl decay chain, with a decay time of ∼2 min [353]. The nuclides $^{265a+b}$Sg, produced in the ^{248}Cm(^{22}Ne,5n) reaction, are more appropriate for radiochemical experiments (see "Liquid-Phase Chemistry of Superheavy Elements" and "Gas-Phase Chemistry of Superheavy Elements").

Bohrium ($Z = 107$) is also inaccessible to direct production in ^{48}Ca-induced reactions, but can be produced indirectly by radioactive decay. The 50-s isotope ^{274}Bh occurs in the decay chain arising from ^{294}117 produced in the ^{249}Bk(^{48}Ca,3n) reaction; only a single atom has been observed, and the reaction involves a target with limited availability [356, 357]. The 9-s isotope ^{272}Bh occurs in the decay chain arising from ^{288}115, produced in the ^{243}Am(^{48}Ca,3n) reaction [285, 286, 354]. The time distribution of observed α decays supports the existence of a second nuclear state with a half-life of 1 s [354], probably an isomer. The 60-s isotope ^{270}Bh occurs in the decay chain arising from ^{282}113 produced in the ^{237}Np(^{48}Ca,3n) reaction [355]. The nuclide ^{271}Bh is a member of the ^{287}115 decay chain, but was not observed in the single detected decay chain for this isotope [285]. The much longer half-lives of ^{48}Ca-produced overshoot Bh isotopes offer distinct advantages in radiochemistry experiments over the more neutron-deficient isotopes produced by other reaction types.

Hassium ($Z = 108$) is the lightest superheavy element that has been produced directly in ^{48}Ca-induced reactions. The 20-s isotope ^{270}Hs has been produced in the ^{226}Ra(^{48}Ca,4n) reaction with a cross section of 8 pb [133]. Difficulties in target handling and a limited cross section favor the production of this isotope via the hot-fusion reaction ^{248}Cm(^{26}Mg,4n) for radiochemistry experiments [179, 180] (see Sect. 2.2 and "Gas-Phase Chemistry of Superheavy Elements"). A single atom of ^{273}Hs has been reported in the ^{285}Fl decay chain, with a decay interval of 350 ms [353]. The 0.2-s isotope ^{275}Hs is produced indirectly as the daughter of the 10% α-decay branch in ^{279}Ds, a member of the ^{287}Fl decay chain [316]. A rare α-decay branch in ^{281}Ds, a member of the ^{289}Fl decay chain, results in the production of ^{277}Hs, a single atom of which has been observed with a lifetime on the order of milliseconds [358, 359]

Meitnerium ($Z = 109$) has been produced only indirectly in ^{48}Ca-induced reactions. A single atom of 8-s ^{278}Mt has been observed as a member of the ^{294}117 decay chain, produced in the ^{249}Bk(^{48}Ca,3n) reaction [356, 357]. The isotopes

^{276}Mt (5 s) and ^{275}Mt (10 ms) are members of the decay chains of element 115 isotopes produced in ^{243}Am(^{48}Ca,*x*n) reactions with $x = 3$ and 4, respectively [285, 286, 354]. The 0.4-s isotope ^{274}Mt is a member of the ^{282}113 decay chain produced in the ^{237}Np(^{48}Ca,3n) reaction [8, 355]. The element Mt presents serious challenges for the radiochemist, from the standpoints of both half-life and production reaction; the best alternatives arise in ^{48}Ca-induced reactions.

Darmstadtium ($Z = 110$) has been produced only indirectly in ^{48}Ca-induced reactions, though neutron-deficient isotopes could arise in irradiations of thorium targets. A single atom of ^{277}Ds has been reported in the decay chain of ^{285}Fl, with a decay interval of ~8 ms [353]. The 13-s SF isotope ^{281}Ds is the terminal member (see ^{277}Hs, above) of the ^{289}Fl decay chain, produced in the ^{244}Pu(^{48}Ca,3n) reaction [331, 349, 358–361]. It is the only known Ds isotope that is appropriate for radiochemical studies. The 0.2-s isotope ^{279}Ds is a member of the ^{287}Fl decay chain, best produced in the ^{242}Pu(^{48}Ca,3n) reaction [316].

Roentgenium ($Z = 111$) has been produced only indirectly in ^{48}Ca-induced reactions, though neutron-deficient isotopes could be produced in irradiations of ^{231}Pa. The isotope ^{278}Rg ($T_{1/2} = 4$ ms) is a member of the ^{282}113 decay chain, produced in the ^{237}Np(^{48}Ca,3n) reaction [8, 355]. The isotopes ^{279}Rg ($T_{1/2} = 170$ ms) and ^{280}Rg ($T_{1/2} = 3.5$ s) are members of the decay chains of element 115 isotopes arising in the ^{243}Am(^{48}Ca,*x*n) reaction with $x = 4$ and $x = 3$, respectively [285, 286, 354]. The isotopes ^{281}Rg ($T_{1/2} = 26$ s) and ^{282}Rg ($T_{1/2} = \sim 0.5$ s) are members of the decay chains of element 117 isotopes arising in the ^{249}Bk(^{48}Ca,*x*n) reaction with $x = 4$ and $x = 3$, respectively [356, 357]

Copernicium ($Z = 112$) has been produced directly in the irradiation of uranium with ^{48}Ca ions. The isotope ^{283}Cn ($T_{1/2} = 3.8$ s) has been produced in the ^{238}U(^{48}Ca,3n) reaction with a peak cross section of 2.5 pb [316]. Initially, the isotope was not observed in the same reaction by the Berkeley group [362, 363], but since that time its production has been confirmed at GSI, though at a lower cross section [364]. The isotope ^{282}Cn ($T_{1/2} = 0.8$ ms) has been produced in the ^{238}U(^{48}Ca,4n) reaction with a cross section of 0.6 pb [316]. An attempt to produce the more neutron-deficient isotope ^{277}Cn via the ^{233}U(^{48}Ca,4n) reaction failed due to a lack of sensitivity. An upper limit of 0.6 pb was set for this reaction [8, 316], presumably a consequence of the decrease in the fission barrier as the evaporation residues depart the *Z*,*N* region of spherical nuclei. Copernicium isotopes are also produced indirectly in ^{48}Ca-induced reactions. In fact, the preferred method of producing ^{283}Cn might be an overshoot reaction, since the cross section for producing the α-emitting parent isotope ^{287}Fl is similar or larger (see below) [316, 365]. The chemical properties of ^{283}Cn were studied in the gas phase [366, 367] (see "Gas-Phase Chemistry of Superheavy Elements"). The thermodynamics of the adsorption of Cn on gold is similar (though slightly less pronounced in binding strength) to that of its chemical homolog Hg, supporting the identification of the atomic number of the nuclide and that of its α-decay parent ^{287}Fl. The isotopes ^{285}Cn ($T_{1/2} = 29$ s) and ^{284}Cn ($T_{1/2} = 100$ ms) are daughters of the flerovium isotopes produced in the ^{244}Pu(^{48}Ca,*x*n) reaction with $x = 3$ and $x = 4$, respectively [331, 349, 358–361]. The isotopes ^{282}Cn and ^{281}Cn ($T_{1/2} = \sim 0.1$ s) are the

daughters of flerovium isotopes produced in the ^{242}Pu(^{48}Ca,xn) reaction with $x = 4$ and $x = 5$, respectively [316, 353, 365]. The only known Cn isotopes with half-lives of sufficient length for chemical studies are produced in ^{48}Ca-induced reactions.

Element 113 was synthesized in 2003 at Dubna, observed with the DGFRS apparatus, which was used to isolate element 113 isotopes following the decays of element 115 isotopes produced in ^{243}Am(^{48}Ca,xn) reactions (see below) [285, 286, 354]. The nuclides ^{284}113 ($T_{1/2} = 0.9$ s) and ^{283}113 ($T_{1/2} = 100$ ms) are the first members of the decay chains arising in the $x = 3$ and $x = 4$ evaporation channels, respectively. The nuclides ^{286}113 ($T_{1/2} = \sim 20$ s) and ^{285}113 ($T_{1/2} = 5.5$ s) are also produced indirectly, in the reaction ^{249}Bk(^{48}Ca,xn) with $x = 3$ and $x = 4$, respectively (see below) [356, 357]. The more neutron-deficient isotope ^{282}113 ($T_{1/2} = 70$ ms) has been produced directly, in the ^{237}Np(^{48}Ca,3n) reaction with a cross section of 1 pb [8, 355]. The element 113 isotopes arising in the ^{48}Ca-irradiation of ^{249}Bk are the ones that have the most relevant half-lives for application in a radiochemistry experiment.

Flerovium ($Z = 114$) was first synthesized in 1999 at Dubna. It was observed with the DGFRS apparatus, which was used to isolate the isotopes ^{289}Fl ($T_{1/2} = 2.1$ s) and ^{288}Fl ($T_{1/2} = 0.7$ s) produced in the reaction ^{244}Pu(^{48}Ca,xn) with $x = 3$ and $x = 4$, respectively, with corresponding peak cross sections of 5 pb and 7 pb, [331, 349, 360, 361]. This work has been independently confirmed at GSI with TASCA [358, 359], but with higher measured peak cross sections, 8 pb and 10 pb, respectively. The error bars of the two determinations overlap. The isotope ^{287}Fl is also produced in the 5n-channel with a cross section of 1 pb. The isotopes ^{287}Fl ($T_{1/2} = 0.48$ s) and ^{286}Fl ($T_{1/2} = 0.13$ s) were produced in the reaction ^{242}Pu(^{48}Ca,xn) with $x = 3$ and $x = 4$ and peak cross sections of 4 pb and 5 pb, respectively [8, 316]. Also with ^{242}Pu as a target, ^{288}Fl is produced in the 2n-channel with a cross section of ~ 0.5 pb [316]. The 3n- and 4n-channel data have been confirmed at Berkeley with BGS, with similar cross sections, 3 pb each [353, 359, 365]. The rare processes ^{244}Pu(^{48}Ca,5n) and ^{242}Pu(^{48}Ca,2n) are not of interest from the standpoint of isotope production for a radiochemistry experiment, but provide a cross-bombardment connection among the flerovium isotopes that pins down their mass assignments and those of their α-decay parents and daughters. Recently, the isotope ^{285}Fl ($T_{1/2} = \sim 0.1$ s) has been reported in the ^{242}Pu(^{48}Ca,5n) reaction with a cross section of ~ 0.6 pb [353]. The flerovium isotopes are also produced indirectly by decays of livermorium isotopes, which are produced with lower cross sections in irradiations of Cm targets (see below). The $A = 289$ nuclide is the flerovium isotope of most interest for a radiochemical experiment; see "Gas-Phase Chemistry of Superheavy Elements" for more details on flerovium chemistry and the isotopes used.

Element 115 was first synthesized in 2003 at Dubna. It was observed with the DGFRS apparatus, which was used to isolate the isotopes ^{288}115 ($T_{1/2} = 250$ ms) and ^{287}115 ($T_{1/2} = \sim 30$ ms), produced in the reaction ^{243}Am(^{48}Ca,xn) with $x = 3$ and $x = 4$, respectively, and corresponding peak cross sections of 8 pb and ~ 2 pb [8, 285, 286, 354]. The 5-member decay chain originating with ^{288}115 terminates

with a one-day spontaneous fission activity, ^{268}Db (which may actually originate from the decay of short-lived ^{268}Rf following the EC decay of ^{268}Db). Dubnium is a chemical homolog of Ta and Nb, and its chemical properties are reasonably well known (see "Liquid-Phase Chemistry of Superheavy Elements" and "Gas-Phase Chemistry of Superheavy Elements"). Collection of recoils from ^{243}Am + ^{48}Ca produced with the same cross section followed by the chemical isolation of a spontaneous fission activity with the same half-life in a group-5 fraction, provides support for its origin as a decay product of an element 115 isotope [330, 337]. The isotopes ^{290}115 ($T_{1/2} = \sim 16$ ms) and ^{289}115 ($T_{1/2} = 0.22$ s) are the first members of the element 117 decay chains arising in ^{249}Bk(^{48}Ca,xn) reactions with $x = 3$ and $x = 4$, respectively. The direct production of a single atom of the isotope ^{289}115 has also been reported in the ^{243}Am(^{48}Ca,2n) reaction with a cross section of ≤ 1 pb [354]. This isotope provides the cross-bombardment connection between isotopes of elements 117 and 115. Element 115 presents a challenge to the radiochemist because of the short half-lives of the known isotopes.

Livermorium ($Z = 116$) was first synthesized in 2000 at Dubna. It was observed with the DGFRS apparatus, which was used to isolate the isotopes ^{293}Lv ($T_{1/2} = 60$ ms) and ^{292}Lv ($T_{1/2} = 20$ ms), produced in the ^{248}Cm(^{48}Ca,xn) reaction with $x = 3$ and $x = 4$, respectively, and corresponding cross sections of 2 pb and 3 pb [316, 350, 368]. This work has been reproduced at GSI with SHIP [369]. The isotopes ^{291}Lv ($T_{1/2} = 18$ ms) and ^{290}Lv ($T_{1/2} = 7$ ms) have also been produced directly, in the ^{245}Cm(^{48}Ca,xn) reaction with $x = 2$ and $x = 3$, respectively, with corresponding cross sections of 1 pb and 4 pb [331, 370]. The isotope ^{289}Lv arising in the 4n-channel was not observed at a limit of $\leq$1 pb. The isotope ^{290}Lv has also been produced indirectly, as the α-decay daughter of ^{294}118, produced in the ^{249}Cf(^{48}Ca,3n) reaction (see below) [370]. Livermorium is currently inaccessible to the radiochemist because of the short half-lives of the known isotopes.

Element 117 was first synthesized in 2010 at Dubna. It was observed with the DGFRS apparatus, which was used to isolate the isotopes ^{294}117 ($T_{1/2} = \sim 80$ ms) and ^{293}117 ($T_{1/2} = 15$ ms), produced in the reaction ^{249}Bk(^{48}Ca,xn) with $x = 3$ and $x = 4$, respectively, and corresponding cross sections of $\sim$0.5 pb and 1.3 pb [356, 357]. Element 117 is currently inaccessible to the radiochemist because of the short half-lives of the known isotopes.

Element 118 was first observed in 2002 at Dubna, but the single atom was insufficient for a conclusive identification because its decay properties matched those of ^{212m}Po [57]. The experiment was continued in 2005, when two more decay sequences were observed, firmly tying the α activity to the decay chain of ^{290}116. The experiment was performed with the DGFRS apparatus, which was used to isolate the isotope ^{294}118 ($T_{1/2} = 0.9$ ms), produced in ^{249}Cf(^{48}Ca,3n) reaction with a cross section of 0.5 pb [370]. Element 118 is currently inaccessible to the radiochemist because of the short half-life of the known isotope.

The experimental peak cross sections for the direct production of transactinides in 3n- and 4n-evaporation channels in ^{48}Ca-induced reactions are plotted in Fig. 3 as a function of the atomic number of the compound nucleus. The fit to the cold-fusion data in Fig. 2 is included for comparison. Unlike the exponential decrease

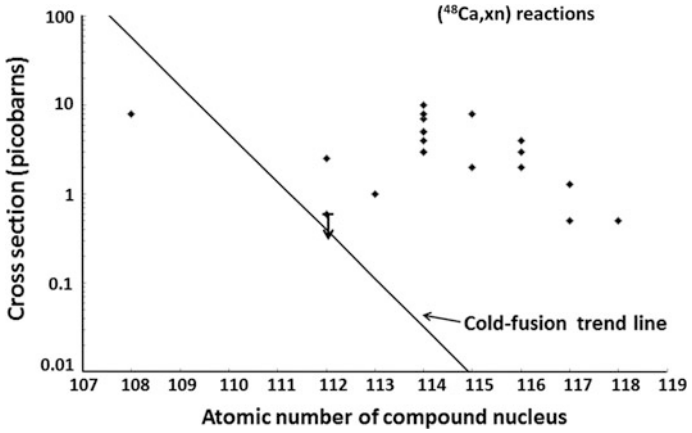

Fig. 3 Cross sections for ^{48}Ca-induced 3n- and 4n-evaporation channels to produce superheavy nuclides, plotted against the atomic number of the compound nucleus. For purposes of comparison, the fit to the cold-fusion data from Fig. 2 is included as a solid line. The ^{48}Ca-induced cross sections do not follow a simple exponential trend, and there are significant advantages over cold-fusion reactions for production of $Z > 112$ isotopes

with increasing atomic number in cold- fusion cross sections, there is a significant deviation from this behavior in the ^{48}Ca-induced reaction cross sections. The $Z = 108$ product of the ^{226}Ra(^{48}Ca,4n) reaction has the neutron and proton numbers associated with the maximum deformed-shell stabilization that dominates the ground-state properties of the cold-fusion superheavy nuclei. In going to the ^{233}U(^{48}Ca,3n) reaction, there is a decrease in cross section of more than an order of magnitude for the production of $Z = 112$, a consequence of the increased fission probability relative to neutron emission in the deexcitation of the compound nucleus. In heavier reacting systems, the trend in cross sections reverses. The cross sections increase with atomic number up to $Z = 114$, beyond which cross sections again begin to fall off. At $Z = 112$, cross sections for ^{48}Ca-induced reactions begin to exceed those for cold fusion; by $Z = 114$, ^{48}Ca-induced reactions offer a two-order-of-magnitude advantage in cross section over cold fusion.

In Fig. 4, the ^{48}Ca-induced reaction cross-section data from Fig. 3 are replotted against the neutron number of the evaporation residue. A polynomial trendline is included to guide the eye. It can be seen that there is less scatter in the data than when plotted against atomic number (Fig. 3). In going from weakly stabilized $N = 169$ nuclei to near-spherical $N = 175$ nuclei there is an increase in cross section of an order of magnitude, only weakly dependent on the atomic number of the evaporation residue. This is driven by the effect on the fission barrier of departing the *Z*,*N* region of weakly stabilized nuclei lying just beyond $N = 162$ and entering a region of near-spherical nuclei (see Fig. 1) [8, 133]. Another indicator that the initial increase in evaporation-residue cross sections is controlled by the fission barrier and Γ_n/Γ_f rather than by cold-fusion-like reaction dynamics

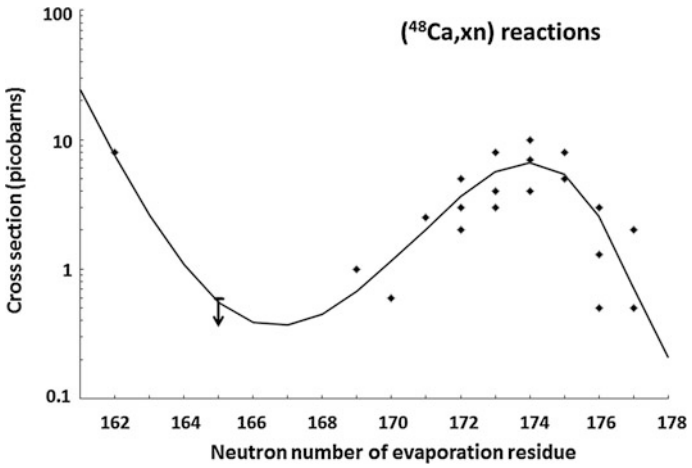

Fig. 4 Cross sections for ^{48}Ca-induced reactions (from Fig. 3) replotted against the neutron number of the evaporation residue. The data support a strong enhancement of the fission barrier as the neutron number increases beyond $N = 168$

lies in the scatter of the data around the trend line. For example, at $N = 174$, the evaporation-residue cross sections span a factor of ~ 2 for isotopes of element 114 and 116. In the cold-fusion plot in Fig. 2, an increase in Z of 2 units results in a decrease of a factor of ~ 13 in cross section.

Superficial examination of Fig. 3 cross sections would lead one to believe that $Z = 114$ is the closed proton shell since that is where the maximum ^{48}Ca-induced transactinide evaporation cross sections are observed, followed by a decline at higher atomic numbers. Actually, as discussed above, the dynamical hindrance of fusion adversely affects ^{48}Ca-induced reaction cross sections, which probably increases with increasing atomic number. It is quite possible that both dynamic hindrance and the reduced survival probability of the compound nucleus at high excitation energies contribute to the fall-off of cross sections beyond $N = 174$, regardless of the location of the proton shell closure. More high-statistics excitation-function information will be required to sort this out.

Attempts have been made to use the α-decay properties of the ^{48}Ca-induced reaction products to benchmark the nuclear mass evaluations arising from the various model calculations and to determine the location of the closed proton shell in transhassium Z,N space. Globally, the decay properties most closely match the predictions of the macroscopic-microscopic model, which predicts a spherical shell closure at $Z = 114$ [52, 58, 371–373]. However, the resiliency of theory is such that the α-decay Q values are also adequately reproduced by other models that predict a higher Z closed shell. Discrimination among the model calculations will only come about through the measurements of the decay properties of nuclides with higher Z and/or N than are currently known [8, 66].

2.5 Superheavy Elements for the Radiochemist

The known superheavy element isotopes are plotted in Fig. 5 as a section of the Chart of the Nuclides, overlaying the microscopic shell corrections from Fig. 1. Even with the relative neutron excess afforded by ^{48}Ca-induced reactions, the known nuclei are located far from the $N = 184$ shell closure. The trend in increasing half-life with increasing neutron number is expected to continue out to the vicinity of the shell. The superheavy nuclei with half-lives sufficiently long to be of interest to the radiochemist are listed in Table 1. When no long-lived isotope of an element is known, the longest-lived nuclide is given.

For the elements beyond $Z = 108$, the best reactions for the synthesis of long-lived nuclides for radiochemical experiments are clearly ^{48}Ca-induced hot fusion. At lower Z, the advantage lies with light heavy-ion-induced hot-fusion reactions. Cold-fusion reactions provide a viable path to a limited number of potential chemical analytes. The ultimate usefulness of the nuclides in Table 1 for radiochemical studies resides in maximizing their production rate. This can only be accomplished through increased beam intensity and advances in target technology. The speed of transport and separation plays an increasingly crucial role for the heaviest elements.

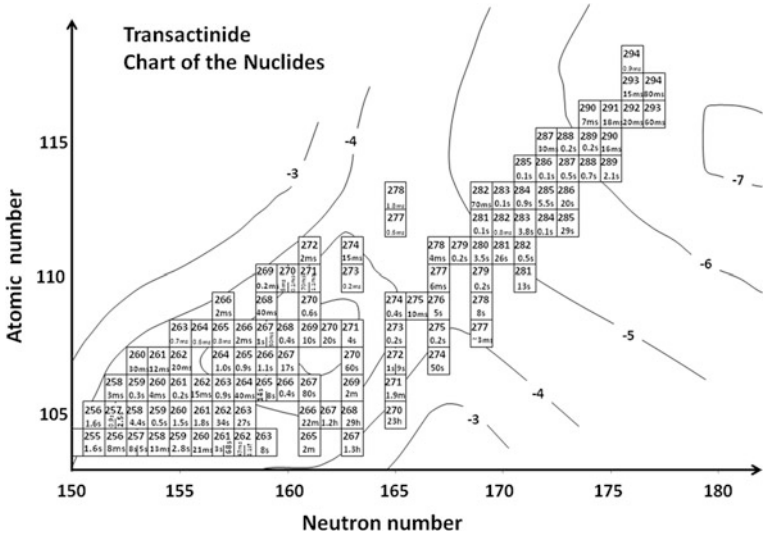

Fig. 5 Chart of the nuclides for the superheavy elements overlaying the microscopic shell corrections from Fig. 1

Table 1 Production of superheavy element isotopes for chemistry experiments. Known nuclides with half-lives longer than 0.7 s are listed along with their decay modes, representative reactions of synthesis and production cross sections. If the element does not have a long-lived isotope, the longest-lived isotope is given

Z	A	Half-life	Decay mode	Reaction	Peak cross section (pb)	Lab energy (MeV)
118	294	0.9 ms	α	^{249}Cf(^{48}Ca,3n)	0.5	251
117	294	~80 ms	α	^{249}Bk(^{48}Ca,3n)	0.5	247
116	293	60 ms	α	^{248}Cm(^{48}Ca,3n)	2	247
115	289	0.22 s	α	^{249}Bk(^{48}Ca,4n)	1.3	252
114	289	2.1 s	α	^{244}Pu(^{48}Ca,3n)	5	243
114	288	0.7 s	α	^{244}Pu(^{48}Ca,4n)	7	243
113	286	~20 s	α	^{249}Bk(^{48}Ca,3n)	0.5	247
113	285	5.5 s	α	^{249}Bk(^{48}Ca,4n)	1.3	252
112	285	29 s	α	^{244}Pu(^{48}Ca,3n)	5	243
112	283	3.8 s	α/SF	^{242}Pu(^{48}Ca,3n)	3	241
112	283	3.8 s	α/SF	^{238}U(^{48}Ca,3n)	2.5	234
111	281	26 s	SF	^{249}Bk(^{48}Ca,4n)	1.3	252
111	280	3.5 s	α	^{243}Am(^{48}Ca,3n)	8	243
110	281	13 s	SF	^{244}Pu(^{48}Ca,3n)	5	243
109	278	~8 s	α	^{249}Bk(^{48}Ca,3n)	0.5	247
109	276	5 s	α	^{243}Am(^{48}Ca,3n)	8	243
108	271	4 s	α	^{248}Cm(^{26}Mg,3n)	2	130
108	270	20 s	α	^{248}Cm(^{26}Mg,4n)	3	136
108	269	10 s	α	^{248}Cm(^{26}Mg,5n)	7	145
108	269	10 s	α	^{208}Pb(^{70}Zn,n)	0.5	344
108	267 m	~1 s	α	^{208}Pb(^{64}Ni,n)	1	310
107	274	~50 s	α	^{249}Bk(^{48}Ca,3n)	0.5	247
107	272	9 s	α	^{243}Am(^{48}Ca,3n)	6	243
107	272 m	1 s	α	^{243}Am(^{48}Ca,3n)	2	243
107	270	~60 s	α	^{237}Np(^{48}Ca,3n)	1	244
107	267	17 s	α	^{249}Bk(^{22}Ne,4n)	100	123
107	266	1.1 s	α	^{249}Bk(^{22}Ne,5n)	25–250	123
107	265	0.9 s	α	^{243}Am(^{26}Mg,4n)	No information	No information
106	271	1.9 min	α/SF	^{242}Pu(^{48}Ca,3n)	0.3	241
106	271	1.9 min	α/SF	^{238}U(^{48}Ca,3n)	0.25	234
106	269	~2 min	α	^{242}Pu(^{48}Ca,5n)	0.6	256
106	267	80 s	SF/α	^{248}Cm(^{26}Mg,3n)	2	130
106	265 (a)	8 s	α	^{248}Cm(^{22}Ne,5n)	180	118
106	265 (a)	8 s	α	^{208}Pb(^{70}Zn,n)	0.5	344
106	265 (b)	14 s	α	^{248}Cm(^{22}Ne,5n)	200	118
106	263	0.9 s	α	^{249}Cf(^{18}O,4n)	300	95

(continued)

Table 1 (continued)

Z	A	Half-life	Decay mode	Reaction	Peak cross section (pb)	Lab energy (MeV)
106	263	0.9 s	α	^{238}U(^{30}Si,5n)	70	133
106	263	0.9 s	α	^{208}Pb(^{64}Ni,n)	16	310
105	270	23 h	SF	^{249}Bk(^{48}Ca,3n)	0.5	247
105	268	29 h	SF	^{243}Am(^{48}Ca,3n)	8	243
105	267	1.2 h	SF	^{243}Am(^{48}Ca,4n)	2	248
105	266	22 min	SF	^{237}Np(^{48}Ca,3n)	1	244
105	263	27 s	SF/α/EC	^{249}Bk(^{18}O,4n)	6000	95
105	262	34 s	α/SF	^{249}Bk(^{18}O,5n)	6000	95
105	262	34 s	α/SF	^{248}Cm(^{19}F,5n)	1300	106
105	261	1.8 s	α/SF	^{249}Bk(^{16}O,4n)	∼5000	92
105	260	1.5 s	α	^{249}Cf(^{15}N,4n)	3000	86
105	258	4.4 s	α/EC	^{209}Bi(^{50}Ti,n)	2900	234
105	258	4.4 s	α/EC	^{241}Am(^{22}Ne,5n)	3600	118
105	257	2.5 s	α/SF	^{209}Bi(^{50}Ti,2n)	2100	244
105	257 m	0.9 s	α	^{209}Bi(^{50}Ti,2n)	∼1000	244
105	256	1.6 s	α	^{209}Bi(^{50}Ti,2n)	∼200	250
104	267	1.3 h	SF	^{242}Pu(^{48}Ca,3n)	0.2	241
104	267	1.3 h	SF	^{238}U(^{48}Ca,3n)	0.2	234
104	265	∼160 s	SF	^{242}Pu(^{48}Ca,5n)	0.6	256
104	263	8 s	SF	^{249}Bk(^{18}O,4n)	180	95
104	262	2.1 s (?)	SF	^{244}Pu(^{22}Ne,4n)	700	114
104	261 (a)	68 s	α	^{248}Cm(^{18}O,5n)	10000	94
104	261 (a)	68 s	α	^{244}Pu(^{22}Ne,5n)	4000	114
104	261 (b)	2.6 s	SF/α	^{248}Cm(^{18}O,5n)	11000	95
104	259	2.8 s	α/SF	^{249}Cf(^{13}C,3n)	6000	87
104	257	4.7 s	α/EC	^{208}Pb(^{50}Ti,n)	5000	272
104	257 m	8 s	α	^{208}Pb(^{50}Ti,n)	∼3000	272
104	255	1.6 s	SF/α	^{208}Pb(^{50}Ti,2n)	5000	276

3 Experimental Techniques

A useful relationship to keep in mind during the following discussion is that given a target with an areal density of 1 mg/cm^2 and a reaction with a cross section of 1 pb, an integrated beam dose of 10^{19} particles (1 μA (particle) for 20 days) leads to the production of approximately 25 atoms. Experiments require high efficiency and selectivity. The limited target thicknesses imposed by the energy loss of heavy ions requires high beam luminosity. See "Experimental Techniques" for more details on experimental techniques.

3.1 Targets

Preparation of appropriate targets is a vital step necessary to perform a successful superheavy element experiment. Targets must be of a uniform thickness that is compatible with the energy loss of heavy ions. While some metal-foil targets can be self-supporting, most thin targets must be prepared on a substrate, which introduces issues of adherence and mechanical resistance to heating and cooling. For experiments that require high beam currents of heavy ions, dissipation of heat becomes an issue. A beam with a current of 1 μA (particle) deposits approximately 1 W of heat for every MeV of energy loss through the target [374]. This usually favors the use of chemical compounds with high melting points as targets. Substrate foils must be thin, strong, and high-melting.

While it is possible to consider chemical experiments in which the heavy-ion beam stops in the target, the use of valuable exotic target materials makes the collection of recoils outside the target material the most commonly used method. Conservation of momentum causes the complete-fusion reaction products to leave the target if it is sufficiently thin. The recoil technique requires that the target be mounted with the heavy-element deposit facing away from the incoming beam (downstream). Targets must be sufficiently thin for recoils to escape yet thick enough to produce evaporation residues at a measurable rate [375].

Besides the issue of thermalized energy, there are two factors that limit the optimum thickness of a target used in a superheavy element experiment. The first of these is the range of projectile energies over which evaporation residues are produced. As discussed above, most of the excitation functions have been measured over a span of less than 20 MeV of projectile energy, which encompasses the complete-fusion excitation-energy range from sub-barrier to a point where the multiple evaporation of neutrons no longer provides a viable alternative to deexcitation by fission. In a representative asymmetric reaction to make element 106, an incident 130 MeV ^{22}Ne ion loses 20 MeV of kinetic energy in approximately 8 mg/cm^2 of Cm_2O_3; in a more symmetric cold-fusion reaction to make element 110, a 320 MeV ^{62}Ni ion loses 20 MeV in only 1.9 mg/cm^2 of Pb metal [374, 376]. The second factor limiting target thickness is the recoil range of the evaporation residues. The slow-moving heavy-element recoils produced in the hot-fusion reaction mentioned above have a range of less than 2 mg/cm^2 in the actinide target, while the fast moving element 110 recoils produced in the cold-fusion reaction have a much longer range in the lead target, approximately 8 mg/cm^2. In the cold-fusion reaction, energy loss of the beam is the factor limiting target thickness, while in the hot-fusion reaction the low recoil velocity of the evaporation residues is the limiting factor.

Regardless of the asymmetry of the reaction, production of superheavy recoils is not significantly increased by increasing the target thickness beyond 2 mg/cm^2. In practice, the momentum acceptance criteria of on-line separators (see Sect. 3.4) are significantly more strict. The areal densities of lead and bismuth targets in on-line cold-fusion physics experiments are usually on the order of 0.5–1.0 mg/cm^2

[377, 378], while the actinide oxide targets in ^{48}Ca irradiations rarely exceed 0.5 mg/cm^2 [8, 358].

With the intense heavy-ion beams delivered by modern accelerators, the maximum beam current that can be delivered to a target is determined by its resistance to energy dissipation processes over extended periods of time. Thin targets are cooled by heat conduction to their support frames and by emissive cooling by black-body radiation [378]. It is also possible to cool target foils through contact with a gas [379, 380], one of the advantages of gas-filled separators (see Sect. 3.4). Figures of merit for various cooling media are available [380]. One of the most effective means of dissipating heat involves distributing the beam intensity over a large area. Rather than actually defocusing the beam, the usual method involves preparing targets in arc-shaped segments, distributed around the periphery of a wheel that is rotated at high velocity so that the areal density of target atoms through the beam spot is maximized. Consequently, the number of ions depositing heat in a given beam-spot-sized target increment is minimized. Targets are rotated synchronously with the time macrostructure of the beam so that the supporting framework is not irradiated [377], which would impede conduction of heat from the foils.

The use of a large area to maximize the intensity of the beam increases the amount of target material incorporated in the target by two orders of magnitude, to $\geq$10 mg. This not only increases the investment in exotic enriched isotopes, but also increases the difficulty in handling high-dose actinide targets like those fabricated from ^{243}Am, ^{249}Bk, and ^{249}Cf.

A wide variety of methods can be applied to the production of targets suitable for heavy-ion irradiations. There are excellent reviews on the subject, e.g., [381, 382]. Methods include vacuum-evaporation, reduction-and-sublimation, electrospray, and electrodeposition onto refractory substrates. The choice of method depends on the chemical form and purity required for the target deposit, and the available quantity of the raw target material.

The production of lead and bismuth targets for cold-fusion experiments is described in the literature [377]. A deposit of 0.5 mg/cm^2 of the metal is vacuum-evaporated onto a thin carbon substrate and overplated with more carbon. The targets are durable and thermally conductive, making edge cooling effective, helping to prevent the melting of Pb (m.p. = 328 °C) and Bi (m.p. = 271 °C). Heavy-ion beam currents approaching 1 μA (particle) have been successfully delivered to these targets. Since cold-fusion is not the most important path to producing long-lived superheavy isotopes for chemical experiments, production of these targets will not be discussed further in this document.

The preferred method for production of actinide targets is electrodeposition (often termed electroplating or molecular plating) [381, 383–385]. This process is efficient, and with care the valuable actinide materials are conserved. A compound of the actinide (usually the nitrate) is dissolved in an organic solvent (e.g., isopropanol), and the solution is placed in a cell which incorporates the target substrate, which must be electrically conductive. A chemically inert electrode is suspended in the solution and an electrical potential is applied such that the target

substrate becomes the cathode. In a single layer deposition procedure, the potential is adjusted to produce a current density of 2–6 mA/cm^2, which usually requires hundreds of volts. The bias/current balance can be adjusted through the control of the water content of the solvent. Following the deposition of the radionuclide, the target is heated to convert the chemically complicated actinide layer to the oxide. For thicker targets, the plating/heating cycle can be repeated several times. The resulting target deposits are adherent to a wide variety of metal substrates, and have good mechanical strength and temperature resistance (see also "Experimental Techniques").

The choice of substrate for a superheavy element production target is key. It must be sufficiently thin such that energy loss and heat dissipation are not excessive, and sufficiently uniform so as not to broaden the energy profile of the heavy ions beyond that produced by range straggling. The mechanical and thermodynamic properties of a number of metal foils have been studied [380], and actinide targets are commonly prepared on Be, Al, Ni, and Mo. The target-making community seems to have moved to Ti as the substrate of choice for heavy-element experiments. Thin foils of Ti are strong and have appropriate thermodynamic properties. A drawback of Ti is its chemical reactivity. It is an excellent getter material and may steal oxygen from the target deposit, cooling gas, or from the ambient background vacuum during an extended irradiation, which can compromise its integrity as a metal.

3.2 Accelerators

Heavy-ion accelerators that can produce intense particle beams at energies near the Coulomb barriers of heavy-element targets are limited in number and it is often difficult to arrange an irradiation of sufficient duration to explore reactions that proceed with cross sections on the order of single-digit picobarns. The appropriate accelerators are of two types, cyclotrons and linear accelerators. Cyclotrons produce a particle beam that can be treated as continuous for practical purposes. Synchronization of the delivered beam with the rotating target wheel requires an imposed interrupt to avoid irradiating the target support frame. Linear accelerators deliver the particle beam in bunches, and the target rotational velocity is adjusted to the macropulse rate and duration. Heavy ions are extracted from an ion source and are accelerated to an energy sufficiently above that required for the reaction that the energy loss in intervening materials (like the target substrate and cooling gas, if any) results in the projectile energy required for the experiment [374, 376].

Unfortunately, the neutron-rich isotopes that are preferred as projectiles in superheavy element synthesis experiments are almost invariably minor components in the natural isotopic mixture of the element (^{40}Ar is a notable exception). As a result, extraction of the desired ions from the ion source can be maximized through the use of enriched isotopic mixtures as feed stock. As an example, early uses of ^{48}Ca involved the profligate consumption of the input material in sputter or

Penning sources [192, 386]. For prolonged irradiations, consumption of the expensive feed stock must be optimized. Recently, ^{48}Ca intensities of >1 μA (particle) were reported at the U400 cyclotron (Flerov Laboratory in Dubna), involving consumption of the 70%-enriched ^{48}Ca input material in an ECR (electron cyclotron resonance) source at the rate of only 0.5 mg/hour [387]. A similar consumption rate has been achieved at GSI.

The use of ECR sources has revolutionized the production of heavy-ion beams. High beam currents are sustainable for extended periods of time, and the high charge states emitted by the ion source eliminate the necessity of further electron stripping in the acceleration process.

3.3 Separation-After-Stopping: The Gas Jet and Radiochemistry

In the irradiation of thin targets with heavy ion beams, reaction products recoil from the target deposit in the general direction defined by the motion of the incoming projectiles. In a superheavy element experiment, the vast majority of these recoiling nuclei are products of interfering quasifission and transfer reactions, transfer-induced fission reactions, reactions with the target substrate, and several other reaction channels. At a beam intensity of 1 μA (particle), given a target with an areal density of 1 mg/cm^2, during a single day of irradiation approximately 5×10^{17} beam particles and on the order of 10^{12} reaction products enter the space behind the target, along with no more than a handful of superheavy element atoms. The isolation of the superheavy "needle in a haystack" is the challenge in a superheavy element synthesis experiment. Methods for accomplishing this can be broken down into two categories: separation-after-stopping and separation-before-stopping.

Separation-after-stopping methods involve slowing recoil nuclei from nuclear kinetic energies (MeV) to atomic energies (eV) prior to isolating and detecting the nuclides of interest. The methods share an insensitivity to reaction kinematics that permit maximum target thicknesses and, consequently, higher production rates. The stopping and transport processes take time, so separation-after-stopping techniques are limited to nuclei with half-lives no shorter than milliseconds [75, 121, 173, 198, 282]. Early examples of these experiments, aimed at the study of the heavy actinides and light transactinides, involved collecting recoil nuclei on fast-moving drums [198, 239, 388, 389], tapes [145, 390], or wheels [197, 213, 336] where mechanical motion quickly removed the product radionuclides from the vicinity of the target to surface-barrier or track detectors for measurement of short-lived spontaneous fission radioactivities.

Gas-jet transport (see also "Experimental Techniques") is the technique that is probably most familiar to the radiochemist, and was used in the discovery of the superheavy element seaborgium (Z = 106) [172]. Recoiling reaction products are

stopped in a volume of gas containing aerosol particles. Product ions attach themselves to the particles and are swept into a capillary for transport to the counters or chemistry devices by differential pressure induced by pumping on the receiving end of the gas jet [202, 389, 391, 392]. The aerosol particles, which have masses on the order of 10^6–10^7 mass units, serve two functions. First, depending on the identity of the stopping gas, recoil products can retain some ionic charge [393] unless neutralized by the beam plasma or quenched by unavoidable trace impurities like water vapor [390]. Charged free atoms are unlikely to remain in the hostile electrical environment near the irradiated target without being lost to collisions with a charged surface. Second, the velocity of transport of the massive aerosol particles as they are swept with the gas down the capillary is large compared to their random (Brownian) translational motion, which is not true of the free reaction-product atoms [394]. Provided flow through the capillary is not turbulent, radionuclide-laden aerosol particles are not lost through collisions with the walls. A variety of materials are used as a source of aerosol particles [391, 395]. The most common are alkali chlorides, produced by flowing the source gas over a high-temperature deposit of the salt before it is introduced into the recoil chamber [172, 396], and carbon clusters for the transport of products to gas-phase chemistry devices (see also "Experimental Techniques", "Liquid-Phase Chemistry of Superheavy Elements" and "Gas-Phase Chemistry of Superheavy Elements").

Gas-jet yields approaching unity have been achieved [202], but are usually somewhat lower for transactinide production experiments, on the order of 30–50%. Transport times are dominated by the volume of gas necessary to stop the recoiling products, and are often estimated by taking the sum of the capillary volume and half the volume of the recoil chamber and dividing by the flow rate of gas through the capillary. Typical transport times are on the order of seconds but can be shorter [394], usually at the cost of efficiency. The time required for the delivery of reaction products by the gas jet is actually characterized by a distribution. For nuclides with half-lives on the order of the characteristic transport time the calculation of a cross section from the rate at which a product is delivered is more complicated than the application of the transportation efficiency to the observed decay rate. Reactions with very heavy ions require a larger volume of gas than do reactions with lighter ions; the recoil chamber pressure is usually limited by the strength of the target substrate or isolation foil and the backing pressure of the cooling gas, if any. At higher beam intensities, an increased plasma density in the recoil chamber due to energy loss of the beam in the stopping gas also seems to decrease jet yields, possibly through destruction of aerosol particles or local charging.

A common application of the gas-jet method involves the delivery of the aerosol particles to thin foils mounted on the perimeter of a stepped wheel [156, 167, 172, 202, 338, 397]. Following a collection period, the wheel is rotated so as to place the deposited activity in front of the first of a series of detectors, exposing a new collection position to the gas jet. Stepped wheels incorporate several collection foils so as to discriminate against the buildup of long-lived radionuclides. The major drawback to the gas-jet-and-wheel method is that there is no way to

significantly discriminate against unwanted reaction products finding their way into the capillary along with the desired products. The presence of lead is ubiquitous in most materials at the ppt-to-ppb level. From this contaminant, heavy-ion reactions give rise to the production of short-lived high-energy α-particle emitters [172, 397] that interfere with the observation of superheavy nuclides, which decay on the wheel at the rate of events per day. The spontaneous fission decay of actinide transfer products, particularly the fission isomers [316], interferes with the positive identification of superheavy decay-chain end members.

Nevertheless, the gas-jet transport system is the workhorse tool in superheavy element radiochemical experiments and will continue to be so in the future. Incorporation of a chemical apparatus at the end of the gas-jet system is discussed in "Experimental Techniques" [184, 391, 394, 395, 398, 399].

A special case of separation-after-stopping is diffusive-source mass spectrometry, which is a mainstay in the production of radioactive-ion beams [400, 401]. As applied to heavy-element experiments, recoils from the target are collected in a high-temperature material from which they are liberated, ionized, and accelerated into a magnetic isotope separator. A common method involves surface ionization of the reaction products during their release from the substrate [390, 402]. The efficiencies for this process can approach unity, depending on the chemical properties of the nuclides [390]. An interesting variation on the concept involves the incorporation of the actinide target material in the high-temperature source itself. This is proposed for the MASHA apparatus, in which a high-temperature fine-grained plutonium oxide ceramic is to be irradiated with ^{48}Ca ions, while Pb-like flerovium ($Z = 114$) reaction products thermally diffuse into an ion source [403]. The heavy-ion beam will stop in the target, contributing to the required heating. The material properties of the ceramic are such that the intensity of the beam is limited only by what can be delivered by the accelerator. The limiting efficiency seems to be defined by the ion source.

3.4 Separation-Before-Stopping: Kinematic Separators

The separation-after-stopping methods take time, and are limited in application to nuclei with half-lives no shorter than several milliseconds. Pushing down to the extremely short half-lives usually comes about at the cost of efficiency, which is unacceptable at very low cross sections. The situation is most severe for the products of irradiations with very heavy ions where recoil ranges are longer, requiring a larger areal density of stopping medium. Prior to their first observation, the range of expectations for the half-lives of the superheavy element nuclides encompassed half-lives far shorter than milliseconds, requiring the development of techniques involving separation-before-stopping, or separation-in-flight.

The kinematic separator takes advantage of the kinematic properties of recoiling compound nuclei, whose direction and velocity are simply defined by the Newtonian laws of motion. The velocities of the recoil species are such that they

can traverse an instrument that is several meters long in a matter of microseconds. Magnetic and electric fields are used to reject unwanted particles. The unreacted beam particles pass through the target in the same direction as the superheavy element recoils. The beam particles have a lower Z and are faster moving, resulting in high charge states that makes their trajectory through electric or magnetic fields less rigid than that of the evaporation residues, so they are more easily deflected (low radius of curvature of the trajectory). Evaporation residues have higher masses and lower charge states, and are least deflected by an applied field (high radius of curvature of the trajectory). Binary reaction products, e.g., products of elastic scattering, quasifission, and fusion-fission, are emitted at a variety of momenta, distributed over a range of angles relative to beam-incident, and with a distribution in charge states. Consequently only a small but sometimes non-negligible fraction of these products will travel through a system of deflecting fields that will deliver them to the same location that receives the evaporation residues.

The kinematic separator selects the evaporation residues on the basis of their momenta. This limits the thickness of targets that can be used in the experiments to much less than the range of the recoil products. For cold-fusion reactions that make superheavy nuclides, the effective limitation on target thickness is 0.5–1.0 mg/cm^2 [377, 378]. For more asymmetric ^{48}Ca-induced reactions where the recoil momentum of the evaporation residues is lower, the limitation is approximately 0.5 mg/cm^2 [8, 358]. Selectivity and efficiency suffer as the asymmetry of the reaction increases, largely due to recoil-range straggling. Therefore, an in-flight implementation of light heavy-ion reactions to produce transactinides is difficult but has been achieved in some cases, e.g., in the ^{22}Ne(^{248}Cm,5n)$^{265a+b}$Sg reaction [159].

There are two types of kinematic separator that are used in superheavy element experiments. For the chemist, the defining difference is whether the reaction products recoil from the target into vacuum or into a low-pressure gas. Energy- or velocity-filter separators are representative of the first type [243, 389, 404]. The SHIP separator in Darmstadt [244] and the VASSILISSA separator in Dubna [405, 406] are examples. SHIP has been used to good effect in the exploration of the superheavy elements produced via cold-fusion (Sect. 2.3). Reaction products leave the target with a distribution of charge states created by atomic collisions with the target material. As they enter the vacuum behind the target, this distribution is frozen. The separator induces small-angle ($<10^\circ$) electric or magnetic deflections to the highly rigid evaporation-residue ions, which results in a greater deflection of the trajectories of the unwanted projectiles. Paired diverting and restoring deflections minimize the dispersion of trajectories caused by the distribution of charge states in the evaporation residues, provided it is not too broad [407].

The second type of separation-before-stopping apparatus is the gas-filled separator [408, 409]. The DGFRS separator in Dubna [410–412], GARIS at RIKEN [270, 413], RITU at Jyväskylä [414], BGS and SASSY at Berkeley [408, 415], and TASCA at GSI [416–418] are all examples of this type. DGFRS has been used to good effect in the exploration of ^{48}Ca-induced reactions that make superheavy nuclides (Sect. 2.4). Reaction products and heavy-ion projectiles leave the target

and enter a volume of low-pressure gas, confined in a magnetic dipole. The distribution of charge states of the fast-moving particles is modified through atomic collisions with the gas molecules. For gas pressures on the order of 0.5–1.0 mbar, recoil products collisionally change their charge states on the order of several times in each centimeter of the flight path [414], so over the meters-long trajectory through the separator, a narrow distribution of charge states is established. Magnetic rigidity $B\rho = mv/q$, so momentum (mv) and charge (q) define a trajectory through the separator. In the calculation of the deflection radius ρ in a gas-filled separator, the charge, which is adjusted continuously around a central value, can be treated as an average value that is not required to be an integer [8]. This means that single large-angle ($>10^{\circ}$) deflections are permitted; the rigidities of slow-moving reaction products and fast-moving projectiles are sufficiently different to effect a separation. Although the gas pressure is low, the pressure required to achieve a statistically significant number of collisions is high enough that electron stopping is significant. The superheavy element recoils lose energy as they pass through the gas, resulting in an average charge state that decreases as the distance from the target increases, which creates an interesting problem in kinematic modeling in the magnetic field [419, 420]. The most commonly used collisional gas is helium [408, 414], though there are advantages to using hydrogen, which can give a better suppression of unwanted products [8].

Achieving a high overall efficiency for the transmission of the products of complete-fusion reactions through a kinematic separator usually results in an increase in the transmission of unwanted particles [421]. In Sect. 3.3, the experimental conditions in a superheavy element irradiation were described: A total of 5×10^{17} beam particles, 10^{12} reaction products and only a few superheavy atoms enter the front end of the kinematic separator in one day. Using the gas-filled separator DGFRS as a representative example, suppression factors of 10^{13}–10^{15} for projectiles and 10^{6} for target-like reaction products (a small fraction of the total reaction cross section) are achieved in ^{48}Ca-induced reactions [8], along with a transmission efficiency of 35–40% for the complete-fusion evaporation residues [420]. Though the suppression factors are impressive, thousands of unwanted projectiles and even more interfering transfer-reaction products are delivered by the separator in one day of running along with, possibly, a single superheavy evaporation residue. This makes the identification of a decay sequence arising from a superheavy nuclide difficult to distinguish from random time-correlated events delivered by the separator at a rate approaching 1 Hz. While the flight time through the separator, typically a few microseconds, is the limiting factor on observable half-life at the short extreme, the random event rate caused by imperfect suppression of unwanted particles by the separator is the limiting factor at the long half-life extreme [422, 423]. Methods of detection, isolation, and characterization of superheavy evaporation residues are dominated by the requirements imposed by the random rate.

A typical detection setup at the focal plane of a kinematic separator includes transmission time-of-flight detectors followed by a stopping position-sensitive semiconductor detector. The time-of-flight detectors are used to tag energy signals

in the semiconductor detector that arise from the implantation of particles flying through the separator, distinguishing them from energy signals due to radioactive decay processes, particularly spontaneous fission. The tagging efficiency of the time-of-flight detectors can exceed 99% [8, 411]. The time-of-flight of a reaction product also gives its velocity, and, combined with the energy signal in the semiconductor detector, gives a rough measure of the mass of the particle. This can be used to discriminate against the products of non-compound reactions. Time-of-flight detectors include pentane-filled multiwire proportional counters [408], secondary-electron foil detectors [424], and microchannel plates [266].

As discussed above, the characteristic decay sequence of a superheavy evaporation residue is a series of α decays terminating in either a spontaneous fission nuclide or in a long-lived actinide isotope [227]. The correlation of sequential α decays in time results in the construction of decay chains. Alpha particles arising in decay processes can be detected with high efficiency with a semiconductor detector [425], approaching that defined by the counting geometry. Position-sensitive semiconductor detectors can be used to reduce the probability that the accidental time-correlation of a sequence of random events will resemble a decay chain by imposing an x–y position correlation requirement. The detectors consist of a series of biased strips on one or more thin, large-area semiconductor wafers; each of these strips acts as an independent detector. In the typical implementation, 12–16 vertical strips identify the position of an energy event in the horizontal direction, and the division of charge between the top and bottom of each strip defines its vertical position, with a resolution on the order of 1 mm [227, 244, 411]. In effect, the detector array consists of hundreds of individual detector "pixels". To be members of the same decay chain, energy events must be correlated in both time and space. Kinematic separators are designed to distribute reaction products across the position-sensitive detector array; there is usually at least one quadrupole set following the analyzing section of the separator to control image size. Position sensitivity provides a reduction in the probability of accidental correlations of unrelated events [422, 426, 427]. A complete decay sequence must consist of a time-of-flight-tagged energy signal in the position-sensitive detector followed by energy signals associated with radioactive decay that must occur within the position interval defined by the resolution of the detector.

Multiple-longitudinal-strip position-sensitive detectors are being replaced by double-sided strip detectors [359, 428] in this application. These detectors have the potential for smaller detector pixels (higher granularity) and, consequently, a reduced random-correlation rate. Digital signal processing allows the observation of shorter sequential-decay intervals, down to 1 μs [429].

There are additional techniques that are used to decrease the random rate. One of these involves the use of a veto detector behind the position-sensitive detector. Light charged particles produced in nuclear reactions in the target or elastically scattered atoms of the filling gas can find their way through the separator to the detector array without triggering the time-of-flight detector. These particles are more penetrating than are the heavy ions or radioactive decay particles, and will

enter a trailing detector array after passing through the thin position-sensitive detector substrate. Time-coincident signals in the position-sensitive detector and the trailing detector result in the veto of the event. Another technique involves shutting off the beam following detection of the implantation of an evaporation residue followed by a high-energy α-particle event in the same detector strip. While the beam is off, the random rate in the detector decreases by more than two orders of magnitude, with contributions from only radioactive-decay processes. The time and energy parameters for the sequential events that trigger the beam-off period and its duration depend on the reaction being studied and have been described in the literature [263, 349, 430].

The range of α particles in the position-sensitive detector matrix is long compared to the depth of the implantation of the evaporation residues; therefore, the efficiency for detecting α particles emitted in decay processes is only on the order of 50% in the focal-plane detector strips. Without modification, half of the α events occurring in the detector will be lost, or only deposit a small fraction of their energy in the semiconductor. Usually, an open box of large-area detectors is constructed with the focal plane detector constituting the back wall [227, 411]. A large fraction of the α-decay events that escape the focal plane will be captured by the box-wall detectors, increasing the efficiency for detecting α particles to >80%. Energy and position calibration of the detector system is accomplished through the use of compound nucleus reactions that produce chains of α-emitters and spontaneous fission activities with known decay properties.

The distribution of random events across a position-sensitive detector and the use of beam interrupt techniques have made it possible to isolate sequential events arising from rare superheavy element decays. However, the possibility of random events simulating a decay sequence is not zero, and increases with an increase in the half-lives of the genetically linked nuclides [427, 431]. Positive identification of α-decay chains with half-life increments beyond minutes requires the observation of several similar decay sequences.

Kinematic separators are also employed in nuclear spectroscopy experiments by way of the recoil tagging method [432–435], which provides a means of enhancing the in-beam prompt γ-ray signature of the decaying compound nucleus over that of other reactions (see "Nuclear Structure of Superheavy Elements" for more details on this technique). Correlation of the events arising in the implantation and subsequent decay of evaporation residues in the focal plane detector can be used to determine the time at which the evaporation residue was created in the target. Time-tagged photon events collected with germanium detectors at the target position are sorted to create a spectrum that includes the γ-rays and X-rays emitted after the last neutron emission that creates the evaporation residue. The detectors are limited in the rate at which they can take data, which limits the beam intensity that can be used in the irradiation. Even with very tight coincidence requirements among the germanium detectors, it is very difficult to observe any but the strongest discrete gamma transitions over the spectral continuum. These constraints currently limit the utility of the method to neutron-evaporation reactions with cross sections in excess of 200 nb [436–438], well beyond what can be achieved in the

transactinides. Even so, the method is relevant to the study of superheavy nuclides in that the construction of high-excitation single-particle level schemes in the heaviest actinides may eventually provide the best evidence of the location of the closed spherical proton shell [55]. See "Nuclear Structure of Superheavy Elements " for a detailed discussion of nuclear spectroscopy and structure aspects.

The increase in half-life with increasing neutron number in the superheavy elements is likely to promote a resurgence in the use of radiochemical techniques in the search for nuclides approaching the $N = 184$ shell closure. This has led to the concept of a hybrid system in which a separation-before-stopping kinematic separator delivers a "cleaned up" superheavy nucleus to the focal plane, where it is stopped in a volume of gas and delivered to a radiochemistry apparatus by means of a separation-after-stopping gas jet [416, 439–441]. This is often referred to as "physical preseparation" [416]. The kinematic separator provides a diminished concentration of interfering radioactivities, which can simplify subsequent chemical procedures, a savings in time and an increase in the significance of an observed decay event at the cost of a decrease in collection efficiency.

4 Other Nuclear Reactions

As discussed in Sect. 2.5, the reactions of most utility for producing long-lived superheavy nuclides for radiochemical studies are those involving irradiation of actinide targets with ^{48}Ca ions, though the use of more asymmetric hot-fusion reactions are particularly attractive for the production of the superheavy elements with $Z = 104$–108. Unfortunately, it is not possible to significantly extend the Chart of the Nuclides by means of these ^{48}Ca-induced reactions, since they require tens of milligrams of actinide target isotopes. The nuclides beyond californium are not available in these quantities, so nuclides with atomic numbers beyond 118 cannot be produced with ^{48}Ca projectiles. The neutron-rich long-lived nuclide ^{250}Cm cannot be produced in significant quantities in a high-flux reactor due to the short half-life and fissionability of its neutron-capture parent, 65-min ^{249}Cm [57]. The ^{250}Cm + ^{48}Ca reaction would produce evaporation residues that could significantly increase the number of long-lived overshoot superheavy nuclei. There is an effort to produce longer lived element 118 isotopes via irradiation of ^{251}Cf [442], but these nuclides are expected to be too short-lived for radiochemistry and their daughters are already known from other ^{48}Ca-induced reactions (Sect. 2.4). The isotope ^{252}Cf is available in large quantities, but the neutron dose associated with this material precludes it being used anywhere near a detector capable of observing the reaction products.

Irradiation of actinide targets with ions heavier than ^{48}Ca to synthesize superheavy complete-fusion products are underway. Recent attempts to produce the evaporation residues of the compound nucleus ^{302}120* in the reactions ^{244}Pu + ^{58}Fe [443] and ^{248}Cm + ^{54}Cr [369] were unsuccessful at the sensitivity level of less than a picobarn. This is, perhaps, not surprising as the reaction $E_{\min}$

values are similar to those for ^{48}Ca-induced reactions, but one would expect that the dynamical hindrance of fusion in the entrance channels to be more severe, with a cross-section trend similar to that observed in cold-fusion reactions (Fig. 2) [444, 445]. Evaporation-residue cross sections for more symmetrical complete-fusion reactions are expected to be unachievably low [309]. Irradiations of ^{249}Bk and ^{249}Cf targets with ^{50}Ti ions provide the best hope of extending the Periodic Table past element 118, but neither reaction will result in overshoot isotopes that will enrich the options available to the radiochemist.

In this section, less conventional methods proposed for the production of long-lived superheavy nuclides for radiochemistry experiments are discussed.

4.1 Complete Fusion with Radioactive-Ion Beams

The line of beta stability passes close to doubly magic ^{298}114 (Fig. 1), which is much more neutron rich ($N/Z = 1.614$) than are nuclides that exist in Nature (e.g., ^{48}Ca, $N/Z = 1.40$; ^{208}Pb, $N/Z = 1.54$; ^{238}U, $N/Z = 1.59$). Therefore, it is not possible to reach the neutron shell closure at $N = 184$ for compound nuclei near $Z = 114$ in fusion reactions with "off-the-shelf" projectiles and targets. The most asymmetric reactions that could hypothetically produce a compound nucleus beyond $N = 184$ are ^{244}Pu + ^{64}Ni and ^{238}U + ^{70}Zn, both of which are associated with a compound nucleus with $Z = 122$. Examination of Figs. 2 and 3 would not lead one to believe that either reaction would have a significant probability of resulting in an evaporation residue.

At this time, the best path for synthesizing longer lived nuclei for radiochemical studies lies in irradiations of actinide targets with neutron-rich radioactive beams. A radioactive-beam facility produces nuclides that are too short-lived to occur in Nature and accelerates them to the desired energy for use in a variety of experiments. The process usually involves irradiation of a stationary target with a beam of a primary projectile followed by separation of the desired secondary species from other reaction products and its subsequent ionization and acceleration (or deceleration). There are several different reaction types that are used to produce the isotopes comprising the secondary beams; they include spallation [400, 446, 447], fragmentation [448–450], and fission [451, 452]. It is beyond the scope of this document to discuss the relative merits of the various radioactive-beam production processes as they relate to the synthesis of superheavy elements. However, it should be mentioned that at the present there are no radioactive-beam facilities that will provide sufficient beam intensities ($>10^{12}$ pps) with a constrained energy distribution to permit the exploration of reactions with picobarn cross sections [453, 454].

The idea of producing superheavy elements by irradiation of targets with neutron-rich short-lived projectiles is not new [453, 455]. Early work included the radiochemical search for heavy elements in a thick tungsten target following an extended irradiation with a high-intensity relativistic proton beam [456, 457]. It

was speculated that spallation products from the p + W reaction would react with other W nuclei to produce heavy elements, though it was already firmly established that the kinetic energies of the vast majority of the fragments were insufficient to overcome the Coulomb barrier for fusion with tungsten [37]. The observed α-emitting isotopes can be explained by the presence of a low-level uranium contaminant in the target material.

Evaporation residues arising in complete-fusion reactions between actinide targets and radioactive-beam particles are controlled by the same $< \Gamma_n/\Gamma_f >$ and dynamical hindrance effects as are the reaction products from stable-ion beam irradiations. It has been observed that fusion cross sections for reactions with neutron-rich radioactive beam particles can be enhanced over those with stable-isotope beams at the same Z, possibly due to an effective lowering of the fusion barrier with the increasing neutron number of the projectile facilitated by neutron flow in the dinuclear reaction intermediate [226, 454, 458]. It is unclear how dynamical hindrance effects and a reduced resistance to deexcitation by fission at high excitation energies in heavier systems will influence the formation of evaporation residues. It has been suggested that the formation of products at the $N = 184$ neutron shell could occur with very high cross sections because of the stabilization of their ground states resulting in a high survival probability during deexcitation [338, 446], but these predictions incorporate an unreasonably optimistic view of the magnitude of the dynamical hindrance of fusion in more symmetrical reacting systems. For our purposes, it seems more reasonable to assume that both cold- and hot-fusion cross sections will follow the trends established above, depicted in Figs. 2 and 4; this is supported by theory [304, 422].

When not constrained to the stable nuclei, beams of particles with neutron numbers out to the neutron-drip line can be considered as possible reactants. Though the lack of suitable accelerator facilities makes this a hypothetical exercise, there are practical concerns governing production of the radioactive species for acceleration as the secondary beam. Continuous production of large quantities of these nuclides is required for the generation of a radioactive beam that is sufficiently intense for a superheavy element synthesis experiment. This limits our discussions to radioactive species close to the line of β stability, because of both primary production rate and half-life. To confine the following discussion, only radioactive ions within four mass numbers of the heaviest stable isotope of each element will be considered as projectiles unless there is a stable isotope of a nearby element at higher neutron number (e.g., ^{46}Ar, at the same neutron number as ^{48}Ca).

Under this constraint, it is not possible to produce new superheavy nuclides at greater neutron excess by cold fusion, or by hot fusion with heavy-ion beams with lower atomic numbers than argon. This is because of the neutron richness of the overshoot isotopes, daughters of the multiple emission of relatively proton-rich α particles in the decays of the ^{48}Ca-induced evaporation residues. Nevertheless, both reaction types offer advantages in the production rates of the known isotopes of superheavy elements with $Z = 106$–108 that are of interest to the radiochemist. As examples: Direct production of the long-lived hassium isotope ^{269}Hs is possible in the cold-fusion irradiation of ^{208}Pb with radioactive ^{62}Fe. From Fig. 2, the cross

section is expected to be approximately 60 pb, approximately a factor of ten higher than that for production in reactions with stable-isotope beams (Table 1). The isotope ^{269}Sg has very attractive properties for chemical studies, but is produced only indirectly as an extreme overshoot nuclide in the decay of ^{285}114, with an effective production cross section of 0.6 pb. The reaction ^{248}Cm(^{26}Ne,5n) produces this nuclide directly, with an expected cross section on the order of 100 pb (Table 1).

When appropriate accelerator facilities become available, irradiations of targets of Pu, Am, and Cm with beams of radioactive Ne and Mg isotopes out to masses 26 and 30, respectively, could be expected to produce long-lived isotopes of the superheavy elements with $Z = 106$–108 with much higher cross sections than can be achieved in irradiations with stable-isotope beams.

Examination of Table 1 indicates that the selection of known nuclides with half-lives long enough to survive a radiochemistry procedure is limited beyond copernicium ($Z = 112$), and non-existent beyond element 115. The irradiation of actinide targets with neutron-rich radioactive beams of Ar and Ca would open up the possibility of exploring the *Z*,*N* space between the known nuclides and the $N = 184$ neutron shell. The neutron-rich Ar isotopes are particularly interesting. ^{46}Ar has the same magic neutron number as ^{48}Ca, and its complete fusion with actinide targets would suffer less from dynamical hindrance in the entrance channel. The irradiation of ^{243}Am with ^{46}Ar produces the element 113 isotopes that are currently only observed indirectly as decay products in the ^{249}Bk + ^{48}Ca reaction. Examination of Fig. 4 would lead to the conclusion that the production cross section would be an order of magnitude higher, on the order of 10 pb. The downturn of evaporation-residue cross sections beyond $N = 175$ in Fig. 4 has been attributed to dynamical hindrance; the production of neutron-rich element 114 isotopes in the irradiation of ^{248}Cm with radioactive Ar ions could proceed with even larger cross sections [454].

The availability of ^{52}Ca projectiles would make it possible to produce $N = 184$ compound nuclei with atomic numbers as low as 116 (in the ^{248}Cm + ^{52}Ca reaction), a significantly lower atomic number than can be achieved with stable-ion beams ($Z = 122$). As discussed above, the neutron excess of the neutron-rich Ca projectiles lowers the Coulomb barrier, partially compensating for the higher excitation energies that result from departure from the $N = 28$ shell closure in ^{48}Ca. The E_{min} in element 114 isotopes produced by irradiation at the Coulomb barrier [94, 95] of ^{244}Pu with even-mass Ca ions is shown in Fig. 6. It is observed that E_{min} does not increase significantly in going from ^{48}Ca-induced reactions to ^{52}Ca-induced reactions. However, reactions to make superheavy nuclides with ^{48}Ca ions are not free of dynamical hindrance limitations, and the impact of neutron excess on the diversion of reaction cross section to quasifission channels is unclear.

When intense beams of neutron-rich, radioactive heavy ions become available, it will be possible to explore transhassium *Z*,*N* space at greater neutron excess than is now possible. This may facilitate the production of isotopes with $Z > 115$ with

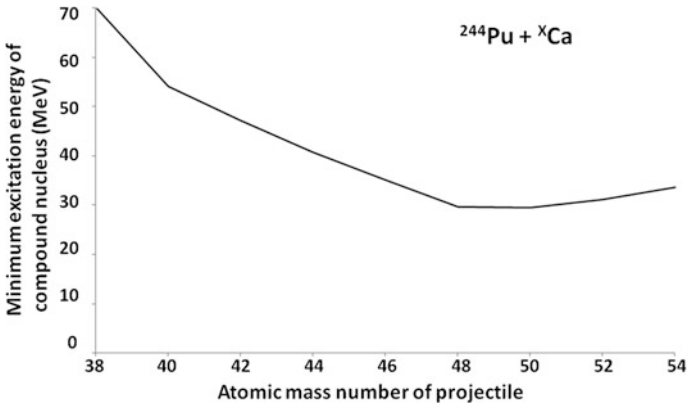

Fig. 6 E_{min} for even-mass Ca-induced complete-fusion reactions with ^{244}Pu as a function of the mass number of the projectile

half-lives suitable for chemical characterization experiments, and longer lived isotopes of the lighter superheavy elements through overshoot reactions.

4.2 Transfer Reactions and Quasifission

Complete-fusion reactions with heavy-element targets have provided the means of producing and studying the superheavy elements. These reactions offer many advantages, not the least of which is the Newtonian constraint on the recoil properties of the products, making it possible to study them on-line with kinematic separators. The major drawback lies in the limited neutron numbers of the projectiles and targets. Even the radioactive beams discussed in the previous section are relatively neutron-poor when compared with the doubly magic ^{298}114 nucleus. There is another way to look at this: In complete-fusion reactions to make neutron-rich species, the problem lies not with the number of neutrons in the projectile, but with the necessity of simultaneously bringing so many protons into the reaction intermediate. It has been proposed [236, 459, 460] that incomplete-fusion reactions, involving the transfer of neutron-rich collections of nucleons from the projectile to the target, may provide an alternative path to the Island of Stability.

The process of incomplete-fusion reactions, also called "transfer reactions", encompasses a variety of mechanisms that are defined by the extent of the interaction between the colliding reaction participants and the duration of time in which the reactant nuclei are in contact [108]. In Coulomb fission there is no exchange of nucleons between the reacting nuclei, but there is enough overlap of the nuclear and Coulomb potentials at closest approach that a heavy-element target nucleus can be induced to fission [461]. Quasi-elastic transfer reactions involve the direct exchange of nucleons between the participants, whose nuclear potentials overlap

so little that the exchange can be thought of as a hand-off of nucleons without the involvement of most of the nuclear material [462, 463]; the angular distribution of the recoiling reaction products is centered around the elastic-scattering grazing angle [464]. As the overlap in the nuclear potentials increases, the quasi-elastic process evolves to the deep-inelastic process [463, 465] involving larger exchanges of nucleons, stronger dissipation of energy and angular momentum [122] and increasing excitation energies in the primary reaction products. Charge and mass flow in the dinuclear deep-inelastic reaction intermediate is determined by the Coulomb, nuclear and centrifugal potentials, their macroscopic dynamics, and gradients in the potential-energy surface as the reaction evolves from the entrance channel to the exit channel. The distribution of angles relative to the beam direction over which the reaction products recoil is still centered near the grazing angle, but becomes broader with the increased magnitude of the mass exchange and the time duration of the interaction, making kinematic separation problematic [466–469]. The radiochemical method has been used to advantage in the study of these reactions. An extreme example of deep-inelastic transfer is quasifission, discussed in Sects. 2.3 and 2.4. Here, the exchange of mass and energy between the reactants is so complete that the mass distribution of reaction products resembles the expectations of the fission of the compound nucleus, even though the reacting system never surmounts the dynamical second barrier and the products are not emitted isotropically in the center of mass [205, 320, 322, 459, 470]. As in fission, shell effects in the nascent reaction products in the exit channel influence the distribution of mass and charge [471, 472].

In Sect. 2.2 it was discussed that the peripheral reactions involving the exchange of a few nucleons compete with complete-fusion reactions with light heavy ions at high impact parameters, corresponding to a small fraction of the reaction cross section. Transfers of small numbers of nucleons proceed much more probably than do exchanges involving large numbers of nucleons, but even with projectiles as light as C, O, and Ne, isotope production involving the transfer of substantial fractions of the projectile are observed [122, 128, 129, 397, 467, 473–476]. Nucleon exchange in these reactions is preferentially from the projectile to the target, driven by the difference of the Coulomb potentials of two touching spheres in the entrance and exit channels [467]. Transfer of a single proton from an ^{18}O projectile to an actinide target nucleus reduces the Coulomb repulsive energy in the dinuclear reaction intermediate by approximately 10 MeV; transfer in the opposite direction results in a corresponding increase. As the number of nucleons exchanged in the reaction increases, the excitation energy of the heavy reaction participant also increases [129, 467] due to the increased dissipation of energy and angular momentum between the participating nuclei.

As discussed previously, targets for use in heavy-ion irradiations are restricted to nuclides with $Z \leq 98$. While "shallow" transfer reactions with light heavy ions have been used with some success to produce new neutron-rich nuclei in the heavy actinides [477, 478], transfers of less than six protons have no application to the production of superheavy nuclei. Since we are interested primarily in neutron-rich exchanges, only projectiles much heavier than Ne should be considered. With

increasing projectile mass, the effect of the exchange of a single proton on the Coulomb potential of the reaction intermediate becomes less important and the drive favoring nucleon exchanges from the light participant to the heavy one decreases. As a result, transfer reactions between heavier reaction participants have been used with some success in the actinide region to produce new neutron-rich nuclei with a lower Z than that of the target [479].

Large exchanges of nucleons are driven by the dinuclear interaction time, the reaction Q value, the gradient of the potential energy surface, and the residual kinetic energy available after the nuclei have come into contact. Charge equilibration in the reaction intermediate is faster than is mass flow [480], so for substantial mass exchange the most probable N/Z of the primary fragments is similar to that of the composite system [469, 481–483], subject to the minimization of the potential energy of the reaction intermediate [108, 467–469, 471, 472]. This means that very massive projectiles, those with the highest value of N/Z, are most favorable for the production of neutron-rich transactinides in transfer reactions. In reactions with the heaviest projectiles, the fraction of the cross section devoted to undesirable complete-fusion reactions goes to zero [484, 485].

Neutron and proton transfer between the two reactants in proximity can be thought of as a tunneling process through the interior barrier of the two-center potential [486]. The interior barrier is lower for neutrons, so the mass flow is accomplished preferably through the agency of the transfer of neutrons [229]. There is a continuous readjustment of N/Z during the mass-diffusion process. Large exchanges of mass are associated with a large dissipation of kinetic energy, which tends to be distributed between the participants in the exit channel proportionally to their masses [122, 466, 487]. However, in specific cases of reactions at or slightly below the Coulomb barrier, exceptions to this rule have been observed [488, 489]. Here, the reaction partner which receives the transferred nucleons is heated while the donating one remains cold.

In discussing an "average" transfer reaction with an actinide target that leads to a transactinide nuclide, N/Z equilibration leads to primary reaction products that are neutron deficient relative to the center of the Island of Stability. The massive exchange of nucleons leads to high excitation energies, resulting in the same $< \Gamma_n / \Gamma_f >$-related depletion of heavy products seen in hot-fusion reactions. The probability of large internuclear transfers of mass is higher at higher reaction energies, but so is the dissipation of energy and angular momentum into the intrinsic modes in the reaction products. As a result, most studies of incomplete-fusion reactions between very heavy ions and actinide targets have been performed near and below the barrier [460, 466–469, 483, 490, 491], favoring small exchanges of mass. Near the barrier, small changes in the reaction energy have little effect on the neutron-richness of the heavy-element products [467].

The high fissility of the product nuclei most strongly depletes those primary products with high excitation energies, with the fission process preferentially claiming transactinide nuclei with E^* greater than 5–8 MeV [229, 467, 483]. This leads to a significant depletion of the products of large projectile-to-target exchanges, approximately an order of magnitude for each exchanged proton [304].

The grazing angle for the heavy-product recoils approaches 0° at the barrier and the angular distribution of the recoil transfer products becomes forward peaked, making it possible to revisit the use of kinematic separators [492]. All existing data are consistent with a maximum cross section for actinide transfer products at projectile energies approximately 10% in excess of the Coulomb barrier. Nevertheless, the statistical nature of the distribution of nuclear charge and excitation energy between the primary products at a given mass asymmetry provides the means by which primary neutron-rich transactinide products could survive deexcitation by fission, even at reaction energies significantly in excess of the barrier.

Both the distribution of charge at a fixed mass asymmetry, and the related distribution of neutron number at a fixed atomic number, can be approximated by Gaussian functions [122, 467]. The width of the cross-section distribution broadens with increasing reaction energy in the vicinity of the barrier, then saturates. Competition between neutron evaporation and fission gives extra breadth to the final distribution of heavy reaction products, but shifts it away from neutron excess [467, 493]. Although "cold" transfers of substantial numbers of nucleons are possible, they are not likely: At $\Delta Z = 4$, in transfer reactions with ^{248}Cm targets, comparison of the final product distribution with expectations from (N/Z) equilibration indicates an average evaporation of 3–4 neutrons [460, 467], meaning that the number of evaporation residues arising from primary Fm products at $E^* = 30$–40 MeV far outweighs the number that arise from primary products at $E^* < 8$ MeV.

Reactions with the heaviest projectiles are expected to produce the most neutron-rich transfers to actinide targets. The near-barrier incomplete-fusion reactions ^{238}U + ^{238}U [466] and ^{238}U + ^{248}Cm [460] were examined for their utility in producing transactinide nuclides. While it was possible to extract cross sections for the primary production of transactinide elements from this work, their excitation energies were so high as to preclude the observation of the extremely rare transactinide evaporation residues. The experiments were radiochemical in nature, and nuclides with half-lives in the range of seconds to minutes were not accessible. New methods are needed to search for the production of most of the nuclides in Table 1 via transfer reactions. The optimum projectile-target combinations and reaction energies for the production of superheavy nuclides have yet to be determined, but incomplete-fusion reactions may provide the only pathway leading to the center of the Island of Stability.

5 Summary and Outlook

Transactinide nuclides have been produced in heavy-ion complete-fusion reactions by a variety of mechanisms. The latest major extension of the Periodic Table has been through the agency of ^{48}Ca-induced reactions with actinide targets, resulting in the synthesis of new elements as far as the next noble gas beyond radon, with $Z = 118$ [370]. The experimental results are consistent with the onset of spherical

nuclear shapes at neutron numbers greater than $N = 172$, supporting the existence of the long-sought Island of Stability, whose location is predicted to be most closely tied to the closed neutron shell at $N = 184$. At this time, all heavy elements through $Z = 114$ are represented by at least one isotope with a half-life greater than one second, suitable for limited chemical studies. The observed decay properties of the most extreme elements lead one to conclude that it is possible to synthesize elements out past $Z = 120$ [133] if the proper reaction mechanisms can be identified.

Actinide nuclides that are available in quantities suitable for low-cross-section heavy-ion bombardments are limited to $Z \leq 98$ (californium). This means that extension of the Periodic Table to the next row, to *eka*-francium ($Z = 119$) and beyond, cannot be accomplished in ^{48}Ca irradiations. Cold-fusion reactions, involving the irradiation of shell-stabilized ^{208}Pb and ^{209}Bi targets with very heavy ions, were used in the discoveries of the elements between bohrium ($Z = 107$) and copernicium ($Z = 112$), inclusive. Unfortunately, the cross sections for the production of evaporation residues decrease exponentially with increasing atomic number (see Fig. 2). The recent report of the observation of element 113 with a cross section of about 20 fb [276–278] represents a practical end to the cold-fusion pathway to new superheavy elements [282]. Recent attempts to produce $Z = 120$ nuclides in the ^{244}Pu(^{58}Fe,*x*n) and ^{248}Cm(^{54}Cr,*x*n) reactions [369, 443], in experiments performed at the same level of sensitivity as successful ^{48}Ca + actinide experiments, were unsuccessful. This is not unexpected, since increasing the atomic number of the projectile leads to an increase in the dynamical hindrance to fusion similar to that which ends transactinide production in cold-fusion reactions. While it could be argued that strong stabilization effects associated with a hypothetical closed proton shell at $Z = 120$ or higher could result in an increase in evaporation-residue cross sections for reactions between actinide targets and ions heavier than ^{48}Ca [8, 282], it seems unlikely that any local upturn in production rate would exceed an order of magnitude (see Figs. 2 and 3). The ^{48}Ca reactions leading to the heaviest known transactinides are characterized by both the reseparation processes that dominate the cold-fusion mechanism and the fissility of the highly excited compound nucleus that dominates the hot-fusion mechanism. The study of evaporation-residue excitation functions is the means by which the complex reaction mechanism can be inferred, information that is necessary to select the optimum conditions to produce elements with $Z \geq 119$; this work is ongoing [8].

Extension of the Periodic Table to new elements is of supreme interest to the chemist. However, if the product isotopes have half-lives that are too short to support chemical investigations, this interest is theoretical rather than practical. From this perspective, the more neutron-rich transactinide nuclei that lie between the known nuclides and the $N = 184$ shell closure are expected to have longer half-lives. Production of these nuclides is problematic, since the complete fusion of actinide targets with available projectiles produces only neutron-poor evaporation residues. The overshoot process, in which a very heavy neutron-deficient nuclide undergoes a series of α decays (a proton-rich process) to produce a

progeny nuclide closer to the valley of beta stability, has been used to produce the longest-lived isotopes of the light transactinides (Table 1). Unfortunately, the limitations on the cross sections for the production of the new elements apply here, and no further progress is expected using the projectile/target combinations that are currently available (Sect. 2.4). In the future, complete-fusion reactions with radioactive-ion beams (Sect. 4.1) and transfer reactions with very heavy ions (Sect. 4.2) may provide pathways to these interesting transactinide isotopes.

In the last 30 years, significant advances in the physical techniques used in transactinide nuclide discovery have made possible the detection of the heaviest elements, produced in heavy-ion reactions with cross sections below 1 pb. Kinematic separators have become very efficient, approaching 60%, so that the observation of position-correlated events in the focal plane can be used to reconstruct the decay sequence of genetically related nuclides with half-lives spanning microseconds to days. Further progress will rely more on improving the suppression of unwanted species rather than improving efficiency. This is particularly important in the interpretation of rare decay sequences involving long-lived nuclei; the probability of an accidental sequence of events mimicking a true decay sequence increases with an increase in half-lives and the random-event rate. Interestingly enough, at the present time the best way to observe very long-lived superheavy nuclides involves chemical separations and counting, a high-efficiency/low-background process.

In any isotope-production experiment, it is impossible to get around the fundamental rate equation, where production rate equals flux times areal density times cross section. The cross sections for the production of transactinide isotopes are small, and the areal density of the target material is limited by the energy loss of heavy ions in matter. The only parameter over which the experimenter has some control is the particle flux. With a cross section of 1 pb and a 1 mg/cm^2 target, a beam current of 1 μA (particle) produces approximately one atom per day of irradiation. A significant increase in luminosity requires not only improvements in particle-accelerator technology, but a fundamental change in the way target materials are irradiated. Advancing the boundaries of the Chart of the Nuclides in the transactinide elements will require these improvements in technique.

References

1. Fermi, E.: Possible production of elements of atomic number higher than 92. Nature **133**, 898–899 (1934)
2. Hahn, O., Strassman, F.: Über den Nachweis und das Verhalten der bei der Bestrahlung des Urans mittels Neutronen entstehenden Erdalkalimetalle. Naturwissenschaften **27**, 11–15 (1939)
3. Meitner, L., Frisch, O.R.: Disintegration of uranium by neutrons: a new type of nuclear reaction. Nature **143**, 239–240 (1939)
4. Von Weisäcker, C.F.: Zur Theorie der Kernmassen. Z. Phys. **96**, 431–458 (1935)

5. Gamov, G.: Mass defect curve and nuclear constitution. Proc. Roy. Soc. London **A126**, 632–644 (1930)
6. Bohr, N., Wheeler, J.A.: The mechanism of nuclear fission. Phys. Rev. **56**, 426–450 (1939)
7. Frenkel, J.: On the splitting of heavy nuclei by slow neutrons. Phys. Rev. **55**, 987 (1939)
8. Oganessian, Yu.: Heaviest nuclei from ^{48}Ca-induced reactions. J. Phys. **G34**, R165–R242 (2007)
9. Thompson, S.G., Tsang, C.F.: Superheavy elements. Science **178**, 1047–1055 (1972)
10. Myers, W.D., Swiatecki, W.J.: Nuclear masses and deformations. Nucl. Phys. **81**, 1–60 (1966)
11. Nilsson, S.G., Thompson, S.G., Tsang, C.F.: Stability of superheavy nuclei and their possible occurrence in nature. Phys. Lett. **28B**, 458–461 (1969)
12. Brack, M., Damgaard, J., Jensen, A.S., Pauli, H.C., Strutinsky, V.M., Wong, C.Y.: Funny hills: the shell-correction approach to nuclear shell effects and its applications to the fission process. Rev. Mod. Phys. **44**, 320–405 (1972)
13. Nilsson, S.G., Tsang, C.F., Sobiczewski, A., Szymanski, Z., Wycech, S., Gustafson, C., Lamm, I.-L., Möller, P., Nilsson, B.: On the nuclear structure and stability of heavy and superheavy elements. Nucl. Phys. **A131**, 1–66 (1969)
14. Haxel, O., Jensen, J.H.D., Suess, H.D.: On the "magic numbers" in nuclear structure. Phys. Rev. **75**, 1766 (1949)
15. Goeppert Mayer, M.: On closed shells in nuclei II. Phys. Rev. **75**, 1969–1970 (1949)
16. Goeppert Mayer, M.: On closed shells in nuclei. Phys. Rev. **74**, 235–239 (1948)
17. Scharff-Goldhaber, G.: Nuclear Physics. Nucleonics **15**(9), 122–124 (1957)
18. Wong, C.Y.: Additional evidence of stability of the superheavy element ^{310}126 according to the shell model. Phys. Lett. **21**, 688–690 (1966)
19. Sobiczewski, A., Gareev, F.A., Kalinkin, B.N.: Closed shells for $Z > 82$ and $N > 126$ in a diffuse potential well. Phys. Lett. **22**, 500–502 (1966)
20. Meldner, H.: Predictions of new magic regions and masses for super-heavy nuclei from calculations with realistic shell model single particle Hamiltonians. Ark. Fys. **36**, 593–598 (1967)
21. Mosel, U., Greiner, W.: On the stability of superheavy nuclei against fission. Z. Phys. **222**, 261–282 (1969)
22. Seaborg, G.T., Loveland, W., Morrissey, D.J.: Superheavy elements: a crossroads. Science **203**, 711–717 (1979)
23. Strutinskii, V.M.: Influence of nucleon shells on the energy of a nucleus. Sov. J. Nucl. Phys. **3**, 449–457 (1966)
24. Myers, W.D.: Droplet model of atomic nuclei. IFI/Plenum, New York (1977)
25. Nilsson, S.G., Nix, J.R., Sobiczewski, A., Szymanski, Z., Wycech, S., Gustafson, C., Möller, P.: On the spontaneous fission of nuclei with Z near 114 and N near 184. Nucl. Phys. **A115**, 545–562 (1968)
26. Bolsterli, M., Fiset, E.O., Nix, J.R., Norton, J.L.: New calculation of fission barriers for heavy and superheavy nuclei. Phys. Rev. **C5**, 1050–1077 (1972)
27. Bassichis, W.H., Kerman, A.K.: Self-consistent calculations of shell effects including the proposed island of stability. Phys. Rev. **C2**, 1768–1776 (1970)
28. Fiset, E.O., Nix, J.R.: Calculation of half-lives for superheavy nuclei. Nucl. Phys. **A193**, 647–671 (1972)
29. Randrup, J., Larsson, S.E., Möller, P., Nilsson, S.G., Pomorski, K., Sobiczewski, A.: Spontaneous-fission half-lives for even nuclei with $Z \geq 92$. Phys. Rev. **C13**, 229–239 (1976)
30. Cowan, J.J., Thielmann, F.-K., Truran, J.W.: The r-process and nucleochronology. Phys. Rep. **208**, 267–394 (1991)
31. Flerov, G.N., Ter-Akopian, G.M.: Superheavy nuclei. Rep. Prog. Phys. **46**, 817–875 (1983)
32. Hillebrandt, W.: The rapid neutron-capture process and the synthesis of heavy and neutron-rich elements. Space Sci. Rev. **21**, 639–702 (1978)

33. Bemis Jr, C.E., Nix, J.R.: Superheavy elements—the quest in perspective. Comments Nucl. Part. Phys. **7**, 65–78 (1977)
34. Nurmia, M.: Superheavies in nature—where and how to look. Phys. Scripta **10A**, 77–80 (1974)
35. Herrmann, G.: The search for superheavy elements in nature. Phys. Scripta **10A**, 71–76 (1974)
36. Flerov, G.N., Perelygin, V.P.: Spontaneous fission of lead and the search for transuranium elements. Sov. J. At. Energy **26**, 603–605 (1969)
37. Seaborg, G.T., Crandall, J.L., Fields, P.R., Ghiorso, A., Keller, O.L., Jr., Penneman, R.A.: Recent advances in the United States of America on the transuranium elements. In: Proceedings of the 4th International Conference on the Peaceful Uses of Atomic Energy, pp. 487–542. United Nations, New York (1972)
38. Herrmann, G.: Superheavy-element research. Nature **280**, 543–549 (1979)
39. Flerov, G.N., Perelygin, V.P., Otgonsuren, O.: Origin of tracks of fission products in lead glasses. Sov. At. Energy **33**, 1144–1149 (1972)
40. Grimm, W., Herrmann, G., Schüssler, H.-D.: Search for superheavy elements in terrestrial matter. Phys. Rev. Lett. **26**, 1040–1043 (1971)
41. Gentry, R.V.: Giant radioactive halos: indicators of unknown radioactivity? Science **169**, 670–673 (1970)
42. Gentry, R.V., Cahill, T.A., Fletcher, N.R., Kaufmann, H.C., Medsker, L.R., Nelson, J.W., Flocchini, R.G.: Evidence for primordial superheavy elements. Phys. Rev. Lett. **37**, 11–15 (1976)
43. Wesolowski, J.J., John, W., Jewel, R., Guy, F.: A search for element 110 in platinum ore via neutron-induced fission. Phys. Lett **B28**, 544–545 (1969)
44. Levine, C.A., Seaborg, G.T.: The occurrence of plutonium in nature. J. Am. Chem. Soc. **73**, 3278–3286 (1951)
45. Peppard, D.F., Studier, M.H., Gergel, M.V., Mason, G.W., Sullivan, J.C., Mech, J.F.: Isolation of microgram quantities of naturally-occurring plutonium and examination of its isotopic content. J. Am. Chem. Soc. **73**, 2529–2535 (1951)
46. Hoffman, D.C., Lawrence, F.O., Mewherter, J.L., Roarke, F.M.: Detection of plutonium-244 in nature. Nature **234**, 132–134 (1971)
47. Kratz, J.V.: The search for superheavy elements. Radiochim. Acta **32**, 25–41 (1983)
48. Strutinsky, V.M.: Shell effects in nuclear masses and deformation energies. Nucl. Phys. **A95**, 420–442 (1967)
49. Strutinsky, V.M.: "Shells" in deformed nuclei. Nucl. Phys. **A122**, 1–33 (1968)
50. Nix, J.R.: Calculation of fission barriers for heavy and superheavy nuclei. Ann. Rev. Nucl. Sci. **22**, 65–120 (1972)
51. Patyk, Z., Sobiczewski, A.: Ground-state properties of the heaviest nuclei analyzed in a multidimensional deformation space. Nucl. Phys. **A533**, 132–152 (1991)
52. Smolanczuk, R., Skalski, J., Sobiczewski, A.: Spontaneous fission half-lives of deformed superheavy nuclei. Phys. Rev. **C52**, 1871–1880 (1995)
53. Cwiok, S., Pashkevich, V.V., Dudek, J., Nazarewicz, W.: Fission barriers of transfermium elements. Nucl. Phys. **A410**, 254–270 (1983)
54. Bjornholm, S., Lynn, J.E.: The double-humped fission barrier. Rev. Mod. Phys. **52**, 725–931 (1980)
55. Reiter, P., Khoo, T.L., Lister, C.J., Seweryniak, D., Ahmad, I., Alcorta, M., Carpenter, M.P., Cizewski, J.A., Davids, C.N., Gervais, G., Greene, J.P., Henning, W.F., Janssens, R.V.F., Lauritsen, T., Siem, S., Sonzogni, A.A., Sullivan, D., Uusitalo, J., Wiedenhoever, I., Amzal, N., Butler, P.A., Chewter, A.J., Ding, K.Y., Fotiades, N., Fox, J.D., Greenlees, P.T., Herzberg, R.-D., Jones, G.D., Korten, W., Leino, M., Vetter, K.: Ground-state band and deformation of the $Z = 102$ isotope ^{254}No. Phys. Rev. Lett. **82**, 509–512 (1999)
56. Audi, G., Bersillon, O., Blachot, J., Wapstra, A.H.: The 2003 Nubase evaluation and the 2003 atomic mass evaluation. Nucl. Phys. **A729**, 3–128 (2003)

57. Firestone, R.B., Shirley, V.S. (eds.): Table of Isotopes, vol. II, 8th edn. Wiley, New York (1996)
58. Muntian, I., Patyk, Z., Sobiczewski, A.: Calculated masses of heaviest nuclei. Phys. At. Nuclei **66**, 1015–1019 (2003)
59. Muntian, I., Hofmann, S., Patyk, Z., Sobiczewski, A.: Properties of heaviest nuclei. Acta Phys. Pol. **B34**, 2073–2082 (2003)
60. Muntian, I., Patyk, Z., Sobiczewski, A.: Fission properties of superheavy nuclei. Acta Phys. Pol. **B34**, 2141–2145 (2003)
61. Bürvenich, T., Bender, M., Maruhn, J.A., Reinhard, P.-G.: Systematics of fission barriers in superheavy elements. Phys. Rev. **C69** 014307(15) (2004)
62. Bender, M., Rutz, K., Reinhard, P.-G., Maruhn, J.A., Greiner, W.: Potential energy surfaces of superheavy nuclei. Phys. Rev. **C58**, 2126–2132 (1998)
63. Bender, M., Rutz, K., Reinhard, P.-G., Maruhn, J.A., Greiner, W.: Shell structure of superheavy nuclei in self-consistent mean-field models. Phys. Rev. **C60** 034304(20) (1999)
64. Berger, J.-F., Bitaud, L., Decharge, J., Girod, M., Dietrich, K.: Superheavy, hyperheavy and bubble nuclei. Nucl. Phys. **A685**, 1c–16c (2001)
65. Bender, M., Nazarewicz, W., Reinhard, P.-G.: Shell stabilization of super- and hyperheavy nuclei without magic gaps. Phys. Lett. **B515**, 42–48 (2001)
66. Cwiok, S., Nazarewicz, W., Heenen, P.H.: Structure of odd-N superheavy elements. Phys. Rev. Lett. **83**, 1108–1111 (1999)
67. Cwiok, S., Hofmann, S., Nazarewicz, W.: Shell structure of the heaviest elements. Nucl. Phys. **A573**, 356–394 (1994)
68. Cwiok, S., Dobaczewski, J., Heenen, P.-H., Magierski, P., Nazarewicz, W.: Shell structure of the superheavy elements. Nucl. Phys. **A611**, 211–246 (1996)
69. Rutz, K., Bender, M., Bürvenich, T., Schilling, T., Reinhard, P.-G., Maruhn, J.A., Greiner, W.: Superheavy nuclei in self-consistent nuclear calculations. Phys. Rev. **C56**, 238–243 (1997)
70. Berger, J.F., Hirata, D., Girod, M.: Microscopic description of superheavy nuclei with the Gogny effective interaction. Acta Phys. Pol. **B34**, 1909–1926 (2003)
71. Armbruster, P.: Shifting the closed proton shell to $Z = 122$—a possible scenario to understand the production of superheavy elements $Z = 112$–118. Eur. Phys. J. **A37**, 159–167 (2008)
72. Chowdbury, P.R., Samanta, C., Basu, D.N.: Search for long lived heaviest nuclei beyond the valley of stability. Phys. Rev. **C77** 044603(10) (2008)
73. Seaborg, G.T.: Man-Made Transuranium Elements. Prentice-Hall, New York (1963)
74. Seaborg, G.T., Loveland, W.D.: The Elements Beyond Uranium. Wiley, New York (1990)
75. Nagame, Y., Hirata, M.: Production and properties of transuranium elements. Radiochim. Acta **99**, 377–393 (2011)
76. Ferguson, D.E., Bigelow, J.E.: Production of ^{252}Cf and other transplutonium isotopes in the United States of America. Actinides Rev. **1**, 213–221 (1969)
77. Hulet, E.K., Lougheed, R.W., Wild, J.F., Dougan, R.J., Moody, K.J., Hahn, R.L., Henderson, C.M., Dupzyk, R.J., Bethune, G.R.: Conclusive Z and A identification of 370-microsecond ^{258}Fm. Phys. Rev. **C34**, 1394–1396 (1986)
78. Hulet, E.K., Wild, J.F., Lougheed, R.W., Evans, J.E., Qualheim, B.J., Nurmia, M., Ghiorso, A.: Spontaneous-fission half-life of ^{258}Fm and nuclear instability. Phys. Rev. Lett. **26**, 523–526 (1971)
79. Lougheed, R.W., Hulet, E.K., Dougan, R.J., Wild, J.F., Dupzyk, R.J., Henderson, C.M., Moody, K.J., Hahn, R.L., Sümmerer, K., Bethune, G.: The discovery of ^{260}Md and the decay properties of ^{258}Fm, $^{258\ m,\ g}$Md, and ^{259}Md. J. Less-Common Met. **122**, 461–468 (1986)
80. Ghiorso, A., Harvey, B.G., Choppin, G.R., Thompson, S.G., Seaborg, G.T.: New element mendelevium, atomic number 101. Phys. Rev. **98**, 1518–1519 (1955)
81. Ghiorso, A., Thompson, S.G., Higgins, G.H., Seaborg, G.T., Studier, M.H., Fields, P.R., Fried, S.M., Diamond, H., Mech, J.F., Pyle, G.L., Huizenga, J.R., Hirsch, A., Manning,

W.M., Browne, C.I., Smith, H.L., Spence, R.W.: New elements einsteinium and fermium, atomic numbers 99 and 100. Phys. Rev. **99**, 1048–1049 (1955)
82. Howard, W.M., Nix, J.R.: Production of superheavy nuclei by multiple capture of neutrons. Nature **247**, 17–20
83. Howard, W.M.: Possible paths for synthesis of superheavy elements in nature. Phys. Scripta **10A**, 138–141 (1974)
84. Sanders, R.: Project Plowshare. Public Affairs Press, Washington (1962)
85. Hoff, R.W.: Production of einsteinium and fermium in nuclear explosions. Lawrence Livermore Laboratory report UCRL-81566 (1978)
86. Hoffman, D.C.: Production of heavy elements in a recent Los Alamos thermonuclear test. Ark. Fys. **36**, 533–537 (1966)
87. Dorn, D.W., Hoff, R.W.: Spontaneous fission in very neutron-rich isotopes. Phys. Rev. Lett. **14**, 440–441 (1965)
88. Mamdouh, A., Pearson, J.M., Rayet, M., Tondeur, F.: Fission barriers of neutron-rich and superheavy nuclei calculated with the ETFSI method. Nucl. Phys. **A679**, 337–358 (2001)
89. Pearson, J.M., Nayak, R.C., Goriely, S.: Nuclear mass formula with Bogolyubov-enhanced shell-quenching: application to r-process. Phys. Lett. **B387**, 455–459 (1996)
90. Meldner, H.W., Nuckolls, J., Wood, L.: An alternative thermonuclear n-capture path to the superheavy island. Phys. Scripta **10A**, 149–155 (1974)
91. Ingley, J.S.: Nuclear explosion experiments to determine nuclear properties of heavy isotopes. Nucl. Phys. **A124**, 130–144 (1969)
92. Wene, C.-O., Johansson, S.A.E.: The importance of delayed fission in the production of very heavy and superheavy elements. Phys. Scripta **10A**, 156–161 (1974)
93. Meldner, H.W.: Superheavy element synthesis. Phys. Rev. Lett. **28**, 975–978 (1972)
94. Bass, R.: Fusion reactions: successes and limitations of a one-dimensional description. In: von Oertzen, W. (ed.) Lecture Notes in Physics 117. Springer, Berlin (1980)
95. Bass, R.: Fusion of heavy nuclei in a classical model. Nucl. Phys. **A231**, 45–63 (1974)
96. Gäggeler, H., Iljinov, A.S., Popeko, G.S., Seidel, W., Ter-Akopian, G.M., Tretyakova, S.P.: A study of fusion reactions between ^{206,207}Pb nuclei and ^{40}Ar ions near the Coulomb barrier. Z. Phys. **A289**, 415–420 (1979)
97. Hinde, D.J., Dasgupta, M., Mukherjee, A.: Severe inhibition of fusion by quasifission in reactions forming ^{220}Th. Phys. Rev. Lett. **89**(282701), 1–4 (2002)
98. Lefort, M.: Nuclear fusion between heavy ions. Rep. Prog. Phys. **39**, 129–173 (1976)
99. Lefort, M.: Complete fusion and its limitation. J. Phys. Coll. C5 (Paris) **37**, 57–81 (1976)
100. Keller, H., Lützenkirchen, K., Kratz, J.V., Wirth, G., Brüchle, W., Sümmerer, K.: Evidence for quasi-fission in ^{40}Ar + ^{208}Pb collisions near the Coulomb-barrier. Z. Phys. **A326**, 313–326 (1987)
101. Back, B.B.: Complete fusion and quasifission in reactions between heavy ions. Phys. Rev. **C31**, 2104–2112 (1985)
102. Cherepanov, E.A., Ijinov, A.S., Mebel, M.V.: Systematics of the effective ratio $< \Gamma_n/\Gamma_f >$ of neutron emission and fission partial widths for transcurium nuclei. J. Phys. **G9**, 931–938 (1983)
103. Simbel, M.H.: Evaluation of Γ_n/Γ_f from cross sections of (HI, xn) reactions. Z. Phys. **A313**, 311–317 (1983)
104. Möller, P., Nix, J.R., Myers, W.D., Swiatecki, W.J.: Nuclear ground-state masses and deformations. At. Data Nucl. Data Tables **59**, 185–381 (1995)
105. Zagrebaev, V.I., Itkis, M.G., Oganessian, Yu.Ts.: Fusion-fission dynamics and perspectives of future experiments. Phys. At. Nuclei **66**, 1033–1041 (2003)
106. Reisdorf, W.: Analysis of fissionability data at high excitation energies. Z. Phys. **A300**, 227–238 (1981)
107. Arimoto, Y., Wada, T., Ohta, M., Abe, Y.: Fluctuation-dissipation model for synthesis of superheavy elements. Phys. Rev. **C59**, 796–809 (1999)
108. Zagrebaev, V.I., Greiner, W.: Unified consideration of deep inelastic, quasi-fission and fusion-fission phenomena. J. Phys. **G31**, 825–844 (2005)

109. Strutinskii, V.M.: Fission width of heated nuclei. Sov. J. Nucl. Phys. **19**, 127–128 (1974)
110. Moretto, L.G.: Statistical attenuation of shell effects in the fission probability of excited superheavy nuclei. Phys. Lett. **34B**, 191–194 (1970)
111. Davidson, N.J., Miller, H.G.: Nuclear shell effects at high temperatures. Phys. Rev. **C48**, 2108–2111 (1993)
112. Pei, J.C., Nazarewicz, W., Sheikh, J.A., Kerman, A.K.: Fission barriers of compound superheavy nuclei. Phys. Rev. Lett. **102** 192501(4) (2009)
113. Lojewski, Z., Pashkevich, V.V., Cwiok, S.: Excitation effects on the nuclear-fission process in the heaviest elements. Nucl. Phys. **A436**, 499–505 (1985)
114. Adeev, G.D., Cherdantsev, P.A.: Shell effects in an excited fissile nucleus. Sov. J. Nucl. Phys. **18**, 381–385 (1974)
115. Cohen, S., Plasil, F., Swiatecki, W.J.: Equilibrium configurations of rotating charged or gravitating liquid masses with surface tension II. Ann. Phys. **82**, 557–596 (1974)
116. Carjan, N., Alexander, J.M.: Predictions of the macroscopic model of nuclei: barriers to fusion and to light fragment emission. Phys. Rev. **C38**, 1692–1697 (1988)
117. Blann, M., Komoto, T.T.: Statistical fission parameters for nuclei at high excitation and angular momenta. Phys. Rev. **C26**, 472–485 (1982)
118. Kubo, K.-I., Manyum, P., Hodgson, P.E.: The spin distribution in heavy-ion fusion. Nucl. Phys. **A534**, 393–402 (1991)
119. Arimoto, Y.: Fusion mechanism in superheavy mass region. J. Nucl. Radiochem. Sci. **3**, 17–18 (2002)
120. Reiter, P., Khoo, T.L., Lauritsen, T., Lister, C.J., Seweryniak, D., Sonzogni, A.A., Ahmad, I., Amzal, N., Bhattacharyya, P., Butler, P.A., Carpenter, M.P., Chewter, A.J., Cizewski, J.A., Davids, C.N., Ding, K.Y., Fotiades, N., Greene, J.P., Greenlees, P.T., Heinz, A., Henning, W.F., Herzberg, R.-D., Janssens, R.V.F., Jones, G.D., Kankaanpaa, H., Kondev, F.G., Korten, W., Leino, M., Siem, S., Uusitalo, J., Vetter, K., Wiedenhoever, I.: Entry distribution, fission barrier, and formation mechanism of ^{254}No. Phys. Rev. Lett. **84**, 3542–3545 (2000)
121. Armbruster, P.: On the production of heavy elements by cold fusion: the elements 106–109. Ann. Rev. Nucl. Part. Sci. **35**, 135–194 (1985)
122. Oganessian, Yu.Ts, Lazarev, Yu.A: Problems involved in the synthesis of new elements. Pure Appl. Chem. **53**, 925–947 (1981)
123. Nishio, K., Ikezoe, H., Nagame, Y., Asai, M., Tsukada, K., Mitsuoka, S., Tsuruta, K., Satou, K., Lin, C.J., Ohsawa, T.: Evidence of complete fusion in the sub-barrier $^{16}O + ^{238}U$ reaction. Phys. Rev. Lett. **93**, 162701(4) (2004)
124. Stephens, F.S., Leigh, J.R., Diamond, R.M.: Some limitations on the production of very neutron-deficient nuclei. Nucl. Phys. **A170**, 321–335 (1971)
125. Blann, M.: Decay of deformed and superdeformed nuclei formed in heavy ion reactions. Phys. Rev. **C21**, 1770–1782 (1980)
126. Silva, R.J., Dittner, P.F., Mallory, M.L., Keller, O.L., Eskola, K., Eskola, P., Nurmia, M., Ghiorso, A.: The new nuclide nobelium-259. Nucl. Phys. **A216**, 97–108 (1973)
127. Shinohara, N., Usuda, S., Ichikawa, S., Suzuki, T., Magara, M., Okashita, H., Yoshikawa, H., Horiguchi, T., Iwata, Y., Shibata, S., Fujiwara, I.: Actinides produced by $^{12}C + ^{242}Pu$ and $^{16}O + ^{238}U$ reactions. Phys. Rev. **C34**, 909–913 (1986)
128. Hahn, R.L., Dittner, P.F., Toth, K.S., Keller, O.L.: Transfer and compound-nucleus reactions that lead to the nuclei ^{245}Cf and ^{244}Cf: Interaction of ^{12}C with ^{239}Pu and ^{238}U. Phys. Rev. **C10**, 1889–1903 (1974)
129. Moody, K.J., Lougheed, R.W., Dougan, R.J., Hulet, E.K., Wild, J.F., Sümmerer, K., Hahn, R.L., van Aarle, J., Bethune, G.R.: Actinide cross sections from the reaction of ^{13}C with ^{254}Es. Phys. Rev. **C41**, 152–159 (1990)
130. Sikkeland, T., Thompson, S.G., Ghiorso, A.: Reactions of uranium-238 with carbon ions. Phys. Rev. **112**, 543–547 (1958)
131. Blann, M.: Precompound decay in heavy-ion reactions. Phys. Rev. **C23**, 205–212 (1981)

132. Schädel, M.: Chemistry of transactinide elements—experimental achievements and perspectives. J. Nucl. Radiochem. Sci. **3**, 113–120 (2002)
133. Oganessian, Yu.: Synthesis of the heaviest elements in ^{48}Ca-induced reactions. Radiochim. Acta **99**, 429–439 (2011)
134. Orlova, O.A., Bruchertseifer, H., Muzychka, Yu.A., Oganesyan, Yu.Ts., Pustyl'nik, B.I., Ter-Akop'yan, G.M., Chepigin, V.I., Val Sek, C.: Study of fusion of ^{48}Ca with the nuclei ^{203,205}Tl, ^{208}Pb, and ^{209}Bi. Sov. J. Nucl. Phys. **30**, 317–321 (1979)
135. Herrmann, G., Seyb, K.-E.: Die schwersten chemischen Elemente. Naturwissenschaften **56**, 590–605 (1969)
136. Barber, R.C., Greenwood, N.N., Hrynkiewicz, A.Z., Jeannin, Y.P., Lefort, M., Sakai, M., Ulehla, I., Wapstra, A.H., Wilkinson, D.H.: Discovery of the transfermium elements. Prog. Part. Nucl. Phys. **29**, 453–530 (1992)
137. Flerov, G.N., Oganesyan, Yu.Ts., Lobanov, Yu.V., Kuznetsov, V.I., Druin, V.A., Perelygin, V.P., Gavrilov, K.A., Tretiakova, S.P., Plotko, V.M.: Synthesis and physical identification of the isotope of element 104 with mass number 260. Phys. Lett. **13**, 73–75 (1964)
138. Flerov, G.N., Oganesyan, Yu.Ts., Lobanov, Yu.V., Kuznetsov, V.I., Druin, V.A., Perelygin, V.P., Gavrilov, K.A., Tret'yakova, S.P., Plotko, V.M.: Synthesis and physical identification of the isotope with mass number 260 of element 104. Sov. At. Energy **17**, 1046–1048 (1964)
139. Oganesyan, Yu.Ts., Lobanov, Yu.V., Tret'yakova, S.P., Lazarev, Yu.A., Kolesov, I.V., Gavrilov, K.A., Plotko, V.M., Poluboyarinov, Yu.V.: Identification of the elements 102 and 104 by means of the collimation method. Sov. At. Energy **28**, 502–509 (1970)
140. Zvara, I., Chuburkov, Yu.T., Tsaletka, R., Zvarova, T.S., Shalaevskii, M.R., Shilov, B.V.: Chemical properties of element 104. Sov. At. Energy **21**, 709–710 (1966)
141. Zvara, I., Chuburkov, Yu.T., Belov, V.Z., Buklanov, G.V., Zakhvataev, B.B., Zvarova, T.S., Maslov, O.D., Caletka, R., Shalaevsky, M.R.: Experiments on chemistry of element 104—kurchatovium—V. Adsorption of kurchatovium chloride from the gas stream on surfaces of glass and potassium chloride. J. Inorg. Nucl. Chem. **32**, 1885–1894 (1970)
142. Zvara, I., Belov, V.Z., Chelnokov, L.P., Domanov, V.P., Hussonnois, M., Korotkin, Yu.S., Schegolev, V.A., Shalayevsky, M.R.: Chemical separation of kurchatovium. Inorg. Nucl. Chem. Lett. **7**, 1109–1116 (1971)
143. Flerov, G.N., Ter-Akopian, G.M.: Synthesis and study of atomic nuclei with $Z > 100$. Prog. Part. Nucl. Phys. **19**, 197–239 (1987)
144. Ghiorso, A., Nurmia, M., Harris, J., Eskola, K., Eskola, P.: Positive identification of two alpha-particle-emitting isotopes of element 104. Phys. Rev. Lett. **22**, 1317–1320 (1969)
145. Somerville, L.P., Nurmia, M.J., Nitschke, J.M., Ghiorso, A., Hulet, E.K., Lougheed, R.W.: Spontaneous fission of rutherfordium isotopes. Phys. Rev. **C31**, 1801–1815 (1985)
146. Nitschke, J.M., Fowler, M., Ghiorso, A., Leber, R.E., Leino, M.E., Nurmia, M.J., Somerville, L.P., Williams, K.E., Hulet, E.K., Landrum, J.H., Lougheed, R.W., Wild, J.F., Bemis Jr, C.E., Silva, R.J., Eskola, P.: Search for an 80 ms spontaneous fission activity in bombardments of ^{249}Bk with ^{15}N. Nucl. Phys. **A352**, 138–146 (1981)
147. Druin, V.A., Bochev, B., Korotkin, Yu.S., Kosyakov, V.N., Lobanov, Yu.V., Minin, E.A., Poluboyarinov, Yu.V., Rykov, A.G., Sagaidak, R.N., Tret'yakova, S.P., Kharitonov, Yu.P.: Synthesis of ^{260}Ku in the irradiation of ^{249}Bk by ^{15}N ions. Sov. At. Energy **43**, 785–790 (1977)
148. Hulet, E.K., Wild, J.F., Dougan, R.J., Lougheed, R.W., Landrum, J.H., Dougan, A.D., Schädel, M., Hahn, R.L., Baisden, P.A., Henderson, C.M., Dupzyk, R.J., Sümmerer, K., Bethune, G.R.: Bimodal symmetric fission observed in the heaviest elements. Phys. Rev. Lett. **56**, 313–316 (1986)
149. Nurmia, M.: Investigations of transuranium elements at Berkeley. In: Bock, R., Hering, W.R. (eds.) Nuclear Reactions Induced by Heavy Ions, pp. 666–672. North-Holland, Amsterdam (1969)
150. Flerov, G.N.: Synthesis and search for heavy transuranium elements. Sov. At. Energy **28**, 390–397 (1970)

151. Akap'ev, G.N., Druin, V.A., Rud', V.I., Sung-Chin-Yang, G.Ya.: The role of α-activity background in study of the α decay of element 104. Sov. J. Nucl. Phys. **12**, 254–256 (1970)
152. Ghiorso, A., Nurmia, M., Harris, J., Eskola, K., Eskola, P.: Defence of the Berkeley work on alpha-emitting isotopes of element 104. Nature **229**, 603–607 (1971)
153. Bemis Jr, C.E., Silva, R.J., Hensley, D.C., Keller Jr, O.L., Tarrant, J.R., Hunt, L.D., Dittner, P.F., Hahn, R.L., Goodman, C.D.: X-ray identification of element 104. Phys. Rev. Lett. **31**, 647–650 (1973)
154. Ghiorso, A., Nurmia, M., Eskola, K., Eskola, P.: ^{261}Rf: new isotope of element 104. Phys. Lett. **32B**, 95–98 (1970)
155. Silva, R., Harris, J., Nurmia, M., Eskola, K., Ghiorso, A.: Chemical separation of rutherfordium. Inorg. Nucl. Chem. Lett. **6**, 871–877 (1970)
156. Nagame, Y., Asai, M., Haba, H., Goto, S., Tsukada, K., Nishinaka, I., Nishio, K., Ichikawa, S., Toyoshima, A., Akiyama, K., Nakahara, H., Sakama, M., Schädel, M., Kratz, J.V., Gäggeler, H.W., Türler, A.: Production cross sections of ^{261}Rf and ^{262}Db in bombardments of ^{248}Cm with ^{18}O and ^{19}F ions. J. Nucl. Radiochem. Sci. **3**, 85–88 (2002)
157. Haba, H., Kaji, D., Komori, Y., Kudou, Y., Morimoto, K., Morita, K., Ooe, K., Ozeki, K., Sato, N., Shinohara, A., Yoneda, A.: RIKEN gas-filled recoil ion separator (GARIS) as a promising interface for superheavy element chemistry—production of element 104, ^{261}Rf, using the GARIS gas-jet system. Chem. Lett. **38**, 426–427 (2009)
158. Haba, H., Kaji, D., Kikunaga, H., Kudou, Y., Morimoto, K., Morita, K., Ozeki, K., Sumita, T., Yoneda, A., Kasamatsu, Y., Komori, Y., Ooe, K., Shinohara, A.: Production and decay properties of the 1.9-s isomeric state in ^{261}Rf. Phys. Rev. **C83**, 034602(7) (2011)
159. Haba, H., Kaji, D., Kudou, Y., Morimoto, K., Morita, K., Ozeki, K., Sakai, R., Sumita, T., Yoneda, A., Kasamatsu, Y., Komori, Y., Shinohara, A., Kikunaga, H., Kudo, H., Nishio, K., Ooe, K., Sato, N., Tsukada, K.: Production of ^{265}Sg in the ^{248}Cm(^{22}Ne,5n)^{265}Sg reaction and decay properties of two isomeric sates in ^{265}Sg. Phys. Rev. **C85**, 024611(11) (2012)
160. Lane, M.R., Gregorich, K.E., Lee, D.M., Mohar, M.F., Hsu, M., Kacher, C.D., Kadkhodyan, B., Neu, M.P., Stoyer, N.J., Sylwester, E.R., Yang, J.C., Hoffman, D.C.: Spontaneous fission properties of ^{262}Rf. Phys. Rev. **C53**, 2893–2899 (1996)
161. Kratz, J.V., Gober, M.K., Zimmermann, H.P., Schädel, M., Brüchle, W., Schimpf, E., Gregorich, K.E., Türler, A., Hannink, N.J., Czerwinski, K.R., Kadkhodayan, B., Lee, D.M., Nurmia, M.J., Hoffman, D.C., Gäggeler, H., Jost, D., Kovacs, J., Scherer, U.W., Weber, A.: New nuclide ^{263}Ha. Phys. Rev. **C45**, 1064–1069 (1992)
162. Flerov, G.N., Oganesian, Yu.Ts., Lobanov, Yu.V., Lazarev, Yu.A., Tretiakova, S.P., Kolesov, I.V., Plotko, V.M.: On the synthesis of element 105. Nucl. Phys. **A160**, 181–192 (1971)
163. Flerov, G.N., Oganesyan, Yu.Ts., Lobanov, Yu.V., Lazarev, Yu.A., Tret'yakova, S.P., Kolesov, I.V., Plotko, V.M.: The synthesis of element 105. Sov. At. Energy **29**, 967–975 (1970)
164. Flerov, G.N.: Fission as a method of isotope synthesis. J. Phys. Soc. Jpn **24**(suppl), 237–243 (1968)
165. Ghiorso, A., Nurmia, M., Eskola, K., Harris, J., Eskola, P.: New element hahnium, atomic number 105. Phys. Rev. Lett. **24**, 1498–1503 (1970)
166. Bemis Jr, C.E., Dittner, P.F., Silva, R.J., Hahn, R.L., Tarrant, J.R., Hunt, L.D., Hensley, D.C.: Production, L x-ray identification, and decay of the nuclide ^{260}105. Phys. Rev. **C16**, 1146–1158 (1977)
167. Gan, Z.G., Qin, Z., Fan, H.M., Lei, X.G., Xu, Y.B., He, J.J., Liu, H.Y., Wu, X.L., Guo, J.S., Zhou, X.H., Yuan, S.G., Jin, G.M.: A new alpha-particle-emitting isotope ^{259}Db. Eur. Phys. J. **A10**, 21–25 (2001)
168. Ghiorso, A., Nurmia, M., Eskola, K., Eskola, P.: Two new alpha-particle emitting isotopes of element 105, ^{261}Ha and ^{262}Ha. Phys. Rev. **C4**, 1850–1855 (1971)
169. Druin, V.A., Bochev, B., Lobanov, Yu.V., Sagaidak, R.N., Kharitonov, Yu.P., Tret'yakova, S.P., Gul'bekyan, G.G., Buklanov, G.V., Erin, E.A., Kosyakov, V.N., Rykov, A.G.:

Spontaneous fission of the heavy isotopes of nielsbohrium (Z = 105) and element 106. Sov. J. Nucl. Phys. **29**, 591–595 (1979)
170. Druin, V.A., Demin, A.G., Kharitonov, Yu.P., Akap'ev, G.N., Rud', V.I., Sung-Ching-Yang, G.Y., Chelnokov, L.P., Gavrilov, K.A.: Study of the decay of isotopes of element 105. Sov. J. Nucl. Phys. **13**, 139–141 (1971)
171. Bemis Jr, C.E., Ferguson, R.L., Plasil, F., Silva, R.J., O'Kelley, G.D., Kiefer, M.L., Hahn, R.L., Hensley, D.C., Hulet, E.K., Lougheed, R.W.: Mass asymmetry and total-kinetic-energy release in the spontaneous fission of ^{262}105. Phys. Rev. Lett. **39**, 1246–1249 (1977)
172. Ghiorso, A., Nitschke, J.M., Alonso, J.R., Alonso, C.T., Nurmia, M., Seaborg, G.T., Hulet, E.K., Lougheed, R.W.: Element 106. Phys. Rev. Lett. **33**, 1490–1493 (1974)
173. Gregorich, K.E., Lane, M.R., Mohar, M.F., Lee, D.M., Kacher, C.D., Sylwester, E.R., Hoffman, D.C.: First confirmation of the discovery of element 106. Phys. Rev. Lett. **72**, 1423–1426 (1994)
174. Nishio, K., Hofmann, S., Hessberger, F.P., Ackermann, D., Antalic, S., Comas, V.F., Gan, Z., Heinz, S., Heredia, J.A., Ikezoe, H., Khuyagbaatar, J., Kindler, B., Kojouharov, I., Kuusiniemi, P., Lommel, B., Mann, R., Mazzocco, M., Mitsuoka, S., Nagame, Y., Ohtsuki, T., Popeko, A.G., Saro, S., Schött, H.J., Sulignano, B., Svirikhin, A., Tsukada, K., Tsuruta, K., Yeremin, A.V.: Measurement of evaporation residue cross-sections of the reaction ^{30}Si + ^{238}U at subbarrier energies. Eur. Phys. J. **A29**, 281–287 (2006)
175. Gregorich, K.E., Gates, J.M, Düllmann, Ch.E., Sudowe, R., Nelson, S.L., Garcia, M.A., Dragojevic, I., Folden III, C.M., Neumann, S.H., Hoffman, D.C., Nitsche, H.: New isotope ^{264}Sg and decay properties of $^{262-264}$Sg. Phys. Rev. **C74**, 044611(4) (2006)
176. Lazarev, Yu.A., Lobanov, Yu.V., Oganessian, Yu.Ts., Utyonkov, V.K., Abdullin, F.Sh., Buklanov, G.V., Gikal, B.N., Iliev, S., Mezentsev, A.N., Polyakov, A.N., Sedykh, I.M., Shirokovsky, I.V., Subbotin, V.G., Sukhov, A.M., Tsyganov, Yu.S., Zhuchko, V.E., Lougheed, R.W., Moody, K.J., Wild, J.F., Hulet, E.K., McQuaid, J.H.: Discovery of enhanced nuclear stability near the deformed shells N = 162 and Z = 108. Phys. Rev. Lett. **73**, 624–627 (1994)
177. Türler, A., Dressler, R., Eichler, B., Gäggeler, H.W., Jost, D.T., Schädel, M., Brüchle, W., Gregorich, K.E., Trautmann, N., Taut, S.: Decay properties of ^{265}Sg (Z = 106) and ^{266}Sg (Z = 106). Phys. Rev. **C57**, 1648–1655 (1998)
178. Oganessian, Yu.Ts.: Synthesis reactions and radioactive properties of transactinoid elements. J. Alloys Compd. **213/214**, 50–60 (1994)
179. Türler, A., Düllmann, Ch.E., Gäggeler, H.W., Kirbach, U.W., Yakushev, A., Schädel, M., Brüchle, W., Dressler, R., Eberhardt, K., Eichler, B., Eichler, R., Ginter, T.N., Glaus, F., Gregorich, K.E., Hoffman, D.C., Jäger, E., Jost, D.T., Lee, D.M., Nitsche, H., Patin, J.B., Pershina, V., Piguet, D., Qin, Z., Schausten, B., Schimpf, E., Schött, H.-J., Soverna, S., Sudowe, R., Thörle, P., Timokhin, S.N., Trautmann, N., Vahle, A., Wirth, G., Zielinski, P.M.: On the decay properties of ^{269}Hs and indications for the new nuclide ^{270}Hs. Eur. Phys. J. **A17**, 505–508 (2003)
180. Düllmann, ChE, Brüchle, W., Dressler, R., Eberhardt, K., Eichler, B., Eichler, R., Gäggeler, H.W., Ginter, T.N., Glaus, F., Gregorich, K.E., Hoffman, D.C., Jäger, E., Jost, D.T., Kirbach, U.W., Lee, D.M., Nitsche, H., Patin, J.B., Pershina, V., Piguet, D., Qin, Z., Schädel, M., Schausten, B., Schimpf, E., Schött, H.-J., Soverna, S., Sudowe, R., Thörle, P., Timokhin, S.N., Trautmann, N., Türler, A., Vahle, A., Wirth, G., Yakushev, A.B., Zielinski, P.M.: Chemical investigation of hassium (element 108). Nature **418**, 859–862 (2002)
181. Dvorak, J., Brüchle, W., Chelnokov, M., Düllmann, Ch.E., Dvorakova, Z., Eberhardt, K., Jäger, E., Krücken, R., Kuznetsov, A., Nagame, Y., Nebel, F., Nishio, K., Perego, R., Qin, Z., Schädel, M., Schausten, B., Schimpf, E., Schuber, R., Semchenkov, A., Thörle, P., Türler, A., Wegrzecki, M., Wierczinski, B., Yakushev, A., Yeremin, A.: Observation of the 3n evaporation channel in the complete hot-fusion reaction ^{26}Mg + ^{248}Cm leading to the new superheavy nuclide ^{271}Hs. Phys. Rev. Lett. **100**, 132503(4) (2008)
182. Eichler, R., Brüchle, W., Dressler, R., Düllmann, Ch.E., Eichler, B., Gäggeler, H.W., Gregorich, K.E., Hoffman, D.C., Hübener, S., Jost, D.T., Kirbach, U.W., Laue, C.A.,

Lavanchy, V.M., Nitsche, H., Patin, J.B., Piguet, D., Schädel, M., Shaughnessy, D.A., Strellis, D.A., Taut, S., Tobler, L., Tsyganov, Y.S., Türler, A., Vahle, A., Wilk, P.A., Yakushev, A.B.: Chemical characterization of bohrium (element 107). Nature **407**, 63–65 (2000)

183. Wilk, P.A., Gregorich, K.E., Türler, A., Laue, C.A., Eichler, R., Ninov, V., Adams, J.L., Kirbach, U.W., Lane, M.R., Lee, D.M., Patin, J.B., Shaughnessy, D.A., Strellis, D.A., Nitsche, H., Hoffman, D.C.: Evidence for new isotopes of element 107: ^{266}Bh and ^{267}Bh. Phys. Rev. Lett. **85**, 2697–2700 (2000)
184. Türler, A.: Heavy-element chemistry—status and perspectives. Eur. Phys. J. **A15**, 271–274 (2002)
185. Gan, Z.G., Guo, J.S., Wu, X.L., Qin, Z., Fan, H.M., Lei, X.G., Liu, H.Y., Guo, B., Xu, H.G., Chen, R.F., Dong, C.F., Zhang, F.M., Wang, H.L., Xie, C.Y., Feng, Z.Q., Zhen, Y., Song, L.T., Luo, P., Xu, H.S., Zhou, X.H., Jin, G.M., Ren, Z.: New isotope ^{265}Bh. Eur. Phys. J. **A20**, 385–387 (2004)
186. Dvorak, J., Brüchle, W., Chelnokov, M., Dressler, R., Düllmann, Ch.E., Eberhardt, K., Gorshkov, V., Jäger, E., Krücken, R., Kuznetsov, A., Nagame, Y., Nebel, F., Novackova, Z., Qin, Z., Schädel, M., Schausten, B., Schimpf, E., Semchenkov, A., Thörle, P., Türler, A., Wegrzecki, M., Wierczinski, B., Yakushev, A., Yeremin, A.: Doubly magic nucleus ^{270}Hs. Phys. Rev. Lett. **97**, 242501(4) (2006)
187. Lazarev, Yu.A., Lobanov, Yu.V., Oganessian, Yu.Ts., Tsyganov, Yu.S., Utyonkov, V.K., Abdullin, F.Sh., Iliev, S., Polyakov, A.N., Rigol, J., Shirokovsky, I.V., Subbotin, V.G., Sukhov, A.M., Buklanov, G.V., Gikal, B.N., Kutner, V.B., Mezentsev, A.N., Sedykh, I.M., Vakatov, D.V., Lougheed, R.W., Wild, J.F., Moody, K.J., Hulet, E.K.: New nuclide ^{267}108 produced by the ^{238}U + ^{34}S reaction. Phys. Rev. Lett. **75**, 1903–1906 (1995)
188. Nishio, K., Hofmann, S., Hessberger, F.P., Ackermann, D., Antalic, S., Arimoto, Y., Comas, V.F., Düllmann, Ch.E., Gorshkov, A., Graeger, R., Hagino, K., Heinz, S., Heredia, J.A., Hirose, K., Ikezoe, H., Khuyagbaatar, J., Kindler, B., Kojouharov, I., Lommel, B., Mann, R., Mitsuoka, S., Nagame, Y., Nishinaka, I., Ohtsuki, T., Popeko, A.G., Saro, S., Schädel, M., Türler, A., Watanabe, Y., Yakushev, A., Yeremin, A.V.: Nuclear orientation in the reaction ^{34}S + ^{238}U and synthesis of the new isotope ^{268}Hs. Phys. Rev. **C82**, 024611(9) (2010)
189. Lazarev, Yu.A., Lobanov, Yu.V., Oganessian, Yu.Ts., Utyonkov, V.K., Abdullin, F.Sh., Polyakov, A.N., Rigol, J., Shirokovsky, I.V., Tsyganov, Yu.S., Iliev, S., Subbotin, V.G., Sukhov, A.M., Buklanov, G.V., Gikal, B.N., Kutner, V.B., Mezentsev, A.N., Subotic, K., Wild, J.F., Lougheed, R.W., Moody, K.J.: α decay of ^{273}110: shell closure at N = 162. Phys. Rev. **C54**, 620–625 (1996)
190. Morita, K., Morimoto, K., Kaji, D., Akiyama, T., Goto, S., Haba, H., Ideguchi, E., Katori, K. Koura, H., Kudo, H., Ohnishi, T., Ozawa, A., Suda, T., Sueki, K., Tokanai, F., Yamaguchi, T., Yoneda, A., Yoshida, A.: Experiment on synthesis of an isotope ^{277}112 by ^{208}Pb + ^{70}Zn reaction. J. Phys. Soc. Jpn **76**, 043201(5) (2007)
191. Gupta, R.K., Parvulescu, C., Sandulescu, A., Greiner, W.: Further possibilities with Pb-targets for synthesizing super-heavy elements. Z. Phys. **A283**, 217–218 (1977)
192. Flerov, G.N., Oganessian, Yu.Ts., Pleve, A.A., Pronin, N.V., Tretyakov, Yu.P.: Acceleration of ^{48}Ca ions and new possibilities of synthesizing superheavy elements. Nucl. Phys. **A267**, 359–364 (1976)
193. Oganessian, Yu.Ts., Utyonkov, V.K., Lobanov, Yu.V., Abdullin, F.Sh., Polyakov, A.N., Shirokovsky, I.V., Tsyganov, Yu.S., Mezentsev, A.N., Iliev, S., Subbotin, V.G., Sukhov, A.M., Subotic, K., Ivanov, O.V., Voinov, A.N., Zagrebaev, V.I., Moody, K.J., Wild, J.F., Stoyer, N.J., Stoyer, M.A., Lougheed, R.W.: Measurements of cross sections for the fusion-evaporation reactions ^{204,206,207,208}Pb + ^{48}Ca and ^{207}Pb + ^{34}S: decay properties of the even-even nuclides ^{238}Cf and ^{250}No. Phys. Rev. **C64**, 054606(8) (2001)
194. Gäggeler, H.W., Jost, D.T., Türler, A., Armbruster, P., Brüchle, W., Folger, H., Hessberger, F.P., Hofmann, S., Münzenberg, G., Ninov, V., Reisdorf, W., Schädel, M., Sümmerer, K.,

Kratz, J.V., Scherer, U., Leino, M.: Cold fusion reactions with ^{48}Ca. Nucl. Phys. **A502**, 561c–570c (1989)
195. Hofmann, S.: New elements—approaching Z = 114. Rep. Prog. Phys. **61**, 639–689 (1998)
196. Denisov, V.Yu., Hofmann, S.: Production of superheavy elements in cold fusion reactions. Acta Phys. Pol. **B31**, 479–484 (2000)
197. Oganessian, Yu.Ts., Iljinov, A.S., Demin, A.G., Tretyakova, S.P.: Experiments on the production of fermium neutron-deficient isotopes and new possibilities of synthesizing element with Z > 100. Nucl. Phys. **A239**, 353–364 (1975)
198. Oganessian, Yu.Ts., Demin, A.G., Iljinov, A.S., Tretyakova, S.P., Pleve, A.A., Penionzhkevich, Yu.E., Ivanov, M.P., Tretyakov, Yu.P.: Experiments on the synthesis of neutron-deficient kurchatovium isotopes in reactions induced by ^{50}Ti ions. Nucl. Phys. **A239**, 157–171 (1975)
199. Oganessian, Yu.Ts., Demin, A.G., Danilov, N.A., Ivanov, M.P., Il'inov, A.S., Kolesnikov, N.N., Markov, B.N., Plotko, V.M., Tret'yakova, S.P., Flerov, G.N.: Experiments on the synthesis of element 107. JETP Lett. **23**, 277–279 (1976)
200. Oganesyan, Yu.Ts., Tret'yakov, Yu.P., Il'inov, A.S., Demin, A.G., Pleve, A.A., Tret'yakova, S.P., Plotko, V.M., Ivanov, M.P., Danilov, N.A., Korotkin, Yu.S., Flerov, G.N.: Synthesis of neutron-deficient isotopes of fermium, kurchatovium and element 106. JETP Lett. **20**, 265–266 (1974)
201. Oganessian, Yu.Ts., Hussonnois, M., Demin, A.G., Kharitonov, Yu.P., Bruchertseifer, H., Constantinescu, O., Korotkin, Yu.S., Tretyakova, S.P., Utyonkov, V.K., Shirokovsky, I.V., Estevez, J.: Experimental studies of the formation and radioactive decay of isotopes with Z = 104-109. Radiochim. Acta **37**, 113–120 (1984)
202. Sikkeland, T., Ghiorso, A., Nurmia, M.J.: Analysis of excitation functions in Cm(C, xn)No reactions. Phys. Rev. **172**, 1232–1238 (1968)
203. Nitschke, J.M., Leber, R.E., Nurmia, M.J., Ghiorso, A.: Observations in the reaction of two magic nuclei: ^{208}Pb and ^{48}Ca. Nucl. Phys. **A313**, 236–250 (1979)
204. Türler, A., Gäggeler, H.W., Jost, D.T., Armbruster, P., Brüchle, W., Folger, H., Hessberger, F.P., Hofmann, S., Münzenberg, G., Ninov, V., Schädel, M., Sümmerer, K., Kratz, J.V., Scherer, U.: Determination of the partial electron-capture and spontaneous-fission half-lives of ^{254}No. Z. Phys. **A331**, 363–364 (1988)
205. Oganessian, Yu.Ts., Penionzhkevich, Yu.E.: Some regularities of the formation of the products of nuclear reactions induced by heavy ions with Z > 40. Nucleonika **21**, 237–249 (1976)
206. Möller, P., Nix, J.R., Armbruster, P., Hofmann, S., Münzenberg, G.: Single-particle enhancement of heavy-element production. Z. Phys. **A359**, 251–255 (1997)
207. Bush, B.W., Bertsch, G.F., Brown, B.A.: Shape diffusion in the shell model. Phys. Rev. **C45**, 1709–1719 (1992)
208. Bock, R., Chu, Y.T., Dakowski, M., Gobbi, A., Grosse, E., Olmi, A., Sana, H., Schwalm, D., Lynen, U., Müller, W., Bjornholm, S., Esbensen, H., Woelfli, W., Morenzoni, E.: Dynamics of the fusion process. Nucl. Phys. **A388**, 334–380 (1982)
209. Swiatecki, W.J.: The dynamics of nuclear coalescence or reseparation. Phys. Scripta **24**, 113–122 (1981)
210. Bjornholm, S., Swiatecki, W.J.: Dynamical aspects of nucleus-nucleus collisions. Nucl. Phys. **A391**, 471–504 (1982)
211. Frobrich, P.: The barrier systematics of fusion and capture of heavy systems within the surface friction model. Phys. Lett. **B215**, 36–40 (1988)
212. Swiatecki, W.: The dynamics of the fusion of two nuclei. Nucl. Phys. **A376**, 275–291 (1982)
213. Gäggeler, H., Sikkeland, T., Wirth, G., Brüchle, W., Bögl, W., Franz, G., Herrmann, G., Kratz, J.V., Schädel, M., Sümmerer, K., Weber, W.: Probing sub-barrier fusion and extra-push by measuring fermium evaporation residues in different heavy ion reactions. Z. Phys. **A316**, 291–307 (1984)

214. Rivet, M.F., Alami, R., Borderie, B., Fuchs, H., Gardes, D., Gauvin, H.: Fusion-fission of heavy systems, influence of the entrance channel mass asymmetry. Z. Phys. **A330**, 295–301 (1988)
215. Volkov, V.V.: The mechanism of compound nucleus formation in complete fusion of two massive nuclei. Phys. At. Nuclei **66**, 1065–1070 (2003)
216. Sierk, A.J., Nix, J.R.: Dynamics of fission and fusion with applications to the formation of superheavy nuclei. Los Alamos preprint LA-UR-73–981 (1973)
217. Morjean, M., Jacquet, D., Charvet, J.L., L'Hoir, A., Laget, M., Parlog, M., Chbihi, A., Chevallier, M., Cohen, C., Dauvergne, D., Dayras, R., Drouart, A., Escano-Rodriguez, C., Frankland, J.D., Kirsch, R., Lautesse, P., Nalpas, L., Ray, C., Schmitt, C., Stodel, C., Tassan-Got, L., Testa, E., Volant, C.: Fission time measurements: a new probe into superheavy element stability. Phys. Rev. Lett. **101**, 072701(4) (2008)
218. Maruyama, T., Bonasera, A., Papa, M., Chiba, S.: Lifetime of heavy composite systems formed by fusion between heavy nuclei. J. Nucl. Radiochem. Sci. **3**, 77–80 (2002)
219. Berdichevsky, D., Reisdorf, W.: Systematic study of the heavy-ion fusion barrier in the frozen approximation. Z. Phys. **A327**, 217–224 (1987)
220. Hinde, D.J., Berriman, A.C., Butt, R.D., Dasgupta, M., Gontchar, I.I., Morton, C.R., Mukherjee, A., Newton, J.O.: Role of entrance-channel dynamics in heavy element synthesis. J. Nucl. Radiochem. Sci. **3**, 31–38 (2002)
221. Aguiar, C.E., Barbosa, V.C., Canto, L.F., Donangelo, R.: Liquid-drop model description of heavy ion fusion at sub-barrier energies. Nucl. Phys. **A472**, 571–590 (1987)
222. Keller, J.G., Schmidt, K.-H., Steltzer, H., Reisdorf, W., Agarwal, Y.K., Hessberger, F.P., Münzenberg, G., Clerc, H.-G., Sahm, C.-C.: Fusion of the system ^{90}Zr + ^{90}Zr. GSI preprint GSI-84-4 (1984)
223. Lesko, K., Henning, W., Rehm, K.E., Rosner, G., Schiffer, J.P., Stephans, G.S.F., Zeidman, B., Freeman, W.S.: Fission following fusion of Ni + Sn. Phys. Rev. **C34**, 2155–2164 (1986)
224. Udagawa, T., Naito, M., Kim, B.T.: Systematics of sub- and near-barrier fusion cross sections and the threshold anomaly. Phys. Rev. **C45**, 876–879 (1992)
225. Vinodkumar, A.M., Loveland, W., Neeway, J.J., Prisbrey, L., Sprunger, P.H., Peterson, D., Liang, J.F., Shapira, D., Gross, C.J., Varner, R.L., Kolata, J.J., Roberts, A., Caraley, A.L.: ^{132}Sn + ^{96}Zr reaction: a study of fusion enhancement/hindrance. Phys. Rev. **C78**, 054608(7) (2008)
226. Kondratyev, V.N., Bonasera, A., Iwamoto, A.: Kinetics in sub-barrier fusion of spherical nuclei. Phys. Rev. **C61**, 044613(11) (2000)
227. Hofmann, S., Münzenberg, G.: The discovery of the heaviest elements. Rev. Mod. Phys. **72**, 733–767 (2000)
228. Antonenko, N.V., Cherepanov, E.A., Nasirov, A.K., Permjakov, V.P., Volkov, V.V.: Compound nucleus formation in reactions between massive nuclei: fusion barrier. Phys. Rev. **C51**, 2635–2645 (1995)
229. Von Oertzen, W.: Cold multi-nucleon transfer between heavy nuclei and the synthesis of new elements. Z. Phys. **A342**, 177–182 (1992)
230. Denisov, V.Yu., Hofmann, S.: Formation of superheavy elements in cold fusion reactions. Phys. Rev. **C61**, 034606 (2000)
231. Lazarev, Yu.A: Influence of pairing correlations on the probability and dynamics of tunneling through the barrier in fission and fusion of complex nuclei. Phys. Scripta **35**, 255–266 (1987)
232. Swiatecki, W., Siwek-Wilczynska, K., Wilczynski, J.: Fusion by diffusion II. Synthesis of transfermium elements in cold fusion reactions. Phys. Rev. **C71** 014602(16) (2005)
233. Quesada, J.M., Broglia, R.A., Bragin, V., Pollarolo, G.: Single-particle and collective aspects of the absorptive potential for heavy ion reactions. Nucl. Phys. **A428**, 305c–312c (1984)
234. Ackermann, D., Scarlassara, F., Bednarczyk, P., Beghini, S., Corradi, L., Montagnoli, G., Müller, L., Napoli, D.R., Petrache, C.M., Varier, K.M., Soramel, F., Spolaore, P., Stefanini,

A.M., Segato, G.F., Signorini, C., Zhang, H.: Mean angular momenta in heavy ion fusion. Nucl. Phys. **A583**, 129–134 (1995)
235. Reisdorf, W., Schädel, M.: How well do we understand the synthesis of heavy elements by heavy-ion induced fusion? Z. Phys. **A343**, 47–57 (1992)
236. Schädel, M., Hofmann, S.: Prospects for the discovery of new elements. J. Radioanal. Nucl. Chem. **203**, 283–300 (1996)
237. Ikezoe, H., Satou, K., Mitsuoka, S., Nishio, K., Jeong, S.C.: Effect of nuclear shell structure on fusion reaction. Phys. At. Nuclei **66**, 1053–1056 (2003)
238. Lazarev, Yu.A., Oganessian, Yu.Ts., Szeglowski, Z., Utyonkov, V.K., Kharitonov, Yu.P., Constantinescu, O., Lien, D.T., Shirokovsky, I.V., Tretyakova, S.P.: Cross sections of the (HI,αn) channel in the cold-fusion-type reactions ^{209}Bi + ^{40}Ar and ^{208}Pb + ^{37}Cl. Nucl. Phys. **A580**, 113–132 (1994)
239. Oganessian, Yu.Ts., Demin, A.G., Danilov, N.A., Flerov, G.N., Ivanov, M.P., Iljinov, A.S., Kolesnikov, N.N., Markov, B.N., Plotko, V.M., Tretyakova, S.P.: On spontaneous fission of neutron-deficient isotopes of elements 103, 105 and 107. Nucl. Phys. **A273**, 505–522 (1976)
240. Smolanczuk, R.: Properties of the hypothetical spherical superheavy nuclei. Phys. Rev. **C56**, 812–824 (1997)
241. Münzenberg, G., Armbruster, P., Folger, H., Hessberger, F.P., Hofmann, S., Keller, J., Poppensieker, K., Reisdorf, W., Schmidt, K.-H., Schött, H.-J., Leino, M.E., Hingmann, R.: The identification of element 108. Z. Phys. **A317**, 235–236 (1984)
242. Münzenberg, G., Armbruster, P., Bertes, G., Folger, H., Hessberger, F.P., Hofmann, S., Poppensieker, K., Reisdorf, W., Quint, B., Schmidt, K.H., Schött, H.J., Sümmerer, K., Zychor, I., Leino, M., Gollerthan, U., Hanelt, E.: Evidence for ^{264}108, the heaviest known even-even isotope. Z. Phys. **A324**, 489–490 (1986)
243. Münzenberg, G., Faust, W., Hofmann, S., Armbruster, P., Güttner, K., Ewald, H.: The velocity filter SHIP, a separator of unslowed heavy ion fusion products. Nucl. Instrum. Methods **161**, 65–82 (1979)
244. Hofmann, S., Faust, W., Münzenberg, G., Reisdorf, W., Armbruster, P., Güttner, K., Ewald, H.: Alpha decay studies of very neutron deficient isotopes of Hf, Ta, W, and Re. Z. Phys. **A291**, 53–70 (1979)
245. Hofmann, S.: Plans to identify heavy elements produced in reactions with cross-sections of 1 pb and below. J. Alloys Compd. **213/214**, 74–80 (1994)
246. Hessberger, F.P., Hofmann, S., Ninov, V., Armbruster, P., Folger, H., Münzenberg, G., Schött, H.J., Popeko, A.G., Yeremin, A.V., Andreyev, A.N., Saro, S.: Spontaneous fission and alpha-decay properties of neutron deficient isotopes $^{257–253}$104 and ^{258}106. Z. Phys. **A359**, 415–425 (1997)
247. Streicher, B., Hessberger, F.P., Antalic, S., Hofmann, S., Ackermann, D., Heinz, S., Kindler, B., Khuyagbaatar, J., Kojouharov, I., Kuusiniemi, P., Leino, M., Lommel, B., Mann, R., Saro, S., Sulignano, B., Uusitalo, J., Venhart, M.: Alpha-gamma decay studies of ^{261}Sg and ^{257}Rf. Eur. Phys. J. **A45**, 275–286 (2010)
248. Hessberger, F.P., Hofmann, S., Ackermann, D., Ninov, V., Leino, M., Münzenberg, G., Saro, S., Lavrentev, A., Popeko, A.G., Yeremin, A.V., Stodel, Ch.: Decay properties of neutron-deficient isotopes ^{256,257}Db, ^{255}Rf, ^{252,253}Lr. Eur. Phys. J. **A12**, 57–67 (2001)
249. Hessberger, F.P., Münzenberg, G., Hofmann, S., Reisdorf, W., Schmidt, K.H., Schött, H.J., Armbruster, P., Hingmann, R., Thuma, B., Vermeulen, D.: Study of evaporation residues produced in reactions of ^{207,208}Pb with ^{50}Ti. Z. Phys. **A321**, 317–327 (1985)
250. Ter-Akopyan, G.M., Iljinov, A.S., Oganessian, Yu.Ts., Orlova, O.A., Popeko, G.S., Tretyakova, S.P., Chepigin, V.I., Shilov, B.V., Flerov, G.N.: Synthesis of the new neutron-deficient isotopes ^{250}102, ^{242}Fm and ^{254}Ku. Nucl. Phys. **A255**, 509–522 (1975)
251. Hessberger, F.P., Münzenberg, G., Hofmann, S., Agarwal, Y.K., Poppensieker, K., Reisdorf, W., Schmidt, K.-H., Schneider, J.R.H., Schneider, W.F.W., Schött, H.J., Armbruster, P., Thuma, B., Sahm, C.-C., Vermeulen, D.: The new isotopes ^{258}105, ^{257}105, ^{254}Lr and ^{253}Lr. Z. Phys. **A322**, 557–566 (1985)

252. Hessberger, F.P., Hofmann, S., Streicher, B., Sulignano, B., Antalic, S., Ackermann, D., Heinz, S., Kindler, B., Kojouharov, I., Kuusiniemi, P., Leino, M., Lommel, B., Mann, R., Popeko, A.G., Saro, S., Uusitalo, J., Yeremin, A.V.: Decay properties of neutron-deficient isotopes of elements from Z = 101 to Z = 108. Eur. Phys. J. **A41**, 145–153 (2009)
253. Demin, A.G., Tretyakova, S.P., Utyonkov, V.K., Shirokovsky, I.V.: On the properties of the element 106 isotopes produced in the reactions Pb + ^{54}Cr. Z. Phys. **A315**, 197–200 (1984)
254. Münzenberg, G., Hofmann, S., Folger, H., Hessberger, F.P., Keller, J., Poppensieker, K., Quint, B., Reisdorf, W., Schmidt, K.H., Schött, H.J., Armbruster, P., Leino, M.E., Hingmann, R.: The isotopes ^{259}106, ^{260}106, and ^{261}106. Z. Phys. **A322**, 227–235 (1985)
255. Oganessian, Yu.Ts., Demin, A.G., Hussonois, M., Tretyakova, S.P., Kharitonov, Yu.P., Utyonkov, V.K., Shirokovsky, I.V., Constantinescu, O., Bruchertseifer, H: On the stability of the nuclei of element 108 with A = 263-265. Z. Phys. **A319**, 215–217 (1984)
256. Folden III, C.M., Dragojevic, I., Düllmann, Ch.E., Eichler, R., Garcia, M.A., Gates, J.M., Nelson, S.L., Sudowe, R., Gregorich, K.E., Hoffman, D.C., Nitsche, H.: Measurement of the ^{208}Pb(^{52}Cr,n)^{259}Sg excitation function. Phys. Rev. **C76**, 027602(4) (2009)
257. Münzenberg, G., Hofmann, S., Hessberger, F.P., Reisdorf, W., Schmidt, K.H., Schneider, J.H.R., Armbruster, P., Sahm, C.C., Thuma, B.: Identification of element 107 by α correlation chains. Z. Phys. **A300**, 107–108 (1981)
258. Münzenberg, G., Armbruster, P., Hofmann, S., Hessberger, F.P., Folger, H., Keller, J.G., Ninov, V., Poppensieker, K., Quint, A.B., Reisdorf, W., Schmidt, K.-H., Schneider, J.R.H., Schött, H.-J., Sümmerer, K., Zychor, I., Leino, M.E., Ackermann, D., Gollerthan, U., Hanelt, E., Morawek, W., Vermeulen, D., Fujita, Y., Schwab, T.: Element 107. Z. Phys. **A333**, 163–175 (1989)
259. Hessberger, F.P., Antalic, S., Ackermann, D., Heinz, S., Hofmann, S., Khuyagbaatar, J., Kindler, B., Kojouharov, I., Lommel, B., Mann, R.: Alpha-decay properties of ^{261}Bh. Eur. Phys. J. **A43**, 175–180 (2010)
260. Folden III, C.M., Nelson, S.L., Düllmann, Ch.E., Schwantes, J.M., Sudowe, R., Zielinski, P.M., Gregorich, K.E., Nitsche, H., Hoffman, D.C.: Excitation function for the production of ^{262}Bh (Z = 107) in the odd-Z projectile reaction ^{208}Pb(^{55}Mn,n). Phys. Rev. **C73**, 014611(11) (2006)
261. Nelson, S.L., Folden III, C.M., Gregorich, K.E., Dragojevic, I., Düllmann, Ch.E., Eichler, R., Garcia, M.A., Gates, J.M., Sudowe, R., Nitsche, H.: Comparison of complementary reactions for the production of ^{261,262}Bh. Phys. Rev. **C78**, 024606(8) (2008)
262. Nelson, S.L., Gregorich, K.E., Dragojevic, I., Garcia, M.A., Gates, J.M., Sudowe, R., Nitsche, H.: Lightest isotope of Bh produced via the ^{209}Bi(^{52}Cr,n)^{260}Bh reaction. Phys. Rev. Lett. **100**, 022501(4) (2008)
263. Hofmann, S., Hessberger, F.P., Ackermann, D., Münzenberg, G., Antalic, S., Cagarda, P., Kindler, B., Kojouharova, J., Leino, M., Lommel, B., Mann, R., Popeko, A.G., Reshitko, S., Saro, S., Uusitalo, J., Yeremin, A.V.: New results on elements 111 and 112. Eur. Phys. J. **A14**, 147–157 (2002)
264. Hofmann, S., Hessberger, F.P., Ninov, V., Armbruster, P., Münzenberg, G., Stodel, C., Popeko, A.G., Yeremin, A.V., Saro, S., Leino, M.: Excitation function for the production of ^{265}108 and ^{266}109. Z. Phys. **A358**, 377–378 (1997)
265. Hofmann, S., Ninov, V., Hessberger, F.P., Armbruster, P., Folger, H., Münzenberg, G., Schött, H.J., Popeko, A.G., Yeremin, A.V., Andreyev, A.N., Saro, S., Janik, R., Leino, M.: The new element 111. Z. Phys. **A350**, 281–282 (1995)
266. Morita, K., Morimoto, K., Kaji, D., Haba, H., Ideguchi, E., Peter, J.C., Kanungo, R., Katori, K., Koura, H., Kudo, H., Ohnishi, T., Ozawa, A., Suda, T., Sueki, K., Tanihata, I., Xu, H., Yeremin, A.V., Yoneda, A., Yoshida, A., Zhao, Y.-L., Zheng, T., Goto, S., Tokanai, F.: Production and decay properties of ^{272}111 and its daughter nuclei. J. Phys. Soc. Japan **73**, 1738–1744 (2004)
267. Hofmann, S., Ninov, V., Hessberger, F.P., Armbruster, P., Folger, H., Münzenberg, G., Schött, H.J., Popeko, A.G., Yeremin, A.V., Andreyev, A.N., Saro, S., Janik, R., Leino, M.: Production and decay of ^{269}110. Z. Phys. **A350**, 277–280 (1995)

268. Münzenberg, G., Armbruster, P., Berthes, G., Folger, H., Hessberger, F.P., Hofmann, S., Keller, J., Poppensieker, K., Quint, A.B., Reisdorf, W., Schmidt, K.-H., Schött, H.-J., Sümmerer, K., Zychor, I., Leino, M.E., Hingmann, R., Gollerthan, R., Hanelt, E.: Observation of the isotopes ^{264}108 and ^{265}108. Z. Phys. **A328**, 49–59 (1987)
269. Dragojevic, I., Gregorich, K.E., Düllmann, Ch.E., Dvorak, J., Ellison, P.A., Gates, J.M., Nelson, S.L., Stavsetra, L., Nitsche, H.: New isotope ^{263}Hs. Phys. Rev. **C79**, 011602(4) (2009)
270. Morita, K., Morimoto, K., Kaji, D., Haba, H., Ideguchi, E., Kanungo, R., Katori, K., Koura, H., Kudo, H., Ohnishi, T., Ozawa, A., Suda, T., Sueki, K., Tanihata, I., Xu, H., Yeremin, A.V., Yoneda, A., Yoshida, A., Zhao, Y.-L., Zheng, T.: Production and decay of the isotope ^{271}Ds (Z = 110). Eur. Phys. J. **A21**, 257–263 (2004)
271. Hofmann, S., Ninov, V., Hessberger, F.P., Armbruster, P., Folger, H., Münzenberg, G., Schött, H.J., Popeko, A.G., Yeremin, A.V., Saro, S., Janik, R., Leino, M.: The new element 112. Z. Phys. **A354**, 229–230 (1996)
272. Münzenberg, G., Armbruster, P., Hessberger, F.P., Hofmann, S., Poppensieker, K., Reisdorf, W., Schneider, J.H.R., Schneider, W.F.W., Schmidt, K.-H., Sahm, C.C., Vermeulen, D.: Observation of one correlated α-decay in the reaction ^{58}Fe on ^{209}Bi -> ^{267}109. Z. Phys. **A309**, 89–90 (1982)
273. Münzenberg, G., Reisdorf, W., Hofmann, S., Agarwal, Y.K., Hessberger, F.P., Poppensieker, K., Schneider, J.R.H., Schneider, W.F.W., Schmidt, K.-H., Schött, H.-J., Armbruster, P., Sahm, C.-C., Vermeulen, D.: Evidence for element 109 from one correlated decay sequence following the fusion of ^{58}Fe with ^{209}Bi. Z. Phys. **A315**, 145–158 (1984)
274. Münzenberg, G., Hofmann, S., Hessberger, F.P., Folger, H., Ninov, V., Poppensieker, K., Quint, A.B., Reisdorf, W., Schött, H.-J., Sümmerer, K., Armbruster, P., Leino, M.E., Ackermann, D., Gollerthan, U., Hanelt, E., Morawek, W., Fujito, Y., Schwab, T., Türler, A.: New results on element 109. Z. Phys. **A330**, 435–436 (1988)
275. Nelson, S.L., Gregorich, K.E., Dragojevic, I., Dvorak, J., Ellison, P.A., Garcia, M.A., Gates, J.M., Stavsetra, L., Ali, M.N., Nitsche, H.: Comparison of complementary reactions for the production of Mt. Phys. Rev. **C79**, 027605(4) (2009)
276. Morita, K., Morimoto, K., Kaji, D., Akiyama, T., Goto, S., Haba, H., Ideguchi, E., Kanungo, R., Katori, K., Koura, H., Kudo, H., Ohnishi, T., Ozawa, A., Suda, T., Sueki, K., Xu, H., Yamaguchi, T., Yoneda, A., Yoshida, A., Zhao, Y.: Experiment on the synthesis of element 113 in the reaction ^{209}Bi(^{70}Zn, n)^{278}113. J. Phys. Soc. Japan **73**(10), 2593–2596 (2004)
277. Morita, K. Morimoto, K., Kaji, D., Akiyama, T., Goto, S., Haba, H., Ideguchi, E., Katori, K. Koura, H., Kikunaga, H., Kudo, H., Ohnishi, T., Ozawa, A., Sato, N., Suda, T., Sueki, K., Tokanai, F., Yamaguchi, T., Yoneda, A., Yoshida, A.: Observation of second decay chain from ^{278}113. J. Phys. Soc. Jpn. **76**, 045001(2) (2007)
278. Morita, K., Morimoto, K., Kaji, D., Haba, H., Ozeki, K., Kudou, Y., Sumita, T., Wakabayashi, Y., Yoneda, A., Tanaka, K., Yamaki, S., Sakai, R., Akiyama, T., Goto, S.-I., Hasebe, H., Huang, M., Huang, T., Ideguchi, E., Kasamatsu, Y., Katori, K., Kariya, Y., Kikunaga, H., Koura, H., Kudo, H., Mashiko, A., Mayama, K., Mitsuoka, S.-I., Moriya, T., Murakami, M., Murayama, H., Namai, S., Ozawa, A., Sato, N., Sueki, K., Takeyama, M., Tokanai, F., Yamaguchi, T., Yoshida, A.: New Result in the Production and Decay of an Isotope, ^{278}113, of the 113th Element. J. Phys. Soc. Jpn. **81**, 103201 (2012)
279. Ginter, T.N., Gregorich, K.E., Loveland, W., Lee, D.M., Kirbach, U.W., Sudowe, R., Folden III, C.M., Patin, J.B., Seward, N., Wilk, P.A., Zielinski, P.M., Aleklett, K., Eichler, R., Nitsche, H., Hoffman, D.C.: Confirmation of production of element 110 by the ^{208}Pb(^{64}Ni,n) reaction. Phys. Rev. **C67**, 064609(5) (2003)
280. Folden III, C.M., Gregorich, K.E., Düllmann, Ch.E., Mahmud, H., Pang, G.K., Schwantes, J.M., Sudowe, R., Zielinski, P.M., Nitsche, H., Hoffman, D.C.: Development of an odd-Z-projectile reaction for heavy element synthesis: ^{208}Pb(^{64}Ni,n)^{271}Ds and ^{208}Pb(^{65}Cu,n)^{272}111. Phys. Rev. Lett. **93**, 212702(4) (2004)
281. Hofmann, S., Hessberger, F.P., Ackermann, D., Antalic, S., Cagarda, P., Cwiok, S., Kindler, B., Kojouharova, J., Lommel, B., Mann, R., Münzenberg, G., Popeko, A.G., Saro, S.,

Schött, H.J., Yeremin, A.V.: The new isotope ^{270}110 and its decay products ^{266}Hs and ^{262}Sg. Eur. Phys. J. **A10**, 5–10 (2001)
282. Hofmann, S.: Synthesis of superheavy elements by cold fusion. Radiochim. Acta **99**, 405–428 (2011)
283. Lazarev, Yu.A., Lobanov, Yu.V., Sagaidak, R.N., Utyonkov, V.K., Hussonnois, M., Kharitonov, Yu.P., Shirokovsky, I.V., Tretyakova, S.P., Oganessian, Yu.Ts.: Study of the stability of the ground states and K-isomeric states of ^{250}Fm and ^{254}102 against spontaneous fission. Phys. Scripta **39**, 422–435 (1989)
284. Ghiorso, A., Lee, D., Somerville, L.P., Loveland, W., Nitschke, J.M., Ghiorso, W., Seaborg, G.T., Wilmarth, P., Leres, R., Wydler, A., Nurmia, M., Gregorich, K., Czerwinski, K., Gaylord, R., Hamilton, T., Hannink, N.J., Hoffman, D.C., Jarzynski, C., Kacher, C., Kadkhodayan, B., Kreek, S., Lane, M., Lyon, A., McMahon, M.A., Neu, M., Sikkeland, T., Swiatecki, W.J., Türler, A., Walton, J.T., Yashita, S.: Evidence for the possible synthesis of element 110 produced by the ^{59}Co + ^{209}Bi reaction. Phys. Rev. **C51**, R2293–R2297 (1995)
285. Oganessian, Yu.Ts., Utyonkov, V.K., Lobanov, Yu.V., Abdullin, F.Sh., Polyakov, A.N., Shirokovsky, I.V., Tsyganov, Yu.S., Gulbekian, G.G., Bogomolov, S.L., Mezentsev, A.N., Iliev, S., Subbotin, V.G., Sukhov, A.M., Voinov, A.A., Buklanov, G.V., Subotic, K., Zagrebaev, V.I., Itkis, M.G., Patin, J.B., Moody, K.J., Wild, J.F., Stoyer, M.A., Stoyer, N.J., Shaughnessy, D.A., Kenneally, J.M., Lougheed, R.W.: Experiments on the synthesis of element 115 in the reaction ^{243}Am(^{48}Ca,xn)$^{291-x}$115. Phys. Rev. **C69**, 021601(5) (2004)
286. Oganessian, Yu.Ts., Utyonkov, V.K., Dmitriev, S.N., Lobanov, Yu.V., Itkis, M.G., Polyakov, A.N., Tsyganov, Yu.S., Mezentsev, A.N., Yeremin, A.V., Voinov, A.A., Sokol, E.A., Gulbekian, G.G., Bogomolov, S.L., Iliev, S., Subbotin, V.G., Sukhov, A.M., Buklanov, G.V., Shishkin, S.V., Chepygin, V.I., Vostokin, G.K., Aksenov, N.V., Hussonois, M., Subotic, K., Zagrebaev, V.I., Moody, K.J., Patin, J.B., Wild, J.F., Stoyer, M.A., Stoyer, N.J., Shaughnessy, D.A., Kenneally, J.M., Wilk, P.A., Lougheed, R.W., Gäggeler, H.W., Schumann, D., Bruchertseifer, H., Eichler, R.: Synthesis of elements 115 and 113 in the reaction of ^{243}Am + ^{48}Ca. Phys. Rev. **C72**, 034611(16) (2005)
287. Ninov, V., Gregorich, K.E., Loveland, W., Ghiorso, A., Hoffman, D.C., Lee, D.M., Nitsche, H., Swiatecki, W.J., Kirbach, U.W., Laue, C.A., Adams, J.L., Patin, J.B., Shaughnessy, D.A., Strellis, D.A., Wilk, P.A.: Observation of superheavy nuclei produced in the reaction of ^{86}Kr with ^{208}Pb. Phys. Rev. Lett. **83**, 1104–1107 (1999)
288. Smolanczuk, R.: Formation of superheavy elements in cold fusion reactions. Phys. Rev. **C63**, 044607(8) (2001)
289. Smolanczuk, R.: Production of superheavy elements. Phys. Rev. **C60**, 021301(3) (1999)
290. Smolanczuk, R.: Excitation functions for the production of superheavy nuclei in cold fusion reactions. Phys. Rev. **C61**, 011601(4) (1999)
291. Smolanczuk, R.: Production mechanism of superheavy nuclei in cold fusion reactions. Phys. Rev. **C59**, 2634–2638 (1999)
292. Morimoto, K., Morita, K., Tanihata, I., Iwasa, N., Kanungo, R., Kato, T., Katori, K., Kudo, H., Suda, T., Sugai, I., Takeuchi, S., Tokanai, F., Uchiyama, K., Wakasaya, Y., Yamaguchi, T., Yeremin, A., Yoneda, A., Yoshida, A.: Search for a Z = 118 superheavy nucleus in the reaction of Kr beam with Pb target at RIKEN. In: Oganessian, Yu.Ts., Akimune, H., Ohta, M., Utsunomiya, H., Wada, T., Yamagata, T. (eds.) Proceedings of Tours Symposium on Nuclear Physics, Tours, France, 4–7 September 2000. AIP Conference Proceedings, vol. 561, pp. 354–357. Am. Inst. Phys., New York (2001)
293. Gregorich, K.E., Ginter, T.N., Loveland, W., Peterson, D., Patin, J.B., Folden, C.M., Hoffman, D.C., Lee, D.M., Nitsche, H., Omtvedt, J.P., Omtvedt, L.A., Stavsetra, L., Sudowe, R., Wilk, P.A., Zielinski, P.M., Aleklett, K.: Cross-section limits for the ^{208}Pb(^{86}Kr, n)^{293}118 reaction. Eur. Phys. J. **A18**, 633–638 (2003)
294. Hofmann, S.: The study of superheavy elements at SHIP: results and plans. Phys. At. Nuclei **66**, 1020–1025 (2003)
295. Ninov, V., Gregorich, K.E., Loveland, W., Ghiorso, A., Hoffman, D.C., Lee, D.M., Nitsche, H., Swiatecki, W.J., Kirbach, U.W., Laue, C.A., Adams, J.L., Patin, J.B., Shaughnessy,

D.A., Strellis, D.A., Wilk, P.A.: Editorial note: observation of superheavy nuclei produced in the reaction of ^{86}Kr with ^{208}Pb [Phys.Rev.Lett. 83, 1104 (1999)]. Phys. Rev. Lett. **89**, 039901(1) (2002)
296. Zagrebaev, V.I.: Synthesis of superheavy nuclei: nucleon collectivization as a mechanism for compound nucleus formation. Phys. Rev. **C64**, 034606(13) (2001)
297. Alburger, D.E., Cumming, J.B.: Search for the β^- decay of ^{48}Ca. Phys. Rev. **C32**, 1358–1361 (1985)
298. Gupta, R.K., Sandulescu, A., Greiner, W.: Synthesis of fermium and transfermium elements using calcium-48 beam. Z. Naturforsch. **32a**, 704–707 (1977)
299. Pacheco, A.J., Fernandez Niello, J.O., DiGregorio, D.E., di Tada, M., Testoni, J.E., Chan, Y., Chavez, E., Gazes, S., Plagnol, E., Stokstad, R.G.: Capture reactions in the ^{40,48}Ca + ^{197}Au and ^{40,48}Ca + ^{208}Pb systems. Phys. Rev. **C45**, 2861–2869 (1992)
300. Sagaidak, R.N., Kniajeva, G.N., Itkis, I.M., Itkis, M.G., Kondratiev, N.A., Kozulin, E.M., Pokrovsky, I.V., Svirikhin, A.I., Voskressensky, V.M., Yeremin, A.V., Corradi, L., Gadea, A., Latina, A., Stefanini, A.M., Szilner, S., Trotta, M., Vinodkumar, A.M., Beghini, S., Montagnoli, G., Scarlassara, F., Ackermann, D., Hanappe, F., Rowley, N., Stuttge, L.: Fusion suppression in mass-asymmetric reactions leading to Ra compound nuclei. Phys. Rev. **C68**, 014603(5) (2003)
301. Trotta, M., Stefanini, A.M., Beghini, S., Behera, B.R., Chizhov, A.Yu., Corradi, L., Courtin, S., Fioretto, E., Gadea, A., Gomes, P.R.S., Haas, F., Itkis, I.M., Itkis, M.G., Kniajeva, G.N., Kondratiev, N.A., Kozulin, E.M., Latina, A., Montagnoli, G., Pokrovsky, I.V., Rowley, N., Sagaidak, R.N., Scarlassara, F., Szanto de Toledo, A., Szilner, S., Voskressensky, V.M., Wu, Y.W.: Fusion hindrance and quasi-fission in ^{48}Ca induced reactions. Eur. Phys. J. **A25**, 615–618 (2005)
302. Zagrebaev, V.I., Aritomo, Y., Itkis, M.G., Oganessian, Yu.Ts., Ohta, M.: Synthesis of superheavy nuclei: how accurately can we describe it and calculate the cross sections?. Phys. Rev. **C65**, 014607(14) (2001)
303. Abe, Y., Shen, C.W., Kosenko, G.I., Boilley, D.: Theory of fusion for superheavy elements. Phys. At. Nuclei **66**, 1057–1064 (2003)
304. Zagrebaev, V.I.: Sequential fusion: sub-barrier fusion enhancement due to neutron transfer. Prog. Theor. Phys. Suppl. **154**, 122–129 (2004)
305. Zagrebaev, V.I.: New approach to description of fusion-fission dynamics in super-heavy element formation. J. Nucl. Radiochem. Sci. **3**, 13–16 (2002)
306. Itkis, M.G., Bogatchev, A.A., Itkis, I.M., Jandel, M., Kliman, J., Kniajeva, G.N., Kondratiev, N.A., Korzyukov, I.V., Kozulin, E.M., Krupa, L., Oganessian, Yu.Ts., Pokrovski, I.V., Ponomarenko, V.A., Prokhorova, E.V., Rusanov, A.Ya., Voskresenski, V.M., Govordovski, A.A., Hanappe, F., Materna, T., Rowley, N., Stuttge, L., Giardina, G., Moody, K.J.: Fusion-fission of superheavy nuclei. J. Nucl. Radiochem. Sci. **3**, 57–62 (2002)
307. Oganessian, Yu.: Sizing up the heavyweights. Nature **413**, 122–125 (2001)
308. Abe, Y., Okazaki, K., Arimoto, Y., Tokuda, T., Wada, T., Ohta, M.: Theoretical predictions of residues cross sections of superheavy elements. Kyoto report YITP-99-41 (1999)
309. Oganessian, Yu.Ts.: Reactions of synthesis of heavy nuclei: Brief summary and outlook. Phys. At. Nucl. **69**, 932–940 (2006)
310. Royer, G., Gherghescu, R.A.: On the formation and alpha decay of superheavy elements. Nucl. Phys. **A699**, 479–492 (2002)
311. Veselsky, M.: Competition of fusion and quasifission in reactions leading to production of superheavy elements. Phys. At. Nuclei **66**, 1086–1094 (2003)
312. Ackermann, D.: Reaction dynamics at the barrier for heavy compound systems. Phys. At. Nuclei **66**, 1114–1117 (2003)
313. Iwamoto, A., Möller, P., Nix, J.R., Sagawa, H.: Collisions of deformed nuclei: a path to the far side of the superheavy island. Nucl. Phys. **A596**, 329–354 (1996)
314. Gupta, R.K., Manhas, M., Greiner, W.: Compactness of the ^{48}Ca induced hot fusion reactions and the magnitudes of quadrupole and hexadecapole deformations. Phys. Rev. **C73**, 054307(13) (2006)

315. Umar, A.S., Oberacker, V.E., Maruhn, J.A., Reinhard, P.-G.: Entrance channel dynamics of hot and cold fusion reactions leading to superheavy elements. Phys. Rev. **C81**, 064607(7) (2010)
316. Oganessian, Yu.Ts., Utyonkov, V.K., Lobanov, Yu.V., Abdullin, F.Sh., Polyakov, A.N., Shirokovsky, I.V., Tsyganov, Yu.S., Gulbekian, G.G., Bogomolov, S.L., Gikal, B.N., Mezentsev, A.N., Iliev, S., Subbotin, V.G., Sukhov, A.M., Voinov, A.A., Buklanov, G.V., Subotic, K., Zagrebaev, V.I., Itkis, M.G., Patin, J.B., Moody, K.J., Wild, J.F., Stoyer, M.A., Stoyer, N.J., Shaughnessy, D.A., Kenneally, J.M., Wilk, P.A., Lougheed, R.W., Il'kaev, R.I., Vesnovskii, S.P.: Measurements of cross sections and decay properties of the isotopes of element 112, 114, and 116 produced in the fusion reactions ^{233,238}U, ^{242}Pu, and ^{248}Cm + ^{48}Ca. Phys. Rev. **C70**, 064609(14) (2004)
317. Rowley, N., Satchler, G.R., Stelson, P.H.: On the "distribution of barriers" interpretation of heavy-ion fusion. Phys. Lett. **B254**, 25–29 (1991)
318. Hinde, D.J., Dasgupta, M., Leigh, J.R., Mein, J.C., Morton, C.R., Newton, J.O., Timmers, H.: Conclusive evidence for the influence of nuclear orientation on quasifission. Phys. Rev. **C53**, 1290–1300 (1996)
319. Ikezoe, H., Mitsuoka, S., Nishio, K., Satou, K., Nishinaka, I.: Dependence of heavy-ion fusion reaction on nuclear deformation and nuclear shell structure. J. Nucl. Radiochem. Sci. **3**, 39–42 (2002)
320. Itkis, M.G., Beghini, S., Bogatchev, A.A., Corradi, L., Dorvaux, O., Gadea, A., Giardina, G., Goverdovski, A.A., Hanappe, F., Itkis, I.M., Jandel, M., Kliman, J., Kniajeva, G.N., Kondratiev, N.A., Korzyukov, I.V., Kozulin, E.M., Krupa, L., Latina, L., Materna, T., Montagnoli, G., Moody, K.J., Oganessian, Yu.Ts., Pokrovsky, I.V., Ponomarenko, V.A., Prokhorova, E.V., Rowley, N., Rusanov, A.Ya., Scarlassara, F., Stefanini, A.M., Stuttge, L., Szilner, S., Trotta, M., Vinodkumar, A.M., Voskressensky, V.M.: Fusion-fission of heavy and superheavy nuclei. Phys. At. Nuclei **66**, 1118–1124 (2003)
321. Itkis, M.G., Oganessian, Yu.Ts., Kozulin, E.M., Kondratiev, N.A., Krupa, L., Pokrovsky, I.V., Polyakov, A.N., Ponomarenko, V.A., Prokhorova, E.V., Pustylnik, B.I., Rusanov, A.Ya., Vakatov, V.I.: Fusion-fission of nuclei with $Z > 100$ at low excitation energies. Nuovo Cim. **111A**, 783–790 (1998)
322. Itkis, I.M., Kozulin, E.M., Itkis, M.G., Knyazheva, G.N., Bogachev, A.A., Chernysheva, E.V., Krupa, L., Oganessian, Yu.Ts., Zagrebaev, V.I., Rusanov, A.Ya., Gönnenwein, F., Dorvaux, O., Stuttge, L., Hanappe, F., Vardaci, E., de Goes Brennand, E.: Fission and quasifission modes in heavy-ion-induced reactions leading to the formation of Hs. Phys. Rev. **C83**, 064613(12) (2011)
323. Denisov, V.Yu., Nörenberg, W.: Entrance channel potentials in the synthesis of the heaviest nuclei. Eur. Phys. J. **A15**, 375–388 (2002)
324. Giardina, G., Hofmann, S., Muminov, A.I., Nasirov, A.K.: Effect of the entrance channel on the synthesis of superheavy elements. Eur. Phys. J. **A8**, 205–216 (2000)
325. Adamian, G.G., Antonenko, N.V., Scheid, W.: Isotopic dependence of fusion cross sections in reactions with heavy nuclei. Nucl. Phys. **A678**, 24–38 (2000)
326. Ohta, M., Arimoto, Y.: An idea for predicting the evaporation residue cross section in superheavy mass region. Phys. At. Nuclei **66**, 1026–1032 (2003)
327. Feng, Z.-Q., Jin, G.-M., Li, J.-Q.: Production of new superheavy $Z = 108$-114 nuclei with ^{238}U, ^{244}Pu, and ^{248,250}Cm targets. Phys. Rev. **C80**, 057601(4) (2009)
328. Zagrebaev, V.I.: Fusion-fission dynamics of super-heavy element formation and decay. Nucl. Phys. **A734**, 164–167 (2004)
329. Patyk, Z., Sobiczewski, A., Armbruster, P., Schmidt, K.-H.: Shell effects in the properties of the heaviest nuclei. Nucl. Phys. **A491**, 267–280 (1989)
330. Schumann, D., Bruchertseifer, H., Eichler, R., Eichler, B., Gäggeler, H.W., Dmitriev, S.N., Oganessian, Yu.Ts., Utyonkov, V.K., Shishkin, S.V., Yeremin, A.V., Lobanov, Yu.V., Tsyganov, Yu.S., Chepygin, V.I., Sokol, E.A., Vostokin, G.K., Aksenov, N.V., Hussonois, M., Itkis, M.G.: Chemical procedure applied for the identification of Rf/Db produced in the ^{48}Ca + ^{243}Am reaction. Radiochim. Acta **93**, 727–732 (2005)

331. Oganessian, Yu.Ts., Utyonkov, V.K., Lobanov, Yu.V., Abdullin, F.Sh., Polyakov, A.N., Shirokovsky, I.V., Tsyganov, Yu.S., Gulbekian, G.G., Bogomolov, S.L., Gikal, B.N., Mezentsev, A.N., Iliev, S., Subbotin, V.G., Sukhov, A.M., Voinov, A.A., Buklanov, G.V., Subotic, K., Zagrebaev, V.I., Itkis, M.G., Patin, J.B, Moody, K.J., Wild, J.F., Stoyer, M.A., Stoyer, N.J., Shaughnessy, D.A., Kenneally, J.M., Lougheed, R.W.: Measurements of cross sections for the fusion-evaporation reactions ^{244}Pu(^{48}Ca,xn)$^{292-x}$114 and ^{245}Cm(^{48}Ca,xn)$^{293-x}$116. Phys. Rev. **C69**, 054607(9) (2004)
332. Viola Jr, V.E., Seaborg, G.T.: Nuclear systematics of the heavy elements—II; lifetimes for alpha, beta and spontaneous fission decay. J. Inorg. Nucl. Chem. **28**, 741–761 (1966)
333. Poenaru, D.N., Plonski, I.-H., Greiner, W.: α-decay half-lives of superheavy nuclei. Phys. Rev. **C74**, 014312(5) (2006)
334. Zhang, H., Zuo, W., Li, J., Royer, G.: α decay half-lives of new superheavy nuclei with a generalized liquid drop model. Phys. Rev. **C74**, 017304(4) (2006)
335. Hoffman, D.C.: Spontaneous fission properties and lifetime systematics. Nucl. Phys. **A502**, 21c–40c (1989)
336. Hulet, E.K., Wild, J.F., Dougan, R.J., Lougheed, R.W., Landrum, J.H., Dougan, A.D., Baisden, P.A., Henderson, C.M., Dupzyk, R.J., Hahn, R.L., Schädel, M., Sümmerer, K., Bethune, G.R.: Spontaneous fission properties of ^{258}Fm, ^{259}Md, ^{260}Md, ^{258}No and ^{260}104: Bimodal fission. Phys. Rev. **C40**, 770–784 (1989)
337. Dmitriev, S.N., Oganessian, Yu.Ts., Utyonkov, V.K., Shishkin, S.V., Yeremin, A.V., Lobanov, Yu.V., Tsyganov, Yu.S., Chepygin, V.I., Sokol, E.A., Vostokin, G.K., Aksenov, N.V., Hussonois, M., Itkis, M.G., Gäggeler, H.W., Schumann, D., Bruchertseifer, H., Eichler, R., Shaughnessy, D.A., Wilk, P.A., Kenneally, J.M., Stoyer, M.A., Wild, J.F.: Chemical identification of dubnium as a decay product of element 115 produced in the reaction ^{48}Ca + ^{243}Am. Mendeleev Comm. **15**, 1–4 (2005)
338. Armbruster, P., Agarwal, Y.K., Brüchle, W., Brügger, M., Dufour, J.P., Gäggeler, H., Hessberger, F.P., Hofmann, S., Lemmertz, P., Münzenberg, G., Poppensieker, K., Reisdorf, W., Schädel, M., Schmidt, K.-H., Schneider, J.H.R., Schneider, W.F.W., Sümmerer, K., Vermeulen, D., Wirth, G., Ghiorso, A., Gregorich, K.E., Lee, D., Leino, M., Moody, K.J., Seaborg, G.T., Welch, R.B., Wilmarth, P., Yashita, S., Frink, C., Greulich, N., Herrmann, G., Hickmann, U., Hildebrand, N., Kratz, J.V., Trautmann, N., Fowler, M.M., Hoffman, D.C., Daniels, W.R., von Gunten, H.R., Dornhöfer, H.: Attempts to produce superheavy elements by fusion of ^{48}Ca with ^{248}Cm in the bombarding energy range of 4.5—5.2 MeV/u. Phys. Rev. Lett. **54**, 406–409 (1985)
339. Illige, J.D., Hulet, E.K., Nitschke, J.M., Dougan, R.J., Lougheed, R.W., Ghiorso, A., Landrum, J.H.: Search for volatile superheavy elements from the reaction ^{248}Cm + ^{48}Ca. Phys. Lett. **B78**, 209–212 (1978)
340. Oganessian, Yu.Ts., Bruchertseifer, H., Buklanov, G.V., Chepigin, V.I., Val Sek, C., Eichler, B., Gavrilov, K.A., Gäggeler, H., Korotkin, Yu.S., Orlova, O.A., Reetz, T., Seidel, W., Ter-Akopian, G.M., Tretyakova, S.P., Zvara, I.: Experiments to produce isotopes of superheavy elements with atomic numbers 114-116 in ^{48}Ca ion reactions. Nucl. Phys. A**294**, 213–224 (1978)
341. Hulet, E.K., Lougheed, R.W., Wild, J.F., Landrum, J.H., Stevenson, P.C., Ghiorso, A., Nitschke, J.M., Otto, R.J., Morrissey, D.J., Baisden, P.A., Gavin, B.F., Lee, D., Silva, R.J., Fowler, M.M., Seaborg, G.T.: Search for superheavy elements in the bombardment of ^{248}Cm with ^{48}Ca. Phys. Rev. Lett. **39**, 385–389 (1977)
342. Otto, R.J., Morrissey, D.J., Lee, D., Ghiorso, A., Nitschke, J.M., Seaborg, G.T., Fowler, M.M., Silva, R.J.: A search for superheavy elements with half-lives between a few minutes and several hundred days, produced in the ^{48}Ca + ^{248}Cm reaction. J. Inorg. Nucl. Chem. **40**, 589–595 (1978)
343. Ter-Akop'yan, G.M., Bruchertseifer, H., Buklanov, G.V., Orlova, O.A, Pleve, A.A., Chepigin, V.I., Val Sek, C.: Experiments on synthesis of odd neutron-deficient isotopes of superheavy elements in reactions induced by ^{48}Ca ions. Sov. J. Nucl. Phys. **29**, 312–317 (1979)

344. Lougheed, R.W., Landrum, J.H., Hulet, E.K., Wild, J.F., Dougan, R.J., Dougan, A.D., Gäggeler, H., Schädel, M., Moody, K.J., Gregorich, K.E., Seaborg, G.T.: A search for superheavy elements using the $^{48}Ca + {}^{254g}Es$ reaction. Phys. Rev. **C32**, 1760–1763 (1985)
345. Oganessian, Yu.Ts., Yeremin, A.V., Gulbekian, G.G., Bogomolov, S.L., Chepigin, V.L., Gikal, B.N., Gorshkov, V.A., Itkis, M.G., Kabachenko, A.P., Kutner, V.B., Lavrentev, A.Yu., Malyshev, O.N., Popeko, A.G., Rohac, J., Sagaidak, R.N., Hofmann, S., Münzenberg, G., Veselsky, M., Saro, S., Iwasa, N., Morita, K.: Search for new isotopes of element 112 by irradiation of ^{238}U with ^{48}Ca. Eur. Phys. J. **A5**, 63–68 (1999)
346. Oganessian, Yu.Ts., Yeremin, A.V., Popeko, A.G., Bogomolov, S.L., Buklanov, G.V., Chelnokov, M.L., Chepigin, V.L., Gikal, B.N., Gorshkov, V.A., Gulbekian, G.G., Itkis, M.G., Kabachenko, A.P., Lavrentev, A.Yu., Malyshev, O.N., Rohac, J., Sagaidak, R.N., Hofmann, S., Saro, S., Giardina, G., Morita, K.: Synthesis of nuclei of the superheavy element 114 in reactions induced by ^{48}Ca. Nature **400**, 242–245 (1999)
347. Oganessian, Yu.Ts., Utyonkov, V.K., Lobanov, Yu.V., Abdullin, F.Sh., Polyakov, A.N., Shirokovsky, I.V., Tsyganov, Yu.S., Gulbekian, G.G., Bogomolov, S.L., Gikal, B.N., Mezentsev, A.N., Iliev, S., Subbotin, V.G., Sukhov, A.M., Buklanov, G.V., Subotic, K., Itkis, M.G., Moody, K.J., Wild, J.F., Stoyer, N.J., Stoyer, M.A., Lougheed, R.W.: Synthesis of superheavy nuclei in the $^{48}Ca + {}^{244}Pu$ reaction. Phys. Rev. Lett. **83**, 3154–3157 (1999)
348. Oganessian, Yu.Ts., Utyonkov, V.K., Lobanov, Yu.V., Abdullin, F.Sh., Polyakov, A.N., Shirokovsky, I.V., Tsyganov, Yu.S., Gulbekian, G.G., Bogomolov, S.L., Gikal, B.N., Mezentsev, A.N., Iliev, S., Subbotin, V.G., Sukhov, A.M., Voinov, A.A., Buklanov, G.V., Subotic, K., Zagrebaev, V.I., Itkis, M.G., Patin, J.B., Moody, K.J., Wild, J.F., Stoyer, M.A., Stoyer, N.J., Shaughnessy, D.A., Kenneally, J.M., Lougheed, R.W.: Heavy element research at Dubna. Nucl. Phys. **A734**, 109–123 (2004)
349. Oganessian, Yu.Ts., Utyonkov, V.K., Lobanov, Yu.V., Abdullin, F.Sh., Polyakov, A.N., Shirokovsky, I.V., Tsyganov, Yu.S., Gulbekian, G.G., Bogomolov, S.L., Gikal, B.N., Mezentsev, A.N., Iliev, S., Subbotin, V.G., Sukhov, A.M., Ivanov, O.V., Buklanov, G.V., Subotic, K., Itkis, M.G., Moody, K.J., Wild, J.F., Stoyer, N.J., Stoyer, M.A., Lougheed, R.W.: Synthesis of superheavy nuclei in the $^{48}Ca + {}^{244}Pu$ reaction: $^{288}114$. Phys. Rev. **C62**, 041604(4) (2000)
350. Oganessian, Yu.Ts., Utyonkov, V.K., Lobanov, Yu.V., Abdullin, F.Sh., Polyakov, A.N., Shirokovsky, I.V., Tsyganov, Yu.S., Gulbekian, G.G., Bogomolov, S.L., Gikal, B.N., Mezentsev, A.N., Iliev, S., Subbotin, V.G., Sukhov, A.M., Ivanov, O.V., Buklanov, G.V., Subotic, K., Itkis, M.G., Moody, K.J., Wild, J.F., Stoyer, N.J., Stoyer, M.A., Lougheed, R.W., Laue, C.A., Karelin, Ye.A., Tatarinov, A.N.: Observation of the decay of $^{292}116$. Phys. Rev. **C63**, 011301(2) (2000)
351. Puri, K.P., Gupta, R.K.: Fusion barriers using the energy-density formalism: simple analytical formula and the calculation of fusion cross sections. Phys. Rev. **C45**, 1837–1849 (1992)
352. Typel, S., Brown, B.A.: Skyrme Hartree-Fock calculations for the α-decay Q values of superheavy nuclei. Phys. Rev. **C67**, 034313(6) (2003)
353. Ellison, P.A., Gregorich, K.E., Berryman, J.S., Bleuel, D.L., Clark, R.M., Dragojevic, I., Dvorak, J., Fallon, P., Fineman-Sotomayor, C., Gates, J.M., Gothe, O.R., Lee, I.Y., Loveland, W.D., McLaughlin, J.P., Paschalis, S., Petri, M., Qian, J., Stavsetra, L., Wiedeking, M., Nitsche, H.: New superheavy element isotopes $^{242}Pu(^{48}Ca,5n)^{285}114$. Phys. Rev. Lett. **105**, 182701(4) (2010)
354. Oganessian, Yu.Ts., Abdullin, F.Sh., Dmitriev, S.N., Gostic, J.M., Hamilton, J.H., Henderson, R.A., Itkis, M.G., Moody, K.J., Polyakov, A.N., Ramayya, A.V., Roberto, J.B., Rykaczewski, K.P., Sagaidak, R.N., Shaughnessy, D.A., Shirokovsky, I.V., Stoyer, M.A., Subbotin, V.G., Sukhov, A.M., Tsyganov, Yu.S., Utyonkov, V.K., Voinov, A.A., Vostokin, G.K.: New insights into the $^{243}Am + {}^{48}Ca$ reaction products previously observed in the experiments on elements 113, 115 and 117. Phys. Rev. Lett. **108**, 022502(5) (2012)
355. Oganessian, Yu.Ts., Utyonkov, V.K., Lobanov, Yu.V., Abdullin, F.Sh., Polyakov, A.N., Sagaidak, R.N., Shirokovsky, I.V., Tsyganov, Yu.S., Voinov, A.A., Gulbekian, G.G.,

Bogomolov, S.L., Gikal, B.N., Mezentsev, A.N., Subbotin, V.G., Sukhov, A.M., Subotic, K., Zagrebaev, V.I., Vostikin, G.K., Itkis, M.G., Henderson, R.A., Kenneally, J.M., Landrum, J.H., Moody, K.J., Shaughnessy, D.A., Stoyer, M.A., Stoyer, N.J., Wilk, P.A.: Synthesis of the isotope $^{282}113$ in the $^{237}Np + ^{48}Ca$ fusion reaction. Phys Rev. **C76**, 011601(5) (2007)

356. Oganessian, Yu.Ts., Abdullin, F.Sh., Bailey, P.D., Benker, D.E., Bennett, M.E., Dmitriev, S.N., Ezold, J.G., Hamilton, J.H., Henderson, R.A., Itkis, M.G., Lobanov, Yu.V., Mezentsev, A.N., Moody, K.J., Nelson, S.L., Polyakov, A.N., Porter, C.E., Ramayya, A.V., Riley, F.D., Roberto, J.B., Ryabinin, M.A., Rykaczewski, K.P., Sagaidak, R.N., Shaughnessy, D.A., Shirokovsky, I.V., Stoyer, M.A., Subbotin, V.G., Sudowe, R., Sukhov, A.M., Tsyganov, Yu.S., Utyonkov, V.K., Voinov, A.A., Vostokin, G.K., Wilk, P.A.: Synthesis of a new element with atomic number Z = 117. Phys. Rev. Lett. **104**, 142502(4) (2010)
357. Oganessian, Yu.Ts., Abdullin, F.Sh., Bailey, P.D., Denker, D.E., Bennett, M.E., Dmitriev, S.N., Ezold, J.G., Hamilton, J.H., Henderson, R.A., Itkis, M.G., Lobanov, Yu.V., Mezentsev, A.N., Moody, K.J., Nelson, S.L., Polyakov, A.N., Porter, C.E., Ramayya, A.V., Riley, F.D., Roberto, J.B., Ryabinin, M.A., Rykaczewski, K.P., Sagaidak, R.N., Shaughnessy, D.A., Shirokovsky, I.V., Stoyer, M.A., Subbotin, V.G., Sudowe, R., Sukhov, A.M., Taylor, R., Tsyganov, Yu.S., Utyonkov, V.K., Voinov, A.A., Vostokin, G.K., Wilk, P.A.: Eleven new heaviest isotopes of elements Z = 105 to Z = 117 identified among the products of $^{249}Bk + ^{48}Ca$ reactions. Phys. Rev. **C83**, 054315(14) (2011)
358. Düllmann, Ch.E., Ackermann, D., Block, M., Brüchle, W., Essel, H.G., Gates, J.M., Hartmann, W., Hessberger, F.P., Huebner, A., Jäger, E., Khuyagbaatar, J., Kindler, B., Krier, J., Kurz, N., Lommel, B., Schädel, M., Schausten, B., Schimpf, E., Steiner, J., Gorshkov, A., Graeger, R., Türler, A., Yakushev, A., Eberhardt, K., Even, J., Hild, D., Kratz, J.V., Liebe, D., Runke, J., Thörle-Pospiech, P., Wiehl, N., Anderson, L.-L., Herzberg, R.-D., Parr, E., Dvorak, J., Ellison, P.A., Gregorich, K.E., Nitsche, H., Lahiri, S., Maiti, M., Omtvedt, J.P., Semchenkov, A., Rudolph, D., Uusitalo, J., Wegrzecki, M.: Production and decay of element 114: high cross sections and new nucleus ^{277}Hs. Phys. Rev. Lett. **104**, 252701(5) (2010)
359. Gates, J.M., Düllmann, Ch.E., Schädel, M., Yakushev, A., Türler, A., Eberhardt, K., Kratz, J.V., Ackermann, D., Andersson, L.-L., Block, M., Brüchle, W., Dvorak, J., Essel, H.G., Ellison, P.A., Even, J., Forsberg, U., Gellanki, J., Gorshkov, A., Graeger, R., Gregorich, K.E., Hartmann, W., Herzberg, R.-D., Hessberger, F.P., Hild, D., Huebner, A., Jäger, E., Khuyagbaatar, J., Kindler, B., Krier, J., Kurz, N., Lahiri, S., Liebe, D., Lommel, B., Maiti, M., Nitsche, H., Omtvedt, J.P., Parr, E., Rudolph, D., Runke, J., Scharffner, H., Schausten, B., Schimpf, E., Semchenkov, A., Steiner, J., Thörle-Pospiech, P., Uusitalo, J., Wegrzecki, M., Wiehl, N.: First superheavy element experiments at the GSI recoil separator TASCA: the production and decay of element 114 in the $^{244}Pu(^{48}Ca,3\text{-}4n)$ reaction. Phys. Rev. **C83**, 054618(17) (2011)
360. Oganessian, Yu.Ts., Utyonkov, V.K., Lobanov, Yu.V., Abdullin, F.Sh., Polyakov, A.N., Shirokovsky, I.V., Tsyganov, Yu.S., Gulbekian, G.G., Bogomolov, S.L., Gikal, B.N., Mezentsev, A.N., Iliev, S., Subbotin, V.G., Sukhov, A.M., Ivanov, O.V., Buklanov, G.V., Subotic, K., Itkis, M.G., Moody, K.J., Wild, J.F., Stoyer, N.J., Stoyer, M.A., Lougheed, R.W.: Synthesis of superheavy nuclei in $^{48}Ca + ^{244}Pu$ interactions. Phys. At. Nuclei **63**, 1679–1687 (2000)
361. Oganessian, Yu.Ts., Utyonkov, V.K., Lobanov, Yu.V., Abdullin, F.Sh., Polyakov, A.N., Shirokovsky, I.V., Tsyganov, Yu.S., Gulbekian, G.G., Bogomolov, S.L., Gikal, B.N., Mezentsev, A.N., Iliev, S., Subbotin, V.G., Sukhov, A.M., Ivanov, O.V., Buklanov, G.V., Subotic, K., Voinov, A.A., Itkis, M.G., Moody, K.J., Wild, J.F., Stoyer, N.J., Stoyer, M.A., Lougheed, R.W., Laue, C.A.: Synthesis of superheavy nuclei in the reactions of ^{244}Pu and ^{248}Cm with ^{48}Ca. Eur. Phys. J. **A15**, 201–204 (2002)

362. Loveland, W., Gregorich, K.E., Patin, J.B., Peterson, D., Rouki, C., Zielinski, P.M., Aleklett, K.: Search for the production of element 112 in the $^{48}Ca + ^{238}U$ reaction. Phys. Rev. **C66**, 044617(5) (2002)
363. Gregorich, K.E., Loveland, W., Peterson, D., Zielinski, P.M., Nelson, S.L., Chung, Y.H., Düllmann, Ch.E., Folden, C.M., Aleklett, K., Eichler, R., Hoffman, D.C., Omtvedt, J.P., Pang, G.K., Schwantes, J.M., Soverna, S., Sprunger, P., Sudowe, R., Wilson, R.C., Nitsche, H.: Attempt to confirm superheavy element production in the $^{48}Ca + ^{238}U$ reaction. Phys. Rev. **C72**, 014605(7) (2005)
364. Hofmann, S., Ackermann, D., Antalic, S., Burkhard, H.G., Comas, V.F., Dressler, R., Gan, Z., Heinz, S., Heredia, J.A., Hessberger, F.P., Khuyagbaatar, J., Kindler, B., Kojouharov, I., Kuusiniemi, P., Leino, M., Lommel, B., Mann, R., Münzenberg, G., Nishio, K., Popeko, A.G., Saro, S., Schött, H.J., Streicher, B., Sulignano, B., Uusitalo, J., Venhart, M., Yeremin, A.V.: The reaction $^{48}Ca + ^{238}U = ^{286}112^*$ studied at the GSI-SHIP. Eur. Phys. J. **A32**, 251–260 (2007)
365. Stavsetra, L., Gregorich, K.E., Dvorak, J., Ellison, P.A., Dragojevic, I., Garcia, M.A., Nitsche, H.: Independent verification of element 114 production in the $^{48}Ca + ^{242}Pu$ reaction. Phys. Rev. Lett. **103**, 132502(4) (2009)
366. Yakushev, A.B., Zvara, I., Oganessian, Yu.Ts., Belozerov, A.V., Dmitriev, S.N., Eichler, B., Hübener, S., Sokol, E.A., Türler, A., Yeremin, A.V., Buklanov, G.V., Chelnokov, M.L., Chepigin, V.I., Gorshkov, V.A., Gulyaev, A.V., Lebedev, V.Ya., Malyshev, O.N., Popeko, A.G., Soverna, S., Szeglowski, Z., Timokhin, S.N., Tretyakova, S.P., Vasko, V.M., Itkis, M.G.: Chemical identification and properties of element 112. Radiochim. Acta **91**, 433–439 (2003)
367. Eichler, R., Brüchle, W., Buda, R., Bürger, S., Dressler, R., Düllmann, ChE, Dvorak, J., Eberhardt, K., Eichler, B., Folden III, C.M., Gäggeler, H.W., Gregorich, K.E., Haenssler, F., Hoffman, D.C., Hummrich, H., Jäger, E., Kratz, J.V., Kuczewski, B., Liebe, D., Nayak, D., Nitsche, H., Piguet, D., Qin, Z., Rieth, U., Schädel, M., Schausten, B., Schimpf, E., Semchenkov, A., Soverna, S., Sudowe, R., Trautmann, N., Thörle, P., Türler, A., Wierczinski, B., Wiehl, N., Wilk, P.A., Wirth, G., Yakushev, A.B., von Zweidorf, A.: Attempts to chemically investigate element 112. Radiochim. Acta **94**, 181–191 (2006)
368. Oganessian, Yu.Ts., Utyonkov, V.K., Moody, K.J.: Synthesis of $^{292}116$ in the $^{248}Cm + ^{48}Ca$ reaction. Phys. At. Nuclei **64**, 1349–1355 (2001)
369. Hofmann, S., Heinz, S., Mann, R., Maurer, J., Khuyagbaatar, J., Ackermann, D., Antalic, S., Barth, W., Block, M., Burkhard, H.G., Comas, V.F., Dahl, L., Eberhardt, K., Gostic, J., Henderson, R.A., Heredia, J.A., Hessberger, F.P., Kenneally, J.M., Kindler, B., Kojouharov, I., Kratz, J.V., Lang, R., Leino, M., Lommel, B., Moody, K.J., Münzenberg, G., Nelson, S.L., Nishio, K., Popeko, A.G., Runke, J., Saro, S., Shaughnessy, D.A., Stoyer, M.A., Thörle-Pospiech, P., Tinschert, K., Trautmann, N., Uusitalo, J., Wilk, P.A., Yeremin, A.V.: The reaction $^{48}Ca + ^{248}Cm = ^{296}116^*$ studied at the GSI-SHIP. Eur Phys. J. **A48**, 62–66 (2012)
370. Oganessian, Yu.Ts., Utyonkov, V.K., Lobanov, Yu.V., Abdullin, F.Sh., Polyakov, A.N., Sagaidak, R.N., Shirokovsky, I.V., Tsyganov, Yu.S., Voinov, A.A., Gulbekian, G.G., Bogomolov, S.L., Gikal, B.N., Mezentsev, A.N., Iliev, S., Subbotin, S.G., Sukhov, A.M., Subotic, K., Zagrebaev, V.I., Vostokin, G.K., Itkis, M.G., Moody, K.J., Patin, J.B., Shaughnessy, D.A., Stoyer, M.A., Stoyer, N.J., Wilk, P.A., Kenneally, J.M., Landrum, J.H., Wild, J.F., Lougheed, R.W.: Synthesis of the isotopes of elements 118 and 116 in the ^{249}Cf and $^{245}Cm + ^{48}Ca$ fusion reactions. Phys. Rev. **C74**, 044602(9) (2006)
371. Baran, A., Lojewski, Z., Sieja, K., Kowal, M.: Global properties of even-even superheavy nuclei in macroscopic-microscopic models. Phys. Rev. **C72**, 044310(13) (2005)
372. Baran, A., Lojewski, Z., Sieja, K.: Masses and half-lives of superheavy elements. Acta Phys. Pol. **B36**, 1369–1372 (2005)
373. Baran, A., Lojewski, Z., Sieja, K.: Superheavy nuclei in different pairing models. Int. J. Mod. Phys. **E15**, 452–456 (2006)

374. Northcliffe, L.C., Schilling, R.F.: Range and stopping power tables for heavy ions. Nucl. Data Tables **A7**, 233–463 (1970)
375. Sikkeland, T., Maly, J., Lebeck, D.F.: Evaporation of 3 to 8 neutrons in reactions between ^{12}C and various uranium nuclides. Phys. Rev. **169**, 1000–1006 (1968)
376. Hubert, F., Bimbot, R., Gauvin, H.: Range and stopping power tables for 2.5–500 MeV/nucleon heavy ions in solids. At. Data Nucl. Data Tables **46**, 1–213 (1990)
377. Folger, H., Hartmann, W., Hessberger, F.P., Hofmann, S., Klemm, J., Münzenberg, G., Ninov, V., Thalheimer, W., Armbruster, P.: Development of ^{170}Er, $^{204,206,207,208}Pb$ and ^{209}Bi target wheels for reaction studies and synthesis of heaviest elements. Nucl. Instrum. Methods **A362**, 64–69 (1995)
378. Marx, D., Nickel, F., Münzenberg, G., Güttner, K., Ewald, H., Faust, W., Hofmann, S., Schött, H.J., Thalheimer, W.: A rotating target wheel with thin targets for heavy ion beams of high current density. Nucl. Instrum. Methods **163**, 15–20 (1979)
379. Oganessian, Yu.Ts.: Transmendelevium elements: the present and the future. In: Proceedings of the Robert A. Welch Foundation Conference on Chemical Research XXXIV, Fifty years with transuranium elements, Chapt. 5, pp. 159–197. Houston, Texas, 22–23 October 1990
380. Nitschke, J.M.: A high intensity heavy-ion recoil-target system. Nucl. Instrum. Methods **138**, 393–406 (1976)
381. Yaffe, L.: Preparation of thin films, sources and targets. Ann. Rev. Nucl. Sci. **12**, 153–188 (1962)
382. Van der Eijk, W., Oldenhof, W., Zehner, W.: Preparation of thin sources; a review. Nucl. Instrum. Methods **112**, 343–351 (1973)
383. Aumann, D.C., Müllen, G.: Preparation of targets of Ca, Ba, Fe, La, Pb, Tl, Bi, Th and U by electrodeposition from organic solutions. Nucl. Instrum. Methods **115**, 75–81 (1974)
384. Müllen, G., Aumann, D.C.: Preparation of targets of Np, Pu, Am, Cm and Cf by electrodeposition from organic solutions. Nucl. Instrum. Methods **128**, 425–428 (1975)
385. Evans, J.E., Lougheed, R.W., Coops, M.S., Hoff, R.W., Hulet, E.K.: The use of electrodeposition methods to prepare actinide targets for cross-section measurements and accelerator bombardments. Nucl. Instrum. Methods **102**, 389–401 (1972)
386. Gavin, B.: Anode sputtering characteristics of the Berkeley 2.5 MV source. IEEE Trans. Nucl. Sci. **NS-23**, 1008–1012 (1976)
387. Kutner, V.B., Bogomolov, S.L., Gulbekian, G.G., Efremov, A.A., Ivanov, G.N., Lebedev, A.N., Levedev, V.Ya., Loginov, V.N., Oganessian, Yu.Ts., Yakushev, A.B., Yazvitsky, N.Yu.: Operation and recent development of ECR ion sources at the FLNR (JINR) cyclotrons. In: Baron, E., Lieuvin, M. (eds.) Proceedings of the 15th International Conference on Cyclotrons and Their Applications, Caen, France, pp. 405–408. Institute of Physics Publishing, Bristol, UK, 15–19 June 1998
388. Nurmia, M., Sikkeland, T., Silva, R., Ghiorso, A.: Spontaneous fission of light fermium isotopes; new nuclides ^{244}Fm and ^{245}Fm. Phys. Lett. **B26**, 78–80 (1967)
389. Münzenberg, G.: Recent advances in the discovery of transuranium elements. Rep. Prog. Phys. **51**, 57–104 (1988)
390. Nitschke, J.M.: OASIS: the SuperHILAC on-line isotope separator. Nucl. Instrum. Methods **206**, 341–351 (1983)
391. Trautmann, N.: Fast radiochemical separations for heavy elements. Radiochim. Acta **70/71**, 237–245 (1995)
392. Gäggeler, H.W.: On-line gas chemistry experiments with transactinide elements. J. Radioanal. Nucl. Chem. **183**, 261–271 (1994)
393. Arje, J., Valli, K.: Helium-jet ion guide for an on-line isotope separator. Nucl. Instrum. Methods **179**, 533–539 (1981)
394. Herrmann, G., Trautmann, N.: Rapid chemical methods for identification and study of short-lived nuclides. Ann. Rev. Nucl. Part. Sci. **32**, 117–147 (1982)
395. Kratz, J.V.: Critical evaluation of the chemical properties of the transactinide elements. Pure Appl. Chem. **75**, 103–138 (2003)

396. Schädel, M., Brüchle, W., Haefner, B.: Fast radiochemical separations with an automated rapid chemistry apparatus. Nucl. Instrum. Methods Phys. Res. **A264**, 308–318 (1988)
397. Schädel, M., Brüchle, W., Brügger, M., Gäggeler, H., Moody, K.J., Schardt, D., Sümmerer, K., Hulet, E.K., Dougan, A.D., Dougan, R.J., Landrum, J.H., Lougheed, R.W., Wild, J.F., O'Kelley, G.D.: High transfer cross sections from reactions with ^{254}Es. Phys. Rev. **C33**, 1547–1550 (1986)
398. Schädel, M.: Chemistry of superheavy elements. Angew. Chem. Int. Ed. **45**, 368–401 (2006)
399. Kadkhodayan, B., Türler, A., Gregorich, K.E., Basiden, P.A., Czerwinski, K.R., Eichler, B., Gäggeler, H.W., Hamilton, T.M., Jost, D.T., Kacher, C.D., Kovacs, A., Kreek, S.A., Lane, M.R., Mohar, M.F., Neu, M.P., Stoyer, N.J., Sylwester, E.R., Lee, D.M., Nurmia, M.J., Seaborg, G.T., Hoffman, D.C.: On-line gas chromatographic studies of chlorides of rutherfordium and homologs Zr and Hf. Radiochim. Acta **72**, 169–178 (1996)
400. Ravn, H.L.: Experiments with intense secondary beams of radioactive ions. Phys. Rep. **54**, 201–259 (1979)
401. Hansen, P.G.: Nuclei far away from the line of beta stability: studies by on-line mass separation. Ann. Rev. Nucl. Part. Sci. **29**, 69–119 (1979)
402. Ravn, H.L.: Progress in targets and ion sources for on-line separators. Nucl. Instrum. Methods **139**, 281–290 (1976)
403. Oganessian, Yu.Ts., Shchepunov, V.A., Dmitriev, S.N., Itkis, M.G., Gulbekyan, G.G., Khabarov, M.V., Bekhterev, V.V., Bogomolov, S.L., Efremov, A.A., Pashenko, S.V., Stepantsov, S.V., Yeremin, A.V., Yavor, M.I., Kalimov, A.G.: The project of the mass separator of atomic nuclei produced in heavy ion induced reactions. Nucl. Instrum. Methods Phys. Res. **B204**, 606–613 (2003)
404. Enge, H.A.: Progress in recoil spectrometers for separation of fast nuclear reaction products. Nucl. Instrum. Methods Phys. Res. **186**, 413–422 (1981)
405. Yeremin, A.V., Andreyev, A.N., Bogdanov, D.D., Ter-Akopian, G.M., Chepigin, V.I., Gorshkov, V.A., Kabachenko, A.P., Malyshev, O.N., Popeko, A.G., Sagaidak, R.N., Sharo, S., Voronkov, E.N., Taranenko, A.V., Lavrentjev, A.Yu.: The kinematic separator VASSILISSA performance and experimental results. Nucl. Instrum. Methods Phys. Res. **A350**, 608–617 (1994)
406. Yeremin, A.V., Bogdanov, D.D., Chepigin, V.I., Gorshkov, V.A., Kabachenko, A.P., Malyshev, O.N., Popeko, A.G., Sagaidak, R.N., Ter-Akopian, G.M., Lavrentjev, A.Yu.: The electrostatic separator VASSILISSA performance and experimental results. Nucl. Instrum. Methods Phys. Res. **B126**, 329–333 (1997)
407. Münzenberg, G.: Ein Geschwindigkeitsfilter für die Analyse von Schwerionen-Reaktionsprodukten. Int. J. Mass Spectrosc. Ion Phys. **14**, 363–387 (1974)
408. Ghiorso, A., Yashita, S., Leino, M.E., Frank, L., Kalnins, J., Armbruster, P., Dufour, J.-P., Lemmertz, P.K.: SASSY, a gas-filled magnetic separator for the study of fusion reaction products. Nucl. Instrum. Methods **A269**, 192–201 (1988)
409. Armbruster, P., Eidens, J., Grüter, J.W., Lawin, H., Roeckl, E., Sistemich, K.: Are gas-filled magnetic separators a useful tool to investigate heavy fast recoils from nuclear reactions? Nucl. Instrum. Methods **91**, 499–507 (1971)
410. Lazarev, Yu.A., Lobanov, Yu.V., Mezentsev, A.N., Oganessian, Yu.Ts., Subbotin, V.G., Utyonkov, V.K., Abdullin, F.Sh., Bechterev, V.V., Iliev, S., Kolesov, I.V., Polyakov, A.N., Sedykh, I.M., Shirokovsky, I.V., Sukhov, A.M., Tsyganov, Yu.S., Zhuchko, V.E.: The Dubna gas-filled recoil separator: a facility for heavy element research. In: Oganessian, Yu.Ts., Penionzhkevich, Yu.E. (eds.) Proceedings of the International School Seminar on Heavy Ion Physics, vol. II, pp. 497–502. Joint Institute for Nuclear Research, Dubna, Russia, 10–15 May 1993
411. Subbotin, V.G., Iliev, S.N., Sukhov, A.M., Tsyganov, Yu.S., Polyakov, A.N., Tomin, V.I., Voinov, A.A.: The detection system of the Dubna gas-filled recoil separator. Acta Phys. Pol. **B34**, 2159–2162 (2003)
412. Tsyganov, Yu.S.: The Dubna gas-filled recoil separator: status and developments. J. Phys. **G25**, 937–940 (1999)

413. Miyatake, H., Nomura, T., Kawakami, H., Tanaka, J., Oyaizu, M., Morita, K., Shinozuka, T., Kudo, H., Sueki, K., Iwata, Y.: INS gas-filled recoil-separator. Nucl. Instrum. Methods Phys. Res. **B26**, 309–313 (1987)
414. Leino, M.: In-flight separation with gas-filled systems. Nucl. Instrum. Methods in Phys. Res. **B126**, 320–328 (1997)
415. Ninov, V., Gregorich, K.E., McGrath, C.A.: The Berkeley gas-filled separator. In: Sherrill, B.M. (ed.) Proceedings of the ENAM98, Exotic Nuclei and Atomic Masses, Bellaire, Michigan (1998); AIP Conference Proceedings vol. 455, pp. 704–707 (1998)
416. Düllmann, ChE: Physical preseparation: a powerful new method for transactinide chemists. Eur. Phys. J. **D45**, 75–80 (2007)
417. Semchenkov, A., Brüchle, W., Jäger, E., Schimpf, E., Schädel, M., Mühle, C., Klos, F., Türler, A., Yakushev, A., Belov, A., Belyakova, T., Kaparkova, M., Kukhtin, V., Lamzin, E., Sytchevsky, S.: The TransActinide Separator and Chemistry Apparatus (TASCA) at GSI—Optimization of ion-optical structures and magnet designs. Nucl. Instrum. Methods **B266**, 4153–4161 (2008)
418. Schädel, M.: Superheavy element chemistry at GSI—status and perspectives. Eur. Phys. J. **D45**, 67–74 (2007)
419. Oganessian, Yu.Ts., Utyonkov, V.K., Lobanov, Yu.V., Abdullin, F.Sh., Polyakov, A.N., Shirokovsky, I.V., Tsyganov, Yu.S., Mezentsev, A.N., Iliev, S., Subbotin, V.G., Sukhov, A.M., Buklanov, G.V., Subotic, K., Lazarev, Yu.A., Moody, K.J., Wild, J.F., Stoyer, N.J., Stoyer, M.A., Lougheed, R.W., Laue, C.A.: Average charge states of heavy atoms in dilute hydrogen. Phys. Rev. **C64**, 064309(6) (2001)
420. Subotic, K., Oganessian, Yu.Ts., Utyonkov, V.K., Lobanov, Yu.V., Abdullin, F.Sh., Polyakov, A.N., Tsyganov, Yu.S., Ivanov, O.V.: Evaporation residue collection efficiencies and position spectra of the Dubna gas-filled recoil separator. Nucl. Instrum. Methods Phys. Res. **A481**, 71–80 (2002)
421. Hofmann, S.: Synthesis and properties of superheavy elements. J. Nucl. Radiochem. Sci. **4**, R1–R13 (2003)
422. Armbruster, P.: On the quest of production of superheavy nuclei in reactions of ^{48}Ca with the heaviest cctinide (*sic*) targets. Eur. Phys. J. **A7**, 23–33 (2000)
423. Hofmann, S.: Techniques for the discovery of new elements. Nucl. Instrum. Methods **B126**, 310–315 (1997)
424. Saro, S., Janik, R., Hofmann, S., Folger, H., Hessberger, F.P., Ninov, V., Schött, H.J., Kabachenko, A.P., Popeko, A.G., Yeremin, A.V.: Large size foil—microchannel plate timing detectors. Nucl. Instrum. Methods Phys. Res. **A381**, 520–526 (1996)
425. Knoll, G.F.: Radiation Detection and Measurement, 2nd edn. Chapter 11. Wiley, New York (1989)
426. Schmidt, K.-H., Sahm, C.-C., Pielenz, K., Clerc, H.-G.: Some remarks on the error analysis in the case of poor statistics. Z. Phys. **A316**, 19–26 (1984)
427. Stoyer, N.J., Stoyer, M.A., Wild, J.F., Moody, K.J., Lougheed, R.W., Oganessian, Yu.Ts., Utyonkov, V.K.: Random probability analysis of heavy-element data. Nucl. Instrum. Methods Phys. Res. **A455**, 433–441 (2000)
428. Wrede, C., Hussein, A., Rogers, J.G., D'Auria, J.: A double sided silicon strip detector as a DRAGON end detector. Nucl. Instrum. Methods Phys. Res. **B204**, 619–624 (2003)
429. Karny, M., Grzywacz, R.K., Batchelder, J.C., Bingham, C.R., Gross, C.J., Hagino, K., Hamilton, J.H., Janas, Z., Kulp, W.D., McConnell, J.W., Momayezi, M., Piechaczek, A., Rykaczewski, K.P., Semmes, P.A., Tantawy, M.N., Winger, J.A., Yu, C.H., Zganjar, E.F.: Fine structure in proton emission from ^{145}Tm discovered with digital signal processing. Phys. Rev. Lett. **90**, 012502(4) (2003)
430. Tsyganov, Yu.S., Subbotin, V.G., Polyakov, A.N., Iliev, S.N., Sukhov, A.M., Voinov, A.A., Tomin, V.I.: Detection system for heavy element research: present status. Nucl. Instrum. Methods Phys. Res. **A525**, 213–216 (2004)
431. Zlokazov, V.B.: Statistical analysis of rare events—synthesis of the element 114. Eur. Phys. J. **A8**, 81–86 (2000)

432. Paul, E.S., Woods, P.J., Davinson, T., Page, R.D., Sellin, P.J., Beausang, C.W., Clark, R.M., Cunningham, R.A., Forbes, S.A., Fossan, D.B., Gizon, A., Gizon, J., Hauschild, K., Hibbert, I.M., James, A.N., LaFosse, D.R., Lazarus, I., Schnare, H., Simpson, J., Wadsworth, R., Waring, M.P.: In-beam γ-ray spectroscopy above ^{100}Sn using the new technique of recoil decay tagging. Phys. Rev. **C51**, 78–87 (1995)
433. Simon, R.S., Schmidt, K.-H., Hessberger, F.P., Hlavac, S., Honusek, M., Münzenberg, G., Clerc, H.-G., Gollerthan, U., Schwab, W.: Evidence for nuclear shape coexistence in ^{180}Hg. Z. Phys. **A325**, 197–202 (1986)
434. Leino, M., Kankaanpaa, H., Herzberg, R.-D., Chewter, A.J., Hessberger, F.P., Le Coz, Y., Becker, F., Butler, P.A., Cocks, J.F.C., Dorvaux, O., Eskola, K., Gerl, J., Greenlees, P.T., Helariutta, K., Houry, M., Jones, G.D., Jones, P., Julin, R., Juutinen, S., Kettunen, H., Khoo, T.L., Kleinboehl, A., Korten, W., Kuusiniemi, P., Lucas, R., Muikku, M., Nieminen, P., Page, R.D., Rahkila, P., Reiter, P., Savelius, A., Schlegel, Ch., Theisen, Ch., Trzaska, W.H., Wollersheim, H.-J.: In-beam study of ^{254}No. Eur. Phys. J. **A6**, 63–69 (1999)
435. Herzberg, R.-D., Amzal, N., Becker, F., Butler, P.A., Chewter, A.J.C., Cocks, J.F.C., Dorvaux, O., Eskola, K., Gerl, J., Greenlees, P.T., Hammond, N.J., Hauschild, K., Helariutta, K., Hessberger, F., Houry, M., Jones, G.D., Jones, P.M., Julin, R., Juutinen, S., Kankaanpaa, H., Kettunen, H., Khoo, T.L., Korten, W., Kuusiniemi, P., Le Coz, Y., Leino, M., Lister, C.J., Lucas, R., Muikku, M., Nieminen, P., Page, R.D., Rahkila, P., Reiter, P., Schlegel, Ch., Scholey, C., Stezowski, O., Theisen, Ch., Trzaska, W.H., Uusitalo, J., Wollersheim, H.J.: Spectroscopy of transfermium nuclei: ^{252}No. Phys. Rev. **C65**, 014303 (2001)
436. Herzberg, R.-D., Amzal, N., Bastin, J.E., Becker, F., Brew, P.M.T., Butler, P.A., Chewter, A.J.C., Cocks, J.F.C., Dorvaux, O., Eskola, K., Gerl, J., Greenlees, P.T., Hammond, N.J., Hauschild, K., Helariutta, K., Hessberger, F., Houry, M., Huerstel, A., Humphreys, R.D., Jones, G.D., Jones, P.M., Julin, R., Juutinen, S., Kankaanpaa, H., Kettunen, H., Khoo, T.L., Korten, W., Kuusiniemi, P., Le Coz, Y., Leino, M., Leppanen, A.P., Lister, C.J., Lucas, R., Muikku, M., Nieminen, P., Page, R.D., Page, T., Rahkila, P., Reiter, P., Schlegel, Ch., Scholey, C., Sletten, G., Stezowski, O., Theisen, Ch., Trzaska, W.H., Uusitalo, J., Wollersheim, H.J.: In-beam spectroscopy of ^{253,254}No. Eur. Phys. J. **A15**, 205–208 (2002)
437. Julin, R.: In-beam spectroscopy of heavy actinides. Nucl. Phys. **A685**, 221c–232c (2001)
438. Taylor, R.B.E., Freeman, S.J., Durell, J.L., Leddy, M.J., Robinson, S.D., Varley, B.J., Cocks, J.F.C., Helariutta, K., Jones, P., Julin, R., Juutinen, S., Kankaanpaa, H., Kanto, A., Kettunen, H., Kuusiniemi, P., Leino, M., Muikku, M., Rahkila, P., Savelius, A., Greenlees, P.T.: γ decay of excited states in ^{198}Rn identified using correlated radioactive decay. Phys. Rev. **C59**, 673–681 (1999)
439. Düllmann, ChE: Superheavy element studies with preseparated isotopes. Radiochim. Acta **99**, 515–526 (2011)
440. Kirbach, U.W., Folden III, C.M., Ginter, T.N., Gregorich, K.E., Lee, D.M., Ninov, V., Omtvedt, J.P., Patin, J.B., Seward, N.K., Strellis, D.A., Sudowe, R., Türler, A., Wilk, P.A., Zielinski, P.M., Hoffman, D.C., Nitsche, H.: The cryo-thermatographic separator (CTS): a new rapid separation and α-detection system for on-line chemical studies of highly volatile osmium and hassium ($Z = 108$) tetroxides. Nucl. Instrum. Methods Phys. Res. **A484**, 587–594 (2002)
441. Stavsetra, L., Gregorich, K.E., Alstad, J., Breivik, H., Eberhardt, K., Folden III, C.M., Ginter, T.N., Johansson, M., Kirbach, U.W., Lee, D.M., Mendel, M., Omtvedt, L.A., Patin, J.B., Skarnemark, G., Sudowe, R., Wilk, P.A., Zielinski, P.M., Nitsche, H., Hoffman, D.C., Omtvedt, J.P.: Liquid-scintillation detection of preseparated ^{257}Rf with the SISAK-system. Nucl. Instrum. Methods Phys. Res. **A543**, 509–516 (2005)
442. Oganessian, Yu.Ts.: Private communication (2011)
443. Oganessian, Yu.Ts., Utyonkov, V.K., Lobanov, Yu.V., Abdullin, F.Sh., Polyakov, A.N., Sagaidak, R.N., Shirokovsky, I.V., Tsyganov, Yu.S., Voinov, A.A., Mezentsev, A.N., Subbotin, V.G., Sukhov, A.M., Subotic, K., Zagrebaev, V.I., Dmitriev, S.N., Henderson, R.A., Moody, K.J., Kenneally, J.M., Landrum, J.H., Shaughnessy, D.A., Stoyer, M.A.,

Stoyer, N.J., Wilk, P.A.: Attempt to produce element 120 in the $^{244}Pu + {}^{58}Fe$ reaction. Phys. Rev. **C79**, 024603(4) (2009)
444. Liu, Z.H., Bao, J.-D.: Optimal reaction for synthesis of superheavy element 117. Phys. Rev. **C80**, 034601(7) (2009)
445. Nasirov, A.K., Mandaglio, G., Giardina, G., Sobiczewski, A., Muminov, A.I.: Effects of the entrance channel and fission barrier in the synthesis of superheavy element $Z = 120$. Phys. Rev. **C84**, 044612(8) (2011)
446. Nomura, T.: The RNB project in Japanese Hadron Facility and possible use of neutron-rich beam for the study of superheavy nuclei. In: Arnould, M., Lewitowicz, M., Oganessian, Yu.Ts., Ohta, M., Utsunomiya, H., Wada, T. (eds.) Proceedings of the Tours Symposium on Nuclear Physics III; AIP Conference Proceedings vol. 425, pp. 29–38. American Institute of Physics, Woodbury, NY (1997)
447. Bricault, P.G., Dombsky, M., Schmor, P.W., Stanford, G.: Radioactive ion beams facility at TRIUMF. Nucl. Instrum. Methods Phys. Res. **B126**, 231–235 (1997)
448. Schmitt, C., Nadtochy, P.N., Heinz, A., Jurado, B., Kelic, A., Schmidt, K.-H.: First experiment on fission transients in highly fissile spherical nuclei produced by fragmentation of radioactive beams. Phys. Rev. Lett. **99**, 042701(4) (2007)
449. Garrett, J.D.: The latest from the new Holifield radioactive ion beam facility at Oak Ridge national laboratory. Nucl. Phys. **A616**, 3c–10c (1997)
450. Morrissey, D.J.: The coupled cyclotron project at the NSCL. Nucl. Phys. **A616**, 45c–45c (1997)
451. Cheifetz, E., Gatti, R.C., Jared, R.C., Thompson, S.G.: Acceleration of fission fragments. Phys. Rev. Lett. **24**, 148–152 (1970)
452. Kester, O., Habs, D., Sieber, T., Gross, M., Kolbe, A., Köster, U., Schempp, A., Ratzinger, U.: Fission fragment accelerators for the Grenoble and Munich high flux reactors. Nucl. Instrum. Methods Phys. Res. **B139**, 28–36 (1998)
453. Münzenberg, G.: Synthesis and investigation of superheavy elements: perspectives on radioactive beams. Philos. Trans. R. Soc. Lond. **A356**, 2083–2104 (1998)
454. Loveland, W.: Synthesis of transactinide nuclei using radioactive beams. Phys. Rev. **C76**, 014612(11) (2007)
455. Armbruster, P.: Nuclear structure in cold rearrangement processes in fission and fusion. Rep. Prog. Phys. **62**, 465–525 (1999)
456. Marinov, A., Batty, C.J., Kilvington, A.I., Newton, G.W.A., Robinson, V.J., Hemingway, J.D.: Evidence for the possible existence of a superheavy element with atomic number 112. Nature **229**, 464–467 (1971)
457. Batty, C.J., Kilvington, A.I., Weil, J.L., Newton, G.W.A., Skarestad, M., Hemingway, J.D.: Search for superheavy elements and actinides produced by secondary reactions in a tungsten target. Nature **244**, 429–430 (1973)
458. Zagrebaev, V.I.: Sub-barrier fusion enhancement due to neutron transfer. Phys. Rev. **C67**, 061601(5) (2003)
459. Oganesyan, Yu.Ts., Penionzhkevich, Yu.E., Tak An, N., Adamek, A., Quoc Bin, N., Mong Sinh, N.: Mass and charge distributions of fission fragments in reactions induced by accelerated Kr and Xe ions. Sov. J. Nucl. Phys. **19**, 119–122 (1974)
460. Schädel, M., Brüchle, W., Gäggeler, H., Kratz, J.V., Sümmerer, K., Wirth, G., Herrmann, G., Stakemann, R., Tittel, G., Trautmann, N., Nitschke, J.M., Hulet, E.K., Lougheed, R.W., Hahn, R.L., Ferguson, R.L.: Actinide production in collisions of ^{238}U with ^{248}Cm. Phys. Rev. Lett. **48**, 852–855 (1982)
461. Holm, H., Greiner, W.: On the influence of nuclear forces on coulomb fission. Nucl. Phys. **A195**, 333–352 (1972)
462. Kratz, J.V., Liljenzin, J.O., Norris, A.E., Seaborg, G.T.: Charge and mass distributions in the reaction of ^{40}Ar ions with ^{238}U. Phys. Rev. **C13**, 2347–2365 (1976)
463. Reus, U., Westmeier, W., Esterlund, R.A., Rox, A., Rajagopalan, M., Patzelt, P.: Evolution from quasi-elastic to deep-inelastic transfer in the system $^{132}Xe + {}^{nat}Fe$. Z. Phys. **A301**, 363–364 (1981)

464. Frahn, W.E.: Generalized Fresnel model for very heavy ion scattering. Nucl. Phys. **A302**, 267–280 (1978)
465. Schröder, W.U., Huizenga, J.R.: Damped heavy-ion collisions. Ann. Rev. Nucl. Sci. **27**, 465–547 (1977)
466. Schädel, M., Kratz, J.V., Ahrens, H., Brüchle, W., Franz, G., Gäggeler, H., Warnecke, I., Wirth, G., Herrmann, G., Trautmann, N., Weis, M.: Isotope distributions in the reaction of ^{238}U with ^{238}U. Phys. Rev. Lett. **41**, 469–472 (1978)
467. Moody, K.J., Lee, D., Welch, R.B., Gregorich, K.E., Seaborg, G.T., Lougheed, R.W., Hulet, E.K.: Actinide production in reactions of heavy ions with ^{248}Cm. Phys. Rev. **C33**, 1315–1324 (1986)
468. Gregorich, K.E., Moody, K.J., Lee, D., Kot, W.K., Welch, R.B., Wilmarth, P.A., Seaborg, G.T.: Actinide production in ^{136}Xe bombardments of ^{249}Cf. Phys. Rev. **C35**, 2117–2124 (1987)
469. Welch, R.B., Moody, K.J., Gregorich, K.E., Lee, D., Seaborg, G.T.: Dependence of actinide production on the mass number of the projectile: Xe + ^{248}Cm. Phys. Rev. **C35**, 204–212 (1987)
470. Toeke, J., Bock. R., Dai, G.X., Gralla, S., Gobbi, A., Hildenbrand, K.D., Kuzminski, J., Müller, W.F.J, Olmi, A., Steltzer, H., Back, B.B., Bjornholm, S.: Quasi fission—the mass drift mode in heavy ion reactions. GSI preprint GSI-84-51 (1984)
471. Schüll, D., Shen, W.C., Freiesleben, H., Bock. R., Busch, F., Bangert, D., Pfeffer, W., Pühlhofer, F.: The influence of the potential energy surface on neutron excess and mass equilibration in the ^{136}Xe + ^{56}Fe system. Phys. Lett. **102B**, 116–120 (1981)
472. Zagrebaev, V.I., Oganessian, Yu.Ts., Itkis, M.G., Greiner, W.: Superheavy nuclei and quasi-atoms produced in collisions of transuranium ions. Phys. Rev. **C73**, 031602(5) (2006)
473. Schädel, M., Brüchle, W., Brügger, M., Gäggeler, H., Moody, K.J., Schardt, D., Sümmerer, K., Hulet, E.K., Dougan, A.D., Dougan, R.J., Landrum, J.H., Lougheed, R.W., Wild, J.F., O'Kelley, G.D., Hahn, R.L.: Heavy isotope production by multinucleon transfer reactions with ^{254}Es. J. Less-Common Metals **122**, 411–417 (1986)
474. Lee, D., von Gunten, H., Jacak, B., Nurmia, M., Liu, Y.-F., Luo, C., Seaborg, G.T., Hoffman, D.C.: Production of heavy actinides from interactions of ^{16}O, ^{18}O, ^{20}Ne and ^{22}Ne with ^{248}Cm. Phys. Rev. **C25**, 286–292 (1982)
475. Lee, D., Moody, K.J., Nurmia, M.J., Seaborg, G.T., von Gunten, H.R., Hoffman, D.C.: Excitation functions for production of heavy actinides from interactions of ^{18}O with ^{248}Cm and ^{249}Cf. Phys. Rev. **C27**, 2656–2665 (1983)
476. Tanaka, S., Moody, K.J., Seaborg, G.T.: Transfer reactions from the interactions of ^{20}Ne and ^{22}Ne with ^{232}Th. Phys. Rev. **C30**, 911–915 (1984)
477. Lougheed, R.W., Hulet, E.K., Wild, J.F., Moody, K.J., Dougan, R.J., Gannett, C.M., Henderson, R.A., Hoffman, D.C., Lee, D.M.: The discovery and spontaneous fission properties of ^{262}No. In: Behrens, J.W., Carlson, A.D. (eds.) Proceedings of 50 years with nuclear fission, vol. II, pp. 694–697. American Nuclear Society, LaGrange Park, IL (1989)
478. Wild, J.F., van Aarle, J., Westmeier, W., Lougheed, R.W., Hulet, E.K., Moody, K.J., Dougan, R.J., Koop, E.-A., Glaser, R.E., Brandt, R., Patzelt, P.: Prompt neutron emission from the spontaneous fission of ^{260}Md. Phys. Rev. **C41**, 640–646 (1990)
479. Moody, K.J., Brüchle, W., Brügger, M., Gäggeler, H., Haefner, B., Schädel, M., Sümmerer, K., Tetzlaff, H., Herrmann, G., Kaffrell, N., Kratz, J.V., Rogowski, J., Trautmann, N., Skalberg, M., Skarnemark, G., Alstad, J., Fowler, M.M.: New nuclides: ^{243}Np and ^{244}Np. Z. Phys. **A328**, 417–422 (1987)
480. Freiesleben, H., Kratz, J.V.: N/Z-equilibration and nucleon exchange in dissipative heavy-ion collisions. Phys. Rep. **106**, 1–120 (1984)
481. Gatty, B., Guerreau, D., Lefort, M., Pouthas, J., Tarrago, X., Galen, J., Cauvin, J., Girard, J., Nifenecker, H.: Evidence for the temporary existence of a "composite" system in deep inelastic nuclear interactions. Z. Phys. **A273**, 65–68 (1975)
482. Hoffman, D.C., Fowler, M.M., Daniels, W.R., von Gunten, H.R., Lee, D., Moody, K.J., Gregorich, K., Welch, R., Seaborg, G.T., Brüchle, W., Brügger, M., Gäggeler, H., Schädel,

M., Sümmerer, K., Wirth, G., Blaich, T., Herrmann, G., Hildebrand, N., Kratz, J.V., Lerch, M., Trautmann, N.: Excitation functions for production of heavy actinides from interactions of ^{40}Ca and ^{48}Ca ions with ^{248}Cm. Phys. Rev. **C31**, 1763–1769 (1985)
483. Leyba, J.D., Henderson, R.A., Hall, H.L., Gannett, C.M., Chadwick, R.B., Czerwinski, K.R., Kadkhodayan, B.A., Kreek, S.A., Haynes, G.R., Gregorich, K.E., Lee, D.M., Nurmia, M.J., Hoffman, D.C.: Heavy actinide production from the interactions of ^{40}Ar with ^{248}Cm and a comparison with the ^{44}Ca-^{248}Cm system. Phys. Rev. **C41**, 2092–2102 (1990)
484. Denisov, V.Yu.: Production of superheavy elements in symmetric reactions. Prog. Part. Nucl. Phys. **46**, 303–305 (2001)
485. Xu, H.M.: Limiting temperatures and disappearance of fusionlike residues. Nucl. Phys. **A568**, 365–396 (1994)
486. Künkel, R., von Oertzen, W., Bohlen, H.G., Gebauer, B., Bösser, H.A., Kohlmeyer, B., Speer, J., Pühlhofer, F., Schüll, D.: Pairing effects in nucleon transfer reactions in the system ^{144}Sm + ^{88}Sr at 4.7 MeV/u. Z. Phys. **A336**, 71–89 (1990)
487. Oganesyan, Yu.Ts., Nadkarni, D.M., Penionzhkevich, Yu.E., Pustyl'nik, B.I., Tak An, N.: Energy dependence of the cross sections for fission and nucleon transfer in interaction of ^{232}Th with accelerated ^{74}Ge ions. Sov. J. Nucl. Phys. **19**, 244–246 (1974)
488. Keller, H., Bellwied, R., Lützenkirchen, K., Kratz, J.V., Brüchle, W., Gäggeler, H., Moody, K.J., Schädel, M., Wirth, G.: Unusual excitation-energy division in quasi-fission reactions between ^{50}Ti, ^{54}Cr and ^{58}Fe with ^{207,208}Pb at the barrier. Z. Phys. **A328**, 255–256 (1987)
489. Klein, P., Kratz, J.V., Gober, M.K., Zimmermann, H.P., Brüchle, W., Reisdorf, W., Schädel, M.: Excitation energy division in ^{51}V + ^{197}Au collisions at and near the barrier. Z. Phys. **A357**, 193–205 (1997)
490. Gäggeler, H., Brüchle, W., Ahrens, H., Folger, H., Franz, G., Kratz, J.V., Schädel, M., Warnecke, I., Wirth, G., Trautmann, N., Herrmann, G., Kaffrell, N., Peuser, P., Tittle, G., Weber, M., Zendel, M.: Search for long-lived superheavy elements in the reaction of ^{136}Xe with ^{238}U. Z. Phys. **A286**, 419–420 (1978)
491. Gäggeler, H., Brüchle, W., Brügger, M., Schädel, M., Sümmerer, K., Wirth, G., Kratz, J.V., Lerch, M., Blaich, T., Herrmann, G., Hildebrand, N., Trautmann, N., Lee, D., Moody, K.J., Gregorich, K.E., Welch, R.B., Seaborg, G.T., Hoffman, D.C., Daniels, W.R., Fowler, M.M., von Gunten, H.R.: Production of cold target-like fragments in the reaction of ^{48}Ca + ^{248}Cm. Phys. Rev. **C33**, 1983–1987 (1986)
492. Heinz, S., Comas, V., Hessberger, F.P., Hofmann, S., Ackermann, D., Burkhard, H.G., Gan, Z., Heredia, J., Khuyagbaatar, J., Kindler, B., Lommel, B., Mann, R., Maurer, J., Nishio, K., Sulignano, B.: Di-nuclear systems studied with the velocity filter SHIP. Eur. Phys. J. **A38**, 227–232 (2008)
493. Breuer, H., Mignerey, A.C., Viola, V.E., Wolf, K.L., Birkelund, J.R., Hilscher, D., Huizenga, J.R., Schröder, W.U., Wilke, W.W.: Charge and mass exchange in ^{56}Fe-induced reactions at 8.3 MeV/nucleon. Phys. Rev. **C28**, 1080–1103 (1983)

Nuclear Structure of Superheavy Elements

Rolf-Dietmar Herzberg

Abstract This chapter is dedicated to the nuclear structure of superheavy elements. It brings together all aspects of nuclear structure that have an influence on the stability of the nucleus on the one hand and that form the basis of experiments performed on superheavy elements to elucidate their nuclear structure on the other hand. The liquid drop model (LDM) is introduced and used to explain the limits of stability against fission, before the shell model is used to explain magic numbers and shell stabilization. Rotational properties of deformed nuclei are introduced and their sensitivity to the underlying nuclear structure is explored. The single particle structure and the influence of pairing on nuclei is discussed before experimental techniques for in-beam gamma and conversion electron spectroscopy are introduced. Finally spectroscopy following alpha decay is discussed.

1 Introduction

The atomic nucleus consisting of Z protons and N neutrons carries 99.9% of an atom's mass, yet it only occupies 10^{-15} of the atomic volume. With all the mass and charge compressed into such a small space it is easy to be tempted into treating the nucleus as a point charge with a positive charge $q = +Ze$ which determines the number of electrons (and thus the chemical element) and neglect its properties in first order when discussing atomic physics. However, if one looks closely the nucleus with its small but finite size has a profound impact on the atomic properties, and this impact is increasingly important the heavier and more highly charged the nucleus is. Details of the electronic structure of superheavy elements

R.-D. Herzberg (✉)
Department of Physics, University of Liverpool, Liverpool L69 7ZE, United Kingdom
e-mail: R.Herzberg@Liverpool.ac.uk

M. Schädel and D. Shaughnessy (eds.), *The Chemistry of Superheavy Elements*,
DOI: 10.1007/978-3-642-37466-1_2,

and consequences of relativistic effects from fast moving electrons are outlined by V. Pershina in "Theoretical Chemistry of the Heaviest Elements".

The largest breakthrough in our understanding of the shell structure of the nucleus came with the successful explanation of the nuclear magic numbers $Z = 2, 8, 20, 28, 50$ and 82 for protons and $N = 2, 8, 20, 28, 50, 82$ and 126 for neutrons in terms of a large and attractive spin-orbit interaction by Goeppert-Mayer and Jensen in 1948 [1, 2]. This led to the first predictions for superheavy shell closures in 1966 by Heiner Meldner [3] who calculated that $Z = 114$ should be the next closed proton configuration. More details of this development from first empirical postulates to detailed theoretical calculations are discussed by G. Herrmann in "Historical Reminiscences: The Pioneering Years of Superheavy Element Research".

This enhanced stability for certain "magic" configurations is analogous to the closed electron shells in noble gases. However, the nucleus can form such closed shell configurations for protons as well as for neutrons, leading to extra stability for doubly magic systems. The heaviest stable nucleus is the doubly magic ^{208}Pb, no other isotopes with $Z > 82$ are stable. However, several primordial isotopes with half-lives comparable to the age of the earth exist: ^{209}Bi ($T_{1/2} = 1.9 \pm 0.2 \times 10^{20}$ year) [4], ^{232}Th ($T_{1/2} = 1.4 \times 10^{10}$ year) [5], ^{235}U ($T_{1/2} = 7.04 \times 10^{8}$ year) [6], and ^{238}U ($T_{1/2} = 4.5 \times 10^{9}$ year) [7]. This exceptional stability can directly be traced to the underlying shell structure. The quest for superheavy elements is therefore identical with the quest for the next closed proton shell and the ultimate limit of stability of matter.

In Sect. 2 we will first look to the liquid drop model (LDM) to understand the limits of nuclear stability. The LDM is used to understand the fission process before we turn to the shell model to discuss the origin and nature of magic shell closures. We use these insights to define superheavy nuclei as those who owe their existence solely to the stabilizing effects of the underlying shell structure. Section 3 looks at rotational properties of deformed nuclei and explores ways in which the observed bands can help to determine the underlying nuclear structure. Section 4 finally turns to the underlying single particle structure and discusses pairing, nuclear g-factors and isomerism. The experimental methods used for nuclear structure studies of superheavy nuclei are explored in Sect. 5.

This chapter is not meant to replace a textbook on nuclear physics. It rather assumes a passing familiarity with nuclear physics and strives to point out those elements and properties, which have a direct bearing on structural studies of superheavy elements. This requires us to make many choices throughout the chapter, hopefully striking a balance between an introduction into the subject that will whet the readers appetite for further study and a reference for those interested in the broad picture only. For a small selection of recommended undergraduate texts on nuclear physics see, e.g., [8–10].

2 Bulk Properties of the Nucleus

2.1 The Liquid Drop Model

The binding energy of a nucleus consisting of Z protons and $N = A - Z$ neutrons is, to first order, well described by the LDM. The model was first proposed by Weizsäcker [11] and Bethe [12] and describes the nucleus as a charged droplet of nuclear incompressible "liquid" of constant density with the strong nuclear force holding the drop together and the Coulomb interaction pushing it apart. The nuclear volume is then directly proportional to the number of constituent nucleons and the nuclear radius is found to be $R(A) = r_0 \times A^{1/3}$ with the constant usually chosen as $r_0 = 1.2$ fm. We can write the mass equivalent energy of the nucleus in the form shown in Eq. 1. Note that in the literature authors often do not give the mass but the binding energy, which results in the opposite sign of all but the first two terms.

$$M(Z,A) = Zm_pc^2 + (A-Z)m_nc^2 - a_VA + a_SA^{2/3} + a_C\frac{Z(Z-1)}{A^{1/3}} + a_A\frac{(A-2Z)^2}{A} - a_P \tag{1}$$

with

$$a_P = \begin{cases} +\delta A^{-1/2} & N,Z \text{ both even} \\ 0 & \\ -\delta A^{-1/2} & N,Z \text{ both odd} \end{cases} \tag{2}$$

The bulk of the mass is made up by the masses of the protons and neutrons. The remaining terms describe the binding energy in a finite nucleus:

- a_VA: The *volume term* accounts for the binding energy of all nucleons as if they were surrounded by infinite nuclear matter. It does not depend on Z since the strong nuclear force acts on neutrons and protons alike. It is proportional to the volume of the nucleus.
- $a_SA^{2/3}$: The *surface term* corrects the binding energy for those nucleons close to the nuclear surface which do not feel an attractive nuclear force on all sides. It is analogous to a surface tension and proportional to the nuclear surface area.
- $a_CZ(Z-1)/A^{1/3}$: The *Coulomb term* accounts for the Coulomb repulsion between the Z protons in the nucleus. For heavy nuclei it is usually approximated as $a_CZ^2/A^{1/3}$.
- $a_A(A-2Z)^2/A = a_A(N-Z)^2/A$: The *asymmetry term* accounts for the difference between protons and neutrons and the Pauli principle.
- $a_P = \pm\delta A^{-1/2}$: The *pairing term* accounts for the tendency of nucleons to form pairs, which are more strongly bound than unpaired nucleons.

To understand the limits of nuclear stability it is clearly the binding energy that is crucial. Thus we examine the binding energy per nucleon $BE(A,Z) = (Zm_pc^2 + (A-Z)m_nc^2 - M(Z,A))/A$ as written in Eq. 3:

$$BE(A,Z) = a_V - a_S A^{-1/3} - a_C \frac{Z(Z-1)}{A^{4/3}} - a_A \frac{(Z-N)^2}{A^2} + \begin{cases} +\delta A^{-3/2} & N,Z \text{ even} \\ 0 & \\ -\delta A^{-3/2} & N,Z \text{ odd} \end{cases} \tag{3}$$

with the parameters a_V, a_S, a_C, a_A, and δ determined from fits to the entire Chart of Nuclei. A common parametrization is $a_V = 15.85$ MeV, $a_S = 18.34$ MeV, $a_C = 0.71$ MeV, $a_A = 23.21$ MeV, $\delta = 12$ MeV [13] . On average the binding energy per nucleon for nuclei around the valley of stability is found to be around 8 MeV. This simple picture will need to be modified significantly to take into account the effect of deformation and the underlying quantum shell structure of the nucleus.

In Fig. 1 we overlay the liquid drop binding energy per nucleon with the known limits of the chart of nuclei. Apart from very light nuclei, we find that nearly all nuclei lie within the contour for a binding energy per nucleon of 7.5 MeV. The notable exception comes at the upper end of the chart where the nuclei beyond Fm ($Z = 100$) all have lower binding energies. The stability of a nucleus against fission in this simple LDM can be parametrized by the fissility parameter

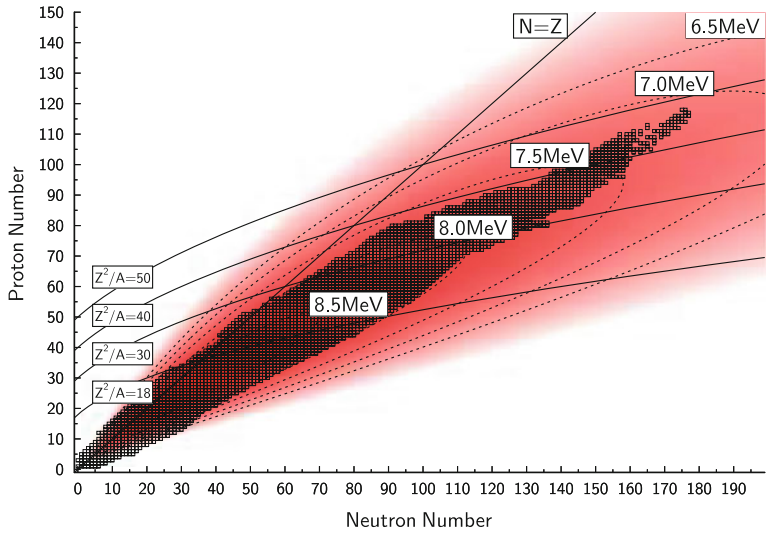

Fig. 1 Binding energy per nucleon in the liquid drop model. Isocontours for binding energies of 8.5, 8, 7.5, 7, and 6.5 MeV are shown, together with the line $N = Z$ and fissility contours $x = Z^2/A = 18, 30, 40, 50$. A fissility $x \simeq 40$ gives the limit of stability in the LDM. Nuclei beyond this line are stabilised entirely by shell effects

$x = Z^2/A$, which will be discussed in detail in Sect. 2.2. We therefore also overlay lines of constant fissility and find that these nuclei also have a high fissility. Indeed, it is in this mass region that the first spontaneously fissioning nuclei are observed.

The curved form of the line of stability with an increasingly strong deviation from the line $N = Z$ towards more neutron-rich nuclei can easily be understood from the LDM. Taking the derivative of $M(Z, A)$ with respect to Z while keeping A constant one obtains the relation for the maximum binding energy obtained for a given mass A at the proton number (Eq. 4)

$$Z \simeq \frac{4a_A + (m_n - m_p)c^2}{2\left(\frac{a_C}{A^{1/3}} + \frac{4a_A}{A}\right)} \simeq \frac{A}{2}\left(\frac{1}{1 + \frac{a_C}{4a_A}A^{2/3}}\right). \tag{4}$$

This form clearly shows the gentle curve of the line of stability towards the neutron-rich side. It is also the bane of experimental studies of superheavy elements, as one has to try to create a nucleus with a very high ratio of neutrons to protons N/Z from a reaction of lighter partners, which will have (much) smaller ratios of N/Z. Thus currently the study of superheavy elements is restricted to neutron deficient isotopes. In future radioactive beam facilities one can hope to use exotic beams with much higher N/Z ratios to create more neutron rich superheavy elements.

2.2 Spontaneous Fission

It is instructive to look in some detail at the fission process. We shall first treat the nucleus in the LDM discussed above. As the fission process leads to the release of a large amount of energy leaving the fission fragments in highly excited states, it is obvious that in first order only the three leading terms (volume, surface, and Coulomb) play an important role in the fission process. Note, however, that the underlying shell structure has a large influence on the detailed fission process and the distribution of the fragments in symmetric and asymmetric fission. As only a few nucleons get emitted in addition to the main fragments the ratio N/A for the fragments resembles that of the fissioning nucleus.

We are neglecting the effects of pairing as they are most important in the vicinity of the ground state and therefore play only a minor role in the fission process during which the nucleus becomes highly excited. Then Eq. 5 gives the binding energy of the nucleus in the LDM.

$$BE = a_V A - a_S A^{2/3} - a_C \frac{Z(Z-1)}{A^{1/3}} \tag{5}$$

We can model the onset of the fission process by evaluating the evolution of these three terms during a smooth transition from the spherical equilibrium shape with radius R to an ellipsoidal shape with long and short axes $a = R(1 + \delta)$ and

$b = c = R/(1+\delta)^{1/2}$. The volume term clearly stays constant with deformation. The surface area to first approximation increases to $S(\delta) = S_0(1 + 2\delta^2/5)$. Similarly the average distance between two protons increases and the Coulomb energy decreases to first order by a factor $E_C(\delta) = E_{C0}(1 - \delta^2/5)$. Equation 6 gives the binding energy as a function of deformation.

$$BE(\delta) = a_V A - a_S A^{2/3}\left(1 + \frac{2}{5}\delta^2\right) - a_C \frac{Z(Z-1)}{A^{1/3}}\left(1 - \frac{1}{5}\delta^2\right) \tag{6}$$

The energy gain then takes the form of Eq. 7.

$$\Delta E(\delta) = BE(\delta) - BE(0) = \frac{\delta^2}{5}\left[a_C \frac{Z(Z-1)}{A^{1/3}} - 2a_S A^{2/3}\right] \simeq \frac{\delta^2 A^{2/3}}{5}(a_C x - 2a_S). \tag{7}$$

The last form approximates $Z(Z-1)$ as Z^2 and writes the term in brackets in terms of the fissility $x = Z^2/A$. Thus Eq. 7 demonstrates the stability of the spherical equilibrium when deformations are small as well as the energetically increasingly favourable conditions for spontaneous fission with increasing fissility. Once deformation grows the first order discussion is no longer valid and higher order terms lead to the formation of a neck, and, finally, separation of the fragments. Other parametrizations for the fission process exist in the literature, see, e.g., [14]. Figure 2 shows the shape and height of the fission barrier for symmetric fission of a spherical nucleus with mass A and charge Z into two spherical fragments with $A/2$ and $Z/2$ and indicates the corresponding nuclear shapes. The height of the fission barrier can be approximated as shown in Eq. 8.

$$\begin{aligned} E_{fiss} \simeq & BE(A,Z) - 2BE(A/2, Z/2) + \Delta E(\delta) \\ = & a_S A^{2/3}\left(1 - 2\left(\tfrac{1}{2}\right)^{2/3}\right) + a_C \frac{Z^2}{A^{1/3}}\left(1 - 2\left(\tfrac{1}{2}\right)^{5/3}\right) + \frac{\delta^2 A^{2/3}}{5}\left[2a_S - a_C \frac{Z^2}{A}\right] \\ = & A^{2/3}\left(0.37 a_C \frac{Z^2}{A} - 0.26 a_S A^{2/3} + \frac{\delta^2}{5}\left[2a_S - a_C \frac{Z^2}{A}\right]\right) \end{aligned} \tag{8}$$

This leads to an energy gain for fissilities $x = \frac{Z^2}{A} \geq \frac{0.26 a_S}{0.37 a_C} \approx 18$.

We can also see that the liquid drop fission barrier vanishes completely for fissilities $x \geq 2a_S/a_C \approx 50$. The contours of constant $x = 18, 30, 40, 50$ are overlaid on Fig. 1 to show the influence of fissility on the limits of nuclear existence. The first spontaneously fissioning nuclei occur around $x \approx 40$, e.g., for ^{256}Rf. This is the limit of stability against spontaneous fission in the LDM. Any nuclei beyond this limit should not be stable against spontaneous fission and decay very quickly with half-lives shorter than 10^{-14} s. Experimentally a large number of nuclei beyond that point exist and decay predominantly though alpha or beta decay with half-lives of up to several seconds.

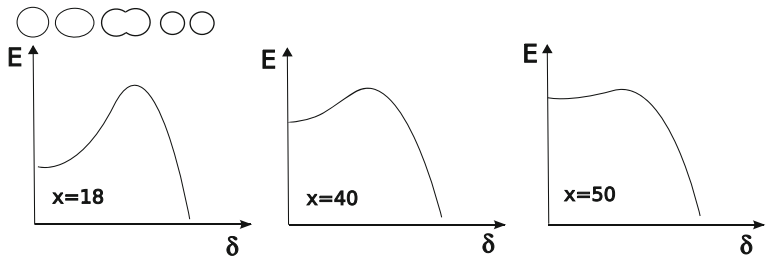

Fig. 2 Schematic illustration of fission barriers as a function of deformation parameter δ for several values of the fissility parameter x. The corresponding nuclear shapes are also indicated

Note that in the literature the fissility is often taken as the ratio of Z^2/A to a critical value $(Z^2/A)_{crit}$, which takes into account the proton-neutron asymmetry as defined in Eq. 9 [15] and is denoted by the capital letter X.

$$X = \frac{(Z^2/A)}{50.88[1 - 1.78((N-Z)/(N+Z))]} \tag{9}$$

This fissility X is a slowly varying quantity which, in the region above uranium, takes on values between 40 and 50.

We illustrate this behaviour in Fig. 3, where the experimentally obtained spontaneous fission half-lives are plotted against X for a number of heavy nuclei and compared to the fission half-life predicted by the LDM alone. The LDM half-

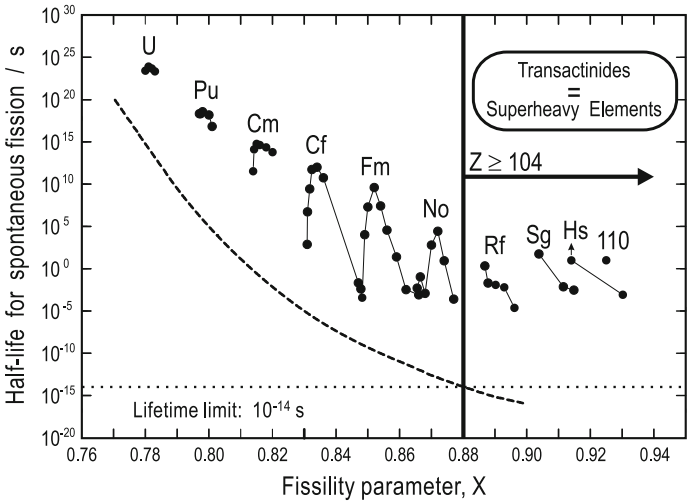

Fig. 3 Experimental spontaneous fission half-lives for even-even nuclei (*circles*) compared to the prediction of the liquid drop model as a function of the fissility parameter $x = Z^2/A$ (*dashed line*). The horizontal *dotted line* shows the minimum lifetime for the formation of a chemical element. Figure reproduced from [19] with permission

life dips below 10^{-14} s around $Z = 104$, as expected. This time is the minimum time required for a hydrogen molecule to form and gives an order of magnitude for the minimum time required for chemical processes.

We use this as a convenient working definition for superheavy nuclei: The superheavy nuclei are those that owe their stability solely to the underlying shell effects. See also the discussion by K. Moody in "Synthesis of Superheavy Elements" and G. Herrmann in "Historical Reminiscences: The Pioneering Years of Superheavy Element Research".

In reality the fission process is a lot more complicated than this simple picture implies. The nucleus has many degrees of freedom for its shape, and the fission barrier is the lowest barrier found in a large deformation parameter space, leading to symmetric and asymmetric fission, as dictated by the intricate interplay of all nucleons in an increasingly deformed potential. However, the simple arguments presented here serve to illustrate the principal limits to nuclear stability. For good starting points for further reading see, e.g., [14, 16–18].

2.3 The Spherical Shell Model

In order to obtain a more realistic understanding of the nucleus as a system of interacting protons and neutrons, we have to look at the underlying shell structure. While the LDM described in the previous section accounts for the bulk of the nuclear binding energy, it is insufficient to explain the experimentally observed deviations from a smooth behaviour observed for certain nucleon configurations. These nuclear "magic numbers" are $N, Z = 2, 8, 20, 28, 50, 82$ and $N = 126$. Experimental evidence for such underlying shell structure comes from several sources:

- Two nucleon separation energies. The binding energy associated with the removal of the last pair of protons or neutrons is very high at magic numbers, whereas it is very low for nuclei with two particles outside a magic shell.
- The probability to observe alpha decay is enhanced at proton and neutron numbers two higher than the magic numbers. This is most obvious in the neutron deficient $N = 84$ isotones where alpha decay first becomes a major decay mode in the nuclear chart. Alpha decays have also been observed for very neutron deficient Te isotopes in the vicinity of ^{100}Sn and they dominate in the heavy mass region beyond Pb. In the heavy mass region one can also observe that the alpha decays have relatively large Q-values above the shell while those for nuclei on the shell are significantly lower. For example the alpha decay of $^{216}_{88}\mathrm{Ra}_{128}$ has an alpha energy of $E_\alpha = 9.349$ MeV whereas the alpha decay of the neutron magic daughter $^{212}_{86}\mathrm{Rn}_{126}$ has an alpha decay energy of only $E_\alpha = 6.264$ MeV.
- Spherical shapes are predominantly found for nuclei with N or Z close to the magic numbers. In these nuclei the first excited state is typically at a very high excitation energy compared to neighbouring nuclei.

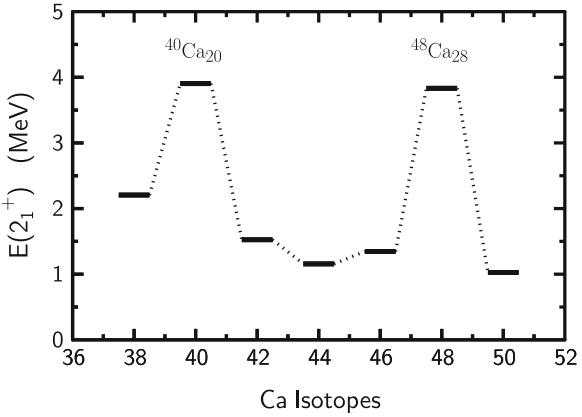

Fig. 4 Energy of the first excited 2^+ state in even nuclei in the calcium chain of isotopes. This chain contains two doubly magic systems with ^{40}Ca and ^{48}Ca. In both cases the first 2^+ state lies at a very high excitation energy compared to the neighboring isotopes

- The energy of the first excited 2^+ state has a local maximum. This experimental finding is illustrated in the calcium isotopes in Fig. 4.

The effect of nuclear shell closures is even more pronounced when both protons and neutrons have magic configurations, resulting in a significant increase in the nuclear binding energy. These doubly magic nuclei close to the line of stability are ^{4}He, ^{16}O, ^{40}Ca, ^{48}Ca, ^{56}Ni, ^{132}Sn, and ^{208}Pb. The more exotic doubly magic ^{48}Ni [20] and ^{100}Sn [21] lie at the extreme neutron deficient edge of the nuclear chart.

The nuclear shell model in its simplest form is based on several assumptions:

- The force between nuclei is attractive and has a short range. The short range is most easily seen by the near-constant nuclear density in the nuclear interior indicating that the attraction is dominant for directly neighboring nucleons.
- At short range the nucleons repel. This is a direct consequence of the Pauli exclusion principle and is usually referred to as the "hard core" of the nuclear interaction.
- Protons and neutrons move in the potential created by all other nucleons around them. Thus the nuclear potential itself is changed through the addition of nucleons. This is distinctly different to the atomic shell where electrons move in the Coulomb potential created by the pointlike nucleus which remains unchanged even if electrons are added to the atom.
- Nucleons move independently of each other and interact rarely. This seems counterintuitive at first. The nucleus is a dense object in which nucleons should "run into each other" all the time. However, nucleons are fermions and the Pauli exclusion principle means that they can only scatter into unoccupied levels. Thus two nucleons deep in the nuclear potential usually do not have sufficient energy to reach unoccupied levels and will not scatter unless they are near the Fermi level where unoccupied levels are more readily available.

Solving the resulting many body problem with a simple harmonic oscillator potential leads to wave functions which can be separated into a radial part $R(r)$ and an angular part characterized by the spherical harmonic functions $Y_{l,m}(\phi, \vartheta)$:

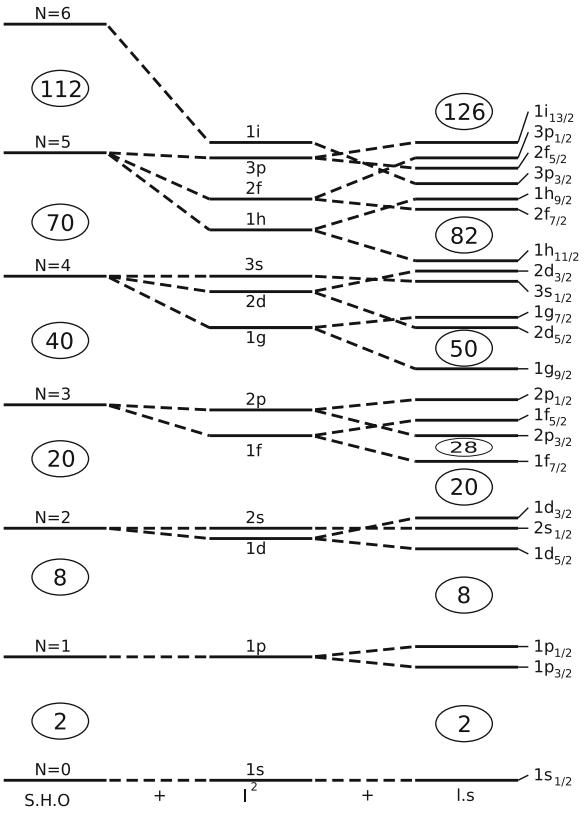

Fig. 5 Schematic representation of the states in the nuclear shell model. The oscillator shells on the *left* are first split into the individual subshells by deviations of the nuclear potential from the harmonic oscillator, before the spin-orbit interaction creates the groupings of states that produce the correct magic numbers above $N = Z = 20$. The diagram is schematic and not to scale

$$\psi(r, \phi\vartheta) = R(r)Y_{l,m}(\phi, \vartheta) \ . \tag{10}$$

We can now characterize the wave functions in that potential through four main quantum numbers, N, l, j, m. The oscillator quantum number N counts the number of oscillator quanta present and takes integer values $0, 1, 2, 3, 4, \ldots$. The orbital angular momentum l takes on integer values $l = N, N-2, N-4, \ldots, 0$ or 1 for states in each shell. The nucleons carry spin $s = 1/2$ which can be coupled to the orbital angular momentum to form the total angular momentum $j = l \pm 1/2$. Finally the projection of the total angular momentum j onto the quantisation axis is given by $m = -j, -j+1, -j+2, \ldots, +j-1, +j$. States are labelled by abbreviating l in the usual spectroscopic notation $s, p, d, f, g, h, i, j, \ldots$ for $l = 0, 1, 2, 3, \ldots$ and listed in the form l_j, such as $d_{5/2}$ and $i_{11/2}$. In case of ambiguities, the states can be distinguished by counting, i.e. we have the $1s_{1/2}$ state stemming from the $N = 0$ oscillator shell, the $2s_{1/2}$ stemming from the $N = 2$ oscillator shell, or the $1p_{3/2}$ and $2p_{3/2}$ stemming from the $N = 1, 3$ oscillator shells, respectively. Table 1 gives a summary of the shells, together with the number of nucleons each state can hold. For a more detailled description the reader is referred to the texts given near the beginning of the chapter.

Table 1 Shell model states for each oscillator shell, their occupancies and the resulting shell closures. Up to $N = 20$ the magic numbers are correctly reproduced.

N	States	Occupancy	Total
0	$1s_{1/2}$	2	2
1	$1p_{1/2}$, $1p_{3/2}$	$2+4=6$	8
2	$2s_{1/2}$, $1d_{3/2}$, $1d_{5/2}$	$2+4+6=12$	20
3	$2p_{1/2}$, $2p_{3/2}$, $1f_{5/2}$, $1f_{7/2}$	$2+4+6+8=20$	40
4	$3s_{1/2}$, $2d_{3/2}$,$2d_{5/2}$, $1g_{7/2}$, $1g_{9/2}$	$2+4+6+8+10=30$	70
5	$3p_{1/2}$, $3p_{3/2}$, $2f_{5/2}$, $2f_{7/2}$, $1h_{9/2}$, $1h_{11/2}$	$2+4+6+8+10+12=42$	112
6	$4s_{1/2}$, $3d_{3/2}$,$3d_{5/2}$, $2g_{7/2}$, $2g_{9/2}$, $1i_{11_2}$, $1i_{13/2}$	$2+4+6+8+10+12+14=56$	168

The closed oscillator shells coincide with the lower magic numbers $N = Z = 2, 8, 20$ but fail to reproduce the experimentally observed ones at higher numbers. The missing ingredient is a strong and attractive spin-orbit interaction, first proposed by Goeppert-Mayer and Jensen in 1948 [1, 2]. The spin-orbit interaction is largest near the nuclear surface and is often written as

$$V_{ls} \propto \frac{\mathrm{d}\, V(r)}{\mathrm{d}\, r} \hat{l} \cdot \hat{s} \tag{11}$$

where $V(r)$ is the radial part of the nuclear potential. This is illustrated in Fig. 6, where a Woods-Saxon shape was assumed for the nuclear potential.

We show in Eq. 12 how one can evaluate the magnitude of the term $l \cdot s$ to be

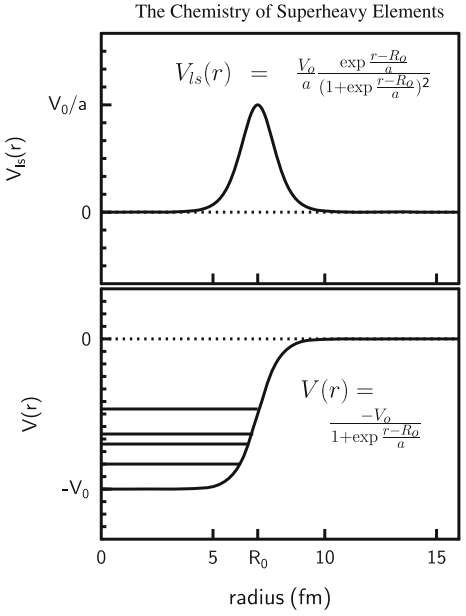

Fig. 6 Schematic representation of the shell model potential and the spin-orbit interaction (*top*) usually taken as proportional to the derivative of the potential, illustrated via a Woods-Saxon potential (*bottom*) with a nuclear radius R_0 and a surface diffuseness a. A few nuclear levels inside the potential are schematically indicated. It is then obvious that the spin-orbit interaction mainly acts near the surface of the nucleus

$$l.s = \begin{cases} l+1 & \text{for} \quad j = l - 1/2 \\ -l & \text{for} \quad j = l + 1/2 \end{cases} \tag{12}$$

This means that the state with the larger j will get lowered, while the state with the smaller j gets raised in energy, resulting in a spin-orbit splitting proportional to $2l + 1$. The magic numbers are now easily explained. The spin orbit interaction acting on the first $f_{5/2}$–$f_{7/2}$ pair in the $N = 3$ oscillator shell lowers the $f_{7/2}$ state to lie energetically between the states of the second oscillator shell and the remaining states in the third shell. As it can hold eight nucleons, it forms the $N = Z = 28$ subshell. The shell at 50 is formed in a similar way: The spin-orbit interaction lowers the $g_{9/2}$ state to lie energetically close to the states in the $N = 3$ shell, adding its 10 nucleons to the 40 already present. The shell at 82 is formed by lowering the $h_{11/2}$ state into the lower shell, and so on. This is illustrated schematically in Fig. 5 where an additional term proportional to l^2 is included. This term simulates a flattening of the potential at small radii and thus gives a better match of the harmonic oscillator potential to the potential of the nucleus, which is better described by a Woods-Saxon shape with a flat bottom.

In order to gain an understanding of the situation for superheavy elements the 82–126 shell is redrawn in Fig. 7, where the effect of large and small spin orbit interaction is illustrated. The predicted shell closure at 114 is realised if a large spin-orbit interaction gives a large splitting between the $2f_{5/2}$ and $2f_{7/2}$ states, and the $1i_{13/2}$ state lies well below the $2f_{5/2}$ state. It is easy to see how a shift in the energy centroids of the various components and a change in spin-orbit interaction strength will lead to the opening and closing of shells at $Z = 114$ and $Z = 120$, leaving only

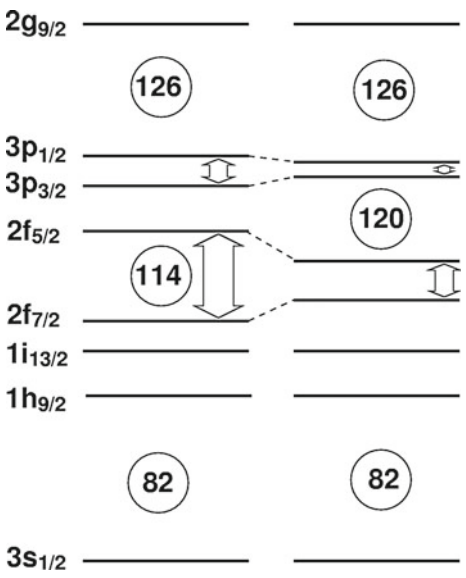

Fig. 7 Shell model level ordering resulting from large (*left*) and small (*right*) spin orbit interaction. The opening and closing of shells at 114 and 120 is clearly seen. Figure reproduced from [22] with permission

$Z = 126$ as a large shell gap. This uncertainty of the positions of the spherical orbitals lies at the heart of the problem of locating the next spherical shell closure.

One word of caution. It is tempting to infer a shell closure from the existence of a large energy gap between levels alone. While this is generally a good approximation at low masses, the high degeneracy of the high-l orbitals starts to play an increasingly important role in heavier nuclei. Stability is not primarily associated with the large energy gap, but really with regions of low level density. This leads to a softening of the magicity illustrated in Fig. 8 [23–25]. Here the shell correction energy is compared for several realistic model calculations for the Sn region (top) and the superheavy region (bottom). In the Sn region the magic numbers 50 and 82 attract extra binding energy, with the doubly magic character clearly in evidence. For the superheavy region the picture is very different. Entire regions of the nuclear chart gain stability through shell effects, leading to much broader "islands" of stability.

2.4 The Deformed Shell Model

Most nuclei are well deformed. From a single particle point of view this means that the total energy of the nucleus can be minimized by arranging the nucleons in a deformed configuration. If the energy gain in this configuration is greater than the energy required to deform the bulk of the nucleus (as seen in the LDM), then the ground state will be deformed and the resulting deformed mean field splits the degeneracy of the spherical single particle levels. The Nilsson model [26] is commonly used to extend the shell model to deformed systems.

If the nucleus deforms axially, the spherical states will split into $(2j + 1)/2$ levels, each still with twofold degeneracy. It is instructive to trace the breaking of the degeneracy back to first principles, namely that the nuclear interaction is short range and attractive. In a deformed nucleus it can therefore be expected that the overlap of the nuclear wavefunction with the bulk of the nucleus determines the energy gain.

Consider a prolate, axially symmetric nucleus with the quantization axis identical to the nuclear symmetry axis. A $g_{9/2}$ proton orbits the nucleus and can occupy any of the m-substates associated with $j = 9/2$, i.e. $\pm 9/2$, $\pm 7/2$, $\pm 5/2$, $\pm 3/2$ and $\pm 1/2$. The projection m of the total angular momentum is usually abbreviated with the letter Ω (see Fig. 9). If we compare the states with $\Omega = 9/2$ and $\Omega = 1/2$ then the former state has j aligned with the nuclear symmetry axis, which means that the nucleon orbits in an equatorial plane nearly perpendicular to that axis. The prolate deformation then means that the nucleon has a small overlap with the other nucleons constituting the nuclear bulk. The $\Omega = 1/2$ state on the other hand has j oriented nearly perpendicular to the symmetry axis, which means that the nucleon occupies a polar orbit resulting in a large overlap with the bulk. It therefore feels a much larger attractive force than the $\Omega = 9/2$ state, and its energy is consequently lowered relative to the $\Omega = 9/2$ state. The remaining states will

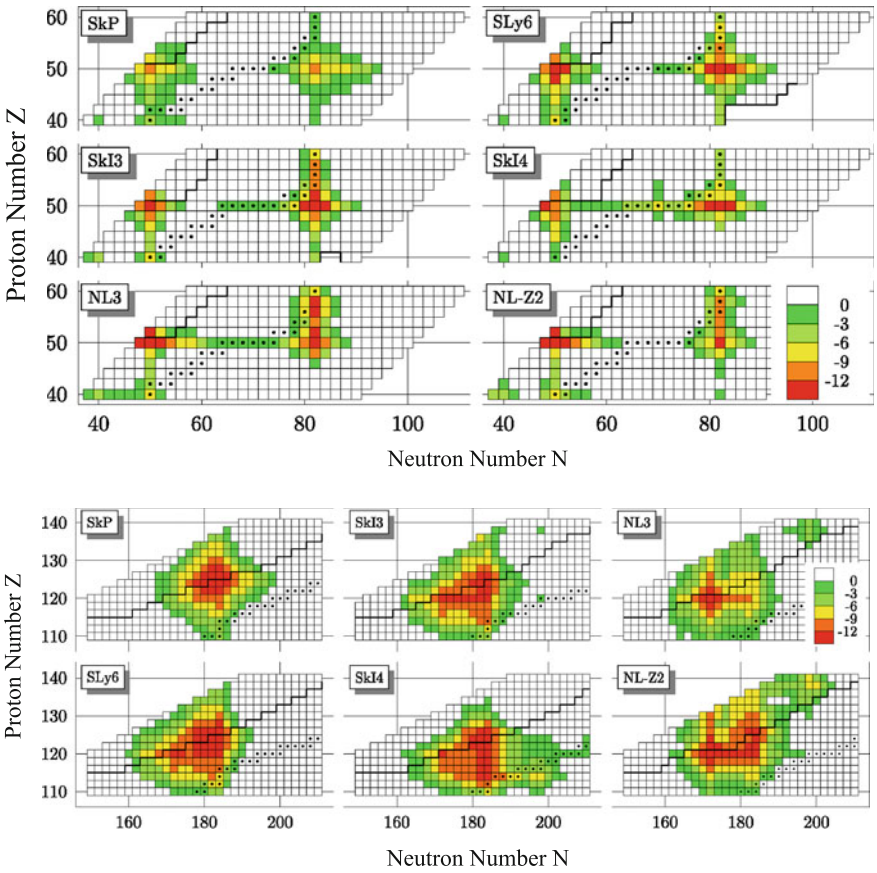

Fig. 8 Shell correction energies for the Sn region (*top*) and the superheavy region (*bottom*) calculated with various interactions. Increasing shell correction energies are colour coded from green (*lowest*) to red (*highest*). The shell stabilization closely traces the magic numbers around Sn while larger islands of stability are formed in the superheavy region. Adapted from [23]

have intermediate energies increasing with increasing Ω, and the resulting levels will still be twofold degenerate in $\pm\Omega$. In the (rare) case of oblate deformation the situation is precisely the opposite, with the nucleon with the largest Ω now circling an equatorial bulge, resulting in this state being lowered by the largest amount.

A complication arises from the possibility of mixing. In a deformed system the states with the same Ω and the same parity can mix leading to a physical state with contributions from several spherical states. For very small and very large deformations this mixing is typically small with a single configuration dominating the wave function. However, for intermediate deformations this mixing can lead to deformed wave functions with large contributions from more than one spherical state. In the Nilsson model the states are therefore labelled with "asymptotic quantum numbers", which become exact only in the limit of very large deformations.

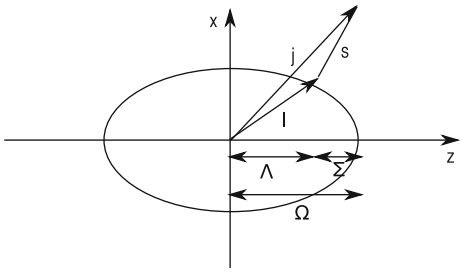

Fig. 9 Schematic representation of the angular momenta in deformed odd mass nuclei and their projections onto the nuclear symmetry axis

The asymptotic labels are given in the form $\Omega^{\pi}[N, n_z, \Lambda]$, see Fig. 9. Here Ω is the projection of the total angular momentum j onto the nuclear symmetry axis, N is the main oscillator quantum number, $\pi = (-1)^N$ is the parity of the state, Λ is the projection of the orbital angular momentum onto the nuclear symmetry axis and n_z counts the number of radial nodes in the wave function. This notation will be used throughout the chapter.

3 Rotational Structure of Nuclei

A spherical nucleus cannot rotate. In order to rotate, the wave function of the system rotated by a small angle α must be distinguishable from the non-rotated wave function. In a spherical system that is impossible and consequently no rotational bands are observed built on spherical configurations, such as the ground states of doubly magic nuclei. A deformed quantum system on the other hand will exhibit rotational behavior. The excitation energy required to set a nucleus rotating is very small compared to the energy required to excite vibrations. Typical excitation energies of the first rotational 2^+ state in superheavy nuclei are only of the order of 40–50 keV. The amount of information available on excited states in superheavy nuclei is rather limited, but has been steadily growing in the last decade. Figure 10 summarises all available information on excited states in nuclei with $Z \geq 96$. While individual rotational levels are often populated in alpha decay, the only rotational bands consisting of several levels observed in nuclei beyond Fm stem from in-beam measurements [27]. It is also obvious that the ground state spins and therefore the ground state configurations are not well determined. The last direct measurement of the ground state spin is in ^{253}Es, where the spin $7/2^+$ was measured directly using laser spectroscopy [28]. All other spins are inferred from systematics and alpha decay chains (see Sect. 5.4).

In this section we first introduce the quantum numbers, notations and conventions usually associated with the description of rotational bands. Then we look at transitions within rotational bands and classify rotational bands according to their K quantum number. We then turn our attention to the influence the

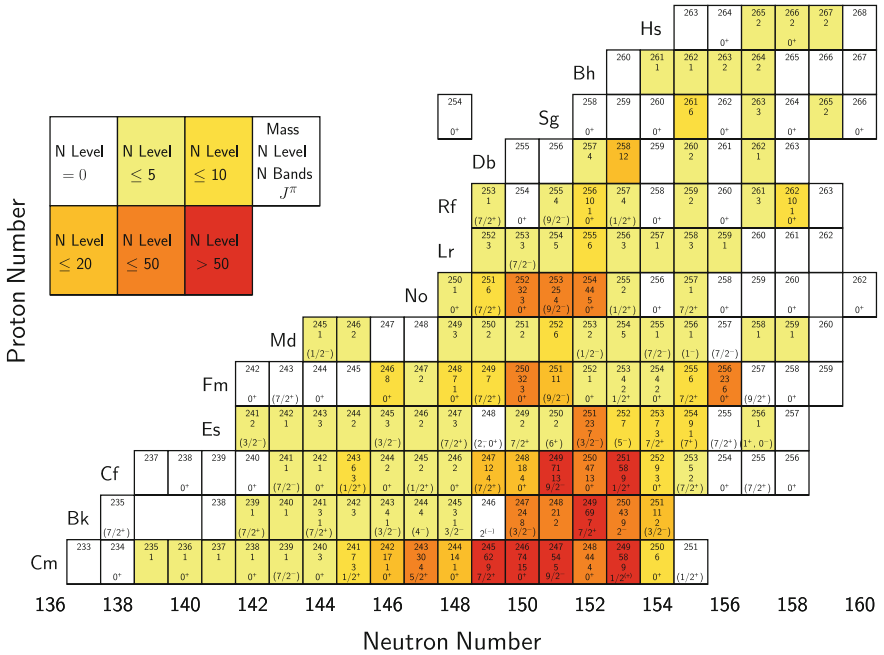

Fig. 10 Summary of experimental information available in the ENSDF data base at the end of 2011 for nuclei from Cm to Hs. The ground state spin, number of known excited levels and number of rotational bands observed are given. In order to help with readability no isotopes with $N > 160$ were included. This figure is an updated version of the one given in [27]

underlying single-particle structure has on the rotational bands, and how this can be used to deduce information about the nucleons responsible. Finally we look at the experimental methods aimed at studying superheavy nuclei.

3.1 Rotational Bands in Even-Even Nuclei

For a definition of the various quantum numbers needed to describe rotational bands we refer to Fig. 11, where we show a well-deformed axially symmetric even-even nucleus. The coordinate axes in the lab system will be labeled with x, y, and z. The coordinate axes in the intrinsic system (in which the nucleus is stationary) are labeled with 1, 2, and 3, with the 3-axis pointing along the symmetry axis.

An intrinsic excitation upon which the rotational band is built, such as, e.g., a vibration or a two-quasiparticle excitation, can be present and is characterized by the projection of its intrinsic angular momentum I on the nuclear symmetry axis. This projection is called the K quantum number. The parity π of the band is also determined entirely by the intrinsic configuration. The entire system can then

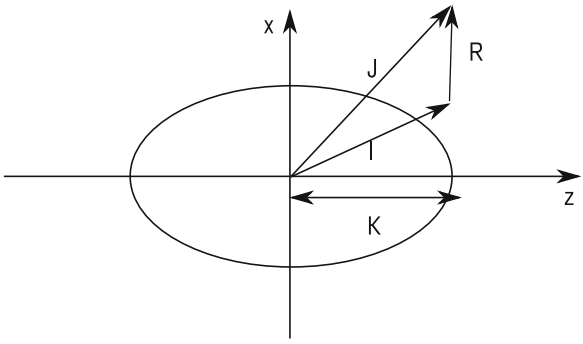

Fig. 11 Schematic representation of the angular momenta in the nucleus. On *top* of an intrinsic excitation with angular momentum I and projection K a collective rotation can be built with orbital angular momentum R. The total angular momentum of the nucleus is J, and all levels in the resulting rotational band have the same K quantum number

exhibit collective rotation around an axis perpendicular to the nuclear symmetry axis with angular momentum R. The total angular momentum J is therefore given by the (quantum mechanically correct) vector sum of $J = I + R$. It is immediately clear that an increase in R can change the length of J, but not K. This has two consequences: A band built on the intrinsic configuration (I, K) will consist of states all of which share the same K quantum number, which is used to characterize the band. Secondly a rotational band with $K > 0$ can not contain a state with angular momentum $J < K$, providing the experimentalist with an easy way to identify K typically as the spin of the bandhead, i.e. the energetically lowest member of the band. The only exception to this rule are negative parity bands with $K = 0$ which have a bandhead spin of $J^\pi = 1^-$.

Figure 12 shows the level scheme of the nucleus ^{254}No. A number of rotational bands is seen, with very different characteristics. The ground state rotational band consists of states with even spins connected by electric quadrupole (E2) transitions. One short band is seen built on a 3^+ state consisting of a characteristic pattern of states with all integer spins greater than three. The sequence 3–5–7 forms one rotational band connected by stretched E2 transitions, as does the sequence 4–6–8. Additionally there are interband transitions $5 \rightarrow 4, 4 \rightarrow 3$ etc. For these transitions both electric quadrupole (E2) and magnetic dipole (M1) transitions are allowed to contribute. The branching ratios of these low-energy transitions carry a lot of information about the underlying structure, which we will exploit in Sect. 4.3. Other bands are seen, and the transitions linking excited bands into the ground state band are indicated. We will return to this level scheme throughout the section as a standard example. In general, rotations are described through the Hamilton operator

$$\hat{H} = \frac{\hbar^2}{2\Theta}\hat{J}^2 \tag{13}$$

where we use Θ as the moment of inertia. This operator has eigenvalues

$$E(J) = \frac{\hbar^2}{2\Theta}J(J+1)\ . \tag{14}$$

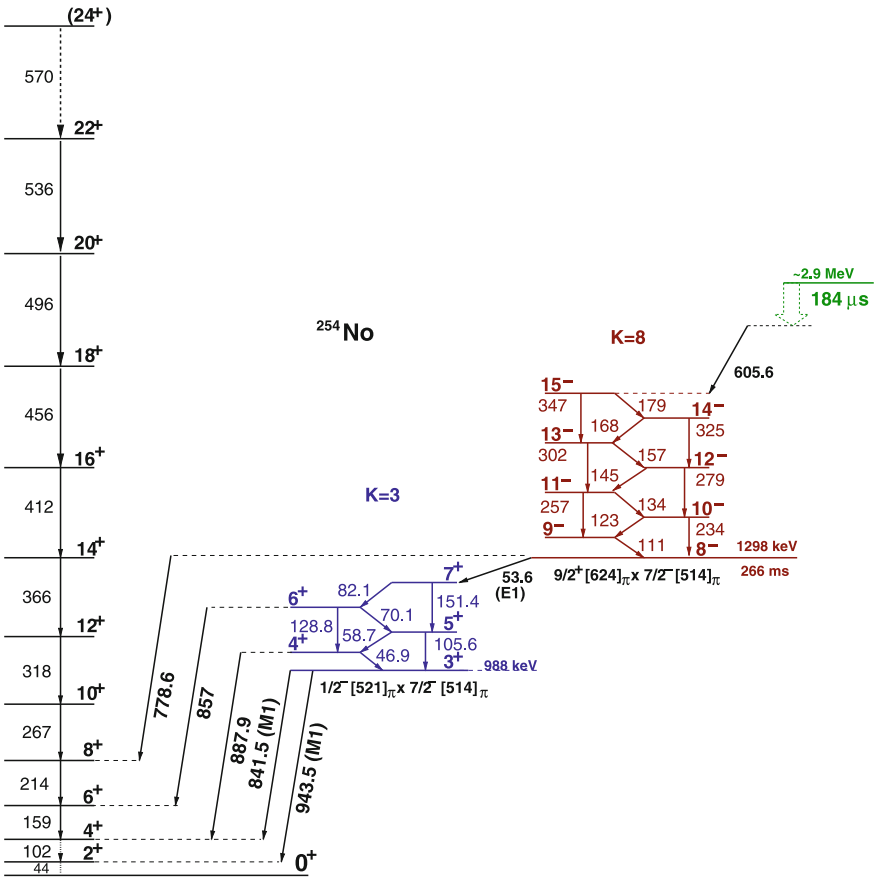

Fig. 12 Level scheme for ^{254}No. The band built on the ground state with spin 0 and $K = 0$ consists of a sequence of stretched $E2$ transitions, while both excited bands are built on configurations with $K > 0$ and consist of both stretched E2 and mixed E2/M1 transitions. The observed branching ratios can be used to determine the underlying nuclear configuration. The numbers give the assigned spins and the energies of the transitions in keV

This leads to a spacing between consecutive levels of the same band of

$$E_T(J \to J-2) = \frac{\hbar^2}{2\Theta}[J(J+1) - (J-2)(J-1)] = \frac{\hbar^2}{\Theta}(2J-1) \tag{15}$$

leading to the characteristic "comb structure" in the gamma spectrum.

We will first restrict ourselves to rotational bands with $K = 0$, such as the ground state rotational bands (gsb) in even-even nuclei. From the level scheme in Fig. 12 we see that the gsb consists solely of levels with even angular momentum, with increasing energetic spacing between them.

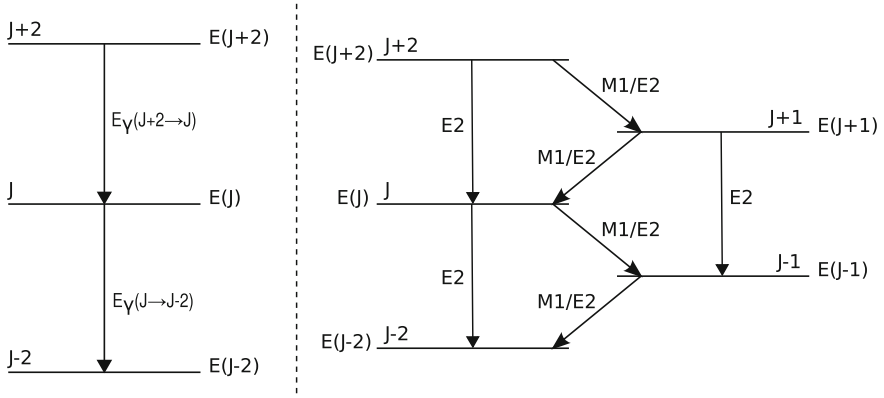

Fig. 13 Definition of labels for transitions in a rotational band. On the *left* we show the case for a single rotational band, e.g., the ground state rotational band in an even-even nucleus. Two stretched electric quadrupole ($E2$) transitions populate and depopulate the band member with angular momentum J. The transition energies E_γ and the level energies $E(J)$ are indicated. On the *right* hand side we show the more frequent case of two strongly coupled bands. Stretched $E2$ transitions connect the members of each band, while the bands are connected by interband transitions of mixed $M1/E2$ character. The branching ratios between the mixed interband transitions and the stretched intraband $E2$ transitions are sensitive to the g-factor of the band-head configuration

To understand the lack of odd spin states we have to look closer at the underlying symmetry. Assume the nucleus has rotated through 180°. From the symmery of the nucleus it is clear that this wave function is now identical to the unrotated one: $|J> = \mathscr{R}(180°)|J>$. However, a closer inspection of the Eigenfunctions (the spherical harmonic functions) of the rotational Hamilton operator shows that they obey the relation $(-1)^J|J> = \mathscr{R}(180°)|J>$. For even spins this is allowed, for odd spins this leads to the condition $|J> = -|J>$, which can only be fulfilled by a wave function identical to 0 everywhere: i.e. no such level can exist. As soon as the symmetry is broken, e.g., by having $K > 0$, this contradiction is removed, and *all* possible values of the angular momentum are realized in the band. However, a band with only even spins immediately leads to the conclusion $K = 0$.

We can now attempt to extract the moment of inertia (MoI) from the observed levels. For this it is useful to define the levels, angular momenta and energies as shown in Fig. 13.

Furthermore, to avoid cluttering the discussion, we restrict ourselves to electric quadrupole transitions and we shall be guided by the relations between energy E, angular frequency ω and moment of inertia Θ found for classical rotations:

$$J = \Theta\omega \qquad \text{and} \qquad E_{rot} = \tfrac{1}{2}\Theta\omega^2 = \tfrac{1}{2}J\omega = \frac{J^2}{2\Theta} \ . \tag{16}$$

The angular frequency can then be found for discrete electric quadrupole transitions as

$$\omega = \frac{J}{\Theta} = \frac{dE}{dJ} \simeq \frac{\Delta E}{\Delta J} = \frac{E_\gamma}{2} \ . \tag{17}$$

We are interested in the MoI that we can attribute to the state with spin J. There are two main ways to extract the MoI from the observed discrete transitions [29]. The kinetic MoI $\mathfrak{I}^{(1)}(J)$ can be extracted from the relationship

$$\frac{\Delta E}{\Delta J} = \frac{1}{2\Theta}[J(J+1) - (J-2)(J-1)] = \frac{2J-1}{2\Theta} = \omega \tag{18}$$

as

$$\Theta = \mathfrak{I}^{(1)} = \frac{2J-1}{2\omega} = \frac{2J-1}{E_\gamma} \ . \tag{19}$$

This form has the advantage that it can easily be assigned to a level from which a single gamma transition is observed. The disadvantage is that the angular momentum of the level has to be known. To get around this limitation it is often convenient to use the dynamic moment of inertia $\mathfrak{I}^{(2)}(J)$ obtained from the relation

$$\begin{aligned} \mathfrak{I}^{(2)} &= \frac{\Delta J}{\Delta \omega} = \frac{2}{\omega(J+2 \to J) - \omega(J \to J-2)} \\ &= \frac{4}{E_\gamma(J+2 \to J) - E_\gamma(J \to J-2)} \end{aligned} \tag{20}$$

In this form one requires no knowledge of the angular momentum, but one needs to have observed two transitions feeding and depopulating the state of interest. One can easily verify that both expressions give identical results for a rigid rotor. However, the rotational properties of a nucleus are not those of a rigid body, but more akin to a nonrotating superfluid [30], which leads to deviations from the rigid rotor results. In particular one finds that the MoI is typically only about half that of a rigid rotor and that the MoI increases as one breaks pairs of nucleons. At the highest excitation energies where several pairs of nucleons have been broken, the MoI approaches a significant fraction of that of the rigid body.

A number of approaches are used throughout the literature to describe this variable MoI. We shall use the one proposed by Harris [31] where the dynamic MoI is expanded as a power series in ω

$$\mathfrak{I}^{(2)} = A + B\omega^2 + C\omega^4 + \ldots \tag{21}$$

The angular momentum of a state can then be found (up to a constant) through integration

$$I = \int \mathfrak{I}^{(2)} d\omega = A\omega + B\omega^3 + \cdots + const. \tag{22}$$

For even-even ground state bands the additive constant is $1/2$, but in general it is not straightforward to deduce reliable spins through this method [29]. However, this approach is often useful to give an indication of the expected angular momentum and can be used in conjunction with other experimental constraints to construct a coherent level scheme.

The Harris fit is also useful to extrapolate a rotational band to unobserved transitions. In the transfermium region the lowest transitions are typically so highly converted that they can not be observed through gamma spectroscopy (see the discussion in Sect. 5). In these cases it is useful to extract the Harris parameters A and B from a fit to the observed MoIs in the ground state rotational band, and solve for the frequency corresponding to the angular momentum of the missing state. In this way the $4^+ \rightarrow 2^+$ and $2^+ \rightarrow 0^+$ energies of various No and Fm nuclei were extracted [27].

3.2 Backbending and Alignment

So far we have treated the rotating nucleus as a body without internal structure, a description that ignores the fact that the nucleus is made up of nucleons which themselves have angular momentum and will therefore interact with the rotating frame via the Coriolis interaction. The Coriolis interaction will act in a way to align the angular momenta of all components of the system with that of the collective rotation. The net effect is one where the nucleus can generate a higher angular momentum without having to spin faster, simply by breaking a pair of nucleons and adding the intrinsic angular momentum of these nucleons to its collective rotation. This effect shows up in a plot of angular momentum versus rotational frequency as a distinctive backbend.

The Coriolis force in a nucleus rotating with angular momentum R acts on a pair of particles with single particle spins j coupled to a pair with total spin $J = 0$. In this pair the nucleons occupy time reversed orbits, i.e. their angular momentum vectors point in opposite directions. It is now clear that the Coriolis force will act differently on the two nucleons trying to align both spins with the collective rotation, effectively breaking the pair and adding $2j$ to the total angular momentum. From the shape of the Coriolis force it is clear that this will happen to those nucleons with the largest spins first, e.g., in the well deformed region around nobelium these are the $j_{15/2}$ neutrons and the $i_{13/2}$ protons.

Figure 14 shows a collection of the measured dynamic MoIs for Pu, Cm, Cf, Fm and No nuclei showing distinct upbends around a rotational frequency of 200 keV in all nuclei, yet it also shows individual differences between nuclei. If we examine the cases of ^{252}No and ^{254}No, we note that the MoI increases more steeply in ^{252}No than in ^{254}No [32]. This behavior can be traced directly to the underlying nucleon configurations and through comparisons with model calculations one sees that in both cases an alignment of $i_{13/2}$ protons and $j_{15/2}$ neutrons is expected. However,

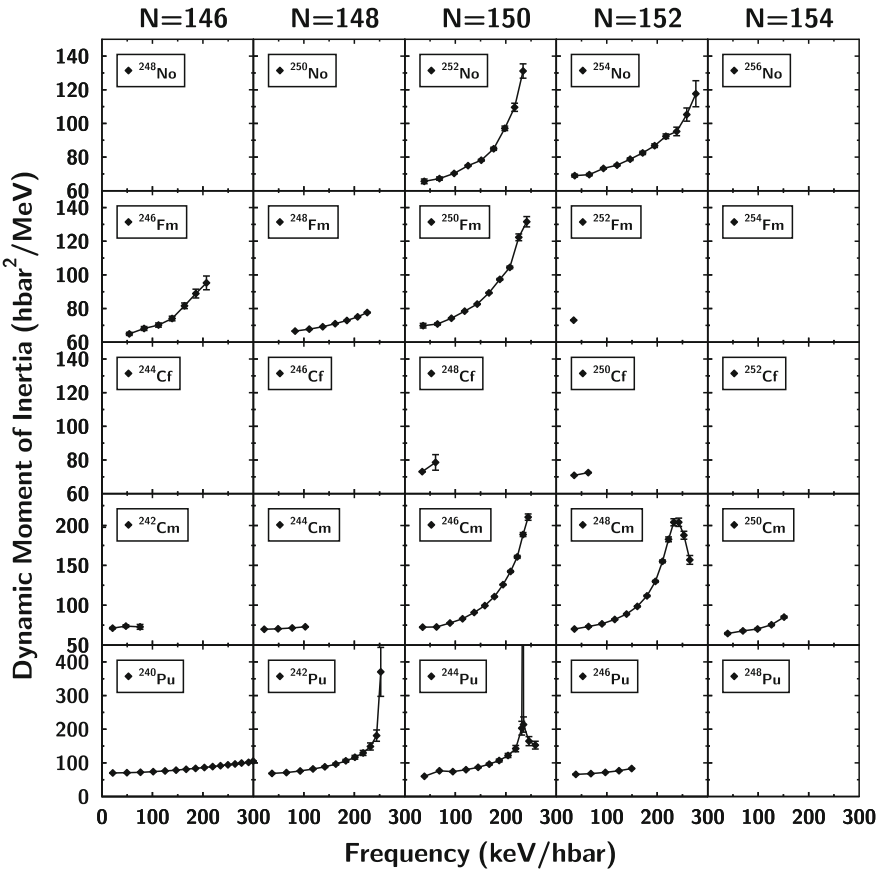

Fig. 14 Moments of inertia for Pu, Cm, Cf, Fm and No nuclei. Upbends around a frequency of 200–300 keV show the alignment of pairs of nucleons with the highest orbital angular momenta (see text). Figure adapted from [27]

in ^{254}No this alignment is expected to occur at the same frequencey, while in ^{252}No the $j_{15/2}$ neutrons are expected to align first. Thus in ^{254}No the available rotational energy is required to account for the breaking and alignment of both pairs and consequently the process is spread out over a larger number of transitions in ^{254}No. This sensitivity of the MoI to the underlying shell structure means that one can get a surprisingly accurate experimental handle on the shell structure simply by observing a number of rotational states, the energies of which are easily extracted with good accuracy in modern gamma ray spectrometers.

The energies of transitions in rotational bands can further be exploited to extract the aligned angular momentum to directly measure the spin of the particle aligning. This requires measurements that go beyond the alignment frequency,

which have not yet been possible for nobelium nuclei. However, in well deformed rare earth nuclei long rotational bands often with more than one backbend can be found.

4 Single Particle Structure of the Nucleus

The ultimate goal of any nuclear structure investigation on a heavy nucleus is to learn something about the underlying single particle structure that is responsible for the added stability at the top end of the Periodic Table. This endeavor is made more complicated by the fact that the single particle structure changes significantly with deformation. As deformed, heavy actinide nuclei are currently providing the bulk of the experimental data on single particle excitations, it is important to understand how one can draw conclusions about spherical levels from a study of deformed ones. This section gives an overview of single particle and quasi-particle states, g-factors and nuclear isomerism.

4.1 Pairing and Quasi Particle States

The shell model describes the nucleus as a system of independent particles coupled by a residual interaction. This residual interaction is generally complicated, but in the case of particles with the same spin j it takes a particularly simple form. Figure 15 shows the schematic level scheme of a pair of $h_{9/2}$ protons, compared with the experimentally observed level scheme of ^{210}Po, which, in the shell model, is described as two $h_{9/2}$ protons outside a closed ^{208}Pb core. In general this energy gained through pairing leads to all nucleons in the nucleus being paired

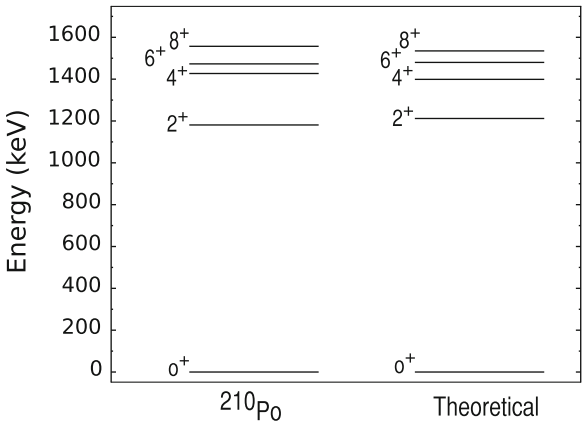

Fig. 15 Schematic level scheme for a pair of $h_{9/2}$ protons (*right*) compared to the low lying levels in ^{210}Po (*left*)

and exciting configurations will involve the breaking of pairs. The situation becomes more complicated in deformed nuclei where the shells lose their degeneracy in j. The minimal energy for the ground state of such nuclei then usually involves a probabilistic distribution of particles across a large number of states, and the description of excitations must take this complicated ground state into account.

The situation can be greatly simplified by translating into a basis where we replace a system of strongly interacting particles by one of non-interacting quasiparticles by means of the Bogoliubov transformation. The details shall be left to the reader to find in one of the many undergraduate textbooks available (e.g., [8–10]), here we shall concentrate on the interpretation.

The Hamilton operator can be written in three terms:

$$\hat{H} = \hat{H}_0 + \hat{V}_{pair} - \lambda \hat{N} \, . \tag{23}$$

The first term accounts for the energy of the independent particles making up the nucleus, the second term describes the interaction between two pairs of particles, and the third term is required to keep the particle number in the nucleus correct. Thus the problem must be solved under the condition that the expectation value of the particle number coincides with the number of particles in the nucleus.

The effect of this transformation is the emergence of quasiparticles which can now take the roles of the independent particles. The correlations introduced by the pairing interaction have been taken into account, at the price of somewhat modified energies of the quasiparticle states. When solving the BCS[1] equations we also find a gap parameter Δ, which in heavy nuclei typically has values $\Delta \simeq 0.5$–0.8 MeV, and is associated with the strength of the particle-hole correlations near the Fermi level, which in this pairing picture is given by the parameter λ.

If the original single particle energies are denoted by ε_i, the Fermi level by λ and the gap parameter Δ, the energy of the corresponding quasiparticle is given by

$$E_i = \sqrt{(\varepsilon_i - \lambda)^2 + \Delta^2} \tag{24}$$

A particle-hole excitation in the presence of pairing can now easily be described by a two-quasiparticle excitation, where the excitation energy of the final state is simply given by the sum of the quasiparticle energies

$$\Delta E = E_i + E_j = \sqrt{(\varepsilon_i - \lambda)^2 + \Delta^2} + \sqrt{(\varepsilon_j - \lambda)^2 + \Delta^2} \geq 2\Delta \, . \tag{25}$$

For energies far from the Fermi level this reduces to the original energy of the particle and the hole, but for excitations near the Fermi surface a minimum energy of 2Δ is required. This is easily seen in Fig. 16 where the low-lying levels of

[1] Named after the scientists who first used this type of pairing to explain superconductivity, J Bardeen, L N Cooper and J R Schrieffer.

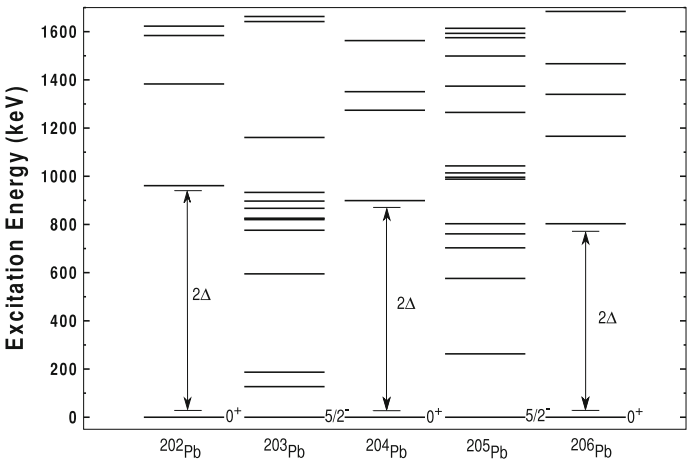

Fig. 16 Low-lying excitation spectra of Pb isotopes. The effects of the pairing interaction are clearly seen in the even isotopes

$^{202-206}$Pb are plotted. In even nuclei the pairing gap is clearly visible, whereas in odd nuclei the single particle spectrum can start at much lower excitation energies.

In well deformed nuclei the two-quasiparticle states retain another property, namely the projection of the contributing spins on the nuclear symmetry axis, K. This means the occurrence of states with large values of K becomes common and can often lead to K-isomerism, which will be discussed later.

4.2 Nuclear g-Factors

Both protons and neutrons carry a magnetic moment. While this is immediately obvious for a rotating charge distribution such as the proton, it is important to remember that this magnetic moment is generated by the charged quarks making up the nucleons. Therefore all constituent nucleons carry a magnetic moment in addition to the bulk magnetic moment of the rotating nucleus itself. The magnetic properties of a state therefore provide us with an experimental handle that we can use to determine the underlying single particle configuration. For a nucleus consisting of hundreds of nucleons this looks to be a daunting task. However, the situation is greatly simplified through the effects of pairing, namely the fact that the nuclear magnetic moment of a pair of nucleons coupled to spin $J = 0$ vanishes. This means that an even-even nucleus has no magnetic moment in its ground state, and the magnetic moment of the ground state of an odd mass nucleus is determined by the magnetic moment of the unpaired particle.

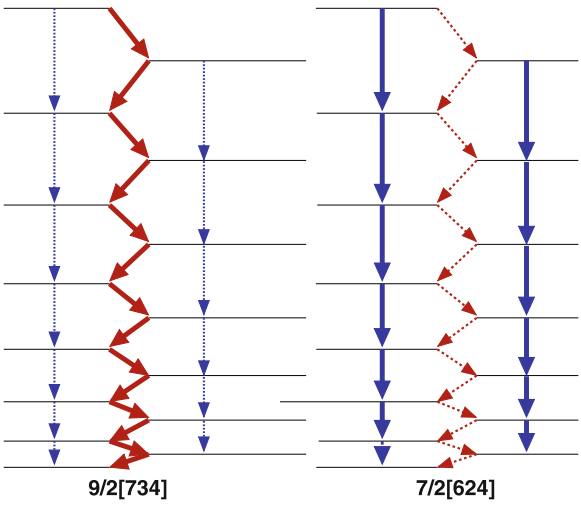

Fig. 17 Predicted intensity pattern in the ground state band of ^{253}No for two different ground state configurations. For the $9/2$ configuration $M1$ interband transitions are dominant whereas for the $7/2$ configuration the $E2$ transitions carry the majority of the intensity. Adapted from [33]

The magnetic moment μ of a spinning charge distribution is proportional to the angular momentum, $\boldsymbol{j}$. The proportionality is given by the g-factor, and the magnetic moment is measured in nuclear magnetons $\mu_N = e\hbar/2m_p$:

$$\mu = g\boldsymbol{j}\,\mu_N\ . \tag{26}$$

The situation is complicated for nucleons as they carry both orbital angular momentum and intrinsic spin, leading to complex expressions for the g-factors. However, they can be calculated readily, and then compared to the observed values to make structural assignments. We will refer to the g-factors due to the individual nucleons as g_K, and to the g-factor due to the nucleus rotating as a whole as g_R. Since only the protons contribute to the magnetic moment of the rotating nucleus we use $g_R \simeq Z/A$ as a good approximation [30].

The experimental handle is then provided by the gamma ray branching ratios between $M1$ and $E2$ transitions in a rotational band built on a state with a g-factor g_K. The intensities of the magnetic dipole transitions are proportional to $(g_K - g_R)^2$, while those of the electric quadrupole transitions are proportional to the electric quadrupole moment Q^2, which does not tend to vary greatly between bands in a given nucleus as it is associated predominantly with the shape of the nucleus as a whole.

Using the definitions of spins and transitions shown in Fig. 13 we find that the branching ratio for gamma transitions depopulating the level with spin J is proportional to $[(g_K - g_R)/Q]^2$, and thus the single particle configuration of the state the band is built upon can be determined by measuring gamma branching ratios in a rotational band. This is illustrated in Fig. 17 where the expected behaviour of the ground state rotational band in ^{253}No is plotted for two different ground state configurations. The $9/2^-[734]$ configuration has a g-factor $g_K = -0.24$ while the

$7/2^+[624]$ configuration has $g_K = 0.28$. Together with $g_R = Z/A \simeq 0.4$ the branching ratios should favour $M1$ transitions for the $9/2^-[734]$ configuration and $E2$ transitions for the $7/2^+[624]$ configuration. Indeed experimental branching ratios favour the $9/2^-$ configuration [34].

4.3 Nuclear Isomers

The half-life of excited nuclear states is typically of the order of picoseconds. However, sometimes one can observe states with significantly longer half-lives, nuclear isomers. In extreme cases the half-life of the isomeric state can exceed the half-life of the ground state. Take as an example the case of ^{180}Ta. This is one of the rarest isotopes that can be found in an isomeric state naturally on earth, where it is to all intents and purposes stable with a half-life $T_{1/2} > 1.2 \times 10^{15}$ y. However, its ground state decays rapidly with a half-life of only $T_{1/2} = 8.125$ h.

To explain isomerism we turn to Fermi's Golden Rule which relates the transition rate to the wave functions of the initial and any final states as well as the density of final states in a given energy interval. In short, a decay can only happen if a suitable final state exists, and, if it does, the transition rate is higher the more the wave function of the final state resembles that of the initial state. We therefore expect isomers to occur in several classes:

Shape Isomers can be found in the second minimum of the fission barriers of actinides. If the nucleus is prepared in the lowest state in the second minimum it is much more deformed than in any of the states in the first minimum. Thus any transition out of the second minimum will require the rearranging of all nucleons, which leads to the observed very small matrix elements and thus the formation of an isomeric state. These isomers are also known as fission isomers.

Spin traps are formed by states which have no states with comparable spins and parities at lower energy that they can decay to. The gamma decay selection rules then lead to very long half-lives as the decays have to proceed through transitions with very high multipolarity. This situation is common in odd–odd nuclei. The above example of ^{180}Ta is such a case where the isomer at an excitation energy of 75 keV above the ground state has a spin $J^\pi = 9^-$ while the ground state itself has spin $J^\pi = 1^+$ requiring an $M8$ transition between them.

K Isomers are the nuclear analogues to the bicycle. They form when the K quantum number has to change during a transition, which requires a change of the orientation of the angular momentum vector. K isomers are found, e.g., when two quasiparticle states with large K form as the lowest quasiparticle excitations. This situation is the most common one in the regions around Hf and No [41].

It is instructive to look at the occurrence of isomers in heavy nuclei. Figure 18 shows the longest lived isomers known in all nuclei from Pb onwards [35]. The heaviest listed nucleus is ^{270}Ds which has an isomer with a half-life $T_{1/2} = 6.0^{+8.2}_{-2.2}$ ms, while its ground state has a half-life $T_{1/2} = 100^{+140}_{-40}$ μs [42].

Fig. 18 Longest lived isomer known in all nuclei above $Z \geq 82$. The size of the symbols indicate half-lives. Figure reproduced from [35] with permission. Copyright 2011 Oldenburg Wissenschaftsverlag GmbH

To us isomerism raises an important question: "Can nuclear isomerism lead to the natural occurrence of superheavy elements in an isomeric state?" This has been a question of much interest recently, see, e.g., [41]. If isomeric states in the region around hafnium and tantalum can live for geological timescales, why should similar isomers not occur in the superheavy region? The neutron numbers in the Hf region are between 100 and 110 with the last neutrons occupying the same orbitals occupied by protons in heavy actinide and transactinide nuclei. Thus conditions in the superheavy region may very well allow long-lived isomeric states that give some hope to find superheavy elements in nature.

4.4 Deformed Gaps

The main focus on shell gaps in the study of superheavy elements has always been the next spherical shell closure for protons and neutrons. However, since the majority of heavy and superheavy nuclei are well deformed, it is also important to understand the effects of deformed shell closures in lighter systems. Here too doubly magic systems can be found, albeit with a different understanding of the magic character.

In Sect. 2.3 we discussed the effect of large energy gaps (see, e.g., Fig. 8) and found that the magic character was not so much down to the large energy gap between two levels, but ultimately the important quantity was the level density, with a low level density leading to extra stability. In the deformed shell model the degeneracy in total angular momentum j is lifted and the state j splits into $(j + 1/2)$ individual components characterized by the projection on the nuclear

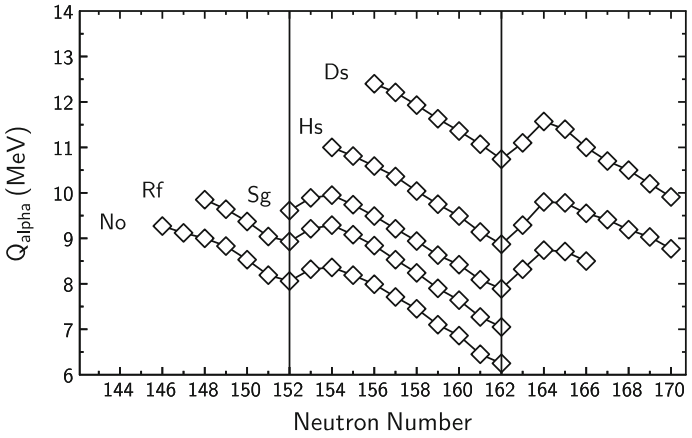

Fig. 19 Q-values calculated with the macroscopic-microscopic model versus neutron number. Data taken from [36, 37]

symmetry axis Ω. Thus, in deformed nuclei the level density appears to be much higher to begin with. However, each level now holds at most two nucleons and any gap in a Nilsson diagram directly leads to a low level density and therefore added stability.

In the region above $Z \simeq 100$ such gaps appear for neutron numbers 152 and 162 as well as proton number 108 (Hs). One consequence of this deformed gap is the occurrance of a local minimum in the alpha decay Q-value at 152 and 162 with local maxima at $N = 154$ and 164 respectively. In Fig. 19 we plot theoretical Q-values from [36, 37] in the region. The dips at $N = 152$ and 162 are clearly visible.

One would therefore expect the nucleus ^{270}Hs to exhibit all the characteristics of a nucleus with extra shell stabilization. This nucleus has recently been synthesized [38, 39] and its decay properties are indeed similar to those predicted.

Other indications of the deformed gap at $N = 152$ come from isomer spectroscopy. In a series of experiments the lowest excited isomeric states in ^{252,254}No and ^{250}Fm were investigated. The $N = 150$ isotones were assigned a neutron configuration while in the $N = 152$ isotope ^{254}No a proton character was established [22, 40]. This is entirely in line with the expectations from theory and supports the conclusions drawn from Q-values alone. Figure 20 shows the energies of the single particle states that play an important role around ^{250}Fm. Note that both protons and neutrons find pairs of levels close to the fermi level that can couple to low-lying states with high K, such as $(9/2^-[734]_\nu \otimes 7/2^+[624]\nu)^{8^-}$ for neutrons, or $(9/2^+[624]_\pi \otimes 7/2^-[514]_\pi)^{8^-}$ and $(7/2^-[514]_\pi \otimes 7/2^+[633]_\pi)^{6^-}$ for proton pairs. In systems with neutron number $N = 158$ one might reasonably expect high K configurations such as $(11/2^-[725]_\nu \otimes 7/2^+[613]_\nu)^{9^-}$ to form low lying isomeric states.

5 Experimental Techniques

The recent progress in nuclear spectroscopy techniques coupled with ever increasing sensitivities has allowed the full arsenal of in-beam nuclear spectroscopy techniques to be unleashed on heavier and heavier systems, produced with ever smaller cross sections. At the time of writing nuclei produced with cross sections as small as a few tens of nb can be studied.

These in-beam techniques are well established as sensitive tools in their own right and, when used for structure studies in superheavy nuclei, are generally complementary to decay studies following alpha or beta decay. In this section we will first look at the experimental conditions for in-beam gamma and electron spectroscopy, before discussing alpha spectroscopy and gamma spectroscopy after alpha decay.

5.1 Experimental Facilities

Experimental setups to study superheavy elements consist primarily of a recoil separator together with detector assemblies at the focal plane for discovery and decay experiments as well as surrounding the target position in case of in-beam studies. Detailed descriptions of each setup currently used in the world are available in the literature. Here we will focus on one example for a setup to explain the roles of the various detector systems in detail before summarising the properties of other widely used setups in a table.

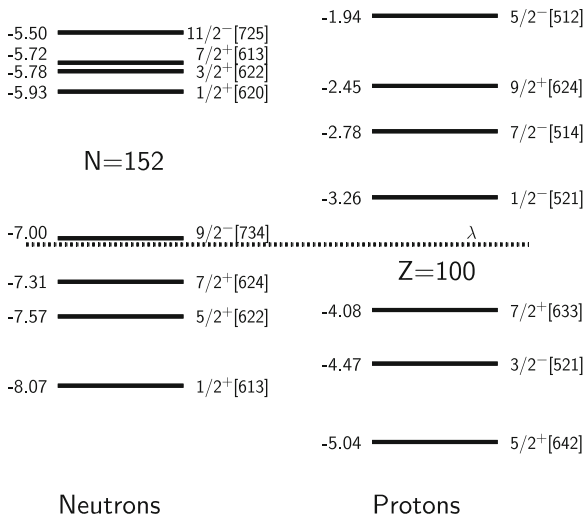

Fig. 20 Single particle energies for ^{250}Fm calculated using a Woods-Saxon potential with "universal" parametrization. The Fermi level is indicated by a *dashed line*. Adapted from [27]

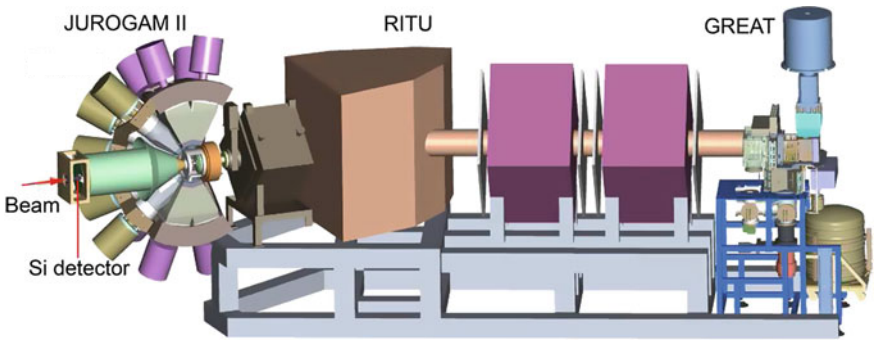

Fig. 21 Experimental in-beam spectroscopy setup at the Accelerator Laboratory of the University of Jyväskylä in Finland. The SAGE spectrometer [43] consisting of a Si detector and a solenoidal magnetic field together with the Jurogam II germanium detector array is on the *left* in front of the recoil separator RITU [44]. The focal plane of RITU is instrumented with the GREAT spectrometer [45]

Figure 21 shows a typical setup at the University of Jyväskylä, Finland. The centrepiece is formed by the gas-filled separator RITU [44], which has a transmission efficiency of approximately 40% for heavy evaporation residues while suppressing the primary beam and unwanted reaction products, e.g., from transfer reactions by more than eight orders of magnitude. The focal plane of RITU is equipped with the GREAT focal plane spectrometer [45]. Reaction products are implanted in two double-sided silicon strip detectors (DSSD) giving a total of 4800 pixels. In front of the implantation detectors sits a Multiwire Proportional Counter (MWPC) to measure the time of flight between the MWPC and the DSSD as well as the energy loss of the incoming ions and several PIN diodes forming a box in the forward direction to measure escaping alpha particles.

These elements are the minimum requirement for superheavy element research: a separator and a means to identify the reaction products. Alternatively a gas catcher is commonly used as a first stage for the transport to specialist detectors for chemical studies or transport to a trap. More details on gas-jet transport systems are given in "Synthesis of Superheavy Elements" and "Experimental Techniques".

For spectroscopy following decay this setup is extended by a variety of germanium detectors surrounding the implantation detector. In the GREAT spectrometer a segmented planar Ge detector is mounted in close proximity behind the DSSD to measure the X-rays and low energy gamma rays emitted at the focal plane. The whole setup is surrounded by several Clover detectors to measure the gamma rays emitted in the focal plane.

For in-beam studies the prompt radiation given off at the target position in front of the recoil separator has to be measured. In our example the detection of both gamma rays and conversion electrons is possible through the combination of the JUROGAM II array with a silicon detector forming the Silicon and GErmanium (SAGE) array. The JUROGAM II germanium array consists of 24 Clover detectors and 30 large single-crystal detectors with a total efficiency of 5.2% at 1.3 MeV.

Table 2 Experimental setups with recoil separators used in laboratories around the world for the study of superheavy elements.

Location	Separator	Configuration	Focal plane instrumentation	In-beam spectroscopy
Darmstadt GSI	SHIP [46, 47]	QQQEDDDDEQQQD[1] vacuum velocity filter	Recoil ID Ge detectors SHIPTRAP [48]	No
	TASCA [49]	DQQ gas-filled separator	Recoil ID Ge detectors (TASISpec) [50] chemistry	No
Dubna FLNR	VASSILISSA [51, 52]	QQQEEEQQQD vacuum E/q separator	Recoil ID Ge detectors (GABRIELA) [53]	No
	DGFRS [54, 55]	DQQ gas-filled separator	Recoil ID chemistry	No
Berkeley LNL	BGS [56]	QGD gas-filled separator	Recoil ID Ge detectors chemistry	GRETINA [57] gamma detection
Argonne ANL	FMA [58]	QQEDEQQ vacuum, mass analyser	Recoil ID Ge detectors	GAMMASPHERE [59, 60] gamma detection
Wako RIKEN	GARIS [61, 62]	DQQD	Recoil ID chemistry	No
Jyväskylä	RITU [44]	QDQQ gas-filled separator	Recoil ID Ge detectors	JUROGAM II [63] gamma detection SAGE [43] gamma and elecron detection

[1] *Q* quadrupole magnet; *D* dipole magnet; *E* electric field; *G* gradient field dipole magnet

A large number of experimental setups exist around the world that are optimized for the study of superheavy elements. The detailled description of each of them could easily fill a full chapter in this book. We shall therefore restrict ourselves to just list them here and give references where the interested reader can find more details. The information is summarized in Table 2. A more detailled overview of the setups relevant for in-beam gamma spectroscopy can be found in [27].

5.2 In-Beam Spectroscopy

In-beam spectroscopy has been the main tool used to uncover the structure of nuclei in great detail. Sophisticated methods to experimentally determine spins, parities, and underlying single particle configurations have been developed over many years and have allowed the detailed investigation of large and complex level

schemes of most nuclei. However, it is not straightforward to unleash this arsenal of spectroscopic tools in order to gain insights into the structure of nuclei with $Z \geq 100$. The main reason is the low cross section of the channel of interest relative to the total reaction cross section. One of the most favourable cases is the reaction of ^{48}Ca on ^{208}Pb which leads in the two-neutron evaporation channel to the production of ^{254}No with a cross section of 2 μb. To pull this weak channel out of the total reaction cross section of a few hundred mb, one has to employ recoil separators in order to identify those reactions leading to the channel of interest. This is not a problem unique to superheavy element spectroscopy. Whenever an experimental handle on a weak channel is required one is faced with the same principal problems. Thus a typical in-beam spectroscopy setup consists of a prompt gamma spectrometer, usually made up out of a large number of Compton suppressed Germanium detectors, coupled to a recoil separator with a suitable focal plane that allows the detection of the recoils of interest. If the focal plane of the separator is further equipped with a detector that allows the identification of the recoils via their characteristic alpha decays, one can employ Recoil Decay Tagging to pull very weak channels out of the background on an event-by-event basis.

The recoil decay tagging (RDT) technique is explained in Fig. 22, top panel. At time 0 a nuclear reaction happens at the target position and the emitted gamma rays are recorded in the Ge-array. The heavy recoil of interest then enters the separator and is transported to its focal plane with a flight time of a few microseconds, where it is implanted in a position sensitive focal plane detector. After a further time, the implanted recoil decays depositing the characteristic alpha decay energy in the same pixel. It is now possible to first use the spatial correlation to identify the implanted nucleus and then to use the well-defined flight time to identify the gamma rays emitted by this nucleus. The three spectra shown in Fig. 23 are taken at various stages of the RDT procedure. In the top panel all gamma rays observed in the reaction of ^{36}Ar on ^{144}Sm leading to a compound nucleus ^{180}Hg are shown [64]. The reaction is dominated by fission and transfer. None of the fission fragments and transfer products reach the focal plane of the recoil separator. The main reaction channel reaching the focal plane is the 2p-2n evaporation channel leading to ^{176}Pt. In the middle panel of Fig. 23 the gamma rays associated with all recoiling nuclei reaching the focal plane are shown. The ground state band of ^{176}Pt dominates the gamma spectrum. The channel of interest in the experiment, however, is the 4n evaporation channel leading to ^{176}Hg. This channel has only a small fraction of the total cross section. If one now further demands that the implanted recoil is followed within 60 ms by the characteristic alpha decay of ^{176}Hg, one obtains the spectrum shown in the bottom panel. As the gamma rays can be identified on an event-by-event basis, this spectrum of ^{176}Hg is extremely clean.

The situation for in-beam spectroscopy of superheavy elements is somewhat different. In the reaction of ^{48}Ca on ^{208}Pb typically only a single channel is open, i.e. the 2n channel leading to ^{254}No. Here the RDT technique is not used to pull a weak gamma ray signal out of an overwhelming background, but to ensure that the

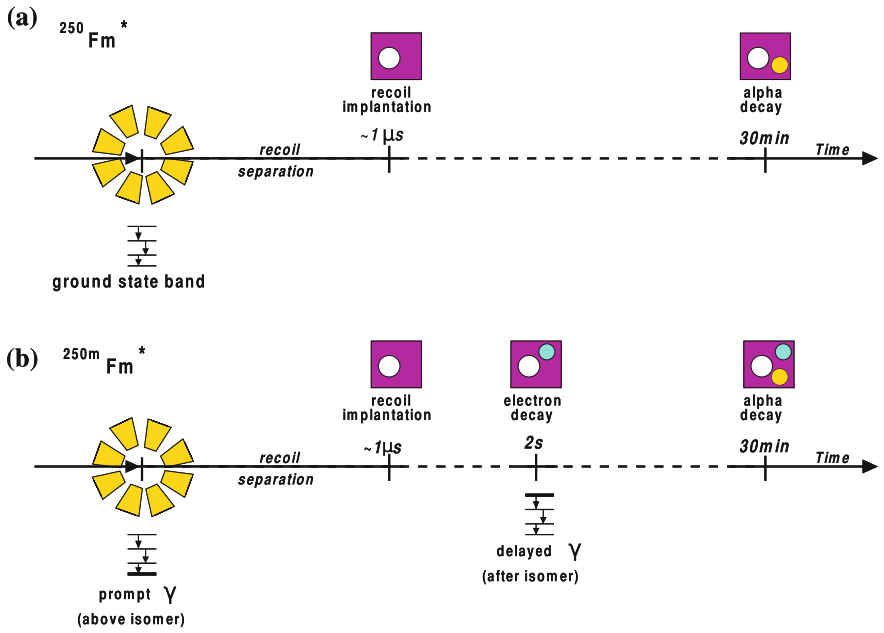

Fig. 22 Schematic illustration of the RDT technique. Prompt gamma rays are observed at the target position. The nucleus then recoils out of the target and flies through the separator where it is implanted in a Si detector. After a while the nucleus decays by a characteristic alpha decay in the same position, identifying the earlier implant. In the *bottom* panel a calorimetric electron signal additionally indicates the decay of an isomeric state

obtained spectrum is really associated with the nucleus in question. Figure 24 shows the gamma spectrum in coincidence with a recoil at the focal plane (top) and the gamma spectrum in coincidence with a recoil at the focal plane which has been correlated to a characteristic ^{254}No alpha decay taking place within 3 min after the implantation in the same pixel (bottom). The ground state rotational band is clearly visible. The intensity falls off for the lower spin members of the band as internal conversion begins to take over (see also Fig. 25). Thus the observed intensity maximum is at the $8^+ \rightarrow 6^+$ transition, and the $4^+ \rightarrow 2^+$ and $2^+ \rightarrow 0^+$ transitions can not be observed in gamma rays.

In the same way as the alpha tag one can use any decay signal at the focal plane to tag a particular reaction channel. The main application has been to tag on isomeric states in the recoiling nucleus. The principle shown in the bottom panel of Fig. 22 is as follows. If an isomeric state with a half-life longer than the flight time through the separator is populated in the reaction, then the isomeric state will decay after the nucleus has been implanted in the focal plane. When the isomer decays an energy signal is left in the implantation pixel from internal conversion electrons, low-energy X-rays, and Auger electrons. This signal is large enough to be detected and will eventually be followed by the ground state alpha decay. Thus

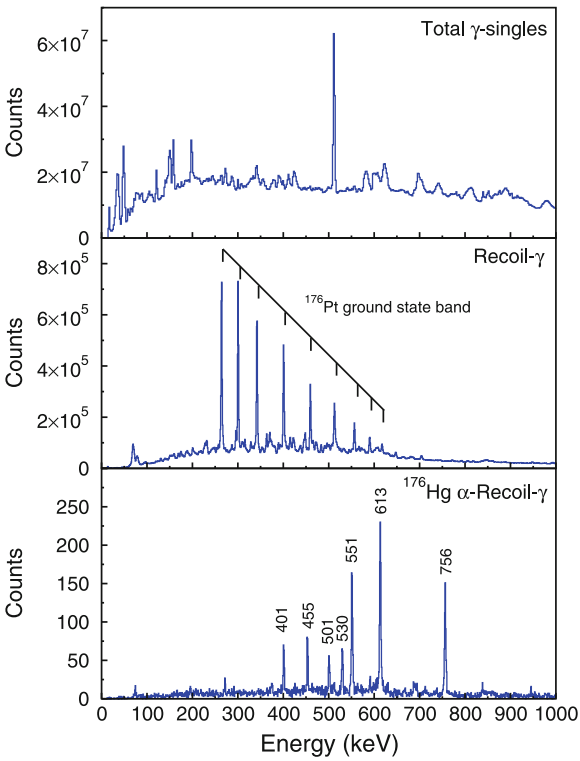

Fig. 23 Illustration of the RDT technique. The *top* panel shows all gamma rays emitted in the reaction of ^{36}Ar on ^{144}Sm. The *middle* panel shows all gamma rays associated with recoiling nuclei reaching the focal plane of the separator. The main reaction channel leading to ^{176}Pt is pulled out of the background. In the *bottom* panel only those gamma rays associated with implanted nuclei followed by the characteristic alpha decay of ^{176}Hg are shown [64]. Note the different scales on the axis. This technique is able to identify gamma rays belonging to a particular reaction channel on an event-by-event basis, which makes it so powerful

the characteristic sequence of implant, low-energy signal, and alpha decay can be used to identify isomers, and, analogous to the RDT technique, pull out the transitions populating the isomer from the prompt radiation measured at the target position. This process is illustrated in Fig. 26 for the decay of two isomeric states in ^{254}No [22]. The top two panels show the electron signals together with their time distributions. The short lived 184 μs isomer feeds mainly into the longer lived 266 ms isomer, and both gamma decay patterns are easily extracted through coincidence with the observed electrons (bottom panels).

5.3 Internal Conversion Electrons

In the heaviest nuclei transitions between excited states are dominated by internal conversion electron emission over gamma emission. It is important to realize that the emission of conversion electrons is a direct process, and does not proceed via an intermediate gamma ray. This is mainly due to the increased probability of finding an atomic electron (its wave function) inside the nucleus where energy can be transferred to it directly. We define the internal conversion coefficient α as the ratio of the number of electrons that get emitted to the number of gamma rays emitted during the decay of a sufficiently large ensemble:

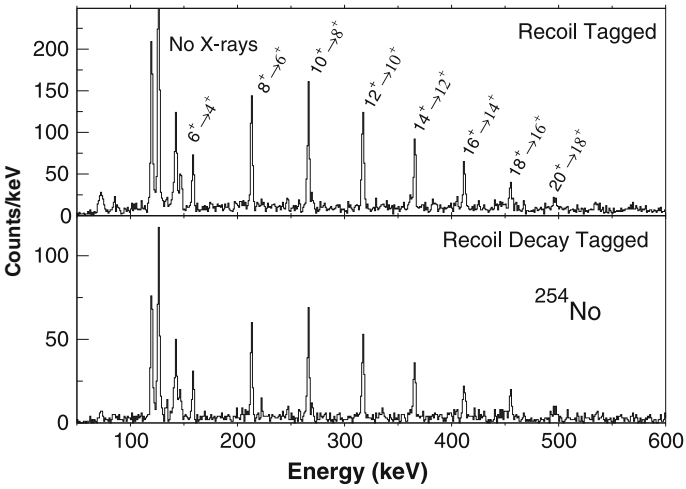

Fig. 24 Gamma ray spectra showing the ground state rotational band of ^{254}No. The *top* spectrum shows all gammas associated with recoils at the focal plane of RITU while the *bottom* spectrum shows only those gammas where the associated implanted nucleus was followed by a characteristic alpha decay of ^{254}No. All peaks in the top spectrum apart from the X-rays of Pb at 76–84 keV are confirmed to belong to ^{254}No

$$\alpha = \frac{I_e}{I_\gamma} \tag{27}$$

This means that a transition with a conversion coefficient of $\alpha = 1$ will proceed through equal numbers of gamma and electron decays if observed in a sufficiently large ensemble. Quantitatively the conversion coefficients increase with Z and increasing multipolarity as well as with decreasing transition energy. The total conversion coefficient is additively composed of the conversion coefficients for the different electron shells, i.e.

$$\alpha_{tot} = \alpha_K + \alpha_{L1} + \alpha_{L2} + \alpha_{L3} + \alpha_{M1} + \ldots \tag{28}$$

The coefficients are tabulated [65], but it is instructive to look at an approximate form valid for energies away from electron binging energy edges and transition energies not exceeding the electron rest energy by too much. Then the K conversion coefficient for an electric or magnetic transition with multipolarity L can be roughly approximated as [66]:

$$\begin{aligned} \alpha_K(EL) &\approx \frac{L}{L+1} Z^3 \left(\frac{e^2}{\hbar c}\right)^4 \left[\frac{2m_0c^2}{E_\gamma}\right]^{L+5/2} \\ \alpha_K(ML) &\approx Z^3 \left(\frac{e^2}{\hbar c}\right)^4 \left[\frac{2m_0c^2}{E_\gamma}\right]^{L+3/2} \end{aligned} \tag{29}$$

This form shows the general features:

- The conversion coefficient increases with decreasing transition energy. Note that as the energy drops below the binding energy of an atomic shell, the conversion coefficient changes rapidly near that threshold.
- The conversion coefficient increases with increasing multipolarity. Dipole transitions are less converted than quadrulole transitions.
- Magnetic transitions are more highly converted than electric transitions of the same multipolarity and energy.

For the spectroscopy of nuclei around $Z \simeq 100$ this means that $E2$ transitions below 200 keV as well as $M1$ transitions below 400 keV are dominated by internal conversion. A realistic case is calculated for fermium and shown in Fig. 25. Here the total conversion coefficients for $E2$ and $M1$ transitions are shown as a function of transition energy. We also show the coefficients for K-conversion in the same graph. It is clear that a measurement of the ratio of the K-conversion coefficient to the total conversion coefficient is sensitive to the multipolarity of the transition. Special attention has to be paid to transitions in the vicinity of binding edges where the conversion coefficient can vary rapidly with energy.

The 44 keV $2^+ \rightarrow 0^+$ transition in ^{254}No has a total conversion coefficient $\alpha \simeq 1500$ which makes this low-lying transition in the level scheme virtually undetectable in gamma rays. Conversely, if doing electron spectroscopy, this should be the strongest transition in the spectrum. Similarly, to deduce g-factors from branching ratios one needs the intensities of the stretched $E2$ transitions easily seen in gamma rays and the interband $M1$ transitions easily seen in electrons. The experimentalist therefore has to choose between gamma and electron spectroscopy, either of which will only reveal a partial picture of the level scheme. Efforts are underway to build a combined gamma and electron spectrometer (SAGE) at the University of Jyväskylä Finland, which will allow the simultaneous in-beam spectroscopy of heavy nuclei using gammas and conversion electrons [43].

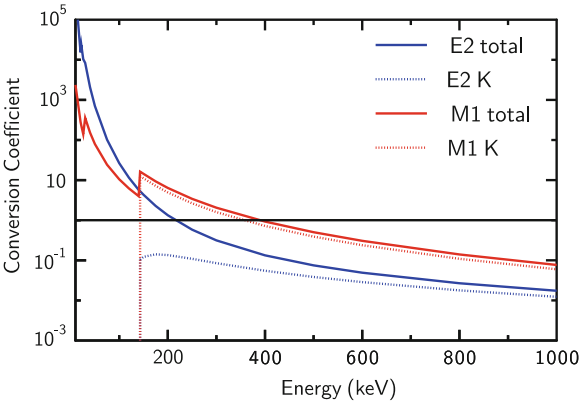

Fig. 25 Internal conversion coefficients for fermium calculated with BrICC [65]. The full lines show the total conversion coefficients for $E2$ and $M1$ transitions while the dashed curves show the K-conversion coefficients only

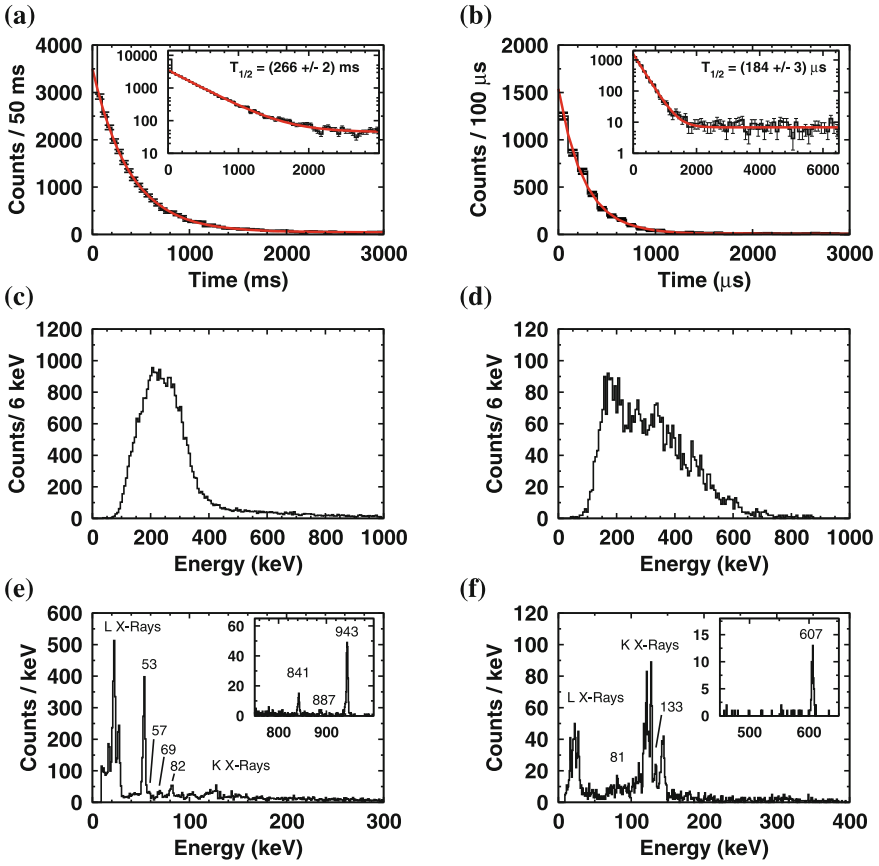

Fig. 26 Isomer spectra for ^{254}No. In panels **a** and **b** we show the time distribution between the implanted recoil and the observation of an electron signal. Note the different timescales for the two isomers. Panels **c** and **d** show the energy spectra of the observed electrons. The two decay paths of the isomers are clearly very different resulting in distinctly different electron signals. In panels **e** and **f** we show the associated gamma rays depopulating the isomers in coincidence with the electrons. The coincidence is able to clearly discriminate between the two different isomers

Selection rules for internal conversion largely follow the same rules as for gamma transitions, with one exception: $E0$ transitions between two states with angular momentum zero are forbidden for gamma rays, but allowed for internal conversion. This is due to the intrinsic angular momentum of the photon of 1 $\hbar$ which makes it impossible to fulfill the triangle rule. Electrons can, however, be ejected from the K shell with zero orbital angular momentum. The intrinsic spin of the electron does not enter the equation as the electron is not created in the process but acts as a spectator.

5.4 Decay Spectroscopy

Alpha decay can reveal a surprising amount of information about the decaying states. We shall not concern ourselves with the basic mechanisms of alpha decay but investigate how it can aid us in unraveling the nuclear single particle structure in the decaying system. The alpha decay half-life is determined by the probability to preform an alpha particle in the nucleus and the probability for that alpha particle to tunnel out of the nucleus. The former depends on the nuclear structure of the mother and the daughter states. The latter dominates the half-life so that we can use the concept of hindrance, i.e. the ratio of the probability that an alpha decay takes place relative to the probability of the same decay taking place in the absence of any influence of nuclear structure on the decay to get at the structural information.

In order to form an alpha particle one needs to assemble a pair of protons and a pair of neutrons. In even-even nuclei this is straightforward, and the most loosely bound pair of each type of particle has the highest probability of ending up in the alpha particle. In odd nuclei however one has a choice between breaking one pair and combining one of these nucleons with the previously single unpaired nucleon, or, alternatively, leaving the unpaired particle in place and forming the alpha particle from the first energetically available pairs. The situation is schematically indicated in Fig. 27. The former decay leaves the daughter nucleus in the ground state, while the latter decay prepares the daughter in an excited state with the odd particle occupying the same single particle orbital as it did in the ground state of the mother. We find experimentally that the latter process is greatly favored over the former. This means that by observing the most likely alpha decay in an odd mass decay chain we can deduce that the configuration and thus the spin and parity of the ground state of the mother and the excited state in the daughter are identical.

The great advantage of this method is that it allows us to trace single particle states from one nucleus to the next, and, since the identification of superheavy

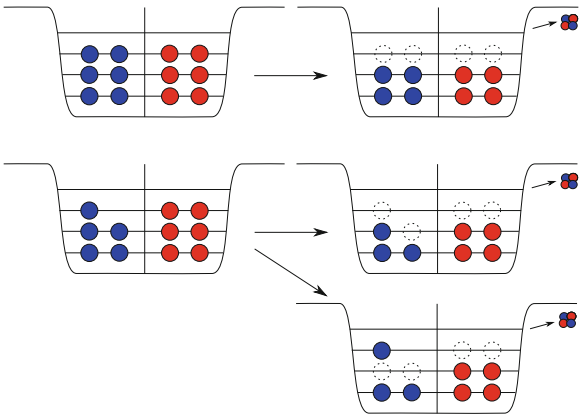

Fig. 27 Schematic illustration of the alpha decay. For an even-even nucleus the least bound pairs of nucleons are combined to form the alpha particle. In an odd–even nucleus the first pairs are usually used to form the alpha (*bottom*) leaving the daughter nucleus in an excited state, rather than breaking one pair (see text)

elements takes place mainly by observing its alpha decay chains, it tends to be readily available. The only observables required are the alpha decay Q-value and the observed half-life. Indeed, a large amount of data is available and the majority of our structural understanding of superheavy nuclei stems from alpha decay work (see, e.g., [27, 54, 67] for recent reviews). One drawback of the method is that it is usually not obvious where the populated state sits in the level scheme of the daughter nucleus, and thus it is difficult to relate the Q-value to the difference in the nuclear masses. In order to make full use of the information available one has to ensure that the radiation emitted during the decay to the ground state of the daughter nucleus is also measured.

5.4.1 Hindrance Factors

When studying alpha decays it is often advantageous to make use of the fact that the half-life of the decay is dominated by the barrier penetration, and that the influence of nuclear structure is of secondary importance. If one can separate the two components, then the influence of the nuclear structure on the decay can be readily studied. To this end one introduces the concept of hindrance. Here one compares the experimentally observed half-life $T_{1/2}^{exp}$ to a theoretical half-life $T_{1/2}^{theo}$ calculated under the assumption that the nuclear structure of mother and daughter have no influence on the decay whatsoever, see Eq. 30.

$$HF = \frac{T_{1/2}^{exp}}{T_{1/2}^{theo}} \tag{30}$$

Several different approaches to find a reasonable value for $T_{1/2}^{theo}$ can be found in the literature. One approach by Taagepera and Nurmia [68], valid for even-even nuclei, gives a semiempirical relationship between the half-life in years, the atomic number of the daughter Z and the alpha decay energy E_α in MeV (Eq. 31).

$$\log_{10} T_{1/2}^{\alpha} = 1.61(Z\sqrt{E_\alpha}) - Z^{2/3}) - 28.9 \tag{31}$$

Another frequently used approach goes back to Viola and Seaborg [69]. A more recent careful fit to a much larger available body of data has been given by Hatsukawa [70].

It is now straightforward to classify the observed alpha decays in terms of their hindrance factors. In even-even nuclei hindrance factors up to HF $\simeq$ 4 are commonly taken as unhindered or favoured transitions. The hindrance factor rises as the alpha decay comes with a change in angular momentum, and rises further still if the parity is changed during the transition. These statements are consciously left vague. While a direct comparison of two alpha lines connecting different states in the same mother-daughter system will give valueable clues about their relative angular momenta, the results of such a comparison should always be taken with a large grain of salt.

In odd mass nuclei hindrance factors rise sharply as the unpaired nucleon will have to either change the orbital it occupied or a pair has to be broken, as discussed in Sect. 5.4. The hindrance factors rise even higher in odd–odd nuclei, accounting for the need of both unpaired nucleons to either change orbital or the need to break one or two pairs.

5.4.2 Alpha Spectroscopy

Instead of implanting a recoiling heavy nucleus into a silicon detector it can be stopped in a gas volume. Transport from this gas-catcher to a gas chromatographic system then requires either a suitably volatile compound to be formed or transport via aerosols. Elements in groups 12–18 may even be transported directly in atomic form [71]. This introduces a chemical selectivity into the system which can be employed to greatly enhance the selectivity of the experiment. One big advantage of such a system is its continuous operation. Experimental details of such techniques are discussed in "Experimental Techniques" and results are outlined in "Gas-Phase Chemistry of Superheavy Elements".

As an example we turn to the chain of hassium isotopes. The state of the current understanding has been summarized recently by Türler [39]. Hassium readily forms the extremely volatile tetroxide HsO_4 which makes the chemical separation of Hs straightforward, provided the isotopes to be studied have a long enough half-life of at least the order of a milli-second. The method gives very clean alpha spectra typically unaffected by electron summing and the population of excited states in the daughters can be used to obtain a good idea of the level scheme of the daughters. In addition, the use of a thermochomatographic setup gave information on the volatility of the observed ^{269,270}Hs [72] which confirmed that hassium behaves similar to its lighter homologs in group 8 of the Periodic Table.

The isotopes ^{269}Hs, ^{265}Sg ^{261}Rf and ^{257}No are connected via alpha decays. However, the data obtained in a large number of experiments did not present an unabiguous picture. Recently, the available data has been reanalysed ([73] and references therein). Figure 28 shows the combined alpha spectra: The top panel shows all alpha decays attributed to ^{265}Sg. The next panel shows only those decays of ^{265}Sg where it was produced as an evaporation residue. This spectrum looks markedly different from that in panel c) where the alpha decays from ^{265}Sg produced in the alpha decay of ^{269}Hs are shown. This alone gives rise to the assumption that two alpha decaying states are present in ^{265}Sg. Further analysis of the daughter alphas show that the state in ^{261}Rf populated predominantly in the decays of ^{269}Hs in turn decays with a half-life of 3 s to ^{257}No. On the other hand, if ^{265}Sg is created as a fusion product, it predominantly decays to a state in ^{261}Rf which decays to ^{257}No with a half-life of 68 s.

On the basis of the combined dataset the following hypothesis was proposed [73]: Two alpha decaying levels in ^{265}Sg exist. Their half-lives are very similar, with 9 and 16 s, respectively. This similarity in half-lives makes a distinction on

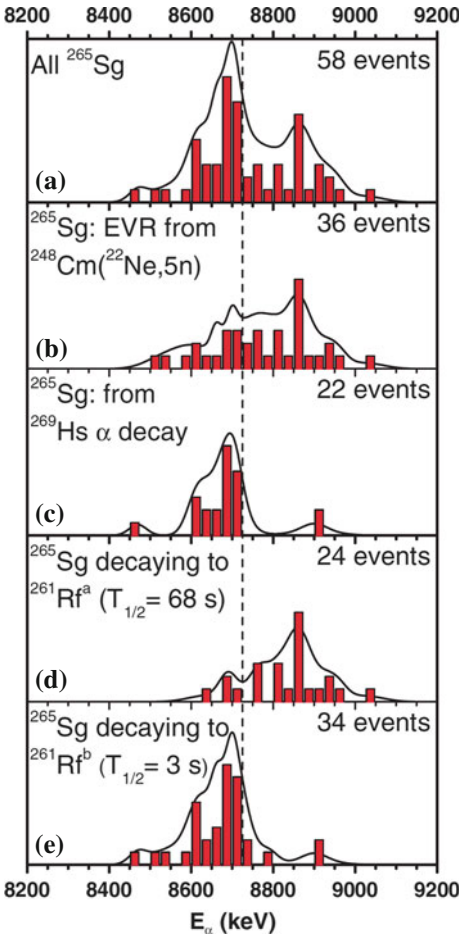

Fig. 28 Alpha spectra of events assigned to the decay of ^{265}Sg. *Solid lines* are superpositions of Gaussians taking into account the detector resolutions of the different detectors. Alpha decays are binned with a resolution of 25 keV. **a** All alpha decays of ^{265}Sg. **b** Only events of ^{265}Sg produced as an evaporation residue. **c** Only events where ^{265}Sg was the alpha decay product of ^{269}Hs. **a** is the sum of **b** and **c**. **d** Only events where ^{265}Sg populated the 68 s activity in ^{261}Rf. **e** Only events where ^{265}Sg populated the 3 s activity in ^{261}Rf. Reprinted figure with permission from [73]. Copyright (2008) by the American Physical Society

the basis of only a small number of events very difficult. These levels are populated to different degrees in the alpha decay of ^{269}Hs and a fusion evaporation reaction. Furthermore, both levels alpha decay to a pair of levels in ^{261}Rf with half-lives of 3 and 68 s, respectively, both of which populate ^{257}No. The proposed decay scheme is shown in Fig. 29. The conclusions of this analysis were recently fully confirmed (and refined) in an experiment performed at RIKEN [74]. This is a good example of the information that can be gathered through the observation of alpha energies and decay times alone.

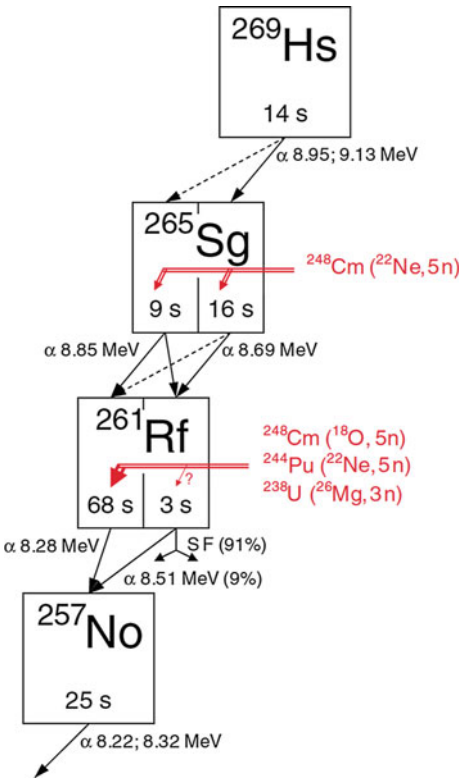

Fig. 29 Current working hypothesis of the decay pattern observed in the chain ^{269}Hs→ ^{265}Sg→ ^{261}Rf→ (^{257}No→). The dominant transitions are indicated with *solid lines*, weak transitions with *dashed lines*. Also shown is the approximate isomeric ratio when ^{265}Sg and ^{261}Rf are produced as evaporation residues. Reprinted figure with permission from [73]. Copyright (2008) by the American Physical Society

5.4.3 Spectroscopy Following Alpha Decay

Alpha decay gives as observables the energy of the decay, and, after kinematic correction the alpha decay Q-value, as well as the half-life. The quantity that is often required, however, is the mass of the decaying nucleus. In case of an even-even nucleus this is straightforward, as the unhindered main decay will connect the ground states of both nuclei and the Q-value directly gives the difference between the mass defects of mother and daughter.

This situation is greatly complicated in the odd–even and odd–odd cases. The presence of unpaired nucleons makes the assumption of a ground state to ground state transition invalid and the Q-value can only give a lower limit to the mass difference, as the alpha decay from the ground state of the mother can populate excited states in the daughter. The only way to obtain a nuclear mass from such a Q-value measurement is if one additionally has information about the excitation energy of the populated state in the daughter nucleus.

Such information is ideally obtained in the same experiment. If an alpha decay populates an excited state in the daughter nucleus, that state will decay to the ground state emitting radiation in prompt coincidence with the alpha particle. As

the probability for alpha decay depends exponentially on the Q-value the populated state will usually sit at fairly low energies in the daughter nucleus, usually well below 1 MeV. The populated state then decays via low energy transitions which are potentially highly converted, leading to the emission of one or more conversion electrons. If the decaying nucleus was implanted in a silicon detector, those electrons will be detected at the same time at the same place in the detector, thus producing an energy summing that can broaden an alpha peak considerably by spreading the alpha signal out to higher apparent energies. In order to obtain the cleanest alpha spectra one prefers to catch the activity on a surface and measure the emitted alpha particles in an external detector, thus greatly reducing the summing. This also leads to a reduction of the number of observed alpha particles due to the finite geometrical acceptance of such a setup.

Another way is to measure the gamma decays following alpha decay. As gamma rays are highly penetrating, they do not deposit a sizeable energy in a thin silicon detector and therefore do not contribute to a broadening of the alpha peak. They allow to build a level scheme for the daughter nucleus, thus fixing the energy of the populated state.

We shall illustrate this with an example. Figures 30 and 31 show the measured gamma ray spectra following the alpha decay of ^{253}No [75] and the systematics of the level schemes deduced from gamma spectroscopy following alpha decay in the $N = 151$ isotones. Three main gamma transitions are observed at 151, 222 and 280 keV in coincidence with the main alpha decay of ^{253}No, which are interpreted as transitions into the ground state rotational band of ^{249}Fm. Two further, much weaker transitions at 209 and 670 keV are in coincidence with alpha decays where the alpha has a different energy, and these are interpreted as hindered alpha decays to excited single particle configurations, which then decay to the ground state via the observed gamma transitions [75]. From this information the level scheme and the assigned configurations shown in Fig. 31 can be deduced.

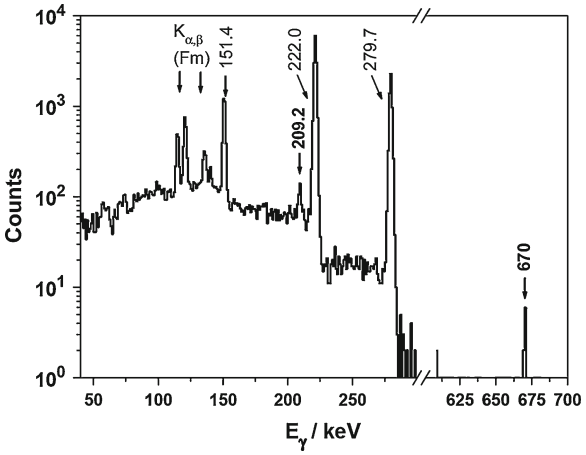

Fig. 30 Gamma rays observed following the alpha decay of ^{253}No. Figure reproduced from [75] with permission

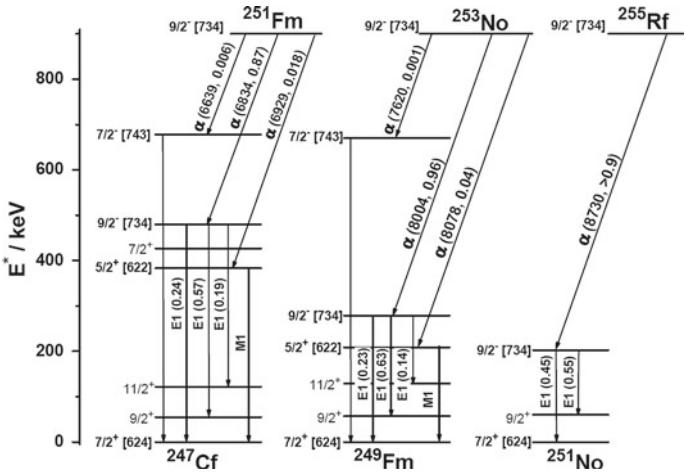

Fig. 31 Deduced level scheme compared to the neighboring $N = 151$ isotones. Taken from [75]

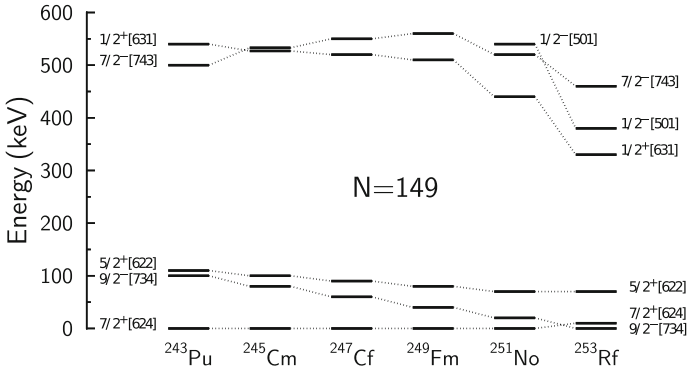

Fig. 32 Comparison of the calculated single neutron spectra for $N = 149$ isotones. The data is taken from [76], the figure is adapted from [27]

This level scheme should be compared to the calculated single particle spectra [76] shown in Fig. 32. The ground state in all cases is $7/2^+$. The lowering in energy of the $9/2^-$ state is nicely reproduced, while the $5/2^+$ and the higher lying $7/2^-$ configurations remain at roughly constant excitation energies.

The need for gamma spectroscopy after alpha decay at the focal plane of recoil separators has gained more and more importance over the last decade. This has lead to the development of a number of dedicated focal plane detection systems that place great emphasis on the detection of gamma rays. Examples include the GABRIELA setup in Dubna [53] and the GREAT spectrometer in Jyväskylä [45]. Currently the setup with the highest gamma ray detection efficiency is the TASISpec spectrometer [50] developed for the focal plane of the TASCA gas-filled separator at GSI [49].

In the TASISpec setup the geometry is optimized so that gamma rays from heavy nuclei implanted in the focal plane can be detected with an absolute efficiency of more than 50%. This paves the way for gamma spectroscopy on the heaviest systems where only a few nuclei are produced.

It is usually through a combination of experimental techniques that the structural assignments can be made. Direct measurements of nuclear masses can be an invaluable tool to determine the position of the level populated in alpha decay in the level scheme [77]. Ultimately, the problems accessing the superheavy region experimentally limits the number of possible experimental probes, and each nucleus has to be treated on an individual basis. This is one of the great experimental challenges for nuclear physics.

6 Conclusions and Outlook

The advances in nuclear experimental techniques over the last decades have allowed a step change in our understanding of the structure of the heaviest nuclei. The study of the rotational properties in in-beam experiments has shown up some of the best examples of rotational nuclei anywhere. Looking at isomeric states and the bands built upon them has allowed the assignment of single particle configurations to excited states which can then be used as a challenge to theory trying to reproduce and understand them. The use of conversion electron spectroscopy opens up a new approach to the study of the underlying single particle structure in the heaviest nuclei.

The rise of gamma spectroscopy after alpha decay has improved our understanding of the single particle configurations of and near the ground states of odd mass nuclei in a way that simply was not possible before. Many excited single particle configurations were identified through weak alpha decay branches and the detection of the subsequent gamma rays.

One obvious application of highly efficient gamma ray detection is in the identification of the elements produced. If an alpha decay populates an excited state in the daugther nucleus, it will decay and sometimes it will emit characteristic X-rays. If these X-rays can be detected, the identification of the Z of the daughter becomes straightforward. In a time when the identification of new elements via alpha decay chains ending in known elements increasingly fails to be applicable, this direct approach to the identification of the elements produced in a reaction will play an important role in the confirmation of claims of discovery.

The superheavy nuclei provide a unique testing ground for our understanding of the nuclus as a complex, strongly interacting many-body system. However, limitations in the number of nuclei that can be produced for study also restrict the number of probes that can be brought to bear. Often assignments are made on the basis of systematics, and need to be continuously confronted with newer measurements, and reevaluated as appropriate. Amongst the open questions is the role of isomers for the possibility of detecting superheavy elements in nature.

Identification of ground state configurations is crucial but experimentally difficult and not always possible on the basis of experimental data alone.

With the advent of modern radioactive beam facilities more neutron-rich systems will become available for study. Here the main challenge lies in the available beam currents, which are not yet high enough to reach a cross section in the picobarn region in a reasonable time. However, modern gamma arrays such as GRETINA and AGATA will be on hand to allow in-beam studies of some of the heaviest nuclei.

Chemical separation is an invaluable tool available for the longer-lived species, as they are chemically identified by the transport to a clean environment where low-backbround studies are possible.

Superheavy elements exist on the edge of physical possibility, both in terms of their electron configurations and their nuclear structure. They are difficult to produce and study, those we have studied so far do not exist long enough to allow any industrial application. Yet they open up a truly interdisciplinary field of study grounded in both chemistry and physics and they can teach us a great deal about the most extreme configurations of protons, neutrons and electrons available.

References

1. Goeppert-Mayer, M.: On closed shells in nuclei. Phys. Rev. **74**, 235–239 (1948)
2. Haxel, O., Jensen, J.H.D., Suess, H.D.: On the "Magic Numbers" in nuclear structure. Phys. Rev. **75**, 1766–1766 (1949)
3. Meldner, H.: Predictions of new magic regions and masses for super-heavy nuclei from calculations with realistic shell model single particle Hamiltonians. Ark. Fys. **36**, 593–598 (1967)
4. de Marcillac, P., Coron, N., Dambler, G., Leblanc, J., Moalic, J.-P.: Experimental detection of α-particles from the radioactive decay of natural bismuth. Nature **422**, 876–878 (2003)
5. Holden, N.E.: Total half-lives for selected nuclides. Pure Appl. Chem. **62**, 941–958 (1990)
6. Browne, E.: Nucl. Data Sheets **98**, 665–800 (2003)
7. Chukreev, F.E., Makarenko, V.E., Martin, M.J.: Nucl. Data Sheets **97**, 129–240 (2002)
8. Heyde, K.: Basic Ideas and Concepts in Nuclear Physics: An Introductory Approach, 3rd edn. Taylor & Francis, Bristol (2004)
9. Casten, R.F.: Nuclear Structure from a Simple Perspective. Oxford University Press, Oxford (2001)
10. Krane, K.S.: Introductory Nuclear Physics. Wiley, New York (1987)
11. von Weizsäcker, C.F.: Zur Theorie der Kernmassen. Z. Phys. **96**, 431–458 (1935)
12. Bethe, H.A., Bacher, R.F.: Nuclear physics A. Stationary states of nuclei. Rev. Mod. Phys. **8**, 82–229 (1936)
13. Wapstra, A.H., Gove, N.B.: The 1971 atomic mass evaluation. At. Data Nucl. Data Tables **9**, 267–468 (1971)
14. Huizenga, J.R., Vandenbosch, R.: Nuclear Fission. Academic Press Inc., New York (1974)
15. Armbruster, P.: On the production of heavy elements by cold fusion: The elements 106 to 109. Ann. Rev. Nucl. Part. Sci. **35**, 135–194 (1985)
16. Wagemans, T.C. (ed.): The Nuclear Fission Process. CRC Press, London (1991)
17. Schmidt, K.-H., Benlliure, J., Junghans, A.R.: Fission of nuclei far from stability. Nucl. Phys. A **693**, 169–189 (2001)

18. Halpern, I.: Nuclear fission. Annu. Rev. Nucl. Sci. **9**, 245–342 (1959)
19. Schädel, M.: The chemistry of superheavy elements. Act. Phys. Pol. B **34**, 1701–1728 (2003)
20. Blank, B., Chartier, M., Czajkowski, S., Giovinazzo, J., Pravikoff, M.S., Thomas, J.-C., de France, G., de Oliveira S.F., Lewitowicz, M., Borcea, C., Grzywacz, R., Janas, Z., Pfützner, M.: Discovery of doubly magic ^{48}Ni. Phys. Rev. Lett. **84**, 1116–1119 (2000)
21. Schneider, R., Friese, J., Reinhold, J., Zeitelhack, K., Faestermann, T., Gernhäuser, R., Gilg, H., Heine, F., Homolka, J., Kienle, P., Körner, H.J., Geissel, H., Münzenberg, G., Sümmerer, K.: Production and identification of ^{100}Sn. Z. Phys. A **348**, 241–242 (1994)
22. Herzberg, R.-D., Greenlees, P.T., Butler, P.A., Jones, G.D., Venhart, M., Darby, I.G., Eeckhaudt, S., Eskola, K., Grahn, T., Gray-Jones, C., Hessberger, F.P., Jones, P., Julin, R., Juutinen, S., Ketelhut, S., Korten, W., Leino, M., Leppänen, A.-P., Moon, S., Nyman, M., Page, R.D., Pakarinen, J., Pritchard, A., Rahkila, P., Saren, J., Scholey, C., Steer, A., Sun, Y., Theisen, Ch., Uusitalo, J.: Nuclear isomers in superheavy elements as stepping stones towards the island of stability. Nature **442**, 896–899 (2006)
23. Bender, M., Nazarewicz, W., Reinhard, P.-G.: Shell stabilization of super- and hyper-heavy nuclei without magic gaps. Phys. Lett. B **515**, 42–48 (2001)
24. Rutz, K. Bender, M., T. Bürvenich, T., Schilling, T., Reinhard, P.-G., Maruhn, J.A., W. Greiner, W.: Superheavy nuclei in self-consistent nuclear calculations. Phys. Rev. C 56, 238–243 (1997).
25. Bender, M. Rutz, K. Reinhard, P.-G., Maruhn, J.A., Greiner, W.: Shell structure of superheavy nuclei in self-consistent mean-field models. Phys. Rev. C 60, 034304(20) (1999).
26. Nilsson, S.G.: Binding states of individual nucleons in strongly deformed nuclei. Dan. Mat. Fys. Medd. **29**, 1–69 (1955)
27. Herzberg, R.-D., Greenlees, P.T.: In-beam and decay spectroscopy of transfermium nuclei. Prog. Part. Nucl. Phys. **61**, 674–720 (2008)
28. Worden, E.F., Gutmacher, R.G., Lougheed, R.W., Conway, J.G., Mehlhorn, R.J.: Hyperfine structure in the 253Es emission spectrum, II. Nuclear spin, nuclear magnetic dipole moment, and energy levels of Es II. J. Opt. Soc. Am. **60**, 1297–1302 (1970).
29. Baktash, C., Nazarewicz, W., Wyss, R.: On the question of spin fitting and quantized alignment in rotational bands. Nucl. Phys. A **555**, 375–407 (1993)
30. Bohr, A., Mottelson, B.R.: Nuclear Structure. World Scientific Publishing Co. Pte. Ltd, Singapore (1998)
31. Harris, S.M.: Higher order corrections to the cranking model. Phys. Rev. **138**, 509–513 (1965)
32. Herzberg, R.D., Amzal, N., Becker, F., Butler, P.A., Chewter, A.J.C., Cocks, J.F.C., Dorvaux, O., Eskola, K., Gerl, J., Greenlees, P.T., Hammond, N.J., Hauschild, K., Helariutta, K., Hessberger, F., Houry, M., Jones, G.D., Jones, P.M., Julin, R., Juutinen, S., Kankaanpaa, H., Kettunen, H., Khoo, T.L., Korten, W., Kuusiniemi, P., Le Coz, Y., Leino, M., Lister, C.J., Lucas, R., Muikku, M., Nieminen, P., Page, R.D., Rahkila, P., Reiter, P., Schlegel, C., Scholey, C., Stezowski, O., Theisen, C., Trzaska, W.H., Uusitalo, J., Wollersheim, H.J. : Spectroscopy of transfermium nuclei: $^{252}_{102}$No. Phys. Rev. C **65**, 014303(7) (2001).
33. Herzberg, R.D., Amzal, N., Bastin, J.E., Becker, F., Brew, P.M.T., Butler, P.A., Chewter, A.J.C., Cocks, J.F.C., Dorvaux, O., Eskola, K., Gerl, J., Greenlees, P.T., Hammond, N.J., Hauschild, K., Helariutta, K., Hessberger, F., Houry, M., Hurstel, A., Humphreys, R.D., Jones, G.D., Jones, P.M., Julin, R., Juutinen, S., Kankaanpaa, H., Kettunen, H., Khoo, T.L., Korten, W., Kuusiniemi, P., Le Coz, Y., Leino, M., Leppanen, A.P., Lister, C.J., Lucas, R., Muikku, M., Nieminen, P., Page, R.D., Page, T., Rahkila, P., Reiter, P., Schlegel, C., Scholey, C., Sletten, G., Stezowski, O., Theisen, C., Trzaska, W.H., Uusitalo, J., Wollersheim, H.J.: In-beam spectroscopy of ^{253,254}No. Eur. Phys. J. A **15**, 205–208 (2002)
34. Herzberg, R.D., Moon, S., Eeckhaudt, S., Greenlees, P.T., Butler, P.A., Page, T., Afanasjev, A.V., Amzal, N., Bastin, J.E., Becker, F., Bender, M., Bruyneel, B., Cocks, J.F.C., Darby, I.G., Dorvaux, O., Eskola, K., Gerl, J., Grahn, T., Gray-Jones, C., Hammond, N.J., Hauschild, K., Heenen, P.H., Helariutta, K., Herzberg, A., Hessberger, F., Houry, M., Hurstel, A.,

Humphreys, R.D., Jones, G.D., Jones, P.M., Julin, R., Juutinen, S., Kankaanpaa, H., Kettunen, H., Khoo, T.L., Korten, W., Kuusiniemi, P., LeCoz, Y., Leino, M., Leppanen, A.P., Lister, C.J., Lucas, R., Muikku, M., Nieminen, P., Nyman, M., Page, R.D., Pakarinen, J., Pritchard, A., Rahkila, P., Reiter, P., Sandzelius, M., Saren, J., Schlegel, C., Scholey, C., Theisen, C., Trzaska, W.H., Uusitalo, J., Wiens, A., Wollersheim, H.J.: Structure of rotational bands in ^{253}No. Eur. Phys. J. A **42**, 333–337 (2009)

35. Herzberg, R.-D., Cox, D.M.: Spectroscopy of actinide and transactinide nuclei. Radiochim. Acta **99**, 441–457 (2011)
36. Muntian, I., Hofmann, S., Patyk, Z., Sobiczewki, A.: Properties of heaviest nuclei. Acta Phys. Pol. B **34**, 2073–2082 (2003)
37. Muntian, I., Patyk, Z., Sobiczewski, A.: Calculated masses of heaviest nuclei (transl. from. Yad. Fiz). Phys. At Nucl. **66**, 1051–1055 (2003)
38. Dvorak, J., Brüchle, W., Chelnokov, M., Dressler, R., Düllmann, Ch.E., Eberhardt, K., Gorshkov, V., Jäger, E., Krücken, R., Kuznetsov, A., Nagame, Y., Nebel, F., Novackova, Z., Qin, Z., Schädel, M., Schausten, B., Schimpf, E., Semchenkov, A., Thörle, P., Türler, A., Wegrzecki, M., Wierczinski, B., Yakushev, A., Yeremin, A.: Doubly magic nucleus $^{270}_{108}\mathrm{Hs}_{162}$. Phys. Rev. Lett. **97**, 242501(4) (2006)
39. Türler, A.: Nuclear structure and reaction studies near doubly magic ^{270}Hs. Radiochim. Acta **100**, 75–83 (2012)
40. Greenlees, P.T., Herzberg, R.D., Ketelhut, S., Butler, P.A., Chowdhury, P., Grahn, T., Gray-Jones, C., Jones, G.D., Jones, P., Julin, R., Juutinen, S., Khoo, T.L., Leino, M., Moon, S., Nyman, M., Pakarinen, J., Rahkila, P., Rostron, D., Saren, J., Scholey, C., Sorri, J., Tandel, S.K., Uusitalo, J., Venhart, M.: High-K structure in ^{250}Fm and the deformed shell gap at $N = 152$ and $Z = 100$. Phys. Rev. C **78**, 021303(5) (2008)
41. Walker, P.M., Dracoulis, G.D.: Energy traps in atomic nuclei. Nature **399**, 35–40 (1999)
42. Hofmann, S., Hessberger, F.P., Ackermann, D., Antalic, S., Cagarda, P., Cwiok, S., Kindler, B., Kojouharova, J., Lommel, B., Mann, R., Münzenberg, G., Popeko, A.G., Saro, S., Schött, H.J., Yeremin, A.V.: The new isotope ^{270}110 and its decay products ^{266}Hs and ^{262}Sg. Eur. Phys. J. A **10**, 5–10 (2001)
43. Papadakis, P., Herzberg, R.D., Pakarinen, J., Butler, P.A., Coleman-Smith, P.J., Cresswell, J.R., Greenlees, P.T., Jones, P., Julin, R., Lazarus, I.H., Letts, S.C., Page, R.D., Parr, E., Peura, P., Pucknell, V.F.E., Rahkila, P., Seddon, D.A., Simpson, J., Sorri, J., Thornhill, J., Wells, D.: Towards combining in-beam gamma-ray and conversion electron spectroscopy. AIP Conf. Proc. **1090**, 14–20 (2009)
44. Leino, M., Äystö, J., Enqvist, T., Heikkinen, P., Jokinen, A., Nurmia, M., Ostrowski, A., Trzaska, W.H., Uusitalo, J., Eskola, K., Armbruster, P., Ninov, V.: Gas-filled recoil separator for studies of heavy elements. Nucl. Instr. Method B **99**, 653–656 (1995)
45. Page, R.D., Andreyev, A.N., Appelbe, D.E., Butler, P.A., Freeman, S.J., Greenlees, P.T., Herzberg, R.-D., Jenkins, D.G., Jones, G.D., Jones, P., Joss, D.T., Julin, R., Kettunen, H., Leino, M., Rahkila, P., Regan, P.H., Simpson, J., Uusitalo, J., Vincent, S.M., Wadsworth, R.: The GREAT spectrometer. Nucl. Instrum. Method B **204**, 634–637 (2003)
46. Münzenberg, G., Faust, W., Hofmann, S., Armbruster, P., Güttner, K., Ewald, H.: The velocity filter SHIP, a separator of unslowed heavy ion fusion products. Nucl. Instrum. Method **161**, 65–82 (1979)
47. Münzenberg, G., Faust, W., Hessberger, F.P., Hofmann, S., Reisdorf, W., Schmidt, K.-H., Schneider, W.F.W., Schött, H., Armbruster, P., Güttner, K., Thuma, B., Ewald, H., Vermeulen, D.: The velocity filter SHIP, performance and survey of current experiments. Nucl. Instrum. Method **186**, 423–433 (1981)
48. Block, M., Ackermann, D., Blaum, K., Chaudhuri, A., Di, Z., Eliseev, S., Ferrer, R., Habs, D., Herfurth, F., Hessberger, F.P., Hofmann, S., Kluge, H.-J., Maero, G., Martin, A., Marx, G., Mazzocco, M., Mukherjee, M., Neumayr, J.B., Plaß, W.R., Quint, W., Rahaman, S., Rauth, C., Rodriguez, D., Scheidenberger, C., Schweikhard, L., Thirolf, P.G., Vorobjev, G.,

Weber, C.: Towards direct mass measurements of nobelium at SHIPTRAP. Eur. Phys. J. D **45**, 39–45 (2007)
49. Semchenkov, A., Brüchle, W., Jäger, E., Schimpf, E., Schädel, M., Mühle, C., Klos, F., Türler, A., Yakushev, A., Belov, A., Belyakova, T., Kaparkova, M., Kukhtin, V., Lamzin, E., Sytchevsky, S.: The TransActinide Separator and Chemistry Apparatus (TASCA) at GSI—optimization of ion-optical structures and magnet designs. Nucl. Instrum. Method B **266**, 4153–4161 (2008)
50. Andersson, L.L., Rudolph, D., Golubev, P., Herzberg, R.D., Hoischen, R., Merchan, E., Ackermann, D., Düllmann, C.E., Eberhardt, K., Even, J., Gerl, J., Hessberger, F.P., Jäger, E., Khuyagbaatar, J., Kojouharov, I., Kratz, J.V., Krier, J., Kurz, N., Prokopowicz, W., Schädel, M., Schaffner, H., Schausten, B., Schimpf, E., Semchenkov, A., Türler, A., Wollersheim, H.J., Yakushev, A., Thörle-Pospiech, P., Hartmann, W., Hübner, A., Lommel, B., Kindler, B., Steiner, J.: TASISpec-A highly efficient multi-coincidence spectrometer for nuclear structure investigations of the heaviest nuclei. Nucl. Instrum. Method A **622**, 164–170 (2010)
51. Yeremin, A.V., Andreyev, A.N., Bogdanov, D.D., Chepigin, V.I., Gorshkov, V.A., Ivanenko, A.I., Kabachenko, A.P., Rubinskaya, L.A., Smirnova, E.M., Stepantsov, S.V., Voronkov, E.N., Ter-Akopian, G.M.: The Vassilissa facility for electrostatic separation and study of complete fusion reaction products. Nucl. Instrum. Method A **274**, 528–532 (1989)
52. Yeremin, A.V., Bogdanov, D.D., Chepigin, V.I., Gorshkov, V.A., Kabachenko, A.P., Malyshev, O.N., Popeko, A.G., Sagaidak, R.N., Ter-Akopian, G.M.: The electrostatic separator VASSILISSA Performance and experimental results. Nucl. Instrum. Method B **126**, 329–333 (1989)
53. Popeko, A.G., Belozerov, A.V., Briancon, Ch., Chepigin, V.I., Dorvaux, O., Hauschild, K., Kabachenko, A.P., Korichi, A., Lopez-Martens, A., Malyshev, O.N., Oganessian, Yu.: Ts., Saro, S., Shutov, A.V., Svirikhin, A.I., Yeremin, A.V.: GABRIELA setup for nuclear spectroscopy of the transfermium element isotopes at the VASSILISSA separator. Phys. At. Nucl. **69**, 1183–1187 (2006)
54. Oganessian, Y.: Heaviest nuclei from ^{48}Ca-induced reactions. J. Phys. G. **34**, R165–R232 (2007)
55. Tsyganov, YuS: The Dubna gas-filled recoil separator: status and developments. J. Phys. G **25**, 937–940 (1999)
56. Ninov, V., Gregorich, K.E., McGrath, C.A.: The Berkeley gas-filled separator. AIP Conf. Proc. **455**, 704–707 (1998)
57. Lee, I.Y., Clark, R.M., Cromaz, M., Deleplanque, M.A., Descovich, M., Diamond, R.M., Fallon, P., Macchiavelli, A.O., Stephens, F.S., Ward, D.: GRETINA: A gamma ray energy tracking array. Nucl. Phys. A **746**, 255–259 (2004)
58. Davids, C.N., Larson, J.D.: The argonne fragment mass analyzer. Nucl. Instrum. Method **40/41**, 1224–1228 (1989)
59. Lee, I.-Y.: The Gammasphere. Prog. Part. Nucl. Phys. **28**, 473–485 (1992)
60. Janssens, R.V.F., Stephens, F.S.: New physics opportunities at Gammasphere. Nucl. Phys. News **6**, 9–17 (1996)
61. Miyatake, H., Nomura, T., Kawakami, H., Tanaka, J., Oyaizu, M., Morita, K., Shinozuka, T., Kudo, H., Sueki, K., Iwata, Y.: INS gas-filled recoil isotope separator. Nucl. Instrum. Method B **26**, 309–313 (1987)
62. Morita, K., Yoshida, A., Inamura, T.T., Koizumi, M., Nomura, T., Fujioka, M., Shinozuka, T., Miyatake, H., Sueki, K., Kudo, H., Nagai, Y., Toriyama, T., Yoshimura, K., Hatsukawa, Y.: RIKEN isotope separator on-line GARIS/IGISOL. Nucl. Instrum. Method B **70**, 220–225 (1992)
63. Greenlees, P.T., Andreyev, A.N., Bastin, J., Becker, F., Bouchez, E., Butler, P.A., Cocks, J.F.C., Le Coz, Y., Eskola, K., Gerl, J., Hauschild, K., Helariutta, K., Herzberg, R.D., Hessberger, F.P., Humphreys, R.D., Hürstel, A., Jenkins, D.G., Jones, G.D., Jones, P., Julin, R., Juutinen, S., Kankaanpää, H., Keenan, A., Kettunen, H., Khoo, T.L., Korten, W., Kuusiniemi, P., Leino, M., Leppanen, A.P., Muikku, M., Nieminen, P., Page, R.D., Page, T.,

Pakarinen, J., Rahkila, P., Reiter, P., Schlegel, C., Scholey, C., Theisen, C., Uusitalo, J., Van de Vel, K., Wadsworth, R., Wollersheim, H.J.: Heavy element spectroscopy at JYFL. AIP Conf. Proc. **764**, 237–242 (2004)
64. Muikku, M., Cocks, J.F.C., Helariutta, K., Jones, P., Julin, R., Juutinen, S., Kankaanpää, H., Kettunen, H., Kuusiniemi, P., Leino, M., Rahkila, P., Savelius, A., Trzaska, W.H., Uusitalo, J., Greenlees, P.T., Page, R.D.: Probing the shape of ^{176}Hg along the yrast line. Phys. Rev. C **58**, R3033–R3036 (1998)
65. Kibedi, T., Burrows, T.W., Trzhaskovskaya, M.B., Davidson, P.M., Nestor Jr, C.W.: Evaluation of theoretical conversion coefficients using Br Icc. Nucl. Instrum. Method A **589**, 202–229 (2008)
66. Musiol, G., Ranft, J., Reif, R., Seeliger, D.: Kern-und Elementarteilchenphysik. VCH Verlagsgesellschaft, Weinheim (1988)
67. Leino, M., Hessberger, F.P.: The nuclear structure of heavy-actinide and trans actinide nuclei. Ann. Rev. Nucl. Part. Sci. **54**, 175–215 (2004)
68. Taagepera, R., Nurmia, M.: Ann. Acad. Sci. Fenn. Ser. A Phys. **78**, 1–17 (1961)
69. Viola, V.E., Seaborg, G.T.: Nuclear systematics of the heavy elements I, energetics and masses. J. Inorg. Nucl. Chem. **28**, 741–761 (1966)
70. Hatsukawa, Y., et al.: Systematics of alpha decay half-lives. Phys. Rev. C **42**, 674–682 (1990)
71. Pitzer, K.S.: Are elements 112, 114, and 118 relatively inert gases? J. Chem. Phys. **63**, 1032–1033 (1975)
72. Düllmann, C.E., Brüchle, W., Dressler, R., Eberhardt, K., Eichler, B., Eichler, R., Gäggeler, H.W., Ginter, T.N., Glaus, F., Gregorich, K.E., Hoffman, D.C., Jäger, E., Jost, D.T., Kirbach, U.W., Lee, D.M., Nitsche, H., Patin, J.B., Pershina, V., Piguet, D., Qin, Z., Schädel, M., Schausten, B., Schimpf, E., Schött, H.-J., Soverna, S., Sudowe, R., Thörle, P., Timokhin, S.N., Trautmann, N., Türler, A., Vahle, A., Wirth, G., Yakushev, A.B., Zielinski, P.M.: Chemical investigation of hassium (element 108). Nature **418**, 859–862 (2002)
73. Düllmann C.E., Türler, A.: ^{248}Cm(^{22}Ne,xn)$^{270-x}$Sg reaction and the decay properties of ^{265}Sg reexamined. Phys. Rev. C **77**, 064320(10) (2008)
74. Haba, H., Kaji, D., Kudou, Y., Morimoto, K., Morita, K., Ozeki, K., Sakai, R., Sumita, T., Yoneda A., Kasamatsu, Y., Komori, Y., Shinohara, A., Kikunaga, H., Kudo, H., Nishio, K., Ooe, K., Sato, N., Tsukada, K.: Production of ^{265}Sg in the ^{248}Cm(^{22}Ne,5n)^{265}Sg reaction and decay properties of two isomeric states in ^{265}Sg. Phys. Rev. C **85**, 024611(11) (2012)
75. Hessberger, F.P.: GSI experiments on synthesis and nuclear structure investigations of the heaviest nuclei. Eur. Phys. J. D **45**, 33–37 (2007)
76. Parkhomenko, A., Sobiczewski, A.: Neutron one-quasiparticle states of heaviest nuclei. Act. Phys. Pol. B **36**, 3115–3137 (2005)
77. Block, M., Ackermann, D., Blaum, B., Droese, C., Dworschak, M., Eliseev, S., Fleckenstein, T., Haettner, E., Herfurth, F., Hessberger, F.P., Hofmann, S., Ketelaer, J., Ketter, J., Kluge, H.-J., Marx, G., Mazzocco, M., Novikov, YuN, Plass, W.R., Popeko, A., Rahaman, S., Rodriguez, D., Scheidenberger, C., Schweikhard, L., Thirolf, P.G., Vorobyev, G.K., Weber, C.: Direct mass measurements above uranium bridge the gap to the island of stability. Nature **463**, 785–788 (2010)

Theoretical Chemistry of the Heaviest Elements

Valeria Pershina

Abstract Theoretical chemical research in the area of the heaviest elements is extremely important. It deals with predictions of properties of exotic species and their behavior in sophisticated and expensive experiments with single atoms and permits the interpretation of experimental results. Spectacular developments in the relativistic quantum theory and computational algorithms have allowed for accurate calculations of electronic structures of the heaviest elements and their compounds. Due to the experimental restrictions in this area, the theoretical studies are often the only source of useful chemical information. The works on relativistic calculations and predictions of chemical properties of elements with $Z \geq 104$ are overviewed. Preference is given to those related to the experimental research. The increasingly important role of relativistic effects in this part of the Periodic Table is demonstrated.

1 Introduction

The main aim of chemical research in the area of the heaviest elements is to assign a new element its proper place in the Periodic Table. Conceptually, it is the atomic number, Z, and electronic configuration of an element that define its position there. Since the latter cannot be measured for the very heavy elements, information on its chemical behavior is often used for this purpose. Unfortunately, with increasing nuclear charge cross-sections and production rates drop so rapidly that such

An erratum to this chapter is available at 10.1007/978-3-642-37466-1_10

V. Pershina (✉)
GSI Helmholtzzentrum für Schwerionenforschung, Darmstadt, Germany
e-mail: V.Pershina@gsi.de

M. Schädel and D. Shaughnessy (eds.), *The Chemistry of Superheavy Elements*,
DOI: 10.1007/978-3-642-37466-1_3,

chemical information can be accessed only for elements with a half-life of the order of at least few seconds and longer (see "Synthesis of Superheavy Elements"). In this case, some fast chemistry techniques are used (see "Experimental Techniques"). They are based on the principle of chromatographic separations either in the gas phase exploiting differences in volatility of elements or their compounds, or in the aqueous phase by solvent extraction or ion-exchange separations using differences in the complex formation. Chemistry of elements 104 (Rf) through 108 (Hs), and of elements 112 (Cn) and 114 (flerovium, Fl) has been successfully studied using these techniques (see "Liquid-Phase Chemistry of Superheavy Elements" and "Gas-Phase Chemistry of Superheavy Elements").

Due to very short half-lives, chemical information obtained from these experiments is limited to the knowledge of only few properties. It mostly answers the question about whether a new element behaves similarly to their lighter congeners in a chemical group, or whether some deviations from the trends occur due to very strong relativistic effects on their valence electron shells. Knowledge of many other important properties such as, e.g., chemical composition, stability, geometrical configuration, ionization potential (IP), electron affinity (EA), etc., cannot be measured at all. Thus, for the heaviest elements, theoretical studies become extremely important and are often the only source of useful chemical information. They are also invaluable in predicting and/or interpreting the outcome of sophisticated and expensive experiments with single atoms. Moreover, it is only the theory that can reveal how relativistic effects influence chemical properties: only a comparison of the observed behavior with that predicted on the basis of relativistic *versus.* non-relativistic calculations does allow assessing the importance and magnitude of relativistic effects.

Theoretical chemical research on the heaviest elements is not less challenging than the experimental one. It should be based on the most accurate relativistic electronic structure calculations in order to reliably predict properties and experimental behavior of the new elements and their compounds. It also needs development of special approaches that bridge calculations with quantities that cannot be so easily predicted from calculations. Due to recent spectacular developments in the relativistic quantum theory, computational algorithms and techniques, very accurate calculations of properties of the transactinide elements and their compounds are now possible, which allow for reliable predictions of their experimental behavior. These theoretical works are overviewed here. Special attention is paid to the predictive power of the theoretical studies for the chemical experiments. The role of relativistic effects is discussed in detail.

Early reviews on predictions of transactinide element properties based on relativistic atomic calculations and extrapolations are those of [1–5]. More recent reviews on the theoretical chemistry of the heaviest elements covering also investigations of molecular, complex, and solid-state properties are those of [6–14]. Chemical and physical properties of the heaviest elements including theoretical aspects are also discussed in [15].

2 Architecture of the Periodic Table

When Seaborg in 1944 introduced his 'actinide' concept [16], the theory played an important role in his decision to place newly discovered elements in a second series where the filling of the 5f-shell takes place, similarly to the 'lanthanide' series where the filling of the 4f-shell takes place. Thus, the filled-shell concept was in accord with the newly found periodicity in chemical properties and resulted in the discovery of the heavy actinides up to No at that time [17]. Since then, the theory advanced to such an extent that the Periodic Table (Fig. 1) is now predicted with sufficient accuracy up to very high Z numbers. That was possible due to the development of very accurate relativistic quantum chemical methods and programs, which could reliably calculate electronic configurations of heavy element atoms and ions. Ground states of the superheavy elements up to $Z = 172$ were predicted in the late 1960s and early 1970s by Mann [18], Fricke, Waber, Greiner [19, 20], Desclaux [21], and later by Nefedov [22] using the Dirac–Fock (DF) and Dirac–Fock-Slater (DFS) methods. The results up to 1975 are summarized in [1, 2] (see also references therein). More accurate multiconfiguration Dirac–Fock (MCDF) [23–31] and Dirac-Coulomb-Breit (DCB) coupled cluster (CC) calculations (see [32, 33] and references therein) performed later basically confirmed those earlier predictions and furnished more accurate values of the electronic energy states.

According to results of these calculations, in the first nine transactinide elements, Rf through Cn, filling of the 6d shell takes place. Followed by them are 7p elements 113 through 118, with element 118 falling into the group of noble

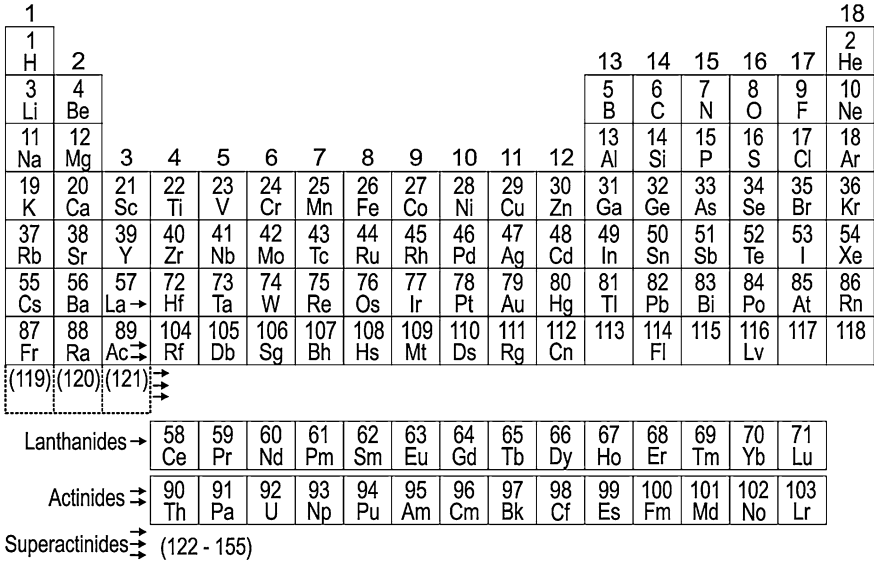

Fig. 1 Modern Periodic Table of the Elements

gases. In elements 119 and 120, the filling of the 8s shell takes place so that these elements will obviously be homologs of alkali and alkali-earth elements in group 1 and 2, respectively. Element 121 has a relativistically stabilized 8p electron in its ground state electron configuration [34], in contrast to the prediction based on a simple extrapolation in the group. In the next element, Z = 122, a 7d electron is added to the ground state, so that it is $8s^2 7d8p$ in contrast to the $7s^2 6d^2$ state of Th [35]. This is the last element where accurate DCB CC calculations exist.

For heavier elements, calculations start to disagree on the ground states (Table 1). The situation there becomes more complicated: 7d, 6f, and 5g levels, and furthermore 9s, $9p_{1/2}$ and $8p_{3/2}$ levels are located energetically so close to each other that clear structures of the pure p, d, f, and g blocks are not distinguishable anymore. The usual classification on the basis of a simple electronic configuration and placement of the elements in this part of the Periodic Table become problematic. Thus, e.g., according to [1, 2], the Periodic Table has a very long 8th period starting from Z = 119 and counting 46 elements, so that the last element of this period is 164, while elements 167 through 172 are $8p_{3/2}$ ones (due to the very large SO effects on the 8p AOs) belonging to the 9th period. The 5g shell is being filled in elements 125 through 144. Elements 165 and 166 are then 9s ones belonging to group 1 and 2, respectively.

Seaborg and Keller have designed another table [3–5], even though they used the same DF calculations of Fricke et al. [1, 2]. In their table, elements of the 8th period are those from Z = 119 through 168, including those from Z = 122 through 153, called superactinides. In difference to the results of [1, 2], the 8p elements are those from Z = 163 to 168, and the 9s elements are those with Z = 169 and 170. Such an arrangement of the elements is, however, not reflecting the filling of the AOs obtained in the original DF calculations, so that the Periodic Table of [1, 2] is more appropriate.

In a recent work based on MCDF (with average level, AL, energy functional) calculations of highly charged states of some elements of the 8th period it was, however, suggested that elements of the 5g series are those from Z = 121 to Z = 138 [31]. Elements 139 and 140 are assigned then to group 13 and 14, respectively, denoting that they are $8p_{1/2}$ elements, while those from Z = 141 to 155 are 6f elements. The 8th period finishes then at element 172. Thus, the Periodic Table of Pyykkö [31] looks quite different to that of Fricke and Waber [1, 2]. One should, however, note that ionized states cannot give information about ground

Table 1 Ground states of elements 121–124 (Z = 120 core +), 140 and 143 (Z = 120 core + $8p_{1/2}^2$ +) and of some of their ions

Method	121	122	123	124…	140	143	Ref.
DCB FSCC	8p	7d8p	–	–	–	–	[34,35]
MCDF/OL	–	–	–	–	$5g^{15}8p^4 6f$	–	[36]
MCDF/AL	8p	7d8p	$6f^2 8p$	$6f^2 8p^2$	$5g^{14}6f^3 7d8p^2$	$5g^{17}6f^2 7d^2$	[30]
MCDF/AL	8p	$8s^2$ (2+)	$6f^1$ (4+)	$6f^1$ (5+)	$5g^{16}8p^2$ (2+)	$5g^{18}7d^3$	[31]
DF	8p	7d8p	6f7d8p	$6f^3 8p$	$5g^{14}6f^3 7d8p^2$	$5f^{17}6f^2 7d^2$	[1, 2]

states of the elements, so that those assignments are rather tentative. An attempt to define ground states of the heaviest elements on the example of Z = 140 using the latest version of the MCDF method (with the optimal level, OL, energy functional) failed [36]. The author arrived to a conclusion that such calculations are presently restricted due to the computer limitations. It was also stated that at the present level of the MCDF theory, the Periodic Table ends at Z = 173, i.e., when the energy of the 1s electron goes below $-2mc^2$. A detail discussion about the end of the Periodic Table depending on the approximation is given in [36].

Thus, at the modern level of the relativistic electronic structure theory, the problem of defining ground states of elements heavier than 122 remains. Very accurate correlated calculations of the ground states with inclusion of the quantum electrodynamic (QED) effects at the self-consistent field (SCF) level are needed in order to reliably predict the future shape of the Periodic Table. At the time of writing, an accepted version of the Table is that of Fig. 1, with the superactinides comprising elements Z = 122 through 155 as suggested in [1, 2].

The structure of the modern Periodic Table cannot be understood without knowing the influence of relativistic effects on electronic valence shells. This is considered in the following section.

3 Relativistic and QED Effects for the Heaviest Elements

With increasing Z of heavy elements causing a stronger attraction to the core, an electron is moving faster, so that its mass increase is

$$m = m_0 / \left[1 - (v/c)^2\right]^{1/2}, \tag{1}$$

where m_0 is the rest mass, v is the velocity of the electron, and c is the speed of light. The Bohr model for a hydrogen-like species gives the following expressions for the velocity, energy, and orbital radius of an electron

$$v = (2\pi e^2/nh)Z, \tag{2}$$

$$E = -(2\pi^2 e^4/n^2 h^2)mZ^2, \tag{3}$$

$$r = Ze^2/mv^2, \tag{4}$$

where n is the principal quantum number, e is the charge of the electron, and h is Planck's constant. With increasing Z along the Periodic Table, the m/m_0 ratio becomes larger. For H it is 1.000027. From the 6th period onwards, this ratio exceeds by 10%, so that relativistic effects cannot be neglected anymore. For example, for Fl, $m/m_0 = 1.79$ and it is 1.95 for element 118. (See also [37] for other examples). The contraction (Eq. 4) and stabilization (Eq. 3) of the hydrogen-

like s and $p_{1/2}$ electrons is a direct relativistic effect and it was shown to originate from the inner K and L shell regions [38]. This effect was found to be also large for the valence region due to the direct action of the relativistic perturbation operator on the inner part of the valence density [39]. Figure 2 shows, e.g., a relativistic contraction of the 7s AO of element 105, Db, $\Delta_R\langle r\rangle_{ns} = \langle r\rangle_{nr} - \langle r\rangle_{rel}/\langle r\rangle_{nr} = 21\%$. Figure 3 shows a relativistic contraction of 25% and stabilization of 5.8 eV of the 7s AO of Cn.

The relativistic contraction and stabilization of the ns AO reach their maximum in the 7th period at Cn [8] (Fig. 4). The shift of the maximum to Cn in the 7th period in contrast to Au in the 6th period is because in Rg and Cn, the ground state electronic configurations are d^9s^2 and $d^{10}s^2$, respectively, while the corresponding electronic configurations in the 6th period are Au($d^{10}s^1$) and Hg($d^{10}s^2$).

The second (indirect) relativistic effect is the destabilization and expansion of outer d and f orbitals: The relativistic contraction of the s and $p_{1/2}$ shells results in a more efficient screening of the nuclear charge, so that the outer orbitals, which never come close to the core, become more expanded and energetically destabilized. (The expansion and destabilization of the (n–1)d AOs with Z are shown in Fig. 3 for group-12 elements, as an example). While the direct relativistic effect originates in the immediate vicinity of the nucleus, the indirect relativistic effect is influenced by the outer core orbitals. It should be realized that though contracted s and $p_{1/2}$ core (innermore) orbitals cause indirect destabilization of the outer orbitals, relativistically expanded d and f AOs cause the indirect stabilization of the valence s and p-AOs. That partially explains the very large relativistic stabilization of the 6s and 7s AOs in Au and Cn, respectively. Since d shells (it is also valid for the f shells) become fully populated at the end of the nd series, a maximum of the indirect stabilization of the valence s and p AOs will occur there [39].

The third relativistic effect is the well-known spin–orbit (SO) splitting of levels with $l > 0$ (p, d, f, etc.) into $j = l \pm ½$. It also originates from the inner shell region in the vicinity of nucleus. The SO splitting for the same l decreases with increasing number of subshells, i.e., it is much stronger for inner (core) shells than

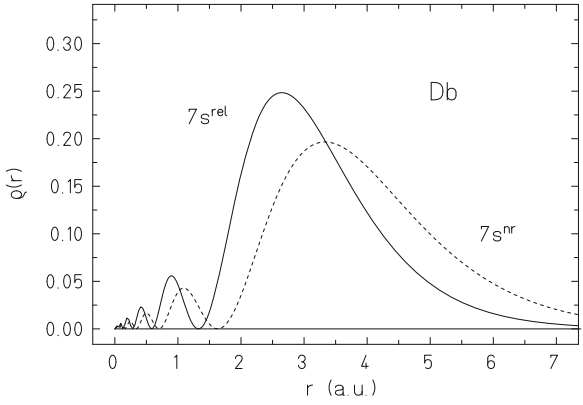

Fig. 2 Relativistic (*solid line*) and non-relativistic (*dashed line*) radial distribution of the 7s valence electrons in Db. From [11]

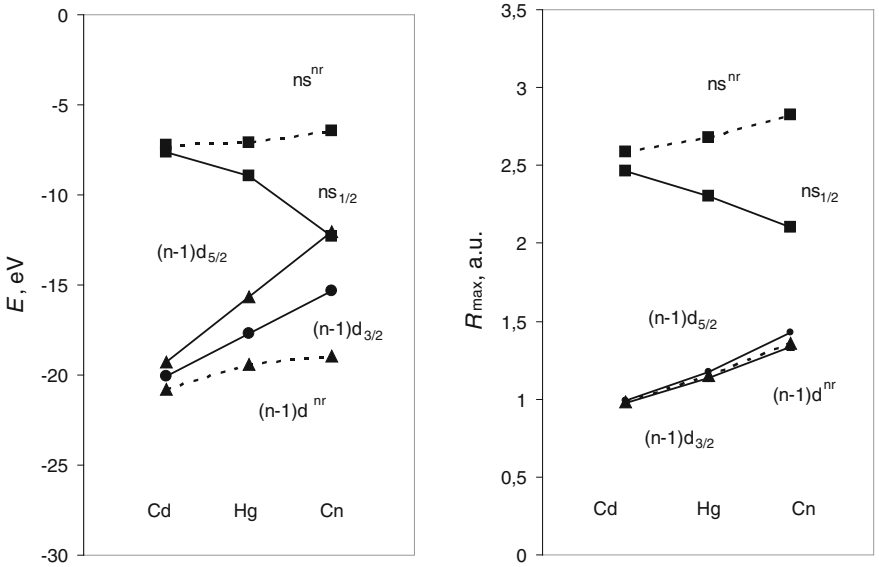

Fig. 3 Relativistic (*solid line*) and nonrelativistic (*dashed line*) energies, E, and the maximum of the radial charge distribution, R_{max}, of the valence ns and (n–1)d AOs of group-12 elements. The data are from [21]. Reprinted with permission from V. Pershina, Radiochim. Acta **99**, 459 (2011). Copyright 2011 Oldenbourg Wissenschaftsverlag GmbH

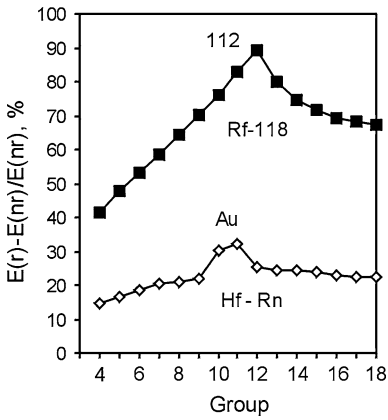

Fig. 4 The relativistic stabilization of the 6s and 7s orbitals in the 6th and 7th rows of the Periodic Table. Re-drawn from [8]. The DF data are from [21]

for outer shells. The SO splitting decreases with increasing l for the same principal quantum number, i.e., the $np_{1/2}$-$np_{3/2}$ splitting is larger than the $nd_{3/2}$-$nd_{5/2}$ and both are larger than the $nf_{5/2}$-$nf_{7/2}$. It is explained by the orbital densities in the vicinity of the nucleus decreasing with increasing l. In transactinide compounds SO coupling becomes similar, or even larger, in size compared to typical bond energies.

All the three effects change approximately as Z^2 for the valence shells down a column of the Periodic Table. It was suggested that relativistic effects depend even on higher powers of Z, especially for the heaviest elements [40]. Dependence of relativistic effects on electronic configuration in the neutral atoms of d- and f-block elements is discussed in [41].

The relativistic destabilization and SO splitting of the 6d AOs increase along the 6d series. Together with the stabilization of the 7s AOs, this results in an inversion of the 7s and $6d_{5/2}$ energy levels in Cn, so that its first ionized electron is $6d_{5/2}$ and not 7s as in Hg (Fig. 3). (The inversion of the 7s and $6d_{5/2}$ levels in the 7th period starts already at Hs). Figure 3 also shows that trends in the relativistic and non-relativistic energies and R_{max} of the ns AOs (the same is valid for the $np_{1/2}$ AOs) are opposite with increasing Z in the groups, which results in the opposite trends in relativistic and nonrelativistic properties defined by those AOs.

In the 7p series, the stabilization of the $7s^2$ is so large that it becomes practically an inert pair. The SO splitting of the 7p AOs increases along the series reaching 11.8 eV at element 118 (Fig. 5).

In the 8p and 9p elements, the SO interaction is so large, that their series split into the $p_{1/2}$ and $p_{3/2}$ ones [1, 2], so that the structure of the Periodic Table has no more clear blocks. For the heavier elements, relativistic effects on their valence orbitals are even more pronounced and could lead to properties that are very different to those of the lighter homologs. Without relativistic effects the properties would, however, also be very different due to the loosely bound valence s and p electrons.

Breit effects (accounting for magnetostatic interaction and retardation effects to the order of $1/c^2$) on energies of valence orbitals and IP are usually small, e.g., 0.02 eV for element 121, but can be as large as 0.1 eV for transition energies

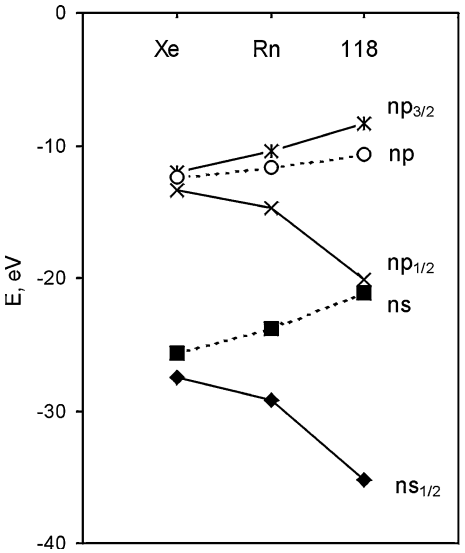

Fig. 5 Relativistic stabilization of the ns and $np_{1/2}$ orbitals and the spin–orbit splitting of the np orbitals for the noble gases Xe, Rn and element 118. The Dirac–Fock atomic energies are from [21] and the Hartree–Fock (nonrelativistic) values are from [8]

between the states including f orbitals [34]. They can also reach few % for the fine-structure level splitting in the 7p elements and are of the order of correlation effects there.

QED effects are known to be very important for inner shells [42, 43] in accurate calculations of X-ray spectra (see [44, 45] for the heaviest elements). For highly charged few electron atoms they were found to approach the Breit correction to the electron–electron interaction. Similar effects were also found for valence ns electrons [46]. A comparison of the valence ns Lamb shift (the vacuum polarization and self-energy) with the ns AO energy and the relativistic, Breit, and nuclear volume contributions to it for coinage metals at the DF level is shown in Fig. 6. The result for the valence ns electron is a destabilization, while for (n–1)d electron is an indirect stabilization. In the middle range (Z = 30–80) both the valence-shell Breit and the Lamb-shift terms behave similarly to the kinetic relativistic effects scaling as Z^2. For the highest Z values the increase is faster.

The nuclear volume effects grow even faster with Z. Consequently, for the superheavy elements, its contribution to the orbital energy should be the second important one after the relativistic contribution. QED corrections for the valence shells in heavy many-electron atoms of elements Rg through Fl, and 118 through 120 calculated using a perturbation theory are given in [47]. Thus, e.g., QED on the DCB IP of element 120 is −0.013 eV, while it is 0.023 eV for Cn. For element 118, QED effects on the binding energy of the 8s electron cause a 9% reduction

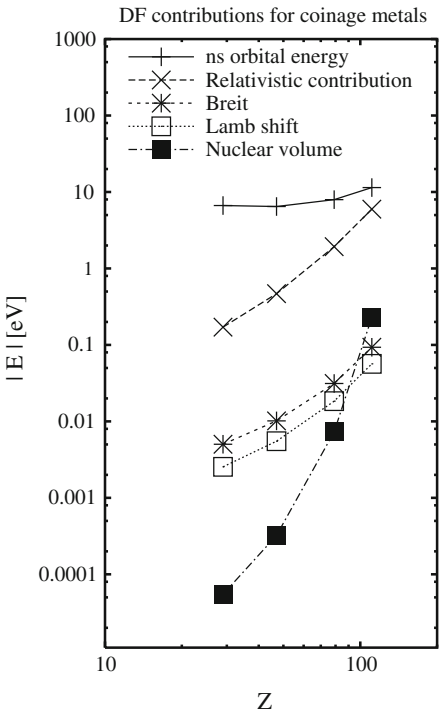

Fig. 6 Comparison of the valence ns Lamb shift with the orbital energy and the relativistic, Breit, and nuclear volume contributions to it for coinage metals. Reproduced with permission from P. Pyykkö, M. Tokman, L.N. Labzowsky, Phys. Rev. A **57**, R689 (1998). Copyright 1998 American Physical Society

(0.006 eV) of EA [48]. Thus, the QED effects are not negligible: they are of the order of 1–2% of the kinetic relativistic effects, which means that the existing studies of relativistic effects are up to 99% [46] (or 101% [36]) correct.

4 Relativistic Quantum Chemical Methods for Atoms and Molecules

4.1 Dirac Equation

Presently the highest level of theory for many-body methods for molecules is the DCB Hamiltonian

$$h_{\mathrm{DCB}} = \sum_i h_D(i) + \sum_{i<j} \left(1/r_{ij} + B_{ij}\right), \tag{5}$$

where the one-electron Dirac operator is

$$h_D(i) = c\vec{\alpha}_i\vec{p}_i + c^2(\beta_i - 1) + V^n(i) \tag{6}$$

Here, $\vec{\alpha}$ and β are the four-dimentional Dirac matrices, and V^n is the nuclear attraction operator. The Breit term in the low photon frequency limit is

$$B_{ij} = -\frac{1}{2}\left[(\vec{\alpha}_i\vec{\alpha}_j)r_{ij}^{-1} + (\vec{\alpha}_i\vec{r}_{ij})(\vec{\alpha}_j\vec{r}_{ij})r_{ij}^{-3}\right]. \tag{7}$$

The operators of the Dirac Eq. (5) are 4×4 matrix operators, and the corresponding wave function is therefore a four-component ($4c$) vector (spinor). The V^n includes the effect of the finite nuclear size, while some finer effect, like QED, can be added to the h_{DCB} perturbatively, although the self-energy QED term is more difficult to treat [36, 47, 48]. The DCB Hamiltonian in this form contains all effects through the second order in α, the fine-structure constant.

Since the relativistic many-body Hamiltonian cannot be expressed in a closed potential form, which means it is unbound, projection one- and two-electron operators are used to solve this problem. The operator projects onto the space spanned by the positive-energy spectrum of the Dirac–Fock-Coulomb (DFC) operator. In this form, the "no-pair" Hamiltonian is restricted then to contributions from the positive-energy spectrum and puts Coulomb and Breit interactions on the same footing in the SCF calculation [49].

Since the Dirac equation is written for one electron, the real problem of methods for a many-electron system is an accurate treatment of the instantaneous electron–electron interaction, called electron correlation. The latter is of the order of magnitude of relativistic effects and contributes to a larger extent to bonding energy and other properties. The DCB Hamiltonian (Eq. 5) accounts for these effects in the first order via the $V_{ij} = 1/r_{ij}$ term. Some higher order of magnitude

correlation effects are taking into account by the configuration interaction (CI), many-body perturbation (MBPT), including the Møller-Plesset (MP) theory, or, presently, at the highest level of theory, coupled cluster with single-double and perturbative triple, CCSD(T), excitations, or Fock-space CC (FSCC) techniques.

4.2 Atomic Codes

The most straightforward way to solve the Dirac many-electron Eq. 5 is that without an approximation. The DCB CC method [32, 33] is based on such a solution and is presently the most powerful method used for atomic calculations.

In the CC approach, correlation effects are taken into account by action of the excitation operator

$$S = \sum_{m \geq 0} \sum_{n \geq 0} \left(\sum_{l \geq m+n} S_l^{(m,n)} \right) \tag{8}$$

defined in the Fock-space CC approach with respect to a closed-shell reference determinant. In addition to the traditional decomposition into terms with different total number of excited electrons (l), S is partitioned according to the number of valence particles (m) or holes (n). Presently, the method is, however, limited to one or two (single-double excitations, CCSD, e.g. $(m,n) \leq 2$) particle valence sectors of the Fock space, i.e., it can treat the states which can be reached from a closed shell by adding or removing no more than two electrons.

Further developments are under way to remove this limitation [32, 33]. Thus, the high-sectors FSCC code is under development, which will allow for treating systems with up to 6 valence electrons/holes in an open shell. Relativistic Hilbert space CC (HSCC) method is also worked on, which could be used for systems with more than a couple of electrons/holes in the active valence shell. The mixed sector (MS) CC method will be a generalization of the previous two (FSCC and HSCC) and will combine their advantages. A further improvement is the introduction of the intermediate Hamiltonian (IH). It is a generalization of the effective Hamiltonian (EH) method and serves as a core of most multi-root multireference approaches. The standard multireference FSCC and HSCC methods (described above) are used in the effective Hamiltonian framework. The most problematic technical problem of the EH method is poor (or no) convergence of iterations due to presence of so-called intruder states. Recently many groups developed different forms of "intruders –free" intermediate Hamiltonian formulations of FSCC and HSCC. These formulations substantially extend the scope and applicability of the multi-root multireference CC methods. The XIH (extrapolated intermediate Hamiltonian) method is a specific (very efficient) form of IH developed by the Eliav-Kaldor group [32, 33].

The DCB FSCC method is very accurate, with an average error of 0.1 eV for excitation energies, since it takes into account most of dynamic correlation effects

omitted in the MCDF method and a core polarization. The DC FSCC and CCSD(T) methods incorporated in the DIRAC program package [50] have a slightly lower accuracy than the DCB FSCC one [32, 33]. Both the DCB and DC FSCC/CCSD(T) methods were applied to the heaviest elements up to Z = 122 (see [32, 33] and references therein, as well as various examples below). Due to the mentioned limitation of the methods, they can, however, presently not handle the elements of the midst of the d, f, or g-series.

In the relativistic *ab initio* DC(B) calculations, in contrast to non-relativistic ones, large basis sets are needed to describe accurately the inner shell region where relativistic perturbation operators are dominant. The condition of the kinetic balance relating the large and small components of the 4*c* wave function should be observed. Kinetically balanced Gaussian type wave functions with a Gaussian distribution for the nuclear potential are presently best suited. The practical basis sets for the heaviest elements are the universal ones [51], those of Visscher [52], Faegri [53, 54], and Dyall [54, 55]. The prolapse-free relativistic Gaussian basis sets for elements up to Z = 119 suitable for 4*c* molecular calculations are those of [56].

A practical instrument for many-electron open shell system is still the MCDF method. There are several modifications of it implemented into computational codes of Desclaux [57], developed further by Indelicato [36], of Grant [58] and Fröse-Fisher [59]. Based on the CI technique, the MCDF method accounts for most of the correlation effects while retaining a relatively small number of configurations. It can treat a large number of open shell configurations and can be applied to elements with any number of valence electrons. It omits, however, dynamic correlation, since excitations of the type $(nj) \rightarrow (n'j)$ cannot be handled, and some core polarization, which makes it less accurate than the DC(B) CC methods. An average error for IP of heavy elements is about 1 eV. Calculations for many heaviest and superheavy elements were performed with the use of the AL version [23–31], as well as with a more accurate OL one [36].

QED are presently included perturbatively on top of the self-consistent-field (SCF) calculations [36, 47, 48].

Atomic calculations for the heaviest elements were also performed using other approaches while studying molecular properties (see Sect. 5). Thus, e.g., electronic states of Fl were calculated using the relativistic complete active space MCSCF (CASMCSCF) CI method [60].

Earlier, chemical properties of the transactinides were predicted using single-configuration DF and DS calculations using approximations of Eqs. 5, 6 and numerical techniques [1, 2, 18–21]. The obtained energy terms were then corrected by the difference with experiment for the lighter homologs to reach the required accuracy. Elements up to Z = 172 were treated with the use of these methods. (Element 184 was also considered, as an example of an even heavier element). Overall, results of the modern *ab initio* correlated atomic calculations agree rather well with the (corrected) DF and DS ones from the early studies.

4.3 Molecular Methods

Methods used for relativistic calculations of the heaviest element systems are, in principle, the same used for any other relativistic system, provided basis sets for the heaviest elements are available. They are described in several issues, with those of [61–63] particularly recommended.

4.3.1 Wavefunction Based (*ab initio*) Methods

4 component (4c) methods. Molecular fully relativistic methods use the same DFC or DC(B) Hamiltonians (Eqs. 5, 6) as the atomic ones. Based on them molecular LCAO codes including correlation effects are at the stage of further development [64, 65]. The problems of electron correlation and proper basis sets make the use of these *ab initio* DF methods limited for molecular applications. Presently, correlation effects are taken into account by the CI, MBPT and CCSD(T) techniques. The basis sets and problems connected with their use are the same as for atomic ab *initio* calculations [51–55].

In these methods, calculations of two-electron integrals require large disk space and computational time. They are, therefore, still too computer time intensive and not sufficiently economical to be applied to the heaviest elements in a routine manner, especially to complex systems studied experimentally. Mostly small molecules, like hydrides or fluorides were studied with their use. The main aim of those works was investigation of the influence of relativistic and correlation effects on properties of model systems. One of successful implementations of this group of methods is a part of the DIRAC program package [50].

2 component (2c) methods. Due to the practical limitations of the 4*c* methods, 2*c* ones are very popular in molecular calculations. In this approximation, the "positronic" and electronic solutions of the Dirac-Hartree–Fock (DHF) method are decoupled [66, 67]. This reduces the number of matrix elements in the Hamiltonian to interactions solely among electrons (positive-energy states) and nuclei and, therefore, saves valuable computer time. Perhaps, the most applied method of decoupling the large and small components of the wave function is the Douglas-Kroll-Hess (DKH) approximation [68].

4.3.2 Relativistic Pseudo-Hamiltonians

An efficient way to solve a many-electron problem is to apply the pseudopotential (PP) approximation. Pseudopotential calculations are less accurate than all-electron, "but they simulate the results of the latter often surprisingly well, for substantially smaller expenses" [69]. The methods are widely used in electronic structure theory for chemically interesting compounds of all elements of the Periodic Table including the heaviest. There are several excellent reviews on this type of methods (see, e.g., [70, 71]).

According to this approximation, frozen inner shells are omitted and replaced in the one-electron part of the Hamiltonian by an additional term, the so-called pseudopotential (V^{PP})

$$H_V = -\frac{1}{2}\sum_{i}^{n_V}\nabla_i^2 + \sum_{i<j}^{n_V}\frac{1}{r_{ij}} + \sum_{i}^{n_V}\sum_{a}^{N_C}\left[V_a^{PP}(r_{ai}) - \frac{Q_a}{r_{ai}}\right] + \sum_{a<b}^{N_C}\frac{Q_a Q_b}{r_{ab}}, \qquad (9)$$

with n_V valence electrons and N_c cores (nuclei). The indices *a, b* run over all cores (nuclei), *i, j* over all valences electrons, Q_a is the charge of core *a*. As a result, the number of basis functions is drastically reduced and, hence the number of two-electron integrals. The additional one-electron pseudopotential integrals are solved by standard integral techniques for the valence basis functions giving rise to additional matrix elements in standard *ab initio* or density functional theory (DFT) schemes at the SCF level.

There are basically two current approaches in molecular applications for approximating V^{PP}: (1) the model core potential (MCP) one, also its extension to the *ab initio* model potential (AIMP) [72, 73] and (2) the semi-local pseudopotential (PP) approximation [74, 75].

In the MCP, or more advanced AIMP, approximations [72, 73], V^{PP} is represented by an adjustable local potential and a projection operator. This potential is constructed so that the inner nodal structure of the pseudo-valence orbitals is conserved, thus closely approximating all-electron valence AOs. Scalar relativistic effects are directly taken into account by relativistic operators such as Douglas-Kroll (DK) one. SO effects can be included with the use of the SO operator, V^{SO}. The resulting one-electron integrals are then easily solved for Gaussian functions. The methods are implemented in some commercial packages and can be applied to most of the elements of the Periodic Table, except of the heaviest, where such potentials still need to be constructed.

In the effective core potential (ECP) approximation, V^{PP} is represented by a semi-local potential [74]. Unlike in the MCP methods, there are no core functions and the pseudo-valence orbitals are nodeless for the radial part, which is an essential approximation. The semi-local ansatz gives rise to rather complicated integrals over the Gaussian functions compared to the MCP methods, though efficient algorithms were developed for their solution. Relativistic and SO effects are treated by relativistic one-electron PPs (RPP) [76]

$$V^{RPP} = \sum_{l,j,m_j} V_{lj}(r)\left|ljm_j\right\rangle\left\langle ljm_j\right|, \qquad (10)$$

or relativistic scalar and SO effects can be separated in the following way

$$V^{RPP} = V^{AREP} + V^{SO}, \qquad (11)$$

where the scalar V^{AREP} is

$$V^{\mathrm{AREP}} = \sum_{l,m_j} V_l(r)|lm_l\rangle\langle lm_l|. \tag{12}$$

The V^{AREP} is usually fitted to one-component (scalar relativistic) or two (four)-component all-electron DHF relativistic atomic wave functions or energies. Such potentials for elements Am through 118 were generated, e.g., by Nash et al. [77]. The ECPs are implemented in the program packages such as Gaussian, Molpro, MOLCAS, or Turbomole, and in the solid-state program CRYSTAL (see [71] and references therein).

Energy-adjusted PPs use atomic spectra (energies) for generating V^{PP} or V^{RPP} [75]. To achieve high accuracy, a large number of valence states has to be taken into account in the fitting procedure, which technically can be demanding and computer time expensive. SOPPs are obtained by adding V^{SO} to V^{AREP} (Eq. 12). These PPs, also including QED effects, were generated for the transactinides till Z = 118 [78, 79].

There are several other PPs differing in the way of fitting pseudopotential parameters. Among these are the popular quasirelativistic (QR) PPs of Hay and Wadt, which are implemented, for example, in the commercial program package "Gaussian" though have not yet been developed for the transactinides [80, 81].

More recently, generalized relativistic effective core potentials, GRECPs, have been developed [82]. An improvement over the original idea of V^{PP} is the division of the valence space into an outer core part and a valence part, and introduction of a special technique to correct an error introduced by smoothing orbitals in the core region. This could give more accurate results than V^{PP} provided a small core definition is used. The method is not widely used, as GREPs are not yet developed for all elements of the Periodic Table, and it has not yet been implemented in standard program packages. It was applied to some simplest heaviest elements molecules.

PPs are also used for 1D, 2D and 3D infinite systems (polymers, surfaces and the bulk). In the solid-state calculations, PPs are constructed from Kohn–Sham rather that Hartree–Fock equations. An overview of this class of the PP methods is given elsewhere [71].

4.3.3 Relativistic Density Functional Theory

DFT is based on the knowledge of the ground state electron density, which uniquely determines the Hamiltonian and, therefore, the ground state energy and other properties [83, 84]. Due to its relative simplicity, DFT became extremely useful in the application to large molecules, clusters, solutions and solids. Systems with the large number of atoms can be treated with sufficient accuracy. The computing time in the DFT for a system of many atoms, N_{at}, grows as N_{at}^2 or N_{at}^3, while in traditional methods, where the many-electron wave function $\Psi(r_1 \ldots r_N)$ is

used, as exp(N_{at}). DFT methods are alternative and complementary, both quantitatively and conceptually, to the traditional ones.

For the relativistic case [85, 86] in the non-collinear spin-polarize (SP) formalism, the Kohn–Sham equation for the total energy lying in the basis of the calculational algorithms is

$$E = \sum_{i=1}^{M} n_i \langle \phi_i | \hat{t} | \phi_i \rangle + \int V^N \rho \mathrm{d}^3 \vec{r} + \frac{1}{2} \int V^H \rho \mathrm{d}^3 \vec{r} + E^{\mathrm{xc}}[\rho, \vec{m}] + \sum_{p>q} \frac{Z_p Z_q}{|\vec{R}_p - \vec{R}_q|} \tag{13}$$

with the electron density

$$\rho(\vec{r}) = \sum_{i=1}^{M} n_i \phi_i^+(\vec{r}) \phi_i(\vec{r}) \tag{14}$$

and the magnetization density

$$\vec{m}(\vec{r}) = -\mu_B \sum_{i=1}^{M} n_i \phi_i^+(\vec{r}) \beta \vec{\Sigma} \phi_i(\vec{r}), \tag{15}$$

where ϕ_i are 4c-Dirac spinors. In Eqs. 13–15, $\hat{t}$ is the Dirac kinetic operator, μ_B is the Bohr-magneton, $V^N$is the nuclear potential, $V^H$is the electronic Hartree potential, and E^{ex} is the exchange correlation energy functional. The 4c spin operator $\vec{\sum} = \left(\sum_x, \sum_y, \sum_z\right)$ is built from the 2c Pauli matrix σ.

Application of the variational principle with the constraint that the number of electrons in the system should be conserved leads to the single particle Kohn–Sham equations in their non-collinear form

$$\left\{ \vec{t} + V^N + \tilde{V}^H + \frac{\delta E^{\mathrm{xc}}[\rho, \vec{m}]}{\delta \rho} - \mu_B \beta \vec{\Sigma} \frac{\delta E^{\mathrm{xc}}[\rho, \vec{m}]}{\delta \vec{m}} \right\} \phi_i = \varepsilon_i \phi_i. \tag{16}$$

According to the SP formalism, nearly each electron is treated by its own wavefunction with a quantum number j and magnetic number m_j. (The collinear approximation is also implemented in the method). This permits treatment of open shell system.

Usually, self-consistent, all-electron calculations are performed within the relativistic local density approximation (LDA). The general gradient approximation (GGA), also in the relativistic form, RGGA, are then included perturbatively in $E^{xc}(\rho, \vec{m})$. The accuracy depends on the adequate knowledge of the potential, whose exact form is, however, unknown. There is quite a number of these potentials and their choice is dependent on the system. Thus, PBE is usually favored by the physics community, PBE0, BLYP, B3LYP, B88/P86, etc., by the chemical community, while LDA is still used extensively for the solid state.

There are two 4c-DFT SP methods based on the solution of Eq. 13. They were extensively used for the heaviest elements. The first one [87] utilizes numerical

4*c* wave functions as a basis set. (The basis set optimization procedure is described in [87]). In the present form, it allows for treating explicitly very large systems such as clusters of up to more than hundred atoms and is, therefore, suitable for treatment of adsorption phenomenon on surfaces of solids. A possibility to treat the large number of atoms economically is foreseen via an embedded cluster procedure [88] (Fig. 7).

The second 4*c*-DFT code is the Beijing Density Functional (BDF) one [89]. As basis sets, 4*c* numerical atomic spinors obtained by finite-difference atomic calculations are used for cores, while basis sets for valence spinors are a combination of numerical atomic spinors and kinetically balanced Slater-type functions. Both the 4*c*-DFT [87] and 4*c*-BDF [89] methods give very similar results.

Earlier, the intrinsically approximate 4*c* Dirac-Slater discrete variational, DS DV, code of Ellis and Rosen [90] with the Slater $E^{\mathrm{ex}} = -3C[3\rho(r)/8\pi]^{1/3} = 0.7$ was used for calculations of transactinide compounds (see [6] for a review). Even though the method was inaccurate in calculating total and, hence, dissociation energies, it provided accurate IPs, EAs and electron transition energies.

2*c*-DFT methods are a cheaper alternative to the 4*c* ones, with a comparable accuracy [91]. One version is available as a part of the Amsterdam Density Functional (ADF) program package [92]. Calculations were performed on some transactinide molecules.

A one-component quasirelativistic DFT method, also a part of the ADF package [92], was extensively used in the calculations for transition element and actinide compounds. (Earlier, the quasirelativistic Hartree–Fock-Slater (QR HFS) method was widely used for such calculations [93]). In this method, the Hamiltonian contains relativistic corrections already in the zeroth-order and is therefore called the zeroth-order regular approximation (ZORA) [94, 95]. The spin operator is also included in the ZORA Fock operator [96]. Other popular quasirelativistic 2*c*-DFT methods are based on the DKH approximation [97, 98] and implemented in many program packages. The following codes should also be mentioned: of Rösch [99, 100], Ziegler [101], and Case and Young [102]. They were, however, not used for the heaviest elements. A review on relativistic DFT methods for solids can be found in [103].

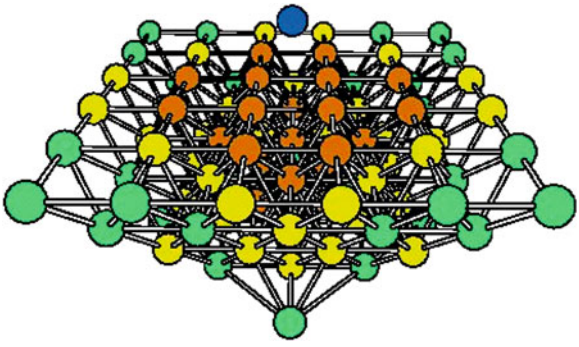

Fig. 7 Embedded M'-M_n system. (The embedded M_n cluster is shown in *red*)

Table 2 Accuracy of different molecular methods showing the importance of relativistic and correlation effects on the equilibrium bond length, R_e (in Å), dissociation energy, D_e (in eV), and vibrational frequency, ω_e (in cm^{-1}), of AuH

Method	R_e	D_e	ω_e	Ref.
HF (NR)	1.831	1.08	1464	[104]
HF (NR) MP2	1.711	1.90	1695	[104]
DHF	1.570	1.78	2067	[104]
DHF MP2	1.497	3.11	2496	[104]
DK CCSD(T)	1.525	2.92	2288	[106]
PP CCSD(T)	1.527	3.21	2306	[107]
RECP CCSD(T)	1.510	3.31	2330	[108]
DFT DKH	1.539	3.33	2330	[99]
DFT ZORA (MP)	1.537	3.33	2258	[109]
4*c*-BDF	1.537	3.34	2259	[109]
Experiment	1.524	3.36	2305	[110]

Accuracy of various relativistic, non-relativistic, correlated and non-correlated methods [99, 104–109] in comparison with experiment [110] is demonstrated in Table 2 for AuH, a sort of a test molecule (see also [111]). Both the PP/RECP and DFT methods seem to perform rather well for this molecule. The data of Table 2 also demonstrate the importance of relativistic and electron correlation effects. Thus, relativistic effects diminish the equilibrium bond length (R_e) by 0.26 Å (the HF–DF difference without correlation), or by 0.21 Å [the (HF + MP2) − (DF + MP2) difference with correlation], and enlarge the dissociation energy (D_e) by 0.70 eV (the HF–DF difference without correlation), or by 2.21 eV [the (HF + MP2) − (DF + MP2) difference with correlation]. Correlation diminishes R_e on the DF level by 0.07 eV, but enhances D_e by 1.34 eV. Thus, even for AuH correlation amounts almost to 50% of the chemical bond strength. These data also demonstrate that there is no additivity of correlation and relativistic effects.

5 Atomic Properties of the Transactinides

Electronic configurations, ionization potentials, atomic/ionic radii, polarizabilities and stability of oxidation states are important chemical properties, whose knowledge is indispensable in assessing similarity of the heaviest elements to their lighter homologs in the chemical groups.

5.1 Electronic Configurations

Predictions of chemical properties of elements Z = 104 through Z = 172 in the ground states made on the basis of DF and DS calculations up to 1975 are summarized in [1, 2]. DF ground states are also reported for Z = 111 through 132 [22]. MCDF calculations for ground and excited states of elements Rf through Hs are

published in [24–29], and for ground states of elements Z = 119–164 in [30]. Excited states of elements Z = 119–169 were also predicted at the MCDF level of theory [31]. The DC(B) CC ground and some excited states were calculated for Rf [112], elements 111–120 [48, 113–133] and 121–122 [34, 35]. DFT + QED calculations were reported for ground states of elements 121–131 [134].

MCDF calculations [23] have shown that Lr is the first element where the strong relativistic stabilization of the $7p_{1/2}$ electron results in a ground state electronic configuration, $7s^2 7p_{1/2}$ ($^2P_{1/2}$), different to that of Lu, $7s^2 6d$ ($^2D_{3/2}$). More accurate DCB CCSD calculations [122] confirmed this result. The next excited state of Lr, $7s^2 6d_{3/2}$ ($^2D_{3/2}$), was found to lie at 0.16 eV higher in energy in good agreement with the "corrected" value of 0.186 eV of the MCDF calculations [23].

For Rf, MCDF calculations [24, 25] have again shown a different electronic configuration, $7s^2 6d7p$ ($^3D_2$), than the one of Hf, $6s^2 5d^2$ ($^3F_2$). The $7s^2 6d7p$ ground state of Rf was, however, not confirmed by more accurate DCB CCSD calculations [112]. Inclusion of correlation effects of higher orders (f-electrons) in the CCSD calculations resulted in the inversion of the $7s^2 6d7p$ and $7s^2 6d^2$ states, with the latter being more stable.

Various calculations have shown that the relativistic stabilization of the 7s-AO in the 7th period results in the availability of the $7s^2$ electron pair in the ground and first ionized states of the 6d and 7p elements, $6d^q 7s^2$ and $7s^2 7p^q$, respectively (Tables 3 and 4). This is in contrast to the 6th period, where Pt and Au have different, $5d^q 6s$, ground states, or Ta, W, Os and Hg have different, $d^{q-1}s$, the 1+ ionized states. (The non-relativistic configuration of element 111 is, for example, $6d^{10}7s$ [113]). The relativistic stabilization of the 7p electrons manifests itself in some excited states different than those of lighter homologs, e.g., $6d7s^2 7p$ ($^3D_2$) of Rf lying 0.3 eV higher in energy in contrast to the $6d^2 7s^2$ ($^3F_3$) state of Hf.

For elements 119 and 120, the calculations have given the 8s and $8s^2$ states beyond the 118 core, respectively, as ground. Element 121 has an $8s^2 8p_{1/2}$ state in difference to Ac, $7s^2 6d$, due to the relativistic stabilization of the $8p_{1/2}$ AO, according to the DCB FSCC calculations [34]. Due to the same reason, the lowest state of the element 121 anion is $8s^2 8p^2$ compared to the $7s^2 7p6d$ state of Ac^-. For element 122, the DCB CCSD calculations [35] have given the $8s^2 7d8p_{1/2}$ ground state in contrast to the $7s^2 6d^2$ state for Th: the relativistic stabilization of the $8p_{1/2}$ orbital is responsible for such a change. All these calculations (except of the MCDF ones for Rf) agree on the ground states of elements up to $Z = 121$. They, however, start to disagree at $Z > 121$ (see Table 1), as was discussed in Sect. 2.

5.2 *Ionization Potentials, Electron Affinities and Oxidation States*

Non-relativistic (HF) and relativistic (DF) AO energies [21] of elements 104 through 118 are shown in Fig. 8. They are helpful in understanding ionization

Table 3 Electronic configurations, stable oxidation states and single ionization potentials of Rf through Cn

Element	Rf[b]	Db[c]	Sg[c]	Bh[c]	Hs[c]	Mt[d]	Ds[d]	Rg[b]	Cn[b]
Chemical group	4	5	6	7	8	9	10	11	12
Stable oxidation States[a]	**4**,3	**5**,4,3	**6**,4	7,5,4,3	**8**,6,4,3	3,6,1	6,4,2,0	**5**,3,-1	**4**,2,**0**
M	$6d^27s^2$	$6d^37s^2$	$6d^47s^2$	$6d^57s^2$	$6d^67s^2$	$6d^77s^2$	$6d^87s^2$	$6d^97s^2$	$6d^{10}7s^2$
IPi, eV	6.01	6.9	7.8	7.7	7.6	8.7	9.6	10.6	11.97
M^+	$6d7s^2$	$6d^27s^2$	$6d^37s^2$	$6d^47s^2$	$6d^57s^2$	$6d^67s^2$	$6d^77s^2$	$6d^87s^2$	$6d^97s^2$
IP* eV	14.37	16.0	17.9	17.5	18.2	(18.9)	(19.6)	(21.5)	22.49
M^{2+}	$7s^2$	$6d^3$	$6d^37s$	$6d^37s^2$	$6d^57s$	?	?	?	$6d^87s^2$
IP_3, eV	23.8[c]	24.6	25.7	26.6	29.3	(30.1)	(31.4)	(31.9)	(32.8)
M^{3+}	7s	$6d^2$	$6d^3$	$6d^27s^2$	$6d^37s^2$	?	?	?	?
IP_{4j} eV	31.9[c]	34.2	35.4	37.3	37.7	(40)	(41)	(42)	(44)
M^{4+}	[Rn]	6d	$6d^2$	$6d^27s$	$6d^2\ s^2$	($6d^5$)	($6d^6$)	($6d^7$)	($6d^8$)
IPs, ev		44.6	47.3	49.0	51.2	(51)	(53)	(55)	(57)
M^{5+}		[Rn]	6d	$6d^2$	$6d^3$				
IP_6, eV			59.2	62.1	64.0				
M^{6+}			[Rn]	6d	$6d^2$				
IP_7, ev				74.9	78.1				
M^{7+}				[Rn]	6d				
IPs, eV					91.8				

[a] bold = most stable states in the gas phase, underlined = most stable in solutions; [b] CCSD calculations: Rf [112]; Rg [113]; Cn [114]; [c] MCDF calculations: Rf [24, 25]; Db [26], Sg [27], Bh and Hs [28]; [d] DF calculations [1, 2]. The values of the IP in the parentheses are extrapolations, see [2]

Table 4 Atomic properties of element 112 through 120 (selected values)

Property	Cn	113	F1	115	Lv	117	118	119	120
Group	12	13	14	15	16	17	18	1	2
Electr. conf.	$d^{10}s^2$	$7s^27p$	$7s^27p^2$	$7s^27p^3$	$7s^27p^4$	$7s^27p^5$	$7s^27p^6$	$8s^1$	$8s^2$
Oxid. state	4,2,0	1,3	2	1,3	2,4	3,1,5,−1	4,2,6	1	2
IP, eV	11.97[a]	7.306[b]	8.626[c]	5.579[d] 5.553[e]	6.881[f]	7.638[g]	8.914[h]	4.788[i]	5.838[j]
EA, eV	0[a]	0.68(5)[b]	0[k]	0.383[d] 0.368[e]	0.905[f]	1.589[g]	0.056[l]	0.663[m]	0.019[j]
α, a.u.	27.40[n]	29.85[o]	30.59[n] 31.0[s]	(66)[p]	(61.17)[p]	(54.24)[p]	46.33[h]	169.00[r]	162.6[j]
AR, Å	1.71[n]	1.22[o]	1.75[n]	2.0[e]	–	1.76[u] 1.77[v]	2.41[h]	2.40[t]	2.0[t]
R_{vdW}, Å	1.99[n]	1.84[o]	2.08[n]	2.46[e]	–	–	2.41[h]	–	–

[a] Ref. [114]; [b] [115]; [c] DCB IHFSCC[129]; [d] [117]; [e] [123]; [f] DCB XIHFSCC[124]; [g] DC CCSD (T) [124]; [h] DCFSCC[119]; [i] DCB FSCC [120]; [j] DCB XIHFSCC (+ QED for IP) [125];[k] [129, 140];[l] [48]; [m] [121]; [n] [127];[o] [126];[p] estimated via a correlation with $R_{max}(np_{3/2})^3$ [130]; [r] DK CCSD(T) [131, 132]; [s] Kramers-restricted (KR) DC [133]; [t] [2]; [u] MCDF [137]; [v] $1/2R_e(M_2)$[91]

process and trends in ionization potentials. The latter, experimental in the case of the 6th row elements, and calculated (best values) in the case of the 7th row elements of the Periodic Table are given in Tables 3, 4 and are shown in Fig. 9.

The DF and DS IPs of elements 104 through 166 are given in [1, 2]. Multiple MCDF IPs of Rf through Hs, Cn, Fl and 117 are presented in [24–28, 135–137], and the first MCDF IPs of elements 113–119 are in [29]. IP(114) was also calculated using relativistic HF MBPT [138], and IPs and EAs of 7p elements were calculated using a multireference (MR) CI method [55]. The DC(B) CC IPs are reported for elements Rf, Rg-122 [34, 35, 48, 112–127]. The accuracy of various calculations of IPs of Pb and Fl is demonstrated in Table 5 [2, 60, 116, 129, 136, 138–140], where the highest level of theory is DCB IHFSCC [116, 129].

The calculated IP(Rf) is smaller than IP(Hf), because the 6d electron of Rf is weaker bound than the 5d one of Hf. For Db and Sg, IPs should be similar to those of Ta and W, due to the similar energies of the ionized electrons in each pair of the homologs. This is, indeed, the case shown by the calculations. IP(Bh) should be smaller than IP(Re). From Hs through Cn, IP of the 6d elements should, however, be larger than IPs of Os through Hg due to the more bound 6d electron in the heaviest elements in comparison with the 6s one in the lighter homologs. The MCDF calculations for Hs [28] and DF ones for Mt [1, 2] have, however, given lower values than expected. For Ds through Cn, the calculated values are larger than those of Pt through Hg, as anticipated. More accurate calculations than the DF and MCDF ones are, therefore, needed for the midst of the 6d-series.

IPs of elements 113 and 114 are also larger than those of Tl and Pb, respectively, due to the relativistically stabilized $7p_{1/2}$ AO. The relativistic stabilization of the $np_{1/2}$ AO in group 13 and 14 is responsible for a trend reversal in the decreasing IPs beyond In and Sn, respectively [126, 127]. IPs of elements 115 through 118 are, on the contrary, smaller than those of Bi through At, and are the

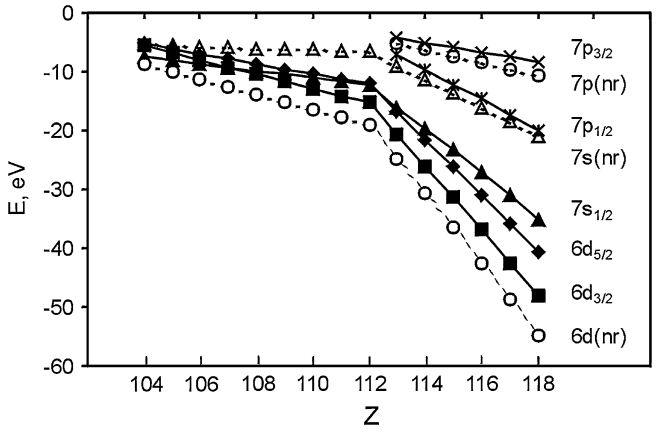

Fig. 8 Relativistic (DF, *solid lines*) and non-relativistic (HF, *dashed lines*) orbital energies of elements 104 through 118. The data are from [21]. From [11]

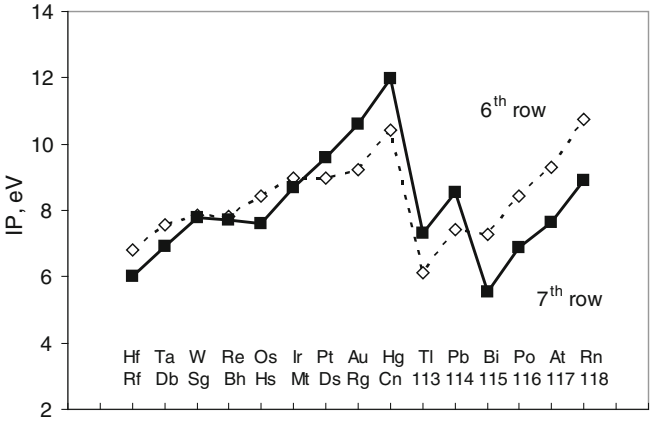

Fig. 9 Ionization potentials of the 6th row elements (*dashed line*, experimental values [141, 142]) and 7th row elements (*solid line*, calculated values, see Tables 3 and 4)

Table 5 A comparison of various calculations of IPs (in eV) of Pb and Fl

Method	Pb	Fl	Ref.
DF	–	8.9 (8.5[a])	[2]
MCDF	7.036	8.125 (8.275[a])	[136]
2*c*-ECP CCSD(T)	7.156 (7.30 fit)	8.529 (8.68[a])	[139]
rel. HF MBPT	7.433	8.487	[138]
CASMC/CI[b]	–	8.419	[60]
DFC CCSD(T)	–	8.36	[140]
DCB IHFSCC	7.484	8.539	[116]
DCB IHFSCC[c]	7.459	8.626	[129]
Exp.	7.417	–	[141]

[a] Extrapolated value; [b] Relativistic Complete Active Space Multiconfiguration/Configuration Interaction method; [c] with a more extended and balanced basis set than in [116]

smallest in their groups, due to the relativistically destabilized $7p_{3/2}$ AO. The drop of the *solid line* in Fig. 9 from element 114 to 115 reflects the magnitude of the 7p AO SO splitting. Overall, Cn has the largest IP in the 7th period, and also in group 12, indicating its largest inertness, while element 118 has a relatively low IP, the lowest in group 18, indicating its maximal chemical activity in this group. It should also be the most electropositive element out of all noble gases.

An upturn in IPs is observed in group 1 from Sc to element 119 and in group 2 from Ba to element 120 due to the relativistic stabilization of the outer $ns_{1/2}$ electrons [143, 144] (Figs. 10, 11). IPs of elements 119 and 120 are relativistically increased, e.g., from 3.31 eV to 4.53 eV for element 119, as DK CCSD calculations show [131, 132].

The IP(121) of 4.447 eV, a DCB FSCC value [34], is the highest in group 3. The DCB IH FSCC value of IP(122) of 5.595 eV [35] is lower than IP(Th) of

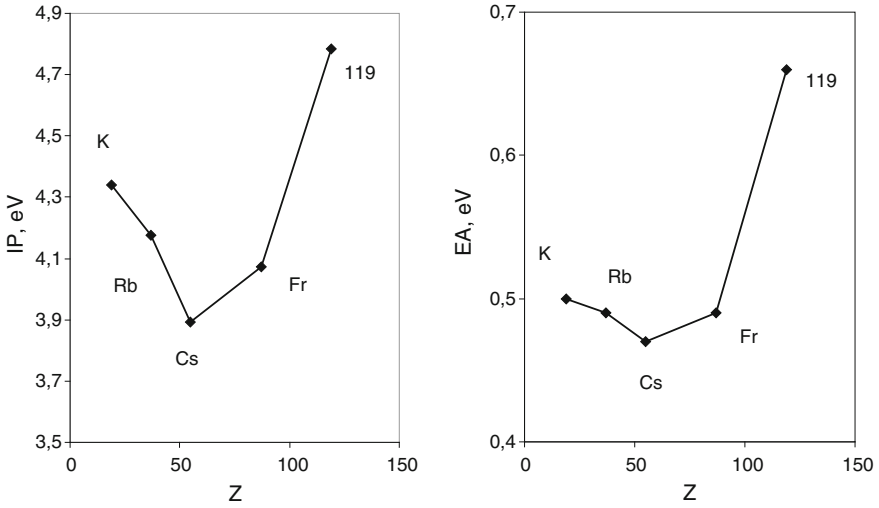

Fig. 10 Ionisation potentials, IP, and electron affinities, EA, of group-1 elements. The data for K through Fr are experimental [141, 142], while those for element 119 are DCB CC calculations [120, 121] (see Table 4). Reprinted with permission from [144]. Copyright 2012 Elsevier

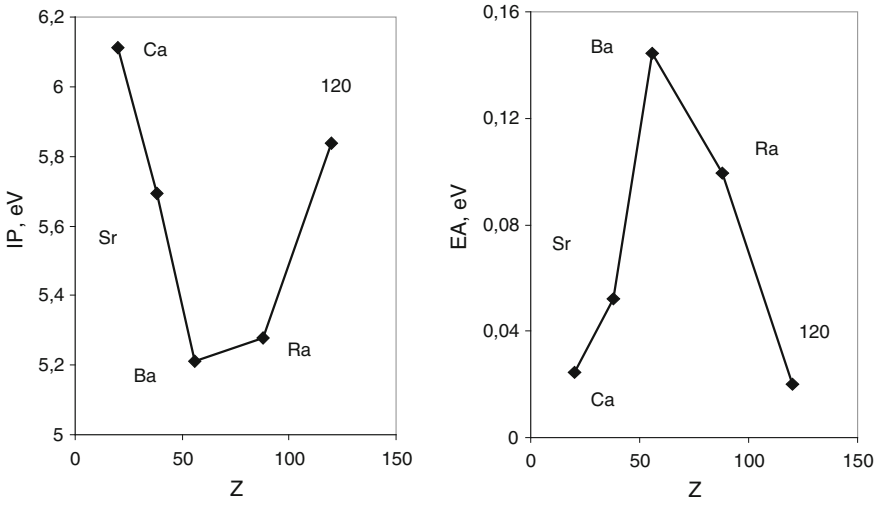

Fig. 11 Ionisation potentials, IP, and electron affinities, EA, of group-2 elements. The data for Ca through Ra are experimental [141, 142], while those for Ra (EA) and element 120 are DC CC calculations [125] (see Table 4). Reprinted with permission from A. Borschevsky, V. Pershina, E. Eliav, U. Kaldor, J. Chem. Phys. **136**, 134317 (2012). Copyright 2012 American Institute of Physics

6.52 eV due to the more bound $8p_{1/2}$ electron of element 122 than the 6d one of Th. The DF and DS values of IPs of even heavier elements can be found in [1, 2].

According to MCDF calculations [25–28], multiple IP should decrease in groups 4 through 8 (Fig. 12). The reason for that is the proximity of the valence 7s and 6d orbitals and relativistic destabilization of the latter with increasing Z in the groups (Fig. 8). That makes energies of the electron transitions between the (n–1)d and ns levels smaller than of the corresponding transitions in their 4d and 5d homologs, resulting in an enhanced stability of the maximum oxidation states.

IPs of internal conversion electrons (1s and 2s) of Cn, Fl, and elements 116 (livermorium, Lv) and 118 were predicted to an accuracy of a few 10 eV using DHF theory and taking into account QED and nuclear-size effects [44]. The $K_{\alpha 1}$ transition energies for different ionization states of Mt were calculated using the same approach and compared with recent experiments on the α-decay of ^{272}Rg [45].

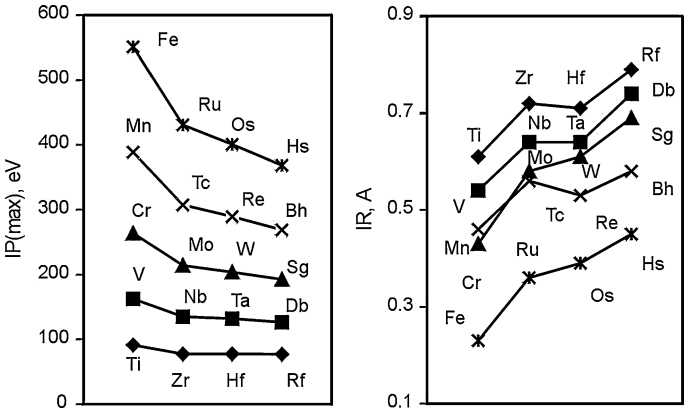

Fig. 12 Ionization potentials to the maximal oxidation state (IP_{max}) and ionic radii (IR) for Rf through Hs obtained from the MCDF calculations [24–28]. From [11]

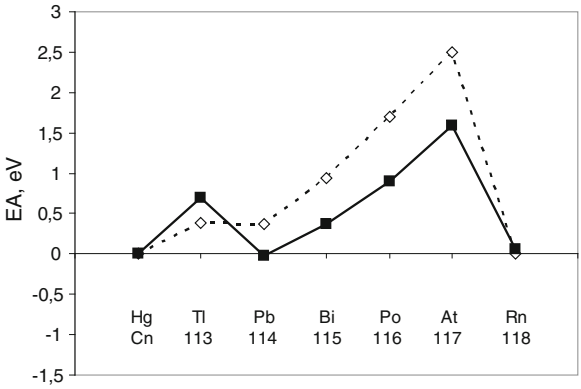

Fig. 13 Electron affinities of the 6th row (open rhomboids connected by the *dashed line* are experimental values [142]) and the 7th row elements of the Periodic Table (filled *squares* connected by the *solid line* are DC(B) CC calculated values, see Table 4)

Electron affinities were calculated for a few of the heaviest elements (Table 4 and Fig. 13). No bound anion was found for Cn by DCB FSCC calculations [114]. EA(113) was shown to be larger than EA(Tl) due to the relativistic stabilization of the $7p_{1/2}$ AO [115]. For Fl having a quasi-closed $7s^2 7p_{1/2}^2$ shell, a negative EA was obtained at various levels of theory (−0.02 eV at DC FSCC [128], −0.215 eV at DHF MRCI [55]), which might be due to the limited, though very large, basis sets. (The negative value has, of course, no physical sense). Thus, it was concluded that Fl has no EA [128]. A zero EA was also obtained by the DHF(B) CCSD(T) calculations [140]. EAs of elements 115 through 117 are smaller than those of the lighter homologs due to the relativistic destabilization of the $7p_{3/2}$ AOs. Element 118 has a positive EA of 0.058 eV, according to the DCB FSCC + QED calculations [48, 118]. The reason for that is the relativistic stabilization of the 8s AO.

EA of element 119 is the largest is group 1 because of the relativistic stabilization of the ns AO (Fig. 10). Also, due to the same reason, a reversal of the decreasing trend in EA beyond Cs is observed in this group. In group 2, on the contrary, EA increases from Ca to Ba, while a reversal of the trend occurs beyond Ba, so that EA of element 120 is about that of Ca (Fig. 11). This trend was explained by the one in the energies of the vacant AOs of a mixed $np_{1/2}$ and (n–1)d character [143] and polarizabilities of the group-2 atoms [125]: Since the extra

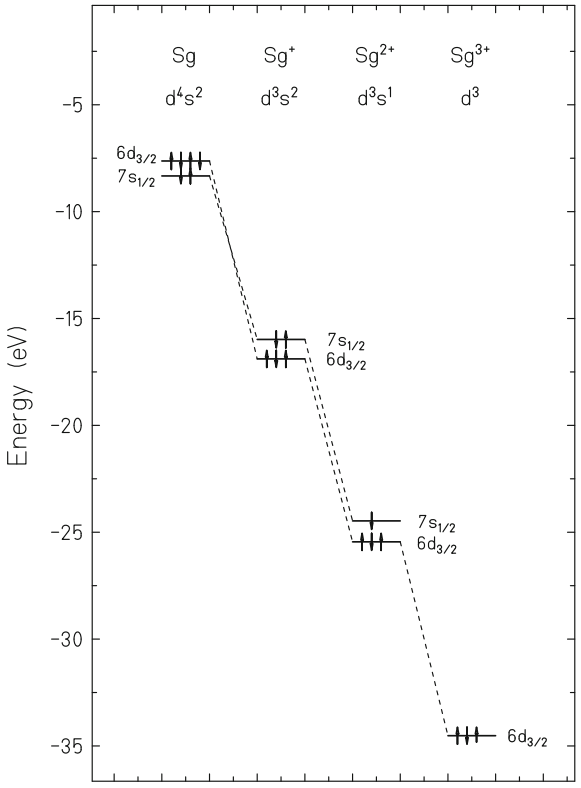

Fig. 14 MCDF orbital energies of the neutral through the third ionized state of Sg. Reprinted with permission from V. Pershina, E. Johnson, B. Fricke, J. Phys. Chem. A **103**, 8463 (1999). Copyright 1999 American Chemical Society

electron is bound to the atom due to the strong correlation (polarization) interaction, the smallest α of element 120 results in its smallest EA. Thus, correlation effects were shown to be very important to stabilize the element 120 negative ion.

Using IP and EA, absolute electronegativities χ were predicted for group 1 and 2 elements including 119 and 120, respectively [143, 144]. They show a reversal of the decreasing trend at Cs and Ba in these groups, respectively. Thus, element 119 should be more electronegative than K, and element 120 should be as electronegative as Ca. EA of element 121 of 0.569 eV should be the highest in group 3, according to the DCB FSCC calculations [34].

Predicted oxidation states of elements Rf through 120 are given in Tables 3, 4. As was mentioned, the proximity of the valence 7s and 6d AOs (Fig. 8) results in the stability of the highest oxidation states at the beginning of the 6d series. For the same reason, lower oxidation states will be unstable there. Thus, e.g., the step-wise ionization process results in the $6d^2$ and not the $7s^2$ configuration for Db^{3+} or Sg^{4+} (see Fig. 14 for Sg, as an example) [145]. Since the 6d AOs of the 6d elements are more destabilized than the (n–1)d AOs of the 4d and 5d elements, the Db^{3+} and Sg^{4+} will even be less stable than Ta^{3+} and W^{4+}.

The destabilization of the 6d AOs at the end of the 6d series is also the reason for the 6d electrons to be chemically active. As a consequence, an increase in the stability of the higher oxidation states is expected, e.g., of the 3+ and 5+ states of Rg and 4+ state of Cn. The 0 state will, however, be predominant in Cn due to its closed-shell structure.

The large relativistic stabilization of the $7s^2$ electrons and, hence, a large 7s–7p gap hindering hybridization, see Fig. 8, is the reason for an enhanced stability of lower oxidation states at the beginning of the 7p-series. Thus, the 1+ oxidation state will be more important for element 113 than the 3+ state.

Due to the relativistic stabilization of the two $7p_{1/2}$ electrons of Fl, the 2+ state should predominate over the 4+ one to a greater extent than in the case of Pb. The 6d AOs should be still accessible for hybridization for elements 113 and 114 and should take part in bonding leading to the formation of compounds of these elements in higher oxidation states like, e.g., $113F_5$ or FlF_6. For elements 115 through 118, on the contrary, lower oxidation states should be more stable than those of the lighter homologs due to the inaccessibility of the relativistically stabilized $7p_{1/2}$ AO for bonding. For element 115, the 1+ state should be more important due to the SO destabilized $7p_{3/2}$ electron. The 3+ state should also be possible, while 5+ not. For Lv, a decrease in the stability of the 4+ oxidation state is expected due to the large SO splitting of the 7p AOs, and the 2+ state should be important because of the two destabilized $7p_{3/2}$ electrons. For element 117, the 1+ and 3+ oxidation states should be the most important, while the 5+ and 7+ states less. The 1- state of element 117 having one-electron hole on the $7p_{3/2}$ AO should, therefore, be less important (its EA is the smallest in the group). For element 118, 2+ and 4+ states are possible, while the 6+ one will be less important, because of the strong binding of the $7p_{1/2}$ electrons. Oxidation states of heavier elements are discussed in [1, 2].

5.3 Atomic/Covalent/Ionic Radii and Polarizability

Radii, atomic (AR) and ionic (IR), are defined by the maximum of the radial charge density, R_{max}, of the outer valence AO in a neutral, or ionized atom, respectively. They were, therefore, estimated in most cases via a correlation between these quantities in the chemical groups. (The DF R_{max} of AOs of elements up to Z = 120 are tabulated by Desclaux [21]). The MCDF R_{max} and defined on their basis AR and IR for Rf through Hs and their lighter homologs in the chemical groups in various oxidation states are given in [23–28], for elements 112 and 114 in [135, 136], and for element 117 in [137]. (The radii for homologs are given in [146–148]). Van der Waals radii, R_{vdW}, in some cases were also estimated via a correlation with R_{max}, AOs as well as from calculations of bond lengths in molecules bound by dispersion forces, like, e.g., Cn_2 [127]. AR of elements Rf through Rg are given in [2], AR and R_{vdW} of elements Cn through 120 are in Table 4. Covalent radii (CR) were obtained for elements till Z = 118 from calculated bond lengths in some covalent compounds [149, 150].

These data show that AR of the 6d elements (the same is valid for R_{vdW}) should be smaller than those of their 5d congeners, with the maximum effect on Rg and Cn undergoing the strongest 7s AO contraction in the respective groups. In group 13 and 14, AR and R_{vdW} exhibit a reversal of the increasing trend at In and Sn, respectively, as that in $R_{max}(np_{1/2})$-AO, so that elements 113 and 114 should have smaller radii than those of the 6p homologs. The reason for that is the relativistic contraction of the $np_{1/2}$ AOs. In elements 115 through 118, the radii should be larger than those of their lighter homologs due to the increasing expansion of the $np_{3/2}$ AOs. In group 1 and 2, a reversal of the increasing trend in AR should occur at Cs and Ba, so that AR of elements 119 and 120 are about AR of Rb and Sr, and those of elements 165 and 166 are about AR of K and Ca, respectively (Fig. 15) [2, 143, 144]. The reason for the trend reversal is the increasing relativistic stabilization of the ns AO. The shell-contraction effects are, however, much smaller in the group-1 series of elements compared to the group-11 ones.

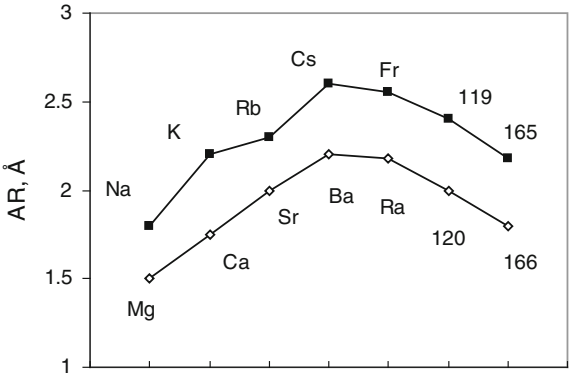

Fig. 15 Atomic radii of alkali and alkaline earth elements. The data for Na through Cs and Mg through Ra are experimental ones [146]. The data for the heaviest elements are from DC and DF calculations (see Table 4). From [13]

Table 6 Estimated ionic radii for CN = 6 (in Å) of Rf through Hs in the maximum oxidation states [24–28]. Experimental data [148] are for the lighter elements

Group 4		Group 5		Group 6		Group 7		Group 8[a]	
Ti^{4+}	0.61	V^{5+}	0.54	Cr^{6+}	0.44	Mn^{7+}	0.46	Fe^{8+}	0.23
Zr^{4+}	0.72	Nb^{5+}	0.64	Mo^{6+}	0.59	Tc^{7+}	0.57	Ru^{8+}	0.36
Hf^{4+}	0.71	Ta^{5+}	0.64	W^{6+}	0.60	Re^{7+}	0.53	Os^{8+}	0.39
Rf^{4+}	0.79[b]	Db^{5+}	0.74[b]	Sg^{6+}	0.65[b]	Bh^{7+}	0.58	Hs^{8+}	0.45

[a] For CN = 4; [b] a correlation of IR with the $\langle \bar{r}_{nl} \rangle$of the 6p AO s gives IR of 0.74 Å for Rf^{4+} , 0.66 Å for Db^{5+} , and 0.63 Å for Sg^{6+} [152]. More realistic values obtained from the geometry optimization of molecular compounds are 0.76 Å for Rf^{4+} and 0.69 Å for Db^{5+}

The IR of group-4 through 8 elements in their highest oxidation states for the coordination number, CN, equal to 6 are given in Table 6 and Fig. 12. They are almost equal for the 4d and 5d elements due to the lanthanide contraction (of 0.020 Å), which is roughly 86% a nonrelativistic effect: The diminished shielding of the nucleus charge by the 4f electrons causes the contraction of the valence shells. The IR of Rf through Hs are about 0.05 Å larger than IR of their 5d congeners. This is due to an orbital expansion of the outer $6p_{3/2}$ AOs responsible for the size of the ions. The IR of the 6d elements are, however, still smaller than IR of the actinides due to the actinide contraction (0.030 Å). The latter is larger than the lanthanide contraction and is mostly a relativistic effect. This is due to the fact that the 5f shell is more diffuse than the 4f shell, so that the contraction of the outermore valence shells is increased by relativity to a larger extent in the case of the 6d elements as compared to the 5d elements. The DF and HF calculations [151] for the 5d and 6d elements with and without the 4f and 5f shells, respectively, have shown that the shell-structure contraction is, indeed, enhanced by relativistic effects and that the orbital and relativistic effects are not additive.

IR of the 119^{+} and 120^{2+} ions were determined via a correlation with $R_{max}[(n–1)p_{3/2}]$ AO in group 1 and 2, respectively [143, 144]. In contrast to the trend in AR in these groups (Fig. 15), the IR reveal a steady increase with Z stipulated by the expansion of the outermost $(n–1)p_{3/2}$ AOs in these ions.

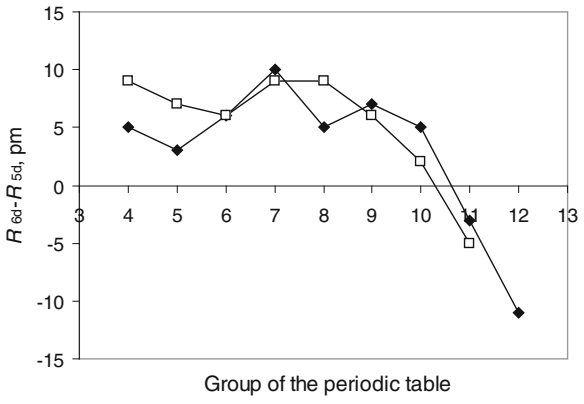

Fig. 16 The difference in the lengths of the single (filled rhomboids) and triple (open *squares*) bonds between the 6d and 5d metals [149, 150]. From [13]

Single and triple bond CR for the group-4 through 8 6d-elements were found to be about 0.06 Å on the average larger than CR of the 5d elements [149, 150] (Fig. 16), in agreement with the IR (Table 6). (The triple bond CR are slightly larger, 0.08 Å on the average). An important finding of those works is a decrease in the CR_{6d}-CR_{5d} difference starting from group 9, reaching negative values in groups 11 and 12, as a result of the relativistic bond contraction caused by the relativistic stabilization of the ns AO. This was called a "transactinide break" [149, 150].

Static dipole polarizabilities (α) were calculated most accurately at the DC CC level of theory for elements Cn through Fl, elements 118 through 120 [119, 125–127, 131, 132]. For elements 115 through 117, α were determined via a correlation with R^3_{max} of the outermost valence AOs in the chemical groups [130]. Results are given in Table 4 and Fig. 17 in comparison with experimental polarizabilities of the homologs in the 6th period.

According to the DC CC calculations [127], polarizability of Cn should be the smallest in group 12 due to the relativistic contraction of the 7s AO. Polarizabilities of element 113 and Fl are also smaller than those of In and Tl, and Sn and Pb, respectively, due to the relativistic stabilization of the $7p_{1/2}$ AO [126, 127]. A reversal of the trends in α is observed in group 13 and 14 beyond In and Sn, respectively, similarly to that in AR, or $R_{max}(np_{1/2})$-AO. A steep increase in α (Fig. 17) from element 114 to 115 reveals the magnitude of the 7p AO SO effect, since the highest occupied (HO) AO in Fl is $7p_{1/2}$, while it is $7p_{3/2}$ in element 115. Thus, the trend becomes opposite in groups 15 through 18 to those in groups 13 and 14, so that for elements 115 through 118, α is the largest in the respective chemical groups due to the largest $R_{max}(np_{3/2})$-AO.

For element 119, α is relativistically decreased from 693.9 to 165.98 a.u., as calculated at the DK CCSD(T) level of theory [131, 132]. A reversal of the increasing trend in α is predicted in groups 1 and 2 beyond Cs and Ba, so that α of elements 119 and 120 are about those of Rb and Ca, respectively [125, 143, 144]. The reason for the trend reversal is the increasing relativistic contraction of the ns AO.

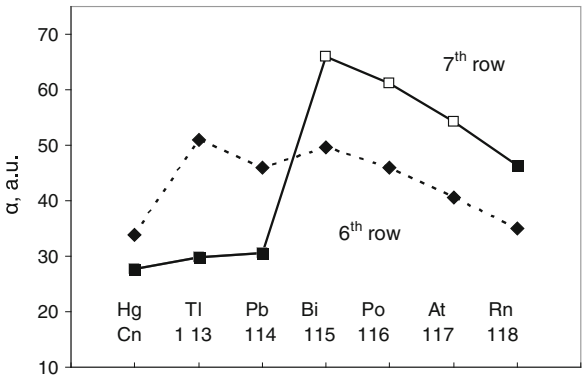

Fig. 17 Polarizabilities of the 6th row (filled rhomboids connected by the *dashed line* are experimental values [142]) and 7th row elements of the Periodic Table (*filled squares* connected by the *solid line* are DC calculated values, open ones are obtained via a correlation with R^3_{max} of their outer AO, see Table 4)

Table 7 Polarizabilities, α (in a.u.), of Hg and Cn calculated within different approximations

Atom	Method	α				Ref.
		HF	MP2	CCSD	CCSD(T)	
Hg	NR PP	82.25	–	–	37.83	[153]
	AR PP	44.78	28.33	35.26	34.42	[153]
	ECP	32.46	27.13	28.82	28.48	[139]
	DC	44.90	27.47	35.31	34.15	[127]
	exp.	–	–	–	33.91	[154]
Cn	NR PP	107.85	–	–	74.66	[153]
	AR PP	29.19	23.57	25.84	25.82	[153]
	ECP	30.30	27.67	28.61	28.68	[139]
	DC	29.46	25.11	27.66	27.64	[127]

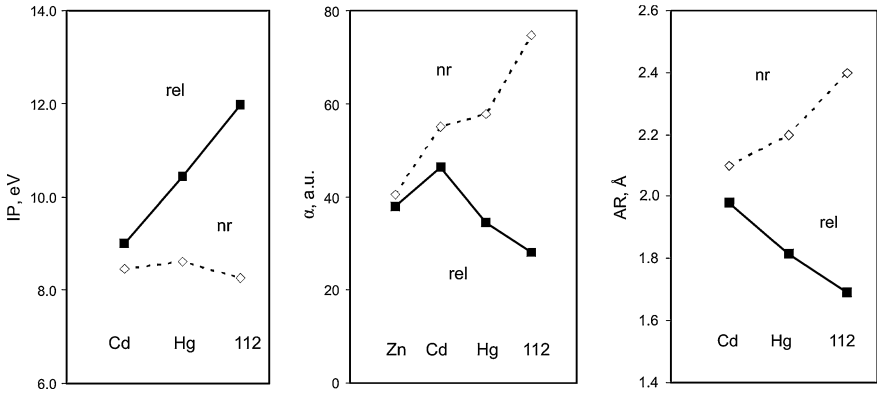

Fig. 18 Relativistic (*solid lines*) and non-relativistic (*dashed lines*) ionization potentials, IP, atomic radii, AR, and polarizabilities, α, of group-12 elements. Reprinted with permission from [155]. Copyright 2000 Elsevier

Finally, Table 7 demonstrates the influence of relativistic and correlation effects on α shown by various calculations—nonrelativistic (NR), average relativistic (AR, i.e., without spin–orbit) PP, relativistic ECP and DC; without electron correlation Hartree–Fock (HF), and with correlation at the different levels of theory (MP2, CCSD and CCSD(T))—for Hg and Cn, as an example. One can see that relativistic effects essentially decrease α of both species, with the effect being much more pronounced for the heavier element (a relativistic decrease from 74.7 to 25.8 a.u., as is shown by the PP CCSD(T) calculations [153]). Correlation effects also decrease α in both cases much more at the nonrelativistic level than at the relativistic. Correlation effects on α of group 13 and 14 elements are similar to those of group-12 elements.

Influence of relativistic effects on atomic properties of group-12 elements, as the most interesting case, is shown in Fig. 18. Thus, relativistic effects are

responsible for the largest IP and smallest both α and AR of Cn in group 12. This means that Cn should be chemically rather inert, much more than the lighter homologs in the group.

6 Electronic Structures and Properties of Gas-Phase Compounds of the Heaviest Elements. The Role of Relativistic Effects

6.1 Rf Through Hs (Elements 104 Through 108)

Elements at the beginning of the 6d series form halides, oxyhalides, oxides and other compounds similarly to their lighter homologs in the chemical groups. Their electronic structures and chemical properties such as ionicity, covalence, bonding, geometrical configurations, thermochemical stability, as well as the influence of relativistic effects on those properties, have been studied in a number of theoretical works. Many of them were also devoted to predictions of the behavior of such compounds in gas-phase chromatography experiments (see "Gas-Phase Chemistry of Superheavy Elements").

6.1.1 Hydrides of Rf and Sg

Group-4 and 6 hydrides, MH_4 (M = Ti, Zr, Hf, and Rf) and MH_6 (M = Cr, Mo, W, and Sg) are the simplest systems which were used in the past as models to study influence of relativistic effects on molecular properties. The early DF one-center expansion (DF-OCE) calculations [156–158] showed relativistic effects to decrease the bond length of RfH_4 and SgH_6, so that $R_e(RfH_4)$ is only 0.03 Å larger than $R_e(HfH_4)$, and $R_e(SgH_6)$ is 0.06 Å larger than $R_e(WH_6)$. The relativistic contraction of orbitals and of bond lengths were shown to be two parallel, but largely independent effects. The calculations revealed a decrease in the dissociation energy of RfH_4 as compared to that of HfH_4 and a slight increase in it of SgH_6 as compared to that of WH_6.

6.1.2 Group-4 Through 8 Halides, Oxyhalides and Oxides

Halides and oxyhalides of the elements at the beginning of the 6d series were studied extensively using a variety of methods, mostly DFT and PPs. The 4*c*-DS DV and DFT calculations were performed for the following compounds: MCl_4 (M = Ti, Zr, Hf, and Rf) [159], MCl_5, $MOCl_3$, MBr_5 and $MOBr_3$ (M = Nb, Ta, and Db) [160–164], MCl_6, $MOCl_4$, MO_2Cl_2 (M = Mo, W, and Sg) [165–167], MO_3Cl (M = Tc, Re, and Bh) [168], and MO_4 (M = Ru, Os, and Hs) [169, 170].

The RECP CCSD calculations were performed for halides and oxyhalides of Rf through Sg, such as $RfCl_4$, MCl_6, $MOCl_4$, MO_2Cl_2, MO_3 (M = W and Sg), MCl_5,

and MBr_5 (M = Ta and Db) [171]. Results of *ab initio* non-correlated DF calculations were reported for $RfCl_4$ and HsO_4 [172, 173].

Results until 1999 are overviewed in [6–9]. For later reviews including more accurate calculations, see [10–14].

Various properties of the transactinide compounds were predicted on the basis of these calculations. Thus, optimal geometries and stability of compounds (dissociation energies) were predicted with a sufficient accuracy. Moreover, electronic density distribution and type of bonding were defined. Some other spectroscopic

Table 8 Bond lengths (in Å) of halides, oxyhalides and oxides of group 4–8 elements as a result of the 4*c*-DFT [159–170] and RECP CCSD(T) [171] calculations in comparison with experiment

Group	Molecule	RECP CCSD(T)		4*c*-DFT[a]		Exp.[b]	
		$M–O/L_{ax}$	$M-L_{eq}$	$M–O/L_{ax}$	$M-L_{eq}$	$M–O/L_{ax}$	$M-L_{eq}$
4	$ZrCl_4$	–	–	–	2.344	–	2.318
	$HfCl_4$	–	–	–	2.344	–	2.317
	$RfCl_4$	–	2.381		2.402	–	–
5	$NbCl_5$	–	–	*2.34*	*2.24*	2.338	2.241
	$TaCl_5$	–	–	*2.37*	*2.23*	2.369	2.227
	$DbCl_5$	–	–	*2.42*	*2.28*	–	–
	$NbOCl_3$	–	–	*1.66*	*2.24*	1.68	2.276
	$TaOCl_3$	–	–	*1.67*	*2.25*	–	–
	$DbOCl_3$	–	–	*1.72*	*2.30*	–	–
	$NbBr_5$	–	–	2.500	2.449	–	–
	$TaBr_5$	2.481	2.435	2.495	2.444	2.473	2.412
	$DbBr_5$	2.536	2.499	2.548	2.496	–	–
	$NbOBr_3$	–	–	1.704	2.442	1.694	2.429
	$TaOBr_3$	–	–	1.716	2.440	–	–
	$DbOBr_3$	–	–	1.788	2.484	–	–
6	$MoCl_6$	–	–	–	*2.25*	–	–
	WCl_6	–	2.319	–	*2.26*	–	2.26
	$SgCl_6$	–	2.359	–	*2.32*	–	–
	$MoOCl_4$	–	–	*1.658*	*2.279*	1.658	2.279
	$WOCl_4$	1.67	2.317	*1.685*	*2.280*	1.685	2.28
	$SgOCl_4$	1.72	2.364	*1.747*	*2.340*	–	–
	MoO_2Cl_2	–	–	*1.698*	*2.259*	1.698	2.259
	WO_2Cl_2	1.700	2.282	*1.710*	*2.270*	1.710	2.270
	SgO_2Cl_2	1.749	2.339	*1.772*	*2.330*	–	–
	WO_3	1.735	–	–	–	–	–
	SgO_3	1.777	–	–	–	–	–
7	TcO_3Cl	–	–	1.69	2.30	–	–
	ReO_3Cl	–	–	1.71	2.28	1.761	2.23
	BhO_3Cl	–	–	1.77	2.37	–	–
8	RuO_4	–	–	1.712	–	1.706	–
	OsO_4	–	–	1.719	–	1.711	–
	HsO_4	–	–	1.799	–	–	–

[a] *Italics*—estimates for the heaviest elements on the basis of IR; [b] for experimental values see the corresponding references in the theoretical works [159–171]

Table 9 Atomization energies, D_e, (in eV), ionization potentials, IP, (in eV), dipole moments, μ (in D), polarizabilities, α (in a.u.), of group 4–8 compounds as a result of various calculations

Group	Molecule	D_e[a]	IP[b]	μ	α	Method	Ref.
4	$ZrCl_4$	21.68	–	–	–	DFT	[159]
		20.32	11.94	–	10.14	BH	
	$HfCl_4$	21.14	–	–	–	DFT	[159]
		20.53	12.03	–	–	BH	
	$RfCl_4$	19.50	10.96	–	–	DFT	[159]
		18.80	-			RECP	[171]
5	$NbCl_5$	*19.25*	10.77	–	–	DS DV	[160]
	$TaCl_5$	*19.46*	10.73	–	–	DS DV	[160]
	$DbCl_5$	17.76	10.83	–	–	DS DV	[160]
	$NbOCl_3$	*21.6*	11.60	0.91	–	DS DV	[163]
	$TaOCl_3$	*22.52*	11.57	0.99	–	DS DV	[163]
	$DbOCl_3$	20.82	11.64	1.27	–	DS DV	[163]
	$NbBr_5$	18.32	9.35	–	172.1	DFT	[164]
		17.86				BH	
	$TaBr_5$	19.41	9.33	–	167.3	DFT	[164]
		18.92				BH	
	$DbBr_5$	18.86	9.37	–	167.0	DFT	[164]
	$NbOBr_3$	20.53	–	–	–	DFT	[164]
	$TaOBr_3$	21.43	–	–	–	DFT	[164]
	$DbOBr_3$	20.36	–	–	–	DFT	[164]
6	$MoCl_6$	–	11.06	–	–	DS DV	[165]
	WCl_6	*21.7*	11.13	–	–	DS DV	[165]
		19.9				RECP	[171]
	$SgCl_6$	20.05	11.17	–	–	DS DV	[165]
		19.9				RECP	[171]
	$MoOCl_4$	*20.54*	–	0.14	–	DS DV	[166]
	$WOCl_4$	*22.96*	–	0.49	–	DS DV	[166]
		21.5		0.24		RECP	[171]
	$SgOCl_4$	*21.24*	–	1.03	–	DS DV	[166]
		21.0		0.77		RECP	[171]
	MoO_2Cl_2	*21.08*	–	1.04	–	DS DV	167
	WO_2Cl_2	*23.5*	–	1.35	–	DS DV	[167]
		21.5		1.51		RECP	[171]
	SgO_2Cl_2	21.6	–	1.83	–	DS DV	[167]
		21.0		2.39		RECP	[171]
	WO_3	18.9	–	–	–	RECP	[171]
	SgO_3	17.8	–	–	–	RECP	[171]
7	TcO_3Cl	23.12	12.25	0.93	33.33	DFT	[168]
	ReO_3Cl	24.30	12.71	1.29	39.88	DFT	[168]
		23.76				BH	
	BhO_3Cl	22.30	13.05	1.95	50.61	DFT	[168]
8	RuO_4	27.48	12.21	–	58.07	DFT	[170]
		19.11	**12.19**		**58.64**	exp.	
	OsO_4	27.71	12.35	–	55.28	DFT	[170]
		21.97	**12.35**		**55.13**	exp.	
	HsO_4	28.44	12.29	–	68.88	DFT	[170]

[a] *Italics*—"experimental" values (calculated via a Born-Haber, BH, cycle); [b] **bold**—measurements

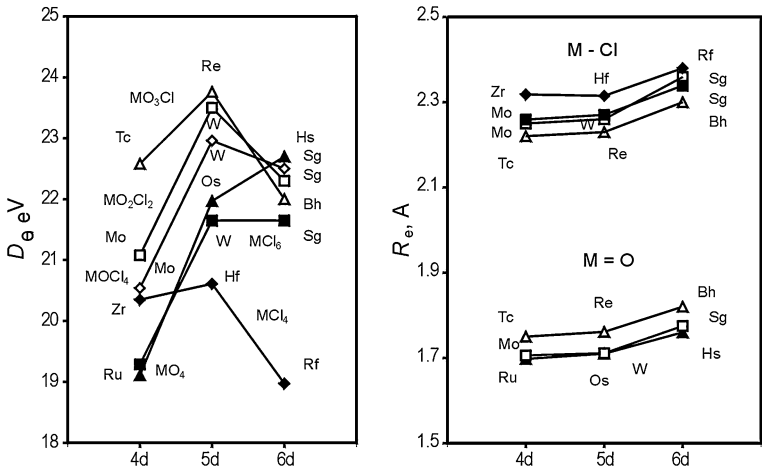

Fig. 19 Atomization energies, D_e, (experimental for the 4d and 5d elements and calculated for the 6d elements) and bond lengths, R_e, for various halides, oxides and oxyhalides of group-4 to 8 elements (see the data in Tables 8 and 9)

properties such as IPs, EAs, energies of electron transitions, polarizabilities and dipole moments were obtained for the stable geometries. Many works were devoted to the study of relativistic effects (both scalar ones and SO interaction) on all those properties by performing additional non-relativistic calculations and comparing them with the relativistic ones. Some works were also devoted to the study of influence of correlation effects on various properties, particularly on bonding. For that purpose, molecular calculations using the DF (HF) approximation (i.e., without correlation), as well as at various levels of electron correlation were performed.

The calculated dissociation energies were used to predict stability of various compounds of the transactinides (at experimental conditions). Using some other properties, like, e.g., polarizabilities, dipole moments and geometrical configurations, volatility of species for gas-phase chromatography experiments were predicted with the use of physico-chemical adsorption models (see further).

Results of the 4*c*-DFT and RECP calculations of various properties—optimized geometries (R_e and bond angles), D_e, IP, α, and μ—of the halides, oxyhalides and oxides of group-4 through 8 elements are summarized in Tables 8, 9. The D_e and R_e are also depicted in Fig. 19.

Overall, very good agreement is observed between the 4*c*-DFT and RECP calculations, as well as between the calculated and experimental values, especially for the bond lengths and geometries. The DFT dissociation energies are slightly overestimated as compared to the experiment, however, they follow perfectly the trends, so that they are rather reliable. Some other properties, including the electronic density distribution, e.g., effective charges, are also nicely reproduced by the calculations. Therefore, predictions for the heaviest elements should be highly reliable.

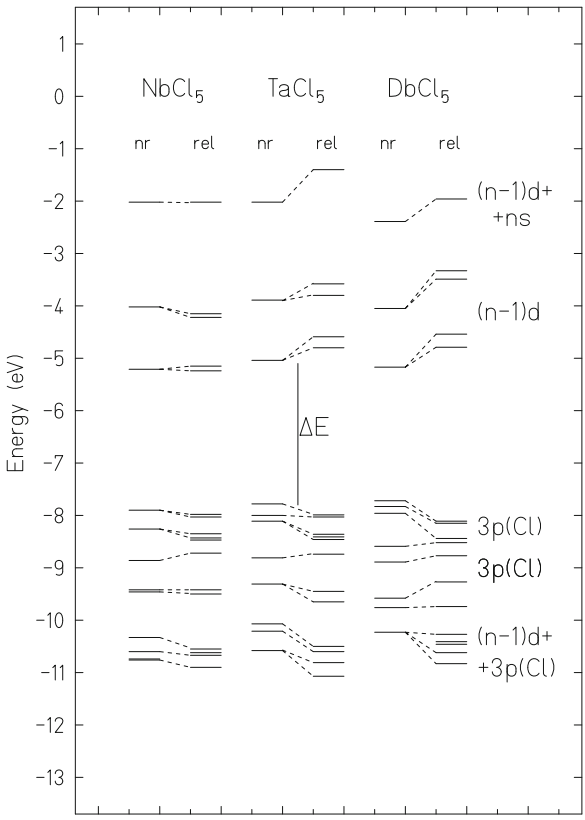

Fig. 20 Relativistic (rel) and non-relativistic (nr) energy levels in MCl_5 (M = Nb, Ta, and Db) obtained from the DS DV calculations. ΔE is the HOMO–LUMO gap. Reprinted with permission from V. Pershina and B. Fricke, J. Chem. Phys. **99**, 9720 (1993). Copyright 1993 American Institute of Physics

The calculations have shown that compounds of the 6d elements are, indeed, homologs of the lighter congeners in the chemical groups and that bonding is defined preferentially by the participation of the valence 6d AOs, with an admixture of the 7s and $7p_{1/2}$ AOs.

A typical schemes of the molecular energy levels of the d-element compounds including those of the transactinides in the relativistic and non-relativistic cases are shown in Fig. 20 for MCl_5 (M = Nb, Ta, and Db), as an example [161]. One can see that the MO schemes, as well as the MO composition (see [160] and [161]), are similar for all the three molecules: the set of bonding MOs is topped by the HOMOs of the preferentially ligand, 3p(Cl), character. Separated from them by the energy gap, ΔE (the HOMO–LUMO gap), lying higher in energy, are the vacant levels of the metal (n–1)d character.

Due to the similarity in the electronic structures, molecular properties of MCl_5 (M = Nb, Ta, and Db) are then also similar. Thus, e.g., IPs defined by the energies of the HOMOs do not differ much (Table 9). Some other properties, like EAs, defined by the LUMOs, or charge-transfer electron transitions change smoothly from the Nb to Db molecule.

The influence of relativistic effects on the MO energies of the group-5 MCl_5, being also typical, is seen from the same Fig. 20 [161].

Thus, relativistic effects increase the HOMO energies (their absolute values), which results in an increase in the molecular IPs. They also decrease the energies (absolute values) of the vacant levels of the (n–1)d character, including LUMOs, which results in a decrease in the EAs. Both effects, consequently, result in an increase in the energies of the electron charge-transfer transitions from the levels of the ligand character to those of the metal character, E[3p(Cl) → (n–1)d(M)]. Since the latter is associated with the reduction of the metal, such an increase leads to an increase in the stability of the maximum oxidation state, i.e., 5+ in group 5. This is demonstrated by a correlation between E[3p(Cl) → (n–1)d(M)] and reduction potentials $E°$(V–IV) for MCl_5 (M = V, Nb, Ta, and Db) in Fig. 21. Thus, non-relativistically, Db^{5+} would have been even less stable than Nb^{5+}. Similar correlations can be shown for compounds of group 4–8 elements in the highest oxidation states. Thus, in groups 4 through 8, relativistic effects increase the stability of the maximum oxidation state.

The RECP and DFT calculations (Tables 8, 9, Fig. 19), in agreement with each other, established that R_e are similar for the 4d and 5d compounds due to the lanthanide contraction, while those of the 6d compounds are about 0.05–0.06 Å larger. (One can also see from Table 8 that the bond lengths estimated on the basis of IR of the heaviest elements in the early DS DV calculations are very realistic). This is in line with their larger IR and CR (see Sect. 5.3). Such an increase in R_e is explained by the orbital and relativistic expansion of the (n–1)d AOs in the groups.

The D_e were shown to increase from the 4d to the 5d compounds and decrease from the 5d to the 6d element compounds for almost all types of species except of group-8 MO_4. In [160–168], such a decrease in D_e of the 6d element compounds was explained by a decrease in the ionic contribution to bonding, while the covalent one steadily increases in the groups. D_e obtained as a sum of the ionic and covalent contributions to chemical bonding calculated within the DS DV scheme turned out to be rather accurate [160–167].

A decrease in ionicity and increase in covalence in groups 4–8 are seen from decreasing Mulliken effective charges, Q_M, and increasing overlap populations (OP), serving as a measure of covalence (Fig. 22). A comparison of results of relativistic and nonrelativistic calculations shows that the reason for this trend is increasingly important relativistic effects. Figure 23 shows relativistic and non-relativistic values of Q_M and OP for MCl_5 (M = V, Nb, Ta, and Db), as an example [161], which change in an opposite way from Ta to Db. A partial OP analysis (Fig. 24) shows that such an increase in covalence (total OP) is due to the increasing contribution of all the relativistic valence AOs, while the contribution of the non-relativistic ns and $np_{1/2}$ AOs decreases from Ta to Db. (In the case of the (n–1)d AOs, the relativistic and nonrelativistic trends are the same, because relativistic effect only enhances the orbital one).

RECP CCSD(T) calculations for the group-6 oxyhalides, with and without SO coupling [171], have shown that larger SO effects on the 6d AOs result in a decrease in D_e of the 6d compounds of 1–1.5 eV in comparison with the 5d ones

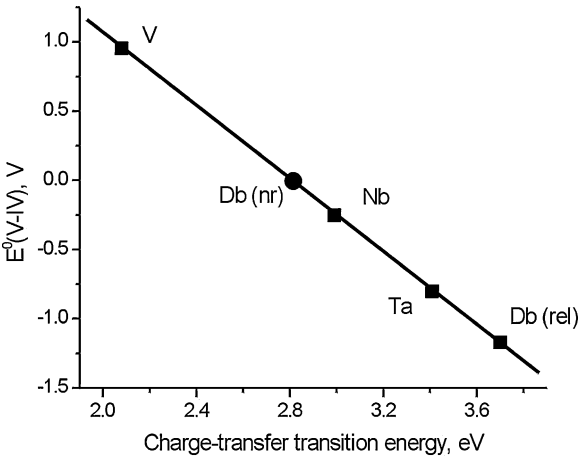

Fig. 21 Correlation between reduction potentials $E°$(V–IV) and energies of the lowest charge-transfer transitions E[3p(Cl) → (n–1)d(M)] in MCl_5 (M = V, Nb, Ta and Db). The non-relativistic value for Db is shown with a filled *circle*. Reproduced from [9]

(Table 10). The effects are larger for the Sg compounds than for the Rf ones due to an increasing $6d_{3/2}$-$6d_{5/2}$ splitting.

Thus, relativistic effects are responsible for the continuation of trends in IP, EA, covalence and stabilities of oxidation states in the groups in going over from the 5d to the 6d elements. (The SO effects are, however, responsible for a trend reversal in D_e). The non-relativistic description of these properties would give opposite and, therefore, wrong trends.

In [171], the importance of electron correlation on Q_M, OP, μ and D_e was demonstrated on the example of group-6 MO_2Cl_2 (Table 10). Correlation effects were shown to significantly decrease Q_M and μ, and increase D_e accounting, e.g., for about 65% in $D_e(SgO_2Cl_2)$. The effects on D_e were found to be larger in the W compounds than in the Sg ones and they become more significant as the number of oxygen atoms increases.

Both the DFT and RECP calculations predict an increase in the stability of compounds of the 6d elements with increasing number of oxygen atoms, e.g., from $SgCl_6$ to $SgOCl_4$ and to SgO_2Cl_2, as is experimentally known for the lighter homologs Mo and W. Thus, SgO_2Cl_2 was recommended in [167] as the most stable type of oxychloride for high-temperature gas phase experiments. $SgCl_6$ and $SgOCl_4$ were shown to be unstable with respect to the loss of Cl transforming into compounds of Sg^V [165, 166].

Among other important trends, one should mention a decrease in the metal–ligand bond strength of the halides with increasing group number, in addition to a decrease in it from the 5d to the 6d compounds within the same group [165]. Thus, $SgCl_6$ was shown to be unstable. Consequently, $BhCl_7$ should not exist. This is also connected with a decrease in the relative stability of the maximum oxidation state along the transactinide series, see Fig. 5 in [165].

Similarly to the chlorides, the trend in the stability of group-5 MBr_5 was predicted from the 4*c*-DFT calculations as Nb < Db < Ta [164]. However, for $MOBr_3$ the trend in the stability is given as Db < < Nb < Ta (see Table 9). Thus,

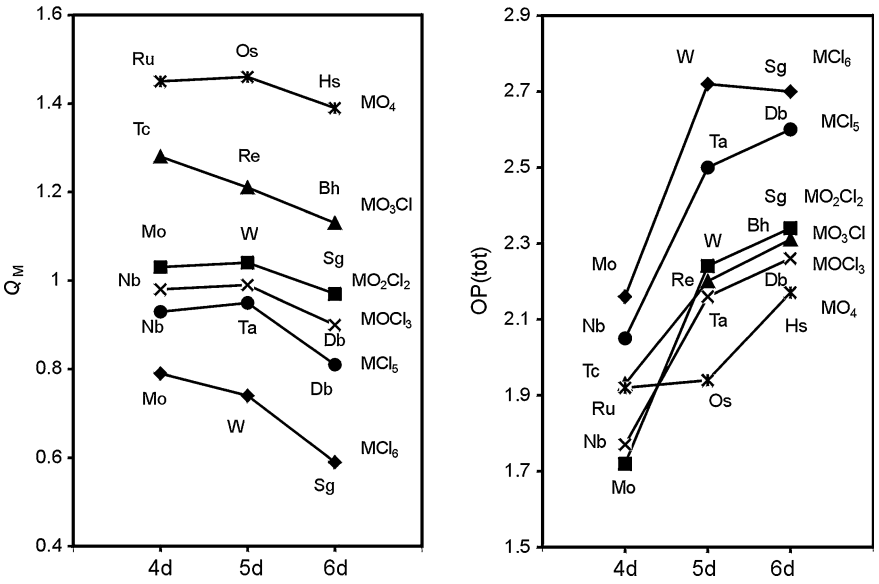

Fig. 22 Effective charges (Q_M) and total overlap populations (OP) in group-4 through 8 (oxy)halides and oxides obtained as a result of the Mulliken population analysis in the DFT calculations [160–170]

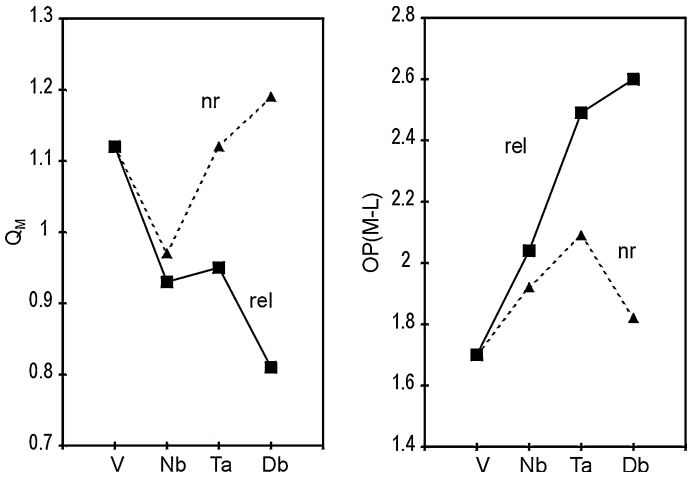

Fig. 23 Relativistic (rel) and non-relativistic (nr) effective charges, Q_M, and overlap populations, OP, in MCl_5 (M = V, Nb, Ta, and Db). L denotes the ligand. The data are from [161]

it was concluded that Db should not have a preference to form oxygen-containing compounds, in difference to the earlier expectations [163]; see also "Gas-Phase Chemistry of Superheavy Elements".

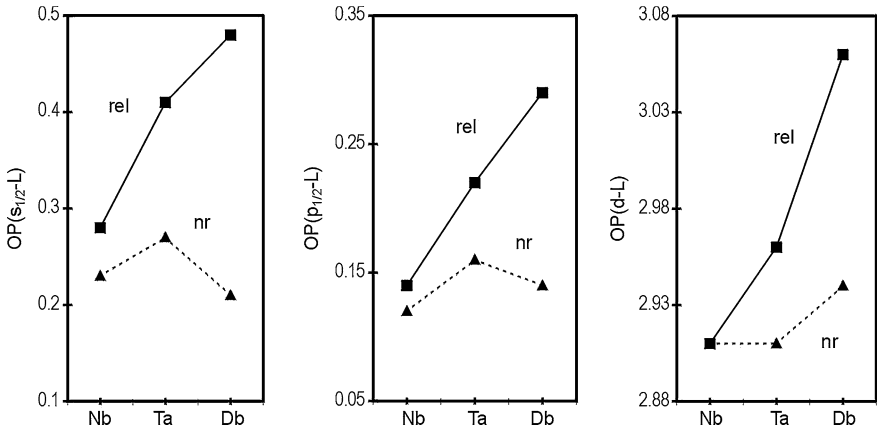

Fig. 24 Relativistic (rel) and non-relativistic (nr) partial overlap populations in MCl_5 (M = Nb, Ta, and Db). L denotes valence orbitals of the ligand. The data are from [161]

Table 10 Correlation and SO effects on the electronic density distribution (Q_M and OP), dipole moments, μ (in D), and atomization energy, D_e (in eV), of MO_2Cl_2 (M = W and Sg)

	Molecule	RECP		DFT
		HF(AREP)[a]	SO-CCSD(T)[b]	DS DV[c]
Q_M	WO_2Cl_2	2.18	1.71	1.08
	SgO_2Cl_2	1.94	1.52	0.97
OP	WO_2Cl_2	2.14	2.03	2.23
	SgO_2Cl_2	2.72	2.55	2.34
μ	WO_2Cl_2	1.70	1.51	1.35
	SgO_2Cl_2	2.64	2.39	1.83
D_e	WO_2Cl_2	11.7	22.2	23.8
	SgO_2Cl_2	14.2	21.0 (22.5[d])	21.8

[a] Average Relativistic, i.e., without SO and correlation [171]; [b] with SO effects and correlation [171] [c] fully relativistic [167]]; [d] without SO effect

Stability of MO_3Cl (M = Tc, Re and Bh) should follow the trend Bh < Tc < Re, according to the 4*c*-DFT calculations [168].

The 4*c*-DFT calculations have also shown that group-8 MO_4 molecules should be all very similar and stable, with the following trend in D_e: RuO_4 < OsO_4 < HsO_4 [169]. However, calculations with larger basis sets, like those used in [170], had to be performed to provide a more accurate value of $D_e(HsO_4)$. $R_e(HsO_4)$, very accurately calculated in [170], should also be larger than R_e of RuO_4 and OsO_4, as in compounds of group 4–7 elements. For these molecules, influence of relativistic effects on properties important for gas-phase experimental investigations was studied in detail [169, 170]. Figure 25 show relativistic and non-relativistic IPs, α, and R_e of these molecules. One can see that relativistic

effects decrease R_e, increase IPs (with the strongest effect on HsO_4) and decrease α. They do, however, not change trends in these properties in the group, since those for the relativistic and non-relativistic (n–1)d AOs are the same. The shape of the IP and α plots with a peak at Os reflects the "zigzag" behavior of the (n–1)d AOs (see Fig. 1 in [169]).

There are also *ab initio* DF [173] and the infinite-order regular approximation with modified metric method (IORAmm/HF) [174] theoretical studies of the electronic structures of MO_4 (M = Os and Hs). These works, however, revealed some deficiency of the calculations that resulted in the prediction of a wrong trend in properties from Os to Hs, as compared to the more accurate calculations [170] and the experiment (see below, as well as discussions in [169]).

All the group 5–7 oxyhalides, as low-symmetry compounds, have dipole moments (see Table 9). As the data show, μ increases from the 4d to 5d and further to 6d compounds, which is connected with an increasing metal–ligand separation. Both relativistic and correlation effects decrease μ (Table 10) due to a decrease in the molecular size and increase in IPs.

The PP calculations were also performed for DbO, along with NbO and TaO. Relativistic effects were shown to stabilize the $^2\Delta_{3/2}$ ground state electronic configuration in DbO, as that in TaO, in contrast to the $^4\Sigma^-$ state of NbO [175, 176].

6.1.3 Other Group-4 Through 8 Compounds

The DS DV calculations were performed for $M(CO)_6$ (M = Mo, W, Sg, and U) [177]. $Sg(CO)_6$ was found to be very similar to $W(CO)_6$ and different from $U(CO)_6$. Bond lengths in covalent compounds of the type MX (M = Rf through element 118; X = H, N, B, and C) and some others were calculated using various approaches, mostly by ADF ZORA (see [149, 150] for a summary). As was mentioned in Sect. 5.3, R_e of the Rf through Hs compounds are about 0.05 Å larger than of their 5d counterparts in good agreement with IR and bond lengths in other types of compounds (Fig. 16).

6.1.4 Predictions of Volatility of Group-4 Through 8 Compounds

Identification of the heaviest elements by studying their volatility is a difficult task. Several quantities are associated with this physical phenomenon, which are not necessarily interrelated. Thus, in gas-phase chromatography experiments, a measure of volatility is either a deposition temperature in a thermochromatography column, T_{ads}, or the temperature of the 50% of the chemical yield, $T_{50\%}$, observed on the outlet of the isothermal column (see "Experimental Techniques" and "Gas-Phase Chemistry of Superheavy Elements", as well as [178]). From these temperatures, an adsorption enthalpy, ΔH_{ads}, is deduced using adsorption models [179], or Monte Carlo simulations [180, 181]. The ΔH_{ads} is supposed to be related to the sublimation enthalpy, ΔH_{sub}, of the macroamount (see "Thermochemical Data from Gas-Phase Adsorption and Methods of their Estimation"). The usage of a correlation between

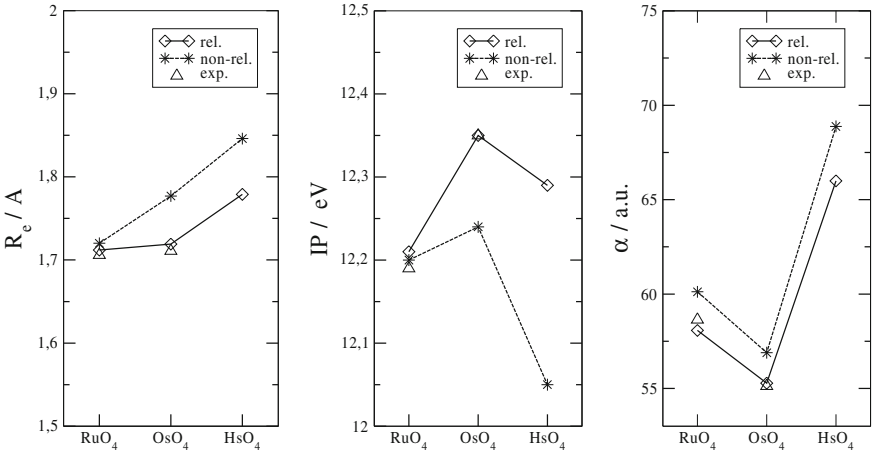

Fig. 25 Relativistic (rel.) and nonrelativistic (non-rel.) bond lengths, R_e, ionization potentials, IP, and polarizabilities, α, of MO_4 (M = Ru, Os, and Hs). Reprinted with permission from V. Pershina, J. Anton, T. Jacob, Phys. Rev. A **78**, 032518 (2008). Copyright 2008 American Physical Society

ΔH_{ads} and ΔH_{sub} is, however, restricted to some groups and types of compounds, while generally not allowed (see below). In macrochemistry, a measure of volatility is an equilibrium vapor pressure over a substance, P_{mm}. Boiling points, T_b, and enthalpy of evaporation, ΔH_{evap}, basically correlate with P_{mm}.

Another difficulty comes from the fact that the studied chemical species are not known. Their composition is usually judged by analogy with the chemical behavior of lighter homologs in the chemical groups. Beside the low statistics of just a few events, a difficulty arises with respect to the interpretation of results, since the surface of the column is not well known. It is often modified with aerosol transport particles or halogenating agents, so that the mechanisms of adsorption and the nature of chemical or physical interactions can only be assumed [178]. Thus, available experimental data are sometimes contradictory and do not correlate with a single property or an electronic structure parameter of the adsorbate.

To determine ΔH_{ads} of a heavy molecule on a complex surface is still a formidable task for quantum chemical calculations. Fully relativistic methods for calculating systems of the heaviest elements interacting with a (complex) surface are not yet available. Especially difficult is the prediction of the physisorption phenomenon caused by weak interactions, where the DFT generally fails.

In the past, DS DV calculations were helpful in establishing some correlation between electronic structure parameters and volatility of halides, oxyhalides and oxides known from macrochemistry [6, 11]. It was established, e.g., that covalent compounds (having higher OP) are more volatile than ionic, and that molecules with dipole moments interact more strongly with a surface than without those, and that the sequence in the adsorption energy is defined by the sequence in dipole moments.

Lately, predictions of the interaction energy of heaviest element molecules with inert surfaces (quartz, silicon nitride, also modified) were made with the use of physisorption models [155, 168–170]. These models are based on the principle of intermolecular interactions subdivided into usual types of long-range forces: dipole–dipole, dipole-polarizability and van der Waals (dispersion) one. Molecular properties required by those models are then calculated with the use of most accurate relativistic methods.

Thus, e.g., for a molecule with a zero dipole moment adsorbed on a dielectric surface by van der Waals forces, the following model of the molecule-slab interaction is used [155]:

$$E(x) = -\frac{3}{16}\left(\frac{\varepsilon - 1}{\varepsilon + 2}\right)\frac{\alpha_{\mathrm{mol}}}{\left(\frac{1}{IP_{\mathrm{slab}}} + \frac{1}{IP_{\mathrm{mol}}}\right)x^3}, \tag{17}$$

where IP_{slab} and IP_{mol} are ionization potentials of the slab and molecule, ε is the dielectric constant of the surface material, and x is molecule-surface separation distance. In a comparative study, x for a lighter element is deduced from the known ΔH_{ads}, while that for a heaviest element is estimated using the difference in their molecular size.

Using this model, ΔH_{ads} of, e.g., group-8 tetroxides on a silicone nitride surface of detectors of a chromatography column were predicted [170]. Since the RuO_4, OsO_4 and HsO_4 molecules are very similar, a very high accuracy of the calculated properties (see Table 9) was required in order to give reliable ΔH_{ads}. The 4*c*-DFT calculations performed with extremely large basis sets revealed an inversion of the trend in α and IPs beyond Os (Fig. 25). Such a trend reversal results in the trend reversal in $-\Delta H_{ads}$, $RuO_4 > OsO_4 < HsO_4$, according to Eq. 17 (Fig. 26). This is in agreement with the experimentally observed trend in $-\Delta H_{ads}$: $OsO_4 < HsO_4$ [182]. Also, the calculated ΔH_{ads} of HsO_4 of -45.1 kJ/mol proved to be in excellent

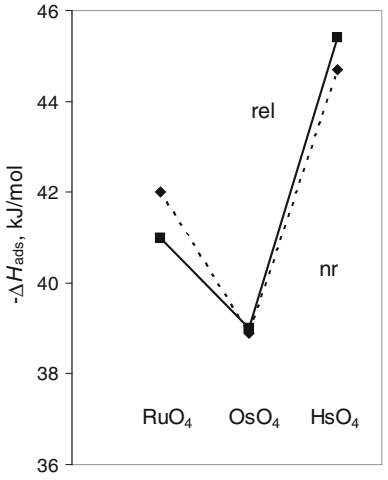

Fig. 26 Relativistic (*solid line*) and nonrelativistic (*dashed line*) adsorption enthalpies of MO_4 (M = Ru, Os, and Hs) on silicon nitride [170]

agreement with the measured ΔH_{ads} of -46 ± 2 kJ/mol. The trend reversal in the molecular properties and ΔH_{ads} is explained by the trend reversal in energies of the (n–1)d AOs at Os (see Fig. 1 in [169]). Relativistic effects were shown to have no influence on the trend in $\Delta H_{ads}(MO_4)$ (Fig. 26), as they have no influence on the trends in the molecular properties (Fig. 25), since relativistic and nonrelativistic (n–1)d AOs change in the same way with increasing Z in group 8 [170].

In [183], thermodynamic equations are given allowing for prediction of T_{ads} of an atom or molecule with respect to T_{ads} of a homolog in a comparative study. One of those equations is shown here for the case of mobile adsorption of molecules with a rotational degree of freedom:

$$e^{-\Delta E_A/\mathrm{RT}} \frac{1}{t_{1/2}^A r_A d_A T_A^{1/2} m_A^{1/2}} = e^{-\Delta E_B/\mathrm{RT}} \frac{1}{t_{1/2}^B r_B d_B T_B^{1/2} m_B^{1/2}}. \quad (18)$$

Here $t_{1/2}$ is half-life of the central atom isotope, r is molecular radius, d is the metal–ligand distance, T is adsorption temperature, m is mass, and ΔE is adsorption energy of a heaviest molecule A with respect to its lighter homolog B. Predictions of $T_{ads}(HsO_4)$ with respect to $T_{ads}(OsO_4)$ were made in [183], as an example. In the same work, various measures of volatility are critically compared, showing that in a comparative study, the most adequate measure of it (in macrochemistry) is the ratio of adsorption/desorption constants, K_{ads}/K_{des}.

For predictions of adsorption of molecules with non-zero dipole moments, equations taking into account long-range interactions, such as molecular dipole-surface charge, dipole-induced dipole, and van der Waals one were deduced. Thus, e.g., the interaction energy of a molecule with a surface charge is [168]

$$E(x) = -\frac{2Qe\mu_{mol}^2}{x^2} - \frac{Q^2e^2\alpha_{mol}}{2x^4} - \frac{3}{2}\frac{\alpha_{mol}\alpha_{slab}}{\left(\frac{1}{IP_{mol}} + \frac{1}{IP_{slab}}\right)}, \quad (19)$$

where μ, IP_{mol} and α_{mol} belong to the molecule and those with index "slab" to the surface; Q is a charge of the surface atom and x is the molecule-surface distance. Using this equation, ΔH_{ads} of group-7 MO_3Cl on a quartz surface of the chromatography column covered with HCl were predicted [168]. The 4*c*-DFT calculated molecular properties required by the model are given in Table 9. Main contributions to the total *E(x)* are given in Table 11 indicating an increase in the energies of all three types of interactions from Tc to Bh. $\Delta H_{ads}(BhO_3Cl) = -78.5$ kJ/mol and $\Delta H_{ads}(TcO_3Cl) = -48.2$ kJ/mol were then determined with

Table 11 Contributions to the interaction energy *E(x)* of the MO_3Cl molecules (M = Tc, Re, and Bh) with Cl^Q (surface) for $Q = {}^-0.4$. From [168]

Molecule	μ-Qe $E10^{16}$ x^2, eV cm^2	α-Qe $E10^{32}$ x^4, eV cm^3	α-α(Cl) $E10^{48}$ x^6, eV cm^6
TcO_3Cl	2.23	5.69	379.06
ReO_3Cl	3.10	6.81	460.65
BhO_3Cl	4.67	8.64	591.17

respect to $\Delta H_{ads}(ReO_3Cl) = -61$ kJ/mol, so that the sequence in volatility was predicted as $TcO_3Cl > ReO_3Cl > BhO_3Cl$. This trend is caused by increasing μ in this row. The predicted sequence and the ΔH_{ads} values are in excellent agreement with the experimental ones of -51 ± 2 kJ/mol for TcO_3Cl and -77 ± 8 kJ/mol for BhO_3Cl [184].

Similarly, a trend in adsorption of group-6 MO_2Cl_2 on a modified quartz surface was predicted as Mo < W < Sg due to increasing dipole moments in this row (Table 9), so that the trend in volatility is Mo > W > Sg [167]. This was also confirmed by results of isothermal gas-phase chromatography experiments [185, 186].

The physisorption adsorption mechanism could, however, not explain results of the gas-phase chromatography experiments with pure halides of group-4 and 5 elements. Thus, e.g., experiments on the chlorides and bromides of group-5 elements, using both thermo- and isothermal chromatography techniques [187–190] revealed that volatility of the Nb and Ta halides is similar, while that of Db is lower. Taking into account the predicted sequence in volatility (as P_{mm} of MBr_5 over the solid) Nb < Ta < Db [162], this unexpected behavior was explained by the formation of either oxyhalides MOL_3, or the $KMBr_5L$ (L = Cl, Br) salt on a quartz surface modified with aerosol transport KCl or KBr particles. To test this assumption, a new theoretical study on the prediction of the adsorption behavior of group 5 bromides at the given experimental conditions was undertaken in [164].

First, it was shown that $DbBr_5$ should, indeed, be formed at the experimental conditions, while $DbOBr_3$ should not (see dissociation energies in Table 9). Further on, the calculations have shown that if the MBr_5 molecule approaches a KCl or KBr surface along the z axis, physisorption described by Eq. 17 occurs. If the molecule, however, approaches such a surface by one of the facets, the MBr_6^- complex is formed (Fig. 27), where an additional Br atom comes from the surface.

The 4c-DFT calculated energies of the $MBr_5 \rightarrow MBr_5L^-$ (L = Br, Cl) reaction with respect to those of Nb, are given in Table 12. The latter are in excellent agreement with the $TaBr_5$-$NbBr_5$ and $DbBr_5$-$NbBr_5$ differences in the experimental ΔH_{ads}, so that the sequence in the strength of the complexes should indeed

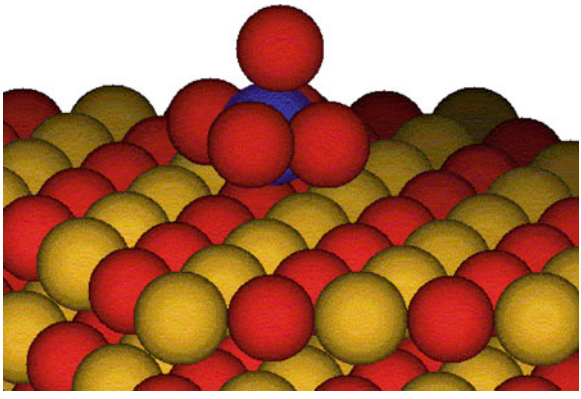

Fig. 27 Formation of MBr_6^- on the KBr surface. Reprinted with permission from V. Pershina, J. Anton, J. Chem. Phys. **136**, 034308(7) (2012). Copyright 2012 American Institute of Physics

Table 12 Energies of the $MBr_5 \rightarrow MBr_5L^-$ (L = Br, and Cl) reaction with respect to those of Nb, $\Delta\Delta E$, as well as relative values (with respect to those of Nb) of measured ΔH_{ads} (in eV)

Reaction energy	Nb	Ta	Db
$\Delta\Delta E(MBr_5 \rightarrow MBr_6^-)$/Nb	0	−0.09	−0.21
$\Delta\Delta E$ $(MBr_5 \rightarrow MBr_5Cl^-)$/Nb	0	−0.09	−0.25
$-\Delta H_{ads}[SiO_2/KCl]/Nb$[a]	0	−0.08	−0.29
$-\Delta H_{ads}[SiO_2/KBr]/Nb$[b]	0	−0.08	+0.19

[a] Experiment [188]; [b] experiment [190], see "Gas-Phase Chemistry of Superheavy Elements"

be Nb < Ta < Db. Thus, obviously, MBr_5L^- (L = Br, Cl) are formed on the KBr/KCl surface in the "one-atom-at-a-time" experiments [187–189]. In this case, the complex of Db should be the strongest, which means that $DbBr_5$ should be the least volatile among the homologs.

The latest experiments on the adsorption of the group-5 pentabromides on the quartz surface (presumably modified with KBr aerosol particles) [190] have, however, shown the following sequence in the adsorption energy $DbBr_5 < NbBr_5 < TaBr_5$, in contrast to the former experiments [188] and recent theoretical predictions [164]. This new experimental result has not yet found its explanation.

6.1.5 Solid State of the 6d Elements

Solid-state calculations were performed on the Rf metal [191]. The structural and electronic properties were evaluated by the first principles DFT in scalar relativistic formalism with and without SO coupling and compared with its 5d homolog Hf. It is found that Rf should crystallize in the hexagonal close packed structure as Hf. However, under pressure, it should have a different sequence of phase transitions than Hf: *hcp* → *bcc* instead of *hcp* → *ω* → *bcc*. An explanation is offered for this difference in terms of the competition between the band structure and the Ewald energy contributions.

6.2 Mt and Ds (Elements 109 and 110)

The group-9 and 10 elements Mt and Ds, respectively, have received little attention so far. The position of these elements in the Periodic Table suggests that they should be noble metals. Volatile hexafluorides and octafluorides might be produced and used for chemical separation experiments. The DS DV calculations for DsF_6 indicate that DsF_6 should be very similar to PtF_6, with very close values of IPs [192]. Relativistic effects were shown to be as large as ligand-field splitting.

Bond lengths in MtH_3, MtC^-, DsH_2, and DsH_3 were calculated using the ADF ZORA program [149, 150]. Using the same method, electronic structures of DsC and DsCO were calculated in [193] suggesting that these compounds are chemically similar to the corresponding 5d homologs.

6.3 Rg (Element 111)

A special interest in the chemistry of Rg is explained by the expectation of unusual properties of its compounds caused by the maximum of the relativistic contraction and stabilization of the 7s AO in this group. The electronic structure of the simplest molecule RgH, a sort of a test system like AuH, was studied at various levels of theory [194–198]. The most representative results are shown in Table 13. (More extended tables are given elsewhere [8, 194, 197]). One can see that a very high accuracy of the calculations is needed to predict the correct trend in R_e from AuH to RgH, because the values are very similar. The 4*c*-DFT R_e [198] is in excellent agreement with the DHF CCSD(T) one [197], as one of most accurate.

The data of Table 13 demonstrate the importance of relativistic and correlation effects on the properties of RgH. A study of influence of relativistic effects on properties of these molecules was performed in [194], see Fig. 28. A comparison of the relativistic (DF or ARPP) with the non-relativistic (HF or NRPP) calculations shows that bonding is considerably increased by relativistic effects doubling the dissociation energy, though the SO splitting diminishes it by 0.7 eV (the ARPP CCSD—SOPP CCSD difference). Thus, it was established, in agreement with the BDF calculations [109], that the trend to an increase in D_e from AgH to AuH should be reversed from AuH to RgH (Fig. 28). The PP CCSD calculations have found that R_e(RgH) is substantially shortened by relativity, $\Delta R_e = -0.4$ Å, and it is the smallest in the series AgH, AuH and RgH, so that the trend to a decrease in R_e is continued with RgH [194]. The BDF calculations [109] have, however, shown R_e(RgH) to be slightly larger than R_e(AuH). The different trends in R_e obtained in these two types of the calculations are connected with a different contribution of the contracted 7s and expanded 6d orbitals to bonding (though the

Table 13 Bond length, R_e (in Å), dissociation energy, D_e (in eV), and force constant, k_e (in mdyn Å^{-1}), as well as vibrational frequency of the bond, ω_e (in cm^{-1}), in the parentheses, for RgH calculated using various approximations in comparison with AuH

Molecule	Method	R_e	D_e	k_e (ω_e)	Ref.
AuH	exp.	1.5236	3.36	3.14	[110]
RgH	HF	2.015	0.90	1.01	[194]
	NRPP CCSD(T)	1.924	1.83	1.11	[194]
	DF	1.520	1.56	4.66	[194]
	ARPP	1.505	2.32	4.98	[194]
	ARPP CCSD(T)	1.498	3.79	4.77	[194]
	SOPP CCSD(T)	1.503	3.05	4.72	[194]
	PP CCSD(T)	1.529	2.83	(2642)	[195]
	SC PP CCSD(T)[a]	1.512	2.87	(2668)	[196]
	DHF CCSD(T)	1.523	2.83	4.23	[197]
	4*c*-BDF	1.546	2.77	3.66	[109]
	SO ZORA(MP)	1.530	2.87	4.26	[109]
	4*c*-DFT	1.520	2.85	(2804)	[198]

[a] Shape-consistent (SP)

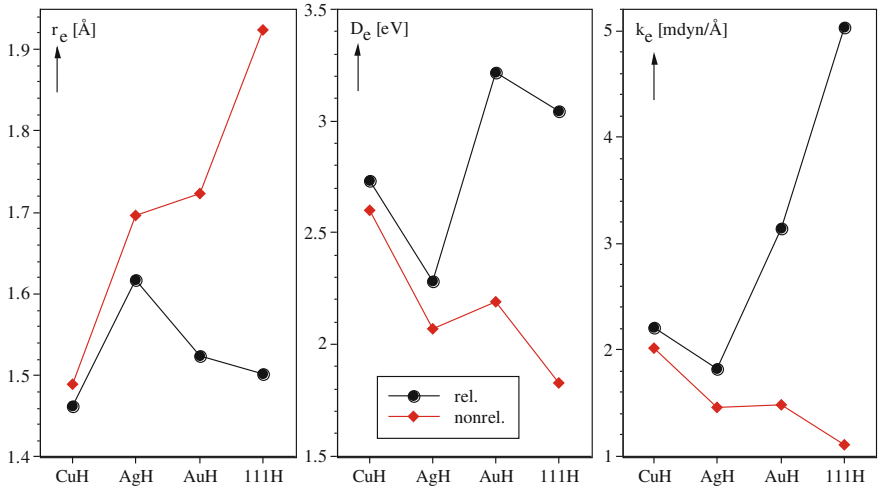

Fig. 28 Nonrelativistic and relativistic bond lengths, r_e (see also Table 13 for various values for RgH), dissociation energies, D_e, and force constants, k_e, of the group-11 hydrides. Reprinted with permission from [194]. Copyright 1996 Elsevier

6d contribution was found to de predominant in both cases). In [109], much larger SO effects were found on R_e (SO increased) and k_e (SO decreased) of RgH. The trend to an increase in k_e was found to be continued with RgH having the largest value of all known diatomic molecules [194]. The μ was shown to be relativistically decreased from AgH to AuH and to RgH indicating that RgH is more covalent and element Rg(I) is more electronegative than Au(I) [109, 194].

Results of the 4*c*-BDF [109] and 4*c*-DFT calculations [198] for other dimers, AuX and RgX (X = F, Cl, Br, O, Au, Rg), indicate that relativistic effects follow a similar pattern to that for RgH except for RgF and RgO, where SO splitting increases D_e. The PP calculations for RgH, RgLi and RgF [197] have, however, shown that SO effects on R_e are very small, but they are large for D_e, decreasing it in all the cases, in difference to the BDF calculations for RgF [109]. Scalar relativistic effects increase D_e(RgLi), but decrease D_e(RgF). They decrease R_e by about 0.4 Å in all the cases. The singlet state was found to be the ground for Rg_2 in comparison with the triplet [198]. The dissociation energy was found to change in the following order: $Au_2 > RgAu > Rg_2$.

In order to study the stability of higher oxidation states, energies of the $MF_6^- \rightarrow MF_4^- + F_2$ and $MF_4^- \rightarrow MF_2^- + F_2$ (M = Cu, Ag, Au, and Rg) decomposition reactions were calculated at the PP MP2 and CCSD levels of theory [199]. Relativistic effects were shown to stabilize higher oxidation states in the high-coordination compounds of Rg due to the destabilization of the 6d AOs and their larger involvement in bonding. RgF_6^- was shown to be the most stable in this group. SO coupling stabilizes the molecules in the following order: $RgF_6^- > RgF_4^- > RgF_2^-$. This order is consistent with the relative involvement of the 6d electrons in bonding for each type of molecule.

6.4 Cn (Element 112)

6.4.1 Relativistic Effects in Group 12 of the Periodic Table

Group-12 elements have all closed-shell $(n–1)d^{10}ns^2$ ground states. Along with the increasing relativistic stabilization of the ns AO in the group (Fig. 3), this results in the fact that the elements become more inert with increasing Z. Thus, bulk Hg is known to be a liquid, however, very different from a condensed noble gas. In the case of Cn, relativistic effects are further amplified, so that this element was expected to be a volatile liquid, or a gas. This was originally assumed by Pitzer in 1975 [200], who found out that the very high excitation energy of 8.6 eV from the s^2 closed shell into the sp valence state of Cn will not be compensated by the energy gain of the chemical bond formation. Thus, Cn should reveal a noble gas character. The high inertness of Cn has also been demonstrated by other atomic properties, such as the highest IP, smallest AR and polarizability in group 12, as discussed in Sect. 5 (Fig. 18).

Experimentally, an inertness/reactivity of Cn was supposed to be investigated by studying its volatility with respect to that of Hg and Rn as adsorption on a gold surface (gold plated detectors) of the chromatography column used in gas-phase chromatography experiments [201–203] ("Gas-Phase Chemistry of Superheavy Elements"). The questions to the modern electronic structure theory, therefore, were: Is Cn metallic in the solid state, or is it more like a solid noble gas? What is its ΔH_{sub}? How volatile and reactive towards gold is the Cn atom in comparison with Hg and Rn?

6.4.2 Van der Waals Systems. Volatility as Sublimation

Homonuclear dimers. In the first approximation, bonding in the solid state of an element is described by bonding in its homonuclear dimer, M_2. Knowledge of the latter was, therefore, important to estimate ΔH_{sub} of the bulk Cn. Moreover, Hg_2 and Cn_2 have been of a special interest in chemical theory in testing the accuracy of quantum chemical methods in treating closed-shell interactions. Accordingly, electronic structures of these dimers were calculated with the use of a various methods, such as 4*c*-BDF, ECP CCSD(T), QP PP CCSD(T) [204] and 4*c*-DFT [155, 198]. Results are summarized in Table 14 and Fig. 29.

Table 14 Bond lengths, R_e (in Å), and dissociation energies, D_e (in eV), of Hg_2 and Cn_2

Method	Hg_2		Cn_2		Ref.
	R_e	D_e	R_e	D_e	
4*c*-BDF (PBE)	3.439	0.053	3.089	0.156	[204]
4*c*-BDF (PBESIC)	3.904	0.025	3.363	0.075	[204]
QR PP CCSD(T)	3.769	0.044	3.386	0.097	[204]
4*c*-DFT (B88/P86)	3.63	0.01	3.45	0.05	[198]
exp.	3.63	0.043	–	–	[110, 205]

The calculations have shown that even though bonding both in Hg_2 and Cn_2 is preferentially of van der Waals type, a partial overlap occurs. The 6d-AOs are active and mixing up with the 7s-AOs of Cn in the HOMO.

Both the DFT and PP calculations agree on an increase in D_e of about 0.04 eV from Hg_2 to Cn_2 with the corresponding bond shortening, in line with the smaller R_{max}[7s(Cn) AO] in comparison with R_{max}[6s(Hg) AO] (Fig. 3). Thus, due to the relativistic 7s AO contraction, Cn_2 should be more stable than Hg_2. This suggests that the bulk of Cn should be more bound than that of Hg (liquid).

Solid state. LDA DFT (non-relativistic, scalar relativistic, SR, and 4*c*-relativistic) band structure calculations were performed on the Cn solid state [206]. The results have shown that Cn prefers the *hcp* structure (as that of Zn and Cd) in difference to Hg (*fcc*). Thus, it should differ from its lighter homolog Hg on a structural level and resemble the solid-state noble gases. A cohesive energy of 1.13 eV (109 kJ/mol) was obtained for Cn at the SR level of theory, which is larger than that of Hg (0.64 eV) and is an order of magnitude larger than those of the solid noble gases. This result is consistent with the larger $D_e(Cn_2)$ with respect to $D_e(Hg_2)$ (see Table 14). Thus, from a theoretical point of view, ΔH_{sub} of 22 kJ/mol obtained via an extrapolation in group 12 [207] is obviously underestimated, as such an extrapolation in this group is not grounded. It was also concluded that Cn is not a metal, but rather a semiconductor with a band gap of at least 0.2 eV. (The LDA results were considered as a lower bound). In this sense, Cn resembles the group 12 metals more closely than it does the noble gases.

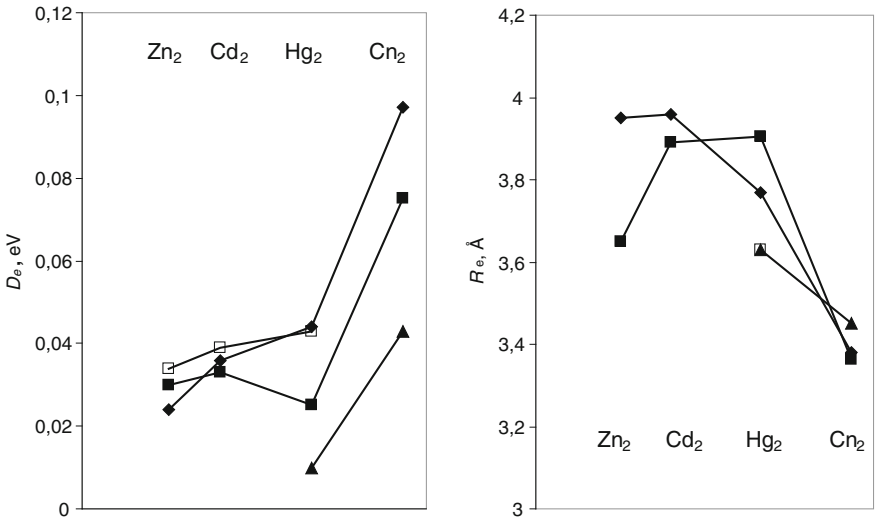

Fig. 29 QR PP CCSD(T) (*filled rhomboids*), 4*c*-BDF (PBESIC) (*filled squares*), 4*c*-DFT (B88/P86) (*filled triangles*) and experimental (*open squares*) dissociation energies, D_e, and bond lengths, R_e, of the group-12 dimers (see Table 14). Reprinted with permission from V. Pershina, Radiochim. Acta, **99**, 459 (2011). Copyright 2011 Oldenbourg Wissenschaftsverlag GmbH

Adsorption on inert surfaces. The knowledge of ΔH_{ads} of Cn on inert surfaces such as quartz and ice (that can be formed in the chromatography column at very low temperatures) was also required for interpreting results of the gas-phase chromatography experiments. With this aim in view, ΔH_{ads} of Hg and Cn, as well as of Rn for comparison, on these surfaces were estimated using a physisorption model (Eq. 17) and DCB FSCC calculated atomic properties [127]. The obtained $-\Delta H_{ads}$ of Hg of 40.5 kJ/mol on quartz and of 25.20 kJ/mol on ice are in good agreement with the experimental values of 42 ± 2 kJ/mol and 25.5 ± 2 kJ/mol, respectively [208, 209]. For Cn, $-\Delta H_{ads} = 43.2 \pm 0.2$ kJ/mol on quartz and $-\Delta H_{ads} = 26.3 \pm 0.1$ kJ/mol on ice were predicted. Thus, Cn was expected to be more strongly bound than Hg by van der Waals forces and to be deposited on ice in the thermochromatography column at slightly higher temperatures than Hg.

By using relativistic *vs.* non-relativistic values of the atomic properties (Fig. 18), the influence of relativistic effects on ΔH_{ads} and the trend in group 12 was elucidated [155]. The trend in ΔH_{ads} was shown to be defined by the trend in AR, since trends in α and IP cancel each other (see Eq. 17). Thus, due to the relativistically more contracted AR(Cn) than AR(Hg), $-\Delta H_{ads}$ of Cn is larger than that of Hg, while non-relativistically, it is the other way around.

6.4.3 Volatility as Measured in Gas-Phase Chromatography Experiments. Interaction with Metals

Heteronuclear dimers. In the simplest approximation, a gold surface can be approximated by only one gold atom. Thus, in order to estimate binding energies of Cn with noble metals, electronic structure calculations were first performed for HgM and CnM, where M = Ag, Au, Pt, Pd, and Cu using the 4*c*-DFT method [210]. It was demonstrated that Cn forms a chemical bond with Au primarily due to the overlap between the double occupied 7s(Cn) AO and single occupied 6s(Au) AO, as well as between the $6d_{5/2}$(Cn) AO and $5d_{5/2}$(Au) AO. Thus, CnAu should be chemically bound having a $\sigma^2\sigma^{*1}\ ^2\Sigma^+$ ground state configuration with two electrons in the bonding and one in the antibonding MOs (Fig. 30).

Overall, Cn should be about 0.2 eV weaker bound with a transition metal atom M than Hg and the bonds should be longer. The latter is a result of the participation of the more expanded 6d(Cn) AOs than the 5d(Hg) AOs in bonding. Among M, bonding with Pd should be the strongest, while with Ag the weakest.

The influence of relativistic effects on properties of MAu (M = Hg and Cn) was studied in [155]. Relativity is shown to increase D_e(HgAu) by 0.13 eV, but to decrease it by about the same amount (0.12 eV) in CnAu due to the contraction of the 7s(Cn) AO. This makes trends in the nonrelativistic *vs.* relativistic D_e values opposite from HgAu to CnAu, so that $D_e^{nr}(CnAu) > D_e^{nr}(HgAu)$, while $D_e^{rel}(CnAu) < D_e^{rel}(HgAu)$. R_e is decreased by relativity in both systems and the trends are the same both for the non-relativistic and relativistic R_e.

Interaction with gold clusters. In [211–213], 4*c*-DFT calculations were performed for Hg and Cn interacting with gold clusters, Au_n. Since the structure of the

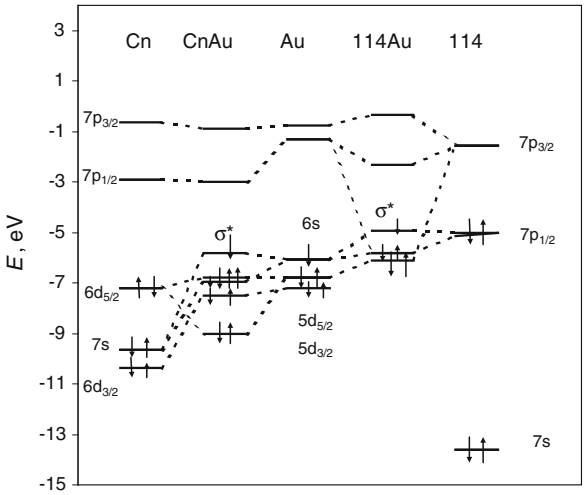

Fig. 30 Bond formation (principal MOs) of the CnAu and FlAu molecules. Reprinted with permission from V. Pershina, Radiochim. Acta, **99**, 459 (2011). Copyright 2011 Oldenbourg Wissenschaftsverlag GmbH

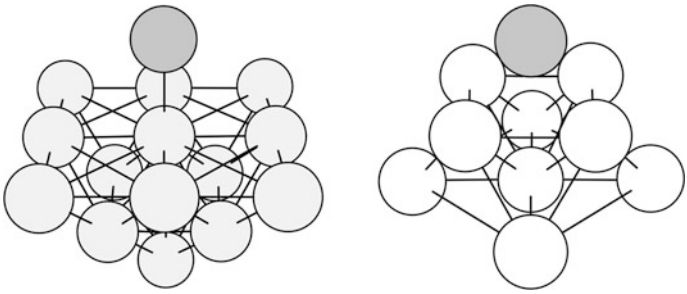

Fig. 31 The M-Au_{14} and M-Au_9 systems simulating adsorption of M in the on-top and hollow sites on the Au(100) surface, respectively. Reprinted with permission from V. Pershina, T. Bastug, Chem. Phys. **311**, 139 (2000). Copyright 2000 Elsevier

gold surface used in the chromatography experiments is not known, two types of ideal surfaces, Au(100) and Au(111), were considered. In the first case, the surface was simulated by the medium-size Au_n clusters and embedded clusters, Au_nAu_m [211, 212]. The ad-atom was positioned at all possible adsorption sites: on-top, bridge and hollow (see Fig. 31 for the on-top and hollow positions on small clusters and Fig. 7 for the on-top position on an embedded cluster). The convergence in E_b(M-Au_nAu_m) with the cluster size was reached for $n > 29$ and $m = 156$ [212].

The obtained potential energy curves are shown in Fig. 32. It was found out that both Cn and Hg adsorb preferentially at the bridge position, and E_b(Cn-Au_n) should be 0.38 eV smaller than E_b(Hg-Au_n) for this position.

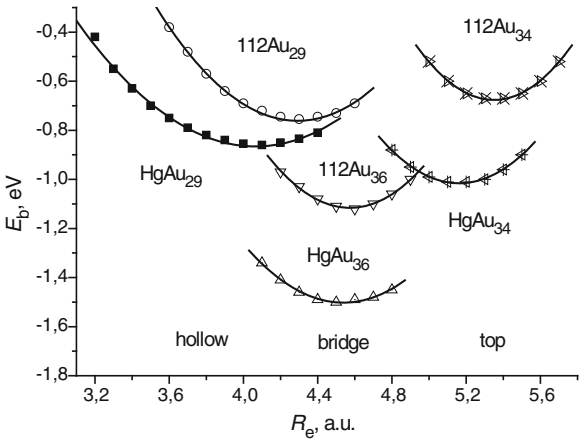

Fig. 32 The 4*c*-DFT calculated potential energy curves for the M-Au$_n$Au$_{156}$ systems (M = Hg and Cn) in the three adsorption positions of M: on-top, hollow and bridge [212]

The difference in the binding energies between Hg-Au$_n$ and Cn-Au$_n$ was calculated as 0.38 eV for the bridge position. With respect to the measured $-\Delta H_{ads}$(Hg) of 1.03 eV on gold [208, 209], this gives $-\Delta H_{ads}$(Cn) = 0.67 eV. This value is in reasonably good agreement with the measured $-\Delta H_{ads}$(Cn) = $0.54^{+0.2}_{-0.01}$ eV (52^{+20}_{-4} kJ/mol) [202, 203]. The obtained absolute values of E_b of Hg and Cn are, however, larger than the experimental $-\Delta H_{ads}$ indicating that the Au(100) surface is obviously a loose approximation for the real one.

Thus, next, adsorption of Cn on the Au(111) surface was considered at the 4*c*-DFT level of theory [213]. The Au(111) surface was modeled by the large Au$_n$ clusters, where the convergence in E_b(M-Au$_n$) with the cluster size was reached for n = 95 for the top, n = 94 for the bridge, n = 120 for the hollow-1 and n = 107 for the hollow-2 positions. The bridge position was found again preferential for Hg, while hollow-2 for Cn. The obtained E_b(Cn-Au$_n$) of 0.46 eV turned out to be in good agreement with the experimental $-\Delta H_{ads}$(Cn) of $0.54^{+0.2}_{-0.01}$ eV [203], indicating that the Au(111) ideal surface is close to the real one.

Works on RECP and 2*c*-DFT (SO corrected) calculations for Hg and Cn interacting with small gold clusters (n = 1–4, and 10) arrived at the same conclusion that the Cn-Au$_n$ bonding is about 0.2 eV weaker than the Hg-Au$_n$ one [214–217].

In [155], the influence of relativistic effects on adsorption of Hg and Cn on gold was investigated on the example of small ad-atom-gold clusters modelling adsorption at the on-top and hollow positions (Fig. 31). Relativistic effects were shown to define the trend to a decrease in E_b(M-Au$_n$) from Hg to Cn, even though they increase E_b(M-Au$_n$) both in the Hg and Cn systems, especially at the hollow position due to the involvement of the 6d(Cn) AOs in bonding. This makes the difference in E_b(M-Au$_n$) between Hg and Cn very small. Relativistic effects were shown to decrease R_e, the distance of the ad-atom to the surface, in all the cases.

Figure 33 summarizes the most interesting cases of the group-12 elements chemistry: D_e(M$_2$), ΔH_{sub}(M), D_e(MAu), E_b(M-Au$_n$) and ΔH_{ads}(M) on gold. Thus,

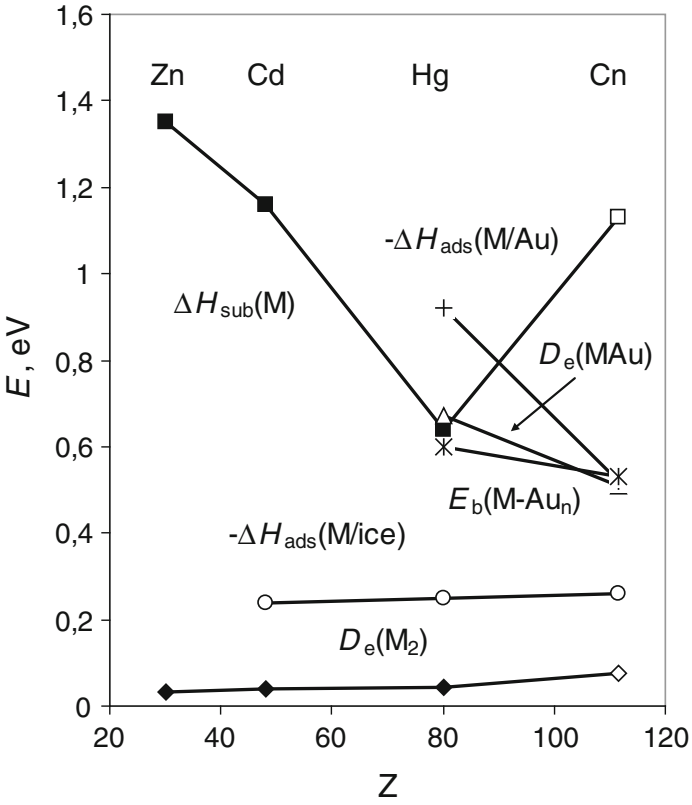

Fig. 33 Binding energies of group-12 elements M (M = Zn, Cd, Hg, and Cn) in various systems: $D_e(M_2)$ (*rhomboids*), $-\Delta H_{ads}$(M/ice) on ice (*circles*), ΔH_{sub}(M) of solids (*squares*), D_e(MAu) (*triangles*); E_b(M-Au$_n$) (*stars*); experimental $-\Delta H_{ads}$(M/Au) on gold (*crosses*). Filled symbols are experimental values, open ones are calculations. Reprinted with permission from V. Pershina, Radiochim. Acta, **99**, 459 (2011). Copyright 2011 Oldenbourg Wissenschaftsverlag GmbH

Cn should be stronger bound by van der Waals forces than Hg both in M_2, solid state and adsorbed state on an inert surface, and this is a relativistic effect caused by the contraction of the 7s(Cn) AO. The M-Au bonding, chemical in nature, should, on the contrary, decrease from Hg to Cn due to the gradual stabilization of the ns AO in group 12. This suggests that a linear correlation between ΔH_{sub} and $-\Delta H_{ads}$ (as that used in [203]) is not valid in this group due to the different type of bonding in these two cases. Therefore, obtained on the basis of this correlation $\Delta H_{sub}(Cn) = 38^{+10}_{-12}$ kJ/mol ($0.39^{+0.1}_{-0.12}$eV), as well as $\Delta H_{sub}(Cn) = 22$ kJ/mol (0.23 eV) obtained via a straightforward extrapolation in group 12 [207] are, obviously, underestimated.

The main conclusion of both the theoretical and experimental studies is that Cn interacts with gold by chemical forces due to the overlap between the valence

orbitals. It forms a metal–metal bond upon adsorption, though weaker than that of Hg, due to relativistic effects. Thus, it behaves like a typical d-element, but not like an inert gas, which is in agreement with its position in group 12 of the Periodic Table.

6.4.4 Other Compounds

The relativistic contraction of the 7s AO is expected to manifest itself also in properties of other Cn compounds. The PP calculations [153] have shown that the relativistic bond length contraction in CnH^+ is similar to that in RgH, and that $R_e(CnH^+)$ is the smallest among all others, CdH^+, HgH^+ and CnH^+, and is similar to $R_e(ZnH^+)$, in agreement with the GRECP calculations [218]. (The RECP CCSD(T) calculations [139] for HgH^+ and CnH^+ have, however, given a larger R_e for the latter compound). Another interesting point is that, in contrast to the group-11 hydrides, the trend in the dissociation energies from Cd to Hg is continued with Cn, i.e., $D_e(CdH^+) < D_e(HgH^+) < D_e(CnH^+)$, while $D_e(AgH) < D_e(AuH) > D_e(RgH)$ [139, 151, 218]. The reason for this difference is greater relativistic effects in CnH^+ than in RgH.

The second (DK2) and third-order DK (DK3) method was also applied to CnH, CnH^+ and CnH^- [219]. It was shown that scalar relativistic effects on the properties of CnH^- are similar to those on 113H and are smaller than those on CnH^+ and CnH. The DK results for CnH differ, however, from the GRECP ones [218]: according to the former, $R_e(HgH) < R_e(CnH)$, and $D_e(HgH) > D_e(CnH)$, while the latter give $R_e(HgH) > R_e(CnH)$, and $D_e(HgM) \approx D_e(CnH)$ (see discussions in [218]).

As was mentioned above, the destabilization of the 6d AOs should result in their larger involvement in bonding. Thus, high-coordination compounds of Cn should be stable and higher oxidation states should be observed. The PP CCSD(T) calculations of the energies of the $MF_4 \rightarrow MF_2 + F_2$ and $MF_2 \rightarrow M + F_2$ (M = Zn, Cd, Hg, and Cn) decomposition reactions supported this assumption [153]. The results are depicted in Fig. 34.

Thus, the 2+ state is important for all three molecules, ZnF_2, CdF_2, and HgF_2, though the first two are more stable than HgF_2. The latter decomposes at 645 °C. The small energy of the decomposition reaction of MF_2 into M and F_2 confirms the prediction that Cn will be more inert than Hg, though the difference to Hg is not that large. A comparison with non-relativistic results shows that this is a pure relativistic effect: non-relativistically, CnF_2 would have been by far more stable (comparable to CdF_2) with decomposition energy of 509.8 kJ/mol.

The 4+ oxidation state is not known for Zn, Cd, and Hg. Results of the PP calculations suggested that HgF_4 should be thermodynamically stable [220, 221]. The energy of the decomposition reaction of CnF_4 of 129.5 kJ/mol indicates that the molecule should be thermodynamically more stable than HgF_4 [153] (Fig. 34). However, no definite conclusion about the existence of CnF_4 can be drawn, since its decomposition energy is between 100 and 200 kJ/mol: experimentally, few

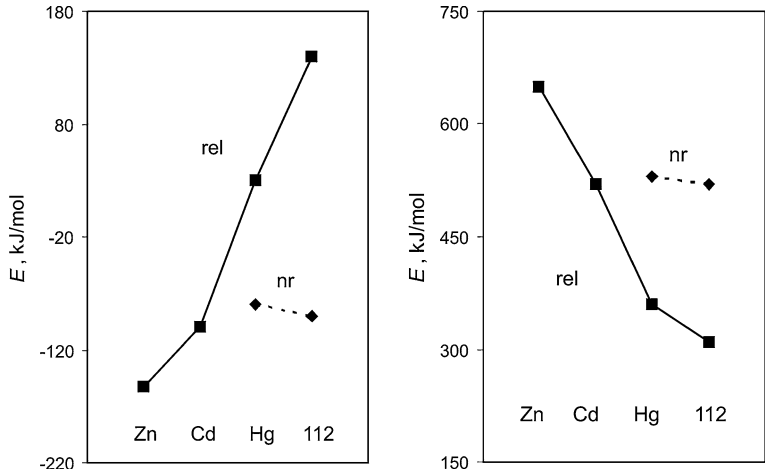

Fig. 34 Relativistic (*solid lines*) and nonrelativistic (*dashed lines*) energies of the decomposition reactions $MF_4 \rightarrow MF_2 + F_2$ and $MF_2 \rightarrow M + F_2$ (M = Zn, Cd, Hg, and Cn). Re-drawn from the data of [153]

compounds with the energy below 100 kJ/mol are known in the solid state. Nonrelativistically, CnF_4 would be definitely unstable with the energy of the decomposition reaction of −93.9 kJ/mol. SO coupling increases energies of both reactions significantly.

A Mulliken population analysis for MF_2 and MF_4 (M = Hg and Cn) suggests that the 6d AOs of Cn are involved in bonding to a larger extent than the 5d AOs of Hg [153]. It was also found that the addition of F^- ions to HgF_2 and to HgF_4 is energetically favorable [220, 221]. By analogy, it is assumed that in combination with appropriate polar solvent, CnF_5^- and/or CnF_3^- may be formed [153].

6.5 7p Elements

6.5.1 Adsorption on Inert Surfaces and Volatility of Atoms

In the 7p elements, the 7s electrons are bound more tightly than the 6s ones in the 6p elements, so they will not take part in the chemical bond formation (Fig. 8). Also, a large SO splitting of the 7p shell into the *nlj* subshells will result in differences in the chemical behavior in comparison with lighter homologs having a complete *nl* shells [1, 2].

Early extrapolations from lighter homologs in the chemical groups have shown that elements 113 through 117 should have smaller ΔH_{sub}, or formation (standard) enthalpies of gaseous atoms, $\Delta H_f(g)$, than their lighter homologs [207], which means that the bulk of the heaviest elements is less bound.

Flerovium, like Cn, was in this sense of particular interest due to the relativistic stabilization of the $7p_{1/2}$ AOs resulting in the quasi-closed shell $7s^27p_{1/2}^2$ ground state and, therefore, inaccessibility of these electrons for chemical bonding. The arguments of Pitzer, similar to those used for Cn, namely, that the $p_{1/2}^2 \rightarrow p^2$ promotion energy to the metal valence state of Fl will not be compensated by the metal–metal bond formation, led to the conclusion that this element should be a relatively inert gas, or a volatile liquid bound by van der Waals forces [200].

Experimentally, volatility of the 7p elements at the beginning of the series, i.e., those with a sufficiently long half-life, is supposed to be studied using gas-phase chromatography techniques. First results were already reported for Fl [222, 223]. Test experiments were conducted on the nearest homolog of element 113, Tl [224].

In order to guarantee transport of elements 113 and 114 from the target chamber to the chemistry set up through Teflon or polyethelene (PE) capillaries, their ΔH_{ads} on these materials need to be known. They were predicted using DC(B) CC calculated atomic properties (Table 4) and a physisorption model of Eq. 17 [126, 127]. The obtained ΔH_{ads} of these elements and their homologs in the groups on these surfaces (also on quartz) are shown in Figs. 35, 36. The ΔH_{ads} were shown to exhibit a trend reversal beyond In in group 13 and beyond Sn in group14 due to the trend reversal in the atomic IP, AR, and α (Figs. 35, 36). The extremely small α of elements 113 and 114, caused by the contraction of the $7p_{1/2}$ AO, is the main reason for their low ΔH_{ads} on inert surfaces. This will allow for easy transport of these elements through the Teflon or PE capillaries.

Adsorption of element 118 and lighter noble gases on various surfaces was also a subject of theoretical investigations with possible future applications. It was interesting to know if it is possible to separate this element from its lighter homologs in group 18 on a specific surface using a chromatography technique. Accordingly, using the DC(B) CC calculated atomic properties (Table 4) and Eq. 17, van der Waals coefficients C_3 and ΔH_{ads} of Ne through element 118 on noble metal (Au and Ag) and non-metal (quartz, ice, Teflon and graphite) surfaces were obtained in [119]. Results for some surfaces are shown in Fig. 37. The C_3 coefficients were shown to steadily increase in group 18, while the increase in $-\Delta H_{ads}$ from Ne to Rn does not continue with element 118: even though α increases in the group (Fig. 37). However, AR $= R_{vdW}$ also increases in this group making ΔH_{ads} of element 118 almost equal to that of Rn (see Eq. 17). It was, therefore, predicted that experimental distinction between Rn and element 118 by adsorption on these surfaces will be impossible. A proper material for separating element 118 could probably be charcoal; further study is needed to test this assumption.

6.5.2 Homonuclear Dimers and Volatility as Sublimation

Homonuclear dimers. Keeping in mind that bonding in M_2 is related to bonding in the solid state, ΔH_{sub} were estimated for the entire series of the 7p elements and their 6p homologs on the basis of the 4*c*-DFT calculations of $D_e(M_2)$ [225, 226].

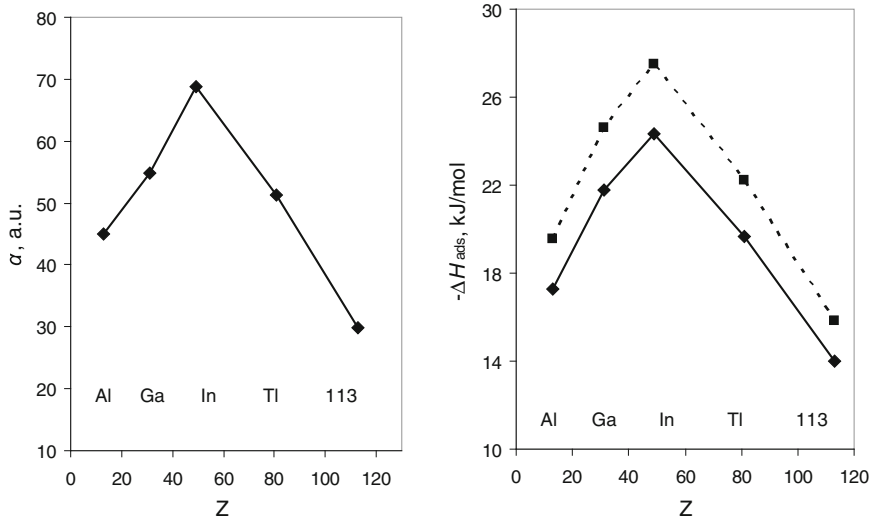

Fig. 35 Polarizabilities, α, and adsorption enthalpies, $-\Delta H_{ads}$, of group-13 elements on Teflon (*solid line*) and polyethylene (*dashed line*): $-\Delta H_{ads}(113)$ is 14 kJ/mol on Teflon and 16 kJ/mol on PE [126]

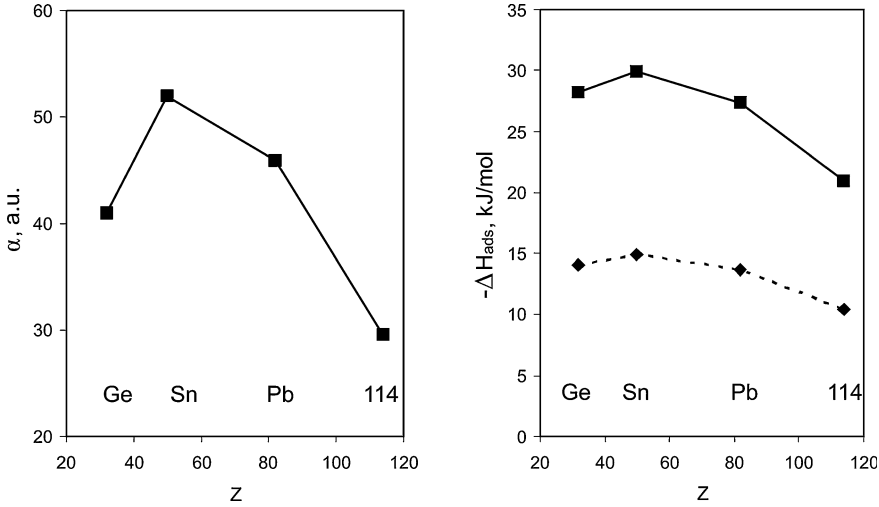

Fig. 36 Polarizabilities, α, and adsorption enthalpies, $-\Delta H_{ads}$, of the group-14 elements on quartz (*solid line*) and Teflon (*dashed line*): $-\Delta H_{ads}(Fl)$ is 21 kJ/mol on quartz and 10.4 kJ/mol on Teflon [127]. From [13]

Some other calculations were also performed for these species: *ab initio* DF for $(113)_2$ [227], 4*c*-BDF, 2*c*-SO ZORA and DC MP2-DFT for the element 113–118 dimers [91, 228–233], and RECP ones for the Fl and element 118 dimers [139].

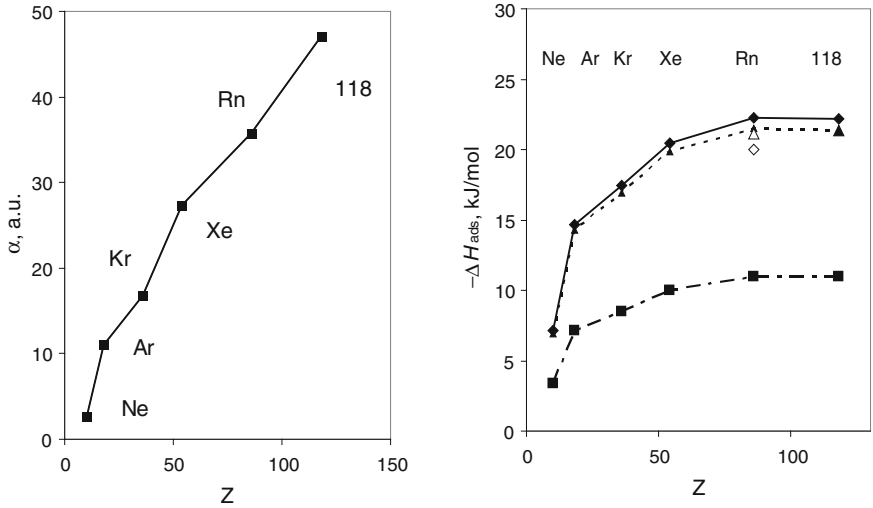

Fig. 37 Polarizabilities, α, and adsorption enthalpies, $-\Delta H_{ads}$, (filled symbols are calculations) of the noble gas atoms on quartz (*rhomboids*, *solid line*), ice (*triangles*, *dashed line*) and Teflon (*squares*, *dashed-dotted line*). Experimental data are for Rn on quartz (an *open rhomboid*) and on ice (an *open triangle*). From [119]

The obtained $D_e(M_2)$ are shown in Fig. 38 [225]. All the 7p-element homonuclear dimers of group-13 through 17 were shown to be weaker bound than their 6p homologs, with the difference in the binding energy between them decreasing from group 15 onwards and a reversal of the trend in group 18, so that $D_e[(118)_2] > D_e(Rn_2)$.

According to *ab initio* DF calculations, $(113)_2$ should be weakly bound because the $7p_{1/2}$ electron yields a weak bond having $2/3\pi$ bonding and $1/3\sigma$ antibonding character [227].

A special case is Fl_2, as that of Cn_2. It was of particular interest due to the strong stabilization and contraction of the $7p_{1/2}$ AO and, therefore, assumed van der Waals nature of the $7p^2_{1/2}$-$7p^2_{1/2}$ bonding. In order to test this hypothesis at the MO level of theory, the electronic structures of Pb_2 and Fl_2 were calculated within various approximations. Results are summarized in Table 15 and shown in Fig. 39.

All the calculations agree on the fact that Fl_2 is stronger bound than a typical van der Waals system. At the 4*c*-DFT level of theory, it is slightly more strongly bound than Cn_2, but much more weakly than Pb_2. A Mulliken population analysis indicates that both the $7p_{1/2}$ and $7p_{3/2}$ AOs of Fl take part in the bond formation: the HOMO of σ character is composed of the $7p_{1/2}$ (98%) and $7p_{3/2}$ (2%) AOs [225, 226]. The participation of the more expanded $7p_{3/2}$(Fl) AO in bonding in comparison with the $6p_{3/2}$(Pb) AO explains an increase in R_e from Pb_2 to Fl_2 (Fig. 39). SO effects were shown to decrease D_e, but increase R_e in both systems [228].

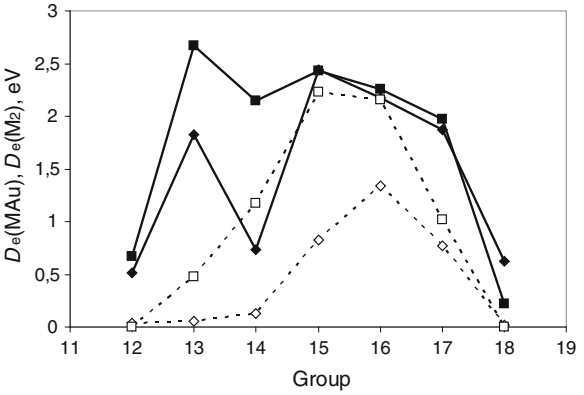

Fig. 38 Calculated dissociation energies of MAu and M_2 (M are elements Hg/Cn through Rn/118). Filled and open *squares* are D_e(MAu) and $D_e(M_2)$ of the 6p elements, respectively, while filled and open rhomboids are D_e(MAu) and $D_e(M_2)$ of the 7p elements, respectively. Reprinted with permission from V. Pershina, A. Borschevsky, J. Anton, T. Jacob, J. Chem. Phys. **133**, 104304 (2010). Copyright 2010 American Institute of Physics

Table 15 Bond lengths, R_e (in Å), dissociation energies, D_e (in eV), and vibrational frequencies, ω_e (in cm^{-1}), of Pb_2 and Fl_2

Molec.	Method	R_e	D_e	ω_e	Ref.
Pb_2	ECP CCSD(T)	3.06	0.64	111	[228]
	RECP CCSD(T)	2.98	0.68	–	[139]
	4*c*-BDF	2.98	1.14	108	[228]
	2*c*-DFT SO ZORA	2.97	1.16	106	[229]
	4*c*-DFT	2.97	1.18	107	[225, 226]
	exp.	2.93	0.86	110	[234]
	exp.	–	1.17	–	[235]
Fl_2	ECP CCSD(T)	3.73	0.07	26	[228]
	4*c*-BDF	3.49	0.12	50	[228]
	2*c*-DFT SO ZORA	3.46	0.12	40	[229]
	4*c*-DFT	3.49	0.13	26	[225, 226]

In $(115)_2$, the $7p_{3/2}$ electrons become active and form a $3/2_u(\pi_u)$ bonding, so that D_e is larger that D_e of $(113)_2$ and Fl_2 [225, 230]. They are also active in Lv_2, but the D_e is larger than that of $(115)_2$ in difference to the 6th period where $D_e(Po)_2 < D_e(Bi_2)$. Thus, the maximum in $D_e(M_2)$ in the 7th row of the Periodic Table is shifted towards group 16 with respect to group 15 in the 6th and upper rows (Fig. 38). This is a pronounced relativistic effect caused by the very large SO splitting of the 7p AOs. As a result of the stabilization of the $7p_{1/2}$ AOs, the system of the highest bonding-antibonding MOs in M_2 consists of only four MOs composed of the $7p_{3/2}$ AOs, so that the half-filled shell (with 4 electrons) falls on Lv_2. In contrast, the $6p_{1/2}$ and $6p_{3/2}$ AOs are not so well separated energetically from each other and form a set of six highest bonding-antibonding MOs, so that the half-filled shell (with 6 electrons) falls on Bi_2 [225].

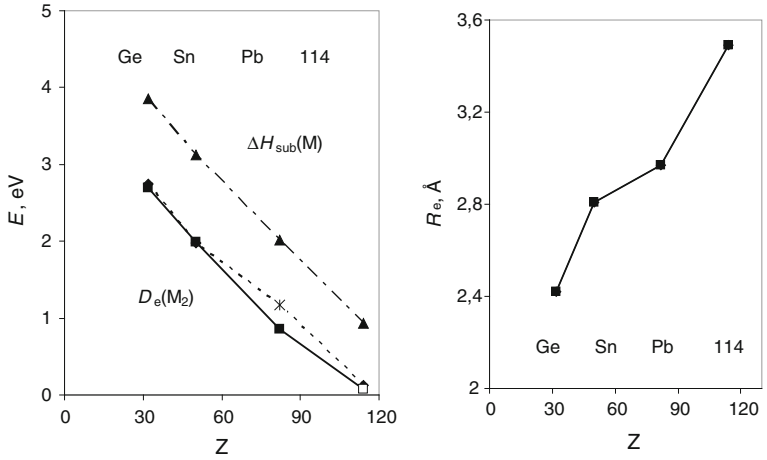

Fig. 39 Dissociation energies, $D_e(M_2)$, (experimental for Ge_2 through Pb_2: Two points for Pb_2 are two different experimental values [234, 235]; and calculated for Fl_2: two points are two different types of calculations, 4*c*-DFT [226] and RECP CCSD(T) [228]); sublimation enthalpies, $\Delta H_{sub}(M)$ [142], and calculated bond lengths, $R_e(M_2)$ [226], where M = Ge, Sn, Pb, and Fl. From [13]

Analogously to the lighter homologs, element 117 should also form $(117)_2$. The calculations found a considerable π bonding character [231, 232]. The bonding is weaker than that of Lv_2 due to the larger number of antibonding electrons. Finally, in $(118)_2$ bonding is of van der Waals type, since the number of bonding and antibonding electrons is the same. It is, however, stronger than that of Rn_2 [139, 225, 233]. This is explained by the larger α of element 118 (46.3 a.u.) than of Rn (35.04 a.u.) [119]. The MO population analysis indicated that no 8s(118) AO takes part in the bond formation in $(118)_2$ [225].

Sublimation (atomization) enthalpies. Solid-state calculations using periodic DFT codes for the 7p elements are still problematic due to very large SO effects on their valence electron shells. An easier way to obtain $\Delta H_f(g)$ is via a correlation with $D_e(M_2)$ in the respective chemical groups. $\Delta H_f(g)$ estimated in this way [225] and those predicted via a linear extrapolation in the groups [207] are given in Table 16, in good agreement with each other. One can see that the $\Delta H_f(g)$ decreases almost linearly with Z in these groups and the values for the 7p elements are the smallest (see Fig. 39 for group 14, as an example).

In [236], E_{coh} of Fl was predicted from SR and SO-GGA-DFT solid-state calculations. The obtained value of 0.5 eV (48.2 kJ/mol), the SO-PW91 result, is in reasonable agreement with the estimates of [207, 225] (Table 16). SO effects were shown to lower E_{coh} and lead to structural phase transitions for the solid Fl (the *hcp* structure in contrast to the *fcc* for Pb). In a nonrelativistic world, all group-14 elements would adopt a diamond structure. An increase in the solid-state nearest-neighbor distance is found from Pb to Fl, as that in their homonuclear dimers, indicating that the nature of the chemical bond in the crystal is similar to that of M_2.

Table 16 Standard enthalpies, $\Delta H_f(g)$ (in kJ/mol), of the 7p elements

Method	E113	Fl	E115	Lv	E117
Extrapolation[a]	138.1	70.3	146.4	92.1	83.7
Correlation[b]	144.7	70.4	152 ± 12	101.3	91.7

[a] Ref. [207]; [b] Ref. [225]

6.5.3 Intermetallic Dimers and Interaction with Metals

Heteronuclear dimers. In order to estimate ΔH_{ads} of the 7p elements on gold, 4*c*-DFT calculations for the MAu dimers were performed in [226, 237]. The obtained D_e(MAu) for the 7p and 6p elements in comparison with $D_e(M_2)$ are shown in Fig. 38. One can see that in groups 13 and 14, D_e(MAu) of the 7p elements are smaller than D_e of the 6p homologs (see also Fig. 40 for group 14 elements, as an example), while in groups 15 through 17, they are about the same. This is in contrast to the trends in $D_e(M_2)$ in these groups, where $D_e(Bi_2) >> D_e[(115)_2]$, $D_e(Po_2) >> D_e(Lv_2)$, and $D_e(At_2) > D_e[(117)_2]$. The relatively strong M-Au bonding of elements 115 through 117 with gold is explained by the relativistic destabilization of the $7p_{3/2}$ AOs fitting energetically better to the 6s(Au) AO, thus making—together with the $7p_{1/2}$ AO—a full σ-bond in MAu in difference to M_2, where only the $7p_{3/2}$ AOs are involved in bonding [225]. In group 18, a reversal of the trend takes place, so that $D_e(118Au) > D_e(RnAu)$, in agreement with the trend in $D_e(M_2)$. This is due to the relativistically more destabilized $7p_{3/2}(118)$ AO than the $6p_{3/2}$(Rn) AO, thus better overlapping with the valence AOs of gold.

According to results of the calculations, Fl should be stronger bound with gold than Cn [213, 237]. This is due to the fact that in FlAu—even though both FlAu

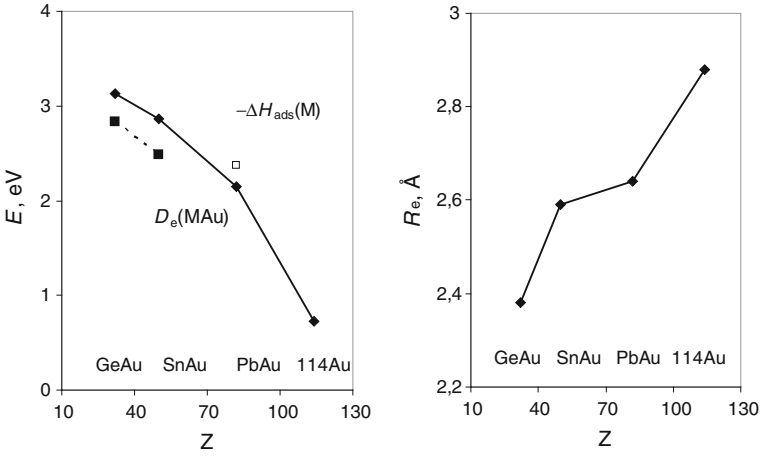

Fig. 40 Dissociation energies, D_e, (*solid line*—calculations [226], *dashed line*—experiment) and calculated bond lengths, R_e, in MAu (M = Ge, Sn, Pb, and Fl). A measured $-\Delta H_{ads}$ of Pb on gold is shown with an open *square*. Reprinted with permission from V. Pershina, Radiochim. Acta, **99**, 459 (2011). Copyright 2011 Oldenbourg Wissenschaftsverlag GmbH

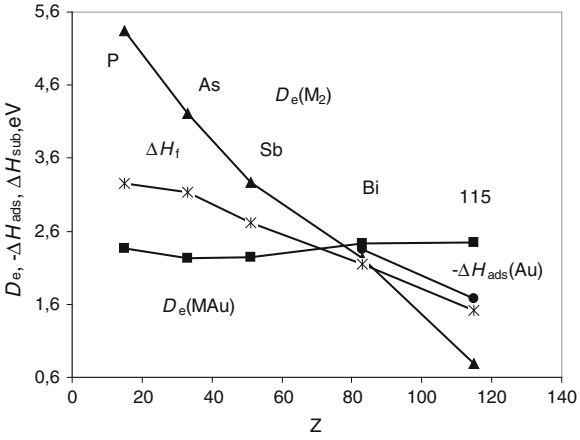

Fig. 41 Calculated dissociation energies, D_e, of MAu (*squares*) [237] and M_2 (*triangles*) [225], formation enthalpies, $\Delta H_f(g)$, of the group 15 elements (*stars*) (for P though Bi are from [142], while for element 115 from [225]) and semi-empirical $-\Delta H_{ads}$ of Bi and element 115 on gold (*circles*) [238]. Reprinted with permission from V. Pershina, A. Borschevsky, J. Anton, T. Jacob, J. Chem. Phys. **133**, 104304 (2010). Copyright 2010 American Institute of Physics

and CnAu are open shell systems with one antibonding σ^* electron—the electron density is donated from the lying higher in energy $7p_{1/2}$(Fl) AO to the 6s(Au) AO, while in CnAu, some excitation energy is needed to transfer some electron density from the closed $7s^2$ shell of Cn to the open 6s shell of Au (Fig. 30).

The calculations have also revealed that the M-Au bond strength *does not decrease linearly with Z* in group 15, 16 and 17. Figure 41 shows, e.g., that in group 15, $D_e(M_2)$ and $\Delta H_f(g)$ decrease, while D_e(MAu) slightly increases with Z. Also, in group 14, a decrease in D_e(MAu) is not strictly linear with Z (Fig. 40).

The 4*c*-DFT calculations were also performed for group-14 intermetallic dimers MM', where M' are group-10 and 11 metals Ni, Pb, Pt, Cu, Ag and Au [226]. (Some of them were supposed to be used as electrode materials in electrochemical deposition experiments [239]). Bonding of Fl with Pt was found to be the strongest, while that with Ag and Ni—the weakest. The trends in D_e and R_e of PbM' and FlM' as a function of M' were shown to be determined by the trends in the energies and R_{max} of the valence (n–1)d AO of the M' atoms, respectively, and are similar for PbM' and FlM' (except for M' = Ni).

Adsorption on gold. The calculated metal–metal bonding in the dimers was used to predict ΔH_{ads} of the heaviest elements on the corresponding metal surfaces. (For lighter elements, semi-empirical ΔH_{ads} are given in [238]). In [240], $-\Delta H_{ads}$ of element 113 on gold of 82 kJ/mol was estimated with respect to the measured $-\Delta H_{ads}$(Tl) of 240 ± 5 kJ/mol [224] using a difference in their D_e(MAu) calculated within the 4*c*-DFT approximation. This gives a preliminary value of $-\Delta H_{ads}(113) = 158.6$ kJ/mol, which is very close to 164.4 kJ/mol predicted via semi-empirical models [238].

In [241], adsorption of the element 113 atom and Tl on a gold surface was modeled by cluster calculations. The 2*c*-DFT calculations were performed for the M-Au$_n$ (M = Tl and element 113, and $n_{max} = 20$) systems, with the gold clusters simulating the Au(100) and Au(111) surfaces. The results show that the difference in the binding energy, E_b(M-Au$_n$), between Tl and element 113 stays within ± 15 kJ/mol of 82 kJ/mol obtained in [240] for MAu. Thus, the cluster calculations performed on a larger scale [241] confirmed the estimate made on the basis of D_e(MAu) [240], so that $-\Delta H_{ads}(113)$ can be finally given as 159 ± 15 kJ/mol.

In [226], $-\Delta H_{ads}$ of Fl on gold of 91 kJ/mol was estimated with respect to the measured $-\Delta H_{ads}$ of Pb [242] using a difference in D_e(MAu) between Pb and Fl.

Also, extensive 4*c*-DFT calculations were performed for M = Pb and Fl interacting with large Au$_n$ clusters simulating the Au(111) surface [213]. All possible adsorption positions were considered. Both Pb and Fl were found to prefer the bridge one, where the convergence in E_b(M-Au$_n$) with the cluster size was reached for $n = 94$. The calculated E_b values turned out to be in very good agreement with experimental data for Pb [242] (Table 17 and Fig. 42) indicating that the Au(111) surface is obviously close to the real one. The obtained $-\Delta H_{ads}$(Fl) of 68.5 kJ/mol is indicative of formation of a chemical bond of Fl with gold. A comparison with group-12 Hg and Cn [213] shows that the trend in E_b(M-Au$_n$) should be Cn < Hg < Fl << Pb (Fig. 42), exactly as that for D_e(MAu) of these elements. Since Hg dissolves into the gold surface gaining another ~0.3 eV [238], the trend in $-\Delta H_{ads}$ should be Cn < Fl < Hg << Pb.

Calculations for the Cn-Au$_n$ and Fl-Au$_n$ systems with the use of other relativistic DFT methods [214–217] came to the same conclusion that Fl should form a rather strong chemical bond with gold, stronger than Cn (Table 17).

Results of the first experiment on adsorption of Fl on gold have, however, given a rather low $-\Delta H_{ads}$ of 34^{+54}_{-11} kJ/mol ($0.35^{+0.6}_{-0.1}$ eV). A conclusion was drawn that this value "suggests the formation of a weak physisorption bond between atomic 114 and a gold surface" [222]. For Cn, it was, however, concluded that "the stronger (than van der Waals—V.P.) adsorption interaction of Cn with gold

Table 17 The Cn-Au$_n$ and Fl-Au$_n$ binding energies (in eV) simulating interactions of M with the Au(100) and Au(111) surfaces (bold values are for the preferential positions)

Method	n	Position	Surface	Cn	Fl	Ref.
4*c*-DFT	1	Top	–	0.51	0.73	[213]
2*c*-DFT	1	Top	–	0.47	0.72	[214–216]
SO DFT	3	Top, bridge	–	0.47	0.77	[214–216]
2*c*-DFT	26	Bridge	Au(100)	0.33	0.55	[216]
2*c*-DFT	37	Hollow-2	Au(111)	–	0.49	[217]
4*c*-DFT	95	Top	Au(111)	0.30	0.47	[213]
4*c*-DFT	94	Bridge	Au(111)	0.42	**0.71**	[213]
4*c*-DFT	107	Hollow-2	Au(111)	**0.46**	0.59	[213]
$-\Delta H_{ads}$ (exp.)	∞	Unknown	Unknown	$0.54^{+0.2}_{-0.04}$	$0.35^{+0.6}_{-0.1}$ ≥ Cn	[202, 222] [223]

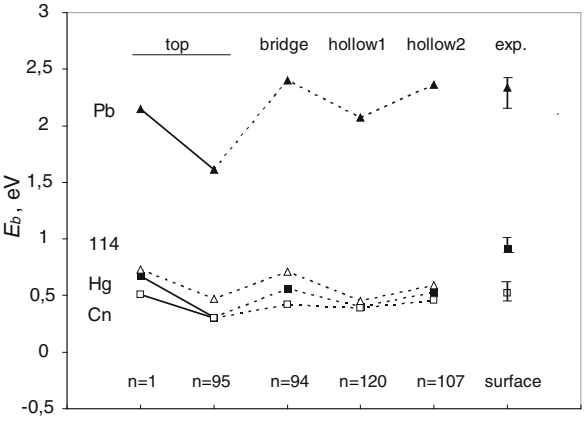

Fig. 42 The 4*c*-DFT calculated binding energies of Pb, Hg, Cn, and Fl with gold clusters in comparison with experimental $-\Delta H_{ads}$ of Pb, Hg and Cn on gold [203, 208, 209, 242]. Reprinted with permission from V. Pershina, J. Anton, T. Jacob, J. Chem. Phys. **131**, 084713 (2009). Copyright 2009 American Institute of Physics

involves formation of a metal bond, which is behavior typical of group-12 elements" [202, 203]. Thus, according to the conclusions of [222], Fl should be chemically more inert than Cn. The subsequent experiment by Yakushev et al. on the adsorption of Fl, conducted at a lower background of interfering products, registered two events of this element adsorbed on gold at room temperature [223]. Such a relatively high T_{ads} is indicative of the chemisorption process and formation of a metal–metal bond. The preliminary estimate of ΔH_{ads} supports the theoretical conclusion that Fl should be at least as reactive as Cn. Further experiments should shed more light on this interesting case.

A summary of the chemical properties of group-14 elements considered above is given in Fig. 43. For elements of this group, a decrease in all types of interactions is observed with increasing Z, so that Fl is the most weakly, but *chemically* bound element in all types of the compounds.

Finally, it is worth comparing properties of Cn and Fl, as both of them were expected to be very inert. Thus, on inert surfaces, Cn should about 6 kJ/mol more strongly adsorb by van der Waals forces than Fl, since $R_{vdW}(Cn) < R_{vdW}(Fl)$. The M–M chemical bond in Fl_2 should be somewhat stronger than that in Cn_2, of preferentially van der Waals character, according to the DFT calculations. (However, *ab initio* DF correlated calculations for both systems would give a more grounded basis for such a comparison). In intermetallic compounds, Fl should be more strongly bound than Cn by chemical forces, since the $7p_{1/2}$(Fl) AO is more readily available for bonding than the 7s(Cn) AO, and the $7p_{3/2}$ AO takes part in the bond formation as well. Also, it should adsorb more strongly than Cn on transition metal surfaces, both by chemical forces. For the solid state of Cn and Fl, a straightforward comparison of cohesive energies obtained by the different DFT calculations [206, 236] is, however, problematic.

In groups 15 through 17, approximately equal D_e(MAu) of the 6p and 7p counterparts suggest that the heaviest elements should adsorb on gold as almost strongly as their lighter homologs, while element 118 should adsorb even more strongly than Rn [237].

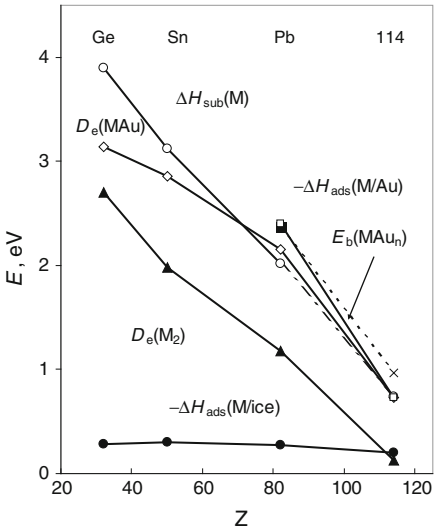

Fig. 43 Calculated dissociation energies D_e of M_2 (filled *triangles* [225]) and MAu (*open rhomboids* [237]); calculated binding energies E_b(M-Au$_n$) (open *squares* [213]); ΔH_{sub}, experimental for Ge, Sn, and Pb, [142] and extrapolated for Fl (*open circles*); experimental $-\Delta H_{ads}$(Pb) on gold (*filled square*) [242]; an estimated $-\Delta H_{ads}$(Fl) (a *cross*) [226]; and calculated $-\Delta H_{ads}$(M) on ice (*filled circles*) [127]. Reprinted with permission from V. Pershina, Radiochim. Acta, **99**, 459 (2011). Copyright 2011 Oldenbourg Wissenschaftsverlag GmbH

At the end of this section, it is again worth discussing validity of the correlation between ΔH_{ads} on some metals and ΔH_{sub} of macroamounts of the adsorbent. As one can see, in groups 13 and 14 there is some, although nonlinear, correlation between these quantities, as that between D_e(MAu) and D_e(M_2) (see, e.g., Fig. 40 for group-14 elements). In groups 15 through 17, no correlation between ΔH_{sub}(M) and $-\Delta H_{ads}$(M) on gold is, however, expected, since M–M and M-Au bonding changes in a different way with Z (see, e.g., Fig. 41 for group-15 elements). There is also no correlation between these quantities in the 6th and 7th periods (see Fig. 10 of [237]). Thus, the case of the 7p elements with strong relativistic effects on their electron shells shows that ΔH_{sub}(M) obtained via a correlation with $-\Delta H_{ads}$(M) can give erroneous results. Also, linear extrapolations of properties such as D_e(MAu) or $-\Delta H_{ads}$(M) from the lighter homologs in the groups should not be used.

6.5.4 Other Compounds of the 7p Elements

Hydrides. DHF, DFC, PP, RECP and 2*c*- and 4*c*-DFT calculations were performed for MH (M = 113–118) [139, 198, 228–230, 243–250] and $113H_3$ [251] and their lighter homologs in the chemical groups. An aim of these studies was the investigation of the influence of relativistic effects on molecular spectroscopic properties. Most representative results are shown in Table 18 and Fig. 44.

Table 18 Bond lengths, R_e (in Å), dissociation energies, D_e (in eV), and SO effects, Δ(SO), on them in MH (M = 113–117) from the RECP calculations [246–248]

Molecule	R_e	ΔR_e(SO)	D_e	ΔD_e(SO)
TlH	1.927	−0.021	1.98	−0.47
113H	1.759	−0.206	1.46	−0.93
PbH	1.884	0.001	1.61	−0.71
FlH	1.972	0.068	0.43	−2.18
BiH	1.836	0.019	2.24	0.08
115H	2.084	0.206	1.82	−0.23
PoH	1.784	0.031	2.27	−0.29
LvH	1.988	0.171	1.81	−0.63
AtH	1.742	0.032	2.31	−0.68
117H	1.949	0.171	1.79	−1.04
RnH	4.387	−0.025	1.84 meV	0.05 meV
118H	3.857	−0.407	5.50 meV	1.94 meV

According to these calculations, in 113H, the 6d and 7s AOs of element 113 participate little in bonding and all the effects are defined by the $7p_{1/2}$ shell. A large relativistic contraction of the $7p_{1/2}$ AO results in a large contraction of the 113-H bond. The SO bond contraction, ΔR_e(SO), is about −0.2 Å. Such a bond contraction is not found in the other MH (M = elements 114–118) (Fig. 44): For FlH through 118H, both the relativistically contracted $7p_{1/2}$ and expanded $7p_{3/2}$ AOs take part in the bond formation, with the contribution of the $7p_{1/2}$ AO gradually decreasing along the 7p series, so that the bonds are longer than those of the homologous MH (M = Pb through Rn). The dissociation energies D_e(MH) (M = 113 through 117) are reduced by the large SO effects (Table 18), with the lowest one at FlH. They also decrease from the 6p to 7p element hydrides. $113H_3$ becomes less stable towards the decomposition into 113H and H_2 than the lighter homologs [251]. In 118H, the van der Waals bond is stabilized by about 2.0 meV by SO effects, with ΔR_e(SO) = −0.025 Å [247]. Trends in the stability of the hydrides were predicted as follows: RnH < < HgH < PbH and 118H < < FlH < CnH.

The RECP CCSD(T) calculations for PbH^+ and FlH^+ have also given a 50% weaker and shorter bond in the latter due to the contraction of the $7p_{1/2}$ AO [139]. The trend for single-charge ions of group 18 is $D_e(RnH^+) > D_e(118H^+)$ and $R_e(RnH^+) < R_e(118H^+)$.

CAS-SCF/SOCI RECP calculations for FlH_2 demonstrated breakdown of the conventional singlet (X^1A_1) and triplet ($^3B_1$) states due to the large relativistic, including SO, effects [252]. The SO effects are shown to destabilize FlH_2 by almost 2.6 eV.

In LvH_2, the SO interaction was found to lengthen the Lv-H bond and lead to a significant H-Lv-H bond angle increase in comparison with PoH_2 according to the RECP calculations [253]. It was concluded that there is a rehybridization of the valence 7p AO with a "supervalent" 8s AO of Lv.

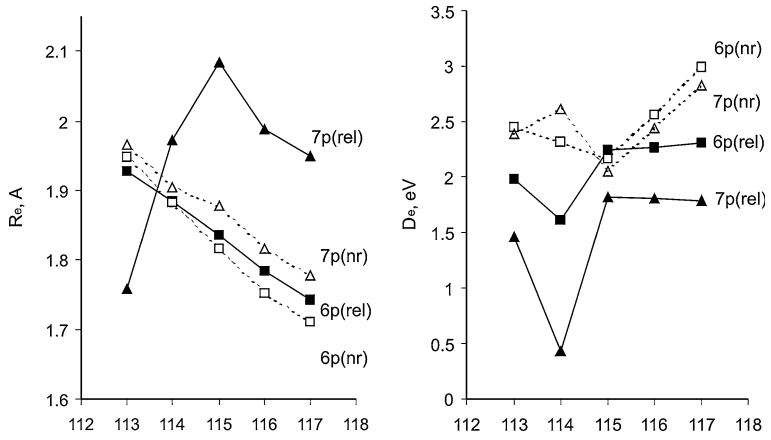

Fig. 44 Bond lengths, R_e, and dissociation energies, D_e, for the 6p- (Tl through At) and 7p-elements (113 through 117) hydrides, MH [228, 246–249]. From [14]

Oxides, hydroxides, halides and halogeno-complexes. Element 113. Results of the 4*c*-DFT calculations have shown Tl and element 113 to form a stable MOH molecule with D_e of 3.68 eV for Tl and 2.42 eV for element 113 [240]. Thus, in the gas-phase chromatography experiments, 113OH should be formed in a pure oxygen flow by analogy with TlOH [224]. $-\Delta H_{ads}$ of 113OH on gold is expected to be lower than $-\Delta H_{ads}$ of the element 113 atom.

PP, DCB, RECP and 4*c*-DFT calculations were performed for MF (M stands for all group 13 metals) [198, 243, 244]. The results show increasing R_e and μ_e from TlF to 113F, in contrast to the decreasing values from TlH to 113H. These different trends in R_e and μ_e for the MF compounds as compared to MH are explained by a more ionic nature of the MF molecules.

A theoretically interesting case is the (113)(117) molecule. The DF calculations have shown that in this molecule both the low-lying $7p_{1/2,1/2}$(113) AO and the destabilized $7p_{3/2,1/2}$(117) AO contribute to electron transfer to the group 13 atom [254]. Thus, rather than the single electron of the group 13 atom completing the valence p shell of the group 17 atom, the electron flow is more the other way around: the high-lying $7p_{3/2,1/2}$ shell donates into the low-lying $7p_{1/2,1/2}$ shell of the group 13 atom. This results in a reversal of the dipole direction and a change of the sign of μ_e.

As in Cn, the relativistic destabilization of the 6d AOs is expected to influence properties of high-coordination compounds of element 113. This was confirmed by the PP and RECP calculations for $113X_3$ (X = H, F, Cl, Br, and I) [74, 244]. As a consequence of the involvement of the 6d AOs, a T-shaped rather than trigonal planar geometric configuration was predicted for these molecules showing that the valence shell electron pair repulsion (VSEPR) theory is not applicable to the heaviest elements. Relativistic effects on bond angles were assumed to be small. However, if Jahn–Teller distortions are involved, relativistic effects may significantly change bond angles, as was shown for AtF_3 [255].

A stable high-coordination compound of element 113, $113F_6^-$, with the metal in the 5+ oxidation state is also foreseen in [244]. $113F_5$ will probably be unstable since the energy of the decomposition reaction $113F_5 \rightarrow 113F_3 + F_2$ is less than −100 kJ/mol. The calculated energies of the reaction $MX_3 \rightarrow MX + X_2$ (M = B through element 113) suggest a decrease in the stability of the 3+ oxidation state in this group.

Element 114 (flerovium, Fl). Electronic structures of FlX (X = F, Cl, Br, I, O) and FlO_2 were calculated using 2*c*-RECP CCSD(T), 2*c*-DFT SO ZORA and 4*c*-BDF methods [228, 229]. Better agreement with experiment for the known compounds of Pb was shown by the RECP CCSD(T) results. Trends in R_e and D_e for the halides and oxides from Pb to Fl were found to be similar to those for the hydrides. In contrast to PbO_2 (D_e = 5.60 eV), FlO_2 (D_e = 1.64 eV) was predicted to be thermodynamically unstable with respect to the decomposition into the metal atom and O_2. According to results of these calculations Fl should not react with O_2 at the experimental conditions, as was theoretically shown in [127].

The *ab initio* DF and PP calculations [256] for the decomposition reactions $MX_4 \rightarrow MX_2 + X_2$ and $MX_2 \rightarrow M + X_2$ (M = Si, Ge, Sn, Pb, and Fl; X = H, F, and Cl) also predicted a decrease in the stability of the 4+ oxidation state in group 14. The instability was shown to be a relativistic effect (see Fig. 45 for MH_4, as an example). The neutral state was found to be more stable for Fl than for Pb. As a consequence, Fl is expected to be less reactive than Pb, but about as reactive as Hg. This is in agreement with the predicted adsorption of Fl on gold that should be much weaker than that of Pb and slightly weaker than that of Hg [213] (Table 17 and Fig. 42). The possibility of the existence of FlF_6^{2-} was also suggested in [256].

Elements 116–117. Estimates of formation enthalpies of MX_2 and MX_4 (X = F, Cl, Br, I, SO_4^{2-}, CO_3^{2-}, NO_3^-, and PO_4^{3-}) for Po and Lv made on the basis of MCDF atomic calculations confirmed the instability of the 4+ state of Lv [257]. The chemistry of Lv is expected to be mainly cationic: an ease of formation of the divalent compounds should approach that of Be or Mn, and tetravalent compounds, e.g., LvF_4, should be formed with the most electronegative atoms.

Influence of SO effects on molecular structure of MX_2 (X = F, Cl, Br, I, At, and element 117) of Lv and its lighter homologs was studied with the use of the quasirelativistic 2*c*-HF and DFT ECP methods [258]. The results have shown that

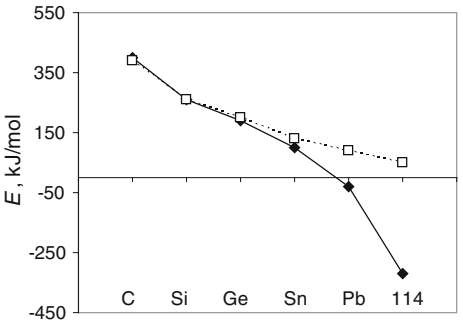

Fig. 45 Relativistic DFC (*solid line*) and nonrelativistic HF (*dashed line*) calculated energies of the decomposition reaction $MH_4 \rightarrow MH_2 + H_2$ (M = C, Si, Ge, Sn, Pb, and Fl) [256]. From [13]

while the molecules are bent at a scalar relativistic level, SO coupling is so strong that only $7p_{3/2}$ AOs of Lv are involved in bonding, which favors linear molecular geometries for MX_2 with heavy terminal halogen atoms.

Electronic structures of IF, AtF and 117F were considered at the DC and RECP levels of theory [74]. D_e(117F) was shown to be the largest among the group-17 fluorides. It was found that D_e(117F) is 0.1 eV increased by SO effects in contrast to the other group 17 fluorides. The SO effects are opposite for all the three spectroscopic constants of 113F and 117F. For $117F_3$, the RECP calculations have shown that the D_{3h} geometry is not the proper one, in difference from AtF_3, thus again indicating that the VSEPR theory is not applicable to the heaviest elements [74, 259]. The SO effect was shown to stabilize this molecule by 1.2 eV, which is unusually large for atoms with open p-shells. A strong ionic character of the bond may be responsible for this huge stabilization.

117Cl is predicted to be bound by a single π bond and have a relativistically (SO) increased bond length [260].

Element 118. The chemistry of element 118 should be interesting due to the very large SO splitting, of 11.8 eV, of the 7p AO [21]. The relativistic destabilization of the four $7p_{3/2}$ electrons suggests that element 118 should be relatively reactive and the most electropositive in the group (see Sect. 5). It was predicted to form a 118-Cl bond [261].

The destabilization of the $np_{3/2}$ AOs should also result in the increasing stability of the 2+ and 4+ oxidation states in group 18. The RECP calculations for the decomposition reactions $MF_2 \rightarrow M + F_2$ and $MF_4 \rightarrow MF_2 + F_2$, where M = Xe, Rn and element 118, confirmed the increasing stability of the fluorides in the group, as a result of the increasing polarizability of the central atom [74, 262]. The SO effects were shown to stabilize $118F_4$ by a significant amount of about 2 eV, though they enlarge R_e by 0.05 Å. Thus, the trends in increasing R_e and D_e in this group are continued with element 118. Also, the following trends in the stability of the fluorides were established: $RnF_2 < HgF_2 < PbF_2$, while $CnF_2 < FlF_2 < 118F_2$.

The influence of the SO interaction on the geometry of group-18 MF_4 was investigated by the RECP SOCI/CCSD calculations [249, 262, 263]. It was shown that a D_{4h} geometrical configuration for XeF_4 (calculated in agreement with experiment) and for RnF_4 (calculated) becomes slightly unstable for $118F_4$. A T_d configuration becomes more stable than the D_{4h} one in $118F_4$ by about 0.2 eV. The reason for this unusual geometry is the availability of only the stereochemically active four $7p_{3/2}$ electrons for bonding. This is another example of the inapplicability of the VSEPR theory for the heaviest elements [263]. It was also predicted that the fluorides of element 118 should most probably be ionic rather than covalent, as in the case of Xe. This prediction might be useful for future gas-phase chromatography experiments.

6.6 Elements with Z > 118

6.6.1 Elements 119 and 120

Chemical properties of elements 119 and 120 predicted on the basis of atomic DF calculations are described in [1, 2]. They are shown to be determined by the valence 8s electrons and are expected to follow those of alkali- and alkali-earth elements in chemical groups 1 and 2, respectively. An increasing relativistic stabilization of the ns AOs of the elements of these groups with increasing Z results in a reversal of trends in such properties as IP, EA, α, and AR, as described in Sect. 5.2. Recently, interest in the chemistry of these elements has been renewed, since these are the next elements that are awaiting discovery after Z = 118. Volatility of atoms of elements 119 and 120 might be studied in the long term using some advanced chromatography (e.g., vacuum) techniques that can cope with extremely short (presumably sub-millisecond) half-lives of their isotopes. In recent theoretical works [143, 144], properties that are of interest for such chromatography studies, i.e., ΔH_{sub} and ΔH_{ads} of elements 119 and 120 on noble metals, were predicted on the basis of 4*c*-DFT calculations of intermetallic compounds.

Homonuclear dimers and sublimation of metals. Calculated binding energies and other spectroscopic properties of the group-1 and 2 M_2 are given in Table 19 [143, 144]. (The calculations are in very good agreement with the measured properties where available. A comparison with other calculations for the lighter homologs of elements 119 and 120 is given in [143, 144]). Plots, demonstrating trends in these properties are shown in Figs. 46, 47.

One can see that in these groups, there is a reversal of trends in $D_e(M_2)$ at Cs and Ba, respectively, though in an opposite way. The reason for the different behavior is a different type of the M–M bonding in these groups: a covalent one in group 1, while a van der Waals one in group 2, even though both are defined by the behavior of the ns AOs.

Table 19 Spectroscopic properties of M_2 (M = K, Rb, Cs, Fr, and element 119) and (M = Ca, Sr, Ba, Ra, and element 120): equilibrium bond lengths, R_e (in Å), dissociation energies, D_e (in eV) and vibrational frequencies, ω_e (in cm^{-1}) [143, 144]

Mol.	Group 1			Mol.	Group 2		
	R_e	D_e	ω_e		R_e	D_e	ω_e
K_2	3.942	0.52	91	Ca_2	4.236	0.14	66
	3.924	*0.52*	*92*		*4.277*	*0.14*	*64*
Rb_2	4.224	0.48	58	Sr_2	4.493	0.13	44
	4.180	*0.48*	*58*		*4.498*	*0.13*	*40*
Cs_2	4.673	0.43	41	Ba_2	4.831	0.23	43
	4.646	*0.45*	*42*		–	–	–
Fr_2	4.610	0.44	33	Ra_2	5.19	0.11	25
$(119)_2$	4.265	0.55	41	$(120)_2$	5.65	0.02	9

[a] Italics are experimental values (see references in [143, 144])

Thus, $(119)_2$ having a σ_g^2 ground state should be most strongly bound by covalent forces and have a shorter bond (about that of Rb_2) caused by the contraction of the 8s AO. On the contrary, $(120)_2$ with a $\sigma_g^2\sigma*_u^2$ ground state should be most weakly, among the homologs, bound by van der Waals forces (the number of bonding and antibonding electrons is the same), and the bond should be the longest. $R_e(M_2)$ of group-1 elements show a reversal of the increasing trend at Cs due to the relativistic contraction of the ns AO. $R_e(M_2)$ of group-2 elements, however, reveal a steady increase in the group which is explained by the participation of the $np_{3/2}$ and (n–1)d AOs in bonding in addition to the ns AOs.

As one can see from Figs. 46, 47, the M–M-bonding correlates with ΔH_{sub} of metals in these groups with the same reversal of trends at Cs and Ba, respectively. Using these correlations and the calculated D_e of $(119)_2$ and $(120)_2$, ΔH_{sub} of element 119 and 120 of 94 kJ/mol and 150 kJ/mol, respectively, were predicted [143, 144]. According to these data, element 119 metal should be as strongly bound as K, while element 120 metal should be most weakly bound in group 2, though stronger than the 119 one.

Intermetallic dimers and adsorption on noble metals. To predict adsorption of elements 119 and 120 on noble metals, e.g., on gold used in chromatography experiments, electronic structures of MAu, where M are group-1 and 2 metals, were calculated using the 4*c*-DFT method [143, 144]. The obtained binding energies and other spectroscopic properties are given in Table 20. (There are no practically experimental data for R_e of the lighter species, expect of that for CaAu. The calculated dissociation energies are somewhat larger, but perfectly follow the experimental trend in group 1. A comparison with other calculations for the lighter

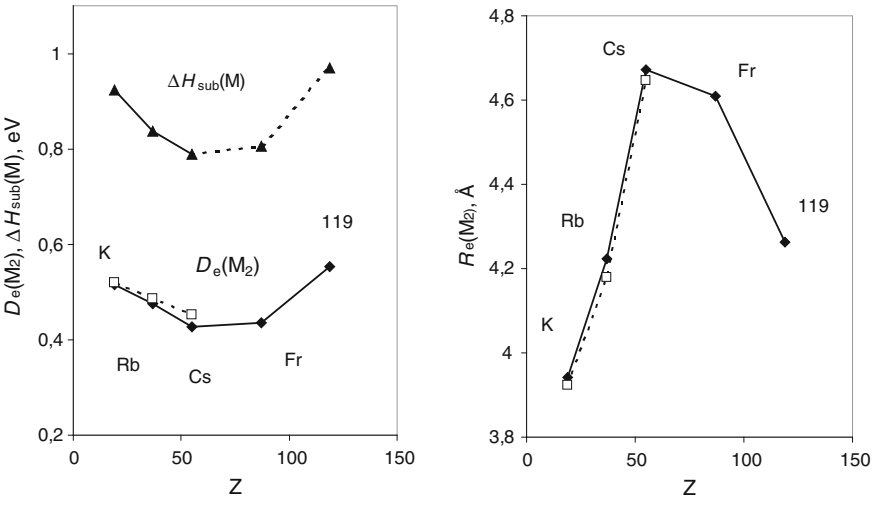

Fig. 46 Dissociation energies, D_e and equilibrium bond lengths, R_e of group-1 M_2 (filled rhomboids are 4*c*-DFT calculations [144], open *squares*—experiment), as well as ΔH_{sub} (filled *triangles* are experiment [142], open ones—estimates). From [144]

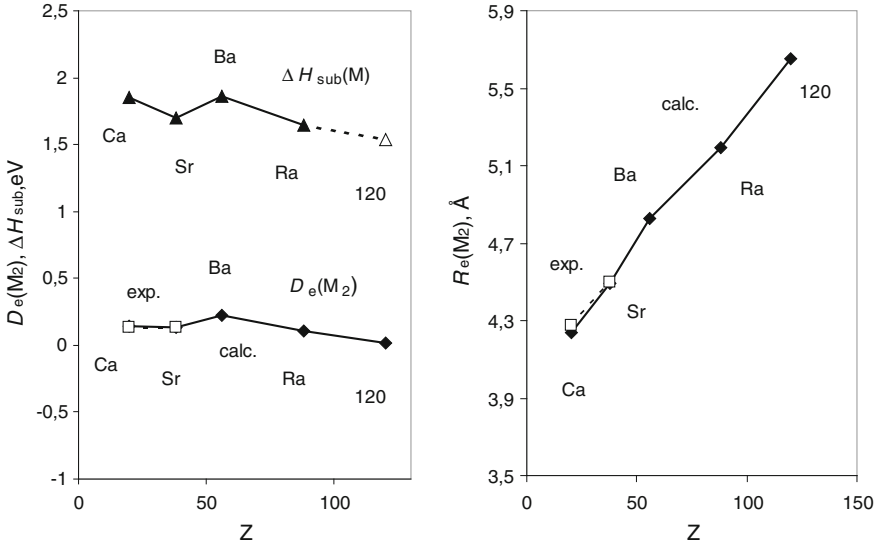

Fig. 47 Dissociation energies, D_e and equilibrium bond lengths, R_e of group-2 M_2 (filled rhomboids are 4*c*-DFT calculations [143], open *squares*—experiment), as well as ΔH_{sub} (filled *triangles* are experiment [142], open ones—estimates). Reprinted with permission from V. Pershina, A. Borschevsky, J. Anton, J. Chem. Phys. **136**, 134317 (2012). Copyright 2012 American Institute of Physics

homologs of elements 119 and 120 are given in [143, 144]). Trends in these properties are shown in Figs. 48, 49.

According to the data of Table 20, elements 119 and 120 should form stable compounds with gold. The D_e(MAu) values show a reversal of the increasing trend at Cs and Ba in group 1 and 2, respectively, so that both 119Au and 120Au should be the weakest among the considered homologs in these group. The trend is defined by the behavior of the ns AOs, whose relativistic stabilization in the groups starts to dominate over the orbital expansion beyond Cs and Ba, respectively. As a result of this stabilization, electronegativities of elements 119 and 120 approach that of Au. This diminishes the electron density transfer from M to Au, and therefore, the bond strength of these dimers. The R_e(MAu) values increase in both groups: since bonding is of preferentially ionic character, the trend is defined by the steadily expanding $(n–1)p_{3/2}$ AOs of the M^+ and M^{2+} ions with Z, respectively. Dipole moments of MAu have also a reversal of the trend in group 1 at Cs and an overall increasing trend in group 2 [143, 144].

The M-Au binding energies in the dimers correlate with the semi-empirical $-\Delta H_{ads}$(M) of K through Cs, and Ca through Ba on gold [238]. Using these correlations in groups 1 and 2, $-\Delta H_{ads}$ of Fr and element 119 on gold of 136 kJ/mol and 106 kJ/mol, respectively, and of Ra and element 120 of 237 kJ/mol and 172 kJ/mol, respectively, were determined. Using correlations with $-\Delta H_{ads}$(M) on other noble metals, ΔH_{ads} of these elements on Ag and Pt were also

Table 20 Spectroscopic properties of MAu (M = K, Rb, Cs, Fr, and element 119) and (M = Ca, Sr, Ba, Ra, and element 120): Equilibrium bond lengths, R_e (in Å), dissociation energies, D_e (in eV), and vibrational frequencies, ω_e (in cm^{-1}) [143, 144]

Mol.	Group 1			Mol.	Group 2		
	R_e	D_e	ω_e		R_e	D_e	ω_e
KAu	2.856	2.76	173	CaAu	2.627	2.71	221
	–	*2.75*	–		*2.67*	*2.55*	*221*
RbAu	2.967	2.75	122	SrAu	2.808	2.63	159
	–	*2.48*	–		–	–	–
CsAu	3.050	2.91	100	BaAu	2.869	3.01	145
	–	*2.53*	–		–	–	–
FrAu	3.097	2.75	89	RaAu	2.995	2.56	105
119Au	3.074	2.44	92	120Au	3.050	1.90	97

[a] Italics are experimental values (see references in [143, 144]

predicted (Figs. 48, 49). The very moderate $-\Delta H_{ads}$ values of elements 119 and 120, the lowest in groups 1 and 2, especially on Ag (63 kJ/mol and 50 kJ/mol, respectively), are indicative of the possibility of adsorption chromatography measurements for these elements.

The ΔH_{sub} and $-\Delta H_{ads}$ values show that there is no proportionality between these quantities in group 1, as they change in the opposite way with Z. In group 2, there is, however, a correlation between ΔH_{sub} and $-\Delta H_{ads}$.

Thermodynamic properties of metals of elements 113 through 120 were predicted in [264] using atomic calculations and mathematical models.

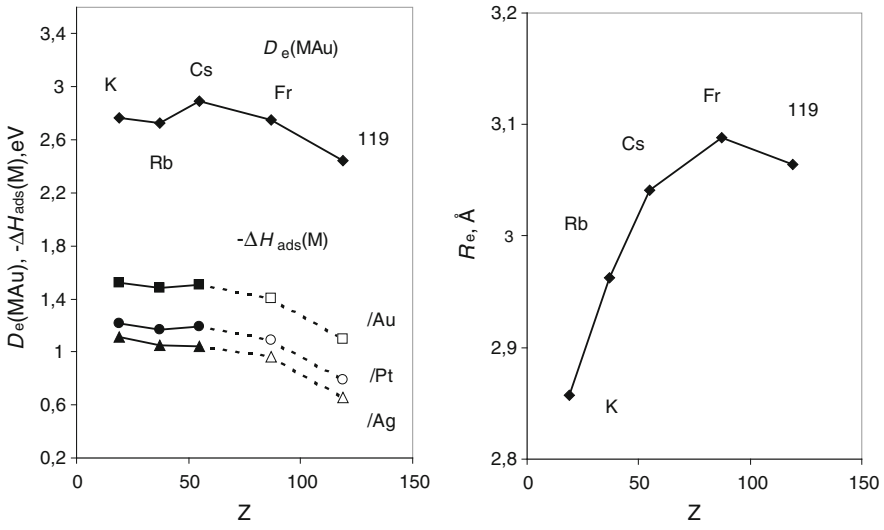

Fig. 48 4*c*-DFT dissociation energies, D_e, and equilibrium bond lengths, R_e, of group-1 MAu, as well as adsorption enthalpies $-\Delta H_{ads}$ (filled symbols are semi-empirical calculations [238], while open ones—obtained via correlations with D_e(MAu) on Au, Pt, and Ag). From [144]

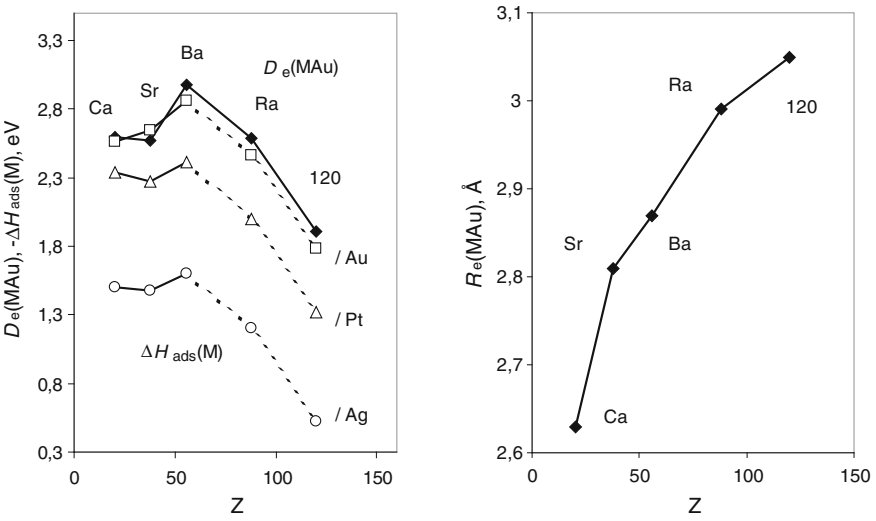

Fig. 49 4*c*-DFT dissociation energies, D_e, and equilibrium bond lengths, R_e, of group-2 MAu, as well as adsorption enthalpies $-\Delta H_{ads}$ (filled symbols are semi-empirical calculations [238], while open ones—obtained via correlations with D_e(MAu) on Au, Pt, and Ag). From [143]

Other compounds. Hydrides and fluorides of elements 119 and 120 were considered within the PP and *ab initio* DF approximations [245, 265, 266]. It was shown that bond distances decrease from the 7th to the 8th period for group-1 and 2 elements due to the relativistic ns AO contraction. The 119F was found to be less ionic than lighter alkaline fluoride homologs in contrast to the expectations based on the periodic trends.

6.6.2 Elements with Z > 120

The chemistry of elements heavier than Z = 120 should be defined by many open shells and their mixing [1, 2]. Due to the very strong relativistic effects, it will be much more different to anything known before. However, without relativistic effects, it would have also been very different due to the very large orbital effects.

Very few molecular calculations exist in this superheavy domain. Properties of elements heavier than 120 predicted on the basis of atomic calculations are discussed in [1–5], as well as at the beginning on this chapter. More recent considerations of their chemistry can be found in [267, 268].

A list of possible molecules of elements in the range Z = 121–164 was suggested in [268], though their verification should be left to future theoretical studies. Interesting examples are those where the elements are in unusual valence states or coordination, like, e.g., $144F_8$ (an analog of PuF_8), or $148O_6$ (an analog of UO_6). Quasi-relativistic multiple-scattering calculations on $125F_6$ have found that

Table 21 Trends in volatility of the group-4 through 8 compounds and the group-12 and 14 atoms

Group	Species	Theoretically predicted	Ref.	Experimentally observed	Ref.
4	MCl_4, MBr_4	Hf < Rf	[9]	Hf < Rf	[272]
5	ML_5 (L = Cl,Br)	Nb < Ta < Db	[162, 164]	(DbO_3Br)	[273]
		$DbCl_5 > DbOCl_3$	[163]	$DbCl_5 > DbOCl_3$	[273]
	$MBr_5 \rightarrow MBr_6^-$	Nb > Ta > Db	[164]	Nb > Ta > Db	[187–189]
				Db > Nb > Ta	[190]
6	MO_2Cl_2	Mo > W > Sg	[167]	Mo > W > Sg	[185, 186]
7	MO_3Cl	Tc > Re > Bh	[168]	Tc > Re > Bh	[184]
8	MO_4	Ru < Os > Hs	[170]	Os > Hs	[182]
12	M	Hg < Cn	[210–213]	Hg < Cn	[202, 203]
14	M	Pb << Fl < Cn	[213, 226]	Fl > Cn	[222]
			[216, 217]	Fl ≤ Cn	[223]

bonding is defined by the $5g^1$ electron, the situation being analogous to NpF_6 with the $5f^1$ electron [269]. There are noncorrelated DF calculations for fluorides of element 126 [270, 271].

Accurate predictions of properties of specific compounds will be quite a challenging task in this area. This may need inclusion of the QED effects to reach the required accuracy.

6.7 Summary of Predictions of Volatility of the Heaviest Elements and their Compounds

Predicted trends in volatility of the heaviest elements and their compounds compared to the experimental observations are summarized in Table 21. One can see that almost all the predictions for group-4 through 8, as well as for group 12 are confirmed by the experiments. In addition, the calculated absolute values of ΔH_{ads} are in very good agreement with the experimental ones, as discussed above. The only open question is volatility of group 4 and 5 pure halides, which might need further experimental or/and theoretical considerations. Predictions for Fl are also awaiting further experimental verifications.

7 Aqueous Chemistry of the Transactinides

7.1 Redox Potentials

Knowledge of the relative stability of oxidation states of elements, i.e., redox potentials, $E°$, is very important for a chemical application. Trends in the stability of various oxidation states of the heaviest elements were predicted earlier on the

basis of atomic DF and DS calculations in combination with models based on a Born-Haber cycle (see [1, 2]). The results, however, depend on the model used and often disagree. Later, oxidation states of Rf, Db, and Sg were estimated [145, 165, 274, 275] using known E° of the lighter homologs [276] and results of atomic MCDF calculations of the IPs [25–28].

For an oxidation–reduction reaction

$$M^{z+n} + ne \leftrightarrow M^{z+}, \tag{20}$$

the redox potential is defined as

$$E^\circ = -\Delta G^\circ / nF, \tag{21}$$

where ΔG° is the free energy of reaction (20) and F is the Faraday number.

E° could then be estimated using a correlation between E° and IP, since

$$\Delta G^\circ = -(\mathrm{IP} + \Delta G^\circ_{\mathrm{hydr}}), \tag{22}$$

where $\Delta G^\circ_{\mathrm{hydr}}$ is a free energy of hydration, being a smooth function of atomic number, and can therefore easily be evaluated. Thus, using the MCDF calculated IPs and experimentally known E° [276, 277] unknown E° of the transactinides in acidic solutions were determined using a linear correlation between these quantities in the chemical groups (see [145, 165, 274, 275] for the values, also a comparison with the homologs). One of those correlations for group-6 species indicating a decrease in the stability of the 4+ state with respect to the 6+ state in group 6, as a decrease in $E^\circ(MO_3/MO_2)$, is shown in Fig. 50, as an example. The E° of the transactinides are given in Table 22.

The obtained values of the redox potentials show the following trends: The stability of the maximum oxidation state increases within groups 4 through 6, while that of lower oxidation states decreases. Along the 7th period, the stability of the maximum oxidation state decreases, because $E^\circ\left(\mathrm{Lr}^{3+}/\mathrm{Lr}^{2+}\right) < E^\circ\left(\mathrm{Rf}^{\mathrm{IV}}/\mathrm{Rf}^{3+}\right) < E^\circ\left(\mathrm{Db}^{\mathrm{V}}/\mathrm{Db}^{\mathrm{IV}}\right) < E^\circ\left(\mathrm{Sg}^{\mathrm{VI}}/\mathrm{Sg}^{\mathrm{V}}\right)$. A similar trend is observed for

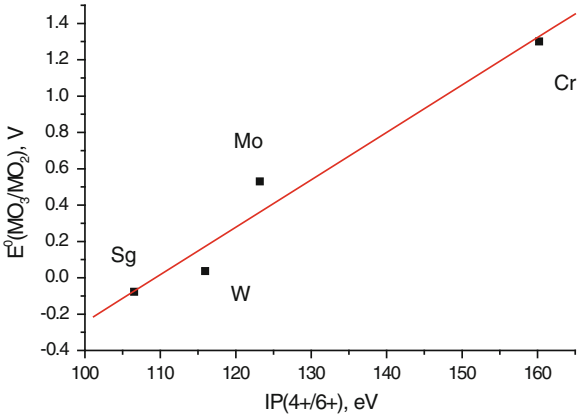

Fig. 50 Correlation between IP(4+/6+) and standard potentials $E^\circ(MO_3/MO_2)$, where M = Cr, Mo, W, and Sg. Reprinted with permission from V. Pershina, E. Johnson, B. Fricke, J. Phys. Chem. A **103**, 8463 (1999). Copyright 1999 American Chemical Society

Table 22 Redox potentials of Lr, Rf, Db, and Sg in aqueous acidic solutions

Potential	Lr[a]	Rf	Db[f]	Sg[g]
$E°(M^{VI}/M^{V})$	–	–	–	−0.046 (MO_3/M_2O_5) −0.05 (M^{VI}, H^+/M)
$E°(M^{V}/M^{IV})$	–	–	−1.0 (M_2O_5/MO_2) −1.13 (MO_2^+/MO^{2+})	−0.11 (M_2O_5/MO_2) −0.35 (M^{V}, H^+/M^{IV},H^+)
$E°(M^{IV}/M^{3+})$	8.1	−1.5 (M^{4+}/M^{3+})[c]	−1.38 (MO_2/M^{3+})	−1.34 (MO_2/M^{3+}) −0.98 ($M(OH)_2^{2+}/M^{3+}$)
$E°(M^{3+}/M^{2+})$	−2.6	−1.7 (M^{3+}/M^{2+})[c]	−1.20	−0.11
$E°(M^{3+}/M)$	−1.96[b]	−1.97 (M^{3+}/M)[d]	−0.56	0.27
$E°(M^{IV}/M)$	–	−1.85 (M^{4+}/M)[e] −1.95 (MO_2/M)[e]	−0.87 (MO_2/M)[d]	−0.134 (MO_2/M) −0.035 ($M(OH)_2^{2+}$/M)
$E°(M^{V}/M)$	–	–	−0.81 (M_2O_5/M)	−0.13 (M_2O_5/M)[d]
$E°(M^{VI}/M)$	–	–	–	−0.12 (MO_3/M) −0.09 (M^{VI}, H^+/M)

[a] [277]; [b] [276]; [c] [275]; [d] roughly estimated from the other $E°$; [e] [165]; [f] [274]; [g] [145]

$E°\left(M^{Zmax}/M\right)$, see Table 22. (The roman numbers denote the valence states in complex compounds). As was shown earlier, the increasing stability of the maximum oxidation state in groups 4, 5 and 6 is a relativistic effect. The estimates of redox potentials confirm that the 3+ and 4+ states for Db and Sg, respectively, will be unstable. Figure 50 shows this for Sg, as an example. One can see that decreasing IPs($M^{4+} \rightarrow M^{6+}$) result in decreasing $E°(M^{VI}/M^{IV})$, so that the 4+ state of Sg with respect to the 6+ state will be even less stable than the 4+ state of the lighter homologs. (See also Sect. 5.2 and "Liquid-Phase Chemistry of Superheavy Elements" for experiments).

7.2 Hydrolysis and Complex Formation

Complex formation of the heaviest elements is studied experimentally by liquid–liquid extractions, or ion exchange separations (see "Liquid-Phase Chemistry of Superheavy Elements"). For a simple complex ML_n, the cumulative complex formation constant

$$\beta_n = [ML_n][M]^{-1}[L]^{-n} \tag{23}$$

is a measure of its stability. For step-wise processes, consecutive constants K_i are used. If various ML_n^{z-n} complexes exist in the aqueous phase, but only one $(ML_i)^{p-}$ complex in the organic phase, the distribution coefficient, K_d, for the anion exchange separations is given by the following equation [278]

$$K_d = \frac{K_{\mathrm{DM}}[RB^+L^-]^p_{\mathrm{org}}\beta_i[L^-]^{i-p}}{\sum_0^N \beta_n[L^-]^n}, \tag{24}$$

where K_{DM} is the association constant with the organic cation. Thus, a sequence in the K_{d} values for a series of species under consideration, e.g., for elements of one group, reflects a sequence in the stability of their complexes.

Complex formation is known to increase in the transition element groups. In aqueous solutions it, however, competes with hydrolysis. This may change trends in the stabilities of complexes and, finally, in their extraction into an organic phase, or sorption by a resin.

One should distinguish between hydrolysis of cations and hydrolysis of complexes [279]. The former is described as a process of a successive loss of protons

$$\mathrm{M(H_2O)}_n^{z+} \leftrightarrow \mathrm{MOH(H_2O)}_{n-1}^{(z-1)+} + \mathrm{H^+}. \tag{25}$$

In acidic solutions, hydrolysis involves either the cation, anion, or both, and is competing with the complex formation described by the following equilibrium

$$x\mathrm{M(H_2O)}_{w^\circ}^{z+} + y\mathrm{OH^-} + i\mathrm{L^-} \leftrightarrow \mathrm{M}_x\mathrm{O}_u\mathrm{(OH)}_{z-2u}\mathrm{(H_2O)}_w\mathrm{L}_i^{(xz-y-i)+} + (xw^\circ + u - w)\mathrm{H_2O}. \tag{26}$$

7.2.1 Theoretical Model for Prediction of Complex Formation

In order to predict a sequence in K_{d} (Eq. 24), one should predict a sequence in the formation constants of a series of species of interest. For a reaction like, e.g., (25) or (26),

$$\log K_i = -\Delta G^{\mathrm{r}}/2.3RT, \tag{27}$$

where ΔG^{r} is the free energy change of the complex formation reaction. To obtain it in a straightforward way, binding or total energies of species in the left and right parts of the reaction should be calculated. Such relativistic calculations, with full geometry optimization for the heaviest elements, are extremely computer time intensive. In addition, the obtained accuracy might be insufficient in predicting stabilities of similar species of homologs. Therefore, the following efficient model was suggested by us.

In a fashion analogous to that of Kassiakoff and Harker [280], the following expression for the free energy of formation of the $\mathrm{M}_x\mathrm{O}_u\mathrm{(OH)}_v\mathrm{(H_2O)}_w^{(xz-2u-v)+}$ species from the elements was adopted

$$-\Delta G^f(u,v,w)/2.3RT = \sum a_i + \sum a_{ij} + \log P - \log(u!v!w!2^w) + (2u+v+1)\log 55.5. \tag{28}$$

The first term on the right hand side of Eq. 28, $\sum a_i$, is the non-electrostatic contribution from M, O, OH, and H_2O, which is related to the overlap population, OP. For a reaction,

$$\Delta \sum a_i = \Delta E^{\mathrm{OP}} = k\Delta \mathrm{OP}, \tag{29}$$

where k is an empirical coefficient. The next term, $\sum a_{ij}$, is a sum of each pairwise electrostatic (Coulomb) interaction:

$$E^C = \sum a_{ij} = -B \sum_{ij} Q_i Q_j / d_{ij}, \tag{30}$$

where d_{ij} is the distance between moieties i and j; Q_i and Q_j are their effective charges and $B = 2.3RTe^2/\varepsilon$, where ε is a dielectric constant. For a reaction, ΔE^{C} is the difference in E^{C} for the species in the left and right parts of the reaction. P in Eq. 28 is the partition function representing the contribution of structural isomers if there are any. The last two terms are statistical: one is a correction for the indistinguishable configurations of the species, and the other is a conversion to the molar scale of concentration for the entropy. Σa_{ij} and Σa_i for each compound are then calculated directly via a Mulliken analysis implemented in most of the quantum chemical methods (e.g., 4*c*-DFT [87]); see Sect. 4.3.3. To predict $\log K_i$ or $\log \beta_i$ for transactinide complexes, coefficients k and B should then be defined by fitting $\log K_i$ to experimental values for the lighter homologs. Using this model, hydrolysis and complex formation constants were predicted for a large number of aqueous compounds of group-4 through 6 elements [281–289] in very good agreement with experiment; see "Liquid-Phase Chemistry of Superheavy Elements". Results of these calculations and comparison with experimental data reveal that a change in the electrostatic metal–ligand interaction energy (ΔE^{C}) of a complex formation reaction contributes predominantly in the change in ΔG^{f}, i.e., in ΔG^{r}. Thus, only by calculating ΔE^{C} can trends in the complex formation be reliably predicted.

7.2.2 Rf

As other group-4 elements, Rf undergoes hydrolysis and complex formation in acidic solutions. These processes for Zr, Hf, and Rf in HF and HCl solutions were studied theoretically using the model described in the previous section [285]. The following reactions were considered: the first hydrolysis step

$$\mathrm{M(H_2O)_8^{4+}} \leftrightarrow \mathrm{MOH(H_2O)_7^{3+}}, \tag{31}$$

the step-wise fluorination

$$\mathrm{M(H_2O)_8^{4+}} \leftrightarrow \mathrm{MF(H_2O)_7^{3+}} \ldots \leftrightarrow \ldots \mathrm{MF_3(H_2O)_5^{+}} \ldots \leftrightarrow \cdots \tag{32}$$

$$\mathrm{MF_4(H_2O)_2} \leftrightarrow \ldots \mathrm{MF_5(H_2O)^{-}} \leftrightarrow \mathrm{MF_6^{2-}}, \tag{33}$$

Table 23 Calculated Coulomb part, ΔE^{C} (in eV), of the free energy change of some typical hydrolysis and complex formation reactions, Eqs. (31–34), for Zr, Hf, and Rf. From [285]

Reactions	Zr	Hf	Rf
$M(H_2O)_8^{4+} \leftrightarrow MOH(H_2O)_7^{3+}$	−4.69	−4.61	−4.11
$M(H_2O)_8^{4+} \leftrightarrow MF(H_2O)_7^{3+}$	0.002	0.015	0.395
$M(H_2O)_8^{4+} \leftrightarrow MF_4(H_2O)_4$	15.86	15.84	16.52
$M(H_2O)_8^{4+} \leftrightarrow MF_6^{2-}$	50.76	50.91	51.10
$M(H_2O)_8^{4+} \leftrightarrow MCl_6^{2-}$	52.15	52.50	53.06
$M(H_2O)_8^{4+} \leftrightarrow MCl_4$	47.99	47.82	47.85

and the complete chlorination

$$M(H_2O)_8^{4+} + \ 6HCl \leftrightarrow MCl_6^{2-}. \tag{34}$$

Calculated ΔE^{C} for some of the reactions of Eqs. (31–34) are given in Table 23. The data of the first row there suggest the following trend in hydrolysis of the group-4 cations Zr > Hf > Rf. The first hydrolysis constant $\log K_{11}$(Rf) ≈ −4 was then determined in good agreement with the experimental value of −2.6 ± 0.7 [290]. The predicted trend is also in agreement with the experimental data for Zr and Hf giving $\log K_{11}$(Zr) = 0.3 and $\log K_{11}$(Hf) = −0.25 [279]. One should note here that a simple model of hydrolysis [279] based on the ratio of a cation charge to its size would give an opposite and, hence, a wrong trend from Zr to Hf, since IR(Zr^{4+}) > IR(Hf^{4+}) [148].

The following useful trends were deduced from the calculated ΔE^{C} (Table 23). For the cation exchange separations (CIX) performed at < 0.1 M HF (no hydrolysis), i.e., for extraction of the positively charged complexes, the K_d values will change in the following way in group-4: Zr ≤ Hf < Rf. This is caused by the decreasing trend in the formation of the positively charged complexes according to Eq. 32: Zr ≥ Hf > Rf. (In the case of formation of complexes with a lower positive charge from complexes with a higher positive charge, a sequence in the K_d values is opposite to a sequence in the complex formation. This is because complexes with a higher charge are better sorbed on the CIX resin than those with a lower charge). This trend was, indeed, observed in the experiments on the CIX separations of group-4 elements at low HF concentrations [291, 292]. For the formation of anionic complexes sorbed by anion exchange (AIX) resins, the trend becomes more complicated depending on pH, i.e., depending on whether the fluorination starts from hydrated or hydrolyzed species. Thus, for experiments conducted in 10^{-3}–10^{-1} M HF (where some hydrolyzed or partially fluorinated species are present), the trend for the formation of MF_6^{2-} (Eq. 33) should be reversed in group 4: Rf ≥ Zr > Hf. Such a trend was observed in the experiments on the AIX separations of group-4 elements from 0.02 M HF [293]. The weaker sorption of Rf from HF solutions of > 10^{-3} M (in 0.1 M HNO_3) on the AIX column was, however, found in [291]. This was explained (and also shown by

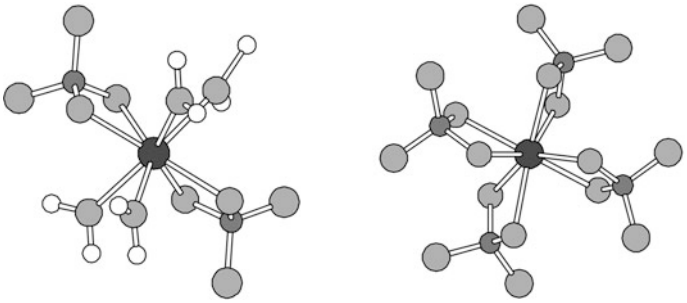

Fig. 51 $M(SO_4)_2(H_2O)_4$ and $M(SO_4)_4^{4-}$ complexes of Zr, Hf, and Rf. Reprinted with permission from V. Pershina, D. Polakova, J.P. Omtvedt, Radiochim. Acta **94**, 407 (2006). Copyright 2006 Oldenbourg Wissenscheftsverlag GmbH

additional experiments) by a strong competition between NO_3^- and Rf complexes for adsorption on the active resin sites. A similar result was obtained in [294], where the formation constant of RfF_6^{2-} was reported at least one order of magnitude smaller than those of ZrF_6^{2-} and HfF_6^{2-}.

For the AIX separations at 4–8 M HCl, where no hydrolysis should occur at such high acidities, the data of Table 23 suggest that the trend in the complex formation and K_d values should be continued with Rf: Zr > Hf > Rf. The AIX separations [294] of group-4 elements from aqueous 4–8 M HCl solutions have, however, shown the following sequence in K_d values: Rf > Zr > Hf. This experimental result cannot find its theoretical explanation.

The TBP extraction of group-4 elements from 8 M HCl showed the K_d of Rf in between those of Zr and Hf: Zr > Rf > Hf [295]. Such an inversion of the trend is consistent with the theoretical trend for the formation of the MCl_4 species, see Table 23. However, the following trend Zr > Hf ≈ Rf was observed in [296]. Some further calculations for the $MCl_4(TBP)_2$ complexes should be performed to study this case in more detail.

Complex formation of group-4 elements in H_2SO_4 solutions was studied theoretically in [288]. In this work, relative values of the free energy change of the $M(SO_4)_2(H_2O)_4$, $M(SO_4)_3(H_2O)_2^{2-}$ and $M(SO_4)_4^{4-}$ (M = Zr, Hf, and Rf) formation reactions from hydrated and partially hydrolyzed cations were calculated using the 4*c*-DFT method. (Figure 51 shows geometrical configurations of two of these complexes). The obtained ΔE^C and trends for one type of the complex formation reaction starting from $M(H_2O)_8^{4+}$ are given in Table 24, as an example.

Table 24 Coulomb part of the free energy change, ΔE^C (in eV), of the complex formation reactions [288]

Reaction	Zr	Hf	Rf	Trend
$M(H_2O)_8^{4+} \leftrightarrow M(SO_4)_2(H_2O)_4$	−35.72	−35.84	−33.60	Hf > Zr > > Rf
$M(H_2O)_8^{4+} \leftrightarrow M(SO_4)_3(H_2O)_2^{2-}$	−42.43	−42.43	−39.37	Zr = Hf > > Rf
$M(H_2O)_8^{4+} \leftrightarrow M(SO_4)_4^{4-}$	−45.14	−45.02	−41.38	Zr > Hf > > Rf
$M(H_2O)_8^{4+} \leftrightarrow RM(SO_4)_4$	−41.04	−40.78	−37.65	Zr > Hf > > Rf

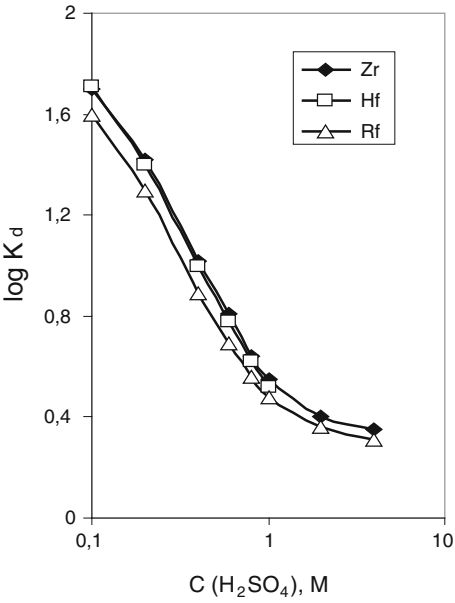

Fig. 52 Predicted logK_d for the extraction of Hf and Rf by amines with respect to the measured one for Zr. Reprinted with permission from V. Pershina, D. Polakova, J.P. Omtvedt, Radiochim. Acta **94**, 407 (2006). Copyright 2006 Oldenbourg Wissenschaftsverlag GmbH

Analogously, ΔE^{C} were obtained for a complex formation reaction starting from the hydrolyzed cations, i.e., $MOH(H_2O)_7^{3+} \leftrightarrow M(SO_4)_n(H_2O)_{8-2n}$. The results have indicated the same trend in the complex formation, Zr > Hf > > Rf, as for the reactions of Table 24. The obtained on their basis logK_d for extraction of Zr, Hf, and Rf by amines are shown in Fig. 52.

Experiments on sorption of Zr, Hf, and Rf from H_2SO_4 solutions by amines confirmed the predicted trend in the complex formation, Zr > Hf > > Rf, and have given the K_d(Rf) values closed to the predicted ones [280, 281].

7.2.3 Db

Like group-4 cations, group-5 ones undergo hydrolysis according to the reaction

$$M(H_2O)_6^{5+} \leftrightarrow M(OH)_6^{-} + 6H^{+}. \quad (35)$$

In [281], hydrolysis of the cations of Nb, Ta, Db, and Pa, for a comparison, was studied theoretically using the model described in Sect. 7.2.1. The calculated relative ΔE^{C} of reaction (35) are given in Table 25. The ΔE^{C} data are indicative of the following trend in hydrolysis of group-5 cations: Nb > Ta > Db > > Pa. This sequence is in agreement with experiments on hydrolysis of Nb, Ta, and Pa [279]. A simple model of hydrolysis does not again reproduce the difference between Nb and Ta having equal IR. The present model based on the real (relativistic) distribution of the electronic density describes correctly the experimental observations.

Table 25 E^C and ΔE^C (in eV) for reaction $M(H_2O)_6^{5+} \leftrightarrow M(OH)_6^-$, where M = Nb, Ta, Db, and Pa. From [281]

Complex	Nb	Ta	Db	Pa
$M(OH)_6^-$	−21.74	−23.33	−21.48	−19.53
$M(H_2O)_6^{5+}$	−21.92	−25.38	−25.37	−29.71
ΔE^C	0.18	2.05	3.89	9.18

Further on, complex formation of group-5 elements in HF, HCl, and HBr solutions was studied theoretically using the same approach [282, 283]. (A motivation for this study was the unexpected behavior of Db (Ha at that time) in the experiments on extraction into triisooctyl amine (TIOA) from mixed HCl/HF solutions [298]: Db was extracted similarly to Pa and not to Ta).

In HCl solutions, a large variety of complexes, such as $M(OH)_2Cl_4^-$, $MOCl_4^-$, $MOCl_5^{2-}$ and MCl_6^- (M = Nb, Ta, Db, and Pa) can be formed with different degrees of hydrolysis according to the following equilibrium

$$M(OH)_6^- + iL^- \leftrightarrow MO_u(OH)_{z-2u}L_i^{(6-i)-}. \quad (36)$$

To predict their stability, 4*c*-DFT calculations for this species were performed in [282, 283]. Obtained ΔE^C for reaction (36) are given in Table 26.

The data of Table 26 suggest the following trend in the complex formation of these elements: Pa > > Nb > Db > Ta. Taking into account the association with the organic cation, the following trend was predicted for sorption of the group-5 complexes by an anion exchanger

$$Pa \gg Nb \geq Db > Ta. \quad (37)$$

Thus, complexes of Pa should be formed in much more dilute HCl solutions, while a much higher acid concentration is needed to form those of Ta. The calculations also predicted the following sequence in the formation of various types of complexes as a function of the acid concentration: $M(OH)_2Cl_4^- > MOCl_4^- > MCl_6^-$ in agreement with experimental data for Nb, Ta, and Pa. The calculations also reproduced the $MF_6^- > MCl_6^- > MBr_6^-$ sequence as a function of the type of ligand (see Table 27).

The theoretical investigations have shown that the trend in the complex formation and extraction (sequence 37) known for Nb, Ta, and Pa turned out to be *reversed* in going to Db. This could not be predicted by any extrapolation of this

Table 26 ΔE^C (in eV) for reaction $M(OH)_6^- \leftrightarrow M(OH)_nCl_m^-$, where M = Nb, Ta, Db, and Pa. From [282, 283]

Metal	$M(OH)_2Cl_4^-$	$MOCl_4^-$	MCl_6^-
Nb	13.56	18.40	19.57
Ta	14.32	19.80	20.78
Db	14.29	19.67	20.46
Pa	11.68	16.29	17.67

Table 27 ΔE^C (in eV) for reaction $M(OH)_6^- \leftrightarrow ML_6^-$, where M = Nb, Ta, Db, and Pa, and L = F, Cl, and Br. From [283]

Complex	F	Cl	Br
NbL_6^-	12.20	19.57	21.40
TaL_6^-	12.69	20.78	22.63
DbL_6^-	12.38	20.46	22.11
PaL_6^-	12.19	17.67	19.91

property within the group, which would have given a continuous, and hence, wrong trend, but came as a result of the relativistic electronic structure calculations for real chemical equilibrium. According to these results, a recommendation was made to repeat the AIX separations in pure HCl or HF solutions. Accordingly, amine separations of the group-5 elements were systematically redone by Paulus et al. [299]. A reversed extraction sequence Pa > Nb ≥ Db > Ta, as that predicted theoretically (sequence 37), was then observed.

7.2.4 Sg

Hydrolysis. Experiments on the CIX separations of Sg from 0.1 M HNO_3 solutions showed that Sg did not elute from the CIX column, in contrast to Mo and W [300]. This non-tungsten-like behavior of Sg was tentatively attributed to its lower tendency to hydrolyze (deprotonate) compared to that of W. To interpret the behavior of Sg in these experiments and to predict its hydrolysis at various pH values, free energies of the following protonation reactions for Mo, W, and Sg

$$\begin{aligned} MO_4^{2-} \leftrightarrow MO_3(OH)^- \leftrightarrow\ & MO_2(OH)_2(H_2O)_2 \leftrightarrow \\ MO(OH)_3(H_2O)_2^+ \leftrightarrow\ & M(OH)_4(H_2O)_2^{2+} \leftrightarrow \ldots \leftrightarrow M(H_2O)_6^{6+} \end{aligned} \quad (38)$$

were considered theoretically [284]. The ΔE^C for these consecutive protonation steps were calculated using the 4*c*-DFT method. The results shown in Table 28 indicate that for the first two protonation steps, the trend in group-6 is reversed: Mo < Sg < W. For the further protonation process, the trend is continued with Sg: Mo < W < Sg.

Table 28 ΔE^C (in eV) for the stepwise protonation of MO_4^{2-} (M = Mo, W, and Sg). From [284]

Reaction	ΔE^C		
	Mo	W	Sg
$MO_4^{2-} + H^+ \leftrightarrow MO_3(OH)^-$	−12.28	−13.13	−12.96
$MO_3(OH)^- + H^+ + 2H_2O \leftrightarrow MO_2(OH)_2(H_2O)_2$	−21.43	−22.08	−21.61
$MO_2(OH)_2(H_2O)_2 + H^+ \leftrightarrow MO(OH)_3(H_2O)_2^+$	−5.84	−6.35	−6.65
$MO(OH)_3(H_2O)_2^+ + H^+ \leftrightarrow M(OH)_4(H_2O)_2^{2+}$	−0.43	−0.76	−1.23
$M(OH)_4(H_2O)_2^{2+} + 4H^+ \leftrightarrow \ldots M(H_2O)_6^{6+}$	41.97	38.71	37.11

Table 29 log$K$ for the step-wise protonation of MO_4^{2-} (M = Mo, W, and Sg). From [284]

Reaction	logK_n		
	Mo	W	Sg
$MO_4^{2-} + H^+ \leftrightarrow MO_3(OH)^-$	3.7	3.8	3.74
$MO_3(OH)^- + H^+ + 2H_2O \leftrightarrow MO_2(OH)_2(H_2O)_2$	3.8	4.3	4.1 ± 0.2
$MO_4^{2-} + 2H^+ + 2H_2O \leftrightarrow MO_2(OH)_2(H_2O)_2$	7.50	8.1	8.9 ± 0.1
$MO_2(OH)_2(H_2O)_2 + H^+ \leftrightarrow MO(OH)_3(H_2O)_2^+$	0.93	0.98	1.02

Thus, the same reversal of the trend is predicted for the protonation of oxyanions of the group-6 elements as that for the complex formation of the group-4 and 5 elements. The predicted trends in the complex formation are in agreement with experiments for Mo and W at various pHs [279]. For the protonation of positively charged complexes, the predicted trend Mo < W < Sg is in line with the experimental observations for Sg [300]. Using the procedure described in Sect. 7.2.1, log$K$ were determined for Sg, as given in Table 29 [284].

Complex formation. Complex formation of Mo, W, and Sg in HF solutions was studied theoretically on the basis of the 4*c*-DFT calculations [286] of the following step-wise fluorination process

$$\begin{aligned} MO_4^{2-}[\text{or } MO_3(OH)^-] + HF \leftrightarrow MO_3F^- \leftrightarrow \\ MO_2F_2(H_2O)_2 \leftrightarrow MO_2F_3(H_2O)^- \leftrightarrow MOF_5^-. \end{aligned} \quad (39)$$

The calculated ΔE^C indicate a very complicated dependence of the complex formation of these elements and trends on the pH and HF concentration. A plot of predicted log$K$ of W and Sg with respect to log$K$(Mo) in AIX separations from HF solutions at all the range of acid concentrations is shown in Fig. 53. There, below 10^{-2} M HF, negatively charged and neutral hydrolyzed complexes are in the aqueous phase, but negatively charged and neutral fluoride complexes are in the organic phase. At higher HF concentrations both neutral and positively charged

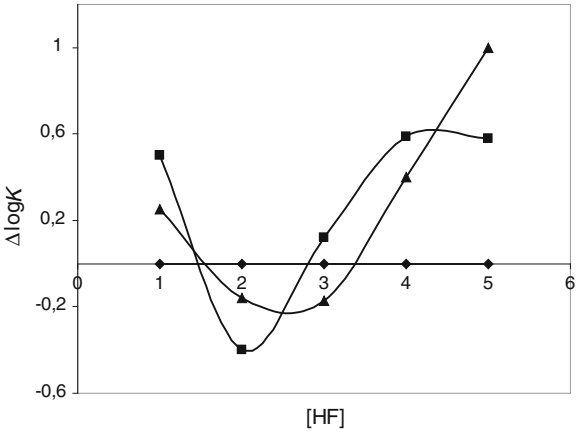

Fig. 53 Predicted relative values of logK_d of W (*squares*) and Sg (*triangles*) with respect to those of Mo (*rhomboids*) by AIX separations from HF solutions as a function of the acid concentration. Points 1 through 5 correspond to the following extracted complexes: MO_3F^-, $MO_2F_2(H_2O)_2$, $MO_2F_3(H_2O)^-$, $MO_2F_4^{2-}$ and MOF_5^-. From [286]

hydrolyzed species occur in the aqueous phase, but negatively charged fluoride complexes are extracted into the organic phase. One can see from Fig. 53 that at the lowest HF concentrations ($< \sim 0.1$ M HF), a reversal of the trends in K_d occurs in the group, while at higher HF molarities ($> \sim 0.1$ M HF), the trend is continued with Sg: Mo < W < Sg. At the range of these HF concentrations, separation between the homologs is the best.

The obtained sequences are in agreement with experiment on Mo and W [301]. Future experiments on the AIX separations of group-6 elements from HF solutions should clarify the extraction position of Sg in the group.

7.2.5 Hs

Experiments [303, 304] with volatile tetroxides of group-8 elements have shown that HsO_4 reacts with the moisturized NaOH surface forming obviously the sodium hassate (VIII), $Na_2[HsO_4(OH)_2]$, by analogy with $Na_2[OsO_4(OH)_2]$ according to the reaction

$$2NaOH + HsO_4 \rightarrow Na_2\left[HsO_4(OH)_2\right]. \quad (40)$$

In [287], the reactivity of RuO_4, OsO_4, and HsO_4 with NaOH was studied on the basis of the 4*c*-DFT calculations of the components of the reaction of Eq. 40 and the model described in Sect. 7.2.1. The ΔE^C values for the $MO_4 \rightarrow Na_2[MO_4(OH)_2]$ reaction of 8.04 eV, 5.09 eV and 5.63 eV for Ru, Os, and Hs, respectively, are indicative of the following trend in the complex formation: Os > Hs > > Ru, in agreement with experiment for Os and Ru. The predicted lower reactivity of HsO_4 with NaOH as compared to that of OsO_4 has so far not clearly been revealed experimentally [305].

7.3 Summary of the Aqueous Chemistry Studies

A summary of the predicted trends in hydrolysis, complex formation and extraction of the heaviest element complexes and their homologs as compared to the experimental results is given in Table 30. As one can see, most of the predictions were confirmed by experiments for the heaviest elements and their homologs, while some of them are still awaiting verification, as in the case of Sg in HF solutions.

The calculations have shown that the theory of hydrolysis [279] based on the relation between the cation size and charge does not explain all the experimental behavior, like, e.g., the difference between Nb and Ta, or Mo and W. Only by performing relativistic calculations for real chemical equilibrium in solutions can complex formation and hydrolysis constants, as well as distribution coefficients between an aqueous and organic phases (or sorption coefficients) and their order in

Table 30 Trends in hydrolysis and complex formation of the group-4 through 8 elements

Group	Extracted complex	Theoretically predicted	Ref.	Experiment. observed	Ref.
4	Hydrolysis of M^{4+}	Zr > Hf > Rf	[285]	Zr > Hf > Rf	[290]
	$MF_x(H_2O)_{8-x}^{z-x}(x \leq 4)$	Zr > Hf > Rf	[285]	Zr > Hf > Rf	[291, 292]
	MF_6^{2-}	Rf ≥ Zr > Hf	[285]	Rf ≥ Zr > Hf	[293]
				Zr > Hf > > Rf	[291, 294]
	MCl_6^{2-}	Zr > Hf > Rf	[285]	Rf > Zr > Hf	[295]
	MCl_4	Rf > Hf > Zr	[285]	Zr > Rf > Hf	[296]
				Zr > Hf ≈ Rf	[297]
	$M(SO_4)_4^{4-}$	Zr > Hf > > Rf	[288]	Zr > Hf > > Rf	[298, 299]
5	Hydrolysis of M^{5+}	Nb > Ta > Db	[281]	Nb > Ta	[270]
	$MOCl_4^-$, MCl_6^-	Nb ≥ Db > Ta	[282]	Nb ≥ Db > Ta	[301]
	MF_6^-, MBr_6^-	Nb > Db > Ta	[283]	Nb > Db > Ta	[301]
6	Hydrolysis of M^{6+}	Mo > W > Sg	[284]	Mo > W > Sg	[302]
	Hydrolysis of $MO_2(OH)_2$	Mo > Sg > W	[284]	Mo > W	[302]
	$MO_2F_2(H_2O)_2$	Mo > Sg > W	[286]	Mo > W	[303, 304, 306, 307]
	MOF_5^-	Mo < W < Sg	[286]	Mo < W	[303]
8	$MO_4(OH)_2^{2-}$	Os > Hs > > Ru	[287]	Os ≥ Hs	[305]

the chemical groups be correctly predicted. Results of such calculations have also shown the predominant contribution in ΔG^r to be a change in the electrostatic metal–ligand interaction energy, ΔE^C. Thus, by calculating only this term can trends in the complex formation be reliably predicted.

7.4 Prospects for Aqueous Chemistry Studies

Experimental aqueous studies of chemical properties of elements heavier than Sg will depend on the development of experimental techniques that can cope with production rates of less than one atom per hour and short half-lives.

From element 107 on, the maximum oxidation state is expected to be relatively unstable in solutions. It would, therefore, be interesting to conduct experiments probing the stability of lower oxidation states. The stability of Bh^{VII} relative to Bh^{IV} could be established by AIX separations of group-7 elements in acidic solutions. In HCl solutions Tc and Re undergo the complexation reaction $MO_4^- + HCl \leftrightarrow MCl_6^{2-}$ simultaneously with reduction. The K_d curves for Tc and Re show peaks at about 7–8 M HCl associated with the reduction [306, 307]. The peak for Tc is at lower HCl concentrations than that of Re indicating an earlier reduction of Tc, which means that Tc is less stable in the 7+ oxidation state (or more stable in the 4+ state) than Re. The position of the peak on the K_d curve

Table 31 Formation enthalpies (in kcal/mol) for some compounds of Hg [303, 304]

Compound	Phase	F	Cl	Br	J
HgX_2	Gas	−70.2	−35.0	−20.4	−3.84
HgX_2	Aqueous	–	−6.9	−10.7	−15.0
HgX_3^-	Aqueous	–	−2.2	−3.0	−3.6
HgX_4^{2-}	Aqueous	–	0.1	−4.1	−4.0

for Bh would, therefore, be indicative of the relative stability of its 7+ oxidation state. It would also be interesting to conduct similar reduction experiments with Hs. Its homologs are known to have the following reduction potentials: $RuO_4 + nHCl \rightarrow RuCl_5OH^{2-} + Cl_2 + nH_2O$ of $E° = 0.14$ V and $OsO_4 + 8HCl \rightarrow H_2OsCl_6 + Cl_2 + 4H_2O$ of $E° = -0.36$ V.

Cn should have a complex ion chemistry, like other elements at the second half of the 6d transition series. A tendency to form stronger bonding with "soft" ligands is foreseen in [1, 2] by analogy with Hg showing the increasing stability of the aqueous complexes from F to Cl to Br and to I (Table 31). The increasing stability constants in this row has, however, another reason, namely the decreasing hydrolysis $HgX_2 + H_2O \leftrightarrow Hg(OH)X$: 1.4% (Cl), 0.08% (Br), 0% (I) [303, 304]. The stability of the gas and crystal phase compounds of Hg, on the contrary, decreases from F to Cl to Br and to I (Table 31).

The formation enthalpy of CnF_2 was calculated at the PP level as −75.33 kcal/mol as compared to the calculated −88.4 kcal/mol for HgF_2 [153]. Thus, taking into account the decreasing stability of the 2+ oxidation state in group 12, experiments could be conducted with probably only CnI^+ and CnI_2. The possibility of formation of CnF_5^- and CnF_3^- was also considered in [153] (by analogy with Hg where the addition of an F^- to HgF_2 or HgF_4 was found energetically favorable), though these compounds will undergo strong hydrolysis in aqueous solutions and will not be stable. Thus, the only possibility would be the formation of $CnBr_5^-$ or CnI_5^-.

Fl should also have a greater tendency to form complexes in solutions than Pb. Since the stability of the 2+ state increases within group 14, Fl would probably form $M^{2+} + X_2 \leftrightarrow MX^+$ (X = Cl, Br, and I) and $M^{2+} + X_2 \leftrightarrow MX_2$ or $MX_2 + X_2 \leftrightarrow MX_3^-$ or MX_4^{2-} by analogy with Pb. (In 11 M HCl, $PbCl_6^{4-}$ is known). As in group 12, the stability of the gas-phase compounds of Pb decreases from F to Cl to Br and to I, while in aqueous solutions it is the other way around. The reason for that is a decreasing hydrolysis from F to Cl to Br and to I (fluoride complexes are not known) according to the reaction $MX_2 \leftrightarrow M(OH)X$, $M(OH)_2$ or $M(OH)_3^-$ [305]. Since the 2+ oxidation state of Fl should be more stable than Pb^{2+}, Fl can be extracted as MBr_3^- or MI_3^-. In [140], the existence of FlF_6^- was suggested, though in solutions this compound will undergo strong hydrolysis. The stability of various complexes of Fl versus stability of the hydrolysis products could be a subject of further theoretical investigations.

8 Conclusions and Outlook

Spectacular developments in the relativistic quantum theory, computational algorithms and computer techniques allowed for accurate calculations of properties of the heaviest elements and their compounds. Nowadays, atomic DC(B) correlated calculations including QED effects reaching an accuracy of few meV for electronic transitions and ionization potentials are available for these elements. These calculations allowed for reliable predictions of electronic configurations of the heaviest elements up to $Z = 122$. For heavier elements, as well as for the midst of the 6d-element series, MCDF calculations are still the source of useful information. On their basis, the end of the Periodic Table from the electronic structure point of view is predicted for $Z = 173$. Treatment of QED effects permitted also relative accurate predictions of inner-shell ionization potentials.

Most of molecular calculations were performed with the use of relativistic DFT and RECP methods that turned out to be complimentary both conceptionally and quantitatively. Their combination is presently the best way to study properties of complex systems of the heaviest elements. DC *ab initio* molecular methods are in the phase of development and their routine application to the heaviest systems is still a matter of future.

Using all those methods, reliable predictions of properties of the heaviest element and their compounds became available. Theoretical calculations permitted establishment of important trends in spectroscopic properties, chemical bonding, stabilities of oxidation states, ligand-field effects, complexing ability and other of the heaviest elements, as well as the role and magnitude of relativistic effects. Detailed studies are offered for elements Rf through 120, as well as for some species of even heavier elements. A high accuracy of total energy calculations allowed for predictions of stability of species, their geometry and energies of chemical reactions in the gas and aqueous phases, as well on surfaces of metals. However, fully relativistic description of adsorption processes on complicated or inert surfaces is still problematic. Therefore, some models were used in practical applications. Also, physico-chemical models were helpful in predicting some other properties that are difficult to handle in a straightforward way, such as, e.g., extraction from aqueous solutions or ion exchange separations. Such studies were performed for elements Rf through Hs, Cn, Fl, and element 113. Some estimates of adsorption enthalpies of even heavier elements, up to $Z = 120$, on noble metals are also available.

Being often conducted in a close link to the experiment, those theoretical works were indispensable for designing chemical experiment and interpreting its outcome. An experimental input was also helpful in improving theoretical models and encouraging a higher accuracy of the calculations. The synergism between the theoretical and experimental research in this field have resulted in better understanding of the chemistry of these exotic species and the role of relativistic effects.

It was shown that the heaviest elements are basically homologs of their lighter congeners in the chemical groups, though their properties may be rather different

due to very large relativistic effects on their electron shells. Relativistic effects were found to be predominant over the orbital one in the electronic structures of the elements of the 7th period and heavier. They are responsible for trends in the chemical groups (a continuation, or a reversal) with increasing Z from the elements of the 6th period. Thus, for elements of the 7th period and heavier, the use of relativistic methods is mandatory. Straightforward extrapolations of properties from lighter congeners may, therefore, result in erroneous predictions.

Although rich information has been collected, a number of open questions still remain. For elements which were chemically identified, a more detailed study, both theoretical and experimental, should follow. New compounds of chemically identified elements, e.g., carbonyls of Sg, or organometallic ones of Hs, should be synthesized and chemically investigated. For the not yet studied elements, like Mt, Ds, Rg, or elements 115 through 118, isotopes suitable for chemical studies should be first found, as well as their nuclear decay properties should be known, so that they can be positively identified. Their separation will also need new technological developments to cope with the very low production rates and short half-lives. In this area, theoretical chemistry will have a number of exciting tasks to predict the experimental behavior in the chemical separation experiments. Even though some basic properties of these elements have been theoretically outlined, more detailed studied should follow taking into account experimental details.

Whether it will ever be possible to experimentally investigate chemical properties of elements heavier than $Z = 118$ remains an open question. The chemistry of these superheavy elements, therefore, rests at the time being on a purely theoretical basis. A number of interesting chemical species for investigations is suggested. Properties of these elements and their compounds will be even more exciting than of those elements which have already been studied, since resemblance with their lighter homologs will be even less pronounced. Some further methodical developments in the relativistic quantum theory resulting in the creation of fully relativistic *ab initio* molecular, cluster, and solid-state codes, also with inclusion of the QED effects on an SCF basis, are needed to achieve a required accuracy of the predicted quantities for those very high Z numbers. The future calculations will also need powerful supercomputers.

References

1. Fricke, B., Waber, J.T.: Theoretical predictions of the chemistry of superheavy elements. Actinide Rev. **1**, 433–485 (1971)
2. Fricke, B.: Superheavy elements. A prediction of their chemical and physical properties. Struct. Bond. **21**, 89–144 (1975)
3. Keller Jr, O.L., Seaborg, G.T.: Chemistry of the transactinide elements. Ann. Rev. Nucl. Sci. **27**, 139–166 (1977)
4. Seaborg, G.T., Keller, O.L., Jr: Future elements. In: Katz, J.J., Seaborg, G.T., Morss, L.R. (eds.) The Chemistry of the Actinide Elements, 2nd edn, vol. 2, pp. 1629–1646. Chapman and Hall, London (1986)

5. Seaborg, G.T.: Evolution of the modern periodic table. J. Chem. Soc. Dalton Trans. 3899–3907 (1996)
6. Pershina, V.: Electronic structure and properties of the transactinides and their compounds. Chem. Rev. **96**, 1977–2010 (1996)
7. Pershina, V., Kratz, J.V.: Experimental and theoretical studies of the chemistry of the heaviest elements. In: Hess, B.A. (ed.) Relativistic Effects in Heavy-Element Chemistry and Physics, pp. 219–244. Wiley, New York (1997)
8. Schwerdtfeger, P., Seth, M.: Relativistic effects on the superheavy elements. In: von Rague Schleyer, P (ed.) Encyclopedia on Calculational Chemistry, vol. 1, pp. 2480–2499. Wiley, New York (1998)
9. Pershina, V., Fricke, B.: Electronic structure and chemistry of the heaviest elements. In: Greiner, W., Gupta, R.K. (eds.) Heavy Elements and Related New Phenomena, pp. 194–162. World Scientific, Singapore (1999)
10. Pershina, V.: The Chemistry of the superheavy elements and relativistic effects. In: Schwerdtfeger, P. (ed.) Relativistic Electronic Structure Theory, Part II, pp. 1–80. Elsevier, Amsterdam (2002)
11. Pershina, V.: Theoretical chemistry of the heaviest elements. In: Schädel, M. (ed.) The Chemistry of Superheavy Elements, pp. 31–94. Kluwer, Dordrecht (2003)
12. Hoffman, D.C., Lee, D.M., Pershina, V.: Transactinide elements and future elements. In: Morss, L.R., Edelstein, N.M., Fuger, J., Katz, J.J. (eds.) The Chemistry of the Actinide and Transactinide Elements, vol. 3, 3d edn, pp. 1652–1752. Springer, Dordrecht (2006)
13. Pershina, V.: Electronic structure and chemistry of the heaviest elements. In: Barysz, M., Ishikawa, Y. (eds.) Relativistic Methods for Chemists, pp. 452–520. Springer, Dordrecht (2010)
14. Pershina, V.: Relativistic electronic structure studies on the heaviest elements. Radiochim. Acta **99**, 459–476 (2011)
15. Cotton, S.A.: After the actinides, then what? Chem. Soc. Rev. **25**, 219–227 (1996)
16. Seaborg, G.T., Metallurgical Laboratory Memorandum MUC-GTS-858, 17 July 1944
17. Seaborg, G.T.: The chemical and radioactive properties of the heavy elements. Chem. Eng. News **23**, 2190–2193 (1945)
18. Mann, J.B.: Stability of 8p electrons in superheavy elements. J. Chem. Phys. **51**, 841–842 (1969)
19. Mann, J.B., Waber, J.T.: SCF relativistic Hartree-Fock calculations on the superheavy elements 118–131. J. Chem. Phys. **53**, 2397–2406 (1970)
20. Fricke, B., Greiner, W., Waber, J.T.: The continuation of the periodic table up to $Z = 172$. The chemistry of superheavy elements. Theoret. Chim. Acta **21**, 235–260 (1971)
21. Desclaux, J.P.: Relativistic Dirac-Fock expectation values for atoms with $Z = 1$ to $Z = 120$. At. Data Nucl. Data Tables **12**, 311–386 (1973)
22. Nefedov, V.I., Yarzhemcky, V.G., Trzhaskovskaya, M.B.: Periodic low as applied to superheavy elements: Specific features arising from relativistic effects. Russ. J. Inorg. Chem. **49**, 1871–1874 (2004)
23. Desclaux, J.P., Fricke, B.: Relativistic prediction of the ground state of atomic lawrencium. J. Phys. **41**, 943–946 (1980)
24. Glebov, V.A., Kasztura, L., Nefedov, V.S., Zhuikov, B.L.: Is element 104 (kurchatovium) a p-element? II. Relativistic calculations of the electronic atomic structure. Radiochim. Acta **46**, 117–121 (1989)
25. Johnson, E., Fricke, B., Keller Jr, O.L., Nestor Jr, C.W., Tucker, T.C.: Ionization potentials and radii of atoms and ions of element 104 (unnilquadium) and of hafnium (2+) derived form multiconfiguration Dirac-Fock calculations. J. Chem. Phys. **93**, 8041–8050 (1990)
26. Fricke, B., Johnson, E., Rivera, G.M.: Ionization potentials and radii of atoms and ions of element 105 (unnilpentium) and ions of tantalum derived from multiconfiguration Dirac-Fock calculations. Radiochim. Acta **62**, 17–25 (1993)
27. Johnson, E., Pershina, V., Fricke, B.: Ionization potentials of seaborgium. J. Phys. Chem. **103**, 8458–8462 (1999)

28. Johnson, E., Fricke, B., Jacob, T., Dong, C.Z., Fritzsche, S., Pershina, V.: Ionization potentials and radii of neutral and ionized species of elements 107 (bohrium) and 108 (hassium) from extended multiconfiguration Dirac-Fock calculations. J. Phys. Chem. **116**, 1862–1868 (2002)
29. Pyper, N.C., Grant, I.P.: Theoretical chemistry of the 7p series of superheavy elements. I. Atomic structure studies by multi-configuration Dirac-Fock theory. Proc. R. Soc. Lond. A **376**, 483–492 (1981)
30. Nefedov, V.I., Trzhaskovskaya, M.B., Yarzhemcky, V.G.: Electronic configurations and the Periodic Table for superheavy elements. Doklady Phys. Chim. **408**, 149–151 (2006)
31. Pyykkö, P.: A suggested periodic table up to $Z \leq 172$, based on Dirac-Fock calculations on atoms and ions. Phys. Chem. Chem. Phys. **13**, 161–168 (2011)
32. Kaldor, U., Eliav, E.: Energies and other properties of heavy atoms and molecules. In: Hernandes-Laguna, A., Maruani, J., Mcweeny, R., Wilson, S. (eds.) Quantum Systems in Chemistry and Physics, vol. I, pp. 161–176. Kluwer, Dordrecht (2000)
33. Eliav, E., Kaldor, U.: Four-component electronic structure methods. In: Barysz, M., Ishikawa, Y. (eds.) Relativistic Methods for Chemists, pp. 279–350. Springer, Dordrecht (2010)
34. Eliav, E., Shmulyian, S., Kaldor, U., Ishikawa, Y.: Transition energies of lanthanum, actinium, and eka-actinium (element 121). J. Chem. Phys. **109**, 3954 (1998)
35. Eliav, E., Landau, A., Ishikawa, Y., Kaldor, U.: Electronic structure of eka-thorium (element 122) compared with thorium. J. Phys. B. **35**, 1693 (2002)
36. Indelicato, P., Bieron, J., Jönnson, P.: Are MCDF calculations 101% correct in the superheavy element range? Theor. Chem. Acc. **129**, 495–505 (2011)
37. Pyykkö, P.: Relativistic effects in structural chemistry. Chem. Rev. **88**, 563–594 (1988)
38. Schwarz, W.H.E., van Wezenbeck, E., Snijders, J.G., Baerends, E.J.: The origin of relativistic effects of atomic orbitals. J. Phys. B. **22**, 1515–1530 (1989)
39. Baerends, E.J., Schwarz, W.H.E., Schwerdtfeger, P., Snijders, J.G.: Relativistic atomic orbital contractions and expansions: magnitude and explanations. J. Phys. B. **23**, 3225–3240 (1990)
40. Onoe, J.: Atomic-number dependence of relativistic effects on chemical bonding. Adv. Quant. Chem. **37**, 311–323 (2000)
41. Autschbach, J., Siekierski, S., Schwerdtfeger, P., Seth, M., Schwarz, W.H.E.: Dependence of relativistic effects on electronic configuration in the neutral atoms of d- and f-block elements. J. Comput. Chem. **23**, 804–813 (2002)
42. Labzowsky, L.N., Goidenko, I.: QED theory of atoms. In: Schwerdtfeger, P. (ed.) Relativistic Electronic Structure Theory, Part I, pp. 401–467. Elsevier, Amsterdam (2002)
43. Lindgren, I.: Relativistic many-body and QED calculations on atomic systems. Int. J. Quant. Chem. **57**, 683–695 (1996)
44. Gaston, N., Schwerdtfeger, P., Nazarewicz, W.: Ionization potential of internal conversion electrons for the superheavy elements 112, 114 116, and 118. Phys. Rev. A **66**, 062505(10) (2002)
45. Thierfelder, C., Schwerdtfeger, P., Hessberger, F.P., Hofmann, S.: Dirac-Hartree-Fock studies of X-ray transitions in meitnerium. Eur. Phys. J. A **36**, 227–231 (2008)
46. Pyykkö, P., Tokman, M., Labzowsky, L.N.: Estimated valence-level Lamb shifts for group 1 and group 11 metal atoms. Phys. Rev. A **57**, R689–R692 (1998)
47. Thierfelder, C., Schwerdtfeger, P.: Quantum electrodynamic corrections for the valence shell in heavy many-electron atoms. Phys. Rev. A **82**, 062503(10) (2010)
48. Goidenko, I., Labsowsky, L., Eliav, E., Kaldor, U., Pyykkö, P.: QED effects to the binding energy of the eka-radon ($Z = 118$) negative ion. Phys. Rev. A **67**, 020102R(1–3) (2003)
49. Sucher, J.: Foundation of the relativistic theory of many-electron atoms. Phys. Rev. A **22**, 348–362 (1980)
50. DIRAC package. Dirac, a relativistic *ab initio* electronic structure program, written by Aa, H.J., Jensen, T.S., Visscher, L. with contributions from Bakken, V., Eliav, E., Enevoldsen, T., Fleig, T., Fossgaard, O., Helgaker, T., Laerdahl, J., Larsen, C.V., Norman, P., Olsen, J.,

Pernpointner, M., Pedersen, J.K., Ruud, K., Salek, P., van Stralen, J.N.P., Thyssen, J., Visser, O., Winther, T. (http://dirac.chem.sdu.dk)
51. Malli, G., da Silva, A.B.F., Ishikawa, Y.: Highly accurate relativistic universal Gaussian basis set: Dirac-Fock-Coulomb calculations for atomic systems up to nobelium. J. Chem. Phys. **101**, 6829–6834 (1994)
52. Visscher, L., Aerts, P.J.C., Visser, O., Nieuwpoort, W.C.: Kinetic balance in contracted basis sets for relativistic calculations. Int. J. Quant. Chem. **40**, 131–139 (1991)
53. Faegri, K.: Relativistic Gaussian basis sets for the elements K-Uuo. Theor. Chem. Acc. **105**, 252–258 (2001)
54. Faegri, K., Dyall, K.G.: Basis sets for relativistic calculations. In: Schwerdtfeger, P. (ed.) Relativistic Electronic Structure Theory, Part I, pp. 259–290. Elsevier, Amsterdam (2002)
55. Dyall, K.: Relativistic double-zeta, triple-zeta, and quadruple-zeta basis sets for the 7p elements, with atomic and molecular applications. Theor. Chem. Acc. **131**, 1172–1174 (2012)
56. Guilherme, L., de Macedo, M., Borin, A.C., da Silva, A.B.F.: Prolapse-free relativistic Gaussian basis sets for the superheavy elements up to Uuo (Z = 118) and Lr (Z = 103). At. Data Nucl. Data Tables **93**, 931–961 (2007)
57. Desclaux, J.P.: A multiconfiguration relativistic Dirac-Fock program. Comp. Phys. Comm. **9**, 31–45 (1975)
58. Grant, I.P.: Variational methods for Dirac wave equations. J. Phys. B **19**, 3187–3206 (1986)
59. Parpia, F.A., Froese-Fisher, S., Grant, I.P.: GRASP92: A package for large-scale relativistic atomic structure calculations. Comp. Phys. Comm. **175**, 745–747 (2006)
60. Balasubramanian, K.: Relativistic computations of the electronic states of the superheavy element 114 and 114^{+}. Chem. Phys. Lett. **341**, 601–607 (2001); *ibid*, Erratum. **351**, 161–162 (2002)
61. Schwerdtfeger, P. (ed.): Relativistic Electronic Structure Theory. Parts I and II. Elsevier, Amsterdam (2002)
62. Dyall, K.G., Faegri, K., Jr.: Relativistic Quantum Chemistry, Oxford University Press, New York (2007)
63. Barysz, M., Ishikawa, Y. (eds.): Relativistic Methods for Chemists, Springer, Dordrecht (2010)
64. Visscher, L.: Post-Dirac-Fock methods. In: Schwerdtfeger, P. (ed.) Relativistic Electronic Structure Theory, Part I, pp. 291–331. Elsevier, Amsterdam (2002)
65. Saue, T.: Post Dirac-Fock-methods-properties. In: Schwerdtfeger, P. (ed.) Relativistic Electronic Structure Theory, Part I, pp. 332–397. Elsevier, Amsterdam (2002)
66. Wolf, A., Reiher, M., Hess, B.A.: Two-component methods and the generalized Douglas-Kroll-Transformation. In: Schwerdtfeger, P. (ed.) Relativistic Electronic Structure Theory, Part I, pp. 622–663. Elsevier, Amsterdam (2002)
67. Barysz, M.: Two-component relativistic theories. In: Barysz, M., Ishikawa, Y. (eds.) Relativistic Methods for Chemists, pp. 165–190. Springer, Dordrecht (2010)
68. Douglas, M., Kroll, N.M.: Quantum electrodynamical corrections to the fine structure of helium. Ann. Phys. **82**, 89–155 (1974)
69. Kutzelnigg, W.: The relativistic many-body problem in molecular theory. Phys. Scr. **36**, 416–431 (1987)
70. Dolg, M.: Relativistic effective core potentials. In: Schwerdtfeger, P. (ed.) Relativistic Electronic Structure Theory, Part I, pp. 793–862. Elsevier, Amsterdam (2002)
71. Schwerdfeger, P.: The pseudopotential approximation in electronic structure theory. Chem. Phys. Chem. **12**, 3143–3155 (2011)
72. Huzinaga, S., Cantu, A.A.: Theory of separability of many-electron systems. J. Chem. Phys. **55**, 5543–5549 (1971)
73. Seijo, L., Barandiaran, Z.: Relativistic *ab initio* model potentials calculations for molecules and embedded clusters. In: Schwerdtfeger, P. (ed.) Relativistic Electronic Structure Theory, Part I, pp. 417–475. Elsevier, Amsterdam (2002)

74. Lee, Y.S.: Two-component relativistic effective core potential calculations for molecules. In: Schwerdtfeger, P. (ed.) Relativistic Electronic Structure Theory, Part II, pp. 352–416. Elsevier, Amsterdam (2002)
75. Cao, X., Dolg, M.: Relativistic pseudopotentials. In: Barysz, M., Ishikawa, Y. (eds.) Relativistic Methods for Chemists, pp. 215–270. Springer, Dordrecht (2010)
76. Lee, Y.L., Ermler, W.C., Pitzer, R.M.: *Ab initio* effective core potentials including relativistic effects. I. Formalism and applications to the Xe and Au atoms. J. Chem. Phys. **67**, 5861–5876 (1977)
77. Nash, C.S., Bursten, B.E., Ermler, W.C.: *Ab initio* relativistic effective potentials with spin-orbit operators. VII. Am through element 118. J. Chem. Phys. **106**, 5153–5142 (1997)
78. Schwerdtfeger, P., Seth, M.: Private communication (2011)
79. Hangle, T., Dolg, M., Hanrath, M., Cao, X., Stoll, H., Schwerdtfeger, P.: Accurate relativistic energy-consistent pseudopotentials for the superheavy elements 111 to 118 including quantum electrodynamic effects. J. Chem. Phys. **136**, 214105 (1–10) (2012)
80. Kahn, L.R., Hay, P.J., Cowan, R.D.: Relativistic effects in *ab initio* effective core potentials for molecular calculations. Applications to the uranium atom. J. Chem. Phys. **68**, 2386–2398 (1978)
81. Hay, P.J.: *Ab initio* studies of exited states of polyatomic molecules including spin-orbit and multiplet effects: The electronic states of UF_6. J. Chem. Phys. **79**, 5469–5483 (1983)
82. Titov, A.V., Mosyagin, N.S.: Generalized relativistic effective core potentials: Theoretical grounds. Int. J. Quant. Chem. **71**, 359–401 (1999)
83. Kohn, W., Becke, A.D., Parr, R.G.: Density functional theory of electronic structure. J. Phys. Chem. **100**, 12974–12980 (1996)
84. Rosen, A.: Twenty to thirty years of DV-Xα calculations: A survey of accuracy and applications. Adv. Quant. Chem. **29**, 1–47 (1997)
85. Engel, E.: Relativistic density functional theory: Foundations and basic formalism. In: Schwerdtfeger, P. (ed.) Relativistic Electronic Structure Theory, Part I, pp. 523–621. Elsevier, Amsterdam (2002)
86. van Wüllen, C.: Relativistic density functional theory. In: Barysz, M., Ishikawa, Y. (eds.) Relativistic Methods for Chemists, pp. 191–214. Springer, Dordrecht (2010)
87. Anton, J., Fricke, B., Engel, E.: Noncollinear and collinear relativistic density-functional program for electric and magnetic properties of molecules. Phys. Rev. A **69**, 012505(10) (2004)
88. Jacob, T., Geschke, D., Fritzsche, S., Sepp, W.-D., Fricke, B., Anton, J., Varga, S.: Adsorption on surfaces simulated by an embedded cluster approach within the relativistic density functional theory. Surf. Sci. **486**, 194–202 (2001)
89. Liu, W., Hong, G., Dai, D., Li, L., Dolg, M.: The Beijing four-component density functional program package (BDF) and its application to EuO, EuS, YbO, and YbS. Theor. Chem. Acc. **96**, 75–83 (1997)
90. Rosen, A., Ellis, D.E.: Relativistic molecular calculations in the Dirac-Slater model. J. Chem. Phys. **62**, 3039–3049 (1975)
91. Mitin, A.V., van Wüllen, C.: Two-component relativistic density-functional calculations of the dimers of the halogens from bromide through element 117 using effective core potential and all-electron methods. J. Chem. Phys. **124**, 064305(7) (2006)
92. ADF, Theoretical Chemistry, Vrije Universiteit Amsterdam, The Netherlands (www.scm.com)
93. Ziegler, T., Tschinke, V., Baerends, E.J., Snijders, J.G., Ravenek, W.: Calculations of bond energies in compounds of heavy elements by a quasi-relativistic approach. J. Phys. Chem. **93**, 3050–3056 (1989)
94. van Lenthe, E., Baerends, E.J., Snijders, J.G.: Relativistic total energy using regular approximation. J. Chem. Phys. **101**, 9783–9792 (1994)
95. Sundholm, D.: Perturbation theory based on quasi-relativistic hamiltonians. In: Schwerdtfeger, P. (ed.) Relativistic Electronic Structure Theory, Part I, pp. 758–792. Elsevier, Amsterdam (2002)

96. Faas, S., van Lenthe, J.H., Hennum, A.C., Snijders, J.G.: An *ab initio* two-component relativistic methods including spin-orbit coupling using the regular approximation. Chem. Phys. **113**, 4052–4059 (2000)
97. Hess, B.A.: Relativistic electronic structure calculations employing a two-component no-pair formalism with external-field projection operators. Phys. Rev. A **33**, 3742–3748 (1986)
98. van Wüllen, C.: Relation between different variants of the generalized Douglas-Kroll transformation through sixth order. J. Chem. Phys. **120**, 7307–7313 (2004)
99. Nasluzov, V.A., Rösch, N.: Density functional based structure optimization for molecules containing heavy elements: Analytical energy gradients for the Douglas-Kroll-Hess scalar relativistic approach to the LCGTO-DF method. Chem. Phys. **210**, 413–425 (1996)
100. Häberlen, O.D., Chung, S.-C., Stener, M., Rösch, N.: From clusters to bulk: A relativistic density functional investigation on a series of gold clusters Au_n, $n = 6,\ldots, 147$. J. Chem. Phys. **106**, 5189–5201 (1997)
101. Ziegler, T., Snijders, J.G., Baerends, E.J.: On the origin of relativistic bond contraction. Chem. Phys. Lett. **75**, 1–4 (1980)
102. Case, D.A., Yang, C.Y.: Relativistic scattered wave calculations on UF_6. J. Chem. Phys. **72**, 3443–3448 (1980)
103. Eschrig, H., Richter, M., Opahle, I.: Relativistic solid state calculations. In: Schwerdtfeger, P. (ed.) Relativistic Electronic Structure Theory, Part I, pp. 723–776. Elsevier, Amsterdam (2002)
104. Collins, C.L., Dyall, K.G., Schaeffer, H.F., III: Relativistic and correlation effects in CuH, AgH, and AuH: Comparison of various relativistic methods. J. Chem. Phys. **102**, 2024–2031 (1995)
105. Dyall, K.G.: Second-order Möller-Plesset perturbation theory for molecular Dirac-Hartree-Foch wavefunctions. Theory for up to two open-shell electrons. Chem. Phys. Lett. **224**, 186–194 (1994)
106. Kaldor, U., Hess, B.A.: Relativistic all-electron coupled-cluster calculations on the gold atom and gold hydride in the framework of the Douglas-Kroll transformation. Chem. Phys. Lett. **230**, 1–7 (1994)
107. Schwerdtfeger, P., Brown, J.R., Laerdahl, J.K., Stoll, H.: The accuracy of the pseudopotential approximation. III. A comparison between pseudopotential and all-electron methods for Au and AuH. J. Chem. Phys. **113**, 7110–7118 (2000)
108. Lee, H.-S., Han, Y.-K., Kim, M.C., Bae, C., Lee, Y.S.: Spin-orbit effects calculated by two-component coupled-cluster methods: Test calculations on AuH, Au_2, TiH and Tl_2. Chem. Phys. Lett. **293**, 97–102 (1998)
109. Liu, W., van Wüllen, C.: Spectroscopic constants of gold and eka-gold (element 111) diatomic compounds: the importance of spin-orbit coupling. J. Chem. Phys. **110**, 3730–3735 (1999)
110. Huber, K.P., Herzberg, G.: Constants of Diatomic Molecules. Van Nostrand Reinhold, New York (1979)
111. Pyykkö, P.: Theoretical chemistry of gold. Angew. Chem. Int. Ed. **43**, 3312–4456 (2004)
112. Eliav, E., Kaldor, U., Ishikawa, Y.: Ground state electron configuration of rutherfordium: Role of dynamic correlation. Phys. Rev. Lett. **74**, 1079–1082 (1995)
113. Eliav, E., Kaldor, U., Schwerdtfeger, P., Hess, B.A., Ishikawa, Y.: Ground state electron configuration of element 111. Phys. Rev. Lett. **73**, 3203–3206 (1994)
114. Eliav, E., Kaldor, U., Ishikawa, Y.: Transition energies in mercury and eka-mercury (element 112) by the relativistic coupled-cluster method. Phys. Rev. A **52**, 2765–2769 (1995)
115. Eliav, E., Kaldor, U., Ishikawa, Y., Seth, M., Pyykkö, P.: Calculated energy levels of thallium and eka-thallium (element 113). Phys. Rev. A **53**, 3926–3933 (1996)
116. Landau, A., Eliav, E., Ishikawa, Y., Kaldor, U.: Electronic structure of eka-lead (element 114) compared with lead. J. Chem. Phys. **114**, 2977–2980 (2001)
117. Eliav, E., Kaldor, U., Ishikawa, Y.: The relativistic coupled-cluster method: transition energies of bismuth and eka-bismuth. Mol. Phys. **94**, 181–187 (1998)

118. Eliav, E., Kaldor, U., Ishikawa, Y., Pyykkö, P.: Element 118: The first rare gas with an electron affinity. Phys. Rev. Lett. **77**, 5350–5352 (1996)
119. Pershina, V., Borschevsky, A., Eliav, E., Kaldor, U.: Adsorption of inert gases including element 118 on noble metal and inert surfaces from *ab initio* Dirac–Coulomb atomic calculations. J. Chem. Phys. **129**, 144106(9) (2008)
120. Eliav, E., Vilkas, M.J., Ishikawa, Y., Kaldor, U.: Ionization potentials of alkali atoms: towards meV accuracy. Chem. Phys. **311**, 163–168 (2005)
121. Landau, A., Eliav, E., Ishikava, Y., Kaldor, U.: Benchmark calculations of electron affinities of the alkali atoms sodium to eka-francium (element 119). J. Chem. Phys. **115**, 2389–2392 (2001)
122. Eliav, E., Kaldor, U., Ishikawa, Y.: Transition energies of ytterbium, lutetium, lawrencium by relativistic coupled-cluster method. Phys. Rev. A **52**, 291–291 (1995)
123. Borschevsky, A., Pershina, V., Eliav, E., Kaldor, U.: Prediction of atomic properties of element 115 and its adsorption on inert surfaces. GSI Annual Report 2010, GSI Report 2011, p. 207
124. Borschevsky, A., Pershina, V., Eliav, E., Kaldor, U.: Benchmark calculations of atomic properties of elements 113–122. Presentation at the TAN2011 Conference, Sochi, 5–11 Sept 2011. (http://tan11.jinr.ru/Final_Programme-TAN11.htm)
125. Borschevsky, A., Pershina, V., Eliav, E., Kaldor, U.: *Ab initio* predictions of atomic properties of element 120, with comparison to lighter homologs, Phys. Rev. A, **87**, 022502-1-8 (2013)
126. Pershina, V., Borschevsky, A., Eliav, E., Kaldor, U.: Atomic properties of element 113 and its adsorption on inert surfaces from *ab initio* Dirac-Coulomb calculations. J. Phys. Chem. A **112**, 13712–13716 (2008)
127. Pershina, V., Borschevsky, A., Eliav, E., Kaldor, U.: Prediction of the adsorption behavior of elements 112 and 114 on inert surfaces from *ab initio* Dirac-Coulomb atomic calculations. J. Chem. Phys. **128**, 024707(9) (2008)
128. Borschevsky, A., Pershina, V., Eliav, E., Kaldor, U.: Electron affinity of element 114, with comparison to Sn and Pb. Chem. Phys. Lett. **480**, 49–51 (2009)
129. Eliav, E.: Private communication (2011)
130. Pershina, V.: Unpublished
131. Lim, I.S., Pernpointer, M., Laerdahl, J.K., Schwerdtfeger, P., Neogrady, P., Urban, M.: Relativistic coupled-cluster static dipole polarizabilities of the alkali metals from Li to element 119. Phys. Rev. A. **60**, 2822–2828 (1999)
132. Lim, I.S., Schwerdtfeger, P., Metz, B., Stol, H.: All-electron and relativistic pseudopotential studies for the group 1 element polarizabilities from K to element 119. J. Chem. Phys. **122**, 104103(12) (2005)
133. Thierfelder, C., Assadollahzadeh, B., Schwerdtfeger, P., Schäfer, S.: Relativistic and electron correlation effects in static dipole polarizabilities for the group-14 elements from carbon to element $Z = 114$: theory and experiment. Phys. Rev. A. **78**, 052506(7) (2008)
134. Umemoto, K., Saito, S.: Electronic configuration of superheavy elements. J. Phys. Soc. Jap. **65**, 3175–3179 (1996)
135. Yu, Y.J., Li, J.G., Dong, C.Z., Ding, X.B., Fritsche, S., Fricke, B.: The excitation energies, ionization potentials and oscillator strengths of neutral and ionized species of Uub ($Z = 112$) and the homologue elements Zn, Cd and Hg. Eur. Phys. J. D **44**, 51–56 (2007)
136. Yu, Y.J., Dong, C.Z., Li, J.G., Fricke, B.: The excitation energies, ionization potentials, and oscillator strengths of neutral and ionized species of Uuq ($Z = 114$) and the homolog elements Ge, Sn, and Pb. J. Chem. Phys. **128**, 124316(7) (2008)
137. Chang, Z., Li., J., Dong, C.: Ionization potentials, electron affinities, resonance excitation energies, oscillator strengths, and ionic radii of element Uus ($Z = 117$) and astatine. J. Phys. Chem. A **114**, 13388–13394 (2010)
138. Dzuba, V.A., Flambaum, V.V., Silvestrov, P.G., Sushkov, O.P.: Many-body perturbation-theory calculations in atoms with open shells. Phys. Rev. A **44**, 2828–2831 (1991)

139. Nash, C.S.: Atomic and molecular properties of elements 112, 114 and 118. J. Phys. Chem. A **109**, 3493–3500 (2005)
140. Schwedtfeger, P., Seth, M.: Relativistic quantum chemistry of the superheavy elements. Closed-shell element 114 as a case study. J. Nucl. Radiochem. Sci. **3**, 133–136 (2002)
141. Moore, C.E.: Atomic energy levels. Natl. Stand. Ref. Data Ser., Natl. Bur. Stand.: Washington, 1971
142. Haynes, W.M. (ed.): CRC Handbook of Chemistry and Physics, 93rd edn. CRC Press, Boca Raton (2012)
143. Pershina, V., Borschevsky, A., Anton, J.: Theoretical predictions of properties of group-2 elements including element 120 and their adsorption on noble metal surfaces. J. Chem. Phys., **136**, 134317 (1–10) (2012)
144. Pershina, V., Borschevsky, A., Anton, J.: Fully relativistic study of intermetallic dimers of group-1 elements K through element 119 and prediction of their adsorption on noble metal surfaces. Chem. Phys. **395**, 87–94 (2012)
145. Pershina, V., Johnson, E., Fricke, B.: Theoretical estimates of redox potentials for group 6 elements, including element 106, seaborgium, in acid solutions. J. Phys. Chem. A **103**, 8463–8470 (1999)
146. Slater, J.C.: Atomic radii in crystals. J. Chem. Phys. **41**, 3199–3204 (1964)
147. Bondi, A.: Van der Walls volumes and radii. J. Phys. Chem. **68**, 441–451 (1964)
148. Shannon, R.D.: Revised effective ionic radii and systematic studies of interatomic distances in halides and chalcogenides. Acta Crystallogr. Sect. A **32**, 751–767 (1976)
149. Pyykkö, P., Atsumi, M.: Molecular single-bond covalent radii for elements 1–118. Chem. Eur. J. **15**, 186–197 (2009)
150. Pyykkö, P., Riedel, S., Patzsche, M.: Triple-bond covalent radii. Chem. Eur. J. **11**, 3511–3620 (2005)
151. Seth, M., Dolg, M., Fulde, P., Schwerdtfeger, P.: Lanthanide and actinide contractions: relativistic and shell structure effects. J. Am. Chem. Soc. **117**, 6597–6598 (1995)
152. Bilewicz, A.: The ionic radii of Rf^{4+}, Db^{5+} and Sg^{6+}. Radiochim. Acta **88**, 833–836 (2000)
153. Seth, M., Schwerdtfeger, P., Dolg, M.: The Chemistry of the superheavy elements. I. Pseudopotentials for 111 and 112 and relativistic coupled cluster calculations for $(112)H^+$ $(112)F_2$, and $(112)F_4$. J. Chem. Phys. **106**, 3623–3632 (1997)
154. Goeben, D., Hohm, U.: Dipole polarizability, Cauchy moments, and related properties of Hg. J. Phys. Chem. **100**, 7710–7712 (1996)
155. Pershina, V., Bastug, T.: Relativistic effects on experimentally studied gas-phase properties of the heaviest elements. Chem. Phys. **311**, 139–150 (2000)
156. Pyykkö, P., Desclaux, J.P.: Dirac-Fock one-center calculations. The model systems TiH_4, ZrH_4, HfH_4, and $(104)H_4$. Chem. Phys. Lett. **50**, 503–507 (1977)
157. Pyykkö, P., Desclaux, J.P.: Dirac-Fock one-center calculations show $(114)H_4$ to resemble PbH_4. Nature **226**, 336–337 (1977)
158. Pyykkö, P., Desclaux, J.P.: Dirac-Fock one-center calculations. VI. The tetrahedral and octahedral model systems CeH_4, ThH_4, CrH_6, MoH_6, WH_6, UH_6 and $(106)H_6$. Chem. Phys. **34**, 261–280 (1978)
159. Varga, S., Fricke, B., Hirata, M., Bastug, T., Pershina, V., Fritzsche, S.: Total energy calculations of $RfCl_4$ and homologues in the framework of relativistic Density Functional Theory. J. Phys. Chem. A **104**, 6495–6498 (2000)
160. Pershina, V., Sepp, W.-D., Fricke, B., Rosen, A.: Relativistic effects in physics and chemistry of element 105. I. Periodicities in properties of group 5 elements. Electronic structure of the pentachlorides. J. Chem. Phys. **96**, 8367–8378 (1992)
161. Pershina, V., Fricke, B.: Relativistic effects in physics and chemistry of element 105. IV. Their influence on the electronic structure and related properties. J. Chem. Phys. **99**, 9720–9729 (1993)
162. Pershina, V., Sepp, W.-D., Fricke, B., Kolb, D., Schädel, M., Ionova, G.V.: Relativistic effects in physics and chemistry of element 105. II. Electronic structure and properties of group 5 elements bromides. J. Chem. Phys. **97**, 1116–1122 (1992)

163. Pershina, V., Sepp, W.-D., Bastug, T., Fricke, B., Ionova, G.V.: Relativistic effects in physics and chemistry of element 105. III. Electronic structure of hahnium oxyhalides as analogs of group 5 elements oxyhalides. J. Chem. Phys. **97**, 1123–1131 (1992)
164. Pershina, V., Anton, J.: Theoretical predictions of properties and gas-phase chromatography behaviour of bromides of group-5 elements Nb, Ta and element 105, Db. J. Chem. Phys. **136**, 034308(7) (2012)
165. Pershina, V., Fricke, B.: Electronic structure and properties of the group 4, 5, and 6 highest chlorides including elements 104, 105, and 106. J. Phys. Chem. **98**, 6468–6473 (1994)
166. Pershina, V., Fricke, B.: Group 6 oxychlorides $MOCl_4$, where M = Mo, W, and element 106 (Sg): electronic structure and thermochemical stability. J. Phys. Chem. **99**, 144–150 (1995)
167. Pershina, V., Fricke, B.: Group 6 dioxydichlorides MO_2Cl_2 (M = Cr, Mo, W, and element 106, Sg): The electronic structure and thermochemical stability. J. Phys. Chem. **100**, 8748–8751 (1996)
168. Pershina, V., Bastug, T.: The electronic structure and properties of group 7 oxychlorides, MO_3Cl, where M = Tc, Re, and element 107. Bh. J. Chem. Phys. **113**, 1441–1446 (2000)
169. Pershina, V., Bastug, T., Fricke, B.: Relativistic effects on the electronic structure and volatility of group-8 tetroxides MO_4, where M = Ru, Os and element 108, Hs. J. Chem. Phys. **122**, 124301(9) (2005)
170. Pershina, V., Anton, J., Jacob, T.: Fully-relativistic DFT calculations of the electronic structures of MO_4 (M = Ru, Os, and element 108, Hs) and prediction of physisorption. Phys. Rev. A **78**, 032518(5) (2008)
171. Han, Y.-K., Son, S.-K., Choi, Y.J., Lee, Y.S.: Structures and stabilities for halides and oxides of transactinide elements Rf, Db, and Sg calculated by relativistic effective core potential methods. J. Phys. Chem. **103**, 9109–9115 (1999)
172. Malli, G.L., Styszynski, J.: *Ab initio* all-electron fully relativistic Dirac-Fock-Breit calculations for molecules of the superheavy transactinide elements: rutherfordium tetrachloride. J. Chem. Phys. **109**, 4448–4455 (1998)
173. Malli, G.: Dramatic relativistic effects in atomization energy and volatility of the superheavy hassium tetroxide and OsO_4. J. Chem. Phys. **117**, 10441–10443 (2002)
174. Filatov, M., Cremer, D.: Calculation of electronic properties using regular approximation to relativistic effects: the polarizabilities of RuO_4, OsO_4, and HsO_4 (Z = 108). J. Chem. Phys. **119**, 1412–2012 (2003)
175. Dolg, M., Wedig, U., Stoll, H., Preuss, H.: Energy adjusted *ab initio* pseudopotentials for the first row transition elements. J. Chem. Phys. **86**, 866–872 (1987)
176. Andrae, D., Häussermann, U., Dolg, M., Stoll, H., Preuss, H.: Energy-adjusted *ab initio* pseudopotentials for the second and third row transition elements. Theor. Chem. Acc. **77**, 123–141 (1990)
177. Nash, C.S., Bursten, B.E.: Comparisons among transition metal, actinide and transactinide complexes: the relativistic electronic structures of $Cr(CO)_6$, $W(CO)_6$, $U(CO)_6$ and $Sg(CO)_6$. New J. Chem. **19**, 669–675 (1995)
178. Zvara, I.: The Inorganic Radiochemistry of Heavy Elements. Springer, Dordrecht (2008)
179. Eichler, B., Zvara, I.: Evaluation of the enthalpy of adsorption from thermodynamic data. Radiochim. Acta **30**, 233–238 (1982)
180. Zvara, I.: Simulation of thermochromatography process by the Monte Carlo method. Radiochim. Acta **38**, 95–101 (1985)
181. Zvara, I.: Problems in thermochromatographic separations of radioelements. J. Radioanal. Nucl. Chem. **204**, 123–134 (1996)
182. Düllmann, Ch., Brüchle, W., Dressler, R., Eberhardt, K., Eichler, B., Eichler, R., Gäggeler, H.W., Ginter, T.N., Glaus, F., Gregorich, K.E., Hoffman, D.C., Jäger, E., Jost, D.T., Kirbach, U.W., Lee, D.E., Nitsche, H., Patin, J.B., Pershina, V., Piguet, D., Qin, Z., Schädel, M., Schausten, B., Schimpf, E., Schött, H.-J., Soverna, S., Sudowe, R., Thörle, P., Timokhin, S.N., Trautmann, N., Türler, A., Vahle, A., Wirth, G., Yakushev, A.B., Zielinski, P.M.: Chemical investigation of hassium (element 108). Nature **418**, 859–862 (2002)

183. Pershina, V.: Predictions of adsorption behaviour of the heaviest elements in a comparative study from the electronic structure calculations. Radiochim. Acta **93**, 125–131 (2005)
184. Eichler, R., Brüchle, W., Dressler, R., Düllman, Ch.E., Eichler, B., Gäggeler, H.W., Gregorich, K.E., Hoffman, D.C., Hübener, S., Jost, D.T., Kirbach, U.W., Laue, C.A., Lavanchy, V.M., Nitsche, H., Patin, J.B., Piguet, D., Schädel, M., Shaughnessy, D.A., Strellis, D.A., Taut, S., Tobler, L., Tsyganov, Y.S., Türler, A., Vahle, A., Wilk, P.A., Yakushev, A.B.: Chemical characterization of bohrium (element 107). Nature **407**, 63–65 (2000)
185. Schädel, M., Brüchle, W., Dressler, R., Eichler, B., Gäggeler, H.W., Günther, R., Gregorich, K.E., Hoffman, D.C., Hübener, S., Jost, D.T., Kratz, J.V., Paulus, W., Schumann, D., Timokhin, S., Trautmann, N., Türler, A., Wirth, G., Yakushev, A.B.: Chemical properties of element 106 (seaborgium). Nature, **388**, 55–57 (1997)
186. Türler, A., Brüchle, W., Dressler, R., Eichler, B., Eichler, R., Gäggeler, H.W., Gärtner, M., Glatz, J.-P., Gregorich, K.E., Hübener, S., Jost, D.T., Lebedev, V.Y., Pershina, V., Schädel, M., Taut, S., Timokhin, N., Trautmann, N., Vahle, A., Yakushev, A.B.: First measurements of a thermochemical property of a seaborgium compound. Angew. Chem. Int. Ed. **38**, 2212–2213 (1999)
187. Zvara, I., Belov, V., Domanov, V.P., Shalaevski, M.R.: Sov. Radiochem. **18**, 371 (1976)
188. Gäggeler, H.W., Jost, D.T., Kovacs, J., Scherer, U.W., Weber, A., Vermeulen, D., Türler, A., Gregorich, K.E., Czerwinski, R.A., Kadkhodayan, B., Lee, D.M., Nurmia, M., Hoffman, D.C., Kratz, J.V., Gober, M.K., Zimmermann, H.P., Schädel, M., Brüchle, W., Schimpf, E., Zvara, I.: Gas phase chromatography experiments with bromides of tantalum and element 105. Radiochim. Acta **57**, 93–100 (1992)
189. Türler, A., Eichler, B., Jost, D.T., Piguet, D., Gäggeler, H.W., Gregorich, K.E., Kadkhodayan, B., Kreek, S.A., Lee, D.M., Mohar, M., Sylwester, E., Hoffman, D.C., Hübener, S.: On-line gas phase chromatography with chlorides of niobium and hahnium (element 105). Radiochim. Acta **73**, 55–66 (1996)
190. Qin, Z., Lin, M.S., Fan, F.L., Huang, W.X., Yan, X.L., Bai, J., Wu, X.L., Lei, F.A., Ding, H.J., Ma, F., Li, G.S., Zhou, H.B., Guo, J.S.: On-line gas chromatographic studies of Nb, Ta, and Db bromides. Radiochim. Acta **100**, 285–290 (2012)
191. Gyanchandani, J., Sikka, S.K.: Structural properties of rutherfordium. An *ab initio* study. Phys. Lett. A **376**, 620–625 (2012)
192. Rosen, A., Fricke, B., Morovic, T., Ellis, D.E.: J. Phys. C-4, Suppl. 4, **40**, C-4/218 (1979)
193. Patzschke, M., Pyykkö, P.: Darmstadtium carbonyl and carbide resemble platinum carbonyl and carbide. The Royal. Soc. Chem., Chem. Commun. 1982–1983 (2004)
194. Seth, M., Schwerdtfeger, P., Dolg, M., Faegri, K., Hess, B.A., Kaldor, U.: Large relativistic effects in molecular properties of the hydride of superheavy element 111. Chem. Phys. Lett. **250**, 461–465 (1996)
195. Dolg, M., Stoll, H., Seth, M., Schwerdtfeger, P.: On the performance of energy-consistent spin-orbit pseudopotentials: (111)H revised. Chem. Phys. Lett. **345**, 490–496 (2001)
196. Han, Y.-K., Hirao, K.: Two-component coupled-cluster calculations for the hydride of element 111: on the performance of relativistic effective core potentials. Chem. Phys. Lett. **328**, 453–458 (2000)
197. Seth, M., Schwerdtfeger, P.: A comparison of relativistic and electron correlation effects for (111)F, (111)H and (111)Li. Chem. Phys. Lett. **318**, 314–318 (2000)
198. Anton, J., Fricke, B., Schwerdtfeger, P.: Non-collinear and collinear four-component relativistic molecular density functional calculations. Chem. Phys. **311**, 97–103 (2005)
199. Seth, M., Cooke, F., Schwerdtfeger, P., Heully, J.-L., Pelissier, M.: The chemistry of the superheavy elements. II. The stability of high oxidation states in group 11 elements: Relativistic coupled cluster calculations for the di-, tetra- and hexafluoro metallates of Cu, Ag, Au, and element 111. J. Chem. Phys. **109**, 3935–3943 (1998)
200. Pitzer, K.S.: Are elements 112, 114, and 118 relatively inert gases? J. Chem. Phys. **63**, 1032–1033 (1975)

201. Yakushev, A.B., Zvara, I., Oganessian, Y.T., Belozerov, A.V., Dmitriev, S.N., Eichler, B., Hübener, S., Sokol, E.A., Türler, A., Yeremin, A.V., Buklanov, G.V., Chelnokov, M.L., Chepigin, V.I., Gorshkov, V.A., Gulyaev, A.V., Lebedev, V.Y., Malyshev, O.N., Popeko, A.G., Soverna, S., Szeglowski, Z., Timokhin, S.N., Tretyakova, S.P., Vasko V.M., Itkis, M.G.: Chemical identification and properties of element 112. Radiochim. Acta **91**, 433–439 (2003)
202. Eichler, R., Aksenov, N.V., Belozerov, A.V., Bozhikov, G. A., Chepigin, V.I., Dmitriev, S.N., Dressler, R., Gäggeler, H.W., Gorshkov, V.A., Haenssler, F., Itkis, M.G., Laube, A., Lebedev, V.Y., Malyshev, O.N., Oganessian, Y.T., Petrushkin, O.V., Piguet, D., Rasmussen, P., Shishkin, S.V., Shutov, S.V., Svirikhin, A.I., Tereshatov, E.E., Vostokin, G.K., Wegrzecki, M., Yeremin, A.V.: Chemical characterization of element 112. Nature **447**, 72–75 (2007)
203. Eichler, R., Aksenov, N.V., Belozerov, A.V., Bozhikov, G.A., Chepigin, V.I., Dmitriev, S.N., Dressler, R., Gäggeler, H.W., Gorshkov, A.V., Itkis, M.G., Haenssler, F., Laube, A., Lebedev, V.Y., Malyshev, O.N., Oganessian, Y.T., Petrushkin, O.V., Piguet, D., Popeko, A.G., Rasmussen, P., Shishkin, S.V., Serov, A.A., Shutov, A.V., Svirikhin, A.I., Tereshatov, E.E., Vostokin, G.K., Wegrzecki, M., Yeremin, A.V.: Thermochemical and physical properties of element 112. Angew. Chem. Int Ed. **47**, 3262–3266 (2008)
204. Liu, W., Dolg, M., Schwerdtfeger, P.: Benchmark relativistic all-electron density functional and *ab initio* pseudopotential study of group12 dimers M_2 (M = Zn, Cd, Hg and eka-Hg). Unpublished
205. Zee, R.D., Blankespoor, S.C., Zweier, T.S.: Direct spectroscopic determination of the Hg_2 bond length and an analysis of the 2540 Å band. J. Chem. Phys. **88**, 4650–4654 (1988)
206. Gaston, N., Opahle, I., Gäggeler, H.W., Schwerdtfeger, P.: Is Eka-Mercury (element 112) a group 12 metal? Angew. Chem. Int. Ed. **46**, 1663–1666 (2007)
207. Eichler, B.: Das Flüchtigkeitsverhalten von Transactiniden im Bereich um Z = 114 (Voraussage). Kernenergie **19**, 307–311 (1976)
208. Soverna, S.: Doctoral Thesis, Universität Bern (2004)
209. Soverna, S., Dressler, R., Düllmann, C.E., Eichler, B., Eichler, R., Gäggeler, H.W., Haenssler, F., Niklaus, J.P., Piguet, D., Qin, Z., Türler, A., Yakushev, A.: Thermochromatographic studies of mercury and radon on transition metal surfaces. Radiochim. Acta **93**, 1–8 (2005)
210. Pershina, V., Bastug, T., Fricke, B., Jacob, T., Varga, S.: Intermetallic compounds of the heaviest elements: the electronic structure and bonding of dimers of element 112 and its homolog Hg. Chem. Phys. Lett. **365**, 176–183 (2002)
211. Pershina, V., Bastug, T., Sarpe-Tudoran, C., Anton, J., Fricke, B.: Predictions of adsorption behaviour of the superheavy element 112. Nucl. Phys. A **734**, 200–213 (2004)
212. Sarpe-Tudoran, C., Fricke, B., Anton, J., Pershina, V.: Adsorption of superheavy elements on metal surfaces. J. Chem. Phys. **126**, 174702(5) (2007)
213. Pershina, V., Anton, J., Jacob, T.: Theoretical predictions of adsorption behavior of elements 112 and 114 and their homologs Hg and Pb. J. Chem. Phys. **131**, 084713(8) (2009)
214. Rykova, E.A., Zeitsevskii, A., Mosyagin, N.S., Isaev, T.A., Titov, A.V.: Relativistic effective core potential calculations of Hg and eka-Hg (E112) interactions with gold: spin-orbit density functional theory modelling of Hg-Au_n and E112-Au_n systems. J. Chem. Phys. **125**, 241102(3) (2006)
215. Zaitsevskii, A., Rykova, E.A., Mosyagin, N.S., Titov, A.V.: Towards relativistic ECP/DFT description of chemical bonding in E112 compounds: spin-orbit and correlation effects in E112X versus HgX (X = H, Au). Cent. Eur. J. Phys. **4**, 448–460 (2006)
216. Zaitsevkii, A., Titov, A.: Relativistic pseudopotential model for superheavy elements: applications to chemistry of eka-Hg and eka-Pb. Russ. Chem. Rev. **78**, 1173–1181 (2009)
217. Zaitsevski, A., van Wüllen, C., Rykova, E.A.: Two-component relativistic density functional modeling of the adsorption of element 114 (eka-led) on gold. Phys. Chem. Chem. Phys. **12**, 4152–4156 (2010)

218. Mosyagin, N.S., Isaev, T.A., Titov, A.V.: Is E112 a relatively inert element? Benchmark relativistic correlation study of spectroscopic constants in E112H and its cation. J. Chem. Phys. **124**, 224302–(1–5) (2006)
219. Nakajima, T., Hirao, K.: Numerical illustration of third-order Douglas-Kroll method: Atomic and molecular properties of superheavy element 112. Chem. Phys. Lett. **329**, 511–516 (2000)
220. Kaupp, M., von Schering, H.G.: Gaseous mercury(IV) fluoride, HgF_4: An *ab initio* study. Angew. Chem., Int. Ed. Engl., **32**, 861–863 (1993)
221. Kaupp, M., Dolg, M., Stoll, H., von Schnering, H.G.: Oxidation state +IV in group 12 chemistry: *ab initio* study of zinc(IV), cadmium(IV), and mercury(IV) fluorides. Inorg. Chem., **33**, 2122–2131 (1994)
222. Eichler, R., Aksenov, N.V., Albin, Y.V., Belozerov, A.V., Bozhikov, G.A., Chepigin, V.I., Dmitriev, S.N., Dressler, R., Gäggeler, H.W., Gorshkov, V.A., Henderson, R.A., Johnsen, A.M., Kenneally, J.M., Lebedev, V.Y., Malyshev, O.N., Moody, K.J., Oganessian, Y.T., Petrushkin, O.V., Piguet, D., Popeko, A.G., Rasmussen, P., Serov, A., Shaughnessy, D.A., Shishkin, S.V., Shutov, A.V., Stoyer, M.A., Stoyer, N.J., Svirikhin, A.I., Tereshatov, E.E., Vostokin, G.K., Wegrzecki, M., Wilk, P.A., Wittwer, D., Yeremin, A.V.: Indication for a volatile element 114. Radiochim. Acta, **88**, 133–139 (2010)
223. Yakushev, A.: Private communication 2011
224. König, S., Gäggeler, H.W., Eichler, R., Haenssler, F., Soverna, S., Dressler, R., Friedrich, S., Piguet, D., Tobler, L.: The production of long-lived Thallium-isotopes and their thermochromatography studies on quartz and gold. PSI Annual report, 2006, Jan 2005, p. 5
225. Pershina, V., Borschevsky, A., Anton, J., Jacob, T.: Theoretical predictions of trends in spectroscopic properties of homonuclear dimers and volatility of the 7p elements. J. Chem. Phys. **132**, 194341(11) (2010)
226. Pershina, V., Anton, J., Fricke, B.: Intermetallic compounds of the heaviest elements and their homologs: The electronic structure and bonding of MḾ, where M = Ge, Sn, Pb, and element 114, and Ḿ = Ni, Pd, Pt, Cu, Ag, Au, Sn, Pb, and element 114. J. Chem. Phys. **127**, 134310(9) (2007)
227. Wood, C.P., Pyper, N.C.: An *ab initio* relativistic calculation for $(E113)_2$. Chem. Phys. Lett. **84**, 614–621 (1981)
228. Liu, W., van Wüllen, Ch., Han, Y.K., Choi, Y.J., Lee, Y.S.: Spectroscopic constants of Pb and eka-lead compounds: comparsion of different approaches. Adv. Quant. Chem. **39**, 325–355 (2001)
229. van Wüllen, C.: Relativistic density functional calculations on small molecules. In: Schwerdtfeger, P. (ed.) Relativistic Electronic Structure Theory, Part II, pp. 598–655. Elsevier, Amsterdam (2002)
230. Liu, W., van Wüllen, C., Wang, F., Li, L.: Spectroscopic constants of MH and M_2 (M = Tl, E113, Bi, E115): Direct comparisons of four- and two-component approaches in the framework of relativistic density functional theory. J. Chem. Phys. **116**, 3626–3634 (2002)
231. Liu, W., Peng, D.: Infinite-order quasirelativistic density functional method based on the exact matrix quasirelativistic theory. J. Chem. Phys. **125**, 044102(1–10) (2006)
232. Peng, D., Liu, W., Xiao, Y., Cheng, L.: Making four- and two-component relativistic density functional methods fully equivalent based on the idea of "from atoms to molecule". J. Chem. Phys. **127**, 104106(15) (2007)
233. Kullie, O., Saue, T.: Range-separated density-functional theory: a 4-component relativistic study of the rare gas dimers He_2, Ne_2, Ar_2, Kr_2, Xe_2, Rn_2 and Uuo_2. Chem. Phys. **395**, 54–62 (2012)
234. Pitzer, K.S., Balasubramanian, K.: Properties of ten electronic states of diatomic lead from relativistic quantum calculations. J. Phys. Chem. **86**, 3068–3070 (1982)
235. Heaven, M.C., Miller, T.A., Bondybey, V.E.: Laser spectroscopy of lead molecules produced by laser vaporization. J. Phys. Chem. **87**, 2071–2075 (1983)

236. Hermann, A., Furthmüller, J., Gäggeler, H.W., Schwerdtfeger, P.: Spin-orbit effects in structural and electronic properties for the solid state of the group-14 elements from carbon to superheavy element 114. Phys. Rev. B **82**, 155116(8) (2010)
237. Pershina, V., Borschevsky, A., Anton, J., Jacob, T.: Theoretical predictions of trends in spectroscopic properties of gold containing dimers of the 6p and 7p elements and their adsorption on gold. J. Chem. Phys. **133**, 104304(10) (2010)
238. Rossbach, H., Eichler, B.: Adsorption von Metallen auf metallische Oberflächen und Möglichkeiten ihrer Nutzung in der Kernchemie, B, pp. 1–20. Akademie der Wissenschaft der DDR, Report No. ZFK-527 (1984)
239. Eichler, B., Kratz, J.V.: Electrochemical deposition of carrier-free radionuclides. Radiochim. Acta **88**, 475–482 (2000)
240. Pershina, V., Anton, J., Jacob, T.: Electronic structures and properties of MAu and MOH, where M = Tl and element 113. Chem. Phys. Lett. **480**, 157–160 (2009)
241. Fox-Beyer, B.S., van Wüllen, C.: Theoretical modelling of the adsorption of thallium and element 113 atoms on gold using two-component density functional methods with effective core potentials. Chem. Phys. **395**, 95–103 (2012)
242. Haenssler, F., Eichler, R., Gäggeler, H.W., Soverna, S., Dressler, R., Piguet, D., Schippering, M.: Thermochromatographic studies of ^{212}Pb on metal surfaces. PSI Annual Report 2005 (2006), p. 3; Eichler, R.: private communication
243. Saue, T., Faegri, K., Gropen, O.: Relativistic effects on the bonding of heavy and superheavy hydrogen halides. Chem. Phys. Lett. **263**, 360–366 (1996)
244. Seth, M., Schwerdtfeger, P., Faegri, K.: The chemistry of superheavy elements. III. Theoretical studies on element 113 compounds. J. Chem. Phys. **111**, 6422–6433 (1999)
245. Thierfelder, C., Schwerdtfeger, P., Kroes, A., Borschevsky, A., Fricke, B. Scalar relativistic and spin-orbit effects in closed-shell superheavy-element monohydrides. Phys. Rev. A **80**, 022501-1-10 (2009)
246. Han, Y.-K., Bae, C., Lee, Y.S.: Two-component calculations for the molecules containing superheavy elements: spin-orbit effects for (117)H, (113)H, and (113)F. J. Chem. Phys. **110**, 8969–8975 (1999)
247. Han, Y.-K., Bae, C., Son, S.-K., Lee, Y.S.: Spin–orbit effects on the transactinide p-block element monohydrides MH (M = element 113–118). J. Chem. Phys. **112**, 2684–2691 (2000)
248. Choi, Y.J., Han, Y.K., Lee, Y.S.: The convergence of spin–orbit configuration interaction calculations for TlH and 113H. J. Chem. Phys. **115**, 3448–3453 (2001)
249. Nash, C.S., Bursten, B.E.: Spin-orbit, VSEPR theory, and the electronic structure of heavy and superheavy group IVA hydrides and group VIIIA tetrafluorides. A partial role reversal for elements 114 and 118. J. Phys. Chem. A **103**, 402–410 (1999)
250. Balasubramanian, K.: Electronic states of the superheavy element 113 and (113)H. Chem. Phys. Lett. **361**, 397–404 (2002)
251. Vest, B., Klinkhammer, K., Thierfelder, C., Lein, M., Schwerdtfeger, P.: Kinetic and thermodynamic stability of the group 13 trihydrides. Inorg. Chem. **48**, 7953–7961 (2009)
252. Balasubramanian, K.: Breakdown of the singlet and triplet nature of electronic states of the superheavy element 114 dihydride ($114H_2$). J. Chem. Phys. **117**, 7426–7432 (2002)
253. Nash, C.S., Crockett, W.W.: An anomalous bond angle in $(116)H_2$. Theoretical evidence for supervalent hybridization. J. Phys. Chem. A **110**, 4619–4621 (2006)
254. Faegri, K., Saue, T.: Diatomic molecules between very heavy elements of group 13 and group 17: a study of relativistic effects on bonding. J. Chem. Phys. **115**, 2456–2464 (2001)
255. Schwerdtfeger, P.: Second-order Jahn—Teller distortions in group 17 fluorides EF_3 (E = Cl, Br, I, and At). Large relativistic bond angle changes in AtF_3. J. Phys. Chem. **100**, 2968–2973 (1996)
256. Seth, M., Faegri, K., Schwerdtfeger, P.: The stability of the oxidation state +4 in group 14 compounds from carbon to element 114. Angew. Chem. Int. Ed. Engl. **37**, 2493–2496 (1998)

257. Grant, I.P., Pyper, N.C.: Theoretical chemistry of superheavy elements E116 and E114. Nature **265**, 715–717 (1977)
258. van Wüllen, C., Langermann, N.: Gradients for two-component quasirelativistic methods. Application to dihalogenides of element 116. J. Chem. Phys. **126**, 114106(9) (2007)
259. Bae, C., Han, Y.-K., Lee, Y.S.: Spin–orbit and relativistic effects on structures and stabilities of group 17 fluorides EF_3 (E = I, At, and element 117): relativity induced stability for the D_{3h} structure of $(117)F_3$. J. Phys. Chem. A **107**, 852–858 (2003)
260. Malli, G.L.: Relativistic and electron correlation effects in molecules of heavy elements. In: Malli, G. (ed.) Relativistic and Electron Correlation Effects in Molecules and Solids, NATO ASI Series, vol. 318, pp. 1–15. Plenum, New York (1994)
261. Pitzer, K.S.: Fluorides of radon and element 118. J. Chem. Soc., Chem. Commun. 760–761 (1975)
262. Han, Y.K., Lee, Y.S.: Structure of RgF_4 (Rg = Xe, Rn, and element 118. $n = 2,4$) calculated by two-component spin-orbit methods. A spin-orbit inducted isomer of $(118)F_4$. J. Phys. Chem. A **103**, 1104–1108 (1999)
263. Nash, C.S., Bursten, B.E.: Spin-orbit coupling versus the VSEPR method: On the possibility of a nonplanar structure for the super-heavy noble gas tetrafluoride $(118)F_4$. Angew. Chem. Int. Ed. **38**, 151–153 (1999)
264. Bonchev, D., Kamenska, V.: Predicting the properties of the 113–120 transactinide elements. J. Phys. Chem. **85**, 1177–1186 (1981)
265. Schwerdtfeger, P.: Relativistic effects in molecular structure of s- and p-block elements. In: Domenicano, A., Hargittai, I. (eds.) Strength from Weakness: Structural Consequences of Weak Interactions in Molecules, Supermolecules, and Crystals, NATO Science Series, pp. 169–190. Kluwer, Dordrecht (2002)
266. Miranda, P.S., Mendes, A.P.S., Gomes, J.S., Alves, C. N., de Souza, A.R., Sambrano, J.R., Gargano, R., de Macedo, L.G.M.: *Ab initio* correlated all electron Dirac-Fock calculations for eka-francium fluoride (E119F). J. Braz. Chem. Soc., **23**, 1104–1113 (2012)
267. Pyykkö, P.: The physics behind chemistry and the periodic table. Chem. Rev. **112**, 371–284 (2012)
268. Pyykkö, P.: Predicting new, simple inorganic species by quantum-chemical calculations: some successes. Phys. Chem. Chem. Phys. **14**, 14734–14742 (2012)
269. Makhyoun, M.A.: On the electronic structure of $5g^1$ complexes of element 125: A quasi-relativistic MS-Xα study. J. Chim. Phys. **85**, 917–924 (1988)
270. Malli, G.L.: Dissociation energy of ekaplutonium fluoride E126F: The first diatomic with molecular spinors consisting of g atomic spinors. J. Chem. Phys. **124**, 071102(2) (2006)
271. Malli, G.L.: Thirty years of relativistic self-consistent field theory for molecules: Relativistic and electron correlation effects for atomic and molecular systems of transactinide superheavy elements up to ekaplutonium E126 with g-atomic spinors in the ground state configuration. Theor. Chem. Acc. **118**, 473–482 (2007)
272. Kadkhodayan, B., Türler, A., Gregorich, K.E., Baisden, P.A., Czerwinski, K.R., Eichler, B., Gäggeler, H.W., Hamilton, T.M., Jost, T.M., Kacher, C.D., Kovacs, A., Kreek, S.A., Lane, M.R., Mohar, M.F., Neu, M.P., Stoyer, N.J., Sylwester, E.R., Lee, D.M., Nurmia, M.J., Seaborg, G.T., Hoffman, D.C.: On-line chromatographic studies of chlorides of Rutherfordium and homologs Zr and Hf. Radiochim. Acta **72**, 169–178 (1996)
273. Türler, A.: Gas phase chemistrty experiments with transactinide elements. Radiochim. Acta **72**, 7–17 (1996)
274. Ionova, G.V., Pershina, V., Johnson, E., Fricke, B., Schädel, M.: Redox reactions for group 5 elements, including element 105, in aqueous solutions. J. Phys. Chem. **96**, 11096–11101 (1992)
275. Johnson, E., Fricke, B.: Prediction of some thermodynamic properties of selected compounds of element 104. J. Phys. Chem. **95**, 7082–7084 (1991)
276. Bratsch, S.G.: Standard electrode potentials and temperature coefficients in water at 298.15 K. J. Phys. Chem. Ref. Data **18**, 1–21 (1989)

277. Bratsch, S.G., Lagowski, J.J.: Actinide thermodynamic predictions. 3. Thermodynamics of compounds and aqua-ions of the 2+, 3+, and 4+ oxidation states and standard electrode potentials at 298.15 K. J. Phys. Chem. **90**, 307–312 (1986)
278. Ahrland, S., Liljenzin, J.O., Rydberg, J.: Solution chemistry. In: Bailar, J. (ed.) Comprehensive Inorganic Chemistry, vol. 5, pp. 519–542. Pergamon Press, Oxford (1973)
279. Baes Jr, C.F., Mesmer, R.E.: The Hydrolysis of Cations. John Wiley, New York (1976)
280. Kassiakoff, A., Harker, D.: The calculations of the ionization constants of inorganic oxygen acids from their structures. J. Am. Chem. Soc. **60**, 2047–2055 (1938)
281. Pershina, V.: Solution chemistry of element 105. Part I: Hydrolysis of group 5 cations: Nb, Ta, Ha and Pa. Radiochim. Acta **80**, 65–74 (1998)
282. Pershina, V.: Solution chemistry of element 105. Part II: Hydrolysis and complex formation of Nb, Ta, Ha and Pa in HCl solutions. Radiochim. Acta **80**, 75–84 (1998)
283. Pershina, V., Bastug, T.: Solution chemistry of element 105. Part III: Hydrolysis and complex formation of Nb, Ta, Db and Pa in HF and HBr solutions. Radiochim. Acta **84**, 79–84 (1999)
284. Pershina, V., Kratz, J.V.: Solution chemistry of element 106: theoretical predictions of hydrolysis of group 6 cations Mo, W, and Sg. Inorg. Chem. **40**, 776–780 (2001)
285. Pershina, V., Trubert, D., Le Naour, C., Kratz, J.V.: Theoretical predictions of hydrolysis and complex formation of group-4 elements Zr, Hf and Rf in HF and HCl solutions. Radiochim. Acta **90**, 869–877 (2002)
286. Pershina, V.: Theoretical treatment of the complexation of element 106, Sg in HF solutions. Radiochim. Acta **92**, 455–462 (2004)
287. Pershina, V.: Theoretical investigations of the reactivity of MO_4 and the electronic structure of $Na_2[MO_4(OH)_2]$, where M = Ru, Os, and Hs (element 108). Radiochim. Acta **93**, 373–376 (2005)
288. Pershina, V., Polakova, D., Omtvedt, J.P.: Theoretical predictions of complex formation of group-4 elements Zr, Hf, and Rf in H_2SO_4 solutions. Radiochim. Acta **94**, 407–414 (2006)
289. Kratz, J.V., Pershina, V.: Experimental and theoretical study of the chemistry of the heaviest elements. In: Hess, B.A. (ed.) Relativistic Effects in Heavy-Element Chemistry and Physics, pp. 219–244. Wiley, West Sussex (2003)
290. Czerwinski, K.R.: Studies of fundamental properties of rutherfordium (element 104) using organic complexing agents. Doctoral Thesis, LBL Berkeley (1992)
291. Strub, E., Kratz, J.V., Kronenberg, A., Nähler, A., Thörle, P., Zauner, S., Brüchle, W., Jäger, E., Schädel, M., Schausten. B., Schimpf, E., Zongwei, Li, Kirbach, U., Schumann, D., Jost, D., Türler, A., Asai, M., Nagame, Y., Sakara, M., Tsukada, K., Gäggeler, H.W., Glanz, J.P.: Fluoride complexation of rutherfordium (Rf, element 104). Radiochim. Acta **88**, 265–271 (2000)
292. Ishii, A., Toyoshima, A., Tsukada, K., Asai, M., Toume, H., Nishinaka, I., Nagame, Y., Miyashita, S., Mori, T., Suganuma, H., Haba, H., Sakamaki, M., Goto, M., Kudo, H., Akiyama, K., Oura, Y., Nakahara, H., Tashiro, Y., Shinohara, A., Schädel, M., Brüchle, W., Pershina, V., Kratz, J.V.: Fluoride complexation of element 104, rutherfordium (Rf), investigated by cation-exchange chromatography. Chem. Lett. **37**, 288–289 (2008)
293. Trubert, D., Le Naour, C., Hussonois, M., Brillard, L., Montroy Gutman, F., Le Du, J.F., Constantinescu, O., Barci, V., Weiss, B., Gasparro, J., Ardisson, G.: In: Abstracts of the 1st Intern. Conf. on Chemistry and Physics of the Transactinides, Seeheim, 26–30 Sept (1999)
294. Toyoshima, A., Haba, H., Tsukada, K., Asai, M., Akiyama, K., Goto, S., Ishii, Y., Nishinaka, I., Sato, T.K., Nagame, Y., Sato, W., Tani, Y., Hasegawa, H., Matsuo, K., Saika, D., Kitamoto, Y., Shinohara, A., Ito, M., Saito, J., Kudo, H., Yokoyama, A., Sakama, M., Sueki, K., Oura, Y., Nakahara, H., Schädel, M., Brüchle, W., Kratz, J.V.: Hexafluoro complex of rutherfordium in mixed HF/HNO_3 solutions. Radiochim. Acta **96**, 125–134 (2008)
295. Haba, H., Tsukada, K., Asai, M., Goto, S., Toyoshima, A., Nishinaka, I., Akiyama, K., Hirata, M., Ichikawa, S., Nagame, Y., Shoji, Y., Shigekawa, M., Koike, T., Iwasaki, M., Shinohara, A., Kaneko, T., Maruyama, T., Ono, S., Kudo, H., Oura, Y., Sueki, K.,

Nakahara, H., Sakama, M., Yokoyama, A., Kratz, J.V., Schädel, M., Brüchle, W.: Anion-exchange behavior of Rf in HCl and HNO_3 solutions. J. Nucl. Radiochem. Sci. **3**, 143–146 (2002)
296. Günther, R., Paulus, W., Kratz, J.V., Seibert, A., Thörle, P., Zauner, S., Brüchle, W., Jäger, E., Pershina, V., Schädel, M., Schausten, B., Schumann, D., Eichler, B., Gäggeler, H.W., Jost, D.T., Türler, A.: Chromatographic study of rutherfordium (element 104) in the system HCl/Tributylphosphate (TBP). Radiochim. Acta **80**, 121–128 (1998)
297. Haba, H., Tsukada, K., Asai, M., Toyoshima, A., Ishii, Y., Toume, H., Sato, T., Nishinaka, I., Ichikawa, T., Ichikawa, S., Nagame, Y., Sato, W., Matsuo, K., Kitamoto, Y., Tashiro, Y., Shinohara, A., Saito, J., Ito, M., Ikezawa, T., Sakamaki, M., Goto, S., Kudo, H., Kikunaga, H., Arai, M., Kamataki, S., Yokoyama, A., Akiyama, K., Sueki, K., Oura, Y., Schädel, M., Brüchle, W., Kratz, J.V.: Extraction behavior of rutherfordium into tributylphosphate from hydrochloric acid. Radiochim. Acta **95**, 1–6 (2007)
298. Omtvedt, J.P., Polyakova, D., Alstad, J., Bjornstad, T., Düllmann, C.E., Folden III, C.M., Garcia, M.A., Gates, J., Gregorich, K.E., Hoffman, D.C., Nelson, S.L., Nitsche, H., Omtwedt, L., Pershina, V., Samadani, F., Skarnemark, G., Stavsetra, L., Sudove, R., Wilson, R.E., Zheng, L., Zielinski, P.M. Radiochim. Acta, to be submitted
299. Li, Z.J., Toyoshima, A., Tsukada, K., Nagame, Y.: Ion-exchange behavior of Zr and Hf as homologues of element 104, Rf, in H_2SO_4 and $H_2SO_4/HClO_4$ mixed solutions. Radiochim. Acta **98**, 7–12 (2010)
300. Kratz, J.V., Zimmermann, H.P., Scherer, U.W., Schädel, M., Brüchle, W., Gregorich, K.E., Gannett, C.M., Hall, H.L., Henderson, R.A., Lee, D.M., Leyba, J.D., Nurmia, M., Hoffman, D.C., Gäggeler, H.W., Jost, D., Baltensperger, U., Ya Nai-Qi, Türler, A., Lienert, C.: Chemical properties of element 105 in aqueous solution: Halide complex formation and anion exchange into Triisoctyl amine. Radiochim. Acta **48**, 121–133 (1989)
301. Paulus, W., Kratz, J.V., Strub, E., Zauner, S., Brüchle, W., Pershina, V., Schädel, M., Schausten, B., Adams, J.L., Gregorich, K.E., Hoffman, D.C., Lane, M.R., Laue, C., Lee, D.M., McGrath, C.A., Shaughnessy, D.K., Strellis, D.A., Sylwester, E.R.: Chemical properties of element 105 in aqueous solution: extraction of the fluoride-, chloride-, and bromide complexes of the group-5 elements into an aliphatic amine. Radiochim. Acta **84**, 69–77 (1999)
302. Schädel, M., Brüchle, W., Jäger, E., Schausten, B., Wirth, G., Paulus, W., Günther, R., Eberhardt, K., Kratz, J.V., Seibert, A., Strub, E., Thörle, P., Trautmann, N., Waldek, W., Zauner, S., Schumann, D., Kirbach, U., Kubica, B., Misiak, R., Nagame, Y., Gregorich, K.E.: Aqueous chemistry of seaborgium ($Z = 106$). Radiochim. Acta **83**, 163–165 (1998)
303. Kronenberg, A.: Entwicklung einer online-Chromatographie für Element 106 (Seaborgium), Doctoral Thesis, University of Mainz (2001)
304. Pfrepper, G., Pfrepper, R., Kronenberg, A., Kratz, J.V., Nähler, A., Brüchle, W., Schädel, M.: Continuous on-line chromatography of short lived isotopes of tungsten as homolog of seaborgium (element 106). Radiochim. Acta **88**, 273–278 (2000)
305. von Zweidorf, A., Angert, R., Brüchle, W., Bürger, S., Eberhartdt, K., Eichler, R., Hummrich, H., Jäger, E., Kling, H.-O., Kratz, J.V., Kuczewski, B., Langrock, G., Mendel, M., Rieth, U., Schädel, M., Schausten, B., Schimpf, E., Thörle, P., Trautmann, N., Tsukada, K., Wiehl, N., Wirth, G.: Evidence for the formation of sodium hassate(VIII). Radiochim. Acta **92**, 855–861 (2004)
306. Caletka, R., Krivan, V.: Anion-exchage behaviour of some elements in HF-HCl medium. J. Radioanal. Nucl. Chem. **142**, 373–382 (1990)
307. Caletka, R., Krivan, V.: Behaviour of 18 elements in HF and HF-NH_4F media on anion exchanger in various ionic forms. J. Radioanal. Nucl. Chem. **142**, 359–371 (1990)
308. Markus, Y. (ed.): Solvent Extraction Reviews, vol. 5. Marcel Dekker, New York (1971)
309. Aylett, B.J.: Group IIB. In: Baylar; J.C. (ed.) Comprehensive Inorganic Chemistry, Vol. 3, pp. 187–328. Pergamon Press, Oxford (1973)
310. Abel, E.W.: Lead. In: Baylar, J.C. (ed.) Comprehensive Inorganic Chemistry, vol. 2, pp. 105–146. Pergamon Press, Oxford (1973)

Fundamental and Experimental Aspects of Single Atom-at-a-Time Chemistry

Claire Le Naour, Darleane C. Hoffman and Didier Trubert

Abstract Investigating the chemical properties of elements that are only produced one-atom-at-a-time raises questions about the validity of the chemical information obtained. Can kinetics and thermodynamics laws be applied when concentrations decrease to a few atoms? What is the meaning of chemical equilibrium with a single atom? An attempt to answer this fundamental question is presented using concepts of statistical thermodynamics and fluctuations theory, and the validity of some experiments on the heaviest actinides and transactinides in aqueous solutions is discussed. Experiments on transactinides are always performed in comparison with their most probable homologs. Such a comparison make sense if effects of the media (composition of electrolyte, ionic strength, temperature) are taken into account, regardless of the concentration of the element under study. Therefore, models that describe non-ideality in aqueous and organic solution are briefly discussed.

1 Introduction

Studies of the chemical properties of the heaviest actinides ($Z > 101$) and all of the transactinides ($Z > 103$), including superheavy elements (SHEs), depend on the use of atom-at-a-time chemistry. They cannot be produced by simple neutron

Didier Trubert was an author for the first edition of this chapter. Didier Trubert—deceased

C. Le Naour (✉) · D. Trubert
Institut de Physique Nucléaire, Orsay, France
e-mail: lenaour@ipno.in2p3.fr

D. C. Hoffman
University of California Berkeley, and Lawrence Berkeley National Laboratory, Berkeley, CA, USA

M. Schädel and D. Shaughnessy (eds.), *The Chemistry of Superheavy Elements*,
DOI: 10.1007/978-3-642-37466-1_4,

capture in reactors and must be synthesized at suitable accelerators using various charged particle induced nuclear reactions; see "Synthesis of Superheavy Elements". The production rates and half-lives decrease rapidly as one goes to higher atomic numbers and more neutron-deficient isotopes. Therefore, chemical experiments must be performed with a few atoms or even a single-atom-at-a-time.

A rather comprehensive summary [1] has been published of the reported discoveries, confirmation, and nuclear properties of the claimed and confirmed transactinide elements with primary emphasis on their chemical properties—experimental, theoretical, and predicted—as of the end of the year 2004. At that time, the elements through 111 (roentgenium, Rg) had been confirmed and named. Subsequently, discovery of element 112 was confirmed by IUPAC and the name copernicium (symbol Cn) was approved in early 2011 [2]. Most recently, the discovery and the proposed names of elements 114 (flerovium, Fl) and 116 (livermorium, Lv) have been accepted [3].

It was emphasized in [1] that the nuclear decay properties of the isotope to be used in these studies must be well known and have unique decay characteristics suitable for detection and positive identification on an 'atom-at-a-time' basis in order to verify that it is from the element whose chemistry is to be studied! It must have a half-life comparable to the proposed chemical separation procedure as well as a 'reasonable' production and detection rate to permit statistically significant results to be obtained, and must give the same results for a few atoms as for macro amounts. For the transactinide elements, production rates range from a few atoms per minute for rutherfordium (Rf, $Z = 104$) to only about one atom per day in the case of elements 108 (hassium, Hs), 112, and 114, the heaviest elements studied to date with chemical techniques. Details of these chemical investigations are outlined in "Liquid-Phase Chemistry of Superheavy Elements" and "Gas-Phase Chemistry of SuperheavyElements".

Not only must we consider whether the concepts of thermodynamics and kinetics used in "classical" chemistry are still valid at such low concentrations, but we must consider whether the chemical information deduced from experiments with a single atom make sense. And how many atoms must be identified to be statistically significant for discovery for confirmation or conversely, even for non-confirmation of a discovery? In many previously reported experiments, positive identification of the element being studied was not established. Without such identification the experiments are meaningless. This is especially difficult (if not impossible) in case of the detection of only spontaneous fission (SF), which effectively destroys information about the fissioning nuclide except for its half-life.

Adloff and Guillaumont [4] considered the validity of results obtained from a very small number of atoms and concluded that results from chemical procedures with fast kinetics in which single atoms undergo many identical chemical reactions between 2-phase systems can be combined to give valid results. Ion-exchange and gas chromatography, and solvent extractions are examples of such systems. And, of course, the chemistry must be fast enough to be accomplished in times comparable to the half-life of the radionuclide being investigated.

Quoting from Ref. [4], "The terminology of the concentration range is rather vague." However, tracer scale usually covers element concentrations ranging from 10^{-10} to 10^{-16} M [4]. At such low concentrations, the number of entities present in 1 cm^3 lies between 10^{10} and 10^4. This number is large enough to apply the law of mass action without any restriction, providing the relevant reaction is kinetically allowed. Thus, because the law of mass action applies, the behavior of the micro-component is expected to be the same at normal concentration and at the tracer scale. In ultra-dilute systems (sub-tracer scale, 10^{-17} to 10^{-20} M), the thermodynamic behavior of an element does not depend on concentrations. However, some discrepancies can occur in particular cases, e.g., as a result of the different degrees of consumption of ligands leading to unusual complexation reactions or in unexpected redox processes [5]. Tracer-scale chemistry is also characterized by a kinetic hindrance for reactions between two micro-components in a given system. This trend excludes polymerization reactions or disproportionation for ultra-trace chemistry.

The aim of the present chapter is to describe what happens when the concentration of the micro-component decreases to some tens of atoms and finally to the ultimate limit of dilution: a single atom. In the following considerations, only reactions of a micro-component with a macro-component will be treated, as they constituted the general case for SHE chemistry.

This chapter is divided into four parts. The first describes results of some previous experiments involving only a few atoms-at-a-time for actinides with $Z > 100$ and the transactinides, i.e., all elements beyond $Z = 103$, beginning with rutherfordium (Rf, element 104). The second deals with kinetic and thermodynamic aspects of the chemistry from tracer to single atom scale. The third, in an illustrative way, concerns experimental approaches. Finally, the effects of the media used and their influence on aqueous phase chemistry will be discussed.

2 Historical Experiments with a Few Atoms

2.1 Discovery and Identification of Mendelevium: A Landmark Experiment

The discovery and identification of element 101 (mendelevium, Md) was a landmark experiment in many ways [1]. It was the first new transuranium element to be produced and identified on the basis of "one-atom-at-a-time" chemistry and it is also the heaviest element (to date) to be chemically identified by direct chemical separation of the element itself. All of the higher Z elements have been first identified by physical/nuclear techniques prior to study of their chemical properties. In fact, one of the criteria for chemical studies is that an isotope with known properties be used for positive identification of the element being studied. Due to relativistic effects [1] chemical properties cannot be reliably predicted and a meaningful study of chemical properties cannot be conducted with *both unknown chemistry and unknown, non-specific nuclear decay properties!*

The discovery of mendelevium was announced and published by Ghiorso, Harvey, Choppin, Thompson, and Seaborg in the Physical Review in 1955 based on detection of a *total of only 17 atoms* [6]. The highly radioactive target, 20 day ^{253}Es, consisted of only about 10^9 atoms and the Md atoms recoiling from the thin target were collected on a catcher foil, which was then removed and dissolved, thus avoiding the necessity of dissolving the precious and highly radioactive target. This was the first use of the recoil technique in the discovery of a new transuranium element; see "Experimental Techniques" for today's use of this technique in SHE chemistry. The Md was separated and chemically identified by its elution from a pre-calibrated cation exchange resin column.

An interesting note is that although this was during the height of the 'cold war' between Russia and the USA, the discoverers at the suggestion of Albert Ghiorso, stated in the discovery paper, "We would like to suggest the name Mendeleev, symbol Mv, for the new element in recognition of the pioneering role of the great Russian chemist, Dmitri Mendeleev, who was the first to use the periodic system of the elements to predict the chemical properties of undiscovered elements, a principle which has been a key to the discovery of the last seven transuranium (actinide) elements". The schematic diagram of the experiment shown in Fig. 1 appeared shortly thereafter in 1955 in the Russian publication Piroda. Later experiments conducted on thousands of atoms confirmed the validity of the original conclusions [1].

2.2 Some Examples of Atom-at-a-Time Investigations of Chemical Properties

Isotopes of heaviest actinides and transactinides are characterized by short half-lives and low production cross sections; see "Synthesis of Superheavy Elements". Study of their chemical properties is therefore a real challenge [1, 7]. It should be

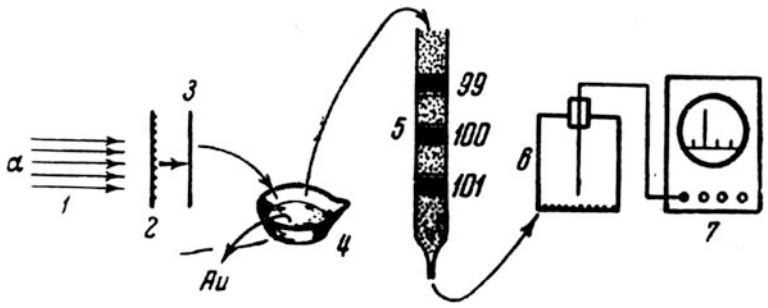

Fig. 1 Schematic diagram from Piroda, 1955. The helium atoms (1) strike the gold target with Es-253 on the back side (2), recoiling product atoms are collected on the gold catcher foil (3), 'symbolically' dissolved in crucible (4) and separated on a pre-calibrated ion-exchange column (5) and measured in the detection and recording system (6), and (7)

noted that although detection is performed on an atom-at-a-time basis, in experiments with heavy actinides there are usually many more atoms than just one single atom present in the system under study. This situation becomes different for SHEs where, from element 106 (seaborgium, Sg) on, the atom-at-a-time situation is the case for any chemical system. On one hand, alpha emitters are produced simultaneously to the transactinide and could interfere in the final detection. On the other hand, dissolution of reaction products is performed in aqueous medium of specific composition and ionic strength that governs the speciation of the elements under study (see "Effects of the Media"). Performing experiments with these elements requires knowledge, not only on the chemical properties of homologs but also on the nuclear decay properties of the studied isotope.

Since the 1970 s, increasingly precise properties of SHEs have been investigated with increasingly sophisticated systems. The first property that was determined in aqueous solution was the most stable oxidation state. Then the behavior of the SHE was carefully compared with that of its most probable homologs and conclusions have been drawn about the relative extractability or adsorbability. Finally, quantitative data on SHE (distribution ratios) are now available in the literature [7].

The complexation of ^{261}Rf in hydrochloric medium was investigated by Hulet et al., using extraction chromatography [8]. It was the first experiment conducted with a fully automated apparatus that allows numerous identical chemical steps to be performed. In 12 M HCl, unlike the trivalent actinides, Rf and its homolog Hf were strongly retained on the column filled with a quaternary amine deposited on fluorocarbon powder. Based on the detection of six events, the similarity of chlorocomplexes of Hf and Rf and their difference from the trivalent actinides Cm and Fm was clearly demonstrated [8].

The first experiment on Db in aqueous solution was performed with the isotope 34-s ^{262}Db produced in the ^{249}Bk(^{18}O,5n) reaction [9]. Reaction products, attached to KCl aerosols, were transferred via a He-jet system and were collected on a glass plate during 60 s. The KCl spot was fumed twice with concentrated nitric acid, washed with 1.5 M HNO_3, dried and finally, the glass plate was placed on a detector for α spectroscopy and SF counting. 801 identical adsorption experiments were performed manually. The detection of 24 events, attributed to ^{262}Db and its daughter allowed Gregorich et al. to conclude that Db displays a property that is characteristic of group 5 elements (Nb, Ta), i.e., strong sorption on glass in concentrated nitric acid unlike group 4 elements and trivalent actinides.

The chemical information deduced from these experiments, illustrative of one-atom-at-a-time chemistry, appears reliable. Intuitively, the numerous repetitive experiments give statistically significant results; see "Liquid-Phase Chemistry of SuperheavyElements" and "Gas-Phase Chemistry of Superheavy Elements" for a comprehensive report of SHE chemistry experiments in the liquid-phase and gas-phase, respectively. The next paragraph will provide proof that kinetics and thermodynamics are valid at the atom scale for most chemical reactions performed with SHEs.

3 Kinetic and Thermodynamics Aspects of Single-Atom Chemistry

Among topics included in radiochemistry, are the chemical properties of radioactive matter in unweighable quantities covering the range from tracer scale or tracer level ($C < 10^{-10}$ M) to a few atoms (sub-tracer level) and even to one single atom in the case of SHEs. In such conditions, the radionuclide M at tracer scale can be considered as the micro-component, whereas components that are not significantly consumed during the course of reactions with M are macro-components [4]. Since single-atom chemistry can be regarded as the limiting case of tracer-scale chemistry, the fundamental aspects of kinetics and thermodynamics of tracer-scale chemistry will be described first.

3.1 Kinetics

In the following, dilution effects on kinetics are illustrated with an elementary reaction of the second order:

$$E_1 + E_2 \underset{k_-}{\overset{k_+}{\rightleftharpoons}} E_3 + E_4 \tag{1}$$

where k_+ and k_- are the forward and backward rate constants, respectively.

The general rate law associated to Eq. 1 is:

$$v = k_+[E_1][E_2] - k_-[E_3][E_4] \tag{2}$$

The mathematical resolution of this equation is rather complicated and can be found in [4, 10]. Assuming $[E_1] = [E_2] = C_0$ at time 0, and neglecting back reaction ($k_+ \gg k_-$), reaction half-time $t_{1/2}$ of the reaction is simply:

$$t_{1/2} = \frac{1}{k_+ C_0} \tag{3}$$

According to Eq. 3, a decrease in the concentration of the species E_1 and E_2 by a factor 10^{-n} increases the reaction half-time by 10^n. A reaction that is fast at macroscopic concentrations becomes too slow to be observed at tracer level. Thus, reactions between two micro-components cannot be observed at the time scale of laboratory experiments. Since the probability of encounter between two species at tracer scale is very low, they coexist in the same state as when they were introduced into the solution. Disproportionation and polymerization reactions are therefore excluded.

The spatial expansion of the system under study must also be considered. For instance, Guillaumont and Adloff, considering disproportionation of Pu(V) from a theoretical point of view, have shown that for 100 atoms of Pu, assuming a very

fast reaction rate ($k = 10^{11}$ M s^{-1}), the half-time $t_{1/2}$ is equal to 50 μs and 1.6 y in a volume of 1 μl and 1 cm^3, respectively [11]. Obviously, a decrease in the rate constant would yield much longer reaction times. Summarizing, the reaction rate of a given number of atoms of a micro-component decreases drastically with the spatial expansion of the system in which they are contained, i.e., the number of atoms per volume unit. Therefore, at critical concentrations, micro-micro-component kinetics prevails largely over thermodynamics in a reaction.

In a reaction between a micro-component and a macro-component, there is no significant consumption of the latter. The rate law associated to the reaction

$$E_1^{\text{micro}} + E_2^{\text{macro}} \underset{\leftarrow}{\rightarrow} E_1E_2 \tag{4}$$

can be written as:

$$\frac{\mathrm{d}[E_1^{\text{micro}}]}{\mathrm{d}t} = -k[E_1^{\text{micro}}][E_2^{\text{macro}}] = k'[E_1^{\text{micro}}] \tag{5}$$

where k' stands for a conditional rate constant.

According to Eq. 5, a reaction between a micro- and a macro-component is always pseudo-first order with respect to the micro-component: the half-time $t_{1/2}$ does not depend on the initial concentration. Hence, the only kinetics data that can be reached at extreme dilution are those related to reactions between the micro-component and a macro-component. Hydrolysis and complexation, central topics in the liquid-phase chemistry of SHEs, belong to this class of reaction.

However, reactions between E_1 and E_2 can only be observed if the half-life of E_1 is compatible with the time characteristics of the reaction under study. For instance, the time needed to achieve the equilibrium must be shorter than the lifetime of the involved radionuclide. Studies of the chemical properties of SHEs give rise not only to the concept of single-atom chemistry but also to one-atom-at-a-time chemistry. For that purpose, chemical processes with high reaction rates are required.

Borg and Dienes [12] have attempted to show the validity of single-atom chemistry from a kinetics point of view using activated complex theory combined with the frequency of exchange between entities. According to this theory, the reaction between species E1 and E2 proceeds via the formation of a cluster of reactant molecules (transition state) that corresponds to a maximum of potential energy [10, 12, 13]. This approach has led to the conclusion that the equilibrium cannot be reached if the activation energy is greater than about 85 kJ. However, the concepts developed in Borg's work are only valid for large numbers of atoms. Energies of activated complexes can only be used for sufficiently high quantities since this concept involves energies estimated from statistical values. Applying a Maxwell–Boltzmann distribution requires that an individual atom or species can acquire energy levels quite different from its most probable or mean values [10, 14]. This fundamental concept forms the basis of the fluctuation theory that is not taken into account in classical thermodynamics and kinetics. Partition functions introduced in statistical thermodynamics and described in the following part, allow fluctuations to be considered.

For the development of concepts of kinetics and of thermodynamics considered in this chapter, the single atom was assumed to be stable. In fact, the probability for a unique atom to exist in specific "specie" can only be determined in a chemical experiment if the atom is radioactive. Therefore, if the atom is stable or has a large half-life, any radiochemical techniques can be used for single-atom chemistry.

The concept of "one-atom-at-a-time chemistry" is different from that of a single-atom chemistry. The main difference is the time. An "observable" chemical reaction of a given radio nuclide can be defined with the following temporal quantities:

$T_{1/2}$: half-life of the radionuclide
t: time necessary for reactants to compete
τ: half-time of equilibrium or steady state chemical reaction
Δt: time for collecting data
A reaction will be observable if: $T_{1/2} > t > \tau > \Delta t$
At the experimental scale, τ and t are macroscopically related.

Problems associated with the disintegration of a single radioactive atom will not be developed here However, an understanding of the decay appears rather important in one-atom-at-a-time chemistry [4, 15].

3.2 Thermodynamics

Let's consider a chemical reaction involving micro-components (m). Since reactions involving the formation of polynuclear compounds are excluded, only the reactions where the stoichiometric coefficient of the micro-component (m) is equal to unity will be examined.

The reaction can be written in the general form:

$$\sum_{i=0}^{i} E_{i(m)} + \sum_{i=0,j=0}^{i,j} \nu_{iMj} E_{iMj} = 0 \tag{6}$$

where ν_i are the stoichiometric coefficients (positive for adducts and negative for products) and M_j denotes the macro-component. In classical thermodynamics, the corresponding law of mass action that defines the relationship between the number of moles of reactants and products is:

$$\prod a_i^{\nu_i} = K \quad \text{and} \quad \Delta G_0 = -RT \ \mathrm{Ln}(K) \tag{7}$$

where K is the equilibrium constant and a_i is the thermodynamical activity of each entity (macro- and micro-component) involved in the equilibrium. Equation 7 can also be expressed in terms of concentrations (corrected with activity coefficients).

However, on one hand, classical thermodynamics of bulk sample stands for the average behavior of a large number of molecules N; macroscopic properties of chemical systems (Gibbs energy, enthalpy variation) deduced from the application of the law of mass action involve therefore high values of N. In these conditions, fluctuations around average values are negligible. On the other hand, thermodynamic functions can be calculated using Boltzmann distribution and canonical partition function. These fundamental notions are introduced in statistical thermodynamics for the description of N molecules in interaction [10, 14].

A macroscopic state of a system is namely considered as a distribution of molecules over fixed energy states: among N molecules, n_1 display energy ε_1, n_2 energy ε_2, n_3 energy ε_3, and so on. For a closed system with N molecules without interaction, the most probable distribution of molecules over the different energy levels is given by a Boltzmann distribution (Eq. 8) that requires the use of the Stirling approximation valid up to N higher than 10.

$$\frac{n_i}{N} = \frac{e^{\frac{-\varepsilon i}{kT}}}{\sum_i e^{\frac{-\varepsilon i}{kT}}} \tag{8}$$

In Eq. 8, the denominator, named z, stands for the molecular partition function. It can be rigorously calculated for simple molecules using experimental spectroscopic data and is related to the average number of states that are accessible to a molecule at a given temperature.

In statistical thermodynamics, a system with interacting particles is depicted with the canonical ensemble that describes a collection of a large number of macroscopic systems under identical conditions (for instance, N particles in a volume V at temperature T). In each system, laws that describe interactions between molecules are identical. They differ by the coordinates of each particular molecule corresponding to a microstate. The static picture of the canonical ensemble is equivalent to the development of a system over time [10, 14]. In other words, the measurement of a macroscopic property reflects a succession of microstates. Thus, the measured property corresponds to a time-averaged mean value and thermodynamic equilibrium corresponds to the most probable macroscopic state.

Similarly to Eq. 8, the most probable configuration for the ensemble composed by $\tilde{N}$ identical systems is given by the canonical distribution:

$$\frac{\tilde{n}_i}{\tilde{N}} = \frac{e^{\frac{-Ei}{kT}}}{\sum_j e^{\frac{-Ej}{kT}}} \tag{9}$$

where the denominator Z stands for the canonical partition function. The fraction of members of the canonical ensemble in a state i at energy E_i can be written as:

$$p_i(N, V, T) = \frac{e^{\frac{-Ei}{kT}}}{Z(N, V, T)} \tag{10}$$

The canonical partition function Z in statistical thermodynamics is fundamental since it is related to thermodynamic parameters like enthalpy and Gibbs energy. For instance, the Gibbs free energy is given by:

$$G - G(0) = -kT \ln Z + kTV \left(\frac{\partial \ln Z}{\partial V} \right)_T \tag{11}$$

When the number of atoms decreases to a few tens of atoms and a fortiori to one atom, the canonical distribution of energy becomes asymmetric and broad [14]. Thus, the most probable energy that corresponds to the state of equilibrium can differ significantly from the mean energy. These deviations from equilibrium, called fluctuations, are not considered in classical thermodynamics since the latter deals only with average quantities. However, it has been demonstrated that second derivatives of thermodynamic functions are connected with fluctuations in energy [14]. Concerning statistical thermodynamics, the Boltzmann distribution predicts that a system may possess an energy different from its most probable value. Fluctuations are therefore taken into account and, in principle, the concept of partition function can be used to express the law of mass action.

Peneloux and Guillaumont introduce this concept for the description of chemical equilibrium in highly diluted system in a short note in 1990 [16]. Then, this approach has been developed in a more detailed way [4, 5]. The aim is to compare the classical expression of an equilibrium constant K related to a large number of species, with the one expressed in terms of average concentration in the case of a few atoms. For that purpose, Guillaumont et al. express partition functions for a single species, for several species involving the same micro-component and for all species that may involve several micro-components, in ideal and real systems. The canonical distribution of quantum states of the system is separated in two parts: one related to micro-components, the other to the macro-components. Then, the average numbers of micro-components involved in the expression of K have been calculated.

The general equations of partition function and canonical distribution have been applied to a reaction of stoichiometry 1–1, which is the case encountered in transactinide chemistry. Guillaumont et al. demonstrated that only in this case, the law of mass action holds, regardless of the number of present species, if the mean concentrations are used. However, when less than hundred atoms are involved in a reaction with a stoichiometry different from 1–1, deviations from the law of mass action can occur. For instance, in highly diluted solution, disproportionation of Pu(IV) and oxidation of U(IV) with Fe(III) have been proved to display an erratic behavior with respect to the law of mass action. Thus, there is no general solution to describe the average populations when few atoms participate in a chemical reaction with a stoichiometry different from 1–1 [4, 5].

In the case of a single atom, the reaction to be considered, derived from Eq. 6 is simply: $E_1 + E_2 = 0$. During the course of reaction, the atom is distributed between species E_1 and E_2. The canonical probability for the single atom to appear in species E_1 or in species E_2 is proportional to the mean concentrations of both

types of species. Therefore, the law of mass action is still valid. Moreover, in a case of a radioactive atom, the half-life must be large enough to allow the occupation of all quantum states corresponding to the different degrees of freedom of each entity. This condition is fulfilled since, generally, the residing times are very short. A dynamic equilibrium is supposed to take place and the entities have time to occupy the energy states of the system.

3.3 Concluding Remarks on Fundamental Aspects of Single-Atom Chemistry

Since the SHE chemistry is correlated with one-atom-at-a-time chemistry, one may ask if it is meaningful to carry out experiments with a single atom. From a theoretical point of view, as was demonstrated above, for a 1:1 stoichiometry reaction the law of mass action and the kinetics laws are valid. However, as there is no macro-component consumption, such a reaction appears as of pseudo-first order. Note that reactions with a 1–1 stoichiometry include all reactions between the micro-component and a single macro-component. This concept can also be extended to stepwise reactions such as the successive formation of metal complexes (hydrolysis, halide complexation); for example:

$$\begin{aligned} &M(H_2O)_x^{n+} + OH^- \leftrightarrows MOH(H_2O)_{x-1}^{(n-1)+} \\ &MOH(H_2O)_{x-y}^{(n-y)+} + OH^- \leftrightarrows MOH(H_2O)_{x-y-1}^{(n-y-1)+} \end{aligned} \tag{12}$$

For higher stoichiometry, these concepts are no longer valid, both for thermodynamics and for kinetics reasons, and each case becomes a particular case seeking its own solution.

All of the theoretical considerations outlined above have been established assuming an "ideal system" without any boundary conditions. It should be pointed out, however, that in practice, all the studied systems, especially in SHE chemistry, have finite dimensions (time and volume). As only ideal system were considered, edge effects, pseudo-colloid formation, sorption phenomena, redox processes with impurities or surfaces, medium effects, etc., have not been taken into account. All these effects, representing the most important part from the deviation from ideality, cannot be predicted with formal thermodynamics and/or kinetics. Thus, radiochemists who intend to perform experiments at the scale of one atom must be aware that the presence of any solid phase (walls of capillary tubes, vessels, etc.) can perturb the experimental system. It is important to check that these edge effects are negligible at tracer levels before performing experiments on the scale of an atom [4, 5]. The following section describes experimental techniques used in SHE chemistry; see "Liquid-Phase Chemistry of Superheavy Elements" and "Gas-Phase Chemistry of Superheavy Elements" for a detailed discussion of SHE chemistry experiments and "Experimental Techniques" for more technical aspects.

4 Experimental Approaches

Prior to experiments with SHE, systematic studies with their most probable homologs at the tracer scale must be carried out to select the experimental conditions (solvent extraction, ion exchanger, aqueous media, gas-phase chromatography columns, etc.). On-line experiments with short-lived isotopes of homologs are also necessary to improve the setup, e.g., to evaluate the eventual impact of edge effects (sorption, etc.) [1, 7]. To ensure strictly identical experimental procedures with transactinides and their homologs, e.g., experiments on 78-s ^{261}Rf and 34-s ^{262}Db have been performed with mixed targets: Gd (often enriched ^{152}Gd or ^{154}Gd) was added to ^{248}Cm for the simultaneous production of 3.29 min ^{169}Hf and 2 min ^{168}Ta, respectively [17, 18]. Similar procedures were applied in chemical studies of Sg, Bh, and Hs. Consequently, a careful comparison with on-line and off-line experiments involving homologs at the tracer scale may allow to draw conclusions about the occurrence—or absence—of edge and sorption effects.

In principle, chemical information on a system can only be obtained with methods that do not alter the species present in solution. However, in order to get this information, an external perturbation must be applied to the system and its response must be analyzed. In the case of radioactive tracer, where the radioactivity measurement is the only way to detect the element (but it does not allow the identification of the form of the species), two types of external perturbation can be applied [4]:

1. by contacting the system with a second phase and subsequently observing the distribution of the radionuclides between the two phases (static or dynamic partition) or
2. by applying an electrical potential or a chemical gradient (transport methods). So far, transport methods have not yet been used in one-atom-at-a-time chemistry since they are not only difficult to carry out but also extremely time consuming.

The aim of a partition experiment, regardless of the concentration involved, is the determination of the partition ratio (K_d) of an element between two phases. For this purpose, measurements of average concentrations of the entities present in each phase have to be performed. Although partition methods are widely used in the field of radiochemistry, chemical properties can only be determined through the variations of K_d with characteristic parameters of the system (ionic strength, ligand concentrations, acidity, temperature, etc.). In the case of a few atoms, it has been shown that the law of mass action involves probabilities for the atom to form a given species in a given phase. Obviously for a single atom, the distribution coefficient is defined in terms of a probability for the element to be in one phase or in the other. This means that measurements must be conducted with the whole phase since the system contains only one entity.

4.1 Static Partition

In a static partition, the atom (necessarily radioactive in the present context) is distributed between two immiscible phases (liquid and/or solid). Since this procedure is sequential, the accuracy in the measurement of the average concentrations increases with the number of trials. For a given system, under given conditions, the determination of one partition ratio requires numerous repetitive experiments, even for the more simple case involving only one chemical species in each phase. The experimental conditions must always ensure that at the end of the experiment, the atom has reached permanent partition equilibrium between the two phases. Moreover, the short half-life of the nucleus must not bring any perturbation since there is only one alternative: either the measurement indicates in which phase the atom is, to ensure this often both phases need to be assayed, or the atom has disintegrated before the measurement and no information is obtained.

Among the static partition techniques, solvent extraction was the most frequently used for heavy elements studies. For instance, experiments involving the two heaviest actinides: ^{255}No ($T_{1/2} = 3.1$ min) and ^{256}Lr ($T_{1/2} = 26$ s) have been performed using extraction with a mixture of TTA/MIBK [19] or with HDEHP [20]. The collection of the short-lived isotopes as well as extraction steps took a few tens of seconds. In a single experiment with Lr, a sample of about ten atoms was available, of which only a tenth remained for detection at the end of the experiment. A statistically reliable result was obtained by performing about 200 identical partition experiments in the presence of trivalent actinides and divalent alkaline earths at tracer scale (e.g., ^{85}Sr, ^{133}Ba, ^{243}Am). The *pH* dependence of extraction of No and Lr, as compared to trivalent actinides and alkaline earths, allowed Silva et al. to draw reliable conclusion about the stable oxidation state of these elements that can only be produced at the scale of a few atoms.

Conversely, experiments on 78-s ^{261}Rf involving extraction with TBP from hydrochloric solution, have led to questionable results because of sorption onto Teflon catchers used in on-line experiments and observed with Hf [21, 22]. Moreover, in the Rf study only the organic phase was analyzed, which contradicts the basic principle mentioned above.

If solvent extraction and ion exchange batch experiments are commonly considered as multi-step procedures, allowing, therefore, the collection of information on the chemical properties of a micro-component, the same conclusion concerning coprecipitation reactions cannot be drawn systematically. The term "coprecipitation" has no precise meaning since it involves many phenomena as syncrystallization (homogeneous incorporation of a micro-component in the lattice of an isomorphous macro-compound), adsorption (chemisorption, electrostatic adsorption), and surface precipitation [4]. When dealing with a few atoms, syncrystallization is strongly hindered. In case of sorption, even if a multi-step mechanism (frequent and rapid sorption—desorption steps) is involved, this technique depends strongly on to many experimental parameters to allow reproducible results. These factors are related to the properties of the solid (surface charge, grain size) and of

the electrolyte solution (ion nature, proton concentration, etc.): especially, the isoelectric point of the solid [23] that determines the sorption properties is strongly correlated with the *pH*. In view of the numerous experimental conditions to reproduce and to parameterize, a distribution coefficient can hardly be formulated [4]. Reischmann et al. [24, 25] have studied the influence of $^{210,\ 218}$Po concentration (10^8 to 40 atoms) on "coprecipitation" with tellurium and arsenic sulfide. Although no evidence for a concentration-dependent behavior of Po was observed, no chemical information can be derived from these experiments.

However, at tracer level, coprecipitation—even if the mechanism remains unknown—is a convenient method for the separation or concentration of different species. The coprecipitation of carrier free Tc and Re with Ph_4AsReO_4 in HNO_3/HF media was used successfully as an additional separation step of these group 7 elements from Nb and Ta [26]. At the same time, the precipitate was used to prepare an alpha source.

4.2 Dynamic Partition

A dynamic partition can be considered as a succession of static partitions. In other words, such partition is characterized by a large number of successive equilibria, governed as a first approximation, by the same constant K_d. In this type of experiments, the displacement of the species, controlled by the K_d, is directly related to the probability of the presence of the atom in the mobile phase. In a single experiment, a significant result can be obtained since it is on its own purely statistical. Techniques—in which dynamic partitions are performed—such as extraction (reverse phase) chromatography, elution ion exchange chromatography, isothermal gas-phase chromatography, and thermochromatography (the latter two are out of the scope of this chapter—see "Experimental Techniques" and "Gas-Phase Chemistry of SuperheavyElements"), are particularly suitable for one-atom-at-a-time chemistry. In solution chromatography, the atom can be observed in a well-defined elution fraction, implying that the position of the elution band can be determined with a single atom.

Extraction chromatography experiments involving the extractant TBP on an inert support have been performed on ^{261}Rf produced in ^{248}Cm(^{18}O,5n) reaction [27]. Numerous preliminary experiments on homologs have been conducted: off-line batch liquid–liquid extraction involving TPB in benzene as organic phase with homologs (^{95}Zr, ^{175}Hf), on-line extraction chromatography with 31-s ^{98}Zr and 3.25 min ^{169}Hf with the Automated Rapid Chemistry Apparatus (ARCA). Based on the results collected with homologs and on 1140 identical experiments including sorption of ^{261}Rf from 12 M HCl on TBP/Voltalef, and elution with 8 M and 2 M HCl, Günther et al. concluded to the extraction sequence Zr > Rf > Hf; see "Hydrolysis Versus Halide Complexation: Studies Using Liquid–Liquid Extraction and Extraction Chromatography Techniques".

Ion exchange chromatography was the technique used for the first chemical experiment on Sg in aqueous solution [28]. A preliminary study on the behavior of groups 4, 5, and 6 as well as trivalent elements was conducted both off- and on-line. The isotope ^{265}Sg was produced by irradiation of ^{248}Cm with Ne ions. 3900 identical separations in a mixture HNO_3/HF were performed with ARCA II and a careful analysis of the observed α-events was conducted. The stability of the +6 oxidation state of Sg and a behavior similar to the one of Mo and W were demonstrated unambiguously; see "Seaborgium (Sg, Element 106)" for more details on the Sg chemistry and "Seaborgium (Sg, Element 106)" for a footnote on an erroneous assignment of spontaneous fission events to ^{266}Sg.

These two illustrative works exemplify not only the SHE chemistry at the one-atom-at-a-time scale, but also the behavior of homologs in batch and on-line experiments. From their results, no concentration-dependant behavior was observed, validating, therefore, the methods used and the conclusions drawn on the chemical behavior of SHE. To go further in this topic, extensive research was conducted using the same chemical techniques in order to get quantitative data. For instance, Nagame et al., conducted experiments with the Automated Ion-exchange separation apparatus coupled with the Detection system for Alpha spectroscopy, AIDA (modified ARCA) that allows chromatographic separations and detection of α-particles to be performed automatically [17]. Batch experiments with ^{88}Zr, ^{175}Hf, ^{234}Th at the tracer scale, followed by on-line experiments with ^{85}Zr and ^{169}Hf, and, finally, on-line experiments with ^{261}Rf and ^{169}Hf, simultaneously, have been performed in order to get information about the adsorption behavior of Rf on anion exchangers as a function of HCl, HNO_3, and HF concentrations. The stability of the chloride complex MCl_6^{2-} in HCl > 8 M, was found to be Rf ≥ Zr > Hf. In HF media, adsorption of Rf was found to be weaker than that of Hf and Zr. In view of the numerous preliminary experiments conducted with homologs, sorption, edge, and concentration effects can be eliminated. Moreover, the studied reaction corresponds to a stoichiometry (1–1) as described in Eq. 12, and the law of mass action is valid whatever the number of atoms. Thus, results obtained with Rf can be considered reliable. Other quantitative data for Rf involving the same type of preliminary experiments with homologs are available in the literature: distribution ratios (K_d) of Rf and Hf in diluted HNO_3 [28] and in mixture HF/HNO_3 [29, 30] have been determined from ion exchange experiments; see "Rutherfordium (Rf, Element 104)".

The feasibility of K_d determinations in the context of one-atom-at-a-time chemistry is very promising and the collection of K_d values will allow establishment of reliable variations of the chemical properties (complexation, hydrolysis) of elements within a group, for comparison with theoretical predictions, and, perhaps, for determination of thermodynamic constants. Moreover, other information can be derived from chromatography experiments. The mathematical treatment of elution curves can be carried out with various models, especially Glueckauf's, which offers the advantages of using simple equations and takes into account the possible dissymmetry of elution bands [31, 32]. The parameters included in Glueckauf's equations allow the determination of the distribution

ratios, and possibly of the diffusion ratios of the species in the mobile phase through the knowledge of the effective height of theoretical plates (EHTP) [31–33]. This latter parameter is characteristic of the efficiency of the column. A systematic study of the width of the elution band as a function of elution rate is required to determine the variations of EHTP. Unfortunately, this type of experiment is very cumbersome and has never been carried out with heavy elements. However, such experiments could provide information about diffusion constants and the related Stoke's radius of species in solution [32, 33].

5 Effects of the Media

The medium used in aqueous chemistry has a huge influence on the reaction thermodynamics and must be taken into account. These effects were often ignored in a large number of papers in the past. The purpose of this paragraph is to remind the reader that the effects of the medium govern the reaction constants not only in pure aqueous solutions but also in partition experiments [34–36]. Temperature effects will not be treated here, but they are also important [35].

Medium effects are imposed by macro-components and by supporting electrolytes if present. All thermodynamic laws are valid and must be applied without restrictions. The micro-component does not act in the calculations of the ionic strength (I_m). Coulomb forces between charged ions mainly impose deviation of experimental constants from zero ionic strength under well-defined conditions. Such deviations have been described in the literature by numerous models, which will not be reiterated here [34, 37]. For high concentrations, neutral species, and multiple interactions between species must also be taken into account.

Since it is independent of the nature of the supporting electrolyte, an extrapolation to zero ionic strength remains the only universal thermodynamic value for a given equilibrium. However, such extrapolation requires the knowledge of numerous parameters, sometimes difficult to determine and/or to estimate.

Recently a model was proposed by Neck et al. [38] to estimate successive hydrolysis constants using the inter-ligand electrostatic repulsion term. This model gives accurate results for actinides (Th, U, Np, and Pu) and can be extrapolated to other complexation reactions as long as data are available on chemical homologs.

In case of low charged species, and approximately below 3 mol kg^{-1} the specific ion interaction theory (SIT) [35] can be applied for the calculations of activity coefficients. Data available on interaction coefficients are scarce. But, paradoxically for actinide ions such data are relatively well known. However, in certain cases, they can be estimated from the model developed by Ciavatta [39, 40].

The knowledge of both thermodynamic constants at zero ionic strength and of the specific interaction coefficients will allow the speciation diagram of the element in the considered medium to be established. At higher electrolyte concentrations, more sophisticated theories taking into account electrostatic or/and hydrodynamic interactions (Pitzer, Mean Spherical Approximation, etc., [35, 37])

have been developed. However, they involve a larger number of characteristic parameters, which unfortunately are unknown for the majority of chemical elements.

Another approach to non-ideality of aqueous solutions does not take into account the nature of interactions between constituents: the simple solution concept allows one to determine thermodynamic properties of concentrated solutions of salts and also the density of various mixtures; the latter parameter being required for the conversion of concentrations from the molar to molal scale [41].

Except for some recent work, most data on SHE chemistry were determined in concentrated media with sometimes undefined ionic strength. A comparison of hydrolysis or complexation constants of homologs, available in the literature at various ionic strengths, must be considered with caution. Most of these constants were determined with weighable amount of elements. Even in one-atom-at-a-time experiments involving the same aqueous media, a direct comparison of results issued from different chemical procedures is delicate. In their work, Günther et al. [27] have reinvestigated the behavior of Rf and homologs in the system HCl/TBP using solvent extraction and extraction chromatography. In batch experiments they obtained similar results as those of Kacher et al. [22]. Their on-line experiments with Rf, Zr, and Hf are reliable since no edge effects have been proved to occur. Part of their discussion is devoted to a comparison with the work of Czerwinski et al. [21]. However, even if the methodology used by the latter would be adequate (which is not the case—see above), data collected in liquid–liquid solvent extraction and extraction chromatography cannot be directly compared, essentially because of medium effects. A system involving liquid–liquid partition can be perfectly defined in thermodynamical terms. From Sergievskii's model indeed, the activity coefficient of a species in the organic phase depends only on the water activity a_{H2O} of the bi-phasic system [42]. Therefore, if the water activity of the system is kept constant, the influence of the aqueous phase on the activity coefficients in the organic phase is also constant. Nevertheless, maintaining the water activity constant (or the ionic strength) does not neutralize all causes of deviations from an ideal solution. In extraction chromatography (or reversed phase chromatography) and in ion-exchange chromatography, the water activity cannot rigorously be defined and maintained constant [34]. However, at low ionic strength, the variations of the water activity in both phases can be neglected. This leads to meaningful thermodynamic data such as the recently determined K_d value of Rf [17, 29, 30].

6 Conclusion

In the case of a single atom, the law of mass action can be applied with mean concentrations proportional to the probabilities of finding an atom in one species or another. However, this derivation of the law of mass action can only be achieved for reactions with a 1-1 stoichiometry. Reactions between a micro-component and

macro-component are always allowed kinetically, the rate of the reaction being of the "pseudo" first order. But, at extreme dilution, the kinetics of reactions involving two micro-components is strongly hindered.

Experimentally, limitations are mainly imposed by the one-atom-at-a-time concept since the time devoted to the collection of data may be important.

The collection of experimental data must also include effects of the media and the temperature (if used). Prior to experiments to be carried out at the level of a single atom, the absence of edge effects must be checked carefully at the tracer scale.

References

1. Hoffman, D.C., Lee, D.M., Pershina, V.: Transactinide elements and future elements. In: Morss, L., Edelstein, N., Fuger, J. (eds.) The Chemistry of the Actinide and Transactinide Elements, 3rd edn., pp. 1652–1752. Springer, Dordrecht (2006) Chapter 14
2. Tatsumi, K., Corish, J.: Name and symbol of the element with atomic number 112 (IUPAC recommendations 2010). Pure Appl. Chem. **82**, 753–755 (2010)
3. Loss, R.D., Corish, J.: Names and symbols of the elements with atomic numbers 114 and 116 (IUPAC recommendations 2012). Pure Appl. Chem. **84**, 1669–1672 (2012)
4. Adloff, J.P., Guillaumont, R.: Fundamentals of Radiochemistry. CRC Press, Boca Raton (1993)
5. Guillaumont, R., Adloff, J.P., Peneloux, A., Delamoye, P.: Sub-tracer scale behavior of radionuclides—application to actinide chemistry. Radiochim. Acta **54**, 1–15 (1991)
6. Ghiorso, A., Harvey, B.G., Choppin, G.R., Thompson, S.G., Seaborg, G.T.: New element, Mendelevium, atomic number 101. Phys. Rev. **98**, 1518–1519 (1955)
7. Kratz, J.V.: Aqueous-phase chemistry of the transactinides. Radiochim. Acta **99**, 477–502 (2011)
8. Hulet, E.K., Lougheed, R.W., Wild, J.F., Nitschke, J.M., Ghiorso, A.: Chloride complexation of element 104. J. Inorg. Nucl. Chem. **42**, 79–82 (1980)
9. Gregorich, K.E., Henderson, R.A., Lee, D.M., Nurmia, M.J., Chasteler, R.M., Hall, H.L., Bennett, D.A., Gannett, C.M., Chadwick, R.B., Leyba, J.D., Hoffmann, D.C., Herrmann, G.: Aqueous chemistry of element 105. Radiochim. Acta **43**, 223–231 (1988)
10. Atkins, P.W.: Physical Chemistry, 6th edn. Oxford University Press, Oxford (1998)
11. Guillaumont, R., Adloff, J.P.: Behavior of environmental plutonium at very low concentration. Radiochim. Acta **58/59**, 53–60 (1992)
12. Borg, R.J., Dienes, G.J.: On the validity of single atom chemistry. J. Inorg. Nucl. Chem. **43**, 1129–1133 (1981)
13. Liboff, R.L.: Introduction to the theory of kinetic equations. Wiley, New York (1969)
14. Koudriavtsev, A.B., Jameson, R.F., Linert, W.: The Law of Mass Action. Springer, Berlin (2001)
15. Schmidt, K.H., Sahm, C.C., Pielenz, K., Clerc, H.G.: Some remarks on the error analysis in the case of poor statistics. Z. Phys. A **316**, 19–26 (1984)
16. Pénéloux, A., Guillaumont, R.: Solutions de dilution extrême et loi d'action de masse. C.R. Acad. Sci. Paris. **310**, série II, 1607–1613 (1990)
17. Nagame, Y., Tsukada, K., Asai, M., Toyoshima, A., Akiyama, K., Ishii, Y., Kaneko-Sato, T., Hirata, M., Nishinaka, I., Ichikawa, S., Haba, H., Enomoto, S., Matsuo, K., Saika, D., Kitamoto, Y., Hasegawa, H., Tani, Y., Sato, W., Shinohara, A., Ito, M., Saito, J., Goto, S., Kudo, H., Kikunaga, H., Kinoshita, N., Yokohama, A., Sueki, K., Oura, Y., Nakahara, H., Sakama, M., Schädel, M., Brüchle, W., Kratz, J.V.: Chemical studies on rutherfordium (Rf) at JAERI. Radiochim. Acta **93**, 519–526 (2005)

18. Trubert, D., Le Naour, C., Monroy Guzman, F., Hussonnois, M., Brillard, L., Le Du, J.F., Constantinescu, O., Gasparro, J., Barci, V., Weiss, B., Ardisson, G.: Chemical isolation of Dubnium (element 105) in fluoride media. Radiochim. Acta **90**, 127–132 (2002)
19. Silva, R., Sikkeland, T., Nurmia, M., Ghiorso, A.: Tracer chemical studies of Lawrencium. Inorg. Nucl. Chem. Lett. **6**, 733–739 (1970)
20. Silva, R.J., McDowell, W.J., Keller, O.R., Tarrant, J.R.: Comparative solution chemistry, ionic radius and single ion hydration energy of Nobelium. Inorg. Chem. **13**, 2233–2237 (1974)
21. Czerwinski, K.R., Kacher, C.D., Gregorich, K.E., Hamilton, T.M., Hannink, N.J., Kadkhodayan, B.A., Kreek, S.A., Lee, D.M., Nurmia, M.J., Türler, A., Seaborg, G.T., Hoffman, D.C.: Solution chemistry of element-104. Part-2. liquid–liquid extractions with Tributylphosphate. Radiochim. Acta **64**, 29–35 (1994)
22. Kacher, C.D., Gregorich, K.E., Lee, D.M., Watanabe, Y., Kadkhodayan, B.A., Wierczinski, B., Lane, M.R., Sylwester, E.R., Keeney, D.A., Hendricks, M., Stoyer, N.J., Yang, J., Hsu, M., Hoffman, D.C., Bilewicz, A.: Chemical studies of rutherfordium (element 104). Part-2. Solvent extraction into tributylphosphate from HBr solutions. Radiochim. Acta **75**, 127–133 (1996)
23. Stumm, W.: Chemistry of the solid-water interface. Wiley Interscience Publication, New York (1992)
24. Reischmann, F.J., Trautmann, N., Herrmann, G.: Chemistry at low concentrations: polonium at a level of 10^8 to 10^5 atoms. Radiochim. Acta **36**, 139–143 (1984)
25. Reischmann, F.J., Rumler, B., Trautmann, N., Herrmann, G.: Chemistry of low concentrations: Polonium at a level of 5000 to 40 atoms. Radiochim. Acta **39**, 185–188 (1986)
26. Schumann, D., Novgorodov, A.F., Misiak, R., Wunderlich, G.: Model Studies for the separation and identification of element 107 (Bohrium, Bh): ion exchange and precipitation experiments with Tc, Re, Nb and Ta nuclides from HNO_3/HF containing aqueous solution. Radiochim. Acta **87**, 7–12 (1999)
27. Günther, R., Paulus, W., Kratz, J.V., Seibert, A., Thörle, P., Zauner, S., Brüchle, W., Jäger, E., Pershina, V., Schädel, M., Schausten, B., Schumann, D., Eichler, B., Gäggeler, H.W., Jost, D.T., Türler, A.: Chromatographic study of Rutherfordium (Element 104) in the system HCl/Tributylphosphate (TBP). Radiochim. Acta **80**, 121–128 (1998)
28. Schädel, M., Brüchle, W., Dressler, R., Eichler, B., Gäggeler, H.W., Günther, R., Gregorich, K.E., Hoffman, D.C., Hübener, S., Jost, D.T., Kratz, J.V., Paulus, W., Schumann, D., Timokhin,S., Trautmann, N., Türler, A., Wirth, G., Yakuschev, A.: Chemical properties of element 106 (seaborgium). Nature. **388**, 55-57 (1997)
29. Schädel, M., Brüchle, W., Schausten, B., Schimpf, E., Jäger, E., Wirth, G., Günther, R., Kratz, J.V., Paulus, W., Seibert, P., Thörle, P., Trautmann, N., Zauner, S., Schumann, D., Andraasy, M., Misiak, R., Gregorich, K.E., Hoffman, D.C., Lee, D.M., Sylwester, E.R., Nagame, Y., Oura, Y.: First aqueous chemistry with Seaborgium (element 106). Radiochim. Acta. **77**, 149-159 (1997)
30. Pfrepper, G., Pfrepper, R., Krauss, D., Yakushev, A.B., Timokhin, S.N., Zvara, I.: Ion exchange equilibria and stoichiometry of complexes of element 104 and Hafnium in Hydrofluoric acid solutions. Radiochim. Acta **80**, 7–12 (1998)
31. Strub, E., Kratz, J.V., Kronenberg, A., Nähler, A., Thörle, P., Zauner, S., Brüchle, W., Jäger, E., Schädel, M., Schausten, B., Schimpf, E., Li, Z., Kirbach, U., Schumann, D., Jost, D.T., Türler, A., Assai, M., Nagame, Y., Sakama, M., Tsukada, K., Gäggeler, H.W., Glatz, J.P.: Fluoride complexation of rutherfordium (Rf, element 104). Radiochim. Acta **88**, 265–271 (2000)
32. Glueckauf, E.: Theory of chromatography, Part 9. The theoretical plate concept in column separations. Trans. Faraday Soc. **51**, 34–44 (1955)
33. Glueckauf, E.: Ion Exchange and Its Application. Society of Chemical Industry, London (1955)
34. Helferich, F.: Ion Exchange. Mc Graw-Hill, New York (1962)

35. Marcus, Y., Kertes, A.S.: Ion exchange and solvent extraction of metal complexes. Wiley-interscience, London (1970)
36. Grenthe, I., Puigdomenech, I. (eds.): Modeling in Aquatic Chemistry. OECD/NEA, Paris (1997)
37. Duplessis, J., Guillaumont, R.: Extraction par solvant et activité thermodynamique. Radiochem. Radioanal. Lett. **31**, 283–292 (1977)
38. Barthel, J.M.G., Krienke, H., Kunz, W.: Physical chemistry of electrolyte solutions modern aspects. Springer, Steinkopff Darmstadt (1998)
39. Neck, V., Kim, J.I.: Solubility and hydrolysis of tetravalent actinides. Radiochim. Acta **89**, 1–16 (2001)
40. Ciaviata, L.: The specific interaction theory in the evaluating ionic equilibria. Ann. Chim. (Roma) **70**, 551–562 (1980)
41. Ciaviata, L.: The specific interaction theory in equilibrium analysis. Some empirical rules for estimate interaction coefficients of metal ion complexes. Ann. Chim. (Roma). **80**, 255–263 (1990)
42. Vdovenko, V.M., Ryazanov, M.A.: Coefficients d'activité dans les systèmes à plusieurs constituants. Radiochimie (French translation of Radiokhimiya) **1**, 40–45 (1965)
43. Sergievskii, V.V.: Extraction of metal nitrates and nitric acid. I. Calculation of the distribution constants in the extraction of uranyl nitrate by ethers, esters, ketones and alcohols. Sov. Radiochem. **20**, 339–342 (1978)

Experimental Techniques

Andreas Türler and Kenneth E. Gregorich

Abstract The chemical investigation of single short-lived atoms of transactinide elements requires the development of unique techniques that encompass synthesis, rapid transport, chemical isolation, and detection of the radioactive decay. Each step presents its challenges and has to be optimized in order to reach the single atom sensitivity. Another issue is the safe and long-term stable operation of such setups. Several techniques were successful in studying the chemical properties of transactinide elements in the liquid phase as well as in the gas phase. Since only single atoms are studied, chromatographic systems are preferred which ensure repeated interactions or repeated phase transitions. Some of the developed systems work continuously where as others perform batch-wise separations. Recently, the coupling of chemical systems to on-line kinematic recoil separators was accomplished taking advantage of the fact, that the product beam is separated from the intense primary projectile beam of the accelerator. Thus, more fragile compounds such as metal–organic transactinide compounds should become available for study.

K. E. Gregorich was author for the first edition of this chapter only.

A. Türler (✉)
Labor für Radio- und Umweltchemie, Universität Bern, Berne, Switzerland
Labor für Radio- und Umweltchemie, Paul Scherrer Institut (PSI), Villigen, Switzerland
e-mail: andreas.tuerler@psi.ch

K. E. Gregorich
Nuclear Science Division, Lawrence Berkeley National Laboratory,
Berkeley, CA 94720, USA

M. Schädel and D. Shaughnessy (eds.), *The Chemistry of Superheavy Elements*,
DOI: 10.1007/978-3-642-37466-1_5,

1 Introduction

The study of chemical properties of the heaviest known elements in the Periodic Table is an extremely challenging task and requires the development of unique experimental methods, but also the persistence to continuously improve all the techniques and components involved. The difficulties are numerous. First, all elements heavier than Fm can only be synthesized artificially "one-atom-at-a-time" at heavy ion accelerators, requiring highest possible sensitivity. Second, due to the relatively short half-lives of all known transactinide nuclides, very rapid and at the same time selective and efficient separation procedures have to be developed. Finally, sophisticated detection systems are needed which allow an efficient detection of the nuclear decay of the separated species, and, therefore, offer unequivocal proof that the observed decay signature originated indeed form a single atom of a transactinide element.

Fast chemical isolation procedures to study the chemical and physical properties of short-lived radioactive nuclides have a long tradition and were applied as early as 1900 by Rutherford [1] to determine the half-life of ^{220}Rn. A rapid development of fast chemical separation techniques [2–7] (see Ref. [5] for an in-depth review) occurred with the discovery of nuclear fission [8]. Indeed, the discovery of new elements up to $Z = 101$ was accomplished by chemical means [9]. Only from there on physical methods prevailed. Nevertheless, rapid gas-phase chemistry played an important role in the claim to discovery of Rf and Db [10]. As of today, the fastest chemical separation systems allow access to the study of α-particle emitting nuclides within less than 1 s as demonstrated by the investigation of ^{224}Pa with a half-life of 0.85 s [11]. Reviews on rapid chemical methods for the identification and study of short-lived nuclides from heavy element synthesis can be found in [12–22].

A chemistry experiment with a transactinide element can be divided into four basic steps:

(1) Synthesis of the transactinide element.
(2) Rapid transport of the synthesized nuclide to the chemical apparatus.
(3) Fast chemical isolation of the desired nuclide and preparation of a sample suitable for nuclear spectroscopy.
(4) Detection of the nuclide via its characteristic nuclear decay properties.

Already the synthesis of heavy and superheavy elements is, from the technological point of view, very demanding. In order to gain access to the longer-lived isotopes of transactinide elements, exotic, highly radioactive target nuclides such as ^{244}Pu, ^{243}Am, ^{248}Cm, ^{249}Bk, ^{249}Cf, or ^{254}Es are bombarded with intense heavy ion beams such as ^{18}O, ^{22}Ne, ^{26}Mg, ^{48}Ca, or ^{50}Ti. On the one hand, as intense beams as possible are to be used; on the other hand, the destruction of the very valuable and highly radioactive targets has to be avoided. In recent years, kinematic recoil separators, mainly gas-filled separators, have been employed as preseparators and were used to deliver a clean product beam to a chemistry

experiment. Experimental arrangements that have successfully been used to irradiate exotic targets and to rapidly transport the synthesized transactinide nuclei to a chemistry set-up are discussed in Sect. 2.

The choice of the chemical separation system has to be based on a number of prerequisites that have to be fulfilled simultaneously to reach the required sensitivity:

- *Speed*: Due to the short half-lives of even the longest lived currently known transactinide nuclides, see "Synthesis of Superheavy Elements", the time required between the production of a nuclide and the start of the measurement is one of the main factors determining the overall yield. In contrast to kinematic separators, chemical instrumentation currently allows the investigation of transactinide nuclides with half-lives of a few seconds or longer. The importance of the speed of separation may diminish in future experiments with the reported longer lived isotopes of superheavy elements Hs, Ds, Cn, and Fl.
- *Selectivity*: Due to the low cross-sections, ranging from the level of a few nanobarns for the production of nuclides of elements Rf and Db, down to a level of a few picobarns or even femtobarns for the production of elements with $Z > 108$, the selectivity of the chemical procedure for the specific element must be very high. Two groups of elements are of major concern as contaminants: Due to the fact that many Po isotopes have similar half-lives and/or α-decay energies as transactinide elements, the separation from these nuclides must be particularly good. Some short-lived Po isotopes are observed as daughter nuclides of precursors, i.e., Pb, Bi, and Rn. Also of concern are some At isotopes. These elements are not only formed in multinucleon transfer reactions with Pb impurities in the target material and/or the target assembly, but also with the target material itself. Here, a chemical purification of the actinide target material and a careful selection of all materials used in the target assembly can already reduce the production of unwanted nuclides by orders of magnitude. Nevertheless, in order to chemically investigate the recently discovered superheavy elements, a kinematic pre-separation might be required to efficiently suppress, e.g., Rn transfer products. A second group of elements, which interfere with the detection of transactinide nuclei, are heavy actinides that decay by spontaneous fission (SF). These are inevitably produced with comparably large cross-sections in multinucleon transfer reactions. The separation from heavy actinides must be particularly good if SF is the only registered decay mode and if no other information, such as the half-life of the nuclide, can be derived from the measurement.
- *Single atom chemistry*: Due to the very low production rates, transactinide nuclei must be chemically processed on a "one-atom-at-a-time" scale. Thus, the classical derivation of the law of mass action is no longer valid, see "Theoretical Chemistry of the Heaviest Elements". R. Guillaumont et al. [23] have derived an expression equivalent of the law of mass action in which concentrations are replaced by probabilities of finding the species in a given state and a given phase. The consequence for single atom chemistry is that the studied atom must be subjected to a repetitive partition experiment to ensure a statistically significant behavior. Here, chromatography experiments are preferred.

- *Repetition*: Since the moment in time at which a single transactinide atom is synthesized can currently not be determined and chemical procedures often work discontinuously, the chemical separation has to be repeated with a high repetition rate. Thus, thousands of experiments have to be performed. This inevitably led to the construction of highly automated chemistry set-ups. Due to the fact, that the studied transactinide elements as well as the interfering contaminants are radioactive and decay with a certain half-life, also continuously operating chromatography systems were developed.
- *Detection*: The unambiguous detection of the separated atom is the most essential part of the whole experiment. Even though some techniques, such as atomic force microscopy (AFM), have reached the sensitivity to manipulate single atoms or molecules (out of many), the detection of the characteristic nuclear decay signature of transactinide nuclei remains currently the only possibility to unambiguously detect the presence of a single atom of a transactinide element after chemical separation. Thus, final samples must be suitable for high resolution α particle and SF-spectroscopy (coincident detection of SF fragments). Most transactinide nuclei show characteristic decay chains that involve the emission of α particles or the SF of daughter nuclei. The detection of such correlated decay chains requires the event-by-event recording of the data. In experiments with physical separators, the use of position sensitive detectors further enhanced the discrimination against randomly correlated events.
- *Speciation*: Due to the fact that transactinide nuclei are detected after chemical separation via their nuclear decay, the speciation cannot be determined. Currently, the speciation in all transactinide chemistry experiments has to be inferred by carefully studying the behavior of lighter, homolog elements. The chemical system must be chosen in such a manner that a certain chemical state is probable and stabilized by the chemical environment.

Basically, four different approaches, which involve the direct detection of the nuclear decay of the isolated nuclides, have been successful in studying the chemical properties of transactinide elements. Two of the systems work in the liquid phase, as discussed in Sect. 3, whereas the other two are designed to investigate volatile transactinide compounds in the gas phase, as discussed in Sect. 4. Chemical information can also be obtained by studying the distribution of long-lived α-decay granddaughters after completion of the on-line experiment. Also these systems will be included in the current review.

2 Targets, Recoil Techniques and Gas-Jets

2.1 Actinide Targets

To date, the highest production rates of isotopes of transactinide elements have been achieved in compound nucleus reactions between light and heavy ion beams (^{18}O, ^{19}F, ^{22}Ne, ^{26}Mg, and ^{48}Ca) with actinide targets (^{238}U, ^{244}Pu, ^{248}Cm, ^{249}Bk,

^{249,250}Cf, and ^{254}Es). The rare target nuclides are produced by successive neutron capture reactions on Cm and Am as starting materials at high flux nuclear reactors such as the HIFR at Oak Ridge, United States, or the SM in Dimitrovgrad, Russia. Elaborate chemical isolation procedures in heavily shielded hot cells are required to isolate the desired rare isotopes from the bulk of the starting material.

Production rates are proportional to both the target thickness and the beam intensity. For nuclear reactions involving the lighter projectiles, target thickness is limiting the compound nucleus recoil ranges (<1 mg/cm^2), because the separation techniques used require the evaporation residues of the compound nucleus to recoil out of the target. With higher Z projectiles, the recoil ranges are larger. But because of the higher rate of projectile energy loss in the target material and the narrow projectile energy range effective for heavy element production, the effective target thicknesses are once again limited to $\sim$1 mg/cm^2. The high levels of radioactivity associated with the milligram amounts of these actinide isotopes present unique challenges for safe handling and irradiation of these targets. The targets must be physically strong to maintain integrity through handling and irradiation. Passage of the beams through the targets produces large amounts of heat, which must be dissipated. In addition, the target material must be chemically stable in the highly ionizing environment created by passage of the beam.

With the recent use of kinematic recoil separators being used as pre-separators for chemical experiments, also the requirements on the targets changed. Kinematic separators ideally separate the projectile beam and transfer reaction products from the desired fusion reaction products. Therefore, this secondary product beam has to fulfill certain characteristics in order to be transmitted efficiently through the separator. These are either relatively well-defined recoil velocities or kinetic energies. Therefore, targets for recoil separators are usually thinner (only up to about 0.6 mg/cm^2), since thicker targets would negatively affect the transmission of the product beam through the separator. Also, these targets are operated in vacuum or a very dilute gas (up to 1 mbar), and therefore the dissipation of the heat is an issue. Due to these limitations, generally rotating target wheels are being used in order to distribute the deposited energy over a larger area.

2.1.1 Target Production Techniques

Several methods have been used in the fabrication of actinide targets for heavy element studies.

Painting. Since the early days of superheavy element experiments, targets have been produced by dissolving the target material in an organic solvent and painting this solution on the target backing material [24]. This technique guarantees minimal losses of the valuable target materials, but the technique does not produce targets of uniform thickness. Also, the adherence of the target material to the backing is sometimes unsatisfactory, resulting in flake off during irradiation.

Polymer-assisted deposition. A modern variant of the painting technique is the polymer-assisted deposition (PAD) technique using spin coating [25, 26]. As

substrate single side polished silicon wafers coated on both sides with a 1-μm thick layer of Si_3N_4 were used. From these, Si_3N_4 windows of the desired shape and size can be obtained by partially removing the Si_3N_4 on the back side and subsequent etching of the Si in hot KOH. The target metal of choice is dissolved in an aqueous polymer solution in which the multidentate polymer chelates the metal. An aliquot is then deposited onto the smooth substrate, spin coated, and finally annealed to remove the polymer and create a homogeneous, crack free, and thin metal oxide film. Stationary Si_3N_4-based targets produced by PAD were able to withstand an ^{40}Ar beam with an intensity of 200 (particle) nA. However, no rare actinide targets have been fabricated so far by using this technique.

Evaporation of volatile actinide compounds. Targets for heavy element chemistry experiments have been produced by the vacuum evaporation of volatile actinide compounds onto stable metallic backing foils. A review of many techniques has been published by Muggleton [27], although he concentrated on high-temperature vacuum evaporation. For vacuum evaporation, a relatively volatile compound of the target element is heated to near its vaporization point, and the evaporated molecules form a uniform deposit on the nearby cooled target backing foil. Heating can be achieved by passing electric current through a refractory metal boat or using resistance heating on various crucibles. For production of targets from metals and more refractory materials, heating can be achieved by electron bombardment. These techniques can produce very pure and uniform targets. The main disadvantage is the relatively low efficiency for collecting the evaporated target material on the target backing foil. This can be a serious disadvantage with the use of extremely rare and radioactive heavy actinide target materials. To circumvent this disadvantage, a thin-film deposition procedure of high material collection efficiency has to be used. Radio-frequency (rf) sputtering with Ar as a working gas was found to meet this condition in a satisfactory way, leading to a material collection efficiency on the substrate of up to 40% [28].

Electrospray. With the electrospray method (see the review by Muggleton [27] and references therein), an actinide compound is dissolved in a nonconducting organic solvent. An extremely fine glass capillary is drawn and an electrode is inserted into the capillary. The capillary is filled with the solvent containing the actinide compound, and the capillary tip is placed within a few centimeters of the target backing foil. Once a high voltage is applied between the electrode and the metal target backing foil, a fine spray is emitted from the capillary, which immediately dries on the backing foil. While large area and thick targets have been produced by this technique with actinide target materials, the spraying of aerosol-sized particles of an extremely radioactive solution poses challenging safety problems. This technique has essentially been supplanted by the molecular plating process.

Ink-jet techniques. Piezoelectric pulsed drop jet devices have been used for target production [29]. These devices are similar to those used in ink-jet printers. So far, they have not been applied in transactinide chemistry experiments.

Molecular plating. Electrodeposition or molecular plating has been the method of choice for production of the small-area actinide targets for use in production of heavy element isotopes for chemical studies. Such techniques have been described by several authors [30–34]. The molecular plating technique can easily be accomplished inside a glove box for containment of the radioactive target material. Up to milligram quantities of actinide elements have been used and the deposition yield can approach 100%. The small volumes used facilitate recovery of actinide materials. Extreme care must be taken to produce targets free of impurities. Recently, also large area target segments for rotating target wheels for use in the ARTESIA set-up and in recoil separators have been fabricated by the molecular plating technique. A comprehensive description of the fabrication process is given in the paper by Eberhardt et al. [35]. Nitrate or chloride compounds of the actinide element are dissolved in a small volume of nitric acid (5–10 μL) and mixed with a surplus of an organic solvent (usually isopropanol, isobutanol or acetone), and a voltage of typically 150 V is applied between the solution and the target backing foil resulting in a current density of up to 1.5 mA/cm^2. A typical plating cell is shown in Fig. 1. Targets up to 1 mg/cm^2 have been produced either by plating successive 0.1 mg/cm^2 layers, and converting the deposit to the oxide form by heating to ∼500 °C before plaiting the next layer or by one-step plating procedures As detailed by Eberhardt et al. [35] temperature control, intense stirring, and chemical cleaning of the target backing foil prior to the deposition process are mandatory prerequisites for a successful target fabrication.

This way, targets of close to 1 mg/cm^2 thickness can be produced in a single deposition cycle. Recently, target segments with the very rare nuclides ^{249}Bk and ^{249}Cf have been produced on ∼2 μm Ti-backings for the gas-filled separator TASCA [36]. These targets were successfully irradiated with ^{50}Ti beams with integrals up to 10^{19} particles. Although targets optically appear to be very uniform

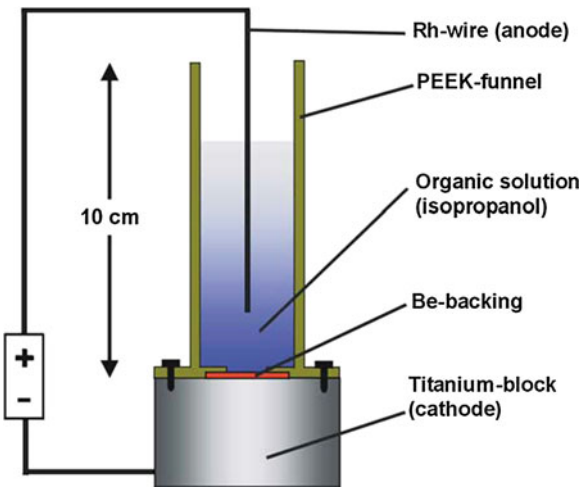

Fig. 1 Schematic of cell used [34] for molecular plating of actinide targets

Fig. 2 Photograph of one segment of a rotating ^{249}Bk target on 5 μm Ti backing fabricated by molecular plating at Mainz University with material supplied by Oak Ridge National Laboratory. (photograph courtesy of Mainz University)

in thickness, as the example of a recently produced target segment of a rotating ^{249}Bk target shows (Fig. 2), detailed investigations by Vascon et al. [37], using atomic force microscopy (AFM), showed that the surface roughness of the underlying target backing and the electrolyte concentration has a significant influence on the smoothness and appearance of the plated layer.

Intermetallic targets. A new technology to produce rare actinide targets with high thermal conductivity was introduced recently by Usoltsev et al. [38]. In a first step, the target material is electroplated on a noble metal surface, i.e., Pd, as described above. In a second step, the foil with the plated material is heated in H_2. Due to the formation of an intermetallic compound with the noble metal support, coupled reduction of the target material with hydrogen at high temperatures becomes thermodynamically possible. As shown by electron microscopy and α-particle spectroscopy, the actinide element forms an alloy and diffuses into the Pd backing, so that the emission of α particles can now be measured also from the back side of the Pd backing foil. The method seems to provide better target stability for stationary targets cooled by direct contact with support grids, as used in gas-phase chemistry experiments on Cn and Fl in Dubna, Russia. However, such targets will not be suitable for separators, due to the very large spread in recoil energies caused by the backing foil. Also, the coupled reduction appears to be reversible. Upon introduction of O_2, the actinide element diffused back to the surface to form an oxide layer.

2.1.2 Target Cooling

The projectile beam loses energy upon passing through the target backing and the target, resulting in deposition of heat in the target. The heat generated must be removed to prevent damage to the target. To allow for the highest beam intensities, highly efficient target cooling is necessary.

Double-window systems and forced gas cooling. The double-window target system has been developed [39] for use with targets on relatively thick backing foils; see Fig. 3. In the double-window system, a vacuum isolation foil is placed

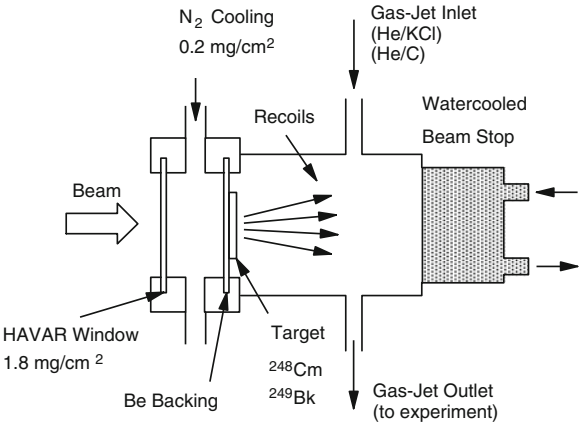

Fig. 3 Double-window target system with forced gas cooling for stationary targets. Reaction products are recoiling form the target and stopped in a volume flushed with an aerosol e.g., He/KCl

just upstream of the target backing foil (with the target material on the downstream side of the backing foil). Cooling gas at pressures near 1 bar is forced at high velocity through a narrow gap between the vacuum isolation foil and the target backing foil, cooling both foils.

Since both the vacuum isolation foil and the target backing foil must hold a pressure difference of greater than 1 bar, relatively thick metal foils, such as 2.5 mg/cm^2 Be or 1.8 mg/cm^2 HAVAR, have been used. These thick foils are especially attractive when considering the mechanical stability of extremely radioactive actinide targets. Variations on the double-window target system have traditionally been used for heavy element production with actinide target materials.

Because of the mechanical stresses associated with the pressure differences across the foils, target areas have been limited to <1 cm^2. Heating of the target by passage of the beam is inversely proportional to the cross-sectional area of the beam. Clearly, an increase in the target size (or area) would allow the use of higher beam intensities.

Yakushev [40] has overcome the small target area limitation by placing a supporting grid over a large area ^{238}U target and using an electrostatic beam wobbler to spread the beam out over a much larger area. While some fraction of the beam is lost on this grid, much larger beam intensities, and therefore higher production rates were achieved. An improved version of the concept was used by Eichler et al. [41–43] to investigate chemical properties of Cn and Fl using ^{242}Pu and ^{244}Pu targets. A schematic drawing of the target assembly and the results of a finite element calculation of the thermal load on a Ti vacuum window are shown in Fig. 4. The incoming beam from the accelerator is indicated by the red arrow.

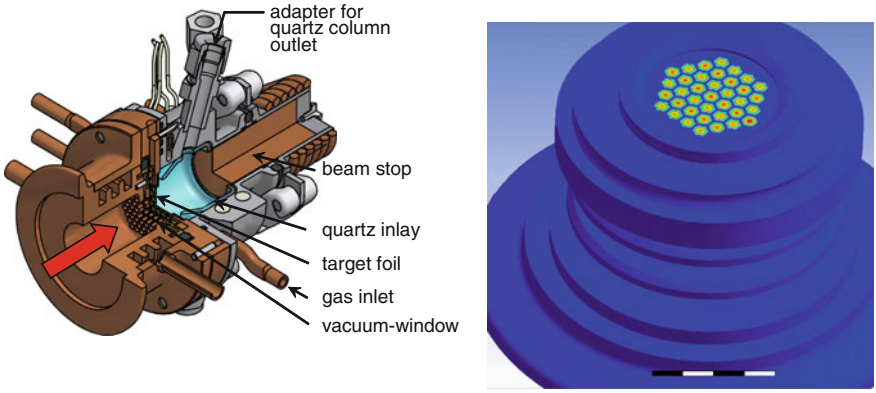

Fig. 4 *Left-hand side*: cartoon of the water-cooled collimator–target–recoil chamber–beam stop assembly as used for experiments described in [41–43] (*red arrow*—incoming beam). *Right-hand side*: Results of a finite element calculation of the thermal load in the Ti vacuum window

2.1.3 Rotating Targets

A method to effectively spread the beam heating over a larger target area is the use of rotating targets. Rotating ^{248}Cm targets have been used in heavy element chemistry experiments at the Gesellschaft für Schwerionenforschung (GSI) [34]. The rotating target and vacuum window assembly ARTESIA [44] has allowed the use of modern high-intensity accelerated beams for heavy element chemistry experiments [45]. A picture of a rotating ^{248}Cm target after irradiation with up to 1 (particle) μA of a ^{26}Mg beam (a factor of four larger than possible with a fixed target) is presented in Fig. 5.

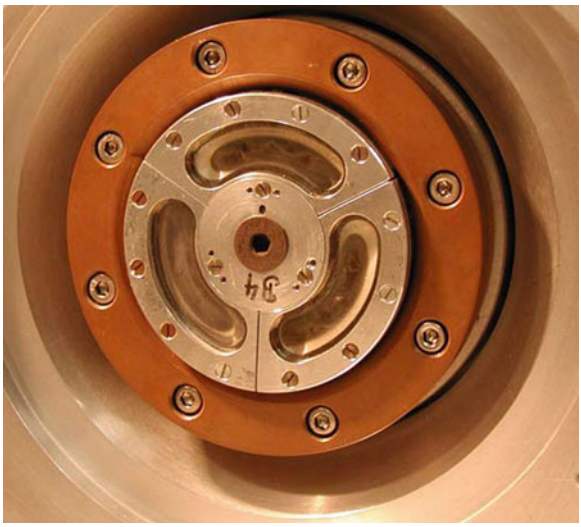

Fig. 5 The GSI rotating ^{248}Cm target wheel ARTESIA

Target wheels of varying diameter are frequently used in recoil separators. Here, usually Ti-backing foils of $\sim$2 μm thickness are employed. With large diameter target wheels relatively high peripheral velocities can be reached, allowing for higher beam currents. However, for very rare actinide nuclides a compromise between target wheel diameter and the available amount of target material has to be found. The newly developed target wheel for the gas-filled separator TASCA has a diameter of 10 cm at centerline of the target segments and the four target segments require a total of about 12 mg for fabrication of a target of about 0.5 mg/cm^2 thickness [46]. At a target wheel speed of 2249 rotations per minute, resulting in a target velocity of 11.77 mm/ms, the target temperature reaches only about 80 °C at $\sim$30 W thermal beam power deposition per cm^2. This can be compared to about 180 °C for the smaller ARTESIA wheel with a diameter of 33.5 mm at centerline of the target segments. Great care has to be taken to defocus the beam to a diameter of about 8 mm and to synchronize the target wheel with the beam pulses of the accelerator, so that one pulse is applied to one target segment. Hitting the target frames with the beam would destroy the delicate targets.

2.2 Recoil Techniques

In the early days of accelerator-based radiochemical separations, thick targets were irradiated, allowing the compound nucleus products to stop in the target material. At the end of an irradiation, the long-lived radionuclides could be chemically separated from the target. Obvious limitations arise with the use of highly radioactive heavy actinide targets in the search for short-lived heavy element isotopes.

2.2.1 Recoil Catcher Foils

When a compound nucleus is formed in the reaction of a projectile beam with a target nucleus, the compound nucleus is formed with the momentum of the beam particle. If the target layer is thin enough, this recoil momentum is sufficient to eject the compound nucleus product from the target. These recoiling reaction products can be stopped in a metal foil placed directly downstream of the target. By using this recoil catcher method, chemical separation of the heaviest elements is facilitated, because only a small fraction of the radioactive target material is transferred to the recoil catcher foil, and the recoil catcher foil material can be chosen to ease its dissolution and chemical removal. Perhaps the first use of the recoil catcher technique for heavy element studies was with the chemical separations used in the 1955 discovery of Md (mendelevium, $Z = 101$) [47]. With the recoil catcher foil technique, the time required for removal of the foil, and dissolution and separation of the foil material results in chemical separation times longer than a few minutes. Since the half-lives of transactinide isotopes are on the order of 1 min or less, this technique has not been used for transactinide chemistry experiments.

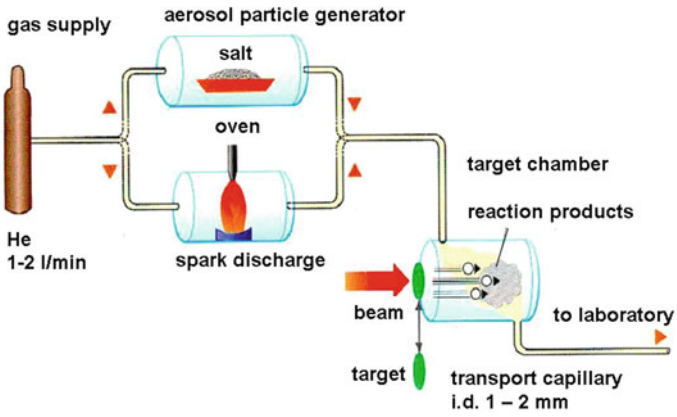

Fig. 6 Components of an aerosol gas-jet transport system

2.2.2 Aerosol Gas-Jets

To achieve faster chemical separation times, the aerosol gas-jet transport technique has been used to deliver transactinide isotopes from the target chamber to various chemical separation devices. Transport times of the order of one second have been achieved. The principles behind the aerosol gas-jet transport technique have been presented by Wollnik [48]. Products of nuclear reactions are allowed to recoil out of a thin target, and are stopped in a gas at a pressure typically above 1 bar. The gas is usually He because of the relatively long recoil ranges. The He gas is seeded with aerosol particles. After stopping in the gas, the reaction products become attached to the aerosol particles. The gas and activity-laden aerosol particles are sucked through a capillary tube to a remote site, by applying vacuum to the downstream end of the capillary. A schematic of the components of an aerosol gas-jet transport system is shown in Fig. 6. At the downstream end of the capillary, the He goes through a supersonic expansion into the vacuum, exiting in a broad cone. The aerosol particles, having much lower random thermal velocities are ejected from the tip of the capillary in a narrow cone, and can be collected on a foil or filter by impaction. The collected aerosol particles, containing the nuclear reaction products, can be made rapidly available for chemical separation.

Many aerosol particle materials have been used, and the material can be specifically chosen to minimize interference with the chemical separation being conducted. Widely used were KCl aerosols which can easily be generated by sublimation of KCl from a porcelain boat within a tube furnace. By choosing a temperature between 650 and 670 °C, specially tailored aerosol particles with a mean mobility diameter of about 100 nm and number concentrations of few times 10^6 particles/cm^3 can be generated. The same technique was applied to produce MoO_3 aerosol particles. Carbon aerosol particles of similar dimensions were generated by spark discharge between two carbon electrodes.

The large transport efficiencies through the capillary for the aerosol gas-jet technique can be explained in terms of the laminar flow profile of the gas inside the capillary [48]. According to Bernoulli's law, the gas pressure at the center of the capillary, where the velocity is highest, is lower than near the capillary walls. Thus, when the sub μm-sized aerosol particles drift away from the center of the capillary, they are subject to a restoring force toward the center of the capillary. Transport efficiencies of over 50% have routinely been achieved for transport capillary lengths over 20 m.

2.2.3 Kinematic Separators and Gas-Jets

Atoms of the transactinide elements are produced at extremely low rates: atoms per minute for Rf and Db, down to atoms per day or week for elements Sg through Fl. They are produced among much larger amounts of "background" activities which hinder the detection and identification of decay of the transactinide atoms of interest. For these reasons, there is a recognized need for a physical pre-separation of the transactinide element atoms before chemical separation. Thus, it was shown that a kinematic separator could be coupled to a transactinide chemistry system with an aerosol gas-jet device [49–53].

Coupling of the Berkeley Gas-Filled Separator (BGS) with a transactinide chemical separation system has been accomplished at the Lawrence Berkeley National Laboratory in some proof-of-principle experiments [50]. For these experiments, 4.0-s ^{257}Rf was produced in the ^{208}Pb(^{50}Ti, n)^{257}Rf reaction, and separated from all other reaction products with the Berkeley Gas-filled Separator [54]. In the focal plane area of the BGS, the ^{257}Rf recoils passed through a 6-μm MYLAR foil and were stopped in a volume of He at a pressure of 2 bar in the recoil transfer chamber (RTC) [49]. The He gas in the RTC was seeded with KCl aerosol particles, and the ^{257}Rf atoms became attached to them. They were transported through a 20-m capillary to the SISAK chemical separation system (see Sect. 3.2.4), where the chemical separation and detection were performed. These proof-of-principle experiments showed the practicality of a physical pre-separation of transactinide nuclides before chemical separation and led to construction of recoil transfer chambers for almost all the currently existing gas-filled separators, such as the Dubna gas-filled separator DGFRS [55], the GARIS separator at RIKEN, Japan [56, 57] and the TASCA separator at the GSI Darmstadt, Germany [53]. A schematic of the working principle and a photograph of an RTC are shown in Figs. 7 and 8, respectively.

In order to take full advantage of physical pre-separation, the Trans Actinide Separator and Chemistry Apparatus (TASCA) was conceived as dedicated separator for transactinide chemistry research. This separator was constructed using the dipole and two quadrupole magnets of the old HECK separator [58]. Extensive simulations of projectile- and product beam trajectories showed that the classical dipole-quadrupole-quadrupole (DQQ) arrangement was the most efficient one. Furthermore, by moving the target as close as possible to the dipole magnet and by removing the shims, the horizontal and vertical acceptance of the separator could

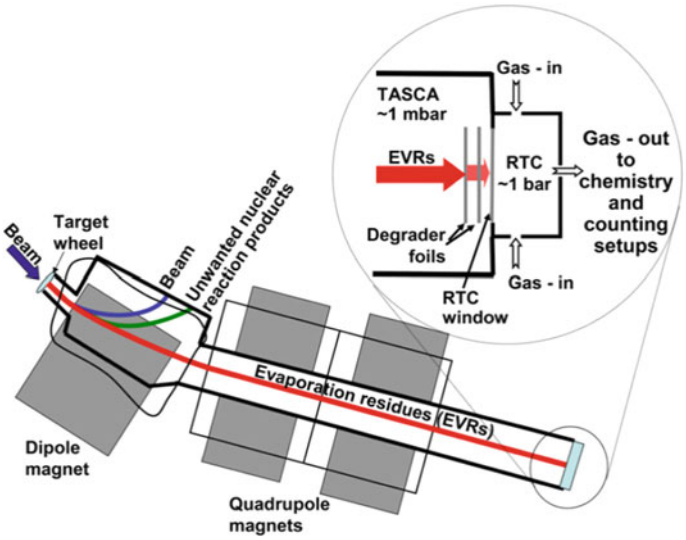

Fig. 7 Schematic of the gas-filled separator TASCA with attached recoil transfer chamber [53]

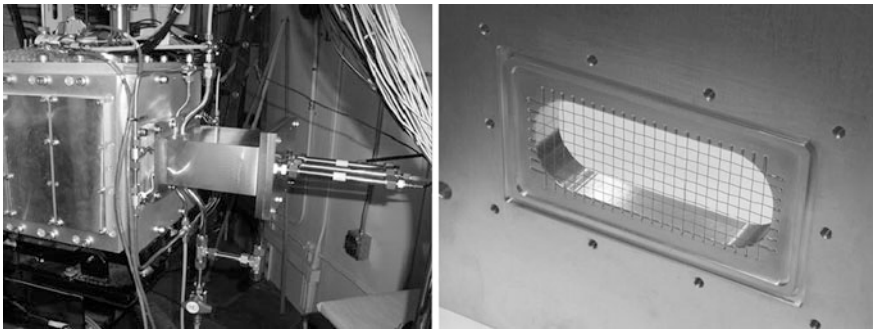

Fig. 8 Recoil transfer chamber installed at the BGS focal plane (*left*), and the support grid for the MYLAR foil (*right*)

be improved significantly. A large exit opening of the dipole vacuum chamber and a specially designed vacuum tube in the quadrupole section with butterfly like cross-section, where the walls of the chamber closely follow the contours of the magnet tips, ensured maximum transmission of evaporation residues (EVRs) to the focal plane. For ^{48}Ca induced reactions on actinide targets, transmissions of up to 60% were observed [59]. TASCA was designed to be operated with the quadrupole magnets polarized either as Q_vQ_h or Q_hQ_v, where v and h indicate vertical or horizontal focusing, respectively. This allows for running TASCA with two different focal-plane image sizes, each with different transmission efficiencies for EVRs. When polarized as Q_hQ_v, the efficiency of TASCA for the transmission of

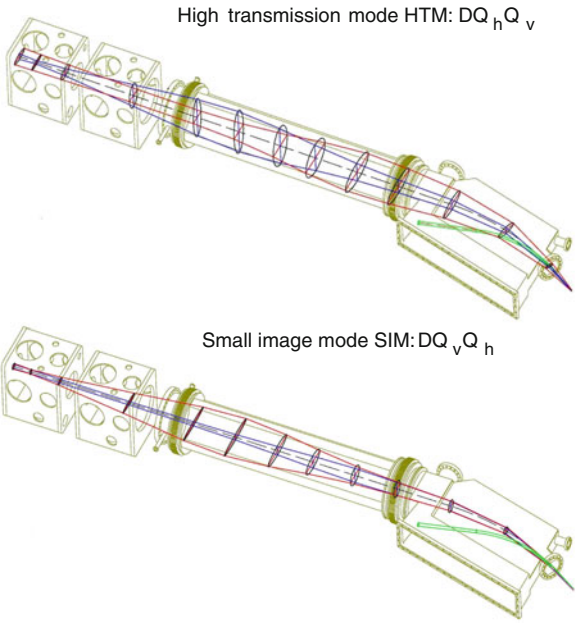

Fig. 9 Beam envelopes calculated for the projectile beam (*green*) and the EVR beam (*red* and *blue*) for the two polarizations Q_hQ_v and Q_vQ_h of TASCA, generating a larger, ellipsoidal image size in the high transmission mode (HTM) or a small, circular image in the small image mode (SIM)

EVRs to the focal plane is maximized, but the focal-plane image is more dispersed, which is an advantage when using a focal plane detector. It is, however, a disadvantage, when relatively short-lived reaction products are stopped in a recoil transfer chamber, because of the large window area generating a large recoil volume. By polarizing the quadrupoles Q_vQ_h, a relatively small, circular focal point can be obtained, allowing for a much smaller recoil chamber volume, and thus a rapid flush time of the recoil transfer chamber. This mode comes at the expense of a reduced transmission of about 35% for EVRs in ^{48}Ca induced reactions. The envelopes of the projectile and EVR beam for the two polarization modes are displayed in Fig. 9. For both operating modes of TASCA, suitable recoil transfer chambers have been constructed [53].

The success of physical preseparation opened up new avenues of research in transactinide chemistry. First, the absence of the primary projectile beam, which, upon passage through the recoil chamber created a plasma and thus harsh ionizing conditions, will allow now for the first time the investigation of more complex transactinide molecules, such as, e.g., metal–organic compounds, such as group-4 hexafluoroacetyacetonates [60], or group-6 hexacarbonyls [61]. Second, the suppression of transfer reaction products allowed the investigation of transactinide nuclei in an almost background free environment, and thus improved the sensitivity and the quality of nuclear data. Examples are the observation of isomeric states in ^{261}Rf [62] and ^{265}Sg [63].

3 Techniques and Instruments for Liquid-Phase Chemistry

Liquid-phase chemical separation techniques have been used for over 100 years, thus their utility for separation and isolation of the chemical elements has been demonstrated. Adaptations of these well-understood separation techniques have been applied to the transactinide elements. These adaptations have been developed to overcome the single-atom and short half-life limitations inherent in the study of transactinide element chemical properties.

3.1 Manual Liquid-Phase Chemical Separations

The early chemical separations with the heaviest elements were performed manually. Today, most of the research has turned to automated chemical separation techniques.

3.1.1 Manual Liquid–Liquid Extractions

Manually performed liquid–liquid extractions have been used for the study of chemical properties of Rf [64–67] and Db [68] in Berkeley. The microscale liquid–liquid extraction technique used in these studies was based on techniques developed for the study of Lr chemical properties [69, 70]. To minimize the separation and sample preparation time, phase volumes were kept to $\sim$20 μL. For these experiments, several specially developed techniques and apparatus were necessary. These include: (a) a special collection turntable for easy collection of the gas-jet samples which also signaled the data acquisition computer at the start and end of collection for each sample; (b) small syringes with hand-made transfer pipettes for rapid pipetting of volumes as small as 15 μL; (c) the ultrasonic mixer, which was made by modification of a commercially available home ultrasonic humidifier; (d) a specially modified centrifuge which reached full speed and returned to a full stop in a few seconds and also signaled the data acquisition computer to record the chemical separation time; (e) techniques for rapidly and reliably drying the organic phase at the center of an Al disk or glass plate; and (f) a set of α-particle detection chambers which could be quickly loaded, evacuated, and which signaled the acquisition computer as to the start and stop of the measurement for each sample. The time from end of collection of aerosols to the beginning of counting of the transactinide chemical fractions was as short as 50 s, and the collection-separation-counting cycle could be repeated every 60–90 s.

For the Rf chemistry, 78-s ^{261}Rf^{a} was produced by the ^{248}Cm(^{18}O,5n)^{261}Rf^{a} reaction. Identification of ^{261}Rf^{a} was made by measuring the 8.29-MeV α particles from the decay of ^{261}Rf^{a} and/or the 8.22–8.32 MeV α particles from the decay of

the 26-s ^{257}No daughter. The detection was made more certain by detecting correlated pairs of α decays from both the ^{261}Rf^{a} parent and the ^{257}No daughter. Detection rates for ^{261}Rf^{a} were as high as five events per hour of experiments. For the Db chemistry, 34-s ^{262}Db was produced by the ^{249}Bk(^{18}O,5n)^{262}Db reaction. Identification of ^{262}Db was made by measuring the 8.45-MeV α particles from the decay of ^{262}Db and/or the 8.59–8.65 MeV α particles from the decay of the 3.9-s ^{258}Lr daughter. The detection was made more certain by detecting correlated pairs of α decays from both the ^{262}Db parent and the ^{258}Lr daughter. Detection rates for the ^{262}Db were approximately one event per hour of experiments.

Because of interference from the radioactive decay of other nuclides (which are typically formed with much higher yields), extraction systems with relatively high decontamination factors from actinides, Bi, and Po must be chosen, and the transactinide activity can only be measured in the selectively extracting organic phase. For this reason, measurement of distribution coefficients is somewhat difficult. By comparing the Rf or Db detection rate under a certain set of chemical conditions to the rate observed under chemical control conditions known to give near 100% yield, distribution coefficients between about 0.2 and 5 can be determined. If the control experiments are performed nearly concurrently, many systematic errors, such as gas-jet efficiency and experimenter technique, are cancelled out. Care must be taken to avoid losses of activities, e.g., on the walls of instruments. Additionally, extraction systems which come to equilibrium in the 5–10 s phase contact time must be chosen.

3.1.2 Manual Column Chromatography

The first liquid-phase transactinide chemical separations were manually performed Rf cation-exchange separations [71] using α-hydroxyisobutyrate (α-HIB) as eluent, performed by Silva et al. in 1970. The newly discovered 78-s ^{261}Rf^{a} was produced in the ^{248}Cm(^{18}O,5n)^{261}Rf^{a} reaction, the recoils were stopped on NH_4Cl-coated Pt foils which were transported to the chemical separation area with a rabbit system. The ^{261}Rf^{a} and other products from the nuclear reaction, along with the NH_4Cl were collected from the Pt disk in a small volume of α-HIB, and run through a small cation-exchange resin column. Under these conditions, all cations with charge states of 4+ or higher were complexed with the α-HIB and eluted from the column. These experiments showed that Rf had a charge state of 4+ (or higher) and that its chemical properties are distinctly different from those of the actinides.

Although manually performed column chromatography separations were used [70] for studies with 3-min ^{260}Lr, further use of column chromatography for studying the chemical properties of the transactinides awaited the development of the automated techniques described below.

3.1.3 Future Techniques for Manual Liquid-Phase Separations

Manually performed liquid-phase chemical separations will possibly be continued to be used, especially for investigations of Rf and Db, with their relatively large production rates. New devices and techniques are under development to minimize the separation and sample preparation time and to minimize the repetitive labor required. One idea being explored is the use of extraction chromatography packings inside small syringes. By picking up the gas-jet sample in a small volume of an appropriate aqueous phase, and pulling it through the chemically selective packing inside the syringe body, and then forcing it back through the packing on to the sample preparation disk, a very fast and simple equivalent of a column separation could be performed.

With the advent of the use of kinematic pre-separators, as described in Sect. 2.2.3 above, the requirements of the chemical separation have been relaxed. It is no longer necessary to have the highest separation factors from interfering Bi, Po, and actinide radioactivities, so simpler separations which are more specific to the transactinide element being studied can be used. These relaxed separation requirements will allow development of simpler chemical separation techniques, and may lead to a new interest in manually performed chemical separations.

3.2 Automated Liquid-Phase Chemical Separations

As chemical investigations progressed from Rf and Db (with detection rates of atoms per hour), through Sg, Hs, and Bh (with detection rates of atoms per day to atoms per week), and on to even heavier elements (with expected detection rates of only a few atoms per month), manually performed chemical separations become impractical. With the automated liquid-phase chemical separation systems that have been developed to date, faster chemical separation and sample preparation times have been achieved. In addition, the precision and reproducibility of the chemical separations have been improved over that obtainable via manually performed separations.

3.2.1 Automated Rapid Chemistry Apparatus (ARCA)

Extensive studies of chemical properties of transactinide elements, Rf, Db, and Sg have been performed with the Automated Rapid Chemistry Apparatus (ARCA), see summaries in Ref. [14, 72, 73]. To improve the speed and reduce cross contamination, the ARCA II was built, featuring two magazines of 20 miniaturized ion-exchange columns [74]. With the large number of columns, cross contamination between samples can be prevented by using each column only once. By miniaturizing the columns, the elution volumes, and therefore the time needed to

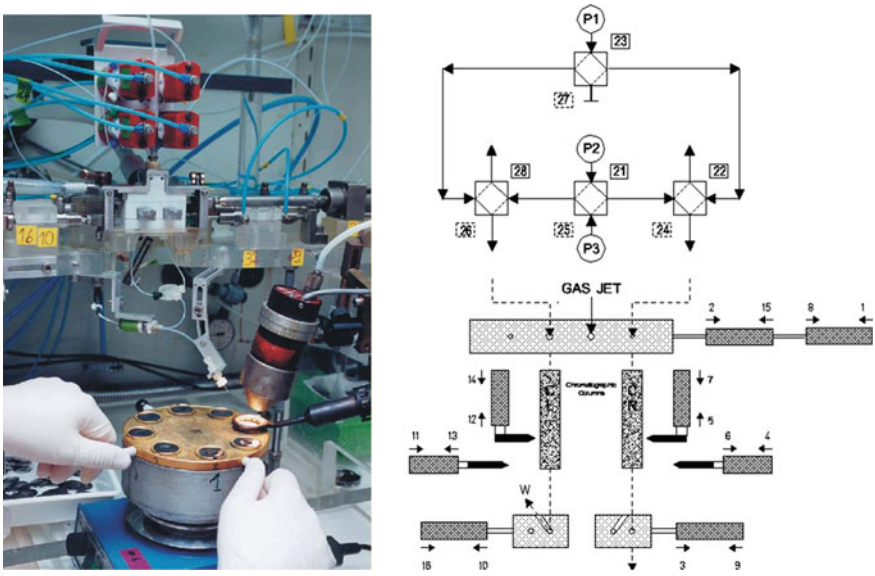

Fig. 10 Photograph (*left*) and schematic (*right*) of the ARCA (for details see text)

dry the final sample to produce a source for α spectroscopy, is much reduced. A photograph and a schematic of the ARCA microprocessor-controlled column chromatography system are presented in Fig. 10.

With ARCA II, activity-bearing aerosols are collected from a gas-jet in a small spot on a slider (seen at the center of the schematic). At the end of a suitable collection time, the slider is moved to position the collection site above one of the miniature ion-exchange columns. A suitable aqueous solution is used to dissolve the aerosols and load the activities onto the ion-exchange material in the column below. Selective elutions of transactinide elements are carried out by directing appropriate solutions through the column. A slider below the ion-exchange column is moved at the appropriate time to collect the chemical fraction of interest on a hot Ta disk. A sample suitable for α-particle pulse–height analysis is prepared by rapid evaporation of the chemical fraction on the Ta disk, which is heated from below by a hot plate, and from above by a flow of hot He gas and a high-intensity lamp. The final samples are then manually placed in a detector chamber for α-particle pulse-height spectroscopy. The two magazines of chromatography columns (CL and CR in the schematic) can be moved independently. During a chemical separation on CL, the right column, CR, is prepared by flowing an appropriate solution through it. After the separation on CL, the magazine is moved forward, placing a new column in the CL position, the next separation is performed on CR while CL is being prepared for the subsequent separation. In this way, up to 40 separations can be carried out, at time intervals of less than 1 min, with each separation performed on a freshly prepared, unused column.

Transactinide chemical separations with ARCA II have been performed with Rf [75, 76], Db [77–81] and Sg [82, 83]. More details and results are discussed in Liquid-Phase Chemistry of Superheavy Elements".

3.2.2 Automated Ion-exchange Separation Apparatus coupled with the Detection System for Alpha Spectroscopy (AIDA)

Building upon the design of ARCA II, an automated column separation apparatus, AIDA has been developed [84]. While the apparatus for collection of aerosols and performing multiple chemical separations on magazines of miniaturized ion-exchange columns is very similar to that in ARCA II, AIDA has automated the tasks of sample preparation and placing the samples in the detector chambers. Using robotic technology, the selected fractions are dried on metal Ta disks and are then placed in vacuum chambers containing large area (passivated implanted planar silicon) PIPS α-particle detectors. The schematic drawing of AIDA is given in Fig. 11. In the ion-exchange process as shown in Fig. 12, two different paths to supply solutions are available; the first eluent goes through the collection site to the microcolumn, while the second strip solution is directed to the column after one-step forward movement of the column magazine to avoid cross-contamination at the collection site.

This robotic sample preparation and counting technology, together with mechanical improvements in the chemical separation system, resulted in an automated column chromatography system that can run almost autonomously.

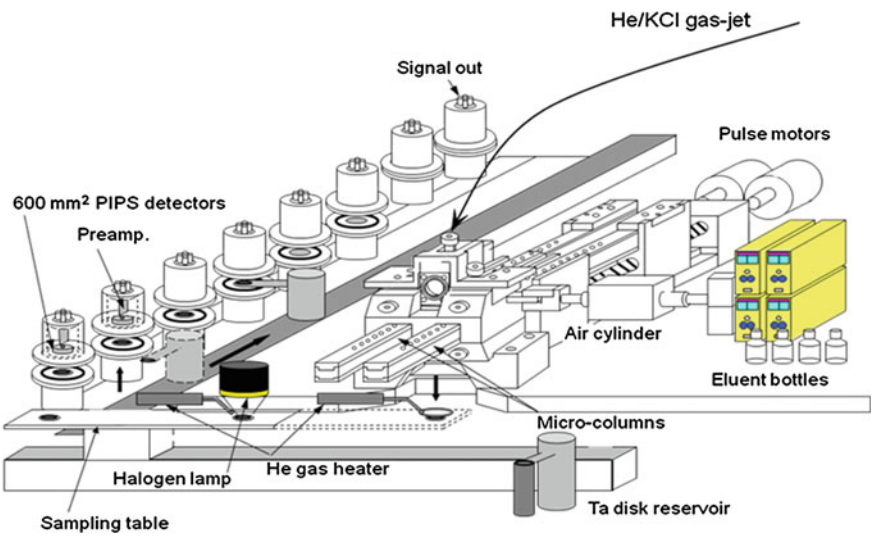

Fig. 11 Schematic drawing of AIDA [84]. Reprinted with permission of [84]. © 2005 Oldenbourg Wissenschaftsverlag GmbH

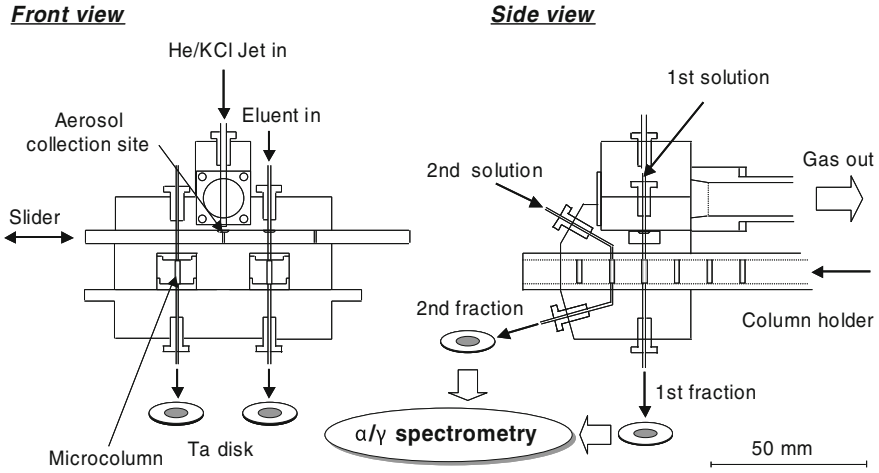

Fig. 12 Schematic of the ion-exchange part in AIDA [84]

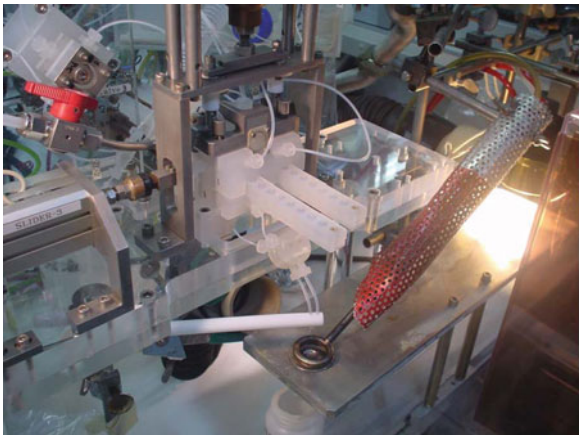

Fig. 13 Photograph of the chromatographic and sample collection part of AIDA

Each separation in columns is accomplished within 20 s and the α-particle measurement can be started within 80 s after the collection of the products at the AIDA collection site. Figure 13 shows the photograph of the chromatographic and sample collection part of AIDA. Chemical experiments with AIDA and results on Rf and Db are summarized in "Liquid-Phase Chemistry of Superheavy Elements" and in [85–92].

To shorten the time for the sample preparation of α sources, the newly developed rapid ion-exchange apparatus AIDA-II was introduced; the apparatus is based on continuous sample collection and evaporation of effluents, and successive α-particle measurement. The ion-exchange part is the same as that of AIDA. The

AIDA-II was successfully applied for the chemical experiments with Db [93]. The effluent is collected as Fraction 1 on a 15 × 300 mm tantalum sheet (0.15-mm thickness) which was continuously moving toward an α-particle detection chamber at 2.0 cm s^{-1}. The sample on the sheet is automatically evaporated to dryness with a halogen heat lamp and then subjected to the α-particle measurement in the chamber equipped with an array of 12 silicon PIN photodiode detectors [93]. Remaining products on the resin were eluted with a strip solution. The eluate is collected on another Ta sheet as Fraction 2 followed by the same procedures for sample preparation and measurement. The α-particle measurement was started 14 and 38 s after the end of product collection for Fractions 1 and 2, respectively. The result is also presented in "Liquid-Phase Chemistry of Superheavy Elements".

3.2.3 Continuous On-Line Chromatography: Identifying the Heavy Element Daughters

One of the difficulties in studying the chemical properties of the transactinide elements is presented by their relatively short half-lives. The time and labor required for performing batch-wise experiments and preparing samples suitable for α-particle pulse-height spectroscopy presents a daunting task. Since the transactinide isotopes typically decay by α-particle emission to relatively long-lived actinides, a technique has been developed to perform continuous chemical separations on the transactinide element isotopes, and detect their presence by observing the α-particle decay of the long-lived daughters. Since the daughter activities are typically produced via multinucleon transfer reactions at rates much greater than the transactinide element production rates, special techniques must be used. The three-column technique has been developed and applied to the study of the solution chemistry of Rf by Szeglowski et al. [94].

In the three column technique, as used by Trubert et al. for the study of chemical properties of Db [95], 34-s ^{262}Db was produced in the ^{248}Cm (^{19}F,5n)^{262}Db reaction and transported to the chemical separation apparatus with an aerosol gas-jet. The activities delivered by the gas-jet were continuously dissolved in an appropriate aqueous solution and passed through a series of three ion-exchange columns. The first column was used to separate all of the directly produced daughter activities, allowing the Db atoms to pass through to the second column, where they are quantitatively retained. As the Db atoms decay to Lr, Md, and Fm (via α- and EC-decay), they are desorbed from the second column and pass to the third column. The third column quantitatively retains the longer lived daughter activities. Since all directly produced Lr, Md, and Fm activities were retained on the first column, this third column should contain only Lr, Md, and Fm atoms that are the decay descendents of Db atoms which were retained on the second column. At the end of a suitable production and chemical separation cycle, the daughter activities are chemically separated from this third column, and assayed for the α-decay of the ^{254}Fm great-granddaughter of ^{262}Db.

The separation technique used for the Db study was adapted from the slightly more complicated technique developed by Pfrepper et al. [96, 97]. In this more general version, once again, the first column is used to remove all of the daughter activities initially present. The chemical conditions are chosen, so that the retention time for the nuclide of interest is on the order of its half-life on the second column, and very short on the third column. If the parent nuclide decays while on the second column, the daughter is strongly adsorbed on the third. On the other hand, if the parent atom survives passage through the second column (and the third), the daughter atom will be found in the effluent from the third column. In this way, the retention time on the second column (and thus the distribution coefficient) of the nuclide of interest is can be measured by comparing the relative amounts of the long-lived daughter activity on the third column and in the effluent of the third column. Three-column systems have been developed in hopes of performing chemical studies with other transactinides [98]; see also "Liquid-Phase Chemistry of Superheavy Elements".

3.2.4 SISAK

The SISAK (Short-lived Isotopes Studied by the AKUFVE-technique, where AKUFVE is s Swedish acronym for an arrangement of continuous investigations of distribution ratios in liquid extraction) system performs continuous liquid–liquid extractions using small-volume separator centrifuges [99]. Activities are delivered to the apparatus with an aerosol gas-jet. The gas-jet is mixed with the aqueous solution to dissolve the activity-bearing aerosols, and the carrier gas is removed in a degasser centrifuge. The aqueous solution is then mixed with an organic solution and the two liquid phases are separated in a separator centrifuge. A scintillation cocktail is then mixed with the organic solution, and this is passed through a detector system to perform liquid scintillation α pulse-height spectroscopy on the flowing solution.

This modular separation and detection system allows the use of well-understood liquid–liquid extraction separations on timescales of a few seconds, with detection efficiencies near 100%. This extremely fast chemical separation and detection system has been used with a sub-second α-active nuclide [100, 101]. However, for the transactinide elements, which are produced in much lower yields with larger amounts of interfering β activities, detection of the α decay of the transactinide isotopes failed. As described in Sect. 2.2.3, pre-separation with the Berkeley Gas-filled Separator before transport to and separation with SISAK allowed the chemical separation and detection of 4-s ^{257}Rf [50]. A schematic of the BGS-RTC-SISAK apparatus is presented in Fig. 14. These proof-of-principle experiments have paved the way for detailed liquid–liquid extraction experiments on short-lived transactinide element isotopes.

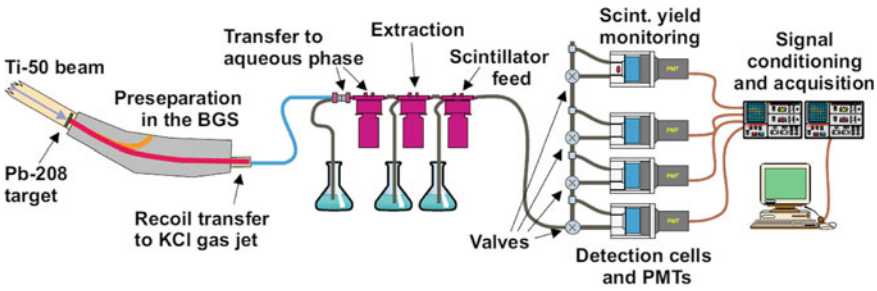

Fig. 14 Schematic of the SISAK liquid–liquid extraction system using the Berkeley Gas-filled Separator as a pre-separator. Reprinted with permission from [50]. © 2002 The Japan Society of Nuclear and Radiochemical Sciences

3.2.5 Future Techniques for Automated Liquid-Phase Chemical Separations

Experiments have been carried out to measure the chemical properties of elements Rf through Hs. Recent experiments have resulted in the identification of isotopes of Cn and Fl with half-lives of at least a few seconds [102]: long enough for future chemical studies. For isotopes of these superheavy elements, production rates are as low as a few atoms per month, making any chemical separations with these elements especially difficult. New, highly efficient aqueous-phase chemical separation systems will have to be developed. Since these separations will be operating for months at a time, they must be designed to run autonomously, presenting unique new challenges to the aqueous-phase chemists.

The development of a new apparatus for the study of electrochemical properties of the heaviest elements has been conducted by Toyoshima et al. [103]. The apparatus is based on a flow electrolytic cell combined with column chromatography. A cross-sectional view of the apparatus is illustrated in Fig. 15. The working electrode is made of bundle of glassy-carbon fibers that is packed in a porous Vycor glass tube (4.8 mm i.d., 7 mm o.d., and 30 mm long) which works as an electrolytic diaphragm. The surface of the carbon fibers was modified with Nafion perfluorinated cation-exchange resin (Nafion dispersion solution DE2020, Wako Chemicals) [103]. A platinum-mesh counter electrode was placed in the electrolyte pool to surround the glass tube. The potential on the working electrode was controlled using a potentiostat referring to the 1.0 M LiCl-Ag/AgCl electrode placed in the pool.

The apparatus was applied to the oxidation of No^{2+} by controlling the applied potential, and A. Toyoshima et al. [104] successfully conducted the oxidation of the No^{3+} ion to the trivalent state No^{3+} in α-hydroxyisobutyric acid (α-HIB) solution based on an atom-at-a-time scale. The isotope ^{255}No with a half-life of 3.1 min was synthesized in a nuclear fusion reaction between ^{12}C ions and a ^{248}Cm target at the JAEA (Japan Atomic Energy Agency) tandem accelerator with a typical production rate of 30 atoms per minute. Nuclear reaction products recoiling

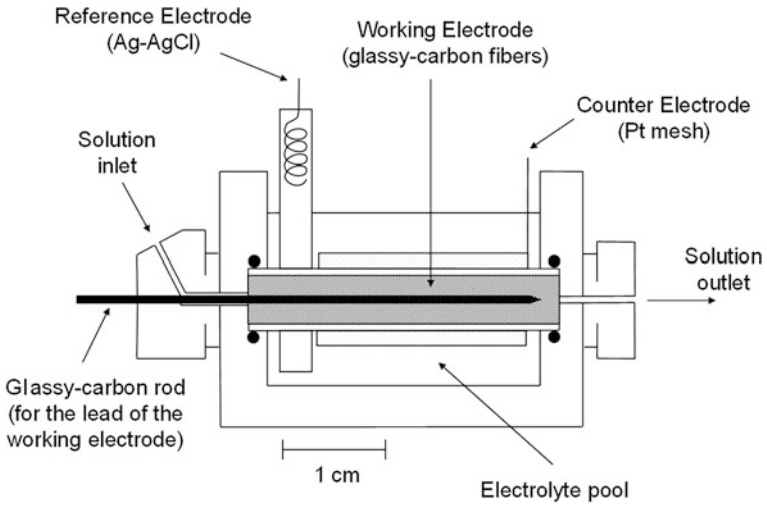

Fig. 15 Schematic view of the electrochemistry apparatus [103]. Reprinted with permission of [103]. © 2008 Oldenbourg Wissenschaftsverlag GmbH

out of the target were attached to potassium chloride (KCl) aerosols seeded in a He gas stream and were then continuously transported to the chemistry laboratory through a Teflon capillary (2.0 mm i.d. × 25 m) within a few seconds. For 10 min, the transported products were deposited on a plastic plate of AIDA. After collection, the products were dissolved with 1080 μL of 0.1 M α-HIB (pH 3.9) and were subsequently fed through a thin Teflon tube into the electrochemical apparatus at a flow rate of 600 μL min^{-1}. The effluent from the column electrode was consecutively collected with a volume of 180 μL on 6 separate Ta disks. The remaining products in the column were stripped with 360 μL of 3.0 M HCl and collected on another 2 Ta disks. The eight samples were evaporated to dryness using hot He gas and halogen heat lamps and were then transferred to an α-spectrometry station of AIDA. The above procedures were accomplished within 3 min and repeated numerous times to obtain sufficient statistics of the α-decay counts of ^{255}No.

Figure 16 shows the oxidation probability of No as a function of the applied potential, that probability defined as $100 \times \left[No^{3+}\right] / \left(\left[No^{2+}\right] + \left[No^{3+}\right]\right)$, where $[No^{2+}]$ and $[No^{3+}]$ represent the radioactivities of ^{255}No measured in the 3.0 M HCl and 0.1 M α-HIB fractions, respectively. The oxidation reaction begins at around 0.7 V and is complete by 1.0 V. The formal redox potential of the $No^{3+} + e^- \leftrightarrows No^{2+}$ reaction corresponding to half of the oxidation probability is evaluated to be approximately 0.75 V under the present conditions. This new technical approach will open up new frontiers of the chemistry of superheavy elements.

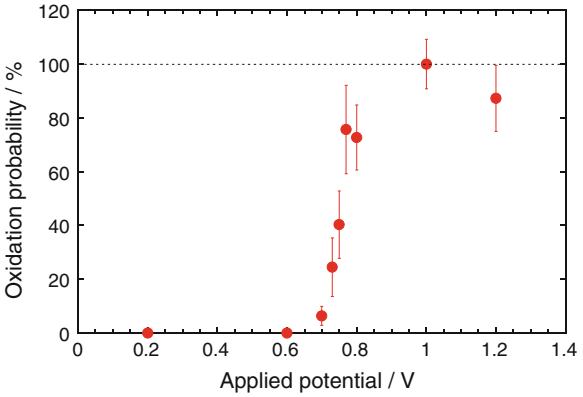

Fig. 16 Oxidation probability of ^{255}No versus applied potential [104]. Reprinted with persmission from Ref. [104]. © 2009 American Chemical Society

4 Techniques and Instruments for Gas-Phase Chemistry

Despite the fact that only few inorganic compounds of the transition elements exist, that are appreciably volatile below an experimentally still easily manageable temperature of about 1000 °C, gas-phase chemical separations played and still play an important role in chemical investigations of transactinide elements. A number of prerequisites that need to be fulfilled simultaneously to accomplish a successful chemical experiment with a transactinide element are almost ideally met by gas chromatography of volatile inorganic compounds. Since the synthesis of transactinide nuclei usually implies a thermalization of the reaction products in a gas volume, a recoil chamber can be connected with a capillary directly to a gas chromatographic system. Gas-phase separation procedures are fast, efficient and can be performed continuously, which is highly desirable in order to achieve high overall yields. Finally, nearly weightless samples can be prepared on thin foils, which allow α spectroscopy and SF spectroscopy of the separated products with good energy resolution and in high, nearly 4π, detection geometry.

Early on, gas-phase chemical separations played an important role in the investigation of the chemical properties of transactinide elements. The technique was pioneered by Zvara et al. at the Dubna laboratory and involved first chemical studies of volatile Rf, Db, and Sg halides and/or oxyhalides [105–107]; see "Gas-Phase Chemistry of Superheavy Elements" for a detailed discussion. The experimental set-ups and the techniques involved are presented in Sect. 4.2. A new technique, named OLGA (On-line Gas chromatography Apparatus), which allowed the α-spectrometric measurement of final products, developed by Gäggeler et al. [108] was then successful in studying volatile transactinide compounds from Rf up to Bh [109–112], see "Gas-Phase Chemistry of Superheavy Elements" for a detailed discussion. In all these experiments, the isolated transactinide nuclides

were unambiguously identified by registering their characteristic nuclear decay, see Sect. 4.3. The technique of synthesizing volatile species *in-situ* in the recoil chamber combined with a new cryo thermochromatography detector [51] was successful in the first chemical identification of Hs (element 108) [45] and in first chemical investigations of Cn in the elemental state [41, 42], see Sect. 4.4.

4.1 Thermochromatography and Isothermal Chromatography

For the experimental investigation of volatile transactinide compounds, two different types of chromatographic separations have been developed, thermochromatography and isothermal chromatography. Sometimes also combinations of the two have been applied. The basic principles of thermochromatography and isothermal chromatography are explained in Fig. 17.

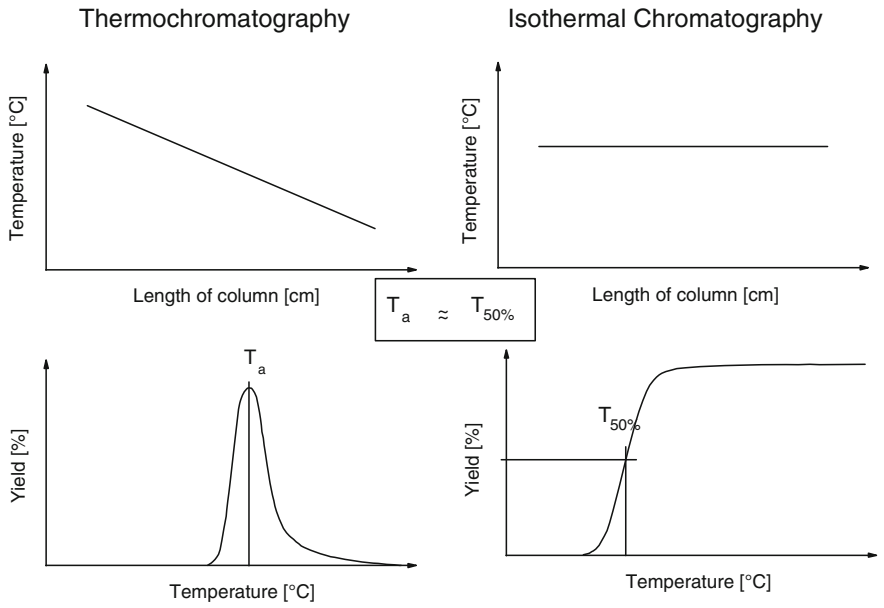

Fig. 17 *Upper panel* temperature profiles employed in thermochromatography and isothermal chromatography; *lower panel* deposition peak and integral chromatogram resulting from thermochromatography and isothermal chromatography, respectively

4.1.1 Thermochromatography

In thermochromatography, see, e.g., Ref. [113] for a review, a carrier gas is flowing through a chromatography column, to which a negative longitudinal temperature gradient has been applied. Open or filled columns can be employed. Species, that are volatile at the starting point, are transported downstream of the column by the carrier gas flow. Due to the decreasing temperature in the column, the time the species spend in the adsorbed state increases exponentially. Different species form distinct deposition peaks, depending on their adsorption enthalpy $\left(\Delta H_a^0\right)$ on the column surface and are thus separated from each other. A characteristic quantity is the deposition temperature (T_a), which depends on various experimental parameters, see "Gas-Phase Chemistry of Superheavy Elements". The mixture of species to be separated can be injected continuously into the column [114–117], or the experiment can be performed discontinuously by inserting the mixture of species through the hot end of the chromatography column, and removing the column through the cold end after completion of the separation. The two variants (continuous or discontinuous) result in slightly different peak shapes. The chromatographic resolution is somewhat worse for the continuous variant. Thermochromatographic separations are the method of choice to investigate species containing long-lived nuclides that decay either by γ emission, EC or β^+ decay, or by the emission of highly energetic β^- particles [118–124]. Thus, the emitted radiation can easily be detected by scanning the length of the column with a detector. The detection of nuclides decaying by α-particle emission or SF decay is more complicated. By inserting SF track detectors into the column, SF decays of short- and long-lived nuclides can be registered throughout the duration of the experiment. After completion of the experiment, the track detectors are removed and etched to reveal the latent SF tracks. Columns made from fused silica have also been used as SF track detectors [107]. However, the temperature range for which SF track detectors can be applied is limited, due to the annealing of tracks with time. It should also be noted, that in thermochromatography all information about the half-life of the deposited nuclide is lost, which is a serious disadvantage, since SF is a nonspecific decay mode of many actinide and transactinide nuclides. However, thermochromatography experiments with transactinides decaying by SF have an unsurpassed sensitivity (provided that the chromatographic separation from actinides is sufficient), since all species are eventually adsorbed in the column and the decay of each nuclide is registered. Thus, the position of each decay in the column contributes chemical information about ΔH_a^0 of the investigated species.

4.1.2 Isothermal Chromatography

In isothermal chromatography, a carrier gas is flowing through a chromatography column of constant, isothermal temperature. Open or filled columns can be

employed. Depending on the temperature and on ΔH_a^0 of the species on the column surface, the species travel slower through the length of the column than the carrier gas. This retention time can be determined either by injecting a short pulse of the species into the carrier gas and measuring the time at which it emerges through the exit of the column [125, 126], or by continuously introducing a short-lived nuclide into the column and detecting the fraction of nuclides that have decayed at the exit of the column [108, 127–130]. A characteristic quantity is the temperature at which half of the introduced nuclides are detected at the exit ($T_{50\%}$). In this case, the retention time in the column is equal to the half-life of the introduced nuclide. The half-life of the nuclide is thus used as an internal clock of the system. The $T_{50\%}$ temperature depends on various experimental parameters; see "Gas-Phase Chemistry of Superheavy Elements". It can be shown, that for similar gas flow rates and column dimensions $T_a \approx T_{50\%}$. By varying the isothermal temperature, an integral chromatogram is obtained. The yield of the species at the exit of the column changes within a short interval of isothermal temperatures from zero to maximum yield. A variant of isothermal chromatography using long-lived radionuclides is temperature programmed chromatography. The yield of different species at the exit is measured as a function of the continuously, but isothermally, increasing temperature [126, 131–134].

On-line isothermal chromatography is ideally suited to rapidly and continuously separate short-lived radionuclides in the form of volatile species from less volatile ones. Since volatile species rapidly emerge at the exit of the column, they can be condensed and assayed with nuclear spectroscopic methods. Less volatile species are retained much longer and the radionuclides eventually decay inside the column.

A disadvantage of isothermal chromatography concerns the determination of ΔH_a^0 on the column surface of transactinide nuclei. In order to determine the $T_{50\%}$ temperature, a measurement sufficiently above and below this temperature is required. Since for transactinide elements this temperature is a priori unknown, several measurements at different isothermal temperatures must be performed, which means that long measurements are required below the $T_{50\%}$ temperature that demonstrate that the transactinide compound is retained long enough that most of the nuclei decayed in the column. Such an approach is very beam time consuming. Furthermore, it must be demonstrated that the experiment was performing as expected and the non-observation of transactinide nuclei was not be due to a malfunctioning of the apparatus.

4.2 Instrumentation for Early Gas-Phase Chemistry Experiments with Transactinide Elements

A schematic drawing of the chemical apparatus constructed for the first chemical isolation of element 104 in Dubna is shown in Fig. 18 [135].

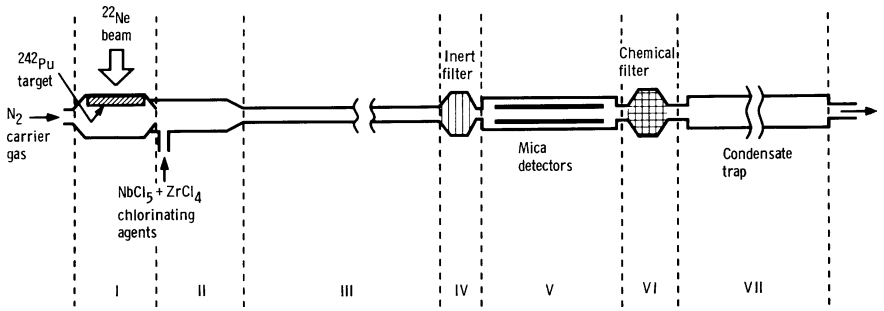

Fig. 18 Schematic of the first gas chromatography apparatus used to chemically isolate element 104 in the form of volatile chlorides (Figure from [10], adapted from [136]). Reprinted with permission from [10]. © 1987 Oldenbourg Wissenschaftsverlag GmbH

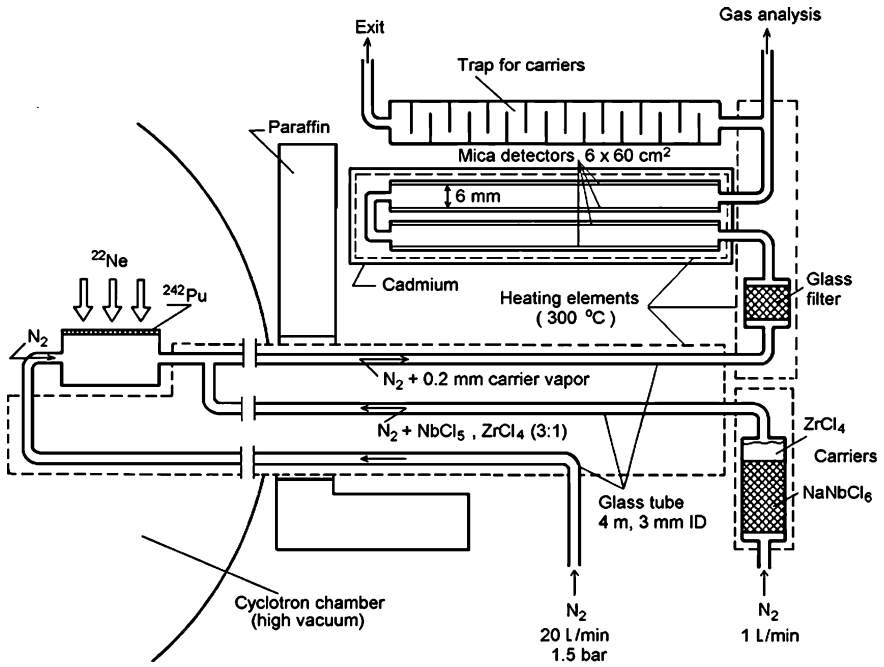

Fig. 19 Diagram of the experimental set-up to isolate short-lived, volatile Rf compounds at the internal beam of the U-300 cyclotron in Dubna [135], Figure from [113]

A diagram showing different sections of the apparatus is displayed in Fig. 19. In section I, a ^{242}Pu target was bombarded at the inner beam of the U-300 cyclotron at Dubna with ^{22}Ne ions. The ^{242}Pu with a thickness of about 800 μg/cm^2 was deposited as oxide on an aluminum foil of 6–9 μm thickness. The target was held between two plates made of an aluminum alloy, into which a number of

closely spaced holes of 1.5 mm diameter were drilled. Both sides of the target were flushed with nitrogen at 250 or 300 °C. In the outer housing of the target chamber, a number of closely spaced holes of 1.5 mm were drilled, which matched the holes of the target holder. An Al foil of 9 μm thickness served as vacuum window. The whole target block was heated with a heater. The space behind the target was limited with an Al foil and was about 11 mm deep and had a volume of about 2 cm^3.

Reaction products recoiling from the target were thermalized in a rapidly flowing stream of N_2 (18 L/min) and were transferred to section II, where the chlorination of the reaction products took place. The transfer efficiency was measured to be >75% and the transfer time was only about 10^{-2} s. In the reaction chamber of section II, vapors of $NbCl_5$ and $ZrCl_4$ were continuously added as chlorinating agents and as carriers [135]. It was found that carriers with a vapor pressure similar to that of the investigated compound yielded optimum transfer efficiencies [114]. The addition of carriers was essential since in this manner the most reactive adsorption sites could be passivated.

Volatile reaction products were flushed into the chromatographic section (section III), which was a 4 m long column with an inner diameter of 3.5 mm. This section consisted of an outer steel column into which tubular inserts of various materials (Teflon™, glass) could be inserted [135]. Section IV contained a filter. This filter had a stainless steel jacket into which, as a rule, crushed column material from section III was filled [135]. This filter was intended to trap large aggregate particles [136]. Aerosols were apparently formed by the interaction of the chloride vapors ($NbCl_5$) with oxygen present in the nitrogen carrier gas. Volatile products passing the filter in section IV now entered the detector in section V. This detector consisted of a narrow channel of mica plates, which recorded SF fragments of the SF decay of a Rf nuclide. The mica plates were removed after completion of the experiment, etched and analyzed for latent fission tracks. The filter in section VI served for the chemisorption of Hf nuclides in ancillary work with long-lived nuclides. In section VII, the chloride carriers were condensed.

The whole apparatus was built to chemically identify an isotope of Rf decaying by SF with a half-life of 0.3 s, that had previously been synthesized and identified by a team of physicists at Dubna. In a number of experiments, Zvara et al. identified multiple SF tracks in the mica detectors when they used glass surfaces and temperatures of 300 °C [135]. They had shown in preparatory experiments with Hf, that indeed the transfer of Hf through the apparatus occurred within less than 0.3 s, and thus that the experimental set-up was suited to study the short-lived Rf isotope [114]. A number of possible sources of SF tracks in the mica detectors other than the SF decay of an Rf isotope were discussed and ruled out. Further experiments with a slightly modified apparatus [137] were conducted immediately after the experiments described here. A total of 63 SF events were attributed to the decay of an Rf nuclide.

Similar thermochromatography set-ups, always relying on the registration of SF tracks, were employed by Zvara et al. to chemically identify the next heavier

transactinide elements Db [12, 106, 138], and Sg [107, 139–141], whereas experiments to chemically identify Bh [142] yielded negative results. However, due to the fact that in all these experiments the separated nuclides were identified by the non characteristic SF decay, and no further information such as the half-life of the investigated nuclide could be measured, most of the experiments fell short of fully convincing the scientific community, that indeed a transactinide element was chemically isolated [10, 20, 143, 144]. Nevertheless, the ideas conceived at Dubna and the techniques invented to chemically study short-lived single atoms, paved the way to gas chromatography experiments that allowed the unambiguous identification of the separated transactinide nuclei.

4.3 *On-line Gas-Phase Chemistry with Direct Identification of Transactinide Nuclei*

One of the most successful approaches to the study of volatile transactinide compounds is the so-called On-Line Gas chromatography Apparatus (OLGA) technique. Contrary to the technique in Dubna, reaction products are rapidly transported through a thin capillary to the chromatography setup with the aid of an aerosol gas-jet transport system, see Sect. 2.2.2. With typical He flow rates of 1–2 L/min and inner diameters of the capillaries of 1.5–2 mm, transport times of less than 10 s were easily achieved. This way, the chromatography system and also the detection equipment could be set up in an accessible, fully equipped chemistry laboratory close to the shielded irradiation vault. The aerosols carrying the reaction products are collected on quartz wool inside a reaction oven. Reactive gases are introduced to form volatile species, which are transported downstream by the carrier gas flow to an adjoining isothermal section of the column, where the chromatographic separation takes place.

A first version of OLGA (I) was developed and built by Gäggeler et al. for the search of volatile superheavy elements, and tested with 25-s ^{211m}Po [129]. Volatile elements were separated in a stream of He and H_2 gas at 1000 °C from nonvolatile actinides and other elements. At the exit of the column, the separated nuclei were condensed on thin metal foils mounted on a rotating wheel ROtating wheel Multidetector Apparatus (ROMA) [145, 146] and periodically moved in front of solid–state detectors, where α particles and SF events were registered in an event-by-event mode. A first attempt to identify the nuclide ^{261}Rf^{a} after chemical isolation as volatile $RfCl_4$ is described by von Dincklage et al. [128]. While the gas chemical isolation of short-lived α particle emitting Hf nuclides was successful, the experiment with Rf failed, since the employed surface barrier detectors were destroyed by the prolonged exposure to the chlorinating agent.

The first successful gas chemical studies of volatile halides of Rf [109] involving the unambiguous detection of time correlated nuclear α decay chains ^{261}Rf^{a} $\longrightarrow$ ^{257}No $\longrightarrow$ ^{253}Fm was accomplished with OLGA(II) [108]. Instead of

condensing the separated molecules on metal foils after passing the chromatography column, they were attached to new aerosol particles and transported through a thin capillary to the detection system. This so-called reclustering process was very effective and allowed to collect the aerosols on thin ($\approx$40 μg/cm^2) polypropylene foils in the counting system (ROMA or MG, Merry Go round [147]). Thus, samples could be assayed from both sides in a 4π geometry, which doubled the counting efficiency. A crucial detail was the use of then newly available PIPS detectors (instead of surface barrier detectors) which were resistant to the harsh chemical environment. At the same time, the Paul Scherrer Institute (PSI) tape system was developed [108], which allowed to significantly reducing the background of long-lived SF activities that accumulated on the wheel systems. However, only a 2π counting geometry could be realized.

An improved version of OLGA(II) was built at Berkeley and was named Heavy Element Volatility Instrument (HEVI) [130]. With both instruments the time needed for separation and transport to detection was about 20 s, the time-consuming process being the reclustering. In order to improve the chromatographic resolution and increase the speed of separation, OLGA(III) was developed [16]. Using a commercial gas chromatography oven and a 2 m long quartz column which ended in a much smaller, redesigned recluster unit, the overall separation time could be reduced by one order of magnitude, while the chromatographic resolution was much better. A schematic of OLGA(III) connected to either a rotating wheel or a tape detection system is shown in Fig. 20.

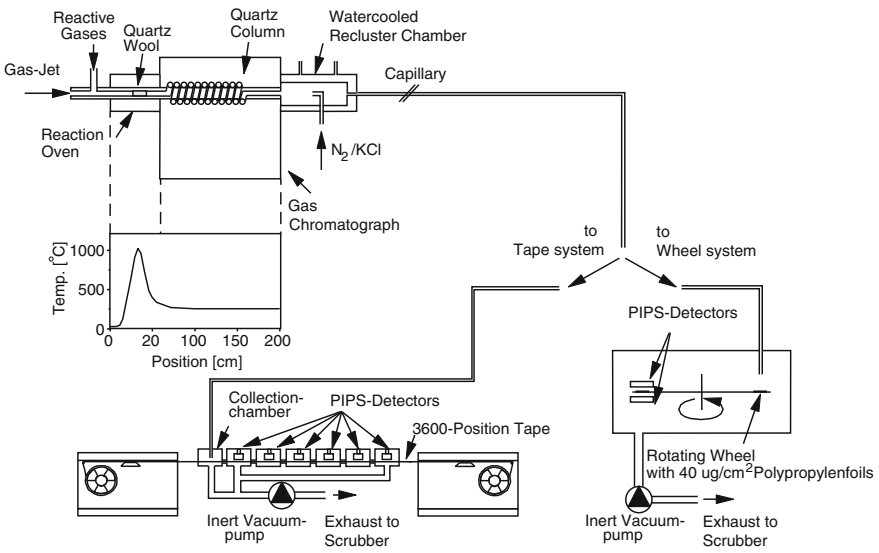

Fig. 20 Schematic of OLGA(III) in combination with the tape detection system or the MG or ROMA wheel detection system [16]. Reprinted with permission of [16]. © 1996 Oldenbourg Verlag GmbH. See text for a more detailed description

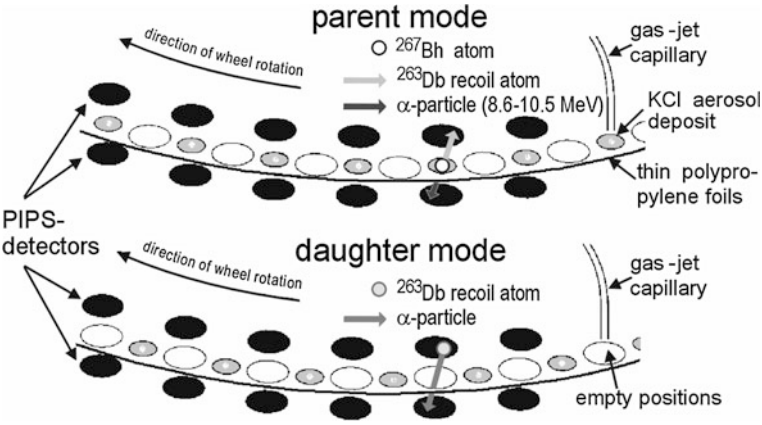

Fig. 21 Parent–daughter mode for rotating wheel systems. See the text for detailed description of operation

OLGA(III) has very successfully been applied to study volatile halides and/or oxyhalides of Rf [148], Db [149], Sg, [111, 150] and Bh [112], see "Gas-Phase Chemistry of Superheavy Elements" for a detailed discussion. In all these experiments, the separated transactinide nuclides were unambiguously identified via their nuclear decay properties. An improved version of OLGA(I), named high-temperature on-line gas chromatography apparatus (HITGAS), has been developed at Forschungszentrum Rossendorf and successfully applied to study oxide hydroxides of group 6 elements including Sg [151, 152].

In order to further reduce the background of unwanted α-decaying nuclides, the so-called parent–daughter recoil counting modus was implemented at the rotating wheel systems. Since the investigated transactinide nuclei decay with a characteristic decay sequence involving the α decay and/or SF decay of daughter nuclei, the significance of the observed decay sequence can be enhanced by observing the daughter decays in a nearly background free counting regime. This can be accomplished in the following manner, see example with ^{267}Bh in Fig. 21. In the parent mode, a ^{267}Bh atom is deposited on the top of a thin foil together with a sample of the aerosol transport material. The wheel is double stepped at preset time intervals to position the collected samples successively between pairs of α-particle detectors. When the ^{267}Bh α-decay is detected in the bottom of a detector pair, it is assumed that the ^{263}Db daughter has recoiled into the face of the top detector. The wheel is single stepped to remove the sources from between the detector pairs, and a search for the ^{263}Db and ^{259}Lr daughters is made for a second preset time interval, before single stepping the wheel again to resume the search for decays of ^{267}Bh.

4.4 In-situ Volatilization and On-line Detection

Even though the OLGA technique has very successfully been applied in gas-phase chemical studies of elements Rf through Bh, the overall efficiency (including the detection of a two member decay chain) was only about 4%, too low to continue studies at the picobarn cross-section level. Obviously, the large number of steps involved, each having a yield below 100%, lead to a poor overall efficiency. These include thermalization of the recoil products in a gas, attachment of products in ionic or atomic form to the surface of aerosol particles, transport of these particles through capillaries, hetero-chemical reactions of the attached species with reactive gases to form volatile compounds, gas adsorption chromatography of the compounds with the surface of the chromatography column, re-attachment of ejected molecules to new particles followed by a transport to the counting device, and finally deposition of the particles on thin foils via impaction.

Therefore, it would be advantageous to perform the chemical synthesis of the volatile molecule in-situ in the recoil chamber. This approach has already been used in the very first chemical studies of transactinides, see Sect. 4.2. Chlorinating and brominating agents were added to a carrier gas in order to form volatile halides of the 6d elements. However, in these early experiments only tracks of SF events were revealed after completion of the experiment. Obviously, such a technique has the disadvantage of not yielding any on-line information during an ongoing experiment. Moreover, most isotopes of transactinide elements decay primarily by α-particle emission.

For studies of element 108 (Hs) and Cn the new device named In-situ Volatilization and On-line detection (IVO) was developed [153]. By adding O_2 to the He carrier gas, volatile tetroxides of group 8 elements were formed in-situ in the recoil chamber. A quartz column containing a quartz wool plug heated to 600 °C was mounted as close as possible to the recoil chamber. The hot quartz wool served as an aerosol filter and provided a surface to complete the oxidation reaction. For future studies with Cn or Fl (element 114) pure He or even a reducing He/H_2 mixture can be employed; see also Sect. 2.2.3 for experiments with in-situ volatilization techniques applied behind recoil separators and making use of recoil transfer chambers.

In order to efficiently detect the nuclear decay of isolated nuclides as well as to obtain chemical information about the volatility of the investigated compounds a completely new technique was devised. This new development is cryo thermochromatography of very volatile species on positive implanted N-type silicon (PIN) diode surfaces that allow α particle and SF spectrometry [51]. The carrier gas containing volatile atoms (i.e., At, Rn, Hg) or molecules (i.e., OsO_4, HsO_4) is flowing through a narrow channel formed by a series of planar silicon diodes. Along this channel a longitudinal negative temperature gradient is established. Due to the close proximity of the silicon diodes facing each other, the probability to register a complete decay chain consisting of a series of α decays is rather high. A first Cryo Thermochromatographic Separator (CTS) was constructed by Kirbach

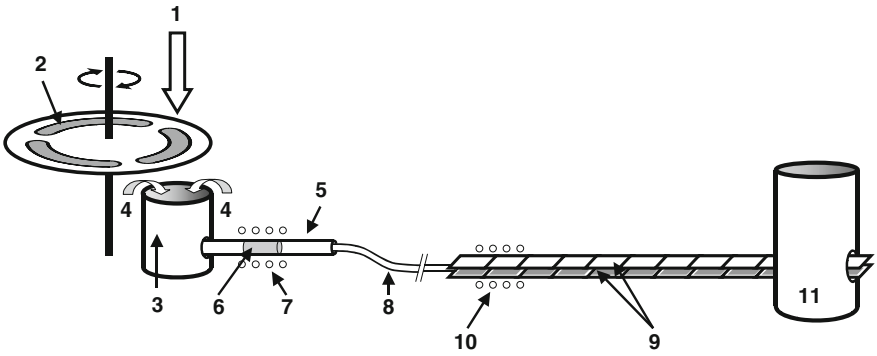

Fig. 22 The ^{26}Mg-beam (1) passed through the rotating vacuum window and ^{248}Cm-target (2) assembly. In the fusion reaction ^{269,270}Hs nuclei were formed which recoiled out of the target into a gas volume (3) and were flushed with a He/O_2 mixture (4) to a quartz column (5) containing a quartz wool plug (6) heated to 600 °C by an oven (7). There, Hs was converted into HsO_4 which is volatile at room temperature and transported with the gas flow through a perfluoroalkoxy (PFA) capillary (8) to the COLD detector array registering the nuclear decay ($\propto$ and spontaneous fission) of the Hs nuclides. The array consisted of 36 detectors arranged in 12 pairs (9), each detector pair consisted of 3 PIN diode sandwiches. Always three individual PIN diodes (*top and bottom*) were electrically coupled. A thermostat (10) kept the entrance of the array at 20 °C; the exit was cooled to −170 °C by means of liquid nitrogen (11). Depending on the volatility of HsO_4, the molecules adsorbed at a characteristic temperature. Figure reproduced from [45]

et al. [51] at the Lawrence Berkeley National Laboratory. A schematic of the experimental set-up used in the first successful chemical identification of Hs as volatile tetroxide is shown in Fig. 22.

In the actual Hs experiment [45] an improved version namely the Cryo On-Line Detector (COLD) was used. This detector was constructed at PSI and consisted of 2 times 36 PIN diodes. A schematic of the COLD is shown in Fig. 23. The COLD featured a steeper temperature gradient and reached a lower end temperature of −170 °C. Two PIN-diodes mounted on ceramic supports were glued together facing each other. Two T-shaped spacers made from silicon confined the gas flow to the active surface of the diodes. The gap between the PIN diodes in the COLD was reduced to 1.5 mm, increasing thus the detection efficiency. The PIN diode sandwiches were enclosed in a Teflon^{TM} coated copper bar, which was placed in a stainless steel housing that was purged with dry N_2. The copper bar was heated at the entrance side with a thermostat to +20 °C and cooled at the exit with a liquid N_2 cold finger. The geometrical efficiency for detecting a single α-particle emitted by a species adsorbed inside the detector array was 77%. The detectors of the COLD array were calibrated on-line with α-decaying ^{219}Rn and its daughters ^{215}Po and ^{211}Bi using a ^{227}Ac source. An improved version named Cryo On-line Multidetector for Physics And Chemistry of Transactinides (COMPACT) with a gap of only 0.6 mm and an inner active detector surface of 93% was successful in identifying the new nuclides ^{270}Hs and ^{271}Hs [154, 155]. By increasing the geometrical detection efficiency, the efficiency of detecting complete α-particle

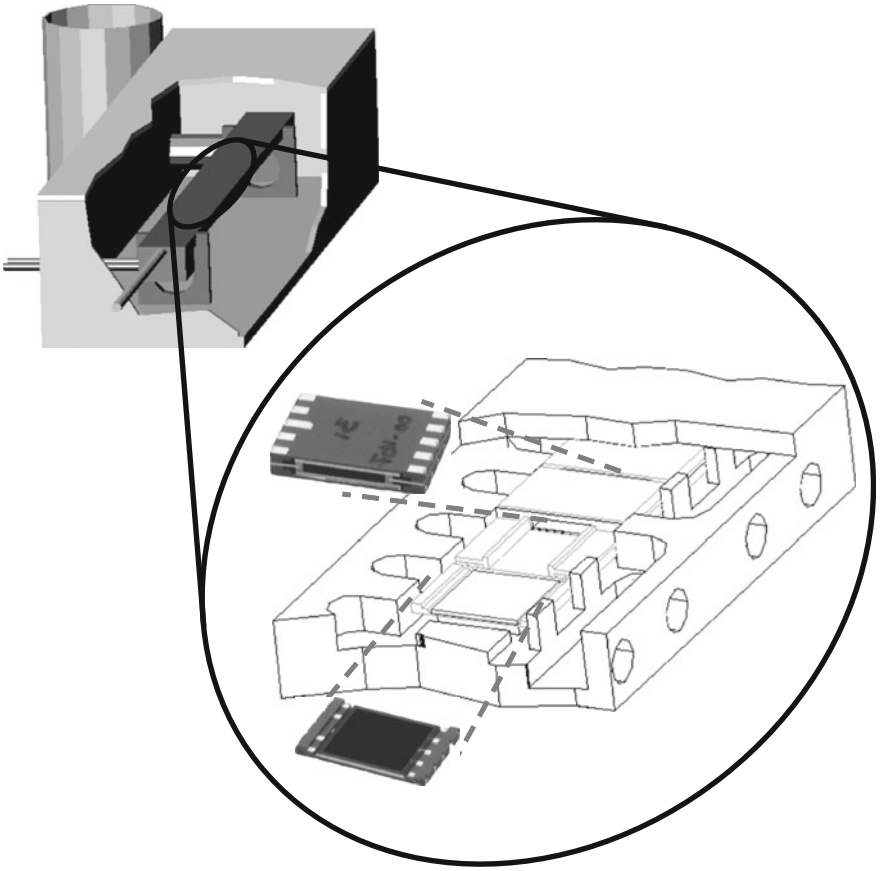

Fig. 23 Schematic of the Cryo On-Line Detector (COLD). For a detailed description see text. Figure from [156]

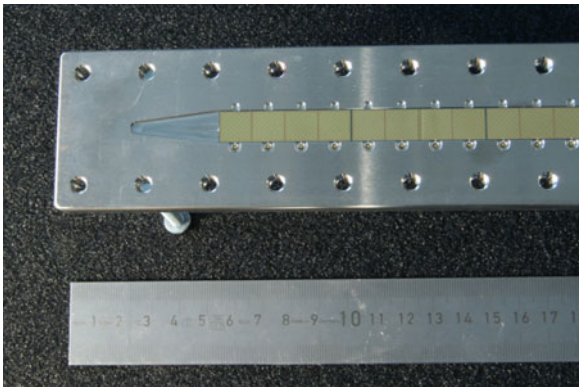

Fig. 24 Photograph of one side of the detector array used in the COMPACT system. Always four PIPS detectors are arranged on one detector chip, with a spacing of 100 μm. The detectors shown here have been covered with a thin layer of Au of few nm thickness. Two such detector panels are mounted facing each other to form a chromatographic channel

decay chains with three or four members was significantly increased, since the detection efficiency for such decay chains is a multiple product of the detection efficiency for a single α-particle.

The concept of CTS, COLD, and COMPACT proved very successful in studying even heavier elements such as Cn and Fl in their elemental state [41–43]. In order to study the interaction of single Cn and Fl atoms with Au, the PIPS detector surfaces were covered with a thin, few nanometer thick layer of Au. In the photograph in Fig. 24, the array of Au covered detectors is displayed. Always four detectors are arranged on a detector chip. The spacing between the individual detectors on one chip is only 100 μm. This array of detectors is covered with an identical second one forming thus the chromatographic channel. The two arrays are sealed with an In wire, which is an ideal sealant at the very low temperatures at which one end of the detector array is operated.

References

1. Rutherford, E.: A radio-active substance emitted from thorium compounds. Philos. Mag. **49**, 1–14 (1900)
2. Herrmann, G., Trautmann, N.: Rapid chemical methods for identification and study of short-lived nuclides. Annu. Rev. Nucl. Part. Sci. **32**, 117–147 (1982)
3. Meyer, R.A.: Rapid automated batchwize radiochemical separation techniques. J. Radioanal. Nucl. Chem. Art. **142**, 135–144 (1990)
4. Skarnemark, G., Alstad, J., Kaffrell, N., Trautmann, N.: Studies of short-lived fission-products by means of the multistage solvent-extraction system SISAK. J. Radioanal. Nucl. Chem. Art. **142**, 145–158 (1990)
5. Rengan, K., Meyer, R.A.: Ultrafast chemical separations, Vol. NAS-NS-3118. Nuclear Science Series. National Academy Press, Washington (1993)
6. Baker, J.D., Meikrantz, D.H., Gehrke, R.J., Greenwood, R.C.: Nuclear decay studies of rare-earth fission-product nuclides using fast radiochemical separation techniques. J. Radioanal. Nucl. Chem. Art. **142**, 159–171 (1990)
7. Gäggeler, H.W.: On-line gas chemistry experiments with transactinide elements. J. Radioanal. Nucl. Chem. **183**, 261–271 (1994)
8. Hahn, O., Strassmann, F.: About the evidence and the behavior in uranium radiation using neutron occuring earth alkaloid metals. Naturwissenschaften **27**, 11–15 (1939)
9. Seaborg, G.T., Loveland, W.D.: The Elements Beyond Uranium. Wiley & Sons, New York (1990)
10. Hyde, E.K., Hoffman, D.C.: A history and analysis of the discovery of elements 104 and 105. Radiochim. Acta **42**, 57–102 (1987)
11. Wierczinski, B., Gregorich, K.E., Kadkhodayan, B., Lee, D.M., Beauvais, L.G., Hendricks, M.B., Kacher, C.D., Lane, M.R., Keeney-Shaughnessy, D.A., Stoyer, N.J., Strellis, D.A., Sylwester, E.R., Wilk, P.A., Hoffman, D.C., Malmbeck, R., Skarnemark, G., Alstad, J., Omtvedt, J.P., Eberhardt, K., Mendel, M., Nähler, A., Trautmann, N.: First chemical on-line separation and detection of a subsecond alpha-decaying nuclide, Pa-224. J. Radioanal. Nucl. Chem. **247**, 57–60 (2001)
12. Zvara, I., Eichler, B., Belov, V.Z., Zvarova, T.S., Korotkin, Y.S., Shalaevski, M.R., Shchegolev, V.A., Hussonnois, M.: Gas chromatography and thermochromatography in the study of transuranium elements. Sov. Radiochem. **16**, 709–715 (1974)

13. Zvara, I.: Thermochromatographic method of separation of chemical elements in nuclear and radiochemistry. Isotopenpraxis **26**, 251–258 (1990)
14. Schädel, M.: Chemistry of the transactinide elements. Radiochim. Acta **70/71**, 207–223 (1995)
15. Trautmann, N.: Fast radiochemical separations for heavy elements. Radiochim. Acta **70–1**, 237–245 (1995)
16. Türler, A.: Gas phase chemistry experiments with transactinide elements. Radiochim. Acta **72**, 7–17 (1996)
17. Gäggeler, H.W.: Fast chemical separation procedures for transactinides. In: Proceedings of "The Robert A. Welch Foundation 41st Confernce on Chemical Research. The Transactinide Elements", pp. 43–63. Houston, Texas, 27–28 Oct 1997
18. Hoffman, D.C., Lee, D.M.: Chemistry of the heaviest elements—one atom at a time. J. Chem. Educ. **76**, 331–347 (1999)
19. Schädel, M.: Chemistry of the superheavy elements. Angew. Chem. Int. Ed. **45**, 368–401 (2006)
20. Kratz, J.V.: Chemistry of transactinides. In: Vértes, A., Nagy, S., Klencsár, Z., Lovas, R.G., Rösch, F. (eds.) Handbook of Nuclear Chemistry, pp. 925–1004. Springer Science + Business Media B.V, Dordrecht Heidelberg London New York (2011)
21. Kratz, J.V.: Aqueous-phase chemistry of the transactinides. Radiochim. Acta **99**, 477–502 (2011)
22. Gäggeler, H.W.: Gas chemical properties of heaviest elements. Radiochim. Acta **99**, 503–513 (2011)
23. Guillaumont, R., Adloff, J.P., Peneloux, A.: Kinetic and thermodynamic aspects of tracer-scale and single atom chemistry. Radiochim. Acta **46**, 169–176 (1989)
24. Drapchinsky, L.V., Kuzmina, T.E., Soloviev, S.M.: Practice of using the multiple painting method. Nucl. Instrum. Methods A **438**, 116–118 (1999)
25. Garcia, M.A., Ali, M.N., Parsons-Moss, T., Ashby, P.D., Nitsche, H.: Metal oxide films produced by polymer-assisted deposition (PAD) for nuclear science applications. Thin Solid Films **516**, 6261–6265 (2008)
26. Ali, M.N., Garcia, M.A., Parsons-Moss, T., Nitsche, H.: Polymer-assisted deposition of homogeneous metal oxide films to produce nuclear targets. Nat. Protoc. **5**, 1440–1446 (2010)
27. Muggleton, A.H.F.: Preparation of Thin Nuclear Targets. J. Phys. E-Sci. Instrum. **12**, 780–807 (1979)
28. Drapchinsky, L.V., Shpakov, V.I.: Preparation of actinide targets by radio-frequency sputtering. Nucl. Instrum. Methods A **362**, 100–103 (1995)
29. Coppieters, L., Vancampenhout, J., Triffaux, J., Vanaudenhove, J.: Development of a piezoelectric pulsed drop jet device for the preparation of nuclear targets. Nucl. Instrum. Methods Phys. Res., Sect. A **224**, 41–49 (1984)
30. Evans, J.E., Lougheed, R.W., Hoff, R.W., Hulet, E.K., Coops, M.S.: Use of electrodeposition methods to prepare actinide targets for cross-section measurements and accelerator bombardments. Nucl. Instrum. Methods **102**, 389–401 (1972)
31. Aumann, D.C., Mullen, G.: Preparation of targets of Ca, Ba, Fe, La, Pb, Tl, Bi, Th and U by electrodeposition from organic solutions. Nucl. Instrum. Methods **115**, 75–81 (1974)
32. Müllen, G., Aumann, D.C.: Preparation of targets of Np, Pu, Am, Cm and Cf by electrodeposition from organic solutions. Nucl. Instrum. Methods **128**, 425–428 (1975)
33. Trautmann, N., Folger, H.: Preparation of actinide targets by electrodeposition. Nucl. Instrum. Methods Phys. Res., Sect. A **282**, 102–106 (1989)
34. Eberhardt, K., Schädel, M., Schimpf, E., Thörle, P., Trautmann, N.: Preparation of targets by electrodeposition for heavy element studies. Nucl. Instrum. Methods Phys. Res., Sect. A **521**, 208–213 (2004)
35. Eberhardt, K., Brüchle, W., Düllmann, C.E., Gregorich, K.E., Hartmann, W., Hübner, A., Jäger, E., Kindler, B., Kratz, J.V., Liebe, D., Lommel, B., Maier, H.-J., Schädel, M., Schausten, B., Schimpf, E., Semchenkov, A., Steiner, J., Szerypo, J., Thörle, P., Türler, A.,

Yakushev, A.: Preparation of targets for the gas-filled recoil separator TASCA by electrochemical deposition and design of the TASCA target wheel assembly. Nucl. Instrum. Methods Phys. Res., Sect. A **590**, 134–140 (2008)
36. Runke, J., Düllmann, C.E., Eberhardt, K., Ellison, P.A., Gregorich, K.E., Hofmann, S., Jäger, E., Kindler, B., Kratz, J.V., Krier, J., Lommel, B., Mokry, C., Nitsche, H., Roberto, J.B., Rykaczewski, K.P., Schädel, M., Thörle-Pospiech, P., Trautmann, N., Yakushev, A.: Preparation of actinide targets for the synthesis of the heaviest elements. J. Radioanal. Nucl. Chem. (2013, in press)
37. Vascon, A., Santi, S., Isse, A.A., Reich, T., Drebert, J., Christ, H., Düllmann, C.E., Eberhardt, K.: Elucidation of constant current density molecular plating. Nucl. Instrum. Methods A **696**, 180–191 (2012)
38. Usoltsev, I., Eichler, R., Dressler, R., Piguet, D., Wittwer, D., Turler, A., Brutsch, R., Olsen, E.A., Omtvedt, J.P., Semchenkov, A.: Preparation of Pd-based intermetallic targets for high intensity irradiations. Nucl. Instrum. Methods Phys. Res., Sect. A **691**, 5–9 (2012)
39. Nitschke, J.M.: High-intensity heavy-ion recoil target system. Nucl. Instrum. Methods **138**, 393–406 (1976)
40. Yakushev, A.B., Zvara, I., Oganessian, Y.T., Belozerov, A.V., Dmitriev, S.N., Eichler, B., Hübener, S., Sokol, E.A., Türler, A., Yeremin, A.V., Buklanov, G.V., Chelnokov, M.L., Chepigin, V.I., Gorshkov, V.A., Gulyaev, A.V., Lebedev, V.Y., Malyshev, O.N., Popeko, A.G., Soverna, S., Szeglowski, Z., Timokhin, S.N., Tretyakova, S.P., Vasko, V.M., Itkis, M.G.: Chemical identification and properties of element 112. Radiochim. Acta **91**, 433–439 (2003)
41. Eichler, R., Aksenov, N.V., Belozerov, A.V., Bozhikov, G.A., Chepigin, V.I., Dmitriev, S.N., Dressler, R., Gäggler, H.W., Gorshkov, V.A., Haenssler, F., Itkis, M.G., Laube, A., Lebedev, V.Y., Malyshev, O.N., Oganessian, Y.T., Petrushkin, O.V., Piguet, D., Rasmussen, P., Shishkin, S.V., Shutov, A.V., Svirikhin, A.I., Tereshatov, E.E., Vostokin, G.K., Wegrzecki, M., Yeremin, A.: Chemical characterization of element 112. Nature **447**, 72–75 (2007)
42. Eichler, R., Aksenov, N.V., Belozerov, A.V., Bozhikov, G.A., Chepigin, V.I., Dmitriev, S.N., Dressler, R., Gäggeler, H.W., Gorshkov, A.V., Itkis, M.G., Haenssler, F., Laube, A., Lebedev, V.Y., Malyshev, O.N., Oganessian, Y.T., Petrushkin, O.V., Piguet, D., Popeko, A.G., Rasmussen, T., Shishkin, S.V., Serov, A.A., Shutov, A.V., Svirikhin, A.I., Tereshatov, E.E., Vostokin, G.K., Wegrzecki, M., Yeremin, A.V.: Thermochemical and physical properties of element 112. Angew. Chem. Int. Ed. **47**, 3262–3266 (2008)
43. Eichler, R., Aksenov, N.V., Albin, Y.V., Belozerov, A.V., Bozhikov, G.A., Chepigin, V.I., Dmitriev, S.N., Dressler, R., Gäggeler, H.W., Gorshkov, V.A., Henderson, R.A., Johnsen, A.M., Kenneally, J.M., Lebedev, V.Y., Malyshev, O.N., Moody, K.J., Oganessian, Y.T., Petrushkin, O.V., Piguet, D., Popeko, A.G., Rasmussen, P., Serov, A.A., Shaughnessy, D.A., Shishkin, S.V., Shutov, A.V., Stoyer, M.A., Stoyer, N.J., Svirikhin, A.I., Tereshatov, E.E., Vostokin, G.K., Wegrzecki, M., Wilk, P.A., Wittwer, D., Yeremin, A.V.: Indication for a volatile element 114. Radiochim. Acta **98**, 133–139 (2010)
44. Schädel, M.: The chemistry of superheavy elements. Acta Phys. Pol., B **34**, 1701–1728 (2003)
45. Düllmann, C.E., Brüchle, W., Dressler, R., Eberhardt, K., Eichler, B., Eichler, R., Gäggeler, H.W., Ginter, T.N., Glaus, F., Gregorich, K.E., Hoffman, D.C., Jäger, E., Jost, D.T., Kirbach, U.W., Lee, D.M., Nitsche, H., Patin, J.B., Pershina, V., Piguet, D., Qin, Z., Schädel, M., Schausten, B., Schimpf, E., Schött, H.J., Soverna, S., Sudowe, R., Thörle, P., Timokhin, S.N., Trautmann, N., Türler, A., Vahle, A., Wirth, G., Yakushev, A.B., Zielinski, P.M.: Chemical investigation of hassium (element 108). Nature **418**, 859–862 (2002)
46. Jäger, E., Brand, H., Düllmann, C.E., Khuyagbaatar, J., Krier, J., Schädel, M., Torres, T., Yakushev, A.: High intensity target wheel at TASCA: target wheel control system and target monitoring. J. Radioanal. Nucl. Chem. (2013, in press)
47. Ghiorso, A., Harvey, B.G., Choppin, G.R., Thompson, S.G., Seaborg, G.T.: New element mendelevium, atomic number 101. Phys. Rev. **98**, 1518–1519 (1955)

48. Wollnik, H.: Principles behind a He-jet system and its application for isotope separation. Nucl. Instrum. Methods **139**, 311–318 (1976)
49. Kirbach, U.W., Gregorich, K., Ninov, V., Lee, D.M., Patin, J.B., Shaughnessy, D.A., Strellis, D.A., Wilk, P.A., Hoffman, D.C., Nitsche, H.: The recoil product transfer chamber (RTC): A new interface for heavy element chemistry studies at the Berkeley gas-filled separator. In: Nuclear Science Division Annual Report 1999. Lawrence Berkeley National Laboratory, Berkeley, (1999)
50. Omtvedt, J.P., Alstad, J., Breivik, H., Dyve, J.E., Eberhardt, K., Folden III, C.M., Ginter, T., Gregorich, K., Hult, E.A., Johansson, M., Kirbach, U.W., Lee, D.M., Mendel, M., Nähler, A., Ninov, V., Omtvedt, L.A., Patin, J.B., Skarnemark, G., Stavsetra, L., Sudowe, R., Wiehl, N., Wierczinski, B., Wilk, P.A., Zielinski, P.M., Kratz, J.V., Trautmann, N., Nitsche, H., Hoffman, D.C.: SISAK liquid–liquid extraction experiments with prespearated ^{257}Rf. J. Nucl. Radiochem. Sci. **3**, 121–124 (2002)
51. Kirbach, U.W., Folden III, C.M., Ginter, T.N., Gregorich, K.E., Lee, D.M., Ninov, V., Omtvedt, J.P., Patin, J.B., Seward, N.K., Strellis, D.A.: The cryo-thermochromatographic separator (CTS): A new rapid separation and ∝-detection system for on-line chemical studies of highly volatile osmium and hassium ($Z = 108$) tetroxides. Nucl. Instrum. Methods Phys. Res., Sect. A **484**, 587–594 (2002)
52. Düllmann, C.E., Folden III, C.M., Gregorich, K.E., Hoffman, D.C., Leitner, D., Pang, G.K., Sudowe, R., Zielinski, P.M., Nitsche, H.: Heavy-ion-induced production and physical preseparation of short-lived isotopes for chemistry experiments. Nucl. Instrum. Methods Phys. Res., Sect. A **551**, 528–539 (2005)
53. Even, J., Ballof, J., Brüchle, W., Buda, R.A., Düllmann, C.E., Eberhardt, K., Gorshkov, A., Gromma, E., Hild, D., Jäger, E., Khuyagbaatar, J., Kratz, J.V., Krier, J., Liebe, D., Mendel, M., Nayak, D., Opel, K., Omtvedt, J.P., Reichert, P., Runke, J., Sabelnikov, A., Samadani, F., Schädel, M., Schausten, B., Scheid, N., Schimpf, E., Semchenkov, A., Thörle-Pospiech, P., Toyoshima, A., Türler, A., Vicente Vilas, V., Wiehl, N., Wunderlich, T., Yakushev, A.: The recoil transfer chamber—An interface to connect the physical preseparator TASCA with chemistry and counting setups. Nucl. Instrum. Methods Phys. Res., Sect. A **638**, 157–164 (2011)
54. Ninov, V., Gregorich, K.E., McGrath, C.A.: The Berkeley gas-filled separator. In: Sherrill, B.M., Morrissey, D.J., Davids, C.N. (eds.) ENAM 98: Exotic Nuclei and Atomic Masses, pp. 704–707. American Institute of Physics, Woodbury, New York (1998)
55. Wittwer, D., Abdullin, F.S., Aksenov, N.V., Albin, Y.V., Bozhikov, G.A., Dmitriev, S.N., Dressler, R., Eichler, R., Gäggeler, H.W., Henderson, R.A., Hubener, S., Kenneally, J.M., Lebedev, V.Y., Lobanov, Y.V., Moody, K.J., Oganessian, Y.T., Petrushkin, O.V., Polyakov, A.N., Piguet, D., Rasmussen, P., Sagaidak, R.N., Serov, A., Shirokovsky, I.V., Shaughnessy, D.A., Shishkin, S.V., Sukhov, A.M., Stoyer, M.A., Stoyer, N.J., Tereshatov, E.E., Tsyganov, Y.S., Utyonkov, V.K., Vostokin, G.K., Wegrzecki, M., Wilk, P.A.: Gas phase chemical studies of superheavy elements using the Dubna gas-filled recoil separator—stopping range determination. Nucl. Instrum. Methods Phys. Res., Sect. B **268**, 28–35 (2010)
56. Haba, H., Kaji, D., Kikunaga, H., Akiyama, T., Sato, N., Morimoto, K., Yoneda, A., Morita, K., Takabe, T., Shinohara, A.: Development of gas-jet transport system coupled to the RIKEN gas-filled recoil ion separator GARIS for superheavy element chemistry. J. Nucl. Radiochem. Sci. **8**, 55–58 (2007)
57. Haba, H., Kikunaga, H., Kaji, D., Akiyama, T., Morimoto, K., Morita, K., Nanri, T., Ooe, K., Sato, N., Shinohara, A., Suzuki, D., Takabe, T., Yamazaki, I., Yokoyama, A., Yoneda, A.: Performance of the gas-jet transport system coupled to the RIKEN gas-filled recoil ion separator GARIS for the ^{238}U(^{22}Ne, 5n)^{255} no reaction. J. Nucl. Radiochem. Sci. **9**, 27–31 (2008)
58. Ninov, V., Armbruster, P., Heßberger, F.P., Hofmann, S., Münzenberg, G., Fujita, Y., Leino, M., Lüttgen, A.: Separation of actinide-made transurania by a gas-filled magnetic separator. Nucl. Instrum. Methods Phys. Res., Sect. A **357**, 486–494 (1995)

59. Gates, J.M., Düllmann, C.E., Schädel, M., Yakushev, A., Türler, A., Eberhardt, K., Kratz, J.V., Ackermann, D., Andersson, L.-L., Block, M., Brüchle, W., Dvorak, J., Essel, H., Ellison, P.A., Even, J., Forsberg, U., Gellanki, J., Gorshkov, A., Graeger, R., Gregorich, K.E., Hartmann, W., Herzberg, R.-D., Heßberger, F.P., Hild, D., Hübner, A., Jäger, E., Khuyagbaatar, J., Kindler, B., Krier, J., Kurz, N., Lahiri, S., Liebe, D., Lommel, B., Maiti, M., Nitsche, H., Omtvedt, J.P., Parr, E., Rudolph, D., Runke, J., Schaffner, H., Schausten, B., Schimpf, E., Semchenkov, A., Steiner, J., Thörle-Pospiech, P., Uusitalo, J., Wegrzecki, M., Wiehl, N.: First superheavy element experiments at the GSI recoil separator TASCA: The production and decay of element 114 in the ^{48}Ca(^{244}Pu,3-4n) reaction. Phys. Rev. C **83**, 054618(17) (2011)
60. Düllmann, C.E., Gregorich, K.E., Pang, G.K., Dragojević, I., Eichler, R., Folden III, C.M., Garcia, M.A., Gates, J.M., Hoffman, D.C., Nelson, S.L., Sudowe, R., Nitsche, H.: Gas chemical investigation of hafnium and zirconium complexes with hexafluoroacetylacetone using preseparated short-lived radioisotopes. Radiochim. Acta **97**, 403–418 (2009)
61. Even, J., Yakushev, A., Düllmann, C.E., Dvorak, J., Eichler, R., Gothe, O., Hild, D., Jäger, E., Khuyagbaatar, J., Kratz, J.V., Krier, J., Niewisch, L., Nitsche, H., Pysmenetska, I., Schädel, M., Schausten, B., Türler, A., Wiehl, N., Wittwer, D.: Rapid synthesis of radioactive transition-metal carbonyl complexes at ambient conditions. Inorg. Chem. **51**, 6431–6433 (2012)
62. Haba, H., Kaji, D., Kikunaga, H., Kudou, Y., Morimoto, K., Morita, K., Ozeki, K., Sumita, T., Yoneda, A., Kasamatsu, Y., Komori, Y., Ooe, K., Shinohara, A.: Production and decay properties of the 1.9-s isomeric state in ^{261}Rf. Phys. Rev. C **83**, 034602(07) (2011)
63. Haba, H., Kaji, D., Kudou, Y., Morimoto, K., Morita, K., Ozeki, K., Sakai, R., Sumita, T., Yoneda, A., Kasamatsu, Y., Komori, Y., Shinohara, A., Kikunaga, H., Kudo, H., Nishio, K., Ooe, K., Sato, N., Tsukada, K.: Production of ^{265}Sg in the ^{248}Cm(^{22}Ne,5n)^{265}Sg reaction and decay properties of two isomeric states in ^{265}Sg. Phys. Rev. C **85**, 024611(11) (2012)
64. Czerwinski, K.R., Gregorich, K.E., Hannink, N.J., Kacher, C.D., Kadkhodayan, B.A., Kreek, S.A., Lee, D.M., Nurmia, M.J., Türler, A., Seaborg, G.T., Hoffman, D.C.: Solution chemistry of element-104.1. Liquid–liquid extractions with triisooctylamine. Radiochim. Acta **64**, 23–28 (1994)
65. Czerwinski, K.R., Kacher, C.D., Gregorich, K.E., Hamilton, T.M., Hannink, N.J., Kadkhodayan, B.A., Kreek, S.A., Lee, D.M., Nurmia, M.J., Türler, A., Seaborg, G.T., Hoffman, D.C.: Solution chemistry of element-104.2. Liquid–liquid extractions with tributylphosphate. Radiochim. Acta **64**, 29–35 (1994)
66. Kacher, C.D., Gregorich, K.E., Lee, D.M., Watanabe, Y., Kadkhodayan, B., Wierczinski, B., Lane, M.R., Sylwester, E.R., Keeney, D.A., Hendricks, M., Stoyer, N.J., Yang, J., Hsu, M., Hoffman, D.C., Bilewicz, A.: Chemical studies of rutherfordium (element 104).2. Solvent extraction into tributylphosphate from HBr solutions. Radiochim. Acta **75**, 127–133 (1996)
67. Kacher, C.D., Gregorich, K.E., Lee, D.M., Watanabe, Y., Kadkhodayan, B., Wierczinski, B., Lane, M.R., Sylwester, E.R., Keeney, D.A., Hendricks, M., Hoffman, D.C., Bilewicz, A.: Chemical studies of rutherfordium (element 104).3. Solvent extraction into triisooctylamine from HF solutions. Radiochim. Acta **75**, 135–139 (1996)
68. Gregorich, K.E., Henderson, R.A., Lee, D.M., Nurmia, M.J., Chasteler, R.M., Hall, H.L., Bennett, D.A., Gannett, C.M., Chadwich, R.B., Leyba, J.D., Hoffman, D.C.: Aqueous chemistry of element 105. Radiochim. Acta **43**, 223–231 (1988)
69. Silva, R., Sikkeland, T., Nurmia, M., Ghiorso, A.: Tracer chemical studies of lawrencium. Inorg. Nucl. Chem. Lett. **6**, 733–739 (1970)
70. Hoffman, D.C., Henderson, R.A., Gregorich, K.E., Bennett, D.A., Chasteler, R.M., Gannett, C.M., Hall, H.L., Lee, D.M., Nurmia, M.J., Cai, S., Agarwal, R., Charlop, A.W., Chu, Y.Y., Seaborg, G.T., Silva, R.J.: Atom-at-a-time radiochemical separations of the heaviest elements—lawrencium chemistry. J. Radioanal. Nucl. Chem. **124**, 135–144 (1988)
71. Silva, R., Harris, J., Nurmia, M., Eskola, K., Ghiorso, A.: Chemical separation of rutherfordium. Inorg. Nucl. Chem. Lett. **6**, 871–877 (1970)

72. Schädel, M.: Aqueous chemistry of transactinides. Radiochim. Acta **89**, 721–728 (2001)
73. Schädel, M.: The chemistry of the transactinide elements—experimental achievements and perspectives. J. Radioanal. Nucl. Chem. **3**, 113–120 (2002)
74. Schädel, M., Brüchle, W., Jäger, E., Schimpf, E., Kratz, J.V., Scherer, U.W., Zimmermann, H.P.: ARCA II—a new apparatus for fast, repetitive HPLC separations. Radiochim. Acta **48**, 171–176 (1989)
75. Günther, R., Paulus, W., Kratz, J.V., Seibert, A., Thörle, P., Zauner, S., Brüchle, W., Jäger, E., Pershina, V., Schädel, M., Schausten, B., Schumann, D., Eichler, B., Gäggeler, H.W., Jost, D.T., Türler, A.: Chromatographic study of rutherfordium (element 104) in the system HCl/tributylphosphate (TBP). Radiochim. Acta **80**, 121–128 (1998)
76. Strub, E., Kratz, J.V., Kronenberg, A., Nähler, A., Thörle, P., Zauner, S., Brüchle, W., Jäger, E., Schädel, M., Schausten, B., Schimpf, E., Li, Z.W., Kirbach, U., Schumann, D., Jöst, D., Türler, A., Asai, M., Nagame, Y., Sakama, M., Tsukada, K., Gäggeler, H.W., Glatz, J.P.: Fluoride complexation of rutherfordium (Rf, element 104). Radiochim. Acta **88**, 265–271 (2000)
77. Kratz, J.V., Gober, M.K., Zimmermann, H.P., Schädel, M., Brüchle, W., Schimpf, E., Gregorich, K.E., Türler, A., Hannink, N.J., Czerwinski, K.R., Kadkhodayan, B., Lee, D.M., Nurmia, M.J., Hoffman, D.C., Gäggeler, H., Jost, D., Kovacs, J., Scherer, U.W., Weber, A.: New nuclide ^{263}Ha. Phys. Rev. C **45**, 1064–1069 (1992)
78. Schädel, M., Brüchle, W., Schimpf, E., Zimmerman, H.P., Gober, M.K., Kratz, J.V., Trautmann, N., Gäggeler, H.W., Jost, D.T., Kovacs, J., Scherer, U.W., Weber, A., Gregorich, K.E., Türler, A., Czerwinski, K.R., Hannink, N.J., Kadkhodayan, B., Lee, D.M., Nurmia, M.J., Hoffman, D.C.: Chemical properties of element 105 in aqueous solution: cation exchange separations with ∝-hydroxyisobutyric acid. Radiochim. Acta **57**, 85–92 (1992)
79. Gober, M.K., Kratz, J.V., Zimmerman, H.P., Schädel, M., Brüchle, W., Schimpf, E., Gregorich, K.E., Türler, A., Hannink, N.J., Czerwinski, K.R., Kadkhodayan, B., Lee, D.M., Nurmia, M.J., Hoffman, D.C., Gäggeler, H.W., Jost, D.T., Kovacs, J., Scherer, U.W., Weber, A.: Chemical properties of element 105 in aqueous solution: extraction into diisobutylcarbinol. Radiochim. Acta **57**, 77–84 (1992)
80. Zimmermann, H.P., Gober, M.K., Kratz, J.V., Schädel, M., Brüchle, W., Schimph, E., Gregorich, K.E., Türler, A., Czerwinski, K.R., Hannink, N.J., Kadkhodayan, B., Lee, D.M., Nurmia, M.J., Hoffman, D.C., Gäggeler, H.W., Jost, D.T., Kovacs, J., Scherer, U.W., Weber, A.: Chemical properties of element 105 in aqueous solution: back extraction from triisooctyl amine into 0.5 M HCL. Radiochim. Acta **60**, 11–16 (1993)
81. Paulus, W., Kratz, J.V., Strub, E., Zauner, S., Brüchle, W., Pershina, V., Schädel, M., Schausten, B., Adams, J.L., Gregorich, K.E., Hoffman, D.C., Lane, M.R., Laue, C., Lee, D.M., McGrath, C.A., Shaughnessy, D.K., Strellis, D.A., Sylwester, E.R.: Chemical properties of element 105 in aqueous solution: extraction of fluoride-, chloride-, and bromide complexes of the group-5 elements into an aliphatic amine. Radiochim. Acta **84**, 69–77 (1999)
82. Schädel, M., Brüchle, W., Schausten, B., Schimpf, E., Jäger, E., Wirth, G., Günther, R., Kratz, J.V., Paulus, W., Seibert, A., Thörle, P., Trautmann, N., Zauner, S., Schumann, D., Andrassy, M., Misiak, R., Gregorich, K.E., Hoffman, D.C., Lee, D.M., Sylwester, E.R., Nagame, Y., Oura, Y.: First aqueous chemistry with seaborgium (Z = 106). Radiochim. Acta **77**, 149–159 (1997)
83. Schädel, M., Brüchle, W., Jäger, E., Schausten, B., Wirth, G., Paulus, W., Günther, R., Eberhardt, K., Kratz, J.V., Seibert, A., Strub, E., Thörle, P., Trautmann, N., Waldek, A., Zauner, S., Schumann, D., Kirbach, U., Kubica, B., Misiak, R., Nagame, Y., Gregorich, K.E.: Aqueous chemistry of seaborgium (Z = 106). Radiochim. Acta **83**, 163–165 (1998)
84. Nagame, Y., Tsukada, K., Asai, M., Toyoshima, A., Akiyama, K., Ishii, Y., Kaneko-Sato, T., Hirata, M., Nishinaka, I., Ichikawa, S., Haba, H., Enomoto, S., Matsuo, K., Saika, D., Kitamota, Y., Hasegawa, H., Tani, Y., Sato, W., Shinohara, A., Ito, M., Saito, J., Goto, S., Kudo, H., Kikunaga, H., Kinoshita, N., Yokoyama, A., Sueki, K., Oura, Y., Nakahara, H.,

Sakama, M., Schädel, M., Brüchle, W., Kratz, J.V.: Chemical studies on rutherfordium (Rf) at JAERI. Radiochim. Acta **93**, 519–526 (2005)
85. Haba, H., Tsukada, K., Asai, M., Goto, S., Toyoshima, A., Nishinaka, I., Akiyama, K., Hirata, M., Ichikawa, S., Nagame, Y., Shoji, Y., Shigekawa, M., Koike, T., Iwasaki, M., Shinohara, A., Kaneko, T., Maruyama, T., Ono, S., Kudo, H., Oura, Y., Sueki, K., Nakahara, H., Sakama, M., Yokoyama, A., Kratz, J.V., Schädel, M., Brüchle, W.: Anion-Exchange Behavior of Rf in HCl and HNO_3 Solutions. J. Nucl. Radiochem. Sci. **3**, 143–146 (2002)
86. Haba, H., Tsukada, K., Asai, M., Toyoshima, A., Ishii, Y., Toume, H., Sato, T., Nishinaka, I., Ichikawa, T., Ichikawa, S., Nagame, Y., Sato, W., Matsuo, K., Kitamoto, Y., Tashiro, Y., Shinohara, A., Saito, J., Ito, M., Ikezawa, T., Sakamaki, M., Goto, S., Kudo, H., Kikunaga, H., Arai, M., Kamataki, S., Yokoyama, A., Akiyama, K., Sueki, K., Oura, Y., Schädel, M., Brüchle, W., Kratz, J.V.: Extraction behavior of rutherfordium into tributylphosphate from hydrochloric acid. Radiochim. Acta **95**, 1–6 (2007)
87. Haba, H., Tsukada, K., Asai, M., Toyoshima, A., Akiyama, K., Nishinaka, I., Hirata, M., Yaita, T., Ichikawa, S.I., Nagame, Y., Yasuda, K.I., Miyamoto, Y., Kaneko, T., Goto, S.I., Ono, S., Hirai, T., Kudo, H., Shigekawa, M., Shinohara, A., Oura, Y., Nakahara, H., Sueki, K., Kikunaga, H., Kinoshita, N., Tsuruga, N., Yokoyama, A., Sakama, M., Enomoto, S., Schädel, M., Brüchle, W., Kratz, J.V.: Fluoride complexation of element 104, rutherfordium. J. Am. Chem. Soc. **126**, 5219–5224 (2004)
88. Toyoshima, A., Haba, H., Tsukada, K., Asai, M., Akiyama, K., Nishinaka, I., Nagame, Y., Saika, D., Matsuo, K., Sato, W., Shinohara, A., Ishizu, H., Ito, M., Saito, J., Goto, S., Kudo, H., Kikunaga, H., Kinoshita, N., Kato, C., Yokoyama, A., Sueki, K.: Elution curve of rutherfordium (Rf) in anion-exchange chromatography with hydrofluoric acid solution. J. Nucl. Radiochem. Sci. **5**, 45–48 (2004)
89. Toyoshima, A., Haba, H., Tsukada, K., Asai, M., Asiyama, K., Goto, S., Ishii, Y., Nishinaka, I., Sato, T.K., Nagame, Y., Sato, W., Tani, Y., Hasegawa, H., Matsuo, K., Saika, D., Kitamoto, Y., Shinohara, A., Ito, M., Saito, J., Kudo, H., Yokoyama, A., Sakama, M., Sueki, K., Oura, Y., Nakahara, H., Schädel, M., Brüchle, W., Kratz, J.V.: Hexafluoro complex of rutherfordium in mixed HF/HNO_3 solutions. Radiochim. Acta **96**, 125–134 (2008)
90. Ishii, Y., Toyoshima, A., Tsukada, K., Asai, M., Toume, H., Nishinaka, I., Nagame, Y., Miyashita, S., Mori, T., Suganuma, H., Haba, H., Sakamaki, M., Goto, S., Kudo, H., Akiyama, K., Oura, Y., Nakahara, H., Tashiro, Y., Shmohara, A., Schädel, M., Brüchle, W., Pershina, V., Kratz, J.V.: Fluoride complexation of element 104, rutherfordium (Rf) investigated by cation-exchange chromatography. Chem. Lett. **37**, 288–289 (2008)
91. Ishii, Y., Toyoshima, A., Tsukada, K., Asai, M., Li, Z.J., Nagame, Y., Miyashita, S., Mori, T., Suganuma, H., Haba, H., Goto, S., Kudo, H., Akiyama, K., Oura, Y., Shinohara, A., Schädel, M., Pershina, V., Kratz, J.V.: Fluorido complex formation of element 104, rutherfordium (Rf). Bull. Chem. Soc. Jpn. **84**, 903–911 (2011)
92. Li, Z.J., Toyoshima, A., Asai, M., Tsukada, K., Sato, T.K., Sato, N., Kikuchi, T., Nagame, Y., Schädel, M., Pershina, V., Liang, X.H., Kasamatsu, Y., Komori, Y., Ooe, K., Shinohara, A., Goto, S., Murayama, H., Murakami, M., Kudo, H., Haba, H., Takeda, Y., Nishikawa, M., Yokoyama, A., Ikarashi, S., Sueki, K., Akiyama, K., Kratz, J.V.: Sulfate complexation of element 104, Rf, in H2SO4/HNO3 mixed solution. Radiochim. Acta **100**, 157–164 (2012)
93. Kasamatsu, Y., Toyoshima, A., Asai, M., Tsukada, K., Li, Z., Ishii, Y., Toume, H., Sato, T.K., Kikuchi, T., Nishinaka, I., Nagame, Y., Haba, H., Kikunaga, H., Kudou, Y., Oura, Y., Akiyama, K., Sato, W., Ooe, K., Fujisawa, H., Shinohara, A., Goto, S., Hasegawa, T., Kudo, H., Nanri, T., Araki, M., Kinoshita, N., Yokoyama, A., Fan, F., Qin, Z., Düllmann, C.E., Schädel, M., Kratz, J.V.: Anionic fluoro complex of element 105 Db. Chem. Lett. **38**, 1084–1085 (2009)

94. Szeglowski, Z., Bruchertseifer, H., Domanov, V.P., Gleisberg, B., Guseva, L.J., Hussonnois, M., Tikhomirova, G.S., Zvara, I., Oganessian, Y.T.: Study of the solution chemistry of element 104—Kurchatovium. Radiochim. Acta **51**, 71–76 (1990)
95. Trubert, D., Hussonnois, M., Brillard, L., Barci, V., Ardisson, G., Szeglowski, Z., Constantinescu, O.: Investigation of the Hf-168 electron-capture decay using fast radiochemical separation. Radiochim. Acta **69**, 149–156 (1995)
96. Pfrepper, G., Pfrepper, R., Yakushev, A.B., Timokhin, S.N., Zvara, I.: "On-line" experiments with cyclotron produced short-lived hafnium isotopes as a test for studies of ion exchange equilibria of element 104 by a continuous chromatography technique. Radiochim. Acta **77**, 201–206 (1997)
97. Pfrepper, G., Pfrepper, R., Krauss, D., Yakushev, A.B., Timokhin, S.N., Zvara, I.: Ion exchange equilibria and stoichiometry of complexes of element 104 and hafnium in hydrofluoric acid solutions. Radiochim. Acta **80**, 7–12 (1998)
98. Pfrepper, G., Pfrepper, R., Kronenberg, A., Kratz, J.V., Nähler, A., Brüchle, W., Schädel, M.: Continuous on-line chromatography of short lived isotopes of tungsten as homolog of seaborgium (element 106). Radiochim. Acta **88**, 273–278 (2000)
99. Omtvedt, J.P., Alstad, J., Eberhardt, K., Fure, K., Malmbeck, R., Mendel, M., Nähler, A., Skarnemark, G., Trautmann, N., Wiehl, N., Wierczinski, B.: Review of the SISAK system in transactinide research: recent developments and future prospects. J. Alloys Compd. **271–273**, 303 (1998)
100. Wilk, P.A., Gregorich, K.E., Hendricks, M.B., Lane, M.R., Lee, D.M., McGrath, C.A., Shaughnessy, D.A., Strellis, D.A., Sylwester, E.R., Hoffman, D.C.: Improved half-life measurement of ^{224}Pa and its ^{209}Bi(^{18}O,3n)^{224}Pa production cross section. Phys. Rev. C **56**, 1626–1628 (1997)
101. Wilk, P.A., Gregorich, K.E., Hendricks, M.B., Lane, M.R., Lee, D.M., McGrath, C.A., Shaughnessy, D.A., Strellis, D.A., Sylwester, E.R., Hoffman, D.C.: Erratum: Improved half-life measurement of ^{224}Pa and its ^{209}Bi(^{18}O,3n)^{224}Pa production cross section [Phys. Rev. C 56, 1626 (1997)]. Phys. Rev. C **58**, 1352 (1998)
102. Oganessian, Y.: Heaviest nuclei from ^{48}Ca induced reactions. J. Phys. G: Nucl. Part. Phys. **34**, R165–R242 (2007)
103. Toyoshima, A., Kasamatsu, Y., Kitatsuji, Y., Tsukada, K., Haba, H., Shinohara, A., Nagame, Y.: Development of an electrochemistry apparatus for the heaviest elements. Radiochim. Acta **96**, 323–326 (2008)
104. Toyoshima, A., Kasamatsu, Y., Tsukada, K., Asai, M., Kitatsuji, Y., Ishii, Y., Toume, H., Nishinaka, I., Haba, H., Ooe, K., Sato, W., Shinohara, A., Akiyama, K., Nagame, Y.: Oxidation of element 102, nobelium, with flow electrolytic column chromatography on an atom-at-a-time scale. J. Am. Chem. Soc. **131**, 9180–9181 (2009)
105. Zvara, I., Chuburkov, Y.T., Caletka, R., Shalaevski, M.R., Shilov, B.V.: Chemical properties of element 104. J. Nucl. Energy **21**, 601–603 (1967)
106. Zvara, I., Belov, V.Z., Korotkin, Y.S., Shalaevski, M.R., Shchegolev, V.A., Hussonnois, M., Zager, B.A.: Experiments on Chemical Identification of Spontaneously Fissionable Isotope of Element 105. In: Dubna Report. vol. P12-5120, p. 13. Joint Institute for Nuclear Research, Dubna, (1970)
107. Zvara, I., Yakushev, A.B., Timokhin, S.N., Honggui, X., Perelygin, V.P., Chuburkov, Y.T.: Chemical identification of element 106 (thermochromatography of oxochlorides). Radiochim. Acta **81**, 179–187 (1998)
108. Gäggeler, H.W., Jost, D.T., Baltensperger, U., Weber, A., Kovacs, A., Vermeulen, D., Türler, A.: OLGA II, an on-line gas chemistry apparatus for applications in heavy element research. Nucl. Instrum. Methods Phys. Res., Sect. A **309**, 201–208 (1991)
109. Türler, A., Gäggeler, H.W., Gregorich, K.E., Barth, H., Brüchle, W., Czerwinski, K.R., Gober, M.K., Hannink, N.J., Henderson, R.A., Hoffman, D.C., Jost, D.T., Kacher, C.D., Kadkhodayan, B., Kovacs, J., Kratz, J.V., Kreek, S.A., Lee, D.M., Leyba, J.D., Nurmia, M.J., Schädel, M., Scherer, U., Schimpf, E., Vermeulen, D., Weber, A., Zimmerman, H.P.,

Zvara, I.: Gas phase chromatography of halides of elements 104 and 105. J. Radioanal. Nucl. Chem. Art. **160**, 327–339 (1992)
110. Gäggeler, H.W., Jost, D.T., Kovacs, J., Scherer, U.W., Weber, A., Vermeulen, D., Türler, A., Gregorich, K.E., Henderson, R.A., Czerwinski, K.R., Kadkhodayan, B., Lee, D.M., Nurmia, M., Kratz, J.V., Gober, M.K., Zimmerman, H.P., Schädel, M., Brüchle, W., Schimpf, E., Zvara, I.: Gas phase chromatography experiments with bromides of tantalum and element 105. Radiochim. Acta **57**, 93–100 (1992)
111. Schädel, M., Brüchle, W., Dressler, R., Eichler, B., Gäggeler, H.W., Günther, R., Gregorich, K.E., Hoffman, D.C., Hübener, S., Jost, D.T., Kratz, J.V., Paulus, W., Schumann, D., Timokhin, S., Trautmann, N., Türler, A.: Chemical properties of element 106 (seaborgium). Nature **388**, 55–57 (1997)
112. Eichler, R., Brüchle, W., Dressler, R., Düllmann, C.E., Eichler, B., Gäggeler, H.W., Gregorich, K.E., Hoffman, D.C., Hubener, S., Jost, D.T., Kirbach, U.W., Laue, C.A., Lavanchy, V.M., Nitsche, H., Patin, J.B., Piguet, D., Schädel, M., Shaughnessy, D.A., Strellis, D.A., Taut, S., Tobler, L., Tsyganov, Y.S., Türler, A., Vahle, A., Wilk, P.A., Yakushev, A.B.: Chemical characterization of bohrium (element 107). Nature **407**, 63–65 (2000)
113. Zvara, I.: The Inorganic Radiochemistry of Heavy Elements—Methods for Studying Gaseous Compounds. Springer, Dordrecht (2008)
114. Zvara, I., Chuburkov, Y.T., Zvarova, T.S., Tsaletka, R.: Experiments on the chemistry of element 104—Kurchatovium I. Development of a method for studying short-lived isotopes. Sov. Radiochem. **11**, 153 (1969)
115. Silva, R.J., Trautmann, N., Zendel, M., Dittner, P.F., Stender, E., Ahrens, H.: A gas-jet recoil-transport system for fission products and its application to a continuous chemical separation procedure in the gas phase. Nucl. Instrum. Methods **147**, 371–378 (1977)
116. Hickmann, U., Greulich, N., Trautmann, N., Gäggeler, H., Gäggeler-Koch, H., Eichler, B., Herrmann, G.: Rapid continuous radiochemical separations by thermochromatography in connection with a gas-jet recoil transport system. Nucl. Instrum. Methods **174**, 507–513 (1980)
117. Zvara, I., Keller, O.L., Silva, R.J., Tarrant, J.R.: Thermochromatography of bromides—proposed technique for study of transactinide element chemistry. J. Chromatogr. **103**, 77–83 (1975)
118. Eichler, B., Domanov, V.P.: Volatilization of radionuclides in air stream and their separation in temperature-gradient tube. J. Radioanal. Nucl. Chem. **28**, 143–152 (1975)
119. Helas, G., Hoffmann, P., Bächmann, K.: Investigation of Mo-chlorides and W-chlorides and ocychlorides by thermochromatography. Radiochem. Radioanal. Lett. **30**, 371–380 (1977)
120. Tsalas, S., Bächmann, K.: Inorganic gas chromatography—the separation of volatile chlorides by thermochromatorgraphy combined with complex formation. Anal. Chim. Acta **98**, 17–24 (1978)
121. Bayar, B., Novgorodov, A.F., Vocilka, I., Zaitseva, N.G.: Fast gas-thermochromatographic separation of mo neutron-deficient isotopes from silver-chloride. Radiochem. Radioanal. Lett. **35**, 109–120 (1978)
122. Polyakov, E.V.: Chemical-Composition of nuclear-reaction products determined by gradient thermochromatography. Sov. Radiochem. **32**, 548–551 (1990)
123. Bayar, B., Vocilka, I., Zaitseva, N.G., Novgorodov, A.F.: Fast gas-thermochromatographic separation of ruthenium neutron-deficient isotopes from silver-chloride. J. Inorg. Nucl. Chem. **40**, 1461–1466 (1978)
124. Zin, K.U., Timochin, S.N., Zvara, I.: Thermochromatographic study of bromides of various elements in relation of their chlorides. Isotopenpraxis **24**, 30–33 (1988)
125. Rudolph, J., Bächmann, K.: Use of radionuclides for determination of adsorption-isotherms of volatile chlorides. J. Radioanal. Chem. **43**, 113–120 (1978)
126. Rudolph, J., Bächmann, K.: Gas-chromatography apparatus for the investigation and separation of radioactively labeled inorganic-compounds at high-temperatures. Mikrochim. Acta **1**, 477–493 (1979)

127. Rudolph, J., Bächmann, K.: Determination of adsorption enthalpies and entropies by on-line-gas chromatography with short-lived nuclides. Radiochim. Acta **27**, 105–108 (1980)
128. Dincklage, R.D.V., Schrewe, U.J., Schmidt-Ott, W.D., Fehse, H.F., Bächmann, K.: Coupling of a He-Jet system to gas-chromatographic columns for the measurement of thermodynamical properties of chemical-compounds of Nb-90 m(18 s), Hf-160(12 s) and Hf-161(17 s). Nucl. Instrum. Methods **176**, 529–535 (1980)
129. Gäggeler, H., Dornhöfer, H., Schmidt-Ott, W.D., Greulich, N., Eichler, B.: Determination of adsorption enthalpies for polonium on surfaces of copper, silver, gold, palladium and platinum. Radiochim. Acta **38**, 103 (1985)
130. Kadkhodayan, B., Türler, A., Gregorich, K.E., Nurmia, M.J., Lee, D.M., Hoffman, D.C.: The heavy element volatility instrument (Hevi). Nucl. Instrum. Methods Phys. Res., Sect. A **317**, 254–261 (1992)
131. Eichler, B.: Preparative thermo gas chromatographic separation of radionuclides in hydrogen and air carrier gas stream. Radiochem. Radioanal. Lett. **22**, 147–155 (1975)
132. Rudolph, J., Bächmann, K., Steffen, A., Tsalas, S.: Inorganic gas-chromatography at high-temperatures. Mikrochim. Acta **1**, 471–481 (1978)
133. Rudolph, J., Bächmann, K.: Determination of adsorption enthalpies and entropies of inorganic halides by temperature-programmed gas-chromatography. J. Chromatogr. **178**, 459–469 (1979)
134. Tsalas, S., Bächmann, K., Heinlein, G.: The application of non-analytical radio gas-chromatography for the determination of adsorption enthalpies and entropies of inorganic bromides. Radiochim. Acta **29**, 217–221 (1981)
135. Zvara, I., Chuburkov, Y.T., Tsaletka, R., Shalaevskii, M.R.: Experiments on the chemistry of element 104—Kurchatovium II. Chemical investigation of the isotope which undergoes spontaneous fission with a half-life of 0.3 sec. Sov. Radiochem. **11**, 161–171 (1969)
136. Chuburkov, Y.T., Zvara, I., Shilov, B.V.: Experiments on the chemistry of element 104—Kurchatovium III. Chemical apparatus in the cyclotron beam. Sov. Radiochem. **11**, 171 (1969)
137. Zvara, I., Chuburkov, Y.T., Belov, V.Z., Buklanov, G.V., Zakhvataev, B.B., Zvarova, T.S., Maslov, O.D., Caletka, R., Shalaevsky, M.R.: Experiments on chemistry of element 104-Kurchatovium—V: Adsorption of kurchatovium chloride from the gas stream on surfaces of glass and potassium chloride. J. Inorg. Nucl. Chem. **32**, 1885–1894 (1970)
138. Zvara, I., Belov, V.Z., Domanov, V.P., Shalaevski, M.R.: Chemical isolation of nielsbohrium and ekatantalum in the form of the anhydrous bromide II. Experiments with a spontaneously fissioning isotope of nielsbohrium. Sov. Radiochem. **18**, 328–334 (1976)
139. Timokhin, S., Yakushev, A.B., Honggui, X., Perelygin, V.P., Zvara, I.: Chemical identification of element 106 by the thermochromatographic method. In: Oganessian, Y.T., Penionzhkevich, Y.E., Kalpakchieva, R. (eds.) International School-Seminar on Heavy Ion Physics, Dubna, 10–15 May 1993, pp. 204–206. Publishing Department, Joint Institute for Nuclear Research, Joliot Curie, 6, 141980, Dubna, Moscow Region, Russia
140. Timokhin, S.N., Yakushev, A.B., Xu, H., Perelygin, V.P., Zvara, I.: Chemical identification of element 106 by thermochromatography. J. Radioanal. Nucl. Chem. Lett. **212**, 31–34 (1996)
141. Yakushev, A.B., Timokhin, S.N., Vedeneev, M.V., Honggui, X., Zvara, I.: Comparative study of oxochlorides of molybdenum, tungsten and element 106. J. Radioanal. Nucl. Chem. **205**, 63–67 (1996)
142. Zvara, I., Domanov, V.P., Hübener, S., Shalaevskii, M.R., Timokhin, S.N., Zhuikov, B.L., Eichler, B., Buklanov, G.V.: Experimental approach to the chemical-identification of element-107 as eka-Rhenium.2. Search for spontaneously fissile isotopes of element-107 in the products of the reaction Bk-249 + Ne-22 by the method of chromathermography. Sov. Radiochem. **26**, 72–76 (1984)
143. Ghiorso, A., Nurmia, M., Eskola, K., Eskola, P.: Comments on chemical separation of Kurchatovium. Inorg. Nucl. Chem. Lett. **7**, 1117–1119 (1971)

144. Kratz, J.V.: Critical evaluation of the chemical properties of the transactinide elements. Pure Appl. Chem. **75**, 103–138 (2003)
145. Sümmerer, K., Brügger, M., Brüchle, W., Gäggeler, H., Jäger, E., Schädel, M., Schardt, D., Schimpf, E.: ROMA—A Rotating Wheel Multidetector Apparatus used in experiments with ^{254}Es as a target. In: GSI Annual Report 1983. vol. 84-1, p. 246. Gesellschaft für Schwerionenforschung mbH, Darmstadt, (1984)
146. Schädel, M., Jäger, E., Schimpf, E., Brüchle, W.: Modeling a nielsbohrium (element-107) online gas-phase separation procedure with rhenium. Radiochim. Acta **68**, 1–6 (1995)
147. Hoffman, D.C., Lee, D., Ghiorso, A., Nurmia, M.J., Aleklett, K., Leino, M.: Fission properties of the 1.5-S spontaneous fission activity produced in bombardment of Cm-248 with O-18. Phys. Rev. C **24**, 495–499 (1981)
148. Türler, A., Buklanov, G.V., Eichler, B., Gäggeler, H.W., Grantz, M., Hüberner, S., Jost, D.T., Lebedev, V.Y., Piguet, D., Timokhin, S.N., Yakushev, A., Zvara, I.: Evidence for relativistic effects in the chemistry of element 104. J. Alloys Compd. **271–273**, 287–291 (1998)
149. Türler, A., Eichler, B., Jost, D.T., Piguet, D., Gäggeler, H.W., Gregorich, K.E., Kadkhodayan, B., Kreek, S.A., Lee, D.M., Mohar, M., Sylwester, E., Hoffman, D.C., Hübener, S.: On-line gas phase chromatography with chlorides of niobium and hahnium (element 105). Radiochim. Acta **73**, 55–66 (1996)
150. Türler, A., Brüchle, W., Dressler, R., Eichler, B., Eichler, R., Gäggeler, H.W., Gärtner, M., Glatz, J.-P., Gregorich, K.E., Hübener, S., Jost, D.T., Lebedev, V.Y., Pershina, V.G., Schädel, M., Taut, S., Timokhin, S.N., Trautmann, N., Vahle, A., Yakushev, A.B.: First measurement of a thermochemical property of a seaborgium compound. Angew. Chem. Int. Ed. **38**, 2212–2213 (1999)
151. Vahle, A., Hübener, S., Dressler, R., Grantz, M.: Development of an apparatus for seaborgium studies by high temperature gas chromatography. Nucl. Instrum. Methods Phys. Res., Sect. A **481**, 637–645 (2002)
152. Hübener, S., Taut, S., Vahle, A., Dressler, R., Eichler, B., Gäggeler, H.W., Jost, D.T., Piguet, D., Türler, A., Brüchle, W., Jäger, E., Schädel, M., Schimpf, E., Kirbach, U., Trautmann, N., Yakushev, A.B.: Physico-chemical characterization of seaborgium as oxide hydroxide. Radiochim. Acta **89**, 737–741 (2001)
153. Düllmann, C.E., Eichler, B., Eichler, R., Gäggeler, H.W., Jost, D.T., Piguet, D., Türler, A.: IVO, a device for In situ volatilization and on-line detection of products from heavy ion reactions. Nucl. Instrum. Methods Phys. Res., Sect. A **479**, 631–639 (2002)
154. Dvorak, J., Brüchle, W., Chelnokov, M., Dressler, R., Düllmann, C.E., Eberhardt, K., Gorshkov, V., Jäger, E., Krücken, R., Kuznetsov, A., Nagame, Y., Nebel, F., Novackova, Z., Qin, Z., Schädel, M., Schausten, B., Schimpf, E., Semchenkov, A., Thörle, P., Türler, A., Wegrzecki, M., Wierczinski, B., Yakushev, A., Yeremin, A.: Doubly magic nucleus ^{270}Hs$_{162}$. Phys. Rev. Lett. **97**, 242501(4) (2006)
155. Dvorak, J., Brüchle, W., Chelnokov, M., Dressler, R., Düllmann, C.E., Dvorakova, Z., Eberhardt, K., Jäger, E., Krücken, R., Kuznetsov, A., Nagame, Y., Nebel, F., Nishio, K., Perego, R., Qin, Z., Schädel, M., Schausten, B., Schimpf, E., Schuber, R., Semchenkov, A., Thörle, P., Türler, A., Wegrzecki, M., Wierczinski, B., Yakushev, A., Yeremin, A.: Observation of the 3*n* evaporation channel in the complete hot-fusion reaction ^{26}Mg + ^{248}Cm leading to the new superheavy nuclide ^{271}Hs. Phys. Rev. Lett. **100**, 132503(4) (2008)
156. Düllmann, C.E.: Chemical investigaton of hassium (Z = 108). PhD thesis, Bern University (2002)

Liquid-Phase Chemistry of Superheavy Elements

Jens Volker Kratz and Yuichiro Nagame

Abstract An overview over the chemical separation and characterization experiments of the four transactinide elements so far studied in liquid phases, rutherfordium (Rf), dubnium (Db), seaborgium (Sg), and hassium (Hs), is presented. Results are discussed in view of the position of these elements in the Periodic Table and of their relation to theoretical predictions. Short introductions on experimental techniques in liquid-phase chemistry, specifically automated rapid chemical separation systems, are also given. Studies of nuclear properties of transactinide nuclei by chemical isolation will be mentioned. Some perspectives for further liquid-phase chemistry on heavier elements are briefly discussed.

1 Introduction

In the liquid-phase chemistry of the transactinide elements and their lighter homologs, carrier-free radionuclides produced in a nuclear reaction are transported to a separation device by a gas-jet technique and are dissolved in an aqueous solution. In general, the latter contains suitable ligands for complex formation. The complexes are then chemically characterized by a partition method that can be liquid–liquid extraction, cation-exchange or anion-exchange chromatography, or reversed-phase extraction chromatography. The ultimate goal of the partition experiments is to determine the so-called distribution coefficient, the K_d value,

J. V. Kratz (✉)
Institut für Kernchemie, Johannes Gutenberg-Universität Mainz, Fritz-Strassmann-Weg 2
55128 Mainz, Germany
e-mail: jvkratz@uni-mainz.de

Y. Nagame
Advanced Science Research Center, Japan Atomic Energy Agency, Tokai,
Ibaraki 319-1195, Japan
e-mail: nagame.yuichiro@jaea.go.jp

M. Schädel and D. Shaughnessy (eds.), *The Chemistry of Superheavy Elements*,
DOI: 10.1007/978-3-642-37466-1_6,

based on an atom-at-a-time scale as a function of ligand concentration. The K_d value is given in its simplest definition, which applies to liquid–liquid extraction, by the ratio of the radioactivity in the organic phase to that in the aqueous phase. In a chromatography experiment, as we will see below, the distribution coefficient is closely related to the key observable, the retention time t_r.

Liquid-phase chemistry is performed mostly in a discontinuous batch-wise manner. It is then necessary, in order to get statistically significant results, to repeat the same experiment several hundred or even several thousand times with a cycle time on the order of a minute. Recent discontinuous studies were either performed manually or with automated rapid chemical separation devices, such as the Automated Rapid Chemistry Apparatus (ARCA II) [1] and the Automated Ion-exchange separation apparatus coupled with the Detection system for Alpha spectroscopy (AIDA) [2]. These discontinuous separations involve a rather time-consuming evaporation step to prepare weightless samples for α spectroscopy. This is avoided with the continuous ion-exchange chromatography with the multi-column technique (MCT), which was first used to study the fluoride complexation of rutherfordium (Rf) [3]. The fast centrifuge system SISAK, Short-lived Isotopes Studied by the AKUFVE-technique, where AKUFVE is a Swedish acronym for an arrangement of continuous investigations of distribution ratios in liquid extraction, were coupled with on-line liquid-scintillation counting (LSC) and was applied for the study of the short-lived nuclide ^{257}Rf [4].

This chapter gives an overview over the chemical separation and characterization experiments of the four transactinide elements so far studied in liquid phases, rutherfordium (Rf), dubnium (Db), seaborgium (Sg), and to some extent hassium (Hs), the chemical properties that were obtained, their relation to theoretical predictions (see "Theoretical Chemistry of the Heaviest Elements"), and some perspectives for further studies. More technical details of these experiments are given in "Experimental Techniques".

2 Rutherfordium (Rf, Element 104)

2.1 First Survey Experiments

According to the actinide concept by Seaborg [5], the 5f series in the Periodic Table ends with element 103, lawrencium (Lr), and a new 6d transition series is predicted to begin with element 104, Rf. After the discovery of a long-lived α-particle emitting isotope with a half-life of $T_{1/2} = 65$ s, ^{261}Rf, by Ghiorso et al. [6] in 1970, Silva et al. [7] confirmed this placement of Rf in the Periodic Table by conducting the first liquid-phase separations with a cation-exchange chromatography column and the chelating agent α-hydroxyisobutyric acid (α-HiB, 2-hydroxy-2-methyl-propionic acid). In this pioneering experiment, ^{261}Rf was produced in irradiation of 47 μg of ^{248}Cm, which was electrodeposited over

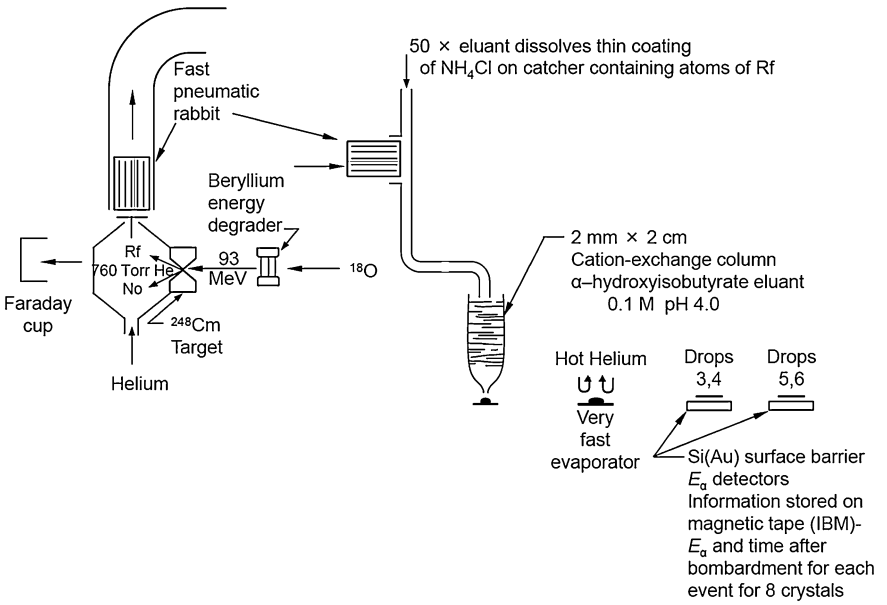

Fig. 1 Sketch of the chemical method used for the first liquid-phase separation of Rf. Adapted from [8]

0.2 mm^2 area onto a Be foil, with 92-MeV ^{18}O ions delivered from the Berkeley Heavy Ion Linear Accelerator. A sketch of the system used is shown in Fig. 1. The recoils from the target were stopped in He gas, were swept out of the recoil chamber through a nozzle, and were deposited on the surface of a rabbit that was coated with a thin layer of NH_4Cl. After fast transport of the rabbit to the chemistry apparatus, the ^{261}Rf was washed from the rabbit with 50 μL ammonium α-HiB (0.1 M, pH = 4.0), and was fed onto the top of a 2 mm diameter by 2 cm long heated (∼80 °C) column of Dowex 50 × 12 cation-exchange resin. This solution was forced into the resin and after adding more eluant the washing was continued. The first two drops (free column volume) containing little or no radioactivity were discarded. The next four drops (taken in two-drop fractions) were collected on platinum disks, evaporated to dryness, and heated to ∼500 °C to burn off any carbon residue. The disks were placed active side down directly over Si(Au) α-particle detectors. The event number, energy, and time distribution of α particles with energies between 6 and 12 MeV emitted by the sources were recorded. The average time from beam off to the start of counting was ∼60 s. Approximately 100 atoms of ^{261}Rf were produced in several hundred experiments. However, only about 1/10 of this number of events were observed after chemistry due to decay, counting geometry, and chemical losses. The overall yield of tracer quantities of the lighter homologs Zr and Hf recovered in drops 3–6 was about 50%.

In contrast, trace quantities of the trivalent ions of rare earth and actinide elements, Tm, Cf, and Cm, did not elute in over 100 column volumes. No^{2+}, as

well as the alkaline earth elements, was retained even more strongly on the resin. α-particle spectra were recorded for four sequential 1 min decay intervals from sources after chemical separation. These contained 17 α-particle events in the energy region 8.2–8.4 MeV. Approximately one-half of these events are due to the decay of 26-s ^{257}No, the daughter of ^{261}Rf. In two experiments, 2 α-decay events occurred in the energy region 8.2–8.4 MeV within a time interval of 1 min, representing a pair of correlated mother (^{261}Rf) and daughter (^{257}No) decays. This number of mother–daughter (α–α) correlations is consistent with the detector geometry used. These data show unambiguously that the chemical behavior of the radioactivity assigned to ^{261}Rf is entirely different from that of trivalent and divalent actinides but is similar to that of Zr and Hf, as one would expect for the next member of the Periodic Table following the actinide series.

The experiment with Rf by Silva et al. [7], even though being "historical", is typical for many liquid-phase experiments performed later. This combines a fast transport system for transfer of the radionuclides from a target-recoil chamber to a chemistry system with a discontinuously performed chemical separation that is repeated hundreds/thousands of times. It also includes the preparation of sources for α spectroscopy by evaporation of the aqueous effluent from the column to dryness and records energy and time of the α events and of α–α correlations for unambiguous isotopic assignment of the radioactivity. Above all, it compares the behavior of a transactinide element with that of its lighter homologs under identical conditions. It has not yet been efficient enough, however, to measure K_d values. This has only been achieved with improved techniques that have been developed more recently, i.e., within the last ∼25 years.

Another first-generation experiment by Hulet et al. [9], testing the chloride complexation of Rf, made use of computer automation to perform all chemical manipulations rapidly, to prepare α sources, and to do α spectroscopy. An extraction chromatographic method was chosen to investigate chloride complexation in high concentrations of HCl, which thereby avoided the hydrolysis reaction possible at lower acidities. The extraction columns contained an inert support loaded with trioctyl-methylammonium chloride (Aliquat 336), since anionic-chloride complexes formed in the aqueous phase are strongly extracted into this ammonium compound. Such complexes are formed in 12 M HCl by the group-4 elements and are extracted, whereas group-1 through group-3 elements, including the actinides, are not appreciably extracted. Thus, these latter radionuclides were eluted from the column with 12 M HCl while Zr and Hf, and Rf, were extracted and subsequently eluted with 6 M HCl, in which chloride complexation is less favored. Figure 2 shows the atoms of ^{261}Rf observed via α decay in three sequential elution fractions.

Only six events from ^{261}Rf were observed in over 100 experiments, one in the feed fraction (12 M HCl), two in elution fraction 2 (6 M HCl), and three in elution fraction 3 (6 M HCl). The percentage of Hf in these same fractions was 12, 59, and 29%. These results showed that the chloride complexation of Rf is consistently stronger than that of the trivalent actinides and is similar to that of Hf. Again, no K_d value was determined in this "early" experiment.

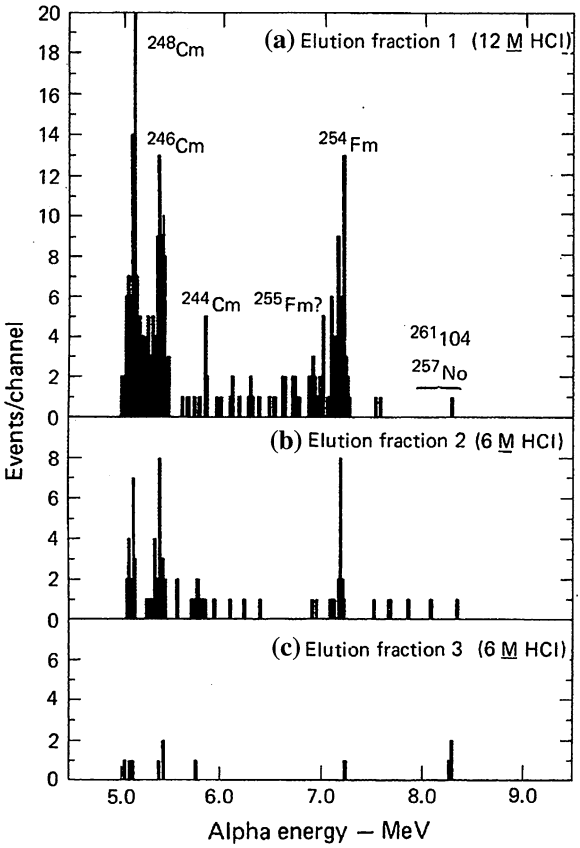

Fig. 2 α spectra showing the decay of a few ^{261}Rf atoms in three sequential elution fractions from a column containing trioctylmethylammonium chloride. Reprinted from [9]

For Rf in aqueous solutions, early experiments exploited the complexing with α-hydroxiisobutyrate (α-HiB) [7] and the formation of chloride anions [9], and thus confirmed a behavior radically different from that of the heavy actinides. Although these were key experiments demonstrating that a new transition element series, the 6d series, begins with element 104, none of these experiments provided a detailed study of Rf chemistry. The results of the first-generation experiments on the chemistry of the early transactinides were summarized by Keller, Jr and Seaborg [10], Hulet [11], Keller, Jr [12], and Silva [13].

2.2 Detailed Studies

A renewed interest in studying the chemical properties of the transactinide elements in more detail both experimentally and theoretically arose in the late 1980s, see, e.g., Hoffman [14–16], Kratz [17, 18], Schädel [19], Kratz [20, 21], Schädel [22], Kratz [23, 24], Schädel [25], Hoffmann et al. [26], and Kratz [27, 28], for

recent reviews on experiments. This extensive series of detailed investigations was made possible by the development of new experimental techniques; see "Experimental Techniques". Computer-controlled automated systems have greatly improved our ability to perform rapidly and reproducibly large numbers of chromatographic separations on miniaturized columns in the liquid phase and to detect the transactinides through their characteristic α decay and preferably by α–α (mother–daughter) correlations. These techniques have produced detailed and sometimes surprising results that called for a detailed theoretical modeling of the chemical properties with improved quantum-chemical calculations; see "Theoretical Chemistry of the Heaviest Elements".

On the other hand, a series of manually performed separations of ^{261}Rf in aqueous solutions was also performed by the research group at the Lawrence Berkeley National Laboratory (LBNL) using the 88-Inch Cyclotron at LBNL [29–34]. Their experiments involving liquid–liquid extractions typically comprised the following steps; a He(KCl)-jet transportation system was used for the transfer of the radionuclides. The KCl aerosol with the reaction products was collected by impaction on a Pt plate or Teflon^{TM} slip for 60 or 90 s, was picked up with 10 μL of the aqueous phase, and was transferred to a 1 mL centrifuge cone containing 20 μL of the organic phase. The phases were mixed ultrasonically for 5 s and were centrifuged for 10 s for phase separation. The organic phase was transferred to a glass cover slip, was evaporated to dryness on a hot plate, and was placed over a Passivated Ion-Implanted Planar Silicon (PIPS) detector. The above procedure took about 1 min and was mainly applied to study the aqueous chemistry of element 104 with the isotope 78-s ^{261}Rf [29–34]. A serious drawback of these latter investigations is that only the organic phase was assayed for ^{261}Rf; the aqueous phase was not counted.

Although an isomeric state of ^{261}Rf with the half-life of 1.9 s has been recently identified [35], only the longer half-life state of ^{261}Rf with $T_{1/2} = 78$ s was used for chemistry and is expressed as ^{261}Rf in this chapter.

2.2.1 Hydrolysis Versus Halide Complexation: Studies Using Liquid–Liquid Extraction and Extraction Chromatography Techniques

Liquid–liquid extractions with triisooctyl amine (TiOA) from 12 M HCl by Czerwinski et al. [30] confirmed the results of Hulet et al. [9]. Cationic species were studied with extraction into thenoyltrifluoroacetone (TTA) [29]. A distribution coefficient for Rf between those of the tetravalent pseudo-homologs Th and Pu indicated that the hydrolysis of Rf is less than that for Zr, Hf, and Pu [29].

Czerwinski et al. performed a series of liquid–liquid extractions with tributylphosphate (TBP) in benzene to study the effect of HCl, Cl^-, and H^+ concentration between 8 and 12 M on the extraction of Zr^{4+}, Hr^{4+}, Th^{4+}, Pu^{4+}, and Rf^{4+} [31]. It was found that Rf was extracted efficiently as the neutral tetrachloride into TBP from 12 M HCl like Zr, Th, and Pu, while the extraction of Hf was relatively low and increased from 20 to 60% between 8 and 12 M HCl. Extraction of Rf

increased from 6 to 100% between 8 and 12 M HCl, thus defining an extraction sequence Zr > Rf > Hf for the neutral group-4 chlorides. Surprising results were obtained when the chloride concentration was varied at a constant H^+ concentration of 8 M. Above 10 M Cl^- concentration, the extraction of Rf decreased and behaved differently from Zr, Hf, and Th, and resembled that of Pu^{4+}. This was interpreted in terms of stronger chloride complexing in Rf than in Zr, Hf, and Th, leading to the formation of $[RfCl_6]^{2-}$ that is not extracted into TBP. Extraction studies at a constant concentration of 12 M Cl^- showed that Rf extraction is sharply increasing with increasing H^+ concentration between 8 and 12 M [31]. Such behavior is not exhibited by Zr and Hf. As some of these extraction experiments suffered from differences in details of the chemical procedures applied to the different elements, e.g., different contact times and volumes used, it is important to confirm these very interesting and somehow unexpected findings in experiments that establish identical conditions for all homologs elements including Rf.

Kacher et al. [33] performed some additional chloride extractions into TBP/benzene with Zr, Hf, and Ti. The reported low extraction yields of Hf in [31] by Czerwinski et al. could not be reproduced by Kacher et al. who reported that they observed that significant amounts of Hf (more than 50% in some cases) stick to Teflon surfaces. (They actually conducted their subsequent experiments with polypropylene equipment, because only negligible adsorption was observed with polypropylene surfaces.) The Hf results from the experiments by Czerwinski et al. [31] were based on on-line data taken at the 88-Inch Cyclotron where the radionuclide was collected on a Teflon disk that, according to [33], accounts for the seemingly low Hf extraction. Surprisingly, a similar loss of Rf due to adsorption in the experiments of Czerwinski et al. [31] was not suspected by Kacher et al. Therefore, the latter authors, based on their new Zr-, Hf-, and Ti-results and on the previous Rf results in [31], suggested a revised sequence of extraction into TBP/benzene from around 8 M HCl as Zr > Hf > Rf > Ti. In a parallel study of liquid–liquid extractions into TBP/benzene from HBr solutions, extraction of Rf was found to be low and was only increased for bromide concentrations beyond 9 M [33]. The extraction behavior of the group-4 elements into TBP from both HCl and HBr solutions was primarily attributed to their different tendencies to hydrolyze [33].

The latter statement refers to concurrent work by Bilewicz et al. [32] who studied the adsorption of Zr, Hf, Th, and Rf on cobalt ferrocyanide surfaces. These ferrocyanides are known to be selective sorbents for heavy univalent cations such as Fr^+, Cr^+, and Rb^+. Some ferrocyanides such as Co ferrocyanide, however, have been found to exhibit also particularly high affinities for tetravalent ions such as Zr^{4+}, Hf^{4+}, and Th^{4+} involving the formation of a new ferrocyanide phase between the 4^+ cation and the $[Fe(CN)_6]^{4-}$ anion. The first hydrolysis step of a 4^+ cation is shown in the following reaction,

$$\left[M(H_2O)_X\right]^{4+} \rightleftarrows M(H_2O)_{X-1}(OH)^{3+} + H^+ \quad (1)$$

On the left hand side of Eq. 1, we have the hydrated 4^+ cation, on the right hand side the first hydrolysis product being a 3^+ cation.

As 3^+ cations essentially do not adsorb on ferrocyanide surfaces, the onset of hydrolysis at decreasing HCl concentration in the aqueous phase will be reflected by a rapid decrease of the adsorbed nuclide. This decrease was observed by Bilewicz et al. [32] below 3 M HCl for Rf, below 1 M HCl for Zr, and below 0.5 M HCl for Hf, establishing seemingly a hydrolysis sequence Rf > Zr > Hf. As, in general, hydrolysis increases with decreasing radius of the cation, the stronger hydrolysis of the larger size of the Rf ion is very surprising and in conflict with the results of Czerwinski et al. [30]. Bilewicz et al. suggested as an explanation that the coordination number CN (X in Eq. 1) for Zr^{4+} and Hf^{4+} is eight, and changes to CN = 6 for Rf due to relativistic effects making the $6d_{5/2}$ orbitals unavailable for ligand bonding of water molecules. Günther et al. [36], however, have shown that this does not withstand a critical examination. It is the present author's opinion that some experimental deficiency and nonincreased tendency of Rf to hydrolyze produced the surprising results of Bilewicz et al. [32]. For example, the contact time of the aqueous phase with the ferrocyanide surface was only 10 s in the Rf experiments. In a kinetic study, the authors found that Zr and Hf adsorbed within 20 and 40 s, respectively, while Th required more than 90 s to achieve nearly complete adsorption [32]. It is conceivable that, within the 10 s interaction of the aqueous phase in the Rf experiments, no equilibrium was established thus making the Rf data meaningless.

A study of the extraction of fluoride complexes of Ti^{4+}, Zr^{4+}, Hf^{4+}, and Rf^{4+} into TiOA was also reported by Kacher et al. [34]. This work presents some evidence for extraction of ^{261}Rf into TiOA from 0.5 M HF. No quantitative assessment of the extraction yield or K_d value, however, was made. Consequently, the conclusion in [34] that the extraction into TiOA for the group 4 elements decreases in the order Ti > Zr ≈ Hf > Rf is not reproducible.

In view of the somewhat unsatisfactory situation with the conflicting Hf results by Czerwinski et al. [31] and Kacher et al. [33] and with the intention to establish an independent set of data characterizing the extraction sequence of Zr, Hf, and Rf from 8 M HCl into TBP, Günther et al. [36] determined distribution coefficients of these elements from HCl solutions. In 8 M HCl, the K_d of Zr is 1180, that for Hf is 64. This difference makes possible a chromatographic separation of Hf from Zr in ARCA II on 1.6 mm i.d. × 8 mm columns filled with TBP on an inert support. This separation was also studied with the short-lived ^{169}Hf from the Gd(^{18}O,xn) reaction yielding $K_d = 53^{+15}_{-13}$ in agreement with the above results from batch extraction experiments. 78-s ^{261}Rf was produced in the ^{248}Cm(^{18}O,5n) reaction at the Philips Cyclotron of the Paul Scherrer Institute (PSI), Switzerland, and from the distribution of α events between the Hf and Zr fraction, a K_d value of 150 was determined for Rf in 8 M HCl. This gives the extraction sequence Zr > Rf > Hf [36]. A theoretical discussion on aspects of hydrolysis and complex formation, including the group 4 elements, can be found in "Hydrolysis and Complex Formation".

2.2.2 Hydrolysis Versus Halide Complexation: Studies Using Ion-Exchange Chromatography

Fluoride complexation of Rf was studied by Szeglowski et al. [3], Pfrepper et al. [37, 38], Kronenberg et al. [39], and Strub et al. [40]. In the work of Szeglowski et al. [3], ^{261}Rf produced in the ^{248}Cm(^{18}O,5n) reaction was transported on line to the chemistry apparatus and was continuously dissolved in 0.2 M HF in a degassing unit, and the solution was passed through three ion-exchange columns. In the first cation-exchange column, actinides produced directly in the reaction were removed from the solution. In the next anion-exchange column, ^{261}Rf was adsorbed, presumably as $[RfF_6]^{2-}$, while the following cation-exchange column retained its cationic decay products. After the end of bombardment, the long-lived descendants ^{253}Fm ($T_{1/2}$ = 3 d) and ^{253}Es ($T_{1/2}$ = 20 d) were desorbed from the third column and detected off-line by α spectroscopy. Their detection was proof that Rf forms anionic fluoride complexes, which are adsorbed on an anion-exchange resin.

Pfrepper et al. [37, 38] developed this technique further, thereby making it a quantitative technique capable of measuring distribution coefficients K_d values of short-lived isotopes by on-line chromatography. In the conventional off-line chromatography, the distribution coefficient is determined via the retention time (elution position) as

$$K_d = [t_r - t_o]\frac{f}{m_r}, \tag{2}$$

with t_r = retention time, t_o = column hold-up time due to the free column volume, f = flow rate of the mobile phase (mL min^{-1}) and m_r = mass of the ion exchanger (g).

As described in [3], in this technique the detection of the transactinide isotope itself, ^{261}Rf, is abandoned and replaced by the detection of its long-lived descendant, 20-d ^{253}Es. This way, one gains the possibility of a continuous on-line mode over many hours. The feeding of ^{261}Rf onto the anion-exchange column is performed under conditions in which the retention time t_r is on the order of the nuclear half-life $T_{1/2}$, i.e., K_d values on the order of 10–50 are selected [37]. Similarly to the principle used in the on-line isothermal gas chromatography, one is using the nuclear half-life as an internal clock. As mentioned in [3], three ion-exchange columns are used in series, first a cation-exchange column that retains the ^{253}Es from the continuously flowing feed solution. This is necessary as ^{253}Es could be produced directly by transfer reactions. It follows the true chromatographic column (C) filled with an anion-exchange resin. The long-lived decay products (D_1) that are formed by radioactive decay of ^{261}Rf during its retention time on the anion-exchange column are eluted from this column as cations and are fixed on the following cation-exchange column. The part of the ^{261}Rf that survives the retention time on the anion-exchange column is eluted from it and passes the following cation-exchange column to be subsequently collected in a reservoir in

which it decays into the long-lived decay products (D_2). D_1 and D_2 are isolated separately after the end of the on-line experiment and assayed off-line for α-decay of ^{253}Es. From the ratio of D_1 and D_2 and the nuclear half-life $T_{1/2}$ of ^{261}Rf, one obtains the distribution coefficient, K_d, as

$$K_d = \left[\frac{T_{1/2}}{\ln 2} \ln \frac{D_1 + D_2}{D_2} - t_o\right] \frac{f}{m_r}. \quad (3)$$

Pfrepper et al. [37] verified the equivalence of Eqs. 2 and 3. They compared K_d values for Hf isotopes obtained, first, in batch experiments and by conventional elution chromatography in the anion-exchange system HS36 (a resin with the quaternary triethyl-ammonium group) –0.27 M HF/x M HNO_3 (x variable) with, second, K_d values obtained in the same system with the multi-column technique (MCT). They used the short-lived Hf isotopes ^{165,166}Hf and detected the daughter nuclides ^{165,166}Tm and ^{166}Yb by γ-ray spectroscopy. In order to determine the ionic charge of the Hf fluoride complexes, the concentration of the counter ion NO_3^- was varied. K_d values were found to be 12.7 ± 1.8 mL g^{-1} with 0.2 M HNO_3 and 2.4 ± 0.8 mL g^{-1} with 0.5 M HNO_3. This corresponds to an ionic charge of –1.9 ± 0.4 for the fluoride complex of Hf as determined from the slope of the plot of log K_d versus the logarithm of the concentration of the counter ion. From this, it was concluded that Hf probably forms $[HfF_6]^{2-}$. This is evidenced also by Fig. 3 in which the K_d values obtained by the on-line MCT are compared with those from a series of batch experiments performed in parallel with the same anion-exchange resin. From the good agreement, it was concluded that with the MCT, determination of the ionic charge of complexes of transactinides must be feasible.

In the application of the MCT to ^{261}Rf [38], Pfrepper et al. used about 20 mg (11 mg) of the anion-exchange resin HS36 in the chromatographic column at an elution rate of approximately 0.35 mL min^{-1} of 0.27 M HF and 0.2 (0.1) M HNO_3. The cation-exchange column (s) that adsorb the descendant nuclides 23-s ^{257}No, 3-d ^{253}Fm, and 20-d ^{253} Es contained 50 mg of the strongly acidic cation

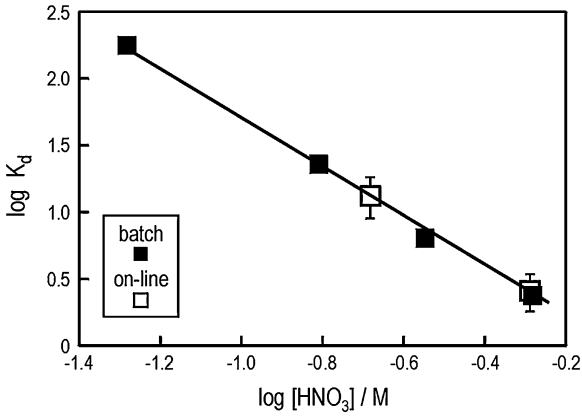

Fig. 3 log K_d of Hf in the system HS36-0.27 M HF/HNO_3 as a function of the HNO_3 concentration, measured in batch and in on-line experiments [37]. Reprinted with permission of Oldenbourg Wissenschaftverlag, München

exchanger Wofatit KPS. For the similar cation-exchange resin Dowex 50 × 12, Pfrepper et al. [37] had shown previously that, for HNO_3 concentrations < 0.3 M, K_d values for trivalent rare-earth cations exceed 10^4 mL g^{-1} resulting in a breakthrough volume in excess of 500 mL. Assuming the same conditions for their ^{261}Rf experiment [38], it was decided to renew the cation-exchange columns collecting the descendant fractions D_1 and D_2 every 12 h. This corresponded to eluent volumes of about 260 mL; while the breakthrough volume was estimated to be about 10^3 mL. Thus, at first sight, breakthrough of the cationic "daughter nuclides" was safely prevented.

^{261}Rf and $^{165–169}$Hf were produced simultaneously by irradiation of a combined target of ^{248}Cm and ^{152,154,158}Gd with ^{18}O ions at the Dubna U-400 Cyclotron. In the γ-ray spectra of D_1 and D_2, the nuclides ^{165}Tm, ^{166}Yb, ^{167}Tm, ^{169}Lu, and ^{169}Yb were detected as the decay products of ^{165,166,167,169}Hf. K_d values on the order of 14.8 and 47 were determined in 0.27 M HF/0.2 M HNO_3 and 0.27 M HF/0.1 M HNO_3, respectively, compatible with an ionic charge of the fluoride complex of –1.85 ± 0.1. For ^{261}Rf, the α decays of its descendant ^{253}Es were evaluated yielding K_d values of about 14 and 50 in 0.27 M HF/0.2 M HNO_3 and 0.27 M HF/0.1 M HNO_3, respectively, giving an ionic charge of –1.9 ± 0.2. It was concluded that Rf has properties of a close homolog of Hf and forms $[RfF_6]^{2-}$, the stoichiometry characteristic of Hf and other group-4 elements [38].

Kronenberg et al. [39] observed that the K_d values of trivalent lanthanide (Tb^{3+}) and actinide cations (^{241}Am and ^{250}Fm) in mixed HF/0.1 M HNO_3 solutions on the cation-exchange resin Dowex 50W × 8 exceed 10^4 mL g^{-1} only for HF concentrations below 10^{-2} M. For higher HF concentrations, the K_d values decrease to 2,000 in 0.05 M HF/0.1 M HNO_3, 1,300 in 0.1 M HF/0.1 M HNO_3, 700 in 0.5 M HF/0.1 M HNO_3, and 500 in 1 M HF/0.1 M HNO_3. A simultaneous rise of K_d values on the anion-exchange resin Dowex 1 × 8 is observed [39] for > 0.05 M HF/0.1 M HNO_3 with values reaching 170 in 0.1 M HF/0.1 M HNO_3, 1,600 in 0.5 M HF/0.1 M HNO_3, and 2,500 in 1 M HF/0.1 M HNO_3 thus indicating that anionic fluoride complexes are formed. The K_d value in 0.27 M HF/0.1 M HNO_3 on a strongly acidic cation-exchange resin can be estimated to be on the order of 800. Thus, the breakthrough volume for lanthanides and actinides in the experiments by Pfrepper et al. [38] was not > 500 mL but rather < 40 mL, i.e., both the Hf and the Rf descendants were breaking through the cation-exchange columns in less than 2 h. It is impossible to reconstruct what this did to the K_d values in the work of Pfrepper et al. [38]. However, the significant difference by orders of magnitude between the K_d values of Hf and Rf in mixed HF/HNO_3 solutions observed recently in [39–41] do cast doubt on the validity of the results in [38], where indistinguishable K_d values for Hf and Rf were reported.

Strub et al. [40] have investigated in batch experiments K_d values of the long-lived tracers ^{95}Zr, ^{175}Hf, and ^{233}Th on a strongly acidic cation-exchange resin, Aminex A5, and on a strongly basic anion-exchange resin, Riedel-de Häen, in 0.1 M HNO_3 solutions containing variable concentrations of HF. On the cation-exchange resin, below 10^{-3} M HF, the K_d values for Zr, Hf, and Th are > 10^3

indicating the presence of cations. In the range 10^{-3} M < [HF] < 10^{-2} M, the K_d values of Zr and Hf decrease due to the formation of neutral or anionic fluoride complexes. The behavior of Zr and Hf is very similar (Hf sticks to the resin even at slightly higher HF concentrations). The elution of Th from the resin is observed at more than one order of magnitude higher HF concentrations, see Fig. 4. These off-line data were compared with on-line data taken with ARCA II at the UNILAC accelerator at the Gesellschaft für Schwerionenforschung (GSI), Darmstadt, where short-lived Hf isotopes $^{166,167,168\cdots}$Hf were produced in xn-reactions of a ^{12}C beam with an enriched ^{158}Dy target. As is shown in Fig. 4, there is general agreement between both sets of data.

On an anion-exchange resin, as expected, there is little adsorption of Zr, Hf, and Th at low HF concentrations. In the range 10^{-3} M < [HF] < 10^{-2} M, the K_d values of Zr and Hf in batch experiments rise simultaneously, i.e., in the same range as they decrease on the cation-exchange resin. This shows that the disappearance of the cationic species at low HF concentrations is followed immediately by the formation of anionic fluoride complexes. For Th, the adsorption on the anion-exchange resin stays low for all HF concentrations, indicating that Th does not form anionic fluoride complexes.

In the Rf experiments performed at the PSI Philips Cyclotron [40], ^{261}Rf was produced in the ^{248}Cm(^{18}O,5n) reaction at 100 MeV. The target contained 10% Gd enriched in ^{152}Gd to produce simultaneously short-lived Hf isotopes. They were used to monitor the behavior of Hf and to perform yield measurements by γ spectroscopy. Rf and Hf were transported by the He(KCl) gas-jet and were collected for 90 s by impaction inside ARCA II [40]. The deposit was dissolved in 200 μL 0.1 M HNO_3/x M HF (x variable) and was fed onto the 1.6 mm i.d. × 8 mm cation-exchange column at a flow rate of 1 mL min^{-1}. The effluent was evaporated to dryness as sample 1. In order to elute remaining Rf and Hf from the column, a second fraction of 200 μL 0.1 M HNO_3/0.1 M HF was collected to strip all group-4 elements from the column. The fraction was prepared as sample 2.

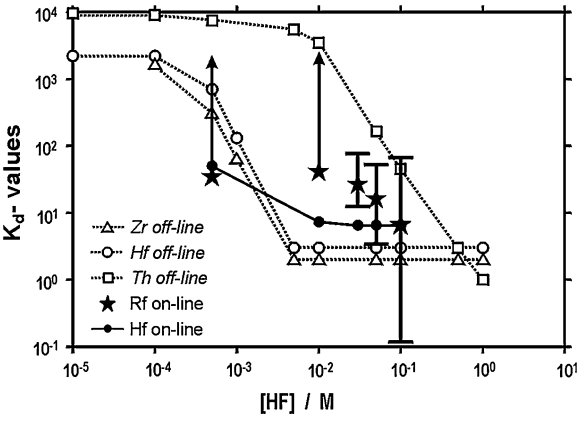

Fig. 4 Adsorption of Zr, Hf, Th, and Rf on the cation-exchange resin, Aminex A6, in 0.1 M HNO_3 at various HF concentrations. Off-line data are shown for Zr, Hf, and Th, and on-line data for Rf and Hf; re-evaluated data from [40]. Reprinted with permission of Oldenbourg Wissenschaftverlag, München

In the anion-exchange experiments, Rf and Hf were transported, collected, and loaded onto the anion-exchange column as in the experiments with the cation-exchange columns. Again, the effluent was evaporated to dryness as sample 1. In order to elute remaining Rf and Hf from the column, a second fraction of 200 μL 5 M HNO_3/0.01 M HF was used. This fraction was prepared as sample 2.

K_d values are often calculated as follows:

$$K_d = \frac{A_S}{A_L} = \frac{A_{S0}\ V_S}{A_{L0}\ m_r}, \tag{4}$$

with A_S specific radioactivity in the solid phase (Bq g^{-1}), A_L specific radioactivity in the liquid phase (Bq mL^{-1}), A_{S0} radioactivity in the solid phase (Bq), A_{L0} radioactivity in the liquid phase (Bq), V_S volume of the solution (mL), and m_r mass of the resin (g). The K_d values using Eq. 4 are obtained such that the radioactivity of sample 1 is attributed to the liquid phase and that of sample 2 to the solid phase. In elution experiments, however, Eq. 4 yields only correct K_d values for the fortunate situation of equal radioactivities in fraction 1 and 2, i.e., cuts between fractions 1 and 2 at the maximum position of the elution curve. To circumvent this deficiency, K_d values shown in Fig. 4 were calculated by a computer program that simulates the elution process. The number of theoretical plates—obtained from the shape of tracer elution curves -, the free column volume, the volume of fraction 1 and an assumed K_d value are the initial input parameters. In an iteration process, the K_d value is varied until the experimentally observed radioactivity in fraction 1 is obtained.

The results of the on-line experiments with Rf and Hf on cation-exchange columns are given in Fig. 4 together with the results of the off-line batch experiments. The on-line data for Hf are consistent with the off-line data.

The K_d values for ^{261}Rf at 5×10^{-4} M HF and at 10^{-2} M HF are lower limits as no ^{261}Rf decays were detected in sample 1. It is seen that the decrease of the K_d values for Rf occur between 0.01 M HF and 0.1 M HF, i.e., at one order of magnitude higher HF concentrations than for Zr and Hf. Under the given conditions, the behavior of Rf is intermediate between that of its pseudo-homolog Th and that of its group members Zr and Hf.

The results of the on-line experiments with the anion-exchange columns are given in Fig. 5. While the off-line data for Hf clearly indicate that anionic fluoride complexes of Hf are formed for $> 10^{-3}$ M HF, one observes that the Hf data taken on-line are systematically lower. The reason for this discrepancy is unknown at present. Seemingly, the behavior of Rf is different from that of Zr and Hf—if compared with the off-line data—as there is almost no adsorption of Rf on the resin. Even for 1 M HF, which is about two orders of magnitude higher than the concentration from whereon maximum K_d values are observed for Zr and Hf, there is no indication of a rise in the K_d values for Rf.

As it would be in contradiction to the results in [3, 34, 38] that there are no anionic fluoride complexes for Rf at any HF concentration, the concentration of HNO_3 was varied [40] between 0.1 M and 0.01 M at a constant HF concentration

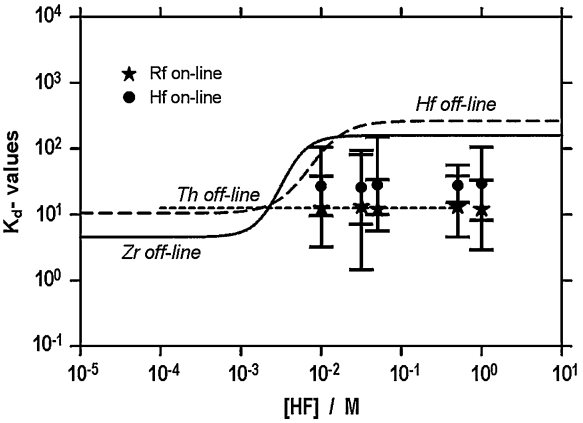

Fig. 5 Adsorption of Zr, Hf, Th, and Rf on the anion-exchange resin, Riedel-de Häen, in 0.1 M HNO_3 at various HF concentrations. The data points of Hf and Rf are taken from the on-line experiments. The lines indicate the trends exhibited by the off-line data [40]. Reprinted with permission of Oldenbourg Wissenschaftverlag, München

of 0.05 M, thus varying the concentration of NO_3^-, which acts as a counter ion competing for the binding sites on the anion exchanger. It was observed [40] that the K_d values of Hf and Rf rise with decreasing NO_3^- concentration, indicating that negatively charged complexes are formed both for Hf and for Rf, and that the counter ion NO_3^- is much more effective in removing Rf from the binding sites on the anion exchanger than in removing Zr and Hf.

This was the starting point for a new series of experiments with anion-exchange chromatography with Aminex A27 in which the HNO_3 and the HF concentration were varied systematically [42]. The following observations were made: (1) There is a steep dependence of the log K_d values of Rf on the log [NO_3^-] concentration at fixed HF concentration (0.01 M). (2) At fixed [NO_3^-] concentration (0.003 M), above 0.1 M HF, increasing the HF concentration is leading to a decrease in the K_d values for Rf. The first observation suggested that the NO_3^- ion acts as a counter ion competing for the binding sites on the anion-exchange resin with the group-4 fluoride complexes. Based on the observation in (2), a second counter ion discussed in [42] is the HF_2^- ion that is the dominant anion above an initial HF concentration of 0.3 M; see also Sect. 2.2.3.

We note, that in the work of A. Kronenberg [38], also two MCT experiments were performed with ^{261}Rf using 0.5 M HF/0.1 M HNO_3 and 0.01 M HF. In the first case, the cation-exchange columns were filled with 330 mg of Dowex 50W × 8 and were used for 3 h to prevent breakthrough of the cationic descendants. The anion-exchange column in between was filled with 50 mg of the anion-exchange resin Dowex 1 × 8 in the nitrate form. In the second case, the cation-exchange columns, filled with 68 mg Dowex 50W × 8, were used for 4 h, and the anion-exchange column was filled with 17 mg of Dowex 1 × 8 in the fluoride form. Each experiment was run for 24 h at an average beam intensity of 3×10^{12} s^{-1}.

The first experiment with 0.5 M HF/0.1 M HNO_3 was performed to corroborate the low K_d values obtained in [40] with ARCA II on an anion-exchange resin, see Fig. 5. A total of 80 α-decay events were observed attributable to ^{253}Es in the sample 1 representing the liquid phase and no event in the strip fraction

representing the solid phase. Taking zero to be compatible with three events at 95% confidence level in Poisson statistics, leads to an upper limit for the K_d value of Rf of < 3 which is rather consistent with the data in [40], but not with the value in 0.27 M HF/0.1 M HNO_3 obtained by Pfrepper et al. [38]. In the second experiment, performed in pure 0.01 M HF without any HNO_3, 90 events attributable to ^{253}Es were observed in the strip fraction representing the solid phase and zero events in the liquid phase. This leads to a lower limit for the K_d value on the order of 300 compatible with the one measured with ARCA II in pure 0.01 M HF by Strub et al. [42]. In summary, one can state that the K_d values for Rf obtained with the MCT [39], i.e., low in 0.5 M HF/0.1 M HNO_3 and high, and comparable to that of Hf, in 0.01 M HF, are consistent with the ones determined with ARCA II in [40].

2.2.3 Complex Formation Studies by Ion-Exchange and Reversed-Phase Extraction Chromatography, and by Liquid–Liquid Extraction

Further detailed studies of liquid-phase experiments with good statistics were extensively performed with AIDA at JAEA, Tokai, Japan [2, 43]; see also "Experimental Techniques" for more experimental details. In the following, the systematic studies of Rf using the JAEA tandem accelerator are presented.

78-s ^{261}Rf was produced in the bombardment of ^{248}Cm with ^{18}O beams at 94 MeV with a cross-section of 13 nb [44]. ^{169}Hf with $T_{1/2} = 3.24$ min was simultaneously produced in the Gd(^{18}O,xn) reaction; a mixed target of ^{248}Cm and Gd was used. In the following, the experimental procedures on the anion-exchange behavior of Rf in HCl solution [45] are summarized. Reaction products recoiling from the target were transported by the He(KCl) gas-jet to the collection site of AIDA. The flow scheme of typical chemical separation procedures is represented in Fig. 6. After collection for 125 s, products were dissolved with 170 μL of hot ($\approx$80 °C) 11.5 M HCl and were fed onto the 1.6 mm i.d. × 7.0 mm chromatographic column filled with the anion-exchange resin MCl GEL CA08Y (particle

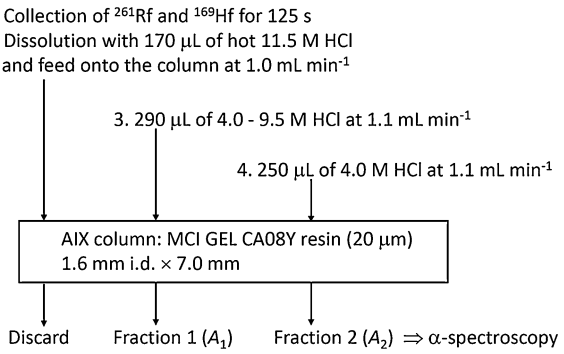

Fig. 6 Flow scheme of the anion-exchange experiment with AIDA

size of about 20 μm) at a flow rate of 1.0 mL min^{-1}. Then, the products were eluted with 290 μL of HCl with concentrations between 4.0 and 9.5 M at a flow rate of 1.1 mL min^{-1}. The effluent was collected on a Ta disk as fraction 1 and, for α-particle measurement, was evaporated to dryness using hot He gas and a halogen heat lamp. The remaining products in the column were eluted with 250 μL of 4.0 M HCl at a flow rate of 1.1 mL min^{-1}. The effluent was collected on another Ta disk and evaporated to dryness as fraction 2. The pair of disks was automatically transported to the α-spectroscopy station equipped with eight 600-mm^2 PIPS detectors. Counting efficiencies of each detector ranged from 30 to 40% depending on geometric differences of the dried α sources. α-particle energy resolution was 80–200 keV FWHM [45]. After the α-particle measurement, the 493 keV γ-radiation of ^{169}Hf was monitored with Ge detectors to determine the elution behavior of Hf and its chemical yield. The anion-exchange experiments with ^{85}Zr and ^{169}Hf, produced from the Ge/Gd mixed target, were conducted under the same conditions as those with ^{261}Rf and ^{169}Hf. The effluents were collected in polyethylene tubes and were assayed by γ-ray spectroscopy [45]. Each separation was accomplished within 20 s and the α-particle measurement was started within 80 s after the collection of the products at the AIDA collection site. The chemical yield of ^{169}Hf, including deposition and dissolution efficiencies of the aerosols, was approximately 60%.

From the 1893 cycles of the anion-exchange experiments, a total of 186 α events from ^{261}Rf and its daughter ^{257}No were registered, including 35 α–α correlation events [45]. Figure 7a shows the adsorption behavior of Rf, Zr, and Hf as a function of HCl concentration. The ordinate shows the adsorption probabilities of these elements, $\%ads = 100A_2/(A_1 + A_2)$, where A_1 and A_2 are the eluted radioactivities observed in fractions 1 and 2, respectively. It should be noted here, that the data of Hf from both targets, Cm/Gd and Gd/Ge, are in very good agreement. The adsorption behavior of Rf is quite similar to those of the group-4 elements Zr and Hf. The adsorption of these elements rapidly increases with increasing HCl concentration above 7 M: typical for the anion-exchange behavior of the group-4 elements. This shows that anionic chloride complexes of the tetravalent Rf, Zr, and Hf are formed above 7 M HCl. On the other hand, the adsorption of the tetravalent pseudo-homolog thorium (Th) in HCl concentrations above 8 M is quite different from that of Rf, Zr, and Hf as shown in Fig. 7b; Th does not form anionic complexes in this region of concentration. The K_d values for Zr, Hf, and Th in Fig. 7b were obtained by a batch method using radiotracers of ^{88}Zr, ^{175}Hf, and ^{234}Th, respectively [45].

An interesting feature is the observed adsorption sequence of Rf followed by Zr and Hf on the anion-exchange resin. This adsorption order reflects the strength of the chloride complex formation as $Rf \geq Zr > Hf$. The present result, however, contradicts the prediction with the relativistic molecular density-functional calculations by Pershina et al. where the sequence of the chloride complex formation is expected to be $Zr > Hf > Rf$ [46]; see "Aqueous Chemistry of the Transactinides".

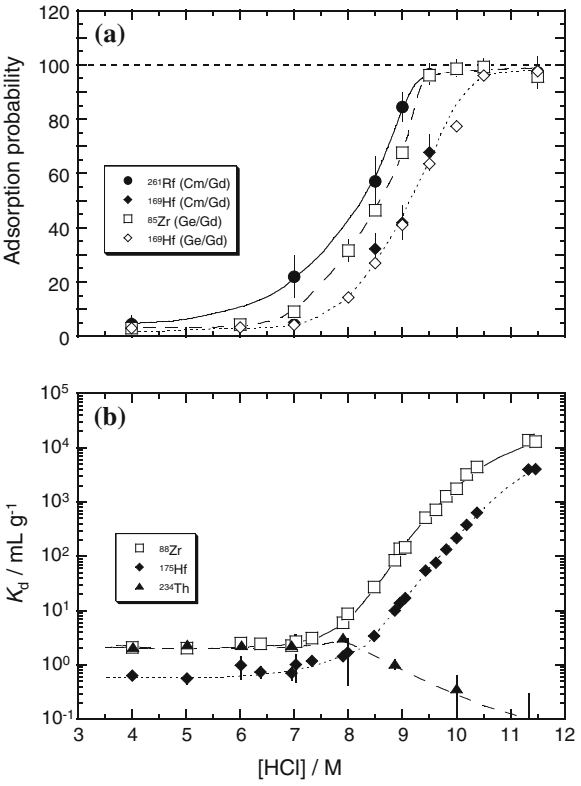

Fig. 7 (**a**) Adsorption probability (%ads) of Rf, Zr, and Hf on the anion-exchange resin CA08Y as a function of HCl concentration. The data for ^{261}Rf and ^{169}Hf obtained from the Cm/Gd target are shown by closed symbols, while those for ^{85}Zr and ^{169}Hf from the Ge/Gd target are by open symbols. (**b**) Distribution coefficients (K_d) for Zr, Hf, and Th on the anion-exchange resin CA08Y as a function of HCl concentration. Adapted from [45]

In order to obtain information on the chemical species and structure of Rf complexes in HCl, measurements of the extended X-ray absorption fine structure (EXAFS) spectra of Zr and Hf chloride complexes were performed at the KEK (High Energy Accelerator Research Organization) Photon Factory [47]. It was found that the Zr and Hf complex structure in HCl solution changes from presumably $[M(H_2O)_8]^{4+}$ (M = Zr and Hf) to the anionic chloride complex $[MCl_6]^{2-}$ with the increase of the HCl concentration from 9 to 12 M. This is consistent with the results of the anion-exchange experiments. Therefore, Haba et al. assume that the structure of the Rf complex, in analogy to those of Zr and Hf, is the octahedral $[RfCl_6]^{2-}$ in conc. HCl. The difference in the strength of the chloride complex formation of Zr and Hf was also demonstrated; the affinity of the Cl^- ion for Zr is higher than that for Hf: $[ZrCl_6]^{2-} > [HfCl_6]^{2-}$ [47], which agrees with the adsorption sequence in Figs. 7a and b and the result by Huffman et al. [48]. This confirms that the sequence in the chloride complex strength among these elements is Rf $\geq$ Zr > Hf.

The non Th^{4+}-like behavior of Rf was also probed with anion-exchange experiments in 8 M HNO_3 [45]. From 217 experiments, a total of 20 α events from ^{261}Rf and ^{257}No were observed including five time-correlated α pairs. Although

Th^{4+} formed anionic complexes and was strongly adsorbed on the anion-exchange resin, Rf was eluted from the column with 8 M HNO_3 as expected for a typical group-4 element and as shown for Zr and Hf in the same series of experiments [45]. The adsorption value for Th was obtained by batch experiments using radiotracer ^{234}Th [45]. The above results definitely confirm that Rf is a member of the group-4 elements, but does not resemble the pseudo-homolog Th.

The extraction behavior of Rf into TBP from hydrochloric acids has also been studied together with those of the lighter group-4 elements Zr and Hf by Haba et al. [49]. The extractability of ^{261}Rf, ^{169}Hf, and ^{85}Zr into TBP was investigated under identical condition in 7.2–8.0 M HCl by reversed-phase extraction chromatography. As shown in Fig. 8, the percent extractions of Rf, Hf, and Zr onto the TBP resin increase steeply with an increase of HCl concentration, and the order of extraction is Zr > Hf ≈ Rf that is in good agreement with the previous work by Günther et al. [36].

The TBP extraction process of the group-4 elements in HCl is expressed by the following chemical equations.

$$\left[M(H_2O)_8\right]^{4+} + 4Cl^- \rightleftarrows MCl_4 + 8H_2O, \quad (5)$$

$$MCl_4 + 2TBP(aq) \rightleftarrows MCl_4(TBP)_2(org). \quad (6)$$

The coordinated H_2O are replaced with Cl^- with an increase of HCl concentration and the formed neutral tetrachloride complex is extracted into the organic phase as $MCl_4(TBP)_2$. Thus, the extractability of the group 4 elements into TBP is expected to depend on the chloride complex formation and on the stability of the TBP

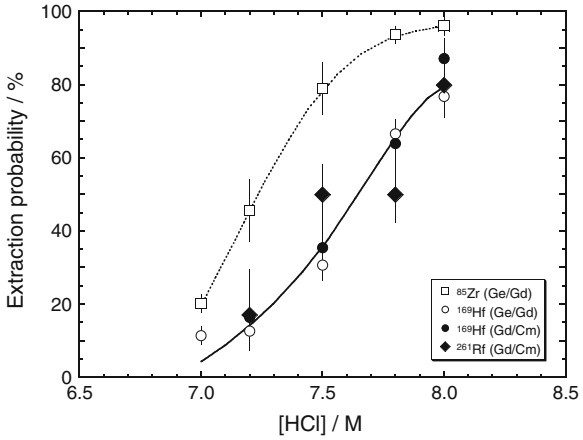

Fig. 8 Percent extractions (%Ext) of Rf, Zr, and Hf on the 20-wt% TBP/CHP20Y resin as a function of HCl concentration. The data for ^{261}Rf and ^{169}Hf obtained from the Cm/Gd target are shown by *closed diamonds* and *closed circles*, respectively, while those for ^{85}Zr and ^{169}Hf from the Ge/Gd target are by *open squares* and *open circles*, respectively. The data for Zr and Hf are connected by a *dotted curve* and a *solid curve*, respectively. Adapted from [49]. Reprinted with permission of Oldenbourg Wissenschaftverlag, München

complex. From the anion-exchange experiments of Rf in 4.0–11.5 M HCl [45] and the detailed structural studies on the Zr and Hf complexes in HCl by the EXAFS spectroscopy [47], it was deduced that Rf forms the same complexes as Zr and Hf: $[Rf(H_2O)_8]^{4+} \rightarrow [RfCl_6]^{2-}$, and that the affinity of Cl^- for these metal ions follows the order of Rf $\geq$ Zr $>$ Hf. This trend would be the same for the formation of MCl_4 as suggested from the smooth variations of the anion-exchange behavior and of the complex structures as a function of HCl concentration [45]. The smaller extractability of Rf in the TBP extraction then would indicate that the stability of the TBP complex of Rf chloride, $RfCl_4(TBP)_2$, is weaker than those of Zr and Hf.

The extraction behavior of Rf into trioctylphosphine oxide (TOPO) from 2.0 to 7.0 M HCl solutions was also investigated together with Zr and Hf [50]. TOPO has a chemical structure similar to that of TBP but it has a higher basicity value as a donor (8.9) than that of TBP (0.16) [51, 52]. The effect of the basicity of the organophosphorus compounds on the stability of the formation of a Rf complex was examined by comparing the extraction sequence of the group-4 elements into TOPO with that into TBP previously studied [49]. The extraction order of the group-4 elements Rf, Zr, and Hf into TOPO was Zr $>$ Hf $\geq$ Rf; the stability of the $RfCl_4 \cdot 2(TOPO)$ complex is lower than those of the corresponding species of Zr and Hf. An effect of the basicity on the formation of the TOPO and TBP complexes was not clearly observed in the extraction sequence among Rf, Zr, and Hf in HCl [50].

Detailed studies of the fluoride complexation of Rf have been extensively performed by Haba et al. [53], Toyoshima et al. [41, 54], and Ishii et al. [55, 56] with AIDA at the JAEA tandem accelerator facility. As the fluoride anion F^- strongly coordinates with metal cations, strong ionic bonds are formed between metal cations and F^-. Thus, information about such as charge density and ionic radii of the metal cations is obtained through the fluoride complex formation process. In addition, the fast reaction kinetics of the fluoride complex formation is an advantage of studying the chemical behavior of short-lived nuclides.

Prior to the on-line experiments with Rf, Haba et al. studied the anion-exchange behavior of the homologs in batch experiments using the radiotracers ^{89}Zr and ^{175}Hf, and with on-line column chromatographic methods applying ^{85}Zr ($T_{1/2} = 7.86$ min) and ^{169}Hf ($T_{1/2} = 3.24$ min), which were produced in the ^{89}Y(p, n) and ^{175}Lu(p, n) reactions, respectively [53]. The K_d values of the homologs on the anion-exchange resin MCI GEL CA08Y (particle size of about 20 μm), obtained by the batch method, are indicated by the dotted line in Fig. 9. It shows the variation of K_d values as a function of the initial concentration of HF, $[HF]_{ini}$. In Fig. 10, elution curves for Zr and Hf by the on-line column experiments are shown as obtained with (a) a 1.6 mm i.d. × 7.0 mm column in 17.4 and 7.7 M HF and with (b) a 1.0 mm i.d. × 3.5 mm column in 9.7 and 5.8 M HF. In these column experiments, Haba and coworkers used two different microcolumns, 1.6 mm i.d. × 7.0 mm and 1.0 mm i.d. × 3.5 mm, to probe a wide range of K_d [53]. According to the Glueckauf equation of chromatography [57], the eluted activity $A(v)$ with the effluent volume v is represented by the following equation:

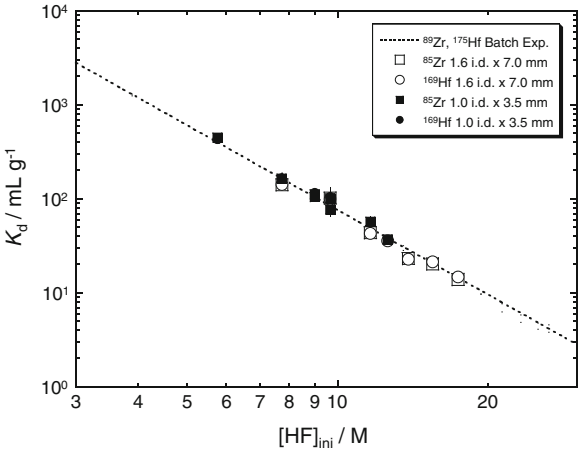

Fig. 9 Variation of the K_d of Zr and Hf on the anion-exchange resin CA08Y obtained in chromatographic experiments as a function of the initial HF concentration. The *dotted line* indicates the results from batch experiments. Adapted from [53]

$$A(v) = A_{max} \exp\left[-\frac{N}{2}\frac{(v_p - v)^2}{v_p v}\right], \tag{7}$$

where the parameters A_{max}, N, and v_p are the maximum peak height, the number of theoretical plates, and the peak volume, respectively. Equation 7 is based on the assumption that the products are adsorbed in a narrow band at the top of the column and the eluting solution makes the band move gradually down the column [57]. This model is applicable to the case where the reaction kinetics is much faster than the elution process. The results of the fit of Eq. 7 are shown as solid or dotted curves in Fig. 10. In the dynamic chromatographic system, the K_d value is expressed as,

$$K_d = \frac{v_p}{m_r}, \tag{8}$$

where m_r is the mass of the dry resin. The variation of the K_d values of Zr and Hf on the anion-exchange resin CA08Y obtained in the chromatographic experiments is plotted by circle and square symbols in Fig. 9 as a function of $[HF]_{ini}$. The K_d values, obtained with the differently sized columns, are consistent with each other. Furthermore, both sets of K_d values obtained by the batch and column experiments agree well with each other, indicating that the chemical reactions reached equilibrium in the column separations.

Then, Haba et al. conducted the Rf fluoride complexing experiments. ^{261}Rf and ^{169}Hf were simultaneously produced in the 94-MeV ^{18}O-induced reactions with a ^{248}Cm/Gd target. Reaction products recoiling from the target were transported by the He(KCl) gas-jet to the collection site of AIDA [53]. The experimental procedures with AIDA were basically the same as those in the chloride formation experiments with Rf; see above and "Experimental Techniques". After collection for 125 s, the products were dissolved with 240 μL HF solution of various

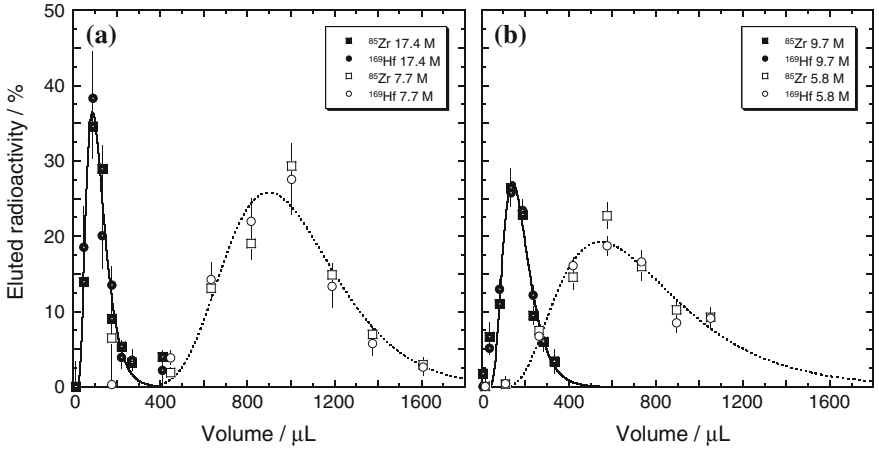

Fig. 10 Elution curves of Zr and Hf from (**a**) 1.6 mm i.d. × 7.0 mm columns in 17.4 and 7.7 M HF and from (**b**) 1.0 mm i.d. × 3.5 mm columns in 9.7 and 5.8 M HF. The *solid* and *dotted curves* are fits by the Glueckauf equation. The number of theoretical plates results as (a) 4.8 ± 0.5 and (b) 4.6 ± 0.5. Adapted from [53]

concentrations (1.9–13.9 M) and were fed onto the chromatographic column filled with the anion-exchange resin MCI GEL CA08Y at a flow rate of 0.74 mL min^{-1}.

From the 4,226 cycles of the anion-exchange experiments, a total of 266 α events from ^{261}Rf and its daughter ^{257}No were registered, including 25 time-correlated α pairs of ^{261}Rf and ^{257}No. Figure 11 depicts the variation of the adsorption probability (%ads) of Rf, Zr, and Hf as a function of $[HF]_{ini}$. The adsorption of Zr is fairly equal to that of Hf over a wide range of HF concentrations and steeply decreases with $[HF]_{ini}$, while that of Rf decreases at much lower $[HF]_{ini}$. The lower adsorption of Rf indicates that the fluoro complex formation of Rf is weaker than those of Zr and Hf. The result is consistent with those reported in [34, 39, 40], where a different behavior of Rf as compared to that of the homologs in the fluoro complex formation was observed.

Although K_d values from column experiments can be evaluated from Eq. 8, it is unrealistic to directly determine the K_d values of Rf from the elusion curves, because of the short half-life and low production yield of ^{261}Rf. Therefore, Haba et al. deduced the K_d values of Rf from the %ads values in the following way, assuming that the kinetics in the complexation and anion-exchange processes of Rf are as fast as those of Zr and Hf and that a single complex anionic species of Rf is involved in the ion-exchange process between the solid and liquid phases [53]. This assumption has subsequently been verified by measuring the elution curve for Rf in 5.4 M HF and by deducing the K_d value according to Eq. 8 by Toyoshima et al. [54] as described in the late part of this section.

The correlations between the %ads values shown in Fig. 11 and the K_d values from Fig. 9 are plotted in Fig. 12 with the same symbols as used in Fig. 11. Solid curves are fits with the free parameters a, b, and c in the equation

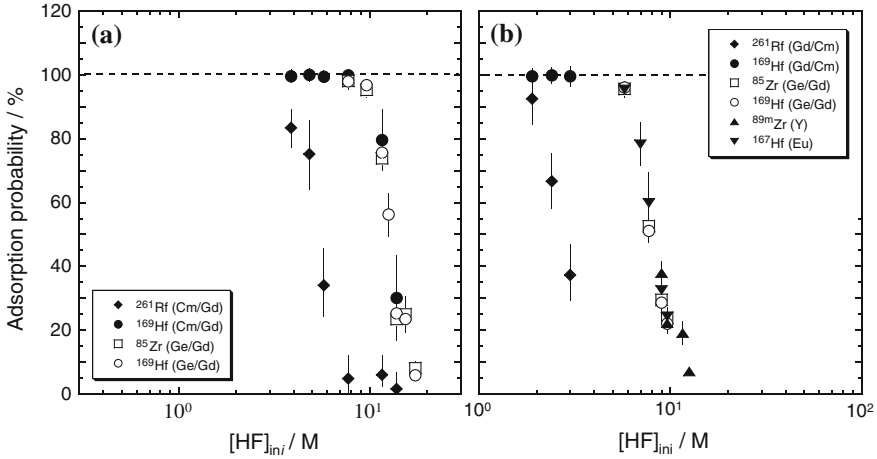

Fig. 11 Adsorption behavior of Rf, Zr, and Hf on the anion-exchange resin CA08Y as a function of the initial HF concentration with (**a**) the 1.6 mm i.d. × 7.0 mm columns and with (**b**) the 1.0 mm i.d. × 3.5 mm columns. Adapted from [53]

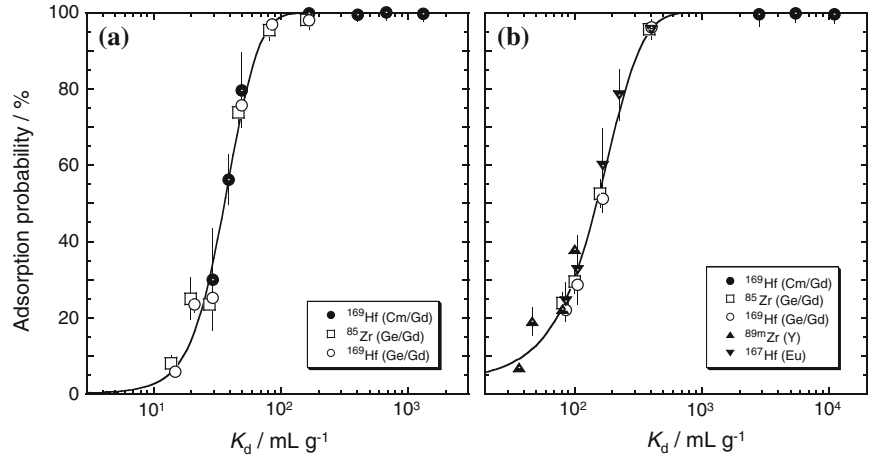

Fig. 12 Variation of the %ads of Zr and Hf on the anion-exchange resin CA08Y with (**a**) the 1.6 mm i.d. × 7.0 mm columns and with (**b**) the 1.0 mm i.d. × 3.5 mm columns as a function of the distribution coefficient K_d. The solid lines are a fit of Eq. 9 to the data [53]. Adapted from [53]

$$\%\text{ads} = 100\exp[-a\exp\{-b(K_d - c)\}]. \tag{9}$$

Thus, %ads of Rf from the dynamic column method with a fixed volume of the effuluent can be transformed into the K_d values. The results are shown in Fig. 13.

Here, the K_d values for Rf, Zr, and Hf in Fig. 13 are plotted as a function of the concentration of HF_2^-, $[HF_2^-]$ [2, 53]. The dissociation of HF is as follows [58],

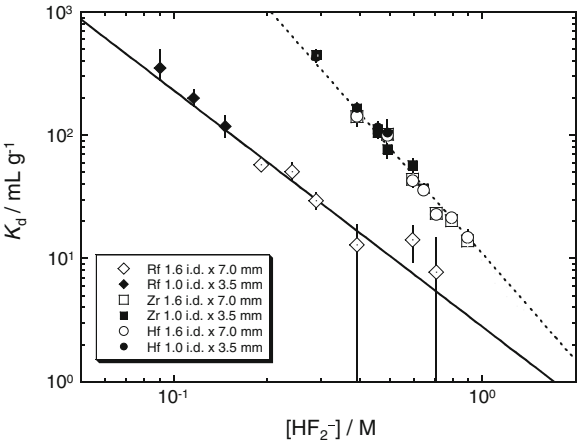

Fig. 13 Distribution coefficients (K_d) for Rf, Zr, and Hf on the anion-exchange resin CA08Y as a function of HF_2^- concentration. The data from the 1.6 mm i.d. × 7.0 mm and 1.0 mm i.d. × 3.5 mm columns are depicted by open and closed symbols, respectively [2, 53]. Adapted from [53]

$$H^+ + F^- \rightleftarrows HF, \tag{10}$$

$$HF + F^- \rightleftarrows HF_2^-. \tag{11}$$

According to the dissociation constants $K_1 = 935\ M^{-1}$ and $K_2 = 3.12\ M^{-1}$ for Eqs. 10 and 11, respectively [58], above 1 M $[HF]_{ini}$, the concentration of the anionic HF_2^- species is more than one order of magnitude higher than that of the free F^-. Thus, the HF_2^- ion acts as a counter anion in the anion-exchange process. As shown in Fig. 13, the K_d values of these elements decrease linearly with $[HF_2^-]$ in the log K_d versus log $[HF_2^-]$ plot. The feature is explained as the displacement of the metal complex from the binding sites of the resin by the counter anion HF_2^- as,

$$R_{n^-}MF_{4+n} + nHF_2^- \rightleftarrows nR{-}HF_2 + MF_{4+n}^{n-}, \tag{12}$$

(M = Rf, Zr, and Hf), where R denotes the resin. It should be noted that the slopes for Zr and Hf are clearly –3 (dashed line), while that for Rf is significantly different, i.e. −2 (solid line). Equation 12 implies then that Rf is likely to be present as the hexafluoro complex, $[RfF_6]^{2-}$, similar to the well-known $[ZrF_6]^{2-}$ and $[HfF_6]^{2-}$ at lower $[HF]_{ini}$, while Zr and Hf are likely to be present in the form of the heptafluoro complexes, $[ZrF_7]^{3-}$ and $[HfF_7]^{3-}$, as suggested in [59, 60]. The activity coefficients of the involved chemical species, however, are not available in the case of the higher concentration of HF. Thus, the definite identification of the anionic fluoro complexes is presently an open question.

Therefore, Toyoshima et al. [41] studied the fluoride complexation of Rf in mixed HF/HNO_3 solutions using dilute HF solution. The anion-exchange behavior of Rf in the concentration ranges of 0.0054–0.74 M HF and of 0.010–0.030 M HNO_3 was investigated in order to clarify the type of anionic fluoro complex of Rf and to evaluate equilibrium constants of its formation reactions. The K_d values were systematically measured as functions of the concentrations of the fluoride ion

(F^-) and of the nitrate ion (NO_3^-). The formation of an anionic fluoro complex of Rf is interpreted in detail by taking into account chemical equilibria of anion-exchange reactions and of formation reactions of fluoro complexes comparing with those of the homologs Zr and Hf. The limit of formation constants for the fluoro complexes of Rf was experimentally evaluated for the first time. Figure 14 shows the variation of the K_d values for Zr, Hf, and Rf in the constant $[F^-]_{eq}$ of 3.0×10^{-3} M as a function of $[NO_3^-]_{eq}$. The K_d values of Zr and Hf obtained in the batch experiments are plotted by open squares and open triangles, respectively. The K_d values of Zr and Hf obtained by Eq. 8 from the on-line column chromatographic experiments are depicted by closed squares and closed triangles, respectively, with the 1.6 mm i.d. $\times$ 7.0 mm column, and by closed diamonds and closed inverted triangles, respectively, with the 1.0 mm i.d. $\times$ 3.5 mm one. The K_d values of Zr and Hf under dynamic conditions are in good agreement with those under the static ones, indicating that all chemical reactions in the studied conditions of the rapid chromatography attained equilibrium. It is found that the K_d values of Zr and Hf are identical with each other and the logarithmic values of K_d linearly decrease with the logarithmic increase of $[NO_3^-]_{eq}$ with a slope of -2.0 ± 0.1; as indicated by the dashed line. The evaluated K_d values of ^{261}Rf are indicated by closed circles and open circles with the 1.6 mm i.d. $\times$ 7.0 mm and 1.0 mm i.d. $\times$ 3.5 mm columns, respectively. The K_d values of Rf are evaluated in the same manner from %ads as mentioned above. As shown in Fig. 14, the K_d values of Rf are much smaller than those of Zr and Hf and they smoothly decrease with an increase of $[NO_3^-]_{eq}$ with the slope of -2.2 ± 0.2; as indicated by the solid line. This feature is interpreted as the displacement of the metal fluoro complex from the binding sites of the resin by the counter anion NO_3^-. The results indicate that, at constant $[F^-]_{eq}$ of 3.0×10^{-3} M, anionic complexes of Rf, Zr, and Hf are present as $[MF_6]^{2-}$ [40].

Figure 15a shows the variation of the K_d values for ^{261}Rf, ^{88}Zr, and ^{175}Hf as a function of $[F^-]_{eq}$. The K_d values of ^{88}Zr under the static conditions at $[NO_3^-]_{eq}$ of

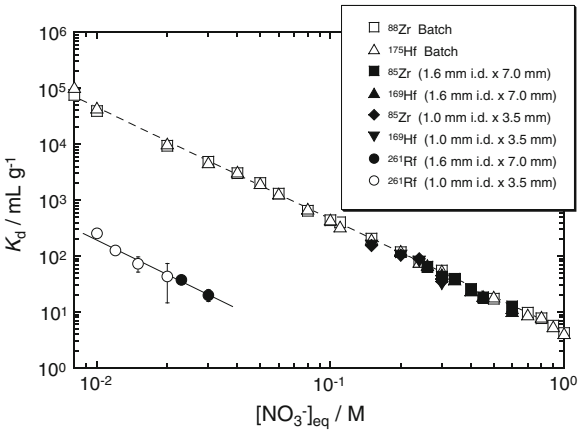

Fig. 14 Distribution coefficients, K_d, of Zr and Hf under static conditions and those of Zr, Hf, and Rf from column chromatography as a function of the equilibrated concentration of NO_3^- ($[NO_3^-]_{eq}$) at fixed $[F^-]_{eq} = 3.0 \times 10^{-3}$ M. Linear relationships of the log K_d versus log $[NO_3^-]_{eq}$ for Rf and the homologs are indicated by the *solid* and *dashed lines*, respectively. Adapted from [41]

0.010, 0.030, 0.10 and 0.30 M are represented by open squares, open diamonds, open squares with diagonal line, and open squares with a cross, respectively, and those of ^{175}Hf are shown by open triangles, open inverted triangles, open left-facing triangles, and open right-facing triangles, respectively. The K_d values for ^{261}Rf at $[NO_3^-]_{eq}$ of 0.01 and 0.015 M are depicted by closed circles and closed squares, respectively. The K_d values of ^{88}Zr and ^{175}Hf are close to each other, and they start to increase at around $[F^-]_{eq} = 1 \times 10^{-5}$ M, gradually reaching constant values between 10^{-4} and 10^{-3} M, and decrease beyond $[F^-]_{eq} = 5 \times 10^{-3}$ M. In contrast to this behavior, the K_d values of Rf increase from 5.0×10^{-4} to 6.0×10^{-3} M, while at $[F^-]_{eq} = 1.3 \times 10^{-2}$ M the K_d value of Rf remains high and is not decreasing as observed for Zr and Hf. In Fig. 15b, the variation of the slopes for Rf, Zr, and Hf in the log K_d versus log $[NO_3^-]_{eq}$ plot is shown by closed circle, open squares and open triangles, respectively, as a function of $[F^-]_{eq}$. The slope for ^{261}Rf is that from Fig. 14. Both the slopes for Zr and Hf are approximately -2 in the $[F^-]_{eq}$ range of 10^{-5}–10^{-2} M. The solid, broken, and dotted curves in Fig. 15a are results of theoretical calculations in which the log K_d is evaluated based on the formation constants K_n ($n = 1 - 6$) in fluoro complex formation and equilibrium constants in the anion-exchange process [41]. From this analysis, it is concluded that the maximum possible value of the formation constant K_6 for Rf is at least one order of magnitude smaller than those for Zr and Hf. Under the assumption that the equilibrium constant of the exchange reaction of $[MF_6]^{2-}$ with the anion-exchange resin is equal for Rf, Zr, and Hf, a K_6 value for Rf results that is approximately three orders of magnitude smaller than those of the lighter homologs. This clearly demonstrates that the formation of the hexafluoro complex of Rf is much weaker than those of the homologs Zr and Hf [41].

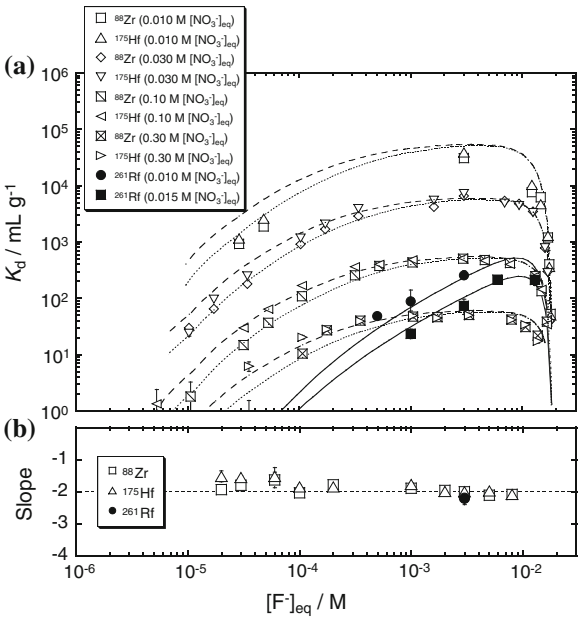

Fig. 15 (**a**) Variation of the K_d values of Zr and Hf under static conditions and of Rf in column chromatography as a function of the equilibrated concentration of F^- ($[F^-]_{eq}$). Values for Zr and Hf are shown for $[NO_3^-]_{eq} = 0.01$, 0.03, 0.1, and 0.3 M, while those for Rf are shown for $[NO_3^-]_{eq} = 0.01$ and 0.015 M. The *solid*, *broken*, and *dotted curves* are theoretical calculations of K_d values. (**b**) Variation of the slopes in the log K_d versus log $[NO_3^-]_{eq}$ plot as a function of $[F^-]_{eq}$. Adapted from [41]

Again, the much weaker complexation of Rf by the fluoride ion is apparent compared to that of its homologs. A qualitative explanation comes from the Hard Soft Acid Base (HSAB) concept [61, 62]. The small fluoride anions are hard donors and prefer the smaller acceptor ions Zr^{4+} and Hf^{4+}. The much larger (softer) Rf acceptor ion tends to prefer larger (softer, more polarizable) donor ligand ions like Cl^-; see [45] and "Hydrolysis and Complex Formation" for a theoretical discussion of fluoride complexation.

The cation-exchange behavior of Rf together with its lighter group 4 homologs Zr and Hf, and the tetravalent pseudo-homolog Th, in HF/HNO_3 mixed solution has been thoroughly studied [55, 56]. The results confirm those from the previous investigation by Strub et al. [40] and from the anion-exchange studies mentioned above. These results demonstrate that the K_d of Rf in HF/0.10 M HNO_3 decreases with increasing concentration of the fluoride ion [F^-]; as shown in Fig. 16. This resembles the behavior of the homologs, indicating the consecutive formation of fluoro complexes of Rf. The K_d values of Rf and the homologs have been also measured as a function of the hydrogen ion concentration [H^+] in the range of [F^-] = 5.29×10^{-7} to 3.17×10^{-6} M. The log K_d values decrease linearly with an increase of log [H^+] with slopes between −2.1 and −2.5. This indicates that these elements are likely to form the same chemical compounds: a mixture of $[MF]^{3+}$ and $[MF_2]^{2+}$ (M = Rf, Zr, Hf and Th) in the studied solution [56]. It is also ascertained that the fluoro complex formation of Rf is significantly weaker than that of Zr and Hf, but it is stronger than that of Th. The adsorption strength on the cation-exchange resin is Zr ≤ Hf < Rf < Th, at a given [F^-] [55, 56].

The observed K_d sequence of Zr ≤ Hf < Rf among the group-4 complexes is in full agreement with that predicted theoretically in [46]. Here, free energy changes of the complex formation reactions were determined on the basis of fully relativistic density functional theory calculations of various hydrated and hydrolyzed fluoro complexes of Zr, Hf, and Rf (see "Hydrolysis and Complex Formation"). It

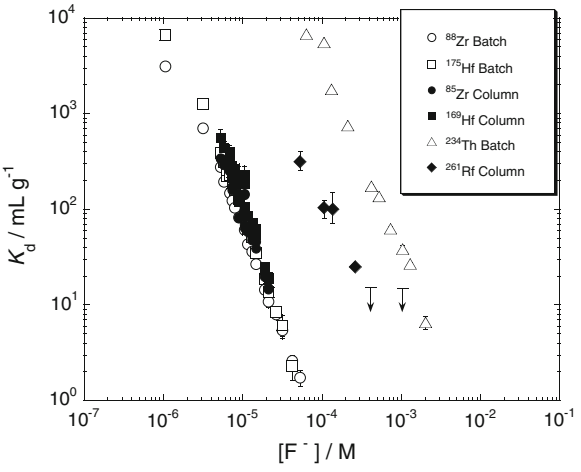

Fig. 16 Variation of the K_d values of Rf, Zr, Hf, and Th on the cation-exchange resin CK08Y in 0.10 M HNO_3 depending on [F^-]. Open symbols indicate data obtained in batch experiments, while solid ones show those from column separation [55, 56]. Adapted from [56]

was shown that at lower HF concentrations and 0.1 M HNO_3, the complex formation occurs preferentially from the hydrolyzed species. The strengths of the formed complexes are predicted as Zr ≥ Hf > Rf. This causes the following trend in the K_d values: Zr ≤ Hf < Rf.

It was also shown in [46] that the electrostatic interaction plays a dominant role in the energies of the complex formation, though it should be determined on the basis of the real electronic density distribution obtained as a result of fully relativistic calculations. Due to a predominant electrostatic interaction, a correlation between crystallographic ionic radii (IR) [63] and the strengths of the formed complexes appears quite natural. IR of the group-4 elements with the coordination number of 6 are [63]: Zr (72 pm) ≈ Hf (71 pm) < Rf (76 pm) [64] ≪ Th (94 pm). In this particular case, this nicely correlates with the sequence in the complex formation Zr ≈ Hf > Rf > Th. Thus, in agreement with the theory, it is shown experimentally that the formation of the positively charged fluoro complexes of Rf is weaker than that of Zr and Hf and stronger than that of Th. The experimentally obtained sequence of the fluoride complexation correlates with the inverse order of the ionic radii. This can be explained on the basis of a predominant electrostatic interaction of the tetravalent group-4 elements and the pseudo group-4 element Th with the fluoride ion F^-. The present result is in agreement with theoretical calculations showing that the ionic radius of Rf^{4+} is in between those of Zr^{4+}/Hf^{4+} and Th^{4+}. Schumann et al. [65] studied the adsorption behavior of Rf on the cation-exchange resin Dowex 50 × 8 from HCl/HF solution, and reported that the sequence of decreasing stability is Zr > Hf ≫ Rf > Th. This result is consistent with one reported in [55, 56].

Recently, Li et al. [66] investigated the sulfate complexation of Rf through cation-exchange chromatography in 0.15−0.69 M H_2SO_4/HNO_3 mixed solutions ($[H^+] = 1.0$ M). The sulfate ion SO_4^{2-} is a strong complexing ligand for group 4 elements. Its strength to form complexes with Zr and Hf is intermediate between

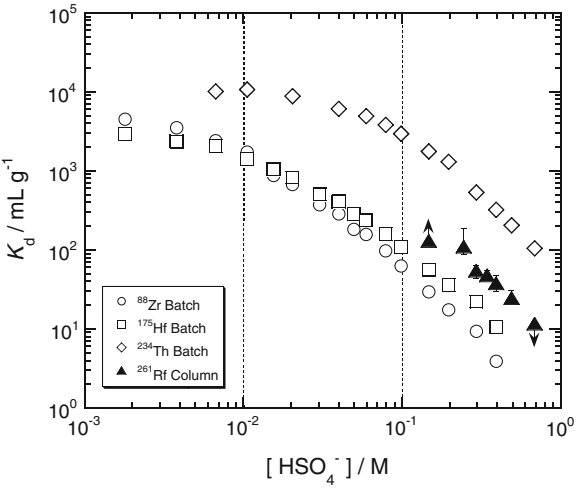

Fig. 17 Variation of K_d of ^{261}Rf on cation-exchange resin derived from its adsorption probabilities as a function of [HSO_4^-] in 0.0018 − 0.69 M H_2SO_4/HNO_3 mixed solutions ($[H^+] = 1.0$ M), together with those of ^{88}Zr, ^{175}Hf, and ^{234}Th obtained in batch experiments. The *arrow*-attached data represent upper or lower limits. Adapted from [66]

those of F^- and Cl^- ions, i.e., $F^- > SO_4^{2-} \gg Cl^- \geq NO_3^-$ [67]. Therefore, it is of great interest to investigate the sulfate complex formation of Rf to clarify whether it is similar to or significantly different from those of the lighter homologs Zr and Hf. Figure 17 clearly shows that the K_d values of ^{261}Rf on the cation-exchange resin decrease with an increase of $[HSO_4^-]$. This indicates a successive formation of Rf sulfate complexes. Despite of some open questions concerning the kinetics in this experiment [66], it demonstrates that Rf has a much weaker tendency to form sulfate complexes than Zr and Hf. Experimental results are in good agreement with theoretical predictions based on relativistic electronic structure density functional theory calculations [68]. According to these predictions, Rf should have a much weaker preference for complex formation than Zr and Hf at the entire range of acid concentrations. This is due to the fact that hydrated, hydrolyzed, and sulfate complexes of Rf are less stable than those of the lighter homologs, which is seen from the calculated free energy changes of complex formation reactions. Theoretical calculations show that the lower stability of the Rf complexes is due to the smaller ionic contribution to the chemical bond. This is caused by the relativistic stabilization of the 7s orbital, as well as the destabilization and spin–orbit splitting of the 6d orbitals. It is also in agreement with the larger ionic radius of Rf (76 pm) [64] in comparison with those of Zr (71 pm) and Hf (72 pm) [63].

The first observation of an elution curve for Rf in anion-exchange chromatography with 5.4 M HF on an atom-at-a-time basis is presented in the following. The K_d value for Rf has been directly determined from the peak volume of the elution curve [54]. In this study, AIDA has been slightly modified to collect consecutively four effluent fractions [54]. Reaction products transported by the He(KCl) gas-jet were deposited on the collection site of AIDA. After collection for 182 s, this site was mechanically moved on the top of microcolumns filled with the anion-exchange resin, MCI GEL CA08Y (particle size of about 20 μm). The collected products were dissolved in 5.4 M HF and were fed onto a 1.6 mm i.d. × 7 mm long chromatographic column at a flow rate of 0.8 mL min^{-1}. The effluent, with volumes of 170, 130, and 130 μL, was consecutively collected on three separate Ta disks labeled as fraction 1, 2, and 3, respectively. Then, the remaining products in the column were eluted with 260 μL of 4.0 M HCl at a flow rate of 1.4 mL min^{-1}. The effluent was collected on another Ta disk as fraction 4. Each fraction was evaporated to dryness using hot He gas and halogen heat lamps. These four Ta disks were in turn automatically subjected to α-spectroscopy with eight 600-mm^2 PIPS detectors. After the α-particle measurement, the γ-radiation of ^{169}Hf was measured with Ge detectors for every third or fourth set of samples to monitor the elution behavior of Hf and its chemical yield.

In Fig. 18, the eluted yields of ^{261}Rf and ^{169}Hf are plotted by solid circles and solid diamonds, respectively, as a function of the half volume of each effluent fraction. In addition, the cumulative yields of ^{261}Rf and ^{169}Hf are indicated by open circles and open squares, respectively, against the total volume of each effluent. The peak volume of the elution curve for ^{261}Rf is observed at around 200 μL, while ^{169}Hf is mostly eluted in the fourth fraction. This shows that the K_d

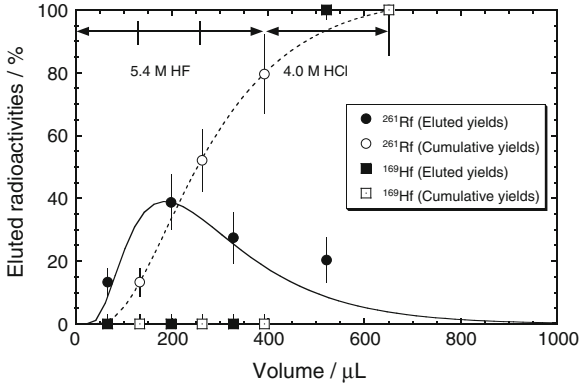

Fig. 18 Elution behavior of ^{261}Rf and ^{169}Hf with 5.4 M HF. The data for ^{261}Rf and ^{169}Hf are indicated by *circles* and *squares*, respectively. The open symbols show the cumulative yield data. The dotted line shows the integrated curve by the Glueckauf equationg [57] to fit the experimental cumulative yields of ^{261}Rf, and the solid line indicates the differential one associated with the differential yields. Adapted from [54]

value for Rf is much smaller than that for Hf. The result is consistent with the already mentioned result [41, 53], i.e., the adsorption of Rf is significantly weaker than those of Zr and Hf at the same concentration of HF.

The elution curve of ^{261}Rf is analyzed by the Glueckauf equation [57]. The dashed line shows the integrated curve of Eq. 7 to fit the experimental cumulative yields of ^{261}Rf except for the value of the fourth fraction (elution with 4.0 M HCl) using $v_p = 186 \pm 35$ μL and $N = 2.6 \pm 1.5$. The solid line is the differential curve of the dashed line, indicating that the elution data, fractions 1–3, are well reproduced by the Glueckauf formula [57]. The K_d value for Rf in anion-exchange chromatography with 5.4 M HF obtained by Eq. 8 has been determined to be 28 ± 6 mLg^{-1} with $m_r = 6.6 \pm 0.3$ mg. The present K_d value is in good agreement with that evaluated from the assumption mentioned previously. This demonstrates that the prescription used in [53] to evaluate the K_d value from the adsorption probability can be reasonably well applied to the fluoride complexation process.

The SISAK system was applied to perform continuous liquid–liquid extraction and detection of short-lived Rf using small-volume centrifuges and a liquid-scintillation detection system; see also "Experimental Techniques". SISAK, employed to extract 4-s ^{257}Rf produced in the ^{208}Pb(^{50}Ti,n) reaction, was coupled to the kinematic recoil separator BGS (Berkeley Gas-filled Separator) at the LBNL 88-inch Cyclotron [4, 69]. Recoiling ^{257}Rf, pre-separated from the primary beam and nuclear reaction by-products, was thermalized in a stopping-gas cell termed Recoil Transfer Chamber (RTC) and was transferred to SISAK through the He(KCl) gas-jet system. Figure 19 shows a schematic diagram of the SISAK set-up. Products delivered to the apparatus with the aerosol gas-jet are mixed with 6 M HNO_3 to dissolve the aerosol-laden products, and the carrier gas is removed in a

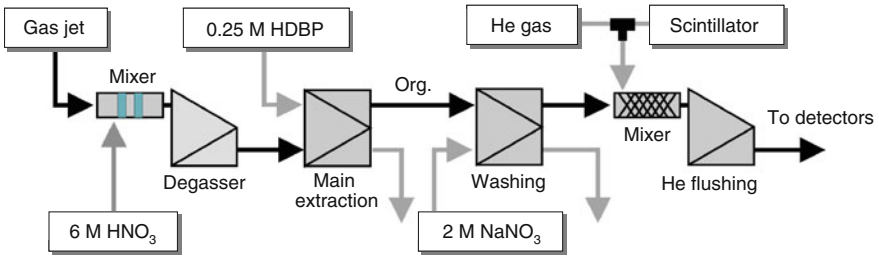

Fig. 19 Schematic diagram of the SISAK liquid–liquid extraction system. Adapted from [4]

degasser centrifuge. The aqueous solution is mixed with an organic solvent, 0.25 M dibutyl-phosphoric acid (HDBP) in toluene. Here Rf is extracted as a Rf nitrate-HDBP compound into the organic toluene. Then the organic phase is washed with 2 M $NaNO_3$ to remove acidic solution. A scintillation cocktail containing the mixture of the organic solvent and the scintillator ingredients is then fed to a detector system to perform liquid scintillation α-spectroscopy for the flowing cocktail. The extraction behavior of Rf was similar to that of the homologs Zr and Hf [4].

The above pilot experiment demonstrated that the SISAK system in combination with liquid scintillation detectors can be used for the investigation of chemical properties of superheavy elements.

3 Dubnium (Db, Element 105)

3.1 First Survey Experiments

First studies of the liquid-phase chemistry of element 105, dubnium (Db), were conducted manually in 1987 by Gregorich et al. [70]. The isotope 34-s ^{262}Db, produced in the ^{249}Bk(^{18}O,5n) reaction [71, 72] at around the bombarding energy of 100 MeV with a cross-section of a few nb, was used. As it is known that group-5 elements adsorb on glass surfaces from strong nitric acid [73], the following adsorption experiment was carried out; the radionuclide bearing aerosols from the He(KCl) gas-jet was collected on a glass plate. At the end of the 60 s collection time, the glass plate was removed from the collection site and was placed on a hot plate. The potassium chloride spot on the glass plate was fumed with 3 μL of 15 M HNO_3. After this nitric acid dried, a second fuming was performed with 7 μL of 15 M HNO_3. When the second drop of nitric acid had dried, the potassium nitrate and the actinide nuclides on the glass plate were removed by washing the plate with 1.5 M HNO_3 from a squirt bottle. Any remaining dilute nitric acid was removed by washing the glass plate with acetone from a second squirt bottle. The glass plate was immediately dried in a stream of hot air from an electric 'heat gun' and placed over one of the Si(Au) surface barrier detectors. The average time from

the end of accumulating the aerosol on a glass plate to the beginning of counting for α and spontaneous fission (SF) decays was 51 s.

In the above experiments, 801 adsorption cycles were performed. The separation from actinides was very successful. The decay rates of $^{252–255}$Fm indicated that only 0.25% of the Fm radioactivities remained on the glass. A total of 26 α events in the energy range from 8.42 to 8.70 MeV were observed during the first 140 s of counting (∼4 half-lives of ^{262}Db). By looking at the time distribution of α events in this energy range out to 500 s, it was estimated that the time interval from 0 to 140 s contained ∼2 background events from longer lived nuclides, leaving ∼24 α events due to the decay of ^{262}Db or its daughter ^{258}Lr. A spectrum containing the α-decay data from the first 30 s of counting for all 801 samples is

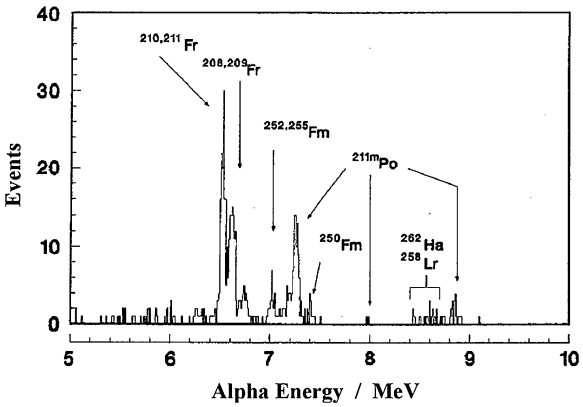

Fig. 20 A summed spectrum containing all of the α-decay data from the first 30 s of counting from the 801 experiments involving the adsorption of ^{262}Db on glass from concentrated nitric acid solution [70]. Reprinted with permission of Oldenbourg Wissenschaftverlag, München

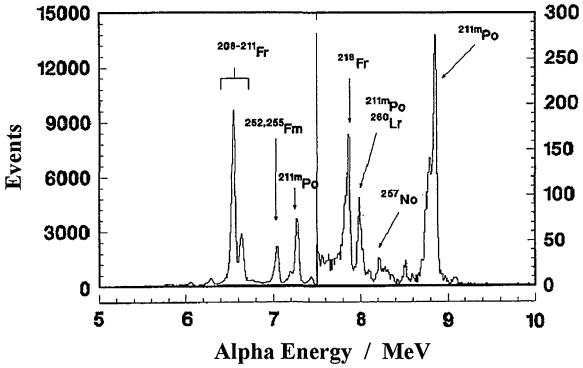

Fig. 21 A representative spectrum of the unseparated product mixture in the 101-MeV ^{18}O bombardment of ^{249}Bk taken on a rotating wheel system. These data were recorded over a 20 s time interval starting 60 s after the end of collection. One should note the change of vertical scale at the center of the spectrum [70]. Reprinted with permission of Oldenbourg Wissenschaftverlag, München

Table 1 α-α parent–daughter correlations in [70]

#	Parent energy (keV)	Parent time[a] (s)	Daughter energy (keV)	Daughter time since parent (s)
1	8640	10.03	8752	4.45
2	8533	131.87	8636	0.08
3	8681	10.82	8661	3.40
4	8437	4.12	8603	2.02
5	8681	2.55	8611	7.88

[a] Time from the beginning of counting to the α event

presented in Fig. 20. For comparison, a summed spectrum of unseparated products from this reaction, taken with a rotating wheel system for a 20 s interval starting 60 s after the end of collection of aerosols, is presented in Fig. 21. It appears that in Fig. 20 there is little fractionation between the Fr-Po radioactivities, which are produced by interaction of the ^{18}O beam with a small Pb impurity in the target, and the Fm radioactivities. There is, however, a large relative enhancement of the radioactivities due to ^{262}Db and its daughter, ^{258}Lr, in the adsorption experiments. Figures 20 and 21 demonstrate that insufficient decontamination from Po can seriously hamper the detection of transactinides.

The 26 α events in Fig. 20 attributed to ^{262}Db and ^{258}Lr contain 5 time-correlated mother–daughter pairs, as indicated in Table 1, as well as ∼14 uncorrelated events and ∼2 background events. A maximum likelihood fit to the half-life of the 16 α singles events, which occurred at times shorter than 140 s from the beginning of counting, together with the 5 parent events of the mother–daughter correlations gives a half-life of 28^{+7}_{-5} s, consistent with the accepted ^{262}Db half-life of 34 s. From detector geometry of 30% of 4π, one would expect the ratio of correlated pairs to uncorrelated events to be 0.214. The measured ratio of 0.36 is within the one sigma uncertainty of 0.18 consistent with the expected ratio. A maximum likelihood fit to the ^{258}Lr half-life based on the time intervals between parent and daughter events gives $2.5^{+1.9}_{-1.0}$ s, which is also in agreement with the accepted value of 4.3 ± 0.5 s.

In the adsorption experiments, Gregorich et al. also observed 26 SF decays in the first 140 s of which 23 were assigned to the decay of ^{262}Db giving a half-life of 32^{+8}_{-6} s, again consistent with the known 34 s half-life. From this, an α-decay branch of 51 ± 14% was deduced for ^{262}Db, with the remainder of the decay being either by SF or by electron capture to ^{262}Rf, which then decays by SF. An overall production cross-section of 3.2 ± 0.5 nb was calculated based on an estimated adsorption yield of 80%. In view of a more recent determination of that cross-section [74], it appears that the adsorption yield was probably overestimated by about a factor of 2.

The other chemical separation attempted in [70] involved the extraction of anionic fluoride species into methyl isobutyl ketone (MIBK). The extraction system with 3.8 M HNO_3 and 1.1 M HF as the aqueous phase, and MIBK as the organic phase was chosen, because MIBK had been found to be an ideal solvent for the rapid preparation of α sources by evaporation. Under these conditions, Ta was extracted into MIBK nearly quantitatively, while Nb was extracted to only a

small extent. It was expected that this trend would continue and Db would be extracted quantitatively.

In these experiments, the radionuclide-bearing aerosols were collected for 90 s on Pt foils. The KCl and the nuclides were dissolved in 20 μL of 3.8 M HNO_3/1.1 M HF. This solution was then placed in a centrifuge cone containing 20 μL of MIBK. The phases were mixed ultrasonically for 2 s and separated in a centrifuge within 4 s. After centrifuging, the MIBK upper phase was pipetted onto a Ni disk that was heated from the edge. After drying, the Ni disk was placed over one of the Si(Au) surface barrier detectors. The average time from the end of the aerosol collection to the start of α and SF counting was 50 s. In tests, performed with ^{172}Ta, the chemical yield was found to be 75%.

In the Db experiments, 335 extractions were performed. No α particles in the energy range of 8.4–8.7 MeV nor any fission were observed within the first 2 min of counting, demonstrating conclusively that, under these conditions, Db is not behaving chemically like its lighter homolog Ta. The nonTa-like behavior of Db might indicate that Db forms polynegative anions like $[DbF_7]^{2-}$ under the chosen conditions. The higher charge would then prevent extraction even into solvents with a relatively high dielectric constant such as MIBK.

3.2 Detailed Studies

3.2.1 Extraction Chromatographic Studies in Mixed Halide Solutions

While polynegative species cannot be extracted into ketones, it is possible to extract them by anion exchange into high molecular-weight ammonium salts. Amine extractions have another advantage for chemical studies of species that are produced as single atoms such as ^{262}Db, so that their chemical behavior must be studied "one-atom-at-a time". Due to their high viscosity, high molecular-weight ammonium salts are best suited as a stationary phase on inert column support materials for High Performance Liquid Chromatography (HPLC). Then the principle of chromatography can be applied to single atoms or ions, and the many adsorption–desorption cycles along the column in the elution of that ion ensure a statistical behavior, so that one can be reasonably certain that the observation represents the 'true' chemistry of the element. Thus, in 1988 Kratz et al. [75] brought their ARCA II equipment [1] (see "Experimental Techniques") to the Berkeley 88-Inch Cyclotron facility to perform a large number of automated reversed-phase extraction chromatography separations with the 1.6 mm i.d. × 8 mm long columns filled with tri-iso-octyl amine (TiOA) on an inert support (Voltalef^{TM}, 32–63 μm, weight ratio 1:5).

The performance of ARCA II was studied with radiotracers of Zr, Nb, Hf, Ta, Pa, and some lanthanides produced on line, and transported to ARCA II with the He(KCl) gas-jet system. To this end, the effluents from the TiOA columns were collected in fractions of three drops in small test tubes and were assayed for γ-ray

spectrometry with two Ge detectors. In agreement with earlier radiotracer studies, chemical yields for Nb, Ta, and Pa were consistently found to be 85 ± 5%.

In the beginning of the ^{262}Db experiments, it was most important to verify that the dubnium halide complexes would be extracted into the TiOA phase under the same conditions as Nb, Ta, and the pseudo-homolog penta-valent Pa, which were known to be extracted either from 12 M HCl/0.02 M HF or from 10 M HCl. ^{262}Db was produced in the ^{249}Bk(^{18}O,5n) reaction at 99 MeV with beam currents of 0.4–0.5 particle microamperes. Its extraction was verified by feeding the

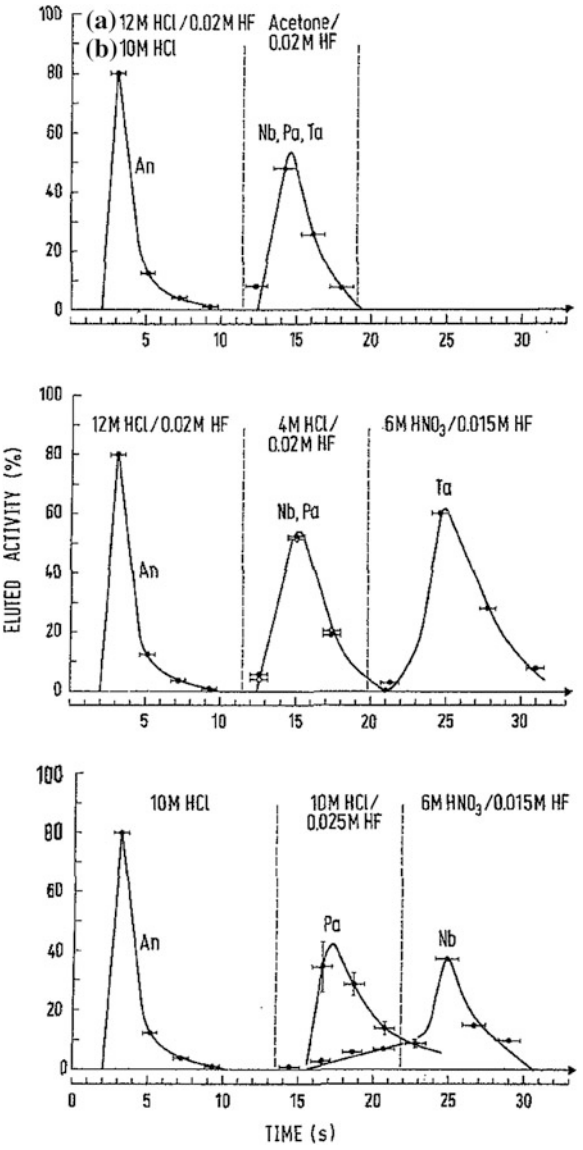

Fig. 22 Elution curves for carrier-free actinides (An), Nb, Ta, and Pa from TiOA/ Voltalef^{TM} columns (1.6 mm i.d. × 8 mm) under the same conditions as in the Db experiments. The horizontal error *bars* are associated with uncertainties in converting drop numbers into effluent volumes, i.e., times. In the upper part, the ^{262}Db is adsorbed on the column from (**a**) 12 M HCl/0.02 M HF, (**b**) 10 M HCl, and is stripped along with the TiOA from the column in acetone/0.02 M HF. In the middle part, the nuclide is extracted as in (**a**), followed by separate elutions of a Nb/Pa fraction, and a Ta fraction. In the lower part, the nuclide is extracted as in (**b**), followed by a Pa, and then a Nb fraction [75]. Reprinted with permission of Oldenbourg Wissenschaftverlag, München

radionuclides to the columns, and by stripping the amine (along with the extracted nuclides) from the columns by dissolving the TiOA in acetone. The acetone strip fraction was evaporated to dryness, and an assay of the samples for α-particle and SF decay started about 45 s after the end of the 60 s collection time. Elution curves for actinides (An), Nb, Ta, and Pa under the same conditions, with carrier-free radionuclides produced online, are shown in the top section of Fig. 22. In a first series of 207 experiments, extraction into the column material occurred from 12 M HCl/0.02 M HF, and 9 α-decay events of ^{262}Db/^{258}Lr including 1 correlated pair, and 12 SF decays were recorded, indicating that ^{262}Db forms anionic complexes that are extracted into TiOA. Small amounts of HF (typically 0.02 M) were added to the HCl solutions. This is suggested in the literature by Korkisch [60] to prevent hydrolysis and to maintain a reproducible solution chemistry of the group 5 elements.

In a second series of 133 experiments, extraction into the amine phase occurred from 10 M HCl. This time, two ^{262}Db/^{258}Lr α events and four SF decays were detected in the acetone strip fraction. This demonstrates that Db behaves similar to Nb, Ta, and Pa also in 10 M HCl. In the next series of 721 collection and separation cycles, the nuclides were adsorbed from 12 M HCl/0.02 M HF on the TiOA column as before, a fraction of Nb/Pa was removed from the column with 4 M HCl/0.02 M HF, followed by the stripping of Ta from the column with 6 M HNO_3/0.015 M HF, as shown in the middle part of Fig. 22. On the average, there was a tailing of about 10% of the Nb/Pa radioactivity into the Ta fraction. Eighty-eight percent of the ^{262}Db/^{258}Lr α-decay events (38 events including 4 α–α correlations) were found in the Nb/Pa fraction, and 12% (5 events, with no correlated pair) in the Ta fraction. This distribution is identical with that of Nb and Pa, and distinctly different from that of Ta. This shows, in contrast to simple extrapolations, that the trend in the chemical properties in group 5 from Nb to Ta does not continue, but is reversed in going from Ta to Db. The distribution of SF decays between the Nb/Pa fraction (39) and the Ta fraction (10) corroborates the above finding.

In a last series of 536 experiments, a separation of Pa from Nb was performed (see the bottom part of Fig. 22). After feeding of the radionuclides in 10 M HCl onto the column, Pa was eluted first with 10 M HCl/0.025 M HF. Under these conditions, a fraction of the Nb radioactivity begins to break through. The change of the eluent to 6 M HNO_3/0.015 M HF was timed such that the Pa fraction contained 80% of Pa and 20% of Nb, while the Nb fraction contained the remaining 20% of Pa and 80% of Nb. The ^{262}Db decays were equally divided between the Pa and Nb fractions; there were 25 α events, including 5 correlated pairs, in the Pa fraction, and 27 α events, including 5 correlated pairs, in the Nb fraction. The Pa/Nb ratio of SF decays was 25:19. These results indicate that the halide complexing strength of dubnium is between that for Nb and Pa.

The half-lives deduced from the 106 α singles, 15 α–α correlations and 109 SF decays were all compatible with the 34 s half-life of ^{262}Db and the 4.3-s half-life of ^{258}Lr. The total production cross-section of ^{262}Db at 99 MeV was 8.3 ± 2.4 nb.

In the discussion of these rather unexpected chemical results [75], it was suggested that the chemical properties of the heaviest elements cannot reliably be

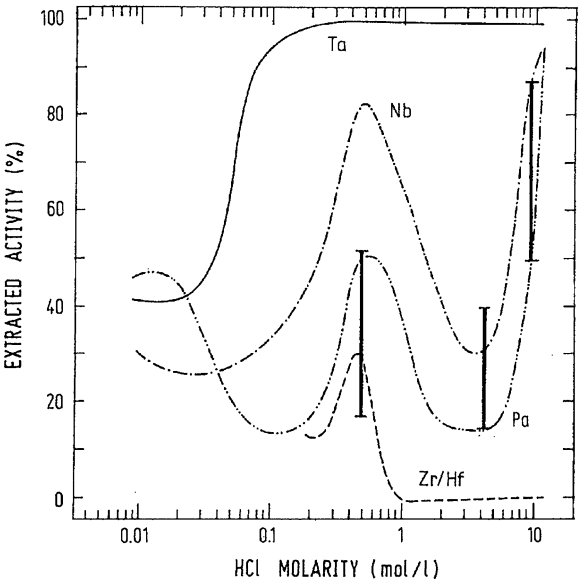

Fig. 23 Fractional extraction, %p, of Nb, Ta, Pa, and Zr/Hf versus. HCl molarity in the system TiOA-HCl/HF. The *bold bars* encompass the upper and lower limits of %p deduced from the Db elution positions. The bar for the extraction of Db from 12 M HCl/0.02 M HF is not included in the figure for clarity. The figure suggests that the element with the unusual behavior is Ta [76]. Reprinted with permission of Oldenbourg Wissenschaftverlag, München

predicted by simple extrapolations of trends within a group of elements, and that relativistic quantum chemical calculations for compounds of Nb, Ta, Pa, and Db are needed to understand in detail the differences in the halide complexing of the group-5 elements.

The TiOA column experiments were continued [75] by feeding the nuclides onto the columns in 12 M HCl/0.01 M HF and eluting a Pa fraction in 0.5 M HCl/0.01 M HF, followed by elution of a Nb fraction in 4 M HCl/0.02 M HF. It was found that ^{262}Db elutes earlier than the bulk of the Nb nuclide, i.e., Db shows a more Pa-like behavior. From the distribution of the ^{262}Db events between fractions 2 and 3 in [75, 76], K_d values or the fractional extraction (%) of ^{262}Db were estimated for 10 M HCl/0.025 M HF and 4 M HCl/0.01 M HF, and for the newly investigated 0.5 M HCl/0.01 M HF. The results are shown in Fig. 23.

It is seen that Db shows a striking non Ta-like behavior and that it follows, at all HCl concentrations below 12 M, the behavior of its lighter homolog Nb and that of its pseudo-homolog Pa. From this similarity, it was concluded that the complex structure of Db would be $[DbOCl_4]^-$ or $[Db(OH)_2Cl_4]^-$ as known for Nb and Pa, and the preferential formation of oxygen containing complexes of Db was also predicted theoretically [77]. The extraction sequence Pa > Db > Nb in [77] was, however, predicted by theory (see "Aqueous Chemistry of the Transactinides"), which is the inverse sequence of that observed experimentally, see Fig. 23. Due to the complicated situation in mixed HCl/HF solutions, with possibilities to form mixed chloride/fluoride complexes or even pure fluoride complexes, it was recommended in [77] to repeat the experiments in the pure HCl system.

The proximity in the Db behavior in the TiOA experiments to that of Pa was the reason for performing a series of extractions of Db into diisobutyl carbinol

(DIBC), a secondary alcohol which is a very specific extractant for Pa. The extraction from concentrated HBr solution in ARCA II was followed by the elution of a Nb fraction in 6 M HCl/0.0002 M HF, and of a Pa fraction in 0.5 M HCl. The number of ^{262}Db decays observed in the Nb fraction indicated that less than 45% of the Db was extracted into DIBC, and the extraction sequence Db < Nb < Pa was established by Gober et al. [78]. This was tentatively attributed to an increasing tendency of these elements to form nonextractable polynegative complex species in the sequence, Pa < Nb < Db.

3.2.2 Extraction Chromatographic Studies in pure Halide Solutions

As suggested by Pershina et al. [77], the amine extractions of the group-5 elements were systematically revisited by Paulus et al. [79] in pure HF, HCl, and HBr solutions. Pershina [80–82], by considering the competition between hydrolysis and halide complex formation (see Sect. 7), predicted the extraction sequence Pa $\gg$ Nb $\geq$ Db > Ta in the pure chloride system. She also predicted the extraction sequence fluorides $\gg$ chlorides > bromides for the halide complexes of the group-5 elements [82]. For tracer nuclides of Pa, Nb, and Ta, these predictions were verified experimentally for a number of amines in batch extractions [79, 83]. Figure 24 shows an example for the quaternary ammonium salt Aliquat 336/Cl^- and aqueous HCl solutions.

Studies with tracer radionuclides of the lighter homologs. Based on these results, new chromatographic column separations with ARCA II were elaborated [79]. In these experiments, most of the amines tested in the HCl system showed slow kinetics for back extraction into the aqueous phase, resulting in elution peaks with an unacceptable tailing of the radioactivities into the subsequent fraction, a feature that was not observed in the mixed HCl/HF system [75]. An acceptable

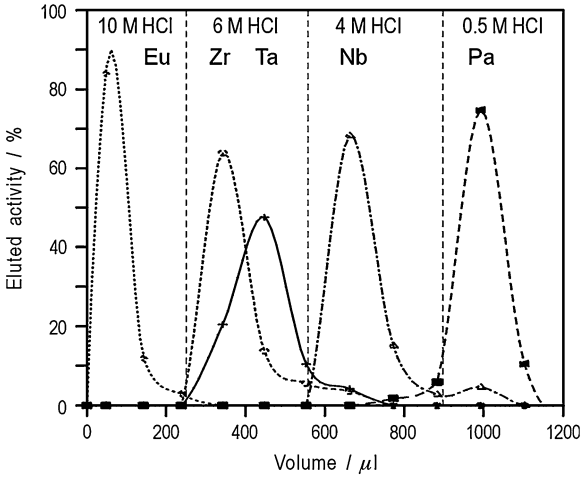

Fig. 24 Elution curves for trivalent cations (Eu), and for Zr, Ta, Nb, and Pa from Aliquat 336/HCl -Voltalef^{TM} (1:5) columns (1.6 mm i.d. × 8 mm) in ARCA II. The radionuclides are fed onto the column in 10 M HCl. This is followed by separate elutions of a Ta fraction (6 M HCl), a Nb fraction (4 M HCl), and a Pa fraction (0.5 M HCl) [77]. Reprinted with permission of Oldenbourg Wissenschaftverlag, München

chromatographic separation was only achieved with the quaternary ammonium salt Aliquat 336/Cl^- at a flow rate of the mobile aqueous phase of 1 mL min^{-1}. Carrier-free radiotracers of Eu, Nb, Ta, Pa, Zr, and Hf were fed onto the column in 10 M HCl. Zr, Hf, and Ta were eluted in 6 M HCl, Nb in 4 M HCl, and Pa in 0.5 M HCl, see Fig. 24. Thus, this system provides conditions for extracting all relevant elements from one HCl solution in a first step and for differentiating between Ta, Nb, and Pa in subsequent elutions.

Similarly, new partition experiments and chromatographic separations were performed with the fluoride salt of Aliquat 336 in HF solutions and with the bromide salt of Aliquat 336 in HBr solutions. The K_d values in the HBr system show the same sequence as in the HCl system: Pa > Nb > Ta. The threshold HBr concentrations above which an appreciable extraction is observed were, however, shifted to higher HBr molarities, i.e., to 6 M HBr for Pa, 9 M for Nb, while Ta is not extracted even from 12 M HBr. Chromatographic separations were performed by loading the radionuclides onto the 1.6 mm i.d. × 8 mm column in 12 M HBr and by eluting Nb in 7 M HBr and Pa in 2 M HBr. The fact that Ta was not extracted from HBr solutions made this system the least attractive for an application to element 105.

With the fluoride salt of Aliquat 336, K_d values on the order of $\geq 10^3$ were observed for all tracer nuclides (Pa, Nb, and Ta) and somewhat lower ones for Zr and Hf even at low HF concentrations. The same extraction sequence Pa > Nb > Ta as in the HCl- and HBr-systems was observed at 0.5 M HF. For increasing HF concentrations, the K_d values stay high for Nb and Ta up to 12 M HF while they decrease for Pa, Zr, and Hf due to the formation of polynegative fluoro complexes such as $[PaF_7]^{2-}$ and $[MF_6]^{2-}$ (M = Zr and Hf), respectively. In chromatographic separations, after feeding the nuclides onto the 1.6 mm i.d. × 8 mm column in 0.5 M HF, a Pa fraction was eluted in 4 M HF and Nb and Ta were subsequently stripped from the column with 6 M HNO_3/0.015 M HF.

Studies of the dubnium behavior. 1,307 experiments were conducted with ^{262}Db produced at the Berkeley 88-Inch Cyclotron in the ^{249}Bk(^{18}O,5n) reaction. Extractions were performed in the Aliquat 336/HCl system with a 50 s cyclic collection time of the KCl aerosol on a Kel-F™ slider in ARCA II. The reaction products were fed onto the column in 167 μL 10 M HCl followed by the elution of a Ta fraction in 183 μL 6 M HCl and by a Nb/Pa fraction in 167 μL 6 M HNO_3/0.015 M HF. The effluents were continuously sprayed through a 60 μm nozzle onto hot Ta disks on which they were evaporated to dryness by hot He gas and infrared light. Start of measurement of the radioactivities was 60 s (Ta fraction) and 76 s (Nb/Pa fraction) after the end of collection.

Six α singles in the Ta fraction and 12 in the Nb/Pa fraction were registered with life times compatible with the 34-s ^{262}Db. In addition, three pairs of correlated mother–daughter decays were registered, one in the Ta fraction and two in the Nb/Pa fraction. From this distribution, the K_d value of 438^{+532}_{-166} for element 105 in 6 M HCl was deduced [79], see Fig. 25. This value is much larger than that of Ta (22), smaller or equal to that of Nb (680), and smaller than that of Pa (1440).

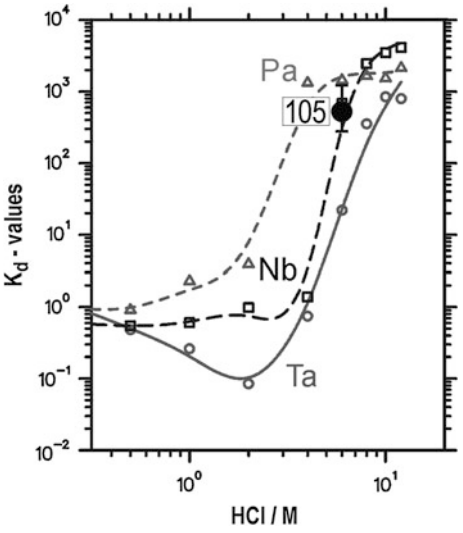

Fig. 25 Extraction behavior of Pa, Nb, and Ta from HCl solutions into Aliquat 336/HCl. The K_d of element 105 (Db) in 6 M HCl (with error *bars* encompassing the 68% confidence limit) is indicated by the *bold dot* [79]. Reprinted with permission of Oldenbourg Wissenschaftverlag, München

Thus, the extraction sequence Pa > Nb ≥ Db > Ta was established exactly as theoretically predicted [81].

In the Aliquat 336/HF system, 377 experiments were performed with ARCA II. The collection time of the He(KF) gas-jet was 50 s. The dissolved reaction products were loaded onto the column in 167 μL 0.5 M HF. In elutions with 133 μL 4 M HF (Pa fraction) and 167 μL 6 M HNO_3/0.015 M HF (Nb/Ta fraction), 4 α–α correlations were detected in the Nb/Ta fraction and none in the Pa fraction. (Due to a contamination of Po, α singles were not evaluated.) The K_d

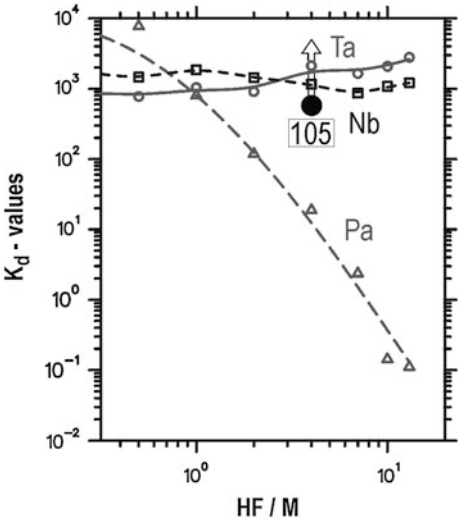

Fig. 26 Extraction behavior of Pa, Nb, and Ta from HF solutions in Aliquat 336/HF. The lower limit for the K_d value of element 105 (Db) in 4 M HF (representing the 68% confidence limit) is indicated by the *bold dot* with the *arrow* [79]. Reprinted with permission of Oldenbourg Wissenschaftverlag, München

value resulting from the probability distributions for zero (Pa fraction) and four (Nb/Ta fraction) observed correlated events is > 570 in 4 M HF which is close to that for Nb and Ta ($\geq 10^3$) and differs markedly from that for Pa (~ 10), see Fig. 26.

It is satisfying to see that not only the extraction sequence in the system Aliquat 336/HCl is correctly predicted by theory [79] but that the calculated free energy changes of the reactions of complex formation are on the order of 12 eV for the fluorides, 20 eV for the chlorides, and 22 eV for the bromides [82] (not taking into account the Gibbs free energy of formation of H_2O which is 3 eV) which, again, is in agreement with the experimental findings. For the fluorides, the equilibrium is always on the right hand side of Eq. (13) even at low HF concentrations; for the chlorides, it takes > 3 M HCl to form extractable chloride complexes and for the bromides, the threshold is shifted to > 6 M HBr (M = Nb, Ta, and Pa, X = F, Cl, and Br),

$$M(H_2O)_6^- + 4HX \rightleftarrows M(OH)_2X_4^- + 4H_2O. \quad (13)$$

3.2.3 Fluoride Complexation Studied by Ion-Exchange Chromatography

The multi-column technique (MCT) was applied to the liquid-phase chemistry of ^{262}Db ($T_{1/2}$ = 34 s) produced in ^{248}Cm(^{19}F,5n), and it was found that Db forms an anionic fluoro complex, which is strongly retained on the anion-exchange resin [84]. The products transported by the gas-jet system were continuously dissolved in 0.2 M HF and passed through a series of three successive ion-exchange columns. In the first cation-exchange column, actinides produced in nucleon transfer reactions and α-decay products of Db were removed from the solution. Anionic complexes of Db were retained in the second anion-exchange column, while the α-decay products of ^{262}Db, ^{258}Lr and ^{254}Fm were adsorbed as cationic complexes in the third cation-exchange column. After the end of a suitable production and chemical separation cycle, the long-lived descendant nuclide ^{254}Fm ($T_{1/2}$ = 3.24 h) was desorbed from the third column using 4.5 M HCl and assayed for α-spectroscopy. Consequently, Trubert et al. [84] isolated almost 70 atoms as an anionic form that is associated with the decay of ^{262}Db, and evaluated the production cross-section of 2.2 nb that is in agreement with that in [44].

The anion-exchange behavior of Db produced in the ^{248}Cm(^{19}F,5n)^{262}Db reaction was investigated by Tsukada et al. [85] together with the homologs Nb and Ta, and the pseudo-homolog Pa, with the anion-exchange resin CA08Y in 13.9 M HF solution. The experimental procedures with AIDA [2] (see "Experimental Techniques") were basically the same as those in the Rf experiments. Prior to the on-line chromatography, batch experiments were conducted with the radiotracers of ^{92m}Nb, ^{177}Ta, and ^{233}Pa. The obtained K_d values are plotted in Fig. 27 as a function of $[HF]_{ini}$.

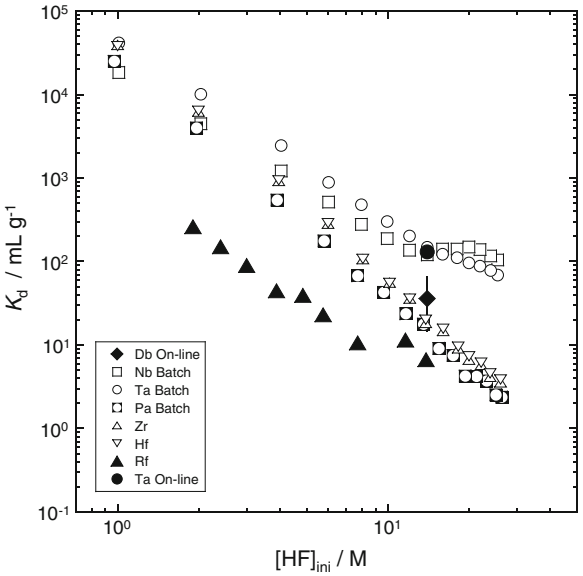

Fig. 27 Variation of the distribution coefficient, K_d, of Db, Nb, Ta, and Pa on the anion-exchange resin CA08Y as a function of $[HF]_{ini}$. The on-line data of Db and Ta are indicated by closed symbols. The K_d values of Rf, Zr, and Hf taken from [53] are also plotted. Adapted from [85]

Then, for Nb and Ta, column experiments were performed with AIDA and K_d values were determined with fits by the Glueckauf equation [57] based on measured elution curves. The K_d values were again correlated with %ads values, and the correlation was used to determine K_d values of ^{262}Db and ^{170}Ta in 13.9 M HF solution. Over 1,702 anion-exchange experiments were conducted with AIDA, and the %ads values of ^{262}Db and ^{170}Ta were determined to be 45^{+21}_{-16}% and 90 ± 2%, respectively. The K_d values of Db, Nb, and Ta obtained in the column experiment at $[HF]_{ini} = 13.9$ M are shown by closed symbols in Fig. 27. The results indicate that the adsorption of Db on the resin is significantly different from that of the homologs and that the adsorption decreases in the sequence Ta ≈ Nb > Db > Pa. The measurement of distribution coefficients at different HF concentrations is necessary to determine the chemical forms of the group-5 elements to compare the experimental adsorption sequence with that from theoretical predictions.

In solutions with more dilute fluoride ion concentration, Kasamatsu et al. [86] have ascertained the well-known significantly different anion-exchange behavior between Nb and Ta in mixed HF/HNO_3. They measured the K_d value of Db in 0.31 M HF/0.10 M HNO_3 solution ($[F^-] = 0.003$ M), where Nb and Ta form $[NbOF_4]^-$ and $[TaF_6]^-$, respectively. Here, ^{262}Db was produced in the ^{248}Cm(^{19}F,5n) reaction with a production rate of about 0.5 atoms per min at the JAEA tandem accelerator [44]. Reaction products recoiling out of the target were continuously transported by the He(KF) gas-jet from the target chamber to the collection site of a newly developed rapid ion-exchange separation apparatus, AIDA-II [87]; see "Experimental Techniques". After collection for 83 s, the products were dissolved with 300 μL of 0.31 M HF/0.10 M HNO_3 and were fed onto the chromatographic column (1.0 mm i.d. × 3.5 mm) filled with the anion-

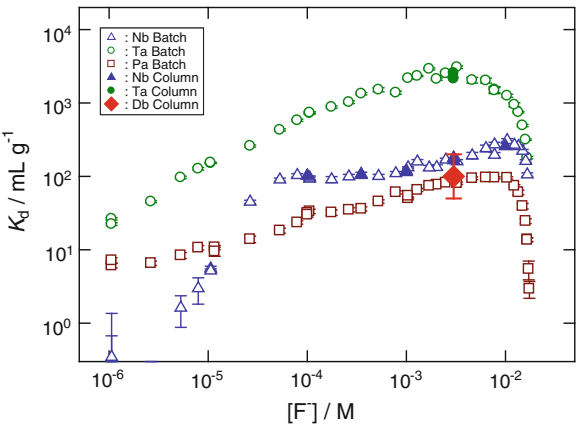

Fig. 28 Distribution coefficients, K_d, of Nb, Ta, Pa, and Db on the anion-exchange resin in HF/0.1 M HNO_3 depending on the fluoride ion concentration. Adapted from [86]

exchange resin MCI GEL CA08Y (particle size of 25 μm) at a flow rate of 1.2 mL min^{-1}. The eluate was collected as fraction 1 on a 15 × 300 mm Ta sheet (0.15 mm thick) that continuously moved toward an α-particle detection chamber at 2.0 cm s^{-1}. Samples on the sheet were automatically evaporated to dryness with a halogen heat lamp, and then assayed in an α-spectroscopic measurement station equipped with an array of 12 silicon PIN detectors [87]. Remaining products on the resin were stripped with 340 μL of 0.015 M HF/6.0 M HNO_3 at 1.0 mL min^{-1}. The eluate was collected on another Ta sheet as fraction 2 and followed by the same procedures. The α-particle measurement was started after 14 and 38 s for each fraction from the beginning of the first elution. The above processes were repeated 1,222 times. The adsorption probability (%ads) of Db was 56^{+16}_{-13}%. The K_d values of Nb and Ta were determined from their elution curves, and the values agree well with those from the batch-wise experiment [88] as shown in Fig. 28. The K_d value of Db was evaluated from its %ads in the same way as described in [53]. It was found that the adsorption of Db on the resin is considerably weaker than that of Ta and is similar to that of Nb and Pa: see Fig. 28. From a discussion on the fluoro complexes of the group-5 elements based on their K_d values [88], this result suggests that Db would form a fluoro-oxo complex $[DbOF_4]^-$, like Nb, but not $[DbF_6]^-$, like Ta. Note that the K_d value of Db is also close to that of Pa that forms $[PaOF_5]^{2-}$ and/or $[PaF_7]^{2-}$ [88–90]. The formation of complexes such as $[DbOF_5]^{2-}$ and $[DbF_7]^{2-}$ could also be suggested for Db. To unequivocally clarify the fluoride complexation of Db, further systematic study of Db as a function of $[F^-]$ and $[NO_3^-]$ is required.

3.2.4 Ion-Exchange Studies Using an Organic Complexing Agent and Resin: Chemical and Nuclear Studies

Another series of experiments with Db used its complexation with the α-hydroxyisobutyric acid (α-HiB) $(CH_3)_2COH$-COOH, that had been used in the first liquid-

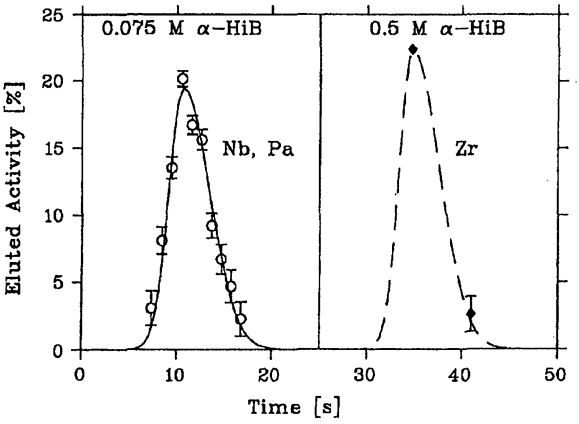

Fig. 29 *Left* frame: Manual HPLC elution (1 mL min^{-1}) of ^{95}Nb (*open circles*) from a 1.7 mm i.d. × 25 mm Aminex A6 column in 0.075 M α-HiB. ^{233}Pa (not shown) elutes in an identical manner. *Right* frame: Elution of ^{95}Zr from the same column in 0.5 M α-HiB. Only two fractions were counted (*black diamonds*). The *dashed curve* has the same shape as the elution curve in the *left* frame. Reproduced from [74]

phase Rf experiment [7]. Chelating by α-HiB depends strongly on the oxidation state of metal ions [74]. Elution from cation-exchange columns in ARCA II with unbuffered dilute α-HiB shows that Nb, Ta, and Pa are eluted promptly, while tetravalent and trivalent metal ions are strongly retained on the resin [74]. This is shown in Fig. 29 for manually performed separations of pentavalent Nb and Pa from tetravalent Zr using 0.075 M α-HiB and a 1.7 mm i.d. × 25 mm column filled with Aminex A6 (particle size 17.5 ± 2 μm). The tracer radionuclides were fed onto the column through a sample loop. After the dead volume of 130 μL (7 s), both Nb and Pa appear in the effluent and are eluted completely in consecutive 150 μL (9 s). The first radioactivity of the tetravalent Zr is detected after the elution of additional 3,150 μL (190 s). After the elution of Nb and Pa in 0.075 M α-HiB, Zr was eluted in 210 μL of 0.5 M α-HiB, see Fig. 29.

In experiments at the UNILAC accelerator in GSI, Darmstadt, the tantalum isotopes $^{168–170}$Ta were transported by the He(KCl) gas-jet and deposited on a polyethylene frit in ARCA II. The dissolution of the collected tantalum

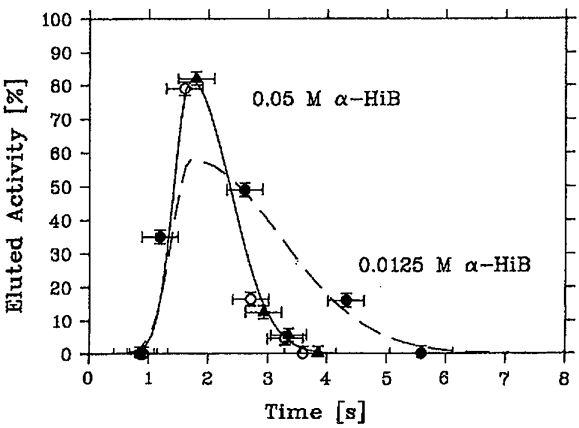

Fig. 30 Automated elution of ^{99m}Nb from 1.6 mm i.d. × 8 mm Aminex A6 columns in ARCA II at a flow rate of 1 mL min^{-1} (16.7 μL s^{-1}). *Open circles* and *closed triangles*, connected by the *solid line*, refer to series of elution with 0.05 M α-HiB. *Black circles* and *dashed curve* indicate elution in 0.0125 M α-HiB. Reproduced from [74]

radioactivity from the frit was investigated as a function of the α-HiB concentration. Because of the smaller column size in ARCA II (1.6 mm i.d. × 8 mm), which might cause an earlier breakthrough of the tetravalent and trivalent metal ions, it was desirable to decrease the α-HiB concentration. Even with 34 μL of 0.025 M α-HiB, dissolution of >75% of the tantalum radioactivity was achieved in 2 s. The time required for the complete elution of Ta from the column was about 4 s. Similar experiments performed at the Mainz TRIGA reactor with ^{99m}Nb confirm this result as shown in Fig. 30. The data for 0.05 M α-HiB show that the elution position and the width are quite reproducible. As the elution obviously takes more time with 0.0125 M α-HiB, see Fig. 30, 0.05 M α-HiB was finally selected for the Db experiment.

The time sequence for the Db separations was as follows; after collection of the transported nuclides on the polyethylene frit in ARCA II for 1 min, the frit was washed with 100 μL of unbuffered 0.05 M α-HiB solution (5 s). This solution was passed through one of 38 cation-exchange columns contained in two magazines, was collected on a Ta disk, and was quickly evaporated to dryness. After flaming and cooling, the Ta disk was inserted into one of 10 detector stations for α-particle energy and SF detection. Start of counting was 39 s after the end of collection. After three separations each, a new column was positioned below the collection frit. Thus, 114 continuous collection and separation cycles were conducted before the program was stopped; the used magazines were removed, and two new magazines were introduced for the next 114 1-min cycles.

In the production experiments with ^{262}Db at the 88-Inch Cyclotron of LBNL, the beam energy in the ^{249}Bk target was 99 MeV. The target originally consisted of 0.54 mg cm^{-2} of 330-d ^{249}Bk and decreased to 0.51 mg cm^{-2} with the remainder of the total thickness being its ^{249}Cf daughter. Db, together with other nuclear reaction products, was transported by the He(KCl) gas-jet (2 L min^{-1}) over 5 m to the collection site in ARCA II and was collected on polyethylene frits. The He(KCl) gas-jet efficiency was measured frequently during the experiments by dissolving the radioactivity in 0.05 M α-HiB and eluting it through an empty column directly onto a Ta disk. After evaporation to dryness and flaming, the production rate of the $^{252–255}$Fm transfer reaction products was determined by α-ray spectrometry. For normalization, separate bombardments of the Bk target were performed in which all of the products recoiling from the target were caught in a Au-catcher foil located directly behind the target. After 1 h of irradiation, the foil was dissolved in aqua regia to which an aliquot of ^{241}Am had been added to trace the chemical yield of actinides. The gold was removed on an anion-exchange column. The actinide fraction, which passed through the column, was collected and dried on a Pt disk for α-particle spectroscopy. By comparing the apparent production rates measured after transport through the He(KCl) gas-jet with the absolute production rates from the Au-catcher experiments, the transport efficiency was determined. In these experiments, the transport efficiency varied between 40 and 53%.

In 525 collection and elution cycles, the α-particle spectrum shown in Fig. 31 was obtained. Apart from ^{249}Cf contamination, sputtered from the target (this

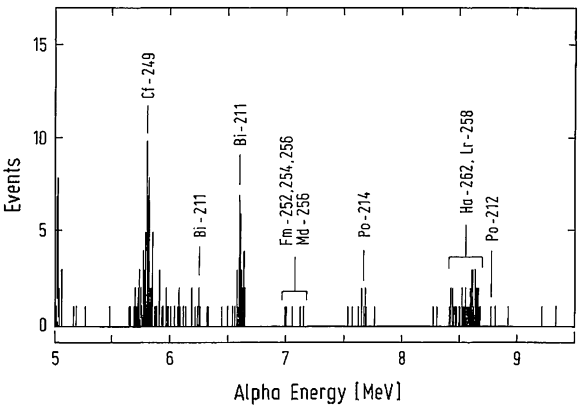

Fig. 31 α-energy spectrum of Db fractions from α-HiB separations observed in the bombardment of a ^{249}Bk target with 99-MeV ^{18}O ions. The symbol Ha should be replaced with Db. Reproduced from [91]

material is not dissolved in the weekly acidic α-HiB solution and is washed mechanically through the column), and from small amounts of Bi and Po radioactivities, produced in transfer reactions on a Pb impurity in the target, the spectrum is very clean.

The spectrum contains 41 α events attributable to element 105, among them nine pairs of ^{262}Db-^{258}Lr mother–daughter decays. The half-lives of $35.7^{+6.9}_{-5.4}$ s for ^{262}Db and $4.2^{+1.5}_{-1.1}$ s for ^{258}Lr were in good agreement with the previously determined values [75]. Also, 23 fissions attributable to Db decays were detected. These event rates are consistent with the detection efficiency and the known production rate [75]. From a chemical point of view, this means that the data are consistent with a high chemical yield of Db in these separations and with the fact that Db resumes the pentavalent oxidation state under the present conditions [74].

The α-HiB procedure was also applied to the products of a ^{249}Bk bombardment with ^{18}O ions at the lower bombarding energy of 93 MeV in an attempt to discover the unknown isotope ^{263}Db produced in the ^{249}Bk(^{18}O,4n) reaction [91]. In a total

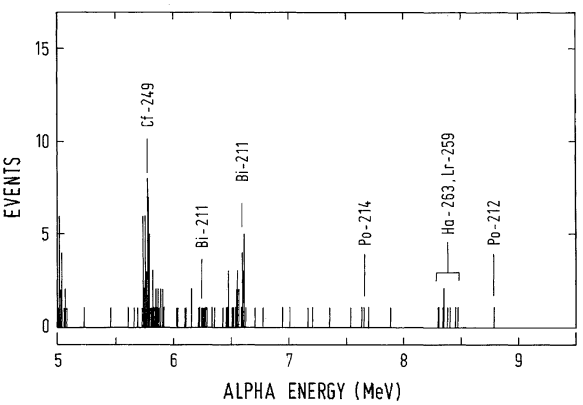

Fig. 32 α-particle energy spectrum of Db fractions from α-HiB separations observed in the bombardment of a ^{249}Bk target with 93-MeV ^{18}O ions. The symbol Ha should be replaced with Db. Reproduced from [91]

of 374 experiments, nine α particles with energies between 8.3 and 8.5 MeV, see Fig. 32, as well as 18 SF events were registered.

The absence of α particles above 8.5 MeV indicates that the ^{262}Db/^{258}Lr pair is no longer present at the lower bombarding energy ($\sigma_{5n} < 1.3$ nb [91]) in agreement with statistical model calculations. Instead, α groups at 8.35 and 8.45 MeV are detected that are assigned to the new isotope ^{263}Db and its daughter ^{259}Lr, respectively [91]. ^{263}Db decays with a half-life of 27^{+10}_{-7}s and has a SF branch of 57^{+13}_{-15}%. The cross-section of 10 ± 6 nb at 93 MeV is on the same order of magnitude as the 5n-channel cross section at 99 MeV and in agreement with statistical evaporation calculations. The mass assignment is supported by the observation of the 8.45 MeV α particles of the daughter, ^{259}Lr, in the chemically separated Db fractions and by the observation of two events [91] in which the α decay of ^{263}Db was followed by the SF decay [92] of the daughter ^{259}Lr.

Based on these results, the cross-section for the production of ^{262}Db at 99 MeV and the SF branch in ^{262}Db as reported earlier [75] had to be revised as it was clear now that both isotopes, 34-s ^{262}Db and 27-s ^{263}Db, are produced at this energy. The new value for the SF branch in ^{262}Db [91] resulted as 33%, and the cross-sections for the production of ^{262}Db and ^{263}Db at 99 MeV resulted as 6 ± 3 nb and 2 ± 1 nb, respectively [91]. This shows that chemical separations of transactinides can also be useful in obtaining new data on nuclear properties of their isotopes.

A search for an EC-branch in the decay of 27-s ^{263}Db was performed in a milking experiment; ^{263}Db was again produced in the ^{249}Bk(^{18}O,4n) reaction and transported to ARCA II by the He(KCl) gas-jet. After 1 min collection, the products were dissolved in 0.05 M α-HiB and were eluted in that solution from a cation-exchange column. The same column was used for five subsequent collection-elution cycles with ^{263}Db. After the fifth elution, an elution of tetravalent ions including those of Rf, if present, was performed with 0.1 M HF. In 155 of such Rf fractions, a total of 22 SF events were observed. From the known α/SF ratio for Fm isotopes and from the Fm contained in the measured α-particle spectra, 8.8 of the SF events had to be attributed to ^{256}Fm. A two-component fit with the ^{256}Fm fixed yielded a half-life of 600^{+300}_{-200} s for ^{263}Rf. Based on the effective production cross-section and on the known cross-section for production of ^{263}Db at 93 MeV, 10 ± 6 nb, an EC-branch in the decay of ^{263}Db on the order of 5% was deduced [93].

This was confirmed in an independent experiment in which ^{263}Db was produced in the reaction ^{249}Bk(^{18}O,4n) at the Philips Cyclotron of the Paul Scherrer Institute (PSI) Villigen, Switzerland. The products were collected for 15 min and then subjected to a chemical separation specific for group-4 elements. The product was dissolved in 0.5 M unbuffered α-HiB and eluted from a cation-exchange column. The effluent was made 9 M in HCl and group-4 tetrachlorides were extracted into TBP/Cyclohexane which was evaporated to dryness on a Ta disk. The Ta disks were assayed for α and SF spectrometry. A SF radioactivity with a half-life of 20 min was observed and again assigned to the nuclide ^{263}Rf, confirming that it is formed by EC decay of ^{263}Db with a decay branch of $3^{+4}_{-1.}$% [94].

Thus, the decay scheme of 27-s ^{263}Db is composed of 41% of α decay with an energy of 8.36 MeV, of 55% of SF, and of 3% of EC into the new isotope ^{263}Rf decaying by SF with a half-life of roughly 15 min. We like to note here, that one decay of ^{263}Rf, observed as a daughter product in an α-decay chain from ^{271}Hs, indicated a much shorter half-live of about 8^{+40}_{-4} s [95, 96].

Recently, chemical identification of Db as a decay product of element 115 produced in the reaction ^{243}Am + ^{48}Ca was performed [97–99]. A 32-cm^2 rotating target consisting of the enriched isotope ^{243}Am in the oxide form was bombarded by a 247-MeV ^{48}Ca beam at the U-400 cyclotron at the Flerov Laboratory of Nuclear Reactions (FLNR), Dubna, Russia. The recoiling reaction products were stopped in a 50 mm diameter Cu catcher foil. After the end of bombardment (EOB), a 7–10 μm thick layer of the Cu catcher was mechanically cut from the surface. The Cu was chemically processed to isolate Db/Rf, which are α-decay descendants of element 115; the layer was dissolved in 10 mL of conc. HNO_3. The resulting solution contained a large amount of Cu and unwanted reaction products. The group 4 and 5 elements were separated from the Cu through coprecipitation with $La(OH)_3$ by introducing ammonium hydroxide and the La^{3+} carrier to the solution. The precipitate was dissolved in 2 M HNO_3, which was loaded onto the strongly acidic cation exchanger Dowex 50 × 8 and subsequently washed with 1 M HF. The group 4 and 5 elements were eluted from the column, while the actinides remained adsorbed on the column. Then the effluent was evaporated and deposited onto a polyethylene foil with subsequent drying in a stream of warm helium. All procedures starting from the EOB until the beginning of detector measurements took 2–3 h [97–99].

In the eight irradiation samples, 15 spontaneous fission events were detected within 174 h. A decay analysis resulted in a single component with a half-life of 32^{+11}_{-7} h that agrees with $T_{1/2}$ obtained in the separate physical experiment [100] within statistical errors. A cross-section for the production of the long-lived SF nuclide from, presumably ^{243}Am(^{48}Ca,3n)^{288}115, was reported to be about 4 pb [97–99]. Schumann et al. concluded that the observed nuclide forms a hydroxide in ammonium solution coprecipitating with $La(OH)_3$ and forms strong anionic fluoride complexes in HF solution, indicating that its chemical properties correspond to that of a group 4 or 5 elements [98].

4 Seaborgium (Sg, Element 106)

In 1993, working at the Dubna gas-filled recoil separator, a Dubna–Livermore collaboration headed by Lazarev et al. [101] succeeded to synthesize, as they believed, two new isotopes of element 106, ^{265}Sg and ^{266}Sg, in the ^{248}Cm(^{22}Ne,5n) and ^{248}Cm(^{22}Ne,4n) reaction at 121 and 116 MeV, respectively. They measured an α energy of 8.63 ± 0.05 MeV for ^{266}Sg and a half-life of 1.2 s for the spontaneously fissioning daughter, ^{262}Rf. For ^{265}Sg, they measured α energies between

8.71 and 8.91 MeV and correlated α decays of the daughter ^{261}Rf (8.29 MeV) and the granddaughter ^{257}No (8.222, 8.27, and 8.32 MeV). The cross-sections were reported to be 80 pb at 116 MeV and 60 pb at 121 MeV for production of ^{266}Sg and 260 pb at 121 MeV for production of ^{265}Sg. These were reported to have an estimated uncertainty of a factor of ∼3. Using the phenomenological formulas of Viola and Seaborg, and of Patyk et al. [102], they estimated a partial α half-life for ^{266}Sg of 10–30 s and of 2–30 s for ^{265}Sg, assuming a hindrance factor between 1 and 3. Measurements of the lifetimes could not be performed as the implantation signals in the position-sensitive surface barrier detector were below the detection threshold. The estimated half-lives were felt to be rather encouraging for the planned chemistry experiments with these Sg isotopes. Note that due to the work by Dvorak et al. [95, 96], Düllmann and Türler [103], and Haba et al. [104], the assignments in [101] need to be corrected; in the chemistry experiments, all decay chains observed in the reaction ^{248}Cm(^{22}Ne,xn)$^{270-x}$Sg which were originally attributed to ^{266}Sg, are originating from ^{265}Sg [103, 104].

In 1995, the first study of the chemical properties of Sg in aqueous solution was performed. A short account of these experiments and their results was published by Schädel et al. [105]. Here, we give a more detailed report on the experiments including the results of a follow-up experiment performed in 1996. These involved the Automated Rapid Chemistry Apparatus, ARCA II [1], that has been successful in studying chemical properties of Db [75, 79] and of Rf [36, 40] in aqueous solutions.

Several chemical systems were tested with the fission products ^{93}Y, ^{97}Zr, and ^{99}Mo, and W isotopes produced in the ^{152}Gd + ^{20}Ne reaction [106] at the PSI Philips cyclotron. α-HiB solutions of 5×10^{-2} M, pH = 2.65 or pH = 5, used to elute W in a rapid and one-stage separation from cation-exchange columns, provided a good separation from Hf and Lu. Likewise, solutions with 0.1 M HCl and

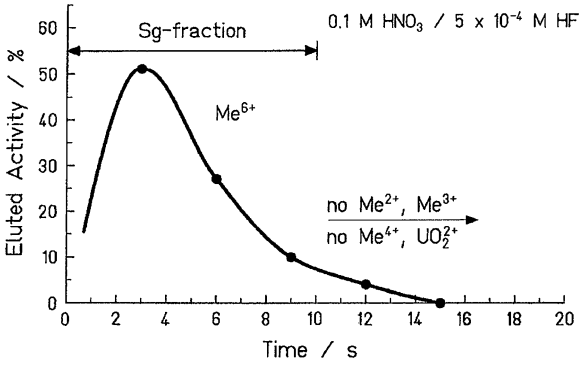

Fig. 33 Elution *curve* for short-lived W isotopes modeling the seaborgium separation in ARCA II using a solution of 0.1 M HNO_3/5 × 10^{-4} M HF with a flow rate of 1 mL min^{-1}. The 1.6 mm i.d. × 8 mm columns are filled with the cation-exchange resin Aminex A6 [108]. Reprinted with permission of Oldenbourg Wissenschaftverlag, München

various HF concentrations between 10^{-4} and 10^{-2} M were eluting W rapidly while Hf was safely retained on the column below 10^{-3} M HF. Hf was observed to be partially eluted for $\geq 2.8 \times 10^{-3}$ M HF in 0.1 M HCl. Finally, the decision was made to use a solution of 0.1 M HNO_3/5 $\times$ 10^{-4} M HF to elute a Sg fraction from cation-exchange columns [107] in order to avoid the formation of mixed chloride–fluoride complexes, which are difficult to model. $[MO_2F_3(H_2O)]^-$ is a likely form of the complexes that are eluted, but neutral species such as MO_2F_2 cannot be excluded. Some problems were encountered with adsorption of the radioactivities on the slider in ARCA II. Among the various materials tested, titanium showed the lowest losses of W and Hf due to adsorption. Figure 33 shows the elution curve for short-lived W isotopes from the reaction of ^{20}Ne with enriched ^{152}Gd. The product was transported to ARCA II with a He(KCl)-jet within about 3 s and deposited on a Ti slider. From here, it was dissolved and washed through the 1.6 mm i.d.$\times$ 8 mm long chromatographic column (filled with the cation exchange resin Aminex A6, 17.5 $\pm$ 2 μm) at a flow rate of 1 mL min^{-1} with 0.1 M HNO_3/5 $\times$ 10^{-4} M HF. Total 85% of the W are eluted within 10 s. No di- or tri-valent metal ions and no group-4 ions are eluted within the first 15 s. Also uranium, in the form of $UO_2^{2+}UO_2^{2+}$, is completely retained on the column.

In the Sg experiments [108], a 950 μg cm^{-2} ^{248}Cm target was bombarded with 3 $\times$ 10^{12} ^{22}Ne ions s^{-1} at 121 MeV to produce ^{265}Sg with a half-life of $\sim$7 s [109] (Todays knowledge [103, 104] shows the presence of two states; one with a half-life of about 9 s and one with about 15 s). Totally, 3,900 identical separations were conducted with a collection and cycle time of 45 s and a total beam dose of 5.48 $\times$ 10^{17} ^{22}Ne ions. The transport efficiency of the He(KCl) jet was 45%. On the average, counting of the samples started 38 s after the end of collection. The overall chemical yield was 80%.

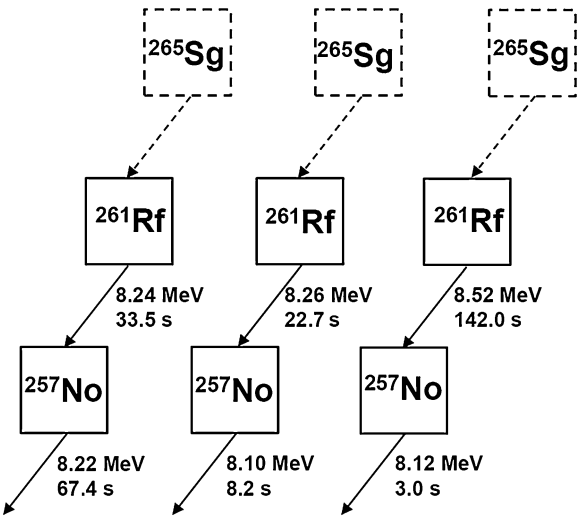

Fig. 34 Nuclear decay chains originating from ^{265}Sg after chemical separation with ARCA II. Adapted from [105]

Three correlated α–α mother–daughter decays were observed that were assigned to the decay of ^{261}Rf and ^{257}No, as the descendants of ^{265}Sg, see Fig. 34. The three correlated events have to be compared with an expectation value of 0.27 for random correlations. This gives a probability of 0.24% that the three events are random correlations. As the mother decays were not observed, it is important to note that ^{261}Rf and ^{257}No can only be observed if the mother, ^{265}Sg, passed through the column because group-4 elements and No are strongly retained on the cation-exchange columns in ARCA II. Most likely, the decay of ^{265}Sg was not observed because it decayed in the time interval between the end-of-separation and the start-of-measurement which was equivalent to four half-lives. That the columns really retained ^{261}Rf was demonstrated in an experiment where ^{261}Rf was produced directly in the ^{248}Cm(^{18}O,5n) reaction at the PSI Philips cyclotron [40], and processed as in the Sg chemistry in 0.1 M HNO_3/5 × 10^{-4} M HF. ^{261}Rf did not elute from the column and was subsequently stripped from the column with 0.1 M HNO_3/10^{-1} M HF. From the observation of the three correlated α-decay chains of ^{265}Sg daughters it was concluded, that, for the first time, a chemical separation of Sg was performed in aqueous solution. Sg shows a behavior typical of a hexavalent element located in group-6 of the Periodic Table. It is different from that of the pseudo group-6 element uranium, which is fixed as UO_2^{2+} on the cation-exchange column. Presumably, Sg forms $[SgO_2F_3(H_2O)]^-$ or the neutral species $[SgO_2F_2]$. However, due to the low fluoride concentration used, the anionic $[SgO_4]^{2-}$ ('seaborgate' in analogy to molybdate, $[MoO_4]^{2-}$, or tungstate, $[WO_4]^{2-}$) could not be excluded.

In order to get experimental information on this latter question, a new series of seaborgium experiments with ARCA II was performed in 1996, which used 0.1 M HNO_3 without HF as the mobile aqueous phase and Aminex A6 as a stationary phase [110]. If the 'seaborgate' ion was isolated in 1995, it was supposed to show up here again. A 691 μg cm^{-2} ^{248}Cm target containing 22 μg cm^{-2} enriched ^{152}Gd was bombarded with 123 MeV ^{22}Ne ions. The simultaneously produced ^{169}W served as a yield monitor. And 45 s cycles were run in which the effluent was evaporated on thin (∼500 μg cm^{-2}) Ti foils mounted on Al frames. These were thin enough to be counted in close geometry by pairs of PIPS detectors, thus, increasing the efficiency for α–α correlations by a factor of four as compared to the 1995 experiment. A beam dose of 4.32 × 10^{17} particles was collected in 4,575 separations. Only one α–α correlation attributable to the ^{261}Rf–^{257}No pair was observed. With an expected number of random correlations of 0.5 this is likely (the probability is 30%) to be a random correlation. From the beam integral and the overall yield as measured simultaneously for ^{169}W (27% including gas-jet transportation and chemical yield), a total of five correlated events were to be expected. This tends to indicate that, in the absence of fluoride ion, there is sorption of Sg on the cation-exchange resin.

This nontungsten like behavior of seaborgium under the given conditions may be attributed to its weaker tendency to hydrolyze:

$$\begin{aligned} \mathrm{M(H_2O)_6^{6+} \rightleftarrows M(OH)(H_2O)_5^{5+} + H^+} \\ \vdots \end{aligned} \tag{14}$$

$$\mathrm{MO(OH)_3(H_2O)_2^+ \rightleftarrows MO_2(OH)_2(H_2O)_2 + H^+} \tag{15}$$

$$\mathrm{MO_2(OH)_2(H_2O)_2 \rightleftarrows MO_3(OH)^- + 2H_2O + H^+} \tag{16}$$

$$\mathrm{MO_3(OH)^- \rightleftarrows MO_4^{2-} + H^+} \tag{17}$$

The measured equilibrium constants for this stepwise de-protonation scheme for Mo and W have been collected from the literature [111]; see also "Aqueous Chemistry of the Transactinides". They show that Mo is more hydrolyzed than W, and that the de-protonation sequence for Mo and W at pH = 1 reaches the neutral species $MO_2(OH)_2(H_2O)_2$. Assuming the de-protonation processes for Sg to be similar to those of Mo and W as in Eqs. 14–17, Pershina and Kratz [111] predict that the hydrolysis of the cationic species to the neutral species decreases in the order Mo > W > Sg. This is in agreement with the experimental data on hydrolysis of Mo and W and with the result for Sg [110]. For Sg, the de-protonation sequence ends earlier with a cationic species such as $SgO(OH)_3(H_2O)_2^+$, which adsorbs on a cation-exchange resin.

It is interesting to recall that a decreasing tendency to hydrolyze (Nb > Ta > Db > Pa) was reported [81] to determine the extraction of the group-5 chlorides into aliphatic amines. Thus, a similar behavior in the neighbouring group 6 would be apparent.

Looking back to the experiments in [108], where fluoride ions were present having a strong tendency to replace OH^- ligands, it appears plausible that, in this preceding experiment, neutral or anionic species were formed:

$$\mathrm{MO_2(OH)_2(H_2O)_2 + 2HF \rightleftarrows MO_2F_2(H_2O)_2 + 2\ H_2O} \tag{18}$$

$$\mathrm{MO_2F_2(H_2O)_2 + F^- \rightleftarrows MO_2F_3(H_2O)^- + H_2O} \tag{19}$$

Thus, the presence of fluoride ions seems to be an important prerequisite for future experiments. Here, the K_d value of Sg on an anion-exchange resin could, e.g., be determined with the MCT [112, 113] as well as with the ion-exchange chromatography [114] and could be compared to those of Mo and W. With the MCT, the K_d value of Sg could be determined on an anion-exchange resin (Dowex 1 × 8) in 0.1 M HNO_3/5 × 10^{-3} M HF. A large amount of work has been invested to prepare such an experiment by measuring K_d values in batch experiments for tracer radioactivities of Zr, Hf, Mo, Ta, W, Th with various resins of different functionality and aqueous solutions containing HCl, HNO_3, HCl/HF, and HNO_3/HF [112, 113]. In Ref. [113], an anion separation scheme in mixed HNO_3/HF solutions was elaborated for a W/Ta separation on an anion-exchange resin with the quaternary ammonium group $-N^+(C_2H_5)_3$ for which relatively low K_d values for W and high K_d values for Ta are observed yielding a W/Ta separation factor of

2270. With this resin, batch and MCT experiments were performed yielding mutually consistent K_d values. By varying the concentration of the counter ion NO_3^- competing for the binding sites on the resin, a slope of –1 in a plot of log K_d versus log [HNO_3] was verified indicating that W, in the presence of HF, forms anions with an electric charge of –1, e.g., $[WO_2F_3]^-$. Thus, the feasibility of a Sg experiment with the MCT was demonstrated.

As the α-decay daughters of ^{265}Sg, i.e., ^{261}Rf, ^{257}No, ^{253}Fm, and ^{253}Es, are cations in HNO_3/HF solutions at sufficiently low HF concentrations, a separation scheme for a possible Sg experiment is to use cation-exchange resins for the filter column F and the daughter column D_1, while the chromatographic column C contains the anion-exchange resin Dowex 1 × 8. In 0.1 M HNO_3/5 × 10^{-3} M HF, ^{261}Rf is still present as a cation [40], and Mo and W have K_d values on Dowex 1 × 8 of 82 and 11.2, respectively [113]. As a continuous dissolution of the KCl aerosol of the transport jet in a degassing unit of the type used in [37, 38] would result in a hold-up time too long for ∼7-s ^{265}Sg, a new apparatus was constructed. Here, the radionuclide-bearing aerosol is deposited for 2 s on a Ta disk by impaction. Thereafter, the Ta disk with the radioactive spot is rotated into a position where the product is dissolved within 2 s in 0.1 M HNO_3/5 × 10^{-3} M HF and is fed into the 3-column system quasi continuously. This MCT experiment has been tested successfully with short-lived W isotopes and awaits its application to ^{265}Sg.

Another attractive future experiment could be an attempt to reduce Sg(VI) to Sg(IV) in 0.1 M HCl/0.1 M HF and to distinguish the two oxidation states on an anion-exchange column where the reduced species, in contrast to the oxidized species, is being eluted [115]. Standard reduction potentials of Sg in acid solutions have been calculated by Pershina et al. [116] (see "Redox Potentials") using the multiconfiguration Dirac–Fock method predicting that the reduction of Sg(VI) to Sg(IV) should be feasible experimentally.

As presently under discussion, the SISAK system coupled to a recoil separator [4] (see Sect. 2.2.3. and "Experimental Techniques") may provide an alternative approach for continuously separating and detecting two oxidation states in Sg. The flow electrolytic column chromatography developed by Toyoshima et al. [117], which was successfully applied in on-line redox experiments of the heaviest actinides [118], may be adaptable to SISAK and may provide an interesting alternative approach for an electrochemical reduction of Sg.

5 Hassium (Hs, Element 108)

Following the example of Zhuikov et al. [119], several groups have adopted the in situ production of volatile tetroxides directly behind the target by adding oxygen (typically 10%) to the carrier gas that contains no aerosol particles [120–122]; see also "Experimental Techniques" and "Gas-Phase Chemistry of Superheavy Elements". Typically, the reaction products were transported with the carrier gas

through a quartz column containing a quartz wool plug heated to some 600 °C at the exit of the recoil chamber providing a hot surface at which the oxidation of the group-8 elements to their tetroxides was completed. The latter were further transported through a Teflon capillary to the detection system. Using thermochromatography at low temperatures, Düllmann et al. [123] measured the temperature at which HsO_4 deposits with their cryo online detector (COLD), which also served as detection system for the isotopes $^{269,\ 270}$Hs. COLD consists of 12 pairs of silicon PIN-diodes mounted at a distance of 1.5 mm to each other inside a copper bar. A temperature gradient from −20 to −170 °C was established along the detector array. The efficiency for detecting a single α particle was 77%. COLD was an improved version of a previous setup called the Cryo-Thermochromatography Separator (CTS) [121]. The deposition temperatures of HsO_4 and OsO_4, the derived adsorption enthalpies, and their relation to theoretical predictions [124–126] are covered in detail in "Gas-Phase Chemistry of Superheavy Elements".

An alternative approach was followed by von Zweidorf et al. [122] (see also "Gas-Phase Chemistry of Superheavy Elements"). In their experiment, the tetroxides were allowed to deposit on a thin layer of humid NaOH faced at a distance of ∼1 mm by an array of PIN-diodes. This system had an efficiency of 45% for detecting a single α particle. For OsO_4, the deposition is due to the formation of an osmate (VIII) of the form $Na_2[OsO_4(OH)_2]$ where OsO_4 acts as an acid anhydride. In the CALLISTO experiment (Continuously working Arrangement for Cluster-Less transport of In-SiTu produced volatile Oxides), ^{269}Hs was produced in the ^{248}Cm(^{26}Mg,5n) reaction. An admixture of ^{152}Gd to one of the three banana-shaped rotating target segments simultaneously produced α-emitting 19.2-s ^{172}Os and 22.4-s ^{173}Os. The evaporation residues were oxidized in situ behind the target in a mixture of He and O_2 and were transported to a deposition and detection

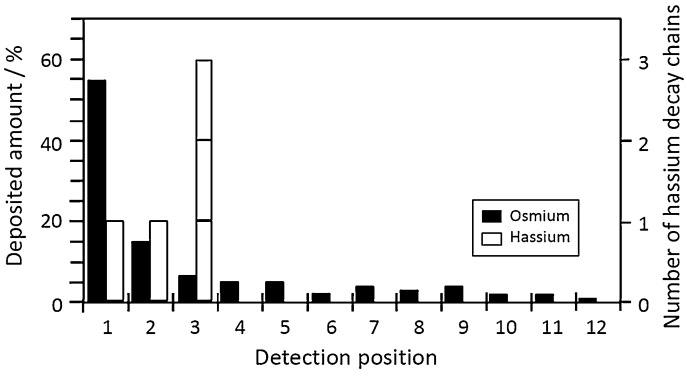

Fig. 35 Distribution of the deposited amount of OsO_4 and HsO_4 on a surface of NaOH facing a phalanx of 16 PIN diode detectors as a function of the detector position. While the ^{172,173}Os α decays are centered in front of detector 1, the ^{269}Hs decays are centered at position 3 [122]. Adapted from [122]

system. The latter consisted of 16 PIN diode detectors facing in close geometry a layer of NaOH which served, in the presence of a certain partial pressure of water in the transport gas, as a reactive surface for the deposition of the volatile tetroxides. In analogy to the formation of the osmate (VIII), the deposition of HsO_4 is likely to involve the reaction

$$2NaOH + HsO_4 \rightleftarrows Na_2\left[HsO_4(OH)_2\right]. \quad (20)$$

Thus, CALLISTO has shown that HsO_4, like OsO_4, is an acid anhydride and forms with NaOH a hassate (VIII), i.e., a salt. Figure 35 shows the distribution of the deposited amount of OsO_4 and HsO_4 as a function of the detector position. While the majority of the Os radioactivity is centered in front of detector 1 and tails into the subsequent positions, the five α-decay chains of ^{269}Hs are centered in front of higher detector numbers with a peak at the detector position 3. In Ref. [122], due to the low statistics, it was not claimed that this indicates a lower reactivity of HsO_4 with respect to moisturized NaOH as compared to OsO_4. However, theoretical work by Pershina [125] (see "Theoretical Chemistry of the Heaviest Elements") predicts interestingly that the hassate(VIII) should be more covalent than the osmate(VIII) and HsO_4 should react slightly weaker with NaOH than OsO_4.

6 Perspectives

Since the fast centrifuge system SISAK is equipped with liquid scintillation counting LSC [127–130], it is in principle capable of investigating short-lived α-decaying nuclides of the transactinides. β/γ- and α-pulses are distinguished by pulse-shape discrimination and pile-up pulses are rejected by a pile-up rejection system. This analog electronics proved to result in insufficient background suppression. Thus, two new approaches are being pursued.

Omtvedt et al. have given a status report on the SISAK liquid–liquid extraction system as used after the physical preseparator BGS at LBNL for chemical studies of transactinides [4, 69, 131]. The article describes the recent extension of SISAK to include a second extraction step in which the nuclide remaining in the aqueous phase after the first extraction stage is transferred to a second organic phase. This way, the amount of radionuclides in the two phases exiting the first extraction stage can be measured by LSC simultaneously, allowing direct determination of the distribution ratio. This report also contains a brief description of the chemical systems developed or being developed. For Rf, an account of extractions from sulphuric acid into tri-octylamine (TOA) in toluene is given where an extraction sequence $Zr > Hf \geq Rf$ is observed in accordance with theoretical calculations [68]. Extractions of Nb and Ta, homologs of Db, from sulphuric acid into TOA in toluene using SISAK are described [132] as well as suitable separation systems for Sg and element 107, Bh [131]. For Hs, following the approach by von Zweidorf

et al. [122], Samadani et al. [133] propose to dissolve the volatile HsO_4 in an aqueous solution of NaOH of variable molarity and to extract the HsO_4(aq) into the organic phase. A proof-of-principle experiment with α-decaying Os isotopes behind the preseparator TASCA, TransActinide Separator and Chemistry Apparatus, GSI was performed recently [134]. The reactions occurring in this experiment are

$$OsO_4(aq) + NaOH(aq) \rightarrow Na[OsO_4(OH)](aq) \tag{21}$$

$$Na[OsO_4(OH)](aq) + NaOH(aq) \rightarrow Na_2\left[OsO_4(OH)_2\right](aq) \tag{22}$$

and

$$OsO_4(aq) \rightarrow OsO_4(org) \tag{23}$$

The distribution ratio for OsO_4 between the two phases is

$$D = \frac{[OsO_4](org)}{[OsO_4](aq) + [OsO_4(OH)]^-(aq) + [OsO_4(OH)_2]^{2-}(aq)} \tag{24}$$

which can be rewritten as

$$D = \frac{K_D}{1 + K_1[OH^-] + K_1K_2[OH^-]^2} \tag{25}$$

where K_1, K_2, and K_D are equilibrium constants for Eqs. 21, 22, and 23, respectively. A fit of Eq. 25 to the experimental data (D vs. [NaOH](aq)) for OsO_4 fixes the numerical values of these equilibrium constants [133]. It will be interesting to compare these for HsO_4, this way testing the predicted lower reactivity of HsO_4 with aqueous NaOH relative to that of OsO_4 [125].

An alternative on-line liquid–liquid extraction system called MicroSISAK is being developed by Hild et al. [135]. It is based on a microreactor produced by methods of microtechnology and precision engineering [136]. The microreactor, consisting of 2 × 15 interdigital channels (30 μm wide) between wavy lamina, acts as a static mixer of the aqueous and organic phases. Its volume is on the order of 3 mm^3. Subsequent phase separation occurs on a hydrophobous Teflon membrane of 0.5 μm pore size. The system can be heated to 60 °C from outside to reach extraction equilibrium in < 1 s. The flow rates of the phases are on the order of 0.2 mL min^{-1}, thus, reducing the flow rate by two orders of magnitude as compared to the existing SISAK system. This helps to avoid production of large volumes of radioactive waste solutions, which are difficult to dispose.

A technique of microchip chemistry was introduced into an on-line solvent extraction system for the future study of superheavy elements by Ooe et al. [137]. Microchips made of glass plates have microscale ditches of typically 1–100 μm in width and depth. Because of a large specific interfacial area and a short diffusion length of solutes, chemical equilibria are rapidly achieved in the microspace, which is suited to the chemical separation of short-lived nuclides. On-line solvent

extraction experiments with rare-earth nuclides were successfully performed [137].

Research groups working at the FLNR, announced the observation of relatively long-lived isotopes of elements 108, 110, 112, 114, and 116 [138]; see also "Synthesis of Superheavy Elements". Due to the half-lives of the observed isotopes in the range of seconds to minutes, chemical investigations of these heaviest elements in the Periodic Table appear now to be feasible. The chemistry of these elements should be extremely interesting due to the predicted dramatic influence of relativistic effects [139–141]. In addition, the chemical identification of the newly discovered superheavy elements is highly desirable as the observed decay chains [138] cannot be linked to known nuclides, which has been heavily criticized [142, 143].

Elements 108–116 are expected to be partially very noble metals; see "Theoretical Chemistry of the Heaviest Elements". Thus, their electrodeposition on suitable electrode materials from aqueous solutions could be an attractive method for their isolation. It is known that the potential associated with the electrochemical deposition of radionuclides in metallic form from solutions of extremely small concentration is strongly influenced by the choice of the electrode material. This is reproduced by Eichler and Kratz [144] in a model in which the interaction between the microcomponent A and the electrode material B is described by the partial molar adsorption enthalpy and entropy of the metal–metal interaction. By combination with the thermodynamic description of the electrode process, a potential is calculated that characterizes the process at 50% deposition:

$$E_{50\%} = E^0 - \Delta H(\mathrm{A-B})/nF + T\Delta S_{\mathrm{vib}}(\mathrm{A-B})/nF - (RT/nF)\ln(A_m/1000) \tag{26}$$

Here, ΔH(A–B) is the partial molar net adsorption enthalpy associated with the transformation of 1 mol of the pure metal A in its standard state into the state of 'zero coverage' on the surface of the electrode material B, ΔS_{vib} is the difference in the vibrational entropies in the above states, n is the number of electrons involved in the electrode process, F is the Faraday constant, and A_{m} the surface of 1 mol of A as a mono layer on the electrode material B [144]. For the calculation of the thermodynamic functions in Eq. 26, a number of models were used by Eichler and Kratz [144]. Calculations were performed for Ni-, Cu-, Pd-, Ag-, Au-, and Pt-electrodes and the microcomponents Hg, Tl, Pb, Bi, and Po, thus confirming the decisive influence of the choice of the electrode material on the deposition potential. For Pd and Au, particularly large, positive values of $E_{50\%}$ were obtained, much larger than the standard electrode potentials (Nernst potentials) tabulated for these elements. This makes these electrode materials the prime choice for practical applications. An application of the same model for superheavy elements still needs to be done, but one can anticipate that the preference for Pd and Au will persist. The latter are metals in which, due to the formation of the metallic bond, almost or completely filled d orbitals are broken up, so that the metals tend in an extreme way toward the formation of intermetallic compounds with sp-metals. The

perspective is to make use of these metals in the form of a tape on which the transactinides are electrodeposited and the deposition zone is subsequently stepped between pairs of Si detectors for α and SF spectroscopy. An attractive candidate for first applications of the method is ^{269}Hs ($T_{1/2} \sim 10$ s) [145]. At the GSI Helmholtz center for heavy ion research, short-lived α-emitting Pb isotopes were produced and transferred to an electrolytic cell and deposited on a palladinated nickel tape. It was shown that the coupling of devices for collection, electrodeposition, and α-spectroscopy is feasible and might be of great use in superheavy element chemistry [146].

References

1. Schädel, M., Brüchle, W., Jäger, E., Schimpf, E., Kratz, J.V., Scherer, U.W., Zimmermann, H.P.: ARCA-II—a new apparatus for fast, repetitive HPLC separations. Radiochim. Acta **48**, 171–176 (1989)
2. Nagame, Y., Tsukada, K., Asai, M., Toyoshima, A., Akiyama, K., Ishii, Y., Kaneko-Sato, T., Hirata, M., Nishinaka, I., Ichikawa, S., Haba, H., Enomoto, S., Matsuo, K., Saika, D., Kitamoto, Y., Hasegawa, H., Tani, Y., Sato, W., Shinohara, A., Ito, M., Saito, J., Goto, S., Kudo, H., Kikunaga, H., Kinoshita, N., Yokoyama, A., Sueki, K., Oura, Y., Nakahara, H., Sakama, M., Schädel, M., Brüchle, W., Kratz, J.V.: Chemical studies on rutherfordium (Rf) at JAERI. Radiochim. Acta **93**, 519–526 (2005)
3. Szeglowski, Z., Bruchertseifer, H., Domanov, V.P., Gleisberg, B., Guseva, L.J., Hussonnois, M., Tikhomirova, G.S., Zvara, I., Oganessian, Yu.: Ts.: study of the solution chemistry of element 104—Kurchatovium. Radiochim. Acta **51**, 71–76 (1990)
4. Omtvedt, J.P., Alstad, J., Breivik, H., Dyve, J.E., Eberhardt, K., Folden III, C.M., Ginter, T., Gregorich, K.E., Hult, E.A., Johansson, M., Kirbach, U.W., Lee, D.M., Mendel, M., Nähler, A., Wierczinski, B., Wilk, P.A., Zielinski, P.M., Kratz, J.V., Trautmann, N., Nitsche, H., Hoffman, D.C.: SISAK liquid-liquid extraction experiments with preseparated ^{257}Rf. J. Nucl. Radiochem. Sci. **3**, 121–124 (2002)
5. Seaborg, G.T.: The chemical and radioactive properties of the heavy elements. Chem. Eng. News **23**, 2190–2193 (1945)
6. Ghiorso, A., Nurmia, M., Eskola, K., Eskola, P.: ^{261}Rf; New isotope of element 104. Phys. Lett. B **32**, 95–98 (1970)
7. Silva, R.J., Harris, J., Nurmia, M., Eskola, K., Ghiorso, A.: Chemical separation of rutherfordium. Inorg. Nucl. Chem. Lett. **6**, 871–877 (1970)
8. Ghiroso, A.: The Discovery of Elements 95-106. In: Proceedings of The Robert A. Welch Foundation, Conference on Chemical Research XXXIV. Fifty Years with Transuranium Elements, Houston, 22–23 Oct 1990, pp. 51–117. The Robert A. Welch Foundation, Houston (1990), and Report XBL 702-6151 (1970)
9. Hulet, E.K., Lougheed, R.W., Wild, J.F., Landrum, J.H., Nitschke, J.M., Ghiorso, A.: Chloride complexation of element 104. J. Inorg. Nucl. Chem. **42**, 79–82 (1980)
10. Keller Jr, O.L., Seaborg, G.T.: Chemistry of the transactinide elements. Ann. Rev. Nucl. Sci. **27**, 139166 (1977)
11. Hulet, E.K.: Chemical properties of the heavier actinides and transactinides. In: Edelstein, N.M. (ed.) Actinides in Perspective, pp. 453–490. Pergamon Press, Oxford (1982)
12. Keller Jr, O.L.: Chemistry of the heavy actinides and light transactinides. Radiochim. Acta **37**, 169–180 (1984)

13. Silva, R.J.: Transeinsteinium elements. In: Katz, J.J., Seaborg, G.T., Morss, L.R. (eds.) The Chemistry of the Actinide Elements, vol. 2, pp. 1085–1117. Chapman and Hall, London (1986)
14. Hoffman, D.C.: Chemistry of the transactinide elements. In: Proceedings of The Robert A. Welch Foundation, Conference on Chemical Research XXXIV. Fifty Years with Transuranium Elements, Houston, Texas, 22–23 Oct 1990, pp. 255–276. The Robert A. Welch Foundation, Houston (1990)
15. Hoffman, D.C.: Atom-at-a-time chemistry. Radiochim. Acta **61**, 123–128 (1993)
16. Hoffman, D.C.: The heaviest elements. Chem. Eng. News **72**, 24–34 (1994)
17. Kratz, J.V.: Chemistry of the transactinide elements. J. Alloys Comp. **213/214**, 20–27 (1994)
18. Kratz, J.V.: Chemie der schwersten Elemente. Chemie in unserer Zeit, 29. Jahrg. Nr. **4**, 194–206 (1995)
19. Schädel, M.: Chemistry of the transactinide elements. Radiochim. Acta **70/71**, 207–223 (1995)
20. Kratz, J.V.: Chemical properties of the transactinide elements. In: Greiner, W., Gupta, R.K. (eds.) Heavy Elements and Related New Phenomena, pp. 129–193. World Scientific, Singapore (1999)
21. Kratz, J.V.: Critical evaluation of the chemical properties of the transactinide elements. Pure Appl. Chem. **75**, 103–138 (2003)
22. Schädel, M. (ed.): The Chemistry of Superheavy Elements. Kluwer Academic Publishers, Dordrecht (2003)
23. Kratz, J.V.: Liquid-phase chemistry. In: Schädel, M. (ed.) The Chemistry of Superheavy Elements, pp. 159–203. Kluwer Academic Publishers, Dordrecht (2003)
24. Kratz, J.V.: Chemistry of transactinides. In: Vértes, A., Nagy, S., Klencsár, Z. (eds.) Handbook of Nuclear Chemistry, vol. 2, pp. 323–395. Kluwer Academic Publishers, Dordrecht (2003)
25. Schädel, M.: Chemistry of superheavy elements. Angew. Chem. Int. Ed. **45**, 368–401 (2006)
26. Hoffman, D.C., Lee, D.M., Pershina, V.: Transactinide elements and future elements. In: Morss, L.R., Edelstein, N.M., J. Fuger, J. (eds.) The Chemistry of the Actinide and Transactinide Elements, 3rd ed., vol. 3, pp. 1652–1752. Springer, Dordrecht (2006)
27. Kratz, J.V.: Chemistry of transactinides. In: Vértes, A., Nagy, S., Klencsár, Z. Lovas, R.G., Rösch, F. (eds.) Handbook of Nuclear Chemistry, 2nd ed., vol. 2, pp. 925–1004, Springer Science + Business Media B.V. , Dordrecht (2011)
28. Kratz, J.V.: Aqueous-phase chemistry of the transactinides. Radiochim. Acta **99**, 477–502 (2011)
29. Czerwinski, K.R.: Ph.D. thesis, University of California, Lawrence Berkeley Laboratory Report LBL-32233 (1992)
30. Czerwinski, K.R., Gregorich, K.E., Hannink, N.J., Kacher, C.D., Kadkhodayan, B., Kreek, S.A., Lee, D.M., Nurmia, M.J., Türler, A., Seaborg, G.T., Hoffman, D.C.: Solution chemistry of element 104: part I. Liquid-liquid extractions with triisooctylamine. Radiochim. Acta **64**, 23–28 (1994)
31. Czerwinski, K.R., Kacher, C.D., Gregorich, K.E., Hamilton, T.M., Hannink, N.J., Kadkhodayan, B., Kreek, S.A., Lee, D.M., Nurmia, M.J., Türler, A., Seaborg, G.T., Hoffman, D.C.: Solution chemistry of element 104: part II. Liquid-liquid extractions with tributylphophate. Radiochim. Acta **64**, 29–35 (1994)
32. Bilewicz, A., Siekierski, S., Kacher, C.D., Gregorich, K.E., Lee, D.M., Stoyer, N.J., Kadkhodayan, B., Kreek, S.A., Lane, M.R., Sylwester, E.R., Neu, M.P., Mohar, M.F., Hoffman, D.C.: Chemical studies of rutherfordium (element 104): part I. Thin film ferrocyanide surfaces for the study of the hydrolysis of rutherfordium. Radiochim. Acta **75**, 121–126 (1996)
33. Kacher, C.D., Gregorich, K.E., Lee, D.M., Watanabe, Y., Kadkhodayan, B., Wierczinski, B., Lane, M.R., Sylwester, E.R., Keeney, D.A., Hendriks, M., Stoyer, N.J., Yang, J., Hsu, M., Hoffman, D.C., Bilewicz, A.: Chemical studies of rutherfordium (element 104): part II.

Solvent extraction into tributylphosphate from HBr solutions. Radiochim. Acta **75**, 127–133 (1996)
34. Kacher, C.D., Gregorich, K.E., Lee, D.M., Watanabe, Y., Kadkhodayan, B., Wierczinski, B., Lane, M.R., Sylwester, E.R., Keeney, D.A., Hendriks, M., Hoffman, D.C., Bilewicz, A.: Chemical studies of rutherfordium (element 104): part III. Solvent extraction into triisooctylamine from HF solutions. Radiochim. Acta **75**, 135–139 (1996)
35. Haba, H., Kaji, D., Kikunaga, H., Kudou, Y., Morimoto, K., Morita, K., Ozeki, K., Sumita, T., Yoneda, A., Kasamatsu, Y., Komori, Y., Ooe, K., Shinohara, A.: Production and decay properties of the 1.9-s isomerric state in ^{261}Rf. Phys. Rev. C **83**, 034602(7) (2011)
36. Günther, R., Paulus, W., Kratz, J.V., Seibert, A., Thörle, P., Zauner, S., Brüchle, W., Jäger, E., Pershina, V., Schädel, M., Schausten, B., Schumann, D., Eichler, B., Gäggeler, H.W., Jost, D.T., Türler, A.: Chromatographic study of rutherfordium (element 104) in the system HCl/Tributylphosphate (TBP). Radiochim. Acta **80**, 121–128 (1998)
37. Pfrepper, G., Pfrepper, R., Yakushev, A.B., Timokhin, S.N., Zvara, I.: ''On-line'' experiments with cyclotron produced short-lived hafnium isotopes as a test for studies of ion exchange equilibria of element 104 by a continuous chromatography technique. Radiochim. Acta **77**, 201–206 (1997)
38. Pfrepper, G., Pfrepper, R., Krauss, D., Yakushev, A.B., Timokhin, S.N., Zvara, I.: Ion exchange equilibria and stoichiometry of complexes of element 104 and hafnium in hydrofluoric acid solutions. Radiochim. Acta **80**, 7–12 (1998)
39. Kronenberg, A., Eberhardt, K., Kratz, J.V., Mohapatra, P.K., Nähler, A., Thörle, P., Brüchle, W., Schädel, M., Türler, A.: On-line anion exchange of rutherfordium in HF/HNO_3 and HF solutions. Radiochim. Acta **92**, 379–386 (2004)
40. Strub, E., Kratz, J.V., Kronenberg, A., Nähler, A., Thörle, P., Zauner, S., Brüchle, W., Jäger, E., Schädel, M., Schausten, B., Schimpf, E., Zongwei, Li, Kirbach, U., Schumann, D., Jost, D., Türler, A., Asai, M., Nagame, Y., Sakama, M., Tsukada, K., Gäggeler, H.W., Glatz, J.P.: Fluoride complexation of rutherfordium (Rf, element 104). Radiochim. Acta **88**, 265–271 (2000)
41. Toyoshima, A., Haba, H., Tsukada, K., Asai, M., Akiyama, K., Goto, S., Ishii, Y., Nishinaka, I., Sato, T.K., Nagame, Y., Sato, W., Tani, Y., Hasegawa, H., Matsuo, K., Saika, D., Kitamoto, Y., Shinohara, A., Ito, M., Saito, J., Kudo, H., Yokoyama, A., Sakama, M., Sueki, K., Oura, Y., Nakahara, H., Schädel, M., Brüchle, W., Kratz, J.V.: Hexafluoro complex of rutherfordium in mixed HF/HNO_3 solutions. Radiochim. Acta **96**, 125–134 (2008)
42. Strub, E., Kratz, J. V., Kronenberg, A., Nähler, A., Thörle, P., Brüchle, W., Jäger, E., Li, Z., Schädel, M., Schausten, B., Schimpf, E., Jost, D., Türler, A., Gäggeler, H.W., Glatz, J.P.: Fluoride complexation of rutherfordium (Rf, Element 104). Institut für Kernchemie, Univ. Mainz, Jahresbericht 2000, IKMz 2001-1, A3 (2001)
43. Nagame, Y.: Radiochemical studies of the transactinide element, rutherfordium (Rf) at JAERI. J. Nucl. Radiochem. Sci. **6**, A21–A28 (2005)
44. Nagame, Y., Asai, M., Haba, H., Goto, S., Tsukada, K., Nishinaka, I., Nishio, K., Ichikawa, S., Toyoshima, A., Akiyama, K., Nakahara, H., Sakama, M., Schädel, M., Kratz, J.V., Gäggeler, H.W., Türler, A.: Production cross sections of ^{261}Rf and ^{262}Db in bombardments of ^{248}Cm with ^{18}O and ^{19}F ions. J. Nucl. Radiochem. Sci. **3**, 85–88 (2002)
45. Haba, H., Tsukada, K., Asai, M., Goto, S., Toyoshima, A., Nishinaka, I., Akiyama, K., Hirata, M., Ichikawa, S., Nagame, Y., Shoji, Y., Shigekawa, M., Koike, T., Iwasaki, M., Shinohara, A., Kaneko, T., Maruyama, T., Ono, S., Kudo, H., Oura, Y., Sueki, K., Nakahara, H., Sakama, M., Yokoyama, A., Kratz, J.V., Schädel, M., Brüchle, W.: Anion exchange behavior of Rf in HCl and HNO_3 solutions. J. Nucl. Radiochem. Sci. **3**, 143–146 (2002)
46. Pershina, V., Trubert, D., Le Naour, C., Kratz, J.V.: Theoretical predictions of hydrolysis and complex formation of group-4 elements Zr, Hf, and Rf in HF and HCl solutions. Radiochim. Acta **90**, 869–877 (2002)

47. Haba, H., Akiyama, K., Tsukada, K., Asai, M., Toyoshima, A., Yaita, T., Hirata, M., Sueki, K., Nagame, Y.: Chloride complexation of Zr and Hf in HCl investigated by extended x-ray absorption fine structure spectroscopy: Toward characterization of chloride complexation of element 104, rutherfordium (Rf). Bull. Chem. Soc. Jpn. **82**, 698–703 (2006)
48. Huffman, E.H., Iddings, G.M., Lilly, R.C.: Anion exchange of Zirconium, Hafnium, Niobium and Tantalum in hydrochloric acid solutions. J. Am. Chem. Soc. **73**, 4474–4475 (1951)
49. Haba, H., Tsukada, K., Asai, M., Toyoshima, A., Ishii, Y., Toume, H., Sato, T., Nishinaka, I., Ichikawa, T., Ichikawa, S., Nagame, Y., Sato, W., Matsuo, M., Kitamoto, Y., Tashiro, Y., Shinohara, A., Saito, J., Ito, M., Ikezawa, T., Sakamaki, M., Goto, S., Kudo, H., Kikunaga, H., Arai, M., Kamataki, S., Yokoyama, A., Akiyama, K., Sueki, K., Oura, Y., Schädel, M., Brüchle, W., Kratz, J.V.: Extraction behaviour of rutherfordium into tributylphosphate from hydrochloric acid. Radiochim. Acta **95**, 1–6 (2007)
50. Toyoshima, A., Kasamatsu, Y., Tsukada, K., Asai, M., Ishii, Y., Toume, H., Nishinaka, I., Sato, T.K., Nagame, Y., Schädel, M., Haba, H., Goto, S., Kudo, H., Akiyama, K., Oura, Y., Ooe, K., Shinohara, A., Sueki, K., Kratz, J.V.: Extraction chromatographic behavior of Rf, Zr, and Hf in HCl solution with styrene-divinylbenzene copolymer resin modified by trioctylphosphine oxide (TOPO). J. Nucl. Radiochem. Sci. **11**, 7–11 (2010)
51. Pai, S.A., Subramanian, M.S.: Synergetic extractions of uranyl ions with 1-phenyl-3-methly-benzoylpyrazolone-5 (HPMBP) and diphenyl sulfoxide (DPSO), tri-n-butyl phosphate (TBP) or tri-n-octylphosphine oxide (TOPO). J. Radioanal. Nucl. Chem. **89**, 423–433 (1985)
52. Rizvi, G.H.: Extraction of actinides with tropolone I. Synergistic extraction of uranium(VI) with tropolone and some neutral donors. J. Radioanal. Nucl. Chem. **170**, 479–487 (1993)
53. Haba, H., Tsukada, K., Asai, M., Toyoshima, A., Akiyama, K., Nishinaka, I., Hirata, M., Yaita, T., Ichikawa, S., Nagame, Y., Yasuda, K., Miyamoto, Y., Kaneko, T., Goto, S., Ono, S., Hirai, T., Kudo, H., Shigekawa, M., Shinohara, A., Oura, S., Nakahara, H., Sueki, K., Kikunaga, H., Kinoshita, N., Tsuruga, N., Yokoyama, A., Sakama, M., Enomoto, S., Schädel, M., Brüchle, W., Kratz, J.V.: Fluoride complexation of element 104, rutherfordium. J. Am. Chem. Soc. **126**, 5219 (2004)
54. Toyoshima, A., Haba, H., Tsukada, K., Asai, M., Akiyama, K., Nishinaka, I., Nagame, Y., Saika, D., Matsuo, K., Sato, W., Shinohara, A., Ishizu, H., Ito, M., Saito, J., Goto, S., Kudo, H., Kikunaga, H., Kinoshita, N., Kato, C., Yokoyama, A., Sueki, K.: Elution curve of rutherfordium (Rf) in anion-exchange chromatography with hydrofluoric acid (HF) solution. J. Nucl. Radiochem. Sci **5**, 45 (2004)
55. Ishii, Y., Toyoshima, A., Tsukada, K., Asai, M., Toume, H., Nishinka, I., Nagame, Y., Miyashita, S., Mori, T., Suganuma, H., Haba, H., Skamaki, M., Goto, S., Kudo, H., Akiyama, K., Oura, Y., Nakahara, H., Tashiro, Y., Shinohara, A., Schädel, M., Brüchle, W., Pershina, V., Kratz, J.V.: Fluoride complexation of element 104, rutherfordium (Rf), investigated by cation-exchange chromatography. Chem. Lett. **37**, 288 (2008)
56. Ishii, Y., Toyoshima, A., Tsukada, K., Asai, M., Li, Z.J., Nagame, Y., Miyashita, S., Mori, T., Suganuma, H., Haba, H., Goto, S., Kudo, H., Akiyama, K., Oura, Y., Shinohara, A., Schädel, M., Pershina, V., Kratz, J.V.: Fluorido complex formation of element 104, rutherfordium (Rf). Bull. Chem. Soc. Jpn. **84**, 903–911 (2011)
57. Glueckauf, E.: Theory of chromatography, Part 9. The "theoretical plate" concept in column separations. Trans. Faraday **51**, 34–44 (1955)
58. Plaisance, M., Guillaumont, R.: Fluoro- et chlorofluoro-complexes de protactiniumpentavalent. Radiochim. Acta **12**, 32–37 (1969)
59. Kim, J.I., Lagally, H., Born, H.-J.: Ion exchange in aqueous and in aqueous-organic solvents: Part I. Anion-exchange behaviour of Zr, Nb, Ta and Pa in aqueous HCl-HF and in HCl-HF-organic solvent. Anal. Chim. Acta **64**, 29–43 (1973)
60. Korkisch, J.: Handbook of Ion Exchange Resins: Their Application to Inorganic and Analytical Chemistry. CRC Press, Boca Raton (1989)
61. Perrson, R.G.: Hard and soft acids bases. J. Am. Chem. Soc. **85**, 3533–3539 (1963)

62. Pearson, R.G.: Hard and soft acids and bases, HSAB, part I. J. Chem. Edu. **45**, 581–587 (1968); Pearson, R.G.: Hard and soft acids and bases., HSAB, part II. J. Chem. Edu. **45**, 643–648 (1968)
63. Shannon, R.D.: Revised effective ionic radii and systematic studies of interatomic distances in halides and chalcogenides. Acta Cryst. **A32**, 751–767 (1976)
64. Pershina, V.: Theoretical chemistry of the heaviest elements. In: Schädel, M. (ed.) The Chemistry of Superheavy Elements, pp. 31–94. Kluwer Academic Publishers, Dordrecht (2003)
65. Schumann, D., Nitsche, H., Taut, St., Jost, D.T., Gäggeler, H.W., Yakushev, A.B., Buklanov, G.V., Domanov, V.P., Lien, D.T., Kubica, B., Misiak, R., Szeglowski, Z.: Sorption behaviour of rutherfordium and thorium from HCl/HF containing aqueous solution. J. All. Comp. **271–273**, 307–311 (1998)
66. Li, Z.J., Toyoshima, A., Asai, M., Tsukada, K., Sato, T.K., Sato, N., Kikuchi, T., Nagame, Y., Schädel, M., Pershina, V., Liang, X.H., Kasamatsu, Y., Komori, Y., Ooe, K., Shinohara, A., Goto, S., Murayama, H., Murakami, M., Kudo, H., Haba, H., Takeda, Y., Nishikawa, M., Yokoyama, A., Ikarashi, S., Sueki, K., Akiyama, K., Kratz, J.V.: Sulfate complexation of element 104, Rf, in H_2SO_4/HNO_3 mixed solution. Radiochim. Acta **100**, 157–164 (2012)
67. Ryabchikov, D.I., Marov, I.N., Ermakov, A.N., Belyaeva, V.K.: Stability of some inorganic and organic complex compounds of zirconium and hafnium. J. Inorg. Nucl. Chem. **26**, 965–980 (1964)
68. Pershina, V., Polakova, D., Omtvedt, J.P.: Theoretical prediction of complex formation of group-4 elements Zr, Hf, and Rf in H_2SO_4 solutions. Radiochim. Acta **94**, 407–414 (2006)
69. Stavsetra, L., Gregorich, K.E., Alstad, J., Breivik, H., Eberhardt, K., Folden III, C.M., Ginter, T.N., Johansson, M., Kirbach, U.W., Lee, D.M., Mendel, M., Omtvedt, L.A., Patin, J.B., Skarnemark, G., Sudowe, R., Wilk, P.A., Zielinski, P.M., Nitsche, H., Hoffman, D.C., Omtvedt, J.P.: Liquid-scintillation detection of preseparated ^{257}Rf with the SISAK system. Nucl. Instr. Meth. Phys. Res. A **543**, 509–516 (2005)
70. Gregorich, K.E., Henderson, R.A., Lee, D.M., Nurmia, M.J., Chasteler, R.M., Hall, H.L., Bennett, D.A., Gannett, C.M., Chadwick, R.B., Leyba, J.D., Hoffman, D.C., Herrmann, G.: Aqueous chemistry of element 105. Radiochim. Acta **43**, 223–231 (1988)
71. Ghiorso, A., Nurmia, M., Eskola, K., Eskola, P.: Two new alpha-particle emitting isotopes of element 105, ^{261}Ha and ^{262}Ha. Phys. Rev. C **4**, 1850–1855 (1971)
72. Bemis, C.E., Ferguson, R.L., Plasil, F., Silva, R.J., O'Kelley, G.D., Keifer, M.L., Hahn, R.L., Hensley, D.C.: Mass asymmetry and total-kinetic-energy release in the spontaneous fission of ^{262}[105]. Phys. Rev. Lett. **39**, 1246–1249 (1977)
73. Weis, M., Ahrens, H., Denschlag, H.O., Fariwar, M., Herrmann, G., Trautmann, N.: Rapidsorption of niobium on glass surfaces. Radiochim. Acta **42**, 201-203 (1987)
74. Schädel, M., Brüchle, W., Schimpf, E., Zimmermann, H.P., Gober, M.K., Kratz, J.V., Trautmann, N., Gäggeler, H., Jost, D., Kovacs, J., Scherer, U.W., Weber, A., Gregorich, K.E., Türler, A., Czerwinski, K.R., Hannink, N.J., Kadkhodayan, B., Lee, D.M., Nurmia, M.J., Hoffman, D.C.: Chemical properties of element 105 in aqueous solution: cation exchange separation with α-hydroxyisobutyric acid. Radiochim. Acta **57**, 85–92 (1992)
75. Kratz, J.V., Zimmermann, H.P., Scherer, U.W., Schädel, M., Brüchle, W., Gregorich, K.E., Gannett, C.M., Hall, H.L., Henderson, R.A., Lee, D.M., Leyba, J.D., Nurmia, M.J., Hoffman, D.C., Gäggeler, H., Jost, D., Baltensperger, U.: Nai-Qi, Ya, Türler, A., Lienert, Ch.: Chemical properties of element 105 in aqueous solution: halide complex formation and anion exchange into triisooctyl amine. Radiochim. Acta **48**, 121–133 (1989)
76. Zimmermann, H.P., Gober, M.K., Kratz, J.V., Schädel, M., Brüchle, W., Schimpf, E., Gregorich, K.E., Türler, A., Czerwinski, K.R., Hannink, N.J., Kadkhodayan, B., Lee, D.M., Nurmia, M.J., Hoffman, D.C., Gäggeler, H., Jost, D., Kovacs, J., Scherer, U.W., Weber, A.: Chemical properties of element 105 in aqueous solution: back extraction from triisooctyl amine into 0.5 M HCl. Radiochim. Acta **60**, 11–16 (1993)

77. Pershina, V., Fricke, B., Kratz, J.V., Ionova, G.V.: The electronic structure of anionic halide complexes of element 105 in aqueous solutions and their extraction by aliphatic amines. Radiochim. Acta **64**, 37–48 (1994)
78. Gober, M.K., Kratz, J.V., Zimmermann, H.P., Schädel, M., Brüchle, W., Schimpf, E., Gregorich, K.E., Türler, A., Hannink, N.J., Czerwinski, K.R., Kadkhodayan, B., Lee, D.M., Nurmia, M.J., Hoffman, D.C., Gäggeler, H., Jost, D., Kovacs, J., Scherer, U.W., Weber, A.: Chemical properties of element 105 in aqueous solution: extraction into diisobutylcarbinol. Radiochim. Acta **57**, 77–84 (1992)
79. Paulus, W., Kratz, J.V., Strub, E., Zauner, S., Brüchle, W., Pershina, V., Schädel, M., Schausten, B., Adams, J.L., Gregorich, K.E., Hoffman, D.C., Lane, M.R., Laue, C., Lee, D.M., McGrath, C.A., Shaughnessy, D.K., Strellis, D.A., Sylwester, E.R.: Chemical properties of element 105 in aqueous solution: extraction of the fluoride-, chloride-, and bromide complexes of the group-5 elements into anapliphatic amine. Radiochim. Acta **84**, 69–77 (1999)
80. Pershina, V.: Solution chemistry of element 105 part I: hydrolysis of group 5 cations: Nb, Ta, Ha and Pa. Radiochim. Acta **80**, 65–73 (1998)
81. Pershina, V.: Solution chemistry of element 105 Part II: hydrolysis and complex formation of Nb, Ta, Ha and Pa in HCl solutions. Radiochim. Acta **80**, 75–84 (1998)
82. Pershina, V., Bastug, T.: Solution chemistry of element 105 part III: hydrolysis and complex formation of Nb, Ta, Ha and Pa in HF and HBr solutions. Radiochim. Acta **84**, 79–84 (1998)
83. Paulus, W., Kratz, J.V., Strub, E., Zauner, S., Brüchle, W., Pershina, V., Schädel, M., Schausten, B., Adams, J.L., Gregorich, K.E., Hoffman, D.C., Lane, M.R., Laue, C., Lee, D.M., McGrath, C.A., Shaughnessy, D.K., Strellis, D.A., Sylwester, E.R.: Extraction of the fluoride-, chloride-, and bromide complexes of the elements Nb, Ta, Pa, and 105 into aliphatic amine. J. Alloys Com. **271–273**, 292–295 (1998)
84. Trubert, D., Naour, C.Le, Guzman, F.M., Hussonnois, M., Brillard, L., Le Du, J.F., Constantinescu, O., Gasparro, J., Barci, V., Weiss, B., Ardisson, G.: Chemical isolation of dubnium (element 105) in fluoride media. Radiochim. Acta **90**, 127–132 (2002)
85. Tsukada, K., Haba, H., Asai, M., Toyoshima, A., Akiyama, K., Kasamatsu, Y., Nishinaka, I., Ichikawa, S., Yasuda, K., Miyamoto, Y., Hashimoto, K., Nagame, Y., Goto, S., Kudo, H., Sato, W., Shinohara, A., Oura, Y., Sueki, K., Kikunaga, H., Kinoshita, N., Yokoyama, A., Schädel, M., Brüchle, W., Kratz, J.V.: Adsorption of Db and its homologues Nb and Ta, and the pseudo-homologue Pa on anion-exchange resin in HF solution. Radiochim. Acta **97**, 83–89 (2009)
86. Kasamatsu, Y., Toyoshima, A., Asai, M., Tsukada, K., Li, Z., Ishii, Y., Toume, H., Sato, T.K., Kikuchi, T., Nishinaka, I., Nagame, Y., Haba, H., Kikunaga, H., Kudou, Y., Oura, Y., Akiyama, K., Sato, W., Ooe, K., Fujisawa, H., Shinohara, A., Goto, S., Hasegawa, T., Kudo, H., Nanri, T., Araki, M., Kinoshita, N., Yokoyama, A., Fan, F., Qin, Z., Düllmann, C.E., Schädel, M., Kratz, J.V.: Anionic fluoro complex of element 105. Db. Chem. Lett. **38**, 1084–1085 (2009)
87. Tsukada, K., Kasamatsu, Y., Asai, M., Toyoshima, A., Ishii, Y., Toume, H., Nagame, Y.: New apparatus AIDA-II for the study of aqueous chemistry of the transactinide elements. JAEA-Rev. **2008–054**, 67–68 (2008)
88. Kasamatsu, Y., Toyoshima, A., Haba, H., Toume, H., Tsukada, L., Akiyama, K., Yoshimura, Y., Nagame, Y.: Adsorption of Nb, Ta and Pa on anion-exchanger in HF and HF/HNO_3 solutions: model experiments for the chemical study of Db. J. Radioanal. Nucl. Chem. **279**, 371–376 (2009)
89. Myasoedov, B.F., Kirby, H.W., Tananaev, I.G.: Protoactinium. In: Morss, L.R., Edelstein, N.M., Fuger, J. (eds.) The Chemistry of the Actinide and Transactinide Elements, 3rd ed., vol. 1, pp. 161–252. Springer, Dordrecht (2006)
90. Di Giandomenico, M.V., Le Naour, C., Simoni, E., Guillaumont, D., Moisy, Ph, Hennig, C., Conradson, S.D., Den Auwer, C.: Structure of early actinides (V) in acidic solutions. Radiochim. Acta **97**, 347–353 (2009)

91. Kratz, J.V., Gober, M.K., Zimmermann, H.P., Schädel, M., Brüchle, W., Schimpf, E., Gregorich, K.E., Türler, A., Hannink, N.J., Czerwinski, K.R., Kadkhodayan, B., Lee, D.M., Nurmia, M.J., Hoffman, D.C., Gäggeler, H., Jost, D., Kovacs, J., Scherer, U.W., Weber, A.: New nuclide ^{263}Ha. Phys. Rev. C **45**, 1064–1069 (1992)
92. Gregorich, K.E., Hall, H.L., Henderson, R.A., Leyba, J.D., Czerwinski, K.R., Kreek, S.A., Kadkhodayan, B., Nurmia, M.J., Lee, D.M., Hoffman, D.C.: Fission branch in ^{259}Lr and confirmation of ^{258}Lr and ^{259}Lr mass assignments. Phys. Rev. C **45**, 1058–1063 (1992)
93. Gregorich, K.E., Kacher, C.D., Mohar, M.F., Lee, D.M., Lane, M.R., Sylvester, E., Hoffman, D.C., Schädel, M., Brüchle, W., Schausten, B., Schimpf, E., Kratz, J.V., Günther, R., Becker, U., Trautmann, N.: Search for the isotope 263 of element 104—a possible EC-branch in ^{263}Ha. GSI Scientific Report 1994, GSI 95-1, 14 (1995)
94. Kratz, J.V., Nähler, A., Rieth, U., Kronenberg, A., Kuczewski, B., Strub, E., Brüchle, W., Schädel, M., Schausten, B., Türler, A., Gäggeler, H.W., Jost, D.T., Gregorich, K.E., Nitsche, H., Laue, C., Sudowe, R., Wilk, P.A.: An EC-branch in the decay of 27-s ^{263}Db: evidence for the isotope ^{263}Rf. Radiochim. Acta **91**, 59–62 (2003)
95. Dvorak, J., Brüchle, W., Chelnokov, M., Dressler, R., Düllmann, Ch.E., Eberhardt, K., Gorshkov, A., Jäger, E., Krücken, R., Kuznetsov, A., Nagame, Y., Nebel, F., Novackova, Z., Qin, Z., Schädel, M., Schausten, B., Schimpf, E., Semchenkov, A., Thörle, P., Türler, A., Wegrzecki, M., Wierczinski, B., Yakushev, A., Yeremin, A.: Double magic nucleus $^{270}_{108}$Hs$_{162}$. Phys. Rev. Lett. **97**, 242501(4) (2006)
96. Dvorak, J., Brüchle, W., Chelnokov, M., Düllmann, Ch.E., Dvorakova, Z., Eberhardt, K., Jäger, E., Krücken, R., Kuznetsov, A., Nagame, Y., Nebel, F., Nishio, K., Perego, R., Qin, Z., Schädel, M., Schausten, B., Schimpf, E., Schuber, R., Semchenkov, A., Thörle, P., Türler, A., Wegrzecki, M., Wierczinski, B., Yakushev, A., Yeremin, A.: Observation of the 3*n* evaporation channel in complete hot-fusion reaction ^{26}Mg + ^{248}Cm leading to the new superheavy nuclide ^{271}Hs. Phys. Rev. Lett. **100**, 132503(4) (2008)
97. Dmitriev, S.N., Oganessyan, Yu Ts, Utyonkov, V.K., Shishkin, S.V., Yeremin, A.V., Lobanov, Y.V., Tsyganov, Y.S., Chepygin, V.I., Sokol, E.A., Vostokin, G.K., Aksenov, N.V., Hussonnois, M., Itkis, M.G., Gäggeler, H.W., Schumann, D., Bruchertseifer, H., Eichler, R., Shaughnessy, D.A., Wilk, P.A., Kenneally, J.M., Stoyer, M.A., Wild, J.F.: Chemical identification of dubnium as a decay product of element 115 produced in the reaction ^{48}Ca + ^{243}Am. Mendeleev Commun. **15**, 1–4 (2005)
98. Schumann, D., Bruchertseifer, H., Eichler, R., Eichler, B., Gäggeler, H.W., Dmitriev, S.N., Oganessian, Yu Ts, Utyonkov, V.P., Shishkin, S.V., Yeremin, A.V., Lobanov, Yu V., Tsyganov, Y.S., Chepygin, V.I., Sokol, E.A., Vostokin, G.K., Aksenov, N.V., Hussonnois, M., Itkis, M.G.: Chemical procedure applied for the identification of Rf/Db produced in the ^{48}Ca + ^{243}Am reaction. Radiochim. Acta **93**, 727–732 (2005)
99. Oganessian, Yu.Ts., Utyonkov, V.K., Dmitriev, S.N., Lobanov, Yu.V., Itkis, M.G., Polyakov, A.N., Tsyganov, Yu.S., Mezentsev, A.N., Yeremin, A.V., Voinov, A.A., Sokol, E.A., Gulbekian, G.G., Bogomolov, S.L., Iliev, S., Subbotin, V.G., Sukhov, A.M., Buklanov, G.V., Shishkin, S.V., Chepygin, V.I., Vostokin, G.K., Aksenov, N.V., Hussonnois, M., Subotic, K., Zagrebaev, V.I., Moody, K.J., Patin, J.B., Wild, J.F., Stoyer, M.A., Stoyer, N.J., Schaughnessy, D.A., Kenneally, J.M., Wilk, P.A., Lougheed, R.W., Gäggeler, H.W., Schumann, D., Bruchertseifer, H., Eichler, R.: Synthesis of elements 115 and 113 in the reaction ^{243}Am + ^{48}Ca. Phys. Rev. C **72**, 034611(16) (2005)
100. Oganessian, Yu.Ts., Utyonkov, V.K., Lobanov, Yu.V., Abdullin, F.Sh., Polyakov, A.N., Shirokovsky, I.V., Tsyganov, Yu.S., Gulbekian, G.G., Bogomolov, S.L., Mezentsev, A.N., Iliev, S., Subbotin, V.G., Sukhov, A.M., Voinov, A.A., Buklanov, G.V., Subotic, K., Zagrebaev, V.I., Itkis, M.G., Patin, J.B., Moody, K.J., Wild, J.F., Stoyer, M.A., Stoyer, N.J., Schaughnessy, D.A., Kenneally, J.M., Lougheed, R.W.: Experiments on the sysnthesis of element 115 in the reaction ^{243}Am(^{48}Ca,xn)$^{291-x}$115. Phys. Rev. C **69**, 021601(5) (2004)
101. Lazarev, YuA, Lobanov, YuV, Oganessian, Yu., Utyonkov, V.K., Abdullin, F.Sh, Buklanov, G.V., Gikal, B.N., Iliev, S., Mezentsev, A.N., Polyakov, A.N., Sedykh, I.M.,

Shirikovsky, I.V., Subbotin, I.G., Sukov, A.M., Tsyganov, Yu.S, Zhuchko, V.E., Lougheed, R.W., Moody, K.J., Wild, J.F., McQuaid, J.H.: Discovery of enhanced nuclear stability near the deformed shells N = 162 and Z = 108. Phys. Rev. Lett. **73**, 624–627 (1994)
102. Patyk, Z., Sobiczewski, A.: Ground-state properties of the heaviest nuclei analyzed in a multidimensional deformation space. Nucl. Phys. A **533**, 132–152 (1991)
103. Düllmann, Ch. E., Türler, A.: ^{248}Cm(^{22}Ne,xn)$^{270-x}$Sg reaction and the decay properties of ^{265}Sg reexamined. Phys. Rev. C **77,** 064320(10) (2008)
104. Haba, H. Kaji, D., Kikunaga, H., Kudou, Y., Morimoto, K., Morita, K., Ozeki, K., Sakai, R., Sumita, T., Yoneda, A., Kasamatsu, Y., Komori, Y., Shinohara, A., Kikunaga, H., Kudo, H., Nishio, K., Ooe, K., Sato, N., Tsukada, K.: Production of ^{265}Sg in the ^{248}Cm(^{22}Ne,5n)^{265}Sg reaction and decay properties of two isomeric states in ^{265}Sg. Phys. Rev. C **85**, 024611(11) (2012)
105. Schädel, M., Brüchle, W., Dressler, R., Eichler, B., Gäggeler, H.W., Günther, R., Gregorich, K.E., Hoffman, D.C., Hübener, S., Jost, D.T., Kratz, J.V., Paulus, W., Schumann, D., Timokhin, S., Trautmann, N., Türler, A., Wirth, G., Yakushev, A.: Chemical properties of element 106 (seaborgium). Nature **388**, 55–57 (1997)
106. Brüchle, W., Schausten, B., Jäger, E., Schimpf, E., Schädel, M., Kratz, J.V., Trautmann, N., Zimmermann, H.P., Bruchertseifer, H., Heller, W.: Fast tungsten separations with ARCA as a test for the chemical characterization of element 106. GSI Scientific Report 1991, GSI 92-1, 315 (1992)
107. Günther, R., Becker, H. U., Eberhardt, K., Zauner, S., Nähler, A., Kratz, J. V., Schädel, M., Brüchle, W., Jäger, E., Schimpf, E., Schausten, B.: Dependence of the transport efficiency of a He(KCl) gasjet on the electrostatical conditions Institut für Kernchemie, Univ. Mainz, Jahresbericht 1994, IKMZ 95-1, 7 (1995)
108. Schädel, M., Brüchle, W., Schausten, B., Schimpf, E., Jäger, E., Wirth, G., Günther, R., Kratz, J.V., Paulus, W., Seibert, A., Thörle, P., Trautmann, N., Zauner, S., Schumann, D., Andrassy, M., Misiak, R., Gregorich, K.E., Hoffman, D.C., Lee, D.M., Sylwester, E.R., Nagame, Y., Oura, Y.: First aqueous chemistry with seaborgium (element 106). Radiochim. Acta **77**, 149–159 (1997)
109. Türler, A., Brüchle, W., Dressler, R., Eichler, B., Gäggeler, H.W., Gregorich, K.E., Jost, D.T., Trautmann, N., Schädel, M.: Decay properties of ^{265}Sg ($Z = 106$) and ^{266}Sg ($Z = 106$). Phys. Rev. C **57**, 1648–1655 (1998)
110. Schädel, M., Brüchle, W., Jäger, E., Schausten, B., Wirth, G., Paulus, W., Günther, R., Eberhardt, K., Kratz, J.V., Seibert, A., Strub, E., Thörle, P., Trautmann, N., Waldek, A., Zauner, S., Schumann, D., Kirbach, U., Kubica, B., Misiak, R., Nagame, Y., Gregorich, K.E.: Aqueous chemistry of seaborgium ($Z = 106$). Radiochim. Acta **83**, 163–165 (1998)
111. Pershina, V., Kratz, J.V.: Solution chemistry of element 106: theoretical predictions of hydrolysis of group 6 cations Mo, W, and Sg. Inorg. Chem. **40**, 776–780 (2001)
112. Pfrepper, G., Pfrepper, R., Kronenberg, A., Kratz, J.V., Nähler, A., Brüchle, W., Schädel, M.: Continuous on-line chromatography of short lived isotopes of tungsten as homolog of seaborgium (element 106). Radiochim. Acta **88**, 273–278 (2000)
113. Kronenberg, A., Mohapatra, P.K., Kratz, J.V., Pfrepper, G., Pfrepper, R.: Anion-exchange behavior of Mo and W as homologs of Sg (element 106) in HCl and HNO_3 as well as in mixed HCl-HF and HNO_3-HF solutions. Radiochim. Acta **92**, 395–403 (2004)
114. Liang, X.H., Tsukada, K., Toyoshima, A., Li, Z.J., Asai, M., Sato, T.K., Sato, N., Nagame, Y.: Adsorption behavior of ^{181}W and ^{93m}Mo as lighter homologues of seaborgium (Sg) in HF/HNO_3 on anion-exchange resin. J. Radioanal. Nucl. Chem. **292**, 917–922 (2012)
115. Strub, E., Kratz, J.V., Brüchle, W., Jäger, E., Schädel, M., Schausten, B., Schimpf, E.: From ARCA to KRAUT: On the homestrecht for a seaborgium reduction experiment. Institut für Kernchemie, Univ. Mainz, Jahresbericht1999, IKMZ 2000-1, A11 (2000)
116. Pershina, V., Johnson, E., Fricke, B.: Theoretical estimates of redox potentials for group 6 elements, including element 106, seaborgium, in acid solutions. J. Phys. Chem. A **103**, 8463–8470 (1999)

117. Toyoshima, A., Kasamatsu, Y., Kitatasuji, Y., Tsukada, K., Haba, H., Shinohara, A., Nagame, Y.: Development of an electrochemistry apparatus for the heaviest elements. Radiochim. Acta **96**, 323–326 (2008)
118. Toyoshima, A., Kasamatsu, Y., Tsukada, K., Asai, M., Kitatsuji, Y., Ishii, Y., Toume, H., Nishinaka, I., Haba, H., Ooe, K., Sato, W., Shinohara, A., Akiyama, K., Nagame, Y.: Oxidation of element 102, nobelium, with flow electrolytic column chromatography on an atom-at-a-time scale. J. Am. Chem. Soc. **131**, 9180–9181 (2009)
119. Zhuikov, B.L., Kruz, H., Zvara, I.: Possibilities of chemical identification of short-lived isotopes of element 108 (in Russian). Report JINRP7-86-322, 26 (1985)
120. Düllmann, ChE, Eichler, B., Eichler, R., Gäggeler, H.W., Jost, D.T., Piguet, D., Türler, A.: IVO, a device for in site volatilization and on-line detection of products from heavy ion reactions. Nucl. Instrum. Meth. A **479**, 631–639 (2002)
121. Kirbach, U.W., Folden Iii, C.M., Ginter, T.N., Gregorich, K.E., Lee, D.M., Ninov, V., Omtvedt, J.P., Patin, J.B., Seward, N.K., Strellis, D.A., Sudowe, R., Türler, A., Wilk, P.A., Zielinski, P.M., Hoffman, D.C., Nitsche, H.: The cryo-thermochromatographic separator (CTS): A new rapid separation and $\propto$-detection system for on-line chemical studies of highly volatile osmium and hassium ($Z = 108$) tetroxides. Nucl. Instr. Meth. Phys. Res. A **484**, 587–594 (2002)
122. Von Zweidorf, A., Angert, R., Brüchle, W., Bürger, S., Eberhardt, K., Eichler, R., Hummrich, H., Jäger, E., Kling, H.-O., Kratz, J.V., Kuczewski, B., Langrock, G., Mendel, M., Rieth, U., Schädel, M., Schausten, B., Schimpf, E., Thörle, P., Trautmann, N., Tsukada, K., Wiehl, N., Wirth, G.: Evidence for the formation of sodium hassate (VIII). Radiochim. Acta **92**, 855–861 (2004)
123. Düllmann, ChE, Brüchle, W., Dressler, R., Eberhardt, K., Eichler, B., Eichler, R., Gäggeler, H.W., Ginter, T.N., Glaus, F., Gregorich, K.E., Hoffman, D.C., Jäger, E., Jost, D.T., Kirbach, U.W., Lee, D.M., Nitsche, H., Patin, J.B., Pershina, V., Piguet, D., Qin, Z., Schädel, M., Schausten, B., Schimpf, E., Schött, H.-J., Soverna, S., Sudowe, R., Thörle, P., Timokhin, S.N., Trautmann, N., Türler, A., Vahle, A., Wirth, G., Yakushev, A.B., Zielinski, P.M.: Chemical investigation of hassium (element 108). Nature **418**, 859–862 (2002)
124. Pershina, V., Bastug, T., Fricke, B., Varga, S.: The electronic structure and properties of group 8 oxides MO_4, where M = Ru, Os, and element 108, Hs. J. Chem. Phys. **115**, 792–799 (2001)
125. Pershina, V.: Theoretical investigations of the reactivity of MO_4 and the electronic structure of $Na_2[MO_4(OH)_2]$, where M = Ru, Os, and Hs (element 108). Radiochim. Acta **93**, 373–376 (2005)
126. Pershina, V., Anton, J., Jacob, T.: Fully relativistic density-functional-theory calculations of the electronic structures of MO_4 (M = Ru, Os, and element 108, Hs) and prediction of physisorption. Phys. Rev. A **78**, 0325181(5) (2008)
127. Persson, H., Skarnemark, G., Skålberg, M., Alstad, J., Liljenzin, J.O., Bauer, G., Haberberger, F., Kaffrell, N., Rogowski, J., Trautmann, N.: SISAK3—an improved system for rapid radiochemical separations by solvent extraction. Radiochim. Acta **48**, 177–180 (1989)
128. Alstad, J., Skarnemark, G., Haberberger, F., Herrmann, G., Nähler, A., Pense-Maskow, M., Trautmann, N.: Development of new centrifuges for fast solvent-extraction of transactinide elements. J. Radioanal. Nucl. Chem. **189**, 133–139 (1995)
129. Wierczinski, B., Eberhardt, K., Herrmann, G., Kratz, J.V., Mendel, M., Nähler, A., Rocker, F., Tharun, U., Trautmann, N., Weiner, K., Wiehl, N., Alstad, J., Skarnemark, G.: Liquid-scintillation spectroscopy of α-particle emitters and detection of spontaneous fission events for on-line studies of actinide and transactinide elements. Nucl. Instr. and Meth. in Phys. Res. A **370,** 532–538 (1996)
130. Wierczinski, B., Alstad, J., Eberhardt, K., Kratz, J.V., Mendel, M., Nähler, A., Omtvedt, J.P., Skarnemark, G., Trautmann, N., Wiehl, N.: Application of fast solvent extraction processes to studies of exotic nuclides. J. Radioanal. Nucl. Chem. **236**, 193–197 (1998)

131. Omtvedt, J.P., Alstad, J., Bjørnstad, T., Düllmann, ChE, Gregorich, K.E., Hoffman, D.C., Nitsche, H., Opel, K., Polakova, D., Samadani, F., Schulz, F., Skarnemark, G., Stavsetra, L., Sudowe, R., Zheng, L.: Chemical properties of the transactinide elements studied in liquid phase with SISAK. Eur. Phys. J. A **45**, 91–97 (2007)
132. Zheng, L., Alstad, J., Bjørnstad, T., Polakova, D., Stavsetra, L., Omtvedt, J.P.: Extraction of Nb and Ta, homologues of Db, from sulphulic acid solutions with TOA in toluene using SISAK. Radiochim. Acta **96**, 41–48 (2008)
133. Samadani, F., Alstad, J., Bjørnstad, T., Stavsetra, L., Omtvedt, J.P.: Development of a SISAK extraction system for chemical studies of element 108, hassium. Radiochim. Acta **98**, 757–764 (2010)
134. Samadani, F., Alstad, J., Schulz, F., Nilssen, J., Omtvedt, J.P., Ottesen, H.B., Qureshi, S., Düllmann, Ch.E., Gates, J.M., Jäger, E., Khuyagbaatar, J., Krier, J., Schädel, M., Schausten, B., Eberhardt, K., Even, J., Hild, D., Kratz, J.V., Roth, Ch., Wiehl, N., Türler, A., Yakushev, A.: Pilot-test experiment with Os of a AISAK setup for Hs-chemistry studies. Institut für Kernchemie, Univ. Mainz, Jahresbericht 2009, IKMZ-2010-1, A7 (2010)
135. Hild, D., Eberhardt, K., Kratz, J.V., Löb, P., Werner, B.: Liquid-liquid-extraction with the MicroSISAK-system. Institut für Kernchemie, Univ. Mainz, Jahresbericht 2008, IKMZ-2009-1, A18 (2009)
136. Ehrfeld, W., Hessel, V., Löwe, H.: Microreactors. Wiley-VCH, Weinheim (2000)
137. Ooe, K., Tashiro, Y., Saika, D., Kitamoto, Y., Matsuo, K., Takabe, T., Kuribayashi, T., Takahashi, N., Yoshimura, T., Sato, W., Takahisa, K., Shinohara, A.: Development of on-line solvent extraction system with microchips for heavy element chemistry. J. Nucl. Radiochem. Sci **8**, 59–62 (2007)
138. Oganessian, Yu.: Ts.: heaviest nuclei from ^{48}Ca-induced reactions. J. Phys. G: Nucl. Part. Phys. **34**, R165–R242 (2007)
139. Pyykkö, P.: Relativistic effects in structural chemistry. Chem. Rev. **88**, 563–594 (1988)
140. Pershina, V.: Electronic structure of properties of the transactinides and their compounds. Chem. Rev. **96**, 1977–2010 (1996)
141. Schwerdtfeger, P., Seth, M.: Relativistic effects of the superheavy elements. In: von R. Schleyer, P., Schreiner, P.R., Allinger, N.L., Clark, T., Gasteiger, J., Kollman, P.A., Schaefer III, H.F. (eds.) Encyclopedia of Computational Chemistry, vol. 4, pp. 2480–2498. Wiley, New York (1998)
142. Armbruster, P.: On the quest of production of superheavy nuclei in reactions of ^{48}Ca with the heaviest actinide targets. Eur. Phys. J. A **7**, 23–33 (2000)
143. Armbruster, P.: On the production of superheavy elements. Ann. Rev. Nucl. Part. Sci. **50**, 411–479 (2000)
144. Eichler, B., Kratz, J.V.: Electrochemical deposition of carrier-free radionuclides. Radiochim. Acta **88**, 475–482 (2000)
145. Türler, A., Düllmann, C.E., Gäggeler, H.W., Kirbach, U.W., Yakushev, A.B., Schädel, M., Brüchle, W., Dressler, R., Eberhardt, K., Eichler, B., Eichler, R., Ginter, T.N., Glaus, F., Gregorich, K.E., Hoffman, D.C., Jäger, E., Jost, D.T., Lee, D.M., Nitsche, H., Patin, J.B., Pershina, V., Piguet, D., Qin, Z., Schausten, B., Schimpf, E., Schött, H.-J., Soverna, S., Sudowe, R., Thorle, P., Timokhin, S.N., Trautmann, N., Vahle, A., Wirth, G., Zielinski, P.M.: On the decay properties of ^{269}Hs and indications for the new nuclide ^{270}Hs. Eur. Phys. J. A **17**, 505–508 (2003)
146. Hummrich, H., Banik, N.L., Breckheimer, M., Brüchle, W., Buda, R., Feist, F., Jäger, E., Kratz, J.V., Kuczewski, B., Liebe, D., Niewisch, L., Schädel, M., Schausten, B., Schimpf, E., Wiehl, N.: Electrodeposition methods in superheavy element chemistry. Radiochim. Acta **96**, 73–83 (2008)

Thermochemical Data from Gas-Phase Adsorption and Methods of Their Estimation

Robert Eichler and Bernd Eichler

Abstract Nowadays, gas-phase chromatography represents one of the fastest and most efficient techniques for the investigation of chemical properties of superheavy elements. The classical gas-adsorption chromatography experiment with transactinide species performed in an isothermal regime or in a temperature gradient, at ambient gas pressures, or under vacuum conditions delivers observables for single atomic species that are dependent on the parameters of the experiment. In Part I of this chapter we present several methods to derive thermodynamic data of the investigated species from these observables, which are not dependent on the experimental parameters and which are therefore intercomparable. A reversal of these methods suggests the behavior of transactinide species based on predicted thermochemical data, which is instrumental for the design of experiments. In Part II of this chapter we demonstrate several methods for the prediction of thermochemical properties of the heaviest elements based on chemical trends established in the Periodic Table. This provides data limits complementary to results of modern relativistic calculations. Finally, only the direct comparison of predicted data to experimental results allows for conclusions to be made on trends of chemical properties among transactinides and their corresponding homologs and for further improvement of the mostly empirical prediction models suggested here.

R. Eichler (✉)
Labor für Radio- und Umweltchemie, Paul Scherrer Institut, Villigen PSI, CH, Switzerland
e-mail: robert.eichler@psi.ch

B. Eichler
Rabenauer Weg 1, Oelsa D-01734, Germany
e-mail: bernd.eichler@tiebel-oelsa.de

M. Schädel and D. Shaughnessy (eds.), *The Chemistry of Superheavy Elements*,
DOI: 10.1007/978-3-642-37466-1_7,

1 Part I: Basic Principles of the Determination of Adsorption Properties Using Gas-Phase Adsorption Chromatographic Methods

1.1 Introduction

Volatilization, combined with gas-adsorption chromatographic investigations, is a well established method in nuclear chemistry. Fast reactions and high transport and separation velocities are crucial advantages of gas chromatography methods over alternative chemistry methods. Additionally, the fast sample preparation for α-spectroscopy and spontaneous fission (SF) measurements directly after the gas-phase separation is a very advantageous feature. Formation probabilities of defined chemical compounds and their volatility can be investigated on the basis of both experimentally determined and theoretically predicted thermochemical data: the latter are discussed in Part II of this chapter.

Volatile elements, as well as a large variety of volatile chemical compounds can be investigated by using a broad assortment of reactive carrier gases. Moreover, different stationary phase materials, available for gas-adsorption chromatography, are further broadening the areas of application; see Table 1. Apart from that, the separation quality can be influenced by the size of the chromatographic surface, e.g., introducing fills into the chromatography column. Experimental investigations were carried out in the temperature range from 85 K [1] to 2400 K [2]. Suitable chemical states and stationary phases exist for almost all elements to allow for their investigation via adsorption chromatography.

As the quantities of elements investigated in nuclear chemistry experiments are often small, down to one-atom-at-a-time, deposition and volatilization are predominately related to adsorption and desorption phenomena, respectively. Essentially, pure condensed phases do not occur. The entire gas-phase transport along the chromatography column is called gas-adsorption chromatography. The gas-phase transport through a chromatography column depends on several factors:

Table 1 Chemical states and the reactive carrier gases and stationary phases applicable for each

Chemical state	Typical reactive carrier gases	Typical stationary phases
Element (atomic state)	H_2, He, Ar	Fused silica, glass, metals, alumina, graphite, ice
Halides	Halogens, hydrogen halides, $SOCl_2$, CCl_4, BBr_3	Fused silica, glass, metals, alumina, alkaline chlorides, alkaline earth chlorides
Oxyhalides	Halogens + O_2, hydrogen halides + O_2	Fused silica, glass, metals, alumina, alkaline chlorides, alkaline earth chlorides
Oxides	O_2	Fused silica, glass, alumina
Oxyhydroxides/ Hydroxides	$O_2 + H_2O$	Fused silica, glass, alumina
Complex compounds	Beta diketones, CO, $AlCl_3$	Fused silica, glass

- Experimental parameters: e.g., flow rate and the type of carrier gas.
- The design of the chromatography columns like shape, material, and filling.
- The temperature, applied to the stationary phase.
- The interaction mechanism between the gaseous atoms and molecules with the stationary phase.

This chapter describes basic physico-chemical relationships between the gas-phase transport of atoms and molecules and their thermochemical properties, which are related to the adsorption–desorption equilibrium. These methods can either be used to predict the behavior of the adsorbates in the chromatographic processes, in order to design experiments, or to characterize the adsorbate from its experimentally observed behavior in a process. While Part I of this chapter is devoted to basic principles of the gas-phase transport and of the gas-adsorption process, the derivation of thermochemical data is discussed in Part II. Symbols used in the following sections of Part I are described in Sect. 1.5. Chapters "Experimental Techniques" and "Gas-Phase Chemistry of Superheavy Elements" discuss technical aspects and experimental results, respectively, which are related to the evaluation methods in gas-adsorption chromatography outlined in this chapter.

1.2 Thermochemical Description of the Transport of Substances in Gas-Adsorption Chromatography

1.2.1 The Adsorption Equilibrium

Here we consider the simple adsorption–desorption reaction equilibrium of a reversible mobile adsorption process:

$$A_{gas} \Leftrightarrow A_{ads} \tag{1}$$

The description of the chromatographic transport of a substance in an ideal linear gas chromatography is based on the differential equation for the transport velocity [3]:

$$\frac{dy}{dt} = \frac{u}{1 + k_i} \tag{2}$$

where k_i represents the partition coefficient corrected by the ratio of both phases, the solid and the gas phase:

$$k_i = \frac{s}{v} \cdot K_{ads} \tag{3}$$

For the formulation of the dimensionless adsorption equilibrium constant the definition of a standard state is crucial. The standard state is freely selectable,

regardless of the possibility of its physical realization. It is defined according to convenience. The standard state of adsorption is assumed to be the ratio of a standard molar volume to the standard molar surface [4].

$$\frac{V}{A} = \frac{c^o_{\text{ads}}}{c^o_{\text{gas}}} = 1cm\ (\text{cgs}) \ \rightarrow \ \frac{V}{100 \cdot A} = \frac{c^o_{\text{ads}}}{c^o_{\text{gas}}} = 1m\ (\text{SI}) \tag{4}$$

$$K = K_{\text{ads}} \cdot \frac{100 \cdot A}{V} = \frac{c_{\text{ads}}}{c_{\text{gas}}} \cdot \frac{c^o_{\text{gas}}}{c^o_{\text{ads}}} \tag{5}$$

The dimensionless equilibrium constant of a simple reversible adsorption reaction is related to thermodynamic standard quantities—the standard adsorption enthalpy and the standard adsorption entropy, which are assumed to be temperature independent:

$$\Delta G^0_{\text{ads}} \ = \ -R \cdot T \cdot ln\,(K) \ = \ \Delta H^0_{\text{ads}} \ - \ T \cdot \Delta S^0_{\text{ads}} \tag{6}$$

For a localized adsorption the concentration of the adsorption sites has to be taken into account [4]. In other cases a reversible change of the chemical state of the adsorbate in the chromatography process has to be considered, e.g., dissociative adsorption and substitutive adsorption as described in Part II of this chapter (Sect. 1.3, Eqs. 55, 56). The reaction enthalpy and entropy have to be introduced into the calculations [5–8] as well as the equilibrium constant for the chemical reaction including the standard states of the occurring chemical states as:

$$K = K_r \cdot K_{\text{ads}} \cdot \frac{100 \cdot A}{V} \tag{7}$$

$$\Delta G^o_{r,\text{ads}} = -R \cdot T \cdot ln(K) = (\Delta H^o_r + \Delta H^o_{\text{ads}}) - T \cdot (\Delta S^o_r + \Delta S^o_{\text{ads}}) \tag{8}$$

The entropy of the mobile adsorption process can be determined from the model given in [4]. It is based on the assumption that during the adsorption process a species in the gas phase, which has three degrees of freedom (translation), is transferred into the adsorbed state with two translational degrees of freedom parallel to the surface and one vibrational degree of freedom vertical to the surface. From statistical thermodynamics the following equation for the calculation of the adsorption entropy is derived:

$$\Delta S^o_{\text{ads}} = R \cdot \left(ln(\frac{100 \cdot A}{V \cdot v_b}) \cdot \sqrt{\frac{R \cdot T}{2 \cdot \pi \cdot M_a}} + \frac{1}{2} \right) \tag{9}$$

As a good approximation it is assumed that the adsorbed species are vibrating in resonance with the lattice phonon vibrations of the solid stationary phase. The phonon frequency can be evaluated from phonon spectra, from the standard entropy of solid metals, from the Debye temperatures, or from the Lindemann equation [9].

1.2.2 Isothermal Gas Chromatography

Combining Eqs. (2–6), including the linear temperature dependency of the carrier gas flow rate, and integrating over the column length the following relation for the retention time in isothermal gas chromatography is obtained [10]:

$$t_r = \frac{L \cdot T_o \cdot \varnothing}{\overline{V}_o \cdot T_{\mathrm{iso}}} \cdot \left[1 + \frac{s}{v} \cdot \frac{V}{100 \cdot A} \cdot \exp\left(-\frac{\Delta H^o_{\mathrm{ads}}}{R \cdot T_{\mathrm{iso}}}\right) \cdot \exp\left(\frac{\Delta S^o_{\mathrm{ads}}}{R}\right)\right] \tag{10}$$

The first addend in Eq. (10) can be neglected. Thus the retention volume is calculated as:

$$ln\left(t_r \cdot \overline{V}_o \cdot \frac{T_{\mathrm{iso}}}{T_o}\right) = ln\left(\frac{L \cdot \varnothing \cdot s \cdot V}{v \cdot 100 \cdot A}\right) + \left(-\frac{\Delta H^o_{\mathrm{ads}}}{R \cdot T_{\mathrm{iso}}}\right) + \left(\frac{\Delta S^o_{\mathrm{ads}}}{R}\right) \tag{11}$$

In experiments with long-lived nuclides species, with $T_{1/2}$ much longer than the experimental duration, the retention time equals the time of the experimental duration. However, for short-lived nuclides, at the temperature where 50% of the species containing a specific nuclide pass the isothermal chromatography column, the retention time equals the half-life of the nuclide:

$$t_r = T_{1/2} \tag{12}$$

Using the mobile adsorption entropy (Eq. 9) ΔH_{ads} can be evaluated from at least a pair of experiments at two different isothermal temperatures under otherwise identical experimental conditions.

1.2.3 Thermochromatography

Gas Thermochromatography

The given description of the gas-phase transport in a tube with a temperature gradient is only valid for the adsorption equilibrium of reversible mobile adsorptions without any superimposed chemical reaction. The temperature profile along the chromatography column is approximated to be linear by:

$$T = T_s - a \cdot y \tag{13}$$

The substitution of the corrected partition coefficient and the introduction of the standard state (Eqs. 3–5) lead to:

$$t_r = -\frac{1}{a} \cdot \int_{T_s}^{T_{\mathrm{dep}}} \frac{\left(1 + \frac{s}{v} \cdot \frac{V}{100 \cdot A} \cdot K(T)\right)}{u(T)} \cdot dT \tag{14}$$

Introducing

$$u(T) = u_o \cdot \frac{T}{T_o} \tag{15}$$

and

$$u_o = \frac{\bar{V}_o}{\varnothing} \tag{16}$$

the integration yields

$$t_r = -\frac{T_o}{a \cdot u_o} \cdot \ln\left(\frac{T_{\mathrm{dep}}}{T_s}\right) + \frac{s \cdot \varnothing \cdot T_o \cdot \frac{V}{100 \cdot A} \cdot \exp\left(\frac{\Delta S^o_{\mathrm{ads}}}{R}\right)}{\overline{V}_o \cdot a \cdot v} \cdot \left[Ei^*\left(-\frac{\Delta H^o_{\mathrm{ads}}}{R \cdot T_{\mathrm{dep}}}\right) - Ei^*\left(-\frac{\Delta H^o_{\mathrm{ads}}}{R \cdot T_s}\right)\right] \tag{17}$$

where Ei*(x) is the exponential integral function of x. This function can be estimated by:

$$Ei^*(x) = \frac{exp(x)}{x} \quad (\text{for } x \gg 1) \tag{18}$$

The first addend in Eq. (17) is negligible for $T_{\mathrm{dep}} \ll T_s$, which is usually the case and

$$Ei^*\left(-\frac{\Delta H^o_{\mathrm{ads}}}{R \cdot T_{\mathrm{dep}}}\right) \gg Ei^*\left(-\frac{\Delta H^o_{\mathrm{ads}}}{R \cdot T_s}\right) \tag{19}$$

Hence, the following simplification [11] is conceivable:

$$\frac{a \cdot t_r \cdot \overline{V}_o}{s \cdot T_{\mathrm{dep}} \cdot \frac{V}{100 \cdot A}} = \left(\frac{R \cdot T_o}{-\Delta H^o_{\mathrm{ads}}}\right) \cdot \exp\left(-\frac{\Delta H^o_{\mathrm{ads}}}{R \cdot T_{\mathrm{dep}}}\right) \cdot \exp\left(\frac{\Delta S^o_{\mathrm{ads}}}{R}\right) \tag{20}$$

Thus, the deposition temperature and the thermodynamic state function of the adsorption are combined and they can easily be determined from each other. The retention time for a short-lived radioactive species is calculated as the radioactive lifetime of the nuclide:

$$t_r = \frac{T_{1/2}}{\ln(2)} \tag{21}$$

or equals the duration of the experiment for a long-lived species, having a $T_{1/2}$ much longer than the experimental duration. Note, that Eqs. (17) and (20) are only valid if the chemical state of the investigated species does not change along the entire temperature range. A simplification of Eq. (17) is not possible if very short-lived nuclides ($T_{1/2} < 1$ s) are investigated. Numerical integration methods have to be used instead. Using the mobile adsorption entropy (Eq. 9) ΔH_{ads} can be

evaluated from one experiment. If several experiments are performed at varied experimental parameters over large ranges, e.g., varying the experimental duration or the gas flow rate, ΔH_{ads} and ΔS_{ads} can be evaluated from an Arrhenius-type plot.

Vacuum Thermochromatography

The model of ideal linear gas chromatography (Eq. 2) also describes the transport of a chemical species along the temperature gradient of a vacuum tube [12]. At molecular flow conditions, the linear velocity of the carrier gas, which is identical to the transport velocity of the adsorbate in the gas phase, has to be substituted by the fraction of the column length over the average retention time of the species in the column:

$$u = \frac{y}{t_r} = \frac{4 \cdot d_i \cdot \sqrt{\frac{2 \cdot \pi \cdot k \cdot T}{m}}}{3 \cdot y} \tag{22}$$

The deposition site of a species in a defined temperature region under conditions where the retention time in the adsorbed state exceeds the duration of the experiment is assumed to be similar to a corresponding effective length of the column at which this species would have exited. This length is the distance of the deposition region, T_{dep}, from the beginning of the column held at T_s. Thus, the average retention time is a function of the column volume and the conductivity (geometric shape) of the column for inert gas-phase species at molecular flow conditions. The probability of residence of the species in the adsorbed state is mainly dependent on the temperature-dependent equilibrium constant and thus, on the thermochemical constants of the adsorption reaction. Increasing the adsorption probability by lowering temperatures decreases the migration velocity of the adsorbate zone. A limited experiment duration or radioactive lifetime of the species leads to a deposition zone of the adsorbate in the column or a zone of increased decay observations, respectively. Applying Eqs. (2) and (22) and substituting the corrected partition coefficient by a gas phase kinetic formulation of the adsorption equilibrium constant:

$$k_i = \frac{4}{d_i} \cdot \frac{h}{k \cdot T} \cdot \sqrt{\frac{k \cdot T}{2 \cdot \pi \cdot m}} \cdot \exp\left(-\frac{\Delta H^o_{ads}}{R \cdot T}\right) \tag{23}$$

gives the following functional dependency between the retention time, the experimental parameters, T_{dep} and ΔH_{ads}:

$$t_r = 2 \cdot A \cdot \left(\frac{1}{3} \cdot \sqrt{T_{\text{dep}}^3} - T_s \cdot \sqrt{T_{\text{dep}}} + \frac{2}{3} \cdot \sqrt{T_s^3} \right) + \\ + B \cdot \left[T_{\text{dep}} \cdot \exp\left(-\frac{\Delta H_{\text{ads}}^o}{R \cdot T_{\text{dep}}} \right) - T_s \cdot \left(-\frac{\Delta H_{\text{ads}}^o}{R \cdot T_{\text{dep}}} \right) \right] + \\ + B \cdot \left(T_s - \left(-\frac{\Delta H_{\text{ads}}^o}{R} \right) \right) \cdot \left[\text{Ei}^* \left(-\frac{\Delta H_{\text{ads}}^o}{R \cdot T_{\text{dep}}} \right) - \text{Ei}^* \left(-\frac{\Delta H_{\text{ads}}^o}{R \cdot Ts} \right) \right] \tag{24}$$

with

$$A = \frac{3}{4 \cdot a^2 \cdot d_i \cdot \sqrt{\frac{2 \cdot \pi \cdot k}{m}}} \tag{25}$$

and

$$B = \frac{3 \cdot h}{2 \cdot a^2 \cdot d_i^2 \cdot k} \tag{26}$$

For practical applications some simplifications [13] result in:

$$t_r = \frac{R \cdot T_s \cdot T_{\text{dep}} \cdot B}{-\Delta H_{\text{ads}}^o} \cdot \exp\left(-\frac{\Delta H_{\text{ads}}^o}{R \cdot T_{\text{dep}}} \right) \tag{27}$$

with B taken from Eq. (26).

Hence, from the experimental parameters and from the measured deposition temperature, the adsorption enthalpy ΔH_{ads}^o can be determined directly. Again this simplification holds only for $t_r \gg 1$ s [14, 15]. For experiments with very short-lived nuclides Eqs. (13, 21–23) have to be substituted into Eq. (2) and the resulting integral has to be solved numerically.

Introducing the mobile adsorption model into this derivation [16] k_i from Eq. (23) changes to:

$$k_i = \frac{4}{d_i} \cdot \frac{V}{100 \cdot A} \exp\left(\frac{\Delta S_{\text{ads}}^o}{R} \right) \cdot \exp\left(-\frac{\Delta H_{\text{ads}}^o}{R \cdot T} \right) \tag{28}$$

Then Eqs. (9, 13, 21, 22, and 28) have to be merged into Eq. (2) and, again, the resulting integral can be solved numerically.

1.3 Microscopic Kinetic Description of the Adsorption Process in Gas Chromatography: Monte-Carlo Methods

This section explains basic principles of Monte-Carlo models, which are also successfully applied for the evaluation of adsorption enthalpies in gas-phase and vacuum adsorption chromatography investigations of the heaviest elements and their lighter homologs (see chapters “Experimental Techniques” and “Gas-Phase

Chemistry of Superheavy Elements"). The application of Monte-Carlo simulation methods in gas-phase adsorption chromatography is based on ideas given in [17]. All models use a microscopic description of the chromatographic adsorption–desorption process on the atomic scale. Hence, they are kinetic models of gas-adsorption chromatography. They can be applied to thermochromatography as well as to chromatography in the isothermal regime. To determine ΔH^o_{ads} of the adsorbate on the stationary phase the experimental parameters and the physical data of the carrier gases and of the adsorbate are used as an input into these models. For a set of ΔH^o_{ads} values, which is the only varied parameter, the simulation yields chromatograms, which have to be compared to the experimental result. The resulting ΔH^o_{ads} value is obtained from the best agreement between the model and experiment. The simulation can be either used for an evaluation of the ΔH^o_{ads} from gas-adsorption chromatographic results or, vice versa, to predict the behavior of an adsorbate in gas chromatography from its known adsorption data and hypothetical experimental data.

1.3.1 Gas Chromatography with Carrier Gases

A flow chart of the Monte-Carlo model is presented in Fig. 1. The formalism can easily be adapted to a PC-based program. The formulas used in the PC-based simulation are given here. For their derivations see [17–22]. The Monte-Carlo principle uses random numbers which are selected between 0 and 1 and are never equal to 1.

The randomized values in the Monte-Carlo simulation of a gas-phase adsorption process for radioactive species are:

1. The radioactive lifetime.

For every given atom a *random* lifetime, which is distributed logarithmically according to the radioactive decay law with the half-life, $T_{1/2}$, of the nuclide is calculated as:

$$t_\lambda = -\frac{\ln(2)}{T_{1/2}} \cdot \ln(1 - random) \tag{29}$$

2. The jump length and the time of flight in the gas phase.

The mean jump length of the adsorbate can be approximated by Golay's approach [18] for cylindrical columns:

$$Y_{jm} = \frac{11 \cdot \overline{V}(p,T)}{48 \cdot \pi \cdot D(p,T)} \tag{30}$$

For rectangular channels the derivations given in [19, 20] shall be considered.

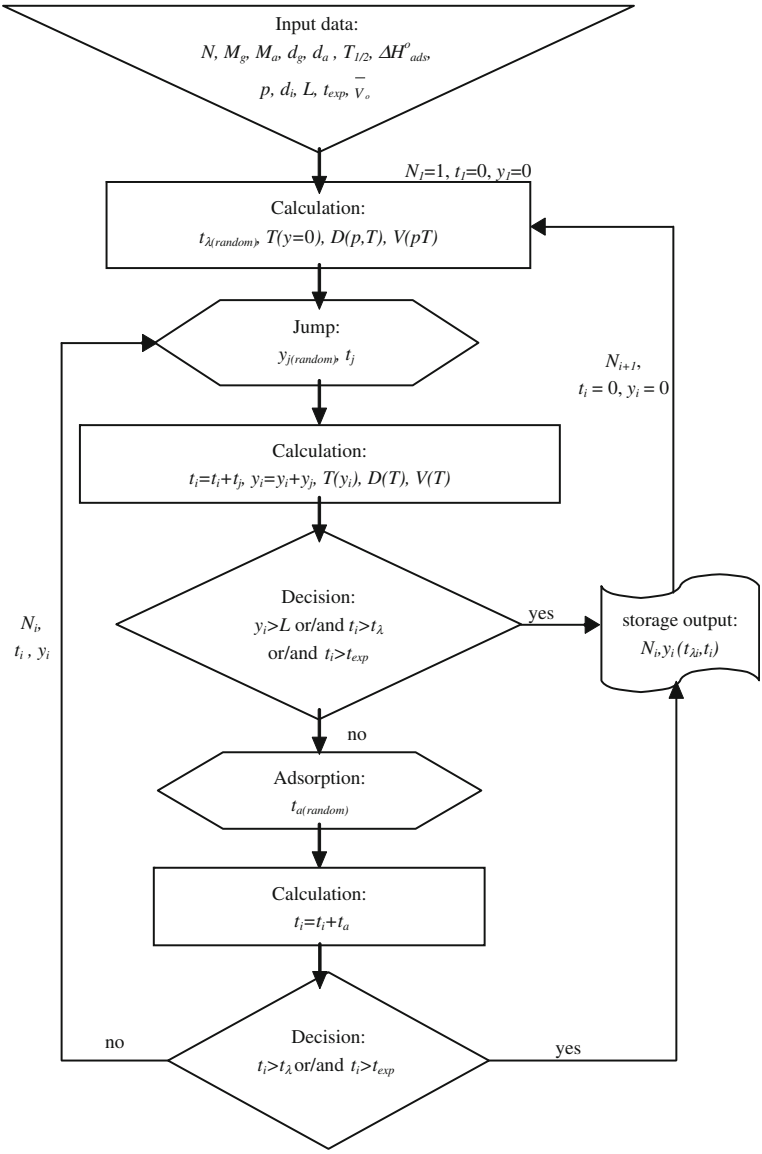

Fig. 1 Flow chart of the PC-based Monte-Carlo simulation of gas chromatography. The indices *i* and *j* stand for the number of the atom and of the individual jump, respectively

The pressure and temperature dependent diffusion coefficient of the adsorbate (*a*) in the carrier gas (*g*) is either tabulated or is approximated, e.g., according to Gilliland's empirical equation [21]:

$$D = 0.43 \cdot 10^{-6} \cdot \frac{T^{1.5}}{p} \cdot \sqrt{\frac{1}{M_g} + \frac{1}{M_a}} \cdot \left(\sqrt[3]{\frac{d_g}{M_g}} + \sqrt[3]{\frac{d_a}{M_a}} \right)^{-2} \left[\mathrm{m}^2 \cdot \mathrm{s}^{-1} \right] \tag{31}$$

The gas flow also depends on the temperature and on the pressure. Assuming an ideal gas behavior of the carrier gas it can be calculated from the flow rate under standard conditions:

$$\overline{V}(p,T) = \overline{V}_o \cdot \frac{T \cdot p_o}{T_o \cdot p} \tag{32}$$

Subsequently, the random jump length along the column, which is distributed logarithmically, is calculated as:

$$y_j = -Y_{\mathrm{jm}} \cdot \ln(1 - \mathrm{random}) \tag{33}$$

Thus, the time the atom remains in the gas phase, i.e., the time of flight can be derived:

$$t_j = \frac{y_j \cdot \pi \cdot d_i^2}{4 \cdot \overline{V}(p,T)} \tag{34}$$

3. The residence time.

The mean number of wall collisions along Y_{jm} is:

$$N_m = Y_{\mathrm{jm}} \cdot \frac{d_i}{2 \cdot \overline{V}(p,T)} \cdot \sqrt{\frac{2 \cdot \pi \cdot R \cdot T}{M_a}} \tag{35}$$

The mean residence time of the atom in the adsorbed state is calculated by a Frenkel-type equation:

$$t_{\mathrm{am}} = \frac{1}{\nu_b} \cdot \exp\left(-\frac{\Delta H^o_{\mathrm{ads}}}{R \cdot T} \right) \tag{36}$$

The overall residence time of the atom in the adsorbed state between two jumps is assumed to be distributed logarithmically and can be calculated as:

$$t_a = -N_m \cdot t_{\mathrm{am}} \cdot \ln(1 - \mathrm{random}) \tag{37}$$

1.3.2 Gas Chromatography in Vacuum

A Monte-Carlo simulation of gas chromatography under vacuum conditions was suggested in [16] and follows the same scheme as of Fig. 1.

The lifetime of each atom or molecule is calculated using Eq. (29). The mean residence time of the atom in the adsorbed state at a defined temperature is

calculated using Eq. (36). The residence time of the atom in the adsorbed state, which is distributed logarithmically, can be calculated as:

$$t_a = -t_{\text{am}} \cdot \ln(1 - \text{random}) \tag{38}$$

The transport of species along the chromatography column is assumed to be dependent only on the solid angle of the desorption direction and on the dimensions of the column.

The solid angles of desorption from a plane surface into the vacuum are calculated according to Knudsen [22] assuming a cosine law:

$$\theta = \arcsin\sqrt{\text{random}} \tag{39}$$

$$\varphi = 2 \cdot \pi \cdot \text{random} \tag{40}$$

It is well presented in [20] that the corresponding straight flight length to the next surface in a cylindrical tube is calculated as:

$$Y_j = d_i \cdot \frac{\cos(\theta)}{\left(1 - \sin^2(\theta) \cdot \sin^2(\varphi)\right)} \tag{41}$$

The corresponding jump length projected to the column wall of a cylindrical tube is calculated as:

$$y_j = d_i \cdot \frac{\cos(\theta) \cdot \sin(\theta) \cdot \sin(\varphi)}{\left(1 - \sin^2(\theta) \cdot \sin^2(\varphi)\right)} \tag{42}$$

The velocity of the atoms can be set as the arithmetic mean velocity from the Maxwell–Boltzmann distribution. It only depends on the temperature and their molecular weight:

$$\overline{v} = \sqrt{\frac{8 \cdot R \cdot T}{\pi \cdot M_a}} \tag{43}$$

Hence, the time the atom is in flight can be calculated as:

$$t_j = \frac{Y_j}{\overline{v}} \tag{44}$$

For simplicity, the column is assumed to be "closed" at the "entrance", i.e., the atoms cannot escape from the side of the column where they entered.

1.4 Summary

Some advantages and disadvantages of the thermodynamic and the kinetic approach are summarized here to facilitate the decision as to which approach should be selected for the subsequent data evaluation from a gas-phase chromatography experiment.

1. Advantages of the thermodynamic model:

   - It is less time consuming.
   - Experiments, where complex stationary phases have been used (e.g., filled columns) can be evaluated.

2. Disadvantages of the thermodynamic model:

   - A linear temperature gradient has to be assumed;
   - Possible "long jumps" cannot be described in the model of linear gas chromatography. Hence separation factors are overestimated, especially in open columns.
   - The radioactive decay time is uniformly approximated through an average lifetime.

3. Advantages of the kinetic Monte-Carlo model:

   - A description of the microscopic chromatographic process at realistic temperature conditions at the surfaces (real temperature gradient) is possible.
   - The probability distribution of the radioactive decay time of the adsorbate is included.
   - The probability that the adsorbate is transported along the column by "long jumps" is taken into account, which is important to describe the chromatographic separation quality, especially in open columns and at high gas flow rates.

4. Disadvantages of the kinetic Monte-Carlo model:

   - The evaluation might be more time consuming, due to the Monte-Carlo programming.
   - The stationary surface geometry has to be simple.

1.5 Symbols

A	…	Inner surface per 1 m column length, m^2
A	…	Negative temperature gradient, K/m
c_{ads}	…	Surface concentration of the adsorbate, particles/m^2
c^0_{ads}	…	Standard surface concentration of the adsorbate, 2.679×10^{23} particles/m^2
c_{gas}	…	Gas concentration of the adsorbate, particles/m^3
c^o_{gas}	…	Standard gas concentration of the adsorbate, 2.679×10^{25} particles/m^3 (ideal gas at STP)
d_a	…	Density of the adsorbate at its melting point, kg/m^3
d_g	…	Density carrier gas at its melting point, kg/m^3

(continued)

(continued)

d_i	…	Inner diameter of the column, m
D	…	Diffusion coefficient of the adsorbate in the carrier gas, m^2/s
$\varnothing$	…	Free open cross-sectional area of the column, m^2
φ, θ	…	Solid angles of desorption
H	…	Planck's constant, J·s
ΔG^o_{ads}	…	Free standard adsorption enthalpy of adsorption, J/mol
$\Delta G^o_{r,\text{ads}}$	…	Free standard adsorption enthalpy with chemical reaction, J/mol
ΔH^o_{ads}	…	Standard adsorption enthalpy at zero surface coverage, J/mol
ΔH^o_r	…	Standard reaction enthalpy, J/mol
K	…	Equilibrium constant of adsorption, dimensionless
K_{ads}	…	Distribution constant, m
k_i	…	Partition coefficient corrected by the phases, dimensionless
K_r	…	Reaction equilibrium constant, dimensionless
K	…	Boltzmann constant, J/K
L	…	Length of the column, m
M	…	Atomic or molecular mass of the adsorbate, kg
M_a	…	Molar weight adsorbate, kg/mol
M_g	…	Molar weight carrier gas, kg/mol
N	…	Number of atoms
N_m	…	Mean number of wall collisions
v_b	…	Maximum lattice phonon vibration frequency, 1/s
P	…	Pressure, Pa
p_o	…	Standard pressure, 101325 Pa
Random	…	Random number
R	…	Gas constant, 8.31441 J/mol·K
S	…	Open surface of the column per 1 m column length, m^2
ΔS^o_{ads}	…	Standard entropy of adsorption at zero surface coverage, J/mol·K
T	…	Time, s
t_a	…	Time the adsorbate keeps adsorbed, s
t_{am}	…	Mean time the adsorbate keeps adsorbed, s
t_{exp}	…	Duration of the experiment, s
t_j	…	Transport time, s
t_λ	…	Lifetime, s
t_r	…	Retention time, s
T	…	Temperature, K
T_{dep}	…	Deposition temperature, K
T_{iso}	…	Isothermal temperature, K
T_o	…	Standard temperature, 298.15 K
$T_{1/2}$	…	Half-life, s
T_s	…	Upper (start) temperature of the gradient, K
U	…	Carrier gas velocity, m/s
u_o	…	Carrier gas velocity at STP, m/s

(continued)

(continued)

V	…	Inner volume of the column, m^3
V	…	Open volume of the column per 1 m column length, m^3
$\overline{V}$	…	Carrier gas flow, m^3/s
$\overline{V}_o$	…	Carrier gas flow at STP, m^3/s
Y	…	Coordinate longitudinal to the column, m
y_j	…	Jump length, m
Y_j	…	Path length, m
Y_{jm}	…	Mean jump length, m

2 Part II: Derivation of Thermochemical Data with Respect to the Periodicity of Properties and Their Interrelations

2.1 Introduction

The discovery of new chemical elements—the transactinides or superheavy elements—stimulated the work on theoretical predictions of their chemical properties. Our intention is to present in Part II of this chapter empirical methods from [23–37] and from our partly unpublished work [38–50], which are used to predict chemical properties of elements and compounds relevant to gas-phase chemical studies of transactinides.

Gas-phase chemical methods can be successfully applied to the chemical characterization of transactinides. They provide a fast separation of transactinides from a wide variety of by-products, which are instantly produced in the nuclear formation reactions of transactinides. These methods are mainly based on the measurement of adsorption properties of the atomic or molecular state of transactinides on different stationary phases.

Due to the extremely low production rates of transactinides in nuclear fusion reactions, all chemical characterizations are carried out at the single atom level (see chapter "Fundamental and Experimental Aspects of Single Atom-at-a-Time Chemistry"). The chemical reaction products are characterized on the basis of their behavior in the separation process or, to be exact, in the gas-phase-adsorption chromatographic process (see Part I of this chapter). In this process the formation probability of defined stable chemical states of transactinides and the subsequent interaction of the formed species with a solid state surface are studied.

The stability and the volatility are chemical properties that define the behavior of a transactinide element or its compound in the gas-adsorption chromatographic process. Therefore, the predictions of these properties are instrumental for the design of experiments (see Chapter "Experimental Techniques" for instrumental aspects) and they are also indispensable for the interpretation of experimental

results; see chapter "Gas-Phase Chemistry of Superheavy Elements". "Empirical" and "exact" methods are both of high importance for the prediction of properties of transactinide elements. The "exact" ab initio methods, which are described in chapter "Theoretical Chemistry of the Heaviest Elements", yield the atomic ground state configuration, ionization potentials, atomic radii, and ionic radii as well as binding energies in isolated single gaseous molecules of defined chemical compounds with high accuracy. However, it still appears impossible to exactly calculate the behavior of a single atom or molecule in a given experimental setup. For the ab initio calculation of the stability of pure solid phases, which is necessary for the evaluation of the volatility[1] of compounds, the accuracy of the available methods is limited. Therefore, up to now, only empirical methods have been used to predict the volatility of compounds. These predictions represent an important part in the multiple step process of the chemical characterization of transactinide elements.

The main steps in this process are:

I. The evaluation of thermochemical data of chemical compounds in the solid and in the gaseous phase.
II. Calculations of the volatilities of the elements and of their compounds.
III. The experimental determination of empirical correlations between the volatility of the pure macroscopic phase and the adsorption behavior of single atoms or molecules on defined surfaces.
IV. The prediction of the adsorption behavior of transactinides or their compounds at zero surface coverage from the predicted volatility (II.) applying the empirical correlations (III.).
V. The physico-chemical description of the gas-adsorption chromatographic process.
VI. Model experiments using short-lived nuclides of lighter homologs for the determination of reaction rates, retention times, and decontamination.
VII. Design of an experimental setup for experiments with transactinides with respect to the predicted properties and its half-life using III. and V.
VIII. The interpretation of the results according to the:

- formation of compounds with similar volatility as known from their homologs,
- relative volatility of equivalent chemical compounds compared with the homologs,
- adsorption enthalpies and the volatilities of fictive macroscopic phases,
- confirmation and/or improvement of prediction methods of the chemical reaction behavior and of the volatility, and
- periodicity of chemical properties and trends along the groups of the Periodic Table.

[1] The term volatility as it is used here clearly and only relates to the macroscopic property sublimation enthalpy. Note, that volatility is often used in a rather sloppy and imprecise way to describe the microscopic adsorption behavior of single atoms on surfaces.

This contribution focuses on steps I–V. Steps VI–VIII are partly discussed in chapters "Experimental Techniques" and "Gas-Phase Chemistry of Superheavy Elements".

2.2 Thermochemical Data

2.2.1 Extrapolative Analysis of Thermochemical Data for Transactinides and Their Compounds

It is assumed that the stability of a chemical state can be expressed in terms of the standard formation enthalpies of gaseous and solid compounds $\Delta_f H^o_{298}(\mathrm{g,s})$ and of their atomic standard formation enthalpies $\Delta_f H^*_{298}(\mathrm{g,s})$. Both values differ only by the presumed elemental state: The first value refers to the standard state of the gaseous element and the second one to the gaseous monatomic state of the element at standard conditions. These values represent relative stability measures in combination with a competing chemical state. Thermochemical state functions describe the behavior of a large number of atoms or molecules. For the description of single atoms we use these values as a measure of the formation probability of different chemical states and to quantify the binding energy in molecules. Gas-adsorption chromatography is a multi-step process, during which a single atom or molecule changes its chemical state in thousands of adsorption–desorption steps. Therefore, the resulting information on the adsorption properties of the investigated chemical species is as reliable as the results from experiments with a very large number of atoms or molecules from a one-step evaporation-deposition experiment. For more detailed information on this topic see Chapter "Fundamental and Experimental Aspects of Single Atom-at-a-Time Chemistry".

Trends of chemical properties of the elements and their compounds exist within the groups of the Periodic Table. Therefore, assuming that all transactinides systematically belong to defined groups, rough estimates about their chemical properties should be feasible. For these estimates, shell effects and relativistic effects, which depend on the atomic number and lead to discontinuous variations of properties along the groups, have to be considered [51–58]. Examples for such effects are: the half occupancy of electron shells, which has a larger effect on the chemical properties of elements with lower atomic numbers, and the sub-shell closure of the *p*-, *d*-, and *f*-electron levels with an increasingly strong spin–orbit coupling for elements at the higher number periods up to the transactinides. A detailed discussion of relativistic effects including the spin–orbit coupling can be found in Chapter "Theoretical Chemistry of the Heaviest Elements". In general, elements with a shell closure or a half-filled electron shell in their ground state configuration form relatively volatile condensed phases and less stable chemical compounds compared to elements in the same group, which do not exhibit such effects. This creates a dilemma for extrapolative predictions of thermochemical

data of transactinides along their groups as these configurations change with atomic or period number. Anyhow, no direct functional dependence exists between thermochemical state functions and electron configurations.

In the following part, several possibilities are outlined, which can be used to master the described dilemma. Hence, more trustworthy extrapolative predictions are obtained by correlating thermochemical state functions mutually. In this case electron shell effects in the homologues are already implemented. To estimate standard formation data of transactinide compounds in their solid and in their gaseous states, the standard enthalpies of monatomic gaseous elements $\Delta H^{*}_{298}\left(\mathrm{E}_{(\mathrm{g})}\right)$ are of fundamental importance. They are used as primary input values for extrapolative predictions and they are mostly equal to the standard sublimation enthalpy $\Delta H^{\circ}_{\mathrm{subl}}$ of these elements. They have to be estimated empirically for the transactinides, though. Experimentally deduced tabulated thermochemical data of the lighter homologs in the corresponding groups of the transactinides in the Periodic Table include relativistic effects in their electronic structure. Hence, rough estimations, e.g., of $\Delta H^{\circ}_{\mathrm{subl}}$ can be obtained by a simple extrapolation by atomic number (Z) along the groups of the Periodic Table [27–30, 34]. These estimations are not to be considered as non-relativistic, because they include the increasing relativistic effects with increasing Z along the lighter elements in the corresponding groups of the Periodic Table. As an example, data included in Table 2 for s- and p-elements are presented in Fig. 2. Note here, the deviation of some of the elements in the first two rows of the Periodic Table.

In an illustrative way, the standard enthalpy of monatomic gaseous elements can be seen as the dissociation enthalpy of a (macromolecular) elemental crystal [59]. This value is a substantial constituent of the binding enthalpy of compounds. Therefore, a coupling between the standard or the atomic standard formation enthalpies of solid and gaseous compounds and the standard enthalpy of monatomic gaseous elements can be expected and is certainly observed, e.g., see Fig. 3.

The enthalpies of formation obtained by this extrapolation are compiled in Table 2. Several results are given for the formation enthalpies, if different values estimated for the standard enthalpies of monatomic gaseous elements were used for the prediction. Correlations between the standard formation enthalpies of the solid state versus the corresponding values of the gaseous state have been used [35–44]. For similar types of compounds of elements along one group with equivalent oxidation states linear correlations can be observed. More generally, this type of correlation is observed for different compounds of transition elements in their highest achievable oxidation state; see Fig. 4.

Another interesting type of linear relations was suggested by Golutvin [60] correlating the standard formation enthalpies of solid and gaseous compounds of elements ($\Delta H^{o}_{\mathrm{eq.}}(\mathrm{g,s})$, see Eq. 45), which are normalized to the oxidation state of the metal ion in this compounds (w) and to the number of metal ions (metal equivalents) in the compounds ($\mathrm{eq}_{\mathrm{metal}}$), with the logarithm of the oxidation state of the metal ion in this compounds.

Table 2 Predicted thermochemical data for transactinides and compounds in kJ/mol

Species	$-\Delta H^{*}_{298}$ (s)	$-\Delta H^{o}_{298}$ (s)	$-\Delta H^{*}_{298}$ (g)	$-\Delta H^{o}_{298}$ (g)	ΔH^{o}_{subl}	ΔS^{o}_{subl}	ΔH^{o}_{Dissl}	$-\Delta H^{o}_{ads}(SiO_2)$	Lit.
Rf			648 ± 40	648 ± 40	648 ± 40				[34]
			557	557	557	141.08	255 ± 14		[50]
$RfCl_4$		1031		909	122			95 ± 8	[44]
					138			104 ± 9	[43]
					126			97 ± 8	[43]
$RfOCl_2$	2204		1745		459			297 ± 17	[39]
Db			700	700	700				[40]
			835 ± 30	835 ± 30	835 ± 30				[34]
			602	602	602	142.81	313 ± 1		[50]
$DbCl_5$		899		805	94			78 ± 8	[44]
$DbOCl_3$		969		789	180.0			136 ± 10	[44]
$DbBr_5$		541		423	118				[40]
		635		526	109				
Sg			834 ± 30	834 ± 30	834 ± 30				[34]
			1030	1030	1030				[30]
			882	882	882	136.40		457 ± 36	[50]
$SgCl_6$	2230		2125		105			85 ± 8	[35]
	2400		2279		121			94 ± 8	
$SgOCl_4$	2413		2318		95			79 ± 8	[35]
	2612		2504		108			86 ± 8	
SgO_2Cl_2	2592		2367		125			97 ± 8	[35]
	2695		2551		144			108 ± 9	
SgO_3	2517		1967		549			380 ± 23	[35]
	2727		2108		519			427 ± 25	

(continued)

Table 2 (continued)

Species	$-\Delta H^{*}_{298}$ (s)	$-\Delta H^{o}_{298}$ (s)	$-\Delta H^{*}_{298}$ (g)	$-\Delta H^{o}_{298}$ (g)	ΔH^{o}_{subl}	ΔS^{o}_{subl}	ΔH^{o}_{Dissl}	$-\Delta H^{o}_{ads}(SiO_2)$	Lit.
Bh			920	920	920				[29]
			850	850	850				[30]
			733	733	733				[34]
			820 ± 20	820 ± 20	820 ± 20	155.07	409 ± 10		[50]
BhO_3		671		385	358			250 ± 18	[41]
BhO_3Cl		650		561	89			75 ± 7	[41]
BhO_3OH		837		710	127			93 ± 11	[41]
Hs			841	841	841				[29]
			791	791	791				[30]
			790	790	790				[34]
			982 ± 2	982 ± 20	982 ± 2	162.44	504 ± 9		[50]
HsO_4	2186		2130		57 ± 11			46 ± 9	[37]
Mt			753	753	753				[29]
			661	661	661				[34]
			746 ± 30	746 ± 30	746 ± 30	160.80	398 ± 2	540 ± 20	[50]
Ds			878	878	878				[29]
			527	527	527				[34]
			510 ± 10	510 ± 10	510 ± 10	149.63	265 ± 3	445 ± 14	[50]
Rg			523	523	523				[29]
			351	351	351				[34]
			384 ± 8	384 ± 8	384 ± 8	132.07	191 ± 2	279 ± 06	[50]
Cn			−85						[34]
			39 ± 3	39 ± 3	39 ± 3	106.51	6 ± 1	12 ± 07	[50]

(continued)

Table 2 (continued)

Species	$-\Delta H^{*}_{298}$ (s)	$-\Delta H^{o}_{298}$ (s)	$-\Delta H^{*}_{298}$ (g)	$-\Delta H^{o}_{298}$ (g)	ΔH^{o}_{subl}	ΔS^{o}_{subl}	ΔH^{o}_{Dissl}	$-\Delta H^{o}_{ads}(SiO_2)$	Lit.
113			142	142	142				[29]
			109 ± 8	109 ± 8	109 ± 8				[30]
			234 ± 14	234 ± 14	234 ± 14	127.82	68 ± 4	89 ± 04	[50]
Fl (114)			42	42	42				[29]
			71 ± 16	71 ± 16	71 ± 16				[30]
			190 ± 18	190 ± 18	190 ± 18	109.27	79 ± 10	52 ± 06	[50]
115			142	142	142				[29]
			151 ± 12	151 ± 12	151 ± 12				[30]
			184 ± 32	184 ± 32	184 ± 32	127.82	154 ± 44	115 ± 03	[50]
Lv (116)			197	197	197				[29]
			83.6 ± 16	83.6 ± 16	83.6 ± 16				[30]
			146 ± 19	146 ± 19	146 ± 19	123.23	153 ± 8	64 ± 05	[50]
117			798 ± 8	798 ± 8	798 ± 8				[30]

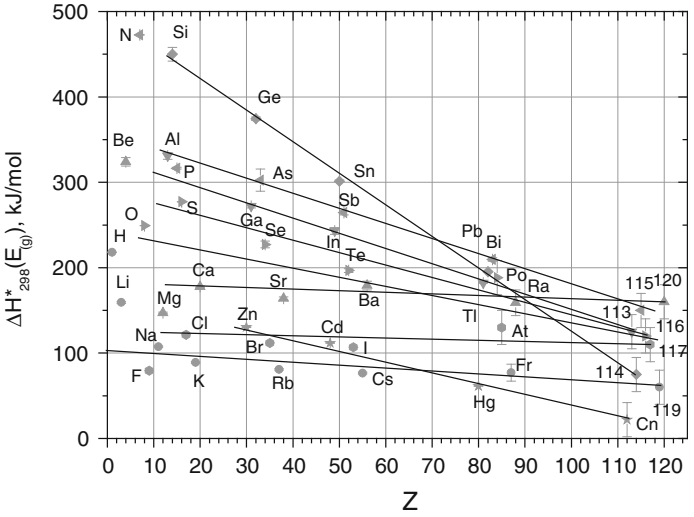

Fig. 2 Extrapolation of the standard enthalpies of monatomic gaseous elements $\Delta H^*_{298}\left(\mathrm{E}_{(g)}\right)$ along the groups of the Periodic Table based on atomic number Z (adapted from [30])

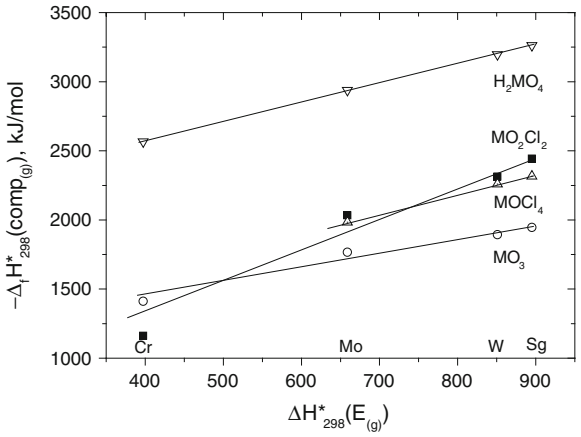

Fig. 3 Extrapolation of the atomic standard formation enthalpies of gaseous compounds $\Delta_f H^*_{298}\left(\mathrm{comp}_{(g)}\right)$ based on the standard enthalpies of monatomic gaseous elements $\Delta H^*_{298}\left(\mathrm{E}_{(g)}\right)$ for group 6 compounds with M = Cr, Mo, W, and Sg (adapted from [35])

$$\Delta_f H^o_{\mathrm{eq.}}(g,s) = \frac{\Delta_f H^o_{298}(g,s)}{w \cdot \mathrm{eq}_{\mathrm{metal}}} \tag{45}$$

Thus, just by assuming the oxidation state of any compound in a selected compound class, the formation enthalpy of a compound in its solid or gaseous state can be predicted. As an example the stability of various bohrium oxides in the gas phase and in the solid phase are predicted as a function of oxidation states in Fig. 5 [36, 41, 42].

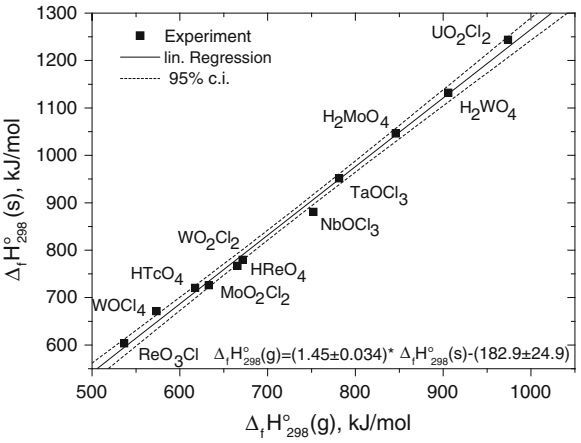

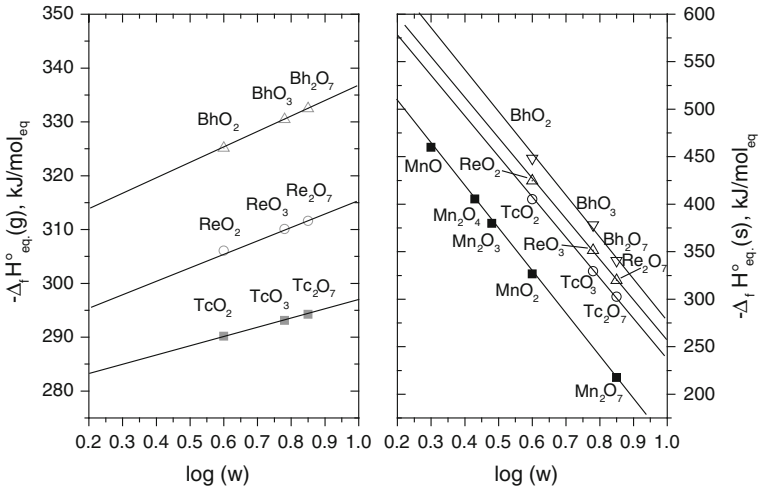

Fig. 4 Correlation of the standard formation enthalpies of oxychlorides and oxyhydroxides in their gaseous ($\Delta_f H^o_{298}(g)$) and solid state ($\Delta_f H^o_{298}(s)$) (adapted from [36])

Fig. 5 Correlations between the normalized standard formation enthalpies $\Delta H^o_{eq.}(g, s)$ of gaseous and solid compounds of group 7 elements and the logarithm of the oxidation state (w) of the metal ion in these compounds (adapted from [41])

2.2.2 Volatility of Compounds

The temperature dependent vapor pressure is frequently used to define volatility. For the adsorbed state the relevant quantity is the desorption pressure, which depends on the temperature and on the surface coverage. The individual crystal lattices, with their characteristic binding properties and, thus, their standard entropy of the pure solid phase, may largely influence the vapor pressure; see, e.g., [39, 44]. Thus, the standard sublimation enthalpy $\left(\Delta H^\circ_{\text{subl}}\right)$ is preferred as a

measure for the volatility of a chemical species. The prediction of the adsorption behavior of a transactinide compound starts with the derivation of the sublimation enthalpy $\left(\Delta H^{\circ}_{\mathrm{subl}}\right)$ of the pure compound. Depending on the availability of data, the standard sublimation enthalpy can be calculated using the following methods:

- Calculations employing the difference between the standard formation enthalpies of compounds in the gaseous and in the solid state:

$$\Delta H^{o,(*)}_{298}(g) - \Delta H^{o,(*)}_{298}(s) = \Delta H^{o}_{\mathrm{subl}} \tag{46}$$

- Correlations between the standard formation enthalpies of the gaseous and of the solid state with the linear regression coefficients a and b given, e.g., in Fig. 4:

$$-\Delta H^{o,(*)}_{298}(s) = a \cdot \Delta H^{o,(*)}_{298}(g) + b \tag{47}$$

The standard sublimation enthalpy is then calculated by:

$$(1-a) \cdot \Delta H^{o,(*)}_{298}(g) + b = \Delta H^{o}_{\mathrm{subl}} \tag{48}$$

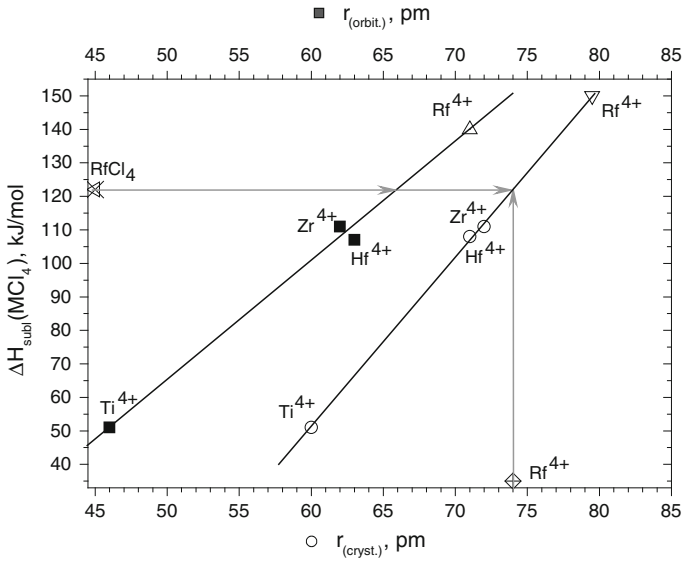

Fig. 6 Radii-volatility correlation for group 4 elements and rutherfordium. The filled squares represent the radii of the outer orbital ($r_{(\mathrm{orbit.})}$, top axis) the open circles show the ionic radii in solid crystals ($r_{(\mathrm{cryst.})}$, bottom axis). Included on the axis are predicted data for $\Delta H_{\mathrm{subl}}(\mathrm{RfCl_4})$ from [44] (crossed triangle) and $r_{(\mathrm{cryst.})}\ \mathrm{Rf}^{4+}$ (crossed diamond) from [59]

Significant correlations exist between ionic radii in the solid state—or radii of electron orbitals of ions—and the sublimation enthalpies for various compound classes; especially for the halides. It is possible to calculate the standard sublimation enthalpy of transactinide compounds from their calculated ionic radii by making use of a radii-volatility correlation and of the corresponding radii of the homologs [43]. However, in this procedure it is important to use consistent sets of radii for all homologs, see, e.g., Fig. 6. The sublimation enthalpy of $RfCl_4$ derived from this approach is included in Table 2.

2.2.3 Empirical Correlations Between Adsorption Properties of Single Atoms or Molecules and the Volatility of Pure Substances

Empirical extrapolative predictions regarding the stability and the volatility of transactinides and of their compounds are, in the next step, followed by the determination of empirical correlations between adsorption properties of extremely small amounts of these elements or compounds and the volatility of the pure macroscopic solid phase of this substance, respectively.

It is assumed that the molar binding energy of an adsorbed single molecule to the surface approximately equals its partial molar adsorption enthalpy at zero surface coverage. In the adsorbed state at zero surface coverage, however, the individual variations of the entropy are partly but not completely suppressed.

The adsorption enthalpy can be expressed as a sum of two independent terms (see also Sect 1.3.2):

- The net adsorption enthalpy, as the enthalpy difference between a pure solid compound and its adsorbed state on a surface at zero surface coverage;
- The desublimation enthalpy.

Hence, for small or equal net adsorption enthalpies it can be expected that the adsorption enthalpy is proportional to the standard sublimation enthalpy, which characterizes the volatility properties of pure solid phases as an integral value:

$$-\Delta H^o_{\mathrm{ads}} \propto -\Delta H^o_{\mathrm{subl}} \tag{49}$$

Small net adsorption enthalpies represent a prerequisite to reversible non-localized mobile adsorption processes without reactions of the species adsorbed on the stationary surfaces. The experimental proof of such correlations for defined classes of pure substances is essential for the prediction of adsorption properties of transactinides and their compounds. Therefore, a variety of gas adsorption chromatographic experiments were carried out with carrier free amounts of different radioisotopes using selected modified surfaces as stationary phases. The use of carrier free amounts is necessary to experimentally obtain adsorption conditions at nearly zero surface coverage.

The selection of proper elements and compounds needs to take into account a very complex situation. The chemical state of the radioisotopes in the reactive carrier gas

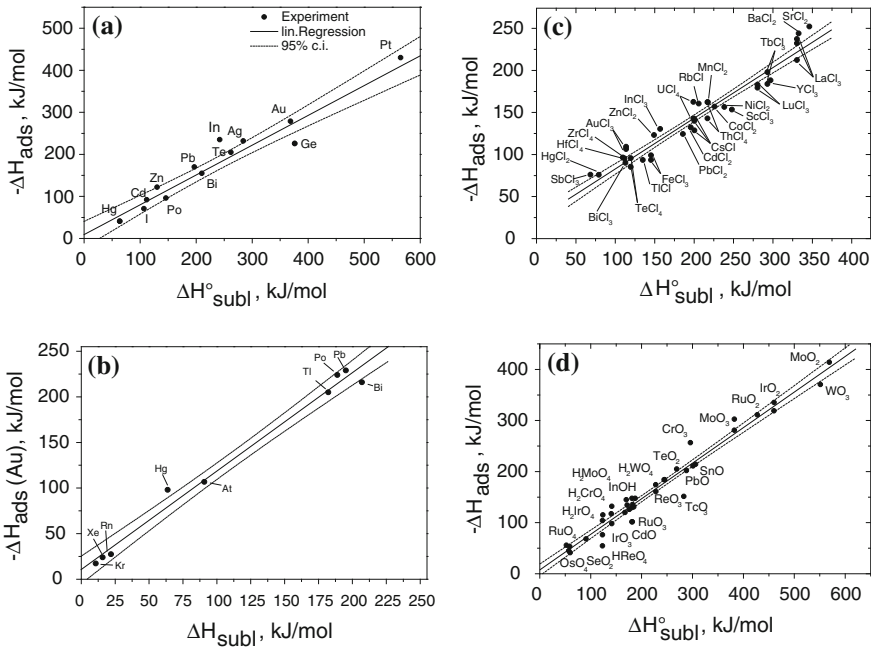

Fig. 7 Correlation of the molecular property adsorption enthalpy ΔH^o_{ads} with the property of the macroscopic solid phase sublimation enthalpy ΔH^o_{subl} for different gas phase chemical systems: Panel (**a**) for elements in H_2 on quartz adapted from [63]; **b** for elements in H_2 or He on gold adapted from [65]; **c** for chlorides and oxychlorides in Cl_2, HCl, CCl_4 (O_2) on quartz adapted from [35], and **d** for oxides and oxyhydroxides in O_2 (H_2O) on quartz adapted from [63]

and the standard sublimation enthalpy of this chemical state must be known. In principle all compounds that are unstable under the selected conditions, have to be rejected as well as compounds that undergo diffusion processes or irreversible reactions with the stationary phase. The following correlations were obtained experimentally for elements and selected compound classes; see Table 1 and Fig. 7 a–d:

1. A: For elements (with H_2, (H_2O)) on quartz [62, 63]

$$-\Delta H^o_{\text{ads}} = (2.9 \pm 16) + (0.73 \pm 0.1) \cdot \Delta H^o_{\text{subl}},\ \text{kJ/mol} \tag{50}$$

2. B: For elements (with He or H_2) on gold [64, 65]

$$-\Delta H^o_{\text{ads}} = (10.3 \pm 6.4) + (1.08 \pm 0.05) \cdot \Delta H^o_{\text{subl}},\ \text{kJ/mol} \tag{51}$$

3. C: For chlorides and oxychlorides (with Cl_2, $SOCl_2$, HCl, (O_2)) on quartz [35]

$$-\Delta H^o_{\text{ads}} = (21.5 \pm 5.2) + (0.600 \pm 0.025) \cdot \Delta H^o_{\text{subl}},\ \text{kJ/mol} \tag{52}$$

4. D: For oxides and oxyhydroxides (with O_2, (H_2O)) on quartz [63, 66]

$$-\Delta H^o_{ads} = (7.0 \pm 8.0) + (0.697 \pm 0.03) \cdot \Delta H^o_{\text{subl}},\ \text{kJ/mol} \tag{53}$$

Experimental observations of these empirical correlations clearly prove the postulated proportionality. These correlations suggest a similarity between the bond (with lower coordination) of the adsorbed particles to the modified surface and the bond to the surface of the pure macroscopic phase of the compound, which is relevant for the desublimation process. The adsorption behavior of atoms and compounds for most of the experiments used in the described correlations were evaluated using differently defined standard adsorption entropies [65–70]. Adsorption data from more recent experimental results were evaluated applying the model of mobile adsorption [4]. Hence, data from previous experiments were re-evaluated using the latter model. These correlations based on estimated standard sublimation enthalpies allow predictions of adsorption enthalpies for selected compounds for the case of zero surface coverage. These results are only valid for experimental conditions using the same reactive gases, and thus, similarly modified stationary surfaces.

For gas chemical studies we assume, in the simplest case, that under a given experimental condition the most stable chemical state is formed and that this state remains unchanged during the entire experiment. Pure and very reactive gas mixtures are used at high concentrations to obtain and stabilize this chemical state. During gas adsorption processes the reactive carrier gas determines the chemical state of the investigated elements and modifies the surface of the stationary chromatographic phase in a characteristic way. Thus, in the case of dissociation reactions, which may occur with very high reaction rates especially at high temperatures, the restoration of the most stable chemical state is possible and is very fast. All deposition and volatilization processes of single atoms or single molecules (the nearest case to zero surface coverage) are basically adsorption and desorption processes, respectively.

Two fundamentally different types of reversible processes can occur in the gas-adsorption chromatography:

- Adsorption and desorption of molecules without any change in the oxidation state and no change in the ligands. For example, the simple adsorption of a group-5 oxychloride can be described by the following equation:

$$MOCl_3(g) \Leftrightarrow MOCl_3(ads) \tag{54}$$

If the interaction of the molecule with the surface is weak (Van der Waals forces), the molecule remains nearly unchanged regarding its binding structure, oxidation state, and number of ligands. This is typical for physisorption. Adsorption processes of molecules with non-saturated coordination show much stronger interactions. These adsorption processes are accompanied by changes of the coordination number of the central atom and, in some cases, by changes of the type of binding (e.g., break-up of a double bond). The oxidation state remains unchanged. This depicts a typical case of chemisorption.

- In a different kind of chemisorption process, a reversible change of the oxidation state or a reversible change of the number of ligands or even the nature of ligands may occur during the adsorption and the desorption of a molecule. For example, for the oxyhydroxide compound of a metal ion in the oxidation state +6 the dissociative adsorption can be described by [7]:

$$H_2MO_4(g) \Leftrightarrow MO_3(ads) + H_2O(g) \tag{55}$$

As another example, the substitutive adsorption of a group 4 tetrachloride is described in [8] by:

$$MCl_4(g) + 1/2O_2(g) \Leftrightarrow MOCl_2(ads) + Cl_2(g) \tag{56}$$

The knowledge of the type of the adsorption process is crucial for the determination of the adsorption enthalpy from experimental results (see Part I of this chapter, Eqs. 7 and 8). One experimental approach to assess the reaction type is the variation of the partial pressure of the reactive carrier gas, which is supposed to be involved in the mechanism of the adsorption reaction [8].

2.3 Empirical Calculation Methods for Adsorption Enthalpies

2.3.1 Physisorption of Noble Gases and Noble-Gas Like Elements

Van der Waals Model

Depending on the type of interaction between an adsorbed particle and a non-metallic solid state surface, there are cases, where adsorption enthalpies can be calculated using empirical and semi-empirical relations. In the cases of atoms with a noble-gas like ground-state configuration and of symmetrical molecules the binding energy (E_B) to a solid surface can be calculated as a function of the polarizability (α), the ionization potential (IP), the distance (r) between the adsorbed atom or molecule and surface, and the relative dielectric constants (ε) [37, 73, 74]:

$$E_B = \frac{3}{16} \cdot \alpha \cdot \frac{(\varepsilon - 1)}{(\varepsilon + 2)} \cdot \frac{1.57 \cdot (IP_1 \cdot IP_2)}{(IP_1 + IP_2)} \cdot \frac{1}{r^3} \tag{57}$$

The binding energy E_B approximately equals the adsorption enthalpy ΔH°_{ads} as:

$$\Delta H^{o}_{ads} = -E_B - 0.5 \cdot R \cdot T \tag{58}$$

Table 3 Adsorption enthalpies on quartz estimated using the physisorption model for Cn, Fl, 118, and HsO_4 [37]

Element	$\alpha^{*}10^{-24}$ (cm^3)	ε (SiO_2)	r (nm)	IP_1, (eV)	IP_2, (eV)	$-\Delta H^{o}_{ads}$(kJ/mol)
Cn	5.33	3.81	0.247	11.7	11.4	29
Fl	6.47	3.81	0.247	11.7	8.5	30
118	8.31	3.81	0.247	11.7	8.7	39
HsO4	8.46	3.81	0.247	11.7	12.27	47

If the elements Cn and Fl (element 114) have a noble-gas like character [54], then, in a fictitious solid state, they would form non-conducting colorless crystals. A physisorptive type of adsorption may occur and their adsorption properties, for example on quartz, can be calculated with this method, see Table 3. For physisorbed noble gas atoms a roughly uniform distance to different surfaces of about 2.47 ± 0.2 Å was deduced from experimental results [47]. A predicted value of the adsorption properties of HsO_4 was based on this model in [37]. In conjunction with molecular and elemental data, which were calculated using density functional theory, this model yields valuable predictive results; see chapter "Theoretical Chemistry of the Heaviest Elements".

The Law of the Corresponding States

Another approach to assess volatility data for noble gas like elements is based on the fundamental law of corresponding states, which was established by van der Waals in 1880. It suggests the existence of a universal equation of states (59) valid for various liquids and gases with high similarity of bonding, interaction, and structure. In the case of the heavier noble gases these requirements are indeed fulfilled. The variables in this equation are the parameters of state reduced by the critical values.

$$\mathrm{f}\left(\frac{p}{p_c}, \frac{V}{V_c}, \frac{T}{T_c}\right) = 0 \tag{59}$$

Based on ab initio atomic calculations, Pitzer [54] first suggested for the elements Cn, Fl, and 118 the possibility of a noble-gas like behavior. Based on these predictions the potential diagrams of these elements should be similar to the noble gas potentials. Hence, in the condensed states van der Waals interactions predominate. Grosse [23] estimated the critical constants (p_c, V_c, T_c) for the elements Rn and 118 using extrapolations along the group 18 based on the period numbers. Improved extrapolations, using the atomic weight and the radii of the outermost electron orbitals [55] have been suggested in [49]; see, e.g., Fig. 8. Note the clear divergence for the light noble gases in [49] for the correlations with p_c and V_c, which is in agreement with the observation of remarkable deviations of He and Ne from the law of corresponding states, having non-zero energy states at 0 K [76].

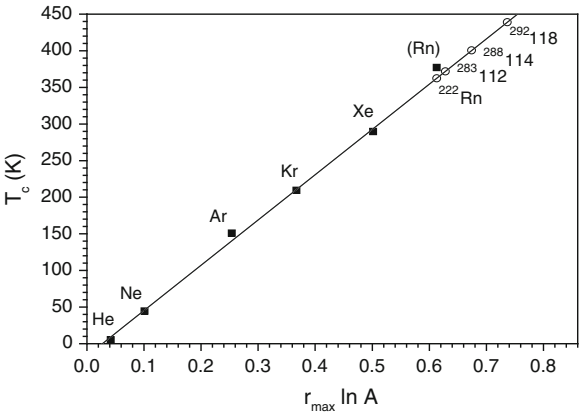

Fig. 8 Correlation of T_c with $r_{max} \cdot \ln(A)$ for noble gases (*black squares*) (adopted from [49]). Linear regression (*black line*) and extrapolated data (*open circles*) are indicated

However, using the data for the heavy noble gases (Ar–Rn) a complete set of critical data is deduced, which is used as follows to describe the volatilization process of the noble gas element 118 and of the potentially noble-gas like elements Cn and Fl. The reduced vapor pressure equation is given as:

$$\log\left(p/p_c\right) = -\frac{\mathrm{a}}{T/T_c} + \mathrm{b} \tag{60}$$

Using the given and extrapolated critical temperatures T_c and critical pressures p_c the coefficients a and b can be deduced. According to the law of corresponding states, these coefficients shall be nearly identical for all ideal solids and liquids. This is true for the heavy noble gases Ar, Kr, Xe, and Rn. Thus, those coefficients a and b from the heavy noble gases are used for predicting vapor pressure coefficients for the elements Cn, Fl, and 118 as:

$$\log\left(\frac{p}{kPa}\right) = -\frac{a \cdot T_c}{T} + b + \log\left(\frac{p_c}{kPa}\right) = -\frac{\mathrm{A}}{\mathrm{T}} + \mathrm{B} \tag{61}$$

From the vapor pressure coefficients of the solid phase the sublimation enthalpy can be estimated; see Table 4, $\Delta H^0_{\mathrm{subl}}(1)$.

A third approach, assumes the potential curves are very similar for elements revealing only van der Waals interaction in the solid state according to Lennard-Jones [77]. A constant proportionality between the depths of the potentials k^{Θ} and the critical temperatures is expected according to:

$$k^{\Theta} = \frac{\left(\Delta H^0_{\mathrm{subl}} + U_0\right)}{R \cdot T_c} = 6.5 \tag{62}$$

with [76, 78]:

$$U_0 = \frac{9}{8} \cdot R \cdot \Theta_D \tag{63}$$

Table 4 Thermochemical data of noble gases and empirically deduced data for elements Rn, Cn, Fl, and 118

Element	T_c, K	p_c, (kPa)	V_c, (cm^3/mol)	Θ_D, K	U_0, (J/mol)	$\Delta H^0_{subl}(1)$, (kJ/mol)	$\Delta H^0_{subl}(2)$, (kJ/mol)	k^{Θ}
He	5.19	227	57					
Ne	44.40	2760	42	64	598.6	1.88	1.88	6.71
Ar	150.87	4898	75	80	748.3	7.73	7.73	6.76
Kr	209.41	5500	91	63	589.3	11.21	11.21	6.77
Xe	289.73	5840	118	55	514.4	15.87	15.87	6.8
Rn	377.5	6280	145	48.7	455.5	20.9		6.8
^{220}Rn	362.43	6312	139	45.09	421.7	19.38	20.07	6.8
^{283}Cn	371.92	6370	150	40.20	376.0	19.89	20.65	6.8
^{288}Fl	400.38	6543	162	40.57	379.5	21.41	22.26	6.8
^{292}118	438.99	6778	170	41.14	384.8	23.45	24.43	6.8

The Debye temperature (Θ_D) can be calculated [76, 78] as:

$$\Theta_D = \frac{163}{V_{0K}^{1/3}} \cdot \sqrt{\frac{b.p.}{A}} \tag{64}$$

The boiling points ($b.p.$) are estimated according to [23] from the critical temperatures as:

$$b.p. = 0.58 \cdot T_c \tag{65}$$

The atomic volume at 0 K (V_{0K}) was shown to be proportional to the critical volume [79]:

$$V_{0K} = 0.239 \cdot V_c \tag{66}$$

For the heavy noble gases very similar $k^{\Theta} \sim 6.8$ are deduced. Hence, the sublimation enthalpies at 0 K (Table 4, $\Delta H^0_{subl}(2)$) for the elements Rn, Cn, Fl, and 118 can be calculated using their critical data. The obtained sublimation enthalpies can be used to predict the potential adsorption behavior of the elements Cn, Fl, and 118 using empirical correlations (Eqs. 50 and 51).

The Adhesion Model

Under the assumption that elements Cn, Fl, and 118 behave as typical heavy noble gases [54] and undergo pure van der Waals interaction with metal surfaces, the adhesion model based on an approach given in [80] can be applied. The adsorption enthalpy of noble-gas like elements was related to the adhesion of atoms to a surface with a certain surface energy. This approach revealed that the adsorption enthalpy of a noble gas (E) on a metal surface is linearly correlated to the adsorption enthalpy of Xe on the same metal.

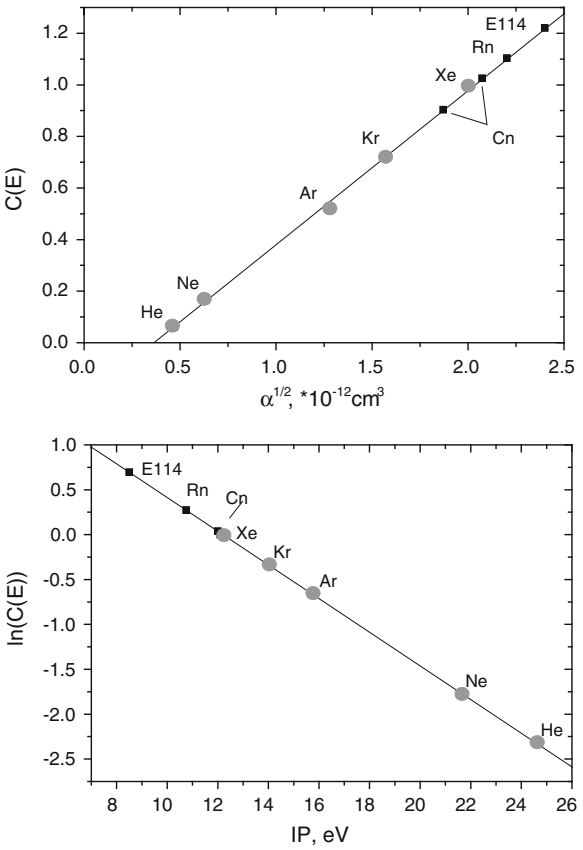

Fig. 9 Empirical correlations of C(*E*) with the atomic dipole polarizabilities α (*upper panel*) and with the ionization potentials *IP* (*lower panel*) (adopted from [16])

$$\Delta H^{o}_{\mathrm{ads}}(E) = C(\mathrm{E}) \cdot \Delta H^{o}_{\mathrm{ads}}(\mathrm{Xe}) \tag{67}$$

This model was successfully applied to reproduce experimental adsorption data for noble gases on metal surfaces. Furthermore, this model was empirically extended in [16] to predict adsorption enthalpies of the elements Rn, Cn, and Fl on metal surfaces, assuming a physisorptive adsorption; see Fig. 9. Please note that two different dipole polarizabilities of Cn as given in the literature lead to two slightly different predictions for the Cn (I, II) adsorption enthalpy on gold, based on correlation depicted in Fig. 9 (upper panel); see Table 5. Experimental adsorption data measured for Rn on various metal surfaces [16] revealed a fairly good agreement with these predictions.

Table 5 Proportionality factors C(E) connecting the adsorption enthalpy of noble-gas like elements on metals with the adsorption enthalpy of Xe on these metals

Element	$\alpha \cdot 10^{-24}$ cm^3	C_1^a (E)	IP eV	C_2^a (E)	$\Delta H^0_{ads}(Au_1)$ (kJ/mol)	$\Delta H^0_{ads}(Au_2)$ (kJ/mol)
He	0.22	0.12	24.6	0.098	2.9	2.3
Ne	0.39	0.17	21.6	0.17	4.1	4.1
Ar	1.64	0.52	15.8	0.52	12.5	12.5
Kr	2.48	0.72	14.0	0.72	17.3	17.3
Xe	4.01	1	12.1	1	24	24
Rn	4.853	1.11	10.5	1.31	26.6	31.4
Cn I	3.5	0.91	12	1.04	21.8	25.0
Cn II	4.3	1.04			25.0	
Fl	5.8	1.2	8.5	2.00	28.8	48

[a] C(E) for noble gases Ne–Xe from [78] and empirically deduced for He and Rn and for assumed noble-gas like elements Cn and Fl using atomic data from [56–58, 73]

2.3.2 Adsorption of Metals on Metal Surfaces

The Metallic Character

One general rule of trends in the Periodic Table is that the metallic character of all elements increases with increasing atomic number Z along the groups of s-elements and of p-elements. The relative difference between the dissociation enthalpy of two-atomic molecules, ΔH°_{diss}, and the sublimation enthalpy, ΔH°_{subl}, of these elements (both values are given in [81] and from section "Thermochemical Data") can be used to estimate the metallic character (m) of elements (see Fig. 10) as suggested in [30]:

$$m = \left(\Delta H^o_{subl} - 0.5 \cdot \Delta H^o_{diss}\right)/\Delta H^o_{subl} \tag{68}$$

For real metals this value is close to 1. This value qualitatively shows whether the association to homo-nuclear two-atomic molecules $\left(\Delta H^o_{diss}\right)$ (non-metallic character) is energetically preferred over the formation of a coordination lattice (metallic character) and vice versa. According to this relation, a metallic character can also be expected for the elements Cn and Fl [30]. Element 117, for example, can be assumed to have a semi-metallic character. However, special precaution is required since the data available for some elements show a large spread. As an example, the range of the literature data on the sublimation of Po is shown here to be limited by two sublimation enthalpies Po(A) [82] and Po(B) [83], which yield quite large variations in the prediction for the Lv character; see Fig. 10.

The Semi-Empirical Macroscopic Adsorption Model

This model assumes that the adsorption enthalpy can be divided into two independent energetic parts—the desublimation enthalpy and the net adsorption enthalpy. Hence, the net adsorption enthalpy characterizes the interaction, which

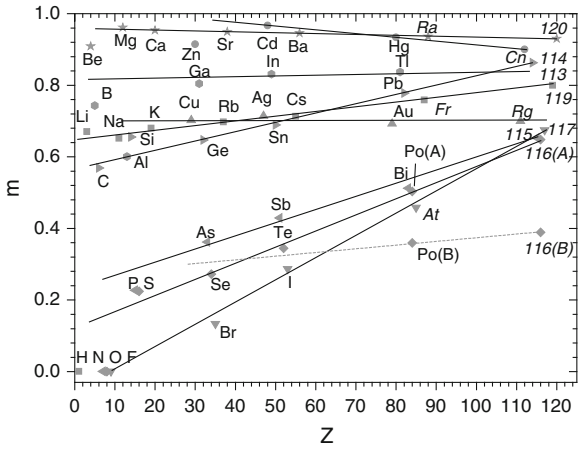

Fig. 10 The metallic character m of *s*- and *p*-elements as a function of the atomic number *Z* and its extrapolation (*in italics*) along the groups of the periodic table to the region of transactinides (adopted from [30])

depends on the nature of both metals. On the other hand, the desublimation enthalpy is an exclusive property of the adsorbate. For the calculation of the net adsorption enthalpies of transactinides on metal surfaces the partial molar enthalpies of solution of the adsorbate in the solid stationary material at infinite dilution and the enthalpy of displacement are required. These values can be obtained using (i) the semi-empirical Miedema model [84–87]; (ii) the Volume-Vacancy model, if the adsorption occurs in the surface; or (iii) the Surface-Vacancy model, if the adsorption occurs on the surface [88–90]. The magnitude of the partial molar enthalpy of solid solution is decisive to the selection of the appropriate Vacancy model. This value is illustrated in Fig. 11. It can be clearly

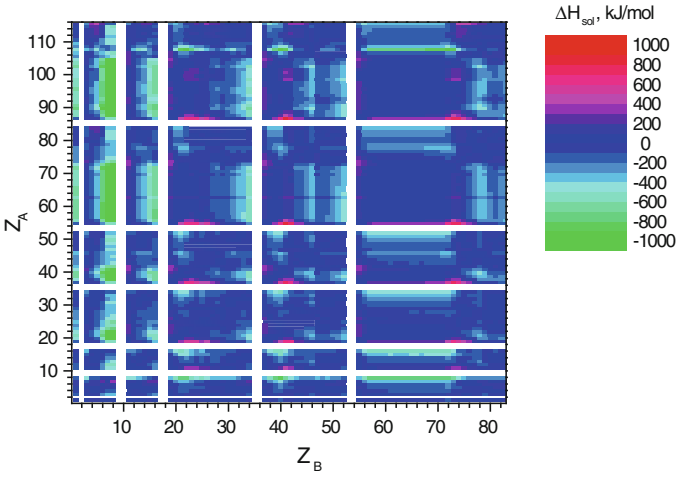

Fig. 11 The partial molar enthalpy of solution (ΔH_{sol}) of element Z_A in element Z_B calculated based on a semi-empirical model suggested by Miedema [82–85]. The halogens and noble gases are excluded

Table 6 Predicted adsorption data of metallic s- and p-elements on different stationary phases

/Surface/element E	ΔH^{o}_{ads}/Quarz/kJ/mol	/Pd/kJ/mol	/Pt/kJ/mol	/Ni/kJ/mol	/Au/kJ/mol	/Cu/kJ/mol
Cn	−12 ± 07	−73	−23	−98	−8	−101
113	−89 ± 04	−228	−169	−251	−115	−221
Fl	−52 ± 06	−225	−169	−91	−93	−189
115	−115 ± 03	−352	−286	−206	−179	−174
116	−64 ± 05	−232	−167	−183	−146	−260

seen from the given figure where the strongest interactions occur between the elements of the Periodic Table.

The data required for the calculations of the net adsorption enthalpies of transactinides are estimated from trends in the Periodic Table [45, 46]. The net adsorption enthalpies and the predicted sublimation enthalpies, e.g., [50], were combined to predict the adsorption enthalpies of transactinides on selected metal surfaces [45, 46, 90]. The metals, which are presented in Table 6, can be used as the stationary phase in gas-adsorption chromatographic experiments for selective gas chemical separations or, in the case of high adsorption interaction, as strong fixation materials for the sample preparation in the measurement of transactinides.

References

1. Eichler, B., Zimmermann, H.P., Gäggeler, H.W.: Adsorption of radon on ice surfaces. J. Phys. Chem. A **104**, 3126–3131 (2000)
2. Beyer, G.J., Novgorodov, A.F., Khalkin, A.F.: On the adsorption of ultra-micro quantities of lanthanides, Sc, Y, Zr, and Hf on polycrystalline Ta surfaces. Radiokhimya **20**, 589–592 (1978) (in Russian)
3. Leipnitz, E., Struppe, H.G.: Handbuch der Gaschromatographie. Verlag Geest und Portig, Leipzig (1970)
4. Eichler, B., Zvara, I.: Evaluation of the enthalpy of adsorption from thermochromatographical data. Radiochim. Acta **30**, 233–238 (1982)
5. Eichler, B., Zude, F., Fan, W., Trautmann, N., Herrmann, G.: Volatilization and deposition of ruthenium oxides in a temperature gradient tube. Radiochim. Acta **56**, 133–140 (1992)
6. Eichler, B., Zude, F., Fan, W., Trautmann, N., Herrmann, G.: Complex transport reactions in a temperature gradient tube—radiochemical study of volatilization and deposition of irridium oxides and hydroxides. Radiochim. Acta **61**, 81–90 (1993)
7. Vahle, A., Hübener, S., Eichler, B.: Thermochromatographic studies of oxide and hydroxide species of molybdenum: Model experiments with respect to the physico-chemical characterization of element 106. Radiochim. Acta **69**, 233–239 (1995)
8. Eichler, B.: The behaviour of radionuclides in gas adsorption chromatographic processes with superimposed chemical reactions (chlorides). Radiochim. Acta **72**, 19–26 (1996)
9. Eichler, B., Kratz, J.V.: Electrochemical deposition of carrier-free radionuclides. Radiochim. Acta **88**, 475–482 (2000)
10. Gäggeler, H., Dornhöfer, H., Schmidt-Ott, W.D., Greulich, N., Eichler, B.: Determination of adsorption enthalpies for polonium on surfaces of copper, silver, gold, palladium and platinum. Radiochim. Acta **38**, 103–106 (1985)

11. Eichler, B., Gäggeler-Koch, H., Gäggeler, H.: Thermochromatography of carrier-free elements: polonium in copper columns. Radiochim. Acta **26**, 193–196 (1979)
12. Eichler, B.: Das Verhalten flüchtiger Radionuklide im Temperaturgradientrohr unter Vacuum. Report ZfK-346, Rossendorf (1977)
13. Gäggeler, H., Eichler, B., Greulich, N., Herrmann, G., Trautmann, N.: Vaccum-thermochromatography of carrier-free species. Radiochim. Acta **40**, 137–143 (1986)
14. Eichler, B., Rhede, E.: Thermochromatographische Untersuchungen mit Aktiniden: 1. Mitteilung: Americium in Titankolonnen. Kernenergie **23**, 191–195 (1980)
15. Eichler, B., Buklanov, G.V., Timokhin, S.N.: Thermochromatographic experiments with actinides in metallic columns in vacuum. Kernenergie **30**, 454–458 (1980)
16. Eichler, R., Schädel, M.: Adsorption of radon on metal surfaces: a model study for chemical investigations of elements 112 and 114. J. Phys. Chem. B **106**, 5413–5420 (2002)
17. Zvara, I.: Simulation of thermochromatographic processes by the Monte Carlo method. Radiochim. Acta **38**, 95 (1986)
18. Golay, M.J.E.: Theory of chromatography in open and coated tubular columns. In: Desty, D.H. (ed.) Gas Chromatography, pp. 36–55. Butterworths, London (1958)
19. Poppe, H.: Mass transfer in rectangular chromatographic channels. J. Chromatogr. A **948**, 3–17 (2002)
20. Zvara, I.: The Inorganic Radiochemistry of Heavy Elements: Methods for Studying Gaseous Compounds. Springer Science + Business Media B.V, New York (2008)
21. Gilliland, E.R.: Diffusion coefficients in gaseous systems. Ind. Eng. Chem. **26**, 681–685 (1934)
22. Knudsen, M.: Die Gesetze der Molekularströmung und der inneren Reibungsströmung der Gase durch Rohren. Ann. Phys. **28**, 75–130 (1909)
23. Grosse, A.V.: Some physical and chemical properties of element 118 (Eka-Em) and element 86 (Em). J. Inorg. Nucl. Chem. **27**, 509–515 (1965)
24. Keller Jr, O.L., Burnett, J.L., Carlson, T.A., Nestor Jr, C.W.: Predicted properties of the super heavy elements. I. Elements 113 and. 114, Eka-thallium and Eka-lead. J. Phys. Chem. **74**, 1127–1134 (1970)
25. David, F.: Redox properties of elements, a systematic study. Radiochem. Radioanal. Lett. **12**, 311–324 (1972)
26. Fricke, B., Waber, J.T.: Theoretical predictions of the chemistry of superheavy elements. Actinides Rev. **1**, 433–485 (1971)
27. Keller Jr, O.L., Nestor Jr, C.W., Carlson, T.A.: Predicted properties of the superheavy elements. II. Element lll, eka- gold. J. Phys. Chem. **77**, 1806–1809 (1973)
28. Keller Jr, O.L., Nestor Jr, C.W., Fricke, B.: Predicted properties of the superheavy elements. III.Element 115, eka-bismuth. J. Phys. Chem. **78**, 1945–1949 (1974)
29. Fricke, B.: Superheavy elements. In: Dunitz, J.D., Hemmerich, P. (eds.) Structure and Bonding, pp. 89–144. Springer, Berlin (1975)
30. Eichler, B.: Das Flüchtigkeitsverhalten von Transactiniden im Bereich um $Z = 114$. Kernenergie **19**, 307–311 (1976)
31. Keller Jr, O.L., Seaborg, G.T.: Chemistry of the transactinide elements. Ann. Rev. Nucl. Sci. **27**, 139–166 (1977)
32. Eichler, B., Reetz, T.: Chemical isolation of new elements. Kernenergie **25**, 218–222 (1982)
33. Pershina, V., Fricke, B.: Electronic structure and properties of the group 4, 5, and 6 highest chlorides including elements 104, 105, and 106. J. Phys. Chem. **98**, 6468–6473 (1994)
34. Ionova, G.V., Pershina, V.G., Suraeva, I.I., Suraeva, N.I.: Estimation of change of thermodynamic properties of transactinoid series metals: sublimation enthalpy. Radiokhimiya **37**, 307–316 (1995)
35. Eichler, B., Türler, A., Gäggeler, H.W.: Thermochemical characterization of seaborgium compounds in gas adsorption chromatography. J. Phys. Chem. A **103**, 9296–9306 (1999)
36. Eichler, R., Brüchle, W., Dressler, R., Düllmeann, C., Eichler, B., Gäggeler, H., Gregorich, K., Hoffman, D., Hübener, S., Patin, J., Piguet, D., Schädel, M., Shaughnessy, D., Strellis, D.,

Taut, S., Tobler, L., Tsyganov, Y., Türler, A., Vahle, A., Wilk, P., Yakushev, A.: Chemical characterization of bohrium (element 107) & (suppl. information). Nature **407**, 63–65 (2000)
37. Düllmann, ChE, Eichler, B., Eichler, R., Gäggeler, H.W., Türler, A.: On the stability and volatility of group 8 tetroxides, mo4 (m = ruthenium, osmium, and hassium (z = 108)). J. Phys. Chem. B **106**, 6679–6684 (2002)
38. Eichler, B.: Voraussage des Verhaltens der Superschweren Elemente und ihrer Chloride bei der thermochromatographischen Abtrennung. In: Joint Institute for Nuclear Research Report, P12-7767, Dubna (1974)
39. Eichler, B., Gäggeler, H.W.: Stability and "Volatility" of element 104 oxychloride. In: PSI solid state research at large scale facilities Annual report 1996, Annex IIIA, p. 77. Villigen (1997)
40. Eichler, B.: On the volatility of hahnium pentabromide. In: PSI condensed matter research using large scale facilities annual report 1993, Annex IIIA, p. 93. Villigen (1994)
41. Eichler, R.: Thermochemical predictions of chemical properties of bohrium (Bh, element 107). In: PSI report TM-18-00-04, Villigen (2001)
42. Eichler, R.: Thermochemical predictions of chemical properties of bohrium (Bh, element 107). In: PSI particles and matter annual report Vol. 1 2000, p. 122.Villigen (2001)
43. Eichler, B., Türler, A., Gäggeler, H.W.: Radius-volatility correlation of tetrachlorides of Ti, Zr, Hf, 104, Th, and U. In: PSI condensed matter research using large scale facilities annual report 1994, Annex IIIA, p. 76. Villigen (1995)
44. Eichler, B., Türler, A., Gäggeler, H.W.: Estimated standard enthalpies of gaseous 104 and 105 and stability and volatility of their chlorides and oxychlorides. In: PSI condensed matter research using large scale facilities annual report 1994, Annex IIIA, p. 77. Villigen (1995)
45. Eichler, B.: Wechselwirkung der Transactinide um Z = 114 mit Metallen. In: Zentralinstitut für Kernforschung Report, ZfK-374, Rossendorf (1978)
46. Eichler, B.: Metallchemie der Transaktinoide. In: Paul Scherrer Institut Report, 00-09, Villigen (2000)
47. Eichler B., Eichler, R., Gäggeler H.W.: Van der Waals Interaction of the Elements 112, 114, and 118 with Solid Surfaces. In: Labor für Radio- und Umweltchemie Annual Report 2000, p. 10. Villigen (2001)
48. Eichler, B.: The Interaction of element 112 with metal surfaces. In: Labor für Radio- und Umweltchemie Annual Report 2000, p. 7. Villigen (2001)
49. Eichler R., Eichler, B.: Thermochemical properties of the elements Rn, 112, 114, and 118. In: Labor für Radio- und Umweltchemie Annual Report 2003, p. 7-8. Villigen (2004)
50. Eichler, B., Verflüchtigungsverhalten der Transaktinoide von Metalloberflächen und aus Schmelzen (Thermochemische Kalkulation). In: Paul Scherrer Institut Report, 03-01, Villigen (2003)
51. Pyykkö, P.: Relativistic effects in structural chemistry. Chem. Rev. **88**, 563–594 (1988)
52. Pershina, V.G.: Electronic structure and properties of the transactinides and their compounds. Chem. Rev. **96**, 1977–2010 (1996)
53. Schwerdtfeger, P., Seth, M.: Relativistic effects of the superheavy elements. In: von Ragué-Schleyer, P., Allinger, N.L., Clark, T., Gasteiger, J., Kollman, P., Schaefer III, H.F., Schreiner, P.R. (eds.) Encyclopaedia of computational chemistry, vol. 4, pp. 2480–2499. John Wiley and Sons, New York (1998)
54. Pitzer, K.S.: Are elements 112, 114, and 118 relatively inert gases? J. Chem. Phys. **63**, 1032–1033 (1975)
55. Desclaux, J.P.: Relativistic Dirac-Fock expectation values for atoms with z = 1 to z = 120. Atom. Dat. **2**, 311–359 (1973)
56. Seth, M., Schwerdtfeger, P., Dolg, M.: The chemistry of the superheavy elements. I. Pseudopotentials for 111 and 112 and relativistic coupled cluster calculations for $(112)H^+$, $(112)F_2$, and $(112)F_4$. J. Chem. Phys. **106**, 3623–3633 (1997)
57. Eliav, E., Kaldor, U., Ishikawa, Y.: Transition energies in mercury and eka-mercury (element 112) by the relativistic coupled cluster method. Phys. Rev. A **52**, 2765–2769 (1995)

58. Landau, A., Eliav, E., Ishikawa, Y., Kaldor, U.: Electronic structure of eka-lead (element 114) compared with lead. J. Chem. Phys. **114**, 2977–2981 (2001)
59. Pauling, L.: The Nature of Chemical Bond, 3rd edn. Cornell University Press, New York (1960)
60. Golutvin, J.M.: Teploti obrazovanija i tipi khimitcheskoi svjasi w neorgenicheskikh kristallakh, Izd. Akademii Nauk SSSR, Moskwa, (1962)
61. Bilewicz, A.: The ionic radii of $Rf4^{+}$, $Db5^{+}$ and $Sg6^{+}$. Radiochim. Acta **88**, 833–835 (2000)
62. Eichler, B., Kim, S.C.: Thermogravimetric determination of the enthalpy of astatine and radon adsorption on palladium surfaces. Isotopenpraxis **21**, 180–183 (1985)
63. Serov, A., Eichler, R., Dressler, R., Piguet, D., Türler, A., Vögele, A., Wittwer, D., Gäggeler, H.W.: Gas chromatography of indium in macroscopic and carrier-free amounts using quartz and gold as stationary phases. Radiochim. Acta **99**, 95–101 (2011)
64. Eichler, R.: Empirical relation between the adsorption properties of elements on gold surfaces and their volatility. Radiochim. Acta **93**, 245–248 (2005)
65. Serov, A., Aksenov, N., Bozhikov, G., Eichler, R., Dressler, R., Lebedev, V., Petrushkin, O., Piguet, D., Türler, A., Vögele, A., Wittwer, D., Gäggeler, H.W.: Adsorption interaction of astatine species with quartz and gold surface. Radiochim. Acta **99**, 593–599 (2011)
66. Eichler, R., Eichler, B., Gäggeler, H.W., Jost, D.T., Dressler, R., Türler, A.: The gas phase oxide and oxyhydroxide chemistry of trace amounts of rhenium. Radiochim. Acta **87**, 151–159 (1999)
67. Zvara, I., Chuburkov, YuT, Belov, V.Z., Maslov, O.D., Tsaletka, R., Shalaevskii, M.R.: Experiments on chemistry of element 104-kurchatovium. Radiokhimiya **12**, 565–572 (1970)
68. Eichler, B., Domanov, V.P.: Reactive desorption techniques and adsorption at various temperatures-used for the separation of radionuclides. J. Radioanal. Chem. **28**, 143–152 (1975)
69. Eichler, B., Domanov, V.P., Zvara, I.: Evaluation of heat of adsorption from thermochromatographic data. II. Chlorides of metals. The adsorption on quartz. In: Joint Institute for Nuclear Research Report, Dubna, GSI-transl.-4/76. Darmstadt (1976)
70. Eichler, B. Domanov, V.P.: Thermochromatographie trägerfreier Kernreaktions-produkte als Chloride. In: Joint Institute for Nuclear Research Report, P12-7775. Dubna (1974)
71. Eichler, B., Reetz, T., Domanov, V.P.: Bestimmung der Adsorptionsenthalpie auf der Grundlage thermochromatographischer Daten. III. Elemente. Adsorption auf Quarz und Metallen. In: Joint Institute for Nuclear Research Report, P12-10047. Dubna (1976)
72. Eichler, B.: Separation of nuclear reaction products from targets of uranium oxides by cyclic phase transformation in the stoichiometric region UOsub(2,00)-UOsub(2,67) and the thermochromatographic separation of volatilized components. J. Inorg. Nucl. Chem. **35**, 4001–4010 (1973)
73. Pauling, L.: A molecular theory of general anesthesia. Science **134**, 15–21 (1961)
74. Frederikse, H.P.R.: Permittivity (dielectric constant) of inorganic solids. In: Linde, D.R. (ed.) Handbook of Chemistry and Physics, 79th edn. 1998/1999, Table 12–48. CRC-Press, Boca Raton (1998)
75. Miller, T.M.: Atomic and Molecular Polarizabilities. In: Linde, D.R. (ed.) Handbook of Chemistry and Physics, 79th edn. 1998/1999, Table 10–160. CRC-Press, Boca Raton, (1998)
76. Clusius, K.: Atomwärmen und Schmelzwärmen von Neon, Argon und Krypton. Z. Phys. Chem. **31**, 459–474 (1936)
77. Lennard-Jones, J.E.: The equations of state of gases and critical phenomena. Physica **4**, 941–956 (1937)
78. Clusius, K., Weigand, K.: Über den Dampfdruck des Xenons und über eien Beziehung von Lennard-Jones, sowie die Konstanz des Verhältnisses Te/Tk bei den Edelgasen. Z. Phys. Chem. **42**, 111–116 (1939)
79. Grosse, A.V.: The compressibilità of solid noble gases and the alkali metals at 0 K. J. Inorg. Nucl. Chem. **26**, 1801–1809 (1964)

80. Miedema, A.R., Nieuwenhuys, B.E.: The heat of adsorption of van der Waals gases on metallic substrates: a special example of metal-non-metal adhesion. Surf. Sci. **104**, 491–509 (1981)
81. Luo, Yu-Ran: Bond dissociation energies, enthalpy of formation of gaseous atoms. In: Haynes, W.M. (ed.) CRC Handbook of Chemistry and Physics, 92nd edn. CRC Press/Taylor and Francis, Boca Raton (2011)
82. Eichler, B.: Die Flüchtigkeitseigenschaften des Poloniums. PSI-Report 02-12, Paul Scherrer Institut ISSN 1019-0643. Villigen (2002)
83. Stull, D., Sinke, G.: Thermodynamic properties of the elements, p. 234. American Chemical Society, Washington (1956)
84. Miedema, A.R.: The electronegativity parameter for transition metals: Heat of formation and charge transfer in alloys. J. Less-Common Met. **32**, 117–136 (1973)
85. Miedema, A.R., Boom, R., De Boer, F.R.: On the heat of formation of solid alloys. J. Less-Common Met. **41**, 283–298 (1975)
86. Boom, R., De Boer, F.R., Miedema, A.R.: On the heat of Mixing of liquid alloys—I. J. Less-Common Met. **45**, 237–245 (1976)
87. Miedema, A.R.: On the heat of formation of solid alloys II. J. Less-Common Met. **46**, 67–83 (1976)
88. Eichler, B.: Bestimmung der Adsorptionswärme gasförmiger Metalle auf festen Metalloberflächen bei Nullbedeckung (Empirisches Modell). In: Zentralinstitut für Kernforschung Report, ZfK-396. Rossendorf (1979)
89. Eichler, B., Rossbach, H.: Adsorption of volatile metals on metal surfaces and its application in nuclear chemistry: I. Calculation of adsorption enthalpies for hypothetical superheavy elements with Z around 114. Radiochim. Acta **33**, 121–125 (1983)
90. Eichler, B., Gäggeler, H.W., Rossbach, H., Hübener, S.: Adsorption of volatile metals on metal surfaces and its application in nuclear chemistry: II. Evaluation of adsorption enthalpies for polonium on surfaces of transition metals and copper, silver and gold. Radiochim. Acta **38**, 131–134 (1985)

Gas-Phase Chemistry of Superheavy Elements

Heinz W. Gäggeler and Andreas Türler

Abstract This chapter summarizes gas chemical studies of transactinides using two approaches, gas thermochromatography and isothermal gas chromatography. Both techniques enabled successful chemical studies of the transactinides, rutherfordium ($Z = 104$, Rf) , dubnium ($Z = 105$, Db), seaborgium ($Z = 106$, Sg), bohrium ($Z = 107$, Bh), hassium ($Z = 108$; Hs), copernicium ($Z = 112$, Cn), and the recently named flerovium ($Z = 114$, Fl). Typically, these chemical investigations were performed one-atom-at-a-time with a total of less than 20 atoms. For their synthesis, hot heavy-ion fusion reactions with actinide targets were used. The elements Rf through Hs show the typical behavior of d-elements, representing the expected trend within their respective group of the Periodic Table. The chemical species investigated were volatile halides, oxyhalides, oxide hydroxides, and oxides. The elements copernicium and flerovium were studied in their elemental state.

1 Introduction

In transactinide chemistry research, gas-phase separation procedures play an important role. Already the very first investigation of rutherfordium has been conducted in form of frontal isothermal gas chromatography in a chlorinating atmosphere [1]. The success of gas chemical separations in transactinide research is quite remarkable, since gas chromatography, in general, is of minor importance in inorganic analytical chemistry.

H. W. Gäggeler (✉) · A. Türler
Labor für Radio- und Umweltchemie, Universität Bern, Bern, CH;
Labor für Radio- und Umweltchemie, Paul Scherrer Institut, Villigen PSI CH,
e-mail: heinz.gaeggeler@psi.ch

M. Schädel and D. Shaughnessy (eds.), *The Chemistry of Superheavy Elements*,
DOI: 10.1007/978-3-642-37466-1_8,

There are several reasons for this exceptional situation. First, production of transactinides at accelerators implies a thermalization of the primary products in a gas, usually helium. It is rather straightforward to connect such a recoil chamber to a gas chromatographic system. Second, gas-phase separation procedures are fast and may be performed in a continuous mode. Third, at the exit of the chromatographic column, separated volatile species can be easily condensed as nearly weightless samples on thin foils. This enables detection of α decay and spontaneous fission (SF) of the separated products with supreme energy resolution.

All these advantages compensate for some disadvantages if compared to liquid-phase separations. They include modest chemical separation factors and a rather limited number of volatile species that are suited for gas chromatographic investigation. One should keep in mind that the retention temperature regime in quartz chromatography columns is limited to maximum temperatures of about 1,000 °C. In addition, due to the short half-lives of transactinide nuclides, the kinetics of the formation of chemical compounds should be fast. So far, mostly inorganic compounds have been synthesized and separated such as halides and oxyhalides. This class of compounds, mostly in form of chlorides and bromides or oxychlorides and oxybromides, respectively, proved to be ideal for the 6*d* elements of groups 4–7.

For the group 6 and 7 elements, also the oxide/hydroxide molecules have been synthesized. For elements of group 8, the tetroxide is the species of choice, since this molecule is very volatile. Very promising for gas-phase chemical studies, although not yet experimentally investigated with transactinides, appears the group of carbonyls of group 6–9 elements. First experiments with homologs revealed a rapid formation of the compound [2] and a similarly volatile behavior as observed for group 8 oxides.

The elements Cn and Fl, having closed- and quasi-closed electron shell configurations (see "Theoretical Chemistry of the Heaviest Elements"), are expected to be rather inert, noble metal-like, in their elemental state, due to the expected strong relativistic stabilization of the 7*s* and $7p_{1/2}$ valence orbitals. Early theoretical studies went as far as attributing them even a noble-gas-like behavior. First experiments with Cn and Fl could confirm a high volatility in the atomic state and only a rather weak interaction with surfaces like Au or Teflon^{TM}. Nevertheless, the concurrently investigated noble-gas Rn showed a significantly higher volatility and a very weak surface interaction that can be explained by van der Waals forces only.

First experiments to study element 113 are being conducted, but no results have been published yet. Currently accessible, but not yet studied experimentally, is element 115, while the longest lived known isotopes of elements 116 and beyond are too short for chemical investigations with current methods. Similar chemical arguments as for Cn and Fl hold for the expected properties of element 116 (livermorium, Lv), while element 118 might exhibit properties similar to Rn. The odd-*Z* elements with atomic numbers 113 and 115 are expected to be less reactive and more volatile compared to their lighter homologs Tl and Bi. However, an accurate prediction of chemical properties, especially in comparison to the behavior of their even-*Z* neighbors is difficult.

2 Rutherfordium (Rf, Element 104)

So far, most gas chemical investigations of this element have been conducted in form of its chloride, oxychloride or bromide. Only in one experiment an attempt was made to search for a p-element behavior of Rf, based on a predicted ground-state configuration of $[Rn]5f^{14}7s^27p^2$ [3] or, from a more recent calculation $[Rn]5f^{14}6d7s^27p$ [4], rather than the expected "d-like" $[Rn]5f^{14}6d^27s^2$. However, the experiment yielded no evidence for a "Pb-like" behavior of Rf [5]. This observation is not surprising, since multi-configuration dirac–fock (MCDF) calculations showed that ionization potentials, atomic, and ionic radii for Rf are very similar to those of Hf [4]. Relativistic coupled-cluster calculations based on the Dirac-Coulomb-Breit Hamiltonian including dynamic correlations (CCSD) resulted in the expected "d-like" $6d^27s^2\ ^3F_2$ state as the ground state of the atom, in contrast to the MCDF calculations. The $6d7s^27p$ state lies 0.274 eV above the ground state [6].

2.1 Volatile Compounds of Group-4 Elements

Due to the high sublimation enthalpies of group-4 elements, gas chromatographic separations of the atoms are not feasible in quartz columns. Under halogenating conditions, however, group-4 elements form mono-molecular pure halides such as tetra fluorides, chlorides, bromides, and iodides.

A good measure of the volatility is the vapor pressure. Figure 1 depicts the vapor pressure curves for Zr and Hf halides in the gas phase over the respective solids. As can be seen, the volatility decreases according to $MCl_4 > MBr_4 > MI_4 > MF_4$ with M = Zr and Hf. Evidently, chlorides and bromides are clearly the best choices for gas chemical studies. Iodides have the disadvantage of a poor thermal stability and fluorides are least volatile.

In principle, in oxygen containing carrier gases also oxyhalides can be synthesized. However, for group-4 elements little is known about these compounds. It was observed that $ZrOCl_2$ and $HfOCl_2$ decompose to tetrachlorides and the oxide

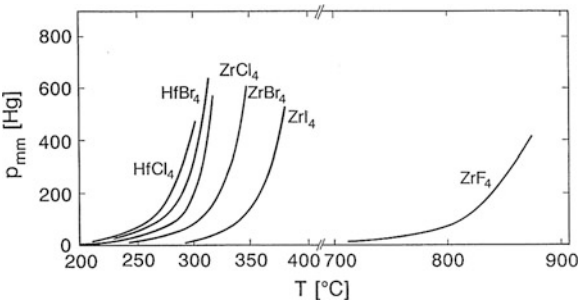

Fig. 1 Vapor pressure curves for Zr and Hf halides over their respective solids. Reproduced from [158]

under elevated temperatures [7]. An alternative process is substitutive adsorption of the pure halides on the surface of the quartz chromatography column where oxychloride formation is possible in the adsorbed state only.

2.2 Early Gas Chemical Studies with Rutherfordium

The first chemical study of Rf [1] was part of the discovery claim of this element by scientists from Dubna. For production of the isotopes ^{259,260}Rf the hot fusion reaction ^{22}Ne + ^{242}Pu was used. In these pioneering studies, isothermal frontal gas chromatography experiments showed that in a chlorinating gas Rf forms a highly volatile molecule; see "Experimental Techniques". As a chlorinating agent, 0.15 mm Hg vapor pressure of $NbCl_5/ZrCl_4$ was added to a flowing N_2 carrier gas. The gas then passed through an isothermal glass column kept at temperatures between 250 and 300 °C. From previous experiments, it was known that actinides do not form sufficiently volatile chlorides that could pass the column at such moderate temperatures.

Behind the column, mica solid-state detectors were positioned. They were kept at lower temperatures in order to adsorb the $RfCl_4$ molecules. It was assumed that the produced isotopes of Rf decay at least partly by spontaneous fission. Mica is known to be well suited for identification of latent fission tracks. In a series of experiments that accumulated a total beam dose of 4×10^{18} beam particles 65 fission tracks were detected along the mica detectors. These fission events were assigned to a spontaneously fissioning isotope of Rf, presumably ^{260}Rf. Later, this assignment was questioned since additional measurements proved that this isotope has a half-life of only 20 ms, too short for a chemical study. It was therefore concluded that ^{259}Rf with a half-life of 3 s and an assumed small fission branch was the isotope that labeled the separated molecule.

After these very first experiments, the Dubna group applied the thermochromatography (TC) technique (see "Experimental Techniques") which permits to compare the volatility of the Rf species, measured via the deposition temperature in the chromatographic tube, with those of the Hf compounds. An example of such a study is depicted in Fig. 2. From the observed very similar deposition temperature of the Rf and Hf chlorides it was concluded that both elements behave very similarly, therefore, convincingly proving that Rf is a d element [8]. Later, the chromatographic peaks shown in Fig. 2 have been analyzed applying a Monte Carlo model. Based on some assumptions on the adsorption process on the chromatography column surface and assuming that indeed the decay of ^{259}Rf with a half-life of 3 s was detected, the following standard enthalpies of adsorption, ΔH^0_a, were deduced: –110 kJ mol^{-1} for Rf and –146 kJ mol^{-1} for Hf [9].

Thermochromatography was also applied to investigate the volatility of Rf and Hf bromides [10]. These experiments yielded evidence that Rf bromide is more volatile than Hf bromide, and also more volatile than Rf chloride.

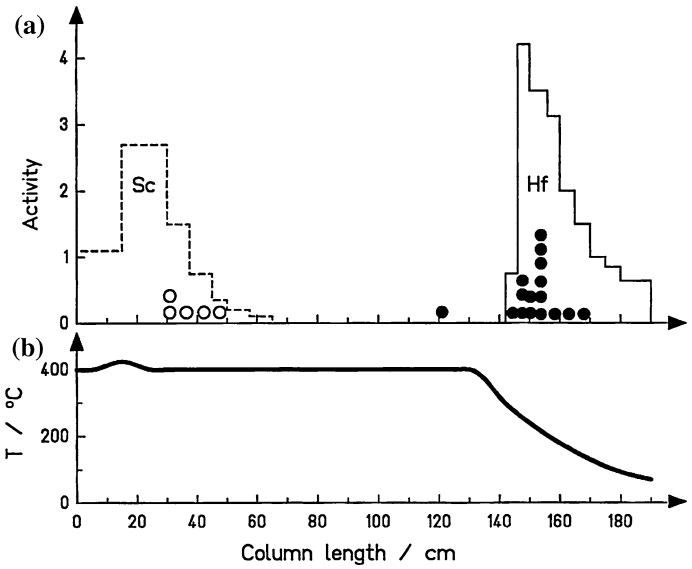

Fig. 2 Results of an experiment to investigate the volatility of ^{259}Rf and ^{170,171}Hf chlorides; **a** distribution of fission tracks (open and closed circles), ^{44m}Sc (a representative of an actinide-like element), and of ^{170,171}Hf; **b** temperature profile along the column. Reproduced from [8]

2.3 On-Line Isothermal Gas Chemical Investigations of Rutherfordium

2.3.1 General Remarks

From the mid 1980s until the early 2000s, predominantly continuous isothermal chromatography (IC) has been applied in gas chemical studies of transactinides. This technique offers the possibility to combine a continuous separation of volatile species with an in-situ detection of the products on the basis of single atom counting. To reach this ambitious goal, novel devices were developed such as the on-line gas chemistry apparatus (OLGA) [11] or, in a modified version, the heavy element volatility instrument (HEVI) [12]; see "Experimental Techniques".

On-line isothermal gas chemistry has originally been developed to search for superheavy elements with atomic numbers between 112 and 118. OLGA I was restricted to an operation with inert gases. Its application concentrated on separations of volatile atoms. As a "reactive" gas, traces of hydrogen gas could be added to a helium carrier gas in order to stabilize the elemental state. Model studies with the *p*-elements Po, Pb, Bi, and At showed that at temperatures of up to 1,000 °C excellent separations of these elements from *d* elements and from *f* elements could be achieved.

Improved versions of OLGA (versions II and III) enabled the applications of corrosive gases, such as hydrogen chloride or hydrogen bromide, chlorine, thionyl

chloride or boron tribromide vapor etc. This made it possible to synthesize volatile halides and measure their retention times in isothermal quartz columns.

2.3.2 Isothermal Gas Chromatography Studies of $RfCl_4$ and $RfBr_4$

For investigations of the chlorides and bromides, commonly the isotope ^{261}Rf was used as a tracer. It has a half-life of 68 s [13, 14] and can be produced in the fusion reaction $^{18}O + ^{248}Cm$ at a bombarding energy of about 100 MeV. ^{261}Rf decays via emission of two sequential α particles via ^{257}No to ^{253}Fm, a long-lived product. Hence, identification of ^{261}Rf after chemical separation bases on the measurement of the two lifetimes and the two α-decay energies of the mother and its daughter nuclide, respectively. From the four signals, an unequivocal identification of every decaying atom of rutherfordium can be achieved. Simultaneous formation of Hf isotopes may be obtained by covering the ^{248}Cm target by a thin layer of Gd.

Figure 3 depicts the result from such a study with the OLGA III device [11]. A flow of He, saturated with carbon aerosol particles, served as a carrier to transport the products from the collection chamber to the chemistry device. The chemical reagent was HCl gas. It was purified from traces of oxygen and was added to the carrier gas at the entrance of the oven system. Rf passed through the quartz column at a lower retention temperature compared to Hf. This observation received considerable attention and was interpreted as evidence for relativistic effects, since the higher volatility of $RfCl_4$ compared to that of $HfCl_4$ is unexpected on the basis of classical extrapolations; see "Thermochemical Data from

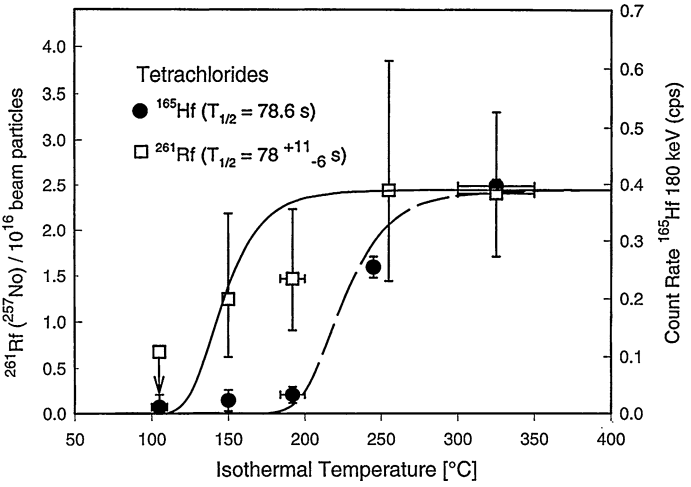

Fig. 3 Relative yields for $^{261}RfCl_4$ and $^{165}HfCl_4$ behind the quartz chromatography column as a function of the isothermal temperature. ^{261}Rf and ^{165}Hf were formed simultaneously in the reaction $^{18}O + ^{248}Cm/^{152}Gd$, respectively. The *solid lines* represent Monte Carlo simulations adapted to the experimental data. Reproduced from [22]

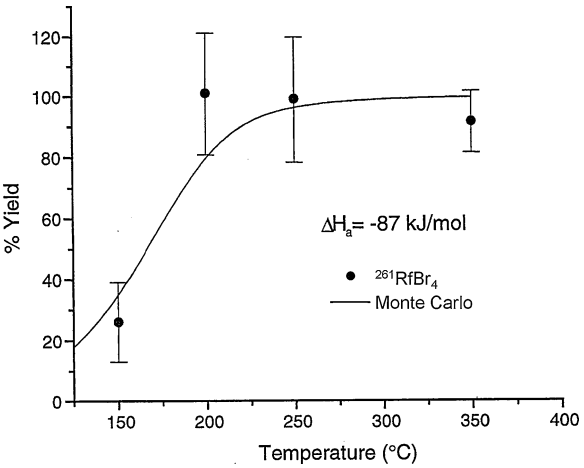

Fig. 4 Chromatographic yield curve for ^{261}Rf bromide using KBr aerosol particles for transport and HBr as reactive gas. Reproduced with permission from [17]. Copyright 2000 Oldenbourg Wissenaschaftsverlag GmbH

Gas-Phase Adsorption and Methods of Their Estimation" for empirical extrapolations and "Theoretical Chemistry of the Heaviest Elements" for theoretical approaches including relativistic effects.

In an earlier study with the device HEVI, chlorides of Zr, Hf, and Rf were investigated employing the reactive gases HCl/CCl_4 (Zr, Hf) and HCl (Rf). MoO_3 particles in a He carrier gas served as aerosol [15]. In contact with HCl, MoO_3 forms a very volatile Mo oxychloride that passes through the chromatographic column without deposition on its surface. For Rf chloride, a higher volatility was found compared to Hf chlorides; see Fig. 3. In addition, the volatility of Zr chloride turned out to be very similar to that of Rf chloride, hence, different to the volatility of Hf chloride. This observation is rather unexpected, since the volatilities of macroamounts of Zr and Hf tetrachlorides are nearly identical, see Fig. 1. Whether formation of oxychlorides explains this discrepancy remains unclear.

A first study of Rf bromide with OLGA II indicated that the Rf compound is more volatile than Hf bromide [16]. For the transport, KCl was used as aerosol particles and HBr/BBr_3 served as a reactive gas. In addition, Rf bromide was found to be less volatile compared to the Rf chloride. In a follow-up study with HEVI, using KBr particles and HBr as a brominating agent, these findings were essentially confirmed, see Fig. 4. The behavior of Zr and Hf bromides was found to be very similar and both being less volatile than the Rf bromide [17].

2.3.3 Oxychlorides of Rf

The oxychlorides of group-4 elements are expected to be less stable than the pure chlorides. $ZrOCl_2$ and $HfOCl_2$ were found to decompose to the tetrachlorides at elevated temperatures [7]. It is therefore not clear whether $ZrOCl_2$ and $HfOCl_2$ exist in the gas phase.

In thermochromatography experiments an increase of the deposition temperature of Zr and Hf was observed as a function of the partial pressure of oxygen in a chlorinating reactive gas mixture [18]. An OLGA III study with oxygen containing chlorinating reactive gas confirmed this observation: Rf and Hf compounds were considerably less volatile compared to oxygen-free conditions; see Fig. 5. It was speculated that the oxychlorides do not exist in the gas phase but only in the adsorbed state. The following transport mechanism was proposed:

$$MCl_{4(g)} + {}^{1}/_{2}\ O_2 \rightleftarrows MOCl_{2(ads)} + Cl_{2(g)} \quad (1)$$

It is interesting to note that, as seen in Fig. 5, $RfOCl_2$ and $HfOCl_2$ behave much more similar compared to the pure chlorides $RfCl_4$ and $HfCl_4$. Further experimental studies are required to corroborate such a reaction mechanism by varying and well controlling the partial pressure of oxygen in different experiments.

2.3.4 Adsorption Enthalpies of Zr, Hf, and Rf Chlorides and Bromides on Quartz

From the measured chromatographic retention temperatures adsorption enthalpies (ΔH_a^0) of single molecules on the surface of the quartz chromatography column can be deduced. This analysis is based on certain thermodynamic assumptions of the adsorption process of single molecules with the surface of the chromatographic column [19]. In addition, a Monte Carlo model enables to describe the migration

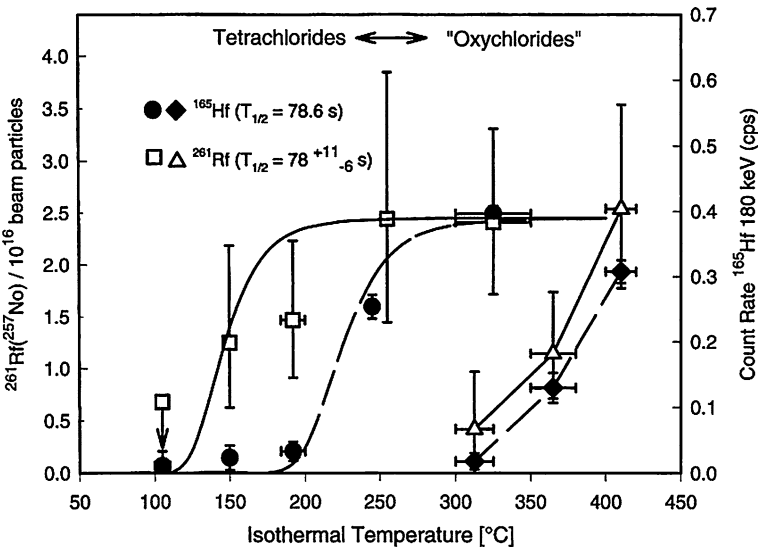

Fig. 5 Yields for ^{261}Rf and ^{165}Hf tetrachlorides (in the left part) obtained with oxygen-free HCl and (in the right part) oxychlorides from $SOCl_2$ vapor and O_2 added as a reactive gas. *Lines* are results from Monte Carlo simulations. Reproduced from [22]. Copyright 1998 Elsevier

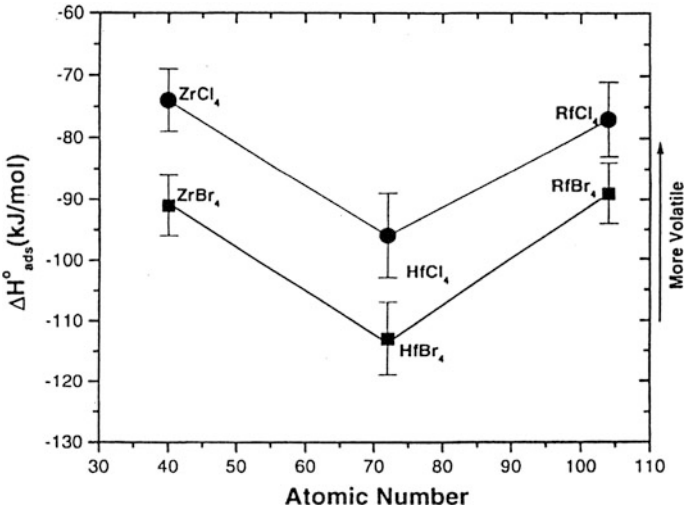

Fig. 6 Adsorption enthalpies of chlorides and bromides of Zr, Hf, and Rf on quartz surfaces, deduced from OLGA and HEVI experiments. Reproduced from [21]

path of each single molecule along the chromatographic column under real experimental conditions [20]; see "Thermochemical Data from Gas-Phase Adsorption and Methods of Their Estimation".

Figure 6 summarizes resulting ΔH_a^0 values from isothermal gas chromatographic investigations of the pure chlorides and bromides of Zr, Hf, and Rf, respectively, using the HEVI and OLGA II devices [21]. A smooth (classical) extrapolation of the ΔH_a^0 values from Zr through Hf shows that one would expect the ΔH_a^0 values for $RfCl_4$ or $RfBr_4$ to be more negative than those of the respective Hf compounds. The experimental values for Rf show a striking reversal of this expected trend. In addition, the bromides have more negative values, hence being less volatile than the corresponding chlorides.

Relativistic calculations of the chemical properties of these compounds predict trends that are in agreement with experimental observations; see "Theoretical Chemistry of the Heaviest Elements". Therefore, it was argued that this "reversal" in the trend of ΔH_a^0 for chlorides and bromides, when going from Zr via Hf to Rf, is evidence for "relativistic effects" in the chemistry of Rf [22].

3 Dubnium (Db, Element 105)

Dubnium is expected to have a $[Rn]5f^{14}6d^37s^2$ electronic ground-state configuration. This makes dubnium a firm member of group 5 of the Periodic Table, positioned below tantalum.

All gas chemical investigations of dubnium have been performed with Db^{5+} in form of the pentahalides (chlorides and bromides) and oxyhalides. As a general rule, all these studies were extremely difficult because of the high tendency of group-5 elements to react with trace amounts of oxygen or water vapor. Hence, gas chemical investigations were only successful if the quartz chromatography columns were very carefully preconditioned with the halogenating reactive gas prior to each experiment. In addition, extensive cleaning procedures to the carrier gas, to remove trace amounts of oxygen and water vapor, were mandatory.

3.1 Volatile Compounds of Group-5 Elements

Group-5 elements are most stable in their maximum oxidation state +5, and, therefore, form pentahalides, see Fig. 7. Most volatile are the pentafluorides, followed by the pentachlorides and the pentabromides. Besides the pure halides, also the oxyhalides (MOX_3) are stable in the gas phase. They should be less volatile compared to the pure halides. This was confirmed experimentally for niobium, see Fig. 8. Under certain experimental conditions both species, the pure halide and the oxyhalide coexist for $NbBr_5$ and $NbOBr_3$ [23], see Fig. 9.

3.2 Early Gas Chemical Studies with Dubnium

As early as 1970, gas chemical experiments with Db were performed in a chlorinating atmosphere [24]. These studies applied the gas thermochromatography technique; see "Experimental Techniques". They indicated that the deposition

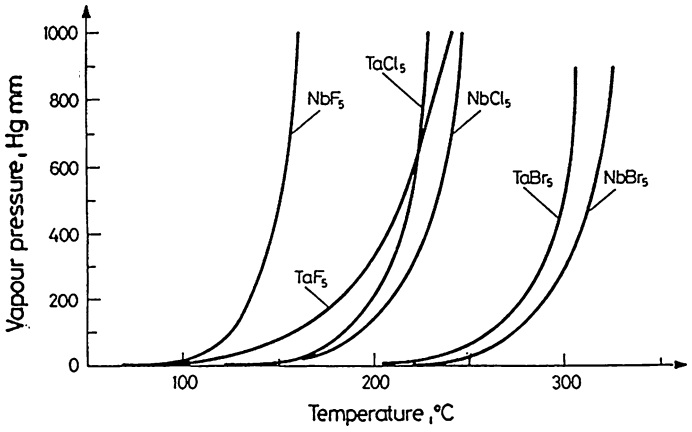

Fig. 7 Vapor pressure curves for Nb and Ta halides over the respective solids. Reproduced from [158]

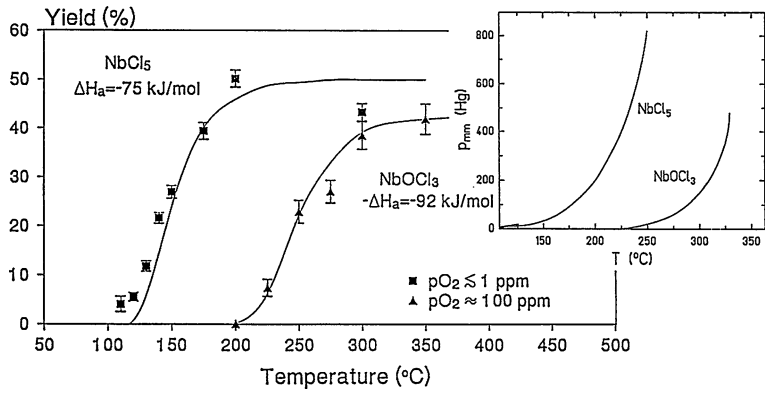

Fig. 8 Vapor pressure curves for $NbCl_5$ and $NbOCl_3$ (upper right corner) and the relative yields of $^{99g}NbCl_5$ and $^{99g}NbOCl_3$ molecules passing through an isothermal quartz column using pure HCl gas and HCl gas with some oxygen, respectively. Reproduced from [158]

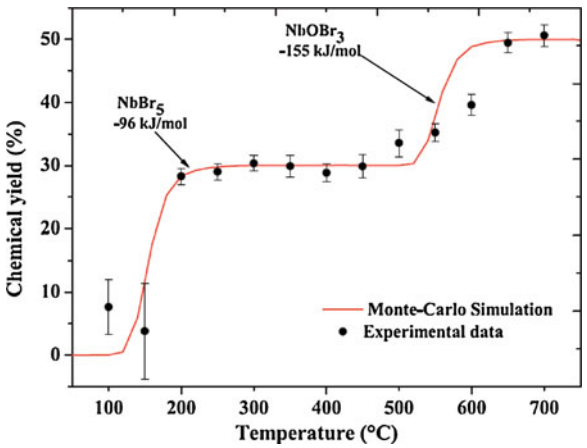

Fig. 9 Chemical yields of $NbBr_5$ and of $NbOBr_3$ measured in an isothermal quartz column using HBr as reactive gas and not highly purified He as carrier gas. Reproduced with permission from [23]. Copyright 2012 Oldenbourg Wissenschaftsverlag GmbH

temperature of Db as a chloride (or oxychloride) is rather similar to that of Hf, if studied under identical conditions, and significantly higher compared to the deposition temperature of Nb. Later studies were conducted in a brominating gas medium, and again yielded evidence that Db bromide is less volatile compared to the homolog compound with Nb [25], see Fig. 10. These investigations were performed with ^{261}Db ($T_{1/2} = 1.8$ s), which has a small fission branch. This nuclide was produced in the $^{243}Am(^{22}Ne,4n)^{261}Db$ reaction.

From the result of this experiment, it was concluded that the boiling point of $DbBr_5$ may exceed the boiling point of $NbBr_5$ by 80–100 °C and may be close to the boiling point of $PaBr_5$. The ionic radius of Db^{5+} was estimated to be close to the radius of Pa^{5+}, which is $\approx$0.9 Å, whereas the radii of Nb^{5+} and Ta^{5+} are both $\approx$0.7 Å.

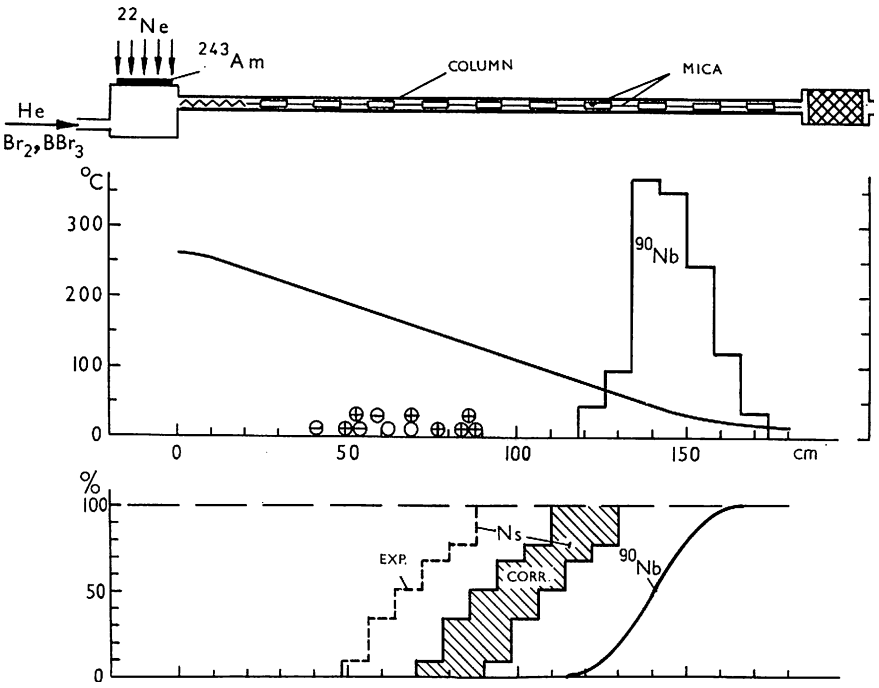

Fig. 10 *Top* Schematic of the early thermochromatography experiment with Db in a brominating atmosphere ($Br_2 + BBr_3$). *Middle* Temperature profile along the column and measured distributions of ^{90}Nb and ^{261}Db. *Bottom* Integral distribution of ^{90}Nb (*solid line*) and of Db (named Ns by the authors at that time; *shaded area*) after corrections for the much shorter half-life of ^{261}Db compared to that of ^{90}Nb. Reproduced from [25]

3.3 On-Line Isothermal Gas Chemical Investigations of Dubnium

3.3.1 Production of Dubnium Isotopes

On-line gas chemical studies of dubnium have been mostly performed with ^{262}Db. This nuclide can be produced in the reaction ^{249}Bk(^{18}O, 5n) at a beam energy of about 100 MeV. It has a half-life of 34 ± 5 s and decays with 67% by emission of two sequential α particles via ^{258}Lr ($T_{1/2} = 4.4$ s) to the long-lived ^{254}Md ($T_{1/2} = 28$ min). In addition, ^{262}Db shows spontaneous fission with a decay branch of 33%; possibly from the short-lived EC-decay daughter ^{262}Rf. Hence, identification of each separated labeled molecule is based on either detection of two characteristic α-particles and their lifetimes or on the detection of a spontaneous fission decay. A more recent chemical study used the isotope ^{258}Db formed in the reaction ^{243}Am(^{20}Ne, 5n)^{258}Db at a beam energy of about 120 MeV [23]. ^{258}Db has a half-life

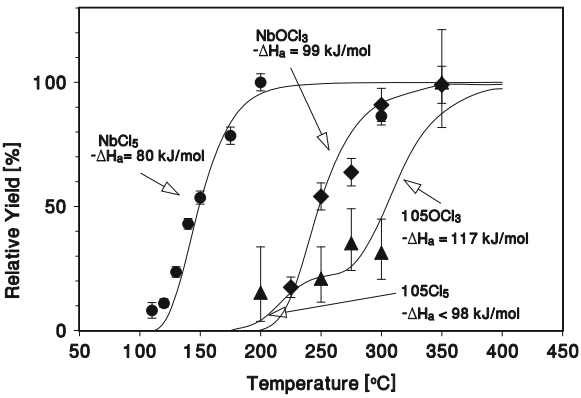

Fig. 11 Relative yield of Db (*triangles*) measured in an isothermal gas chromatographic experiment with purified HCl as reactive gas. Reproduced with permission from [26]. Copyright 1996 Oldenbourg Wissenschaftsverlag GmbH. For comparison, the data for Nb measured under identical gas chemical conditions from Fig. 8 are also shown

of 4.3 s and decays by α emission (67%). Its daughter ^{254}Lr has a half-life of 13 s and decays by α emission (78%) to the granddaughter nuclide ^{250}Md, which decays mostly (93%) by EC to the long-lived product ^{250}Fm ($T_{1/2}$ = 30 min).

3.3.2 Chlorides and Oxychlorides

Several attempts failed to form the pure pentachloride of Db in on-line isothermal gas chromatographic investigations. Obviously, despite very thorough cleaning procedures, minute amounts of oxygen and/or water vapor in the system were still sufficient to form at least partly dubnium oxychloride, most likely $DbOCl_3$. Figure 11 depicts a measured chromatographic curve in conjunction with the data for Nb from Fig. 8 [26].

As chlorinating agent HCl gas was used, purified with activated charcoal at 900 °C. The shape of the yield curves suggests two components, a species with a lower volatility passing through the column above 350 °C and one with a higher volatility that is retained in the column only below 200 °C. The two species are tentatively assigned to $DbOCl_3$ and $DbCl_5$, respectively.

3.3.3 Bromides and Oxybromides

The volatility of Db bromides was studied with HBr as a reactive gas using the isotope ^{262}Db formed in the ^{249}Bk(^{18}O, 5n) reaction [27]. In this experiment, the retention behaviors of Nb and Ta bromides were investigated as well. Interestingly, the volatile Ta bromide was formed only when HBr was saturated with BBr_3 vapor. Results are shown in Fig. 12. A trend in volatility of Nb ≈ Ta > Db was deduced. This sequence is very surprising since $DbBr_5$ is expected to be more volatile compared to $NbBr_5$ and $TaBr_5$, respectively, based on considerations of

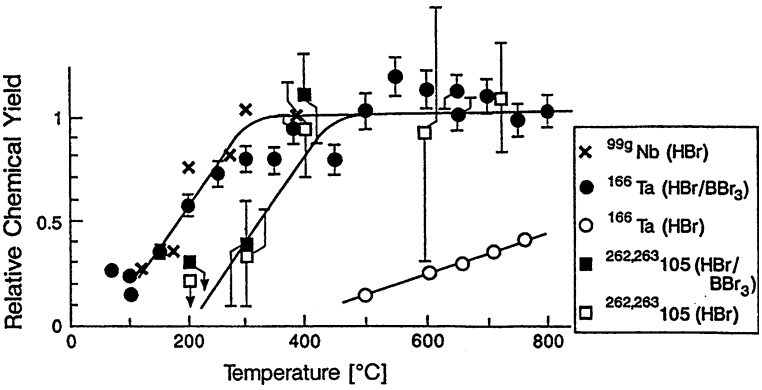

Fig. 12 Yields of Nb, Ta, and Db in a gas chromatographic experiment with HBr (Nb, Db) and HBr/BBr_3 (Db, Ta) as reactive gas. Reproduced with permission from [27]. Copyright 1992 Oldenbourg Wissenschaftsverlag GmbH

the adsorption on quartz surfaces by dispersion forces [28–30]. Evidence for a lower volatility of Db bromide relative to that of Nb bromide has already been found in previous thermochromatographic studies; see Fig. 10. It was stated [26] that formation of Db oxybromide with trace amounts of water vapor in the carrier gas cannot be fully excluded.

More recently, the experimental study of Db bromide was repeated with an improved purification of the He carrier gas. Under this condition, the data shown in Fig. 13 were collected, which indicated that Db bromide is more volatile than observed previously (see Fig. 12). The volatility sequence deduced from this experiment, together with independent studies on the behavior of Nb and Ta under identical chemical conditions, was Db > Nb > Ta [23]. This experimental

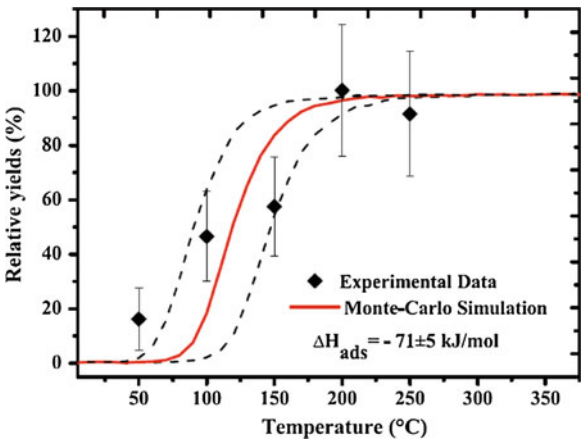

Fig. 13 Yields of ^{258}Db in a gas chromatographic experiment with HBr gas added to highly purified carrier gas He. Reproduced with permission from [23]. Copyright 2012 Oldenbourg Wissenschaftsverlag GmbH

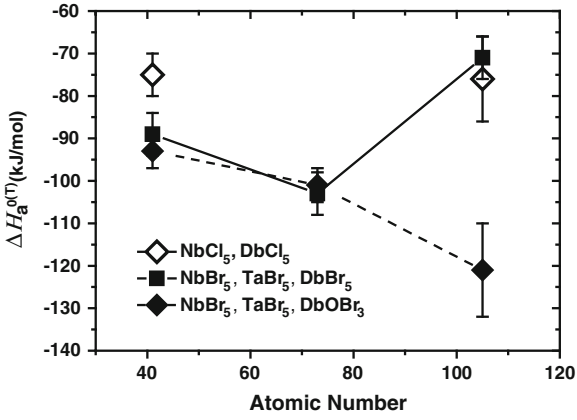

Fig. 14 Adsorption enthalpies of pentachlorides and -bromides of Nb, Ta and Db on quartz surfaces from isothermal chromatography experiments. Data from [23] for $NbBr_5$, $TaBr_5$, $DbBr_5$ (filled *squares*), [27] for $NbBr_5$, $TaBr_5$, $DbOBr_3$ (filled *diamonds*), and [31] $NbCl_5$, $DbCl_5$ (open *diamonds*)

observation is in conflict with previous studies, but only concerning the behavior of Db; see Fig. 14. The deduced adsorption enthalpies for $NbBr_5$ and $TaBr_5$ were in excellent agreement. It was concluded that indeed the previous studies [25, 27] were performed with Db oxybromide rather than the Db bromide. A different explanation is proposed by Pershina et al. [30] where the formation of MBr_5L^- (L = Br or Cl) complexes is discussed on the KCl or KBr covered surface (see "Theoretical Chemistry of the Heaviest Elements, Predictions of Volatility of Group-4 through 8 Compounds"), which would indeed suggest a less volatile Db compared to Nb and Ta. It was also concluded that if the pure bromides were observed experimentally for Nb and Ta, also $DbBr_5$ should be formed, since Db showed the lowest affinity toward oxygen [30], in contrast to earlier predictions [29].

3.3.4 Adsorption Enthalpies of Nb, Ta, and Db Chlorides, Oxychlorides, Bromides, and Oxybromides on Quartz

Figure 14 depicts ΔH_a^0-values of group-5 chlorides and bromides measured with the OLGA technique (for an overview of several experimental investigations and a re-analysis of the data, see [26]). The trend of the ΔH_a^0-values for bromides when going from Nb via Ta to Db is very similar to the situation in group 4 depicted in Fig. 6. For the pentachlorides no data exist yet for Ta. For $DbCl_5$, the value determined by Kadkhodayan [31] is given, which is afflicted with a rather large uncertainty, but appears quite plausible with respect to the value determined for $DbBr_5$ by Qin et al. [23]. In Table 1, ΔH_a^0-values measured for group 5 halides and oxyhalides are summarized.

Table 1 Comparison of $-\Delta H_a^{0(T)}$ values measured for group-5 halides and oxyhalides in various experiments

Technique	References	Years	Aerosol material	$-\Delta H_a^{0(T)}$·(kJ·mol^{-1})					
Chlorides				$NbCl_5$	$NbOCl_3$	$TaCl_5$	$TaOCl_3$	$DbCl_5$	$DbOCl_3$
TC	[161]	1973	–	85[a]				88[a]	
TC	[162]	1991	–	95[a]				118[a]	
IC, HEVI	[31]	1993	MoO_3	75 ± 5[b]			157 ± 12[b]	76 ± 10[b]	
IC, OLGA III	[163]	1996	C	80 ± 1	99 ± 1			≤97	117 ± 3
Bromides				$NbBr_5$	$NbOBr_3$	$TaBr_5$	$TaOBr_3$	$DbBr_5$	$DbOBr_3$
TC	[161]	1973	–	87[a]				82[a]	
TC	[162]	1991	–	83[a]				108[a]	
IC, OLGA II	[27]	1992	KCl	93 ± 4[c]		101 ± 4[c]			121 ± 11[c]
IC, OLGA III	[23]	2012	KBr	89 ± 5	155 ± 5	103 ± 5		71 ± 5	

[a] Data evaluated in Ref. [164]
[b] Data from Ref. [31] reanalyzed with $\tau_0 = 2{\cdot}10^{-13}$ s [163]
[c] Data from Ref. [27] reanalyzed with $\tau_0 = 2{\cdot}10^{-13}$ s [163]

4 Seaborgium (Sg, Element 106)

For over 20 years, ^{263}Sg with a half-life of 0.9 s was the longest lived known Sg isotope. In addition to the minute production rates, this short half-life effectively prevented a chemical identification of Sg. In 1992, Timokhin et al. from Dubna studied the chemical identification of Sg as a volatile oxychloride making use of an on-line thermochromatography method [32]. This claim was substantiated by ancillary experiments [33, 34] and further studies of the behavior of the group-6 homologs Mo and W [35]. Shortly thereafter, an international collaboration of chemists conducted on-line isothermal chromatography experiments with Sg oxychlorides [36]. The presence of Sg after chemical isolation in the gas-phase was established by directly identifying the nuclide ^{265}Sg via the observation of its characteristic, genetically linked, nuclear decay chain[1] [36]. Also, a first thermochemical property of a Sg compound, namely the adsorption enthalpy of Sg oxychloride on the chromatographic surface was measured in these experiments [38]. In a subsequent experiment, Sg was also characterized as a volatile oxide hydroxide in on-line isothermal chromatography experiments [39].

4.1 Volatile Compounds of Group-6 Elements

Seaborgium is expected to be a member of group 6 of the Periodic Table, and thus a homolog of Cr, Mo, and W. In the elemental state, all group-6 elements are extremely refractory. The melting and boiling points are strongly increasing down the group (W has the highest melting point of all metals). While both Mo and W are chemically very similar, there is not much similarity with Cr. Both Mo and W have a wide variety of oxidation states and their chemistry is among the most complex of the transition elements. There exist a number of volatile inorganic Mo and W compounds that are suitable for gas chromatographic investigations. Mo and W form volatile halides, oxyhalides, oxide hydroxides, and also carbonyls.

[1] Due to an erroneous assignment of mass numbers and decay properties in the physics discovery experiment [37], it was believed that also in the chemistry experiments two different isotopes of Sg, namely ^{265}Sg and ^{266}Sg were observed [36, 38, 39]. After, the discovery of ^{270}Hs (the α-decay mother of ^{266}Sg) it became evident, that all decay chains observed in the Sg chemistry experiments are due to ^{265}Sg only [13, 14]. There is now conclusive evidence for two isomeric states in ^{265}Sg [40]. ^{265}Sg^{a} decays with a half-life of about 9 s preferentially to ^{261}Rf^{a}, which further decays by α-particle emission and a half-life of 68 s to ^{257}No, whereas ^{265}Sg^{b} with a half-life of about 14 s decays preferentially to ^{261}Rf^{b}, which undergoes spontaneous fission with a half-life of about 3 s [40, 41]. Both states are formed in the direct synthesis reaction ^{248}Cm(^{22}Ne,5n)^{265}Sg^{a,b}. See detailed discussion in Sect. 6.5 and Fig. 31.

4.1.1 Halides and Oxyhalides

Among all hexahalides only the compounds MF_6 (M = Mo, W), WCl_6, and WBr_6 are known. $MoCl_6$ is not stable and exists probably only in a chlorine atmosphere in the gas phase. WCl_6 can be volatilized as a monomeric vapor while WBr_6 is decomposing to WBr_5 on moderate heating. Of the pentahalides, the pentafluorides and the pentachlorides are known; W also forms the pentabromide. While MoF_5 and WF_5 have the typical tetrameric structure of the pentafluorides, $MoCl_5$ and WCl_5 form dimeric species in the solid. $MoCl_5$ is monomeric in the gas phase.

In contrast to the pure halides, the oxyhalides of group-6 elements are more stable and show a similarly high volatility. For the 6^+ oxidation state, the two stoichiometric types MOX_4 and MO_2X_2 (M = Mo, W; X = F, Cl) exist. The Mo compounds are less stable than those of W. Of the oxyfluorides $MoOF_4$, MoO_2F_2, and WOF_4 are known, whereas the existence of WO_2F_2 is doubtful. Of the oxychlorides all four varieties exist. However, $MoOCl_4$ decomposes to $MoOCl_3$ already at room temperature. WO_2Cl_2 disproportionates at temperatures above 200 °C to form WO_3 and $WOCl_4$. Though there is no indication that single molecules of WO_2Cl_2 are unstable even at elevated temperatures.

In the 5^+ oxidation state, four principal compounds of the type MOX_3 (M = Mo, W; X = Cl, Br) are known. The vapor pressure of Mo and W chlorides and oxychlorides over their respective solids as a function of temperature is shown in Fig. 15. All vapor pressures of the pure chlorides $MoCl_5$, WCl_5, and WCl_6 are very similar. The volatility of MoO_2Cl_2 is higher than that of $MoOCl_4$, whereas the situation is reversed for W, where $WOCl_4$ is more volatile than WO_2Cl_2. According to tabulated enthalpies of sublimation, $MoOCl_4$ should be more volatile than MoO_2Cl_2 [42]. This change in the sequence of vapor pressures can be explained by the solid-phase entropies.

4.1.2 Oxides and Oxide Hydroxides

By analogy to Mo and W, the oxides and oxide hydroxides of Sg are expected to be moderately volatile, whereas the heavy actinides and the groups 4 and 5 transactinides Rf and Db do not form volatile oxides and oxide hydroxides. For

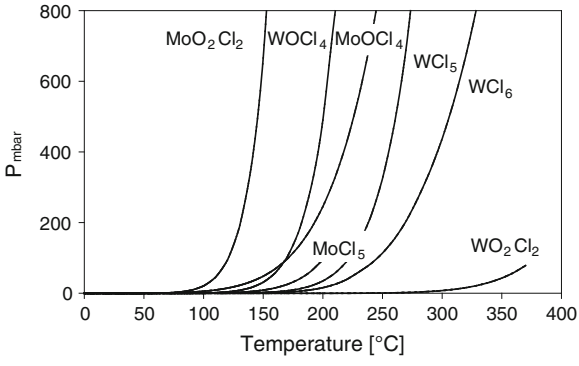

Fig. 15 Vapor pressure of Mo and W chlorides and oxychlorides over their respective solids as a function of temperature. $MoCl_5$ is melting at 197 °C whereas WO_2Cl_2 disproportionates at temperatures above 200 °C. Data from [42]

this reason this class of compounds should be very selective with regard to a gas chromatographic isolation of Sg from the plethora of by-products of the nuclear formation reaction. Mo and W form many stable oxides, but in excess of oxygen, the trioxides MO_3 (M = Mo, W) should be the main component. Macroscopic amounts of MoO_3 and WO_3 sublimate preferentially as polymers of the type $(MO_3)_n$. However, carrier-free amounts can be volatilized in dry oxygen only as monomers. In moist oxygen, the more volatile oxide hydroxides $MO_2(OH)_2$ (M = Mo, W) can be formed. Extensive studies using thermochromatography and on-line isothermal chromatography [43, 44] in dry and moist oxygen have revealed that the transport of Mo and W in moist oxygen is not governed by simple reversible adsorption reactions of $MO_2(OH)_2$, but by a dissociative adsorption according to the reaction

$$MO_2(OH)_2 \rightleftarrows MO_{3(ads)} + H_2O_{(g)} \quad M = Mo, W. \tag{2}$$

4.1.3 Carbonyls

A characteristic feature of d-group elements is their ability to form complexes with π-acceptor type ligands such as CO. All group-6 elements Cr, Mo, and W form very volatile and stable hexacarbonyls and constitute the only complete family of carbonyls. Direct production of carbonyls from the elements and CO is only accomplished at high pressures and temperatures. However, formation of carbonyls is possible in hot atom reactions under ambient condition. Nuclides formed in nuclear reactions (via fission or heavy ion reactions) are thermalized in a stopping gas to which CO gas is added, and then highly volatile carbonyls are formed in situ [45, 2]. When fission products were thermalized in a mixture of N_2/CO, the formation and transport of $Mo(CO)_6$ was observed. Up to 80% yield could be obtained compared to a N_2/KCl-cluster gas-jet transport, when the gas mixture contained 75% CO. Thermochromatography experiments revealed a very volatile species on quartz for which adsorption enthalpies of -42.5 kJ·mol^{-1} were evaluated, very similar to OsO_4; see Sect. 6.1. Thermochromatography experiments with α-emitting ^{163,164}W and ^{170,171}Os, preseparated with the gas-filled recoil separator TASCA and stopped in a recoil transfer chamber, resulted in adsorption enthalpies of –46.5 and –43.5 kJ·mol^{-1} and were assigned to the species $W(CO)_6$ and $Os(CO)_5$, respectively. The feasibility of a future experiment to study $Sg(CO)_6$ and $Hs(CO)_5$ was, thus, fully demonstrated.

4.2 Gas Chemical Studies with Seaborgium

4.2.1 Thermochromatography of Oxychlorides

Early on, separation procedures to chemically isolate Sg concentrated on the inorganic gas chromatography of chlorides and/or oxychlorides [46]. In a number

of studies, the gas chromatographic behavior of halide and oxyhalide species of Mo and W were investigated with respect to a physico-chemical characterization of Sg [47–55].

In experiments by the Dubna group [32–35], the reaction ^{249}Cf(^{18}O, 4n) was employed to produce 0.9-s ^{263}Sg. A very similar setup as in experiments to chemically identify Rf and Db was used. Reaction products were thermalized behind the target in a rapidly flowing stream of Ar gas and flushed to the adjoining thermochromatography column; see "Experimental Techniques". Volatile oxychlorides were synthesized by adding air saturated with $SOCl_2$ as a reactive agent. The formed oxychloride species migrated downstream the fused silica chromatography column, to which a longitudinal, negative temperature gradient was applied, and finally deposited according to their volatility. In contrast to earlier experiments, no mica plates were inserted, but the fused silica column itself served as SF track detector. The deposition of Sg was registered after completion of the experiment by searching for latent SF tracks left by the SF decay of ^{263}Sg. Indeed, in several experiments a number of SF tracks were found in the column in the temperature region 150–250 °C. They were attributed to the decay of Sg nuclides. Therefore, like its lighter homologs Mo and W, Sg must form volatile oxychloride compounds. The SF tracks were only found, when the quartz wool plug, which was inserted as a filter for aerosols, was absent. This was attributed to the increased surface, and thus a much longer retention time. In Fig. 16, the locations of those 41 registered SF events are shown that were observed in the course of three experiments corresponding to a total beam dose of 6.1×10^{17} ^{18}O beam particles. The dotted histogram shows the data corrected for the relative detection efficiency caused by the increasingly strong annealing of fission tracks at increasing, elevated temperatures. The solid lines denoted with "[106]" and with ^{176}W show the deposition peak for 2.5-h ^{176}W and the expected shape of the "[106]" deposition peak fitting the SF data. Based on the results of ancillary experiments with short-lived W nuclides, it was concluded that in a first, fast step volatile MO_2Cl_2 (M = W, Sg) molecules were formed and in a second, slower step the deposited MO_2Cl_2 was converted to more volatile $MOCl_4$.

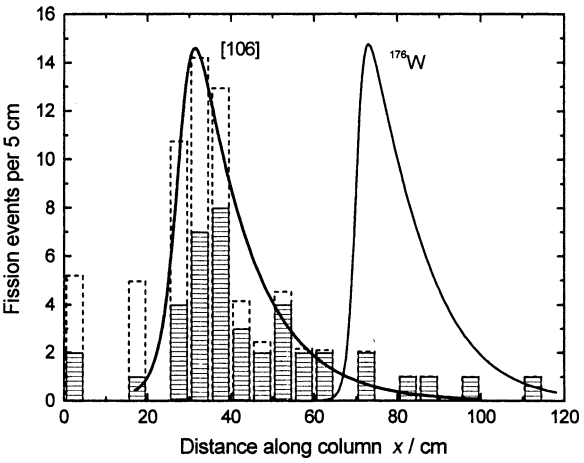

Fig. 16 Measured distribution of spontaneous fission events attributed to the decay of an isotope of element 106 (Sg). The dotted histogram shows the data corrected for the relative detection efficiency due to annealing of fission tracks. The thick solid curves show the smoothed corrected thermochromatograms for Sg, denoted "[106]", and for ^{176}W. Figure reproduced with permission from [35]. Copyright 1998 Oldenbourg Wissenschaftsverlag GmbH

Therefore, the Sg deposition peak was attributed to the compound SgO_2Cl_2, whereas the ^{176}W deposition peak was attributed to $WOCl_4$. Due to the occurrence of two different species as well as due to the large differences in half-life no information about the relative volatility of MO_2Cl_2 (M = Mo, W, Sg) or $MOCl_4$ (M = Mo, W, Sg) was obtained within group 6.

4.2.2 Isothermal Chromatography of Oxychlorides

In 1995 and 1996, an international collaboration of radiochemists conducted on-line isothermal chromatography experiments with Sg oxychlorides using the OLGA technique (see "Experimental Techniques") at the Gesellschaft für Schwerionenforschung (GSI) in Darmstadt [36, 38]. In this work, the Sg-isotopes $^{265}Sg^{a,b}$ were synthesized in the reaction $^{248}Cm(^{22}Ne,5n)$. Nuclear reaction products, recoiling from the target, were stopped in He gas loaded with carbon aerosols, and—adsorbed to their surface—were continuously transported through a thin capillary to the OLGA set-up. The aerosols carrying the reaction products were collected on quartz wool inside the reaction oven kept at 1000 °C. Reactive gases—Cl_2 saturated with $SOCl_2$ and traces of O_2—were introduced in order to form volatile oxychlorides (thermodynamic calculations [54] indicate that Mo and W most probably form the dioxide dichloride MO_2Cl_2, M = Mo, W). Simultaneously, the carbon aerosols were converted to CO_2. The chromatographic separation takes place downstream in the adjoining isothermal section of the column. At temperatures of 300 °C and above, group-6 oxychloride molecules travel through the column essentially without delay. In order to increase the sensitivity of the experiment, the mother–daughter recoil counting modus was implemented at the rotating wheel system ROMA; see "Experimental Techniques". In a first experiment conducted at isothermal temperatures of the chromatography column of 300 °C and of 400 °C, the nuclides $^{265}Sg^{a,b}$ were unambiguously identified after chemical isolation by the observation of α-decay chains [57].

In a second experiment at 350 °C isothermal temperature, the results of the first experiment were confirmed by observing further $^{265}Sg^{a,b}$ α-decay chains [57]. Without changing any other experimental parameter, the isothermal temperature was then lowered to 250 °C and the yield of ^{265}Sg was measured with a comparable sensitivity as at higher isothermal temperatures. In order to assure that the experimental setup performed as expected, the nuclide ^{168}W was simultaneously produced from a small ^{152}Gd admixture to the ^{248}Cm target material and its yield was monitored. In Fig. 17, the relative yields measured for oxychlorides of short-lived Mo, W, and Sg nuclides are shown as a function of isothermal temperature (the Sg data points measured at 300, 350 and 400 °C are summarized in one data point). The yield curve for ^{168}W was measured with the same chromatography column and under identical experimental conditions as they were then used for the isolation of Sg, whereas the yield curve for ^{104}Mo was determined in an earlier measurement. The solid lines show the results of a Monte Carlo simulation

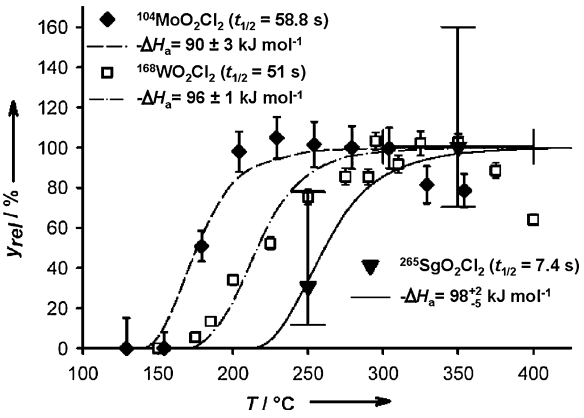

Fig. 17 Relative yield of MO_2Cl_2 (M = Mo, W, Sg) as a function of isothermal temperature in the chromatography column [38]

procedure where the migration of a molecule through the chromatography column has been modeled [20].

From the measured Sg data, a first thermochemical property of a Sg compound could be deduced, namely $-\Delta H_a^0(SgO_2Cl_2) = 98^{+2}_{-5}$ kJ·mol^{-1} (68% error interval). For WO_2Cl_2, $-\Delta H_a^0(WO_2Cl_2) = 96 \pm 1$ kJ·mol^{-1} was deduced, whereas for MoO_2Cl_2 $-\Delta H_a^0(MoO_2Cl_2) = 90 \pm 3$ kJ·mol^{-1} resulted. The sequence in volatility of MO_2Cl_2 (M = Mo, W, Sg) on the stationary phase is $MoO_2Cl_2 > WO_2Cl_2 \approx SgO_2Cl_2$. The probability that SgO_2Cl_2 is equally volatile or even more volatile than MoO_2Cl_2 was estimated to be less than 15%.

The experimentally determined ΔH_a^0-values, measured with trace amounts (at zero surface coverage), were directly correlated with their macroscopic sublimation enthalpies (ΔH_s^0) using an empirical model; see "Thermochemical Data from Gas-Phase Adsorption and Methods of Their Estimation". It was therefore possible to directly estimate a sublimation enthalpy and to obtain a value of $\Delta H_s^0(SgO_2Cl_2) = 127^{+10}_{-21}$ kJ·mol^{-1} from only a few investigated molecules. $\Delta H_s^0(SgO_2Cl_2)$ is a very important quantity in order to estimate, e.g., ΔH_s^0(Sg). Seaborgium is expected to have an equally or even higher ΔH_s^0 than W, the least volatile element in the Periodic Table; see "Thermochemical Data from Gas-Phase Adsorption and Methods of Their Estimation".

4.2.3 Isothermal Chromatography of Sg Oxides/Oxide Hydroxides

In moist oxygen containing gases, the transport of group-6 elements Mo, W, and presumably also Sg, along chromatography columns occurs via a dissociative adsorption reaction and not via a simple reversible adsorption. Retention times for these dissociative processes in an isothermal chromatography column are generally longer, even at very high temperatures. With the high temperature on-line gas chromatography apparatus (HITGAS) [58] retention times of about 8–9 s were determined from measurements with short-lived Mo and W nuclides at isothermal temperatures above 1,000 °C. By condensing the separated volatile species

directly on metal foils mounted on the circumference of the rotating wheel of the ROMA detection system (see "Experimental Techniques"), the time-consuming reclustering step could be avoided. However, this reduced the detection efficiency, since, due to the thickness of the metal foils, final samples could be assayed only in a 2π geometry. Furthermore, contaminants, like various Po isotopes, cannot be removed in the oxide/hydroxide chemical system, which makes detection of genetically linked α-decay chains difficult. Fortunately, $^{265}Sg^{b}$ decays by α-particle emission to the relatively short-lived $^{261}Rf^{b}$ ($T_{1/2} = 2.6$ s), which preferentially decays by spontaneous fission.

In an experiment conducted at GSI, a ^{248}Cm target was bombarded with 119 MeV ^{22}Ne ions. Reaction products recoiling from the target were stopped in He gas loaded with MoO_3 aerosol particles and were swept to the HITGAS set-up. At the entrance to the chromatography column, moist O_2 was added to the gas jet. The temperature of the quartz chromatography column was 1,052 °C in the reaction zone and 1,027 °C in the isothermal part. Loosely packed quartz wool in the reaction zone served as a filter for aerosol particles. A total beam dose of $6.3{\cdot}10^{17}$ ^{22}Ne ions was accumulated. The search for genetically linked decay chains $^{265}Sg^{b} \longrightarrow \alpha\ ^{261}Rf^{b} \longrightarrow sf$ revealed two candidate events. The probability that both of these events were entirely random was only 2%[2] [39]. Therefore, as expected, Sg appeared to be volatile under the conditions of the experiment, presumably as Sg oxide hydroxide. In the O_2–$H_2O_{(g)}$/$SiO_{2(s)}$-system Sg showed typical group-6 element properties. Under the given conditions, this coincides also with a U(VI)-like behavior. U is also known to form a volatile oxide hydroxide.

In Fig. 18, the relative yields of Mo and W oxide hydroxides in open quartz columns using humid O_2 as reactive carrier gas component are shown as a function of isothermal temperature. The solid lines are the result of a Monte Carlo model

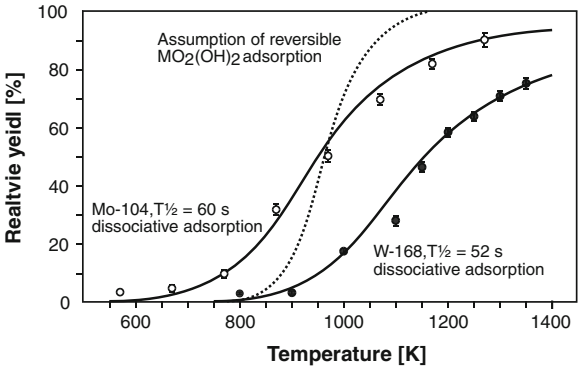

Fig. 18 Relative yields in isothermal gas chromatography of ^{104}Mo (○) and ^{168}W (●) oxide hydroxides in quartz columns using humid oxygen as reactive carrier gas component. Sg was observed at an isothermal temperature of 1027 °C (1,300 K). Figure reproduced with permission from [39]. Copyright 2001 Oldenbourg Wissenschaftsverlag GmbH

[2] In the original publication, the decay chains were erroneously attributed to ^{266}Sg. However, this does not affect the significance of the observation of Sg or the interpretation of the chemical result.

based on a microscopic description of the dissociative adsorption process [43] with $\Delta H^0_{\text{diss.ads}}$ ($MoO_2(OH)_2$) = −54 kJ·mol^{-1} and $\Delta H^0_{\text{diss.ads}}$ ($WO_2(OH)_2$) = −56 kJ·mol^{-1}. The dashed line represents a hypothetical yield curve assuming that group-6 oxide hydroxides are transported by simple reversible adsorption with $\Delta H^{0(T)}_a$ = −220 kJ·mol^{-1} [39].

In order to answer the question about the sequence of volatility of oxide hydroxides within group 6, further experiments have to be conducted at lower isothermal temperatures.

5 Bohrium (Bh, Element 107)

The fourth transactinide element, bohrium, is expected to be a homolog of Mn, Tc, and Re and thus to belong to group 7 of the Periodic Table. Two early attempts to chemically identify Bh as volatile oxides or oxide hydroxides failed [59, 60]. For the synthesis of Bh nuclides, the reactions ^{249}Bk(^{22}Ne,4-5n)^{267,266}Bh and ^{254}Es(^{16}O,4–5n)^{265,266}Bh were employed. The decay properties of the nuclides $^{265–267}$Bh were entirely unknown at the time. With the identification of the nuclides ^{266}Bh ($T_{1/2} \approx 1$ s) and ^{267}Bh ($T_{1/2} = 17^{+14}_{-6}$ s) [61] in bombardments of ^{249}Bk with ^{22}Ne ions and the recognition that the rapid formation of volatile oxide hydroxides is apparently hindered [62], Eichler et al. paved the way to the first successful chemical identification of Bh as oxychloride compound [63]. However, due to the very low formation cross-sections of only about 70 pb for ^{267}Bh (produced in the reaction ^{249}Bk(^{22}Ne,4n)) [61], any experiment aiming at a chemical identification of Bh was predestined to be a “tour de force”. Nevertheless, in a 1 month long experiment conducted at the Paul Scherrer Institute (PSI), Switzerland, an international collaboration of radiochemists observed a total of 6 α-decay chains originating from ^{267}Bh after chemical isolation and they established the sequence in volatility $TcO_3Cl > ReO_3Cl > BhO_3Cl$ [64].

5.1 Volatile Compounds of Group-7 Elements

In contrast to elements in groups 4 and 5, but similar to group 6, the 7 valence electrons of group 7 elements allow for a large number of stable oxidation states and thus a wide variety of inorganic compounds. An increased stabilization is observed for the half-filled d-shells. This is especially evident for the 3d shell of Mn, which is considerably more volatile than its neighbors Cr and Fe in the same period. However, Mn behaves chemically markedly different from its homologs Tc and Re. Compounds of Mn are chemically most stable in the oxidation state +2, whereas compounds in the oxidation states +4 and +7 are strong oxidizing agents. Compounds of Tc and Re in high oxidation states are much more stable toward reduction and the oxidation state +2 is of minor importance. Due to the lanthanide

Table 2 Typical mononuclear compounds of group-7 elements

Compound	Mn	Tc	Re
Oxides	MnO, MnO_2	TcO_2, TcO_3	ReO_2, ReO_3
Hydoxides	$MnOH$, $Mn(OH)_2$		
Oxide hydroxides		$HTcO_4$	$HReO_4$
Sulfides	MnS, MnS_2	TcS_3	ReS_3
Halides X = F, Cl, Br, I	MnX_2, MnX_3, MnX_4	TcX_3, TcX_4, TcX_5, TcX_6	ReX_3, ReX_4, ReX_5, ReX_6
Oxyhalides X = F, Cl, Br, I		$TcOX_3$, $TcOX_4$, TcO_3X	$ReOX_3$, $ReOX_4$, ReO_3X

contraction, atomic and ionic radii of Tc and Re are very similar, and thus these elements are chemically very much alike. Some typical mononuclear compounds of group-7 elements are listed in Table 2. Of all the compounds listed in Table 2 the oxides, oxide hydroxides, and the oxychlorides turned out to be the most promising candidates for a chemical separation and identification of Bh.

5.1.1 Oxides and Oxide Hydroxides

Oxides and oxide hydroxides of Tc and Re are typically formed in an O_2/H_2O containing gas phase. They were extensively studied, mostly using the method of thermochromatography [65–76]. The technique has also been applied to develop Tc and Re generator systems for nuclear medical applications [77, 78]. In their works, Schädel et al. [79] and Eichler et al. [62] studied the oxide and the oxide/hydroxide chemistry of trace amounts of Re in an O_2/H_2O-containing system with respect to its suitability for a first gas chemical identification of Bh. They investigated the behavior of long-lived Re nuclides in thermochromatographic systems as well as the one of short-lived Re nuclides in on-line isothermal chromatography. The results of these studies [62] are summarized in Fig. 19 and can be described as follows:

Thermochromatography of oxides and oxide hydroxides

In thermochromatography experiments three different processes can be distinguished, reflected in the deposition peaks B, C, and D in Fig. 19, depending on the pretreatment of the column surface and the oxidation potential of the carrier gas. These are:

1. The rapid formation of the perrhenic acid ($HReO_4$) and a gas chromatographic transport of the rather volatile $HReO_4$ governed by mobile adsorption processes to relatively low deposition temperatures of less than 100 °C (deposition peak D in Fig. 19). This behavior is observed if the employed quartz columns are pretreated in excess of 1,000 °C with H_2 and with O_2/H_2O or H_2O_2 as reactive component of the carrier gas.
2. The rapid formation of the rhenium trioxide (ReO_3) and a gas chromatographic transport of ReO_3 governed by mobile adsorption processes to deposition

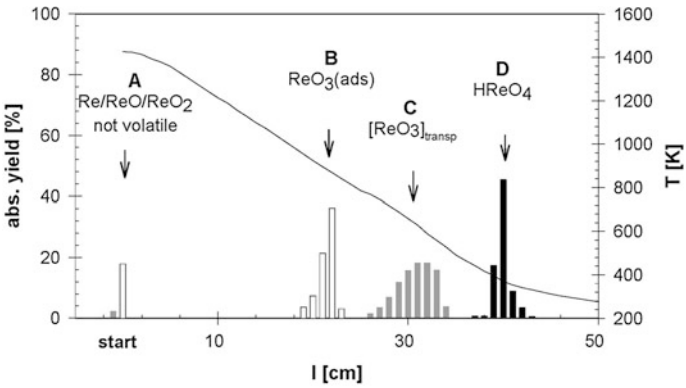

Fig. 19 Merged thermochromatograms of Re in the system He, O_2, H_2O. Figure reproduced with from [62]. Copyright 1999 Oldenbourg Wissenschaftsverlag GmbH

temperatures of about 500 °C (deposition peak B in Fig. 19). This behavior is observed if the employed quartz columns are pretreated in excess of 1,000 °C with O_2 and with O_2, O_2/H_2O, or H_2O_2 as reactive component of the carrier gas.

3. The formation of the rhenium trioxide (ReO_3) and a consecutive transport of ReO_3 by mobile adsorption and a superimposed transport reaction. The latter leads to a reversible formation of more volatile $HReO_4$ via a surface catalyzed reaction, and thus through the intermediate $HReO_4$, to a transport of ReO_3 to lower adsorption temperatures (deposition peak C in Fig. 19). This behavior is observed if the employed quartz columns are pretreated in excess of 1,000 °C with O_2 and with O_2 as reactive component of the carrier gas.

In addition to the just described components, a small fraction of Re remains as a nonvolatile compound at the starting position (peak A in Fig. 19). Due to their high volatility, the oxide hydroxides appear to be especially interesting for an on-line gas chromatographic study of Bh. A high volatility of the investigated compound gives rise to high separation factors from less volatile by-products, such as heavy actinides, but also from Po, Pb, and Bi nuclides. Due to their very similar α-decay energies, they usually hamper a sensitive detection of transactinides.

Isothermal chromatography of oxides and oxide hydroxides

Based on thermochromatographic studies, on-line methods for the gas chromatographic isolation of volatile group-7 oxides or oxide hydroxides were investigated using the OLGA technique [62]; see "Experimental Techniques". The nuclide ^{169m}Re ($T_{1/2}$ = 16 s), with its α-decay branch (E_α = 5.0 MeV), is ideally suited to model the behavior of its heavier group-7 homolog Bh and it was produced in the fusion reaction ^{156}Dy(^{19}F, 6n). Transfer reaction products, such as $^{152–155}$Er and $^{151–154}$Ho, served as model elements for the behavior of heavy actinides.

Reaction products were transported attached to carbon aerosol particles in He from the target site to the OLGA set-up. In order to obtain the volatile $HReO_4$

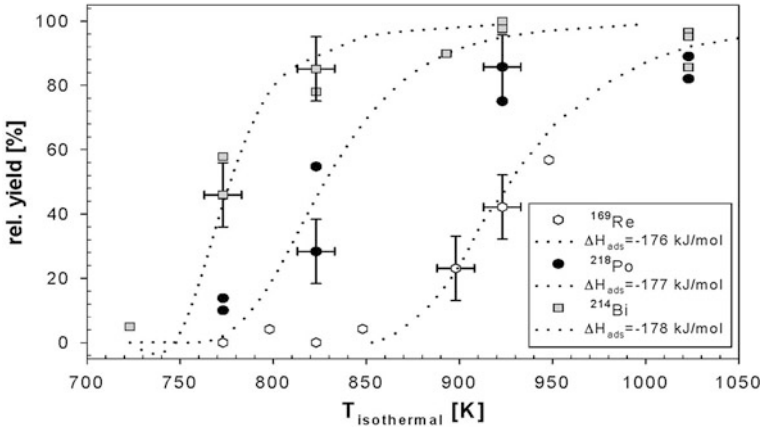

Fig. 20 Temperature versus yield curve from isothermal chromatography of $^{169m}ReO_3$, ^{218}Po ($T_{1/2} = 3.05$ min, presumably as $^{218}PoO_2$), and ^{214}Bi ($T_{1/2} = 19.9$ min, presumably as BiOOH). Figure reproduced with permission from [62]. Copyright 1999 Oldenbourg Wissenschaftsverlag GmbH

100 mL·min^{-1} O_2 (containing 500 ppm O_3), saturated with H_2O_2 at room temperature, were added as reactive components. The carbon aerosols were stopped on a quartz wool plug in the reaction oven at 1,100 °C (1373 K in Fig. 20), where the reaction products were oxidized and the aerosols were converted to CO_2. The yield of volatile Re oxides was measured as a function of the temperature in the adjoining isothermal section of the column. The resulting temperature versus yield curve is shown in Fig. 20. Unfortunately, high yields of a volatile Re compound were only observed at temperatures of 627 °C (900 K in Fig. 20) and above. The deduced $-\Delta H_a^0(ReO_3) = 176 \pm 10$ kJ·mol^{-1} was in good agreement with $-\Delta H_a^0(ReO_3) = 190 \pm 10$ kJ·mol^{-1} (evaluated from peak B shown in Fig. 19), which was measured in thermochromatography experiments. This adsorption enthalpy value identified the volatile species as ReO_3 [62]. The much more volatile $HReO_4$ was not observed at the given experimental conditions. A kinetic hindrance of the formation of $HReO_4$ was excluded, since also much longer lived Re nuclides were not observed after chemical separation.

Po and Bi as possibly interfering contaminants were also investigated under the same experimental conditions and, as shown in Fig. 20, were found to be similarly volatile as ReO_3. In conclusion, an on-line isolation of very volatile group-7 oxide hydroxides was not accomplished. The isolation of less volatile trioxides appeared not to be promising due to the interference of Po and Bi by-products hampering the unambiguous identification of Bh nuclides after chemical isolation. Nevertheless, the oxide system provided an excellent separation from lanthanides [62] and actinides [59, 60], separation factors of $\geq 10^3$ were deduced. Preseparation with a recoil separator (see e.g. an application in one of the Fl experiments in Sect. 8) may provide a path to much cleaner samples and a variety of Bh experiments in the gas phase.

5.1.2 Chlorides and Oxychlorides

Since the oxide and the oxide hydroxide systems are not well suited to rapidly isolate single atoms of group-7 elements [62], chlorides and oxychlorides were investigated as potential candidate compounds for an on-line gas chemical isolation of Bh [63]. This approach had already been successful in studies of volatile Db and Sg oxychlorides; see Sects. 3 and 4. However, a number of different chloride/oxychloride species exist within group 7, and thus the chemical speciation of the formed compounds appears to be complicated. For Re the pure chlorides $ReCl_3$, $ReCl_4$, $ReCl_5$, and $ReCl_6$ are known, as well as the oxychlorides $ReOCl_3$, $ReOCl_4$, and ReO_3Cl.

Thermochromatography of chlorides and oxychlorides

Only few thermochromatographic studies of chloride and oxychloride compounds of group-7 elements Tc and Re were known [49, 80, 81]. Therefore, Eichler et al. [63] reinvestigated the thermochromatographic behavior of Tc and Re in quartz columns in the gas chemical system $He_{(g)}/O_{2(g)}/HCl_{(g)}$. They used trace amounts of the nuclides ^{101}Tc and ^{104}Tc, obtained from a thin ^{252}Cf fission source, and ^{183,184}Re produced from proton irradiations of $^{nat.}$W. Because of the existence of a large variety of chloride and oxychloride compounds of the group-7 elements Tc and Re, many different deposition zones were expected in thermochromatography experiments. Surprisingly, only one single deposition zone for Tc and Re was observed at rather low deposition temperatures, indicating the formation of a very volatile compound; see Fig. 21.

Variation of the carrier gas mixture He (vol% 0–60), O_2 (vol% 0–80%), and HCl (vol% 10–100) did not yield any other volatile compound. The deposition zone of Tc was observed at a lower temperature as the one for Re and it coincided with the condensation zone of H_2O, which was formed in the reaction of HCl and O_2 at $\approx$1130 °C in the reaction oven. For this reason, only an upper limit of the

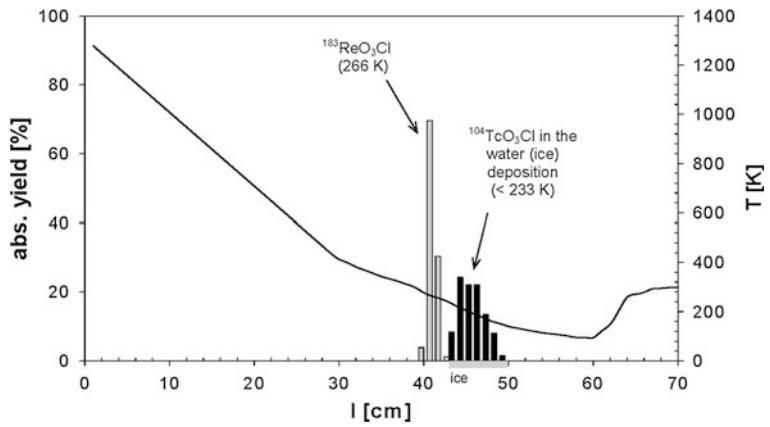

Fig. 21 Merged thermochromatograms of ^{104}Tc and ^{183}Re in the gas chemical system $He_{(g)}/O_{2(g)}/HCl_{(g)}/SiO_{2(s)}$. Figure reproduced with permission from [63]. Copyright 2000 Oldenbourg Wissenschaftsverlag GmbH

adsorption enthalpy of the Tc compound was established. An empirical correlation of measured adsorption enthalpies of trace amounts of a number of chloride and oxychloride species with their macroscopic boiling point identified the formed volatile species quite clearly as the trioxychlorides (MO_3Cl, M = Tc, Re). The observed properties of group-7 oxychlorides in thermochromatography experiments appeared quite promising for a first chemical identification of Bh. Therefore, the gas chemical system $He_{(g)}/O_{2(g)}/HCl_{(g)}$ was further investigated in on-line isothermal chromatography using short-lived Tc and Re nuclides.

Isothermal chromatography of chlorides and oxychlorides

As in studies of group-7 oxides and oxide hydroxides short-lived ^{169m}Re was used. Short-lived $^{106–108}$Tc, $^{98–101}$Nb, and $^{99–102}$Zr were obtained from a ^{252}Cf fission source. As reactive gases, HCl and O_2 were added to the He/C-aerosol gas-jet shortly before the reaction oven. Nuclear reaction products were oxidized and chlorinated together with the carbon aerosols. At the column exit, the separated, volatile molecules were adsorbed on the surface of CsCl aerosol particles of a second gas-jet ("reclustering") and were rapidly transported to a detection system. Yields of 80% were observed compared to ^{169m}Re entering the OLGA III set-up. However, this approach did not work for the more volatile TcO_3Cl. Obviously, the adsorption enthalpy of TcO_3Cl on a CsCl surface was too low to allow an efficient reclustering. Using aerosols with a reducing surface, such as $FeCl_2$, significantly improved the yield. This interesting property allowed a distinction between a "Tc-like" and a "Re-like" behavior in a first experiment with Bh; see below. Ancillary experiments with ^{218}Po and ^{218}Bi were conducted to investigate the separation of volatile MO_3Cl compounds (M = Tc and Re) from Po and Bi contaminants. As shown in Fig. 22, the separation of Tc and Re trioxychlorides from the less volatile

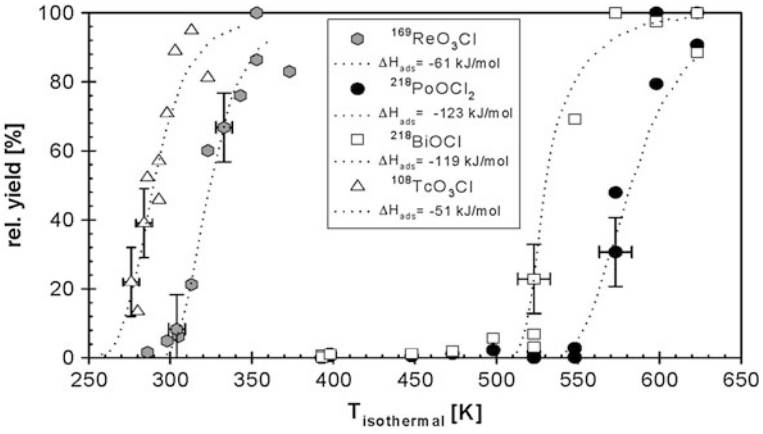

Fig. 22 Yield curves versus isothermal temperature measured for oxychloride compounds of the nuclides ^{108}Tc (Δ), ^{169}Re (⬢), ^{218}Po (●), and ^{218}Bi (□) in the chemical system $He_{(g)}/O_{2(g)}/HCl_{(g)}/SiO_{2(s)}$. The dotted lines indicate the results of simulations with the microscopic model of Zvara [20] with the adsorption enthalpies indicated. Figure reproduced with permission from [63]. Copyright 2000 Oldenbourg Wissenschaftsverlag GmbH

BiOCl or $PoOCl_2$ is excellent. Separation factors from lanthanides, serving as a model for heavy actinides, were $>10^3$. $^{99-102}$Zr and $^{98-101}$Nb, serving as model elements for the lighter transactinides Rf and Db, were separated at isothermal temperatures up to 200 °C with separation factors of $>10^2$. An average overall process time of about 3 s was evaluated for Re. Thus, the gas chemical system $He_{(g)}/O_{2(g)}/HCl_{(g)}/SiO_{2(s)}$ was shown to fulfill all requirements for a first successful chemical identification of Bh [63].

5.2 Gas Chemical Studies of Bohrium

5.2.1 Thermochromatography of Oxides and/or Oxide Hydroxides

A first attempt to chemically identify element 107 as eka-rhenium was conducted by Zvara and co-workers already in 1984 [59]. As in earlier experiments with Rf, Db, and Sg, see above Sects. 2.2, 3.2 and 4.2.1, respectively, they searched for latent tracks in thermochromatographic columns imprinted by the stopping of a fission fragment from the decay of a spontaneously fissioning isotope of Bh. Moist air with a water vapor pressure of 600 Pa at a flow rate of 0.75 $L \cdot min^{-1}$ passed behind a 150 $\mu g \cdot cm^{-2}$ thick ^{249}Bk target that was irradiated with ^{22}Ne ions. Eight experiments were conducted with varying conditions concerning the operation of the thermochromatographic column. In the last three experiments an optimum purification from actinides was achieved. No SF tracks were observed in a temperature range from 800 °C down to 20 °C, while the nuclide ^{177}Re (produced from an admixture of ^{159}Tb to the target material) was adsorbed at around 200 °C. This negative result was interpreted that either the half-lives of the produced Bh nuclides were shorter than 2 s or that the production cross-sections were lower than 100 pb [59]. Even though the reached cross-section limits are very close to the cross-sections measured later by Wilk et al. [61], the studies by Eichler et al. [62] showed that the rapid formation of a volatile oxide hydroxide is hindered.

5.2.2 On-line Gas Chromatography of Oxides

Later, in a different attempt, Schädel et al. [60] bombarded a ^{254}Es target with ^{16}O ions to produce the isotopes ^{266}Bh and ^{265}Bh at the 88-Inch Cyclotron of the Lawrence Berkeley National Laboratory (LBNL). Reaction products recoiling from the target were thermalized in He containing 20% O_2. Attached to the surface of KCl aerosols, they were transported to the on-line chromatography set-up OLGA. In the reaction oven of OLGA, kept at 1,050 °C, the KCl aerosols were stopped and were destroyed on a quartz wool plug. The water content of the gas mixture was kept below 100 ppm in order to form only the trioxide species, as determined in test experiments with Re. Volatile oxides, which passed through the second part of the column with a negative temperature gradient ranging from

1,050 °C down to 500 °C at the exit of the column, were deposited on thin Ni catcher foils (0.67 mg·cm^{-2}) that were coated with 50 μg·cm^{-2} Ta. The catcher foils were mounted on the circumference of a rotating wheel and stepped periodically between pairs of surface barrier detectors to register α decays and SF decays. A spectrum of all α events from all runs (93 and 96 MeV bombarding energy) and all detectors revealed that a small portion of heavy actinide isotopes had passed through the gas chromatographic column, but that the decontamination factor was better than 10^3. Even though a couple of α decays were registered with energies between 8.4 and 9.2 MeV, none of these could be conclusively attributed to the decay of a Bh isotope. No genetically linked decay chains were observed. Assuming a transport time of about 1 s and a half-life of the produced Bh isotopes of more than 2 s, cross-section limits of about 3–10 nb were reached (95% confidence level). These upper limits were larger than the calculated production cross-sections by more than one order of magnitude. As outlined by the authors, the experiment clearly failed to chemically identify Bh.

5.2.3 Isothermal Chromatography of Oxychlorides

In an experiment at the PSI Philips cyclotron, the first successful chemical isolation and identification of Bh was accomplished [64]. A target of 670 μg·cm^{-2} ^{249}Bk covered with a 100 μg·cm^{-2} layer of ^{159}Tb was prepared at the LBNL on a thin 2.77 mg·cm^{-2} Be foil. The target was irradiated for about 4 weeks with typically 1.6×10^{12} particles of ^{22}Ne per second. The beam energy in the middle of the target was 119 ± 1 MeV, producing 17-s ^{267}Bh in the reaction ^{249}Bk(^{22}Ne, 4n). ^{176}Re was simultaneously produced in the reaction ^{159}Tb(^{22}Ne, 5n) and it served as a yield monitor for the chemical separation process. Nuclear reaction products recoiling from the target were attached to carbon aerosol clusters and were transported with the carrier gas flow through a capillary to the modified OLGA III set-up. As reactive gases, a mixture of HCl and O_2 were added. After chemical separation, final products were attached to CsCl aerosols and were transported to the rotating wheel detection system ROMA, where α particle and SF decays were registered event by event in almost 4π geometry. Measurements were performed at isothermal temperatures of 180, 150, and 75 °C. At each isothermal temperature, a beam integral of 1×10^{18} ^{22}Ne particles was accumulated.

Throughout the experiment close to 180.000 samples were measured. A total of six genetically linked decay chains attributed to the decay of ^{267}Bh were observed; four at an isothermal temperature of 180 °C, two at 150 °C and none at 75 °C. Due to a small contamination with Po and Bi nuclides, and a statistical treatment of this background, 1.3 of the 4 decay chains observed at 180 °C had to be attributed to accidental correlations unrelated to the decay of ^{267}Bh. At 150 °C this correction was only 0.1 out of 2 observed decay chains. The properties of the observed decay chains are shown in Fig. 23.

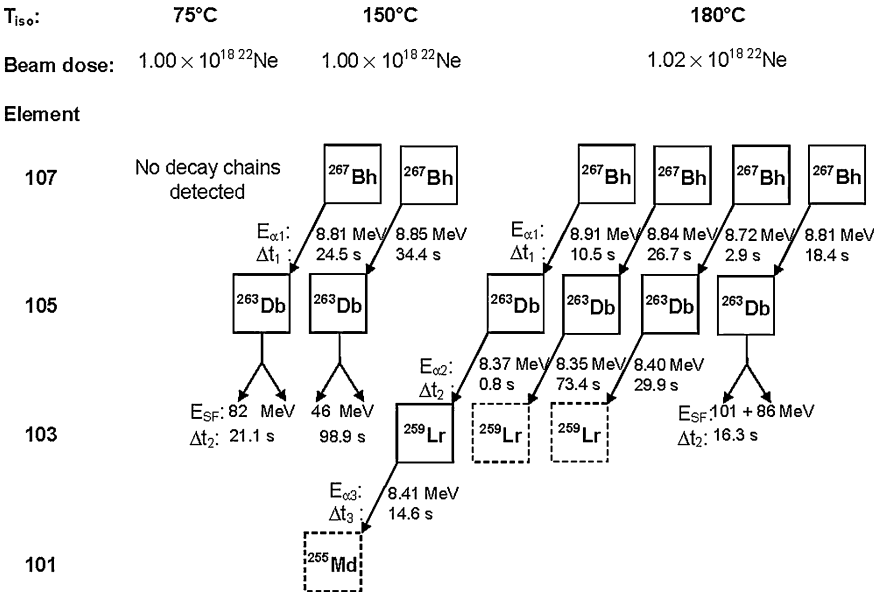

Fig. 23 The six nuclear decay chains attributed to the decay of ^{267}Bh leading to ^{263}Db and ^{259}Lr. Given are the observed decay energies and the lifetimes between end of sample collection (Δt_1) and after the previous α decay (Δt_2, Δt_3). These decays were observed at 180 and 150 °C, which allowed the unambiguous identification of Bh after chemical separation, presumably as volatile BhO_3Cl. No ^{267}Bh was detected at 75 °C isothermal temperature. Figure reproduced from [64]

Interestingly, for $^{169}ReO_3Cl$ a relatively high yield of 80% was observed at 75 °C as compared with the yield at 180 °C isothermal temperature. This indicates that BhO_3Cl, which was not observed at 75 °C, is less volatile than ReO_3Cl. The fact that ^{267}Bh was identified after chemical separation already excludes a "Tc-like" behavior of Bh, since CsCl was used as the recluster aerosol material, which was not suitable to recluster the very volatile TcO_3Cl [63]. The relative yield of $^{108}TcO_3Cl$, $^{169}ReO_3Cl$, and (most likely) $^{267}BhO_3Cl$ as a function of isothermal temperature is shown in Fig. 24. The deduced enthalpies of adsorption on the column surface were $-\Delta H_a^0(TcO_3Cl) = 51 \pm 3$ kJ·mol^{-1}, $-\Delta H_a^0(ReO_3Cl) = 61 \pm 3$ kJ·mol^{-1}, and $-\Delta H_a^0(BhO_3Cl) = 75^{+6}_{-9}$ kJ·mol^{-1} (68% confidence interval). Therefore, the sequence in volatility is $TcO_3Cl > ReO_3Cl > BhO_3Cl$. The probability that BhO_3Cl is equally or more volatile than ReO_3Cl is less than 10%.

This sequence in volatility agrees well with predictions from fully relativistic density–functional calculations for group-7 oxychlorides that have been performed by V. Pershina et al. [82]; see "Theoretical Chemistry of the Heaviest Elements". The results of these calculations showed that the electronic structure of BhO_3Cl is very similar to that of TcO_3Cl and ReO_3Cl. Increasing dipole moments and electric dipole polarizabilities in the group suggest a decreasing volatility in the sequence $TcO_3Cl > ReO_3Cl > BhO_3Cl$. However, also classical extrapolations down the

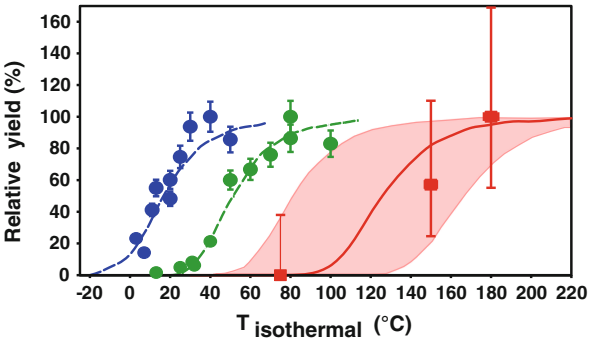

Fig. 24 Relative yields of the compounds $^{108}TcO_3Cl$ (●), $^{169}ReO_3Cl$ (●), and (most likely) $^{267}BhO_3Cl$ (■) as a function of isothermal temperature. The error bars indicate a 68% confidence interval. The solid lines indicate the results of simulations with the microscopic model of I. Zvara [20] with the adsorption enthalpies given in the text. The dashed lines represent the calculated relative yield concerning the 68% confidence interval of the standard adsorption enthalpy of BhO_3Cl from –66 to –81 kJ·mol^{-1}. Figure reproduced from [64]

groups of the Periodic Table, making use of empirical correlations of thermochemical properties, predict BhO_3Cl to be more stable and less volatile than ReO_3Cl or TcO_3Cl [83]. As in the case of Sg oxychlorides, the experimentally determined ΔH_a^0 value can be used to estimate a macroscopic sublimation enthalpy (ΔH_s^0) of BhO_3Cl, using an empirical linear correlation function; see "Thermochemical Data from Gas-Phase Adsorption and Methods of Their Estimation". Therefore, it was possible to directly estimate $\Delta H_s^0(BhO_3Cl) = 89^{+21}_{-18}$ kJ·mol^{-1} from only a few investigated molecules.

6 Hassium (Hs, Element 108)

The experimental chemical investigation and characterization of the next heavier transactinide element Hassium (Hs, element 108) has, for some years, constituted a daunting task, even though from the very beginning, the selection of a volatile compound was absolutely clear. Hassium, as a presumed member of group 8 of the Periodic Table, and thus a homolog of Fe, Ru, and Os, should form stable and at the same time very volatile HsO_4 molecules, very similar to OsO_4.

The discovery of Hs was reported in 1984 [84] with the identification of the nuclide ^{265}Hs with a half-life of only 1.5 ms, far too short for all of the currently available chemical separator systems. Only in 1996, the much longer lived isotope ^{269}Hs with a half-life of the order of about 10 s was observed in the α-decay chain of the nuclide ^{277}Cn [85]. However, the production cross-section of only about 1 pb for the reaction $^{208}Pb(^{70}Zn,1n)^{277}Cn$ was discouragingly small. A somewhat larger production cross-section of about 7 pb could be expected for the direct production of ^{269}Hs in the reaction $^{248}Cm(^{26}Mg,5n)$ [86].

Thus, the state-of-the-art techniques, that have successfully been applied to chemically identify Bh, had to be improved by at least one order of magnitude! This goal was indeed accomplished by introducing novel techniques for irradiation, separation, and detection. The first successful Hs chemistry experiment was conducted in the spring of 2001 again in the framework of an international collaboration at GSI, Darmstadt, and proved that Hs behaves like a typical member of group 8 and forms volatile Hs-oxide molecules, very likely HsO_4 [87]. This novel technique was later also used to perform nuclear studies of new Hs-isotopes [88, 89].

6.1 Volatile Compounds of Group-8 Elements

Group-8 elements Fe, Ru, and Os are known to exist in a large number of oxidation states: Fe is known in all states from –2 through +6 (also +8 has been reported), Ru in the states –2 through +8 (with the exception of +1) and Os in all states from –2 through +8, explaining the large variety of compounds. Ru and Os are the elements with the highest maximum valency within their periods and the only elements, which can form an 8+ oxidation state (with the exception of Xe, which is known to form tetrahedral XeO_4 [90]). While the chemistry of Ru and Os is quite similar, Fe behaves differently. The reason is the existence of the lanthanide series, which is inserted in the sixth period of the Periodic Table. Therefore, investigations of the chemical properties for a future Hs chemistry experiment concentrated on Ru and Os. The most important volatile compounds of Ru and Os are the tetroxides MO_4 (M = Ru, Os). There also exist a number of volatile Ru and Os halides and oxyhalides. The fluorides and oxyfluorides are of importance, but experimentally difficult to handle. Quite naturally, early considerations [91, 92] and experimental developments [56, 70, 93–105] for a first Hs chemistry exclusively concentrated on the tetroxides. This strategy is justified, since classical extrapolations [106] as well as fully relativistic density functional theory calculations on the group-8 tetroxides [107] predict the existence of a volatile and very stable HsO_4.

6.1.1 Thermochromatography of Oxides

The volatilization and deposition of carrier-free radionuclides of the elements Re, Os, Ir, Mo, Tc, and Ru in a thermochromatography column were studied using air as a carrier gas [70]. The columns were filled with quartz powder (200 μm). Os was completely volatilized and adsorbed at –40 °C. The deduced enthalpy of adsorption on the quartz surface was $-\Delta H_a^0(OsO_4) = 50 \pm 5$ kJ·mol^{-1}. Ru was deposited at much higher temperatures around 400 °C and was identified as RuO_3. Later, in different on-line thermochromatography experiments, consistently values for $-\Delta H_a^0(OsO_4)$ between 39 and 41 kJ·mol^{-1} were determined [87, 94, 105].

The transport of Ru oxides in a temperature gradient tube appears to be more complicated. First indications that also Ru can be volatilized in the form of RuO_4 were obtained in [94], but such a behavior was not observed in [95]. In contrast to

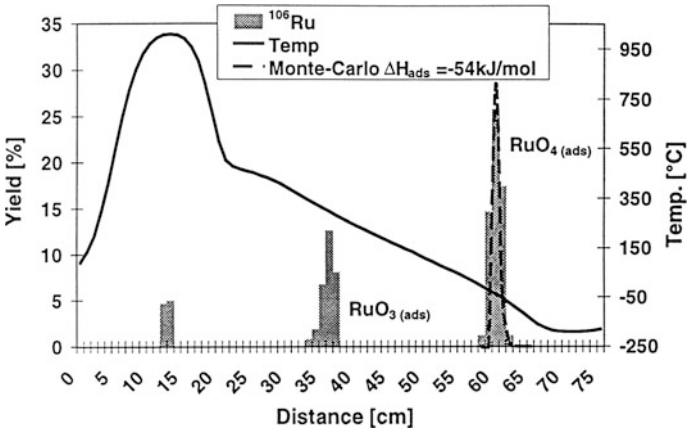

Fig. 25 Thermochromatography of ^{106}Ru in O_2 gas (20 mL min^{-1}) in an empty quartz column. The solid line represents the temperature profile in the column. Two different Ru zones were observed after completion of the experiment (for details see text). Some of the Ru was not volatilized at the starting position. The dashed lines indicate the modeled deposition zone of a species transported by mobile adsorption with $-\Delta H_a^0(RuO_4) = 54$ kJ·mol^{-1}. Figure reproduced from [56]

Os, the transport of Ru appears to occur by chemical transport reactions where the chemical species change during the chromatographic process. In experiments by Düllmann et al. [56] using O_2 as carrier gas, two deposition peaks were observed, see Fig. 25. The location of the deposition peak at higher temperatures varied over a wide range in different experiments and disappeared completely in experiments lasting more than 1 hour. This peak was therefore attributed to Ru transported by a transport reaction of the type

$$RuO_{3(ads)} \rightleftarrows RuO_{4(g)} + {}^1\!/\!_2\ O_{2(g)}. \quad (3)$$

However, RuO_3 does not exist in macroscopic quantities. The second peak at lower deposition temperatures was attributed to RuO_4 transported by mobile adsorption, with an adsorption enthalpy of $-\Delta H_a^0(RuO_4) = 55 \pm 4$ kJ·mol^{-1}.

6.1.2 Isothermal Chromatography of Oxides

In order to directly detect the nuclear decay of Hs isotopes in a future experiment, test experiments with short lived, α-particle emitting Os isotopes were conducted. The experiments by A. Yakushev et al. [103] with $^{171-174}$Os ($T_{1/2} = 8.3$–45 s) demonstrated several important aspects of a future Hs experiment. First, by installing an oven as closely as possible to the recoil chamber high yields of OsO_4 were obtained simply by using a mixture of Ar/O_2 as carrier gas. The addition of aerosol particles was not necessary. Indeed, OsO_4 was already formed "in-situ" in the recoil chamber [102], but the chemical yield of short-lived Os nuclides could

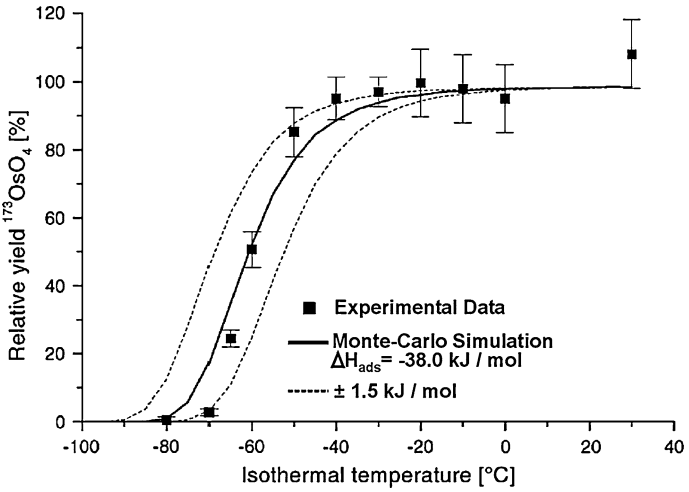

Fig. 26 Relative yields of $^{173}OsO_4$ ($T_{1/2} = 22.4$ s) as a function of isothermal temperature. Figure reproduced from [104]. Copyright 2002 Elsevier Science B.V.

substantially be improved by heating the attached oven [104]. The OsO_4 molecules were transported with minimal losses by the carrier gas at room temperature through an open quartz chromatography column. At the exit, the Ar/O_2 stream was mixed with a stream of Ar loaded with Pb aerosols on which the OsO_4 was adsorbed and reduced to nonvolatile OsO_2. The Pb aerosols were collected on a stepwise moving tape by impaction and transported in front of 6 PIPS detectors to register the α-particle decay of the isolated Os nuclides. The overall yield (not including the detection efficiency) was measured to be 50–60%.

Experiments by von Zweidorf et al. [102] also employed the in-situ production of Ru- and Os tetroxides in oxygen containing carrier gases, but were aimed at studies of the adsorption properties of volatile tetroxides on different surfaces at room temperature. Glass fiber filters soaked with 1 M NaOH yielded the best results, but also freshly prepared Na surfaces provided good adsorption of OsO_4.

Using a similar set-up as in [103], Düllmann et al. [104] measured a yield versus isothermal temperature breakthrough curve of $^{173}OsO_4$, see Fig. 26. This setup was named in-situ volatilization and on-line detection (IVO). Volatile OsO_4 was synthesized in-situ in the recoil chamber and transported by the He/O_2 carrier gas to a quartz chromatography column that could be operated between ambient temperature and –80 °C. At the exit of the column, volatile molecules were adsorbed on the surface of Pb aerosols and transported to the ROMA counting system. In order to prevent the build-up of ice in the column, all gases had to be carefully dried. In agreement with thermochromatography experiments [87, 94, 105] $-\Delta H_a^0(OsO_4) = 38.0 \pm 1.5$ kJ·mol^{-1} was determined. The decontamination from interfering elements, e.g., Po was determined to be $>10^4$. The yield of the IVO technique

was of the order of 50% and, therefore, about a factor of three more efficient than the OLGA system used in experiments with Bh. But the gain of at least one order of magnitude was not yet accomplished.

6.2 Early Attempts to Chemically Identify Hassium

A first unsuccessful attempt to chemically identify Hs as volatile HsO_4 was reported by Zhuikov et al. [97, 98] from Dubna. The reaction $^{40}Ar + {}^{235}U$ was employed to produce short-lived α-decaying isotopes of element 110 and their Hs daughter nuclides. These were rapidly isolated as volatile tetroxides to detect their SF decay. Atoms recoiling from the target were stopped in air and were transported to a thermochromatography column, where the purification from actinides took place on a hot quartz wool filter. OsO_4 was adsorbed quantitatively on Lavsan (polyethylenphtalat) fission track detectors covered with 50 $\mu g \cdot cm^{-2}$ of Pb. No SF decays were registered resulting in a cross-section limit of 10 pb for nuclides with half-lives longer than 150 ms.

In a second experiment, using the reaction $^{249}Cf(^{22}Ne,4n)^{267}Hs$, Zhuikov et al. [97, 98] searched also for short-lived α-particle emitting isotopes of Hs. Recoiling atoms were thermalized in a mixture of Ar + 2% O_2 and were continuously swept from the target chamber through a Teflon capillary to a quartz column kept at 1000–1100 °C. The column was filled with CaO to retain nonvolatile nuclear reaction products; e.g., actinides, Ra, Fr, and Po. Volatile species were then transported through a Teflon capillary and were blown onto the surface of a Si detector covered with 50 $\mu g \cdot cm^{-2}$ of Pb. At the opposite side, an annular Lavsan track detector (also coated with 50 $\mu g \cdot cm^{-2}$ of Pb) was located for registering fission fragments. The whole counting device was placed inside a shielding of Cd and paraffin in order to decrease the background. In model experiments with Os, OsO_4 was efficiently absorbed on the Pb surfaces. The decontamination from actinides was excellent (separation factor $> 10^6$) as well as that from Po ($>10^3$). Nevertheless, no α particles in the energy range above 8.5 MeV and no SF events were registered. An upper limit of 100 pb for the cross-sections of α-decaying nuclides with half-lives in the range between 50 ms and 12 h and of 50 pb for spontaneously fissioning nuclides was established.

A similar experiment was reported by Dougan et al. [100]. A setup called On-line Separation and Condensation AppaRatus (OSCAR) was installed at the LBNL 88-Inch Cyclotron. Nuclear reaction products were collected with a KCl aerosol gas-jet and were transported from the target chamber to the OSCAR set-up where O_2 was added. The aerosol particles were destroyed on a hot quartz wool plug and the formation of tetroxides occurred at a temperature of 650 °C. Nonvolatile reaction products were retained on the quartz wool plug, whereas the volatile tetroxides were swept by the carrier gas flow to a condensation chamber. Here, they were deposited on a Ag disk, which was cooled with liquid N_2. An annular Si surface barrier detector registered α particles and SF decays of nuclides adsorbed

on the disk surface. The OSCAR setup was used to search for α-decaying ^{272}Hs, the expected EC decay daughter of ^{272}Mt (estimated EC-decay half-life: 25 min), produced in the ^{254}Es(^{22}Ne, 4n) reaction. However, no α decays between 8.7 and 11.0 MeV were observed and an upper limit for the cross-section of 1 nb was derived.

The experiments by Zhuikov et al. [97, 98] and Dougan et al. [100] clearly demonstrated that the chemical selectivity would have been sufficient for a first chemical identification of Hs. However, the overall efficiency and the longtime stability of the experiments to reach the required sensitivity were not sufficient.

6.3 On-Line Thermochromatography of Hassium

In order to reach the required sensitivity, and to obtain, at the same time, meaningful chemical information about Hs and its compounds, different experimental developments had to be combined. First, the most promising approach to synthesize relatively long-lived Hs isotopes appeared to be the reaction ^{248}Cm(^{26}Mg,4,5n)^{270,269}Hs. Second, the rate of production could be increased by using an intense ^{26}Mg beam impinging on rotating ^{248}Cm targets. Such a technically very challenging irradiation setup was constructed and put into operation by Schädel et al.; see "Experimental Techniques". Third, the "in-situ" production [104] allowed for highest possible chemical yields of group-8 tetroxides. Fourth, in order to compare the volatility of HsO_4 with those of its lighter homologs of group 8, thermochromatography is the method of choice, since the position of every detected atom contributes chemical information. So far, the only problem of the thermochromatographic technique was the unambiguous identification of the decaying nuclide. This problem was solved by Kirbach et al. [105] who have built a rectangular thermochromatography column consisting of PIN diodes. In the actual Hs experiment an improved version namely the cryo on-line detector (COLD) was used; see "Experimental Techniques".

The required gain in sensitivity of one order of magnitude compared to the OLGA set-up used in experiments with Bh was thus accomplished. With the rotating target wheel, synthesis of about three atoms of ^{269}Hs per day could be expected, assuming a cross-section of 7 pb. The overall efficiency of the setup (including detection of a 3 member α-decay chain) amounted to 30–50%, resulting in the expected detection of about one decay chain per day of experiment.

In an experiment to produce Hs isotopes conducted in May of 2001 at GSI, valid data were collected during 64.2 h. During this time 1.0×10^{18} ^{26}Mg beam particles passed through the ^{248}Cm target. Only α lines originating from ^{211}At, ^{219,220}Rn, and their decay products were identified. While ^{211}At and its decay daughter ^{211}Po were deposited mainly in the first two detectors, ^{219,220}Rn and their decay products accumulated in the last three detectors, where the temperature was sufficiently low to partly adsorb Rn. During the experiment, seven correlated decay chains were detected, see Fig. 27.

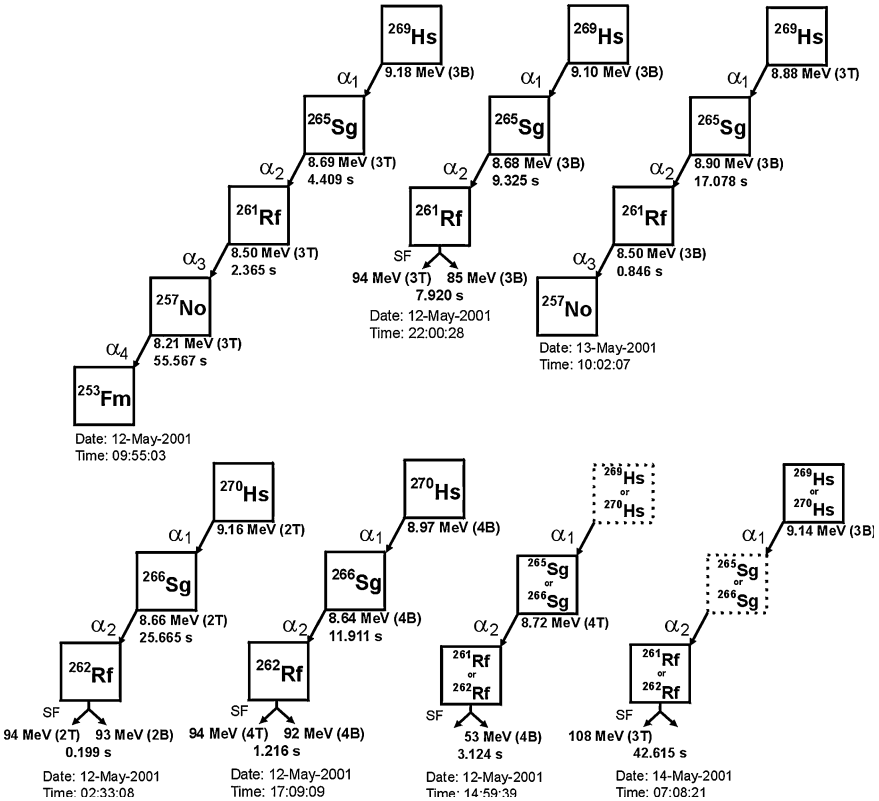

Fig. 27 The seven nuclear decay chains attributed to the decay of ^{269}Hs leading to ^{265}Sg^{a,b}, ^{261}Rf^{a,b}, and ^{257}Lr in the COLD detector after chemical isolation of volatile tetroxides. Figure reproduced from [87]. Based on an erroneous assignment of mass numbers and decay properties of Sg isotopes in the physics discovery experiment [37] (see Footnote 1 in Sect. 4), decay chains 4 and 5 were attributed to ^{270}Hs. With the discovery of ^{270}Hs, which will be discussed later, it became obvious that all seven decay chains must be attributed to ^{269}Hs

All decay chains were observed in detectors 2 through 4 and were assigned to the decay of either ^{269}Hs or the yet unknown ^{270}Hs. The characteristics of decay chains 1 through 3 agreed well with the literature data on ^{269}Hs and its daughter nuclides [85, 108], while two other decay chains were attributed to the decay of ^{270}Hs. This assignment was based on an erroneous assignment of mass numbers and decay properties of Sg isotopes in the physics discovery experiment [37] (see Footnote 1 in Sect. 4). The last two decay chains were incomplete and a definite assignment to ^{269}Hs or ^{270}Hs could not be made at the time. With the discovery of ^{270}Hs [88], which will be discussed later, it became obvious that all seven decay chains must be attributed to ^{269}Hs. No additional three-member decay chains with a total period of $\leq$300 s were registered in detectors 2–10. The background count rate of α particles with energies between 8.0 and 9.5 MeV was about 0.6 h^{-1} per

detector. This leads to very low probabilities of $\leq 7 \times 10^{-5}$ and $\leq 2 \times 10^{-3}$ for any of the first five chains and any of the last two chains, respectively, being of random origin. In addition, four fission fragments with energies >50 MeV that were not correlated with a preceding α particle were registered in detectors 2 through 4.

The longitudinal distribution of the seven decay chains originating from Hs is depicted in Fig. 28. The maximum of the Hs distribution was found at a temperature of –44 ± 6 °C. The distribution of $^{172}OsO_4$ ($T_{1/2} = 19.2$ s) measured before and after the experiment showed a maximum in detector 6 at a deposition temperature of –82 ± 7 °C. As in experiments with lighter transactinide elements the Monte Carlo model of Zvara [20], that describes the microscopic migration of a molecule in a gas chromatographic column, was used to evaluate the adsorption enthalpy of HsO_4 and OsO_4 on the silicon nitride detector surface. The modeled distributions with $-\Delta H_a^0(HsO_4) = 46 \pm 2$ kJ·mol^{-1} (68% confidence interval) and $-\Delta H_a^0(OsO_4) = 39 \pm 1$ kJ·mol^{-1} are shown as solid lines in Fig. 28.

The higher deposition temperature of about 40 °C, and thus the ≈ 7 kJ·mol^{-1} higher adsorption enthalpy seems to indicate a slightly lower volatility of HsO_4 compared to its lighter homolog OsO_4. This experimental result was somewhat unexpected since according to both, classical extrapolations and relativistic molecular calculations, HsO_4 was predicted to be about as volatile as OsO_4 [107, 109]. New calculations of the electronic structures of MO_4 (M = Ru, Os, and Hs), using the 4c-DFT method with a significantly increased number of basis functions, resulted in a notably larger polarizability of HsO_4, and thus an increase of $-\Delta H_a^0(HsO_4)$ by 6.2 kJ·mol^{-1} [110], while confirming older values for RuO_4 and OsO_4 [107, 109]. Now excellent agreement with the experimentally determined adsorption enthalpies was obtained. The high volatility of the Hs oxide species clearly suggests that it is HsO_4 since, by analogy with the known properties of the

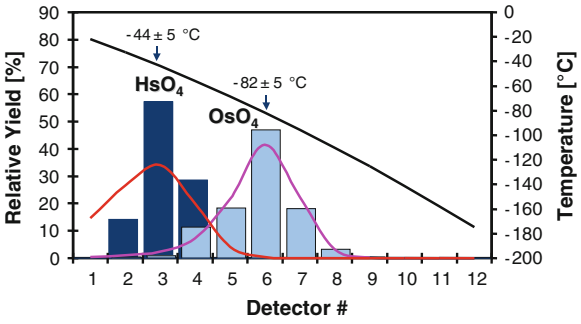

Fig. 28 Relative yields of HsO_4 and OsO_4 for each of the 12 detector pairs. Measured values are represented by bars: $^{269}HsO_4$: *dark blue*; $^{172}OsO_4$: *light blue*. The solid black line indicates the temperature profile (*right-hand scale*). The maxima of the deposition distributions were evaluated as –44 ± 6 °C for HsO_4 and –82 ± 7 °C for OsO_4. *Solid lines* represent results of a simulation of the adsorption process with standard adsorption enthalpies of −46.0 kJ·mol^{-1} for $^{269}HsO_4$ (*red line*) and −39.0 kJ·mol^{-1} for $^{172}OsO_4$ (*purple line*)

Os oxides, all other Hs oxides are expected to be much less volatile and unable to reach the detector system. The observed formation of a volatile Hs oxide (very likely HsO_4) provides strong experimental evidence that Hs behaves chemically as an ordinary member of group 8 of the Periodic Table.

6.4 Reactive Surface Deposition of Hassium, Formation of Sodium Hassate (VIII)

In an independent experiment, von Zweidorf et al. [111] used the Continuously Working Arrangement For CLuster-Less Transport of In-SiTu Produced Volatile Oxides (CALLISTO) setup to demonstrate that the volatile Hs compound formed in-situ with oxygen containing carrier gases reacts readily with a thin layer of hydroxide in the presence of water; see also "Hassium (Hs, Element 108)". This behavior is well-known for OsO_4, which behaves as an acid anhydride. With aqueous NaOH it forms a sodium osmate(VIII) of the stoichiometry $Na_2[OsO_4(OH)_2]$. In an experiment similar to the one of Ch. Düllmann et al. [87], the reaction $^{248}Cm(^{26}Mg, 5n)^{269}Hs$ was employed to form volatile $^{269}HsO_4$ by stopping the fusion reaction products in a mixture of He/O_2 and passing the gas stream through a hot quartz wool filter. The addition of water vapors significantly improved the deposition yield of tetroxides on freshly prepared NaOH surfaces. Therefore, the He/O_2 gas stream (1 $L \cdot min^{-1}$ He, 0.1 $L \cdot min^{-1}$ O_2), containing HsO_4 and OsO_4, was mixed with 0.1 $L \cdot min^{-1}$ He saturated with water at 30 °C. The detection system consisted of four detection arrays, each containing four silicon PIN-diodes of 10 mm × 8 mm active area facing a stainless steel plate, coated with NaOH at a distance of about 1 mm. The gas stream was passing through three of these arrays, whereas the fourth one was in so-called "service mode". Every 60 min, one of the stainless steel plates had to be replaced with a freshly coated one, since the reactive surfaces were loosing deposition efficiency with time. Presumably, this was due to the neutralization of the alkaline surface with CO_2. Carbon dioxide was probably formed under the influence of the heavy ion beam by a reaction of the carbon beam dump with the oxygen of the jet gas. The flow of the gas stream was controlled by four computer controlled valves. The working principle of the deposition and detection system is illustrated in Fig. 29. A disadvantage of the one-sided detection system is the reduced detection geometry compared to a two-sided geometry in a cryo thermochromatography detector. The one-sided detection system significantly lowers the probability to detect complete nuclear decay chains.

In total, five nuclear decay chains attributed to the decay of Hs isotopes were registered [111]. For reasons discussed in Sect. 6.3, all five decay chains can safely be assigned to the decay of ^{269}Hs. The distribution of the five Hs events in relation to the lighter homolog Os on the 3 times 4 detectors, i.e., 12 positions are depicted in Fig. 30. The gas stream always entered the detection setup before detector position 1 and left after passing detector 12.

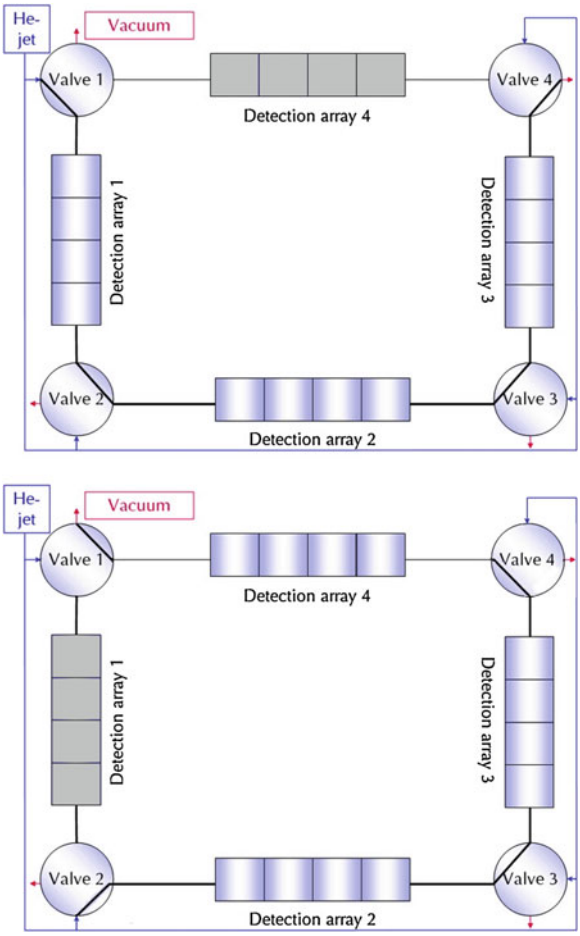

Fig. 29 Comparison of two different states of the deposition and detection system of CALLISTO. In the upper part of the figure, detection array 4 is in "service mode", in the lower part of the figure, detection array 1 is in "service mode", allowing replacing the steel plate of array 1 with a freshly prepared NaOH surface. Figure reproduced from [159] with permission of the author

In the case of osmium, the formation of the osmate(VIII) was associated with a maximum at the first detection position (Fig. 30). Assuming similar properties of OsO_4 and HsO_4, the deposition of hassium was explained as due to the formation of an analogous sodium hassate(VIII) according to the reaction mechanism:

$$2\ \mathrm{NaOH} + \mathrm{HsO_4} \rightleftarrows \mathrm{Na_2}\left[\mathrm{HsO_4(OH)_2}\right] \tag{4}$$

The authors [111] concluded, that for the first time, an acid–base reaction was performed with the tetroxide of hassium leading to the formation of a hassate(VIII). Evidence for a lower reactivity of HsO_4 with respect to moisturized NaOH as compared to OsO_4 as tentatively suggested by the maximum of the Hs distribution on detector 3 was not judged as significant due to the few detected events.

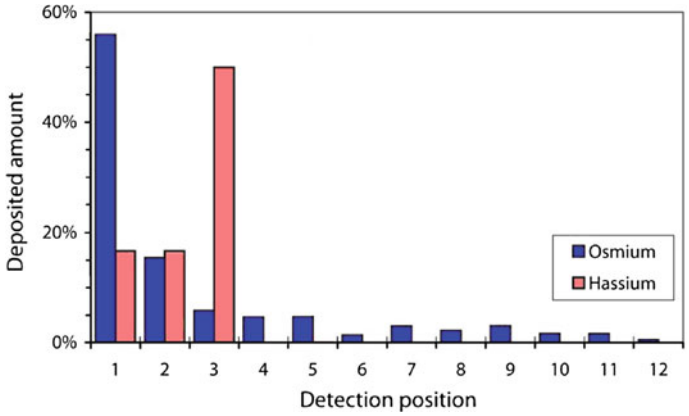

Fig. 30 Deposition pattern of OsO_4 (*blue*) and $^{269}HsO_4$ (*red*) on NaOH surface form a moist gas stream. The Os α activity was mostly due to the decay of 19.2 s ^{172}Os and 22.4 s ^{173}Os. Figure adapted from [159] with permission of the author

6.5 Discovery of the Isotopes ^{270}Hs and ^{271}Hs

The nuclide ^{270}Hs is of special importance to nuclear structure physics (see "Nuclear Structure of Superheavy Elements"), since it was predicted to be a deformed, doubly magic nucleus [112, 113]. Superheavy nuclides owe their existence exclusively to nuclear shell effects, which stabilize them against spontaneous fission decay. Macroscopic–microscopic calculations of the ground-state shell corrections energies, i.e., the correction to be applied to the liquid-drop binding energy, in the region from $Z = 82$ and $N = 126$ up to $Z = 120$ and $N = 190$ reveal three regions of increased stability [114]. These are (i) centered on the nuclides ^{208}Pb, the last known, spherical doubly magic nucleus with –14 MeV shell correction energy, (ii) a smaller region centered around ^{270}Hs with about –7 MeV, and (iii) a slightly larger region around ^{298}Fl with also about –7 MeV shell correction energy; see "Syntheses of Superheavy Elements" and "Nuclear Structure of Superheavy Elements". The new area of increased stability at $Z = 108$ and $N = 162$ corresponds to gaps in the single particle spectra and appears only if quadrupole and hexadecapole deformations are taken into consideration. The experimental study of the decay properties of ^{270}Hs and to measure, e.g., its α-decay energy is therefore pivotal to calibrate theoretical models. The stabilization of neutron shells is reflected by local minima of Q_α near and at magic neutron numbers, while magic proton numbers are characterized by unusually large Q_α-values of parent nuclei decaying into the proton shell. While the nucleus ^{298}Fl is currently not reachable with experimentally feasible synthesis reactions, there are several possibilities to synthesize ^{270}Hs. The reaction ^{26}Mg + ^{248}Cm, which already proved suitable to synthesize ^{269}Hs in the 5n reaction channel, should also be suitable to produce ^{270}Hs in the 4n evaporation channel with similar production cross-section. For such an asymmetric reaction,

chemical isolation of hassium in the form of volatile tetroxides offers a superior overall efficiency compared to electrostatic and magnetic separator systems.

In an experimental campaign, the reaction ^{26}Mg + ^{248}Cm was investigated at five different beam energies [88, 89]. For these experiments, performed at GSI, a heated recoil chamber, which was operated at 400 °C, was constructed in order to optimize the rapid formation of tetroxides. Also, the new cryo thermochromatography detector cryo on-line multidetector for physics and chemistry of transactinides (COMPACT), with an improved detection efficiency, was developed. Version 1 had a detection efficiency for a single α particle of 78% and version 2 of 93%. This way, the probability to detect all members of a decay chain was significantly improved. In two experiments, a total of 26 decay chains assigned to Hs isotopes were identified.

Thirteen of these decay chains could be assigned to the, by now, well-known ^{269}Hs, produced in the 5n evaporation channel. These data, together with a re-evaluation of the older literature data, lead to a disentanglement of the complicated decay chains of ^{269}Hs [13, 14]. An updated decay scheme is shown in Fig. 31. The observation of two different α-decay energies in ^{265}Sg that feed two different isomeric states in ^{261}Rf lead to the postulation of two isomeric states also in ^{265}Sg. A more detailed discussion can be found in [115]. Recently, the two isomeric states in ^{265}Sg were independently confirmed in an experiment by H. Haba et al. [40].

Seven decay chains observed at lower beam energies exhibited a new feature. The α-particle decay was in all cases followed shortly in time by spontaneous fission with a half-life of 0.3 s. This decay sequence was assigned to the new nuclide ^{270}Hs, produced in the 4n channel, and its spontaneously fissioning daughter ^{266}Sg [88, 89].

At the three lowest beam energies, a total of six decay chains were observed, which again were different from the previously measured ones. In five cases, the α particle was followed by a spontaneous fission decay with a relatively long half-life of 84 s. In one case, an α particle of $E_\alpha = 9.30$ MeV was followed after 149 s by a second α particle with a relatively low $E_\alpha = 8.20$ MeV, instead of spontaneous fission. The decay chain was then terminated 12 s later by spontaneous fission. In [88], this decay chain was tentatively assigned to ^{271}Hs, produced in the 3n channel. The large difference in ΔE_α of 1.1 MeV was interpreted as a signature for crossing the $N = 162$ neutron shell from right to left. Consequently, the daughter of ^{271}Hs, the nuclide ^{267}Sg, decays mainly by spontaneous fission, but to a minor extent also by α-particle emission to the nuclide ^{263}Rf. In these series of experiments, altogether five new nuclides have been observed; among them the deformed doubly magic nucleus ^{270}Hs. An in-depth review of the work can be found in [115]; "Nuclear Structure of Superheavy Elements" provides a detailed discussion on nuclear structure aspects of the heaviest elements. In Fig. 32, the decay properties of $^{269–271}$Hs and their daughters are displayed.

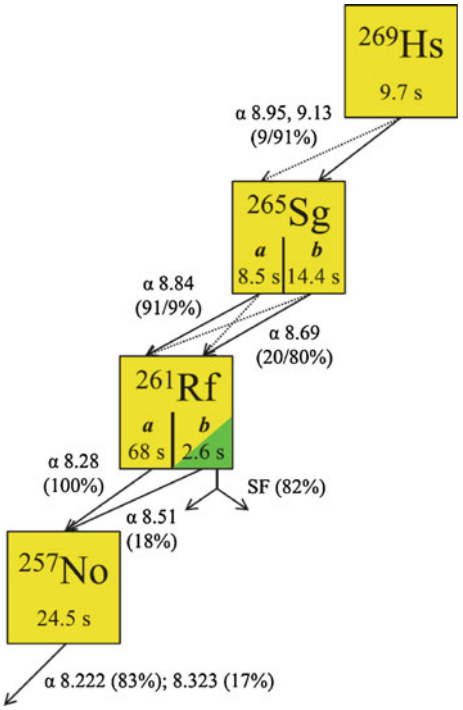

Fig. 31 Decay chains of ^{269}Hs. Reevaluation of the literature data [13, 14] and [115] together with data from [40]. Figure reproduced with permission from Ref. [40]. Copyright 2012 by The American Physical Society

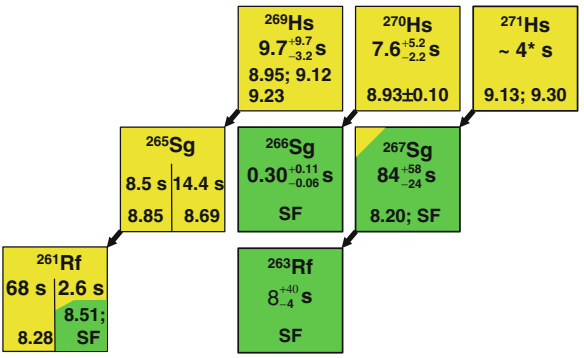

Fig. 32 Decay properties of ^{269,270,271}Hs and their daughters. Figure updated with data from [40]

7 Copernicium (Cn, Element 112)

With the reported synthesis of partly long-lived isotopes of elements Cn ($Z = 112$) through element 118 in ^{48}Ca induced reactions on ^{238}U, ^{242,244}Pu, ^{243}Am, ^{245,248}Cm, ^{249}Bk, and ^{249}Cf targets [116–120], the focus of chemists working in this field shifted to the chemical exploration of these superheavy elements, rather than continuing with Mt, Ds, and Rg. One of the main driving forces for entering

this new era are strong relativistic effects that are expected to strongly influence chemical properties [121]; see "Theoretical Chemistry of the Heaviest Elements". These elements have filled $6d^{10}$ and $7s^2$ electron shells and the $7p$ shell is being filled. Early attempts to chemically identify elements with atomic numbers 112 and higher failed; see "Historical Reminiscences: The Pioneering Years of Superheavy Element Research" for a historical perspective. Only recently, the required sensitivity was reached performing chemistry experiments at the picobarn cross-section level; for recent reviews see, e.g., [122–124].

7.1 Volatility of Group-12 to 18 Elements and Compounds

Due to the expected high volatility of elements with atomic numbers 112 to 118 in their elemental state [125] (see also "Theoretical Chemistry of the Heaviest Elements and Thermochemical Data from Gas-Phase Adsorption and Methods of Their Estimation"), gas-phase chemical studies play an important role in investigating their chemical properties. Very early on, it was speculated that, because of relativistic effects and due to their closed $7s^26d^{10}$ and $7s^26d^{10}7p_{½}^2$ (sub)shells, Cn and Fl (Fl, $Z = 114$), respectively, might be very volatile; possibly even as volatile as radon [126]. More recent predictions claim that both elements should still retain some metallic character, and thus adsorb quite well on certain metal surfaces [127]. Semiempirical extrapolations [128] point to Pd, Cu, and Au as ideal surfaces for the adsorption of superheavy elements.

Besides the elemental state, also volatile compounds of superheavy elements have been considered. Bächmann et al. [91] extrapolated the boiling points of hydrides, methyl-, and ethyl compounds of elements 113 through 117. Trautmann et al. [129] showed, that short-lived ^{216}Po ($T_{1/2} = 0.15$ s), a member of group 16, was volatilized using ethyl radicals, probably as diethylpolonium.

Isotopes of the group 14 to 16 elements Pb (e.g., ^{212}Pb, ^{213}Pb), Bi (e.g., ^{212}Bi, ^{213}Bi), and Po (e.g., ^{211m}Po, ^{212m}Po) severely interfere with the detection of transactinide nuclei. Therefore, due to the high α-decay energies of the above-mentioned isotopes of Pb, Bi, and Po, a very clean separation of transactinide elements from these elements must be accomplished.

7.2 First Attempts to Chemically Identify Copernicium

A first attempt to chemically identify Cn in the elemental state was made by Yakushev et al. [130] in Dubna. The isotope ^{283}Cn was produced by bombarding a $^{nat.}$U target with ^{48}Ca ions. At the time of the experiment, it was assumed that ^{283}Cn decays by SF with a half-life of about 3 min [116, 117]. Simultaneously, short-lived Hg isotopes were produced from a small admixture of Nd to the target material. In test experiments, short-lived Hg isotopes were isolated in the elemental form from other reaction products and were quantitatively transported in He through a 30 m long Teflon^{TM} capillary at room temperature.

Adsorption of Hg nuclides on silicon detectors, as in the successful experiment with HsO_4, proved experimentally not feasible, since Hg was adsorbed on such surfaces only at temperatures of –150 °C and below. However, Hg adsorbed quantitatively on Au, Pt, and Pd surfaces at room temperature. As little as 1 cm^2 of Au or Pd surface was sufficient to adsorb Hg atoms nearly quantitatively from a stream of 1 $L \cdot min^{-1}$ He. Therefore, detector chambers containing a pair of Au or Pd coated PIPS detectors were constructed. The detector chambers were positioned inside an assembly of 84 ^{3}He-filled neutron detectors (in a polyethylene moderator) in order to simultaneously detect neutrons accompanying spontaneous fission events, see Fig. 33.

In an experiment conducted in the year 2000, a total beam dose of 6.85×10^{17} ^{48}Ca ions was accumulated. The chemical yield for the simultaneously produced ^{185}Hg ($T_{1/2} = 49$ s) was 80%. If Cn behaved chemically like Hg and all efficiencies measured for Hg were also valid for Cn, detection of $3.4^{+4.3}_{-2.2}$ SF events could be expected, assuming the cross-section value for the production of ^{283}Cn measured in [116]. However, no SF events were observed. Therefore, no unambiguous answer as to any chemical and physical property of Cn was obtained [130].

In a follow-up experiment, the question whether Cn remained in the gas phase and passed over the Au and Pd surfaces was addressed [131]. Therefore, a special

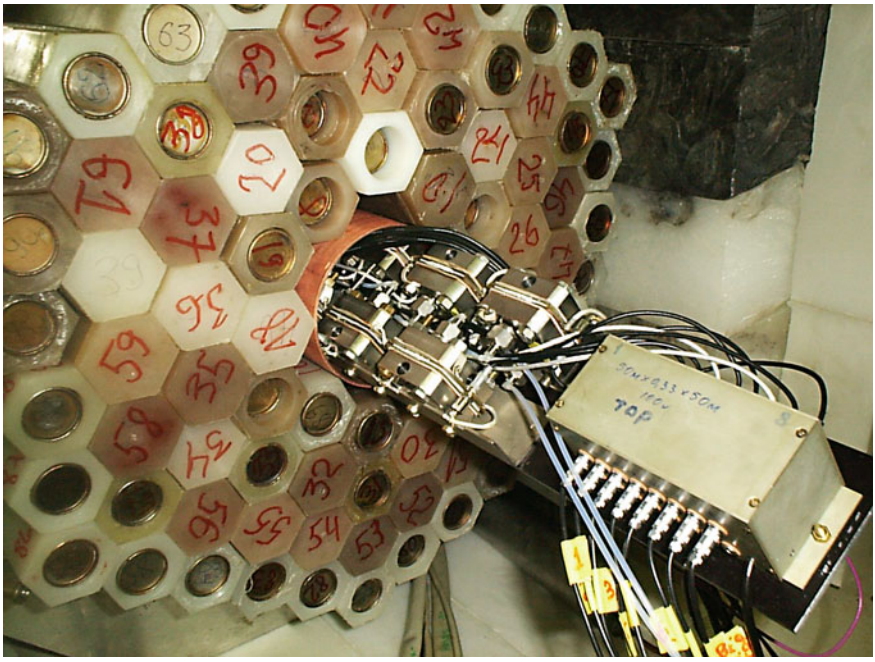

Fig. 33 Detector arrangement for the detection of ^{283}Cn consisting of pairs of Au and Pd coated PIPS detectors inside an assembly of 84 ^{3}He filled neutron detectors. Photograph reproduced from [130]

ionization chamber to measure SF fragments of nuclei remaining in the gas was added at the exit of the Au or Pd coated PIPS detector array. A total beam dose of 2.8×10^{18} ^{48}Ca ions was accumulated. Again zero SF events were registered on the Au and Pd coated PIPS detectors, confirming the result of the first experiment. However, eight high energy events were detected in the ionization chamber. They were ascribed to SF decays, because they were accompanied by neutrons registered in the surrounding neutron counters (see Fig. 33), while only one background count was expected [131]. Therefore, the majority of the events were attributed to the decay of an isotope of Cn, since there is no other known volatile element with nuclides which decay by SF. From this experiment, it appeared that the interaction of Cn with a Au and Pd surface is much weaker than for Hg [131].

A new experiment to measure the enthalpy of adsorption of Cn on Au surfaces was conducted at GSI Darmstadt [132]. This can be done with a cryo thermochromatography detector array similar to that used for the chemical study of Hs (see Sect. 6.3); with one difference being that the surfaces of the detectors were covered with a thin Au layer. The temperature gradient along the detector started at +35 °C and reached down to –185 °C; the adsorption temperature of Rn. A total beam dose of 2.8×10^{18} ^{48}Ca ions was accumulated on a 1.6 mg·cm^{-2} thick ^{238}U target. After stopping the products in a carrier gas (He), they were transported through a 25 m long capillary within about 25 s to the detector array. Seven events were detected with energies higher than 40 MeV that were attributed to fission fragments from the SF decay of ^{283}Cn. Since the detector array was operated in a 2π-counting mode, no fission fragment coincidences could be measured. The position of most of these events was identical to the deposition peak of Rn, measured simultaneously during the experiment. It should be mentioned, however, that the measured energies were lower than expected. It was argued that a thin ice layer, onto which the atoms were adsorbed, might have caused a reduction of the measured kinetic energies. It was therefore concluded that all three chemical studies yielded a consistent picture, namely that Cn is very similar to Rn [132].

To the very big surprise, later physics studies could not confirm the SF-decay of ^{283}Cn. They rather showed that this isotope decays via α emission with a half-life of about 4 s to ^{279}Ds, which then decays by SF with a half-life of 0.2 s [119]. This situation asked for new chemistry experiments, since the transport time from the site of nuclei production at the accelerator to the detector array, in all chemistry experiments performed so far, was too long for identification of a 4-s isotope.

Therefore, additional chemistry experiments were performed at GSI, Darmstadt, and at FLNR in Dubna, using the same reaction and setup as applied for the previous chemistry experiment with some improvements (shorter transport time of about 2 s and 4π-counting geometry). In two experiments, using the ^{48}Ca on ^{238}U (1.6 mg·cm^{-2}) reaction at center-of-target (c.o.t) beam energies of 231 and 234 MeV, respectively, and a total beam dose of 5.9×10^{18}, no decay chain was observed that could be ascribed to ^{283}Cn [133]. The cross-section limit reached was 1.3 pb. This sensitivity was interpreted as insufficient to be in disagreement with physics experiments which produced ^{283}Cn in this reaction with—on average—1.5

pb [119, 134]. Hence, the chemistry results of the first experiments described above could not be confirmed because no SF events were detected.

This example nicely shows how difficult it is to perform chemistry experiments at the cutting edge of current technology. If only trace amounts are available for study it is mandatory to base the chemical interpretation on an unequivocal identification of separated single atoms. This identification should not base solely on the detection of single fission fragments, as it was done in these first chemistry experiments. For the moment being, however, it remains unclear what kind of signals have been measured in these experiments (for a summary of these early physics and chemistry experiments with Cn see [122]).

7.3 On-Line Thermochromatography of Copernicium

After the unsuccessful ^{48}Ca on ^{238}U experiments, an attempt was made investigating the chemical properties of Cn using a reaction that first produces Fl ($Z = 114$). The reason for this rather unusual strategy was the observation that cross-sections significantly increase when going from Cn to Fl using ^{48}Ca-induced fusion reactions [119]. A prerequisite of this approach is, however, that first a Fl isotope is formed that has a too short half-life for chemical study, or more important, that decays fast enough into a Cn daughter nucleus with a sufficiently long half-life. The ideal case that fulfills this requirement is the reaction ^{48}Ca + ^{242}Pu. The decay chain observed in physics experiments from the reaction channel ^{242}Pu(^{48}Ca,3n)^{287}Fl is depicted in Fig. 34.

The setup shown in Fig. 35 was used for this study. Each side inside the detector array consisted of 32 (1 × 1) cm^2 silicon detectors, one side being coated by a 50 nm thin Au layer. This enabled the detection of α-decay chains with high efficiency and SF events via the detection of coincident fission fragments. A transportation time of about 2 s was achieved by reducing the length of the transport capillary between collection chamber at the accelerator and the

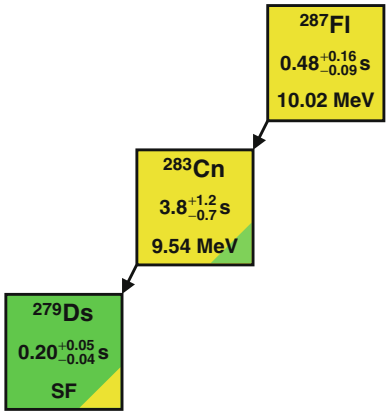

Fig. 34 Decay properties of ^{287}Fl and its daughters [119] used for the first chemical experiment with Cn

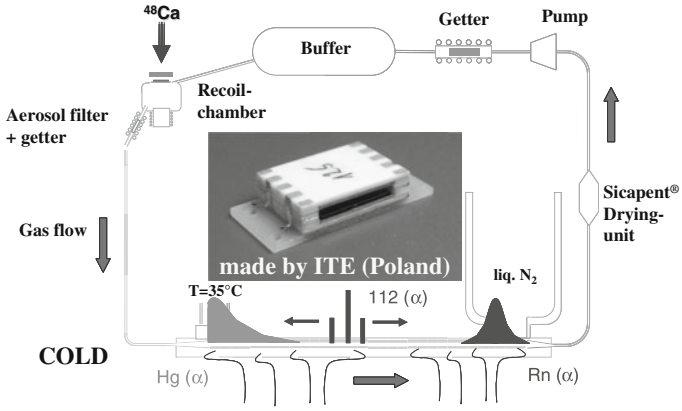

Fig. 35 IVO device used for the experiments with Cn and Fl. The unit is operated in a closed-loop mode to enable highest possible purification from water vapor and from trace contaminants. The detector array consisted of 32 (1 × 1) cm^2 silicon detector pairs (see insert) along which a stationary temperature gradient was established. Figure reproduced with permission from [122]. Copyright 2011 Oldenbourg Wissenschaftsverlag GmbH

chromatography setup. Moreover, the setup was operated in a closed loop mode to reduce the water vapor content of the carrier gas. This was decisive to reduce the formation of ice layers at low temperatures. Still, it was impossible to exclude ice formation at temperatures below about −100 °C.

With a mean transport time of 2.2 s, the yield of ^{287}Fl is reduced to 5% while for ^{283}Cn it is still 68%. In the course of two bombardments of a 1.4 mg·cm^{-2} thick ^{242}Pu target with ^{48}Ca projectiles of 236 MeV (c.o.t. energy) five decay chains were detected. They started with the α decay of ^{283}Cn followed by SF decays within less than one second [135, 136]; see Fig. 36. The observed signature with an α event of very high energy followed by a SF event shortly afterward is very unique and makes the probability that these observed decay chains are of random origin very small. Since no signal can be detected upon deposition of an atom on the surface of the detector, no information may be gained on the half-life of the first decaying product. However, with a transport time of about 2 s, a minimum value of the order of seconds is plausible.

The deposition positions of the five atoms along the detector array are depicted in Fig. 37. The results shown here represent the outcome of three different experiments with varying values of the temperature range inside the detector array and the velocity of the carrier gas, respectively. Also shown are the deposition patters of α-decaying isotopes of Hg and Rn. They were formed in nuclear reactions with a minor admixture of Nd to the ^{242}Pu target (for Hg) or in transfer reactions with the Pu target material (for Rn). In the first experiment, the temperature range inside the detector array ranged from –24 to –185 °C. Under this condition, the first decay chain of ^{283}Cn was observed at the beginning of the column in the second detector, a region where also the major Hg deposition was found.

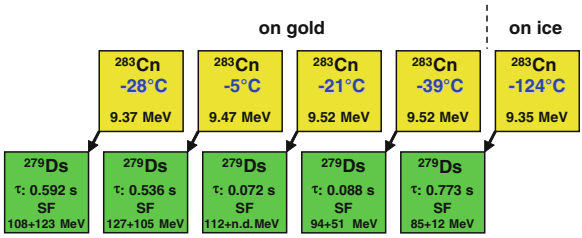

Fig. 36 Decay chains attributed to ^{283}Cn observed in the experiments to study the chemical property of Cn (from [136]). Indicated is the deposition temperature at which the decay of the Cn-atoms was observed. The first four decay chains were observed on the Au surface, whereas the last one occurred in the region where the detectors were covered by a thin layer of ice. τ is the lifetime, i.e., the measured time difference between the α decay of the mother nucleus and the SF event. *n.d.* not detected due to incomplete geometrical efficiency of the detector array

To search for a possible difference in chemical behavior between Hg and Cn the temperature at the beginning of the detector array was increased to the maximum value at which a semiconductor detector is still operational (+35 °C). Indeed, in the second experiment one decay chain of ^{283}Cn was observed at –5 °C (detector 7 in panel b of Fig. 37), which is at the edge of Hg deposition. Therefore, a third experiment was conducted with increased gas flow rate (increase from about 1 to 2 L·min^{-1}). Under this experimental condition, two atoms of ^{283}Cn were detected on the Au covered detector array at –29 °C and –39 °C, respectively (detector 11 and 14 in panel c of Fig. 37). One further atom was found on the ice covered part at –124 °C. All three atoms were observed where only little, if any, Hg deposition occurred.

All three parts of the experiment can be nicely described with a Monte Carlo model (see "Thermochemical Data from Gas-Phase Adsorption and Methods of Their Estimation") assuming one adsorption enthalpy of –52 kJ·mol^{-1} (ordinate on the right hand side of Fig. 37). Hence, this experimental study yields a consistent picture that Cn adsorbs on an Au surface with an adsorption enthalpy which is stronger than that of Rn but weaker compared to that of Hg [136].

The resulting value for the adsorption enthalpy of Cn on the Au surface of -52 kJ·mol^{-1} is in reasonably good agreement with a theoretical prediction that yielded -44 kJ·mol^{-1}, applying a fully relativistic four-component functional theory calculation [127], and a range of –33 to –39 kJ·mol^{-1} using the relativistic pseudopotential approach [137].

Based on an empirical correlation between adsorption enthalpies of single atoms on Au surfaces with their sublimation enthalpy (see Fig. 38), for Cn a value of $\Delta H^0_S = 39^{+23}_{-10}$kJ·mol^{-1} (= $4.8^{+2.8}_{-1.2}$ kcal·mol^{-1}) results [136]. This value is significantly lower compared to a theoretical prediction based on solid–state theory using relativistic Dirac–Kohn–Sham calculations, which predicted that Cn is a semiconductor with a cohesive energy of about 110 kJ·mol^{-1} [138].

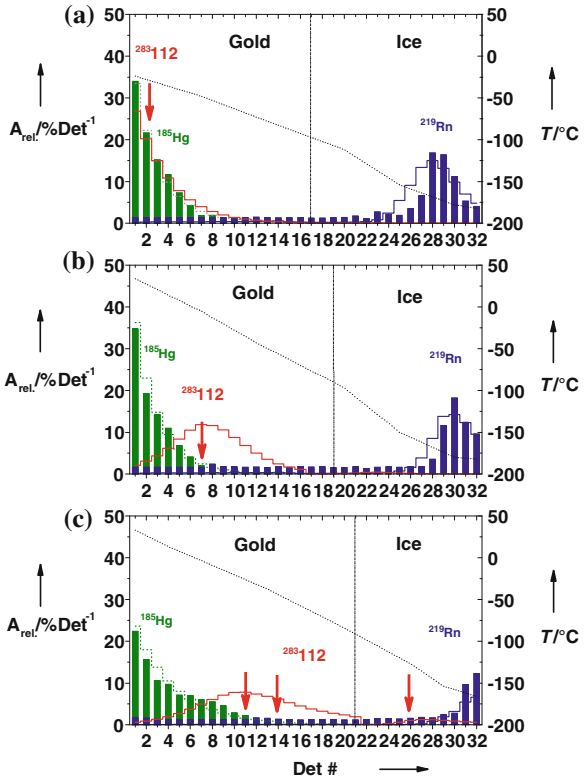

Fig. 37 Deposition of the five detected atoms (indicated by arrows) assigned to ^{283}Cn in ^{48}Ca + ^{242}Pu experiments. The dotted lines indicate the temperature gradient inside the detector array (*right axis* in °C). The three panels a, b, and c reflect the three different regimes in terms of temperature range inside the detector array and gas flow rates (see *text*). The solid red lines depict results of a Monte Carlo model prediction (*left axis* in rel. units) including the given experimental parameters and assuming the deposited atoms to have always an adsorption enthalpy with the Au surface of –52 kJ·mol^{-1} [122, 136]. The vertical dashed lines at detectors 17, 19, and 21, respectively, indicate the start of the ice layer formation toward lower temperatures corroborated by reduced resolutions in the α spectra

Figure 39 depicts the trend of sublimation enthalpies within elements of group 12. The experimental result of Cn nicely supports the classical expectation, already predicted in 1976 by Eichler [125]. Hence, from the experimental study it follows that Cn is a very volatile noble metal which still exhibits a metallic character.

Two additional atoms of Cn were detected in later experiments conducted at FLNR. The first atom, ^{283}Cn, was observed using the same setup, reaction, and beam parameters (^{242}Pu target thickness 1.4 mg·cm^{-2}, beam dose 3.4x10^{18}, ^{48}Ca c.o.t.-beam energy 235 MeV). The decay of ^{283}Cn was observed at a temperature of –7 °C. It's signature was the emission of a 9.3 MeV α particle followed by a SF decay 73 ms later; in agreement with the data depicted in Fig. 37 [139].

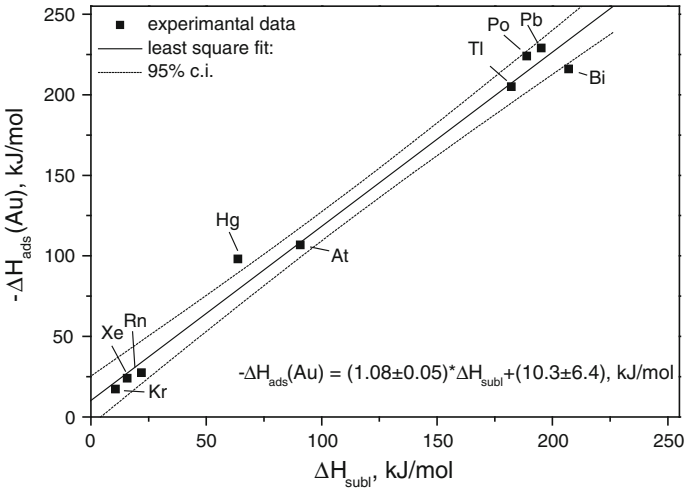

Fig. 38 Correlation between microchemical adsorption enthalpies of *p* and *s*-elements on Au surfaces and their respective macrochemical sublimation enthalpies, reprinted with permision from [160]. Copyright 2005 Oldenbourg Wissenschaftsverlag GmbH

The second atom of Cn, ^{285}Cn, was detected in an experiment behind the Dubna gas-filled magnetic separator using the reaction ^{48}Ca + ^{244}Pu (target thickness 0.44 mg·cm^{-2}, c.o.t.-beam energy 244 MeV). A gas (He/Ar mixture) collection chamber was mounted in the focal plane of the separator to stop products from fusion reactions and to transport them along a capillary to the detector array. In this experiment, one decay chain assigned to ^{285}Cn (E_α = 9.15 MeV) → ^{281}Ds (SF_{coinc}. after 3.4 s) was observed at –93 °C [140]; obviously on the ice covered part of the detector array. This position is, within chemical resolution, still in agreement with previous observations for Cn; see Fig. 37. The novel strategy of using recoil separators as the first step, which reduces the amount of unwanted products formed in nucleon transfer reactions by several orders of magnitude, substantially increases the significance of detected decay chains from the wanted few atoms from complete fusion reactions. This approach was developed at the Lawrence Berkeley Laboratory [141]. Currently, it is also applied at GSI using the TASCA gas-filled magnetic separator [142] for a study of the chemical property of Fl [143].

To conclude, several experiments conducted with different techniques resulted in seven observed atoms of Cn. They yield the consistent picture that this element is a very volatile noble metal.

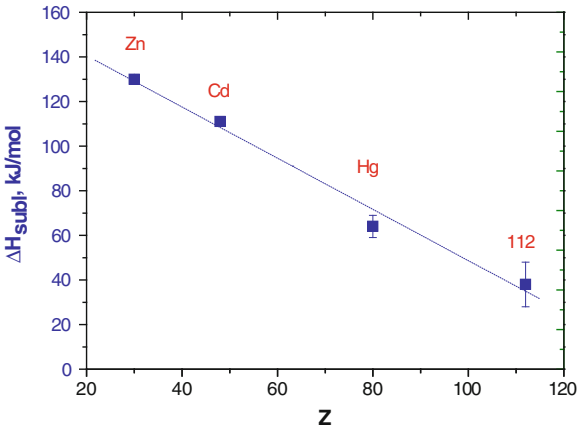

Fig. 39 Sublimation enthalpies of the group 12 elements Zn, Cd, and Hg from the literature and extrapolated sublimation enthalpy of Cn ($Z = 112$) using the correlation depicted in Fig. 38

8 Flerovium (Fl, Element 114)

The next heavier element currently under investigation is Fl which, as a homolog of Pb, is placed in group 14 of the Periodic Table. Suitable nuclides for chemical experiments are ^{287}Fl ($T_{1/2} = 0.48^{+0.16}_{-0.09}$ s) [119], ^{288}Fl ($T_{1/2} = 0.69^{+0.17}_{-0.11}$s) [144], and ^{289}Fl ($T_{1/2}$ =2.1$^{+0.8}_{-0.4}$s) [144]. They can be synthesized in the reactions ^{48}Ca + ^{242}Pu and ^{244}Pu [119]. In the experiment which registered three decay chains of ^{283}Cn in the COLD setup (see Fig. 37c) [136], also a three-member decay chain (not shown in Fig. 36) was registered in detector pair 19 held at –88 °C (see Fig. 40). This decay chain was attributed to an atom of ^{287}Fl reaching the detector despite its short half-live of only 0.5 s. The transport efficiency was estimated to be 5% [145].

An additional experiment conducted in 2007 at FLNR employed a ^{244}Pu target in combination with the COLD setup. This experiment revealed two further decay chains that were attributed to ^{288}Fl [145] see Fig. 40. The transport efficiencies of ^{288}Fl and ^{289}Fl can be estimated using the above-mentioned half-lives of ^{288}Fl and ^{289}Fl to be 11 and 48%, respectively. These efficiencies are higher than the previously mentioned 5% because of the longer half-lives of ^{288}Fl and ^{289}Fl as compared to ^{287}Fl. Indeed, the two events were attributed to the decay of ^{288}Fl. One α-decay event of 9.95 MeV occurred on the bottom detector of detector pair 18 followed 0.109 s later by one SF fragment in the neighboring top detector 19 held at −90 °C. The deposition of ^{288}Fl occurred most likely on the gold covered (top) detector 19 where the SF fragment was observed, whereas the α particle was emitted across the gap and registered in detector 18 bottom. The second decay chain started with an α particle of 9.81 MeV in the top detector of pair 3 and ended 0.104 s later with a single fission fragment observed in bottom detector 6 at –4 °C. The observation that the decay of a daughter atom is displaced from that of the mother atom was explained by the recoil of the daughter atom out of the detector during the α-particle emission, followed by a transport of the recoiling daughter

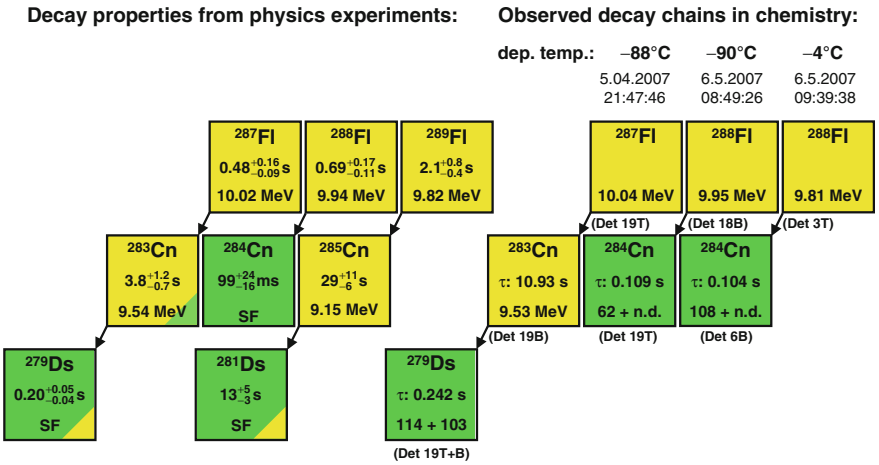

Fig. 40 *Left side* decay properties of $^{287–289}$Fl from physics experiments [119, 144], showing half-lives (with 68% c.i. error limits), from a recent compilation of all experimental results, and mean α-decay energies. Typical uncertainties on α-decay energies are ±0.06 MeV. Yellow colored nuclei decay by α-particle emission, green colored nuclei by spontaneous fission. For ^{279}Ds and ^{281}Ds a small α-decay branch of the order of 10% has been observed. Right side: decay chains attributed to ^{287}Fl and ^{288}Fl observed in the chemistry experiments of [145]. For each decay chain, the deposition temperature, the date and time and the detector number are given (T for the gold covered top detectors and B for the bottom detectors). For Cn and Ds isotopes the life time τ between subsequent α-particle emissions or terminating SF events is given. Also indicated are SF fragment energies in MeV (*n.d.* not detected)

with the carrier gas [145]. Several candidates for decay chains of ^{289}Fl were registered. However, large amounts of various Rn isotopes were produced in multi-nucleon transfer reactions of the ^{244}Pu target with the ^{48}Ca beam. The Rn passed through the thermochromatography column and decayed partly in-flight in every detector sandwich where it created a background of α-particle events, including the region where decays of ^{289}Fl and its daughter ^{285}Cn were expected. This prevented a clear identification of the rather long decay chain from ^{289}Fl [145].

The decay properties of the three events attributed to the decay of ^{287}Fl and ^{288}Fl, along with the literature data from physics experiments, are depicted in Fig. 40. The location of these three detected events, attributed to deposition of atoms of Fl in relation to the elements Cn, Hg, and Rn, is shown in Fig. 41, panels 1 through 4. The dashed line (right hand ordinate) indicates the temperature gradient established during the experiments. The ordinate on the left hand indicates relative yields per detector pair in percentage of a given element. The vertical dash-dotted line indicates the temperature, at which the dew point in the gas was reached. Left of the dash-dotted line, the surface of the COLD detector was either Au (top detectors) or SiO_2 (bottom detectors), right of the dash dotted line the surfaces were covered by a thin layer of ice.

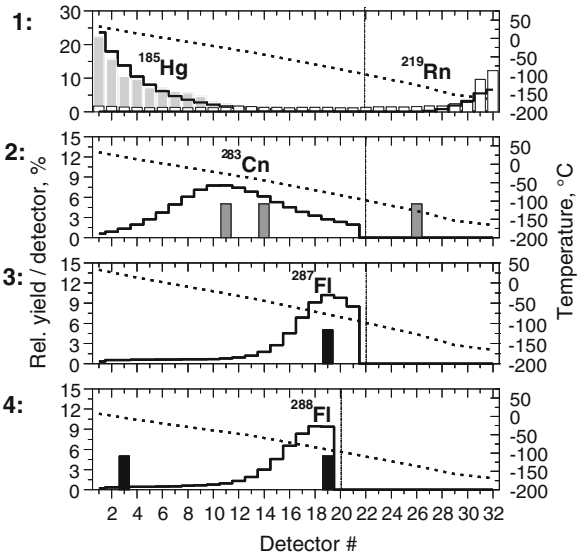

Fig. 41 Deposition patterns of the elements Hg, Rn, Cn, and Fl in the COLD detector as observed in experiments by Eichler et al. [145]. For a detailed discussion see *text*

In panel 1 of Fig. 41, the deposition of the nuclide ^{185}Hg ($T_{1/2}$ = 49 s) (gray bars), produced from an admixture of $^{nat.}$Nd to the target material, is shown. Single atoms of Hg show the expected diffusion controlled deposition pattern from irreversible adsorption on the Au surface of the top detectors. Due to the high flow rates, and since only one side of the detector channel was Au covered, the distribution of Hg extends far into the COLD detector. The nuclide ^{219}Rn (white bars), being produced in transfer reactions, was deposited on the ice surface only at very low temperatures close to the exit of COLD; as expected for the noble gas Rn. The deposition patterns of both ^{185}Hg and ^{219}Rn could be satisfactorily described by a microscopic model of the adsorption chromatographic process. It was based on a Monte Carlo approach [20] (solid lines) with $-\Delta H_{ads}^{Au}(\mathrm{Hg}) \geq 50$ kJ·mol^{-1} and $-\Delta H_{ads}^{ice}(\mathrm{Rn}) = 19$ kJ·mol^{-1}, respectively; in good agreement with the literature data. In panel 2, the location of three decays of ^{283}Cn in COLD (see Fig. 37c) is depicted that were observed in the same experiment as the decay chain attributed to ^{287}Fl (panel 3). In panels 3 and 4, the location of the deposition of one atom of ^{287}Fl and two atoms of ^{288}Fl, respectively, is shown. From these three events, a most probable adsorption enthalpy of $-\Delta H_{\mathrm{ads}}^{\mathrm{Au}}(\mathrm{Fl}) = 34^{+20}_{-3}$ kJ·mol^{-1} (68% c.i.) was deduced [145] assuming that the event observed at – 4 °C originated from a decay during transport along the column. The corresponding calculated model distributions are truncated at the dash-dotted line indicating the dew point.

An adsorption enthalpy of $-\Delta H_{\mathrm{ads}}^{\mathrm{Au}}(\mathrm{Fl}) = 34^{+20}_{-3}$ kJ·mol^{-1} is surprisingly low, since Fl, as the homolog of Pb, is expected to be more reactive than Cn and should thus deposit at higher temperatures than Cn, and not at lower or equal temperatures as observed in these experiments. Theoretical calculations, which predicted the adsorption of Cn ($-\Delta H_{\mathrm{ads}}^{\mathrm{Au}}(\mathrm{Cn}) = 44$ kJ·mol^{-1}, see Sect. 7.3 and "Theoretical

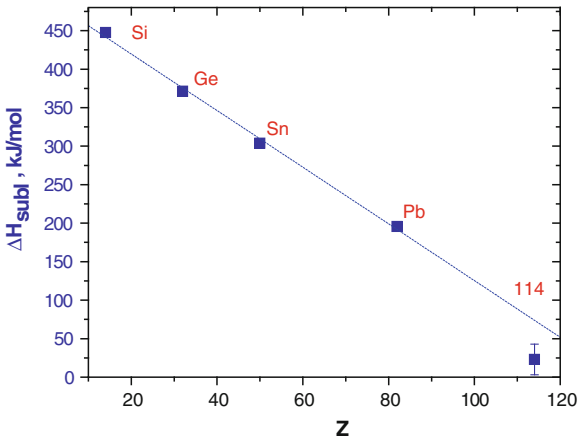

Fig. 42 Sublimation enthalpies of the group 14 elements Si, Ge, Sn, and Pb from the literature and the extrapolated sublimation enthalpy of Fl ($Z = 114$) (from Ref. [145] and using the correlation depicted in Fig. 38)

Chemistry of the Heaviest Elements") sufficiently accurate, predict $-\Delta H_{ads}^{Au}(Fl) = 68$ kJ·mol^{-1}, somewhat less volatile than Cn [146]. It was argued, that on transition metal surfaces Fl should adsorb stronger than Cn, due to chemical forces; since the $7p_{1/2}$(Fl) atomic orbital is less stabilized than the $7s$(Cn) atomic orbital. On the other hand, relativistic solid–state calculation yield cohesive energies (equivalent to sublimation enthalpies) which are higher for Cn (1.1 eV [138]) compared to Fl (0.5 eV [147]). This prediction is at variance with the calculation from [146] under the assumption that sublimation enthalpies correlate with the adsorption enthalpies on Au surfaces; see Fig. 38.

The observation that Fl exhibits an unexpected high volatility (see Fig. 42), together with the fact that a background in the detector array made the positive identification of ^{289}Fl events impossible, caused some skepticism [148]; see "Theoretical Chemistry of the Heaviest Elements, 7p Elements" for a theoretical discussion.

In order to remove the background of undesired reaction products, the chemical "techniques" (collection chambers, gas-jets, chromatography systems, detectors, etc.), which had so far been developed and successfully applied for lighter transactinides, coupled to a physical recoil (pre-)separator, such as a gas-filled separator. At GSI, Darmstadt, the dedicated gas-filled separator TASCA (Trans-Actinide Separator and Chemistry Apparatus) was constructed and was successfully commissioned [142]. With TASCA, recoiling fusion products are separated from the incoming beam and from transfer reaction products with a dipole magnet and are focused on a relatively small product beam spot by two quadrupole magnets. The device is operated as a gas-filled separator, which allows charge focusing. At the end of the separator, the product beam, which consists of single ions in case of superheavy elements, is passing through a thin window, supported by a honeycomb structure, and is thermalized in a gas volume. The windows can stand pressures well above 1 bar; the pressure difference between the millibar pressure range in the separator and the pressure in the gas jet. These so-called

Recoil Transfer Chambers (RTC) replace the so far used target chambers [149]. The lower overall efficiency, which now also includes the transmission through the separator, is compensated by the removal of the primary beam and interfering transfer reaction products. A first chemical experiment with Fl at GSI using thermochromatography on Au surfaces has been conducted behind the TASCA separator in fall of 2009 [143].

Two events attributed to the decay of Fl were observed. Both α-particle decays of Fl isotopes occurred at room temperature. A detailed comparison with the experiment at FLNR cannot be made, especially since no analysis of the experiment behind TASCA has been published so far. Despite of this, it is quite remarkable that two independent experiments were able to separate and detect Fl in a chemistry experiment, demonstrating the power of gas chemical investigations and the frontier of chemical research of superheavy elements.

Clearly, further experiments are needed here to elucidate the true chemical properties of Fl in the elemental state.

9 Conclusions and Outlook

In the near future, first results concerning the chemistry of element 113 can be expected. First experiments have been conducted by Dmitriev et al. at FLNR, Dubna studying the adsorption of element 113 on Au surfaces. Only preliminary results have been communicated [150].

The knowledge about the chemistry of transactinide elements will grow and new classes of compounds, such as volatile carbonyls [45], open new perspectives, especially to first chemical studies of Mt. In the α-decay chain of ^{288}115 and ^{294}117 sufficiently long-lived isotopes of Mt, ^{276}Mt ($T_{1/2} \approx 0.7$ s) and ^{278}Mt ($T_{1/2} \approx 8$ s), have been identified and become available for chemical studies. For the not yet studied elements, like Ds, Rg, and element 115, isotopes with $T_{1/2}$ suitable for chemical studies have also been identified. The nuclide ^{289}115 with $T_{1/2} \approx 0.4$ s was produced recently in the reaction ^{243}Am(^{48}Ca,2n) [151] as well as the α-decay daughter of ^{293}117 produced in the reaction ^{249}Bk(^{48}Ca,4n) [120, 152, 153]. For elements 116 through 118, new isotopes suitable for chemical studies must first be discovered. Their separation will also need new technological developments to cope with the very low production rates and short half-lives. Here, vacuum thermochromatography [154, 155, 156] coupled to a preseparator might give access to nuclides with half-lives of the order of only 100 ms.

On the long run, new accelerators delivering higher beam intensities and even more exotic target materials such as ^{250}Cm, ^{251,252}Cf, and ^{254}Es will allow to produce nuclides closer to the line of beta stability in so-called superheavy element factories. Possible electron-capture branches in the members of the α-particle decay chains may lead to the formation of longer lived nuclides of Mt, Ds, Rg, and Cn [157], that could be stored and studied in traps.

References

1. Zvara, I., Chuburkov, Y.T., Caletka, R., Shalaevski, M.R., Shilov, B.V.: Chemical properties of element 104. J. Nucl. Energy **21**, 601–603 (1967)
2. Even, J., Yakushev, A., Düllmann, C.E., Dvorak, J., Eichler, R., Gothe, O., Hild, D., Jäger, E., Khuyagbaatar, J., Kratz, J.V., Krier, J., Niewisch, L., Nitsche, H., Pysmenetska, I., Schädel, M., Schausten, B., Türler, A., Wiehl, N., Wittwer, D.: Rapid synthesis of radioactive transition-metal carbonyl complexes at ambient conditions. Inorg. Chem. **51**, 6431–6433 (2012)
3. Keller, O.L.: Chemistry of the heavy actinides and light transactinides. Radiochim. Acta **37**, 169–180 (1984)
4. Johnson, E., Fricke, B., Keller, O.L., Nestor, C.W., Tucker, T.C.: Ionization-potentials and radii of atoms and ions of element 104 (Unnilquadium) and of Hafnium(2 +) derived from multiconfiguration Dirac-Fock calculations. J. Chem. Phys. **93**, 8041–8050 (1990)
5. Zhuikov, B.L., Chuburkov, Y.T., Timokhin, S.N., Jin, K.U., Zvara, I.: Is element-104 (Kurchatovium) a P-element. 1. Chromatography of atoms with hydrogen as carrier gas. Radiochim. Acta **46**, 113–116 (1989)
6. Eliav, E., Kaldor, U., Ishikawa, Y.: Ground-state electron configuration of Rutherfordium—role of dynamic correlation. Phys. Rev. Lett. **74**, 1079–1082 (1995)
7. Morozov, A.I., Karlova, E.V.: Physico-chemical properties of anhydous Zirconium and Hafnium oxychlorides. Zh. Neorg. Khim. **16**, 25 (1971)
8. Zvára, I., Belov, V.Z., Chelnokov, L.P., Domanov, V.P., Hussonois, M., Korotkin, Y.S., Schegolev, V.A., Shalayevsky, M.R.: Chemical separation of kurchatovium. Inorg. Nucl. Chem. Lett. **7**, 1109–1116 (1971)
9. Türler, A.: Gas phase chemistry of the transactinide elements Rutherfordium, Dubnium, and Seaborgium. Universität Bern, Habilitationsschrift (1999)
10. Zvara, I., Timokhin, S.N., Chuburkov, Y.T., Domanov, V.P., Gorski, B.: Comparative study of the chlorides and bromides of element 104 with Hf(Zr) by thermochromatography. In: Joint Institute for Nuclear Research, Laboratory of Nuclear Reactions, Scientific Report 1989–1990, vol. E7-91-75, pp. 34-35. Joint Institute for Nuclear Research, Dubna (1991)
11. Gäggeler, H.W., Jost, D.T., Baltensperger, U., Weber, A., Kovacs, A., Vermeulen, D., Türler, A.: OLGA II, an on-line gas chemistry apparatus for applications in heavy element research. Nucl. Instrum. Methods Phys. Res., Sect. A **309**, 201–208 (1991)
12. Kadkhodayan, B., Türler, A., Gregorich, K.E., Nurmia, M.J., Lee, D.M., Hoffman, D.C.: The heavy element volatility instrument (Hevi). Nucl. Instrum. Methods Phys. Res., Sect. A **317**, 254–261 (1992)
13. Düllmann, C.E., Türler, A.: $^{248}Cm(^{22}Ne,xn)^{270-x}Sg$ reaction and the decay properties of ^{265}Sg reexamined. Phys. Rev. C **77**, 064320(10) (2008)
14. Düllmann, C.E., Türler, A.: Erratum: $^{248}Cm(^{22}Ne, xn)^{270-x}Sg$ reaction and the decay properties of ^{265}Sg reexamined. [Phys. Rev. C 77, 064320 (2008)] Phys. Rev. C **78**, 029901(E) (2008)
15. Kadkhodayan, B., Türler, A., Gregorich, K.E., Baisden, P.A., Czerwinski, K.R., Eichler, B., Gäggeler, H.W., Hamilton, T.M., Jost, D.T., Kacher, C.D., Kovacs, A., Kreek, S.A., Lane, M.R., Mohar, M.F., Neu, M.P., Stoyer, N.J., Sylwester, E.R., Lee, D.M., Nurmia, M.J., Seaborg, G.T., Hoffman, D.C.: On-line gas chromatographic studies of chlorides of rutherfordium and homologs Zr and Hf. Radiochim. Acta **72**, 169–178 (1996)
16. Türler, A., Gäggeler, H.W., Gregorich, K.E., Barth, H., Brüchle, W., Czerwinski, K.R., Gober, M.K., Hannink, N.J., Henderson, R.A., Hoffman, D.C., Jost, D.T., Kacher, C.D., Kadkhodayan, B., Kovacs, J., Kratz, J.V., Kreek, S.A., Lee, D.M., Leyba, J.D., Nurmia, M.J., Schädel, M., Scherer, U., Schimpf, E., Vermeulen, D., Weber, A., Zimmerman, H.P., Zvara, I.: Gas phase chromatography of halides of elements 104 and 105. J. Radioanal. Nucl. Chem. Art. **160**, 327–339 (1992)

17. Sylwester, E.R., Gregorich, K.E., Lee, D.M., Kadkhodayan, B., Türler, A., Adams, J.L., Kacher, C.D., Lane, M.R., Laue, C.A., McGrath, C.A., Shaughnessy, D.A., Strellis, D.A., Wilk, P.A., Hoffman, D.C.: On-line gas chromatographic studies of Rf, Zr, and Hf bromides. Radiochim. Acta **88**, 837–843 (2000)
18. Domanov, V.P., Zin, K.U.: Thermochromatographic study on chlorination products from traces of Zr, Hf, and Nb in the presence of oxygen. Sov. Radiochem. **31**, 160–163 (1989)
19. Eichler, B., Zvara, I.: Evaluation of the enthalpy of adsorption from thermochromatographical data. Radiochim. Acta **30**, 233–238 (1982)
20. Zvara, I.: Simulation of thermochromatographic processes by the Monte Carlo method. Radiochim. Acta **38**, 95–101 (1985)
21. Gregorich, K.E.: Radiochemistry of Rutherfordium and Hahnium. In: Proceedings of The Robert A. Welch Foundation, 41st Conference of Chemical Research–The Transactinide Elements, Houston, Texas, 27–28 October 1997, pp. 95–124. The Robert A. Welch Foundation, Houston (1997)
22. Türler, A., Buklanov, G.V., Eichler, B., Gäggeler, H.W., Grantz, M., Hüberner, S., Jost, D.T., Lebedev, V.Y., Piguet, D., Timokhin, S.N., Yakushev, A., Zvara, I.: Evidence for relativistic effects in the chemistry of element 104. J. Alloys Compd. **271–273**, 287–291 (1998)
23. Qin, Z., Lin, M.S., Fan, F.L., Huang, W.X., Yan, X.L., Bai, J., Wu, X.L., Lei, F.A., Ding, H.J., Ma, F., Li, G.S., Zhou, H.B., Guo, J.S.: On-line gas chromatographic studies of Nb, Ta, and Db bromides. Radiochim. Acta **100**, 285–289 (2012)
24. Zvara, I., Belov, V.Z., Korotkin, Y.S., Shalaevski, M.R., Shchegolev, V.A., Hussonnois, M., Zager, B.A.: Experiments on chemical identification of spontaneously fissionable isotope of element 105. In: Dubna Report P12-5120, p. 13. Joint Institute for Nuclear Research, Dubna, (1970)
25. Zvara, I., Belov, V.Z., Domanov, V.P., Shalaevski, M.R.: Chemical isolation of Nielsbohrium and Ekatantalum in the form of the anhydrous Bromide II. Experiments with a spontaneously fissioning isotope of Nielsbohrium. Sov. Radiochem. **18**, 328–334 (1976)
26. Türler, A.: Gas phase chemistry experiments with transactinide elements. Radiochim. Acta **72**, 7–17 (1996)
27. Gäggeler, H.W., Jost, D.T., Kovacs, J., Scherer, U.W., Weber, A., Vermeulen, D., Türler, A., Gregorich, K.E., Henderson, R.A., Czerwinski, K.R., Kadkhodayan, B., Lee, D.M., Nurmia, M., Kratz, J.V., Gober, M.K., Zimmerman, H.P., Schädel, M., Brüchle, W., Schimpf, E., Zvara, I.: Gas phase chromatography experiments with bromides of tantalum and element 105. Radiochim. Acta **57**, 93–100 (1992)
28. Pershina, V., Sepp, W.-D., Fricke, B., Kolb, D., Schädel, M., Ionova, G.V.: Relativistic effects in physics and chemistry of element 105. II. Electronic structure and properties of group 5 bromides. J. Chem. Phys. **97**, 1116–1122 (1992)
29. Pershina, V., Sepp, W.-D., Bastug, T., Fricke, B., Ionova, G.V.: Relativistic effects in physics and chemistry of element 105. III. Electronic structure of hahnium oxyhalides as analogs of group 5 elements oxyhalides. J. Chem. Phys. **97**, 1123–1131 (1992)
30. Pershina, V., Anton, J.: Theoretical predictions of properties and gas-phase chromatography behaviour of bromides of group-5 elements Nb, Ta, and element 105, Db (vol. 136, 034308, 2012). J. Chem. Phys. **136**, 034308(7) (2012)
31. Kadkhodayan, B.: On-line gas chromatographic studies of Rutherfordium (element 104), Hahnium (element 105), and Homologs. In Report LBL-33961, p. 150. Lawrence Berkeley Laboratory, Berkeley (1993)
32. Timokhin, S., Yakushev, A.B., Honggui, X., Perelygin, V.P., Zvara, I.: Chemical identification of element 106 by the thermochromatographic method. In: Oganessian, Y.T., Penionzhkevich, Y.E., Kalpakchieva, R. (eds.) International School-Seminar on Heavy Ion Physics, 10–15 May 1993, pp. 204–206. Joint Institute for Nuclear Research, Dubna (1993)

33. Yakushev, A.B., Timokhin, S.N., Vedeneev, M.V., Honggui, X., Zvara, I.: Comparative study of oxochlorides of molybdenum, tungsten and element 106. J. Radioanal. Nucl. Chem. **205**, 63–67 (1996)
34. Timokhin, S.N., Yakushev, A.B., Xu, H., Perelygin, V.P., Zvara, I.: Chemical identification of element 106 by thermochromatography. J. Radioanal. Nucl. Chem. Lett. **212**, 31–34 (1996)
35. Zvara, I., Yakushev, A.B., Timokhin, S.N., Honggui, X., Perelygin, V.P., Chuburkov, Y.T.: Chemical identification of element 106 (thermochromatography of oxochlorides). Radiochim. Acta **81**, 179–187 (1998)
36. Schädel, M., Brüchle, W., Dressler, R., Eichler, B., Gäggeler, H.W., Günther, R., Gregorich, K.E., Hoffman, D.C., Hübener, S., Jost, D.T., Kratz, J.V., Paulus, W., Schumann, D., Timokhin, S., Trautmann, N., Türler, A.: Chemical properties of element 106 (seaborgium). Nature **388**, 55–57 (1997)
37. Lazarev, Y.A., Lobanov, Y.V., Oganessian, Y.T., Utyonkov, V.K., Abdullin, F.S., Buklanov, G.V., Gikal, B.N., Iliev, S., Mezentsev, A.N., Polyakov, A.N., Sedykh, I.M., Shirokovsky, I.V., Subbotin, V.G., Sukhov, A.M., Tsyganov, Y.S., Zhuchko, V.E., Lougheed, R.W., Moody, K.J., Wild, J.F., Hulet, E.K., McQuaid, J.H.: Discovery of enhanced nuclear stability near the deformed shells $N = 162$ and $Z = 108$. Phys. Rev. Lett. **73**, 624–627 (1994)
38. Türler, A., Brüchle, W., Dressler, R., Eichler, B., Eichler, R., Gäggeler, H.W., Gärtner, M., Glatz, J.-P., Gregorich, K.E., Hübener, S., Jost, D.T., Lebedev, V.Y., Pershina, V.G., Schädel, M., Taut, S., Timokhin, S.N., Trautmann, N., Vahle, A., Yakushev, A.B.: First measurement of a thermochemical property of a seaborgium compound. Angew. Chem. Int. Ed. **38**, 2212–2213 (1999)
39. Hübener, S., Taut, S., Vahle, A., Dressler, R., Eichler, B., Gäggeler, H.W., Jost, D.T., Piguet, D., Türler, A., Brüchle, W., Jäger, E., Schädel, M., Schimpf, E., Kirbach, U., Trautmann, N., Yakushev, A.B.: Physico-chemical characterization of seaborgium as oxide hydroxide. Radiochim. Acta **89**, 737–741 (2001)
40. Haba, H., Kaji, D., Kudou, Y., Morimoto, K., Morita, K., Ozeki, K., Sakai, R., Sumita, T., Yoneda, A., Kasamatsu, Y., Komori, Y., Shinohara, A., Kikunaga, H., Kudo, H., Nishio, K., Ooe, K., Sato, N., Tsukada, K.: Production of ^{265}Sg in the ^{248}Cm(^{22}Ne,5n)^{265}Sg reaction and decay properties of two isomeric states in ^{265}Sg. Phys. Rev. C **85**, 024611(11) (2012)
41. Haba, H., Kaji, D., Kikunaga, H., Kudou, Y., Morimoto, K., Morita, K., Ozeki, K., Sumita, T., Yoneda, A., Kasamatsu, Y., Komori, Y., Ooe, K., Shinohara, A.: Production and decay properties of the 1.9-s isomeric state in ^{261}Rf. Phys. Rev. C **83**, 034602(7) (2011)
42. Knacke, O., Kubaschewski, O., Hesselmann, K. (eds.): Thermochemical Properties of Inorganic Substances, vol. II. Springer-Verlag, Berlin (1991)
43. Vahle, A., Hübener, S., Dressler, R., Eichler, B., Türler, A.: Reaction gas chromatography of oxide and hydroxide species of molybdenum—simulation and experiment. Radiochim. Acta **78**, 53–57 (1997)
44. Vahle, A., Hübener, S., Funke, H., Eichler, B., Jost, D.T., Türler, A., Brüchle, W., Jäger, E.: Gas chromatographic studies of oxide and hydroxide species of tungsten—model experiments with respect to the physico-chemical characterization of seaborgium (element 106). Radiochim. Acta **84**, 43–51 (1999)
45. Even, J.: Developments for transactinide chemistry experiments behind the gas-filled separator TASCA. PhD-thesis. Universitätsbibliothek Mainz (2011)
46. Zvara, I., Eichler, B., Belov, V.Z., Zvarova, T.S., Korotkin, Y.S., Shalaevski, M.R., Shchegolev, V.A., Hussonnois, M.: Gas chromatography and thermochromatography in the study of transuranium elements. Sov. Radiochem. **16**, 709–715 (1974)
47. Helas, G., Hoffmann, P., Bächmann, K.: Investigation of Mo-Chlorides and W-Chlorides and Ocychlorides by thermochromatography. Radiochem. Radioanal. Lett. **30**, 371–380 (1977)

48. Bayar, B., Votsilka, I., Zaitseva, N.G., Novgorodov, A.F.: Rapid gas-thermochromatographic isolation of neutron-deficient isotopes of molybdenum from silver chloride. Sov. Radiochem. **20**, 64–69 (1978)
49. Tsalas, S., Bächmann, K.: Inorganic gas chromatography—the separation of volatile chlorides by thermochromatorgraphy combined with complex formation. Anal. Chim. Acta **98**, 17–24 (1978)
50. Rudolph, J., Bächmann, K., Steffen, A., Tsalas, S.: Inorganic gas-chromatography at high-temperatures. Mikrochim. Acta **1**, 471–481 (1978)
51. Rudolph, J., Bächmann, K.: Use of radionuclides for determination of adsorption-isotherms of volatile chlorides. J. Radioanal. Chem. **43**, 113–120 (1978)
52. Rudolph, J., Bachmann, K.: Gas-chromatography apparatus for the investigation and separation of radioactively labeled inorganic-compounds at high-temperatures. Mikrochim. Acta **1**, 477–493 (1979)
53. Tsalas, S., Bächmann, K., Heinlein, G.: The application of non-analytical radio gas-chromatography for the determination of adsorption enthalpies and entropies of inorganic bromides. Radiochim. Acta **29**, 217–221 (1981)
54. Gärtner, M., Böettger, M., Eichler, B., Gäggeler, H.W., Grantz, M., Hübener, S., Jost, D.T., Piguet, D., Dressler, R., Türler, A., Yakushev, A.B.: On-line gas chromatography of Mo, W and U (oxy)chlorides. Radiochim. Acta **78**, 59–68 (1997)
55. Lebedev, V.Y., Yakushev, A.B., Timokhin, S.N., Vedeneev, M.B., Zvara, I.: Chemical state of molybdenum, tungsten and element 106 in chlorinating gases. Czech J. Phys. **49**, 589–595 (1999)
56. Düllmann, C.E., Türler, A., Eichler, B., Gäggeler, H.W.: Thermochromatographic investigation of ruthenium with oxygen as carrier gas. In: 1st International Conference on Chemistry and Physics of the Transactinide Elements, Seeheim, Germany, pp. P-M-13, 26–30 September 1999
57. Türler, A., Dressler, R., Eichler, B., Gäggeler, H.W., Jost, D.T., Schädel, M., Brüchle, W., Gregorich, K.E., Trautmann, N., Taut, S.: Decay properties of ^{265}Sg(Z = 106) and ^{266}Sg(Z = 106). Phys. Rev. C **57**, 1648–1655 (1998)
58. Vahle, A., Hübener, S., Dressler, R., Grantz, M.: Development of an apparatus for seaborgium studies by high temperature gas chromatography. Nucl. Instrum. Methods Phys. Res., Sect. A **481**, 637–645 (2002)
59. Zvara, I., Domanov, V.P., Hübener, S., Shalaevskii, M.R., Timokhin, S.N., Zhuikov, B.L., Eichler, B., Buklanov, G.V.: Experimental approach to the chemical-identification of element-107 as Eka-Rhenium.2. Search for spontaneously fissile isotopes of element-107 in the products of the reaction Bk-249 + Ne-22 by the method of chromathermography. Sov. Radiochem. **26**, 72–76 (1984)
60. Schädel, M., Jäger, E., Brüchle, W., Sümmerer, K., Hulet, E.K., Wild, J.F., Lougheed, R.W., Dougan, R.J., Moody, K.J.: Radiochemical search for neutron-rich isotopes of Nielsbohrium in the ^{16}O + ^{254}Es reaction. Radiochim. Acta **68**, 7–12 (1995)
61. Wilk, P.A., Gregorich, K.E., Türler, A., Laue, C.A., Eichler, R., Ninov, V., Adams, J.L., Kirbach, U.W., Lane, M.R., Lee, D.M., Patin, J.B., Shaughnessy, D.A., Strellis, D.A., Nitsche, H., Hoffman, D.C.: Evidence for new isotopes of element 107: ^{266}Bh and ^{267}Bh. Phys. Rev. Lett. **85**, 2697–2700 (2000)
62. Eichler, R., Eichler, B., Gäggeler, H.W., Jost, D.T., Dressler, R., Türler, A.: The gas phase oxide and oxyhydroxide chemistry of trace amounts of rhenium. Radiochim. Acta **87**, 151–159 (1999)
63. Eichler, R., Eichler, B., Gäggeler, H.W., Jost, D.T., Piguet, D., Türler, A.: Gas phase chemistry of technetium and rhenium oxychlorides. Radiochim. Acta **88**, 87–93 (2000)
64. Eichler, R., Brüchle, W., Dressler, R., Düllmann, C.E., Eichler, B., Gäggeler, H.W., Gregorich, K.E., Hoffman, D.C., Hubener, S., Jost, D.T., Kirbach, U.W., Laue, C.A., Lavanchy, V.M., Nitsche, H., Patin, J.B., Piguet, D., Schädel, M., Shaughnessy, D.A., Strellis, D.A., Taut, S., Tobler, L., Tsyganov, Y.S., Türler, A., Vahle, A., Wilk, P.A.,

Yakushev, A.B.: Chemical characterization of bohrium (element 107). Nature **407**, 63–65 (2000)
65. Merinis, J., Bouissieres, G.: Separation par Volatilisation des Radioisotopes de Mercure, de Platine, d'Iridium, d'Osmium et de Rhenium formée par Spallation dans une Cible d'Or. Anal. Chim. Acta **25**, 498–504 (1961)
66. Schäfer, H.: Chemische Transportreaktionen. Verlag Chemie, Weinheim (1962)
67. Bayar, B., Novgorodov, A.F., Zaitseva, N.G.: Rapid gas-thermochromatographic separation of radioactive elements. I. Production of radioactive Re isotopes. Radiochem. Radioanal. Lett. **15**, 231–242 (1973)
68. Bayar, B., Votsilka, I., Zaitseva, N.G., Novgorodov, A.F.: Fast gas thermochromatographic method of isolating radioactive elements. II. Gold: universal target for express production of radioactive preparations of rhenium, osmium, iridium, and mercury. Sov. Radiochem. **16**, 333–338 (1974)
69. Bayar, B., Novgorodov, A.F., Vocilka, I., Zaitseva, N.G.: Rapid gas-thermochromatographic separation of radioactive elements. II. Gold as a universal target for the rapid production of radioactive Re, Os, Ir, and Hg isotopes. Radiochem. Radioanal. Lett. **19**, 43–53 (1974)
70. Eichler, B., Domanov, V.P.: Volatilization of radionuclides in air stream and their separation in temperature-gradient tube. J. Radioanal. Nucl. Chem. **28**, 143–152 (1975)
71. Bayar, B., Vocilka, I., Zaitseva, N.G., Novgorodov, A.F.: Fast gas-thermochromatographic separation of radioactive elements. 5. Production of volatile Re oxides and hydroxides in Re-W System and their gas-thermochromatographic behavior. Radiochem. Radioanal. Lett. **34**, 75–87 (1978)
72. Adilbish, M., Zaitseva, N.G., Kovach, Z., Novgordov, A.F., Sergeev, Y.Y., Tikhonov, V.I.: Volatilization from molten gold and thermochromatographic separation of ultramicroquantities of rhenium and osmium ocides at low pressures of oxygen-containing gases. Sov. Radiochem. **20**, 652–662 (1978)
73. Steffen, A., Bächmann, K.: Gas chromatographic study of volatile oxides and hydroxides of Re, Tc, Os, Ru and Ir -II: thermochromatographic investigations. Talanta **25**, 677–683 (1978)
74. Novgorodov, A.F., Adilbish, M., Zaitseva, N.G., Kovalev, A.S., Kovach, Z.: Behavior of nuclear reaction products upon sublimation from irradiated Ag and Au under a dynamic vacuum of $1–10^{-1}$ Pa for O_2 or H_2O. Sov. Radiochem. **22**, 590–601 (1980)
75. Domanov, V.P., Hübener, S., Shalaevskii, M.R., Timokhin, S.N., Petrov, D.V., Zvara, I.: Experimental approach to the identification of element-107 as Ekarhenium.1. Continuous gas-thermochromatographic isolation of radiorhenium. Sov. Radiochem. **25**, 23–28 (1983)
76. Eichler, B.: The behaviour of radionuclides in gas adsorption chromatographic processes with superimposed chemical reactions (chlorides). Radiochim. Acta **72**, 19–26 (1996)
77. Rösch, F., Novgorodov, A.F., Qaim, S.M.: Thermochromatographic separation of (99 m)Tc from enriched molybdenum targets and its large-scale production for nuclear medical application. Radiochim. Acta **64**, 113–120 (1994)
78. Novgorodov, A.F., Bruchertseifer, F., Brockmann, J., Lebedev, N.A., Rösch, F.: Thermochromatographic separation of no-carrier-added Re-186 or Re-188 from tungsten targets relevant to nuclear medical applications. Radiochim. Acta **88**, 163–167 (2000)
79. Schädel, M., Jäger, E., Schimpf, E., Brüchle, W.: Modeling a Nielsbohrium (element-107) online gas-phase separation procedure with rhenium. Radiochim. Acta **68**, 1–6 (1995)
80. Merinis, J., Bouissieres, G.: Migration of radioelements in a temperature gradient tube. Radiochim. Acta **12**, 140–152 (1969)
81. Neidhart, B., Bächmann, K., Krämer, S., Link, I.: Selective separation of fission technetium using solid chlorides. Radiochem. Radioanal. Lett. **12**, 59–69 (1972)
82. Pershina, V., Bastug, T.: The electronic structure and properties of group 7 oxychlorides MO_3Cl, where M = Tc, Re, and element 107. Bh. J. Chem. Phys. **113**, 1441–1446 (2000)
83. Eichler, R.: Die chemische Characterisierung des Transactinoids Bohrium (Bh, element 107). Ph.D. thesis, University of Bern, Switzerland (2000)

84. Münzenberg, G., Armbruster, P., Folger, H., Heßberger, F.P., Hofmann, S., Keller, J., Poppensieker, K., Reisdorf, W., Schmidt, K.H., Schott, H.J., Leino, M.E., Hingmann, R.: The identification of element-108. Z. Phys. A: Hadrons Nucl. **317**, 235–236 (1984)
85. Hofmann, S., Ninov, V., Heßberger, F.P., Armbruster, P., Folger, H., Münzenberg, G., Schött, H.J., Popeko, A.G., Yeremin, A.V., Saro, S., Janik, R., Leino, M.: The new element 112. Z. Phys. A: Hadrons Nucl. **354**, 229–230 (1996)
86. Kratz, J.V.: Chemical properties of the transactinide elements. In: Greiner, W., Gupta, R.K. (eds.) Heavy Elements and Related New Phenomena, vol. 1, pp. 129–193. World Scientific, Singapore (1999)
87. Düllmann, C.E., Brüchle, W., Dressler, R., Eberhardt, K., Eichler, B., Eichler, R., Gäggeler, H.W., Ginter, T.N., Glaus, F., Gregorich, K.E., Hoffman, D.C., Jäger, E., Jost, D.T., Kirbach, U.W., Lee, D.M., Nitsche, H., Patin, J.B., Pershina, V., Piguet, D., Qin, Z., Schädel, M., Schausten, B., Schimpf, E., Schött, H.J., Soverna, S., Sudowe, R., Thörle, P., Timokhin, S.N., Trautmann, N., Türler, A., Vahle, A., Wirth, G., Yakushev, A.B., Zielinski, P.M.: Chemical investigation of hassium (element 108). Nature **418**, 859–862 (2002)
88. Dvorak, J., Brüchle, W., Chelnokov, M., Dressler, R., Düllmann, C.E., Eberhardt, K., Gorshkov, V., Jäger, E., Krücken, R., Kuznetsov, A., Nagame, Y., Nebel, F., Novackova, Z., Qin, Z., Schädel, M., Schausten, B., Schimpf, E., Semchenkov, A., Thörle, P., Türler, A., Wegrzecki, M., Wierczinski, B., Yakushev, A., Yeremin, A.: Doubly magic nucleus $^{270}Hs_{162}$. Phys. Rev. Lett. **97**, 242501(4) (2006)
89. Dvorak, J., Brüchle, W., Chelnokov, M., Dressler, R., Düllmann, C.E., Dvorakova, Z., Eberhardt, K., Jäger, E., Krücken, R., Kuznetsov, A., Nagame, Y., Nebel, F., Nishio, K., Perego, R., Qin, Z., Schädel, M., Schausten, B., Schimpf, E., Schuber, R., Semchenkov, A., Thörle, P., Türler, A., Wegrzecki, M., Wierczinski, B., Yakushev, A., Yeremin, A.: Observation of the 3*n* evaporation channel in the complete hot-fusion reaction $^{26}Mg + {}^{248}Cm$ leading to the new superheavy nuclide ^{271}Hs. Phys. Rev. Lett. **100**, 132503(4) (2008)
90. Gundersen, G., Hedberg, K., Huston, J.L.: Molecular structure of xenon tetroxide, XeO_4. J. Chem. Phys. **52**, 812–815 (1970)
91. Bächmann, K., Hoffmann, P.: Chemische Probleme bei der Darstellung überschwerer Elemente durch Kernreaktionen. Radiochim. Acta **15**, 153–163 (1971)
92. Fricke, B.: Superheavy elements. A prediction of their chemical and physical properties. Struct. Bond. **21**, 89–144 (1975)
93. Eichler, B.: Preparative thermo gas chromatographic separation of radionuclides in hydrogen and air carrier gas stream. Radiochem. Radioanal. Lett. **22**, 147–155 (1975)
94. Domanov, V.P., Zvara, I.: Continuous-flow thermochromatographic separation of unsupported radioisotopes of platinum elements in a stream of air from nuclear-reaction products in an accelerator heavy-ion beam. Sov. Radiochem. **26**, 731–739 (1984)
95. Eichler, B., Zude, F., Fan, W., Trautmann, N., Herrmann, G.: Volatilization and deposition of ruthenium oxides in a temperature-gradient tube. Radiochim. Acta **56**, 133–140 (1992)
96. Zude, F., Fan, W., Trautmann, N., Herrmann, G., Eichler, B.: Thermochromatography of platinum elements in oxygen—radiochemical studies of the behavior of rhodium, palladium, osmium and platinum. Radiochim. Acta **62**, 61–63 (1993)
97. Zhuikov, B.L., Chepigin, V.I., Kruz, H., Ter-Akopian, G.M., Zvara, I.: Experiments for chemical isolation and detecting of spontaneously fissioning and α-active isotopes of element 108. Unpublished report, Joint Institute for Nuclear Research, Dubna (1985)
98. Chepigin, V.I., Zhuikov, B.L., Ter-Akopian, G.M., Zvara, I.: In: Fizika tiazhelykh ionov—1985. Sbornik annotacii, p. 15. Joint Institute for Nuclear Research, Dubna (1986)
99. Zhuikov, B.L., Kruz, H., Zvara, I.: In: Fizika tiazhelykh ionov—1985. Sbornik annotacii, p. 26. Joint Institute for Nuclear Research, Dubna (1986)
100. Dougan, R.J., Moody, K.J., Lougheed, R.W., Wild, J.F., Bethune, G.R.: OSCAR: an apparatus for on-line gas-phase separations. In: Lawrence Livermore National Laboratory Annual Report FY87, vol. UCAR 10062/87, pp. 4–17. Lawrence Livermore National Laboratory, Livermore (1987)

101. Hulet, E.K., Moody, K.J., Lougheed, R.W., Wild, J.F., Dougan, R.J., Bethune, G.R.: Search for ^{272}109 in a new region of stability. In: Lawrence Livermore National Laboratory Annual Report FY87, vol. UCAR 10062/87, pp. 4–9. Lawrence Livermore National Laboratory, Livermore (1987)
102. von Zweidorf, A., Kratz, J.V., Trautmann, N., Schädel, M., Nähler, A., Jäger, E., Schausten, B., Brüchle, W., Schimpf, E., Angert, R., Li, Z., Wirth, G.: The synthesis of volatile tetroxides of osmium and ruthenium. In: 1st International Confernence on Chemistry and Physics of the Transactinide Elements, Seeheim, Germany, pp. P-M-17, 16–30 September 1999
103. Yakushev, A.B., Vakatov, V.I., Vasko, V., Lebedev, V.Y., Timokhin, S.N., Tsyganov, Y.S., Zvara, I.: On-line experiments with short-lived osmium isotopes as a test of the chemical identification of the element 108—Hassium. In: 1st International Conference on Chemistry and Physics of the Transactinide Elements, Seeheim, Germany, p. P-M-17, 26-30 September 1999
104. Düllmann, C.E., Eichler, B., Eichler, R., Gäggeler, H.W., Jost, D.T., Piguet, D., Türler, A.: IVO, a device for in situ volatilization and on-line detection of products from heavy ion reactions. Nucl. Instrum. Methods Phys. Res., Sect. A **479**, 631–639 (2002)
105. Kirbach, U.W., Folden III, C.M., Ginter, T.N., Gregorich, K.E., Lee, D.M., Ninov, V., Omtvedt, J.P., Patin, J.B., Seward, N.K., Strellis, D.A.: The cryo-thermochromatographic separator (CTS): a new rapid separation and α-detection system for on-line chemical studies of highly volatile osmium and hassium (Z = 108) tetroxides. Nucl. Instrum. Methods Phys. Res., Sect. A **484**, 587–594 (2002)
106. Düllmann, C.E., Eichler, B., Eichler, R., Gäggler, H.W., Türler, A.: On the stability and volatility of group 8 tetroxides, MO_4 (M = ruthenium, osmium, and hassium (Z = 108)). J. Phys. Chem. B **106**, 6679–6684 (2002)
107. Pershina, V., Bastug, T., Fricke, B., Varga, S.: The electronic structure and properties of group 8 oxides MO_4, where M = Ru, Os, and element 108 Hs. J. Chem. Phys. **115**, 792–799 (2001)
108. Hofmann, S., Heßberger, F.P., Ackermann, D., Antalic, S., Cagarda, P., Cwiok, S., Kindler, B., Kojouharova, J., Lommel, B., Mann, R., Münzenberg, G., Popeko, A.G., Saro, S., Schött, H.J., Yeremin, A.V.: The new isotope ^{270}110 and its decay products ^{266}Hs and ^{262}Sg. Eur. Phys. J. A **10**, 5–10 (2001)
109. Pershina, V., Bastug, T., Fricke, B.: Relativistic effects on the electronic structure and volatility of group-8 tetroxides MO_4, where M = Ru, Os, and element 108, Hs. J. Chem. Phys. **122**, 124301(9) (2005)
110. Pershina, V., Anton, J., Jacob, T.: Fully relativistic density-functional-theory calculations of the electronic structures of MO(4) (M = Ru, Os, and element 108, Hs) and prediction of physisorption. Phys. Rev. A **78**, 032518(5) (2008)
111. von Zweidorf, A., Angert, R., Brüchle, W., Bürger, S., Eberhardt, K., Eichler, R., Hummrich, H., Jäger, E., Kling, H.-O., Kratz, J.V., Kuczewski, B., Langrock, G., Mendel, M., Rieth, U., Schädel, M., Schausten, B., Schimpf, E., Thörle, P., Trautmann, N., Tsukada, K., Wiehl, N., Wirth, G.: Evidence for the formation of sodium hassate (VIII). Radiochim. Acta **92**, 855–861 (2004)
112. Patyk, Z., Skalski, J., Sobiczewski, A., Cwiok, S.: Potential-energy and spontaneous-fission half-lives for heavy and superheavy nuclei. Nucl. Phys. A **502**, C591–C599 (1989)
113. Patyk, Z., Sobiczewski, A.: Ground-state properties of the heaviest nuclei analyzed in a multidimensional deformation space. Nucl. Phys. A **533**, 132–152 (1991)
114. Sobiczewski, A., Muntian, I., Patyk, Z.: Problem of "deformed" superheavy nuclei. Phys. Rev. C **63**, 034306(12) (2001)
115. Türler, A.: Nuclear structure and reaction studies near doubly magic ^{270}Hs. Radiochim. Acta **100**, 75–83 (2012)
116. Oganessian, Y.T., Yeremin, A.V., Gulbekian, G.G., Bogomolov, S.L., Chepigin, V.I., Gikal, B.N., Gorshkov, V.A., Itkis, M.G., Kabachenko, A.P., Kutner, V.B., Lavrentev, A.Y., Malyshev, O.N., Popeko, A.G., Rohach, J., Sagaidak, R.N., Hofmann, S., Münzenberg, G.,

Veselsky, M., Saro, S., Iwasa, N., Morita, K.: Search for new isotopes of element 112 by irradiations of ^{238}U with ^{48}Ca. Eur. Phys. J. A **5**, 63–68 (1999)
117. Oganessian, Y.T., Yeremin, A.V., Popeko, A.G., Bogomolov, S.L., Buklanov, G.V., Chelnokov, L.P., Chepigin, V.I., Gikal, B.N., Gorshkov, V.A., Gulbekian, G.G., Itkis, M.G., Kabachenko, A.P., Lavrentev, A.Y., Malyshev, O.N., Rohach, J., Sagaidak, R.N., Hofmann, S., Saro, S., Giardina, G., Morita, K.: Synthesis of nuclei of the superheavy element 114 in reactions incuded by ^{48}Ca. Nature **400**, 242–245 (1999)
118. Oganessian, Y.T., Utyonkov, V.K., Lobanov, Y.V., Abdullin, F.S., Polyakov, A.N., Shirokovsky, I.V., Tsyganov, Y.S., Gulbekian, G.G., Bogomolov, S.L., Gikal, B.N., Mezentsev, A.N., Iliev, S., Subbotin, V.G., Sukhov, A.M., Ivanov, O.V., Buklanov, G.V., Subotic, K., Itkis, M.G., Moody, K.J., Wild, J.F., Stoyer, N.J., Stoyer, M.A., Lougheed, R.W.: Synthesis of superheavy nuclei in the ^{48}Ca + ^{244}Pu reaction: ^{288}114. Phys. Rev. C **62**, 041604(4) (2000)
119. Oganessian, Y.: Heaviest nuclei from ^{48}Ca induced reactions. J. Phys. G: Nucl. Part. Phys. **34**, R165–R242 (2007)
120. Oganessian, Y.T., Abdullin, F.S., Bailey, P.D., Benker, D.E., Bennett, M.E., Dmitriev, S.N., Ezold, J.G., Hamilton, J.H., Henderson, R.A., Itkis, M.G., Lobanov, Y.V., Mezentsev, A.N., Moody, K.J., Nelson, S.L., Polyakov, A.N., Porter, C.E., Ramayya, A.V., Riley, F.D., Roberto, J.B., Ryabinin, M.A., Rykaczewski, K.P., Sagaidak, R.N., Shaughnessy, D.A., Shirokovsky, I.V., Stoyer, M.A., Subbotin, V.G., Sudowe, R.: Synthesis of a new element with atomic number Z = 117. Phys. Rev. Lett. **104**, 142502(4) (2010)
121. Schwerdtfeger, P., Seth, M.: Relativistic effects of the superheavy elements. In: von Ragué Schleyer, P. (ed.) Encyclopedia on Calculational Chemistry, vol. 4, pp. 2480–2499. Wiley, New York (1998)
122. Gäggeler, H.W.: Gas chemical properties of heaviest elements. Radiochim. Acta **99**, 503–513 (2011)
123. Schädel, M.: Chemistry of the superheavy elements. Angew. Chem. Int. Ed. **45**, 368–401 (2006)
124. Türler, A, Pershina, V.: Advances in the Production and Chemistry of the Heaviest Elements. Chem. Rev. **113**, 1237–1312 (2013)
125. Eichler, B.: Das Flüchtigkeitsverhalten von Transactiniden im Bereich um Z = 114 (Voraussage). Kernenergie **19**, 307–311 (1976)
126. Pitzer, K.S.: Are elements 112, 114, and 118 relatively inert gases? J. Chem. Phys. **63**, 1032–1033 (1975)
127. Pershina, V., Anton, J., Jacob, T.: Theoretical predictions of adsorption behavior of elements 112 and 114 and their homologs Hg and Pb. J. Chem. Phys. **131**, 084713(8) (2009)
128. Eichler, B., Rossbach, H.: Adsorption of volatile metals on metal-surfaces and its application in nuclear chemistry 1. Calculation of adsorption enthalpies for hypothetical superheavy elements with Z around 114. Radiochim. Acta **33**, 121–125 (1983)
129. Trautmann, W., Hoffmann, P., Bächmann, K.: Gas-phase transport of polonium using ethyl radicals. J. Organomet. Chem. **92**, 191–196 (1975)
130. Yakushev, A., Buklanov, G.V., Chelnokov, L.P., Chepigin, V.I., Dmitriev, S.N., Gorshkov, V.A., Hübener, S., Lebedev, V.Y., Malyshev, O.N., Oganessian, Y.T., Popeko, A.G., Sokol, E.A., Timokhin, S.N., Türler, A., Vasko, V.M., Yeremin, A.V., Zvara, I.: First attempt to chemically identify element 112. Radiochim. Acta **89**, 743–745 (2001)
131. Yakushev, A.B., Zvara, I., Oganessian, Y.T., Belozerov, A.V., Dmitriev, S.N., Eichler, B., Hübener, S., Sokol, E.A., Türler, A., Yeremin, A.V., Buklanov, G.V., Chelnokov, M.L., Chepigin, V.I., Gorshkov, V.A., Gulyaev, A.V., Lebedev, V.Y., Malyshev, O.N., Popeko, A.G., Soverna, S., Szeglowski, Z., Timokhin, S.N., Tretyakova, S.P., Vasko, V.M., Itkis, M.G.: Chemical identification and properties of element 112. Radiochim. Acta **91**, 433–439 (2003)
132. Gäggeler, H.W., Brüchle, W., Düllmann, C.E., Dressler, R., Eberhardt, K., Eichler, B., Eichler, R., Folden III, C.M., Ginter, T.N., Glaus, F., Gregorich, K.E., Haenssler, F., Hoffman, D.C., Jäger, E., Jost, D.T., Kirbach, U.W., Kratz, J.V., Nitsche, H., Patin, J.B.,

Pershina, V., Piguet, D., Qin, Z., Rieth, U., Schädel, M., Schimpf, E., Schausten, B., Soverna, S., Sudowe, R., Thörle, P., Trautmann, N., Türler, A., Vahle, A., Wilk, P.A., Wirth, G., Yakushev, A.B., von Zweidorf, A.: Chemical and nuclear studies of hassium and element 112. Nucl. Phys. A **734**, 208–212 (2004)

133. Eichler, R., Brüchle, W., Buda, R., Bürger, S., Dressler, R., Düllmann, C.E., Dvorak, J., Eberhardt, K., Eichler, B., Folden III, C.M., Gäggeler, H.W., Gregorich, K.E., Haenssler, F., Hoffman, D.C., Hummrich, H., Jäger, E., Schimpf, E., Semchenov, A., Soverna, S., Sudowe, R., Trautmann, N., Thörle, P., Türler, A., Wierczinski, B., Wiehl, N., Wilk, P.A., Wirth, G., Yakushev, A., von Zweidorf, A.: Attempts to chemically investigate element 112. Radiochim. Acta **94**, 181–191 (2006)
134. Hofmann, S., Ackermann, D., Antalic, S., Burkhard, H.G., Comas, V.F., Dressler, R., Gan, Z., Heinz, S., Heredia, J.A., Heßberger, F.P., Khuyagbaatar, J., Kindler, B., Kojouharov, I., Kuusiniemi, P., Leino, M., Lommel, B., Mann, R., Münzenberg, G., Nishio, K., Popeko, A.G., Saro, S., Schött, H.J., Streicher, B., Sulignano, B., Uusitalo, J., Venhart, M., Yeremin, A.: The reaction $^{48}Ca + {}^{238}U \rightarrow {}^{286}112^*$ studied at the GSI-SHIP. Eur. Phys. J. A **32**, 251–260 (2007)
135. Eichler, R., Aksenov, N.V., Belozerov, A.V., Bozhikov, G.A., Chepigin, V.I., Dmitriev, S.N., Dressler, R., Gäggler, H.W., Gorshkov, V.A., Haenssler, F., Itkis, M.G., Laube, A., Lebedev, V.Y., Malyshev, O.N., Oganessian, Y.T., Petrushkin, O.V., Piguet, D., Rasmussen, P., Shishkin, S.V., Shutov, A.V., Svirikhin, A.I., Tereshatov, E.E., Vostokin, G.K., Wegrzecki, M., Yeremin, A.: Chemical characterization of element 112. Nature **447**, 72–75 (2007)
136. Eichler, R., Aksenov, N.V., Belozerov, A.V., Bozhikov, G.A., Chepigin, V.I., Dmitriev, S.N., Dressler, R., Gäggeler, H.W., Gorshkov, A.V., Itkis, M.G., Haenssler, F., Laube, A., Lebedev, V.Y., Malyshev, O.N., Oganessian, Y.T., Petrushkin, O.V., Piguet, D., Popeko, A.G., Rasmussen, T., Shishkin, S.V., Serov, A.A., Shutov, A.V., Svirikhin, A.I., Tereshatov, E.E., Vostokin, G.K., Wegrzecki, M., Yeremin, A.V.: Thermochemical and physical properties of element 112. Angew. Chem. Int. Ed. **47**, 3262–3266 (2008)
137. Zaitsevskii, A.V., van Wüllen, C., Titov, A.V.: Relativistic pseudopotential model for superheavy elements: applications to chemistry of eka-Hg and eka-Pb. Russ. Chem. Rev. **78**, 1173–1181 (2009)
138. Gaston, N., Opahle, I., Gäggeler, H.W., Schwerdtfeger, P.: Is eka-mercury (element 112) a group 12 metal? Angew. Chem. Int. Ed. **46**, 1663–1666 (2007)
139. Eichler, R.: New Attempt to Chemically Investigate $^{283}112$ and $^{287}114$. In: Türler, A., Schwikowski, M., Blattmann, A. (eds.) Annual Report 2009, p. 3. Labor für Radio- und Umweltchemie der Universität Bern und des Paul Scherrer Instituts, Villigen PSI, Bern (2010)
140. Wittwer, D., Abdullin, F.S., Aksenov, N.V., Albin, Y.V., Bozhikov, G.A., Dmitriev, S.N., Dressler, R., Eichler, R., Gäggeler, H.W., Henderson, R.A., Hubener, S., Kenneally, J.M., Lebedev, V.Y., Lobanov, Y.V., Moody, K.J., Oganessian, Y.T., Petrushkin, O.V., Polyakov, A.N., Piguet, D., Rasmussen, P., Sagaidak, R.N., Serov, A., Shirokovsky, I.V., Shaughnessy, D.A., Shishkin, S.V., Sukhov, A.M., Stoyer, M.A., Stoyer, N.J., Tereshatov, E.E., Tsyganov, Y.S., Utyonkov, V.K., Vostokin, G.K., Wegrzecki, M., Wilk, P.A.: Gas phase chemical studies of superheavy elements using the Dubna gas-filled recoil separator—stopping range determination. Nucl. Instrum. Methods Phys. Res., Sect. B **268**, 28–35 (2010)
141. Stavsetra, L., Gregorich, K.E., Alstad, J., Breivik, H., Eberhardt, K., Folden III, C.M., Ginter, T.N., Johansson, M., Kirbach, U.W., Lee, D.M.: Liquid-scintillation detection of preseparated ^{257}Rf with the SISAK-system. Nucl. Instrum. Methods Phys. Res., Sect. A **543**, 509–516 (2005)
142. Schädel, M.: Superheavy element chemistry at GSI—status and perspectives. Eur. Phys. J. D **45**, 67–74 (2007)
143. Yakushev, A., Gates, J.M., Gorshkov, A., Graeger, R., Ackermann, D., Block, M., Brüchle, W., Düllmann, C.E., Essel, H.G., Heßberger, F.P., Hübner, A., Jäger, E., Khuyagbaatar, J.,

Kindler, B., Krier, J., Kurz, N., Lommel, B., Schädel, M., Schausten, B., Schimpf, E., Eberhardt, K., Eibach, M., Even, J., Hild, D., Kratz, J.V., Niewisch, L.J., Runke, J., Töhrle-Pospiech, P., Wiehl, N., Dvorak, J., Nitsche, H., Omtvedt, J.P., Semchenkov, A., Forsberg, U., Rudolph, D., Uusitalo, J., Andersson, L.-L., Herzberg, R.-D., Parr, E., Qin, Z., Wegrzecki, M.: COMPACT coupled to TASCA for element 114 chemistry*. In: GSI Scientific Report 2009, vol. NUSTAR-SHE-11, p. 180. Gesellschaft für Schwerionenforschung mbH, Darmstadt (2010)

144. Düllmann, C.E., Schädel, M., Yakushev, A., Türler, A., Eberhardt, K., Kratz, J.V., Ackermann, D., Andersson, L.-L., Block, M., Brüchle, W., Dvorak, J., Essel, H.G., Ellison, P.A., Even, J., Gates, J.M., Gorshkov, A., Graeger, R., Gregorich, K.E., Hartmann, W., Herzberg, R.-D., Heßberger, F.P., Hild, D., Hübner, A., Jäger, E., Khuyagbaatar, J., Kindler, B., Krier, J., Kurz, N., Lahiri, S., Liebe, D., Lommel, B., Maiti, M., Nitsche, H., Omtvedt, J.P., Parr, E., Rudolph, D., Runke, J., Schausten, B., Schimpf, E., Semchenkov, A., Steiner, J., Thörle-Pospiech, P., Uusitalo, J., Wegrzecki, M., Wiehl, N.: Production and decay of element 114: high cross sections and the new nucleus ^{277}Hs. Phys. Rev. Lett. **104**, 252701(5) (2010)
145. Eichler, R., Aksenov, N.V., Albin, Y.V., Belozerov, A.V., Bozhikov, G.A., Chepigin, V.I., Dmitriev, S.N., Dressler, R., Gäggeler, H.W., Gorshkov, V.A., Henderson, R.A., Johnsen, A.M., Kenneally, J.M., Lebedev, V.Y., Malyshev, O.N., Moody, K.J., Oganessian, Y.T., Petrushkin, O.V., Piguet, D., Popeko, A.G., Rasmussen, P., Serov, A.A., Shaughnessy, D.A., Shishkin, S.V., Shutov, A.V., Stoyer, M.A., Stoyer, N.J., Svirikhin, A.I., Tereshatov, E.E., Vostokin, G.K., Wegrzecki, M., Wilk, P.A., Wittwer, D., Yeremin, A.V.: Indication for a volatile element 114. Radiochim. Acta **98**, 133–139 (2010)
146. Pershina, V.: Relativistic electronic structure studies on the heaviest elements. Radiochim. Acta **99**, 459–476 (2011)
147. Hermann, A., Furthmüller, J., Gäggeler, H.W., Schwerdtfeger, P.: Spin-orbit effects in structural and electronic properties for the solid state of the group-14 elements from carbon to superheavy element 114. Phys. Rev. B **82**, 155116(8) (2010)
148. Düllmann, C.E.: Superheavy elements at GSI: a broad research program with element 114 in the focus of physics and chemistry. Radiochim. Acta **100**, 67–74 (2012)
149. Even, J., Ballof, J., Brüchle, W., Buda, R.A., Düllmann, C.E., Eberhardt, K., Gorshkov, A., Gromma, E., Hild, D., Jäger, E., Khuyagbaatar, J., Kratz, J.V., Krier, J., Liebe, D., Mendel, M., Nayak, D., Opel, K., Omtvedt, J.P., Reichert, P., Runke, J., Sabelnikov, A., Samadani, F., Schädel, M., Schausten, B., Scheid, N., Schimpf, E., Semchenkov, A., Thörle-Pospiech, P., Toyoshima, A., Türler, A., Vicente Vilas, V., Wiehl, N., Wunderlich, T., Yakushev, A.: The recoil transfer chamber—an interface to connect the physical preseparator TASCA with chemistry and counting setups. Nucl. Instrum. Methods Phys. Res., Sect. A **638**, 157–164 (2011)
150. Tereshatov, E.E., Shaughnessy, D.A., Gostic, J.M., Henderson, R.A.: Synthesis and investigation of the chemical properties of odd-Z superheavy elements. Abstr. Pap. Am. Chem. Soc. **241**, 1 (2011)
151. Oganessian, Y.T., Abdullin, F.S., Dmitriev, S.N., Gostic, J.M., Hamilton, J.H., Henderson, R.A., Itkis, M.G., Moody, K.J., Polyakov, A.N., Ramayya, A.V., Roberto, J.B., Rykaczewski, K.P., Sagaidak, R.N., Shaughnessy, D.A., Shirokovsky, I.V., Stoyer, M.A., Subbotin, V.G., Sukhov, A.M., Tsyganov, Y.S., Utyonkov, V.K., Voinov, A.A., Vostokin, G.K.: New insights into the ^{243}Am + ^{48}Ca reaction products previously observed in the experiments on elements 113, 115, and 117. Phys. Rev. Lett. **108**, 022502(5) (2012)
152. Oganessian, Y.T., Abdullin, F.S., Bailey, P.D., Benker, D.E., Bennett, M.E., Dmitriev, S.N., Ezold, J.G., Hamilton, J.H., Henderson, R.A., Itkis, M.G., Lobanov, Y.V., Mezentsev, A.N., Moody, K.J., Nelson, S.L., Polyakov, A.N., Porter, C.E., Ramayya, A.V., Riley, F.D., Roberto, J.B., Ryabinin, M.A., Rykaczewski, K.P., Sagaidak, R.N., Shaughnessy, D.A., Shirokovsky, I.V., Stoyer, M.A., Subbotin, V.G., Sudowe, R., Sukhov, A.M., Taylor, R., Tsyganov, Y.S., Utyonkov, V.K., Voinov, A.A., Vostokin, G.K., Wilk, P.A.: Eleven new

heaviest isotopes of elements Z = 105 to Z = 117 identified among the products of ^{249}Bk + ^{48}Ca reactions. Phys. Rev. C **83**, 054315(14) (2011)
153. Oganessian, Y.T., Abdullin, F.S., Alexander, C., Binder, J., Boll, R.A., Dmitriev, S.N., Ezold, J., Felker, K., Gostic, J.M., Grzywacz, R.K., Hamilton, J.H., Henderson, R.A., Itkis, M.G., Miernik, K., Miller, D., Moody, K.J., Polyakov, A.N., Ramayya, A.V., Roberto, J.B., Ryabinin, M.A., Rykaczewski, K.P., Sagaidak, R.N., Shaughnessy, D.A., Shirokovsky, I.V., Shumeiko, M.V., Stoyer, M.A., Stoyer, N.J., Subbotin, V.G., Sukhov, A.M., Tsyganov, Y.S., Utyonkov, V.K., Voinov, A.A., Vostokin, G.K.: Production and decay of the heaviest nuclei ^{293,294}117 and ^{294}118. Phys. Rev. Lett. **109**, 162501(5) (2012)
154. Eichler, R., Schädel, M.: Adsorption of radon on metal surfaces: a model study for chemical investigations of elements 112 and 114. J. Phys. Chem. B **106**, 5413–5420 (2002)
155. Hohn, A., Eichler, R., Eichler, B.: Investigations on adsorption and transport behaviour of carrier-free silver, gold and platinum in quartz columns under vacuum conditions. Radiochim. Acta **92**, 513–516 (2004)
156. Gäggeler, H., Eichler, B., Greulich, W., Herrmann, G., Trautmann, N.: Vacuum-Thermochromatography of Carrier-free species. Radiochim. Acta **40**, 137–143 (1986)
157. Zagrebaev, V.I., Karpov, A.V., Greiner, W.: Possibilities for synthesis of new isotopes of superheavy elements in fusion reactions. Phys. Rev. C **85**, 014608(8) (2012)
158. Gäggeler, H.W.: On-line gas chemistry experiments with transactinide elements. J. Radioanal. Nucl. Chem. **183**, 261–271 (1994)
159. von Zweidorf, A.: Gaschemische Untersuchungen in situ gebildeter flüchtiger Oxide des Rutheniums, Osmiums und Hassiums. ibidem-Verlag, Stuttgart (2003) and Ph.D. thesis, Universität Mainz (2003)
160. Eichler, R.: Empirical relation between the adsorption properties of elements on gold surfaces and their volatility. Radiochim. Acta **93**, 245–248 (2005)
161. Zvara, I.: Studies of the heaviest elements at Dubna. In: Report JINR, vol. E12-7547, p. 28. Joint Institute for Nuclear Research, Dubna (1973)
162. Zvara, I., Timokhin, S.N., Chuburkov, Y.T., Yakushev, A.B., Gorski, B.: A comparative study of chlorides and bromides of element 105 (Ns), Ta and Nb by the thermochromatographic method. In: Scientific Report 1989–1990, vol. E7-91-75, p. 36. Joint Institute for Nuclear Research, Laboratory of Nuclear Reactions, Dubna (1991)
163. Türler, A., Eichler, B., Jost, D.T., Piguet, D., Gäggeler, H.W., Gregorich, K.E., Kadkhodayan, B., Kreek, S.A., Lee, D.M., Mohar, M., Sylwester, E., Hoffman, D.C., Hübener, S.: On-line gas phase chromatography with chlorides of niobium and hahnium (element 105). Radiochim. Acta **73**, 55–66 (1996)
164. Zvara, I.: Gas phase chemistry studies of transactinoid elements and the relativistic effects. Czech J. Phys. **49**, 563–571 (1999)

Historical Reminiscences: The Pioneering Years of Superheavy Element Research

Günter Herrmann

Abstract This chapter deals with the pioneering years of superheavy element research, from the mid 1960s to the mid 1980s. The prediction that superheavy nuclides could form an island around element 114 with half-lives long enough to have survived in Nature since nucleosynthesis led to intensive searches—not unlike "gold fever"—for such relic nuclei in all sorts of natural environments. Positive claims were raised from time to time but could not stand up under further scrutiny. Numerous attempts to synthesize superheavy nuclei by large leaps from the mainland of elemental stability to the island of superheavy elements went without success as well. The discovery of three more transactinide elements, 107–109, from 1981 to 1984 encouraged chemists to resume research on the chemistry of transactinide elements with a new approach: automated chemical procedures.

1 Introduction

In 1955, Wheeler [1] performed a courageous extrapolation of nuclear masses and decay half-lives and concluded that nuclei twice as heavy as the then heaviest known nuclei existed; he subsequently called them *superheavy nuclei.* Two years later, Scharff-Goldhaber [2] mentioned in a discussion of the nuclear shell model that beyond the well-established proton shell at $Z = 82$ (lead), the next proton shell should be completed at $Z = 126$ in analogy to the known $N = 126$ neutron shell. Together with a new $N = 184$ shell, these shell closures should lead to a local region of relative stability. These speculations, however, did not impact contemporary research since such extremely heavy nuclei were experimentally beyond reach.

G. Herrmann (✉)
Institut für Kernchemie, Johannes Gutenberg-Universität, Fritz-Straßmann-Weg 2, D-55128 Mainz, Germany
e-mail: guen.herrmann@t-online.de

M. Schädel and D. Shaughnessy (eds.), *The Chemistry of Superheavy Elements*,
DOI: 10.1007/978-3-642-37466-1_9,

The situation changed in 1966 due to the publication of three theoretical papers. In a study of nuclear masses and deformations, Myers and Swiatecki [3] emphasized the enormous stabilization against fission gained by shell closures. Nuclei at the next proton shell closure beyond $Z = 82$ should have fission barriers even higher than that of uranium, making them quite stable against spontaneous fission. This was in sharp contrast to the liquid-drop nuclear model, which predicts vanishing fission barriers in the same region, and therefore prompt instability due to disruption by fission. Remarkably, although the discussion in this paper focused on $Z = 126$ as the next proton shell, a closure at $Z = 114$ was already mentioned as an alternative, with reference to unpublished calculations by H. Meldner. He presented his results [4] at the symposium "Why and How Should We Investigate Nuclides far off the Stability Line?", in 1966 in Lysekil, Sweden [5], the seminal event for superheavy element research. Simultaneously, Sobiczewski et al. [6] also derived that 114 should be the next magic proton number. Other groups using different theoretical approaches soon agreed. A fantastic perspective was thus opened—an island of superheavy elements located not too far from the then heaviest known element, 103, and hence perhaps within reach.

First theoretical estimates [7–10] of decay half-lives around the doubly magic, spherical nucleus $Z = 114$, $N = 184$ revealed a topology as depicted in Fig. 1 [10]. Three major decay modes were considered: spontaneous fission, α decay, and β^- decay or electron capture. Spontaneous fission half-lives were found to peak sharply at the doubly magic nucleus, descending by orders of magnitude within short distances in the Z–N plane, thus causing the island-like shape. In contrast, half-lives for α decay should decrease rather uniformly with increasing

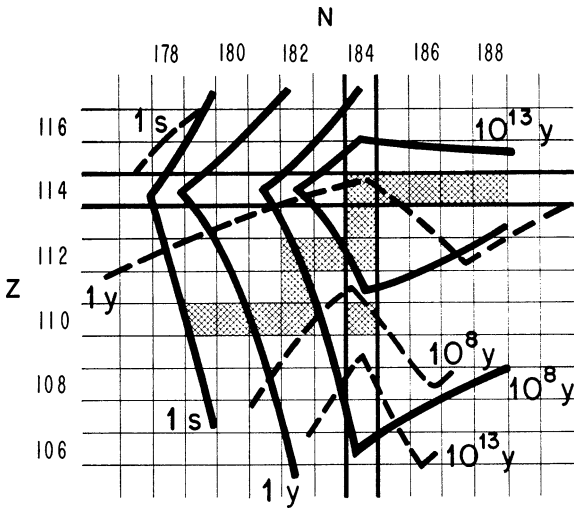

Fig. 1 Topology of the island of superheavy nuclei around the shell closures at proton number $Z = 114$ and neutron number $N = 184$ as predicted in 1969. Thick solid lines are contours of spontaneous fission half-lives; broken lines refer to α-decay half-lives. Shaded nuclei are stable against β decay. Reproduced from [10]

proton number, with some zigzag at the nuclear shell closures. The β-stable nuclei would cross the plane as a diagonal belt. For $Z = 114$, $N = 184$ an enormous spontaneous fission half-life of 2×10^{19} y was estimated, but only 10 y were estimated for α decay. In a limited region, long half-lives for both decay modes were expected to meet, most spectacularly at $Z = 110$, $N = 184$ where an overall half-life of 2×10^{8} y should result—sufficiently long for the occurrence of superheavy elements in Nature! Additional stability was expected for odd elements such as 111 or 113 [8, 11] due to the well-known hindrance of spontaneous fission and α decay for odd proton numbers.

These predictions of very long half-lives immediately stirred up a gold-rush period of hunting for superheavy elements in natural samples. Everybody was encouraged to participate. Almost nothing was needed to perform these experiments except for only a little money. Almost no equipment was needed, no research group or permission by a laboratory director was required, no accelerator beam time or proposal to funding agencies was needed—not even a garage. Just an intelligent choice of a natural sample and a corner in the kitchen at home could be sufficient to make an outstanding discovery: new and superheavy elements in Nature. The detector could be a simple microscope from school days now used to detect fission fragment tracks, which had accumulated in the sample since geological times. Such tracks (Fig. 2) are caused by radiation damage in the surrounding solid when the energetic fragments are slowed down to rest, and they can be made visible by chemical etching.

Due to the topology of the island, superheavy nuclei should decay by spontaneous fission, either immediately or after a sequence of other decay steps. In a detailed theoretical exploration, [12] of the *Z*–*N* plane around the island, the longest lived nuclide again turned out to be $Z = 110$, $N = 184$, decaying with a 3×10^{9} y half-life via α-particle emission to ^{290}108. From there, two subsequent β^{-} transitions should lead via ^{290}109 to ^{290}110, where the chain should terminate by spontaneous fission with a 140 d half-life. The doubly magic ^{298}114, with a half-life of 790 y, should also decay into ^{290}110 by two α-particle emissions via ^{294}112 as the intermediate step.

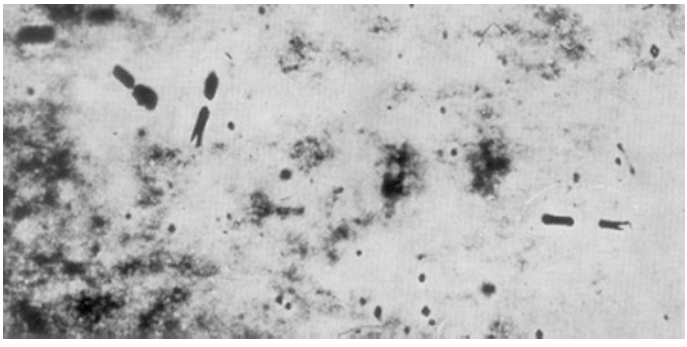

Fig. 2 Tracks of fission fragments in mica showing the characteristic forward–backward orientation of the two fragments emerging from the same fission event. Courtesy of Brandt (1974)

Since spontaneous fission is extremely rare in Nature, detection of fission events in natural samples would give a strong hint as to the existence of superheavy elements. α-particle spectra would be less specific, because the energies predicted for superheavy nuclei should fall into the range covered by decay products of uranium and thorium, and elaborate chemical treatment would be required to distinguish them.

The first attempts to synthesize superheavy nuclei in the laboratory were already under way in the late 1960s. Complete fusion of medium-heavy projectiles with very heavy targets—the successful approach in the extension of the Periodic Table—was considered the most promising approach. However, a large gap had to be bridged in a single step from conceivable targets, such as uranium or curium, to the island. The then existing heavy-ion accelerators could not provide the required medium-element projectiles in adequate intensities if at all. These demands had a strong impact on accelerator technology in order to upgrade the existing facilities and build novel ones.

The situation is illustrated in a cartoon, Fig. 3, which entertained the audiences of related conferences in the early 1970s. Several sailors are shown attempting to cross the sea of instability, fighting against hostile forces. Already on the way are the crews of the JINR (Joint Institute for Nuclear Research at Dubna, Soviet Union) with the Heavy-ion U-300 Cyclotron (Xe), and the IPN (Institut de Physique Nucléaire at Orsay, France) with the ALICE cyclotron (Kr); those of the LBL (Lawrence Berkeley Laboratory at Berkeley, USA) are just launching the SuperHILAC linear accelerator (Ge), whereas the UNILAC linear accelerator (U) of the GSI (Gesellschaft für Schwerionenforschung at Darmstadt, Germany) is still under construction.

Turning now to chemistry, the crucial question was: where are the superheavy elements located in the Periodic Table and how well do they fit into its architecture? The answer had immediate implications for the ongoing "search for" campaigns, for the selection of natural samples as well as for the design of chemical identification procedures. In a naive continuation of the Table, element

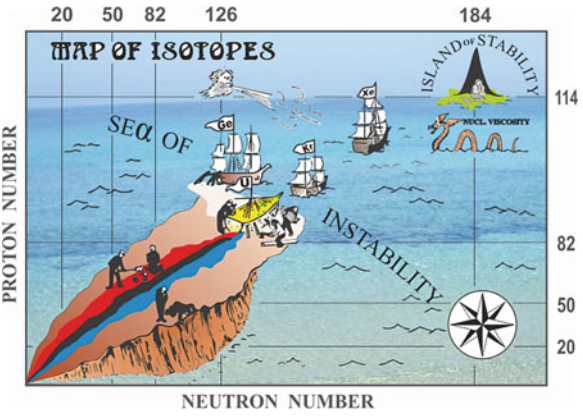

Fig. 3 Allegorical view of heavy-ion accelerator projects launched in the early 1970s for a journey to the island of superheavy elements. The facilities are identified by flags showing their most advanced projectile beam, see text. Newly colored version of a cartoon originally provided by Flerov [13]

110 is located below platinum, 112 below mercury, 114 below lead, and 118 becomes the next noble gas below radon. Quantum–mechanical calculations of ground-state electronic configurations [14, 15] supported this view. The electron configurations should indeed be analogous to that of the homologs; e.g., two 7*s* valence electrons were predicted for element 112, as there are two 6*s* electrons in mercury.

Extrapolations within the respective groups of the Periodic Table should thus be an appropriate approach to predict the chemical behavior of superheavy elements [14] even in some detail, such as for the 7*p* elements 113 and 114, eka-thallium and eka-lead, respectively [16]. Specific chemical properties were needed as the basis for identification, but properties common to several superheavy elements were also of interest for group separations in enrichment procedures; for example, the high volatility expected for elements 112–116 in the metallic states [17] or the strong bromide complexes of elements 108–116 [18].

Deviations from straightforward extrapolations within the Periodic Table could be caused by relativistic effects in the electron shells of superheavy elements. The inner electrons rotate around the nucleus with such a high velocity that they gain substantial mass; the *s*- and *p*-orbitals shrink, whereas higher lying orbitals expand. As a consequence [19], the two *s* electrons in element 112 and also the two $p_{1/2}$ electrons in element 114 could form closed electron shells, and thus eka-mercury and eka-lead would be chemically inert gases like element 118, eka-radon. Beyond element 121, eka-actinium, a series of 6*f* elements may occur, in analogy to the 5*f* actinide elements following actinium. But the 5*g* orbital may also be filled in competition to form a series of 32 superactinide elements [20].

Within a few years, many aspects of superheavy nuclei and elements were predicted. A review [21] covering the literature until the end of 1973 was based on 329 references, and status reports [22–27] published from time-to-time illustrated how the field had further developed.

2 Search for Superheavy Elements in Nature

Since the solar system and the Earth's crust were formed about 4×10^9 y ago, a half-life of some 10^8 y for superheavy nuclei would be long enough for their survival until present day. Heavy elements beyond iron are created in gigantic stellar collisions and explosions, the supernovae, which produce free neutrons in tremendous densities and initiate the so-called *r*-process of nucleosynthesis where *r* stands for "rapid". Starting at seed nuclei around iron, several neutrons are captured to form very neutron-rich isotopes which decay quickly by β^- transitions to the next heavier element. These daughter products again capture neutrons and undergo β^- decay and so forth. In this way, the *r*-process path proceeds parallel to the belt of stable nuclei from iron to the heaviest elements but shifted to much higher neutron numbers, with discontinuities at magic neutron numbers, as is sketched in Fig. 4.

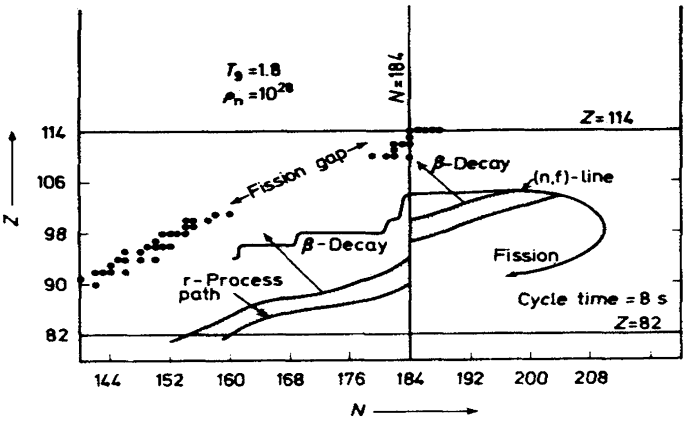

Fig. 4 Nucleosynthesis of superheavy nuclei by the *r*-process. Shown in the *Z*–*N* plane is the *r*-process path of very neutron-rich nuclei formed during a supernova event by rapid neutron capture alternating with β^- decay. After the event, the *r*-process nuclei decay via long β^--decay chains toward the belt of β-stable nuclei (*arrows*). Those originating at $Z \approx 104$ end up around closed-shell nuclei with $Z \approx 114$, $N \approx 184$ (*dots*). From [28]

As soon as the stellar explosion ceases, the very short-lived nuclei decay toward the region of β-stability by a chain of fast β^- transitions, thereby further increasing their atomic number. Somewhere at very high atomic numbers, the *r*-process is terminated by fission. Figure 4 shows these results [28] for a stellar temperature of 1.8×10^9 K (T_9), a neutron density of 10^{28} cm^{-3} (ρ_n) and a cycle time of only 8 s for the whole process. This study predicted continuation of the process up to $Z \approx 104$, sufficient to feed magic nuclei with $Z = 114$, $N = 184$ by decay. Other early treatments [29–31] denied the production of superheavy elements in the *r*-process. The question remained controversial for quite some time [32].

But even if the half-lives of superheavy nuclides did not exceed the 10^8 y level, there was hope to discover them in Nature. Although now extinct, they may have left detectable traces such as fission tracks or fission products in certain samples. Another possible source could be the cosmic radiation impinging on Earth whose heavy component may be formed by a *r*-process nucleosynthesis in our galaxy not longer than 10^7 y ago [33], and may hence contain superheavy nuclei with half-lives down to some 10^5 years.

In this context, attention was also drawn [11] to quite a number of earlier reports on natural α-particle emitters with energies that did not match any known natural radioactive source but fell into the region predicted for superheavy nuclides. Were the superheavies already there, but unrecognized?

2.1 Terrestrial Samples

Any search for superheavy elements in terrestrial material begins with the choice of a sample. Relevant geochemical aspects are discussed in Refs. [34, 35]. First searches were reported in 1969 by the Berkeley [10] and the Dubna groups [36]. In Berkeley, a search for element 110, eka-platinum, in natural platinum ores with standard analytical techniques remained negative at a concentration limit of 1 ppb, and low-level counting techniques did not reveal any activity above background. In Dubna, however, fission tracks discovered in old lead glasses were tentatively attributed to element 114, eka-lead, present in concentrations of 10^{-11}–10^{-12} gram per gram of sample with an assumed half-life of 1×10^9 y of the radioactive source. As a convention, 1×10^9 y is the half-life assumed for the conversion of measured specific activities (count rate per gram of sample) into the more instructive concentration (gram of radionuclide per gram of sample). Examinations of the same and of other lead-bearing samples for spontaneous fission events with large proportional counters in Dubna seemed to confirm these findings, but further measurements [37] of thin samples sandwiched between two plastic fission track detectors showed that the events were background caused by cosmic-ray induced reactions of lead.

Other groups [38] found no evidence for spontaneous fission activities in lead and other samples at a lower detection limit of 10^{-13} g/g achieved with the sandwich technique. Even limits down to 10^{-17} g/g can be reached by etching fission tracks in suitable minerals where they would have accumulated over millions of years. Such searches in a variety of minerals [35, 39] remained inconclusive, however.

A versatile technique for spontaneous fission detection is counting the neutrons emitted in the fission process. Although neutron detection is less efficient than fission fragment or α-particle counting, it can compete because much larger samples, up to tens of kilograms, can be inspected. With a simple arrangement of six ^{3}He-filled neutron counters, a sensitivity of 10^{-11} g/g was reached in 2 days of counting [40], allowing a quick survey of a great variety of samples. Activities were found with all heavy metals in the Periodic Table from platinum to bismuth, but with identical decay rates. Furthermore, as Fig. 5 shows, the rates for lighter elements fall on a curve representing cross-sections for high-energy spallation reactions as a function of atomic number. This shows that a background of neutrons is created by cosmic-rays impinging on the samples during counting, which requires additional shielding.

More advanced versions of neutron counting were based on the expectation that spontaneous fission events of superheavy nuclei should be accompanied by the emission of about 10 neutrons [41, 42], distinctly more than two to four observed for any other spontaneous fission decay. Such neutron bursts can be recognized by recording neutron multiplicities—events with several neutrons in coincidence—with ^{3}He-filled counting tubes [43, 44] or large tanks filled with a liquid scintillator sensitive to neutrons [45].

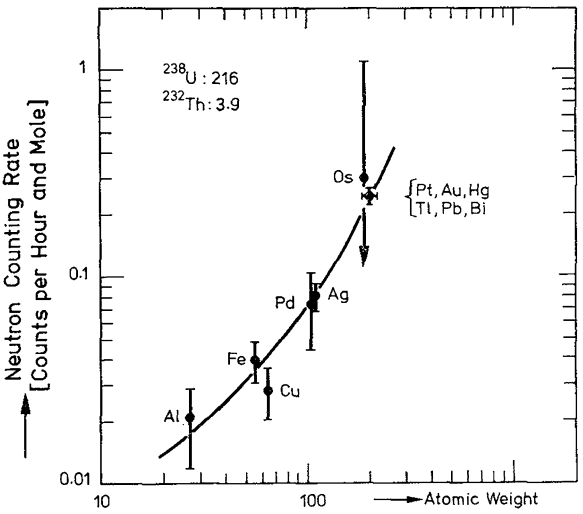

Fig. 5 Neutron counting as detection method for spontaneous fission events of superheavy nuclei. The recorded neutron rates (*points*) were found to follow the relative cross-sections of cosmic-ray induced spallation reactions (*curve*), and were thus due to background events. The numbers are the rates measured for natural uranium and thorium. From [40]

Figure 6 shows a neutron multiplicity detector [43] with 20 ^{3}He counting tubes neutron arranged in two rings around the central sample chamber, which accommodated upto 100 kg of a sample. The tubes were embedded in paraffin for slowing down the neutrons. Bursts of $\geq$10 neutrons from an emitter source at 10^{-14} g/g concentration should result in about one event per day with multiplicity of four or larger. A similar sensitivity was reached [45] with a scintillator-based neutron detector. To suppress background by cosmic-ray induced neutron showers, the detectors were operated below ground and with an electronic anticoincidence shielding triggered by incoming high-energy particles. With such an instrument no positive results at the 10^{-14} g/g level were obtained for lead ores or samples from industrial lead processing. The publication Ref. [45] gives an illustrative example of how researchers can be misled by a contamination of a sample by tiny amounts of the common nuclide 2.5-y ^{252}Cf which decays by spontaneous fission and thus emits neutrons.

A quite unconventional approach to fission-event detection is a device called the "spinner." The instrument, Fig. 7, consists of a glass cylinder with glass arms filled with about one liter of the sample solution. Upon rotation, a negative pressure develops in the solution through the action of centrifugal forces. The solvent does not evaporate, however, but remains in a metastable state until a strongly ionizing event in the solution destroys this state and produces a bubble which is detected optically. The spinner can be operated with very low background rates, as low as one event per month corresponding to a detection limit of 10^{-13}–10^{-14} g/g. No fission events were observed [46] with salts from the elements platinum to lead in the Periodic Table, and galena (natural lead sulfide).

Attempts were made to further improve the detection limits by enrichment of superheavy elements from very large samples. Among the "hottest" natural samples were brines from hot springs at the Cheleken Peninsula in the Caspian Sea

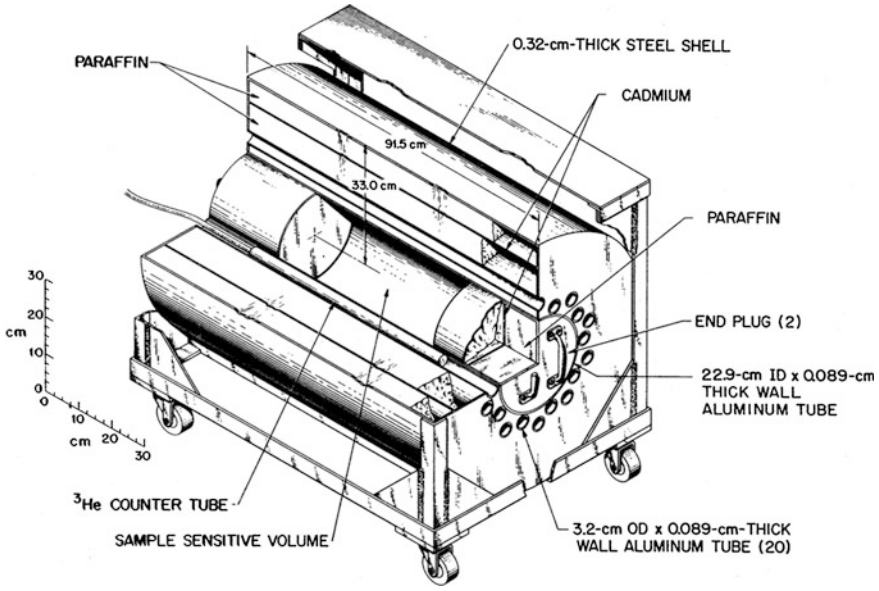

Fig. 6 Large neutron counter with ^{3}He counting tubes for the recording of neutron multiplicities in the spontaneous fission decay of superheavy nuclei (see text). Reproduced from [43]

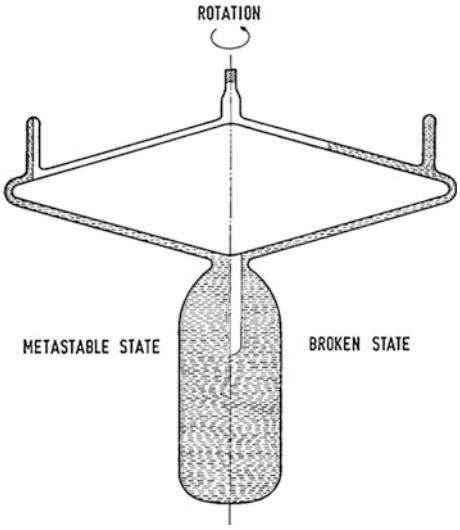

Fig. 7 The spinner detector. The container is filled with a solution of the sample. Upon rotation, a metastable state develops (at *left*) which breaks down after an ionizing event, as is indicated by the formation of a central bubble (at *right*). From [46]

which are known to be rich in volatile elements, probably due to material escaping from large depths in the Earth's mantle. They may contain superheavy elements

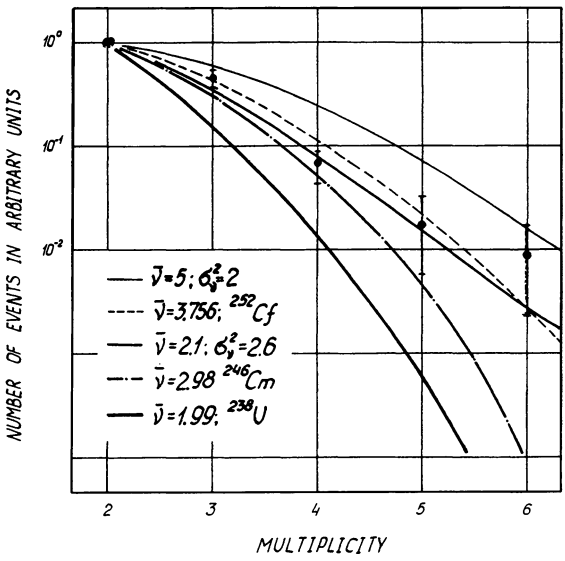

Fig. 8 Spontaneous fission activity in hot spring water at the Cheleken Peninsula after concentration by ion exchange. Shown is the measured neutron multiplicity distribution (*dots*) compared with measured distributions for ^{238}U, ^{246}Cm and ^{252}Cf spontaneous fission and calculated distributions for two sets of ν and σ^2, the average number of neutrons per fission and its variance, respectively. From [47]

deposited in deeper layers. After processing some 2,000 m^3 of spring water through 850 kg of an anion-exchange resin, a weak spontaneous fission activity appeared in the resin, and fractions eluted from the resin showed rates up to five events per day with neutron multiplicities as depicted in Fig. 8 [47]. Evidently, natural ^{238}U can be ruled out as the source, but not a contamination by 2.5-y ^{252}Cf. Attempts to concentrate the activity further for identification of its atomic number failed [48]. A search for such activities in similar brines, Salton Sea in California and Atlantis II at the floor of the Red Sea, gave no positive evidence [49].

The extreme case of the search for element 114 is flue dust collected during the industrial processing of lead from galena [50]. Eka-lead should be more volatile than lead, and hence enriched in flue dust. Samples collected from 10^3 to 10^4 tons of galena were concentrated further by chemical and mass separations. They were finally exposed to reactor neutrons but no induced fission events were found with fission track detectors. The deduced concentration limit of 10^{-19}–10^{-23} g/g is by far the lowest achieved in searches for superheavy elements in Nature.

Very unexpected news arrived in the summer of 1976—evidence for element 126, and possibly 124 and 116 in Nature. The evidence was obtained [51] in a study of radioactive halos, a phenomenon known since the early days of radioactivity research. They appear in certain minerals as spherical zones of discoloration around a central mineral grain and are due to radiation damage by α-particles emitted from uranium or thorium present in the grain. Cuts through such halos reveal a well-resolved ring structure reflecting the ranges of α particles in the surrounding mineral. There are, however, ranges which cannot be associated with known natural nuclides. In particular, in biotite from Madagascar, giant halos were observed [52] with ranges equivalent to about 14 MeV α particles, an energy predicted for α transitions at $Z \approx 126$. Such halos occur around relatively large inclusions of monazite crystals

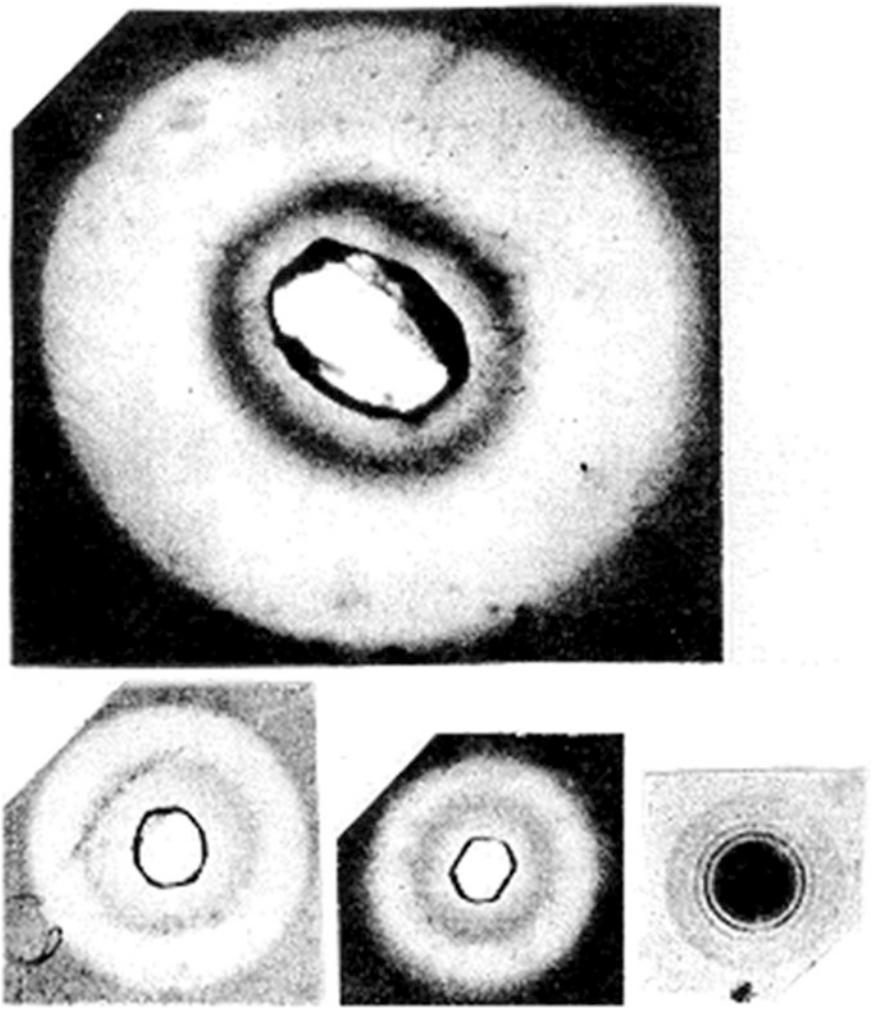

Fig. 9 Radioactive halos around large central monazite inclusions in biotite from Madagascar. Top: giant halo, bottom: thorium and uranium halos; at right: well-resolved uranium halo around a small central grain for comparison. All photographs are on the same scale; the outer diameter of the halo at top is 250 μm. From [53]

(a lanthanide-thorium-uranium phosphate), as Fig. 9 shows, together with haloes of the thorium and uranium decay series around large and also small central crystals.

In order to verify the presence of elements around $Z \approx 126$, the monazite inclusions were irradiated with sharply collimated proton beams to excite the X-ray spectra of the elements. As can be seen in Fig. 10, two well-separated groups of strong peaks appear [51], the L X-rays of uranium and thorium (at left), and the K X-rays of the lanthanide elements (at right). In between, with energies

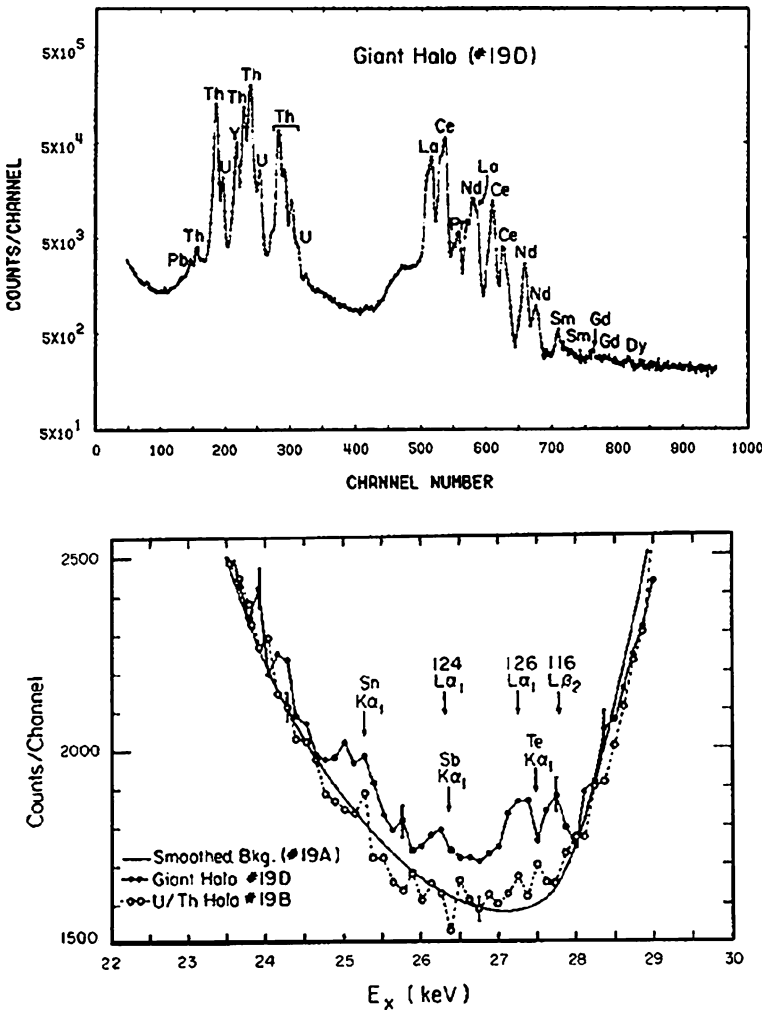

Fig. 10 Proton-induced X-ray spectrum of a monazite inclusion in the center of a giant radioactive halo (at *top*). The region in the gap around channel 400 is shown enlarged at the bottom (*dots*) together with the spectrum of a U-Th halo (*circles*) and a smoothed background (*line*). From [51]

between 24 and 29 keV, much weaker peaks were identified and assigned to the $L_{\alpha 1}$ X-rays of the elements 116, 124 and 126. Surprisingly high concentrations, 10–100 ppm in the grain, result from the observed peak intensity. If such concentrations would also hold for bulk monazite, tons of superheavy elements would become easily accessible in some regions of the Earth, e.g., at Indian beaches.

The occurrence of elements 126 and 124 in monazites would perhaps not be unlikely because in a superactinide series of elements they would be homologs of

uranium and thorium [14]. Element 116, however, would be a homolog of polonium. Since polonium is known to be strongly enriched by some marine invertebrates, it was suggested [54] to search for element 116 in crustacea such as lobsters, shrimps, and crabs in coastal waters at beaches rich in monazite sand—perhaps a gourmet's recommendation.

Objections against these findings were soon raised. The strongest peak attributed to element 126 could experimentally be accounted for [55] by a prompt γ ray emitted during the proton bombardment in the (p,n) reaction with ^{140}Ce, cerium is a major component of monazite. The weaker peaks were shown to stem from K X-rays of traces of ordinary elements such as antimony and tellurium [56]. When the X-ray spectra were selectively excited by monochromatic synchrotron radiation tuned to the X-ray absorption edges of the supposed elements, the evidence for superheavy elements vanished [57, 58]. Furthermore, attempts failed [59] to detect them in bulk monazites through isolation of an $A > 294$ fraction with a mass separator. Chemical enrichments [60] from bulk samples also remained without success. The conclusion is that giant halos are not due to superheavy elements, but a generally accepted explanation of what they are is still lacking.

2.2 Extra-Terrestrial Samples

Lunar rocks showed no indication of spontaneous fission activity in neutron multiplicity counting of a 3 kg sample [45].

Much attention was paid to the evidence for extinct superheavy elements appearing in a class of primitive meteorites, the carbonaceous chondrites. These are low-temperature condensates from a solar gas that have more or less escaped subsequent differentiating processes, and may therefore represent the material from which the solar system was made. They contain a surplus of the neutron-rich xenon isotopes 131–136 [61], at first attributed to the spontaneous fission of the now extinct ^{244}Pu. But when this assignment became questionable, it was suggested [62, 63] that superheavy elements might be the progenitors. Correlations between the concentrations of excess xenon and of volatile elements such as thallium, bismuth, and indium in meteorites pointed to elements 115, 114, or 113 [64, 65]. The strange xenon was found to be strongly enriched [66] in a host phase comprising less than 0.5% of the meteorite, isolated after dissolution of its bulk in strong acids.

Light xenon isotopes from 129 to 124 were also over-abundant in such meteorites [61, 67, 68] and enriched [66] in the tiny host phase although they are not formed in fission. Whether there are two anomalous xenon components of different origin remained controversial for years [69]. Eventually, the fission origin of the anomalous xenon was ruled out [70] because in a host phase containing the excess xenon, no excess was detected for the adjacent, but nonvolatile fission products barium 130–138.

Stimulated by these studies, samples of primitive meteorites were inspected by neutron multiplicity counting. In the Allende meteorite available in large

quantities, a weak fission activity at the 10^{-14} g/g level was reported [71–73] but could not be enriched chemically [74–76].

Another class of "search for" experiments is the measurement of heavy element abundances in the cosmic radiation by exposure to particle track detectors—nuclear emulsions or plastic sheets—in balloon flights at high altitudes with analysis of the recorded tracks for atomic number and abundance. A survey [33] of all data obtained until 1970 showed one single event beyond $Z \approx 100$. With the data collected in the Skylab space station, the limit became more stringent: no superheavy nucleus in spite of the 204 recorded tracks with atomic number 74–87 [77]. A similar limit was deduced [78] after exposure in a satellite. In a study of cosmic-ray induced tracks in olivine crystals enclosed in iron-stone meteorites, which were exposed in space over millions of years, unusually long tracks were found and attributed to superheavy elements [79, 80]. However, this conclusion could not be maintained [81, 82] after calibration experiments of track dimensions with energetic ^{238}U beams delivered by accelerators.

The largest collector surface for elements impinging on the Globe is of course the Sea. Heavy elements deposited in seawater are enriched in certain sediments, such as iron-manganese hydroxides called manganese nodules. Fission tracks were found [83] in feldspar inclusions in such nodules, but no evidence was obtained [40, 45] for spontaneous fission activities by counting nodules with neutron detectors.

In summary, there was no evidence beyond a doubt for superheavy elements in Nature. Since improved theoretical calculations of half-lives tended with time to reach much shorter values than those required for occurrence in Nature, the enthusiasm for further searches ceased in the early 1980s. This colorful intermezzo in superheavy element research appeared to be finished, but remarkably, a search for primordial element 108 (hassium) in its homolog osmium was recently undertaken [84].

3 Early Attempts to Synthesize Superheavy Elements

First attempts to synthesize superheavy nuclei in the late 1960s followed the approach that was so successful for actinide elements: complete fusion of a projectile and a target nucleus chosen to attain by amalgamation the desired proton number. As long as elements around 126 were the goal, the perspective looked promising. Fusion cross-sections as large as tens of millibarns were extrapolated [85, 86] from data for heavy actinides, including the ^{232}Th(^{80}Kr, 2n) reaction directly leading to the doubly magic $Z = 126$, $N = 184$ nucleus. With element 114 as the focus, the situation is different in that the doubly magic nucleus $Z = 114$, $N = 184$ is extremely neutron rich. Its neutron-to-proton ratio cannot be achieved by any realistic projectile-target combination. Close approach to $Z = 114$ is connected with a neutron number far below $N = 184$, whereas to meet $N = 184$ requires an overshooting of $Z = 114$ by about 10 protons [85, 87].

Evidence for success would be the observation of very energetic α particles or spontaneous fission activities not common among ordinary nuclei. But such evidence would require further examination. Unfortunately, the identification of a new element by means of its radioactive decay into well-known nuclides of a known element—very successful for actinide elements—would not be possible in a region far apart from already explored territory.

The first attempt to synthesize element 114 was made in 1969 in Berkeley [10] by bombarding neutron-rich ^{248}Cm with ^{40}Ar projectiles. The experiment was negative at a cross-section limit of about 10 nanobarns. The compound nucleus ^{288}114 contains only 174 neutrons, and it should evaporate four neutrons to $^{284}114_{170}$, which is probably located outside the island. With the large variety of heavy-ion beams soon becoming available, attempts to reach the island by complete fusion reactions were carried out on a broad basis. Within a few years, twenty different reactions were tried [24] covering compound nuclei with proton numbers from 110 to 128 and neutron numbers from 168 to 194.

To give an example, high-energy α particles with energies of 13–15 MeV—as predicted for elements around 126—from short-lived emitters were observed at the ALICE Orsay in bombardments of thorium with krypton. This was taken as evidence for the synthesis of a compound nucleus of element 126 [88]. But attempts in the same laboratory to secure the evidence by a direct mass identification failed [89]. In these control experiments, the magnetic rigidity, kinetic energy and time-of-flight of fragments produced in interactions of ^{84}Kr with ^{232}Th, ^{208}Pb and ^{238}U were measured.

Very surprising news appeared in the early 1970s—can superheavy nuclei be made by heavy-ion reactions without using a heavy-ion accelerator? A long-lived spontaneous fission activity was chemically isolated and assigned [90] to element 112, eka-mercury, from tungsten plates bombarded over a long time in the beam dump of the 24 GeV proton beam at the CERN in Geneva. A two-stage production process was postulated: proton-induced spallation of tungsten generates energetic recoil atoms, which fuse with tungsten to produce superheavy nuclei. Attempts to confirm the results in other laboratories failed [46, 91, 92], a conclusion finally shared by most of the original authors [93].

Finally, the efforts focused on experiments with ^{48}Ca projectiles, which are doubly magic ($Z = 20$, $N = 28$) and very neutron rich, but also very rare and expensive. After survey experiments with this projectile at Berkeley [94, 95] and Dubna [96, 97], the ^{48}Ca + ^{248}Cm reaction was considered to be the most promising because the compound nucleus $Z = 116$, $N = 180$ provides a relatively close approach to the neutron shell with moderate overshooting of the proton shell. Also, the predicted decay chain after evaporation of four neutrons [12] appeared to be suitable for detection. The decay chain should start at the evaporation residue ^{292}116 with α decay having a few seconds half-life, followed within several minutes by two electron captures of ^{288}114 and ^{288}113, and end at ^{288}112 by spontaneous fission with 50 min half-life.

Figure 11 refers to a series of ^{48}Ca + ^{248}Cm experiments by an international collaboration [98] performed at the UNILAC and the SuperHILAC. With a variety

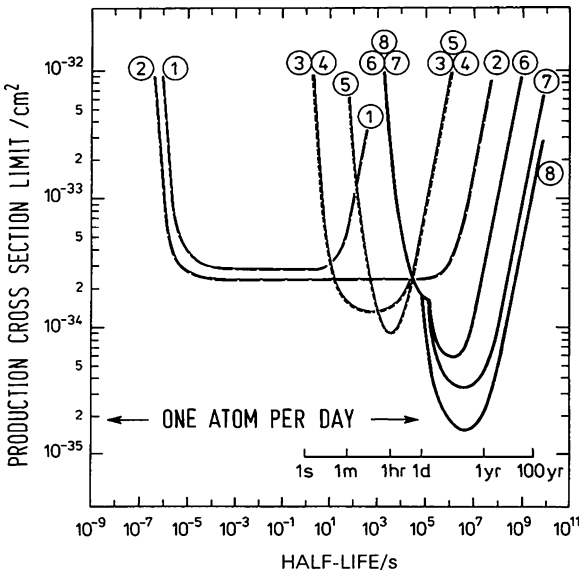

Fig. 11 Search for superheavy nuclides in the reaction of ^{48}Ca with ^{248}Cm. Upper limits of production cross-sections are plotted versus half-life. The curves refer to different separation techniques: recoil-fragment separators (*curves* 1, 2), fast on-line chemistry (3–5), and off-line chemistry with low-background counting (6–8), see also text. From [98]

of techniques, a half-life range of 14 orders of magnitude, from 1 μs to 10 y, was covered. The upper limits of the production cross-sections achieved in these negative experiments are plotted versus the assumed half-life of the product. Each technique has a specific half-life region of highest sensitivity, but is less sensitive at shorter half-lives because of decay before detection, and at longer ones by a decay rate which is too low for detection.

The region of very short half-lives (curves 1 and 2) was inspected with two recoil-fragment separators with fragment detection by surface-barrier detectors. For intermediate half-lives (3–5), chemical on-line separations were applied, and off-line chemistry was used in the detection of long-lived products (6–8). The chemical procedures were based on volatilization at high temperature (3 and 8) for elements 112 through 116 [17], and at room temperature (4 and 6) for 112 and 114 [19]. Anion exchange of bromide complexes (5 and 7) was applied for elements 108–116 [18]. The cross-section limit was generally about 200 picobarns, with some extra sensitivity gained for long-lived products by fission fragment-fission neutron coincidence counting [99].

The ^{48}Ca + ^{254}Es reaction with $Z = 119$ as the compound nucleus was also studied [100] with negative results.

Was there an alternative? Would it help to offer a projectile with far more protons and neutrons than what was required to fill the gap between target and superheavy nuclei? In deep-inelastic reactions, massive projectile and target nuclei

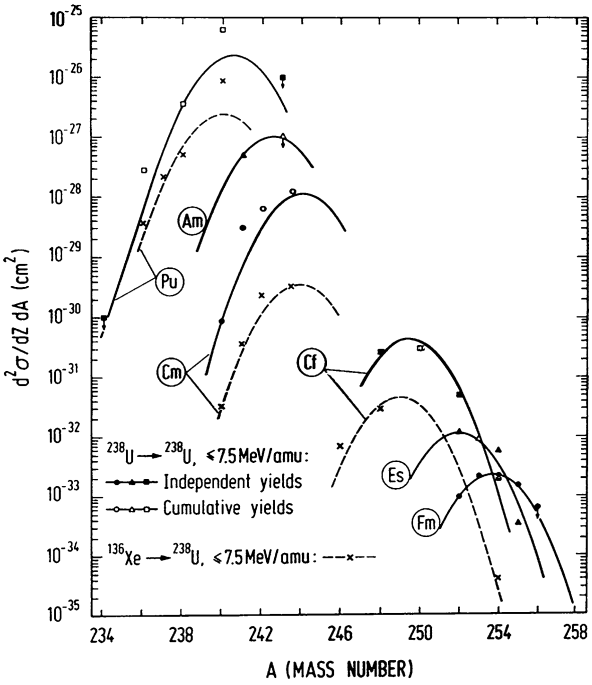

Fig. 12 Production cross-sections of transuranium nuclides in the interaction of ^{238}U with ^{238}U (*solid lines*) plotted versus mass number. Also shown are data for the ^{136}Xe + ^{238}U interaction (*dashed lines*). From [101]

stick together in a dumbbell shaped, dinuclear collision complex, but their mutual electrostatic repulsion drives the complex apart before complete amalgamation is reached. During the contact nucleons are exchanged between the partners, and with some probability one part grows considerably at the expense of the other one. Would this also happen if a $^{238}U_{146}$ beam interacts with a $^{238}U_{146}$ target; could one partner in the dinuclear collision grow to become doubly magic $^{298}114_{184}$, whereas the other one would shrink to $^{178}70_{108}$, a known neutron-rich isotope of ytterbium?

A radiochemical study [101] of the element distribution in the ^{238}U + ^{238}U reaction at the UNILAC revealed the expected broad distribution of reaction products. Figure 12 shows the production cross-sections for nuclides beyond uranium. They decrease from plutonium to fermium by eight orders of magnitude, indicating severe losses by fission of freshly formed transfer products. Nonetheless, an extrapolation to surviving $Z = 114$ fragments gives about 10 picobarn cross-sections, not a completely hopeless situation. For the complementary products below uranium where fission decay is not significant, the yields decrease exponentially from $Z = 92$ down to $Z = 73$. This trend is well reproduced [102] by a theoretical model treating nucleon transfer in the intermediate collision complex as a diffusion process. Extrapolation of the model to $Z = 70$ gives about 100 microbarn total production cross-section.

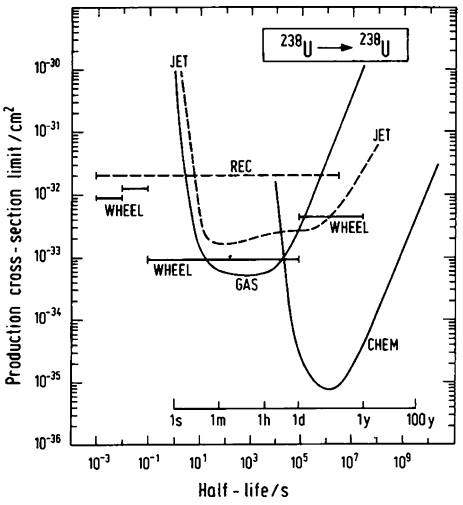

Fig. 13 Search for superheavy nuclides in the $^{238}U + ^{238}U$ reaction: upper limits for the production cross-section obtained with various techniques (see text), plotted versus half-life. Reproduced from [105]

Direct searches for superheavy elements in the $^{238}U + ^{238}U$ reaction were also undertaken at the UNILAC by several groups. All these efforts unfortunately did not result in positive evidence of the production of superheavy elements. Figure 13 gives a summary of these searches. The curve labeled CHEM [103] was obtained with off-line chemical separations and inspection for α and spontaneous fission activities; here, the 10 picobarn level was reached for half-lives between several days and years. The curve labeled GAS [104] holds for an on-line search of species, which are volatile at room temperature. WHEEL [105] refers to fission track detection in the unseparated product mixture deposited on a rotating catcher, REC [106] to the inspection of unseparated recoil atoms implanted in a surface barrier detector, and JET [107, 108] after their on-line transport from target to detector by a gas jet system.

Attempts to find superheavy elements in the $^{238}U + ^{248}Cm$ reaction [109] failed, too, although the production cross-sections for transcurium isotopes increase by three orders of magnitude [110] compared with the $^{238}U + ^{238}U$ reaction.

Two decades later the reaction of ^{48}Ca with ^{248}Cm was repeated by a Dubna-Livermore collaboration [84, 111], this time successfully with the discovery of element 116. The isotopes $^{293}116$ and $^{292}116$, α-particle emitters with 61 and 18 ms half-lives, were produced by the $^{248}Cm(^{48}Ca,3n)$ and $(^{48}Ca,4n)$ reactions with 1.0 and 3 picobarn cross-sections, respectively. This level is two orders of magnitude below the level reached in the earlier experiments shown in Fig. 11 [98]. The previous approach appeared to not be sensitive enough to these low cross-sections.

4 New Elements, New Chemistry

Besides the hunting for "superheavies", attempts to extend the Periodic Table element-after-element continued also in these years and in 1974 reached element 106 (seaborgium). It was synthesized in Berkeley [112] by the ^{249}Cf(^{18}O,4n)^{263}106 reaction and was identified to be an α-particle emitter with a half-life of only 0.9s. The evaporation of four neutrons after fusion of projectile and target indicates an excitation energy of 40–50 MeV energy, which is typical for actinide-based fusion reactions, thus, called "hot fusions". But such excitations are unwanted in the synthesis of fragile nuclei at the limit of stability. Fortunately, they can largely be avoided by using the closed-shell nuclei ^{208}Pb and ^{209}Bi as targets [113], which, as an additional advantage, are generally available and inactive. This "cold fusion" approach requires medium-weight, neutron-rich projectiles, which were not generally available at the then existing heavy-ion accelerators but were offered in appropriate energies and intensities at the new UNILAC accelerator at the GSI in Darmstadt.

Element 107 (bohrium) was the first element discovered at the GSI by cold fusion [114]. Its synthesis succeeded in 1981 by the ^{209}Bi(^{54}Cr,n) reaction leading to ^{262}107, which decays with 4.7 ms half-life by α-particle emission into a chain of well-known nuclides; the assignments of proton and mass number of the new element were, therefore, beyond any doubt. Essential for this success was SHIP, the powerful recoil-fragment separator, which separated online the very few wanted nuclei from a huge bulk of waste particles. In addition, it had a sophisticated detection system, which recorded the decay events that followed a suspected event at the spot where it was collected. Two more elements, 108 (hassium) and 109 (meitnerium), were discovered by the SHIP group in the following 3 years. These nuclei also decay by α-particle emission with millisecond half-lives. No evidence was obtained for the onset of spontaneous fission, which was expected in this region due to the decreasing barrier heights against fission, as predicted by the liquid-drop nuclear model. In a comprehensive analysis of the observations, Armbruster concluded that these nuclei are already shell stabilized in the ground state; they "correspond to what superheavy elements are to be" [115]. Thus, the superheavies were already there, but not as spherical nuclei like those supposed to exist around element 114, but as deformed nuclei with elongated shapes. Extra stability around $Z = 108$ and $N = 162$, due to shell stabilization of deformed nuclei, was already indicated in theoretical studies [116, 117] and was confirmed later by further work.

The new elements should belong to the 6*d* transition elements beginning with element 104 (rutherfordium) for which a colorful chemistry is expected, quite different from the monotone chemistry of the preceding heavy actinides. Very little was known, however, about the chemistry of the transactinides. In aqueous solutions, cationic and anionic species of element 104 had been studied with standard column techniques [118, 119], and in the gaseous state, halide compounds of 104 and 105 by their volatilization and deposition on solid surfaces [120–122].

The elements 104 and 105 behaved, in all cases, like homologs of hafnium zirconium (104) and tantalum niobium (105), respectively.

Four more transactinides, 106–109, were added and the possibility to proceed to still heavier elements was positive; a strong motivation to initiate extended chemical studies. Furthermore, with increasing atomic number, a new and unique chemical aspect should become more and more visible: chemical consequences of increasingly strong relativistic effects in the electron shells. How will they change the architecture of the Periodic Table; by minor irregularities or by drastic breaks? Will, for example, eka-lead (element 114) at ambient temperature behave like a metallic element or an inert gas?

Research on the chemistry of transactinide elements was resumed in the mid 1980s at Berkeley by the first study of element 105 in aqueous solution [123]. The α-particle emitter, 35-s ^{262}Db, produced by the ^{249}Bk(^{18}O,5n) reaction, served as a probe. The investigated chemical topic was the adsorption on glass in very strong nitric acid, a characteristic property of tantalum and niobium. Dubnium was found to share this property. Due to the very low production rate of ^{262}Db, some 800 manually performed experiments were required to obtain a statistically satisfying result based on 24 α-decay events altogether. This example showed that automated, computer-controlled online procedures were needed for a broad exploration of the open territory.

Automated procedures had already been developed and were applied in studies of short-lived fission products [124], but additional and stringent conditions have to be met for their applications to the heaviest elements. This work at the one-atom-at-a-time level with short-lived nuclei sets extremely strong constraints on the choice of chemical procedures. The chemistry and also the α-particle spectroscopy required for identification have to be fast in terms of the half-life of the radionuclide. In addition, the procedures should be robust enough for running them over days or weeks in order to catch and study the few produced atoms. Developments in this direction were mainly pushed by groups at GSI/Darmstadt—University of Mainz (Germany) and Paul Scherrer Institut/Villigen—University of Bern (Switzerland), with groups at the Lawrence Berkeley Laboratory—University of California joining for experiments with the heaviest elements. First results were obtained with the last actinide element, 103 (lawrencium). The isotope 3-min ^{260}Lr was used for investigations in aqueous solution [125] and in the gas phase [126]. Improved versions of the key instruments for experiments in aqueous solution [127] and with gases [128] were published. The first applications to a transactinide element—halide complexes of element 105 in aqueous solution [129] and halide species in the gas phase [130]—showed clearly the potential of automated procedures. What followed? See this book.

Acknowledgment The author is grateful to Brigitta Schausten, Dawn Shaughnessy and Matthias Schädel for their editing of the article.

References

1. Wheeler, J.A.: Fission physics and nuclear theory. In: Proceedings of International Conference Peaceful Uses of Atomic Energy, Geneva 1955, vol. 2, pp. 155–163, 220–226. United Nations, New York (1956)
2. Scharff-Goldhaber, G.: Nuclear physics. Nucleonics **15**(9), 122–124 (1957)
3. Myers, W.D., Swiatecki, W.J.: Nuclear masses and deformations. Nucl. Phys. **81**, 1–60 (1966)
4. Meldner, H.: Predictions of new magic regions and masses for super-heavy nuclei from calculations with realistic shell model single particle Hamiltonians. In Ref. [5], pp. 593–598
5. Proceedings International Symposium. Why and How Should We Investigate Nuclides far off the Stability Line, Lysekil 1966. Arkiv Fysik **36** (1967)
6. Sobiczewski, A., Gareev, F.A., Kalinkin, B.N.: Closed shells for $Z > 82$ and $N > 126$ in a diffuse potential well. Phys. Lett. **22**, 500–502 (1966)
7. Nilsson, S.G., Nix, J.R., Sobiczewski, A., Szymański, Z., Wycech, S., Gustafson, C., Möller, P.: On the spontaneous fission of nuclei with *Z* near 114 and *N* near 184. Nucl. Phys. **A115**, 545–562 (1968)
8. Grumann, J., Mosel, U., Fink, B., Greiner, W.: Investigation of the stability of superheavy nuclei around $Z = 114$ and $Z = 164$. Z. Phys. **228**, 371–386 (1969)
9. Nilsson, S.G., Tsang, C.F., Sobiczewski, A., Szymański, Z., Wycech, S., Gustafson, C., Lamm, I.-L., Möller, P., Nilsson, B.: On the nuclear structure and stability of heavy and superheavy elements. Nucl. Phys. **A131**, 1–66 (1969)
10. Nilsson, S.G., Thompson, S.G., Tsang, C.F.: Stability of superheavy nuclei and their possible occurence in nature. Phys. Lett. **28B**, 458–461 (1969)
11. Meldner, H., Herrmann, G.: Superheavy elements in nature? Z. Naturforschung **24a**, 1429–1430 (1969)
12. Fiset, E.O., Nix, J.R.: Calculation of half-lives for superheavy nuclei. Nucl. Phys. **A193**, 647–671 (1972)
13. Flerov, G.N.: Proceedings of Nobel Symposium 27, Super-Heavy Elements—Theoretical Predictions and Experimental Generation, Ronneby 1974, Phys. Scr. **10A**, 1 (1974)
14. Fricke, B., Greiner, W., Waber, J.T.: The continuation of the periodic table up to $Z = 172$. The chemistry of superheavy elements. Theoret. Chim. Acta **21**, 235–260 (1971)
15. Fricke, B.: Superheavy elements. Struct. Bond. **21**, 89–144 (1975)
16. Keller, O.L., Burnett, J.L., Carlson, T.A., Nestor, C.W.: Predicted properties of the super heavy elements. I. Elements 116 and 114, eka-thallium and eka-lead. J. Phys. Chem. **74**, 1127–1134 (1970)
17. Eichler, B.: Das Flüchtigkeitsverhalten von Transactiniden im Bereich um $Z = 114$ (Voraussage). Kernenergie **19**, 307–311 (1976)
18. Kratz, J.V., Liljenzin, J.O., Seaborg, G.T.: A chemical group separation procedure for superheavy elements and various other reaction products from heavy-ion bombarded uranium targets. Inorg. Nucl. Chem. Lett. **10**, 951–957 (1974)
19. Pitzer, K.S.: Are elements 112, 114, and 118 relatively inert gases? J. Chem. Phys. **63**, 1032–1033 (1975)
20. Waber, J.T., Cromer, D.T., Liberman, D.: SCF Dirac-Slater calculations of the trans-lawrencium elements. J. Chem. Phys. **51**, 664–668 (1969)
21. Herrmann, G.: Superheavy elements. In: Maddock, A.G. (ed.) International Review of Science, Inorganic Chemistry, Radiochemistry, vol. 8, pp. 221–272. Butterworths, London (1975)
22. Thompson, S.G., Tsang, C.F.: Superheavy elements. Science **178**, 1047–1055 (1972)
23. Seaborg, G.T., Loveland, W., Morrissey, D.J.: Superheavy elements—a crossroads. Science **203**, 711–717 (1979)
24. Herrmann, G.: Superheavy-element research. Nature **280**, 543–549 (1979)
25. Kratz, J.V.: The search for superheavy elements. Radiochim. Acta **32**, 25–41 (1983)

26. Flerov, G.N., Ter-Akopyan, G.M.: Superheavy nuclei. Rep. Prog. Phys. **46**, 817–875 (1983)
27. Herrmann, G.: Synthesis of the heaviest chemical elements—results and perspectives. Angew. Chem. Int. Ed. Engl. **27**, 1417–1436 (1988); transl. from Angew. Chem. **100**, 1471–1491 (1988)
28. Schramm, D.N., Fowler, W.A.: Synthesis of superheavy elements in the *r*-process. Nature **231**, 103–106 (1971)
29. Viola, V.E.: On the production of nuclides with $A > 250$ in stellar nucleosynthesis. Nucl. Phys. **A139**, 188–202 (1969)
30. Schramm, D.N., Fiset, E.O.: Superheavy elements and the *r*-process. Astrophys. J. **180**, 551–570 (1973)
31. Howard, W.M., Nix, J.R.: Production of superheavy nuclei by multiple capture of neutrons. Nature **247**, 17–20 (1974)
32. Meyer, B.S., Möller, P., Howard, W.M., Mathews, G.J.: Fission barriers for *r*-process nuclei and implications for astrophysics. In: Behrens, J.W., Carlson, A.D. (eds.) Proceedings of Conference 50 Years with Nuclear Fission, Gaithersburg 1989, pp. 587–591. Amer. Nucl. Soc., La Grange Park (1989)
33. Price, B.P., Fowler, P.H., Kidd, J.M., Kobetich, E.J., Fleischer, R.L., Nichols, G.E.: Study of the charge spectrum of extremely heavy cosmic rays using combined plastic detectors and nuclear emulsions. Phys. Rev. **D3**, 815–823 (1971)
34. Vdovenko, V.M., Sobotovich, M.: The problem of the possible existence of super-heavy elements in nature. Sov. Phys. Doklady **14**, 1179–1182 (1969); transl. from Dokl. Akad. Nauk SSSR Fiz. Ser. **189**, 980–983 (1969)
35. Haack, U.: Suche nach überschweren Transuranelementen. Untersuchung irdischer Minerale mit Hilfe der Spaltspurmethode. Naturwissenschaften **60**, 65–70 (1973)
36. Flerov, G.N., Perelygin, V.P.: Spontaneous fission of lead and the search for transuranium elements. Sov. J. Atom. Energy **26**, 603–605 (1969); transl. from Atomnaya Energiya **26**, 520–522 (1969)
37. Flerov, G.N., Perelygin, V.P., Otgonsurén, O.: Origin of tracks of fission products in lead glasses. Sov. J. Atom. Energy **33**, 1144–1149 (1972); transl. from Atomnaya Energiya **33**, 979–984 (1972)
38. Geisler, F.H., Phillips, P.R., Walker, R.M.: Search for superheavy elements in natural and proton-irradiated materials. Nature **244**, 428–429 (1973)
39. Price, P.B., Fleischer, R.L., Woods, R.T.: Search for spontaneously fissioning elements in nature. Phys. Rev. **C1**, 1819–1821 (1970)
40. Grimm, W., Herrmann, G., Schüssler, H.-D.: Search for superheavy elements in terrestrial matter. Phys. Rev. Lett. **26**, 1040–1043, err. 1408 (1971)
41. Nix, J.R.: Predicted properties of the fission of super-heavy nuclei. Phys. Lett. **30B**, 1–4 (1969)
42. Schmitt, H.W., Mosel, U.: Fission properties of heavy and superheavy nuclei. Nucl. Phys. **A186**, 1–14 (1972)
43. Macklin, R.L., Glass, F.M., Halperin, J., Roseberry, R.T., Schmitt, H.W., Stoughton, R.W., Tobias, M.: Neutron multiplicity counter. Nucl. Instr. Meth. **102**, 181–187 (1972)
44. Ter-Akopyan, G.M., Popeko, A.G., Sokol, E.A., Chelnokov, L.P., Smirnov, V.I., Gorshkov, V.A.: A neutron multiplicity counter for rare spontaneous fission events. Nucl. Instr. Meth. Phys. Res. **190**, 119–124 (1981)
45. Cheifetz, E., Jared, R.C., Giusti, E.R., Thompson, S.G.: Search for superheavy elements in nature. Phys. Rev. **C6**, 1348–1361 (1972)
46. Behringer, K., Grütter, A., von Gunten, H.R., Schmid, A., Wyttenbach, A., Hahn, B., Moser, U., Reist, H.W.: Search for superheavy elements. Phys. Rev. **C9**, 48–55 (1974)
47. Flerov, G.N., Korotkin, Yu.S., Ter-Akopyan, G.M., Zvara, I., Oganessian, Yu.Ts., Popeko, A.G., Chuburkov, Yu.T., Chelnokov, L.P., Maslov, O.D., Smirnov, V.I., Gerstenberger, R.: Results of the searches for superheavy nuclei in the Cheleken penninsula geothermal waters. Z. Phys. **A292**, 43–48 (1979)

48. Chuburkov, Yu.T., Popeko, A.G., Skobelev, N.K.: Concentrating a new natural spontaneously fissile nuclide from Cheleken geothermal brine. Sov. Radiochem. **30**, 108–117 (1988); transl. from Radiokhimiya **30**, 112–121 (1988)
49. Ter-Akopyan, G.M., Sokol, E.A., Fam Ngoc Chuong, Ivanov, M.P., Popeko, G.S., Molzahn, D., Lund, T., Feige, G., Brandt, R.: Search for spontaneous fission activity in Salton sea and Atlantis II hot brines. Z. Phys. **A316**, 213–215 (1984)
50. McMinn, J., Ihle, H.R., Wagner, R.: Use of an electromagnetic isotope separator in the search for element 114 in nature. Nucl. Instr. Meth. **139**, 175–180 (1976)
51. Gentry, R.V., Cahill, T.A., Fletcher, N.R., Kaufmann, H.C., Medsker, L.R., Nelson, J.W., Flocchini, R.G.: Evidence for primordial superheavy elements. Phys. Rev. Lett. **37**, 11–15 (1976)
52. Gentry, R.V.: Radiohalos in a radiochronological and cosmological perspective. Science **184**, 62–66 (1970)
53. Gentry, R.V.: Radioactive halos. Ann. Rev. Nucl. Sci. **23**, 347–362 (1973)
54. Wolke, R.L.: Proposed experiment to corroborate the existence of superheavy element 116 in nature. Phys. Rev. Lett. **37**, 1098–1100 (1976)
55. Bosch, F., El Goresy, A., Krätschmer, W., Martin, B., Povh, B., Nobiling, R., Traxel, K., Schwalm, D.: Comment on the reported evidence for primordial superheavy elements. Phys. Rev. Lett. **37**, 1515–1517 (1976)
56. Wölfli, W., Lang, J., Bonani, G., Suter, M., Stoller, Ch., Nissen, H.-U.: Evidence for primordial superheavy elements? J. Phys. **G3**, L33–L37 (1977)
57. Sparks, C.J., Raman, S., Yakel, H.L., Gentry, R.V., Krause, M.O.: Search with synchrotron radiation for superheavy elements in giant-halo inclusions. Phys. Rev. Lett. **38**, 205–208 (1977)
58. Sparks, C.J., Raman, S., Ricci, E., Gentry, R.V., Krause, M.O.: Evidence against superheavy elements in giant-halo inclusions re-examined with synchrotron radiation. Phys. Rev. Lett. **40**, 507–511, err. 1112 (1978)
59. Stéphan, C., Epherre, M., Cieślak, E., Sowiński, M., Tys, J.: Search for superheavy elements in monazite ore from madagascar. Phys. Rev. Lett. **37**, 1534–1536 (1976)
60. Stakemann, R., Heimann, R., Herrmann, G., Tittel, G., Trautmann, N.: Search for superheavy elements in monazites using chemical enrichment. Nature **297**, 136–137 (1982)
61. Reynolds, J.H., Turner, G.: Rare gases in the chondrite Renazzo. J. Geophys. Res. **69**, 3263–3281 (1964)
62. Anders, E., Heymann, D.: Elements 112–119: were they present in meteorites? Science **164**, 821–823 (1969)
63. Dakowski, M.: The possibility of extinct superheavy elements occuring in meteorites. Earth Planet. Sci. Lett. **6**, 152–154 (1969)
64. Anders, E., Larimer, J.W.: Extinct superheavy element in meteorites: attempted characterization. Science **175**, 981–983 (1972)
65. Anders, E., Higuchi, H., Gros, J., Takahashi, H., Morgan, J.W.: Extinct superheavy element in the allende meteorite. Science **190**, 1262–1271 (1975)
66. Lewis, R.S., Srinivasan, B., Anders, E.: Host phase of a strange xenon component in Allende. Science **190**, 1251–1262 (1975)
67. Manuel, O.K., Hennecke, E.W., Sabu, D.D.: Xenon in carbonaceous chondrites. Nature Phys. Sci. **240**, 99–101 (1972)
68. Manuel, O.K., Sabu, D.D.: Strange xenon, extinct superheavy elements, and the solar neutrino puzzle. Science **195**, 208–209 (1977)
69. Begemann, F.: Isotopic anomalies in meteorites. Rep. Prog. Phys. **43**, 1309–1356 (1980)
70. Lewis, R.S., Anders, E., Shimamura, T., Lugmair, G.W.: Barium isotopes in Allende meteorite: evidence against an extinct superheavy element. Science **222**, 1013–1015 (1983)
71. Popeko, A.G., Skobelev, N.K., Ter-Akopyan, G.M., Goncharov, G.N.: Search for superheavy elements in meteorites. Phys. Lett. **52B**, 417–420 (1974)

72. Flerov, G.N., Ter-Akopyan, G.M., Popeko, A.G., Fefilov, B.V., Subbotin, V.G.: Observation of a new spontaneously fissile nuclide in certain meterorites. Sov. J. Nucl. Phys. **26**, 237–240 (1977); transl. from Yadern. Fiz. **26**, 449–454 (1977)
73. Amirbekyan, A.V., Davtyan, L.S., Markaryan, D.V., Khudaverdyan, A.G.: Once again on the new spontaneously fissile nuclide in the Allende meteorite. Sov. J. Nucl. Phys. **36**, 786–787 (1982); transl. from Yadern. Fiz. **36**, 1356–1359 (1982)
74. Zvara, I., Flerov, G.N., Zhuĭkov, B.L., Reetz, T., Shalaevskiĭ, M.R., Skobelev, N.K.: Experiments on chemical concentration of a new spontaneously fissile nuclide from material of the Allende meteorite. Sov. J. Nucl. Phys. **26**, 240–243 (1977); transl. from Yadern. Fiz. **26**, 455–460 (1977)
75. Lund, T., Becker, H.-J., Jungclas, H., Molzahn, D., Vater, P., Brandt, R.: Are the superheavy elements in the meteorite Allende? Inorg. Nucl. Chem. Lett. **15**, 413–416 (1979)
76. Lund, T., Tress, G., Khan, E.U., Molzahn, D., Vater, P., Brandt, R.: Further attempts to isolate superheavy elements in the meteorite Allende. J. Radioanal. Nucl. Chem. Lett. **93**, 363–370 (1985)
77. Shirk, E.K., Price, P.B.: Charge and energy spectra of cosmic rays with $Z > 60$: the skylab experiment. Astrophys. J. **220**, 719–733 (1978)
78. Fowler, P.H., Walter, R.N.F., Masheder, M.R.W., Moses, R.T., Worley, A., Gay, A.M.: Ariel 6 measurements of the flux of ultraheavy cosmic rays. Astrophys. J. **314**, 739–747 (1987)
79. Otgonsurén, O., Perelygin, V.P., Stetsenko, S.G., Gavrilova, N.N., Fiéni, C., Pellas, P.: Abundances of $Z > 52$ nuclei in galactic cosmic rays: long-term averages based on studies of pallasites. Astrophys. J. **210**, 258–266 (1976)
80. Perelygin, V.P., Stetsenko, S.G.: Search for the tracks of galactic cosmic nuclei with $Z > 110$ in meteorite olivins. JETP Lett. **32**, 608–610 (1980); transl. from Pisma Zh. Eksp. Teor. Fiz. **32**, 622–625 (1980)
81. Perron, C., Bourot-Denise, M., Perelygin, V.P., Birkholz, W., Stetsenko, S.G., Dersch, R., Zhu, T.C., Vater, P., Brandt, R.: Reveletion of heavy ion tracks in olivine: orientation dependent annealing or etching? Nucl. Tracks Radiat. Meas. **15**, 231–234 (1988)
82. Perelygin, V.P., Stetsenko, S.G.: Results of a calibration of olivines from meteorites by means of ^{238}U nuclei at the Bevalac accelerator. JETP Lett. **49**, 292–296 (1989); transl. from Pisma Zh. Eksp. Teor. Fiz. **49**, 257–260 (1989)
83. Otgonsurén, O., Perelygin, V.P., Flerov, G.N.: Search for far transuranic elements in ferromanganese nodules. Sov. Phys. Doklady **14**, 1194–1197 (1970); transl. from Dokl. Akad. Nauk SSSR Fiz. Ser. **189**, 1200–1203 (1969)
84. Oganessian, Yu.: Heaviest nuclei from ^{48}Ca-induced reactions. J. Phys. **G34**, R165–R242 (2007)
85. Sikkeland, T.: Synthesis of nuclei in the region of $Z = 126$ and $N = 184$. In: Ref. [5], pp. 539–552
86. Wong, C.Y.: On the production of the superheavy nucleus ^{310}126. Nucl. Phys. **A103**, 625–643 (1967)
87. Lefort, M.: Recherche des éléments superlourds par synthèse nucléaire. Ann. Physique **5**, 355–376 (1970)
88. Bimbot, R., Deprun, C., Gardès, D., Gauvin, H., Le Beyec, Y., Lefort, M., Pèter, J., Tamain, B.: Complete fusion induced by krypton ions: Indications for synthesis of superheavy nuclei. Nature **234**, 215–216 (1971)
89. Colombani, P., Gatty, B., Jacmart, J.C., Lefort, M., Peter, J., Riou, M., Stéphan, C., Tarrago, X.: Superheavy compound nuclei investigated with in-flight mass spectroscopy. Phys. Lett. **42B**, 208–210 (1972)
90. Marinov, A., Batty, C.J., Kilvingston, A.I., Newton, G.W.A., Robinson, V.J., Hemingway, J.D.: Evidence for the possible existence of a superheavy element with atomic number 112. Nature **229**, 464–467 (1971)
91. Unik, J.P., Horwitz, E.P., Wolf, K.L., Ahmad, I., Fried, S., Cohen, D., Fields, P.R., Bloomquist, C.A.A., Henderson, D.J.: Production of actinides and the search for super-

heavy elements using secondary reactions induced by GeV protons. Nucl. Phys. **A191**, 233–244 (1972)
92. Westgaard, L., Erdal, B.R., Hansen, P.G., Kugler, E., Sletten, G., Sundell, S., Fritsch, T., Henrich, E., Theis, W., Wolf, G.K., Camplan, J., Klapisch, R., Meunier, R., Poszkanzer, A.M., Stéphan, C., Tys, J.: Search for super-heavy elements produced by secondary reactions in uranium. Nucl. Phys. **A192**, 519–523 (1972)
93. Batty, C.J., Kilvingston, A.I., Weil, J.L., Newton, G.A.W., Skarestad, M., Hemingway, J.D.: Search for superheavy elements and actinides produced by secondary reactions in a tungsten target. Nature **244**, 429–430 (1973)
94. Hulet, E.K., Lougheed, R.W., Wild, J.F., Landrum, J.H., Stevenson, P.C., Ghiorso, A., Nitschke, J.M., Otto, R.J., Morrissey, D.J., Baisden, P.A., Gavin, B.F., Lee, D., Silva, R.J., Fowler, M.M., Seaborg, G.T.: Search for superheavy elements in the bombardment of ^{248}Cm with ^{48}Ca. Phys. Rev. Lett. **39**, 385–389 (1977)
95. Illige, J.D., Hulet, E.K., Nitschke, J.M., Dougan, R.J., Lougheed, R.W., Ghiorso, A., Landrum, J.H.: Search for volatile superheavy elements from the reaction ^{248}Cm + ^{48}Ca. Phys. Lett. **78B**, 209–212 (1978)
96. Oganessian, Yu.Ts., Bruchertseifer, H., Buklanov, G.V., Chepigin, V.I., Choy Val Sek, Eichler, B., Gavrilov, K.A., Gäggeler, H., Korotkin, Yu.S., Orlova, O.A., Reetz, T., Seidel, W., Ter-Akopyan, G.M., Tretyakova, S.P., Zvara, I.: Experiments to pro-duce isotopes of superheavy elements with atomic numbers 114–116 in ^{48}Ca ion reactions. Nucl. Phys. **A294**, 213–224 (1978)
97. Ter-Akopyan, G.M., Bruchertseifer, H., Buklanov, G.V., Orlova, O.A., Pleve, A.A., Cherpigin, V.I., Choy Val Sek: Experiments on synthesis of odd neutron deficient isotopes of superheavy elements in reactions induced by ^{48}Ca ions. Sov. J. Nucl. Phys. **29**, 312–316 (1979); transl. from Yad. Fiz. **29**, 608–614 (1979)
98. Armbruster, P., Agarwal, Y.K., Brüchle, W., Brügger, M., Dufour, J.P., Gäggeler, H., Hessberger, F.P., Hofmann, S., Lemmertz, P., Münzenberg, G., Poppensieker, K., Reisdorf, W., Schädel, M., Schmidt, K.-H., Schneider, J.H.R., Schneider, W.F.W., Sümmerer, K., Vermeulen, D., Wirth, G., Ghiorso, A., Gregorich, K.E., Lee, D., Leino, M., Moody, K.J., Seaborg, G.T., Welch, R.B., Wilmarth, P., Yashita, S., Frink, C., Greulich, N., Herrmann, G., Hickmann, U., Hildebrand, N., Kratz, J.V., Trautmann, N., Fowler, M.M., Hoffman, D.C., Daniels, W.R., von Gunten, H.R., Dornhöfer, H.: Attempts to produce superheavy elements by fusion of ^{48}Ca with ^{248}Cm in the bombarding energy range of 4.5–5.2 MeV/u. Phys. Rev. Lett. **54**, 406–409 (1985)
99. Peuser, P., Tharun, U., Keim, H.-J., Trautmann, N., Herrmann, G., Wirth, G.: A low background detection system for fragments and neutrons from spontaneous fission sources. Nucl. Instr. Meth. Phys. Res. **A239**, 529–535 (1985)
100. Lougheed, R.W., Landrum, J.H., Hulet, E.K., Wild, J.F., Dougan, R.J., Dougan, A.D., Gäggeler, H., Schädel, M., Moody, K.J., Gregorich, K.E., Seaborg, G.T.: Search for superheavy elements using the ^{48}Ca + ^{254}Es^{g} reaction. Phys. Rev. **C32**, 1760–1763 (1985)
101. Schädel, M., Kratz, J.V., Ahrens, H., Brüchle, W., Franz, G., Gäggeler, H., Warnecke, I., Wirth, G., Herrmann, G., Trautmann, N., Weis, M.: Isotope distribution in the reaction of ^{238}U with ^{238}U. Phys. Rev. Lett. **41**, 469–472 (1978)
102. Riedel, C., Nörenberg, W.: Theoretical estimates for the production of transuranium elements in heavy-ion collisions. Z. Phys. **A290**, 385–391 (1979)
103. Herrmann, G.: Search for superheavy elements in damped collisions of ^{238}U with ^{238}U. Pure Appl. Chem. **53**, 949–964 (1981)
104. Hildebrand, N., Frink, C., Greulich, N., Hickmann, U., Kratz, J.V., Trautmann, N., Herrmann, G., Brügger, M., Gäggeler, H., Sümmerer, K., Wirth, G.: A cryosystem for the detection of alpha and spontaneous-fission activities in volatile species. Nucl. Instr. Meth. Phys. Res. **A260**, 407–412 (1987)
105. Gäggeler, H., Trautmann, N., Brüchle, W., Herrmann, G., Kratz, J.V., Peuser, P., Schädel, M., Tittel, G., Wirth, G., Ahrens, H., Folger, H., Franz, G., Sümmerer, K., Zendel, M.:

Search for superheavy elements in the $^{238}U + ^{238}U$ reaction. Phys. Rev. Lett. **45**, 1824–1827 (1980)
106. Hildenbrand, K.D., Freiesleben, H., Pühlhofer, F., Schneider, W.F.W., Bock, R., v. Harrach, D., Specht, H.J.: Reaction between ^{238}U and ^{238}U at 7.42 MeV/nucleon. Phys. Rev. Lett. **39**, 1065–1068 (1977)
107. Jungclas, H., Hirdes, D., Brandt, R., Lemmertz, P., Georg, E., Wollnik, H.: Search for superheavy elements in the interaction of ^{136}Xe and ^{238}U with ^{nat}U using the gas jet transport technique. Phys. Lett. **79B**, 58–60 (1978)
108. Aumann, D.C., Faleschini, H., Friedmann, L., Weismann, D.: Search for volatile superheavy elements in heavy-ion reactions. Phys. Lett. **82B**, 361–364 (1979)
109. Kratz, J.V., Brüchle, W., Folger, H., Gäggeler, H., Schädel, M., Sümmerer, K., Wirth, G., Greulich, N., Herrmann, G., Hickmann, U., Peuser, P., Trautmann, N., Hulet, E.K., Lougheed, R.W., Nitschke, J.M., Ferguson, R.L., Hahn, R.L.: Search for superheavy elements in damped collisions between ^{238}U and ^{248}Cm. Phys. Rev. **C33**, 504–508 (1986)
110. Schädel, M., Brüchle, W., Gäggeler, H., Kratz, J.V., Sümmerer, K., Wirth, G., Herr-mann, G., Stakemann, R., Tittel, G., Trautmann, N., Nitschke, J.M., Hulet, E.K., Lougheed, R.W., Hahn, R.L., Ferguson, R.L.: Actinide production in collisions of ^{238}U with ^{248}Cm. Phys. Rev. Lett. **48**, 852–855 (1982)
111. Oganessian, Yu.Ts., Utyonkov, V.K., Lobanov, Yu.V., Abdullin, F.Sh., Polyakov, A.N., Shirokovsky, I.V., Tsyganov, Yu.S., Gulbekian, G.G., Bogomolov, S.L., Gikal, B.N., Mezentsev, A.N., Iliev, S., Subbotin, V.G., Sukhov, A.M., Voinov, A.A., Buklanov, G.V., Subotic, K., Zagrebaev, V.I., Itkis, M.G., Patin, J.B., Moody, K.J., Wild, J.F., Stoyer, M.A., Stoyer, N.J., Shaughnessy, D.A., Kenneally, J.M., Wilk, P.A., Lougheed, R.W., Ilkaev, R.I., Vesnovskii, S.P.: Measurements of cross sections and decay properties of the isotopes of elements 112, 114, and 116 produced in the fusion reactions of $^{233,238}U$, ^{242}Pu, and $^{248}Cm + ^{48}Ca$. Phys. Rev. **C70**, 064609–1/064609–14 (2004)
112. Ghiorso, A., Nitschke, J.M., Alonso, J.R., Alonso, C.T., Nurmia, M., Seaborg, G.T., Hulet, E.K., Lougheed, R.W.: Element 106. Phys. Rev. Lett. **33**, 1490–1493 (1974)
113. Oganessian, Yu.Ts., Iljinov, A.S., Demin, A.G., Tretyakova, S.P.: Experiments on the production of fermium neutron-deficient isotopes and new possibilities of synthesizing elements with $Z > 100$. Nucl. Phys. **A239**, 353–364 (1975)
114. Münzenberg, G., Hofmann, S., Heßberger, F.P., Reisdorf, W., Schmidt, K.H., Schneider, J.H.R., Armbruster, P., Sahm, C.C., Thuma, B.: Identification of element 107 by α correlation chains. Z. Phys. **A300**, 107–108 (1981)
115. Armbruster, P.: On the production of heavy elements by cold fusion: the elements 106–109. Ann. Rev. Nucl. Part. Sci. **35**, 135–194 (1985)
116. Čwiok, S., Pashkevich, V.V., Dudek, J., Nazarevicz, W.: Fission barriers of trans-fermium elements. Nucl. Phys. **A410**, 254–270 (1983)
117. Möller, P., Leander, G.A., Nix, J.R.: On the stability of transeinsteinium elements. Z. Phys. **A323**, 41–45 (1986)
118. Silva, R., Harris, J., Nurmia, M., Eskola, K., Ghiorso, A.: Chemical separation of rutherfordium. Inorg. Nucl. Chem., Lett. **6**, 871–877 (1970)
119. Hulet, E.K., Lougheed, R.W., Wild, J.F., Landrum, J.H., Nitschke, J.M., Ghiorso, A.: Chloride complexation of element 104. J. Inorg. Nucl. Chem. **42**, 79–82 (1980)
120. Zvara, I., Belov, V.Z., Domanov, V.P., Korotkin, Yu.S., Chelnokov, L.P., Shalaevs-kii, M.R., Shegolev, V.A., Hussonnois, M.: Chemical isolation of kurchatovium. Sov. Radiochem. **14**, 115–118 (1972); transl. from Radiokhimiya **14**, 119–122 (1972)
121. Zvara, I., Eichler, B., Belov, V.Z., Zvarova, T.S., Korotkin, Yu.S., Shalaevskii, M.R., Shegolev, V.A., Hussonnois, M.: Gas chromatography and thermochromatography in the study of transuranic elements. Sov. Radiochem. **16**, 709–715 (1974); transl. from Radiokhimiya **16**, 720–727 (1974)
122. Zvara, I., Belov, V.Z., Domanov, V.P., Shalaevskii, M.R.,: Chemical isolation of nilsbohrium as ekatantalum in the form of the anhydrous bromide. II: Experiments with a

spontaneously fissioning isotope of nilsbohrium. Sov. Radiochem. **18**, 328–334 (1976); transl. from Radiokhimiya **18**, 371–377 (1976)
123. Gregorich, K.E., Henderson, R.A., Lee, D.M., Nurmia, M.J., Chasteler, R.M., Hall, H.L., Bennett, D.A., Gannett, C.M., Chadwick, R.B., Leyba, J.D., Hoffman, D.C., Herrmann, G.: Aqueous chemistry of element 105. Radiochim. Acta **43**, 223–231 (1988)
124. Herrmann, G., Trautmann, N.: Rapid chemical methods for the identification and study of short-lived nuclides. Ann. Rev. Nucl. Part. Sci. **32**, 117–147 (1982)
125. Brüchle, W., Schädel, M., Scherer, U.W., Kratz, J.V., Gregorich, K.E., Lee, D., Nurmia, M., Chasteler, R.M., Hall, H.L., Henderson, R.A., Hoffman, D.C.: The hydration enthalpies of Md^{3+} and Lr^{3+}. Inorg. Chim. Acta **146**, 267–276 (1988)
126. Jost, D.T., Gäggeler, H.W., Vogel, Ch., Schädel, M., Jäger, E., Eichler, B., Gregorich, K.E., Hoffman, D.C.: Search for lawrencium as a p-element using gas chromatography techniques. Inorg. Chim. Acta **146**, 255–259 (1988)
127. Schädel, M., Brüchle, W., Jäger, E., Schimpf, E., Kratz, J.V., Scherer, U.W., Zimmermann, H.P.: ARCA II, a new apparatus for fast, repetitive HPLC separations. Radio-chimica Acta **48**, 171–176 (1989)
128. Gäggeler, H.W., Jost, D.T., Baltensperger, U., Weber, A., Kovacs, A., Vermeulen, D., Türler, A.: OLGA II, an on-line gas chemistry apparatus for applications in heavy element research. Nucl. Instr. Meth. Phys. Res. **A309**, 201–208 (1991)
129. Kratz, J.V., Zimmermann, H.P., Scherer, U.W., Schädel, M., Brüchle, W., Gregorich, K.E., Gannett, C.M., Hall, H.L., Henderson, R.A., Lee, D.M., Leyba, J.D., Nurmia, M.J., Hoffman, D.C., Gäggeler, H., Jost, D., Baltensperger, U., Nai-Qi, Ya., Türler, A., Lienert, Ch.: Chemical properties of element 105 in aquaeous solution. Halide complex formation and anion exchange into triisooctylamine. Radiochim. Acta **48**, 121–133 (1989)
130. Gäggeler, H.W., Jost, D.T., Kovacs, J., Scherer, U.W., Weber, A., Vermeulen, D., Türler, A., Gregorich, K.E., Henderson, R.A., Czerwinski, K.R., Kadkhodayan, B., Lee, D.M., Nurmia, M.J., Hoffman, D.C., Kratz, J.V., Gober, M.K., Zimmermann, H.P., Schädel, M., Brüchle, W., Schimpf, E., Zvara, I.: Gas phase chromatography experiments with bromides of tantalum and element 105. Radiochim. Acta **57**, 93–100 (1992)

Publisher's Erratum to: Theoretical Chemistry of the Heaviest Elements

Valeria Pershina

Publisher's Erratum to: Chapter "Theoretical Chemistry of the Heaviest Elements" in: M. Schädel and D. Shaughnessy (eds.), *The Chemistry of Superheavy Elements*, DOI 10.1007/978-3-642-37466-1_3

Some mistakes were introduced during the production of this book. Please find the corrected information in the following table.

The online version of the original chapter can be found under DOI 10.1007/978-3-642-37466-1_3

V. Pershina (✉)
GSI Helmholtzzentrum für Schwerionenforschung, Darmstadt, Germany
e-mail: V.Pershina@gsi.de

DOI: 10.1007/978-3-642-37466-1_10,

Page	Line	Incorrect in the text	Should read as
154	6	IPi	IP_1
Table 3, left column			
	8	IP*	IP_2,
	12	IP_{4j}	IP_4,
	14	IPs, ev	IP_5, eV
	20	IPs	IP_8
154	Third line from bottom	[k] [129, 140]	[k] [128, 140]
Footnote of Table 4			
157	Third and second lines from bottom	A. Borschevky, V. Pershina, E. Eliav, U. Kaldor, J. Chem. Phys. **136**, 134317 (2012).	V. Pershina, A. Borschevsky, J. Anton, J. Chem. Phys. **136**, 134317 (2012).
Fig. 11, caption			
161	11	R_{max}, AOs	R_{max} of AOs
163	21	element 114–115	element 114 to element 115
167	3	10.14	103.6
Table 9, 6th column			
168	14 from bottom	were predicted	was predicted
179	Last line in the table	−0.08	−0.14
Table 12, third column			
182	Third line from bottom (above the table)	of a various	of various
215	8 (main text)	[294]	[295]
	12 (main text)	[295]	[296]
	14 (main text)	[296]	[297]
216	8 (main text)	[280, 281]	[298, 299]
217	5 (main text)	[298]	[300]
218	6 (main text)	[299]	[301]
218	10 (main text)	[300]	[302]
219	6 (main text)	[300]	[302]

(continued)

(continued)

Page	Line	Incorrect in the text	Should read as
220	7	[301]	[303, 304]
220	11	[303, 304]	[305]
221	Fourth line from bottom	[306, 307]	[308]
222	Caption of Table 31	[303, 304]	[309]
222	11 (main text)	[303, 304]	[309]
222	Fifth line from bottom	[305]	[310]

Index

M. Schädel and D. Shaughnessy (eds.), *The Chemistry of Superheavy Elements*,
DOI: 10.1007/978-3-642-37466-1, © Springer-Verlag Berlin Heidelberg 2014

D

S

T